

PALACKÝ UNIVERSITY OLMOUC

Faculty of Science

Laboratory of Growth Regulators



**Modulation of nuclear receptors' activity
in relation to human cancer**

Dissertation thesis

Author:	Mgr. Miroslav Peřina
Study programme:	P0511D030004 Experimental biology
Study course:	Experimental biology
Form of study:	Full-time
Supervisor:	Mgr. Radek Jorda, Ph.D.
Year of study beginning:	2020

Declaration

"I hereby declare that I prepared the dissertation independently, indicating all sources used and co-authorships. I agree with the publication of the thesis according to Act no. 111/1998 Coll., Universities, as amended. I have been made aware that my work is subject to rights and obligations arising from law no. 121/2000 Coll., Copyright Act, as amended."

In Olomouc, 12. 4. 2024

.....

Acknowledgement

"I would like to thank my supervisor, MSc. Radek Jorda, Ph.D., for his professional guidance, helpful attitude and for the time he has devoted to me. At the same time, I would like to thank Prof. RNDr. Vladimír Kryštof, Ph.D. and MSc. Eva Řezníčková, Ph.D. for their valuable advice and Assoc. Prof. Frédéric Santer, Ph.D. for his guidance during my internship abroad. I would also like to thank all the members of the Department of Experimental Biology, Palacký University Olomouc, for their help and advice, especially MSc. Jakub Bělíček, MSc. Veronika Vojáčková, MSc. Markéta Kovalová, Ph.D., MSc. Hana Dostálová, Msc. Denisa Veselá, Ph.D. and Jana Hudcová for their support. Finally, my biggest thanks go to my wife MSc. Martina Peřinová and my family."

Bibliographical identification

Author's first name and surname	Miroslav Peřina
Title	Modulation of nuclear receptors' activity in relation to human cancer
Type of thesis	Dissertation
Department	Laboratory of Growth Regulators, Palacký University Olomouc
Supervisor	Mgr. Radek Jorda. Ph.D.
The year of presentation	2024

Abstract

The next-generation hormone therapies improved outcomes of prostate cancer patients, but nearly all eventually progress to develop resistance. Therefore, the discovery of novel agents is needed to improve the treatment efficacy. The main part of the dissertation thesis investigated the biological activity of the library of dihydrotestosterone derivatives with different modifications on the A-ring (119 compounds in total) prepared by Éva Frank's (University of Szeged, Hungary) synthetic group. The A-ring fused pyrazole modification of dihydrotestosterone was the most potent structural motif, with representatives displaying strong antagonist activity against androgen receptor transactivation and potent antiproliferative activity, surpassing standard androgen receptors' antagonists enzalutamide and galeterone. Lead compound potently downregulated and degraded androgen receptor, even in patients' samples *ex vivo*. Molecular docking studies provided the structural basis of compounds' activity, revealing interactions and potential for further optimization. In the other part of the dissertation, given the role of the glucocorticoid receptor in acquired resistance, novel hydrocortisone's derivatives were also analysed and dual antagonists of androgen and glucocorticoid receptors were described. The lead compound suppressed the signalling of both receptors, the interactions were proved in cells and modelled by molecular docking. Overall, the dissertation study provided valuable insights into the design and development of novel androgen receptor-targeted compounds for the treatment of prostate cancer, highlighting their potential as alternative or complementary therapies to existing standards of care.

Keywords	Androgen receptor, prostate cancer, antagonist
Number of pages	97
Number of appendices	5
Language	English

Bibliografická identifikace

Jméno a příjmení autora	Miroslav Peřina
Název práce	Modulace activity jaderných receptorů ve vztahu k lidským nádorovým onemocněním
Typ práce	Disertační
Pracoviště	Laboratoř růstových regulátorů, Přírodovědecká fakulta, Univerzita Palackého v Olomouci
Vedoucí práce	Mgr. Radek Jorda. Ph.D.
Rok obhajoby práce	2024

Abstrakt

Hormonální terapie nové generace zlepšily výsledky léčby pacientů s karcinomem prostaty, ale téměř u všech nakonec dochází k rozvoji rezistence. Pro zlepšení účinnosti léčby karcinomu prostaty je proto zapotřebí vývoj nových léčiv. V hlavní části disertační práce byla analyzována biologická aktivita knihovny dihydrotestosteronových derivátů s různými modifikacemi na A-kruhu (celkem 119 sloučenin) připravené syntetickou skupinou Évy Frank (University of Szeged, Maďarsko). Modifikace dihydrotestosteronu fúzí s pyrazolem byla obecně nejúčinnějším strukturním motivem analyzovaných sloučenin, jejíž zástupci vykazovali silnou antagonistickou aktivitu vůči transaktivaci androgenového receptoru a silnou antiproliferativní aktivitu vůči buňkám karcinomu prostaty, převyšující standardní antagonisty enzalutamid a galeteron. Nejúčinnější látka vyvolala snížení exprese a degradaci androgenového receptoru, a to i ve vzorcích pacientů *ex vivo*. Molekulárním dokováním byl popsán strukturní základ aktivity sloučenin a objasněna interakce s ligand-vazebnou doménou androgenového receptoru i potenciál pro další optimalizaci. V další části disertační práce, vzhledem k roli glukokortikoidového receptoru u získané rezistence, byly také analyzovány deriváty hydrokortizonu a popsáni duální antagonisté androgenového a glukokortikoidového receptoru. Vedoucí sloučenina potlačila signalizaci obou receptorů a interakce s nimi byly detailně popsány. Obecně poskytla disertační práce cenné poznatky pro návrh a vývoji nových sloučenin cílených pro léčbu karcinomu prostaty a zdůraznila jejich potenciál jako alternativních nebo doplňkových terapií ke stávajícím standardním přístupům.

Klíčová slova	Androgenový receptor, karcinom prostaty, antagonist
Počet stran	97
Počet příloh	5
Jazyk	Anglický

CONTENT

LIST OF ABBREVIATIONS	7
1 OBJECTIVES OF THE THESIS	10
2 NUCLEAR RECEPTORS	11
2.1 Androgen receptor	13
2.2 Androgen receptor's activation and regulation	15
2.3 Androgen receptor's role in prostate cancer development and progression	18
2.4 Androgen receptor's role in the castration-resistant prostate cancer	20
3 Targeting androgen receptor in management of prostate cancer	22
3.1 Androgen deprivation therapy	23
3.2 Steroidal antiandrogens	25
3.2.1 Investigational steroidal compounds	28
3.3 Non-steroidal antiandrogens	30
3.3.1 First-generation non-steroidal antiandrogens	30
3.3.2 Second-generation non-steroidal antiandrogens	31
3.3.3 Investigational non-steroidal antiandrogens	33
3.4 Co-activators' inhibition	34
3.5 Targeting other domains of androgen receptor	36
3.6 Targeted degradation of androgen receptor	37
3.6.1 Monovalent inducers of androgen receptor's degradation	38
3.6.2 Molecular glues and autophagic degraders of androgen receptor	40
3.6.3 Proteolysis targeting chimeras	40
3.7 Resistance to known therapies and its management	42
3.8. Development of novel therapies for prostate cancer	44
4 MATERIALS AND METHODS	46
4.1 Commercial compounds	46
4.2 Cell cultures	46
4.2.1 Androgen and glucocorticoid receptors' transactivation assay	46
4.2.2 Cell viability assay	47
4.2.3 Colony formation assay	47
4.2.4 Cell lysis, electrophoresis and Western blot	47
4.2.5 Fractionation of cellular compartments	48
4.2.6 Cellular thermal shift assay	48
4.2.7 Cell cycle analysis	49
4.2.8 Analysis of mRNA expression	49
4.2.9 Androgen receptor preparation and micro-scale thermophoresis	49
4.2.10 Molecular docking	50
5 SURVEY OF RESULTS AND DISCUSSION	51
5.1 Screening and discovery of novel androgen receptor's antagonists	52
5.2 Compounds' effect on downstream signalling and the cell cycle	58
5.3 Androgen receptor's downregulation and degradation	60
5.4 Analysis of compounds' interaction with androgen receptor	62
5.5 Optimisation of cell fractionation and cellular thermal shift assay	63
5.6 Dual targeting of androgen and glucocorticoid receptors	68
6 CONCLUSION AND PERSPECTIVES	71
7 REFERENCE	73
8 CURRICULUM VITAE	91
9 APPENDICES	96

LIST OF ABBREVIATIONS

11 β -HSD2	11 β -hydroxysteroid dehydrogenase 2
3 β -HSD	3 β -hydroxysteroid dehydrogenase
ACE2	angiotensin-converting enzyme 2
ADT	androgen deprivation therapy
AE	adverse effect
AF-1	activation function 1
AF-2	activation function 2
AKR1C3	aldo-keto reductase 3
AKT	protein kinase B
AR	androgen receptor
ARE	androgen response element
AR-FL	full-length androgen receptor
AR-V7	androgen receptor splicing variant 7
AR-Vs	androgen receptor splicing variants
BET	bromodomain and extra-terminal motif
BPH	benign prostatic hyperplasia
BrCa	breast cancer
BSA	bovine serum albumin
CAR	constitutive androstane receptor
CBP	cAMP response element-binding protein-binding protein
CDK	cyclin-dependent kinases
CETSA	cellular-thermal shift assay
cf-DNA	circulating free DNA
c-MYC	cellular myelocytomatosis oncogene
CNA	copy number alteration
CNS	central nervous system
COUP2TF1	chicken ovalbumin upstream promoter transcription factor 1
CPA	cyproterone acetate
CRBN	cereblon
CRPC	castration-resistant prostate cancer
CSPC	castration-sensitive prostate cancer
CSS	charcoal-stripped serum
CYP 11A1	cytochrome P450 cholesterol side chain cleavage enzyme
CYP17A1	cytochrome P450 17 α -hydroxylase, 17,20-lyase
DAX1	dosage-sensitive adrenal hypoplasia X-linked 1
DBD	DNA binding domain
DDR	DNA damage repair
DHEA	dehydroepiandrosterone
DHT	5 α -dihydrotestosterone
DMEM	Dulbecco's modified Eagle medium
EAR2	erythroblast transformation member 2
ER	oestrogen receptor
ERR	estrogen-related receptor
FBS	foetal bovine serum
FDA	US Food and Drug Administration
FSH	follicle-stimulating hormone
FXR	farnesoid X receptor
GNCF	germ cell nuclear factor

GnRH	gonadotropin-releasing hormone
GR	glucocorticoid receptor
HGPIN	high-grade prostatic intraepithelial neoplasia
HNF4	hepatocyte nuclear factor
HPLC/MS	high-performance liquid chromatography with mass spectrometry
HR	hinge region
HRE	hormone response element
HSP	heat shock protein
KLK3	kallikrein-related peptidase 3
LBD	ligand binding domain
LBP	ligand binding pocket
LH	luteinizing hormone
LHR1	liver homolog receptor 1
LHRH	luteinizing hormone-releasing hormone
LXR	liver X receptor
mCRPC	metastatic castration-resistant prostate cancer
mCSPC	metastatic castration sensitive prostate cancer
MDM2	mouse double minute 2 homolog
MFS	metastasis-free survival
mPCa	metastatic prostate cancer
MR	mineralocorticoid receptor
MST	micro-scale thermophoresis
NES	nuclear export signal
nmCRPC	non-metastatic castration-resistant prostate cancer
Nkx3.1	NK homeobox, family 3, A
NOR1	neuron-derived orphan receptor
NR	nuclear receptor
NTD	N-terminal domain
NURR1	nuclear receptor-related 1
NURR77	nuclear receptor-related 77
OS	overall survival
PARP	poly ADP-ribose polymerase
PCa	prostate cancer
PDT	photodynamic therapy
PFS	progression-free survival
PI3K	phosphatidylinositol-3-kinase
PIN	prostatic intraepithelial neoplasia
PNR	photoreceptor-specific nuclear receptor
PPAR	peroxisome proliferator-activated receptor
PR	progesterone receptor
PROTAC	proteolysis-targeting chimera
PSA	prostate-specific antigen
PSMA	prostate-specific membrane antigen
PTEN	phosphatase and tensin homolog
PTM	post-translational modifications
PTT	photothermal therapy
PXR	pregnane X receptor
RAR	retinoic acid receptor
REVERB	reverse ERB receptor
RIPA	radioimmunoprecipitation buffer

RPMI	Roswell Park Memorial Institute 1640 Medium
ROR	retinoic acid receptor-related orphan receptor
RXR	retinoid X receptor
SAR	structure and activity relationship
SARD	selective androgen receptor degrader
SARM	selective androgen receptor modulator
SDS	sodium-dodecyl sulphate
SDS-PAGE	SDS-polyacrylamide gel electrophoresis
SF1	steroidogenic factor 1
SHBG	sex hormone-binding globulin
SHP	small heterodimer partner
TF	transcription factor
THR	thyroid hormone receptor
TLX	T-cell leukaemia homeobox protein
TMPRSS2	transmembrane serine protease 2
TR	testicular receptor
TR2	testicular receptor 2
UPS	ubiquitin-proteasome system
VDR	vitamin D receptor
VHL	von Hippel-Lindau protein

1 OBJECTIVES OF THE THESIS

Nuclear receptors (NRs) are crucial regulators of physiological processes and diseases, with the androgen receptor (AR) having a pivotal role in prostate cancer (PCa) (Dhiman *et al.*, 2018; Velho *et al.*, 2021). Over the years, the treatment of PCa has undergone significant advancements and targeting of AR has been utilized to improve patients' outcomes. Initially, antiandrogens were steroid-based (Dawson *et al.*, 2000), the next development focused on non-steroidal compounds, which were successfully approved, but the steroid-based AR antagonists are less exploited. Several steroidal compounds, mostly modified on the D-ring of the androstane core have been investigated (Cortés-Benítez *et al.*, 2016; Shi *et al.*, 2018; Jorda *et al.*, 2019a, Jorda *et al.*, 2019b), but apart of approved androgens' synthesis inhibitor abiraterone (Jarman *et al.*, 1998) only galeterone (Njar and Brodie, 2015) entered clinical trials, unfortunately without successful approval. (Taplin *et al.*, 2019). For the abovementioned reasons, investigation of novel agents is desirable and identification of new predictive biomarkers of resistance is needed to improve treatment efficacy.

Compared to D-ring fused or substituted steroid derivatives, compounds containing a heterocycle moiety on the A-ring have been recently much less investigated. In collaboration with Éva Frank's (University of Szeged, Hungary) synthetic group, the main objective of the dissertation thesis was to characterise the biological activity of already published and novel A-ring substituted 5 α -dihydrotestosterone (DHT)-derivatives, searching for potent and selective AR modulators, predominantly antagonists. The compounds were intended to be analysed for their agonist and antagonist activities towards AR, their binding into the AR, antiproliferative activity in PCa cell lines (both AR-positive and AR-negative ones), the influence of the AR level or downstream signalling (**Appendix I. – III.**).

The other objective was to evaluate the biological activity of hydrocortisone's derivatives prepared by the synthetic group of Gyula Schneider and Erzsébet Mernyák (University of Szeged, Hungary). Compounds were intended to be analysed for their agonist or antagonist activity towards both the androgen and glucocorticoid (GR) receptors and appropriate PCa cell lines (**Appendix IV.**).

As a part of this thesis, several D-ring-attached steroidal isoxazoles and triazoles (similar to abiraterone) were planned to be characterised for their presumed CYP17A1 inhibitory effect and AR-antagonist activity (**Appendix V.**).

2 NUCLEAR RECEPTORS

NRs have historically been at the forefront of cancer research. The family comprises 48 transcription factors (TFs) pivotal in regulating a multitude of physiological processes, including metabolism, immunity, development and cell proliferation. However, they also act as critical regulators of diseases and serve as biomarkers for tumour classification and targets for hormone therapy (Mangelsdorf *et al.*, 1995; Dhiman *et al.*, 2018). Unlike other transcription factors, many NRs directly bind small lipophilic ligands (easily diffusing through the cytoplasmic membrane) in the cytosol or possibly in the nucleus, the main place of their action (Evans, 1988; Zhao *et al.*, 2019) The NR family of transcription factors can be divided into three categories by their ligands: the endocrine NRs (utilizing endocrine hormones as their endogenous ligands), the orphan NRs (no natural ligand described yet) and the adopted NRs (formerly considered orphans, but later their natural ligands were discovered) (**Table 1**) (Yang *et al.*, 2021).

Table 1 Groups of nuclear receptors based on their ligands. Oestrogen receptor (ER), vitamin D receptor (VDR), retinoic acid receptor (RAR), androgen receptor (AR), mineralocorticoid receptor (MR), glucocorticoid receptor (GR), progesterone receptor (PR), thyroid hormone receptor (THR), REVERB – reverse ERB receptor, testicular receptor TR, neuron-derived orphan receptor (NOR1), nuclear receptor related 1 (NURR1), nuclear receptor related 77 (NURR77), hepatocyte nuclear Factor (HNF4), constitutive androstane receptor (CAR), retinoic acid receptor-related orphan receptor (ROR), oestrogen-related receptor (ERR), peroxisome proliferator-activated receptor (PPAR), retinoid X receptor (RXR), liver X receptor (LXR), steroidogenic factor 1 (SF1), pregnane X receptor (PXR), farnesoid X receptor (FXR), dosage-sensitive adrenal hypoplasia X-linked 1 (DAX1), small heterodimer partner (SHP), testicular receptor 2 (TR2), chicken ovalbumin upstream promoter transcription factor (COUPTF), liver homolog receptor 1 (LHR1), erythroblast transformation member 2 (EAR2), T-cell leukaemia homeobox protein (TLX), photoreceptor-specific nuclear receptor (PNR), germ cell nuclear factor (GCNF) (Dhiman *et al.*, 2018; Yang *et al.*, 2021).

Human nuclear receptors	
Endocrine	ER α , ER β , VDR, RAR α , RAR β , RAR γ , AR, MR, GR, PR, THR α , THR β
Adopted	REVERB α , REVERB β , TR4, NOR1, NURR1, NURR77, HNF4 α , HNF4 γ , CAR, ROR α , ROR β , ROR γ , ERR α , ERR β , ERR γ , PPAR α , PPAR β , PPAR γ , RXR α , RXR β , RXR γ , LXR α , LXR β , SF1, PXR, FXR
Orphan	DAX1, SHP, TR2, COUPTF1, COUPTF2, LHR1, EAR2, TLX, PNR, GNCF

Upon ligand binding, conformational changes occur within NR proteins, leading to diverse functional outcomes. These changes facilitate NR binding to specific DNA target motifs (hormone response elements – HREs) within the genome and modulate the transcription of target genes. It's important to note that NR-mediated effects on gene expression aren't solely dependent on HREs; ligand-bound NRs can also interact with other TFs within chromatin complexes (Danielian *et al.*, 1992).

The NR can quickly react to changes in the cellular environment, making them important parts of signalling pathways. Many tissues in the body express different types of NRs responding to various signals, which is why they play crucial roles in both normal body functions and diseases (Becnel *et al.*, 2015). Early research of NRs linked steroid hormones' receptors to PCa (AR) and BrCa (ER) development and progression (Bluemn *et al.*, 2012; Thomas and Gustafsson, 2015). Later it was found, that the presence or absence of certain NRs, like the ER and (PR), can affect patient survival and response to treatment in BrCa. Using specific detection, the NRs' expression can be used for tumour classification and prediction of their response to hormone therapy (Bardou *et al.*, 2003).

In the past, much attention has been given to studying the specific roles of particular NRs in different types of cancer. However, gene regulation in cells involves complex interactions among multiple proteins and most tissues express several NRs that are linked to cancer. These findings suggest that NRs likely cooperate in cancer cells, forming a network with various chromatin modifiers, signalling molecules, transcriptional co-regulators, and pioneer factors (Kittler *et al.*, 2013; Dhiman *et al.*, 2018). More importantly, it was found that tissue-specific expression of crucial NRs might play oncogenic, tumour-suppressive or both roles in the cancerogenesis of different cancers. For example, the clear oncogenic role of AR in PCa (Sharma *et al.*, 2013) differs from its possible tumour-suppressive role in bladder cancer (Boorjian *et al.*, 2004).

Taken together, NRs are pivotal in the development and perpetuation of cancer characteristics. Numerous drugs targeting NRs have been extensively employed in treating cancer, or are currently undergoing evaluation in clinical trials (Yang *et al.*, 2021). With advancing knowledge regarding the involvement of NRs in physiological and pathological cellular processes, there is a promise of the emergence of novel approaches capable of targeting these receptors with enhanced efficacy and reduced adverse effects (AEs) in cancer therapy.

2.1 Androgen receptor

The AR, also known as NR3C4 (nuclear receptor subfamily 3, group C, member 4), is a NR that binds the androgen hormones, primarily testosterone and DHT. Acting as a TF, it plays a crucial role in the physiological development of both primary and secondary male sexual characteristics. The *AR* gene is located on the X chromosome, specifically on the long arm in the *Xq11 to Xq12* loci (Velho *et al.*, 2021). It consists of 8 exons and introns and the protein product comprises 919 amino acids forming three main domains along with a hinge region, resulting in a final molecular weight of 110 kDa (Tan *et al.*, 2015). Exon 1 encodes the N-terminal domain (NTD), exons 2 and 3 encode the DNA binding domain (DBD), and exons 4 to 8 encode the ligand binding domain (LBD) and hinge region (HR). The complete structure of the AR is illustrated in **Figure 1**.

The NTD is the largest part of AR, spanning 555 amino acids (Velho *et al.*, 2021). It plays an important role in receptor activation, cooperating with the LBD. Within the NTD, there is a so-called activation function 1 (AF-1), located between amino acids 142 and 485. Two regions within AF-1, Tau-1 (amino acid residues 110 to 370) and Tau-5 (amino acid residues 360 to 485), are essential for achieving full receptor activation. Additionally, specific sequences within the NTD, including FQNLF (amino acid residues 23 - 27) and WHTLF (amino acid residues 433 - 437), are necessary for establishing a direct interaction between the NTD and LBD. This interaction is crucial for regulating many androgen-dependent genes (Davey and Grossmann, 2016). Moreover, this domain interaction aids receptor dimerization and stabilisation, with subsequent impairment of ligand dissociation from LBD.

The DBD spans from the 556 - 623 amino acid residues and is highly conserved (Tan *et al.*, 2015). Its core is formed from a cysteine-rich region containing two zinc fingers (Cys2-His2 type) which enable the binding of the receptor to the HREs on the DNA. Within the DBD and the HR (624 - 665), there is a nucleus-transport signal region (residues 617 - 633). This transport of the activated AR is crucial, as passive movement through the nuclear membrane is limited. Therefore, upon the ligand binding, the AR undergoes a conformational change with the nucleus-transport signal region exposure. Additionally, the HR enhances DNA binding and serves as a target for acetylation, methylation, and ubiquitination (Wen *et al.*, 2020).

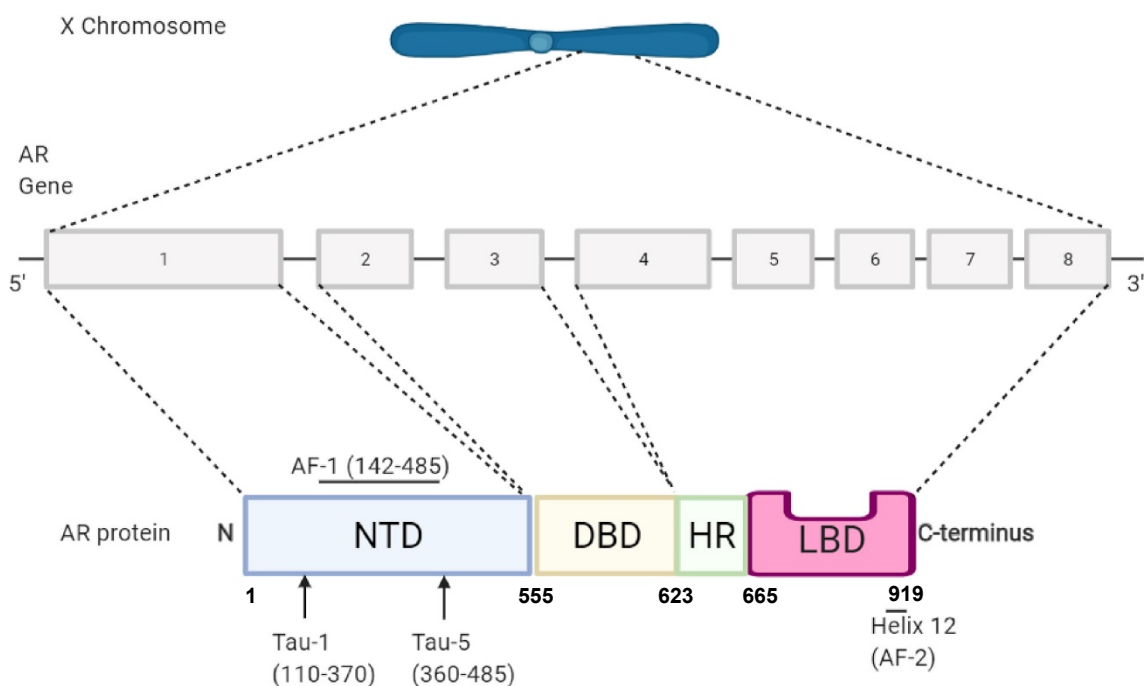


Figure 1 The AR gene/protein structure. The AR gene is transcribed from the X chromosome with 8 exons. The exon 1 codes for the NTD, exons 2 and 3 code for the DBD and exons 4-8 code for the HR and the LBD. AF-1 resides within the NTD, with two activation domains Tau-1 and Tau-5, while Activation Function-2 (AF-2) resides mainly within the final helix H12 of the LBD. Taken from Maylin *et al.*, 2021.

The LBD spans from amino acid residues 666 - 919. Unlike the NTD, its structure has been extensively described using crystallography since the early 21st century (Matias *et al.*, 2000). This domain comprises 11 α -helices and 2 antiparallel folded β -sheets. The entire structure is sandwiched into 3 layers. The first layer contains helices H1 and H3, while H2, commonly found in the LBD of most NRs, is absent in the AR and is replaced by a long flexible linker. The middle layer consists of H4, H5, a β -folded sheet, H8 and H9. The third layer includes H10 and H11. The direct binding site of the ligand, known as the ligand binding pocket (LBP), is surrounded by the N-terminal segments of H3, H5, and H11. The AF-2, formed by helix H12, acts as the "lid" of the LBP (**Figure 2**). After ligand binding, AF-2 closes the LBP by altering its conformation. Additionally, the LBD regulates the AR nuclear/cytoplasmic shuttling by ligand detection (Tyagi *et al.*, 2000) with a nearby located nuclear export signal (NES) (Saporita *et al.*, 2003). In addition to the classic AR structure described above, several other variants were described, both in healthy and malignant cells (Velho *et al.*, 2021). These morphologically different variants are known as AR splicing variants (AR-Vs), arising from alternative splicing of intron regions during the pre-mRNA splicing (Nakazawa *et al.*, 2014). They confer the resistance towards antiandrogens, which is described in detail in section 2.4.

2.2 Androgen receptor's activation and regulation

The current model of testosterone action is initiated by its synthesis, primarily by the Leydig cells in the testes (secondary in target tissues from adrenal androgens), under the regulation of luteinizing hormone (LH) secreted by the anterior pituitary gland. LH secretion is upstream regulated by gonadotropin-releasing hormone (GnRH). (Dai *et al.*, 2017). Once synthesised, testosterone is transported bound to serum sex hormone-binding globulin (SHBG) or albumin (Baker *et al.*, 2002), with only the free form entering prostate cells. Upon internalisation, testosterone is converted into a more potent metabolite DHT, which activates the AR (described below), to regulate the transcription, leading to the proliferation, survival and growth of prostate cells (Dehm and Tindall, 2006). The presence of androgens and functional AR is crucial for male sexual differentiation, prostate development and physiological processes (Heinlein and Chang, 2004). AR's significance in disease is considerable, as it is implicated in conditions ranging from complete androgen insensitivity syndrome and spinal bulbar muscular atrophy (Brinkmann, 2001) to PCa or BrCa. In the PCa, the dependence on AR signalling is clear and it has been exploited for therapeutic intervention for decades.

The nature of the AR ligand can be agonist (enhances the transcriptional activity), or antagonist (suppresses the transcriptional activity), or its effects may be mixed or variable. AR can bind a wide range of ligands by a flexible accommodation of the LBP (Gao *et al.*, 2005). Generally, natural agonists are small lipophilic molecules derived from cholesterol. The activation of AR follows similar principles within the known physiological agonists (testosterone or DHT) or synthetic analogues (metribolone (R1881) and initiates by the interaction between the AR and the ligand in the cytosol of the cell (Tan *et al.*, 2015). In the cytosol, AR is found as an inactive monomer bound to chaperones from the heat shock protein (HSP) family (HSP90, HSP70) or co-chaperones (p23) (Cano *et al.*, 2013). Upon ligand binding to the LBP, the receptor is released from HSP. Through the signal sequence in the DBD and the HR, the ligand-bound AR monomer is transported into the nucleus and dimerizes with another AR molecule (Chen *et al.*, 2012). Posttranslational modifications (PTM) (primarily phosphorylation) play a crucial role in AR activation and can take place in the cytosol or nucleus. Following dimerization, AR binds to androgen response elements (AREs) in the promoter region of downstream target genes (e.g., prostate-specific antigen (PSA)), by a zinc finger motif. This binding results in the formation of an AR-dimer complex with

coactivators and other DNA-binding proteins, leading to full activation of AR's transcriptional activity. DHT is stronger agonist compared to testosterone due to the absence of the C4-C5 double bond on the A-ring, exhibiting altered geometry and altering the distance and angle of the hydrogen bond with the key residue Arg752 (**Figure 2**). This modification favours the interaction of the LBP with DHT over testosterone (Pereira de Jésus-Tran *et al.*, 2006) and reduces the dissociation rate of DHT by up to 5 times (Grino *et al.*, 1990). An important synthetic agonist of AR, metribolone, is among the most potent orally active AR agonists (Takeda *et al.*, 2007). The agonists display the same orientations and interactions in the LBP with conserved hydrogen bonds with N705, Q711, R752 and T877 along with hydrophobic interactions (**Figure 2**).

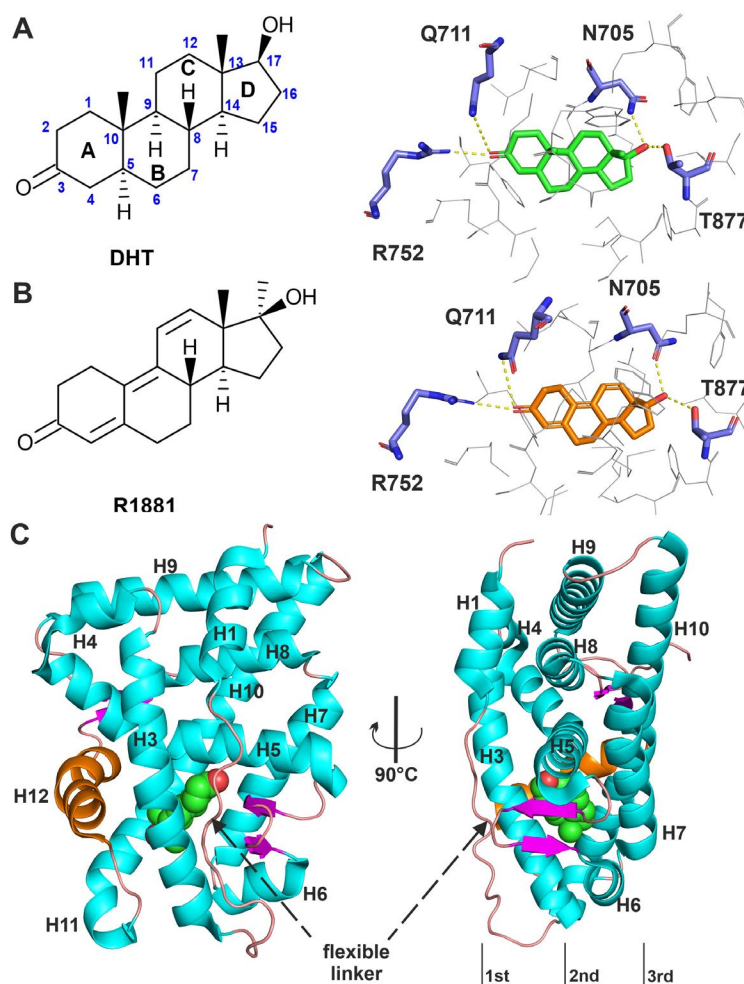


Figure 2 (A) Structure of DHT and its interactions in AR LBD from the co-crystal structure (PDB 1I37). (B) Structure of R1881 and its interactions in AR LBD from the co-crystal structure (PDB 1E3G). The AR-LBD residues forming hydrogen bonds (yellow dotted lines) with (N705, Q711, R752, and T877) are labelled and shown as blue sticks, and the residues forming hydrophobic interactions are shown as grey lines. (C) Structure of the AR-LBD (PDB 1E3G) consists of 11 α -helices (cyan), two-stranded β -sheets (magenta) arranged in a typical three-layer (1st, 2nd, 3rd) sandwich fold and the regulatory helix12 (orange) and the linkers, including the long flexible linker (salmon).

Beyond its regulation by androgens, the AR is also modulated by PTMs, serving not only as a TF but also as a central node integrating various signal transduction pathways, possibly targeted by therapy. Thus far, several PTMs of AR have been discovered, encompassing phosphorylation, acetylation, methylation, ubiquitination and SUMOylation (**Figure 3**) (Wen *et al.*, 2020). These alterations are indispensable for upholding the protein's stability, nuclear translocation and full transcriptional activity. The most prominent AR post-translational regulation is phosphorylation, with at least 19 phosphorylation sites on AR protein, with the majority being regulated by androgens, located predominantly on serine residues (Koryakina *et al.*, 2015; Wen *et al.*, 2020) and activating the AR functions. The AR phosphorylation sites are well described, with known therapy implications. The highly studied phosphorylation on S81 can be both androgen-dependent (Chen *et al.*, 2006) and independent (Yang *et al.*, 2007), but it is generally impaired by androgen deprivation *in vivo* (Russo *et al.*, 2018). It increases AR protein stability, nuclear localization and transactivation. S81 is phosphorylated by several cyclin-dependent kinases (CDKs) (Chen *et al.*, 2006; Jorda *et al.*, 2018; Liu *et al.*, 2017; Gordon *et al.*, 2010), further modulated by Sema4D/plexin-B1 (Williamson *et al.*, 2016) or Caveolin-1 (Karantanos *et al.*, 2016) in the nucleus (**Figure 3**).

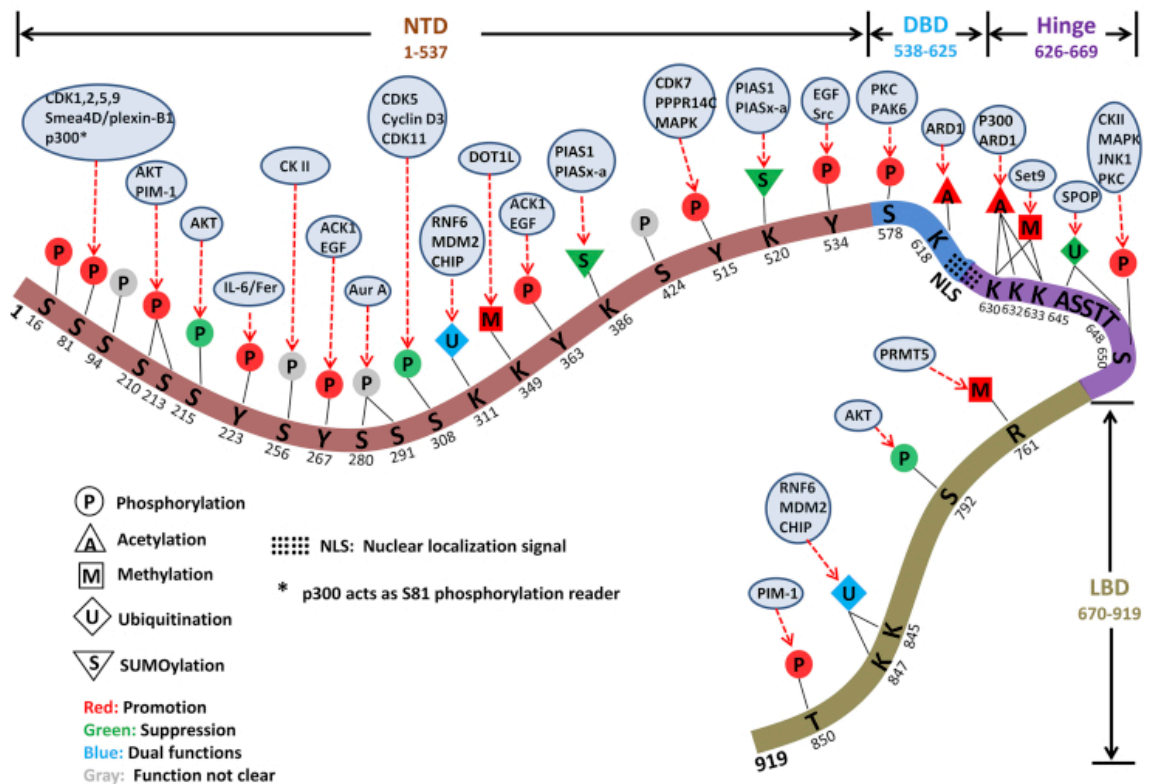


Figure 3 A diagram summarizing PTMs of the AR. Modifications: phosphorylation (P), acetylation (A), methylation (M), ubiquitination (U) and SUMOylation (S) are shown and the character of effect is distinguished by colours. Taken from Wen *et al.*, 2020.

2.3 Androgen receptor's role in prostate cancer development and progression

The prostate, a walnut-sized gland of men, produces seminal fluid to support sperm transport. It comprises four zones: anterior fibromuscular stroma, central zone, peripheral zone, and periurethral transition zone. Most PCa arise from the peripheral zone, while the transition zone is implicated in benign prostatic hyperplasia (BPH) (Shen *et al.*, 2010). The prostate epithelium consists of luminal, basal, and neuroendocrine cells, with emerging evidence suggesting that PCa originates from either luminal or basal cell types (Stoyanova *et al.*, 2013; Wang *et al.*, 2013). The prenatal prostate development relies on androgens and a functional AR (Wilson *et al.*, 1993), which also support the survival of secretory epithelia in fully-developed organ. In normal prostate tissue, cell death and proliferation rates are balanced (Berges *et al.*, 1995). While castration reduces prostatic DHT levels, leading to apoptosis of secretory epithelial cells, stromal cells are rather androgen-independent. On the contrary, elevated serum androgens increase prostate cells' proliferation, but they may not alone promote prostate carcinogenesis (Hsing, 2001).

Androgen-responsive genes (affected by androgen treatment) are regulated through AR transcriptional activity. Identification of these genes led to progress in PCa diagnosis and treatment, but it could still unveil new biomarkers and treatment strategies. The most known AR downstream target is PSA (kallikrein-related peptidase 3 (*KLK3*), whose expression is tightly regulated by AR through ARE in the PSA promoter (Cleutjens *et al.*, 1997). It's a serine protease secreted into the prostate ducts to prevent semen coagulation. The importance of AR activity for PSA expression was demonstrated in AR-negative PCa cell line PC-3, where re-expression of AR induced PSA production (Kollara *et al.*, 2003). The PSA protein still remains the most recruited biochemical marker for prostatic diseases, particularly PCa and the treatment response. In a normal prostate, PSA levels are significantly higher than in serum, entering the serum through leakage only. During PCa progression, abnormal ductal structure allows PSA secretion into extracellular space, elevating serum PSA levels (Heinlein and Chang, 2004).

While historically only a few downstream targets of AR were known (*KLK3*, *KLK2* and *NKX3-1*) (Prescott *et al.*, 1998), advances by the human genome project and microarray technologies have enabled the discovery of numerous AR downstream genes through expression analyses of PCa cells and tissues (a core set of more than 200 genes) (Jin *et al.*, 2013). Alongside the discovery of androgen-responsive genes, the downstream

molecular pathways and cellular processes governed by androgens became apparent. Functional annotation revealed that a majority of the genes are involved in: (I) production or modification of secretory proteins, protein folding, trafficking, and secretion (*KLK2, KLK3, NDRG1, FKBP5, HERC3, SEC24D, TMPRSS2*) (Xu *et al.*, 2001); (II) cell-cycle, energy metabolism and biosynthetic pathways (*DHCR24, ALDH1A3, CDK8, BARD1*) (Massie *et al.*, 2011); (III) signalling (*PIK3R3, BCHE, SGK, MERTK, TMPRSS2*) and regulators of transcription such as *GATA2, CTBP1, ETV1, CREB3L4, HOXB13* and *NKX3-1*. These findings underscore the role of androgens in supporting the survival and growth of prostatic cells and the production of seminal fluid (Toivanen and Shen, 2017).

Accordingly, growth control in the normal prostate is tightly regulated but it is lost in neoplasia (Lamb *et al.*, 2014). Not only is androgen signalling indispensable to prostate development and normal function, but it is also a key driver of PCa initiation and progression. Therefore, numerous studies characterised the expression and function of AR target genes in PCa, for example, the *FKBP5*, which was expressed higher in prostate tumour samples relative to BPH and may be a potential diagnostic marker for PCa (Velasco *et al.*, 2004). The malignant progression of prostate tumours is an intricate process driven by the accumulation of somatic mutations in the prostate epithelial cells' genome. These mutations, occurring in oncogenes or tumour suppressor genes, play pivotal roles in regulating cell growth, DNA damage repair (DDR), cell proliferation, and cell death (Ahmed and Eeles, 2015; Robinson *et al.*, 2015). PCa is categorized as a C-class tumour, with prevalent genetic changes including copy number alterations (CNAs) and gene structural rearrangements (Baca *et al.*, 2013; Hieronymus *et al.*, 2014).

During the initial stages, a premalignant lesion known as prostatic intraepithelial neoplasia (PIN) emerges, with high-grade PIN (HGPIN) recognized as a precursor to invasive PCa (Bostwick and Cheng, 2012). HGPIN exhibits numerous proliferative abnormalities compared to normal and hyperplastic epithelium, with overexpression of oncogenic proteins such as anti-apoptotic Bcl2 and GSTP1. Additionally, dysregulation of proliferation markers like Ki-67 and cyclin-dependent kinase inhibitor p27 (Kip1), along with loss of tumour suppressor proteins like PTEN and Nkx3.1, are observed in HGPIN (Packer *et al.*, 2016). The AR signalling pathway is implicated in promoting PCa through chromosomal translocations (Fraser *et al.*, 2017), particularly *TMPRSS2-ERG* gene fusions, generated by AR-induced chromosomal proximity and erroneous DNA repair (Stopsack *et al.*, 2020). These fusions are commonly detected in HGPIN lesions, suggesting their involvement in early PCa development (Tomlins *et al.*, 2005).

Furthermore, the downregulation of several miRNA families along with activation of telomerase, *PTEN* deletion, and loss of *RBI*, contribute to the progression from HGPIN to carcinoma (Packer *et al.*, 2016; Antonarakis *et al.*, 2012). Further genetic alterations, including AR mutations and amplification, overexpression of oncogenes like *CXCR4* and *EZH2*, and mutations in *FOXA1*, *BRCA1/2*, and *ATM*, are associated with PCa progression from early stages to metastatic disease (Rebello *et al.*, 2021).

2.4 Androgen receptor's role in the castration-resistant prostate cancer

Various acquired resistance mechanisms are AR-mediated, but many are also AR-independent. While ADT and AR antagonists (abiraterone and enzalutamide) initially block tumour progression, most patients eventually develop castration-resistant prostate cancer (CRPC) due to the cells' adaptation to low androgen levels (Chandrasekar *et al.*, 2015). Upon the ADT, numerous genes display differential expression, but many of them were not down-regulated after short-term castration in patients. It indicated that the ADT may not be sufficient to completely block the AR activity, which can then lead to PCa cell survival in a low androgen environment (Montgomery *et al.*, 2008). The AR signalling plays a critical role in CRPC development and resistance to current therapy renders metastatic CRPC (mCRPC) a lethal form of the disease (Angulo *et al.*, 2022). The AR-dependent acquired resistance mechanisms include AR mutations, AR amplification and overexpression, AR-alternative splicing, altered expression of AR-coregulators or intratumoral androgen biosynthesis.

Point mutations in the AR LBD are common in PCa, particularly in mCRPC and the frequently observed ones include F877L, H875Y, T877A, and L702H. These variants were detected in circulating free DNA (cf-DNA) samples from mCRPC patients, typically emerging with disease progression upon treatment with enzalutamide or abiraterone (Antonarakis *et al.*, 2016). They are all associated with AR promiscuity (loss of specificity to androgens), being activated by other hormones like oestrogens, progesterone or glucocorticoids. Additionally, mutated AR can switch non-steroidal antiandrogens (enzalutamide and apalutamide) into agonists, leading to resistance to these treatments (Culig *et al.*, 1999; Rathkopf *et al.*, 2017) (resistance patterns are summarised in **Table 2**). Currently, mutated AR can be targeted only by darolutamide, but the future holds promises in clinical trials of proteolysis targeting chimeras (PROTACs) or compounds targeting NTD or DBD (Li *et al.*, 2019; He *et al.*, 2022).

Table 2 Resistance patterns of different AR point mutations (Antonarakis *et al.*, 2016; Culig *et al.*, 1999; Rathkopf *et al.*, 2017; Schmidt *et al.*, 2021).

Condition / mutation	L702H	H875Y	F877L	T877A
enzalutamide treatment		✓	✓	✓
abiraterone treatment	✓			✓
steroid hormones' promiscuity	✓	✓	✓	✓
enzalutamide and apalutamide agonist activity			✓	

Overexpression of AR, as the most common alternation (in 30–50% of patients) is frequently observed in CRPC at the time of diagnosis, typically identified through tumour biopsies (Robinson *et al.*, 2015). Analysis of cf-DNA in plasma samples from patients treated with enzalutamide reveals a higher incidence of AR amplification compared to abiraterone (Annala *et al.*, 2018). Amplification serves as a compensatory mechanism against AR inhibition, leading to reduced treatment efficacy over time. AR overexpression can be induced by increased protein stability or decreased degradation (Vellky *et al.*, 2020). Elevated AR expression increases tumour cell sensitivity to minimal androgen levels, increasing the risk of disease progression (Coutinho *et al.*, 2016). AR-signalling in CRPC can be reactivated and sustained by extensive S81 phosphorylation, which became indeed a useful biomarker of AR activity in CRPC (Russo *et al.*, 2018).

Resistant PCa is also linked to the expression of AR-Vs, which are constitutively active forms, usually lacking the LBD (target of antagonists). Various AR-Vs, including AR-V1, AR-V567es, AR-V3, and notably androgen receptor splicing-variant 7 (AR-V7), are found in CRPC (**Figure 4**). Among these, AR-V7 is the most prevalent, detected in approximately 40% of cases at the protein level (Antonarakis *et al.*, 2016). Patients with AR-V7 expression typically experience shorter progression-free survival (PFS). These variants function independently of androgen binding and can confer resistance by forming active homodimers or heterodimers with full-length AR (AR-FL) (Wadosky *et al.*, 2019). Detection of AR-V7 in the nucleus of circulating tumour cells points out CRPC patients for taxane-based chemotherapy, since cabazitaxel showed promising outcomes in these patients (Ashizawa *et al.*, 2022) and there are also investigational drugs targeting other than the LBD.

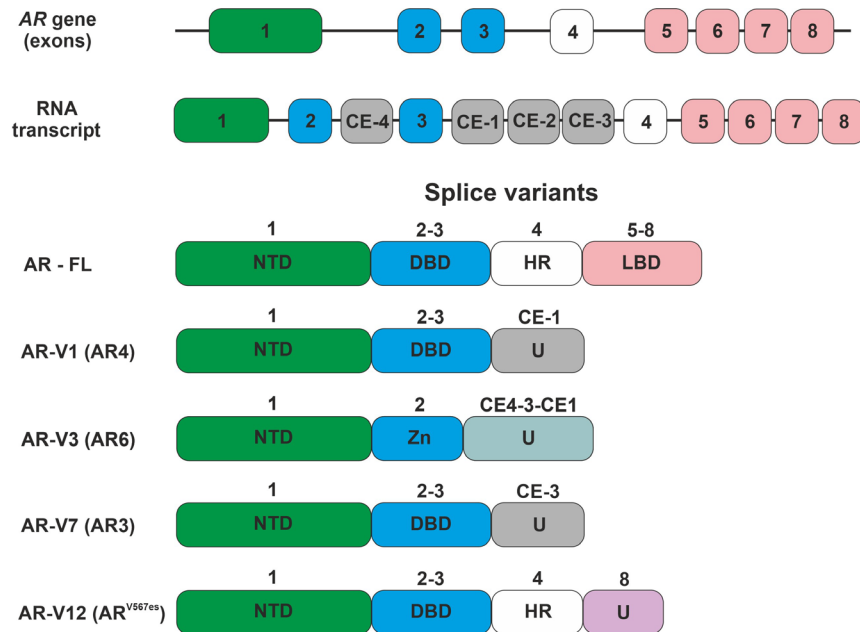


Figure 4 The AR gene is composed of 8 exons coding the different domains and the RNA transcript might be spliced in distinct ways to combine the standard exons (1–8), resulting in cryptic exons (CE-1, CE-2, CE-3, CE-4). CE inclusion results in unique (U) regions with sequences not found in the wt-AR. The composition of the four most prominent AR-Vs with constitutive activity is shown. In AR-V3/AR6, the splice variant bears only one zinc finger (Zn) and, thus, a truncated DBD. The numbers of included exons are shown above each splice variant (Antonarakis *et al.*, 2016; Wadosky *et al.*, 2019).

Furthermore, a significant mechanism contributing to abnormal AR signalling in CRPC involves intra-tumoral androgen synthesis, driven by the upregulation of key enzymes in steroidogenesis. Notably, enzymes such as cytochrome P450 cholesterol side chain cleavage enzyme (CYP11A1) and CYP17A1 are often overexpressed, facilitating the production of weak androgens like dehydroepiandrosterone (DHEA) and androstenedione. These weak androgens can then be converted into testosterone through the catalysis of enzymes 3 β -hydroxysteroid dehydrogenase (3 β -HSD) or aldo-keto reductase 3 (*AKR1C3*), which are also highly expressed by CRPC cells (Penning *et al.*, 2014). Following ADT, there may be an intratumoral increase in testosterone precursors (progesterone, cholesterol) (Armandari *et al.*, 2014), all supporting the hypothesis of a compensatory mechanism for treatment.

3 Targeting androgen receptor in management of prostate cancer

Over the years, the treatment of PCa has undergone significant advancements and targeting of AR signalling, a significant driver of PCa growth, has been utilized for revolutionizing patient outcomes and improving survival rates. The prognosis for both localized and metastatic PCa (mPCa) has significantly improved over the past decades,

reflecting the success of scientific advancements in this field. Previously limited to palliative care, treatment options now include curative robotic-assisted radical prostatectomy, stereotactic radiotherapy, and brachytherapy. Chemotherapy and androgen-suppressive therapies have also extended life expectancy, alongside the advancements in diagnostic imaging and staging (Denmeade and Isaacs, 2002).

Modern management of PCa considers various factors for tailored treatment, including disease stage, histopathological characteristics, molecular features, and patient-specific factors. For localized disease, options include active surveillance, surgery, radiotherapy, and hormone therapy based on the risk assessment. Multimodal approaches are recommended for locally advanced disease (Kane *et al.*, 2017). The treatment landscape for mPCa has evolved significantly. While standard treatment involved ADT, new agents like next-generation hormone therapies, radionuclides, taxanes, and poly ADP-ribose polymerase (PARP) inhibitors have expanded treatment options, with evolving strategies from single-agent to combination therapies even in mPCa, often leading to temporary remission (Cornford *et al.*, 2017; Gillessen *et al.*, 2020). The focus has been mainly to directly target either the ligand (synthesis of testosterone) or the receptor (AR transcription activity). However, there have been instances where alternative methods have been explored to indirectly inhibit AR signalling. In the following sections, different strategies targeting this crucial signalling pathway will be described, along with their effectiveness and constraints.

3.1 Androgen deprivation therapy

The concept of androgen ablation in prostate disease dates back to the 19th century, with experiments in animals establishing the relationship between hormones and prostate function (Lytton, 2001). The subsequent research elucidated the testosterone synthesis regulation and was awarded by two Nobel Prizes in Physiology and Medicine (Denmeade and Isaacs, 2002). The hypothalamus plays a crucial role by the secretion of the luteinizing hormone-releasing hormone (LHRH), stimulating the pituitary gland to release follicle-stimulating hormone (FSH) and LH. While LH acts on receptors on the Leydig cells in the testes to control testosterone synthesis, FSH influences the Sertoli cells, prompting the expression of LH receptors (Tolkach *et al.*, 2013).

The discovery and synthesis of LHRH led to the development of synthetic peptide agonists (Schally *et al.*, 2000), which induced transient testosterone flare and downregulated pituitary receptors for LHRH, leading to reduced testosterone levels,

effective in the treatment of PCa. Synthetic peptide LHRH agonists included leuprolide (Lupron), and goserelin (Zoladex) which were developed for clinical use (Xu *et al.*, 2012). Unfortunately, LHRH agonists come with drawbacks such as high cost, impotence, hot flashes and loss of libido. Additionally, the testosterone peak following the initial use of LHRH agonists might trigger tumour flare in patients with advanced disease (Rhee *et al.*, 2015). To mitigate these AEs, combined therapy with androgen signalling inhibitors was suggested and also LHRH antagonists were developed.

LHRH direct antagonists, such as cetrorelix (Cetrotide), abarelix (Plenaxix) and orgalutran (Ganirelix), controlled the testosterone levels better and faster than agonists. In the example of abarelix, it was shown that LHRH antagonists do not induce the harmful flare in serum testosterone, in contrast, they perform rapid medical castration (Crawford *et al.*, 2009). In 2008, a new generation LHRH antagonist, degarelix (Firmagon) was developed and approved by the US Food and Drug Administration (FDA) for advanced PCa, being a potent and long-acting suppressor of testosterone levels in patients without serious AEs (Klotz *et al.*, 2008; Cui *et al.*, 2014). All the above-mentioned approaches of androgen ablation were compared and showed to be equally effective in reducing tumour growth and upon the decades of surgical orchiectomy, LHRH antagonists have become the preferred method (Hussain *et al.*, 2013).

There were efforts to develop new approaches targeting testosterone synthesis. Ketoconazole (antifungal agent) (**Figure 5**), has been repurposed as a second-line treatment for patients who failed androgen ablation. By inhibiting the enzyme CYP17A, ketoconazole blocks both gonadal and adrenal steroidogenesis. Treatment with ketoconazole reduced the PSA level, however, without any improvement in patients' overall survival (OS) and with AEs such as gastrointestinal, liver and skin problems (Vasaitis *et al.*, 2011). Abiraterone acetate, the first FDA-approved drug targets both adrenal and intra-tumoral androgen synthesis, and inhibits CYP450 17 α -hydroxylase and 17,20-lyase activities. Clinical trials have shown that it effectively suppresses serum testosterone, exhibiting significant antitumor activity (Jarman *et al.*, 1998). However, abiraterone treatment leads to elevated levels of adrenocorticotrophic hormone, necessitating co-administration of low-dose prednisone to mitigate this AE. It was shown that the active metabolite of abiraterone acetate, Δ (4)-abiraterone, displays potent clinical activity by inhibition of steroidogenesis and moderate AR antagonism (Vasaitis *et al.*, 2011). Other drugs targeting androgen biosynthesis have also emerged. Orteronel (TAK-700) and seviteronel (VT-464) (**Figure 5**) exhibit selective inhibition of the 17,20-lyase

activity of CYP17A1 and induce decreased circulating androgens, leading to prolonged PFS (Madan *et al.*, 2020). Galeterone, the CYP17A1 inhibitor and also the steroidal antiandrogen is discussed in section 3.2. Additionally, finasteride, an inhibitor of the 5 α -reductase enzyme, reduces DHT synthesis by blocking the conversion of testosterone to DHT in cells and it is used for the treatment of BPH (Denmeade and Isaacs, 2002).

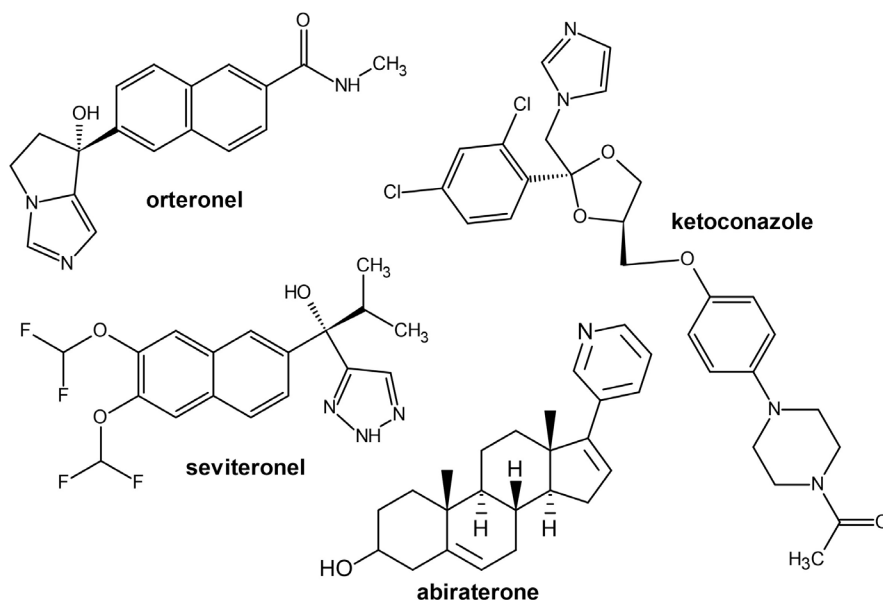


Figure 5 Clinically used inhibitors of testosterone synthesis targeting the CYP17A1.

3.2 Steroidal antiandrogens

First AR antagonists were developed in response to failures of androgen synthesis inhibitors. To directly bind and block the AR LBD and interfere with its transcriptional activity, initial antiandrogens incorporated a steroidal skeleton, analogous to the androgens, to ensure receptor binding (Helsen *et al.*, 2014). Several steroidal antiandrogens like cyproterone acetate (CPA), megestrol acetate, medroxyprogesterone acetate and spironolactone (**Figure 6**) were utilized to achieve maximal androgen blockade. However, their clinical use was limited due to significant drawbacks such as hepatotoxicity, interference with libido and potency, cardiovascular side effects, and low efficacy (Dawson *et al.*, 2000; Schröder *et al.*, 2004).

These AEs were attributed to their low selectivity towards other steroid receptors, such as the PR and GR, where they acted as weak or partial agonists. Their antigonadotrophic effects resulted in reduced secretion of LH and FSH, leading to decreased plasma levels of testosterone and oestradiol, affecting libido and potency (Schröder *et al.*, 1993). CPA has been one of the most clinically studied cancer drugs

in PCa, especially for palliative treatment (Saranyutanon *et al.*, 2019). The molecule displayed greater binding affinity to the AR compared to first-generation nonsteroidal antiandrogens and also an antigonadotrophic character. However, studies showed that CPA as monotherapy is inferior, and combination with goserelin acetate is not superior (Thorpe *et al.*, 1996). The antiandrogenic activity of spironolactone and megestrol acetate was comparable to CPA, but they acted also at the periphery to inhibit 5- α -reductase activity (Sert *et al.*, 2003; Saranyutanon *et al.*, 2019). The clinical use of megestrol acetate is limited by increased appetite and the patient's weight and also by dysregulation of corticoid hormones (Orme *et al.*, 2003). Medroxyprogesterone acetate is used as a treatment for hot flushing in menopausal women (Irani *et al.*, 2010).

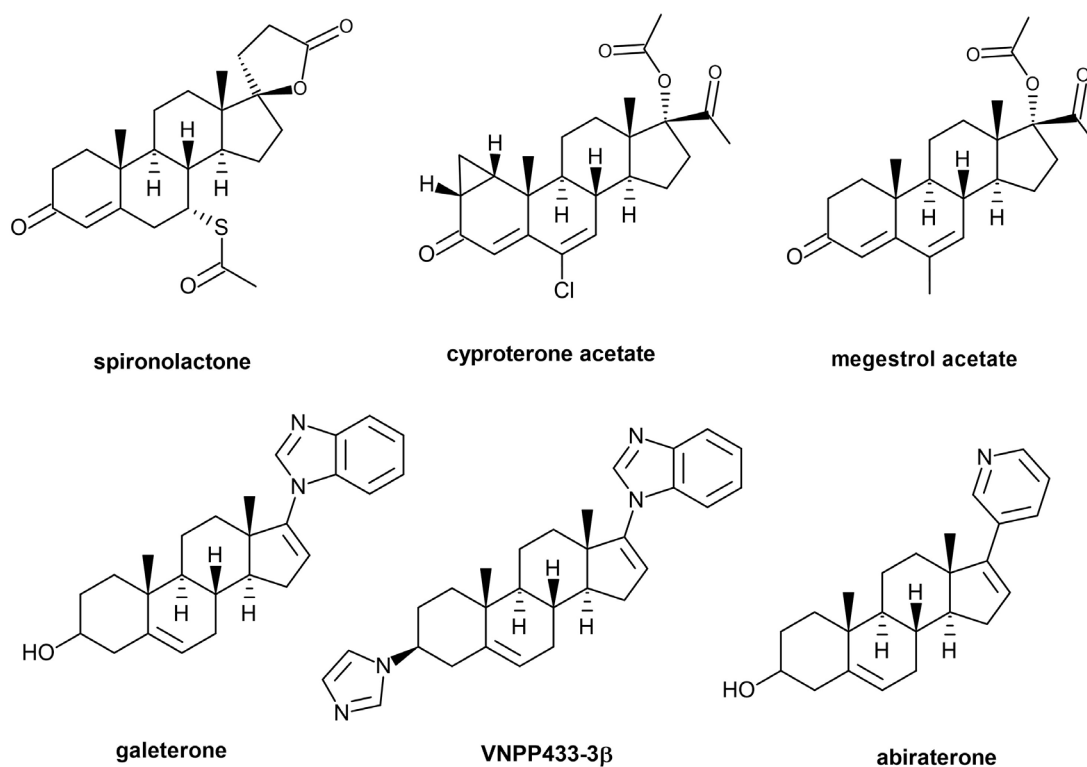


Figure 6 Initial steroidal AR antagonists (upper line) and new-generation of steroidal AR antagonists/androgen synthesis inhibitors.

Compared to the above-mentioned steroidal antagonists, the modern multi-targeted drug galeterone (TOK-001) (**Figure 6**) is a selective modulator that alters androgen signalling in a variety of ways. It works as a powerful AR antagonist and a selective CYP17A1 inhibitor, inducing AR protein degradation in PCa cells (Kwegyir-Afful *et al.*, 2015; 2016). Galeterone therapy in PCa models led to a considerable decrease in the levels of both AR-FL and AR-V7. Galeterone is also effective against AR point mutations

T877A and F876L mutations (Pozas *et al.*, 2022). Galeterone's phase I and phase II trials in patients with CRPC showed sufficient tolerance and potential efficacy, with the majority of patients displaying a drop in PSA level, which led to the phase III clinical study (Bastos and Antonarakis, 2016), focusing on the splice variant AR-V7. Patients with mCRPC who exhibited AR-V7 were treated with galeterone, but the trial was stopped after it was determined that the survival endpoints were unlikely to be met. However, galeterone is still in ongoing clinical trial (ClinicalTrials.gov ID: NCT04098081) for pancreatic cancer in combination with gemcitabine (Kwegyir-Afful *et al.*, 2017).

In subsequent research aimed at enhancing galeterone's effectiveness against PCa, potent analogues were discovered through structural modifications of the C-3 hydroxy group (Purushottamachar *et al.*, 2013; 2016). Additionally, it was found that galeterone and its analogues not only inhibit the AR axis, but also effectively target oncogenic eukaryotic protein translation by degradation of mitogen-activated protein kinase interacting kinases 1 and 2, eventually inhibiting the initiation factor 4E (Kwegyir-Afful *et al.*, 2016). This signalling is frequently associated with drug resistance in various human cancers (Bhat *et al.*, 2015) and it was demonstrated that galeterone and analogues are effective even in drug-resistant PCa cell lines, including enzalutamide-resistant CRPC (D'Abronzio and Ghosh, 2018). Furthermore, the discovery of galeterone analogue VNPP433-3 β (**Figure 6**), as a molecular glue that induces the proximity of AR-FL and mouse double minute 2 homolog (MDM2) revealed its role in the mediation of the ubiquitination and degradation of AR by MDM2 (Thomas *et al.*, 2023).

Recent findings suggested that the formulation of galeterone and analogues could significantly impact potency, due to their weakly basic nature and low solubility. In an *in vivo* rat study, KinetiSol amorphous solid dispersions exhibited a two-fold higher potency compared to a spray-dried dispersion with an equal drug load (Thompson *et al.*, 2023). Concerning the challenges related to solubility and bioavailability, the monohydrochloride salt of galeterone and the mono- and di-hydrochloride salts of VNPP433-3 β were prepared, to improve their *in vivo* pharmacokinetics. The galeterone salt demonstrated increased *in vitro* antiproliferative activity (7.4-fold), but decreased plasma exposure, compared to VNPP433-3 β salts with the same antiproliferative activities, but significantly improved oral pharmacokinetic profiles. Therefore, the HCl salts of VNPP433-3 β represent promising candidates for further clinical assessment (Thankan *et al.*, 2023).

3.2.1 Investigational steroidal compounds

Inspired by the promising potency of galeterone and its analogues, several other steroid compounds were developed, mainly bearing D-ring substitution/fusion with diverse heterocyclic cores. For example, a set of 17β -N-arylcarbamoyleandrosterone derivatives displayed potent antiproliferative activity, however towards both the AR-positive and negative PCa cell lines (compared to non-cancerous cells). The compound **6g** exhibited reasonable antiproliferative activity ($GI_{50} \approx 10 \mu\text{M}$ in LNCaP and PC-3), but was androgen-independent, which suggested targeting distinct pathways than AR (Cortés-Benítez *et al.*, 2016). A series of other steroidal D-ring pyridines exhibited reasonable growth inhibition against AR-negative PC-3 cells ($GI_{50} \approx 1.55 \mu\text{M}$), but much lower potency towards AR-positive LNCaP cells. Compound **3j** inhibited colony formation and migration of PC-3 cells, but did not target the AR as well (Shi *et al.*, 2018).

Novel oxazoline, benzoxazole and benzimidazole androstane derivatives inspired by abiraterone and galeterone proved the benefit of the isoxazole substitution at the C-17 on the D-ring. Compounds displayed moderate antiproliferative activity, equal towards AR-positive and negative cell lines and CYP17A1 binding (Latysheva *et al.*, 2020). It inspired further investigations of these compounds as potential anti-PCa agents with isoxazole substitution. The modified derivatives diminished the AR transcriptional activity and displayed antiproliferative activity selective to AR-positive cell lines (GI_{50} in the low μM range). The candidate compound **24j** suppressed AR signalling, decreased the AR protein level and showed clear AR targeting (**Appendix V.**, Rudovich *et al.*, 2022). A series of novel D-ring spirofused and linked 1,3,4-thiadiazine steroid derivatives displayed antiproliferative activity against AR-positive PCa cells (22Rv1) and blocked the AR downstream signalling, inducing apoptosis. The linked thiadiazine-substituted androstenes (**7j**) exhibited better antiproliferative activity ($GI_{50} \approx 4 \mu\text{M}$) than spiro-derivatives and notably, than the antiandrogen bicalutamide (Komendantova *et al.*, 2019).

Most importantly, two series of steroidal AR-antagonists were developed and characterised in our department. At first, novel 4,5,6,7-tetrahydropyrazolo[1,5-*a*]pyridine-fused steroidal compounds on the D-ring showed the ability to suppress the AR-downstream signalling with slight selectivity towards AR-positive PCa cell lines (compound **11**), but weak antiproliferative activity (Jorda *et al.*, 2019a). Additionally, series of galeterone analogues including steroid-fused azacycles on the D-ring displayed strong targeting of the AR with potent antiproliferative activity towards AR-positive cell

lines (single-digit micromolar GI_{50}). The candidate compound **3f** reduced AR transactivation and downstream signalling and the flexible docking proved a similar position within AR-LBD compared to galeterone, with better binding energy (Jorda *et al.*, 2019b). All the structures of investigational steroidal compounds are shown in **Figure 7**.

The collaborating group of Éva Frank published a synthesis of novel D-ring pyrazolyl derivatives as potent CYP17A1 inhibitors and antiproliferative agents in the BrCa cell lines (single-digit micromolar GI_{50} s) (Kovács *et al.*, 2016). Further, they also presented androstano-arylpyrimidines fused on A or D ring with specificity towards PCa cell lines, but they were evaluated only in AR-negative ones, suggesting that other pathways than AR are targeted (Baji *et al.*, 2017a) (**Figure 7**). Part of the compounds analysed in the frame of this thesis was previously synthesized and characterised, but without any biological analysis towards the AR or AR-positive PCa cell lines at all. They comprised the monosubstituted A-ring fused pyrazoles (Baji *et al.*, 2017b), A-ring quinolines (Baji *et al.*, 2016) and 1-aryl-5-methyl A-ring fused pyrazoles (Mótyán *et al.*, 2019) of DHT, which were analysed for their effect on AR-axis (**Appendix II., III.**).

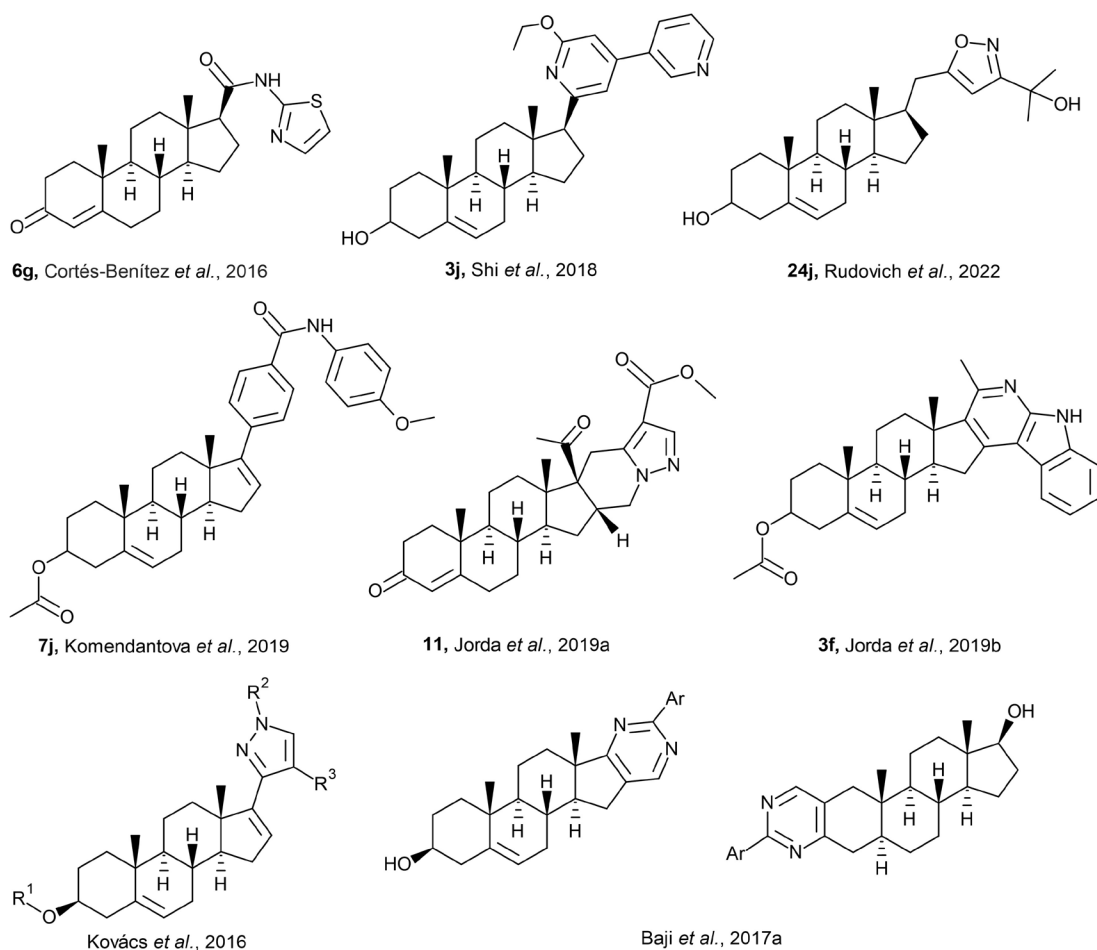


Figure 7 Structures of novel investigational steroidal compounds.

3.3 Non-steroidal antiandrogens

Due to the AEs observed upon treatment with steroidal antiandrogens (central impact on androgen secretion, loss of libido and sexual potency, hepatotoxicity etc.), pharmaceutical companies began to search for alternative, nonsteroidal anti-androgens without these side effects, but with the same mechanism (occupation the AR-LBD). In contrast to steroidal antiandrogens, non-steroidal counterparts have a more specific target range, resulting in fewer side effects (Saranyutanon *et al.*, 2019), however, they also display several limitations, as listed below. The representatives of two generations of non-steroidal antiandrogens as well as their approval dates and PCa conditions are summarised in **Table 3** and the structures of all representatives are shown in **Figure 8**.

3.3.1 First-generation non-steroidal antiandrogens

Flutamide was discovered as the first antiandrogen of this kind (Airhart *et al.*, 1978), which underwent clinical testing, receiving FDA approval for PCa treatment (Crawford *et al.*, 1989), followed by its derivative nilutamide (Namer *et al.*, 1988), with better pharmacokinetic properties. They both displayed beneficial effect in PCa patients in combination with ADT, but only slightly improving the OS. Later, a more potent derivative, bicalutamide (**Figure 8**), was developed (Chen *et al.*, 2009) (**Table 3**). Conversely, bicalutamide operates through a distinct mechanism, it binds to an allosteric site on the AR-LBD, inducing a conformational change and inhibiting the transcriptional activity (Osguthorpe and Hagler, 2011). It also exhibits a higher affinity for AR compared to other first-generation representatives. Thanks to the good safety profile and dosage once a day, bicalutamide is commonly used in monotherapy (Chen *et al.*, 2009).

Initially perceived as advantageous due to their low impact on libido or potency, it later emerged that these agents could traverse the blood-brain barrier, and increase LH levels in the bloodstream, leading to elevated serum testosterone levels. Even though they were tolerated and potent during the early stages of the disease, they are considered inferior therapies in terms of OS and PFS (Seidenfeld *et al.*, 2000). Ultimately, patients develop resistance to these drugs and progress to the lethal stage of CRPC. While these agents temporarily reduced the AR expression, in some individuals with CRPC they exhibited agonist activity, particularly due to AR mutations (T877A or W741L), converting them to agonists (Culig *et al.*, 1999; Chen *et al.*, 2009). To address these limitations in treatment, second-generation antiandrogens with enhanced binding affinity and specificity were developed.

Table 3 Nonsteroidal AR antagonists' approval and type of PCa.

Generic name	Another name	Approval date (clinical stage)	Treatments	Reference
<i>First-generation</i>				
Flutamide	Eulexin	27 Jan 1989	mCRPC	Airhart <i>et al.</i> , 1978, Crawford <i>et al.</i> , 1989
Bicalutamide	Casodex	04 Oct 1995	mCRPC	Cockshott <i>et al.</i> , 1990
Nilutamide	Nilandron	09 Sep 1996	mCRPC (+castration)	Namer <i>et al.</i> , 1988, Dijkman <i>et al.</i> , 1997
<i>Second-generation</i>				
		31 Aug 2012	mCRPC	Tran <i>et al.</i> , 2009
Enzalutamide	MDV3100	13 Jul 2018	nmCRPC	Hussain <i>et al.</i> , 2018
		16 Dec 2019	mCSPC	Davis <i>et al.</i> , 2019
Apalutamide	ARN-509	14 Feb 2018	nmCRPC	Clegg <i>et al.</i> , 2012
		17 Sep 2019	mCSPC/ mCRPC	Smith <i>et al.</i> , 2018; Chi <i>et al.</i> , 2019
Darolutamide	ODM-201	30 Jul 2019	nmCRPC	Moilanen <i>et al.</i> , 2015
		Phase III	mCSPC	Fizazi <i>et al.</i> , 2020

3.3.2 Second-generation non-steroidal antiandrogens

The second-generation of FDA-approved antiandrogens include enzalutamide, apalutamide and darolutamide. The use of these second-generation AR antagonists has indeed led to improved patient OS by more effective targeting of aberrant AR signalling in CRPC patients (Scher *et al.*, 2012) (**Table 3**). However, despite their initial efficacy, these agents have only yielded temporary responses due to the swift emergence of resistance (Watson *et al.*, 2015; Schmidt *et al.*, 2021).

Enzalutamide (MDV3100) (**Figure 8**) was the first FDA-approved second-generation AR antagonist for the treatment of CRPC, boasting significantly higher AR-binding affinity, compared to the first-generation counterparts. It competes with androgens for AR-LBD binding, inhibits nuclear translocation, DNA binding, and co-activator recruitment (Tran *et al.*, 2009). Extending overall survival (OS) and metastasis-free survival (MFS) in CRPC (Hussain *et al.*, 2018) and castration-sensitive PCa (CSPC) (Davis *et al.*, 2019), it has been a golden standard of PCa treatment. Despite its

widespread clinical use, enzalutamide's elevated steady-state brain levels are linked to central nervous system (CNS)-related events like seizures (Pilon *et al.*, 2017).

Apalutamide (ARN-509) (**Figure 8**), another member of the second generation emerged subsequently, showing a lower steady-state brain level with fewer seizure side effects (Clegg *et al.*, 2012), but retaining all the potent activities towards the AR axis as enzalutamide (Tran *et al.*, 2009). Apalutamide notably increases the MFS of CRPC and OS of mPCa's (Smith *et al.*, 2018; Chi *et al.*, 2019) and is frequently used in combination with abiraterone and prednisone (Saad *et al.*, 2021). Unfortunately, the weak binding to AR with the F876L mutation poses a risk of treatment resistance in the case of both enzalutamide and apalutamide (Saranyutanon *et al.*, 2019).

In contrast to enzalutamide and apalutamide, the most recently approved second-generation AR antagonist darolutamide (ODM-201) (**Figure 8**) possesses a distinct chemical structure and is unable to penetrate the blood-brain barrier, suggesting a reduced potential for CNS side effects. It also exhibits higher AR affinity compared to the other two mentioned, effectively blocking the nuclear translocation of the AR (Moilanen *et al.*, 2015). Clinical trials showed that darolutamide not only delivers significant antitumor effects with longer OS but also maintains a favourable safety profile in patients with nmCRPC (Shore *et al.*, 2018; Fizazi *et al.*, 2020). Another phase III study of darolutamide plus ADT in metastatic castration-sensitive prostate cancer (mCSPC) patients is currently ongoing (NCT04736199) (**Table 3**). Additional *in vitro* data highlighted darolutamide's effective inhibition of AR-FL harbouring a majority of gain-of-function mutations (Lallous *et al.*, 2021).

Taken together, the successful second-generation non-steroidal AR antagonists trio demonstrated potent efficacy in AR's suppression across patients with various stages of PCa (Lokeshwar *et al.*, 2021). However, concerns persist regarding enzalutamide-induced seizures and the shorter serum half-life of darolutamide, necessitating higher doses, which can lead to cardiovascular toxicity (Morgans *et al.*, 2021). Additionally, prolonged use of AR antagonists leads to drug resistance, prompting ongoing research into new AR antagonists and alternative therapeutic approaches.

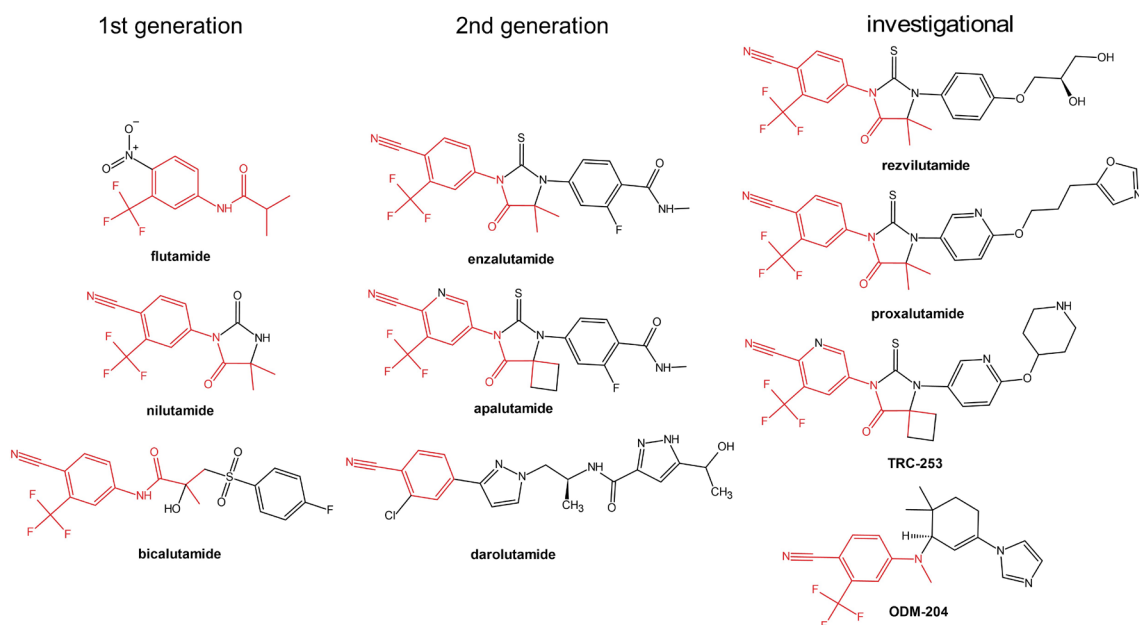


Figure 8 Structures and development of non-steroidal AR antagonists. The common motif is shown in red.

3.3.3 Investigational non-steroidal antiandrogens

The limited sustainability of clinical response with inevitable acquired resistance has supported the clinical investigation of more potent therapeutic agents (Schmidt *et al.*, 2021). A novel derivative of enzalutamide, rezvilutamide (SHR3680) (**Figure 8**), demonstrated comparable anti-tumour potency with reduced brain distribution and a lower risk of seizures. In a phase I/II study involving patients with progressive mCRPC, rezvilutamide exhibited favourable tolerability, safety, and promising anti-tumour activity (Qin *et al.*, 2022). In interim analyses of a phase III clinical trial (NCT03520478), rezvilutamide plus ADT significantly improved PFS and OS in high-volume mCSPC patients (Gu *et al.*, 2022). Following successful clinical evaluation, rezvilutamide was approved in China for treating mCSPC with high tumour burden. There are other ongoing trials in mCRPC previously treated with abiraterone (NCT04603833) or in high-risk locally advanced PCa (NCT05009290) (Keam, 2023).

Proxalutamide (GT-0918) (**Figure 8**), another derivative similar to enzalutamide, demonstrated three times higher binding affinity to AR in preclinical studies. It effectively downregulated AR levels in CRPC and exhibited efficacy against both wt-AR and AR mutants conferring resistance to previous antagonists (Zhou *et al.*, 2020). Proxalutamide has completed a phase I clinical trial in mCRPC (NCT02826772), indicating superior tolerance and promising antitumor activity (Zhou *et al.*, 2023),

currently enrolling participants for phase II (NCT03899467). Interestingly, since AR regulates the expression of angiotensin-converting enzyme 2 (ACE2) and the cell surface transmembrane serine protease 2 (TMPRSS2) (Samuel *et al.*, 2020), blockade of androgen signalling with AR antagonists may mitigate coronavirus infectivity and proxalutamide is now entering phase III studies for treating SARS-CoV-2 (NCT04869228) (Qiao *et al.*, 2023).

BMS-641988, another AR antagonist, showed AR-binding affinity and antitumour activity comparable to proxalutamide (Attar *et al.*, 2009). In a phase I clinical trial for CRPC patients, BMS-641988 exhibited moderate anti-tumour activity and seizures, leading to the study's termination (Rathkopf *et al.*, 2011).

Another novel AR TRC-253 (JNJ-63576253) (**Figure 8**), a thiohydantoin structural derivative of apalutamide, acts as a competitive antagonist with high affinity for both wt-AR and AR mutants in LBD. A Phase I/IIA dose-escalation study (NCT02987829) in mCRPC patients revealed that elevated doses of TRC-253 were linked to AEs, including anaemia (Rathkopf *et al.*, 2019; Zhang *et al.*, 2021).

ODM-204 (**Figure 8**), finally, represents an orally bioavailable non-steroidal dual inhibitor of the CYP17A1 enzyme and AR signalling. It potently inhibited steroid biosynthesis *in vivo*, along with promising antitumor efficacy in human PCa xenografts (Oksala *et al.*, 2019). Subsequent phase I–II trials conducted in patients with progressive mCRPC (NCT02344017) revealed that it was well tolerated and displayed preliminary antitumor activity. Unfortunately, challenges related to pharmacokinetics impede its further development (Peltola *et al.*, 2020).

3.4 Co-activators' inhibition

As reiterated, the AR is a crucial transcription factor, whose regulation involves a cooperation with co-regulator proteins, forming the ultimate transcription complex. Co-regulator proteins influence the transcription mainly through epigenetic modifications of chromatin, mainly through histone acetylation/deacetylation (Velho *et al.*, 2021). It is governed by three classes of proteins: histone-acetyltransferases (writers), histone deacetylases (erasers), and bromodomain and extra-terminal motif (BET) proteins (readers) that bind to acetylated histones (Dawson *et al.*, 2012). Hormone-bound AR in active conformation binds coactivators to an AF-2 region and the most prominent AR co-activators are cAMP response element-binding protein (CREB)-binding protein (CBP) and its homolog p300 (histone acetyltransferases) and BET proteins, resulting

in potent activity to run the transcription from AREs (Shang *et al.*, 2002, Ogryzko *et al.*, 1996). AR co-activators can govern the upregulation of oncogenic drivers like *c-MYC* and *AKT* (Zhang *et al.*, 2017), can play a pivotal role in CRPC development (Heemers and Tindall, 2007) and inhibition of this axis has been proposed to combat resistance mechanisms in PCa.

Molibresib (GSK525762, I-BET-762) is an orally bioavailable BET inhibitor which demonstrated antitumor activity in preclinical studies, including PCa models (Zhao *et al.*, 2013). A phase I trial in CRPC patients who already received at least 3 prior therapies, showed a partial response or stable disease with improved PFS and OS in the majority of subjects. On the other hand, treatment-related AEs were observed in the majority of patients as well, leading to therapy discontinuation or dose reductions. Investigations evaluating molibresib in combination with abiraterone or enzalutamide in mCRPC patients were terminated (NCT03150056) (Cousin *et al.*, 2022).

Birabresib (MK-8628/OTX015) is a bromodomain inhibitor that competes with bromodomain proteins' binding to acetylated histones. Preclinical studies indicated its efficacy in PCa (Asangani *et al.*, 2016) and a phase Ib trial included patients with mCRPC (NCT02259114). Clinical antitumor activity was observed, with the majority of patients showing stable disease. Dose-limiting toxicities were milder compared to molibresib, with common treatment-related AEs (Lewin *et al.*, 2018).

ZEN-3694, a second-generation pan-BET/bromodomain inhibitor, showed potent inhibitory activity on the AR signalling pathway, downregulating AR-Vs, cellular myelocytomatosis oncogene (*c-MYC*), GR, and other CRPC oncogenes. A phase Ib/II trial combining ZEN-3694 with enzalutamide displayed a benefit (increased PFS) for mCRPC patients who had progressed on abiraterone and/or enzalutamide (Aggarwal *et al.*, 2020) and a phase II study combining it with enzalutamide or pembrolizumab is enrolling patients (NCT04471974). Other promising candidates from this group include inobrodib (CCS1477) and NEO2734, targeting p300/CBP or BET and CBP/p300, respectively. Both compounds effectively inhibited the expression of AR (FL, Vs) and *c-MYC* and showed potency in bicalutamide-resistant xenograft models, surpassing molibresib (Spriamo *et al.*, 2020). There is an ongoing phase I/IIa trial (NCT03568656) assessing the safety and efficacy of inobrodib alone or in combination with abiraterone or enzalutamide, in mCRPC patients (DeBono *et al.*, 2019) and a phase I trial of NEO2734 (NCT05488548) is recruiting patients to validate the efficacy in patients harbouring hotspot mutations in *SPOP* (Yan *et al.*, 2019).

3.5 Targeting other domains of androgen receptor

Currently, the majority of approved and evaluated AR antagonists target the LBD, however, these compounds are susceptible to LBD mutations and alternative splicing variants. Recently, the NTD of AR has emerged as a promising novel target due to its crucial role in AR transcription (Li *et al.*, 2019). Several candidate drugs acting as NTD AR antagonists (anitens) have emerged, including mainly the EPI-compounds (EPIs), which inhibit the AR transactivation by binding to the AF1 domain in the AR-NTD (Ban *et al.*, 2021). They were derived from marine sponges (Yang *et al.*, 2016) and it is discussed whether the initially isolated mixture of diastereoisomers (EPI-001) could have been a metabolic product of bisphenol A diglycidyl ester, generated by the sponges in polluted seawater (Avgeris *et al.*, 2022). EPI-506 (ralaniten acetate), the triacetate pro-drug of EPI-002 (**Figure 9**) was the first AR-NTD inhibitor which entered clinical trials (NCT02606123), but was discontinued due to moderate potency and poor bioavailability (Maurice-Dror *et al.*, 2022). Next-generation EPIs, such as EPI-7386 (masofaniten) (**Figure 9**) demonstrated enhanced potency in AR-Vs positive xenografts and favourable pharmaceutical properties. Moreover, it has successfully proceeded through phase I clinical trials for mCRPC, where it was well tolerated and showed preliminary antitumor activity in heavily pre-treated mCRPC (NCT04421222). Part Ib is opened for enrolment of pre-treated mCRPC patients and treatment-naive nmCRPC ones (Pachynski *et al.*, 2023). Additionally, synergistic activity of EPIs and enzalutamide has been observed in preclinical models of enzalutamide-resistant CRPC (Hirayama *et al.*, 2020) Further research on ligand-based optimization of NTD-targeting drugs is recommended due to the NTD's intrinsic disorder, which makes it unsuitable for structure-based drug discovery. The EPI core is a generally promising structure for chemical modifications and already led to the development of a targeted degrader (more in section 3.6.3).

The DBD of the AR represents an alternative binding site, vital for ARE recognition and AR dimerization. However, due to its conservation among other steroid receptors, targeting this domain can lead to unintended effects on other receptors (Xu *et al.*, 2015). Despite challenges, progress has been made in developing DBD-targeting AR antagonists. Pyrvinium, initially an anti-pinworm medication, was re-purposed as a non-competitive antagonist of AR-DBD by binding at the DBD-ARE interface. It showed potent inhibition of AR signalling including AR-Vs and inhibited CRPC xenograft

growth, but decreased both prostate weight and bone mineral density. It indeed affected PR and GR, which hindered its clinical evaluation (Lim *et al.*, 2014; Pal *et al.*, 2019). Other studies have explored other potential DBD binders, yet none have advanced to clinical trials. Several compounds target the P box, disrupting interactions between the DBD and AREs in both AR-FL and AR-Vs. Notably, specific amino acids at positions 590 and 594 in the AR DBD could confer high selectivity towards AR, sparing other NRs. Dimerization of AR-FL and AR-Vs is essential for transcriptional activity, since AR-Vs monomers showed no activity compared to AR-FL monomers (Riley *et al.*, 2023). Through docking and pharmacophore modelling, VPC-17281 and VPC-17160 emerged as promising leads, exhibiting stronger inhibition of AR-V7 than AR-FL and suppressing growth in PCa cell lines carrying AR-Vs (Xu *et al.*, 2023).

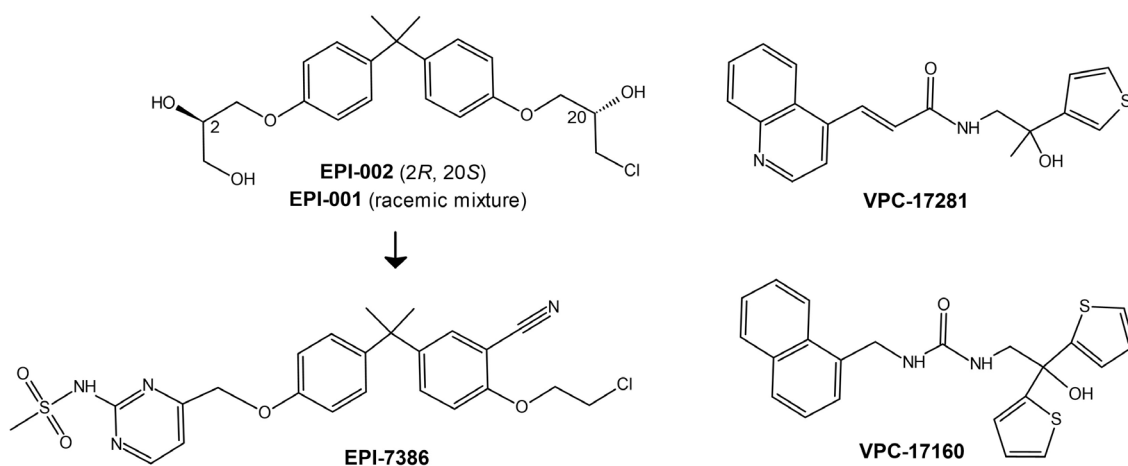


Figure 9 AR-NTD (left) and AR-DBD (right) - targeting molecules.

3.6 Targeted degradation of androgen receptor

Targeting proteins for degradation is an innovative approach based on a complete elimination of the target protein, rather than inhibition of the function only. This strategy traces back to the development of HSP90 inhibitors as anticancer agents (Kundrat and Regan, 2010). The approach increased its efficacy and attractiveness with the introduction of PROTACs and molecular glues, which hijack the ubiquitin-proteasome system (UPS) essential for the degradation of misfolded proteins. Significant progress has been accomplished in recent years, reaching also clinical evaluation (Alabi and Crews, 2021).

AR degradation presents a complementary approach to AR antagonists, offering several advantages etc. overcoming resistance to AR antagonists in PCa cells with AR point mutations (Salami *et al.*, 2018), operating in an event-driven manner rather than

occupancy manner observed in antagonists. To maintain appropriate AR levels, it undergoes physiologic degradation *via* the UPS and alternative PTEN-caspase-3 pathway (Lee *et al.*, 2003). The UPS involves covalent attachment of ubiquitin to the target protein, marking it for degradation by 26S proteasome. The key component of the UPS is the E3 ligase, with the most established ones being cereblon (CRBN), and von Hippel–Lindau (VHL), an inhibitor of apoptosis protein and (MDM2) (Collins *et al.*, 2017). Notably, MDM2 phosphorylate the AR at Ser213 and Ser791 through the PI3K/AKT pathway, facilitating its recognition for subsequent degradation. Additionally, the AR HR includes the PEST sequence, serving as the degradation motif. Alternatively, the tumour suppressor PTEN can interact with AR-DBD and expose it for caspase-3 recognition and cleavage in the cytoplasm (Lin *et al.*, 2004).

AR degraders can be sorted based on degradation mechanisms to bifunctional AR PROTACs (including also specific nongenetic inhibitor of apoptosis protein erasers and hydrophobic tagged chimeric degraders), molecular glues, autophagic degraders of AR and others. The terminology of small molecules triggering degradation lacks a precise definition. The mechanism of action of PROTACs and molecular glues (bivalent molecules) is well-understood and implied by their terms. However, the other substances (antagonists or modulators), inducing AR protein degradation through distinct mechanisms (destabilisation, folding disruption) are not properly categorised, being termed as "monomer AR degraders" (Chen *et al.*, 2024), which does not properly capture their nature. Hence, we suggest referring to them as "monovalent inducers of AR degradation" instead.

3.6.1 Monovalent inducers of androgen receptor's degradation

Efforts have been dedicated to discover compounds with distinct pharmacodynamic properties compared to non-steroidal antagonists, including selective AR modulators (SARMs), which offer tissue selectivity. Acting as partial or weak agonists in androgenic tissues, SARMs primarily exert anabolic effects on muscles and bones, showing therapeutic potential in osteoporosis, muscular dystrophy, BPH, BrCa, and PCa (Solomon *et al.*, 2019). For instance, minor modifications of bicalutamide resulted in enobosarm, a potent SARM evaluated in BrCa (Marhefka *et al.*, 2004). LY2452473 (OPK-88004) (**Figure 10**), the SARM developed for PCa exhibited antagonist AR activity, reduced PSA levels, and enhanced anabolic effects and completed phase II in clinical evaluation (NCT02499497) (Pencina *et al.*, 2021).

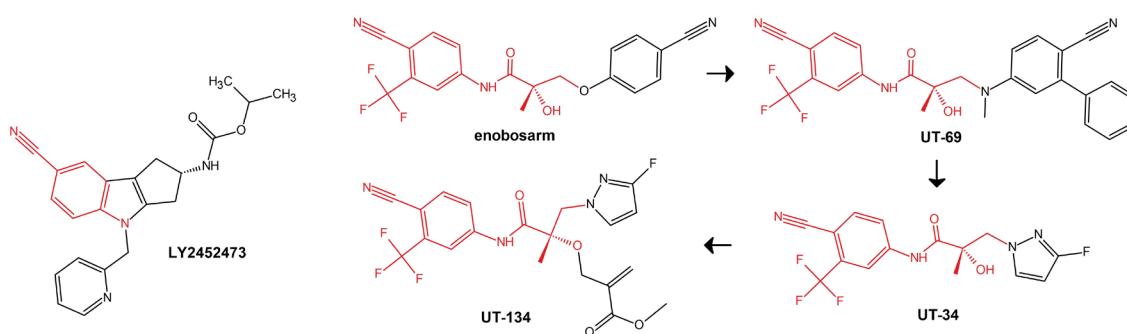


Figure 10 Structure of SARMs (LY2452473 and enobosarm) and development of SARDs. The common motif is shown in red.

The compound UT-69, derived from enobosarm, acted as a monomeric selective AR degrader (SARD) (**Figure 10**). It inhibited AR transactivation, blocked downstream signalling and promoted AR degradation by binding to both the LBD and the AF1 domain in the NTD. Despite being effective against wt-AR and Vs, UT-69's oral administration was hindered by metabolic instability. Further optimizations led to potent and orally highly bioavailable derivative UT-34, which bound to AF-1 rather than LBD, leading to AR degradation, inducing tumour regression in preclinical models (Ponnusamy *et al.*, 2019) phase I/II clinical study in mCRPC (NCT05917470). Recently, UT-143 (**Figure 10**) has been reported to irreversibly suppress both AR-FL and AR-V7 transactivation, through the selective and covalent binding to cysteines (C406 and C327) in the AF-1 (Thiyagarajan *et al.*, 2023).

Other monomeric AR degraders act by distinct mechanisms, such as the above-mentioned dissociation of HSPs from the AR, promoting AR degradation. For example, a derivative of natural antibiotic geldanamycin, 17-allylamino-17-demethoxygeldanamycin inhibited HSP90 chaperone function, degrading both wt-AR and mutants *in vivo*, however, a phase II trial in mCRPC (NCT00118092) found it ineffective (Heath *et al.*, 2008). ASC-J9, a curcumin derivative, was established as an AR degrader, acting by dissociation from chaperone and promoting the AR-MDM2 association, which displayed potency in preclinical models of CRPC (Cheng *et al.*, 2018) and advanced to phase II clinical trials for acne and androgenetic alopecia treatment (NCT00525499). Niclosamide, an approved anti-helminthic drug, acts as an AR degrader and targets both the AR-FL and Vs (Liu *et al.*, 2021). While niclosamide showed preclinical activity in CRPC, its bioavailability was initially poor (Schweizer *et al.*, 2018; NCT02532114), however, it proceeded through the phase I clinical trial for CRPC

(NCT02807805) in a novel orally bioavailable formulation and the phase II of this drug is warranted (Parikh *et al.*, 2021).

Various other compounds have demonstrated the ability to reduce AR protein levels *via* the UPS, although many lack a clear degradation mechanism. For instance, darolutamide derivatives downregulated both AR-FL and Vs, while galeterone and analogues induced AR degradation by interfering with balanced ubiquitination (Ha *et al.*, 2022). AR protein stability is crucial for its function and antagonists, typically blocking AR nuclear localization, may decrease its activating phosphorylation at S81, thereby promoting AR protein degradation (Hsu *et al.*, 2011). Conversely, docetaxel, used in advanced PCa, can enhance AR protein stability by increasing phosphorylation at S81, potentially contributing to chemotherapy resistance, which can be overcome by the AR degradation (by ASC-J9) restoring docetaxel sensitivity (Luo *et al.*, 2019).

3.6.2 Molecular glues and autophagic degraders of androgen receptor

Molecular glues, a recent innovation in targeted protein degradation, induce proximity and formation of a complex between the AR and ubiquitin ligases, leading to AR ubiquitination and subsequent degradation by UPS (Dong *et al.*, 2021). For instance, VNPP433-3 β , a new-generation galeterone analogue, facilitates this process by inducing the formation of the AR-MDM2 complex (Thomas *et al.*, 2023). These glues, typically small molecules, possess promising pharmacokinetic properties, however, systematic drug discovery strategies for AR molecular glues are lacking, with galeterone derivatives being the only reported examples to date (Wang *et al.*, 2022).

Autophagic degradation of AR involves directing specifically ubiquitinated AR to autophagosomes *via* the autophagy receptor p62, followed by lysosomal degradation (Mitani *et al.*, 2015). Riluzole, used for treating amyotrophic lateral sclerosis, promotes selective autophagy by enhancing the interaction between AR and p62, leading to AR (FL, Vs and mutants) degradation. Additionally, riluzole as the only example activates endoplasmic reticulum stress (Wadosky *et al.*, 2019) increasing the AR degradation.

3.6.3 Proteolysis targeting chimeras

Introduction of PROTACs revolutionised induced protein degradation (Sakamoto *et al.*, 2001). Operating through an event-driven mechanism, PROTACs (comprising a target-protein ligand, linker and E3 ligand) selectively degrade target proteins by hijacking the UPS, even with temporary binding. The AR was selected for PROTACs investigation due

to its pivotal role in PCa progression and played a central role in the evolution of PROTAC technology with ARV-110 (bavdegalutamide) being the first AR PROTAC in clinical trials, showing potential to overcome resistance in CRPC (Ha *et al.*, 2022).

Numerous novel PROTACs targeting the AR have emerged, differing in the AR binder and the E3-ubiquitin ligase binder. The known PROTACs can be categorized into sub-groups based on the AR domain they target (LBD (predominantly), DBD or NTD). Regarding the AR binding component, the LBD PROTACs can utilize AR endogenous agonists, synthetic agonists (such as S-6) or antagonists. Conversely, E3 ubiquitin ligase components include early peptide E3 ligands, small-molecule affinity binders of CRBN and VHL proteins, inhibitors of apoptosis proteins and MDM2 proteins, or hydrophobic tags (Zeng *et al.*, 2020; Chen *et al.*, 2024).

The first AR LBD-PROTACs were constructed from DHT and peptides (phosphopeptide from I κ B α (Sakamoto *et al.*, 2001) or VHL-targeting peptide (Schneekloth *et al.*, 2004) and faced limitations due to their high molecular weight and poor pharmacokinetics. Recognizing the significance of AR mutations in CRPC, ARCC-4 (**Figure 11**) based on enzalutamide moiety and VHL ligand was developed and its superiority over enzalutamide in CRPC cells was demonstrated (Salami *et al.*, 2018). This breakthrough, including the degradation of clinically relevant AR mutants led to the development of AR-PROTACs with improved pharmacokinetic properties by Arvinas. Starting from ARCC-4, the E3 binder was first modified to CRBN, then the molecule was modified several times to improve *in vitro* degradation potency and *in vivo* pharmacokinetics, finally obtaining bavdegalutamide (ARV-110) (**Figure 11**) (Ha *et al.*, 2022). It started a new journey for AR PROTACs toward clinical practice. The phase I trial (NCT03888612) results showed that ARV-110 is well-tolerated by CRPC patients, effectively degrading AR and suppressing tumour growth (Petrylak *et al.*, 2020). Consequently, bavdegalutamide (as the first-in-class AR PROTAC) entered phase II clinical study in October 2020, which already demonstrated its antitumor efficacy among PCa patients even with T877A and H875Y mutations, despite not being initially designed to degrade mutated AR. Notably, bavdegalutamide failed to degrade AR with the point mutation Leu702His or AR-V7 (Ha *et al.*, 2022; Gao *et al.*, 2022).

Therefore, Arvinas is devoted to refine the drawbacks and develop AR-V7 targeting PROTAC. The structure of another AR PROTAC supported by Arvinas, ARV-766 (luxdegalutamide) was designed for optimal genotype coverage, by modifications in the AR ligand and E3 ligase ligand of ARV-110 (Snyder *et al.*, 2023). Preclinical data

demonstrated the potency to robustly suppress tumour growth even under high concentrations of androgen. Clinical studies of ARV-766, as a monotherapy or in combination with abiraterone, have recently progressed from phase I to phase II in patients with mCRPC (Petrylak *et al.*, 2023).

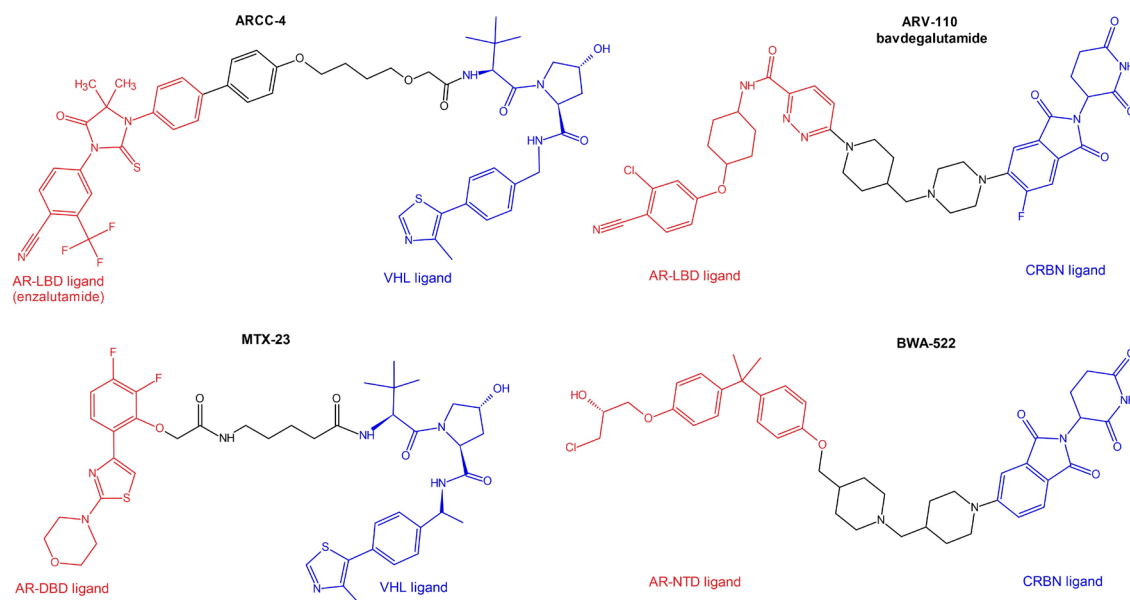


Figure 11 PROTACs targeting the AR-LBD (upper) with the AR-DBD PROTAC **MTX-23** and AR-NTD PROTAC **BWA-522**. The AR ligand is shown in red, the linker in black and the E3 ligand in blue.

The DBD PROTACs are less explored, however, the example is compound MTX-23 (**Figure 11**) based on the DBD ligand VPC-14228 linked to a VHL ligand. MTX-23 preclinically displayed the degradation of AR variants, including V-7, inhibited cell proliferation and tumour growth *in vivo*, especially in CRPC cell line and enzalutamide-resistant PCa xenografts (Lee *et al.*, 2021). Next, the well-established NTD antagonist EPI-506 (a pro-drug of EPI-002) was successfully utilized to develop the AR PROTAC BWA-522 (**Figure 11**), which incorporates a CRBN head. It degraded both AR-FL and AR-V7, effectively suppressing AR downstream signalling *in vitro*. Moreover, BWA-522 achieved sufficient oral bioavailability in mice and was potent against PCa xenografts *in vivo* (Zhang *et al.*, 2023).

3.7 Resistance to known therapies and its management

The novel AR-targeted drugs have significantly improved PCa management, providing effective alternatives to cytotoxic chemotherapy and leading to improved clinical outcomes in both CSPC and CRPC. However, the long-term efficacy of these agents

is limited by acquired resistance, a similar challenge observed with abiraterone. As already mentioned, CRPC develops on the basis of acquired resistance by many mechanisms collectively contributing to the re-activation of AR signalling (Vellky and Ricke, 2020). Prolonged exposure to AR signalling inhibitors, such as enzalutamide and abiraterone, may force CRPC cells to undergo de-differentiation into AR-negative PCa, accompanied by significant transcriptional and chromatin structural rewiring (Feng *et al.*, 2023).

Researchers actively explore ways to overcome resistance and enhance existing therapies and identify new targets (AR-V7, AKT, HIF1 α etc.). The search for predictive biomarkers of resistant tumours resulted in the approval of PARP inhibitors (olaparib and rucaparib) for pre-treated mCRPC (Iannantuono *et al.*, 2023). The outcomes of ongoing clinical trials offer hope for advancing precision medicine in PCa and refining treatment strategies to enhance patient outcomes.

The most frequent acquired mechanisms of resistance are loss of AR expression and GR upregulation, which are discussed below. Strong and prolonged inhibition of the AR has led to an increase in PCa cases transitioning into AR-negative disease, associated with poor prognosis (Formaggio *et al.*, 2021). The resistance to enzalutamide usually involves other genes in adaptation (e.g., *SOX2*, *TP53*, *RB1*, *N-MYC*, *EZH2*), compared to resistance to ADT, typically involving only genes within the AR pathway. At the stage of CRPC, the plasticity of PCa cells increases and the de-differentiation process leads to a transition into AR-negative disease, involving extensive transcriptional and chromatin changes resulting in resistance and decreased response to treatment (Feng *et al.*, 2023).

The incidence of AR-negative disease in mCRPC patients has increased from 11% to 36% with androgen receptor inhibitors' treatment (abiraterone, enzalutamide) (Bluemn *et al.*, 2017), suggesting a continuing trend, possibly even extended in AR PROTACs. The tumour biopsy is required for diagnosis of AR-negative disease, and the most prevalent and recognised subtype is the neuroendocrine PCa, characterized by elevated neuroendocrine proteins and reduced expression of AR-regulated epithelial markers (Beltran *et al.*, 2014). Its standard treatment involves platinum-based chemotherapy (cisplatin/carboplatin with docetaxel or etoposide). Unfortunately, response rates to these regimens are high but not long-lasting, with poor prognosis (Aparicio *et al.*, 2013), therefore, there is a clinical priority to explore strategies to prevent the AR-negative PCa onset and maintain sensitivity to therapy.

In recent decades, numerous strategies to re-activate AR expression in advanced PCa were developed, mainly targeting the RB1 and p53 signalling network (EZH2 or p38 inhibition, SOX2 silencing, azacytidine treatment) (Ku *et al.*, 2017), although they lack robust *in vivo* validation. Future research could benefit from clinically relevant models to better understand AR-negative disease and the potential for restoring AR expression.

Numerous studies indicated that GR can activate transcription programs similar to AR, potentially bypassing AR blockade and contributing to therapy resistance in CRPC (Isikbay *et al.*, 2014). Prolonged ADT, AR inhibition or docetaxel treatment often result in the restoration of histone H3 lysine 27 acetylation on the GR enhancer, leading to increased GR expression, both *in vitro* and in relapsed patient samples (Palit *et al.*, 2019). This GR upregulation is associated with the re-expression of AR-responsive genes, promoting PCa tumour proliferation despite AR blockade. Additionally, GR agonists like dexamethasone can induce resistance to enzalutamide, while GR antagonists may restore enzalutamide sensitivity in CRPC (Puhr *et al.*, 2018). Considering the frequent use of glucocorticoids (prednisone, dexamethasone) in primary or mPCa patients, there's an urgent need to develop new therapeutic strategies with a focus on GR expression. Recent studies suggest that targeting the GR pathway alongside antiandrogen therapy could enhance PCa treatment outcomes, and there's ongoing development of novel compounds acting as AR/GR antagonists (Wu *et al.*, 2019; Li *et al.*, 2024), as well as combinations of AR antagonists with selective GR antagonists. Even though the approach was found safe and well tolerated, yet, no clinical trial showed beneficial outcomes in targeting both the AR and GR in CRPC patients (Abida *et al.*, 2024).

3.8. Development of novel therapies for prostate cancer

Various novel approaches like PROTACs and targeting different regions (NTD or DBD) are explored to overcome resistance mechanisms observed in clinical trials. However, the development of novel LBD antagonists is also plausible, with emphasis on desired properties such as limited resistance, favourable pharmacokinetics and minimal side effects. The absence of a crystal structure of the wt-LBD with an antagonist hampers the structure-based development, even though the structures of AR mutants in complex with antagonists provided a basis to build the model for prediction of antagonist binding to AR-wt (Wahl and Smieško, 2018). Among the important questions to be addressed in the future is the detailed interactions between the selective ligands and the AR-LBD, since there are at least two possible orientations of the tail group of second-generation

nonsteroidal antagonists in the LBP (Gim *et al.*, 2021). Overall, the continued development of novel AR antagonists holds promise for improving outcomes of PCa patients, particularly those who do not respond to current treatments or developed resistance.

Apart from the AR axis, several other approaches might be used to target and treat PCa, including phototherapy, immunotherapy and targeting other signalling pathways (PARP, AKT or CDK). Phototherapy, including photodynamic therapy (PDT) or photothermal therapy (PTT), offers benefits such as minimal invasiveness, precise tumour targeting, low systemic toxicity, and low risk of resistance development, however, irradiation of the deep-seated solid tumours may be challenging (Shi and Sadler, 2020). PDT utilize a non-toxic photoactive compound accumulating in a tumour which is activated by irradiation, leading to tumour destruction and it is in a clinical trial for recurrent PCa (NCT03067051). PTT, on the other hand, involves heating tumour tissue (by near-infrared laser irradiation) to temperatures around 41–45 °C, sensitizing tumour cells to chemotherapy, demonstrated by combination with doxorubicin chemotherapy and the targeting with gold nanoparticles in a pilot clinical trial showed potent PCa tumour ablation (Rastinehad *et al.*, 2019).

Targeting a specific membrane antigen is crucial for treatment selectivity and prostate-specific membrane antigen (PSMA) is highly expressed in PCa and serves as a vital target for diagnosis and therapy. PSMA ligands such as monoclonal antibodies, aptamers, and small-molecule inhibitors offer the potential to build conjugates for imaging and targeted therapy (He *et al.*, 2022). PSMA imaging agents like ⁶⁸Ga-PSMA-11 for positron emission tomography have shown improved sensitivity in PCa diagnosis (Afshar-Oromieh *et al.*, 2013). Targeted radionuclide therapy with ¹⁷⁷Lu-PSMA-617, demonstrated potent anticancer activity with higher PSA response rates and fewer AEs compared to cabazitaxel in mCRPC and was FDA-approved (Sartor *et al.*, 2021). Several PSMA-targeted radionuclide therapies are currently being evaluated in ongoing clinical trials (Jang *et al.*, 2023). PSMA can also be targeted by antibody-drug conjugates or PSMA-based Chimeric Antigen Receptor-T Cell Therapy, both of which are undergoing evaluation in clinical trials (Deluce *et al.*, 2022).

4 MATERIALS AND METHODS

4.1 Commercial compounds

The compounds which were used as standards are listed in **Table 4**.

Table 4 List of commercially available compounds, vendor and their purity.

Compound	CAS number	Vendor	Purity (%), determination
enzalutamide	915087-33-1	MedChemExpress	99.96% (HPLC/MS)
galeterone	851983-85-2	Merck	≥98 %, (HPLC)
R1881	965-93-5	Merck	≥98 % (HPLC)
MG-132	133407-82-6	MedChemExpress	99.97% (HPLC/MS)

4.2 Cell cultures

The PCa cell lines comprised the LNCaP and C4-2 (American Tissue Culture Collection), 22Rv1, LAPC-4, DU145 (generous gift from Assoc. Prof. Jan Bouchal from Faculty Hospital Olomouc) LNCaP-Abl and DuCaP (generous gift from Prof. Zoran Culig, Medical University Innsbruck, Austria) and PC-3 (German Collection of Microorganisms and Cell Cultures). All the PCa cell lines were cultivated in RPMI, supplemented with foetal bovine sera (FBS) specified for each experiment, only LAPC-4 was routinely cultivated with 1 nM R1881 and LNCaP-Abl with steroid-depleted serum (charcoal-stripped serum, CSS). The AR-positive breast cancer cell lines comprised T47D and MCF7 (European Collection of Authenticated Cell Culture) and SKBR3 (American Tissue Culture Collection) and were cultivated in DMEM. The reporter cell lines 22Rv1-ARE14 and AZ-GR were generous gifts from Prof. Zdeněk Dvořák from the Department of Cell Biology, UP. All the media were supplemented with 100 IU/ml penicillin, 100 µg/ml streptomycin, 4 mM glutamine and 1 mM sodium pyruvate. Cells were cultivated in a humidified incubator at 37 °C and in a 5% CO₂ atmosphere.

4.2.1 Androgen and glucocorticoid receptors' transactivation assay

The Nunc™ MicroWell™ 96-well optical flat-bottom plate (Thermo Fisher Scientific) was used for luciferase assays, in which 22Rv1-ARE14 or AZ-GR cells were seeded (40 000 or 20 000 cells/well, respectively). On the second day, the cultivation medium (supplemented with FBS) was discarded and cells were washed with PBS. Cells were then incubated in the absence or presence of analysed compounds dissolved in a medium

supplemented with CSS and 1 nM R1881 or 100 nM dexamethasone in the case of 22Rv1-ARE14 or AZ-GR, respectively. Upon 24 h of incubation, cells were washed with PBS again and lysed for 10 min in a lysis buffer (10 mM Tris pH = 7.4, 2 mM DCTA, 1% Nonidet P40, 2 mM DTT) at 37 °C. Next, reaction buffer (20 mM tricine pH = 7.8, 1.07 mM MgSO₄·7H₂O, 5 mM ATP, 9.4 mM luciferin) was added and the luminescence of the samples was measured using a Tecan M200 Pro microplate reader (Biotek). Assays were performed in duplicate.

4.2.2 Cell viability assay

For the viability assays, cells were seeded into the 96-well tissue culture plates, the other day, solutions of compounds were added in different concentrations in replicates for 72 h. Upon treatment, the resazurin solution (Sigma Aldrich) was added for 4 h, and the fluorescence of resorufin was subsequently measured at 544 nm/590 nm (excitation/emission) using a Fluoroskan Ascent microplate reader (Labsystems). Percentual viability or GI₅₀ value was calculated from the dose-response curves that resulted from the measurements using GraphPad Prism 5.

4.2.3 Colony formation assay

PCa cells 22Rv1 and DU145 (5000 cells per well), LAPC-4 and PC-3 (10 000 cells per well) were seeded into 6-well plates. After two days of cultivation, the medium was replaced with fresh medium containing different concentrations of the compounds. Cells were cultivated for 10 days in the presence of compounds. After the treatment, the medium was discarded and colonies were fixed with 70% ethanol for 15 min, washed with PBS and stained with crystal violet (1% solution in 96% ethanol) for 1 h. Finally, wells were washed with PBS and colonies' photographs were captured.

4.2.4 Cell lysis, electrophoresis and Western blot

After all treatments, cells were harvested by centrifugation, washed twice with PBS, pelleted and kept frozen at - 80 °C. Pellets were thawed and resuspended in ice-cold RIPA lysis buffer supplemented with phosphatase and protease inhibitors. Ultrasound sonication (10 s with 30% amplitude) of cells was performed on ice and soluble proteins in supernatants were obtained by centrifugation at 14 000 g for 30 min. Cellular fractionation experiments were performed using the Qproteome Cell Compartment Kit (Qiagen). Protein concentration in supernatants was measured and balanced within samples. Proteins were denatured by the addition of sodium dodecyl sulphate (SDS)-

loading buffer, separated by SDS- polyacrylamide gel electrophoresis (PAGE) and electroblotted onto nitrocellulose membranes. Immunodetection of proteins was performed as usual, membranes were blocked in BSA solution, incubated overnight with primary antibodies, washed and incubated with secondary antibodies conjugated with peroxidase. Then, peroxidase activity was detected by SuperSignal West Pico reagents (Thermo Scientific) using a CCD camera LAS-4000 (Fujifilm). Particular primary antibodies are listed in publications (appendices), secondary antibodies were purchased from Cell Signalling Technology: anti-rabbit secondary antibody (porcine anti-rabbit immunoglobulin serum); anti-mouse secondary antibody (rabbit anti-mouse IgG, clone D3V2A). All antibodies were diluted in 4% BSA and 0.1% Tween 20 in TBS.

4.2.5 Fractionation of cellular compartments

Cellular fractionation experiments were performed using the Qproteome Cell Compartment Kit (Qiagen). The protocol was subsequently optimised with in-house buffers, as described in section 5.5. Cells were first harvested by trypsinisation, washed in PBS and divided into aliquots. Then, the basic cytosolic buffer A (150 mM NaCl, 50 mM HEPES (pH 7.4) with protease inhibitors and 0.1% IGEPAL[®] CA-630 was added. After the 5 min incubation on ice, the suspension was centrifuged at 600 g for 6 min. The obtained supernatant represented the cytosolic fraction, while the pellet was further incubated with buffer B (nuclear, 20 mM HEPES, pH 7.9, 1.5 mM MgCl₂, 0.5 M NaCl, 0.2 mM EDTA, 20% glycerol, 1% Triton[™] X100), sonicated and centrifuged at 14 000 g for 15 min. The supernatant represented soluble nuclear proteins, while the pellet contained insoluble proteins bound to chromatin and cell debris.

4.2.6 Cellular thermal shift assay

CETSA experiments were performed according to the optimised protocol (section 5.5). LAPC-4 or C4-2 cells were harvested by trypsinisation, re-suspended in PBS with 5 mM glucose and divided into test tubes, where they were treated with tested compounds for 1 h. Upon the treatment, cells were counted and equally aliquoted into PCR strips, heated at the temperature gradient from 37 °C to 60 °C for 3 min, cooled down to 4 °C and they were snap-frozen in liquid nitrogen. The lysis by freeze-thaw cycles was performed and the supernatants containing soluble proteins were obtained by centrifugation at 14 000 g for 30 min, and mixed with SDS-loading buffer, separated by SDS-PAGE and immunoblotted for thermostable AR level.

4.2.7 Cell cycle analysis

Cells were treated with test compounds for 24 h, they were harvested by trypsinisation, washed with PBS and fixed with 70% ethanol. After rehydration, cells were permeabilised by 2 M HCl, 0.5% Triton X-100. Following neutralization and washing with PBS, the cells were stained with propidium iodide and analysed by flow cytometry with a 488 nm laser (BD FACS Verse with BD FACSuite software, version 1.0.6.). Cell cycle distribution was analysed using ModFit LT (Verity Software House, version 5.0).

4.2.8 Analysis of mRNA expression

Cells were treated and harvested into lysis buffer and total RNA was isolated using RNeasy plus mini kit (QIAGEN) based on the manufacturer's instruction. RNA concentration and purity were evaluated using a DeNovix DS-11 spectrophotometer, while the quality of RNA was determined by gel electrophoresis. The RNA (0.5–1 µg) was reverse transcribed into first-strand cDNA which was carried out by SensiFast cDNA Synthesis Kit (Bioline). RNA Spike I template (TATAA) was used as a control. Quantitative RT-PCR was performed on a CFX96 Real-Time PCR Detection System (Bio-rad) with a SensiFAST SYBR No-Rox Kit (Bioline). The suitable primers were designed using Primer-BLAST (Ye *et al.*, 2012) and synthesized by Generi Biotech. Primary data were analysed using Bio-rad CFX Maestro 2.2. Relative gene expression levels were determined using the $\Delta\Delta C_t$ method (Livak and Schmittgen, 2001). Expression was normalized per *ACTB* and *SDHA* (the most stable by Bio-rad CFX Maestro 2.2). Used primers: *ACTB* (F: GCACCACACCTTCTACAAT; R: GTCTCAAACATGATCTGG GT); *AR-FL* (F: TTCGCCCCTGATCTGGTTTT; R: TGCCTCATTCGGACAC ACTG); *KLK3* (F: CCACACCCGCTCTACGATATG; R: GGAGGTCCACACACT GAAGTT); *SDHA* (F: TACAAGGTGCGGATTGATGA; R: GTTTTGTCGATCACG GGTCT).

4.2.9 Androgen receptor preparation and micro-scale thermophoresis

AR-LBD (with His6-tag) was expressed and purified using recombinant plasmid pET-15b-hAR-663-919, which was a generous gift from Elizabeth Wilson (Addgene plasmid # 89083) by the original protocol (Askew *et al.*, 2007). The recombinant AR was purified into the storage buffer (25 mM Tris, 300 mM NaCl, pH 8.0, 5 mM DTT) and concentrated up to 0.5 mg/ml using a centrifugal filter unit with 10 kDa cut-off (Merck). MST method was used to prove the binding of **3d** in the AR-LBD, which was labelled with the His-

Tag Labelling Kit RED-tris-NTA (NanoTemper) (100 nM dye + 800 nM His-tagged protein) for 30 min. The labelled protein was used for MST measurements with or without **3d** in a final concentration of 400 nM His-tagged protein in the storage buffer, supplemented with 0.1% Tween. Measurements were done on a Monolith NT.115 instrument (NanoTemper Technologies).

4.2.10 Molecular docking

Molecular docking was performed with the crystal structure of AR-LBD with DHT (PDB: 2PIV) or AR-antagonist model (Wahl and Smieško, 2018), for GR the docking was performed into the crystal structure of GR-LBD with mifepristone (PDB:1NHZ). The 3D structures of all compounds were obtained and their energy was minimised by molecular mechanics with Avogadro 1.90.0, a software used for the drawing and characterisation of chemical structures. Polar hydrogens were added to ligands and proteins with the AutoDock Tools program (Morris *et al.*, 2009) and docking studies were performed using AutoDock Vina 1.05 (Trott *et al.*, 2010). Interactions between ligand and amino acid residues were modelled in PLIP software (Adasme *et al.*, 2021). Figures were generated in Pymol ver. 2.0.4 (Schrödinger, LLC).

5 SURVEY OF RESULTS AND DISCUSSION

Steroid-based compounds have gained attractivity in recent years with several examples, mostly modified in the D-ring of the androstane core, as AR modulators with anti-PCa properties, investigated also at our department (Cortés-Benítez *et al.*, 2016; Shi *et al.*, 2018; Jorda *et al.*, 2019a, Jorda *et al.*, 2019b).

However, compared to D-ring fused or substituted steroid derivatives, compounds containing a heterocycle moiety in the A-ring have been recently much less investigated. In collaboration with Éva Frank's (University of Szeged, Hungary) synthetic group, we explored the biological activity and structure and activity relationship (SAR) of 5 α -dihydrotestosterone (DHT)-derivatives with modifications on the A-ring (**Figure 12**).

The results part of the thesis comprises the deep screening of AR antagonists within novel and already published (Baji *et al.*, 2017b; Baji *et al.*, 2016; Mótyán *et al.*, 2019) compounds based on DHT with diverse A-ring substitution. At first, the effect of compounds on AR-transactivation was investigated using gene reporter assay and antiproliferative potency towards PCa cell lines was assessed by resazurin-based assay. The most potent compounds were analysed in detail for their binding into the AR, the influence of the AR level and downstream signalling (**Appendix I. – III.**). For a detailed assessment of the compounds' behaviour, several methods established at the department were used, while the isolation of the cellular fractions (cytosol and nuclei) and the cellular-thermal shift assay were optimised based on the published protocols to fit best for the NR's analysis as a part of this thesis.

Finally, the biological activity of hydrocortisone's derivatives prepared by the synthetic group of Gyula Schneider and Erzsébet Mernyák (University of Szeged, Hungary) was also performed. Given the crucial role of GR in resistant PCa and recently described dual and selective antagonists of AR/GR, further development of similar compounds was supported. As a part of this dissertation thesis, novel 17 α - and/or 21-ester or carbamate derivatives of hydrocortisone were characterised. Compounds were analysed for their activity towards both the AR and GR and the lead compound suppressing the signalling of both receptors was successfully found (**Appendix IV.**). As a part of this thesis, several D-ring-attached steroidal isoxazoles and triazoles (similar to abiraterone) were also developed and characterised, displaying presumed CYP17A1 inhibitory effect and moderate AR-antagonist activity (**Appendix V.**).

5.1 Screening and discovery of novel androgen receptor's antagonists

An ideal AR antagonist should possess key properties to ensure effective therapeutic outcomes. These properties include a high affinity for the AR to effectively compete with endogenous androgens, selectivity towards the AR to minimize off-target effects and reduce AEs, potency to suppress the growth and proliferation of PCa cells with minimal toxicity to healthy tissue, favourable pharmacokinetic properties etc (He *et al.*, 2022).

A broad library of DHT derivatives (**Figure 12**) was efficiently prepared in two steps. Generally, Claisen-Schmidt condensation of the DHT precursor with variously substituted aldehydes led to the regio- and stereoselective formation of α,β -unsaturated ketones, which underwent cyclization with different binucleophilic reagents, without or with microwave irradiation applied to the reaction mixture. The heterocyclic products were obtained with good yields. Next, in some cases the 17β -hydroxyl group was oxidized, leading to the corresponding 17-ones. In addition to the routine solution-phase analysis of the products, the structures of several compounds were determined by single-crystal X-ray diffraction. Altogether, compounds bearing different nitrogen-containing five or six-membered heterocycles as a fusion to the A-ring of DHT with a similar series of terminal substituents (119 compounds in total) were thoroughly characterised.

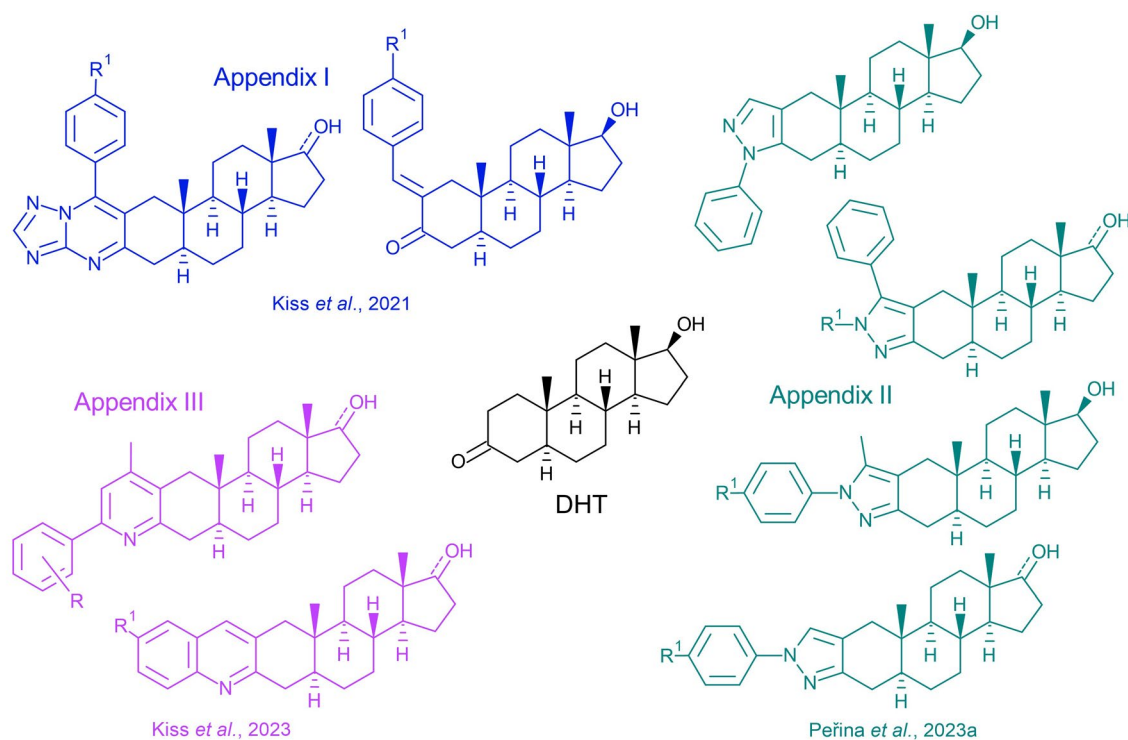


Figure 12 Schematic representation of the A-ring fused DHT derivatives from Éva Frank's synthetic group analysed in publications (**Appendix I. -III.**).

The analysed library of the A-ring DHT derivatives comprised particularly:

- α,β -enones with C17-OH group (9 compounds)
- triazolo[1,5-*a*]pyrimidines with C17-OH or C17-keto group (18)
- pyrazolo[1,5-*a*]pyrimidines (4)
- N-monosubstituted pyrazole derivatives (16)
- 1-aryl-5-methyl pyrazole derivatives (16)
- 1,5-disubstituted pyrazole derivatives (24)
- monosubstituted quinoline derivatives (9)
- mono- and di-substituted pyridine derivatives (23)

Since the AR modulators are known to influence AR-dependent transcription, at first the activity of analysed compounds towards the R1881-stimulated AR's transcriptional activity was assessed, upon 24 h treatment. Compounds were screened at point concentrations (including 10 μ M, as frequently used in previous studies) using an AR-dependent reporter cell line, 22Rv1-ARE14, stable-transfected with a reporter plasmid containing *KLK3* promoter with ARE sequence controlling luciferase expression (Bartonkova *et al.*, 2015). Subsequently, compounds were analysed for their antiproliferative in AR-positive and AR-negative cell lines, to display their potency to block the proliferation of PCa cells.

Table 5 Overview of activities of A-ring fused DHT derivatives. The characteristics of every group is shown as a mean of the effect (AR transactivation in agonist/antagonist setting or per cent of viable cells) within the whole group of compounds.

The A-ring fusion	Structure	Original label	AR activity (antagonist mode) (%)*	AR activity (agonist mode) (%)*	Viability of AR+ lines†	Viability of AR-line†	Ref.
α,β -enones C17-OH		2a - 2k	50	no	90 2f, 2j	n.a.	Appendix 1
triazolo[1,5-a]pyrimidines, C17-OH		8a - 8k	78	majority no	91	n.a.	
triazolo[1,5-a]pyrimidines, C17=O		11a - 11k	88	majority no	98	n.a.	
pyrazolo-pyrimidines		6a, 7a, 9a, 10a	74	no	107	n.a.	
The A-ring fusion	Structure	Original label	AR activity (antagonist mode) (%)*	AR activity (agonist mode) (%)*	Viability of AR+ lines‡	Viability of AR-cell line‡	Ref.
monosubstituted (N-2) pyrazoles, C17-OH		1a-1h	55	64	62	90 1d	Appendix 2
monosubstituted (N-1) pyrazoles, C17-OH		2a-2h	77	78	98	102	
1-aryl-5-methyl pyrazoles, C17-OH		3a - 3h	25	21	54	81 3c, 3g	
1-aryl-5-methyl pyrazoles, C17=O		4a - 4h	60	24	71	103	
5-aryl-1-methyl pyrazoles, C17-OH		8a - 8h	52	11	40	97	
5-aryl-1-methyl pyrazoles, C17=O		10a - 10h	70	13	43	98	
1,5 -biaryl pyrazoles, C17-OH		8i - 8 k	141	64	42	25	
1,5 -biaryl pyrazoles, C17=O		10i - 10k	157	66	63	70 10i	
quinolines		1a-1i	83	30	79	96	Appendix 3
6'-substituted pyridines		2a - 2h	101	70	82	105	
4',6'-disubstituted pyridines		3a - 3o	112	60	79	106	

*mean of the percentual AR transcriptional activity upon treatment (calculated for the whole group of compounds, normalised to the level of 1 nM R1881, n.a., not analysed.

† percentual viability upon 72-h treatment with 10 μ M compounds, norm. to control.

‡ percentual viability upon 72-h treatment with 20 μ M compounds, norm. to control.

The first part of the analysed library comprised α,β -enones, triazolo[1,5-*a*]pyrimidines and pyrazolo[1,5-*a*]pyrimidines. As shown in **Table 5** and **Appendix I., Table 3** α,β -enones belonged to the most active compounds (6 compounds reduced R1881-stimulated AR transactivation to 50 % at 10 μ M concentration, most potently the compounds **2a**, **2d**, **2f**. Within the α,β -enones, there was not any compound with agonist properties at 10 μ M. On the other hand, triazolo[1,5-*a*]pyrimidines and pyrazolo[1,5-*a*]pyrimidine DHT-derivatives were active only partially and some of them displayed agonist activities. It was obvious that heterocyclization of **2a** reduced the antiandrogenic effect (**8a**). While the C17-OH derivatives were not all generally more potent antagonists than the C17-keto counterparts, within the examples of **8e**, **8i**, **8j** and **11e**, **11i**, **11j** C17-OH variants displayed slightly higher potency.

The antagonist activity of *p*-chlorobenzylidene derivative **2f** (**Figure 13**) ($IC_{50} = 3.54 \mu$ M) reached up to single-digit micromolar values and showed to be comparable with values obtained for standards, i.e. galeterone ($IC_{50} = 5.82 \mu$ M) and enzalutamide ($IC_{50} = 1.50 \mu$ M) (Yu *et al.*, 2014; Tran *et al.*, 2009) (**Appendix I., Supplementary Material, S38-S41**). Antiproliferative properties were tested in two AR-positive PCa cell lines (22Rv1-ARE14, C4-2), at 10 μ M compounds for 72 h. While the majority of the compounds induced no decrease in PCa cells proliferation, the most potent derivative **2f** (**Figure 13**) displayed mid-micromolar values ($GI_{50} = 9.9 \pm 1.8 \mu$ M and $15.7 \pm 4.4 \mu$ M) in 22Rv1-ARE14 and C4-2, respectively and outperformed the used standards with $GI_{50} > 50 \mu$ M (**Appendix I., Supplementary Material, S42-S47**). Considering the limited cytotoxicity of AR antagonists (Latysheva *et al.*, 2020; Chen *et al.*, 2022), displaying rather a cytostatic effect, the results might correspond with previous studies. That is why the prolonged antiproliferative effect of **2f** was further evaluated by clonogenic assay in 22Rv1-ARE14 cells. As shown in **Appendix I., Fig. 5**, **2f** significantly inhibited the formation of cell colonies in a dose-dependent manner.

The next group of analysed derivatives comprised already published A-ring fused pyrazoles of DHT bearing the mono-substitution in positions N2 or N1 (series **1** and **2**) and 1-aryl-5- methyl pyrazoles (**3** and **4**), together with newly prepared 1-methyl-5-aryl pyrazoles (**8** and **10**). The monosubstituted pyrazoles from series **1** and **2** displayed only moderate effect on R1881-stimulated AR-transcriptional activity, being only weak antagonists in 10 μ M concentration. Unfortunately, most compounds (except regioisomers **1f** and **2f**) undesirably activated the AR in agonist mode (**Table 5**, **Appendix II., Table 2**). Representatives from series **3** and **8** that bear the C-17 hydroxy

group and combine methyl and aryl substitution at N1 or C5 position of pyrazole (**3a–3h**, **8a–8h**) showed to act as strong antagonists. In total, 12 out of 16 compounds were able to decrease the AR-transcriptional activity below 50 % of R1881-stimulated control (**Table 5, Appendix II., Tables 3, 4**). Compounds from series **3** were generally more potent antagonists than their regioisomers from series **8**. Importantly, none of the compounds displayed agonist activities except **8b**. The most potent derivative was **3d** (**Figure 13**) with 1-fluorophenyl-5-methyl pyrazole moiety reaching the low micromolar antagonist potency ($IC_{50} = 1.18 \mu\text{M}$), outperforming the analysed standards enzalutamide and galeterone (Yu *et al.*, 2014; Tran *et al.*, 2009).

Antagonist activities were observed also for series **4** and **10** bearing the C-17 keto group (counterparts of **3** and **8**, combining methyl and aryl substitution at the N1 or C5 position of the pyrazole ring, respectively). All compounds (**4a–4h**, **10a–10h**) acted predominantly as AR antagonists but were less potent than compounds from series **3** and **8** (**Table 5, Appendix II., Tables 3, 4**). Previous results showed that the combination of a small substituent (Me group) with a bulky one (phenyl or *para*-substituted phenyl moiety) in the 1,5 positions of the pyrazole ring is fundamental to reach strong antagonist activity. This scenario was obvious from the results with derivatives **8l**, **10l** (1,5-dimethyl-substituted) and **8i**, **10i** (1,5-diaryl-substituted) that displayed only agonist activities towards AR transactivation.

Antiproliferative properties of the pyrazole derivatives were screened on the panel of three PCa cell lines, namely LAPC-4, 22Rv1 (AR-positive) and DU145 (AR-negative). In general, effects corresponded with previous assays showing that compounds from series **3**, **4**, **8**, and **10** belonged to the most active ones, while compounds from series **1** and **2** did not exert any effect on the viability of PCa cells, consistently with the weak agonist activity of these derivatives. The most potent derivatives in 22Rv1 cells were compounds **3a**, **3d**, **8d–g** (<30 % viable cells in 20 μM concentration), while LAPC4 cells were the most sensitive to compounds **3d**, **4e** and **10a–h** (<40 % viable cells in 20 μM concentration). The results confirmed the selective targeting of AR because DU145 stayed unaffected upon treatment with the majority of compounds, with the exceptions of antagonists **3c**, **3g** and compounds **8i–k**, **10i** displaying potent antiproliferative activity towards DU145 and no AR-antagonist properties (**Table 5, Appendix II., Table 5**), suggesting another mechanism of action. In a consequence of the relatively low antiproliferative potential of AR antagonists (Latysheva *et al.*, 2020; Chen *et al.*, 2022), their effect was evaluated on the colony-formation assay in LAPC-4 cells during the

10-day treatment. As shown in **Appendix II., Table 2, Table 3, Table 4, Figures. S4 and S5**, all compounds from series **3, 4, 8** and **10** were potent in blocking the formation of cell colonies in 5 μM concentration, the majority outperforming the enzalutamide (Tran *et al.*, 2009). Consistently with previous results, compounds from series **2** and **8i–I, 10i–I** displayed only a weak effect comparable to enzalutamide. On the other hand, many compounds from series **1** effectively inhibited colonies growth, being only weak antagonists, indicating the targeting of other processes in cells. Further, the antiproliferative effect of the most potent compound **3d** (**Figure 13**) in different cell lines was dose-dependent, with increased potency in AR-positive PCa cell lines with GI_{50} values in low micromolar ranges with LAPC-4 cells being the most sensitive ($\text{GI}_{50} = 7.9 \pm 1.6 \mu\text{M}$) (**Appendix II., Figure S9**).

The last analysed group in the library comprised already published steroidal A-ring-fused quinolines (**1a–1i**) and novel A-ring-fused 6'-substituted pyridine derivatives (**2a–2h**) and A-ring-fused 4',6'-disubstituted pyridine derivatives (**3a–3o**). Approximately one-half of the quinolines were able to decrease the AR-transcriptional activity in the antagonist mode, but with much lower potency compared to earlier derivatives, with only 3 compounds (**1a, 1d, 1i**) able to diminish the R1881-activated AR transcriptional activity to approx. 50 % at 10 μM . In the agonist mode, it was found that four compounds displayed agonist activity (**1b, 1g, 1c, 1i**), while the rest of this group was found not to have AR agonist activity (**Table 5, Appendix III., Table 3**), including **1d** (**Figure 13**), which was found to be the most potent one with $\text{IC}_{50} = 10.51 \mu\text{M}$, comparable potency to galeterone (7.59 μM) (Yu *et al.*, 2014) (**Appendix III., Figure 7**). There was no clear SAR within series **2** and **3**, of the pyridines, which generally show very few and only weak antagonists. It was clear that the monosubstitution at the C-6' position by an aromatic moiety led to compounds exerting strong agonist activities in series **2**, except for compounds **2f** and **2g**. In series **3**, the combination of a methyl moiety at the 4'-position with an aryl substitution in the C-6' position yielded compounds with moderate antagonist properties (**3a–3c**) (**Appendix III., Table 3**). A similar beneficial effect was earlier observed in very potent disubstituted A-ring fused pyrazoles. In contrast, substitutions by the bi-aryl motif (in both C-4' and C-6' positions of the pyridine) yielded compounds with strong agonist activities, also correlating with the previous research. All compounds were evaluated in 20 μM concentration for their effect on PCa cell lines' (LAPC-4, 22Rv1, LNCaP and DU145) proliferation using the resazurin-based cell viability assay after 72 h treatment. The results confirmed previous studies and correlated with weak antagonist

properties, because the majority of compounds decreased the viability only to 70–80% of the vehicle-treated cells (Latysheva *et al.*, 2020; Chen *et al.*, 2022). Generally, the viability of DU145 was not influenced by most of the compounds, which supports the targeting of the AR. Corresponding with the AR-antagonist activity, compounds **1d** and **1i** indeed displayed reasonable antiproliferative activity predominantly in 22Rv1 (decreasing the viability to approx. 20%), but also in LAPC-4 and LNCaP (**Appendix III., Table 4**). Compound **1d** (**Figure 13**) outperformed the standard antagonists galeterone and enzalutamide. There was a clear difference between the sensitivity of the AR-positive cell lines and the AR-negative DU145 (**Appendix III., Figure 7**). The antiproliferative activity of these derivatives in 10 μ M towards the LAPC-4 cell line using the CFA for 10 days showed profound antiproliferative activity of compounds **1a**, **1c**, **1d**, **1g**, **1h** and **1i**, decreasing the colony formation to 16–30% of control treated by vehicle (**Appendix III., Figure 5**).

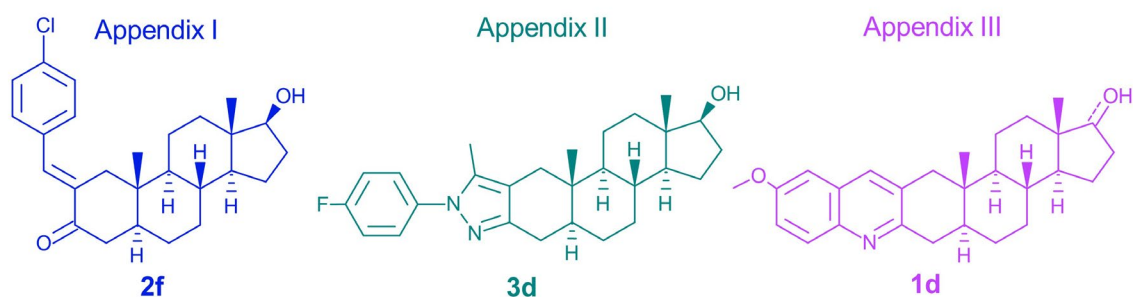


Figure 13 Structures of the most potent compounds from each group.

5.2 Compounds' effect on downstream signalling and the cell cycle

The crucial process in AR signalling is its translocation into the nucleus in response to androgens (Chen *et al.*, 2012), where it drives the transcription of target genes and AR modulators have been shown to block the transport and accumulation of AR in the nucleus (Tran *et al.*, 2009; Yu *et al.*, 2014). Therefore, the effect of **2f** on AR distribution in R1881-stimulated cells was analysed. As shown in **Appendix I., Fig. 7**, **2f** and galeterone markedly decreased the transport of AR to the nucleus, compared to androgen-activated control. While AR remained in cytosol upon the treatment of cells with **2f**, galeterone induced also partial AR degradation (Kwegyir-Afful *et al.*, 2015).

With the most potent AR antagonists from novel compounds, further analysis of the AR downstream signalling was performed by western-blot analysis of AR transcription targets, PSA and Nkx3.1. In the case of the *p*-chlorobenzylidene derivative

2f, the treatment of 22Rv1-ARE14 and C4-2 did not lead to changes in the protein expression of AR itself, while expression of PSA and Nkx3.1 decreased in a dose-dependent manner compared to R1881-stimulated cells. It was consistent with the effect on AR-transactivation and comparable with galeterone (Yu *et al.*, 2014). Moreover, cleaved PARP (indicating ongoing apoptosis) was not detected, corresponding with mild cytotoxicity of the investigated compound (**Appendix I., Figure 9**).

The most potent pyrazole derivatives were analysed in detail in three PCa cell lines (LNCaP, LNCaP-Abl, LAPC-4). Apart from other potent compounds, candidate **3d** displayed potent blockage of AR signalling mainly in LAPC-4 (expressing wt-AR), with sharp decreases in both Nkx3.1 and PSA protein levels and AR-phosphorylation level at serine 81 as well as moderate decrease in AR level, in agreement with antagonist activity (He *et al.*, 2022). Moreover, **3d** displayed activity in LNCaP cells (bearing the AR Thr877Ala mutation) and importantly, even in CRPC model LNCaP – Abl (cells established by long-term cultivation in androgen-depleted medium, resulted in AR hypersensitivity (Culig *et al.*, 1999), being able to block the S81 phosphorylation and down-regulate both the AR and PSA (**Appendix II., Figure 4**). Moreover, the changes in AR level and downstream targets were precisely monitored in different concentrations and time of treatment, where the dose-dependent suppression of AR signalling up to 10 μ M concentration of **3d** (comparable to galeterone's effect) was observed in LAPC-4 (**Appendix II., Figure 5**), as well as in 22Rv1 and LNCaP (**Appendix II., Supplementary Figure S6**) (Kwegyir-Afful *et al.*, 2015). Long-term treatment of LAPC-4 showed a significant decrease in the AR expression (discussed in section 5.3).

In case of the DHT-quinolines, upon steroid withdrawal and subsequent stimulation of AR signalling by R1881, compounds **1d** and **1a** moderately diminished the AR phosphorylation on S81 (Jorda *et al.*, 2018; Lv *et al.*, 2020) and suppressed the AR signalling in 10 μ M concentration (decrease of the PSA protein level) in LAPC-4, similar to the effect of galeterone (Kwegyir-Afful *et al.*, 2015) (**Appendix III., Figure 7**). Similar activity of the lead compound **1d** was observed mainly on the PSA level even in LNCaP and 22Rv1 (**Appendix III., Supplementary Figure 4**).

To further describe the effect of candidate compounds on PCa cells' proliferation and mechanism of action, the cell cycle analysis was performed. Upon 48 h of treatment, a reduced number of cells in the S-phase of the cell cycle was detected upon treatment with pyrazole derivative **3d** in AR-positive LAPC-4 and 22Rv1 cells, but with no effect in AR-negative DU145 cells (**Appendix II., Supplementary Figure S10**). The S-phase

cells' decrease corresponded with published AR-regulation of the cell cycle (Gregory *et al.*, 2001). Interestingly, the effect of **3d** was comparable with PROTAC bavdegalutamide and while in the LAPC-4 cells the 48-h treatment led to an increase in G2/M phase cells, in 22Rv1, the G1 cells' percentage was increased, leading to a similar increase in cell death in higher concentration. This suggested that the consequences of treatment might be slightly different among the PCa cell lines, but the complete inactivity in DU145 cells proved the AR-targeting (Puhr *et al.*, 2018). In the case of quinoline derivative **1d**, cell cycle analysis after 24 h of treatment showed an increased number of cells in the G1 phase with reduced S-phase cells' percentage in LAPC-4 and LNCaP. The effect was consistent with proliferation blockage and was more profound compared to galeterone or enzalutamide (**Appendix II., Supplementary Figure S5**).

5.3 Androgen receptor's downregulation and degradation

Long-term treatment of LAPC-4 with the most potent pyrazole derivative **3d** showed a significant decrease in AR protein level after 48 and 72 h (**Appendix II., Figure 5B**), as observed for bavdegalutamide as well. Similar effect was published for galeterone (Yu *et al.*, 2014; Kwegyir-Afful *et al.*, 2015) and several other monomer AR-degraders (Wu *et al.*, 2023). Moreover, the expression of PSA and Nkx3.1 was completely switched off upon 72-h treatment with **3d**. Importantly, the longer treatment with **3d** caused only proliferation inhibition without massive induction of apoptosis as documented by monitoring of PARP and procaspases proteins expression and fragmentation (**Appendix II., Supplementary Figure S7**). It was therefore confirmed that the AR downregulation is not evoked by cell death, which was induced only in prolonged treatment (72 h) by the AR-signalling inhibition.

Using the rescue experiment (Tang *et al.*, 2009), the ability of **3d** to bind to AR-LBP was verified. Upon saturation of AR-LBP with **3d** for 1 h, bavdegalutamide (a rapid and effective AR degrader) degradation activity in the following 4 h treatment was impaired, (**Appendix II., Figure 5C**), which confirmed the competition for binding to the AR-LBP (Burslem *et al.*, 2018). To further evaluate the functional consequences of diminished AR transactivation, qPCR analysis of mRNA expression of *AR* and *KLK3* (PSA) was performed. In the 24 h treatment, lead compound **3d** decreased *KLK3* mRNA expression in both 22Rv1 and LAPC-4 cells (activated by 1 nM R1881) more potently than enzalutamide or galeterone (**Appendix II., Figure 7B**). Moreover, the expression level of *AR* transcript decreased moderately, as well (**Appendix II., Supplementary**

Figure S11). Upon the discovery of *AR* mRNA downregulation, an experiment with proteasome inhibition was needed, to distinguish whether the novel derivatives target the *AR* transcription or the AR-protein stability. The proteasome inhibitor MG-132 was recruited to block its activity and as a result, ubiquitinated proteins (including AR) accumulated within the cells because they could not be efficiently degraded (Jin *et al.*, 2020) (**Figure 14A**). As was already demonstrated, **3d** was able to markedly decrease the AR protein level upon 24 h treatment in 10 μ M concentration, similar to bavdegalutamide in the range of hundreds of nM to 1 μ M. Oppositely, treatment with 10 μ M proteasome inhibitor MG-132 induced an increase in AR protein level and co-treatment with the analysed AR degraders blocked the AR degradation (**Figure 14A**), suggesting that the **3d** indeed induced proteasomal degradation and changed the AR turnover, similarly to galeterone (Kwegyir-Afful *et al.*, 2015). In contrast with that, the treatment with **3d** revealed a dose-response decrease in *AR* mRNA expression to approx. 50 % in 10 μ M (also comparable to galeterone (Kwegyir-Afful *et al.*, 2015), while the 1 μ M bavdegalutamide did not lead to a significant decrease (**Figure 14B**). Altogether, it was shown that compared to pure AR degrader bavdegalutamide (Neklesa *et al.*, 2018), candidate compound **3d** both down-regulates the transcription of *AR* and induces the AR protein degradation. Most importantly, it was shown that compound **3d** downregulated the AR (similar to enzalutamide and bavdegalutamide) in short-term *ex vivo* culture of patient-derived samples (**Appendix II., Figure 8, Supplementary Figure S12**).

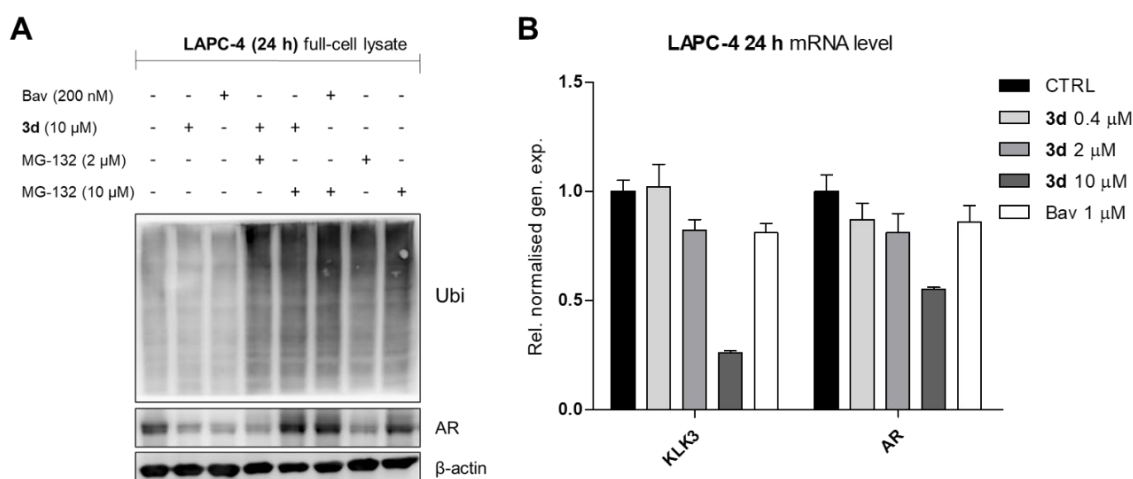


Figure 14 (A) Western blot analysis of AR and overall ubiquitinated proteins. The LAPC-4 cells were treated with **3d**, bavdegalutamide, MG-132 or combinations for 20 h. Upon the treatment, Full-cell lysate in 1% SDS was prepared. β -actin served as a loading control. (B) The dose-dependent effect of compound **3d** and standard PROTAC bavdegalutamide on relative normalized mRNA expression of *AR* and its downstream gene *KLK3* (PSA). Cells were cultivated in CSS medium overnight, then treated with compounds in the presence of 1 nM R1881 for 24 h. Bav, bavdegalutamide.

5.4 Analysis of compounds' interaction with androgen receptor

Previous findings showed that steroidal agonists (testosterone, DHT and R1881) can induce thermal stabilisation of AR performed by CETSA (Shaw *et al.*, 2018), therefore the assay was recruited and optimised to be useful in NR's thermal stability analysis, as described in section 5.5. The optimised assay proved the direct in-cell (C4-2) binding of **2f** (Appendix I, Figure 6) to the AR in a dose-dependent manner. The control experiment with 100 nM R1881 confirmed a previously published increase in AR's thermal stability as well as (Shaw *et al.*, 2018).

Even though the optimised CETSA was useful to prove the direct binding, it is a tedious and time-consuming method. That is why the bacterial expression of recombinant human His6-tagged AR-LBD was performed, based on the previously published protocol (Askew *et al.*, 2007). Innovatively, AR-LBD was expressed without any ligand present during the expression (it is mainly expressed in the presence of DHT), to have empty LBP. Next, the binding of **3d** in purified recombinant AR-LBD was examined by the MST using the Protein Labelling Kit RED-NHS (Nanotemper). The binding of the **3d** induced significant changes in the protein mobility marked by the labelling dye-fluorescence (Wienken *et al.*, 2010) (Appendix II, Fig. S8) and thus confirmed the direct binding of **3d** into the AR-LBD. Further, using the same procedure, the interaction of **1d** was also confirmed by MST and the change was consistent with the effect of 25 μ M galeterone (Appendix II, Figure 8B).

To particularly describe the binding and the binding pose of novel antagonists in the LBP, molecular docking was recruited. The binding of all candidate compounds was assessed by flexible docking into AR-LBD co-crystal structure with natural agonist DHT (PDB: 2PIV). The key residues in the extremities of the cavity (Asn705, Gln711, Arg752, and Thr877) were set flexible, which allowed the rearrangement of the cavity to fit ligands. Candidate compound **2f** showed a similar pose and interactions with the AR binding site (Appendix I, Figure 8) as DHT, with conserved bonds to Arg752 and Asn705 and better binding energy (-12.7 kcal/mol) in comparison with the natural ligand DHT (-10.9 kcal/mol). The binding of the candidate compound **3d** revealed more extensive binding in AR-LBD with poses similar to steroidal antagonists cyproterone (Bohl *et al.*, 2007) or galeterone (Njar and Brodie, 2015). Moreover, it was confirmed by similar positions of interacting residues as in the published antagonist model (Wahl and Smieško, 2018). The first two poses of **3d** displayed high

binding energy ($\Delta G_{Vina} = -11.8$ kcal/mol and -11.6 kcal/mol, respectively) and similar orientation with identical interactions in the 1'-(4''-fluorophenyl)-5'-methylpyrazolo part of **3d** (Arg752 and Gly583 halogen bond with fluorine with other hydrophobic interactions) (**Appendix II., Figure 6A, B**), but the key difference was observed in the interaction of the 17 β -OH on the D-ring of **3d**. In the first pose, the group formed a conserved hydrogen bond with Thr877 (known from the binding of DHT), while in the second pose, the steroid core was positioned at a different angle towards Asn705 (independent of Thr877), forming a hydrogen bond with the 17 β -OH group (**Appendix II., Figure 8B**). Most importantly, both poses showed similar binding to cyproterone and the second pose independent of Thr877 (mutated in LNCaP cell line to alanine) is also observed in the second generation of non-steroidal antiandrogens (Prekovic *et al.*, 2016; Xu *et al.*, 2022), explaining the potency even in PCa with AR mutations. The flexible molecular docking of the quinoline **1d** in the same setting showed a very similar binding pose, with the best binding energy $\Delta G_{Vina} = -10.2$ kcal/mol. Overall, the A-ring fused 6'-methoxyquinoline part was sandwiched between the helix 2 and 3 and the methoxy moiety formed hydrogen bonds between the oxygen and Arg752 and Gln711. The steroid core was stabilised by conserved interactions (Bohl *et al.*, 2007; Gim *et al.*, 2021) and the 17 β -OH on the D-ring formed a conserved bond with Thr877, with a possible interaction with Asn705 as well (**Appendix III., Figure 8C**).

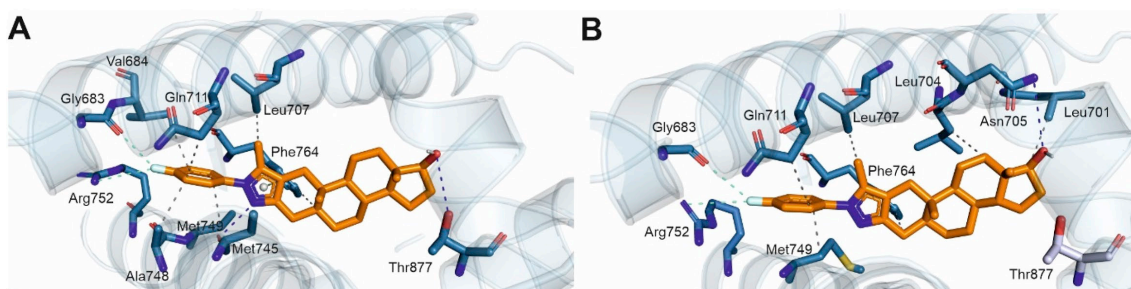


Figure 15 Binding poses of the most potent pyrazole derivative **3d** in the AR-LBD, dependent (A) and independent (B) of Thr877.

5.5 Optimisation of cell fractionation and cellular thermal shift assay

The cell's compartment fractionation is a useful assay, enabling the analysis of the sub-cellular localisation of protein target (AR). The trial experiment was performed using the Qproteome Cell Compartment Kit (Qiagen) (**Appendix I., Figure 7**). Subsequently, a protocol using in-house buffers was optimised to increase the throughput of the assay. Inspired by protocols for crude subcellular fractionation (Abmayr *et al.*, 2006; Holden and Horton, 2009), 22Rv1 cells were washed and directly lysed from the adherent

monolayer on the Petri dish. The monolayer was incubated with the lysis buffer A (cytosolic, 150 mM NaCl, 50 mM HEPES (pH 7.4), 45 µg/ml digitonin with protease inhibitors) for 5 minutes on ice, which should release the cytosol fraction (Abmayr *et al.*, 2006; Holden and Horton, 2009), that was collected (sample 1) (**Figure 16A**). Unfortunately, the digitonin did not disrupt cells properly, which took place during the subsequent scratching in another portion of buffer A, releasing the cellular content (sample 2). Upon centrifugation at 600 g for 6 min, the pellet contained all proteins (sample 3), while the supernatant only the cytosolic ones (sample 4). The pellet was further incubated with the RIPA (nuclear) lysis buffer (150 mM NaCl, 50 mM HEPES (pH 7.4) 0.5% sodium deoxycholate, 0.1% sodium dodecyl sulphate) in which it completely dissolved (sample 5), but contained all the types of proteins (**Figure 16A**).

Another protocol was used to isolate sub-cellular fractions from the Petri dish monolayer of 22Rv1 cells (Baghirova *et al.*, 2015). Cells were washed with PBS and incubated with the lysis buffer A (cytosolic, 150 mM NaCl, 50 mM HEPES (pH 7.4), 0.1% IGEPAL[®] CA-630 with protease inhibitors) for 5 min on ice. Upon the incubation, the cells detached and they were gently washed from the dish bottom (sample 1) (**Figure 16B**) and centrifuged at 600 g for 6 min. The obtained supernatant (sample 2) contained only cytosolic proteins, while the pellet was further incubated with buffer B (nuclear, 20 mM HEPES, pH 7.9, 1.5 mM MgCl₂, 0.5 M NaCl, 0.2 mM EDTA, 20% glycerol, 1% Triton[™] X100), sonicated and centrifuged at 14 000 g for 15 min. The obtained supernatant (sample 3) contained soluble and membrane nuclear proteins and the insoluble pellet contained DNA-bound proteins (sample 4) (**Figure 16B**).

Since the previous attempts showed limitations of direct lysis on the Petri dish, to compare different detergents (Baghirova *et al.*, 2015; Senichkin *et al.*, 2021) in the cytosolic buffer, cells were initially harvested by trypsinisation and washed in PBS and aliquoted. Then, the basic cytosolic buffer A (150 mM NaCl, 50 mM HEPES (pH 7.4) with protease inhibitors) was applied with three different detergents: 45 µg/mL digitonin or 0.1% IGEPAL[®] CA-630 or 0.1 % NP-40. After the 5 min incubation on ice, the suspension was centrifuged at 600 g for 6 min. The obtained supernatant should represent the cytosolic fraction (c), while the pellet was further incubated with buffer B (nuclear, 20 mM HEPES, pH 7.9, 1.5 mM MgCl₂, 0.5 M NaCl, 0.2 mM EDTA, 20% glycerol, 1% Triton[™] X100), sonicated and centrifuged at 14 000 g for 15 min to obtain soluble nuclear fraction (n). While Igepal or NP-40 (Baghirova *et al.*, 2015; Senichkin *et al.*, 2021) were suitable for the selective cytosol extraction, digitonin (Abmayr *et al.*, 2006;

Holden and Horton, 2009) did not succeed in the cell lysis (**Figure 16C**). The combination of the Igepal/Triton buffers fractionated the cells for the cytosolic, nuclear and insoluble cytoskeleton/DNA-bound proteins (**Figure 16D**). The optimised buffers (section 4.2.5) were used to assess the NR's localisation (**Appendix IV., Figure 4**).

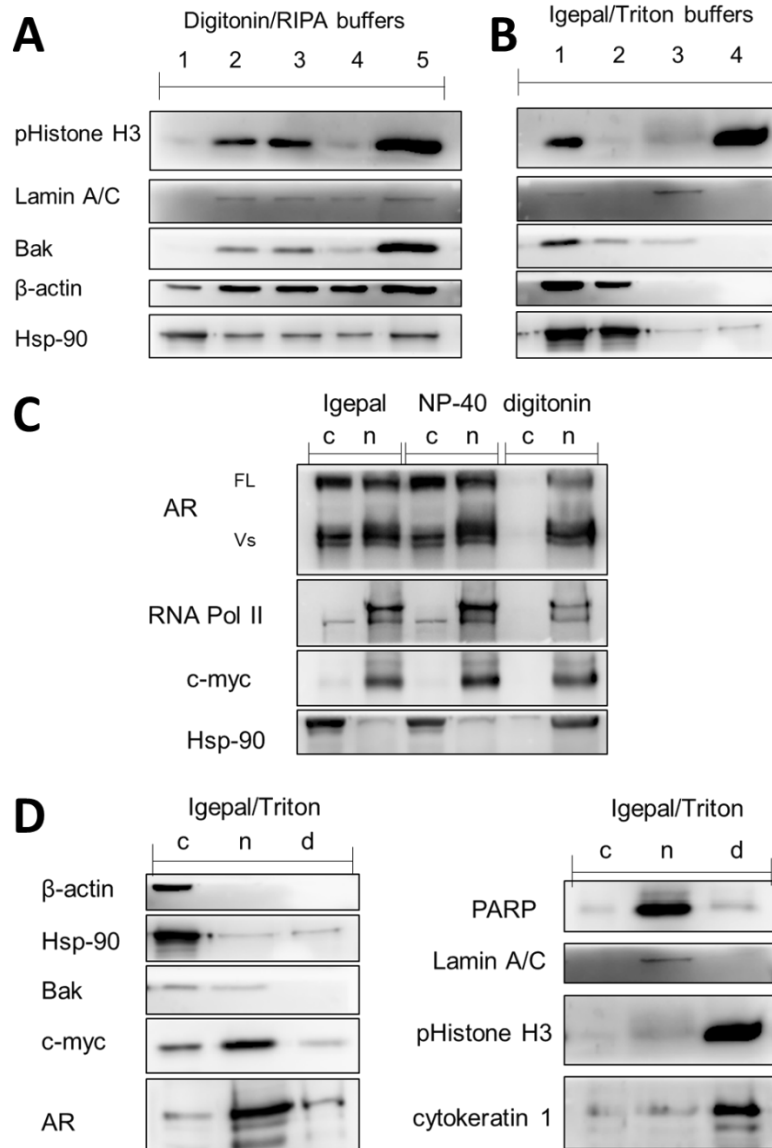


Figure 16 Comparison of digitonin and RIPA buffers (**A**) with Igepal/Triton buffers (**B**) for 22Rv1 cell fractionation from Petri dish with the same procedure (lysis in the first buffer, scratching of the cells, low speed-centrifugation to separate nuclei, their lysis in the second buffer, high-speed centrifugation. Numbers correspond with obtained cellular fractions. (**C**) Fractionation of trypsinized cells incubated with different combinations of lysis buffers with the same general procedure to obtain cytosolic (c) and nuclear (n) fractions. (**D**) Igepal/ Triton combination for the best fractionation of cytosol (c), soluble nuclear proteins (n) and DNA-bound nuclear proteins (d) with the membrane debris.

The binding of candidate AR antagonists was first evaluated by CETSA, whose advantage is the use of untagged AR from cell lysate or within intact cells, showing the

thermal stabilisation upon target engagement. At first, the CETSA experiment was based on the original publication (Jafari *et al.*, 2014) using a purified AR-FL protein (Merck Millipore) in a protein buffer and a crude cell lysate of C4-2 cells (high AR expression) in RIPA lysis buffer. The aggregation temperature was screened in the range of 40 – 60 °C (3 min in CFX96 Touch (BioRad), then the samples were cooled for 3 min at 4 °C and centrifuged at 14 000 g for 30 min. The supernatants were subsequently mixed with SDS-loading buffer, separated by SDS-PAGE and immunoblotted with AR-antibody.

It was shown that the thermal stability of recombinant protein is insufficient, while the lysate from C4-2 cells displayed an appropriate response, with the aggregation temperature around 44 °C (**Figure 17A**). The optimisation continued with the C4-2 cell lysate from the harvested cells cultivated in FBS-supplemented media or in CSS-supplemented media (steroid-depleted). No clear thermal stabilisation was observed upon the incubation of the R1881 or **2f** with both lysates for 1 h (**Figure 17B**).

Even though the CETSA can be performed in lysate, the presence of detergents might change the protein solubility. The next setup was the CETSA in treated intact cells (Shaw *et al.*, 2018; Henderson *et al.*, 2020) cultivated in CSS-supplemented media. The cells were harvested by trypsinisation, diluted in PBS with 5 mM glucose, counted and divided into test tubes, and treated with R1881 or **2f** for 3 h. The subsequent procedure followed the same principle, with a temperature gradient from 45 °C to 57 °C. Obtained samples were lysed by 3 freeze-thaw cycles (Almqvist *et al.*, 2016) and processed. Apparently, R1881 and candidate compound **2f** increased temperature stability, but after the normalisation of the signal to the control, no effect was observed (**Figure 17C**).

The prolonged incubation of cells in PBS with high concentrations of compounds probably influenced the integrity of the cells and caused an imbalance of the basal AR level. To avoid it, finally, C4-2 cells were harvested, re-suspended in PBS with 5 mM glucose, divided into test tubes and treated with R1881 only for 1 h. Next, cells were counted and aliquoted into PCR strips, heated at the temperature gradient from 37 °C to 60 °C and processed as before. The immunoblotting revealed that 100 nM R1881 induced thermal stabilisation from 43 °C to 54 °C (**Figure 17D**), corresponding with previous findings (Shaw *et al.*, 2018). The CETSA was also found to confirm the binding of non-steroidal AR-antagonists CCPI (Lv *et al.*, 2021) and enzalutamide (Shaw *et al.*, 2018), however, by showing a decrease in AR thermal stability. The candidate compound **2f** displayed AR-stabilisation in C4-2 in a concentration manner (from 10 µM – 100 µM)

(Appendix I, Figure 6), despite being characterised as a competitive antagonist, and it might originate from extensive interaction of the steroid scaffold with AR-LBD.

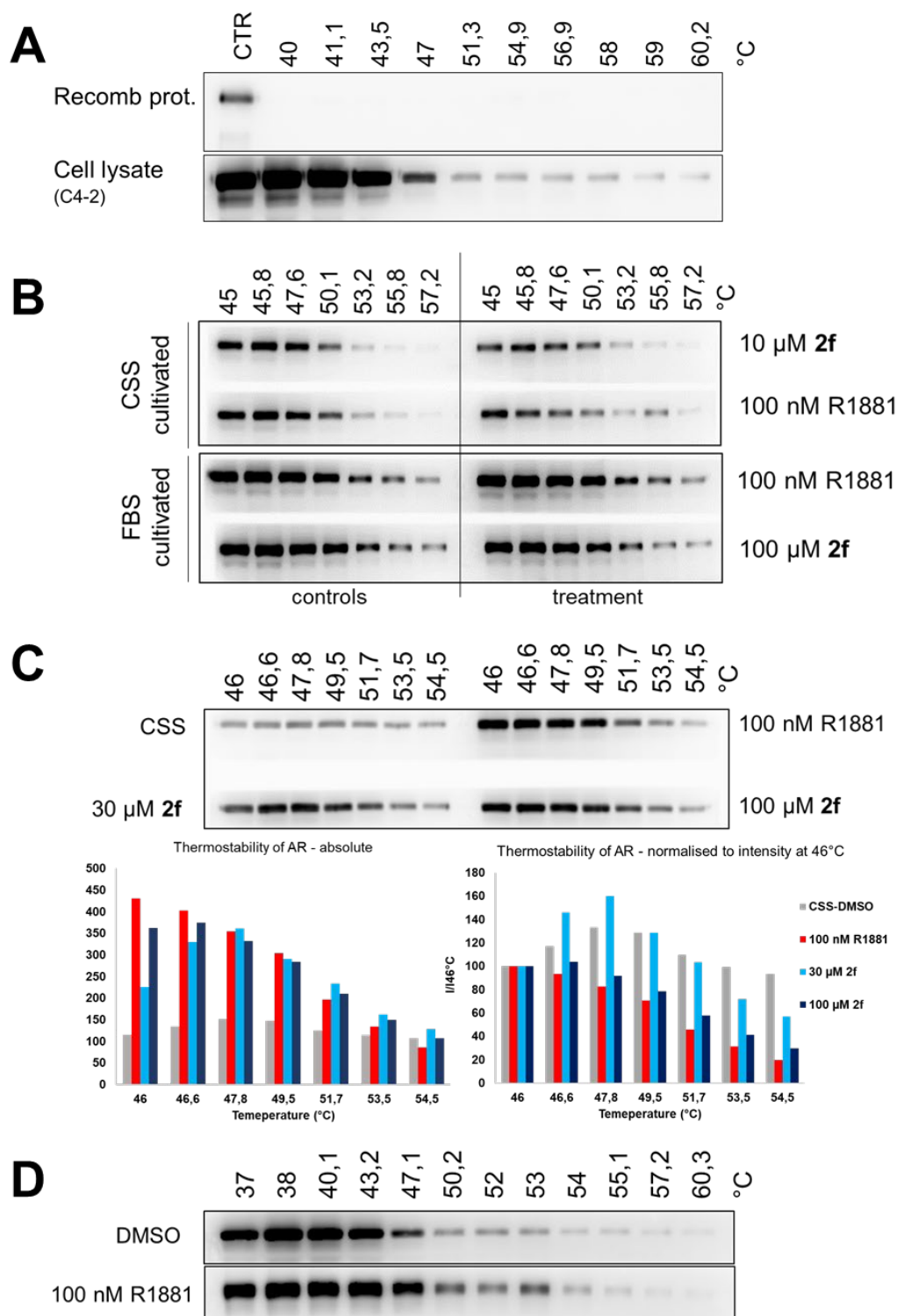


Figure 17 Optimisation of the CETSA protocol. **(A)** First trial of thermal shift using recombinant AR protein and C4-2 cell lysate. **(B)** CETSA with 1 h incubation of compounds with RIPA-buffer lysate from cells cultivated in FBS or CSS-supplemented media **(C)** CETSA performed in cells treated for 3 h with subsequent lysis by freeze-thaw cycles. **(D)** CETSA performed in cells treated for 1 h and normalised after the treatment with subsequent lysis by freeze-thaw cycles.

5.6 Dual targeting of androgen and glucocorticoid receptors

To combat the resistance of CRPC, namely the AR-negative PCa with GR upregulation, GR-targeting treatments were recently described with dual and selective antagonists of AR/GR (Rosette *et al.*, 2020). In the frame of this thesis, novel 17 α - and/or 21-ester or carbamate derivatives of hydrocortisone (GR agonist) were developed and evaluated for their biological activity towards AR and GR in different PCa cells. The group of analysed compounds comprised 17 α -monoesters of hydrocortisone, C-21 esters and carbamates. The effect of compounds on both NRs was evaluated using AR and GR reporter cell lines, 22Rv1-ARE14 (Bartonkova *et al.*, 2015) and AZ-GR (Novotna *et al.*, 2012) respectively. Within prepared compounds, some AR agonists were described, in agreement that hydrocortisone can activate AR (Bartonkova *et al.*, 2015) and that glucocorticoids can act as AR agonists in AR mutants (Zhao *et al.*, 2000). However, the attention was focused on two 17 α -butyryloxy,21-(alkyl)carbamoyloxy derivatives **14** and **15** that displayed strong antagonist properties towards both AR and GR (**Appendix IV., Figure 2**). Antagonist activities of the lead compounds towards AR reached low micromolar values ($IC_{50} = 3.96 \mu\text{M}$ and $11.38 \mu\text{M}$ for **14** and **15**, respectively), comparable to standards, i.e. enzalutamide ($IC_{50} = 3.32 \mu\text{M}$) and galeterone ($IC_{50} = 7.59 \mu\text{M}$) (Norris *et al.*, 2017). Additionally, antagonist activities towards GR reached single-digit micromolar values ($IC_{50} = 4.44 \mu\text{M}$ and $8.11 \mu\text{M}$ for **14** and **15**, respectively), weaker than for standard mifepristone ($IC_{50} = 0.59 \mu\text{M}$) (Du *et al.*, 2019). No clear agonist activity was observed for compounds **14** and **15** neither towards the AR, nor the GR (**Appendix IV., Figure 2**).

Antiproliferative properties of the hydrocortisone derivatives were tested in four PCa cell lines, namely LAPC-4, 22Rv1 (expressing both AR and GR), C4-2 (only AR), and DU145 (AR-negative and GR overexpressing). While the compounds without clear AR/GR activities did not display antiproliferative activities, the most potent derivatives **14** and **15** displayed mid-micromolar values ($GI_{50} = 25 \mu\text{M} - 40 \mu\text{M}$ upon treatment for 72 h) in all AR-positive cells, comparable with standards galeterone and mifepristone. Compound **14** (**Figure 18**) was the only one which reached measurable $GI_{50} = 80 \mu\text{M}$ in R-negative DU145 cells (**Appendix IV., Supplementary Figure S6**). The CFA was performed to assess the prolonged antiproliferative potency in 22Rv1, LAPC-4 and DU145. Generally, compound **14** exhibited strong colony-formation inhibition in AR-positive PCa cell lines, comparable with standard galeterone (Kwegyir-

Afful *et al.*, 2019), but weaker colony-formation inhibition in AR-negative and GR-overexpressing PCa cell line, compared to both galeterone and mifepristone (**Appendix IV., Figure 3**).

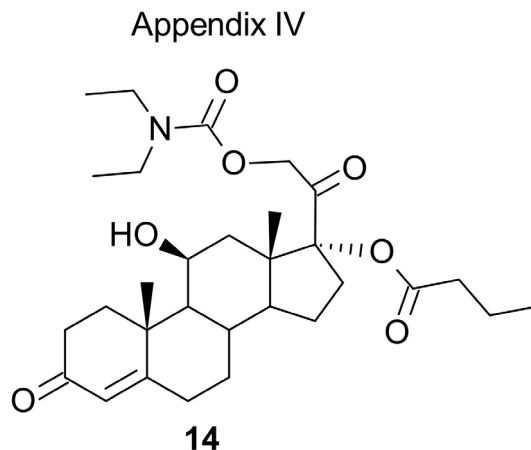


Figure 18 Structure of the most potent AR/GR antagonist **14**.

Interaction with both NRs was confirmed by the optimised CETSA and followed the previous studies. Subsequently, **14** decreased the translocation of AR and GR to the nucleus similarly to galeterone (Yu *et al.*, 2014) and mifepristone (Peeters *et al.*, 2008), respectively (**Appendix IV., Figure 4**). Both compounds **14** and **15** were able to reduce AR a GR downstream signalling by diminishing the levels of their transcriptional targets (PSA and Nkx3.1 of AR and SGK-1 and 11- β -HSD2 of GR). In LAPC-4 (**Appendix IV., Figure 5A**) and 22Rv1 (**Appendix IV., Supplementary Figure S9**) S81phosphorylation and PSA and Nkx3.1 decreased, comparable with galeterone's effect (Yu *et al.*, 2014). Analysis of DU145 (**Appendix IV., Figure 5B**) revealed the blockage of activating phosphorylation of GR on S211 and decreases in the protein levels of 11- β -HSD2 and SGK-1 upon treatment with 20 μ M **14**, similar to mifepristone (Peeters *et al.*, 2008).

Molecular docking into the GR (PDB 1NHZ) (Kauppi *et al.*, 2003) showed extensive binding of **14** in a similar way as mifepristone, but with stronger binding energy ($\Delta G_{\text{vina}} = -11.5$ kcal/mol and -10.8 kcal/mol, respectively). Direct hydrogen bonds from the 3-carbonyl in the A-ring to Gln570 and Arg611 were found. Interestingly, the 21-(*N,N*-diethylcarbamoyloxy) was orientated in the same direction as the dimethylaniline side chain of mifepristone (**Appendix IV., Figure 6A, B**), disrupting the helix-12 position (Kauppi *et al.*, 2003). Molecular docking into the AR-antagonist model (Wahl and Smieško, 2018) revealed the same binding of compound **14** as cyproterone

(Bohl *et al.*, 2007) (**Appendix IV., Figure 6C, D**) with similar binding energy ($\Delta G_{vina} = -12.5$ kcal/mol and -12.1 kcal/mol, respectively) and key interaction residues.

The enzalutamide resistance is connected with increased GR expression *in vitro* (Culig, 2017) and it was shown that the first changes in GR level could be observed just 7 days after the treatment with a sub-lethal concentration of enzalutamide (Isikbay *et al.*, 2014; Puhr *et al.*, 2018). Candidate compounds **14** and **15** did not cause a significant increase in GR or AR levels during the same periods. Importantly, compound **14** reduced the enzalutamide-induced GR upregulation upon 3- and 7-day treatment (**Appendix IV., Supplementary Figure S7**). Overall, the findings and the clinical trial of enzalutamide and mifepristone in CRPC (Serritella *et al.*, 2022) support the development and deep characterisation of novel dual AR and GR antagonists (Li *et al.*, 2024) as anticancer agents in PCa cases with upregulation of GR activity.

6 CONCLUSION AND PERSPECTIVES

The approved next-generation hormone therapies targeting AR markedly increased the effectiveness of the PCa therapy (He *et al.*, 2022). Despite the initial effectiveness of treatment of PCa, nearly all patients eventually progress to develop resistance. Therefore, the discovery of novel strategies is needed to improve the effectiveness in resistant PCa cases (Deluce *et al.*, 2022). Since the steroidal compounds containing a heterocycle moiety in the A-ring have been recently much less investigated towards the AR and PCa (Jorda *et al.*, 2019b; Njar and Brodie, 2015; Baji *et al.*, 2016; Mótyán *et al.*, 2019), the main part of the dissertation thesis investigated biological activity of library of DHT derivatives with modifications on the A-ring prepared by Éva Frank's (University of Szeged, Hungary) synthetic group. Altogether, DHT derivatives bearing different nitrogen-containing five or six-membered heterocycles as a fusion to the A-ring with a series of terminal substituents (119 compounds in total) were thoroughly characterised, searching for a potent AR antagonist to effectively suppress the growth and proliferation of PCa cells with minimal toxicity to healthy tissue. For a detailed assessment of the compounds' behaviour, methods established at the department were used, while the isolation of the cellular fractions (cytosol and nuclei) and the cellular-thermal shift assay were optimised based on the published protocols.

Divided by the particular groups, it was clear that α,β -enones demonstrated potent antiandrogenic effects, with compound **2f** being particularly effective outperforming standard treatments like enzalutamide and galeterone (Yu *et al.*, 2014; Tran *et al.*, 2009), while triazolo[1,5-*a*]pyrimidines and pyrazolo[1,5-*a*]pyrimidines showed partial activity, with some representatives exhibiting agonist properties (**Appendix I**). The A-ring fused pyrazoles were generally the most potent group of analysed compounds with representatives bearing the C-17 hydroxy group and 1'-aryl-5'-methyl substitution showing the strongest antagonist properties. Antiproliferative effects were observed, selective for AR-positive cell lines, with the lead compound **3d** displaying significant potency. The potent downregulation and degradation of AR must be underscored, as well as the potent activity of **3d** in patients' samples *ex vivo* (**Appendix II**). The A-ring-fused quinolines showed moderate antagonist activity, with **1d** which showed reasonable antiproliferative potency, particularly in AR-positive cell lines. The pyridine derivatives exhibited varying activity, with both agonist/antagonist properties (**Appendix III**).

From the mechanistic point of view, the most potent derivative **3d** displayed strong antagonist activity, surpassing standard AR antagonists like enzalutamide and galeterone, selectively targeted AR-positive cells, sparing AR-negative cell lines. Molecular docking studies provided insights into the structural basis of compounds' activity, revealing interactions within the AR-LBD and potential for further optimization.

Additionally, the biological activity of hydrocortisone's derivatives was also analysed and compounds were described as dual antagonists of AR/GR. The lead compound suppressed the signalling of both receptors, the interactions were proved in cells and modelled by molecular docking (**Appendix IV.**). Since GR signalling is a resistance mechanism (Puhr *et al.*, 2018; Wu *et al.*, 2019), the findings support the development and deep characterisation of dual AR and GR antagonists as anticancer agents in PCa cases with upregulation of GR activity (Li *et al.*, 2024).

Finally, as a part of this thesis, several D-ring-attached steroidal isoxazoles and triazoles (similar to abiraterone) were characterised and their CYP17A1 inhibitory effect and AR-antagonist activity was proved (**Appendix V.**).

Overall, the dissertation study provided valuable insights into the design and development of novel AR-targeted compounds for the treatment of PCa, highlighting their potential as alternative or complementary therapies to existing standards of care. Various novel approaches like PROTACs (Alabi and Crews, 2021). and targeting different regions (Li *et al.*, 2019) are explored to overcome resistance mechanisms observed in clinical trials. Based on the frequent LBD mutations and splicing variants (Angulo *et al.*, 2022), the most promising therapies seem to be N-terminal or DNA-binding domains-targeting drugs. However, the development of novel LBD antagonists is also plausible, with emphasis on desired properties such as limited resistance, favourable pharmacokinetics and minimal side effects (He *et al.*, 2022) The structure-based development is however hampered by the absence of a crystal structure of the wt-LBD with an antagonist (Wahl and Smieško, 2018). Apart from the AR axis, there are several other approaches for the PCa treatment, including phototherapy (Shi and Sadler, 2020), targeting prostate-specific membrane antigen (PSMA) by immunotherapy in clinical trials or approved radionuclide therapy (¹⁷⁷Lu-PSMA-617) (He *et al.*, 2022). and many other clinical trials of compounds holding promise for the future.

7 REFERENCE

- Abida W, Hahn AW, Shore N, Agarwal N, Sieber P, Smith MR, Dorff T, Monk JP, Rettig MB, Patel R, Page A, Duff M, Xu R, Wang J, Barkund S, Pankov A, Wang A, Junttila M, Multani PS, Daemen A, Chow Maneval E, Logothetis CJ, Morris MJ. Phase 1 Study of ORIC-101, a Glucocorticoid Receptor Antagonist, in Combination with Enzalutamide in Patients with Metastatic Castration-Resistant Prostate Cancer Progressing on Enzalutamide. *Clin Cancer Res.* 2024 Jan 16.
- Abmayr SM, Yao T, Parmely T, Workman JL. Preparation of nuclear and cytoplasmic extracts from mammalian cells. *Curr Protoc Mol Biol.* 2006 Aug;Chapter 12:Unit 12.1.
- Afshar-Oromieh A, Zechmann CM, Malcher A, Eder M, Eisenhut M, Linhart HG, Holland-Letz T, Hadaschik BA, Giesel FL, Debus J, Haberkorn U. Comparison of PET imaging with a (68)Ga-labelled PSMA ligand and (18)F-choline-based PET/CT for the diagnosis of recurrent prostate cancer. *Eur J Nucl Med Mol Imaging.* 2014 Jan;41(1):11-20.
- Aggarwal RR, Schweizer MT, Nanus DM, Pantuck AJ, Heath EI, Campeau E, Attwell S, Norek K, Snyder M, Bauman L, Lakhotia S, Feng FY, Small EJ, Abida W, Alumkal JJ. A Phase Ib/IIa Study of the Pan-BET Inhibitor ZEN-3694 in Combination with Enzalutamide in Patients with Metastatic Castration-resistant Prostate Cancer. *Clin Cancer Res.* 2020 Oct 15;26(20):5338-5347.
- Ahmed M, Eeles R. Germline genetic profiling in prostate cancer: latest developments and potential clinical applications. *Future Sci OA.* 2015 Dec 18;2(1):FSO87.
- Airhart RA, Barnett TF, Sullivan JW, Levine RL, Schlegel JU. Flutamide therapy for carcinoma of the prostate. *South Med J.* 1978 Jul;71(7):798-801.
- Alabi SB, Crews CM. Major advances in targeted protein degradation: PROTACs, LYTACs, and MADTACs. *J Biol Chem.* 2021 Jan-Jun;296:100647.
- Almqvist H, Axelsson H, Jafari R, Dan C, Mateus A, Haraldsson M, Larsson A, Martinez Molina D, Artursson P, Lundbäck T, Nordlund P. CETSA screening identifies known and novel thymidylate synthase inhibitors and slow intracellular activation of 5-fluorouracil. *Nat Commun.* 2016 Mar 24;7:11040.
- Angulo JC, Ciria Santos JP, Gómez-Caamaño A, Poza de Celis R, González Sala JL, García Garzón JM, Galán-Llopis JA, Pérez Sampietro M, Perrot V, Planas Morin J; ANARESISTANCE study group. Development of castration resistance in prostate cancer patients treated with luteinizing hormone-releasing hormone analogues (LHRHa): results of the ANARESISTANCE study. *World J Urol.* 2022 Oct;40(10):2459-2466.
- Annala M, Vandekerckhove G, Khalaf D, Taavitsainen S, Beja K, Warner EW, Sunderland K, Kollmannsberger C, Eigl BJ, Finch D, Oja CD, Vergidis J, Zulfikar M, Azad AA, Nykter M, Gleave ME, Wyatt AW, Chi KN. Circulating Tumor DNA Genomics Correlate with Resistance to Abiraterone and Enzalutamide in Prostate Cancer. *Cancer Discov.* 2018 Apr;8(4):444-457.
- Antonarakis ES, Armstrong AJ, Dehm SM, Luo J. Androgen receptor variant-driven prostate cancer: clinical implications and therapeutic targeting. *Prostate Cancer Prostatic Dis.* 2016 Sep;19(3):231-41.
- Antonarakis ES, Keizman D, Zhang Z, Gurel B, Lotan TL, Hicks JL, Fedor HL, Carducci MA, De Marzo AM, Eisenberger MA. An immunohistochemical signature comprising PTEN, MYC, and Ki67 predicts progression in prostate cancer patients receiving adjuvant docetaxel after prostatectomy. *Cancer.* 2012 Dec 15;118(24):6063-71.
- Aparicio AM, Harzstark AL, Corn PG, Wen S, Araujo JC, Tu SM, Pagliaro LC, Kim J, Millikan RE, Ryan C, Tannir NM, Zurita AJ, Mathew P, Arap W, Troncoso P, Thall PF, Logothetis CJ. Platinum-based chemotherapy for variant castrate-resistant prostate cancer. *Clin Cancer Res.* 2013 Jul 1;19(13):3621-30.
- Armandari I, Hamid AR, Verhaegh G, Schalken J. Intratumoral steroidogenesis in castration-resistant prostate cancer: a target for therapy. *Prostate Int.* 2014 Sep;2(3):105-13.
- Asangani IA, Wilder-Romans K, Dommeti VL, Krishnamurthy PM, Apel IJ, Escara-Wilke J, Plymate SR, Navone NM, Wang S, Feng FY, Chinnaiyan AM. BET Bromodomain Inhibitors

- Enhance Efficacy and Disrupt Resistance to AR Antagonists in the Treatment of Prostate Cancer. *Mol Cancer Res.* 2016 Apr;14(4):324-31.
- Ashizawa T, Nagata M, Nakamura S, Hirano H, Nagaya N, Lu Y, Horie S. Efficacy of cabazitaxel and androgen splicing variant-7 status in circulating tumour cells in Asian patients with metastatic castration-resistant prostate cancer. *Sci Rep.* 2022 Oct 26;12(1):18016.
- Askew EB, Gampe RT Jr, Stanley TB, Faggart JL, Wilson EM. Modulation of androgen receptor activation function 2 by testosterone and dihydrotestosterone. *J Biol Chem.* 2007 Aug 31;282(35):25801-16.
- Attar RM, Jure-Kunkel M, Balog A, Cvijic ME, Dell-John J, Rizzo CA, Schweizer L, Spires TE, Platero JS, Obermeier M, Shan W, Salvati ME, Foster WR, Dinchuk J, Chen SJ, Vite G, Kramer R, Gottardis MM. Discovery of BMS-641988, a novel and potent inhibitor of androgen receptor signaling for the treatment of prostate cancer. *Cancer Res.* 2009 Aug 15;69(16):6522-30.
- Avgeris I, Pliatsika D, Nikolaropoulos SS, Foustieris MA. Targeting androgen receptor for prostate cancer therapy: From small molecules to PROTACs. *Bioorg Chem.* 2022 Nov;128:106089.
- Baca SC, Prandi D, Lawrence MS, Mosquera JM, Romanel A, Drier Y, Park K, Kitabayashi N, MacDonald TY, Ghandi M, Van Allen E, Kryukov GV, Sboner A, Theurillat JP, Soong TD, Nickerson E, Auclair D, Tewari A, Beltran H, Onofrio RC, Boysen G, Guiducci C, Barbieri CE, Cibulskis K, Sivachenko A, Carter SL, Saksena G, Voet D, Ramos AH, Winckler W, Cipicchio M, Ardlie K, Kantoff PW, Berger MF, Gabriel SB, Golub TR, Meyerson M, Lander ES, Elemento O, Getz G, Demichelis F, Rubin MA, Garraway LA. Punctuated evolution of prostate cancer genomes. *Cell.* 2013 Apr 25;153(3):666-77.
- Baghirova S, Hughes BG, Hendzel MJ, Schulz R. Sequential fractionation and isolation of subcellular proteins from tissue or cultured cells. *MethodsX.* 2015 Nov 7;2:440-5.
- Baji A, Gyovai A, Wölfling J, Minorics R, Ocsosvzki I, Zupkó I, Frank É. Microwave-assisted one-pot synthesis of steroid-quinoline hybrids and an evaluation of their antiproliferative activities on gynecological cancer cell lines. *RSC Adv.* 2016 Mar; 6: 27501-27516.
- Baji Á, Kiss T, Wölfling J, Kovács D, Igaz N, Gopisetty MK, Kiricsi M, Frank É. Multicomponent access to androstano-arylpyrimidines under microwave conditions and evaluation of their anti-cancer activity in vitro. *J Steroid Biochem Mol Biol.* 2017a Sep;172:79-88.
- Baji Á, Kovács F, Mótyán G, Schneider G, Wölfling J, Sinka I, Zupkó I, Ocsosvzki I, Frank É. Investigation of pH and substituent effects on the distribution ratio of novel steroidal ring D- and A-fused arylpyrazole regioisomers and evaluation of their cell-growth inhibitory effects in vitro. *Steroids.* 2017b Oct;126:35-49.
- Baker ME. Albumin, steroid hormones and the origin of vertebrates. *J Endocrinol.* 2002 Oct;175(1):121-7.
- Ban F, Leblanc E, Cavga AD, Huang CF, Flory MR, Zhang F, Chang MEK, Morin H, Lallous N, Singh K, Gleave ME, Mohammed H, Rennie PS, Lack NA, Cherkasov A. Development of an Androgen Receptor Inhibitor Targeting the N-Terminal Domain of Androgen Receptor for Treatment of Castration Resistant Prostate Cancer. *Cancers (Basel).* 2021 Jul 12;13(14):3488.
- Bardou VJ, Arpino G, Elledge RM, Osborne CK, Clark GM. Progesterone receptor status significantly improves outcome prediction over estrogen receptor status alone for adjuvant endocrine therapy in two large breast cancer databases. *J Clin Oncol.* 2003 May 15;21(10):1973-9.
- Bartonkova I, Novotna A, Dvorak Z. Novel stably transfected human reporter cell line AIZ-AR as a tool for an assessment of human androgen receptor transcriptional activity. *PLoS One.* 2015 Mar 26;10(3):e0121316.
- Bastos DA, Antonarakis ES. Galeterone for the treatment of advanced prostate cancer: the evidence to date. *Drug Des Devel Ther.* 2016 Jul 15;10:2289-97.
- Becnel LB, Darlington YF, Ochsner SA, Easton-Marks JR, Watkins CM, McOwiti A, Kankanamge WH, Wise MW, DeHart M, Margolis RN, McKenna NJ. Nuclear Receptor Signaling Atlas: Opening Access to the Biology of Nuclear Receptor Signaling Pathways. *PLoS One.* 2015 Sep 1;10(9):e0135615.

- Beltran H, Tomlins S, Aparicio A, Arora V, Rickman D, Ayala G, Huang J, True L, Gleave ME, Soule H, Logothetis C, Rubin MA. Aggressive variants of castration-resistant prostate cancer. *Clin Cancer Res*. 2014 Jun 1;20(11):2846-50.
- Berges RR, Vukanovic J, Epstein JI, CarMichel M, Cisek L, Johnson DE, Veltri RW, Walsh PC, Isaacs JT. Implication of cell kinetic changes during the progression of human prostatic cancer. *Clin Cancer Res*. 1995 May;1(5):473-80.
- Bhat M, Robichaud N, Hulea L, Sonenberg N, Pelletier J, Topisirovic I. Targeting the translation machinery in cancer. *Nat Rev Drug Discov*. 2015 Apr;14(4):261-78.
- Bluemn EG, Coleman IM, Lucas JM, Coleman RT, Hernandez-Lopez S, Tharakan R, Bianchi-Frias D, Dumpit RF, Kaipainen A, Corella AN, Yang YC, Nyquist MD, Mostaghel E, Hsieh AC, Zhang X, Corey E, Brown LG, Nguyen HM, Pienta K, Ittmann M, Schweizer M, True LD, Wise D, Rennie PS, Vessella RL, Morrissey C, Nelson PS. Androgen Receptor Pathway-Independent Prostate Cancer Is Sustained through FGF Signaling. *Cancer Cell*. 2017 Oct 9;32(4):474-489.e6.
- Bluemn EG, Nelson PS. The androgen/androgen receptor axis in prostate cancer. *Curr Opin Oncol*. 2012 May 24;3(3):251-257.
- Bohl CE, Wu Z, Miller DD, Bell CE, Dalton JT. Crystal structure of the T877A human androgen receptor ligand-binding domain complexed to cyproterone acetate provides insight for ligand-induced conformational changes and structure-based drug design. *J Biol Chem*. 2007 May 4;282(18):13648-55.
- Boorjian S, Ugras S, Mongan NP, Gudas LJ, You X, Tickoo SK, Scherr DS. Androgen receptor expression is inversely correlated with pathologic tumor stage in bladder cancer. *Urology*. 2004 Aug;64(2):383-8.
- Bostwick DG, Cheng L. Precursors of prostate cancer. *Histopathology*. 2012 Jan;60(1):4-27.
- Brinkmann AO. Molecular basis of androgen insensitivity. *Mol Cell Endocrinol*. 2001 Jun 20;179(1-2):105-9.
- Burslem GM, Smith BE, Lai AC, Jaime-Figueroa S, McQuaid DC, Bondeson DP, Toure M, Dong H, Qian Y, Wang J, Crew AP, Hines J, Crews CM. The Advantages of Targeted Protein Degradation Over Inhibition: An RTK Case Study. *Cell Chem Biol*. 2018 Jan 18;25(1):67-77.e3.
- Cano LQ, Lavery DN, Bevan CL. Mini-review: Foldosome regulation of androgen receptor action in prostate cancer. *Mol Cell Endocrinol*. 2013 Apr 30;369(1-2):52-62.
- Chandrasekar T, Yang JC, Gao AC, Evans CP. Mechanisms of resistance in castration-resistant prostate cancer (CRPC). *Transl Androl Urol*. 2015 Jun;4(3):365-80.
- Chen QH, Munoz E, Ashong D. Insight into Recent Advances in Degrading Androgen Receptor for Castration-Resistant Prostate Cancer. *Cancers (Basel)*. 2024 Feb 4;16(3):663.
- Chen S, Gulla S, Cai C, Balk SP. Androgen receptor serine 81 phosphorylation mediates chromatin binding and transcriptional activation. *J Biol Chem*. 2012 Mar 9;287(11):8571-83.
- Chen S, Xu Y, Yuan X, Bubley GJ, Balk SP. Androgen receptor phosphorylation and stabilization in prostate cancer by cyclin-dependent kinase 1. *Proc Natl Acad Sci U S A*. 2006 Oct 24;103(43):15969-74.
- Chen Y, Clegg NJ, Scher HI. Anti-androgens and androgen-depleting therapies in prostate cancer: new agents for an established target. *Lancet Oncol*. 2009 Oct;10(10):981-91. doi: 10.1016/S1470-2045(09)70229-3.
- Chen Y, Zhou Q, Hankey W, Fang X, Yuan F. Second generation androgen receptor antagonists and challenges in prostate cancer treatment. *Cell Death Dis*. 2022 Jul 21;13(7):632.
- Cheng MA, Chou FJ, Wang K, Yang R, Ding J, Zhang Q, Li G, Yeh S, Xu D, Chang C. Androgen receptor (AR) degradation enhancer ASC-J9[®] in an FDA-approved formulated solution suppresses castration resistant prostate cancer cell growth. *Cancer Lett*. 2018 Mar 28;417:182-191.
- Chi KN, Agarwal N, Bjartell A, Chung BH, Pereira de Santana Gomes AJ, Given R, Juárez Soto Á, Merseburger AS, Özgüroğlu M, Uemura H, Ye D, Deprince K, Naini V, Li J, Cheng S, Yu MK, Zhang K, Larsen JS, McCarthy S, Chowdhury S; TITAN Investigators. Apalutamide for Metastatic, Castration-Sensitive Prostate Cancer. *N Engl J Med*. 2019 Jul 4;381(1):13-24.

- Clegg NJ, Wongvipat J, Joseph JD, Tran C, Ouk S, Dilhas A, Chen Y, Grillot K, Bischoff ED, Cai L, Aparicio A, Dorow S, Arora V, Shao G, Qian J, Zhao H, Yang G, Cao C, Sensintaffar J, Wasielewska T, Herbert MR, Bonnefous C, Darimont B, Scher HI, Smith-Jones P, Klang M, Smith ND, De Stanchina E, Wu N, Ouerfelli O, Rix PJ, Heyman RA, Jung ME, Sawyers CL, Hager JH. ARN-509: a novel antiandrogen for prostate cancer treatment. *Cancer Res.* 2012 Mar 15;72(6):1494-503.
- Cleutjens KB, van der Korput HA, van Eekelen CC, van Rooij HC, Faber PW, Trapman J. An androgen response element in a far upstream enhancer region is essential for high, androgen-regulated activity of the prostate-specific antigen promoter. *Mol Endocrinol.* 1997 Feb;11(2):148-61.
- Cockshott ID, Cooper KJ, Sweetmore DS, Blacklock NJ, Denis L. The pharmacokinetics of Casodex in prostate cancer patients after single and during multiple dosing. *Eur Urol.* 1990 Aug;18 Suppl 3:10-7.
- Collins I, Wang H, Caldwell JJ, Chopra R. Chemical approaches to targeted protein degradation through modulation of the ubiquitin-proteasome pathway. *Biochem J.* 2017 Mar 15;474(7):1127-1147.
- Cornford P, Bellmunt J, Bolla M, Briers E, De Santis M, Gross T, Henry AM, Joniau S, Lam TB, Mason MD, van der Poel HG, van der Kwast TH, Rouvière O, Wiegel T, Mottet N. EAU-ESTRO-SIOG Guidelines on Prostate Cancer. Part II: Treatment of Relapsing, Metastatic, and Castration-Resistant Prostate Cancer. *Eur Urol.* 2017 Apr;71(4):630-642.
- Cortés-Benítez F, Cabeza M, Ramírez-Apan MT, Alvarez-Manrique B, Bratoeff E. Synthesis of 17 β -N-arylcarbamoyleandroster-4-en-3-one derivatives and their anti-proliferative effect on human androgen-sensitive LNCaP cell line. *Eur J Med Chem.* 2016 Oct 4;121:737-746.
- Cousin S, Blay JY, Garcia IB, de Bono JS, Le Tourneau C, Moreno V, Trigo J, Hann CL, Azad AA, Im SA, Cassier PA, French CA, Italiano A, Keedy VL, Plummer R, Sablin MP, Hemming ML, Ferron-Brady G, Wyce A, Khaled A, Datta A, Foley SW, McCabe MT, Wu Y, Horner T, Kremer BE, Dhar A, O'Dwyer PJ, Shapiro GI, Piha-Paul SA. Safety, pharmacokinetic, pharmacodynamic and clinical activity of molibresib for the treatment of nuclear protein in testis carcinoma and other cancers: Results of a Phase I/II open-label, dose escalation study. *Int J Cancer.* 2022 Mar 15;150(6):993-1006
- Coutinho I, Day TK, Tilley WD, Selth LA. Androgen receptor signaling in castration-resistant prostate cancer: a lesson in persistence. *Endocr Relat Cancer.* 2016 Dec;23(12):T179-T197.
- Crawford ED, Eisenberger MA, McLeod DG, Spaulding JT, Benson R, Dorr FA, Blumenstein BA, Davis MA, Goodman PJ. A controlled trial of leuprolide with and without flutamide in prostatic carcinoma. *N Engl J Med.* 1989 Aug 17;321(7):419-24. Erratum in: *N Engl J Med* 1989 Nov 16;321(20):1420.
- Crawford ED, Hou AH. The role of LHRH antagonists in the treatment of prostate cancer. *Oncology (Williston Park).* 2009 Jun;23(7):626-30.
- Cui Y, Zong H, Yan H, Li N, Zhang Y. Degarelix versus goserelin plus bicalutamide therapy for lower urinary tract symptom relief, prostate volume reduction and quality of life improvement in men with prostate cancer: a systematic review and meta-analysis. *Urol Int.* 2014 Mar;93(2):152-9.
- Culig Z, Hoffmann J, Erdel M, Eder IE, Hobisch A, Hittmair A, Bartsch G, Utermann G, Schneider MR, Parczyk K, Klocker H. Switch from antagonist to agonist of the androgen receptor bicalutamide is associated with prostate tumour progression in a new model system. *Br J Cancer.* 1999 Sep;81(2):242-51.
- Culig Z. Molecular Mechanisms of Enzalutamide Resistance in Prostate Cancer. *Curr Mol Biol Rep.* 2017 Oct;3(4):230-235..
- D'Abronzio LS, Ghosh PM. eIF4E Phosphorylation in Prostate Cancer. *Neoplasia.* 2018 Jun;20(6):563-573.
- Dai C, Heemers H, Sharifi N. Androgen Signaling in Prostate Cancer. *Cold Spring Harb Perspect Med.* 2017 Sep 1;7(9):a030452.
- Danielian PS, White R, Lees JA, Parker MG. Identification of a conserved region required for hormone dependent transcriptional activation by steroid hormone receptors. *EMBO J.* 1992 Mar;11(3):1025-33. Erratum in: *EMBO J* 1992 Jun;11(6):2366.

- Davey RA, Grossmann M. Androgen Receptor Structure, Function and Biology: From Bench to Bedside. *Clin Biochem Rev.* 2016 Feb;37(1):3-15.
- Davis ID, Martin AJ, Stockler MR, Begbie S, Chi KN, Chowdhury S, Coskinas X, Frydenberg M, Hague WE, Horvath LG, Joshua AM, Lawrence NJ, Marx G, McCaffrey J, McDermott R, McJannett M, North SA, Parnis F, Parulekar W, Pook DW, Reaume MN, Sandhu SK, Tan A, Tan TH, Thomson A, Tu E, Vera-Badillo F, Williams SG, Yip S, Zhang AY, Zielinski RR, Sweeney CJ; ENZAMET Trial Investigators and the Australian and New Zealand Urogenital and Prostate Cancer Trials Group. Enzalutamide with Standard First-Line Therapy in Metastatic Prostate Cancer. *N Engl J Med.* 2019 Jul 11;381(2):121-131
- Dawson MA, Kouzarides T, Huntly BJ. Targeting epigenetic readers in cancer. *N Engl J Med.* 2012 Aug 16;367(7):647-57.
- Dawson NA, Conaway M, Halabi S, Winer EP, Small EJ, Lake D, Vogelzang NJ. A randomized study comparing standard versus moderately high dose megestrol acetate for patients with advanced prostate carcinoma: cancer and leukemia group B study 9181. *Cancer.* 2000 Feb 15;88(4):825-34.
- de Bono JS, Cojocaru E, Plummer ER, Knurovski T, Clegg K, Ashby F, Pegg N, West W, Brooks AN. An open-label phase I/IIa study to evaluate the safety and efficacy of CCS1477 as monotherapy and in combination in patients with advanced solid/metastatic tumors. *J Clin Oncol.* 2019;37(15_suppl):TPS5089-TPS5089.
- Dehm SM, Tindall DJ. Molecular regulation of androgen action in prostate cancer. *J Cell Biochem.* 2006 Oct 1;99(2):333-44.
- Deluce JE, Cardenas L, Lalani AK, Maleki Vareki S, Fernandes R. Emerging Biomarker-Guided Therapies in Prostate Cancer. *Curr Oncol.* 2022 Jul 18;29(7):5054-5076.
- Denmeade SR, Isaacs JT. A history of prostate cancer treatment. *Nat Rev Cancer.* 2002 May;2(5):389-96.
- Dhiman VK, Bolt MJ, White KP. Nuclear receptors in cancer - uncovering new and evolving roles through genomic analysis. *Nat Rev Genet.* 2018 Mar;19(3):160-174.
- Dijkman GA, Janknegt RA, De Reijke TM, Debruyne FM. Long-term efficacy and safety of nilutamide plus castration in advanced prostate cancer, and the significance of early prostate specific antigen normalization. International Anandron Study Group. *J Urol.* 1997 Jul;158(1):160-3.
- Dong G, Ding Y, He S, Sheng C. Molecular Glues for Targeted Protein Degradation: From Serendipity to Rational Discovery. *J Med Chem.* 2021 Aug 12;64(15):10606-10620.
- Du X, Eksterowicz J, Zhou H, Rew Y, Zhu L, Yan X, Medina JC, Huang T, Chen X, Sutimantanapi D, Jahchan N, Kong W, Sun J, Zavorotinskaya T, Ye Q, Fantin VR, Sun D. Discovery of a Potent Steroidal Glucocorticoid Receptor Antagonist with Enhanced Selectivity against the Progesterone and Androgen Receptors (OP-3633). *J Med Chem.* 2019 Jul 25;62(14):6751-6764.
- Evans RM. The steroid and thyroid hormone receptor superfamily. *Science.* 1988 May 13;240(4854):889-95.
- Feng K, Liu C, Wang W, Kong P, Tao Z, Liu W. Emerging proteins involved in castration-resistant prostate cancer via the AR-dependent and AR-independent pathways (Review). *Int J Oncol.* 2023 Nov;63(5):127.
- Fizazi K, Shore N, Tammela TL, Ulys A, Vjaters E, Polyakov S, Jievaltas M, Luz M, Alekseev B, Kuss I, Le Berre MA, Petrenciuc O, Snapir A, Sarapohja T, Smith MR; ARAMIS Investigators. Nonmetastatic, Castration-Resistant Prostate Cancer and Survival with Darolutamide. *N Engl J Med.* 2020 Sep 10;383(11):1040-1049.
- Formaggio N, Rubin MA, Theurillat JP. Loss and revival of androgen receptor signaling in advanced prostate cancer. *Oncogene.* 2021 Feb;40(7):1205-1216.
- Fraser M, Sabelnykova VY, Yamaguchi TN, Heisler LE, Livingstone J, Huang V, Shiah YJ, Yousif F, Lin X, Masella AP, Fox NS, Xie M, Prokopec SD, Berlin A, Lalonde E, Ahmed M, Trudel D, Luo X, Beck TA, Meng A, Zhang J, D'Costa A, Denroche RE, Kong H, Espiritu SM, Chua ML, Wong A, Chong T, Sam M, Johns J, Timms L, Buchner NB, Orain M, Picard V, Hovington H, Murison A, Kron K, Harding NJ, P'ng C, Houlahan KE, Chu KC, Lo B, Nguyen F, Li CH, Sun RX, de Borja R, Cooper CI, Hopkins JF, Govind SK, Fung C, Waggott

- D, Green J, Haider S, Chan-Seng-Yue MA, Jung E, Wang Z, Bergeron A, Dal Pra A, Lacombe L, Collins CC, Sahinalp C, Lupien M, Fleshner NE, He HH, Fradet Y, Tetu B, van der Kwast T, McPherson JD, Bristow RG, Boutros PC. Genomic hallmarks of localized, non-indolent prostate cancer. *Nature*. 2017 Jan 19;541(7637):359-364.
- Gao W, Bohl CE, Dalton JT. Chemistry and structural biology of androgen receptor. *Chem Rev*. 2005 Sep;105(9):3352-70.
- Gao X, Burris III HA, Vuky J, Dreicer R, Sartor AO, Sternberg CN, Percent IJ, Hussain MHA, Kalebasty AR, Shen J, Heath EI, Abesada-Terk G, Gandhi SG, McKean M, Lu H, Berghorn E, Gedrich R, Chirnomas SD, Vogelzang NJ, Petrylak DP. Phase 1/2 study of ARV-110, an androgen receptor (AR) PROTAC degrader, in metastatic castration-resistant prostate cancer (mCRPC). *J Clin Oncol*. 2022; 40(6_suppl): 17-17.
- Gillessen S, Attard G, Beer TM, Beltran H, Bjartell A, Bossi A, Briganti A, Bristow RG, Chi KN, Clarke N, Davis ID, de Bono J, Drake CG, Duran I, Eeles R, Efstathiou E, Evans CP, Fanti S, Feng FY, Fizazi K, Frydenberg M, Gleave M, Halabi S, Heidenreich A, Heinrich D, Higano CTS, Hofman MS, Hussain M, James N, Kanavaras R, Kantoff P, Kauli RB, Leibowitz R, Logothetis C, Maluf F, Millman R, Morgans AK, Morris MJ, Mottet N, Mrabti H, Murphy DG, Murthy V, Oh WK, Ost P, O'Sullivan JM, Padhani AR, Parker C, Poon DMC, Pritchard CC, Reiter RE, Roach M, Rubin M, Ryan CJ, Saad F, Sade JP, Sartor O, Scher HI, Shore N, Small E, Smith M, Soule H, Sternberg CN, Steuber T, Suzuki H, Sweeney C, Sydes MR, Taplin ME, Tombal B, Türkeri L, van Oort I, Zapatero A, Omlin A. Management of Patients with Advanced Prostate Cancer: Report of the Advanced Prostate Cancer Consensus Conference 2019. *Eur Urol*. 2020 Apr;77(4):508-547.
- Gim HJ, Park J, Jung ME, Houk KN. Conformational dynamics of androgen receptors bound to agonists and antagonists. *Sci Rep*. 2021 Aug 5;11(1):15887.
- Gordon V, Bhadel S, Wunderlich W, Zhang J, Ficarro SB, Mollah SA, Shabanowitz J, Hunt DF, Xenarios I, Hahn WC, Conaway M, Carey MF, Gioeli D. CDK9 regulates AR promoter selectivity and cell growth through serine 81 phosphorylation. *Mol Endocrinol*. 2010 Dec;24(12):2267-80.
- Gregory CW, Johnson RT Jr, Presnell SC, Mohler JL, French FS. Androgen receptor regulation of G1 cyclin and cyclin-dependent kinase function in the CWR22 human prostate cancer xenograft. *J Androl*. 2001 Jul-Aug;22(4):537-48.
- Grino PB, Griffin JE, Wilson JD. Testosterone at high concentrations interacts with the human androgen receptor similarly to dihydrotestosterone. *Endocrinology*. 1990 Feb;126(2):1165-72.
- Gu W, Han W, Luo H, Zhou F, He D, Ma L, Guo H, Liang C, Chong T, Jiang J, Chen Z, Wang Y, Zou Q, Tian Y, Xiao J, Huang J, Zhu S, Dong Q, Zhang X, Li H, Yang X, Chen C, Li J, Jin C, Zhang X, Ye D; CHART Investigators. Rezvolutamide versus bicalutamide in combination with androgen-deprivation therapy in patients with high-volume, metastatic, hormone-sensitive prostate cancer (CHART): a randomised, open-label, phase 3 trial. *Lancet Oncol*. 2022 Oct;23(10):1249-1260.
- Ha S, Luo G, Xiang H. A Comprehensive Overview of Small-Molecule Androgen Receptor Degradators: Recent Progress and Future Perspectives. *J Med Chem*. 2022 Dec 22;65(24):16128-16154.
- He Y, Xu W, Xiao YT, Huang H, Gu D, Ren S. Targeting signaling pathways in prostate cancer: mechanisms and clinical trials. *Signal Transduct Target Ther*. 2022 Jun 24;7(1):198.
- Heath EI, Hillman DW, Vaishampayan U, Sheng S, Sarkar F, Harper F, Gaskins M, Pitot HC, Tan W, Ivy SP, Pili R, Carducci MA, Erlichman C, Liu G. A phase II trial of 17-allylamino-17-demethoxygeldanamycin in patients with hormone-refractory metastatic prostate cancer. *Clin Cancer Res*. 2008 Dec 1;14(23):7940-6.
- Heemers HV, Tindall DJ. Androgen receptor (AR) coregulators: a diversity of functions converging on and regulating the AR transcriptional complex. *Endocr Rev*. 2007 Dec;28(7):778-808.
- Heinlein CA, Chang C. Androgen receptor in prostate cancer. *Endocr Rev*. 2004 Apr;25(2):276-308.

- Helsen C, Van den Broeck T, Voet A, Prekovic S, Van Poppel H, Joniau S, Claessens F. Androgen receptor antagonists for prostate cancer therapy. *Endocr Relat Cancer*. 2014 Aug;21(4):T105-18.
- Henderson MJ, Holbert MA, Simeonov A, Kallal LA. High-Throughput Cellular Thermal Shift Assays in Research and Drug Discovery. *SLAS Discov*. 2020 Feb;25(2):137-147.
- Hieronymus H, Schultz N, Gopalan A, Carver BS, Chang MT, Xiao Y, Heguy A, Huberman K, Bernstein M, Assel M, Murali R, Vickers A, Scardino PT, Sander C, Reuter V, Taylor BS, Sawyers CL. Copy number alteration burden predicts prostate cancer relapse. *Proc Natl Acad Sci U S A*. 2014 Jul 29;111(30):11139-44.
- Hirayama Y, Tam T, Jian K, Andersen RJ, Sadar MD. Combination therapy with androgen receptor N-terminal domain antagonist EPI-7170 and enzalutamide yields synergistic activity in AR-V7-positive prostate cancer. *Mol Oncol*. 2020 Oct;14(10):2455-2470.
- Holden P, Horton WA. Crude subcellular fractionation of cultured mammalian cell lines. *BMC Res Notes*. 2009 Dec 10;2:243.
- Hsing AW. Hormones and prostate cancer: what's next? *Epidemiol Rev*. 2001 Mar;23(1):42-58.
- Hussain M, Tangen CM, Berry DL, Higano CS, Crawford ED, Liu G, Wilding G, Prescott S, Kanaga Sundaram S, Small EJ, Dawson NA, Donnelly BJ, Venner PM, Vaishampayan UN, Schellhammer PF, Quinn DI, Raghavan D, Ely B, Moynour CM, Vogelzang NJ, Thompson IM Jr. Intermittent versus continuous androgen deprivation in prostate cancer. *N Engl J Med*. 2013 Apr 4;368(14):1314-25.
- Hussain M, Fizazi K, Saad F, Rathenborg P, Shore N, Ferreira U, Ivashchenko P, Demirhan E, Modelska K, Phung D, Krivoshik A, Sternberg CN. Enzalutamide in Men with Nonmetastatic, Castration-Resistant Prostate Cancer. *N Engl J Med*. 2018 Jun 28;378(26):2465-2474.
- Iannantuono GM, Chandran E, Floudas CS, Choo-Wosoba H, Butera G, Roselli M, Gulley JL, Karzai F. Efficacy and safety of PARP inhibitors in metastatic castration-resistant prostate cancer: A systematic review and meta-analysis of clinical trials. *Cancer Treat Rev*. 2023 Nov;120:102623.
- Irani J, Salomon L, Oba R, Bouchard P, Mottet N. Efficacy of venlafaxine, medroxyprogesterone acetate, and cyproterone acetate for the treatment of vasomotor hot flushes in men taking gonadotropin-releasing hormone analogues for prostate cancer: a double-blind, randomised trial. *Lancet Oncol*. 2010 Feb;11(2):147-54.
- Isikbay M, Otto K, Kregel S, Kach J, Cai Y, Vander Griend DJ, Conzen SD, Szmulewitz RZ. Glucocorticoid receptor activity contributes to resistance to androgen-targeted therapy in prostate cancer. *Horm Cancer*. 2014 Apr;5(2):72-89.
- Jafari R, Almqvist H, Axelsson H, Ignatushchenko M, Lundbäck T, Nordlund P, Martinez Molina D. The cellular thermal shift assay for evaluating drug target interactions in cells. *Nat Protoc*. 2014 Sep;9(9):2100-22.
- Jang A, Kendi AT, Sartor O. Status of PSMA-targeted radioligand therapy in prostate cancer: current data and future trials. *Ther Adv Med Oncol*. 2023 Mar 4;15:17588359231157632.
- Jarman M, Barrie SE, Llera JM. The 16,17-double bond is needed for irreversible inhibition of human cytochrome p45017alpha by abiraterone (17-(3-pyridyl)androsta-5, 16-dien-3beta-ol) and related steroidal inhibitors. *J Med Chem*. 1998 Dec 31;41(27):5375-81.
- Jin HJ, Kim J, Yu J. Androgen receptor genomic regulation. *Transl Androl Urol*. 2013 Sep;2(3):157-177.
- Jin J, Wu Y, Chen J, Shen Y, Zhang L, Zhang H, Chen L, Yuan H, Chen H, Zhang W, Luan X. The peptide PROTAC modality: a novel strategy for targeted protein ubiquitination. *Theranostics*. 2020 Aug 8;10(22):10141-10153.
- Jorda R, Bučková Z, Řezníčková E, Bouchal J, Kryštof V. Selective inhibition reveals cyclin-dependent kinase 2 as another kinase that phosphorylates the androgen receptor at serine 81. *Biochim Biophys Acta Mol Cell Res*. 2018 Feb;1865(2):354-363.
- Jorda R, Lopes SMM, Řezníčková E, Ajani H, Pereira AV, Gomes CSB, M V D Pinho E Melo T. Tetrahydropyrazolo[1,5-a]pyridine-fused steroids and their in vitro biological evaluation in prostate cancer. *Eur J Med Chem*. 2019a Sep 15;178:168-176.
- Jorda R, Řezníčková E, Kielczewska U, Maj J, Morzycki JW, Siergiejczyk L, Bazgier V, Berka K, Rárová L, Wojtkielewicz A. Synthesis of novel galeterone derivatives and evaluation of

- their in vitro activity against prostate cancer cell lines. *Eur J Med Chem.* 2019b Oct 1;179:483-492.
- Kane CJ, Eggener SE, Shindel AW, Andriole GL. Variability in Outcomes for Patients with Intermediate-risk Prostate Cancer (Gleason Score 7, International Society of Urological Pathology Gleason Group 2-3) and Implications for Risk Stratification: A Systematic Review. *Eur Urol Focus.* 2017 Oct;3(4-5):487-497.
- Karantanos T, Karanika S, Wang J, Yang G, Dobashi M, Park S, Ren C, Li L, Basourakos SP, Hoang A, Efstathiou E, Wang X, Troncoso P, Titus M, Broom B, Kim J, Corn PG, Logothetis CJ, Thompson TC. Caveolin-1 regulates hormone resistance through lipid synthesis, creating novel therapeutic opportunities for castration-resistant prostate cancer. *Oncotarget.* 2016 Jul 19;7(29):46321-46334.
- Kauppi B, Jakob C, Färnegårdh M, Yang J, Ahola H, Alarcon M, Calles K, Engström O, Harlan J, Muchmore S, Ramqvist AK, Thorell S, Ohman L, Greer J, Gustafsson JA, Carlstedt-Duke J, Carlquist M. The three-dimensional structures of antagonistic and agonistic forms of the glucocorticoid receptor ligand-binding domain: RU-486 induces a transconformation that leads to active antagonism. *J Biol Chem.* 2003 Jun 20;278(25):22748-54.
- Keam SJ. Rezvilutamide: First Approval. *Drugs.* 2023 Feb;83(2):189-193.
- Kittler R, Zhou J, Hua S, Ma L, Liu Y, Pendleton E, Cheng C, Gerstein M, White KP. A comprehensive nuclear receptor network for breast cancer cells. *Cell Rep.* 2013 Feb 21;3(2):538-51.
- Klotz L, Boccon-Gibod L, Shore ND, Andreou C, Persson BE, Cantor P, Jensen JK, Olesen TK, Schröder FH. The efficacy and safety of degarelix: a 12-month, comparative, randomized, open-label, parallel-group phase III study in patients with prostate cancer. *BJU Int.* 2008 Dec;102(11):1531-8.
- Kollara A, Diamandis EP, Brown TJ. Secretion of endogenous kallikreins 2 and 3 by androgen receptor-transfected PC-3 prostate cancer cells. *J Steroid Biochem Mol Biol.* 2003 Apr;84(5):493-502.
- Komendantova AS, Scherbakov AM, Komkov AV, Chertkova VV, Gudovanniy AO, Chernoburova EI, Sorokin DV, Dzichenka YU, Shirinian VZ, Volkova YA, Zavarzin IV. Novel steroidal 1,3,4-thiadiazines: Synthesis and biological evaluation in androgen receptor-positive prostate cancer 22Rv1 cells. *Bioorg Chem.* 2019 Oct;91:103142.
- Koryakina Y, Knudsen KE, Gioli D. Cell-cycle-dependent regulation of androgen receptor function. *Endocr Relat Cancer.* 2015 Apr;22(2):249-64.
- Kovács D, Wölfling J, Szabó N, Szécsi M, Schelz Z, Zupkó I, Frank É. Synthesis of novel 17-(4'-formyl)pyrazolylandrosta-5,16-dienes and their derivatives as potent 17 α -hydroxylase/C17,20-lyase inhibitors or antiproliferative agents depending on the substitution pattern of the heteroring. *Eur J Med Chem.* 2016 Sep 14;120:284-95.
- Ku SY, Rosario S, Wang Y, Mu P, Seshadri M, Goodrich ZW, Goodrich MM, Labbé DP, Gomez EC, Wang J, Long HW, Xu B, Brown M, Loda M, Sawyers CL, Ellis L, Goodrich DW. Rb1 and Trp53 cooperate to suppress prostate cancer lineage plasticity, metastasis, and antiandrogen resistance. *Science.* 2017 Jan 6;355(6320):78-83.
- Kundrat L, Regan L. Balance between folding and degradation for Hsp90-dependent client proteins: a key role for CHIP. *Biochemistry.* 2010 Sep 7;49(35):7428-38.
- Kwegyir-Afful AK, Bruno RD, Purushottamachar P, Murigi FN, Njar VC. Galeterone and VNPT55 disrupt Mnk-eIF4E to inhibit prostate cancer cell migration and invasion. *FEBS J.* 2016 Nov;283(21):3898-3918.
- Kwegyir-Afful AK, Ramalingam S, Purushottamachar P, Ramamurthy VP, Njar VC. Galeterone and VNPT55 induce proteasomal degradation of AR/AR-V7, induce significant apoptosis via cytochrome c release and suppress growth of castration resistant prostate cancer xenografts in vivo. *Oncotarget.* 2015 Sep 29;6(29):27440-60.
- Kwegyir-Afful AK, Ramalingam S, Ramamurthy VP, Purushottamachar P, Murigi FN, Vasaitis TS, Huang W, Kane MA, Zhang Y, Ambulos N, Tiwari S, Srivastava P, Nnane IP, Hussain A, Qiu Y, Weber DJ, Njar VCO. Galeterone and The Next Generation Galeterone Analogs, VNPP414 and VNPP433-3 β Exert Potent Therapeutic Effects in Castration-/Drug-Resistant

- Prostate Cancer Preclinical Models In Vitro and In Vivo. *Cancers (Basel)*. 2019 Oct 24;11(11):1637.
- Lallous N, Snow O, Sanchez C, Parra Nuñez AK, Sun B, Hussain A, Lee J, Morin H, Leblanc E, Gleave ME, Cherkasov A. Evaluation of Darolutamide (ODM201) Efficiency on Androgen Receptor Mutants Reported to Date in Prostate Cancer Patients. *Cancers (Basel)*. 2021 Jun 11;13(12):2939.
- Lamb AD, Massie CE, Neal DE. The transcriptional programme of the androgen receptor (AR) in prostate cancer. *BJU Int*. 2014 Mar;113(3):358-66.
- Latysheva AS, Zolottsev VA, Veselovsky AV, Scherbakov KA, Morozevich GE, Pokrovsky VS, Novikov RA, Timofeev VP, Tkachev YV, Misharin AY. New steroidal oxazolines, benzoxazoles and benzimidazoles related to abiraterone and galeterone. *Steroids*. 2020 Jan;153:108534.
- Lee DK, Chang C. Endocrine mechanisms of disease: Expression and degradation of androgen receptor: mechanism and clinical implication. *J Clin Endocrinol Metab*. 2003 Sep;88(9):4043-54.
- Lee GT, Nagaya N, Desantis J, Madura K, Sabaawy HE, Kim WJ, Vaz RJ, Cruciani G, Kim IY. Effects of MTX-23, a Novel PROTAC of Androgen Receptor Splice Variant-7 and Androgen Receptor, on CRPC Resistant to Second-Line Antiandrogen Therapy. *Mol Cancer Ther*. 2021 Mar;20(3):490-499.
- Lewin J, Soria JC, Stathis A, Delord JP, Peters S, Awada A, Aftimos PG, Bekradda M, Rezai K, Zeng Z, Hussain A, Perez S, Siu LL, Massard C. Phase Ib Trial With Birabresib, a Small-Molecule Inhibitor of Bromodomain and Extraterminal Proteins, in Patients With Selected Advanced Solid Tumors. *J Clin Oncol*. 2018 Oct 20;36(30):3007-3014.
- Li C, Han X, Yan Q, Ji Y, Zhang R, Yuan D, Yang F, Wang J, Wu M, Zhou J. Design and Synthesis of Dual-Target Inhibitors Targeting Androgen Receptors and Glucocorticoid Receptors to Overcome Antiandrogen Resistance in Castration-Resistant Prostate Cancer. *J Med Chem*. 2024 Mar 14;67(5):3419-3436.
- Li C, Han X, Yan Q, Ji Y, Zhang R, Yuan D, Yang F, Wang J, Wu M, Zhou J. Design and Synthesis of Dual-Target Inhibitors Targeting Androgen Receptors and Glucocorticoid Receptors to Overcome Antiandrogen Resistance in Castration-Resistant Prostate Cancer. *J Med Chem*. 2024 Mar 14;67(5):3419-3436.
- Li D, Zhou W, Pang J, Tang Q, Zhong B, Shen C, Xiao L, Hou T. A magic drug target: Androgen receptor. *Med Res Rev*. 2019 Sep;39(5):1485-1514.
- Lim M, Otto-Duessel M, He M, Su L, Nguyen D, Chin E, Alliston T, Jones JO. Ligand-independent and tissue-selective androgen receptor inhibition by pyrvinium. *ACS Chem Biol*. 2014 Mar 21;9(3):692-702.
- Lin HK, Hu YC, Lee DK, Chang C. Regulation of androgen receptor signaling by PTEN (phosphatase and tensin homolog deleted on chromosome 10) tumor suppressor through distinct mechanisms in prostate cancer cells. *Mol Endocrinol*. 2004 Oct;18(10):2409-23.
- Liu C, Armstrong CM, Ning S, Yang JC, Lou W, Lombard AP, Zhao J, Wu CY, Yu A, Evans CP, Tepper CG, Li PK, Gao AC. ARVib suppresses growth of advanced prostate cancer via inhibition of androgen receptor signaling. *Oncogene*. 2021 Sep;40(35):5379-5392.
- Liu X, Gao Y, Ye H, Gerrin S, Ma F, Wu Y, Zhang T, Russo J, Cai C, Yuan X, Liu J, Chen S, Balk SP. Positive feedback loop mediated by protein phosphatase 1 α mobilization of P-TEFb and basal CDK1 drives androgen receptor in prostate cancer. *Nucleic Acids Res*. 2017 Apr 20;45(7):3738-3751.
- Livak KJ, Schmittgen TD. Analysis of relative gene expression data using real-time quantitative PCR and the 2(-Delta Delta C(T)) Method. *Methods*. 2001 Dec;25(4):402-8.
- Lokeshwar SD, Klaassen Z, Saad F. Treatment and trials in non-metastatic castration-resistant prostate cancer. *Nat Rev Urol*. 2021 Jul;18(7):433-442.
- Luo J, Tian J, Chou F, Lin C, Xing EZ, Zuo L, Niu Y, Yeh S, Chang C. Targeting the androgen receptor (AR) with AR degradation enhancer ASC-J9 $\text{\textcircled{R}}$ led to increase docetaxel sensitivity via suppressing the p21 expression. *Cancer Lett*. 2019 Mar 1;444:35-44.

- Lv S, Song Q, Chen G, Cheng E, Chen W, Cole R, Wu Z, Pascal LE, Wang K, Wipf P, Nelson JB, Wei Q, Huang W, Wang Z. Regulation and targeting of androgen receptor nuclear localization in castration-resistant prostate cancer. *J Clin Invest*. 2021 Feb 15;131(4):e141335.
- Lytton B. Prostate cancer: a brief history and the discovery of hormonal ablation treatment. *J Urol*. 2001 Jun;165(6 Pt 1):1859-62.
- Madan RA, Schmidt KT, Karzai F, Peer CJ, Cordes LM, Chau CH, Steinberg SM, Owens H, Eisner J, Moore WR, Dahut WL, Gulley JL, Figg WD. Phase 2 Study of Sevitronel (INO-464) in Patients With Metastatic Castration-Resistant Prostate Cancer After Enzalutamide Treatment. *Clin Genitourin Cancer*. 2020 Aug;18(4):258-267.e1.
- Mangelsdorf DJ, Thummel C, Beato M, Herrlich P, Schütz G, Umesono K, Blumberg B, Kastner P, Mark M, Chambon P, Evans RM. The nuclear receptor superfamily: the second decade. *Cell*. 1995 Dec 15;83(6):835-9.
- Marhefka CA, Gao W, Chung K, Kim J, He Y, Yin D, Bohl C, Dalton JT, Miller DD. Design, synthesis, and biological characterization of metabolically stable selective androgen receptor modulators. *J Med Chem*. 2004 Feb 12;47(4):993-8.
- Massie CE, Lynch A, Ramos-Montoya A, Boren J, Stark R, Fazli L, Warren A, Scott H, Madhu B, Sharma N, Bon H, Zecchini V, Smith DM, Denicola GM, Mathews N, Osborne M, Hadfield J, Macarthur S, Adryan B, Lyons SK, Brindle KM, Griffiths J, Gleave ME, Rennie PS, Neal DE, Mills IG. The androgen receptor fuels prostate cancer by regulating central metabolism and biosynthesis. *EMBO J*. 2011 May 20;30(13):2719-33.
- Maurice-Dror C, Le Moigne R, Vaishampayan U, Montgomery RB, Gordon MS, Hong NH, DiMascio L, Perabo F, Chi KN. A phase 1 study to assess the safety, pharmacokinetics, and anti-tumor activity of the androgen receptor n-terminal domain inhibitor epi-506 in patients with metastatic castration-resistant prostate cancer. *Invest New Drugs*. 2022 Apr;40(2):322-329.
- Maylin ZR, Nicolescu RC, Pandha H, Asim M. Breaking androgen receptor addiction of prostate cancer by targeting different functional domains in the treatment of advanced disease. *Transl Oncol*. 2021 Aug;14(8):101115.
- Mitani T, Minami M, Harada N, Ashida H, Yamaji R. Autophagic degradation of the androgen receptor mediated by increased phosphorylation of p62 suppresses apoptosis in hypoxia. *Cell Signal*. 2015 Oct;27(10):1994-2001.
- Moilanen AM, Riikonen R, Oksala R, Ravanti L, Aho E, Wohlfahrt G, Nykänen PS, Törmäkangas OP, Palvimo JJ, Kallio PJ. Discovery of ODM-201, a new-generation androgen receptor inhibitor targeting resistance mechanisms to androgen signaling-directed prostate cancer therapies. *Sci Rep*. 2015 Jul 3;5:12007.
- Montgomery RB, Mostaghel EA, Vessella R, Hess DL, Kalthorn TF, Higano CS, True LD, Nelson PS. Maintenance of intratumoral androgens in metastatic prostate cancer: a mechanism for castration-resistant tumor growth. *Cancer Res*. 2008 Jun 1;68(11):4447-54.
- Morgans AK, Shore N, Cope D, McNatty A, Moslehi J, Gomella L, Sartor O. Androgen receptor inhibitor treatments: Cardiovascular adverse events and comorbidity considerations in patients with non-metastatic prostate cancer. *Urol Oncol*. 2021 Jan;39(1):52-62.
- Morris GM, Huey R, Lindstrom W, Sanner MF, Belew RK, Goodsell DS, Olson AJ. AutoDock4 and AutoDockTools4: Automated docking with selective receptor flexibility. *J Comput Chem*. 2009 Dec;30(16):2785-91.
- Mótyán G, Gopisetty MK, Kiss-Faludy RE, Kulmány Á, Zupkó I, Frank É, Kiricsi M. Anti-Cancer Activity of Novel Dihydrotestosterone-Derived Ring A-Condensed Pyrazoles on Androgen Non-Responsive Prostate Cancer Cell Lines. *Int J Mol Sci*. 2019 May 2;20(9):2170.
- Namer M, Amiel J, Toubol J. Anandron (RU 23908) associated with orchiectomy in stage D prostate cancer. Preliminary results of a randomized, double-blind study. *Am J Clin Oncol*. 1988;11 Suppl 2:S191-6.
- Neklesa TK, Snyder LB, Willard RR, Vitale N, Raina K, Pizzano J, Gordon D, Bookbinder M, Macaluso J, Dong H, Liu Z, Ferraro C, Wang G, Wang J, Crews CM, Houston J, Crew AP, Taylor I. Abstract 5236: ARV-110: An androgen receptor PROTAC degrader for prostate cancer. *Cancer Res*. 2018 Jul 1;78(13_Supplement):5236.

- Njar VC, Brodie AM. Discovery and development of Galeterone (TOK-001 or VN/124-1) for the treatment of all stages of prostate cancer. *J Med Chem.* 2015 Mar 12;58(5):2077-87.
- Norris JD, Ellison SJ, Baker JG, Stagg DB, Wardell SE, Park S, Alley HM, Baldi RM, Yllanes A, Andreano KJ, Stice JP, Lawrence SA, Eisner JR, Price DK, Moore WR, Figg WD, McDonnell DP. Androgen receptor antagonism drives cytochrome P450 17A1 inhibitor efficacy in prostate cancer. *J Clin Invest.* 2017 Jun 1;127(6):2326-2338.
- Novotna A, Pavek P, Dvorak Z. Construction and characterization of a reporter gene cell line for assessment of human glucocorticoid receptor activation. *Eur J Pharm Sci.* 2012 Dec 18;47(5):842-7.
- Ogryzko VV, Schiltz RL, Russanova V, Howard BH, Nakatani Y. The transcriptional coactivators p300 and CBP are histone acetyltransferases. *Cell.* 1996 Nov 29;87(5):953-9.
- Oksala R, Moilanen A, Riikonen R, Rummakko P, Karjalainen A, Passiniemi M, Wohlfahrt G, Taavitsainen P, Malmström C, Ramela M, Metsänkylä HM, Huhtaniemi R, Kallio PJ, Mustonen MV. Discovery and development of ODM-204: A Novel nonsteroidal compound for the treatment of castration-resistant prostate cancer by blocking the androgen receptor and inhibiting CYP17A1. *J Steroid Biochem Mol Biol.* 2019 Sep;192:105115.
- Orme LM, Bond JD, Humphrey MS, Zacharin MR, Downie PA, Jansen KM, Mitchell SL, Robinson JM, Grapsas NA, Ashley DM. Megestrol acetate in pediatric oncology patients may lead to severe, symptomatic adrenal suppression. *Cancer.* 2003 Jul 15;98(2):397-405.
- Osguthorpe DJ, Hagler AT. Mechanism of androgen receptor antagonism by bicalutamide in the treatment of prostate cancer. *Biochemistry.* 2011 May 17;50(19):4105-13.
- Pachynski RK, Iannotti N, Laccetti AL, Carthon BC, Chi KN, Smith MR, Vogelzang NJ, Tu W, Kwan EM, Wyatt AW, Villaluna K, Younginger B, Cesano A. Oral EPI-7386 in patients with metastatic castration-resistant prostate cancer. *J Clin Oncol.* 2023 Feb 41(6_suppl):177.
- Packer JR, Maitland NJ. The molecular and cellular origin of human prostate cancer. *Biochim Biophys Acta.* 2016 Jun;1863(6 Pt A):1238-60.
- Pal SK, Tew BY, Lim M, Stankavich B, He M, Pufall M, Hu W, Chen Y, Jones JO. Mechanistic Investigation of the Androgen Receptor DNA-Binding Domain Inhibitor Pyrvinium. *ACS Omega.* 2019 Feb 28;4(2):2472-2481.
- Palit SA, Vis D, Stelloo S, Lieftink C, Prekovic S, Bekers E, Hofland I, Šuštić T, Wolters L, Beijersbergen R, Bergman AM, Győrffy B, Wessels LF, Zwart W, van der Heijden MS. TLE3 loss confers AR inhibitor resistance by facilitating GR-mediated human prostate cancer cell growth. *Elife.* 2019 Dec 19;8:e47430.
- Parikh M, Liu C, Wu CY, Evans CP, Dall'Era M, Robles D, Lara PN, Agarwal N, Gao AC, Pan CX. Phase Ib trial of reformulated niclosamide with abiraterone/prednisone in men with castration-resistant prostate cancer. *Sci Rep.* 2021 Mar 18;11(1):6377.
- Peeters BW, Ruijt GS, Craighead M, Kitchener P. Differential effects of the new glucocorticoid receptor antagonist ORG 34517 and RU486 (mifepristone) on glucocorticoid receptor nuclear translocation in the AtT20 cell line. *Ann N Y Acad Sci.* 2008 Dec;1148:536-41.
- Peltola KJ, Bono P, Jones RH, Vjaters E, Nykänen P, Vuorela A, Oksala R, Pohjanjousi P, Mustonen MVJ, Fizazi K, Massard C. ODM-204, a Novel Dual Inhibitor of CYP17A1 and Androgen Receptor: Early Results from Phase I Dose Escalation in Men with Castration-resistant Prostate Cancer. *Eur Urol Focus.* 2020 Jan 15;6(1):63-70.
- Pencina KM, Burnett AL, Storer TW, Guo W, Li Z, Kibel AS, Huang G, Blouin M, Berry DL, Basaria S, Bhasin S. A Selective Androgen Receptor Modulator (OPK-88004) in Prostate Cancer Survivors: A Randomized Trial. *J Clin Endocrinol Metab.* 2021 Jul 13;106(8):2171-2186.
- Penning TM. Androgen biosynthesis in castration-resistant prostate cancer. *Endocr Relat Cancer.* 2014 Aug;21(4):T67-78.
- Pereira de Jesus-Tran K, Côté PL, Cantin L, Blanchet J, Labrie F, Breton R. Comparison of crystal structures of human androgen receptor ligand-binding domain complexed with various agonists reveals molecular determinants responsible for binding affinity. *Protein Sci.* 2006 May;15(5):987-99.
- Petrylak DP, Gao X, Vogelzang NJ, Garfield MH, Taylor I, Moore MD, Peck RA, Burris HA. First-in-human phase I study of ARV-110, an androgen receptor (AR) PROTAC degrader in

- patients (pts) with metastatic castrate-resistant prostate cancer (mCRPC) following enzalutamide (ENZ) and/or abiraterone (ABI). *J Clin Oncol*. 2020 May;38(15_suppl):3500-3500.
- Petrylak DP, Stewart TF, Gao X, Berghorn E, Lu H, Chan E, Gedrich R, Lang JM, McKean M. A phase 2 expansion study of ARV-766, a PROTAC androgen receptor (AR) degrader, in metastatic castration-resistant prostate cancer (mCRPC). *J Clin Oncol*. 2023 Feb;41(6_suppl):TPS290-TPS290.
- Pilon D, Behl AS, Ellis LA, Robitaille MN, Lefebvre P, Dawson NA. Assessment of Real-World Central Nervous System Events in Patients with Advanced Prostate Cancer Using Abiraterone Acetate, Bicalutamide, Enzalutamide, or Chemotherapy. *Am Health Drug Benefits*. 2017 May;10(3):143-153.
- Ponnusamy S, He Y, Hwang DJ, Thiyagarajan T, Houtman R, Bocharova V, Sumpter BG, Fernandez E, Johnson D, Du Z, Pfeiffer LM, Getzenberg RH, McEwan IJ, Miller DD, Narayanan R. Orally Bioavailable Androgen Receptor Degradable, Potential Next-Generation Therapeutic for Enzalutamide-Resistant Prostate Cancer. *Clin Cancer Res*. 2019 Nov 15;25(22):6764-6780.
- Pozas J, Álvarez Rodríguez S, Fernández VA, Burgos J, Santoni M, Manneh Kopp R, Molina-Cerrillo J, Alonso-Gordoa T. Androgen Receptor Signaling Inhibition in Advanced Castration Resistance Prostate Cancer: What Is Expected for the Near Future? *Cancers (Basel)*. 2022 Dec 9;14(24):6071.
- Prekovic S, van Royen ME, Voet AR, Geverts B, Houtman R, Melchers D, Zhang KY, Van den Broeck T, Smeets E, Spans L, Houtsmuller AB, Joniau S, Claessens F, Helsen C. The Effect of F877L and T878A Mutations on Androgen Receptor Response to Enzalutamide. *Mol Cancer Ther*. 2016 Jul;15(7):1702-12.
- Prescott JL, Blok L, Tindall DJ. Isolation and androgen regulation of the human homeobox cDNA, NKX3.1. *Prostate*. 1998 Apr 1;35(1):71-80.
- Puhr M, Hoefler J, Eigentler A, Ploner C, Handle F, Schaefer G, Kroon J, Leo A, Heidegger I, Eder I, Culig Z, Van der Pluijm G, Klocker H. The Glucocorticoid Receptor Is a Key Player for Prostate Cancer Cell Survival and a Target for Improved Antiandrogen Therapy. *Clin Cancer Res*. 2018 Feb 15;24(4):927-938.
- Purushottamachar P, Kwegyir-Afful AK, Martin MS, Ramamurthy VP, Ramalingam S, Njar VC. Identification of Novel Steroidal Androgen Receptor Degrading Agents Inspired by Galeterone β -Imidazole Carbamate. *ACS Med Chem Lett*. 2016 May 23;7(7):708-13.
- Purushottamachar P., Godbole A.M., Gediya L.K., Martin M.S., Vasaitis T.S., Kwegyir-Afful A.K., Ramalingam S., Ates-Alagoz Z., Njar V.C. Systematic structure modifications of multitarget prostate cancer drug candidate galeterone to produce novel androgen receptor down-regulating agents as an approach to treatment of advanced prostate cancer. *J. Med. Chem*. 2013;56:4880-4898.
- Qiao Y, Wotring JW, Zheng Y, Zhang CJ, Zhang Y, Jiang X, Pretto CD, Eyunni S, Parolia A, He T, Cheng C, Cao X, Wang R, Su F, Ellison SJ, Wang Y, Qin J, Yan H, Zhou Q, Ma L, Sexton JZ, Chinnaiyan AM. Proxalutamide reduces SARS-CoV-2 infection and associated inflammatory response. *Proc Natl Acad Sci U S A*. 2023 Jul 25;120(30):e2221809120.
- Qin X, Ji D, Gu W, Han W, Luo H, Du C, Zou Q, Sun Z, He C, Zhu S, Chong T, Yao X, Wan B, Yang X, Bai A, Jin C, Zou J, Ye D. Activity and safety of SHR3680, a novel antiandrogen, in patients with metastatic castration-resistant prostate cancer: a phase I/II trial. *BMC Med*. 2022 Mar 4;20(1):84.
- Rastinehad AR, Anastos H, Wajswol E, Winoker JS, Sfakianos JP, Doppalapudi SK, Carrick MR, Knauer CJ, Taouli B, Lewis SC, Tewari AK, Schwartz JA, Canfield SE, George AK, West JL, Halas NJ. Gold nanoshell-localized photothermal ablation of prostate tumors in a clinical pilot device study. *Proc Natl Acad Sci U S A*. 2019 Aug 26;116(37):18590-18596.
- Rathkopf D, Liu G, Carducci MA, Eisenberger MA, Anand A, Morris MJ, Slovin SF, Sasaki Y, Takahashi S, Ozono S, Fung NK, Cheng S, Gan J, Gottardis M, Obermeier MT, Reddy J, Zhang S, Vakkalagadda BJ, Alland L, Wilding G, Scher HI; Prostate Cancer Clinical Trials Consortium. Phase I dose-escalation study of the novel antiandrogen BMS-641988 in patients with castration-resistant prostate cancer. *Clin Cancer Res*. 2011 Feb 15;17(4):880-7.

- Rathkopf DE, Saleh MN, Tsai FY, Bilen MA, Rosen LS, Gottardis M, Infante JR, Adams BJ, Liu L, Theuer CP, Freddo JL, Agarwal N. An open label phase 1/2A study to evaluate the safety, pharmacokinetics, pharmacodynamics, and preliminary efficacy of TRC253, an androgen receptor antagonist, in patients with metastatic castration-resistant prostate cancer. *J Clin Oncol*. 2019;37(15_suppl):e16542-e16542.
- Rathkopf DE, Smith MR, Ryan CJ, Berry WR, Shore ND, Liu G, Higano CS, Alumkal JJ, Hauke R, Tutrone RF, Saleh M, Chow Maneval E, Thomas S, Ricci DS, Yu MK, de Boer CJ, Trinh A, Kheoh T, Bandekar R, Scher HI, Antonarakis ES. Androgen receptor mutations in patients with castration-resistant prostate cancer treated with apalutamide. *Ann Oncol*. 2017 Sep 1;28(9):2264-2271.
- Rebello RJ, Oing C, Knudsen KE, Loeb S, Johnson DC, Reiter RE, Gillissen S, Van der Kwast T, Bristow RG. Prostate cancer. *Nat Rev Dis Primers*. 2021 Feb 4;7(1):9.
- Rhee H, Gunter JH, Heathcote P, Ho K, Stricker P, Corcoran NM, Nelson CC. Adverse effects of androgen-deprivation therapy in prostate cancer and their management. *BJU Int*. 2015 Apr;115 Suppl 5:3-13.
- Riley CM, Elwood JML, Henry MC, Hunter I, Daniel Lopez-Fernandez J, McEwan IJ, Jamieson C. Current and emerging approaches to noncompetitive AR inhibition. *Med Res Rev*. 2023 Sep;43(5):1701-1747.
- Robinson D, Van Allen EM, Wu YM, Schultz N, Lonigro RJ, Mosquera JM, Montgomery B, Taplin ME, Pritchard CC, Attard G, Beltran H, Abida W, Bradley RK, Vinson J, Cao X, Vats P, Kunju LP, Hussain M, Feng FY, Tomlins SA, Cooney KA, Smith DC, Brennan C, Siddiqui J, Mehra R, Chen Y, Rathkopf DE, Morris MJ, Solomon SB, Durack JC, Reuter VE, Gopalan A, Gao J, Loda M, Lis RT, Bowden M, Balk SP, Gaviola G, Sougnez C, Gupta M, Yu EY, Mostaghel EA, Cheng HH, Mulcahy H, True LD, Plymate SR, Dvigne H, Ferraldeschi R, Flohr P, Miranda S, Zafeiriou Z, Tunariu N, Mateo J, Perez-Lopez R, Demichelis F, Robinson BD, Schiffman M, Nanus DM, Tagawa ST, Sigaras A, Eng KW, Elemento O, Sboner A, Heath EI, Scher HI, Pienta KJ, Kantoff P, de Bono JS, Rubin MA, Nelson PS, Garraway LA, Sawyers CL, Chinnaiyan AM. Integrative clinical genomics of advanced prostate cancer. *Cell*. 2015 May 21;161(5):1215-1228. Erratum in: *Cell*. 2015 Jul 16;162(2):454.
- Rosette C, Agan FJ, Rosette N, Mazzetti A, Moro L, Gerloni M. The Dual Androgen Receptor and Glucocorticoid Receptor Antagonist CB-03-10 as Potential Treatment for Tumors that have Acquired GR-mediated Resistance to AR Blockade. *Mol Cancer Ther*. 2020 Nov;19(11):2256-2266.
- Rudovich AS, Peřina M, Krech AV, Novozhilova MY, Tumilovich AM, Shkel TV, Grabovec IP, Kvasnica M, Mada L, Zavialova MG, Mekhtiev AR, Jorda R, Zhabinskii VN, Khripach VA. Synthesis and Biological Evaluation of New Isoxazolyl Steroids as Anti-Prostate Cancer Agents. *Int J Mol Sci*. 2022 Nov 4;23(21):13534.
- Russo JW, Liu X, Ye H, Calagua C, Chen S, Voznesensky O, Condulis J, Ma F, Taplin ME, Einstein DJ, Balk SP, Chen S. Phosphorylation of androgen receptor serine 81 is associated with its reactivation in castration-resistant prostate cancer. *Cancer Lett*. 2018 Dec 1;438:97-104.
- Saad F, Efstathiou E, Attard G, Flaig TW, Franke F, Goodman OB Jr, Oudard S, Steuber T, Suzuki H, Wu D, Yeruva K, De Porre P, Brookman-May S, Li S, Li J, Thomas S, Bevans KB, Mundle SD, McCarthy SA, Rathkopf DE; ACIS Investigators. Apalutamide plus abiraterone acetate and prednisone versus placebo plus abiraterone and prednisone in metastatic, castration-resistant prostate cancer (ACIS): a randomised, placebo-controlled, double-blind, multinational, phase 3 study. *Lancet Oncol*. 2021 Nov;22(11):1541-1559.
- Sakamoto KM, Kim KB, Kumagai A, Mercurio F, Crews CM, Deshaies RJ. Protacs: chimeric molecules that target proteins to the Skp1-Cullin-F box complex for ubiquitination and degradation. *Proc Natl Acad Sci U S A*. 2001 Jul 17;98(15):8554-9.
- Salami J, Alabi S, Willard RR, Vitale NJ, Wang J, Dong H, Jin M, McDonnell DP, Crew AP, Neklesa TK, Crews CM. Androgen receptor degradation by the proteolysis-targeting chimera ARCC-4 outperforms enzalutamide in cellular models of prostate cancer drug resistance. *Commun Biol*. 2018 Aug 2;1:100.

- Samuel RM, Majd H, Richter MN, Ghazizadeh Z, Zekavat SM, Navickas A, Ramirez JT, Asgharian H, Simoneau CR, Bonser LR, Koh KD, Garcia-Knight M, Tassetto M, Sunshine S, Farahvashi S, Kalantari A, Liu W, Andino R, Zhao H, Natarajan P, Erle DJ, Ott M, Goodarzi H, Fattahi F. Androgen Signaling Regulates SARS-CoV-2 Receptor Levels and Is Associated with Severe COVID-19 Symptoms in Men. *Cell Stem Cell*. 2020 Dec 3;27(6):876-889.e12.
- Saporita AJ, Zhang Q, Navai N, Dincer Z, Hahn J, Cai X, Wang Z. Identification and characterization of a ligand-regulated nuclear export signal in androgen receptor. *J Biol Chem*. 2003 Oct 24;278(43):41998-2005.
- Saranyutanon S, Srivastava SK, Pai S, Singh S, Singh AP. Therapies Targeted to Androgen Receptor Signaling Axis in Prostate Cancer: Progress, Challenges, and Hope. *Cancers (Basel)*. 2019 Dec 23;12(1):51.
- Sartor O, de Bono J, Chi KN, Fizazi K, Herrmann K, Rahbar K, Tagawa ST, Nordquist LT, Vaishampayan N, El-Haddad G, Park CH, Beer TM, Armour A, Pérez-Contreras WJ, DeSilvio M, Kpamegan E, Gericke G, Messmann RA, Morris MJ, Krause BJ; VISION Investigators. Lutetium-177-PSMA-617 for Metastatic Castration-Resistant Prostate Cancer. *N Engl J Med*. 2021 Sep 16;385(12):1091-1103.
- Schally AV, Comaru-Schally AM, Plonowski A, Nagy A, Halmos G, Rekasi Z. Peptide analogs in the therapy of prostate cancer. *Prostate*. 2000 Oct 1;45(2):158-66.
- Scher HI, Fizazi K, Saad F, Taplin ME, Sternberg CN, Miller K, de Wit R, Mulders P, Chi KN, Shore ND, Armstrong AJ, Flaig TW, Fléchon A, Mainwaring P, Fleming M, Hainsworth JD, Hirmand M, Selby B, Seely L, de Bono JS; AFFIRM Investigators. Increased survival with enzalutamide in prostate cancer after chemotherapy. *N Engl J Med*. 2012 Sep 27;367(13):1187-97.
- Schmidt KT, Huitema ADR, Chau CH, Figg WD. Resistance to second-generation androgen receptor antagonists in prostate cancer. *Nat Rev Urol*. 2021 Apr;18(4):209-226.
- Schneekloth JS Jr, Fonseca FN, Koldobskiy M, Mandal A, Deshaies R, Sakamoto K, Crews CM. Chemical genetic control of protein levels: selective in vivo targeted degradation. *J Am Chem Soc*. 2004 Mar 31;126(12):3748-54.
- Schröder FH, Whelan P, de Reijke TM, Kurth KH, Pavone-Macaluso M, Mattelaer J, van Velthoven RF, Debois M, Collette L; Members of the EORTC Genito-Urinary Group. Metastatic prostate cancer treated by flutamide versus cyproterone acetate. Final analysis of the "European Organization for Research and Treatment of Cancer" (EORTC) Protocol 30892. *Eur Urol*. 2004 Apr;45(4):457-64.
- Schröder FH. Cyproterone acetate--mechanism of action and clinical effectiveness in prostate cancer treatment. *Cancer*. 1993 Dec 15;72(12 Suppl):3810-5.
- Schweizer MT, Haugk K, McKiernan JS, Gulati R, Cheng HH, Maes JL, Dumpit RF, Nelson PS, Montgomery B, McCune JS, Plymate SR, Yu EY. A phase I study of niclosamide in combination with enzalutamide in men with castration-resistant prostate cancer. *PLoS One*. 2018 Jun 1;13(6):e0198389.
- Seidenfeld J, Samson DJ, Hasselblad V, Aronson N, Albertsen PC, Bennett CL, Wilt TJ. Single-therapy androgen suppression in men with advanced prostate cancer: a systematic review and meta-analysis. *Ann Intern Med*. 2000 Apr 4;132(7):566-77. Erratum in: *Ann Intern Med*. 2005 Nov 15;143(10):764-5.
- Senichkin VV, Prokhorova EA, Zhivotovsky B, Kopeina GS. Simple and Efficient Protocol for Subcellular Fractionation of Normal and Apoptotic Cells. *Cells*. 2021 Apr 9;10(4):852.
- Serritella AV, Shevrin D, Heath EI, Wade JL, Martinez E, Anderson A, Schonhoft J, Chu YL, Karrison T, Stadler WM, Szmulewitz RZ. Phase I/II Trial of Enzalutamide and Mifepristone, a Glucocorticoid Receptor Antagonist, for Metastatic Castration-Resistant Prostate Cancer. *Clin Cancer Res*. 2022 Apr 14;28(8):1549-1559.
- Sert M, Tetiker T, Kirim S. Comparison of the efficiency of anti-androgenic regimens consisting of spironolactone, Diane 35, and cyproterone acetate in hirsutism. *Acta Med Okayama*. 2003 Apr;57(2):73-6.
- Shang Y, Myers M, Brown M. Formation of the androgen receptor transcription complex. *Mol Cell*. 2002 Mar;9(3):601-10. Erratum in: *Mol Cell*. 2003 Jun;11(6):1697.

- Sharma NL, Massie CE, Ramos-Montoya A, Zecchini V, Scott HE, Lamb AD, MacArthur S, Stark R, Warren AY, Mills IG, Neal DE. The androgen receptor induces a distinct transcriptional program in castration-resistant prostate cancer in man. *Cancer Cell*. 2013 Jan 14;23(1):35-47.
- Shaw J, Leveridge M, Norling C, Karén J, Molina DM, O'Neill D, Dowling JE, Davey P, Cowan S, Dabrowski M, Main M, Gianni D. Determining direct binders of the Androgen Receptor using a high-throughput Cellular Thermal Shift Assay. *Sci Rep*. 2018 Jan 9;8(1):163.
- Shen MM, Abate-Shen C. Molecular genetics of prostate cancer: new prospects for old challenges. *Genes Dev*. 2010 Sep 15;24(18):1967-2000.
- Shi H, Sadler PJ. How promising is phototherapy for cancer? *Br J Cancer*. 2020 Sep;123(6):871-873.
- Shi YK, Wang B, Shi XL, Zhao YD, Yu B, Liu HM. Synthesis and biological evaluation of new steroidal pyridines as potential anti-prostate cancer agents. *Eur J Med Chem*. 2018 Feb 10;145:11-22.
- Shore ND, Tammela TL, Massard C, Bono P, Aspegren J, Mustonen M, Fizazi K. Safety and Antitumour Activity of ODM-201 (BAY-1841788) in Chemotherapy-naïve and CYP17 Inhibitor-naïve Patients: Follow-up from the ARADES and ARAFOR Trials. *Eur Urol Focus*. 2018 Jul;4(4):547-553.
- Smith MR, Saad F, Chowdhury S, Oudard S, Hadaschik BA, Graff JN, Olmos D, Mainwaring PN, Lee JY, Uemura H, Lopez-Gitlitz A, Trudel GC, Espina BM, Shu Y, Park YC, Rackoff WR, Yu MK, Small EJ; SPARTAN Investigators. Apalutamide Treatment and Metastasis-free Survival in Prostate Cancer. *N Engl J Med*. 2018 Apr 12;378(15):1408-1418.
- Snyder L, Lee SH, Neklesa TK, Chen X, Dong H, Ferraro C, Gordon DA, Macaluso J, Pizzano J, Wang J, Willard RR, Vitale N, Peck R, Moore MD, Crews CM, Houston J, Crew AP, Taylor I. Abstract ND03: Discovery of ARV-766, an androgen receptor degrading PROTAC® for the treatment of men with metastatic castration-resistant prostate cancer. *Cancer Res*. 2023 Apr 1;83(7_Supplement):ND03.
- Solomon ZJ, Mirabal JR, Mazur DJ, Kohn TP, Lipshultz LI, Pastuszak AW. Selective Androgen Receptor Modulators: Current Knowledge and Clinical Applications. *Sex Med Rev*. 2019 Jan;7(1):84-94.
- Spriano F, Gaudio E, Cascione L, Tarantelli C, Melle F, Motta G, Priebe V, Rinaldi A, Golino G, Mensah AA, Aresu L, Zucca E, Pileri S, Witcher M, Brown B, Wahlestedt C, Giles F, Stathis A, Bertoni F. Antitumor activity of the dual BET and CBP/EP300 inhibitor NEO2734. *Blood Adv*. 2020 Sep 8;4(17):4124-4135.
- Stopsack KH, Nandakumar S, Wibmer AG, Haywood S, Weg ES, Barnett ES, Kim CJ, Carbone EA, Vasselmann SE, Nguyen B, Hullings MA, Scher HI, Morris MJ, Solit DB, Schultz N, Kantoff PW, Abida W. Oncogenic Genomic Alterations, Clinical Phenotypes, and Outcomes in Metastatic Castration-Sensitive Prostate Cancer. *Clin Cancer Res*. 2020 Jul 1;26(13):3230-3238.
- Stoyanova T, Cooper AR, Drake JM, Liu X, Armstrong AJ, Pienta KJ, Zhang H, Kohn DB, Huang J, Witte ON, Goldstein AS. Prostate cancer originating in basal cells progresses to adenocarcinoma propagated by luminal-like cells. *Proc Natl Acad Sci U S A*. 2013 Dec 10;110(50):20111-6.
- Takeda AN, Pinon GM, Bens M, Fagart J, Rafestin-Oblin ME, Vandewalle A. The synthetic androgen methyltrienolone (r1881) acts as a potent antagonist of the mineralocorticoid receptor. *Mol Pharmacol*. 2007 Feb;71(2):473-82.
- Tan MH, Li J, Xu HE, Melcher K, Yong EL. Androgen receptor: structure, role in prostate cancer and drug discovery. *Acta Pharmacol Sin*. 2015 Jan;36(1):3-23.
- Tang YQ, Han BM, Yao XQ, Hong Y, Wang Y, Zhao FJ, Yu SQ, Sun XW, Xia SJ. Chimeric molecules facilitate the degradation of androgen receptors and repress the growth of LNCaP cells. *Asian J Androl*. 2009 Jan;11(1):119-26.
- Taplin ME, Antonarakis ES, Ferrante KJ, Horgan K, Blumenstein B, Saad F, Luo J, de Bono JS. Androgen Receptor Modulation Optimized for Response-Splice Variant: A Phase 3, Randomized Trial of Galeterone Versus Enzalutamide in Androgen Receptor Splice Variant-

- 7-expressing Metastatic Castration-resistant Prostate Cancer. *Eur Urol.* 2019 Dec;76(6):843-851.
- Thankan RS, Thomas E, Purushottamachar P, Weber DJ, Njar VCO. Salinization Dramatically Enhance the Anti-Prostate Cancer Efficacies of AR/AR-V7 and Mnk1/2 Molecular Glue Degraders, Galeterone and VNPP433-3 β Which Outperform Docetaxel and Enzalutamide in CRPC CWR22Rv1 Xenograft Mouse Model. *Bioorg Chem.* 2023 Oct;139:106700.
- Thiyagarajan T, Ponnusamy S, Hwang DJ, He Y, Asemota S, Young KL, Johnson DL, Bocharova V, Zhou W, Jain AK, Petricoin EF, Yin Z, Pfeffer LM, Miller DD, Narayanan R. Inhibiting androgen receptor splice variants with cysteine-selective irreversible covalent inhibitors to treat prostate cancer. *Proc Natl Acad Sci U S A.* 2023 Jan 3;120(1):e2211832120.
- Thomas C, Gustafsson JÅ. Estrogen receptor mutations and functional consequences for breast cancer. *Trends Endocrinol Metab.* 2015 Sep;26(9):467-76.
- Thomas E, Thankan RS, Purushottamachar P, Weber DJ, Njar VCO. Targeted Degradation of Androgen Receptor by VNPP433-3 β in Castration-Resistant Prostate Cancer Cells Implicates Interaction with E3 Ligase MDM2 Resulting in Ubiquitin-Proteasomal Degradation. *Cancers (Basel).* 2023 Feb 14;15(4):1198.
- Thompson SA, Gala U, Davis DA Jr, Kucera S, Miller D, Williams RO 3rd. Can the Oral Bioavailability of the Discontinued Prostate Cancer Drug Galeterone Be Improved by Processing Method? KinetiSol® Outperforms Spray Drying in a Head-to-head Comparison. *AAPS PharmSciTech.* 2023 Jun 21;24(6):137.
- Thorpe SC, Azmatullah S, Fellows GJ, Gingell JC, O'Boyle PJ. A prospective, randomised study to compare goserelin acetate (Zoladex) versus cyproterone acetate (Cyprostat) versus a combination of the two in the treatment of metastatic prostatic carcinoma. *Eur Urol.* 1996;29(1):47-54.
- Toivanen R, Shen MM. Prostate organogenesis: tissue induction, hormonal regulation and cell type specification. *Development.* 2017 Apr 15;144(8):1382-1398.
- Tolkach Y, Joniau S, Van Poppel H. Luteinizing hormone-releasing hormone (LHRH) receptor agonists vs antagonists: a matter of the receptors? *BJU Int.* 2013 Jun;111(7):1021-30.
- Tomlins SA, Rhodes DR, Perner S, Dhanasekaran SM, Mehra R, Sun XW, Varambally S, Cao X, Tchinda J, Kuefer R, Lee C, Montie JE, Shah RB, Pienta KJ, Rubin MA, Chinnaiyan AM. Recurrent fusion of TMPRSS2 and ETS transcription factor genes in prostate cancer. *Science.* 2005 Oct 28;310(5748):644-8.
- Tran C, Ouk S, Clegg NJ, Chen Y, Watson PA, Arora V, Wongvipat J, Smith-Jones PM, Yoo D, Kwon A, Wasielewska T, Welsbie D, Chen CD, Higano CS, Beer TM, Hung DT, Scher HI, Jung ME, Sawyers CL. Development of a second-generation antiandrogen for treatment of advanced prostate cancer. *Science.* 2009 May 8;324(5928):787-90.
- Tyagi RK, Lavrovsky Y, Ahn SC, Song CS, Chatterjee B, Roy AK. Dynamics of intracellular movement and nucleocytoplasmic recycling of the ligand-activated androgen receptor in living cells. *Mol Endocrinol.* 2000 Aug;14(8):1162-74.
- Vasaitis TS, Bruno RD, Njar VC. CYP17 inhibitors for prostate cancer therapy. *J Steroid Biochem Mol Biol.* 2011 May;125(1-2):23-31.
- Velasco AM, Gillis KA, Li Y, Brown EL, Sadler TM, Achilleos M, Greenberger LM, Frost P, Bai W, Zhang Y. Identification and validation of novel androgen-regulated genes in prostate cancer. *Endocrinology.* 2004 Aug;145(8):3913-24.
- Velho PI, Bastos DA, Antonarakis ES. New approaches to targeting the androgen receptor pathway in prostate cancer. *Clin Adv Hematol Oncol.* 2021 Apr;19(4):228-240.
- Vellky JE, Ricke WA. Development and prevalence of castration-resistant prostate cancer subtypes. *Neoplasia.* 2020 Nov;22(11):566-575.
- Wadosky KM, Shourideh M, Goodrich DW, Koochekpour S. Riluzole induces AR degradation via endoplasmic reticulum stress pathway in androgen-dependent and castration-resistant prostate cancer cells. *Prostate.* 2019 Feb;79(2):140-150.
- Wahl J, Smieško M. Endocrine Disruption at the Androgen Receptor: Employing Molecular Dynamics and Docking for Improved Virtual Screening and Toxicity Prediction. *Int J Mol Sci.* 2018 Jun 15;19(6):1784.

- Wang A, Luo X, Wang Y, Meng X, Lu Z, Yang Y. Design, Synthesis, and Biological Evaluation of Androgen Receptor Degrading and Antagonizing Bifunctional Steroidal Analogs for the Treatment of Advanced Prostate Cancer. *J Med Chem*. 2022 Sep 22;65(18):12460-12481.
- Wang ZA, Mitrofanova A, Bergren SK, Abate-Shen C, Cardiff RD, Califano A, Shen MM. Lineage analysis of basal epithelial cells reveals their unexpected plasticity and supports a cell-of-origin model for prostate cancer heterogeneity. *Nat Cell Biol*. 2013 Mar;15(3):274-83.
- Watson PA, Arora VK, Sawyers CL. Emerging mechanisms of resistance to androgen receptor inhibitors in prostate cancer. *Nat Rev Cancer*. 2015 Dec;15(12):701-11.
- Wen S, Niu Y, Huang H. Posttranslational regulation of androgen dependent and independent androgen receptor activities in prostate cancer. *Asian J Urol*. 2020 Jul;7(3):203-218.
- Wienken CJ, Baaske P, Rothbauer U, Braun D, Duhr S. Protein-binding assays in biological liquids using microscale thermophoresis. *Nat Commun*. 2010 Oct 19;1:100.
- Williamson M, de Winter P, Masters JR. Plexin-B1 signalling promotes androgen receptor translocation to the nucleus. *Oncogene*. 2016 Feb 25;35(8):1066-72. doi: 10.1038/onc.2015.160.
- Wilson JD, Griffin JE, Russell DW. Steroid 5 alpha-reductase 2 deficiency. *Endocr Rev*. 1993 Oct;14(5):577-93.
- Wu M, Xie Y, Cui X, Huang C, Zhang R, He Y, Li X, Liu M, Cen S, Zhou J. Rational drug design for androgen receptor and glucocorticoids receptor dual antagonist. *Eur J Med Chem*. 2019 Mar 15;166:232-242.
- Wu M, Zhang R, Zhang Z, Zhang N, Li C, Xie Y, Xia H, Huang F, Zhang R, Liu M, Li X, Cen S, Zhou J. Selective androgen receptor degrader (SARD) to overcome antiandrogen resistance in castration-resistant prostate cancer. *Elife*. 2023 Jan 19;12:e70700.
- Xu D, Zhan Y, Qi Y, Cao B, Bai S, Xu W, Gambhir SS, Lee P, Sartor O, Flemington EK, Zhang H, Hu CD, Dong Y. Androgen Receptor Splice Variants Dimerize to Transactivate Target Genes. *Cancer Res*. 2015 Sep 1;75(17):3663-71.
- Xu LL, Su YP, Labiche R, Segawa T, Shanmugam N, McLeod DG, Moul JW, Srivastava S. Quantitative expression profile of androgen-regulated genes in prostate cancer cells and identification of prostate-specific genes. *Int J Cancer*. 2001 May 1;92(3):322-8.
- Xu Q, Zhang Z, Huang C, Bao Q, Zhang R, Wu M, Xiao X, Han X, Li X, Zhou J. Development of novel androgen receptor antagonists based on the structure of darolutamide. *Bioorg Chem*. 2022 Jul;124:105829.
- Xu S, Kondal MD, Ahmad A, Zhu R, Fan L, Zaborniak P, Madden KS, de Souza JV, Bronowska AK. Mechanistic Investigation of the Androgen Receptor DNA-Binding Domain and Modulation via Direct Interactions with DNA Abasic Sites: Understanding the Mechanisms Involved in Castration-Resistant Prostate Cancer. *Int J Mol Sci*. 2023 Jan 9;24(2):1270.
- Xu Y, Jiang YF, Wu B. New agonist- and antagonist-based treatment approaches for advanced prostate cancer. *J Int Med Res*. 2012 Aug;40(4):1217-26.
- Yan Y, Ma J, Wang D, Lin D, Pang X, Wang S, Zhao Y, Shi L, Xue H, Pan Y, Zhang J, Wahlestedt C, Giles FJ, Chen Y, Gleave ME, Collins CC, Ye D, Wang Y, Huang H. The novel BET-CBP/p300 dual inhibitor NEO2734 is active in SPOP mutant and wild-type prostate cancer. *EMBO Mol Med*. 2019 Nov 7;11(11):e10659.
- Yang CS, Xin HW, Kelley JB, Spencer A, Brautigan DL, Paschal BM. Ligand binding to the androgen receptor induces conformational changes that regulate phosphatase interactions. *Mol Cell Biol*. 2007 May;27(9):3390-404.
- Yang YC, Banuelos CA, Mawji NR, Wang J, Kato M, Haile S, McEwan IJ, Plymate S, Sadar MD. Targeting Androgen Receptor Activation Function-1 with EPI to Overcome Resistance Mechanisms in Castration-Resistant Prostate Cancer. *Clin Cancer Res*. 2016 Sep 1;22(17):4466-77.
- Yang Z, Chang YJ, Yu IC, Yeh S, Wu CC, Miyamoto H, Merry DE, Sobue G, Chen LM, Chang SS, Chang C. ASC-J9 ameliorates spinal and bulbar muscular atrophy phenotype via degradation of androgen receptor. *Nat Med*. 2007 Mar;13(3):348-53.
- Yang Z, Gimple RC, Zhou N, Zhao L, Gustafsson JÅ, Zhou S. Targeting Nuclear Receptors for Cancer Therapy: Premises, Promises, and Challenges. *Trends Cancer*. 2021 Jun;7(6):541-556.

- Yang Z, Gimple RC, Zhou N, Zhao L, Gustafsson JÅ, Zhou S. Targeting Nuclear Receptors for Cancer Therapy: Premises, Promises, and Challenges. *Trends Cancer*. 2021 Jun;7(6):541-556.
- Ye J, Coulouris G, Zaretskaya I, Cutcutache I, Rozen S, Madden TL. Primer-BLAST: a tool to design target-specific primers for polymerase chain reaction. *BMC Bioinformatics*. 2012 Jun 18;13:134.
- Yu Z, Cai C, Gao S, Simon NI, Shen HC, Balk SP. Galeterone prevents androgen receptor binding to chromatin and enhances degradation of mutant androgen receptor. *Clin Cancer Res*. 2014 Aug 1;20(15):4075-85.
- Zeng S, Huang W, Zheng X, Liyan Cheng, Zhang Z, Wang J, Shen Z. Proteolysis targeting chimera (PROTAC) in drug discovery paradigm: Recent progress and future challenges. *Eur J Med Chem*. 2021 Jan 15;210:112981.
- Zhang B, Liu C, Yang Z, Zhang S, Hu X, Li B, Mao M, Wang X, Li Z, Ma S, Zhang S, Qin C. Discovery of BWA-522, a First-in-Class and Orally Bioavailable PROTAC Degrader of the Androgen Receptor Targeting N-Terminal Domain for the Treatment of Prostate Cancer. *J Med Chem*. 2023 Aug 24;66(16):11158-11186.
- Zhang P, Wang D, Zhao Y, Ren S, Gao K, Ye Z, Wang S, Pan CW, Zhu Y, Yan Y, Yang Y, Wu D, He Y, Zhang J, Lu D, Liu X, Yu L, Zhao S, Li Y, Lin D, Wang Y, Wang L, Chen Y, Sun Y, Wang C, Huang H. Intrinsic BET inhibitor resistance in SPOP-mutated prostate cancer is mediated by BET protein stabilization and AKT-mTORC1 activation. *Nat Med*. 2017 Sep;23(9):1055-1062.
- Zhang Z, Connolly PJ, Lim HK, Pande V, Meerpoel L, Teleha C, Branch JR, Ondrus J, Hickson I, Bush T, Luistro L, Packman K, Bischoff JR, Ibrahim S, Parrett C, Chong Y, Gottardis MM, Bignani G. Discovery of JNJ-63576253: A Clinical Stage Androgen Receptor Antagonist for F877L Mutant and Wild-Type Castration-Resistant Prostate Cancer (mCRPC). *J Med Chem*. 2021 Jan 28;64(2):909-924.
- Zhao L, Zhou S, Gustafsson JÅ. Nuclear Receptors: Recent Drug Discovery for Cancer Therapies. *Endocr Rev*. 2019 Oct 1;40(5):1207-1249.
- Zhao XY, Malloy PJ, Krishnan AV, Swami S, Navone NM, Peehl DM, Feldman D. Glucocorticoids can promote androgen-independent growth of prostate cancer cells through a mutated androgen receptor. *Nat Med*. 2000 Jun;6(6):703-6.
- Zhao Y, Yang CY, Wang S. The making of I-BET762, a BET bromodomain inhibitor now in clinical development. *J Med Chem*. 2013 Oct 10;56(19):7498-500.
- Zhou T, Qin S, Xu W, Tang S, Chen G, Li S, Hou J, Gao X, Shi G, Sun Z, Jin J, Chen L, Sun W, Liu B, Wang J, Meng Q, Wang D, Hu Z, He D, Yang Y, Song X, Fu C, Wang Y, Ye D, Zhang W. Proxalutamide in metastatic castration-resistant prostate cancer: Primary analysis of a multicenter, randomized, open-label, phase 2 trial. *Int J Cancer*. 2023 Aug 15;153(4):792-802.
- Zhou T, Xu W, Zhang W, Sun Y, Yan H, Gao X, Wang F, Zhou Q, Hou J, Ren S, Yang Q, Yang B, Xu C, Zhou Q, Wang M, Chen C, Sun Y. Preclinical profile and phase I clinical trial of a novel androgen receptor antagonist GT0918 in castration-resistant prostate cancer. *Eur J Cancer*. 2020 Jul;134:29-40.

8 CURRICULUM VITAE

MSc. Miroslav Peřina



Date of birth: 18. 6. 1996
Address: Zvolenov 544, 751 01 Tovačov
Telephone: +420 608 602 900
Email: miroslav.perina01@upol.cz

Education

- 2020 – present Palacký University in Olomouc – Ph.D. degree study of Experimental Biology, Topic: *Modulation of nuclear receptors' activity in relation to human cancer*
- 2018 – 2020 Palacký University in Olomouc - master's degree study of Biochemistry (graduated with honours) Topic: *Selective inhibition of cyclin-dependent kinases in haematological malignancies*
- 2015 – 2018 Palacký University in Olomouc - bachelor's degree study of Biochemistry, Faculty of Science (graduated with honours). Topic: *Expression and purification of CDK2/CycA and its characterisation*

Work experience

- 2021 – present Department of Experimental Biology, Faculty of Science, Palacký University in Olomouc
- 2016 – 2020 Laboratory of Growth regulators – Palacký University in Olomouc and Institute of experimental botany AV ČR

Teaching

- 2023 – present Supervisor of the Bachelor's thesis. Topic: *Expression and purification of the ligand-binding domain of the human androgen receptor*, Mgr. Monika Pitnerová
- 2020 – present KEB/MKBCH Methods in Clinical Biochemistry (practical course)

Research interest

Protein expression and purification, Protein crystallography and structural biology, Cell cycle, Signalling pathways, Cancer treatment, Drug design and discovery, Kinase inhibitors, Nuclear receptors, Nuclear receptors' antagonists, Prostate cancer, Antiandrogens.

Skills, experience

Protein expression in bacterial, insect and human cell systems. Protein purification by affinity chromatography, gel filtration chromatography, protein electrophoresis, Western blot. Tissue cultures of human cancer cell lines, insect cell lines. Analysis of biological effects of synthetic compounds on human cancer cells (signalling, colony-forming assays, viability and apoptosis assays, cell cytometry). Interaction of small molecules with proteins (cellular thermal shift assay, ITC, nanoDSF, MST). Molecular modelling (molecular docking, PyMol).

Conferences

- 2023 Peřina M, Kiss MA, Mótyán G, Szczyrbová E, Eliáš M, Študent V Jr, Kurfürstová D, Kovalová M, Mada L, Bouchal J, Frank É, Jorda R. A-ring-fused pyrazoles of dihydrotestosterone in prostate cancer. CZECH ANUAL CANCER RESEARCH MEETING 2023, Olomouc (20. - 22. 11. 2023) – oral presentation
- 2022 Peřina M, Kiss MA, Mótyán G, Szczyrbová E, Eliáš M, Študent V Jr, Kurfürstová D, Kovalová M, Mada L, Bouchal J, Frank É, Jorda R. A-ring-fused pyrazoles of dihydrotestosterone targeting prostate cancer cells via the downregulation of the androgen receptor. CZECH ANUAL CANCER RESEARCH MEETING 2022, Olomouc (1. - 2. 12. 2022) – poster presentation
- 2022 Peřina M, Supíková K, Bělíček J, Kovalová M. Production of transferases for ligand discovery and structural biology. EMBO WORKSHOP: Chemical biology 2022, Heidelberg, Germany (5. 9. – 8. 9. 2022) – poster presentation
- 2022 Peřina M, Kiss A, Mernyák E, Mada L, Schneider G, Jorda R. Hydrocortisone esters targeting androgen and glucocorticoid receptors in prostate cancer. CHEMISTRY AND BIOLOGY OF PHYTOHORMONES AND RELATED SUBSTANCES 2022, Malenovice (15. -17. 5. 2022) – oral presentation
- 2021 Peřina M, Kiss MA, Bazgier V, May NV, Baji Á, Jorda R, Frank É. Synthesis of dihydrotestosterone derivatives modified in the A-ring with (hetero)arylidene, pyrazolo[1,5-a]pyrimidine and triazolo[1,5-a]pyrimidine moieties and their targeting of the androgen receptor in prostate cancer. CHEMISTRY AND BIOLOGY OF PHYTOHORMONES AND RELATED SUBSTANCES 2021, Malenovice (12. -14. 9. 2021) – oral presentation awarded with a price

2019 Peřina M, Řezníčková E, Jorda R, Kryštof V. Biological differences among CDK4/6 inhibitors. EFMC-ACSMEDI MedChem Frontiers, Kraków, Poland (10. 6. – 13. 6. 2019) poster presentation

Internships

2023 3 months-long internship at the **Department of Experimental Urology, Medical University Innsbruck**, Austria. Supervised by assoc. Prof. Frédéric Santer, Ph.D. Biological analysis of the AR-splicing variants in human prostate cancer development and therapy.

2020 1-week work internship at the **BIOCEV**, Prague. Supervised by assoc. prof. Daniel Rosel and Michal Dibus, Ph.D. Expression of human PKN3 in human cells (handling, lipofection) for affinity purification and enzyme analysis.

2018-2019 2-weeks work internships at the **Institute of Organic Chemistry and Biochemistry of the CAS**, Prague. Supervised by assoc. prof. Pavlína Maloy Řezáčová and Jana Škerlová, Ph.D. Bacterial expression and affinity purification of human CDK2/CycA, protein crystallisation.

Research Projects

2023 IGA_PrF_2023_012 – Small molecular inhibitors of oncogene kinase FLT3. Principal investigator Principal investigator

2022 **Principal investigator** in project: UPOL DSGC-2021-0158 (2022) Protein production for experimental and structural biology, part of the: Improving Schematics of Doctoral Student Grant Competition and their Pilot Implementation' (No. CZ.02.2.69/0.0/0.0/19_073/0016713), from the Ministry of Education, Youth and Sports of the Czech Republic

2021 2021 IGA_PrF_2021_007 – Molecular effects of enzyme inhibitors
Principal investigator: prof. RNDr. Vladimír Kryštof, Ph.D.

2020 - 2021 GAČR 19-09086S - Dual FLT3/CDK9 inhibition as a possible therapeutical approach for mixed lineage leukemia. Principal investigator: prof. RNDr. Vladimír Kryštof, Ph.D.

Awards

2022 The Dean's Award (Faculty of Science) main prize in the Chemistry - PhD. Section

2019 The Dean's award (Faculty of Science) 1. prize in the Chemistry – Masters Section

2019 The Czech Centers' award for science popularisation (FameLab Czech Republic 2019)

Publications

15 publications, 3 first author, 81 citations, *h*-index 6 (Scopus) (updated April 8th 2024)

Jorda R, Havlíček L, Šturc A, Tušková D, Daumová L, Alam M, Škerlová J, Nekardová M, **Peřina M**, Pospíšil T, Šíroká J, Urbánek L, Pachl P, Řezáčová P, Strnad M, Klener P, Kryštof V. 3,5,7-Substituted Pyrazolo[4,3-*d*]pyrimidine Inhibitors of Cyclin-Dependent Kinases and Their Evaluation in Lymphoma Models. **J Med Chem.** 2019 May 9;62(9):4606-4623.

Jansa J, Jorda R, Škerlová J, Pachl P, **Peřina M**, Řezníčková E, Heger T, Gucký T, Řezáčová P, Lyčka A, Kryštof V. Imidazo[1,2-*c*]pyrimidin-5(6H)-one inhibitors of CDK2: Synthesis, kinase inhibition and co-crystal structure. **Eur J Med Chem.** 2021 Apr 15;216:113309.

Kiss MA, **Peřina M**, Bazgier V, May NV, Baji Á, Jorda R, Frank É. Synthesis of dihydrotestosterone derivatives modified in the A-ring with (hetero)arylidene, pyrazolo[1,5-*a*]pyrimidine and triazolo[1,5-*a*]pyrimidine moieties and their targeting of the androgen receptor in prostate cancer. **J Steroid Biochem Mol Biol.** 2021 Jul;211:105904.

Dayal N, Řezníčková E, Hernandez DE, **Peřina M**, Torregrosa-Allen S, Elzey BD, Škerlová J, Ajani H, Djukic S, Vojáčková V, Lepšík M, Řezáčová P, Kryštof V, Jorda R, Sintim HO. 3*H*-Pyrazolo[4,3-*f*]quinoline-Based Kinase Inhibitors Inhibit the Proliferation of Acute Myeloid Leukemia Cells In Vivo. **J Med Chem.** 2021 Aug 12;64(15):10981-10996.

Vlková K, Gucký T, **Peřina M**, Řezníčková E, Kryštof V. Synthesis and biological activity evaluation of novel 2,6,9-trisubstituted purine conjugates as potential protein kinases inhibitors. **Bioorg Med Chem Lett.** 2022 Mar 15;60:128603.

Jorda R, Havlíček L, **Peřina M**, Vojáčková V, Pospíšil T, Djukic S, Škerlová J, Grúz J, Renešová N, Klener P, Řezáčová P, Strnad M, Kryštof V. 3,5,7-Substituted Pyrazolo[4,3-*d*]Pyrimidine Inhibitors of Cyclin-Dependent Kinases and Cyclin K Degradars. **J Med Chem.** 2022 Jul 14;65(13):8881-8896.

Rudovich AS, **Peřina M**, Krech AV, Novozhilova MY, Tumilovich AM, Shkel TV, Grabovec IP, Kvasnica M, Mada L, Zavialova MG, Mekhtiev AR, Jorda R, Zhabinskii VN, Khripach VA. Synthesis and Biological Evaluation of New Isoxazolyl Steroids as Anti-Prostate Cancer Agents. **Int J Mol Sci.** 2022 Nov 4;23(21):13534.

Řezníčková E, Krajčovičová S, **Peřina M**, Kovalová M, Soural M, Kryštof V. Modulation of FLT3-ITD and CDK9 in acute myeloid leukaemia cells by novel proteolysis targeting chimera (PROTAC). **Eur J Med Chem.** 2022 Dec 5;243:114792.

Vlková K, Pádrtová R, Gucký T, **Peřina M**, Řezníčková E, Kryštof V. Synthesis and biological activity evaluation of novel 3,5,7-trisubstituted pyrazolo[1,5-a]pyrimidines. **Bioorg Med Chem Lett**. 2022 Dec 8;80:129096.

Tomanová M, Kozlanská K, Jorda R, Jedinák L, Havlíková T, Řezníčková E, **Peřina M**, Klener P, Dolníková A, Cankař P, Kryštof V. Synthesis and Structural Optimization of 2,7,9-Trisubstituted purin-8-ones as FLT3-ITD Inhibitors. **Int J Mol Sci**. 2022 Dec 18;23(24):16169.

Gonzalez G, Kvasnica M, Svrčková K, Štěpánková Š, Santos JRC, **Peřina M**, Jorda R, Lopes SMM, Melo TMVDPE. Ring-fused 3 β -acetoxyandrost-5-enes as novel neuroprotective agents with cholinesterase inhibitory properties. **J Steroid Biochem Mol Biol**. 2023 Jan;225:106194.

Peřina M, Kiss MA, Mótyán G, Szczyrbová E, Eliáš M, Študent V Jr, Kurfürstová D, Kovalová M, Mada L, Bouchal J, Frank É, Jorda R. A-ring-fused pyrazoles of dihydrotestosterone targeting prostate cancer cells via the downregulation of the androgen receptor. **Eur J Med Chem**. 2023 Jan 13;249:115086.

Peřina M, Kiss A, Mernyák E, Mada L, Schneider G, Jorda R. Synthesis of hydrocortisone esters targeting androgen and glucocorticoid receptors in prostate cancer in vitro. **J Steroid Biochem Mol Biol**. 2023 May;229:106269.

Kovalová M, Havlíček L, Djukic S, Škerlová J, **Peřina M**, Pospíšil T, Řezníčková E, Řezáčová P, Jorda R, Kryštof V. Characterization of new highly selective pyrazolo[4,3-d]pyrimidine inhibitor of CDK7. **Biomed Pharmacother**. 2023 May;161:114492.

Kiss MA, **Peřina M**, Bereczki L, Baji Á, Bělíček J, Jorda R, Frank É. Dihydrotestosterone-based A-ring-fused pyridines: Microwave-assisted synthesis and biological evaluation in prostate cancer cells compared to structurally related quinolines. **J Steroid Biochem Mol Biol**. 2023 Jul;231:106315.

9 APPENDICES

- I. Kiss MA*, **Peřina M***, Bazgier V, May NV, Baji Á, Jorda R, Frank É. Synthesis of dihydrotestosterone derivatives modified in the A-ring with (hetero)arylidene, pyrazolo[1,5-a]pyrimidine and triazolo[1,5-a]pyrimidine moieties and their targeting of the androgen receptor in prostate cancer. **J Steroid Biochem Mol Biol**. 2021 Jul;211:105904.

*shared first authorship

IF (2021): 5.0 (Q1, clinical biochemistry, endocrinology; Q2, molecular medicine)
MP (40% contribution), as a shared first author, performed cellular experiments analyzing the biological activity of the tested substances, the effect on the AR, its signalling and the binding of candidate substances. He interpreted the obtained data and participated in writing the manuscript.

- II. **Peřina M***, Kiss MA*, Mótyán G, Szczyrbová E, Eliáš M, Študent V Jr, Kurfürstová D, Kovalová M, Mada L, Bouchal J, Frank É, Jorda R. A-ring-fused pyrazoles of dihydrotestosterone targeting prostate cancer cells via the downregulation of the androgen receptor. *Eur J Med Chem*. 2023a Mar 5;249:115086.

*shared first authorship

IF (2022): 6.7 (Q1, chemistry, medicine, pharmacology)
MP (40% contribution), as shared first author, optimized and performed biochemical and cellular experiments analyzing the biological activity of the tested substances, the effect on the AR and its signalling and degradation, the binding of substances and the viability of prostate cancer cell lines after treatment. Using computer modelling, he created a model of the binding pose. He interpreted the obtained data and significantly participated in the writing of the manuscript and its revision.

- III. Kiss MA, **Peřina M**, Bereczki L, Baji Á, Bělíček J, Jorda R, Frank É. Dihydrotestosterone-based A-ring-fused pyridines: Microwave-assisted synthesis and biological evaluation in prostate cancer cells compared to structurally related quinolines. **J Steroid Biochem Mol Biol**. 2023 Jul;231:106315.

IF (2022): 4.1 (Q2, clinical biochemistry, endocrinology; molecular medicine)
MP (30% contribution), as a co-author, performed biochemical and cellular experiments analyzing the biological activity of the tested substances, the effect on the androgen receptor, its signalling and proof of binding of the substances. Using computer modelling, he created a model of the binding pose. He interpreted the data and participated in the writing of the manuscript.

- IV. Peřina M**, Kiss A, Mernyák E, Mada L, Schneider G, Jorda R. Synthesis of hydrocortisone esters targeting androgen and glucocorticoid receptors in prostate cancer in vitro. **J Steroid Biochem Mol Biol.** 2023b May;229:106269.

IF (2022): 4.1 (Q2, clinical biochemistry, endocrinology, molecular medicine)

MP (40% contribution) as the first author optimised and performed biochemical experiments analyzing the biological activity of the tested substances, the effect on the AR and GR and their signalling and substance binding. He created a model of the binding pose, studied the viability and proliferation of prostate cancer cell lines, interpreted the data and wrote the manuscript and its revision.

- V. Rudovich AS, Peřina M**, Krech AV, Novozhilova MY, Tumilovich AM, Shkel TV, Grabovec IP, Kvasnica M, Mada L, Zavialova MG, Mekhtiev AR, Jorda R, Zhabinskii VN, Khripach VA. Synthesis and Biological Evaluation of New Isoxazolyl Steroids as Anti-Prostate Cancer Agents. **Int J Mol Sci.** 2022 Nov 4;23(21):13534.

IF (2022): 5.6 (Q1, medicine, organic chemistry; Q2, molecular biology)

MP (30% contribution), as a co-author performed biochemical and cellular experiments analyzing the biological activity of the tested substances, the effect on the AR and its signalling, and binding of substances. He created a model of the binding pose, interpreted the data and participated in the writing of the manuscript.

Appendix I.

Kiss MA*, **Peřina M***, Bazgier V, May NV, Baji Á, Jorda R, Frank É. Synthesis of dihydrotestosterone derivatives modified in the A-ring with (hetero)arylidene, pyrazolo[1,5-a]pyrimidine and triazolo[1,5-a]pyrimidine moieties and their targeting of the androgen receptor in prostate cancer. **J Steroid Biochem Mol Biol.** 2021 Jul;211:105904.

*shared first authorship



Contents lists available at ScienceDirect

Journal of Steroid Biochemistry and Molecular Biology

journal homepage: www.elsevier.com/locate/jsbmb

Synthesis of dihydrotestosterone derivatives modified in the A-ring with (hetero)arylidene, pyrazolo[1,5-*a*]pyrimidine and triazolo[1,5-*a*]pyrimidine moieties and their targeting of the androgen receptor in prostate cancer

Márton A. Kiss^{a,1}, Miroslav Peřina^{b,1}, Václav Bazgier^{c,d}, Nóra V. May^e, Ádám Baji^a, Radek Jorda^{b,*}, Éva Frank^{a,*}

^a Department of Organic Chemistry, University of Szeged, Dóm tér 8, Szeged, H-6720, Hungary

^b Department of Experimental Biology, Faculty of Science, Palacký University Olomouc, Šlechtitelů 27, Olomouc, 78371, Czech Republic

^c Department of Physical Chemistry, Faculty of Science, Palacký University Olomouc, Šlechtitelů 241/27, Olomouc, 77900, Czech Republic

^d Laboratory of Growth Regulators, The Czech Academy of Sciences, Institute of Experimental Botany & Palacký University, Šlechtitelů 27, Olomouc, 78371, Czech Republic

^e Centre for Structural Science, Research Centre for Natural Sciences, Magyar tudósok körútja 2, Budapest, H-1117, Hungary

ARTICLE INFO

Keywords:

2-arylidene-dihydrotestosterone
Azolo[1,5-*a*]pyrimidines
Heterocyclization
Crystal structures
Androgen receptor
Flexible docking
Transcriptional activity

ABSTRACT

One of the main directions of steroid research is the preparation of modified derivatives in which, in addition to changes in physicochemical properties, receptor binding is significantly altered, thus a bioactivity different from that of the parent compound predominates. In the frame of this work, 2-arylidene derivatives were first synthesized by regioselective modification of the A-ring of natural sex hormone, 5 α -dihydrotestosterone (DHT). After Claisen-Schmidt condensations of DHT with (hetero)aromatic aldehydes in alkaline EtOH, heterocyclizations of the α,β -enones were performed with 3-amino-1,2,4-triazole, 3-aminopyrazole and 3-amino-5-methylpyrazole in the presence of *t*-BuOK in DMF to afford 7'-epimeric mixtures of A-ring-fused azolo-dihydropyrimidines, respectively. Depending on the electronic demand of the substituents of the arylidene moiety, spontaneous or 2,3-dichloro-5,6-dicyanobenzoquinone (DDQ)-induced oxidation of the heteroring led to triazolo[1,5-*a*]pyrimidines and pyrazolo[1,5-*a*]pyrimidines in good yields, while, using the Jones reagent as a strong oxidant, 17-oxidation also occurred. The crystal structures of an arylidene and a triazolopyrimidine product have been determined by single crystal X-ray diffraction and both were found to crystallize in the monoclinic crystal system at *P*2₁ space group. Most derivatives were found to diminish the transcriptional activity of androgen receptor (AR) in reporter cell line. The candidate compound (17 β -hydroxy-2-(4-chloro)benzylidene-5 α -androstan-3-one, **2f**) showed to suppress androgen-mediated AR transactivation in a dose-dependent manner. We confirmed the cellular interaction of **2f** with AR, described the binding in AR-binding cavity by the flexible docking and showed the ability of the compound to suppress the expression of AR-regulated genes in two prostate cancer cell lines.

Abbreviations: 3AMP, 3-amino-5-methylpyrazole; 3AP, 3-aminopyrazole; 3AT, 3-aminotriazole; ATP, adenosine triphosphate; AR, androgen receptor; ARE, androgen response element; *n*-BuOH, normal butanol; *t*-BuOK, potassium *tert*-butylate; CETSA, cellular-thermal shift assay; CPPI, 3-(4-chlorophenyl)-6,7-dihydro-5H-pyrrolo[1,2-*a*]imidazole; CSS, charcoal stripped serum; CRPC, castration-resistant prostate cancer; CYP17A1, steroid 17 α -hydroxylase/17,20-lyase; DCTA, *trans*-1,2-diaminocyclohexane-*N,N,N',N'*-tetraacetic acid; DDQ, 2,3-dichloro-5,6-dicyanobenzoquinone; DHT, 5 α -dihydrotestosterone; DMF, *N,N*-dimethylformamide; DTT, dithiothreitol; ESI-MS, electrospray ionization mass spectrometry; EtOH, ethanol; HMBC, heteronuclear multiple bond correlation; HSQC, heteronuclear single quantum correlation; LBD, ligand-binding domain; LHRH, luteinizing hormone-releasing hormone; MW, microwave; NOESY, nuclear overhauser effect spectroscopy; NMR, nuclear magnetic resonance; ORTEP, Oak Ridge Thermal-Ellipsoid Plot program for crystal structure illustrations; PARP, poly(ADP-ribose)polymerase; PBS, phosphate-buffered saline; PCR, polymerase chain reaction; PSA, prostate-specific antigen; RIPA, radioimmunoprecipitation assay buffer; SDS-PAGE, sodium dodecyl sulphate-polyacrylamide gel electrophoresis; TLC, thin layer chromatography.

* Corresponding authors.

E-mail addresses: radek.jorda@upol.cz (R. Jorda), frank@chem.u-szeged.hu (É. Frank).

¹ These authors contributed equally to this work.

<https://doi.org/10.1016/j.jsbmb.2021.105904>

Received 18 March 2021; Received in revised form 20 April 2021; Accepted 27 April 2021

Available online 29 April 2021

0960-0760/© 2021 The Authors. Published by Elsevier Ltd. This is an open access article under the CC BY license (<http://creativecommons.org/licenses/by/4.0/>).

1. Introduction

The androgen receptor (AR) is a ligand-activated transcription factor that belongs to the superfamily of steroid and thyroid hormone receptors and plays a crucial role in the normal development of male reproductive tissues. High expression and/or relaxation of AR regulation is strongly implicated in prostate cancer (PCa). Current therapeutic strategies for the treatment of PCa include androgen deprivation and radiation therapy (e.g. anti-LHRH agents), surgery, chemotherapy (e.g. docetaxel, cabazitaxel) or the use of steroidal (e.g. abiraterone) or non-steroidal antiandrogens (e.g. enzalutamide) (Fig. 1) or PARP inhibitors [1]. Unfortunately, the disease rapidly progresses to castration-resistant prostate cancer (CRPC) stage, which is defined by AR-pathway alterations including AR gene amplification, overexpression, mutation, splice variants, and the increase in adrenal and intratumoral androgens.

AR splicing variants [2], which lack the ligand-binding domain as a result of alternative splicing of the AR gene, are emerging as a crucial mechanism in CRPC progression. Among these variants, AR-V7 is the most clinically meaningful and the most frequently expressed receptor variant in PCa samples [3]. Several anti-AR-V7 strategies have been described, including inhibition of the transcription of the AR gene, inhibition of splicing to generate AR-V7, destabilization of the AR-V7 transcript and protein, AR degradation, blocking of AR synthesis, inhibition of the constitutive activity of AR-V7 in the nucleus, interference with intracellular trafficking of AR, and inhibition of downstream signalling related to AR-V7 activation [4,5].

Several steroidal compounds, mostly modified in the D-ring of the androstane core have been investigated as AR modulators or for their anti-PCa properties [6–11], but only galeterone [12] and abiraterone [13] (Fig. 1) have entered clinical trials. Both agents showed to target adrenal and tumour androgen production by inhibition of the steroidogenic enzyme CYP17A1, and galeterone is capable to induce AR and AR-V7 degradation in PCa by competitive antagonism of AR [14]. In the clinic, galeterone is shown to be well tolerated and demonstrates pharmacodynamic changes consistent with its selective, multifunctional AR signaling inhibition [15]. Unfortunately, recent results from phase 3 clinical trials on AR-V7 and metastatic CRPC patients have not confirmed galeterone's efficacy [16]. In addition, the fact that

abiraterone-treated patients generally relapse within one year indicated the resistance mechanism to abiraterone that is accompanied by upregulation of CYP17A1 and induction of AR and AR splice variants [2,17]. For the above reasons, investigations of other ligands are desirable.

We previously described several D-ring-attached steroidal azoles, structurally similar to abiraterone, displaying CYP17A1 inhibitory effect [18–20]. Recently, some A-ring-fused arylpyrazoles [21] and arylpyrimidines [22] of 5 α -dihydrotestosterone (DHT) have also been demonstrated to exert anticancer activity against multiple cancer cell lines including PCas. Some recent articles reported steroidal compounds with pyrazolo[1,5-*a*]pyrimidine and triazolo[1,5-*a*]pyrimidine moieties [23, 24] but without deeper pharmacological investigations. In the current work, additional A-ring-modified derivatives of DHT containing (hetero)arylidene, pyrazolo[1,5-*a*]pyrimidine and triazolo[1,5-*a*]pyrimidine moieties have been synthesized and their ability to affect the transcriptional activity of AR in reporter cell line was investigated. Structural determination of all compounds was accomplished by ¹H and ¹³C NMR spectroscopy and electrospray ionization mass spectrometry (ESI-MS), while for two representative molecules, by single crystal X-ray diffraction. Candidate compound was further studied and showed to interact with AR and to suppress expression of Nkx3.1 and PSA in PCa. Finally, interaction within the AR's cavity was performed by the flexible docking.

2. Results and discussion

2.1. Synthesis and characterization of the target compounds

As a first synthetic modification, DHT was reacted with benzaldehyde (1a), substituted benzaldehydes 1b–h and heteroaromatic aldehydes 1i and 1j, respectively, in order to obtain 2-(hetero)arylidene-3-ones 2a–j suitable for cyclization with binucleophilic reagents (Table 1, entries 1–12). Arylaldehydes were selected to ensure that their reactivity covered a wide spectrum, i.e. in addition to benzaldehyde 1a, derivatives containing both electron donating (CH₃ and OMe) and electron withdrawing groups (Cl, CN, NO₂) were used. The synthesis of a structurally related 2-methylidene derivative 2k from DHT with excess acetaldehyde 1k has been reported previously [21] (Table 1, entry 13).

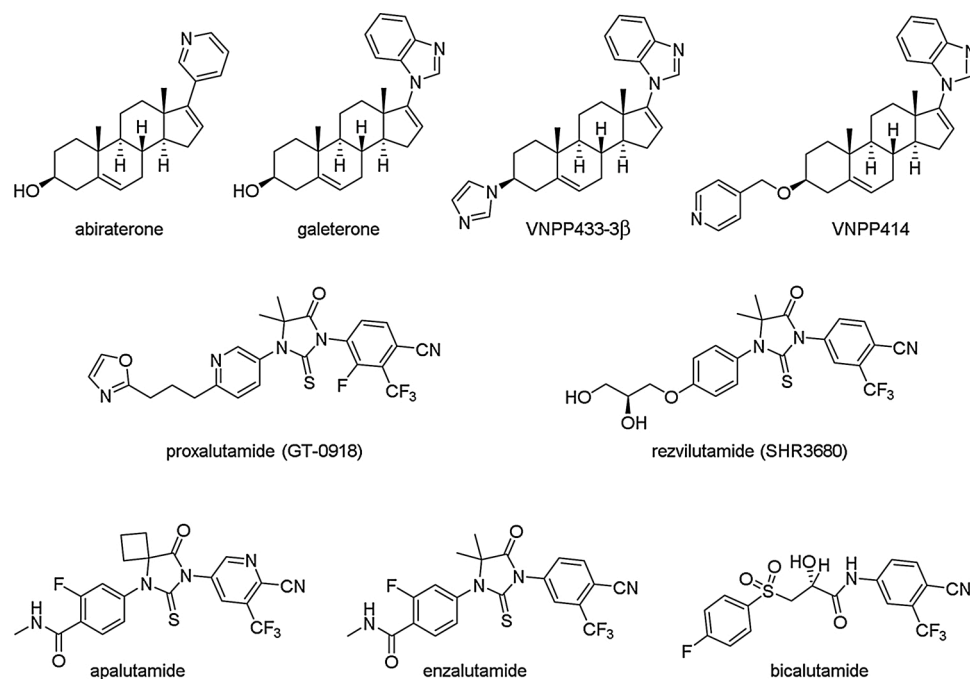
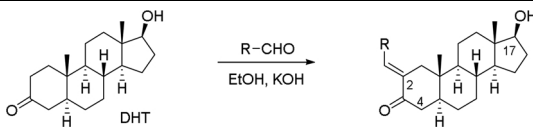


Fig. 1. Representatives of steroidal and non-steroidal anti-PCa agents, which reduce endogenous androgen production by the inhibition of CYP17A1 and/or act as AR antagonists.

Table 1
Synthesis of A-ring-modified α,β -enones **2a–k** from DHT.



Entry	R-CHO ^a	R	Temperature (°C)	Time	Product	Yield (%) ^b
1	1a	Ph	reflux	30 min	2a	74
2	1a	Ph	r.t.	3 h	2a	92
3	1a	Ph	80 (MW)	10 min	2a	69
4	1b	<i>p</i> -CH ₃ C ₆ H ₄	r.t.	4 h	2b	87
5	1c	<i>m</i> -CH ₃ C ₆ H ₄	r.t.	4 h	2c	89
6	1d	<i>p</i> -MeO-C ₆ H ₄	r.t.	4 h	2d	89
7	1e	<i>p</i> -F-C ₆ H ₄	r.t.	3 h	2e	91
8	1f	<i>p</i> -Cl-C ₆ H ₄	0	3 h	2f	90
9	1g	<i>p</i> -CN-C ₆ H ₄	0	1 h	2g ^c	–
10	1h	<i>p</i> -NO ₂ C ₆ H ₄	0	1 h	2h ^c	–
11	1i	furan-2-yl	0	3 h	2i	84
12	1j	tiophen-2-yl	0	3 h	2j	83
13	1k	CH ₃	–10	3.5 h	2k ^d	70

^a 1.2 equiv.

^b After purification by column chromatography.

^c In addition to compound **2**, the significant formation of the 4-arylidene and 2,4-diarylidene derivatives were detected.

^d The synthesis has been reported previously [21].

Although Claisen-Schmidt condensation of arylaldehydes to the C16 position of 17-ketosteroids was found to lead to the corresponding D-ring substituted products in alkaline EtOH both at room temperature [25] and under reflux [26], in the case of the A-ring, a regioselectivity problem may arise from the two α -carbon atoms (C2 and C4) adjacent to the C3 carbonyl group available for substitution. The reaction conditions may vary depending on the different electronic nature and thus reactivity of the aldehydes used.

For a preliminary experiment, the reaction of DHT and benzaldehyde **1a** in 1:1.2 M ratio was carried out in alkaline EtOH at both reflux and room temperatures (r. t.). Although at 25 °C longer time (3 h) was needed than in boiling EtOH (30 min) for complete conversion, the selectivity was found to be better, and the 2-benzylidene derivative **2a** was obtained selectively in excellent yield (94 %, Table 1, entry 1). Higher temperature (entry 2) and especially microwave (MW) irradiation (80 °C, 10 min, entry 3) favoured the formation of the 4-isomer as an undesired by-product.

During the Claisen-Schmidt condensation of DHT performed with other arylaldehydes **1b–h**, the reaction rates were found to be affected significantly by the different R substituents in the aromatic ring. Longer reaction time (4 h) at room temperature was needed for the regioselective formation of the desired products **2b–d** in cases of arylaldehydes **1b–d** containing electron donating groups (CH₃, OMe), which can be explained by the decreased electrophilicity of these reagents (Table 1, entries 4–6). While *p*-fluorobenzaldehyde (**1e**) displayed similar reactivity to benzaldehyde (entry 7), a lower temperature was required to achieve adequate regioselectivity when **1f** with an electron-withdrawing Cl atom or heteroaryl aldehydes (**1g**, **1h**) were used, due to the higher reactivity of these carbonyl compounds. It is also important to note that arylaldehydes **1g** and **1h** having a strong electron-withdrawing group (CN or NO₂) were so reactive even at low temperature that the transformations resulted in the inseparable mixtures of 2- (**2g** or **2h**) and 4-arylidene derivatives as well as 2,4-disubstituted products (entries 9 and 10), therefore these reactions were abandoned.

The structure of the novel arylidene (**2a–f**) and heteroarylidene derivatives (**2i** and **2j**) in solution was confirmed by ¹H and ¹³C NMR measurements, which indicated the presence of the characteristic signals of the aromatic ring from the aryl- and heteroarylaldehydes (Supplementary Material, S1-S30). Since the usually more stable and thus favoured (*E*)-configuration along the double bond was earlier evidenced by NOESY correlations between the 1-H and 21-CH₃ protons for **2k** [21],

the same stereochemistry in solution appears to be certain for the structural analogues (**2a–f**, **2i**, **2j**) containing a larger (hetero)aromatic ring than the CH₃ group of **2k**.

The solid phase structure of **2a** was determined by single crystal X-ray diffraction. The molecule crystallized in the monoclinic crystal system in *P*2₁ space group. ORTEP representation together with atom numbering of the compound and the packing arrangements viewed from the crystallographic direction 'a' is depicted in Fig. 2. The unit cell, containing two molecules, is shown in Fig. S1 and the packing arrangements viewed from the 'a', 'b' and 'c' crystallographic directions are shown in Fig. S2. The torsion angle measured for C2-C26-C1'-C6' was found to be 16.5° showing that the phenyl ring is in a plane with the DHT rings. Bond distances and angles are collected in Tables S1 and S2. The molecules are arranged in columns by the help of O2-H2O...O1 connection between neighboring molecules (Fig. S3). Some selected hydrogen bond data is shown in Table S3. Because of the steric hindrance of the C18 and C19 methyl groups, the molecules above each other are shifted away and C4-H4A... π and C5-H5... π secondary interactions are forming between C–H protons and the phenyl rings (Fig. S3). The crystal does not contain any solvent accessible voids.

As a continuation, the ring-closure reactions of the synthesized steroidal α,β -enones with different aminoazole reagents were planned to carry out. The initial experiments were performed with the benzylidene derivative **2a**, in order to find the optimum conditions for the synthesis of pyrazolo[1,5-*a*]pyrimidines and triazolo[1,5-*a*]pyrimidines (Scheme 1). Although *t*-BuOK has often been used as catalyst in polar protic solvents, such as EtOH or *n*-BuOH, for similar heterocyclizations of α,β -unsaturated ketones, long reaction times (6–30 h) under reflux were generally required for complete conversions [23,27]. Since the progress of the reaction of **2a** with 3-amino-5-methylpyrazole (3AMP), 3-aminopyrazole (3AP) or 3-aminotriazole (3AT) also proved to be very slow under these conditions, MW irradiation was first applied to obtain rate acceleration. In the latter cases, however, the formation of a significant amount of by-products was observed. As a next attempt, EtOH was replaced with DMF in the presence of *t*-BuOK, which in each case led to almost complete conversion indicated by a sharp colour change of the mixtures, within 45 min at 140 °C (Scheme 1). The same reactions in DMF required 3 h when KOH was used as a base. TLC monitoring confirmed the formation of two new substances in each reaction. The NMR spectroscopic analysis showed that the less polar compounds were the target products **6a–8a**, while the more polar molecule proved to be

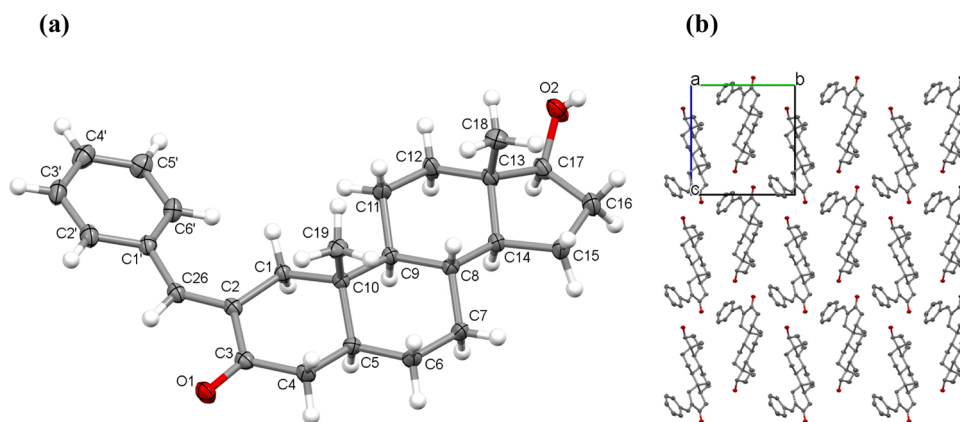
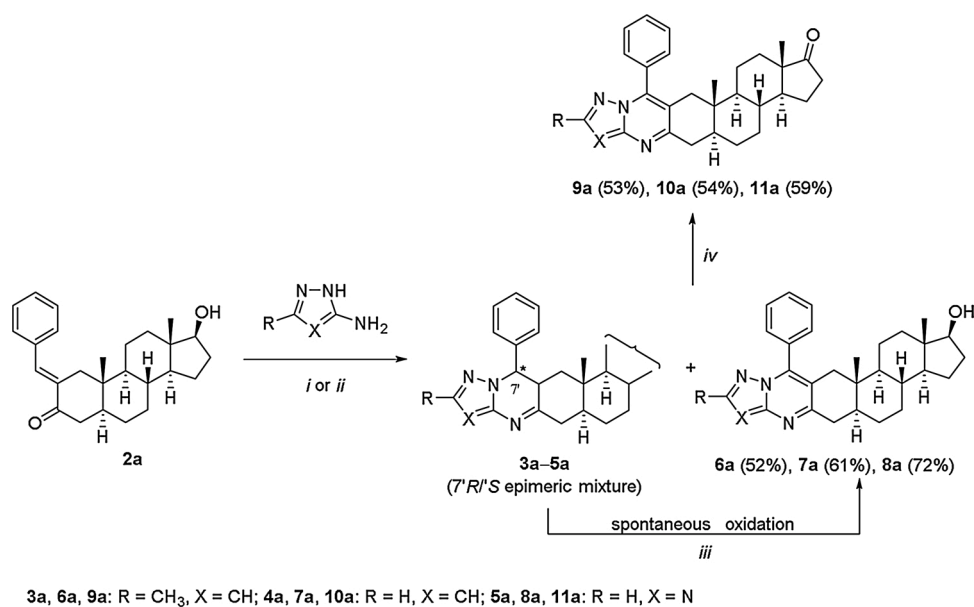


Fig. 2. Crystal structure of **2a** showing the (a) ORTEP representation of the molecule with atom numbering (displacement parameters are drawn at 50 % probability level) and (b) the packing arrangement of the molecules (without hydrogen atoms) viewed from crystallographic direction 'a'.



Scheme 1. Synthesis of pyrazolo[1,5-*a*]pyrimidines and triazolo[1,5-*a*]pyrimidines from 2-benzylidene derivative (**2a**) of DHT. *Reagents and conditions:* Azoles: 3AMP (R = CH₃, X = CH), 3AP (R = H, X = CH), 3AT (R = H, X = N); (i) *t*-BuOK, DMF, 140 °C, 45 min; (ii) KOH, DMF, 140 °C, 3 h; (iii) stirred in air, 25 °C, 24 h; (iv) Jones reagent, acetone, r.t., 30 min..

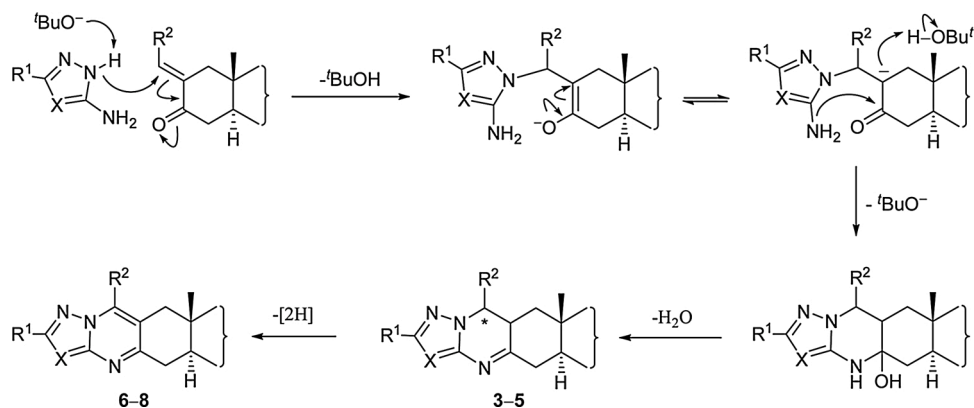


Fig. 3. Proposed mechanism for the formation of azolo[1,5-*a*]pyrimidines.

its unoxidized precursor as an inseparable mixture of two epimers **3a–5a**. Since the autooxidation also occurred during the reaction, the reaction mixtures were stirred for an additional 24 h at room temperature after conversion of the benzylidene derivative **2a** in order to complete the oxidation to **6a–8a**. The yields of the desired products were found to be the highest (**8a**, 72%) when 3AT was used for the cyclization, while only moderate yield (**6a**, 52 %) was obtained in case of 3AMP. During the reactions with pyrazole reagents, small amounts of unconverted starting material **2a** were also detected, suggesting the lower reactivity of these reagents compared to 3AT. Nevertheless, according to the TLC monitoring of the reaction mixtures, the moderate yields were not justified unless the formation of some polar by-product adhering to the silica gel reduced the yield of the desired compounds.

The presumed mechanism may provide an answer to the experimental findings (Fig. 3). Since the azole reagents are very weak acids, a strong base is needed (KOH or *t*-BuOK) to deprotonate the ring-N atom, so that the *aza*-Michael addition to the enone can occur more efficiently. The increase in reaction rate by using *t*-BuOK in a polar aprotic (DMF) instead of a polar protic solvent (EtOH or *n*-BuOH) can be explained by the higher basicity of *t*-BuOK under this condition, as the solvent can interact only with the potassium centre. The isolated yields of the desired products can be affected by the acidic strength of the azoles, as well as the tendency of the polar intermediate formed by heterocyclization to lose water (Fig. 3). The latter compound can reduce the yield of the azolo[1,5-*a*]pyrimidines as highly polar by-product.

In contrast to the spontaneous oxidation of the heterocyclic moiety of **3a–5a**, complete oxidation of the crude products with the Jones reagent in acetone affected both the dihydropyrimidine ring and the 17-OH group, and resulted in the corresponding heteroaromatic 17-keto derivative **9a–11a** in moderate yields (Scheme 1).

It is important to note that a one-pot three-component reaction of DHT, benzaldehyde (**1a**), and 3AP was also attempted [28], but these types of reactions were discarded due to long reaction times, purification difficulties, and similar product yields. The fact that α,β -enone intermediates may also be of pharmacological interest also supported the stepwise pathway.

Since the highest product yield was obtained when 3AT was applied for heterocyclization, the other (hetero)arylidene derivatives (**2b–f**, **2i**, **2j**) were converted to A-ring-fused triazolo[1,5-*a*]pyrimidines only using this reagent under the previously optimized conditions. According to the experimental results summarized in Table 2, in most of the cases the cyclization and subsequent spontaneous oxidation led to the desired products (**8b–e**, **8i–k**) in good yields (entries 1–4 and 6–8). However, 2,3-dichloro-5,6-dicyano-1,4-benzoquinone (DDQ) was required as mild oxidizing agent to convert **5f** (Fig. 3), which contains an electron-

withdrawing Cl atom on the benzene ring, to **8f** (entry 5). DDQ could also be used for other derivatives to accelerate the heteroaromatization, as oxidation occurred rapidly in dioxane under MW irradiation at 120 °C within 5 min. When the product mixture containing **5** and **8** of each reaction was treated with the Jones reagent as strong oxidizing agent, not only the dihydropyrimidine ring but also the 17 β -hydroxyl group was oxidized to a ketone to give derivatives **11** (Table 2).

The structure of all heterocyclic products was confirmed by 1D and 2D NMR as well as ESI-MS measurements. A comparison of the proton spectra of the 17-OH (**6a**, **7a**, **8**) and 17-keto derivatives (**9a**, **10a**, **11**) showed that the proton peaks of the angular C18 and C19 methyl groups were interchanged. Since 19-H₃ is in similar chemical environment for all compounds, the location of its peak does not change significantly, however, for 17-ones, the 18-H₃ protons are deshielded due to the strong electron-attracting effect of the carbonyl group, so that the singlet signal corresponding to these equivalent protons appears at a higher chemical shift. It can also be attributed to the presence of the carbonyl group in compounds **9a**, **10a** and **11**, that the multiplet peaks of the 16-H₂ protons are shifted downfield (2.08 and 2.45 ppm), separately from the signals of the other backbone protons. In the aliphatic region of the spectra, proton signals belonging to C1 and C4 with characteristic splitting can be observed. While the signals of 1-H₂ appear as two doublets with the same coupling constant due to the germinal coupling, 4-H₂ gives two doublet peaks because of both geminal coupling and coupling to a single proton on the adjacent C5 carbon atom. The spectrum of compounds **9a**, **10a** and **11** lacks the triplet of the 17-H proton characteristic of derivatives **6a**, **7a** and **8**, which proves that oxidation has occurred. The aromatic region of the spectrum of all compounds shows the signals of the protons on the pyrimidine ring, as well as a singlet of 2'-H for triazole derivatives **8** and **11**, two inter-coupling doublets of the 2'-H and 3'-H for unsubstituted pyrazoles **7a** and **10a** and a singlet of 3'-H for methylpyrazoles **6a** and **9a**. ¹H-¹³C correlations were performed based on 2D NMR measurements (HSQC and HMBC) of one representative of each pyrazolopyrimidine (**7a**) and triazolopyrimidine derivative (**8a**) (Supplementary Material, S-11 and S-13). It should be noted that for some derivatives, certain carbon atoms belonging to the condensed heterocycle were observed as weak signals in the ¹³C NMR (J MOD) spectra in spite of the high number of scans, presumably due to the long relaxation time of these carbon nuclei.

Crystal structure of **8j** was determined by single crystal X-ray diffraction. The molecule crystallized in the monoclinic crystal system in *P*₂₁ space group and the asymmetric unit contains two molecules and one dichloromethane solvent molecule. ORTEP representation together with atom numbering of the compound and the packing arrangements viewed from the crystallographic direction 'a' is depicted in Fig. 4. The

Table 2
Synthesis of A-ring-fused triazolo[1,5-*a*]pyrimidines of DHT.

Entry	Enone	R ¹	17-OH product	Yield (%) ^b	17=O product ^c	Yield (%) ^b
1	2b	<i>p</i> -CH ₃ C ₆ H ₄	8b	76	11b	62
2	2c	<i>m</i> -CH ₃ C ₆ H ₄	8c	77	11c	66
3	2d	<i>p</i> -MeO-C ₆ H ₄	8d	71	11d	59
4	2e	<i>p</i> -F-C ₆ H ₄	8e	73	11e	57
5	2f ^a	<i>p</i> -Cl-C ₆ H ₄	8f	65	11f	62
6	2i	furan-2-yl	8i	59	11i	55
7	2j	thiophen-2-yl	8j	62	11j	57
8	2k ^d	CH ₃	8k	69	11k	52

^a After the heterocyclization, DDQ was used to oxidize the heteroring.

^b After chromatographic purification.

^c Jones oxidation was performed not with the purified **8**, but with the crude product containing both **5** and **8**, of the heterocyclization.

^d Ref [21].

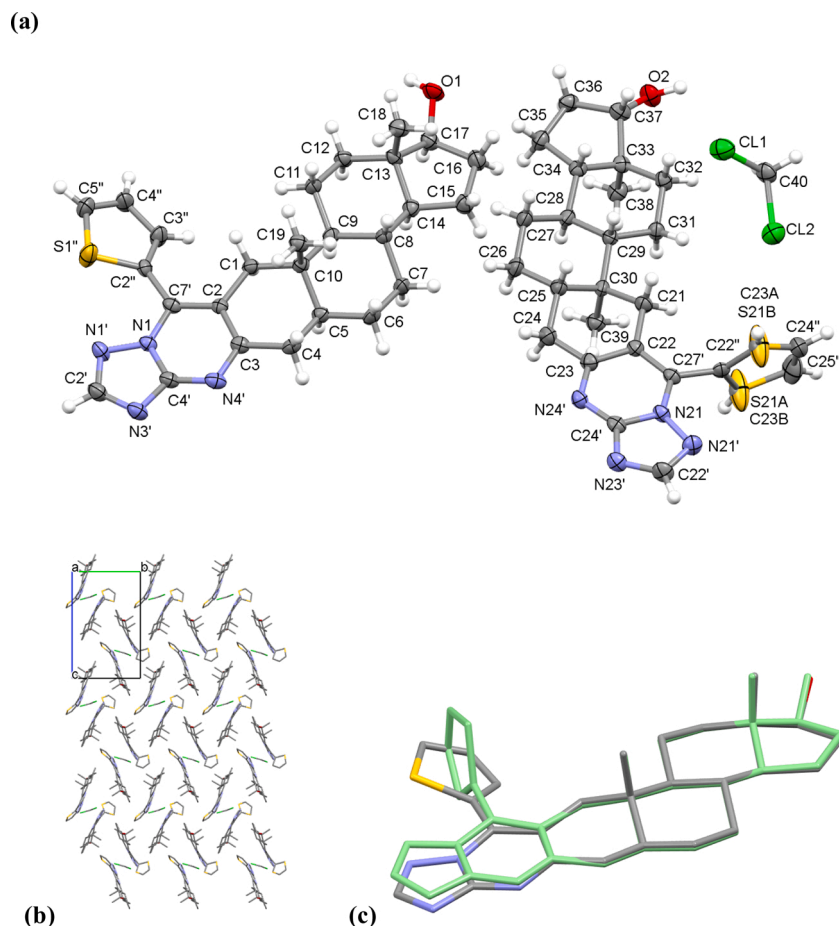


Fig. 4. Crystal structure of **8 j** showing the (a) ORTEP representation of the asymmetric unit with atom numbering (displacement parameters are drawn at 50 % probability level) and the (b) packing arrangement of the molecules (without hydrogen atoms) viewed from crystallographic direction 'a' and (c) overlay of the two molecules of the asymmetric unit (molecule 1 is coloured by element and molecule 2 is green).

unit cell containing four molecules is shown in **Fig. S4**, and the packing arrangements viewed from the 'a', 'b' and 'c' crystallographic directions are shown in **Fig. S5**. The two molecules of the asymmetric unit have different conformations. Overlay of the two structures in **Fig. 4c** clearly shows the different thiophene ring positions. Angles between thiophene and pyrimidine ring planes are 30.86° for molecule 1 and 83.47° for molecule 2. In case of molecule 2, the thiophene ring was found in two disordered positions where the S21 and C23 atoms are interchanged. The occupancy of the major component containing C23A and S21A was found to be 76 %, while the minor component containing C23B and S21B atoms is 24 %. The rotational freedom of this ring is due to the fact that it interacts only from one direction with a neighbour by C24'-H24'...O1, while this freedom was not found for molecule 1 where the thiophene ring is involved in two hydrogen bonds with C5''-H5''...O2 and C4''-H4''...Cl1 (**Fig. S6** and **Table S3**). Selected bond distances and angles are collected in **Tables S1** and **S2**. The packing of the molecules arranged by hydrogen bonds is shown in **Fig. S3** and the data of the secondary interactions are collected in **Table S3**. The dichloromethane molecules are placed in voids of 72.2 \AA^3 , which is 2.9 % of the unit cell volume.

2.2. The effect of steroids on AR transcriptional activity and viability of PCa cells

AR modulators are known to influence AR-dependent transcription; therefore, we examined the metribolone (R1881)-stimulated transcriptional activity of AR after 24 h treatment with our novel DHT-derivatives. Compounds were screened at three concentrations using

an AR-dependent reporter cell line, 22Rv1-ARE14, which was transfected with a reporter plasmid containing androgen response element (ARE) sequence and luciferase sequence [29].

The analysed library of novel A-ring modified DHT-derivatives comprised 9 α,β -enones (series 2), 18 triazolo[1,5-*a*]pyrimidines (series 8 and 11), and 4 pyrazolo[1,5-*a*]pyrimidines (6a, 7a, 9a, and 10a). As shown in **Table 3**, α,β -enones from series 2 belong to the most active compounds (6 compounds reduced R1881-stimulated AR transactivation to 50 % at 10 μM concentration) with *p*-chlorobenzylidene derivative **2f** being the most potent steroid, whereas thiophene-2-yl derivative **2j** and ethylidene derivative **2k** belong to the least potent α,β -enones. DHT-derivatives from other series were active only partially (9 compounds reduced activity to 75 % of control) and only 3 members (**8k**, **11k**, and **11i**) were completely inactive. It is obvious that heterocyclization of **2a** with 3AT reduced the antiandrogenic effect (**8a**). We also observed that the methylation of the pyrazolo[1,5-*a*]pyrimidine **7a** resulted in the less active derivative **6a**. The same tendency displayed also 17-keto pairs of pyrazolo[1,5-*a*]pyrimidines **9a** and **10a**. The antagonistic activity of compounds **2f** ($\text{IC}_{50} = 3.54 \mu\text{M}$) and **2a** ($\text{IC}_{50} = 6.92 \mu\text{M}$) reached up to single-digit micromolar values and showed to be comparable with values obtained for standards, i.e. galeterone ($\text{IC}_{50} = 5.82 \mu\text{M}$) and enzalutamide ($\text{IC}_{50} = 1.50 \mu\text{M}$) (Supplementary Material, S38-S41).

Antiproliferative properties of all novel steroids were tested in two AR-positive PCa cell lines (22Rv1-ARE14, C4-2), both originated from metastatic lesions. Resulting data are presented as residual viability at 10 μM compounds after 72 h of treatment compared to untreated control. Antiproliferative activities of the most potent derivative **2f**

Table 3

AR antagonistic activity and antiproliferative activity of novel DHT-derivatives.

Compound	Transcriptional AR activity (% ± SD) in 22Rv1-ARE14 after 24 h treatment ^a			Viability (% ± SD, 10 μM) after 72 h ^b		
	10 μM	2 μM	0.4 μM	22Rv1-ARE14	C4-2	
α,β-enones C17-OH group	2k	67.0 ± 3.9	98.2 ± 3.0	>100	87.0 ± 1.9	
	2a	36.4 ± 5.3	69.9 ± 0.9	81.3 ± 10.3	92.9 ± 1.1	92.8 ± 4.2
	2b	42.2 ± 5.6	73.6 ± 7.0	90.1 ± 7.9	91.2 ± 1.2	97.2 ± 2.8
	2c	49.3 ± 3.5	89.2 ± 2.7	100.0 ± 1.9	90.3 ± 1.9	> 100
	2d	38.9 ± 1.9	70.2 ± 5.5	91.0 ± 2.9	91.3 ± 1.9	93.7 ± 2.7
	2e	64.9 ± 4.2	86.1 ± 9.7	99.1 ± 9.9	80.2 ± 3.3	98.9 ± 2.2
	2f	34.2 ± 6.5	86.3 ± 4.6	>100	42.2 ± 12.8	74.0 ± 13.6
	2i	40.6 ± 7.3	78.7 ± 5.5	93.9 ± 9.1	> 100	91.9 ± 2.0
	2j	77.5 ± 8.7	>100	>100	> 100	57.4 ± 2.0
	8k	>100	>100	>100	87.5 ± 2.6	> 100
	8a	77.6 ± 2.2	89.5 ± 3.0	91.2 ± 3.9	76.7 ± 1.3	93.5 ± 1.3
triazolo[1,5- <i>a</i>]pyrimidines C17-OH group	8b	77.6 ± 3.0	86.1 ± 8.4	97.4 ± 4.0	70.8 ± 1.5	92.1 ± 1.9
	8c	86.1 ± 2.4	>100	>100	93.3 ± 1.2	94.2 ± 1.9
	8d	76.9 ± 1.5	91.6 ± 3.0	99.5 ± 4.8	91.1 ± 0.8	92.7 ± 1.6
	8e	86.7 ± 8.1	98.7 ± 2.2	98.1 ± 3.6	90.5 ± 2.1	88.4 ± 0.6
	8f	65.8 ± 5.2	94.3 ± 6.4	95.7 ± 4.1	94.1 ± 1.7	87.1 ± 4.0
	8i	67.1 ± 8.9	86.6 ± 3.7	97.9 ± 8.2	> 100	99.9 ± 2.5
	8j	59.9 ± 6.6	80.5 ± 8.6	97.5 ± 11.1	94.0 ± 2.2	90.9 ± 1.1
	11k	>100	96.7 ± 7.2	95.6 ± 8.3	> 100	97.1 ± 2.3
	11a	86.9 ± 6.7	87.0 ± 1.8	90.0 ± 9.9	96.9 ± 0.3	100.0 ± 3.6
	11b	68.7 ± 2.1	84.0 ± 7.2	100.4 ± 5.6	93.7 ± 1.8	97.3 ± 7.4
	triazolo[1,5- <i>a</i>]pyrimidines C17-keto group	11c	75.0 ± 4.6	82.0 ± 10.1	91.3 ± 0.5	88.6 ± 1.0
11d		74.2 ± 1.7	81.2 ± 2.8	84.6 ± 0.6	93.3 ± 1.9	96.5 ± 3.9
11e		93.1 ± 9.7	96.5 ± 2.1	98.3 ± 8.4	> 100	> 100
11f		67.8 ± 2.4	85.3 ± 2.7	96.7 ± 1.1	90.5 ± 0.8	97.3 ± 2.5
11i		>100	>100	>100	100.3 ± 2.0	99.7 ± 5.2
11j		88.6 ± 4.4	99.4 ± 7.4	>100	92.5 ± 1.0	> 100
6a		86.3 ± 4.4	>100	>100	> 100	99.1 ± 1.2
pyrazolo[1,5- <i>a</i>] pyrimidines	7a	69.9 ± 2.5	>100	>100	> 100	99.7 ± 1.5
	9a	82.2 ± 1.7	>100	>100	> 100	> 100
	10a	62.5 ± 4.8	92.1 ± 6.6	>100	> 100	> 100
	Enzalutamide	14.3 ± 0.9	42.7 ± 2.2	75.4 ± 1.5	94.5 ± 1.2	90.0 ± 2.1
Galeterone	34.6 ± 2.3	73.4 ± 2.9	92.4 ± 4.4	> 100	> 100	

^a Transcriptional activity normalized to signal of 1 nM R1881 = 100 %, measured at least in triplicate.

^b Viability of treated cells normalized to the viability of control cell treated with vehicle, measured at least in triplicate.

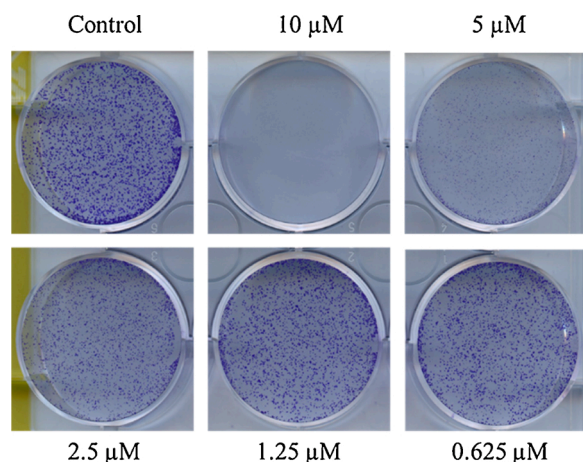


Fig. 5. Colony formation assay of 22Rv1-ARE14 PCA cells. Cells were treated with indicated concentrations of **2f** for 10 days. Medium was replaced by fresh medium with compound after 5 days. Representative result from two replicates is shown.

displayed mid-micromolar values ($GI_{50} = 9.9 \pm 1.8 \mu\text{M}$ and $15.7 \pm 4.4 \mu\text{M}$) in 22Rv1-ARE14 and C4-2, respectively. Compound **2f** showed to have higher antiproliferative activity than used standards with $GI_{50} > 50 \mu\text{M}$ (Supplementary Material, S42-S47).

The prolonged antiproliferative effect of **2f** was further evaluated by clonogenic assay in 22Rv1-ARE14 cells. As shown in Fig. 5, **2f** is able to significantly inhibit formation of cell colonies in a dose dependent manner after 10 days of treatment.

2.3. Effect of **2f** on the stability of AR and its cellular localization

Previous findings showed that steroidal agonists (testosterone, DHT and R1881) can induce thermal stabilisation of AR performed by cellular-thermal shift assay (CETSA) [30]. This technology was previously found to confirm binding of nonsteroidal AR-antagonists CCPI and enzalutamide [30,31], therefore we performed this assay for **2f** (Fig. 6). In control experiment, the incubation of C4-2 cells with 100 nM R1881 confirmed previously published increase in thermal stability of AR [30]. Similar results were obtained with multiple concentrations of **2f** that, in our opinion, originate from more extensive interaction with AR-LBD.

The AR becomes strongly concentrated in the nucleus in response to androgens [32] where it drives the transcription of target genes. Several AR modulators showed to block the transport and accumulation of AR to nucleus [33–35] as a result of its targeting. Therefore, we investigated the effect of **2f** on AR distribution in R1881-stimulated cells. As shown in Fig. 7, **2f** and galeterone markedly decreased the transport of AR to the nucleus in comparison to androgen-activated cells. While AR remained in cytosol upon the treatment of cells with **2f**, galeterone induced also partial AR degradation (see densitometric analysis).

2.4. Molecular docking of DHT derivative **2f** to AR-LBD

The AR contains a narrow nonpolar active site with two hydrogen-bonding capacities: arginine (R752) towards carbonyl group on the A-ring, while threonine (T877) and asparagine (N705) towards the hydroxyl group on the D-ring of DHT. To confirm the location of ligand **2f** within the AR's cavity, the flexible docking study was performed [10]. Very importantly, candidate compound **2f** showed similar interactions with AR binding site as DHT. This basic motif allows binding of **2f** to the

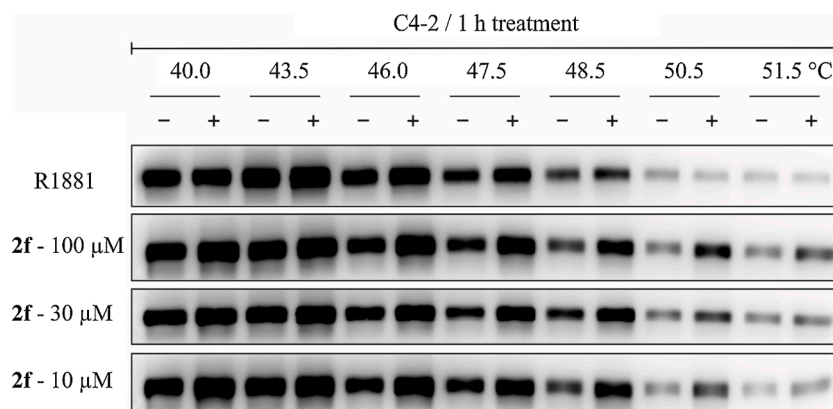


Fig. 6. Western blots showing protein level of AR (soluble fraction) after indicated heat shocks of C4-2 cells after 1 h treatment in absence (-) or presence (+) of 100 nM R1881 or **2f** in different concentrations.

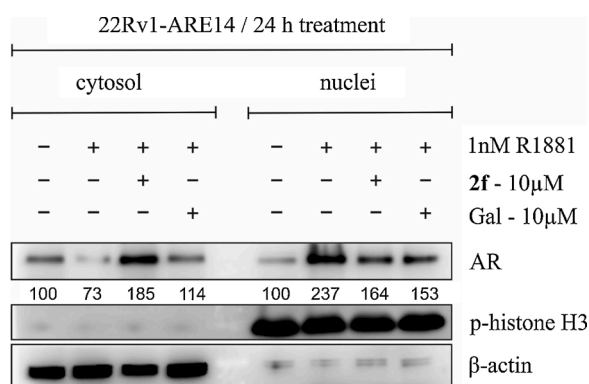


Fig. 7. Western blotting analysis showing AR distribution in 22Rv1-ARE14 cells. The cells were cultivated in CSS medium for 24 h and then treated with 1 nM R1881 alone or in combination with **2f** or galeterone (Gal) for additional 24 h. Cellular fractions were isolated using the Qproteome Cell Compartment Kit (Qiagen) and subjected for immunoblot analysis of appropriate proteins. Phosphorylated histone H3 and β -actin levels were used as controls of equal protein loading and quality of separation, respectively. Quantification was performed using Multigaugue 3.0 software. Representative result from two replicates is shown.

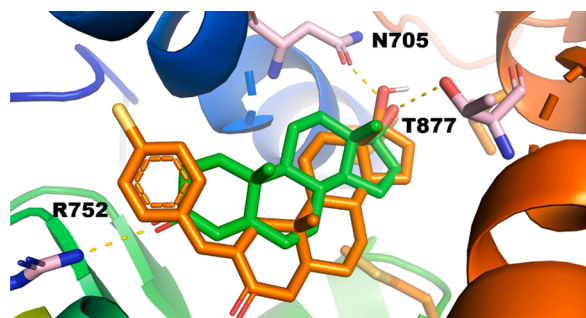


Fig. 8. Detailed view of the active site of the AR (PDBID:2PIV) with DHT as natural ligand (green compound, binding energy dG -10.9 kcal/mol) and candidate compound **2f** (orange, binding energy dG Vina -12.7 kcal/mol). Hydrogen bonds (depicted as yellow dashed lines) can be observed between compound **2f** and amino acids N705 and T877, similarly to DHT, that also makes the hydrogen bond with the amino acid R752.

same hydrogen bonds to arginine (R752) and asparagine (N705) as template (Fig. 8). Candidate compound **2f** showed stronger binding energy (dG Vina -12.7 kcal/mol,) in comparison with the natural ligand DHT (dG Vina -10.9 kcal/mol).

2.5. Effects of **2f** on the expression of AR-regulated targets

We showed that compound **2f** is able to reduce AR-transcriptional activity in a dose-dependent manner and to inhibit colony formation of studied PCa cell lines. We further analysed whether **2f** can affect the protein expression of well-known AR transcriptional targets, namely PSA and Nkx3.1 in treated 22Rv1 and C4-2 cells. Immunoblotting analysis (Fig. 9) revealed that protein expression of AR remained unchanged (both full length AR (FL) and V7-splice variant in 22Rv1-ARE14 and predominant full length AR in C4-2), while expression of PSA and Nkx3.1 decreased in dose-dependent manner compared to control, R1881-stimulated cells. This trend is in agreement with luciferase AR-transcriptional assay and is comparable with results observed for galeterone. Moreover, we did not detect the cleaved PARP usually indicating ongoing apoptosis that corresponds with mild cytotoxicity of investigated steroids.

3. Conclusions

A-ring-fused pyrazolo[1,5-*a*]pyrimidine and triazolo[1,5-*a*]pyrimidine derivatives of DHT were efficiently prepared in two steps. Claisen-Schmidt condensation of the steroid precursor with variously substituted aldehydes led to the regio- and stereoselective formation of α,β -unsaturated ketones, which underwent cyclization with 3AT, 3AP and 3AMP, respectively, as binucleophilic reagents. The heterocyclic products were obtained in good yields by spontaneous or induced oxidation.

In addition to the solution phase NMR analysis of the products, the structures of compounds **2a** and **8j** were determined by single crystal X-ray diffraction and both were found to crystallize in the monoclinic crystal system at $P2_1$ space group. In crystal **2a**, the phenyl ring was found to be planar to the DHT part of the molecule. In case of **8j**, the asymmetric unit of the crystal contains two molecules and one CH_2Cl_2 solvent molecule. The thiophene ring is in plane with the DHT rings in one of the molecules, while it turns to almost perpendicular to the DHT ring planes in the second molecule and it occupies two disordered positions. Differences in freedom of rotation can be traced back to secondary interactions with neighbouring molecules.

Our biological experiments revealed us that mainly substituted α,β -enones from series **2** inhibited R1881-stimulated AR transactivation in micromolar concentrations. Candidate compound **2f** showed to interact with the AR in cells and to reduce its transport to the nucleus that resulted in the suppression of expression of AR-regulated proteins observed in androgen-stimulated PCa cell lines. Moreover, we performed a flexible docking study to describe the proposed binding mode of **2f** in the AR-LBD cavity.

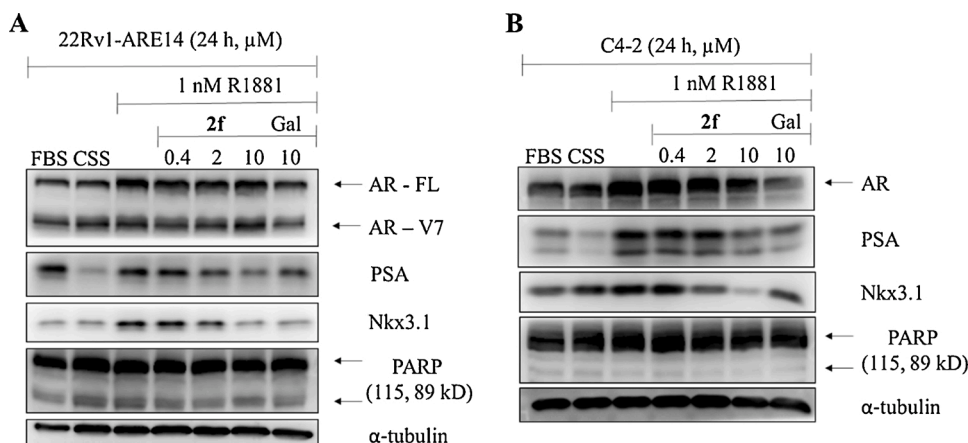


Fig. 9. Western blotting analysis of AR-regulated proteins in treated 22Rv1-ARE14 and C4-2 cell lines. In 22Rv1-ARE14, expression of both full length AR (FL) and V7-splice variant is shown, whereas in C4-2 only predominant full length AR is shown. The cells were deprived of androgens (cultivated in CSS medium) for 24 h and then treated with 1 nM R1881 alone or in combination with different concentrations of 2f or galeterone for 24 h. Alpha-tubulin was control of equal protein loading. Representative result from two replicates is shown.

4. Experimental

4.1. General

Chemicals, reagents and solvents were purchased from commercial suppliers (Sigma-Aldrich, TCI and Alfa Aesar) and used without further purification. Melting points (Mp) were determined on an SRS Optimelt digital apparatus and are uncorrected. For MW-assisted syntheses, a CEM Discover SP laboratory MW reactor was used with a max. power of 200 W (running a dynamic control program). Elementary analysis data were obtained with a PerkinElmer CHN analyzer model 2400. The transformations were monitored by TLC using 0.25 mm thick Kieselgel-G plates (Si 254 F, Merck). The compound spots were detected by spraying with 5 % phosphomolybdic acid in 50 % aqueous phosphoric acid. Flash chromatographic purifications were carried out on silica gel 60, 40–63 μm (Merck). NMR spectra were recorded with a Bruker DRX 500 instrument at room temperature in CDCl_3 using residual solvent signal as an internal reference. Chemical shifts are reported in ppm (δ scale), and coupling constants (J) are given in Hz. Multiplicities of the ^1H signals are indicated as a singlet (s), a broad singlet (bs), a doublet (d), a double doublet (dd), a triplet (t), or a multiplet (m). ^{13}C NMR spectra are ^1H -decoupled and the J-MOD pulse sequence was used for multiplicity editing. In this spin-echo type experiment, the signal intensity is modulated by the different coupling constants J of carbons depending on the number of attached protons. Both protonated and unprotonated carbons can be detected (CH_3 and CH carbons appear as positive signals, while CH_2 and C carbons as negative signals).

Automated flow injection analyses were performed with an HPLC/MSD system. System accessories: a micro-well plate autoinjector, an Agilent 1100 micro vacuum degasser, a quaternary pump, and a 1946A MSD equipped with an electrospray ion source (ESI) operated in positive ion mode. ESI parameters were: nebulizing gas N_2 , at 35 psi; drying gas N_2 , at 350 $^\circ\text{C}$ and 12 L/min; capillary voltage 3000 V; fragmentor voltage 70 V. The MSD was operated with a mass range of m/z 60 – 620 in scan mode. Samples (0.2 μL) were injected directly into the solvent flow (0.3 mL/min) of acetonitrile/ H_2O = 70:30 (v/v) with the simultaneous addition of 0.1 % formic acid with an automated needle wash. Agilent LC/MSD Chemstation was used as software to control the system.

4.2. Chemistry

4.2.1. General procedure for the Claisen-Schmidt condensation of DHT with different (hetero)aryl aldehydes (1a–j)

DHT (871 mg, 3 mmol) and KOH (281 mg, 5 mmol) were dissolved in absolute EtOH (15 mL) and the mixture was stirred until a homogeneous solution was produced. To this, arylaldehyde (1a–j, 3.60 mmol, 1.20 equiv.) was added and the mixture was stirred for a given time at room

temperature (1a–e) or at 0 $^\circ\text{C}$ (1f–j) achieved by an ice bath. After completion of the reaction, the mixture was poured into ice cold water and neutralized with a diluted solution of HCl. The resulting precipitate was filtered off, washed with water, and dried. The crude product was purified by column chromatography (silica gel, CH_2Cl_2 to EtOAc/ CH_2Cl_2 = 5:95 using gradient elution).

4.2.1.1. 17 β -Hydroxy-2-benzylidene-5 α -androstan-3-one (2a). According to Section 4.2.1., benzaldehyde (1a, 370 μL) was used for the reaction. The reaction time was 3 h and 2a was obtained as a white solid. This reaction was repeated several times to obtain a sufficient amount of starting material. Yield: 1.05 g (92 %); Mp 185–187 $^\circ\text{C}$; ^1H NMR (CDCl_3 , 500 MHz): δ 0.73 (s, 3H, 18- H_3), 0.80 (s, 3H, 19- H_3), 0.85–1.02 (overlapping m, 3 H), 1.11 (m, 1 H), 1.22–1.50 (overlapping m, 7 H), 1.58–1.63 (overlapping m, 2 H), 1.71–1.85 (overlapping m, 3 H), 2.07 (m, 1 H), 2.19 (d, 1H, J = 15.6 Hz, one of 1- H_2), 2.24 (dd, 1H, J = 18.6 Hz, J = 13.2 Hz, one of 4- H_2), 2.46 (dd, 1H, J = 18.6 Hz, J = 5.2 Hz, the other of 4- H_2), 3.12 (d, 1H, J = 15.6 Hz, the other of 1- H_2), 3.65 (t, 1H, J = 8.6 Hz, 17-H), 7.33 (m, 1 H), 7.36–7.42 (overlapping m, 4 H), 7.56 (s, 1H, 2a-H); ^{13}C NMR (CDCl_3 , 125 MHz): δ 11.2 (C-18), 12.0 (C-19), 21.2 (CH_2), 23.5 (CH_2), 28.7 (CH_2), 30.7 (CH_2), 31.2 (CH_2), 35.6 (CH), 36.2 (C-10), 36.8 (CH_2), 42.0 (CH_2), 42.6 (CH), 43.0 (2C, CH_2 and C-13), 51.1 (CH), 53.9 (CH), 82.0 (C-17), 128.5 (2C, C-2' and C-6'), 128.7 (C-4'), 130.4 (2C, C-3' and C-5'), 135.4 and 135.8 (C-1' and C-2) 137.4 (C-2a), 201.6 (C-3); ESI-MS 379 [$\text{M}+\text{H}$] $^+$; Anal. Calcd. for $\text{C}_{26}\text{H}_{34}\text{O}_2$ C 82.49; H 9.05. Found C 82.57; H 9.12.

4.2.1.2. 17 β -Hydroxy-2-(4-methyl)benzylidene-5 α -androstan-3-one (2b). According to Section 4.2.1., *p*-tolualdehyde (1b, 420 μL) was used for the reaction. The reaction time was 4 h, and 2b was obtained as a white solid. Yield: 1.03 g (87 %); Mp 202–205 $^\circ\text{C}$; ^1H NMR (CDCl_3 , 500 MHz): δ 0.73 (s, 3H, 18- H_3), 0.79 (s, 3H, 19- H_3), 0.85–1.02 (overlapping m, 3 H), 1.12 (m, 1 H), 1.21–1.50 (overlapping m, 7 H), 1.58–1.64 (overlapping m, 2 H), 1.70–1.85 (overlapping m, 3 H), 2.07 (m, 1 H), 2.19 (dd, 1H, J = 15.7 Hz, J = 2.5 one of 1- H_2), 2.22 (dd, 1H, J = 18.6 Hz, J = 13.0 Hz, one of 4- H_2), 2.37 (s, 3H, 4'- CH_3), 2.45 (dd, 1H, J = 18.6 Hz, J = 5.3 Hz, the other of 4- H_2), 3.11 (d, 1H, J = 15.7 Hz, the other of 1- H_2), 3.66 (t, 1H, J = 8.6 Hz, 17-H), 7.21 (d, 2H, J = 8.1 Hz, 3'-H and 5'-H), 7.30 (d, 2H, J = 8.1 Hz, 2'-H and 6'-H), 7.55 (s, 1H, 2a-H); ^{13}C NMR (CDCl_3 , 125 MHz): δ 11.2 (C-18), 12.0 (C-19), 21.2 (CH_2), 21.5 (4'- CH_3), 23.6 (CH_2), 28.7 (CH_2), 30.7 (CH_2), 31.2 (CH_2), 35.6 (CH), 36.2 (C-10), 36.8 (CH_2), 42.1 (CH_2), 42.6 (CH), 42.9 (CH_2), 43.0 (C-13), 51.1 (CH), 53.9 (CH), 82.0 (C-17), 129.3 (2C, C-2' and C-6'), 130.6 (2C, C-3' and C-5'), 133.0 (C-1'), 134.6 (C-4'), 137.6 (C-2a), 139.0 (C-2) 201.6 (C-3); ESI-MS 393 [$\text{M}+\text{H}$] $^+$; Anal. Calcd. for $\text{C}_{27}\text{H}_{36}\text{O}_2$ C 82.61; H 9.24. Found C 82.47; H 9.08.

4.2.1.3. 17 β -Hydroxy-2-(3-methyl)benzylidene-5 α -androstan-3-one (2c). According to Section 4.2.1., *m*-tolualdehyde (**1c**, 420 μ L) was used for the reaction. The reaction time was 4 h, and **2c** was obtained as a white solid. Yield: 1.05 g (89 %); Mp 145–147 °C; $^1\text{H NMR}$ (CDCl_3 , 500 MHz): δ 0.73 (s, 3H, 18-H₃), 0.80 (s, 3H, 19-H₃), 0.86–1.02 (overlapping m, 3 H), 1.12 (m, 1 H), 1.22–1.50 (overlapping m, 7 H), 1.58–1.65 (overlapping m, 2 H), 1.71–1.85 (overlapping m, 3 H), 2.07 (m, 1 H), 2.18 (d, 1H, J = 15.7 Hz, one of 1-H₂), 2.24 (dd, 1H, J = 18.6 Hz, J = 13.2 Hz, one of 4-H₂), 2.37 (s, 3H, 3'-CH₃), 2.45 (dd, 1H, J = 18.6 Hz, J = 5.3 Hz, the other of 4-H₂), 3.12 (d, 1H, J = 15.7 Hz, the other of 1-H₂), 3.65 (t, 1H, J = 8.6 Hz, 17-H), 7.14 (d, 1H, J = 7.6 Hz, 4'-H), 7.20 (m, 2H, 2'-H and 6'-H), 7.29 (t-like m, 1H, 5'-H), 7.53 (s, 1H, 2a-H); $^{13}\text{C NMR}$ (CDCl_3 , 125 MHz): δ 11.2 (C-18), 12.0 (C-19), 21.2 (CH₂), 21.6 (3'-CH₃), 23.6 (CH₂), 28.7 (CH₂), 30.7 (CH₂), 31.2 (CH₂), 35.6 (CH), 36.2 (C-10), 36.8 (CH₂), 42.0 (CH₂), 42.7 (CH), 42.9 (CH₂), 43.0 (C-13), 51.1 (CH), 53.9 (CH), 82.0 (C-17), 127.3, 128.4, 129.5 and 131.4 (C-2', C-4', C-5' and C-6'), 135.3 (C-1'), 135.8 (C-2), 137.7 (C-2a), 138.2 (C-3'), 201.6 (C-3); ESI-MS 393 [M+H]⁺; Anal. Calcd. for C₂₇H₃₆O₂ C 82.61; H 9.24. Found C 82.70; H 9.28.

4.2.1.4. 17 β -Hydroxy-2-(4-methoxy)benzylidene-5 α -androstan-3-one (2d). According to Section 4.2.1., *p*-anisaldehyde (**1d**, 440 μ L) was used for the reaction. The reaction time was 4 h, and **2d** was obtained as a white solid. Yield: 1.09 g (89 %); Mp 186–188 °C; $^1\text{H NMR}$ (CDCl_3 , 500 MHz): δ 0.74 (s, 3H, 18-H₃), 0.80 (s, 3H, 19-H₃), 0.86–1.02 (overlapping m, 3 H), 1.13 (m, 1 H), 1.20–1.50 (overlapping m, 7 H), 1.58–1.67 (overlapping m, 2 H), 1.71–1.87 (overlapping m, 3 H), 2.07 (m, 1 H), 2.22 (m, 2H, one of 1-H₂ and one of 4-H₂), 2.45 (dd, 1H, J = 18.8 Hz, J = 5.3 Hz, the other of 4-H₂), 3.08 (d, 1H, J = 15.7 Hz, the other of 1-H₂), 3.66 (t, 1H, J = 8.6 Hz, 17-H), 3.84 (s, 3H, 4'-OCH₃), 6.93 (d, 2H, J = 8.8 Hz, 3'-H and 5'-H), 7.38 (d, 2H, J = 8.8 Hz, 2'-H and 6'-H), 7.55 (s, 1H, 2a-H); $^{13}\text{C NMR}$ (CDCl_3 , 125 MHz): δ 11.2 (C-18), 12.1 (C-19), 21.2 (CH₂), 23.6 (CH₂), 28.7 (CH₂), 30.7 (CH₂), 31.2 (CH₂), 35.6 (CH), 36.1 (C-10), 36.9 (CH₂), 42.2 (CH₂), 42.4 (CH), 42.8 (CH₂), 43.0 (C-13), 51.1 (CH), 54.0 (CH), 55.5 (4'-OCH₃), 82.0 (C-17), 114.1 (2C, C-3' and C-5'), 128.4 (C-1'), 132.4 (2C, C-2' and C-6'), 133.3 (C-2), 137.6 (C-2a), 160.1 (C-4') 201.4 (C-3); ESI-MS 409 [M+H]⁺; Anal. Calcd. for C₂₇H₃₆O₃ C 79.37; H 8.88. Found C 79.25; H 9.01.

4.2.1.5. 17 β -Hydroxy-2-(4-fluoro)benzylidene-5 α -androstan-3-one (2e). According to Section 4.2.1., 4-fluorobenzaldehyde (**1e**, 390 μ L) was used for the reaction. The reaction time was 3 h, and **2e** was obtained as a white solid. Yield: 1.08 g (91 %); Mp 107–111 °C; $^1\text{H NMR}$ (CDCl_3 , 500 MHz): δ 0.74 (s, 3H, 18-H₃), 0.81 (s, 3H, 19-H₃), 0.85–1.02 (overlapping m, 3 H), 1.12 (m, 1 H), 1.22–1.51 (overlapping m, 7 H), 1.57–1.65 (overlapping m, 2 H), 1.72–1.86 (overlapping m, 3 H), 2.07 (m, 1 H), 2.17 (d, 1H, J = 15.7 Hz, one of 1-H₂), 2.24 (dd, 1H, J = 18.6 Hz, J = 13.2 Hz, one of 4-H₂), 2.45 (dd, 1H, J = 18.6 Hz, J = 5.3 Hz, the other of 4-H₂), 3.05 (d, 1H, J = 15.7 Hz, the other of 1-H₂), 3.66 (t, 1H, J = 8.6 Hz, 17-H), 7.09 (m, 2H, J = 8.1 Hz, 3'-H and 5'-H), 7.36 (m, 2H, 2'-H and 6'-H), 7.51 (s, 1H, 2a-H); $^{13}\text{C NMR}$ (CDCl_3 , 125 MHz): δ 11.2 (C-18), 12.1 (C-19), 21.2 (CH₂), 23.6 (CH₂), 28.7 (CH₂), 30.8 (CH₂), 31.3 (CH₂), 35.7 (CH), 36.3 (C-10), 36.9 (CH₂), 42.0 (CH₂), 42.7 (CH), 42.9 (CH₂), 43.1 (C-13), 51.2 (CH), 54.0 (CH), 82.0 (C-17), 115.7 (d, 2C, J = 21.5 Hz, C-3' and C-5'), 132.0 (C-1'), 132.3 (d, 2C, J = 8.3 Hz, C-2' and C-6'), 135.3 (C-2), 136.2 (C-2a), 161.8 (d, J = 250.0 Hz, C-4'), 201.3 (C-3); ESI-MS 397 [M+H]⁺; Anal. Calcd. for C₂₆H₃₃FO₂ C 78.75; H 8.39. Found C 78.84; H 8.29.

4.2.1.6. 17 β -Hydroxy-2-(4-chloro)benzylidene-5 α -androstan-3-one (2f). According to Section 4.2.1., 4-chlorobenzaldehyde (**1f**, 506 mg) was used for the reaction. The reaction time was 3 h, and **2f** was obtained as a white solid. Yield: 1.12 g (90 %); Mp 195–197 °C; $^1\text{H NMR}$ (CDCl_3 , 500 MHz): δ 0.73 (s, 3H, 18-H₃), 0.80 (s, 3H, 19-H₃), 0.85–1.01 (overlapping m, 3 H), 1.11 (m, 1 H), 1.22–1.50 (overlapping m, 7 H), 1.56–1.65

(overlapping m, 2 H), 1.72–1.86 (overlapping m, 3 H), 2.06 (m, 1 H), 2.22 (d, 1H, J = 15.7 Hz, one of 1-H₂), 2.22 (dd, 1H, J = 18.7 Hz, J = 13.3 Hz, one of 4-H₂), 2.45 (dd, 1H, J = 18.7 Hz, J = 5.3 Hz, the other of 4-H₂), 3.03 (d, 1H, J = 15.7 Hz, the other of 1-H₂), 3.65 (t, 1H, J = 8.6 Hz, 17-H), 7.30 (d, 2H, J = 8.6 Hz, 3'-H and 5'-H), 7.37 (d, 2H, J = 8.6 Hz, 2'-H and 6'-H), 7.48 (s, 1H, 2a-H); $^{13}\text{C NMR}$ (CDCl_3 , 125 MHz): δ 11.2 (C-18), 12.0 (C-19), 21.2 (CH₂), 23.5 (CH₂), 28.7 (CH₂), 30.7 (CH₂), 31.2 (CH₂), 35.6 (CH), 36.3 (C-10), 36.8 (CH₂), 42.0 (CH₂), 42.6 (CH), 42.9 (CH₂), 43.0 (C-13), 51.1 (CH), 53.9 (CH), 82.0 (C-17), 128.8 (2C, C-3' and C-5'), 131.6 (2C, C-2' and C-6'), 134.2 (C-4'), 134.6 (C-1'), 136.0 (C-2), 136.0 (C-2a), 201.4 (C-3); ESI-MS 413 [M+H]⁺; Anal. Calcd. for C₂₆H₃₃ClO₂ C 75.61; H 8.05. Found C 75.49; H 7.92.

4.2.1.7. 17 β -Hydroxy-2-(2-furylidene)-5 α -androstan-3-one (2i). According to Section 4.2.1., furfural (**1i**, 300 μ L) was used for the reaction. The reaction time was 3 h, and **2i** was obtained as a pale yellow solid. Yield: 926 mg (84 %); Mp 197–199 °C; $^1\text{H NMR}$ (CDCl_3 , 500 MHz): δ 0.77 (s, 3H, 18-H₃), 0.86 (s, 3H, 19-H₃), 0.88–1.04 (overlapping m, 3 H), 1.16 (m, 1 H), 1.22–1.33 (overlapping m, 2 H), 1.37–1.50 (overlapping m, 4 H), 1.62 (m, 1 H), 1.72–1.80 (overlapping m, 3 H), 1.90 (m, 1 H), 2.08 (m, 1 H), 2.18 (d, 1H, J = 17.5 Hz, one of 1-H₂), 2.22 (dd, 1H, J = 19.0 Hz, J = 13.2 Hz, one of 4-H₂), 2.41 (dd, 1H, J = 19.0 Hz, J = 5.4 Hz, the other of 4-H₂), 3.25 (d, 1H, J = 17.5 Hz, the other of 1-H₂), 3.67 (t, 1H, J = 8.6 Hz, 17-H), 6.51 (dd, 1H, J = 3.4 Hz, J = 1.8 Hz, 4'-H), 6.62 (d, 1H, J = 3.4 Hz, 3'-H), 7.40 (d, 1H, J = 1.8 Hz, 5'-H), 7.57 (s, 1H, 2a-H); $^{13}\text{C NMR}$ (CDCl_3 , 125 MHz): δ 11.2 (C-18), 12.4 (C-19), 21.3 (CH₂), 23.6 (CH₂), 28.7 (CH₂), 30.8 (CH₂), 31.3 (CH₂), 35.6 (C-10), 35.7 (CH), 37.0 (CH₂), 42.1 (CH), 42.2 (CH₂), 42.5 (CH₂), 43.1 (C-13), 51.2 (CH), 54.1 (CH), 82.1 (C-17), 112.4 (C-3'), 116.3 (C-4'), 124.3 (C-2a), 131.9 (C-2), 144.8 (C-5'), 152.6 (C-2'), 200.3 (C-3); ESI-MS 369 [M+H]⁺; Anal. Calcd. for C₂₄H₃₂O₃ C 78.22; H 8.75. Found C 78.11; H 8.82.

4.2.1.8. 17 β -Hydroxy-2-(2-thiophenylidene)-5 α -androstan-3-one (2j). According to Section 4.2.1., thiophene-2-carbaldehyde (**1j**, 340 μ L) was used for the reaction. The reaction time was 3 h, and **2j** was obtained as a pale yellow solid. Yield: 962 mg (83 %); Mp 216–219 °C; $^1\text{H NMR}$ (CDCl_3 , 500 MHz): δ 0.77 (s, 3H, 18-H₃), 0.86 (s, 3H, 19-H₃), 0.90–1.04 (overlapping m, 3 H), 1.18 (m, 1 H), 1.23–1.33 (overlapping m, 2 H), 1.37–1.53 (overlapping m, 4 H), 1.63 (m, 1 H), 1.72–1.82 (overlapping m, 3 H), 1.91 (m, 1 H), 2.08 (m, 1 H), 2.18 (d, 1H, J = 16.5 Hz, one of 1-H₂), 2.24 (dd, 1H, J = 19.1 Hz, J = 13.1 Hz, one of 4-H₂), 2.43 (dd, 1H, J = 19.1 Hz, J = 5.4 Hz, the other of 4-H₂), 3.11 (d, 1H, J = 16.5 Hz, the other of 1-H₂), 3.68 (t, 1H, J = 8.6 Hz, 17-H), 7.14 (dd, 1H, J = 5.1 Hz, J = 3.7 Hz, 4'-H), 7.35 (d, 1H, J = 3.7 Hz, 3'-H), 7.54 (d, 1H, J = 5.1 Hz, 5'-H), 7.84 (s, 1H, 2a-H); $^{13}\text{C NMR}$ (CDCl_3 , 125 MHz): δ 11.2 (C-18), 12.5 (C-19), 21.3 (CH₂), 23.6 (CH₂), 28.7 (CH₂), 30.7 (CH₂), 31.2 (CH₂), 35.6 (CH), 35.9 (C-10), 36.9 (CH₂), 41.8 (CH), 42.4 (CH₂), 42.6 (CH₂), 43.1 (C-13), 51.1 (CH), 54.0 (CH), 82.0 (C-17), 127.8 (C-4'), 130.3 (C-2a), 130.7 (C-3'), 131.5 (C-2'), 133.6 (C-5'), 139.3 (C-2), 200.3 (C-3); ESI-MS 385 [M+H]⁺; Anal. Calcd. for C₂₄H₃₂O₂S C 74.96; H 8.39. Found C 74.84; H 8.27.

4.2.2. General procedure for the synthesis of A-ring-fused pyrazolo[1,5-a]pyrimidine (**6a**, **7a**) and triazolo[1,5-a]pyrimidine derivatives (**8a–f**, **8i–k**) of DHT

1 mmol arylidene (**2a–f**), heteroarylidene (**2i**, **2j**) or methylidene derivative (**2k**) [21], binucleophilic reagent (3-amino-5-methylpyrazole - 3AMP, 3-aminopyrazole - 3AP or 3-aminotriazole - 3AT, 2 equiv.) and *t*-BuOK (224 mg, 2 equiv.) were dissolved in DMF (10 mL) and the mixture was stirred at 140 °C for 45 min. After complete conversion of the starting material, the mixture was stirred for another 24 h at room temperature, while spontaneous oxidation of the heteroring occurred in most of the cases. During work-up, the mixture was poured into water, neutralized with diluted HCl and extracted with CH₂Cl₂ (3 × 10 mL). The combined organic layer was washed with water (2 × 20 mL) and

brine (20 mL), dried over anhydrous Na₂SO₄ and the solvent was evaporated *in vacuo*. The crude product was purified by column chromatography except in the reaction of **2f** with 3AT, where oxidation of the heteroring with DDQ was needed. Thus, in this latter case, the residue was dissolved in 1,4-dioxane (10 mL) and DDQ (499 mg, 1.1 equiv.) was added. The mixture was irradiated in a closed vessel at 120 °C for 5 min, then poured into ice-cold water. NH₄Cl was added and the resulting precipitate was filtered off and dried. The crude product was purified by column chromatography.

4.2.2.1. 17β-Hydroxy-2'-methyl-7-phenylpyrazolo[1,5-a]pyrimidino [5',6':3,2]-5α-androstane (6a). Substrate: **2a** (379 mg); Reagent: 3AMP (194 mg). For purification of the crude product, EtOAc/CH₂Cl₂ = 20:80 eluent was used. Yield: 237 mg (52 %, off white solid); Mp 259–261 °C; ¹H NMR (CDCl₃, 500 MHz): δ 0.71 (s, 3H, 18-H₃), 0.74 (s, 3H, 19-H₃), 0.86–1.04 (overlapping m, 4 H), 1.23–1.45 (overlapping m, 6 H), 1.58–1.76 (overlapping m, 5 H), 2.05 (m, 1 H), 2.18 (d, 1H, *J* = 16.0 Hz, 1α-H), 2.41 (s, 3H, 2'-CH₃), 2.56 (d, 1H, *J* = 16.0 Hz, 1β-H), 2.72 (dd, 1H, *J* = 18.9 Hz, *J* = 12.6 Hz, 4β-H), 3.03 (dd, 1H, *J* = 18.9 Hz, *J* = 5.6 Hz, 4α-H), 3.61 (t, 1H, *J* = 8.6 Hz, 17α-H), 6.40 (d, 1H, *J* = 2.4 Hz, 3'-H), 7.44 (bs, 2H, 2''-H and 6''-H), 7.53–7.59 (m, 3H, 3''-H, 4''-H and 5''-H); ¹³C NMR (CDCl₃, 125 MHz): δ 11.1 (C-18), 11.7 (C-19), 14.9 (2'-CH₃), 20.8 (C-11), 23.4 (C-15), 28.5 (C-6), 30.5 (C-16), 31.1 (C-7), 35.3 (C-10), 35.6 (C-8), 36.6 (C-4), 37.1 (C-12), 40.0 (C-1), 41.6 (C-5), 42.8 (C-13), 50.9 (C-14), 53.5 (C-9), 81.8 (C-17), 94.1 (C-3'), 114.1 (C-2), 128.9 (2C) and 129.3 (2C): C-2'', C-6'', C-3'' and C-5'', 129.9 (C-4''), 130.5 (C-4''), 144.4 (C), 148.3 (C), 154.6 (C), 158.4 (C-3); ESI-MS 456 [M+H]⁺; Anal. Calcd. for C₃₀H₃₇N₃O C 79.08; H 8.19. Found C 79.01; H 8.07.

4.2.2.2. In the PDF, section 4.2.2.2. and 4.2.2.5. are next to each other, but the text seems completely different (this is just an example). Could the line spacing and editing be unified? 17β-Hydroxy-7'-phenylpyrazolo[1,5-a]pyrimidino[5',6':3,2]-5α-androstane (7a). Substrate: **2a** (379 mg); Reagent: 3AP (166 mg). For purification of the crude product, EtOAc/CH₂Cl₂ = 20:80 eluent was used. Yield: 270 mg (61 %, yellow solid); Mp 140–142 °C; ¹H NMR (CDCl₃, 500 MHz): δ 0.72 (s, 3H, 18-H₃), 0.78 (s, 3H, 19-H₃), 0.80 (m, 1H, 9α-H), 0.92–0.99 (overlapping m, 2H, 7α-H and 14α-H), 1.02 (m, 1H, 12α-H), 1.23–1.47 (overlapping m, 6H, 15β-H, 11-H₂, 6β-H, 8β-H and 16β-H), 1.58–1.79 (overlapping m, 5H, 5α-H, 6α-H, 7β-H, 12β-H and 15α-H), 2.06 (m, 1H, 16α-H), 2.23 (d, 1H, *J* = 16.2 Hz, 1α-H), 2.65 (d, 1H, *J* = 16.2 Hz, 1β-H), 2.76 (dd, 1H, *J* = 19.2 Hz, *J* = 12.7 Hz, 4β-H), 3.09 (dd, 1H, *J* = 19.2 Hz, *J* = 5.6 Hz, 4α-H), 3.62 (t, 1H, *J* = 8.6 Hz, 17α-H), 6.63 (d, 1H, *J* = 2.4 Hz, 3'-H), 7.45 (bd, 2H, 2''-H and 6''-H), 7.54–7.61 (m, 3H, 3''-H, 4''-H and 5''-H), 7.99 (d, 1H, *J* = 2.4 Hz, 2'-H); ¹³C NMR (CDCl₃, 125 MHz): δ 11.2 (C-18), 11.8 (C-19), 20.9 (C-11), 23.6 (C-15), 28.6 (C-6), 30.8 (C-16), 31.2 (C-7), 35.5 (C-10), 35.8 (C-8), 36.8 (2C: C-4 and C-12), 40.1 (C-1), 41.8 (C-5), 43.0 (C-13), 51.2 (C-14), 53.8 (C-9), 82.0 (C-17), 94.8 (C-3'), 115.2 (C-2), 129.2 (2C) and 129.3 (2C): C-2'', C-6'', C-3'' and C-5'', 130.3 (C-1''), 130.4 (C-4''), 144.9 (C-2'), 145.8 and 146.9 (C-3a' and C-7'), 159.0 (C-3); ESI-MS 442 [M+H]⁺; Anal. Calcd. for C₂₉H₃₅N₃O C 78.87; H 7.99. Found C 79.01; H 8.07.

4.2.2.3. 17β-Hydroxy-7'-phenyl[1,2,4]triazolo[1,5-a]pyrimidino [5',6':3,2]-5α-androstane (8a). Substrate: **2a** (379 mg); Reagent: 3AT (168 mg). For purification of the crude product, EtOAc/CH₂Cl₂ = 50:50 eluent was used. Yield: 317 mg (72 %, white solid); Mp 257–260 °C; ¹H NMR (CDCl₃, 500 MHz): δ 0.71 (s, 3H, 18-H₃), 0.75 (s, 3H, 19-H₃), 0.82 (m, 1H, 9α-H), 0.90–1.06 (overlapping m, 3H, 7α-H, 12α-H and 14α-H), 1.22–1.46 (overlapping m, 6H, 6β-H, 8β-H, 11-H₂, 15β-H and 16β-H), 1.57–1.77 (overlapping m, 5H, 5α-H, 6α-H, 7β-H, 12β-H and 15α-H), 2.05 (m, 1H, 16α-H), 2.32 (d, 1H, *J* = 16.2 Hz, 1α-H), 2.71 (d, 1H, *J* = 16.2 Hz, 1β-H), 2.81 (dd, 1H, *J* = 19.4 Hz, *J* = 12.8 Hz, 4β-H), 3.13 (dd, 1H, *J* = 19.4 Hz, *J* = 5.3 Hz, 4α-H), 3.62 (t, 1H, *J* = 8.5 Hz, 17α-H), 7.48 (m, 2H, 2''-H and 6''-H), 7.60 (m, 3H, 3''-H, 4''-H and 5''-H), 8.33 (s, 1H,

2'-H); ¹³C NMR (CDCl₃, 125 MHz): δ 11.1 (C-18), 11.8 (C-19), 20.9 (C-11), 23.5 (C-15), 28.3 (C-6), 30.6 (C-16), 31.1 (C-7), 35.3 (C-10), 35.6 (C-8), 36.6 (C-12), 37.6 (C-4), 40.0 (C-1), 41.5 (C-5), 42.9 (C-13), 50.9 (C-14), 53.5 (C-9), 81.9 (C-17), 118.1 (C-2), 129.1 (C-1''), 129.2 (4C, C-2'', C-3'', C-5'' and C-6''), 130.9 (C-4''), 146.0 (C-7'), 153.7 (C-3a'), 155.1 (C-2'), 165.9 (C-3); ESI-MS 443 [M+H]⁺; Anal. Calcd. for C₂₈H₃₄N₄O C 75.98; H 7.74. Found C 76.12; H 7.66.

4.2.2.4. 17β-Hydroxy-7'-(4''-tolyl)-[1,2,4]triazolo[1,5-a]pyrimidino [5',6':3,2]-5α-androstane (8b). Substrate: **2b** (393 mg); Reagent: 3AT (168 mg). For purification of the crude product, EtOAc/CH₂Cl₂ = 40:60 eluent was used. Yield: 349 mg (76 %, white solid); Mp 135–138 °C; ¹H NMR (CDCl₃, 500 MHz): δ 0.72 (s, 3H, 18-H₃), 0.76 (s, 3H, 19-H₃), 0.83 (m, 1 H), 0.92–1.08 (overlapping m, 3 H), 1.26–1.47 (overlapping m, 6 H), 1.59–1.79 (overlapping m, 5 H), 2.07 (m, 1 H), 2.35 (d, 1H, *J* = 16.3 Hz, 1α-H), 2.49 (s, 3H, 4''-CH₃), 2.78 (d, 1H, *J* = 16.3 Hz, 1β-H), 2.83 (dd, 1H, *J* = 19.6 Hz, *J* = 13.0 Hz, 4β-H), 3.15 (dd, 1H, *J* = 19.6 Hz, *J* = 5.3 Hz, 4α-H), 3.63 (t, 1H, *J* = 8.6 Hz, 17α-H), 7.41 (m, 4H, 2''-H, 3''-H, 5''-H and 6''-H), 8.39 (s, 1H, 2'-H); ¹³C NMR (CDCl₃, 125 MHz): δ 11.2 (C-18), 11.8 (C-19), 21.0 (C-11), 21.8 (4''-CH₃), 23.5 (C-15), 28.4 (C-6), 30.7 (C-16), 31.1 (C-7), 35.4 (C-10), 35.7 (C-8), 36.7 (C-12), 37.8 (C-4), 40.2 (C-1), 41.5 (C-5), 42.9 (C-13), 51.0 (C-14), 53.6 (C-9), 82.0 (C-17), 118.8 (C-2), 125.7 (C-1''), 129.2 (2C, C-2'' and C-6''), 129.9 (2C, C-3'' and C-5''), 141.5 (C-4''), 146.6 (C-7'), 166.9 (C-3); the signals for C-2' and C-3a' were not observed; ESI-MS 457 [M+H]⁺; Anal. Calcd. for C₂₉H₃₆N₄O C 76.28; H 7.95. Found C 76.35; H 8.07.

4.2.2.5. 17β-Hydroxy-7'-(3''-tolyl)-[1,2,4]triazolo[1,5-a]pyrimidino [5',6':3,2]-5α-androstane (8c). Substrate: **2c** (393 mg); Reagent: 3AT (168 mg). For purification of the crude product, EtOAc/CH₂Cl₂ = 40:60 eluent was used. Yield: 351 mg (77 %, white solid); Mp 160–163 °C; ¹H NMR (CDCl₃, 500 MHz): δ 0.72 (s, 3H, 18-H₃), 0.77 (s, 3H, 19-H₃), 0.81–1.07 (overlapping m, 4 H), 9α-H), 1.24–1.47 (overlapping m, 6 H), 1.59–1.89 (overlapping m, 5 H), 2.06 (m, 1 H), 2.30 (d, 1H, *J* = 16.3 Hz, 1α-H), 2.47 (s, 3H, 3''-CH₃), 2.71 (d, 1H, *J* = 16.3 Hz, 1β-H), 2.81 (dd, 1H, *J* = 19.5 Hz, *J* = 12.7 Hz, 4β-H), 3.14 (dd, 1H, *J* = 19.5 Hz, *J* = 5.6 Hz, 4α-H), 3.63 (t, 1H, *J* = 8.6 Hz, 17α-H), 7.25 (m, 2H), 7.40 (d-like m, 1 H): 2''-H, 4''-H and 6''-H, 7.49 (t-like m, 1H, 5''-H), 8.34 (s, 1H, 2'-H); ¹³C NMR (CDCl₃, 125 MHz): δ 11.2 (C-18), 11.8 (C-19), 20.9 (C-11), 21.7 (3''-CH₃), 23.5 (C-15), 28.4 (C-6), 30.7 (C-16), 31.1 (C-7), 35.3 (C-10), 35.7 (C-8), 36.7 (C-12), 37.7 (C-4), 40.1 (C-1), 41.6 (C-5), 42.9 (C-13), 51.0 (C-14), 53.6 (C-9), 82.0 (C-17), 118.1 (C-2), 126.2 (C-6''), 129.1 (C-1''), 129.2, 129.5 and 131.7 (C-2'', C-4'' and C-5''), 139.1 (C-4''), 146.4 (C-7'), 153.8 (C-3a'), 155.2 (C-2'), 165.8 (C-3); ESI-MS 457 [M+H]⁺; Anal. Calcd. for C₂₉H₃₆N₄O C 76.28; H 7.95. Found C 76.15; H 7.88.

4.2.2.6. 17β-Hydroxy-7'-(4''-methoxyphenyl)-[1,2,4]triazolo[1,5-a]pyrimidino[5',6':3,2]-5α-androstane (8d). Substrate: **2d** (409 mg); Reagent: 3AT (168 mg). For purification of the crude product, EtOAc/CH₂Cl₂ = 40:60 eluent was used. Yield: 337 mg (71 %, off white solid); Mp 158–161 °C; ¹H NMR (CDCl₃, 500 MHz): δ 0.73 (s, 3H, 18-H₃), 0.75 (s, 3H, 19-H₃), 0.82 (m, 1 H), 0.92–1.09 (overlapping m, 3 H), 1.26–1.47 (overlapping m, 6 H), 1.59–1.80 (overlapping m, 5 H), 2.07 (m, 1 H), 2.35 (d, 1H, *J* = 16.3 Hz, 1α-H), 2.77 (d, 1H, *J* = 16.3 Hz, 1β-H), 2.82 (dd, 1H, *J* = 19.6 Hz, *J* = 13.0 Hz, 4β-H), 3.15 (dd, 1H, *J* = 19.6 Hz, *J* = 5.3 Hz, 4α-H), 3.64 (t, 1H, *J* = 8.6 Hz, 17α-H), 3.91 (s, 3H, 4''-OMe), 7.11 (d, 2H, *J* = 8.8 Hz, 3''-H and 5''-H), 7.47 (d, 2H, *J* = 8.8 Hz, 2''-H and 6''-H), 8.36 (s, 1H, 2'-H); ¹³C NMR (CDCl₃, 125 MHz): δ 11.2 (C-18), 11.8 (C-19), 21.0 (C-11), 23.6 (C-15), 28.4 (C-6), 30.8 (C-16), 31.2 (C-7), 35.4 (C-10), 35.8 (C-8), 36.8 (C-12), 37.8 (C-4), 40.4 (C-1), 41.7 (C-5), 43.0 (C-13), 51.1 (C-14), 53.7 (C-9), 55.6 (4''-OMe), 82.0 (C-17), 114.6 (2C, C-3'' and C-5''), 118.4 (C-2), 120.9 (C-1''), 131.2 (2C, C-2'' and C-6''), 146.2 (C-7'), 153.3 (C-3a'), 154.4 (C-2'), 161.5 (C-4''), 166.3 (C-3); ESI-MS 473 [M+H]⁺; Anal. Calcd. for C₂₉H₃₆N₄O₂ C 73.70; H 7.68. Found C 73.82; H 7.57.

4.2.2.7. 17 β -Hydroxy-7'-(4''-fluorophenyl)-[1,2,4]triazolo[1,5-a]pyrimidino[5',6':3,2]-5 α -androsterane (8e). Substrate: **2e** (397 mg); Reagent: 3AT (168 mg). For purification of the crude product, EtOAc/CH₂Cl₂ = 50:50 eluent was used. Yield: 335 mg (73 %, off white solid); Mp 135–138 °C; ¹H NMR (CDCl₃, 500 MHz): δ 0.73 (s, 3H, 18-H₃), 0.76 (s, 3H, 19-H₃), 0.80–1.08 (overlapping m, 4 H), 1.25–1.48 (overlapping m, 6 H), 1.59–1.81 (overlapping m, 5 H), 2.07 (m, 1 H), 2.32 (d, 1H, J = 16.2 Hz, 1 α -H), 2.70 (d, 1H, J = 16.2 Hz, 1 β -H), 2.81 (dd, 1H, J = 19.5 Hz, J = 12.7 Hz, 4 β -H), 3.15 (dd, 1H, J = 19.5 Hz, J = 5.6 Hz, 4 α -H), 3.63 (t, 1H, J = 8.6 Hz, 17 α -H), 7.31 (m, 2H, 3''-H and 5''-H), 7.51 (m, 2H, 2''-H and 6''-H), 8.34 (s, 1H, 2'-H); ¹³C NMR (CDCl₃, 125 MHz): δ 11.2 (C-18), 11.8 (C-19), 21.0 (C-11), 23.5 (C-15), 28.4 (C-6), 30.7 (C-16), 31.1 (C-7), 35.4 (C-10), 35.7 (C-8), 36.7 (C-12), 37.7 (C-4), 40.2 (C-1), 41.6 (C-5), 42.9 (C-13), 51.0 (C-14), 53.6 (C-9), 82.0 (C-17), 116.6 (d, 2C, J = 22.1 Hz, C-3'' and C-5''), 118.1 (C-2), 125.1 (d, J = 3.5 Hz, C-1''), 131.7 (d, 2C, J = 8.6 Hz, C-2'' and C-6''), 145.0 (C-7'), 154.0 (C-3a'), 155.4 (C-2'), 164.0 (d, J = 252.1 Hz, C-4''), 165.8 (C-3); ESI-MS 461 [M+H]⁺; Anal. Calcd. for C₂₈H₃₃FN₄O C 73.02; H 7.22. Found C 72.95; H 7.13.

4.2.2.8. 17 β -Hydroxy-7'-(4''-chlorophenyl)-[1,2,4]triazolo[1,5-a]pyrimidino[5',6':3,2]-5 α -androsterane (8f). Substrate: **2f** (413 mg); Reagent: 3AT (168 mg). For purification of the crude product after oxidation with DDQ, EtOAc/CH₂Cl₂ = 50:50 eluent was used. Yield: 311 mg (65 %, white solid); Mp 157–160 °C; ¹H NMR (CDCl₃, 500 MHz): δ 0.73 (s, 3H, 18-H₃), 0.76 (s, 3H, 19-H₃), 0.84 (m, 1 H), 0.92–1.09 (overlapping m, 3 H), 1.24–1.48 (overlapping m, 6 H), 1.60–1.81 (overlapping m, 5 H), 2.07 (m, 1 H), 2.32 (d, 1H, J = 16.2 Hz, 1 α -H), 2.71 (d, 1H, J = 16.2 Hz, 1 β -H), 2.82 (dd, 1H, J = 19.7 Hz, J = 12.8 Hz, 4 β -H), 3.15 (dd, 1H, J = 19.7 Hz, J = 5.3 Hz, 4 α -H), 3.64 (t, 1H, J = 8.6 Hz, 17 α -H), 7.45 (d, 2H, J = 8.2 Hz, 3''-H and 5''-H), 7.60 (d, 2H, J = 8.2 Hz, 2''-H and 6''-H), 8.33 (s, 1H, 2'-H); ¹³C NMR (CDCl₃, 125 MHz): δ 11.2 (C-18), 11.9 (C-19), 21.1 (C-11), 23.6 (C-15), 28.5 (C-6), 30.8 (C-16), 31.2 (C-7), 35.5 (C-10), 35.8 (C-8), 36.8 (C-12), 37.7 (C-4), 40.2 (C-1), 41.7 (C-5), 43.0 (C-13), 51.1 (C-14), 53.7 (C-9), 82.0 (C-17), 118.0 (C-2), 127.6 (C-1''), 129.6 (2C, C-2'' and C-6''), 130.9 (2C, C-3'' and C-5''), 137.2 (C-4''), 144.8 (C-7'), 154.1 (C-3a'), 155.6 (C-2'), 165.7 (C-3); ESI-MS 477 [M+H]⁺; Anal. Calcd. for C₂₈H₃₃ClN₄O C 70.50; H 6.97. Found C 70.69; H 7.07.

4.2.2.9. 17 β -Hydroxy-7'-(furan-2''-yl)-[1,2,4]triazolo[1,5-a]pyrimidino[5',6':3,2]-5 α -androsterane (8i). Substrate: **2i** (369 mg); Reagent: 3AT (168 mg). For purification of the crude product, EtOAc/CH₂Cl₂ = 40:60 eluent was used. ¹H NMR (CDCl₃, 500 MHz): δ 0.78 (s, 3H, 18-H₃), 0.79 (s, 3H, 19-H₃), 0.94–1.06 (overlapping m, 3 H), 1.16–1.53 (overlapping m, 6 H), 1.62–1.81 (overlapping m, 5 H), 1.90 (m, 1 H), 2.10 (m, 1 H), 2.75 (d, 1H, J = 17.1 Hz, 1 α -H), 2.84 (dd, 1H, J = 19.4 Hz, J = 12.7 Hz, 4 β -H), 3.11 (dd, 1H, J = 19.4 Hz, J = 5.5 Hz, 4 α -H), 3.36 (d, 1H, J = 17.1 Hz, 1 β -H), 3.69 (t, 1H, J = 8.6 Hz, 17 α -H), 6.78 (dd, 1H, J = 3.6 Hz, J = 1.7 Hz, 4''-H), 7.83 (d, 1H, J = 1.7 Hz, 3''-H), 8.10 (d, 1H, J = 3.6 Hz, 5''-H), 8.48 (s, 1H, 2'-H); ¹³C NMR (CDCl₃, 125 MHz): δ 11.2 (C-18), 12.0 (C-19), 21.2 (C-11), 23.6 (C-15), 28.3 (C-6), 30.8 (C-16), 31.2 (C-7), 35.0 (C-10), 35.7 (C-8), 36.9 (C-12), 37.9 (C-4), 40.7 (C-1), 40.9 (C-5), 43.0 (C-13), 51.1 (C-14), 54.0 (C-9), 82.0 (C-17), 112.6 (C-3''), 117.1 (C-2), 121.8 (C-4''), 135.4 (C-2''), 143.9 (C-7'), 146.0 (C-5''), 153.4 (C-3a'), 154.5 (C-2'), 165.7 (C-3); ESI-MS 433 [M+H]⁺; Anal. Calcd. for C₂₆H₃₂N₄O₂ C 72.19; H 7.46. Found C 72.27; H 7.33.

4.2.2.10. 17 β -Hydroxy-7'-(thiophen-2''-yl)-[1,2,4]triazolo[1,5-a]pyrimidino[5',6':3,2]-5 α -androsterane (8j). Substrate: **2j** (385 mg); Reagent: 3AT (168 mg). For purification of the crude product, EtOAc/CH₂Cl₂ = 40:60 eluent was used. Yield: 280 mg (62 %, yellow solid); Mp 164–167 °C; ¹H NMR (CDCl₃, 500 MHz): δ 0.75 (s, 3H, 18-H₃), 0.76 (s, 3H, 19-H₃), 0.89–1.04 (overlapping m, 3 H), 1.13 (m, 1 H), 1.25–1.49 (overlapping m, 5 H), 1.54–1.87 (overlapping m, 6 H), 2.08 (m, 1 H), 2.53 (d, 1H, J = 16.2 Hz, 1 α -H), 2.83 (dd, 1H, J = 19.6 Hz, J = 12.7 Hz, 4 β -H), 3.08 (d,

1H, J = 16.2 Hz, 1 β -H), 3.16 (dd, 1H, J = 19.6 Hz, J = 5.7 Hz, 4 α -H), 3.66 (t, 1H, J = 8.6 Hz, 17 α -H), 7.32 (dd, 1H, J = 5.0 Hz, J = 3.8 Hz, 4''-H), 7.80 (m, 2H, 3''-H and 5''-H), 8.46 (s, 1H, 2'-H); ¹³C NMR (CDCl₃, 125 MHz): δ 11.2 (C-18), 11.9 (C-19), 21.2 (C-11), 23.5 (C-15), 28.3 (C-6), 30.7 (C-16), 31.1 (C-7), 35.6 (C-10), 35.7 (C-8), 36.8 (C-12), 37.8 (C-4), 41.3 (C-5), 41.4 (C-1), 43.0 (C-13), 51.0 (C-14), 53.8 (C-9), 82.0 (C-17), 118.8 (C-2), 127.4 (C-3''), 128.1 (C-2''), 131.4 (C-4''), 133.9 (C-5''), 140.4 (C-7'), 153.0 (C-3a'), 153.9 (C-2'), 166.2 (C-3); ESI-MS 449 [M+H]⁺; Anal. Calcd. for C₂₆H₃₂N₄OS C 69.61; H 7.19. Found C 69.75; H 7.06.

4.2.2.11. 17 β -Hydroxy-7'-methyl-[1,2,4]triazolo[1,5-a]pyrimidino[5',6':3,2]-5 α -androsterane (8k). Substrate: **2k** [21] (316 mg); Reagent: 3AT (168 mg). For purification of the crude product, EtOAc/CH₂Cl₂ = 50:50 eluent was used. Yield: 261 mg (69 %, white solid); Mp > 200 °C (decomp.); ¹H NMR (CDCl₃, 500 MHz): δ 0.79 (s, 3H, 18-H₃), 0.82 (s, 3H, 19-H₃), 0.86–1.05 (overlapping m, 3 H), 1.16 (m, 1 H), 1.27–1.57 (overlapping m, 5 H), 1.61–1.81 (overlapping m, 5 H), 1.91 (m, 1 H), 2.09 (m, 1 H), 2.37 (d, 1H, J = 16.0 Hz, 1 α -H), 2.77 (dd, 1H, J = 19.3 Hz, J = 13.0 Hz, 4 β -H), 2.78 (s, 3H, 7'-CH₃), 2.89 (d, 1H, J = 16.0 Hz, 1 β -H), 3.02 (dd, 1H, J = 19.3 Hz, J = 5.1 Hz, 4 α -H), 3.68 (t, 1H, J = 8.6 Hz, 17 α -H), 8.42 (s, 1H, 2'-H); ¹³C NMR (CDCl₃, 125 MHz): δ 11.2 (C-18), 12.2 (C-19), 13.8 (7'-CH₃), 21.1 (C-11), 23.5 (C-15), 28.3 (C-6), 30.7 (C-16), 31.1 (C-7), 35.1 (C-10), 35.7 (C-8), 36.8 (C-12), 37.4 (C-4), 39.3 (C-1), 41.3 (C-5), 43.0 (C-13), 51.1 (C-14), 54.0 (C-9), 82.0 (C-17), 118.0 (C-2), 145.4 (C-7'), 152.9 (C-3a'), 154.4 (C-2') 164.7 (C-3); ESI-MS 381 [M+H]⁺; Anal. Calcd. for C₂₃H₃₂N₄O C 72.60; H 8.48. Found C 72.55; H 8.32.

4.2.3. General procedure for the synthesis of heterocyclic 17-keto steroids by Jones oxidation

The crude product (**6a**, **7a**, **8a–f** or **8i–k**) of the heterocyclization (4.2.2.) was dissolved in acetone (10 mL) and Jones reagent (0.2 mL) was added dropwise into the solution, which was then stirred at room temperature for 30 min, after which it was poured into ice-cold water. NH₄Cl was added and the resulting precipitate was filtered off and dried. The crude product was purified by column chromatography.

2-Methyl-7'-phenylpyrazolo[1',5'-a]pyrimidino[5',6':3,2]-5 α -androsteran-17-one (9a). Yield: 241 mg (53 %, off white solid); Mp > 250 °C (decomp.); ¹H NMR (CDCl₃, 500 MHz): δ 0.76 (s, 3H, 19-H₃), 0.83 (s, 3H, 18-H₃), 0.87 (m, 1 H), 1.06 (m, 1 H), 1.20 (m, 1 H), 1.31–1.41 (overlapping m, 4 H), 1.49–1.57 (overlapping m, 2 H), 1.69–1.77 (m, overlapping m, 3 H), 1.88 (m, 1 H), 1.96 (m, 1 H), 2.07 (m, 1H, 16 α -H), 2.21 (d, 1H, J = 16.0 Hz, 1 α -H), 2.41 (s, 3H, 2'-CH₃), 2.44 (dd, 1H, J = 19.0 Hz, J = 8.6 Hz, 16 β -H), 2.56 (d, 1H, J = 16.0 Hz, 1 β -H), 2.75 (dd, 1H, J = 19.0 Hz, J = 12.5 Hz, 4 β -H), 3.09 (dd, 1H, J = 16.0 Hz, J = 5.3 Hz, 4 α -H), 6.43 (s, 1H, 3'-H), 7.45 (bs, 2H, 2''-H and 6''-H), 7.54–7.60 (m, 3H, 3''-H, 4''-H and 5''-H); ¹³C NMR (CDCl₃, 125 MHz): δ 11.7 (C-19), 13.8 (C-18), 15.0 (2'-CH₃), 20.5 (C-11), 21.9 (C-15), 28.3 (C-6), 29.8 (CH₂), 30.4 (CH₂), 31.5 (CH₂), 35.2 (C-8), 35.5 (C-10), 35.9 (C-4), 39.9 (C-1), 41.5 (C-5), 47.7 (C-13), 51.4 (C-14), 53.5 (C-9), 94.1 (C-3'), 113.9 (C-2), 114.2 (C-3a'), 129.1 (2C) and 129.3 (2C): C-2'', C-6'', C-3'' and C-5'', 130.1 (C-1''), 130.4 (C-4''), 158.0 (C-3), 221.1 (C-17), the signal for C-7' carbonyl-C was not observed owing to the long relaxation time of this carbon nucleus; ESI-MS 440 [M+H]⁺; Anal. Calcd. for C₂₉H₃₃N₃O C 79.23; H 7.57. Found C 79.11; H 7.47.

4.2.3.2. 7'-Phenylpyrazolo[1',5'-a]pyrimidino[5',6':3,2]-5 α -androsteran-17-one (10a). Yield: 237 mg (54 %, yellow solid); Mp > 250 °C (decomp.); ¹H NMR (CDCl₃, 500 MHz): δ 0.79 (s, 3H, 19-H₃), 0.84 (s, 3H, 18-H₃), 0.86 (m, 1 H), 1.06 (m, 1 H), 1.20 (m, 1 H), 1.31–1.42 (overlapping m, 4 H), 1.50–1.57 (overlapping m, 2 H), 1.72–1.78 (m, overlapping m, 3 H), 1.89 (m, 1 H), 1.97 (m, 1 H), 2.07 (m, 1H, 16 α -H), 2.25 (d, 1H, J = 16.1 Hz, 1 α -H), 2.44 (dd, 1H, J = 19.2 Hz, J = 8.6 Hz, 16 β -H),

2.65 (d, 1H, $J = 16.1$ Hz, 1 β -H), 2.78 (dd, 1H, $J = 19.2$ Hz, $J = 12.7$ Hz, 4 β -H), 3.11 (dd, 1H, $J = 19.2$ Hz, $J = 5.6$ Hz, 4 α -H), 6.62 (bs, 1H, 3'-H), 7.45 (bd, 2H, 2''-H and 6''-H), 7.54–7.61 (m, 3H, 3''-H, 4''-H and 5''-H), 7.99 (d, 1H, $J = 2.2$ Hz, 2'-H); ^{13}C NMR (CDCl₃, 125 MHz): δ 11.8 (C-19), 13.8 (C-18), 20.6 (C-11), 21.9 (C-15), 28.4 (C-6), 30.5 (CH₂), 31.6 (CH₂), 35.3 (C-8), 35.6 (C-10), 35.9 (C-4), 36.8 (CH₂), 40.0 (C-1), 41.8 (C-5), 47.7 (C-13), 51.6 (C-14), 53.7 (C-9), 94.9 (C-3'), 114.9 (C-2), 129.2 (2C) and 129.3 (2C): C-2'', C-6'', C-3'' and C-5'', 130.3 (C-1''), 130.4 (C-4''), 144.9 (C-2'), 145.8 and 147.0 (C-3a' and C-7'), 158.7 (C-3), 220.6 (C-17); ESI-MS 440 [M+H]⁺; Anal. Calcd. for C₂₉H₃₃N₃O C 79.23; H 7.57. Found C 79.11; H 7.47.

4.2.3.3. 7'-Phenyl-[1,2,4]triazolo[1,5-a]pyrimidino[5',6':3,2]-5 α -androstan-17-one (11a). Yield: 258 mg (59 %, white solid); Mp > 300 °C (decomp.); ^1H NMR (CDCl₃, 500 MHz): δ 0.78 (s, 3H, 19-H₃), 0.84 (s, 3H, 18-H₃), 0.90 (m, 1 H), 1.08 (m, 1 H), 1.19–1.44 (overlapping m, 5 H), 1.49–1.60 (overlapping m, 2 H), 1.78 (overlapping m, 3 H), 1.90 (m, 1 H), 1.98 (m, 1 H), 2.08 (m, 1H, 16 α -H), 2.37 (d, 1H, $J = 16.3$ Hz, 1 α -H), 2.46 (dd, 1H, $J = 19.2$ Hz, $J = 8.8$ Hz, 16 β -H), 2.74 (d, 1H, $J = 16.3$ Hz, 1 β -H), 2.85 (dd, 1H, $J = 19.6$ Hz, $J = 12.6$ Hz, 4 β -H), 3.20 (dd, 1H, $J = 19.6$ Hz, $J = 5.4$ Hz, 4 α -H), 7.50 (m, 2H, 2''-H és 6''-H), 7.63 (m, 3H, 3''-H, 4''-H and 5''-H), 8.42 (s, 1H, 2'-H); ^{13}C NMR (CDCl₃, 125 MHz): δ 11.8 (C-19), 13.8 (C-18), 20.6 (CH₂), 21.9 (CH₂), 28.2 (C-6), 30.4 (CH₂), 31.5 (CH₂), 35.2 (C-8), 35.4 (C-10), 35.9 (CH₂), 37.7 (C-4), 40.0 (C-1), 41.4 (C-5), 47.6 (C-13), 51.4 (C-14), 53.5 (C-9), 119.2 (C-2), 128.4 (C-1''), 129.3 (4C, C-2'', C-3'', C-5'' and C-6''), 131.3 (C-4''), 146.7 (C-7'), 151.8 (C-3a'), 152.9 (C-2'), 167.5 (C-3), 220.7 (C-17); ESI-MS 441 [M+H]⁺; Anal. Calcd. for C₂₈H₃₂N₄O C 76.33; H 7.32. Found C 76.19; H 7.45.

4.2.3.4. 7'-(4''-Tolyl)-[1,2,4]triazolo[1,5-a]pyrimidino[5',6':3,2]-5 α -androstan-17-one (11b). Yield: 284 mg (62 %, white solid); Mp 283–286 °C; ^1H NMR (CDCl₃, 500 MHz): δ 0.78 (s, 3H, 19-H₃), 0.85 (s, 3H, 18-H₃), 0.90 (m, 1 H), 1.09 (m, 1 H), 1.21–1.60 (overlapping m, 7 H), 1.74–1.80 (overlapping m, 3 H), 1.92 (m, 1 H), 1.98 (m, 1 H), 2.09 (m, 1H, 16 α -H), 2.38 (d, 1H, $J = 16.2$ Hz, 1 α -H), 2.46 (dd, 1H, $J = 19.2$ Hz, $J = 8.5$ Hz, 16 β -H), 2.49 (s, 3H, 4''-CH₃), 2.78 (d, 1H, $J = 16.2$ Hz, 1 β -H), 2.85 (dd, 1H, $J = 19.6$ Hz, $J = 12.7$ Hz, 4 β -H), 3.20 (dd, 1H, $J = 19.6$ Hz, $J = 5.4$ Hz, 4 α -H), 7.39–7.44 (overlapping m, 4H, 2''-H, 3''-H, 5''-H and 6''-H), 8.43 (bs, 1H, 2'-H); ^{13}C NMR (CDCl₃, 125 MHz): δ 11.8 (C-19), 13.8 (C-18), 20.7 (CH₂), 21.8 (4''-CH₃), 21.9 (CH₂), 28.2 (C-6), 30.4 (CH₂), 31.5 (CH₂), 35.2 (C-8), 35.4 (C-10), 35.9 (CH₂), 37.7 (C-4), 40.1 (C-1), 41.4 (C-5), 47.6 (C-13), 51.4 (C-14), 53.5 (C-9), 119.1 (C-2), 125.3 (C-1''), 129.2 (2C, C-2'' and C-6''), 130.0 (2C, C-3'' and C-5''), 141.8 (C-4''), 146.9 (C-7'), 151.8 (C-3a'), 152.8 (C-2'), 167.3 (C-3), 220.8 (C-17); ESI-MS 455 [M+H]⁺; Anal. Calcd. for C₂₉H₃₄N₄O C 76.62; H 7.54. Found C 76.76; H 7.41.

4.2.3.5. 7'-(3''-Tolyl)-[1,2,4]triazolo[1,5-a]pyrimidino[5',6':3,2]-5 α -androstan-17-one (11c). Yield: 301 mg (66 %, white solid); Mp 263–265 °C; ^1H NMR (CDCl₃, 500 MHz): δ 0.79 (s, 3H, 19-H₃), 0.85 (s, 3H, 18-H₃), 0.89 (m, 1 H), 1.07 (m, 1 H), 1.20–1.60 (overlapping m, 7 H), 1.73–1.81 (overlapping m, 3 H), 1.89–2.00 (overlapping m, 2 H), 2.08 (m, 1H, 16 α -H), 2.32 (d, 1H, $J = 16.2$ Hz, 1 α -H), 2.45 (dd, 1H, $J = 19.2$ Hz, $J = 8.6$ Hz, 16 β -H), 2.47 (s, 3H, 3''-CH₃), 2.72 (d, 1H, $J = 16.2$ Hz, 1 β -H), 2.83 (dd, 1H, $J = 19.5$ Hz, $J = 12.7$ Hz, 4 β -H), 3.17 (dd, 1H, $J = 19.5$ Hz, $J = 5.5$ Hz, 4 α -H), 7.26 (m, 2 H), 7.41 (d-like m, 1 H): 2''-H, 4''-H and 6''-H, 7.50 (t-like m, 1H, 5''-H), 8.35 (s, 1H, 2'-H); ^{13}C NMR (CDCl₃, 125 MHz): δ 11.8 (C-19), 13.8 (C-18), 20.6 (CH₂), 21.7 (3''-CH₃), 21.9 (CH₂), 28.3 (C-6), 30.4 (CH₂), 31.5 (CH₂), 35.2 (C-8), 35.4 (C-10), 35.9 (CH₂), 37.6 (C-4), 40.0 (C-1), 41.5 (C-5), 47.7 (C-13), 51.4 (C-14), 53.5 (C-9), 117.9 (C-2), 126.1 (C-6''), 129.0 (C-1''), 129.2, 129.5 and 131.8 (C-2'', C-4'' and C-5''), 139.2 (C-4''), 146.5 (C-7'), 153.7 (C-3a'), 155.2 (C-2'), 165.6 (C-3), 220.9 (C-17); ESI-MS 455 [M+H]⁺; Anal. Calcd. for C₂₉H₃₄N₄O C 76.62; H 7.54. Found C 76.55; H 7.60.

4.2.3.6. 7'-(4''-Methoxyphenyl)-[1,2,4]triazolo[1,5-a]pyrimidino[5',6':3,2]-5 α -androstan-17-one (11d). Yield: 280 mg (59 %, white solid); Mp 273–275 °C; ^1H NMR (CDCl₃, 500 MHz): δ 0.76 (s, 3H, 19-H₃), 0.85 (s, 3H, 18-H₃), 0.91 (m, 1 H), 1.08 (m, 1 H), 1.22–1.42 (overlapping m, 5 H), 1.47–1.60 (overlapping m, 2 H), 1.73–1.80 (overlapping m, 3 H), 1.91 (m, 1 H), 1.98 (m, 1 H), 2.09 (m, 1H, 16 α -H), 2.40 (d, 1H, $J = 16.2$ Hz, 1 α -H), 2.46 (dd, 1H, $J = 19.2$ Hz, $J = 8.8$ Hz, 16 β -H), 2.79 (d, 1H, $J = 16.2$ Hz, 1 β -H), 2.83 (dd, 1H, $J = 19.6$ Hz, $J = 12.6$ Hz, 4 β -H), 3.19 (dd, 1H, $J = 19.6$ Hz, $J = 5.3$ Hz, 4 α -H), 3.92 (s, 3H, 4''-OMe), 7.13 (d, 2H, $J = 8.7$ Hz, 3''-H and 5''-H), 7.49 (d, 2H, $J = 8.7$ Hz, 2''-H and 6''-H), 8.42 (bs, 1H, 2'-H); ^{13}C NMR (CDCl₃, 125 MHz): δ 11.8 (C-19), 13.8 (C-18), 20.7 (CH₂), 21.9 (CH₂), 28.1 (C-6), 30.4 (CH₂), 31.5 (CH₂), 35.2 (C-8), 35.4 (C-10), 35.9 (CH₂), 37.7 (C-4), 40.2 (C-1), 41.4 (C-5), 47.7 (C-13), 51.4 (C-14), 53.5 (C-9), 55.6 (4''-OMe), 114.6 (2C, C-3'' and C-5''), 118.7 (C-2), 120.2 (C-1''), 131.2 (2C, C-2'' and C-6''), 146.5 (C-7'), 152.2 (C-3a'), 153.3 (C-2'), 161.6 (C-4''), 166.9 (C-3), 221.0 (C-17); ESI-MS 471 [M+H]⁺; Anal. Calcd. for C₂₉H₃₄N₄O₂ C 74.01; H 7.28. Found C 74.15; H 7.17.

4.2.3.7. 7'-(4''-Fluorophenyl)-[1,2,4]triazolo[1,5-a]pyrimidino[5',6':3,2]-5 α -androstan-17-one (11e). Yield: 261 mg (57 %, white solid); Mp > 250 °C (decomp.); ^1H NMR (CDCl₃, 500 MHz): δ 0.78 (s, 3H, 19-H₃), 0.85 (s, 3H, 18-H₃), 0.90 (m, 1 H), 1.08 (m, 1 H), 1.21–1.47 (overlapping m, 5 H), 1.51–1.61 (overlapping m, 2 H), 1.73–1.93 (overlapping m, 4 H), 1.98 (m, 1 H), 2.08 (m, 1H, 16 α -H), 2.35 (d, 1H, $J = 16.2$ Hz, 1 α -H), 2.46 (dd, 1H, $J = 19.2$ Hz, $J = 8.7$ Hz, 16 β -H), 2.70 (d, 1H, $J = 16.2$ Hz, 1 β -H), 2.83 (dd, 1H, $J = 19.2$ Hz, $J = 12.9$ Hz, 4 β -H), 3.17 (dd, 1H, $J = 19.2$ Hz, $J = 5.5$ Hz, 4 α -H), 7.31 (m, 2H, 3''-H and 5''-H), 7.51 (m, 2H, 2''-H and 6''-H), 8.34 (s, 1H, 2'-H); ^{13}C NMR (CDCl₃, 125 MHz): δ 11.8 (C-19), 13.8 (C-18), 20.7 (CH₂), 21.9 (CH₂), 28.2 (C-6), 30.4 (CH₂), 31.5 (CH₂), 35.2 (C-8), 35.5 (C-10), 35.9 (CH₂), 37.6 (C-4), 40.1 (C-1), 41.5 (C-5), 47.7 (C-13), 51.4 (C-14), 53.6 (C-9), 116.6 (d, 2C, $J = 22.1$ Hz, C-3'' and C-5''), 117.8 (C-2), 125.0 (d, $J = 3.6$ Hz, C-1''), 131.7 (d, 2C, $J = 8.7$ Hz, C-2'' and C-6''), 145.1 (C-7'), 154.0 (C-3a'), 155.5 (C-2'), 164.0 (d, $J = 252.0$ Hz, C-4''), 165.5 (C-3) 220.8 (C-17); ESI-MS 459 [M+H]⁺; Anal. Calcd. for C₂₈H₃₁FN₄O C 73.34; H 6.81. Found C 73.28; H 6.74.

4.2.3.8. 7'-(4''-Chlorophenyl)-[1,2,4]triazolo[1,5-a]pyrimidino[5',6':3,2]-5 α -androstan-17-one (11f). Yield: 293 mg (62 %, white solid); Mp > 300 °C (decomp.); ^1H NMR (CDCl₃, 500 MHz): δ 0.78 (s, 3H, 19-H₃), 0.85 (s, 3H, 18-H₃), 0.89 (m, 1 H), 1.08 (m, 1 H), 1.21–1.61 (overlapping m, 7 H), 1.74–1.82 (overlapping m, 3 H), 1.91 (m, 1 H), 1.98 (m, 1 H), 2.09 (m, 1H, 16 α -H), 2.37 (d, 1H, $J = 16.2$ Hz, 1 α -H), 2.46 (dd, 1H, $J = 19.2$ Hz, $J = 8.8$ Hz, 16 β -H), 2.72 (d, 1H, $J = 16.2$ Hz, 1 β -H), 2.85 (dd, 1H, $J = 19.6$ Hz, $J = 12.6$ Hz, 4 β -H), 3.20 (dd, 1H, $J = 19.6$ Hz, $J = 5.3$ Hz, 4 α -H), 7.47 (d, 2H, $J = 8.2$ Hz, 3''-H and 5''-H), 7.61 (d, 2H, $J = 8.2$ Hz, 2''-H and 6''-H), 8.40 (bs, 1H, 2'-H); ^{13}C NMR (CDCl₃, 125 MHz): δ 11.9 (C-19), 13.8 (C-18), 20.7 (CH₂), 21.9 (CH₂), 28.2 (CH₂), 30.4 (CH₂), 31.5 (CH₂), 35.2 (C-8), 35.5 (C-10), 35.9 (CH₂), 37.7 (C-4), 40.1 (C-1), 41.4 (C-5), 47.6 (C-13), 51.4 (C-14), 53.5 (C-9), 118.8 (C-2), 126.9 (C-1''), 129.7 (2C, C-2'' and C-6''), 130.9 (2C, C-3'' and C-5''), 137.5 (C-4''), 145.2 (C-7'), 152.6 (C-3a'), 153.8 (C-2'), 166.8 (C-3), 220.7 (C-17); ESI-MS 475 [M+H]⁺; Anal. Calcd. for C₂₈H₃₁ClN₄O C 70.80; H 6.58. Found C 70.71; H 6.45.

4.2.3.9. 7'-(Furan-2''-yl)-[1,2,4]triazolo[1,5-a]pyrimidino[5',6':3,2]-5 α -androstan-17-one (11i). Yield: 238 mg (55 %, light brown solid); Mp > 200 °C (decomp.); ^1H NMR (CDCl₃, 500 MHz): δ 0.81 (s, 3H, 19-H₃), 0.90 (s, 3H, 18-H₃), 1.03 (m, 1 H), 1.12 (m, 1 H), 1.32–1.65 (overlapping m, 7 H), 1.74–1.83 (overlapping m, 3 H), 1.92 (m, 1 H), 2.01 (m, 1 H), 2.12 (m, 1H, 16 α -H), 2.48 (dd, 1H, $J = 19.4$ Hz, $J = 8.7$ Hz, 16 β -H), 2.78 (d, 1H, $J = 17.1$ Hz, 1 α -H), 2.87 (dd, 1H, $J = 19.4$ Hz, $J = 12.6$ Hz, 4 β -H), 3.13 (dd, 1H, $J = 19.4$ Hz, $J = 5.3$ Hz, 4 α -H), 3.38 (d, 1H, $J = 17.1$ Hz, 1 β -H), 6.79 (dd, 1H, $J = 3.6$ Hz, $J = 1.7$ Hz, 4''-H), 7.86 (d, 1H, $J = 1.7$ Hz, 3''-

Table 4
Crystal data and structure refinement for compounds **2a** and **8j**.

	2a	8j
Empirical formula	C ₂₆ H ₃₄ O ₂	C ₅₃ H ₆₆ Cl ₂ N ₈ O ₂ S ₂
Molecular formula	C ₂₆ H ₃₄ O ₂	2 (C ₂₆ H ₃₂ N ₄ OS) CH ₂ Cl ₂
Formula weight	378.53	982.15
Temperature (K)	153(2)	153(2)
Radiation and wavelength λ (Å)	Mo-Kα, 0.71073	Mo-Kα, 0.71075
Crystal system	monoclinic	monoclinic
Space group	P 2 ₁	P 2 ₁
Unit cell dimensions		
a (Å)	7.0071(5)	12.4299(8)
b (Å)	12.0136(9)	11.2453(7)
c (Å)	12.7119(10)	17.5904(11)
β (°)	95.767(7)	92.572(7)
Volume Å ³	1064.68(14)	2456.3(3)
Z	2/1	2/1
Density (calculated) (Mg/m ³)	1.181	1.328
Absorption coefficient, μ (mm ⁻¹)	0.072	0.268
F(000)	412	1044
Crystal colour	colourless	colourless
Crystal description	block	chunk
Crystal size (mm)	0.50 × 0.50 × 0.50	0.35 × 0.30 × 0.30
Absorption correction	numerical	numerical
Max. and min. transmission	0.981, 0.987	0.989, 0.994
θ–range for data collection (°)	3.192 ≤ θ ≤ 30.480	3.281 ≤ θ ≤ 25.347°
Reflections collected	26,315	31,944
Completeness to 2θ	0.999	0.997
Independent reflections (R(int))	6433 (0.0250)	8944 (0.0587)
Reflections I > 2σ(I)	5960	7107
Refinement method	full-matrix least-squares on F ²	full-matrix least-squares on F ²
Data / restraints / parameters	6433 / 1 / 260	8944 / 1 / 605
Goodness-of-fit on F ²	1.081	1.018
Final R indices [I > 2σ(I)], R ₁ , wR ₂	0.0407, 0.0945	0.0474, 0.0849
R indices (all data), R ₁ , wR ₂	0.0449, 0.0962	0.0676, 0.0905
Max. and mean shift/esd	0.000; 0.000	0.001; 0.000
Largest diff. peak and hole (e. Å ⁻³)	0.417; -0.145	0.423; -0.380

H), 8.14 (d, 1H, *J* = 3.6 Hz, 5''-H), 8.53 (s, 1H, 2'-H); ¹³C NMR (CDCl₃, 125 MHz): δ 12.0 (C-19), 13.9 (C-18), 20.9 (CH₂), 22.0 (CH₂), 28.1 (CH₂), 30.4 (CH₂), 31.7 (CH₂), 35.1 (C-10), 35.2 (C-8), 36.0 (CH₂), 37.8 (C-4), 40.6 (C-1), 40.7 (C-5), 47.7 (C-13), 51.5 (C-14), 54.0 (C-9), 112.8 (C-3''), 117.2 (C-2), 122.3 (C-4''), 135.6 (C-2''), 143.7 (C-7''), 146.3 (C-5''), 152.7 (C-3a'), 153.7 (C-2'), 166.1 (C-3), 221.0 (C-17); ESI-MS 431 [M+H]⁺; Anal. Calcd. for C₂₆H₃₀N₄O₂ C 72.53; H 7.02. Found C 72.41; H 6.94.

4.2.3.10. 7'-(Thiophen-2''-yl)-[1,2,4]triazolo[1,5-a]pyrimidino [5',6':3,2]-5α-androstan-17-one (11j). Yield: 264 mg (57 %, yellow solid); Mp > 300 °C (decomp.); ¹H NMR (CDCl₃, 500 MHz): δ 0.77 (s, 3H, 19-H₃), 0.87 (s, 3H, 18-H₃), 0.98 (m, 1 H), 1.10 (m, 1 H), 1.29–1.66 (overlapping m, 7 H), 1.74–1.86 (overlapping m, 3 H), 1.93 (m, 1 H), 2.00 (m, 1 H), 2.11 (m, 1H, 16α-H), 2.47 (dd, 1H, *J* = 19.1 Hz, *J* = 8.9 Hz, 16β-H), 2.56 (d, 1H, *J* = 16.1 Hz, 1α-H), 2.85 (dd, 1H, *J* = 19.6 Hz, *J* = 12.6 Hz, 4β-H), 3.09 (d, 1H, *J* = 16.1 Hz, 1β-H), 3.18 (dd, 1H, *J* = 19.6 Hz, *J* = 5.5 Hz, 4α-H), 7.33 (t, 1H, *J* = 4.4 Hz, 4''-H), 7.80 (m, 2H, 3''-H and 5''-H), 8.47 (s, 1H, 2'-H); ¹³C NMR (CDCl₃, 125 MHz): δ 11.8 (C-19), 13.8 (C-18), 20.9 (CH₂), 21.9 (CH₂), 28.1 (CH₂), 30.4 (CH₂), 31.6 (CH₂), 35.2 (C-8), 35.6 (C-10), 35.9 (CH₂), 37.7 (C-4), 41.2 (C-5), 41.3 (C-1), 47.7 (C-13), 51.4 (C-14), 53.7 (C-9), 118.6 (C-2), 127.5 (C-3''), 127.8 (C-2''), 131.6 (C-4''), 134.1 (C-5''), 140.6 (C-7'), 152.7 (C-3a'), 153.7 (C-2'), 166.2 (C-3) 221.0 (C-17); ESI-MS 447 [M+H]⁺; Anal. Calcd. for C₂₆H₃₀N₄OS C 69.92; H 6.77. Found C 70.05; H 6.65.

7'-Methyl-[1,2,4]triazolo[1,5-a]pyrimidino[5',6':3,2]-5α-androstan-17-one (11k). Yield: 197 mg (52 %, white solid); Mp > 250 °C (decomp.); ¹H NMR (CDCl₃, 500 MHz): δ 0.84 (s, 3H, 19-H₃), 0.91 (s, 3H, 18-H₃), 0.98 (m, 1 H), 1.09 (m, 1 H), 1.30–1.44 (overlapping m, 3 H), 1.51–1.65 (overlapping m, 3 H), 1.69–1.76 (overlapping m, 2 H), 1.82 (m, 1 H), 1.92 (m, 2 H), 2.00 (m, 1 H), 2.10 (m, 1H, 16α-H), 2.39 (d, 1H, *J* = 16.0

Hz, 1α-H), 2.48 (dd, 1H, *J* = 19.3 Hz, *J* = 8.7 Hz, the 16β-H), 2.79 (s, 3H, 7'-CH₃ and m, 1H, 4β-H), 2.90 (d, 1H, *J* = 16.2 Hz, 1β-H), 3.04 (dd, 1H, *J* = 19.4 Hz, *J* = 5.1 Hz, 4α-H), 8.44 (s, 1H, 2'-H); ¹³C NMR (CDCl₃, 125 MHz): δ 12.1 (C-19), 13.8 (7'-CH₃), 13.9 (C-18), 20.8 (CH₂), 21.9 (CH₂), 28.1 (C-6), 30.4 (CH₂), 31.6 (CH₂), 35.2 (C-8), 35.9 (2C, C-10 and CH₂), 37.3 (C-4), 39.2 (C-1), 41.2 (C-5), 47.7 (C-13), 51.5 (C-14), 51.9 (C-9), 118.1 (C-2), 145.6 (C-7'), 152.4 (C-3a'), 153.9 (C-2'), 164.9 (C-3), 220.8 (C-17); ESI-MS 379 [M+H]⁺; Anal. Calcd. for C₂₃H₃₀N₄O C 72.98; H 7.99. Found C 73.12; H 7.89.

4.3. X-ray data collection, structure solution and refinement for compound **2a** and **8j**

Single crystals suitable for single crystal X-ray diffraction measurements have been obtained by evaporation from methanol, resulting in crystal **2a** and from CH₂Cl₂/diethyl-ether leading to crystal **8j**. The crystals were mounted on loops and X-ray diffraction data were collected at 153(2) K on a Rigaku RAXIS-RAPID II diffractometer using Mo-Kα radiation. Numerical absorption correction [39] was carried out using the program CrystalClear [40] SHELX [41] program package under WinGX [42] software were used for structure solution and refinement. The structures were solved by direct methods. The models were refined by full-matrix least squares on F². Refinement of non-hydrogen atoms was carried out with anisotropic temperature factors (except for disordered carbon atoms C23A and C23B in crystal **8j** where isotropic temperature factor was used). Hydrogen atoms were placed into geometric positions. They were included in structure factor calculations but they were not refined. The isotropic displacement parameters of all the hydrogen atoms were approximated from the U(eq) value of the atom they were bonded to. In crystal **8j**, two molecules and one dichloromethane have been found in the asymmetric unit. In molecule **2** the thiophene rings was found in two disordered positions

with an occupancy of 76 % for C23A and S21A and 24 % for C23B and S21B atoms. Constraints have been used for the refinement of the position and ADP of disordered atoms. As the configuration of the chiral atoms of DHT was known and the reactions did not lead to novel asymmetric center, the absolute configuration was not investigated. The summary of data collection and refinement parameters are collected in Table 4. Selected bond lengths and angles of compounds calculated by PLATON software [43] are collected in Tables S1 and S2. The graphical representation and the edition of CIF files were done by Mercury [44] and EnCIFer [45] softwares. The crystallographic data files for the two compounds have been deposited with the Cambridge Crystallographic Database as CCDC 2062396-2062397.

4.4. Cell lines

The 22Rv1-ARE14 reporter cell line [29] and C4-2 were kindly provided by prof. Zdeněk Dvořák and by Dr. Marián Hajdúch, respectively (both from Palacký University Olomouc, Czech Republic). 22Rv1-ARE14 and C4-2 cell lines were grown in RPMI-1640 medium. All media were supplemented with 10 % normal or charcoal-stripped fetal bovine serum (steroid-depleted serum), 4 mM glutamine, 100 IU/mL penicillin, 100 mg/mL streptomycin and 1 mM sodium pyruvate. Cells were cultivated in a humidified incubator at 5% CO₂ atmosphere and 37 °C.

4.5. AR-transcriptional luciferase assay

22Rv1-ARE14 cells were seeded into the Nunc™ MicroWell™ 96-well optical-bottom plate (Thermo Fisher Scientific) (40 000 cells/well). The next day, the cultivation medium was discarded and cells were washed with PBS. Cells were then incubated in the absence or presence of tested compounds dissolved in RPMI-1640 medium supplemented with charcoal-stripped serum and 1 nM R1881. After 24 h incubation, cells were washed with PBS and lysed for 10 min in a lysis buffer (10 mM Tris pH = 7.4, 2 mM DCTA, 1% nonidet P40, 2 mM DTT) at 37 °C. After lysis, reaction buffer (20 mM tricine pH = 7.8, 1.07 mM MgSO₄ · 7H₂O, 5 mM ATP, 9.4 mM luciferin) was added to the wells and the luminescence of the samples was measured using a Tecan M200Pro microplate reader (Biotek). Assays were performed in triplicate.

4.6. Cell viability assay

For the viability assays, 22Rv1-ARE14 (10000 cells per well) and C4-2 (5000 cells per well) were seeded into the 96-well tissue culture plates and were cultivated overnight. Solutions of analysed compounds were then added in different concentrations in triplicate for 72 h. After treatment, the resazurin solution (Sigma Aldrich) was added to a final concentration of 10 µg per ml for 4 h, and then the fluorescence of resorufin was measured at 544 nm/590 nm (excitation/emission) using a Fluoroskan Ascent microplate reader (Labsystems). Finally, GI₅₀ value was calculated from the dose response curves that resulted from the assays using GraphPad Prism 5.

4.7. Colony formation assay

PCa cells 22Rv1-ARE14 (2000 cells per well) and C4-2 (5000 cells per well) were seeded into 6-well plates and cultivated overnight. The following day, the medium was removed and replaced with fresh medium containing different concentrations of the compound. Media containing compounds were replaced once within 10 days. After that, the medium was discarded and colonies were fixed with 70 % ethanol for 15 min, washed with PBS and stained with crystal violet (1 % solution in 96 % ethanol) for 1 h. Finally, wells were washed with PBS until colonies were visible and its photograph was captured.

4.8. Thermal shift assay

CETSA experiment was inspired by published protocol [30,31]. C4-2 cells were deprived of androgens (by cultivation in charcoal stripped serum for 24 h), then were harvested, washed twice with PBS and treated with R1881 or several concentrations of 2f for 1 h at 37 °C in PBS with 5 mM glucose. Following the incubation the treated cells were aliquoted into PCR strips and heated at different temperatures for 3 min in CFX96 Touch Real-time PCR detection system (BioRad). Finally, all samples were supplemented with protease inhibitors and lysed by freeze-thaw cycles using liquid nitrogen. Samples were clarified by centrifugation at 14000 g for 20 min and supernatants were collected and denatured and separated by SDS-PAGE and immunoblotted.

4.9. Immunoblotting

Briefly, the cells were harvested and lysed using standard protocol in RIPA buffer supplemented with protease and phosphatase inhibitors. Cells were also disrupted by ultrasound sonication (10 s with 30 % amplitude). Cellular fractionation was performed using the Qproteome Cell Compartment Kit (Qiagen). Protein concentration was balanced within samples and then proteins were separated by SDS-PAGE and electroblotted onto nitrocellulose membranes. Membranes were blocked in 4% BSA and incubated with primary antibodies overnight. The next day, membranes were washed and incubated with secondary antibodies conjugated with peroxidase. Then, peroxidase activity was detected by SuperSignal West Pico reagents (Thermo Scientific) using a CCD camera LAS-4000 (Fujifilm). Specific antibodies were purchased from Merck (anti-α-tubulin, clone DM1A; anti phospho-histone H3 (Ser10); anti-β-actin, clone C4), or Cell Signaling Technology (anti-AR, clone D6F11; anti-PSA/KLK3, clone D6B1; anti-Nkx3.1, clone D2Y1A; anti-PARP, clone 46D11; anti-rabbit secondary antibody). All antibodies were diluted in 4% BSA and 0.1 % Tween 20 in TBS.

4.10. Molecular docking

Molecular docking is useful theoretical method for prediction and interpretation of new designed derivatives based on dihydrotestosterone ligand. Androgen receptor PDBID:2PIV [36] was selected as crystal structure as an input to molecular docking. The docking studies were performed using AutoDock Vina 1.05 [37]. Amino acids up to 6 Å from the active site were set as flexible. These settings enabled amino acid movement, increased the permitted volume of active site, and allowed the placement of DHT derivatives into the otherwise smaller highly-packed cavity for native ligands (e.g. DHT). All 3D structures of DHT derivatives were obtained with Marvin 15.1.5, a software used for the drawing, displaying and characterization of chemical structure, substructures and reactions. Polar hydrogens were added to all ligands and proteins with the AutoDock Tools (ADT) [38] program prior to docking with Autodock Vina program.

Author statement

Conceptualization, É.F. and R.J.; Chemical synthesis and optimization experiments, M.A.K. and Á.B.; Pharmacological studies, M.P.; Single crystal X-ray analysis, N.V.M.; Flexible docking, V.B.; Structural analysis, M.A.K.; Formal analysis and interpretation of data, Á.B. and M. P.; Methodology, resources, supervision, É.F. and R.J.; Writing—original draft preparation, M.P., N.V.M. and M.A.K.; Writing—review and editing, É.F. and R.J. All authors have read and agreed to the published version of the manuscript.

Acknowledgement

N.V.M. thanks the financial support for the National Research, Development and Innovation Office (OTKA K124544). The authors (RJ,

MP, VB) gratefully acknowledge financial support from the Grant Agency of the Czech Republic (GA20-15621S) and Palacký University Olomouc (IGA_PrF_2021_007). VB was supported by the ELIXIR CZ research infrastructure project (MEYS Grant No: LM2018131) including access to computing and storage facilities“.

Appendix A. Supplementary data

Supplementary material related to this article can be found, in the online version, at doi:<https://doi.org/10.1016/j.jsbmb.2021.105904>.

References

- [1] A. Paschalis, J.S. de Bono, Prostate cancer 2020: “The Times They Are a’ Changing”, *Cancer Cell* 38 (2020) 25–27, <https://doi.org/10.1016/j.ccell.2020.06.008>.
- [2] S. Cao, Y. Zhan, Y. Dong, Emerging data on androgen receptor splice variants in prostate cancer, *Endocr. Relat. Cancer* 23 (2016) T199–T210, <https://doi.org/10.1530/ERC-16-0298>.
- [3] C. Lu, J. Luo, Decoding the androgen receptor splice variants, *Transl. Androl. Urol.* 2 (2013) 178–186, <https://doi.org/10.3978/j.issn.2223-4683.2013.09.08>.
- [4] T. Uo, S.R. Plymate, C.C. Sprenger, The potential of AR-V7 as a therapeutic target, *Expert Opin. Ther. Targets* 22 (2018) 201–216, <https://doi.org/10.1080/14728222.2018.1439016>.
- [5] S. Saranyananon, S.K. Srivastava, S. Pai, S. Singh, A.P. Singh, Therapies targeted to androgen receptor signaling axis in prostate cancer: progress, challenges, and hope, *Cancers (Basel)* 12 (2019) 51, <https://doi.org/10.3390/cancers12010051>.
- [6] P. Purushottamachar, A.M. Godbole, L.K. Gediya, M.S. Martin, T.S. Vasaitis, A. K. Kwegyir-Afful, S. Ramalingam, S. Ates-Alagoz, V.C. Njar, Systematic structure modifications of multitarget prostate cancer drug candidate galeterone to produce novel androgen receptor down-regulating agents as an approach to treatment of advanced prostate cancer, *J. Med. Chem.* 56 (2013) 4880–4898, <https://doi.org/10.1021/jm400048v>.
- [7] F. Cortés-Benítez, M. Cabeza, M.T. Ramírez-Apan, B. Alvarez-Manrique, E. Bratoeff, Synthesis of 17 β -N-arylcabamoylandrost-4-en-3-one derivatives and their anti-proliferative effect on human androgen-sensitive LNCaP cell line, *Eur. J. Med. Chem.* 121 (2016) 737–746, <https://doi.org/10.1016/j.ejmech.2016.05.059>.
- [8] Y.K. Shi, B. Wang, X.L. Shi, Y.D. Zhao, B. Yu, H.M. Liu, Synthesis and biological evaluation of new steroidal pyridines as potential anti-prostate cancer agents, *Eur. J. Med. Chem.* 145 (2018) 11–22, <https://doi.org/10.1016/j.ejmech.2017.12.094>.
- [9] L.L. Romero-Hernández, P. Merino-Montiel, S. Meza-Reyes, J.L. Vega-Baez, Ó. López, J.M. Padrón, S. Montiel-Smith, Synthesis of unprecedented steroidal spiro heterocycles as potential antiproliferative drugs, *Eur. J. Med. Chem.* 143 (2018) 21–32, <https://doi.org/10.1016/j.ejmech.2017.10.063>.
- [10] R. Jorda, E. Rezníčková, U. Kielczewska, J. Maj, J.W. Morzycki, L. Siergiejczyk, V. Bazziger, K. Berka, L. Rárová, A. Wojtkiewicz, Synthesis of novel galeterone derivatives and evaluation of their *in vitro* activity against prostate cancer cell lines, *Eur. J. Med. Chem.* 179 (2019) 483–492, <https://doi.org/10.1016/j.ejmech.2019.06.040>.
- [11] R. Jorda, S.M.M. Lopes, E. Rezníčková, H. Ajani, A.V. Pereira, C.S.B.M.V.D. Gomes, T. Pinho, E. Melo, Tetrahydropyrazolo[1,5-*a*]pyridine-fused steroids and their *in vitro* biological evaluation in prostate cancer, *Eur. J. Med. Chem.* 178 (2019) 168–176, <https://doi.org/10.1016/j.ejmech.2019.05.064>.
- [12] V.C. Njar, A.M. Brodie, Discovery and development of Galeterone (TOK-001 or VN/124-1) for the treatment of all stages of prostate cancer, *J. Med. Chem.* 58 (2015) 2077–2087, <https://doi.org/10.1021/jm501239f>.
- [13] M. Jarman, S.E. Barrie, J.M. Llera, The 16,17-double bond is needed for irreversible inhibition of human cytochrome p45017 α by abiraterone (17-(3-pyridyl)androsta-5,16-dien-3 β -ol) and related steroidal inhibitors, *J. Med. Chem.* 41 (1998) 5375–5381, <https://doi.org/10.1021/jm981017j>.
- [14] A.K. Kwegyir-Afful, S. Ramalingam, P. Purushottamachar, V.P. Ramamurthy, V. C. Njar, Galeterone and VNPT55 induce proteasomal degradation of AR/AR-V7, induce significant apoptosis via cytochrome c release and suppress growth of castration resistant prostate cancer xenografts *in vivo*, *Oncotarget* 6 (2015) 27440–27460, <https://doi.org/10.18632/oncotarget.4578>.
- [15] B. Montgomery, M.A. Eisenberger, M.B. Rettig, F. Chu, R. Pili, J.J. Stephenson, N. J. Vogelzang, A.J. Koletsy, L.T. Nordquist, W.J. Edenfield, K. Mamlook, K. J. Ferrante, M.E. Taplin, Androgen receptor modulation optimized for response (ARMOR) Phase I and II studies: galeterone for the treatment of castration-resistant prostate cancer, *Clin. Cancer Res.* 22 (2016) 1356–1363, <https://doi.org/10.1158/1078-0432.CCR-15-1432>.
- [16] M.E. Taplin, E.S. Antonarakis, K.J. Ferrante, K. Horgan, B. Blumenstein, F. Saad, J. Luo, J.S. de Bono, Androgen receptor modulation optimized for response-splice variant: a Phase 3, randomized trial of galeterone versus enzalutamide in androgen receptor splice variant-7-expressing metastatic castration-resistant prostate cancer, *Eur. Urol.* 76 (2019) 843–851, <https://doi.org/10.1016/j.eururo.2019.08.034>.
- [17] E.A. Mostaghel, B.T. Marck, S.R. Plymate, R.L. Vessella, S. Balk, A.M. Matsumoto, P.S. Nelson, R.B. Montgomery, Resistance to CYP17A1 inhibition with abiraterone in castration-resistant prostate cancer: induction of steroidogenesis and androgen receptor splice variants, *Clin. Cancer Res.* 17 (2011) 5913–5925, <https://doi.org/10.1158/1078-0432.CCR-11-0728>.
- [18] D. Kovács, J. Wölfling, N. Szabó, M. Szécsi, Z. Schelz, I. Zupkó, É. Frank, Synthesis of novel 17-(4'-formyl)pyrazolylandrosta-5,16-dienes and their derivatives as potent 17 α -hydroxylase/C17,20-lyase inhibitors or antiproliferative agents depending on the substitution pattern of the heteroring, *Eur. J. Med. Chem.* 120 (2016) 284–295, <https://doi.org/10.1016/j.ejmech.2016.05.006>.
- [19] D. Kovács, J. Wölfling, N. Szabó, M. Szécsi, I. Kovács, I. Zupkó, É. Frank, An efficient approach to novel 17-5'-(1',2',4')-oxadiazolyl androstenes via the cyclodehydration of cytotoxic O-steroidacylamidoximes, and an evaluation of their inhibitory action on 17 α -hydroxylase/C17,20-lyase, *Eur. J. Med. Chem.* 70 (2013) 649–660, <https://doi.org/10.1016/j.ejmech.2013.10.038>.
- [20] D. Kovács, J. Wölfling, N. Szabó, M. Szécsi, R. Minorics, I. Zupkó, É. Frank, Efficient access to novel androsteno-17-(1',3',4')-oxadiazoles and 17 β -(1',3',4')-thiadiazoles via N-substituted hydrazone and N,N'-disubstituted hydrazine intermediates, and their pharmacological evaluation *in vitro*, *Eur. J. Med. Chem.* 98 (2015) 13–29, <https://doi.org/10.1016/j.ejmech.2015.05.010>.
- [21] G. Mótyán, M.K. Gopisetty, R.E. Kiss-Faludy, Á. Kulmány, I. Zupkó, É. Frank, M. Kiricsi, Anti-cancer activity of novel dihydrotestosterone-derived ring A-condensed pyrazoles on androgen non-responsive prostate cancer cell lines, *Int. J. Mol. Sci.* 20 (2019) 2170, <https://doi.org/10.3390/ijms20092170>.
- [22] Á. Baji, T. Kiss, J. Wölfling, D. Kovács, N. Igaz, M.K. Gopisetty, M. Kiricsi, É. Frank, Multicomponent access to androstano-arylpyrimidines under microwave conditions and evaluation of their anti-cancer activity *in vitro*, *J. Steroid Biochem. Mol. Biol.* 172 (2017) 79–88, <https://doi.org/10.1016/j.jsbmb.2017.06.001>.
- [23] P.P. Kaishap, S. Baruah, K. Shekarrao, S. Gogoi, R.C. Boruah, A facile method for the synthesis of steroidal and nonsteroidal 5-methyl pyrazolo[1,5-*a*]pyrimidines, *Tetrahedron Lett.* 55 (2014) 3117–3121, <https://doi.org/10.1016/j.tetlet.2014.04.011>.
- [24] A. Arenas-González, L.A. Mendez-Delgado, P. Merino-Montiel, J.M. Padrón, S. Montiel-Smith, J.L. Vega-Báez, S. Meza-Reyes, Synthesis of monomeric and dimeric steroids containing [1,2,4]triazolo[1,5-*a*]pyrimidines, *Steroids* 116 (2016) 13–19, <https://doi.org/10.1016/j.steroids.2016.09.014>.
- [25] G.M. Allan, H.R. Lawrence, J. Cornet, C. Bubert, D.S. Fischer, N. Vicker, A. Smith, H.J. Tutill, A. Purohit, J.M. Day, M.F. Mahon, M.J. Reed, B.V.L. Potter, Modification of Estrone at the 6, 16, and 17 Positions: novel potent inhibitors of 17 β -hydroxysteroid dehydrogenase type 1, *J. Med. Chem.* 49 (2006) 1325–1345, <https://doi.org/10.1021/jm050830t>.
- [26] V. Jayachandran, S. Vivek Kumar, R. Ranjith Kumar, Synthesis of novel 16-spiro steroids: 7-(Aryl)tetrahydro-1H-pyrrolo[1,2-*c*][1,3]thiazolo estrone hybrid heterocycles, *Steroids* 82 (2014) 29–37, <https://doi.org/10.1016/j.steroids.2014.01.003>.
- [27] L.-H. Huang, Y.-F. Zheng, C.-J. Song, Y.-G. Wang, Z.-Y. Xie, Y.-W. Lai, Y.-Z. Lu, H.-M. Liu, Synthesis of novel D-ring fused 7'-aryl-androstano[17,16-*d*][1,2,4]triazolo[1,5-*a*]pyrimidines, *Steroids* 77 (2012) 367–374, <https://doi.org/10.1016/j.steroids.2011.12.012>.
- [28] P. Saikia, P.P. Kaishap, R. Prakash, K. Shekarrao, S. Gogoi, R.C. Boruah, R. C. A facile one-pot synthesis of 7-substituted pyrazolo[1,5-*a*]pyrimidines by base induced three-component reaction, *Tetrahedron Lett.* 55 (2014) 3896–3900, <https://doi.org/10.1016/j.tetlet.2014.05.021>.
- [29] I. Bartonkova, A. Novotna, Z. Dvorak, Novel stably transfected human reporter cell line AIZ-AR as a tool for an assessment of human androgen receptor transcriptional activity, *PLoS One* 10 (2015), e0121316, <https://doi.org/10.1371/journal.pone.0121316>.
- [30] J. Shaw, M. Leveridge, C. Norling, J. Karén, D.M. Molina, D. O'Neill, J.E. Dowling, P. Davey, S. Cowan, M. Dabrowski, M. Main, D. Gianni, Determining direct binders of the androgen receptor using a high-throughput cellular thermal shift assay, *Sci. Rep.* 8 (2018) 163, <https://doi.org/10.1038/s41598-017-18650-x>.
- [31] S. Lv, Q. Song, G. Chen, E. Cheng, W. Chen, R. Cole, Z. Wu, L.E. Pascal, K. Wang, P. Wipf, J.B. Nelson, Q. Wei, W. Huang, Z. Wang, Regulation and targeting of androgen receptor nuclear localization in castration-resistant prostate cancer, *J. Clin. Invest.* (2020), <https://doi.org/10.1172/JCI141335>.
- [32] S. Chen, S. Gulla, C. Cai, S.P. Balk, Androgen receptor serine 81 phosphorylation mediates chromatin binding and transcriptional activation, *J. Biol. Chem.* 287 (2012) 8571–8583, <https://doi.org/10.1074/jbc.M111.325290>.
- [33] Z. Yu, C. Cai, S. Gao, N.I. Simon, H.C. Shen, S.P. Balk, Galeterone prevents androgen receptor binding to chromatin and enhances degradation of mutant androgen receptor, *Clin. Cancer Res.* 20 (2014) 4075–4085, <https://doi.org/10.1158/1078-0432.CCR-14-0292>.
- [34] Z. Wu, K. Wang, Z. Yang, L.E. Pascal, J.B. Nelson, K. Takubo, P. Wipf, Z. Wang, A novel androgen receptor antagonist JJ-450 inhibits enzalutamide-resistant mutant ARF876L nuclear import and function, *Prostate* 80 (2020) 319–328, <https://doi.org/10.1002/pros.23945>.
- [35] C. Tran, S. Ouk, N.J. Clegg, Y. Chen, P.A. Watson, V. Arora, J. Wongvipat, P. M. Smith-Jones, D. Yoo, A. Kwon, T. Wasielewska, D. Welsbie, C.D. Chen, C. S. Higano, T.M. Beer, D.T. Hung, H.I. Scher, M.E. Jung, C.L. Sawyers, Development of a second-generation antiandrogen for treatment of advanced prostate cancer, *Science* 324 (2009) 787–790, <https://doi.org/10.1126/science.1168175>.
- [36] E. Estébanez-Perpiñá, L.A. Arnold, P. Nguyen, E.D. Rodrigues, E. Mar, R. Bateman, R.J. Fletterick, A surface on the androgen receptor that allosterically regulates coactivator binding, *Proc. Natl. Acad. Sci.* 104 (2007) 16074–16079, <https://doi.org/10.1073/pnas.0708036104>.
- [37] O. Trott, A.J. Olson, AutoDock Vina: Improving the speed and accuracy of docking with a new scoring function, efficient optimization, and multithreading, *J. Comput. Chem.* 31 (2010) 455–461, <https://doi.org/10.1002/jcc.21334>.
- [38] G.M. Morris, R. Huey, W. Lindstrom, M.F. Sanner, R.K. Belew, D.S. Goodsell, A. J. Olson, AutoDock4 and AutoDockTools4: automated docking with selective receptor flexibility, *J. Comput. Chem.* 30 (2009) 2785–2791, <https://doi.org/10.1002/jcc.21256>.
- [39] T. Higashi, Numerical Absorption Correction, NUMABS, 2002.

- [40] CrystalClear S.M. 1.4.0 Rigaku/MSI Inc., 2008.
- [41] SHELXL-2013 Program for Crystal Structure Solution, University of Göttingen, Germany, 2013.
- [42] L.J. Farrugia, WinGX and ORTEP for Windows: an update, *J. Appl. Crystallogr.* 45 (2012) 849–854, <https://doi.org/10.1107/S0021889812029111>.
- [43] A.L. Spek, Single-crystal structure validation with the program PLATON, *J. Appl. Crystallogr.* 36 (2003) 7–13, <https://doi.org/10.1107/S0021889802022112>.
- [44] C.F. Macrae, P.R. Edgington, P. McCabe, E. Pidcock, G.P. Shields, R. Taylor, M. Towler, J. van De Streek, Mercury: visualization and analysis of crystal structures, *J. Appl. Crystallogr.* 39 (2006) 453–457, <https://doi.org/10.1107/S002188980600731X>.
- [45] F.H. Allen, O. Johnson, G.P. Shields, B.R. Smith, M. Towler, CIF applications. XV. enCIFer : a program for viewing, editing and visualizing CIFs, *J. Applied Crystallogr.* 37 (2004) 335–338, <https://doi.org/10.1107/S0021889804003528>.

Supplementary Material for

**Synthesis of dihydrotestosterone derivatives modified in the A-ring with
(hetero)arylidene, pyrazolo[1,5-*a*]pyrimidine and triazolo[1,5-*a*]pyrimidine moieties and
their targeting of the androgen receptor in prostate cancer**

Márton A. Kiss^{1,‡}, Miroslav Peřina^{2,‡}, Václav Bazgier^{3,4}, Nóra V. May⁵, Ádám Baji¹, Radek Jorda^{2,*}, Éva Frank^{1,*}

¹*Department of Organic Chemistry, Doctoral School of Chemistry, University of Szeged, Dóm tér 8, H-6720 Szeged, Hungary*

²*Department of Experimental Biology, Faculty of Science, Palacký University Olomouc, Šlechtitelů 27, 78371 Olomouc, Czech Republic*

³*Department of Physical Chemistry, Faculty of Science, Palacký University Olomouc, Šlechtitelů 241/27, 77900 Olomouc, Czech Republic.*

⁴*Laboratory of Growth Regulators, The Czech Academy of Sciences, Institute of Experimental Botany & Palacký University, Šlechtitelů 27, 78371 Olomouc, Czech Republic*

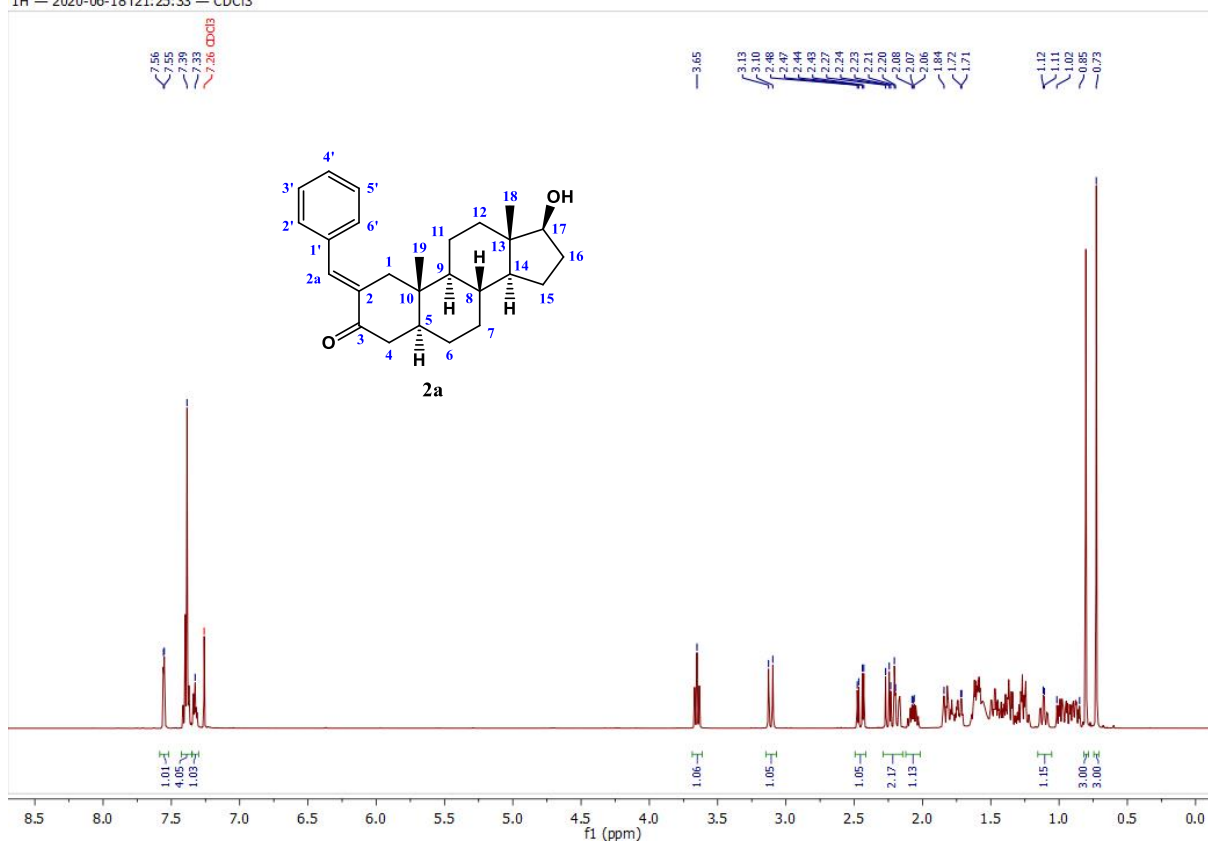
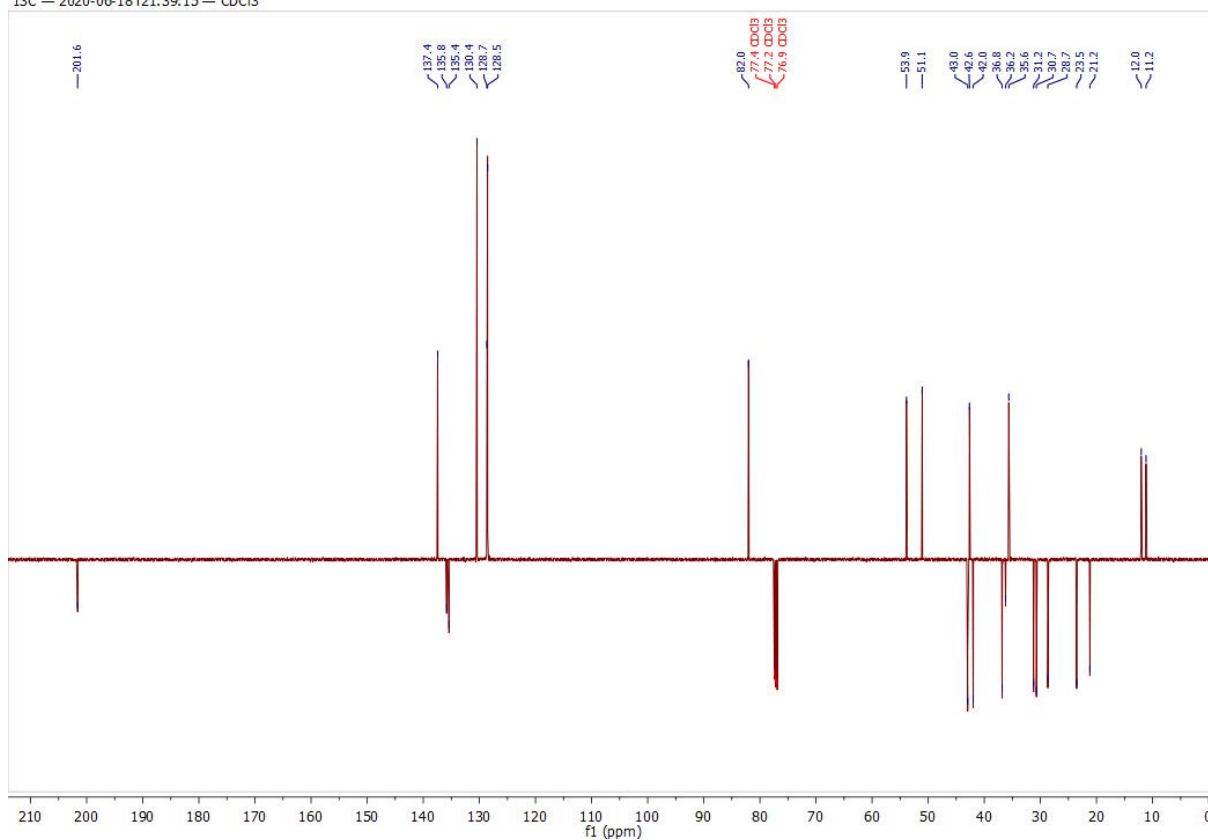
⁵*Centre for Structural Science, Research Centre for Natural Sciences, Magyar tudósok körútja 2, H-1117 Budapest, Hungary*

[‡]These authors contributed equally to this work.

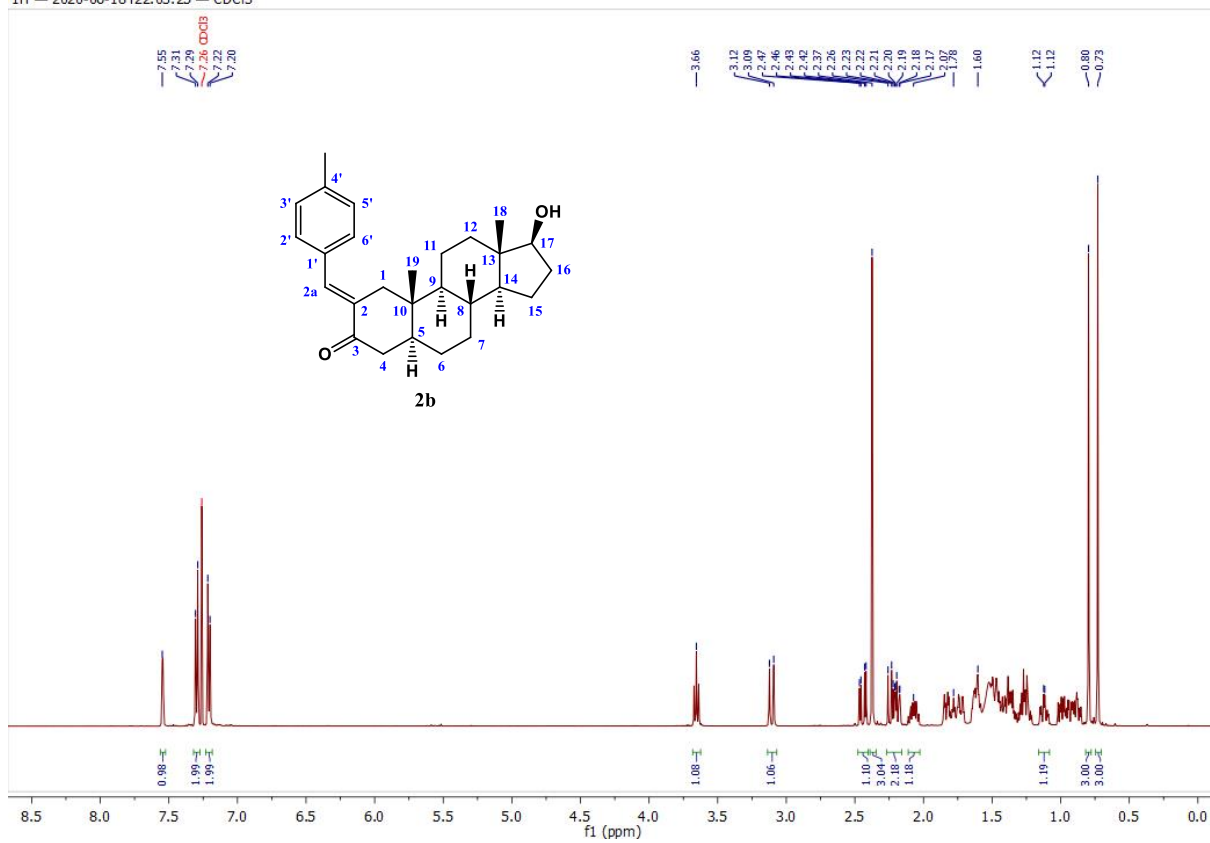
*Corresponding authors: frank@chem.u-szeged.hu; Tel.: +36 62 544 275;
radek.jorda@upol.cz; Tel.: +420 585 634 854

Table of Contents

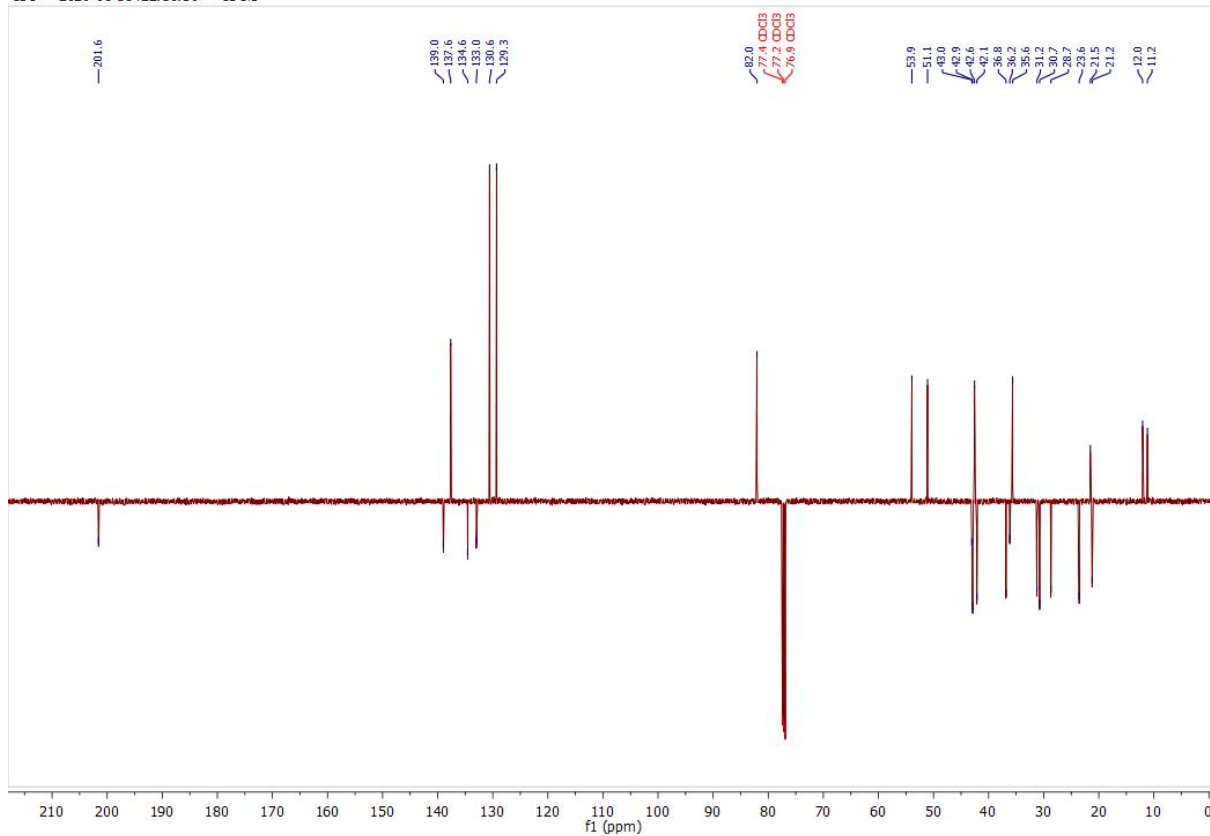
¹H and ¹³C NMR spectra of the synthesized compounds	S1-S32
Figure S1. Unit cell containing two molecules in the crystal of 2a	S33
Figure S2. Packing arrangements in crystal 2a viewed from the crystallographic directions 'a', 'b' and 'c'	S33
Figure S3. Crystal packing in crystal 2a showing (a) O-H...O and C-H...O interactions and (b) C-H... π connections of neighbouring molecules in different view points	S34
Figure S4. Unit cell containing two molecules in the crystal of 8j	S35
Figure S5. Packing arrangements in crystal 8j viewed from the crystallographic directions 'a', 'b' and 'c'	S35
Figure S6. Packing arrangements in crystal 8j showing the main interactions O/C-H...N and C-H...Cl interactions between neighbouring molecules	S36
Table S1. Bond length obtained for the compound 2a in crystal I and two molecules of 8j in crystal II	S37
Table S2. Bond angles obtained for molecules in crystal 2a and 8j	S38
Table S3. Hydrogen-bond geometry of crystal 2a and 8j	S39
Transcriptional activity (22Rv1-ARE14 gene reporter assay, 24 h)	S40-S43
Viability of 22Rv1-ARE14 (72 h) and C4-2 (72 h)	S44-S49

^1H and ^{13}C NMR spectra of the synthesized compounds1H — 2020-06-18T21:25:33 — CDCl₃13C — 2020-06-18T21:39:15 — CDCl₃

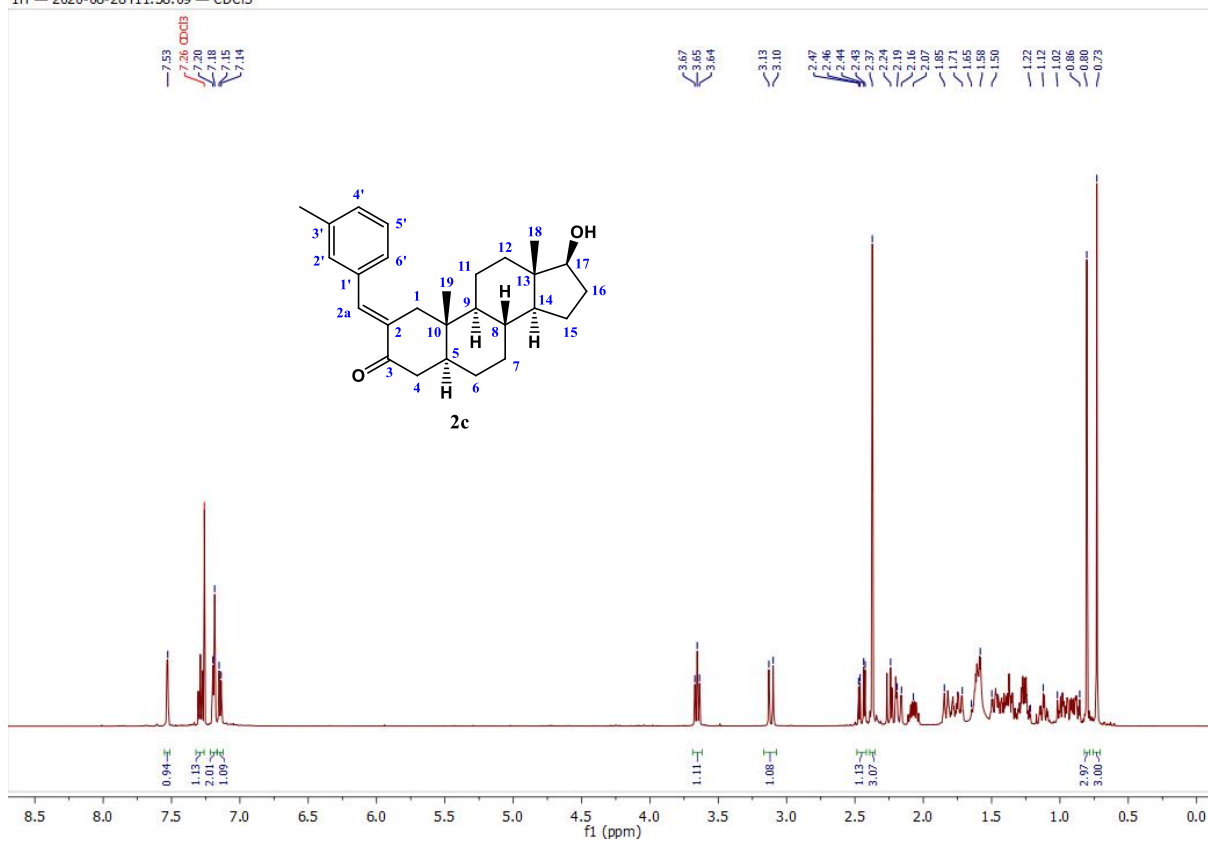
1H — 2020-06-18T22:03:25 — CDCl3



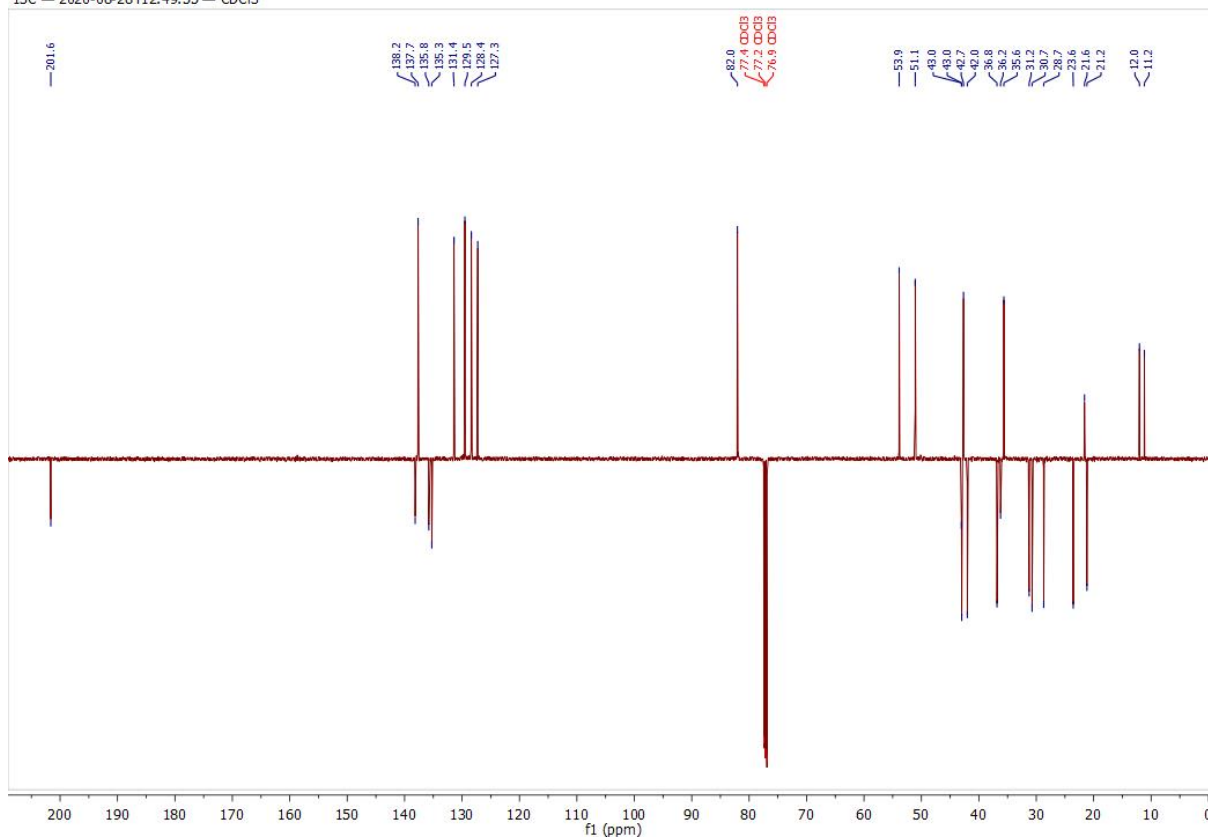
13C — 2020-06-18T22:16:50 — CDCl3



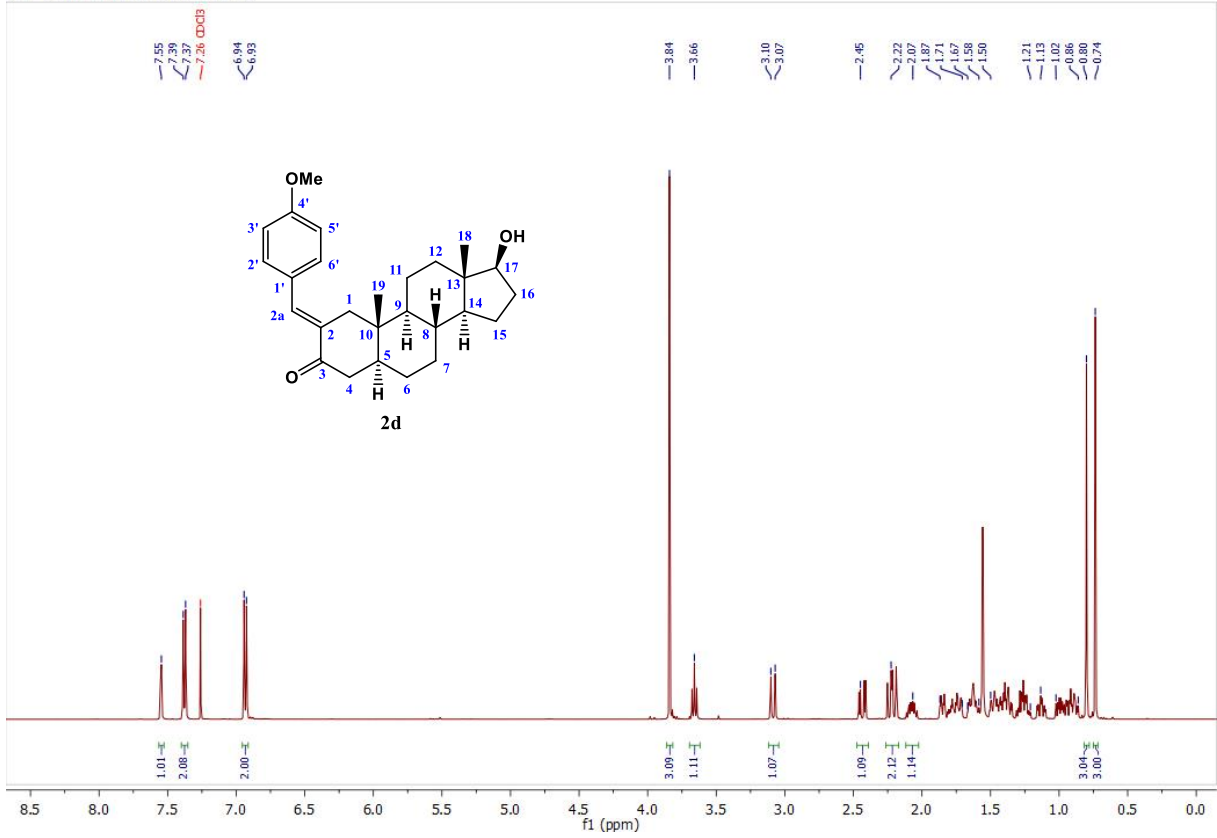
1H — 2020-08-28T11:58:09 — CDCl3



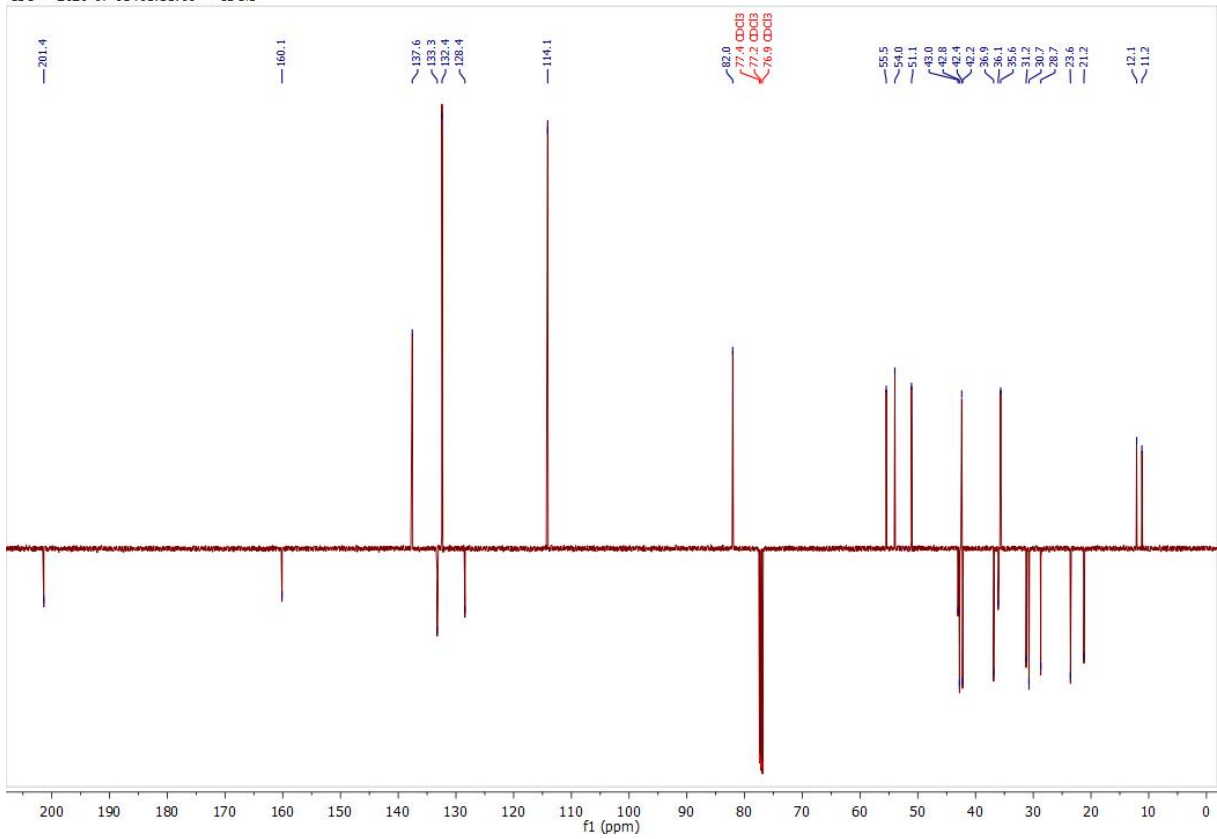
13C — 2020-08-28T12:49:55 — CDCl3

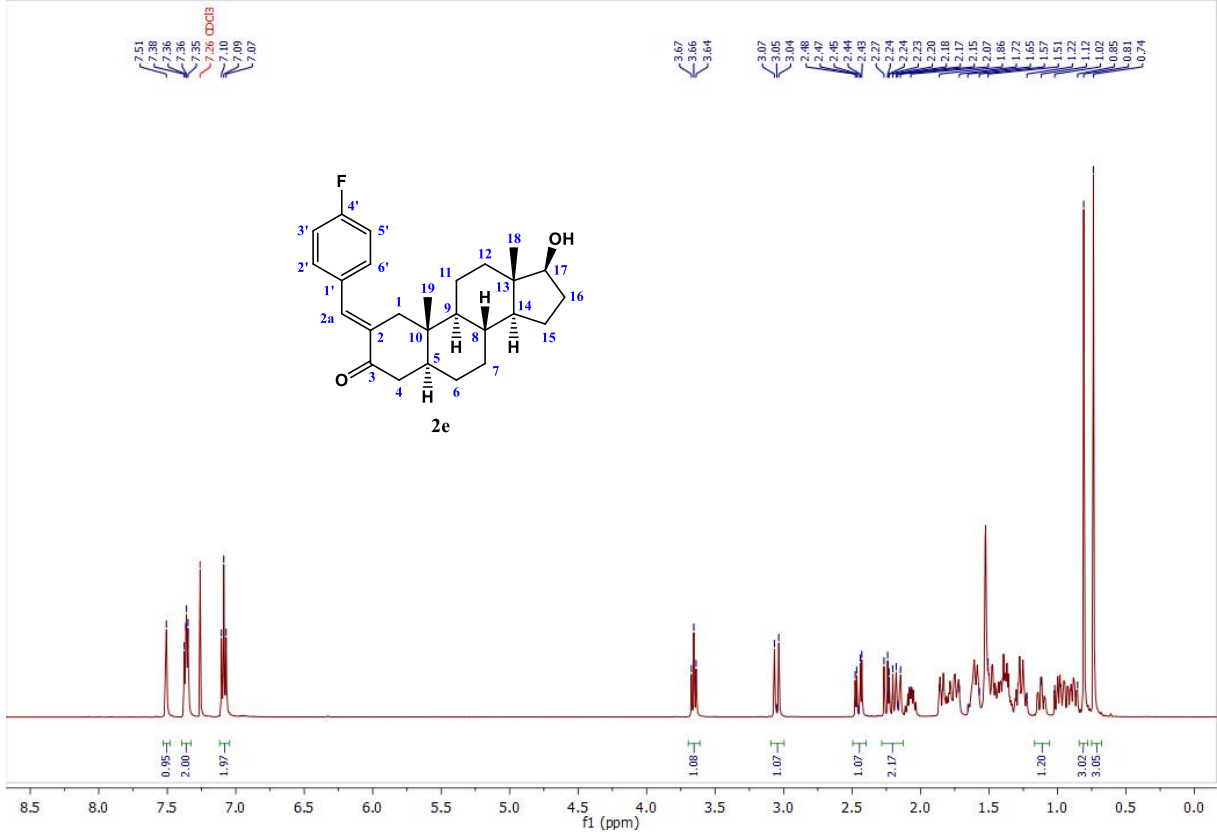
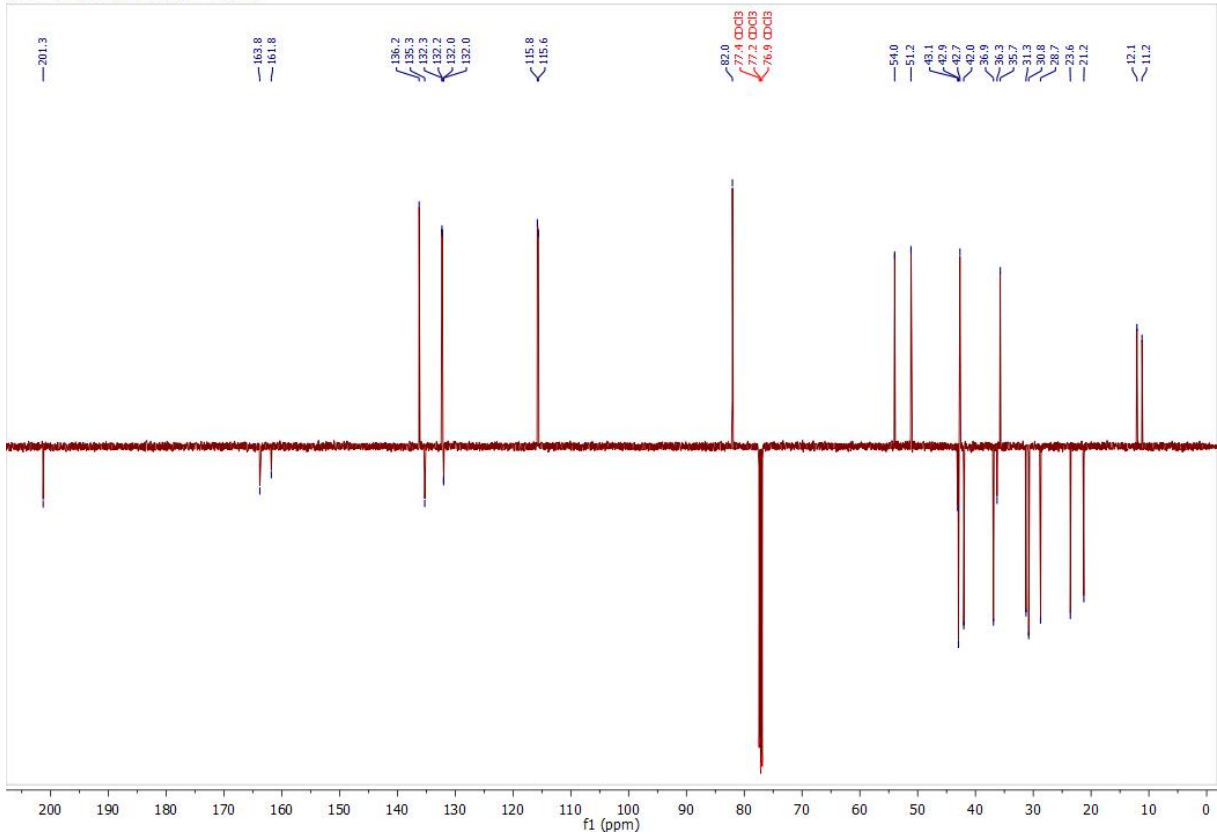


1H — 2020-07-01T05:19:43 — CDCl3

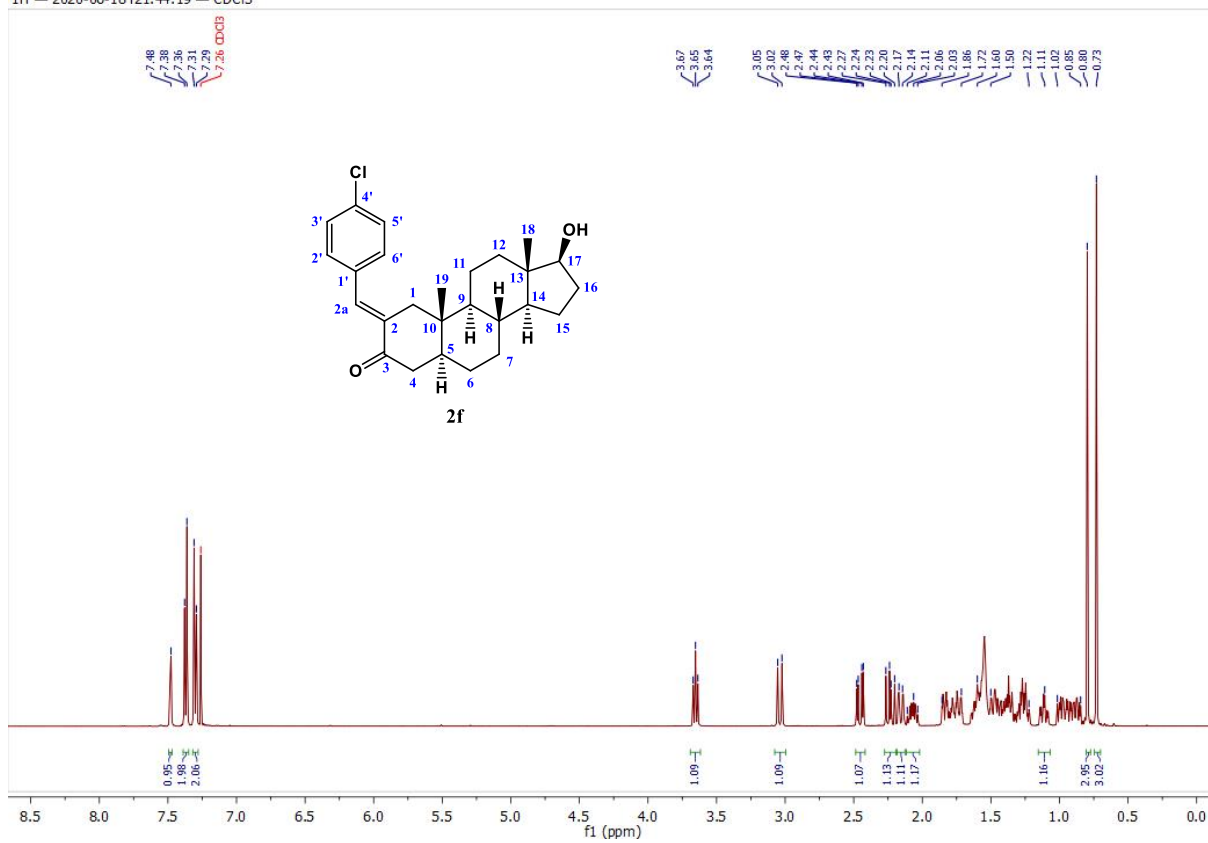


13C — 2020-07-01T05:33:09 — CDCl3

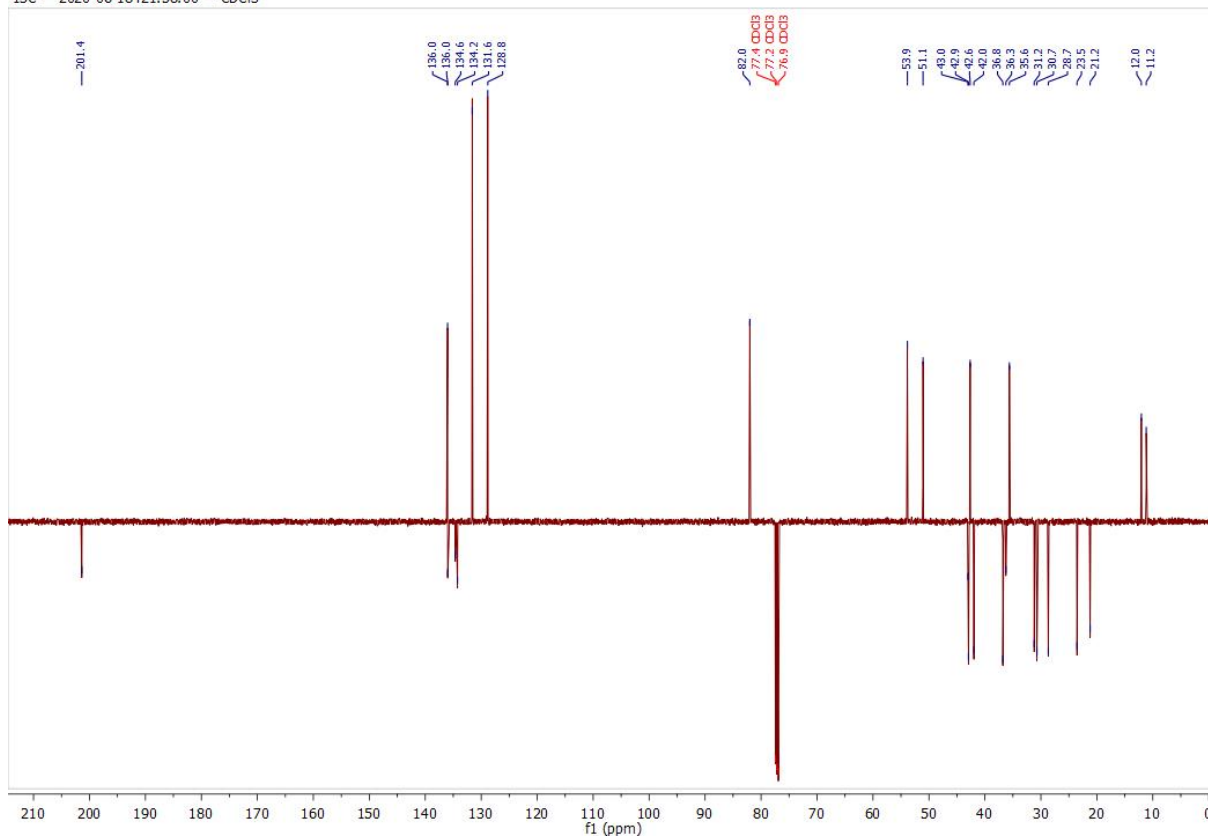


1H — 2020-07-30T00:41:32 — CDCl₃13C — 2020-07-30T00:54:57 — CDCl₃

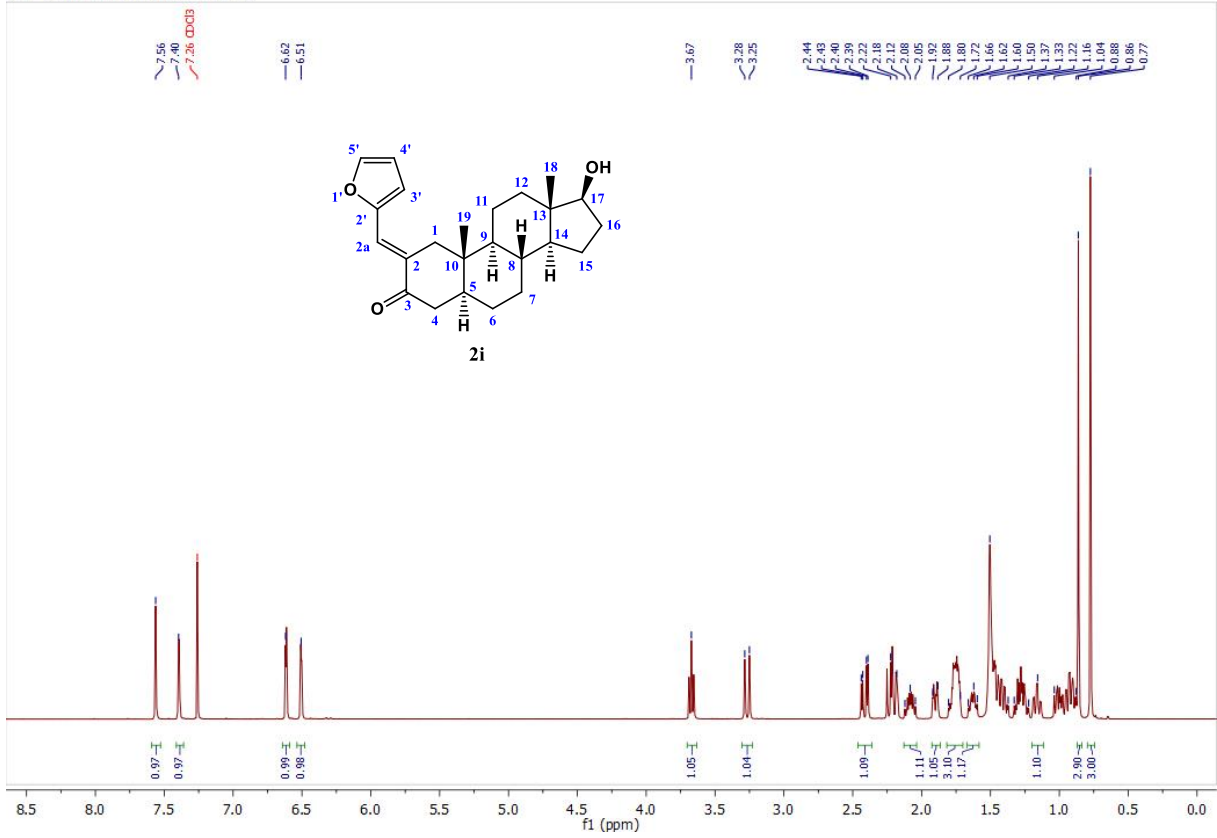
1H — 2020-06-18T21:44:19 — CDCl3



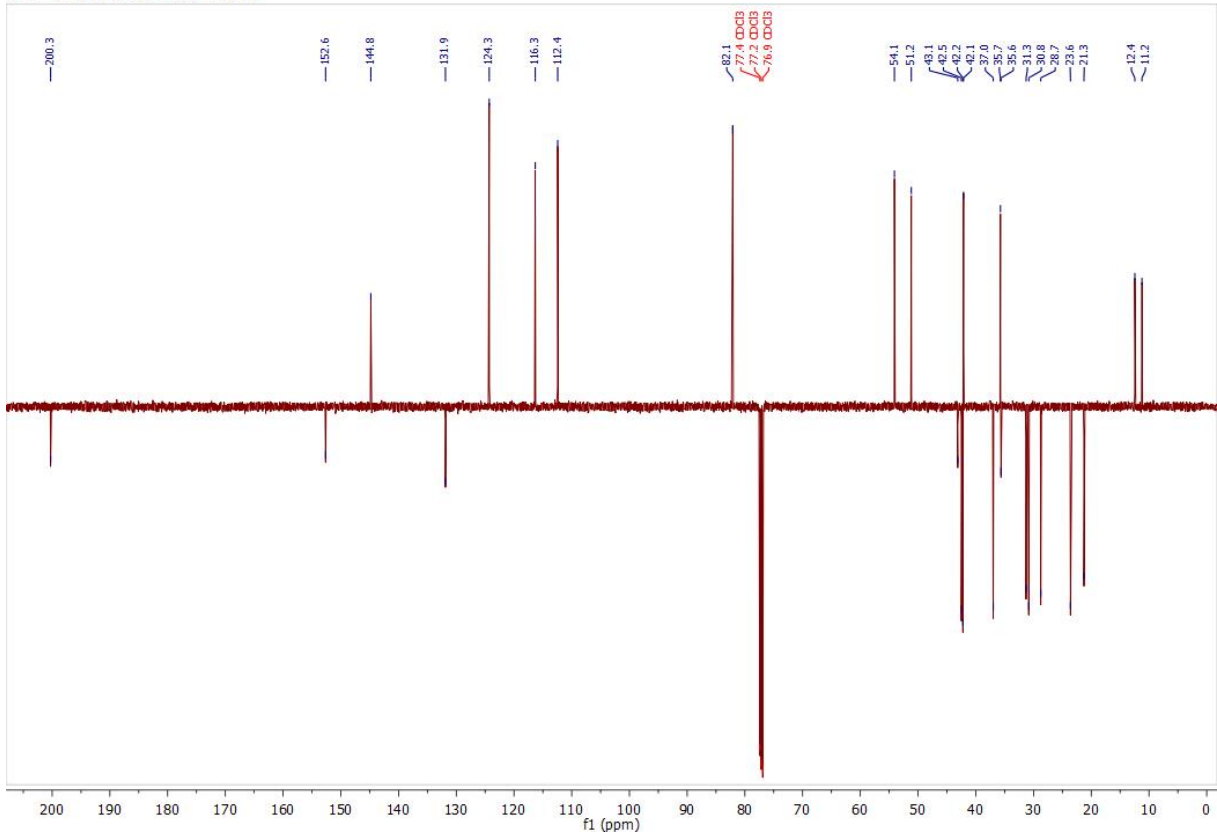
13C — 2020-06-18T21:58:00 — CDCl3



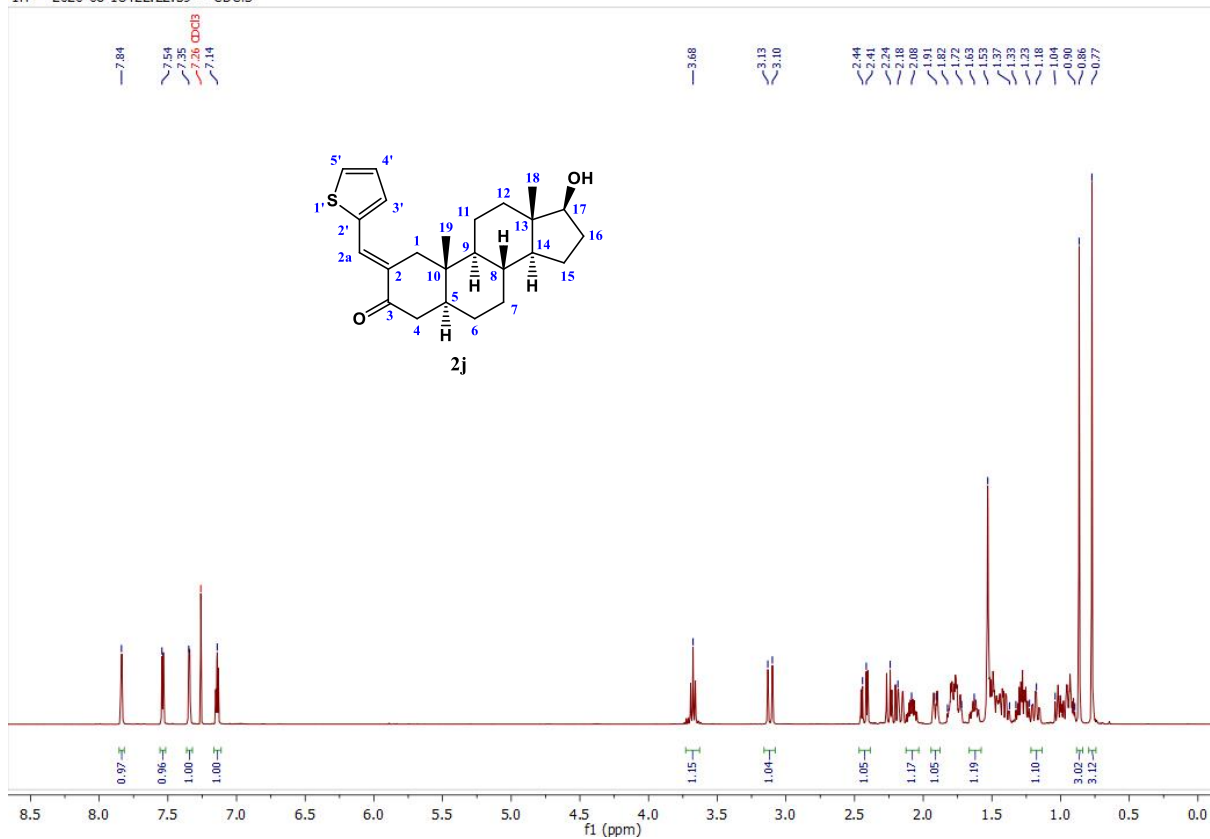
1H — 2020-07-15T20:27:43 — CDCl3



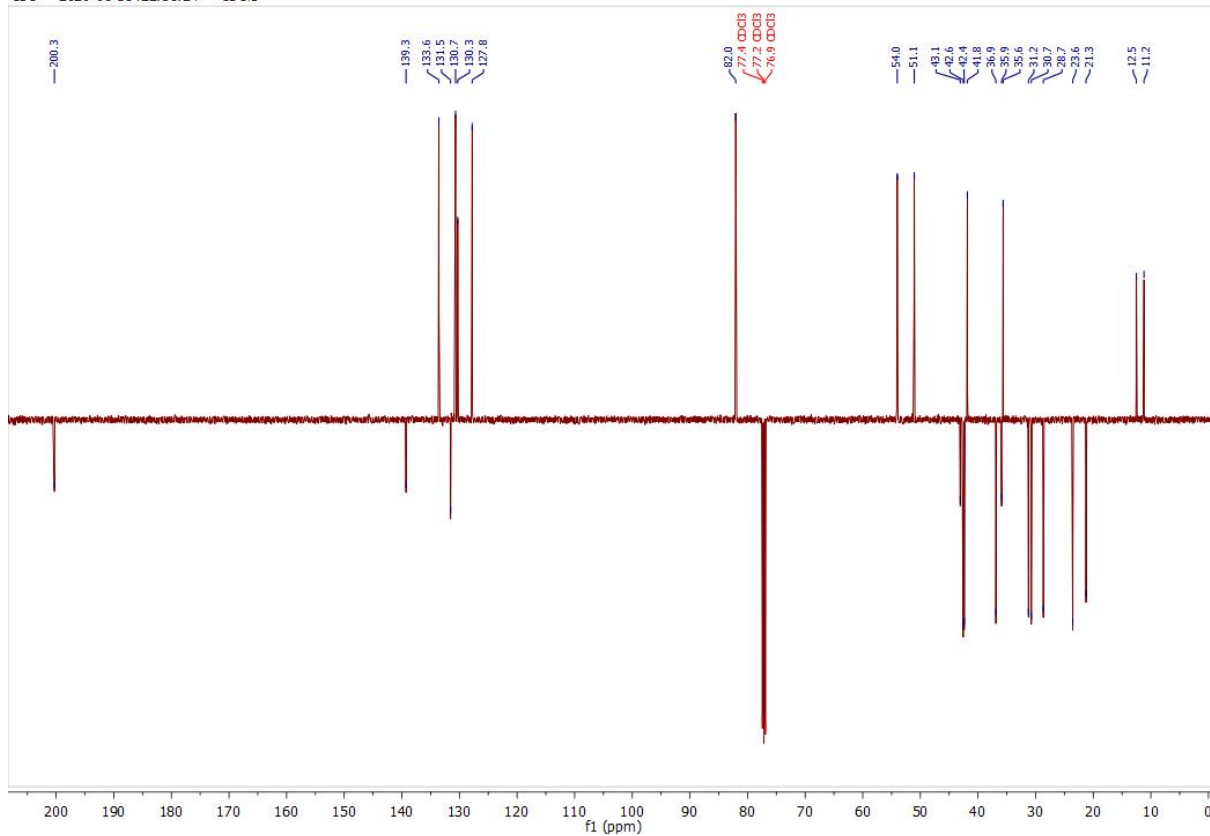
13C — 2020-07-15T20:41:11 — CDCl3



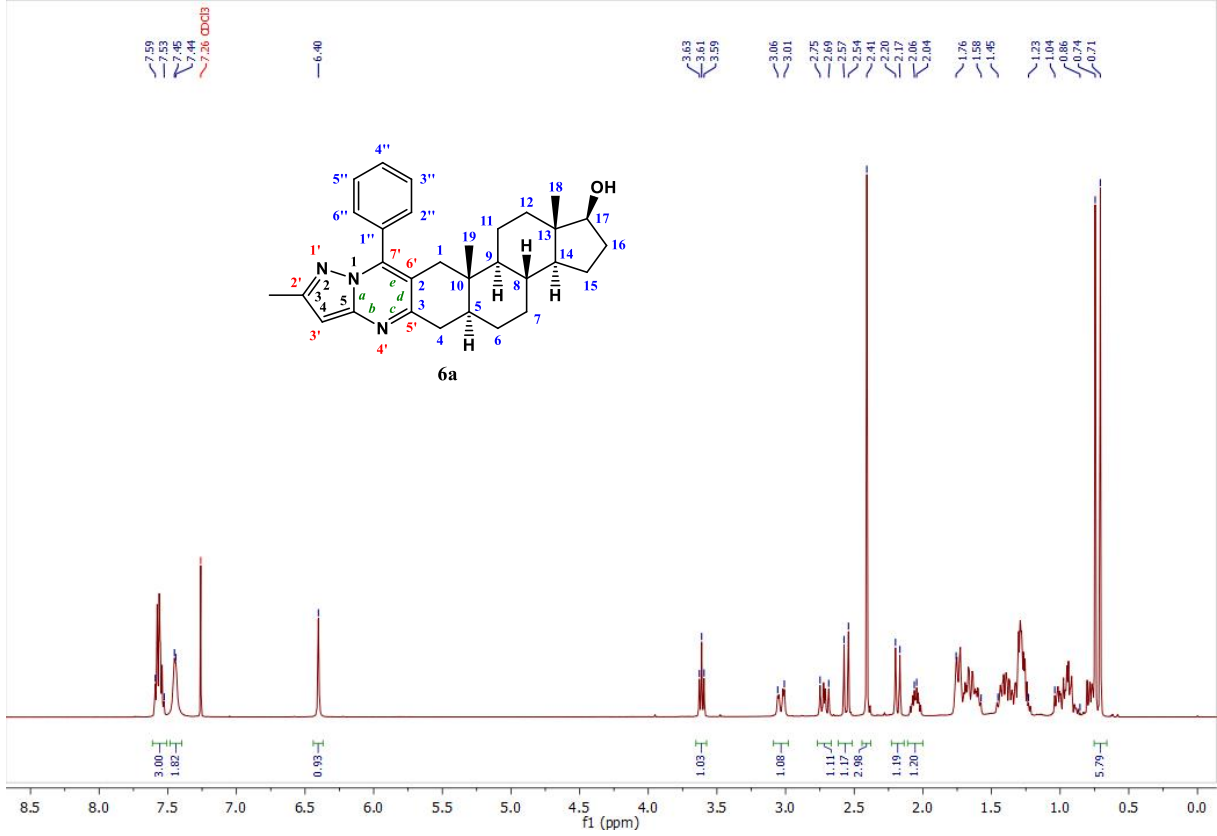
1H — 2020-06-18T22:22:59 — CDCl3



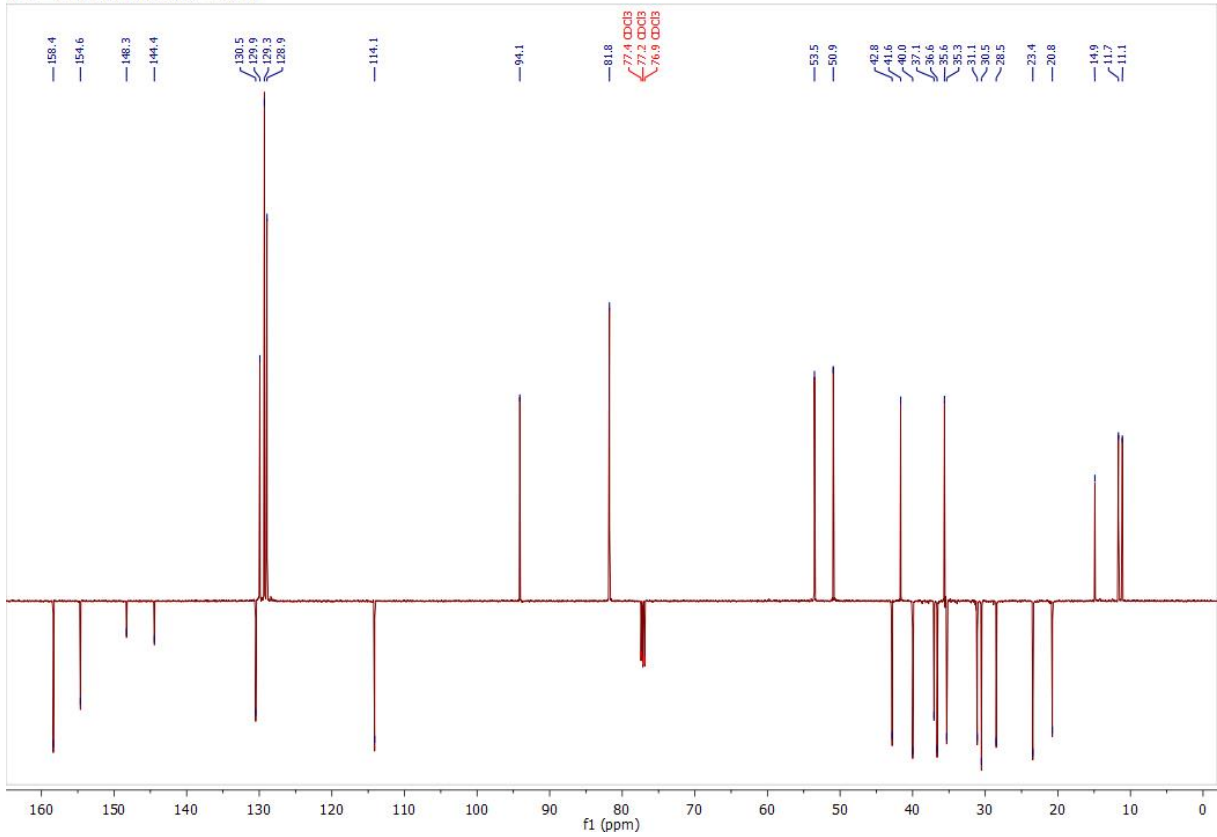
13C — 2020-06-18T22:36:24 — CDCl3



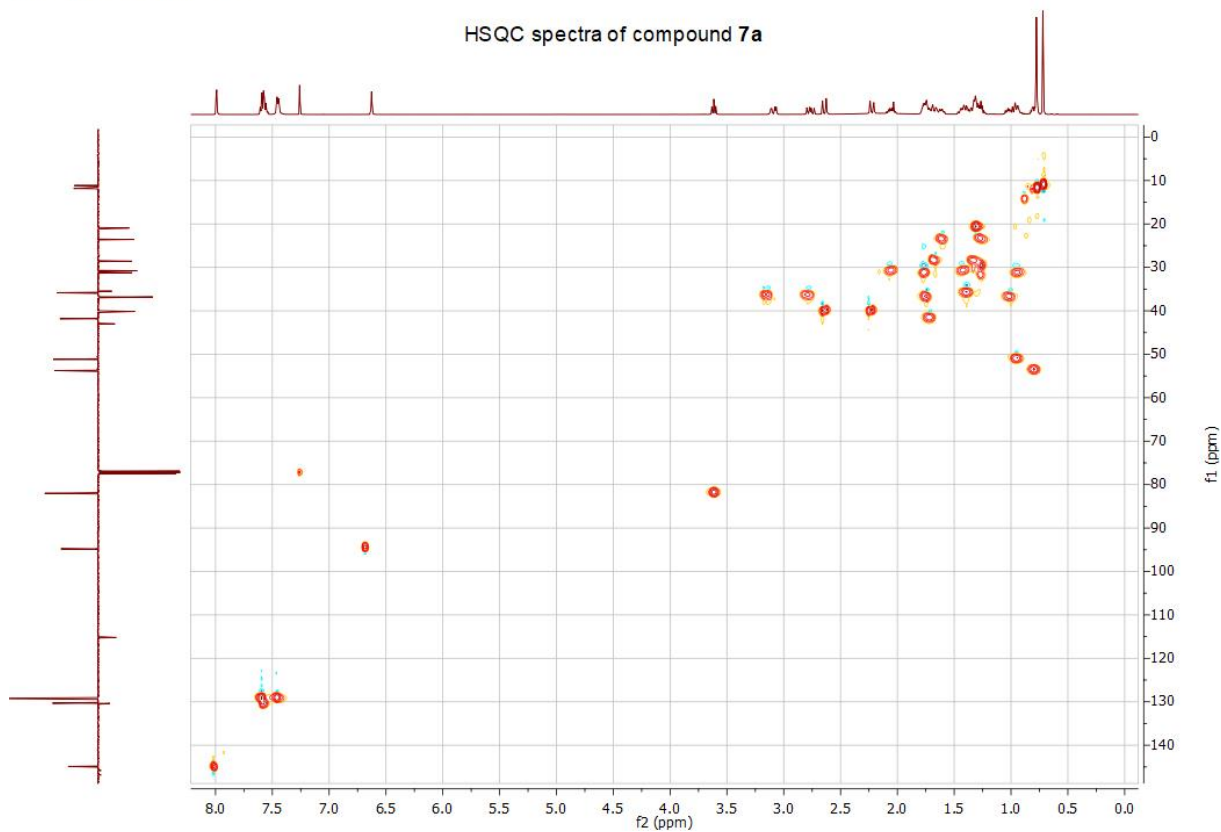
1H — 2020-08-28T14:33:26 — CDCl3



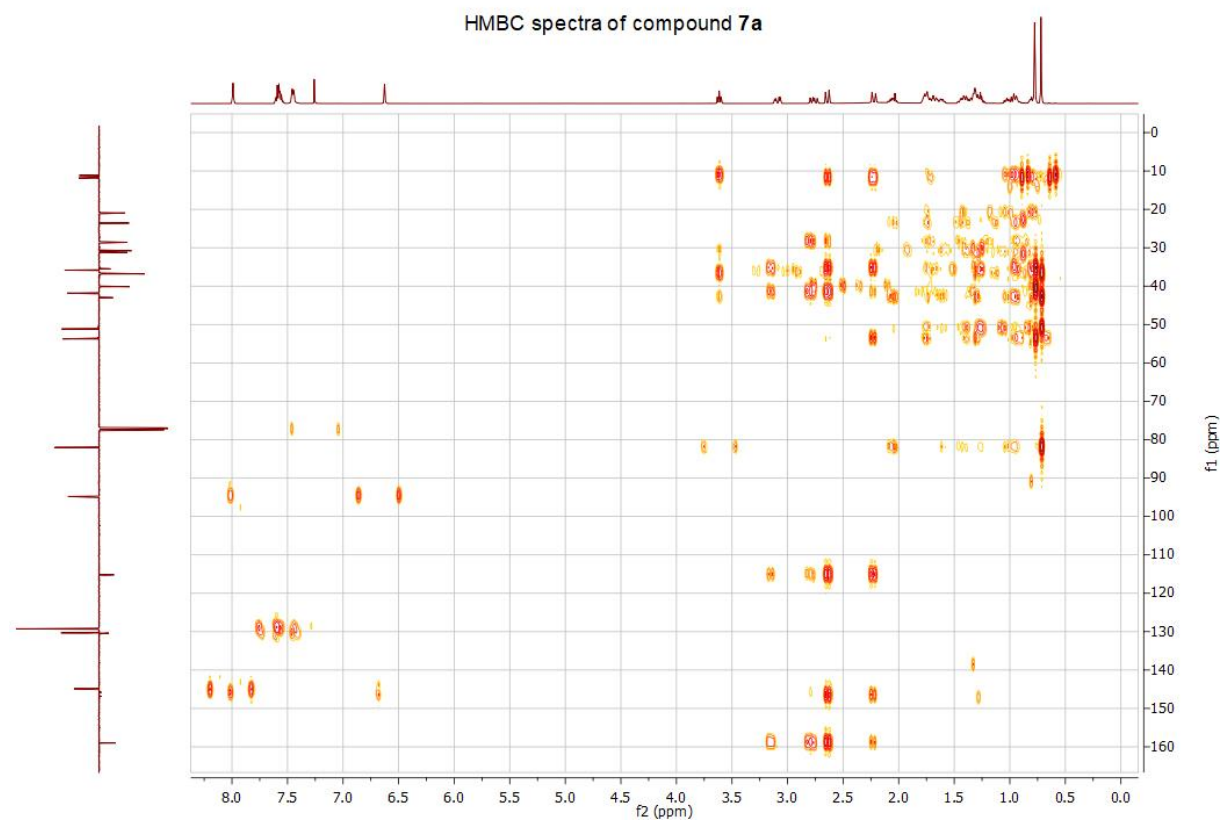
13C — 2020-01-18T07:05:52 — CDCl3



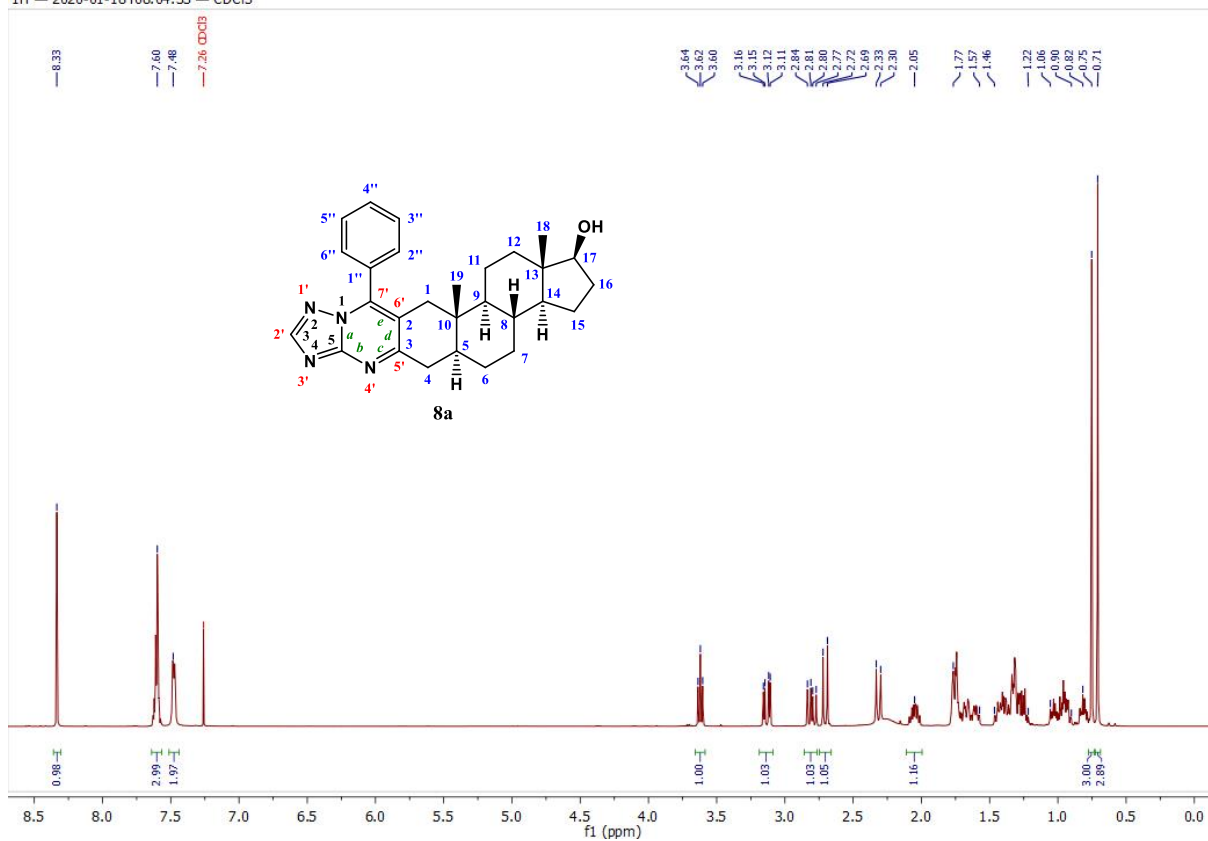
1H — 2020-01-10T16:11:25 — CDCl3



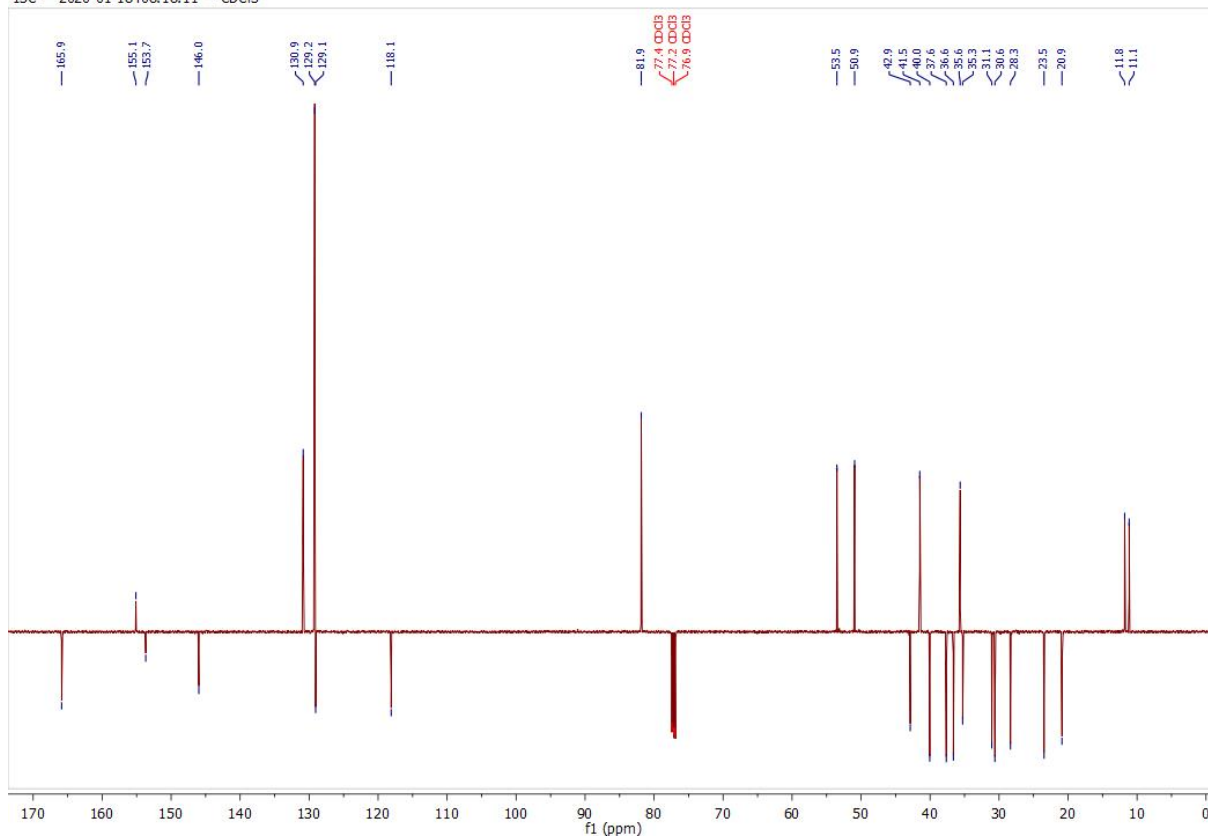
1H — 2020-01-10T16:43:04 — CDCl3



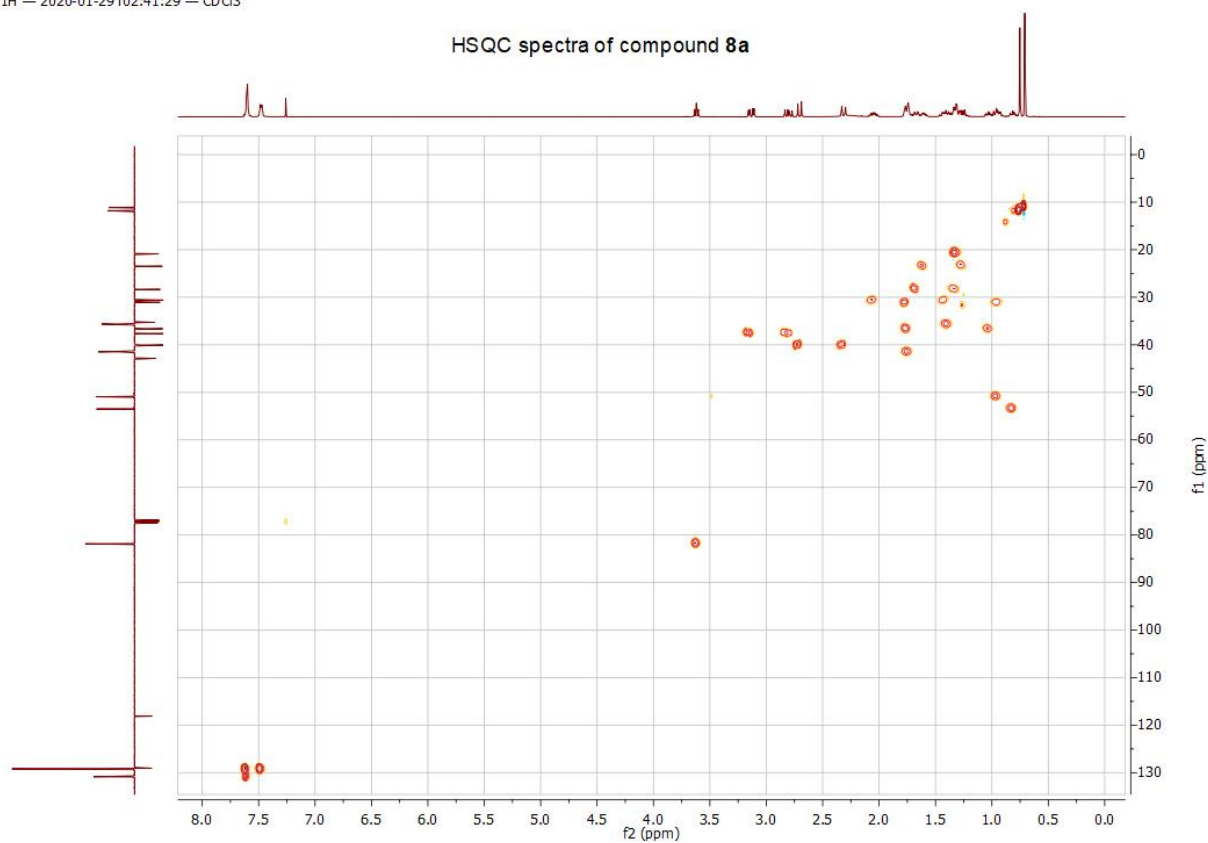
1H — 2020-01-18T08:04:33 — CDCl3



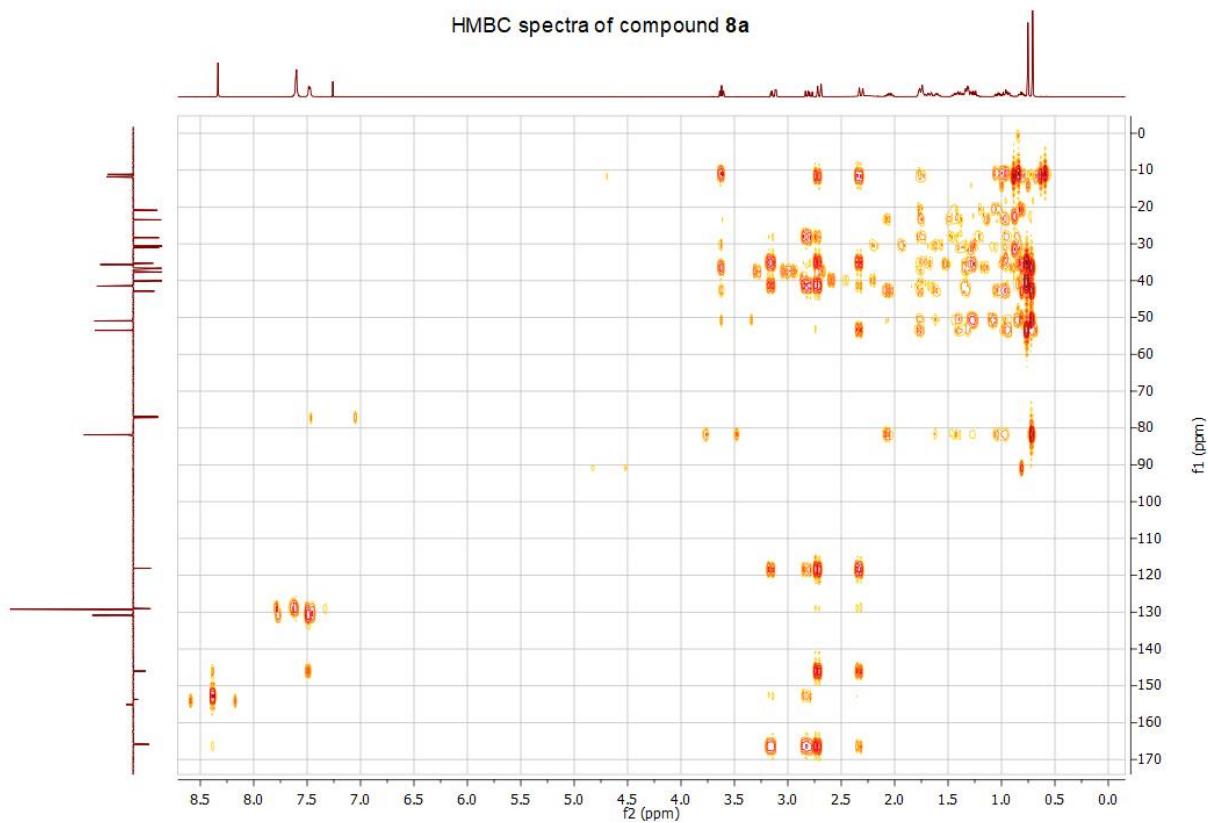
13C — 2020-01-18T08:18:11 — CDCl3



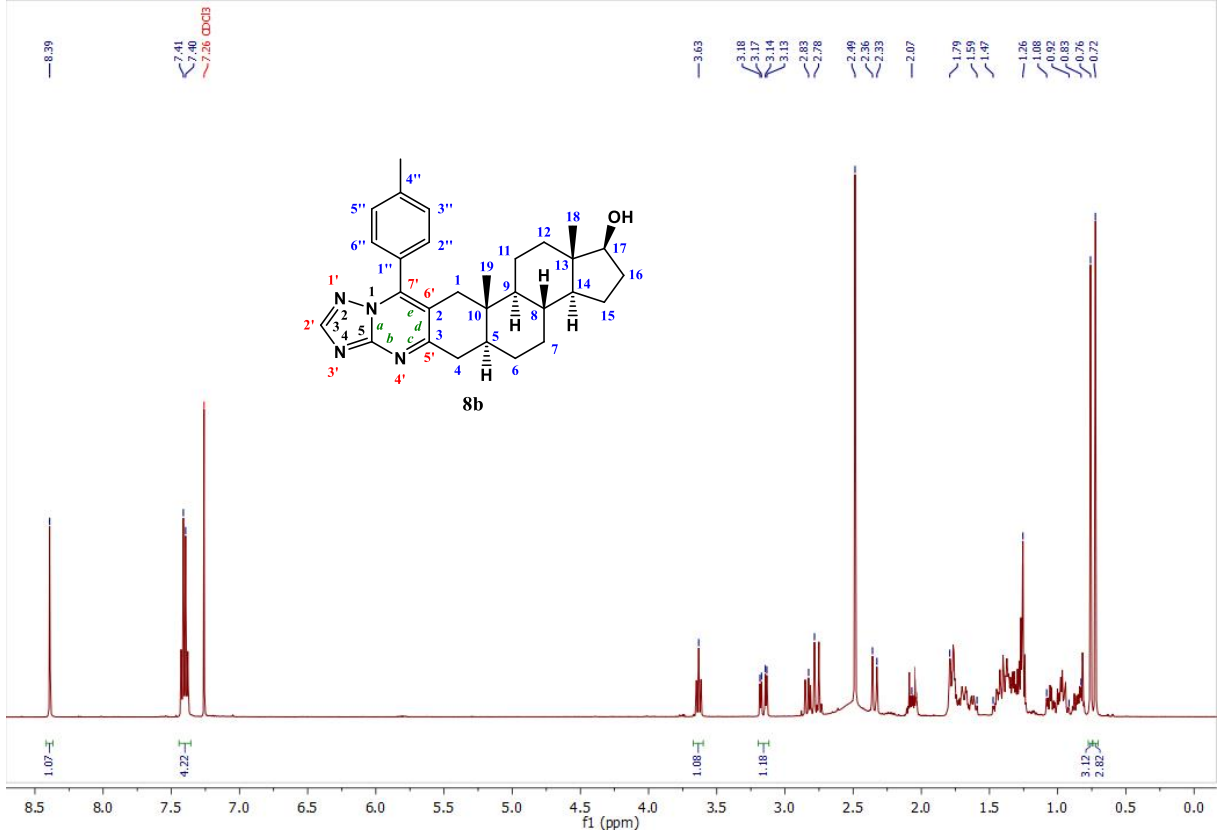
1H — 2020-01-29T02:41:29 — CDCl3



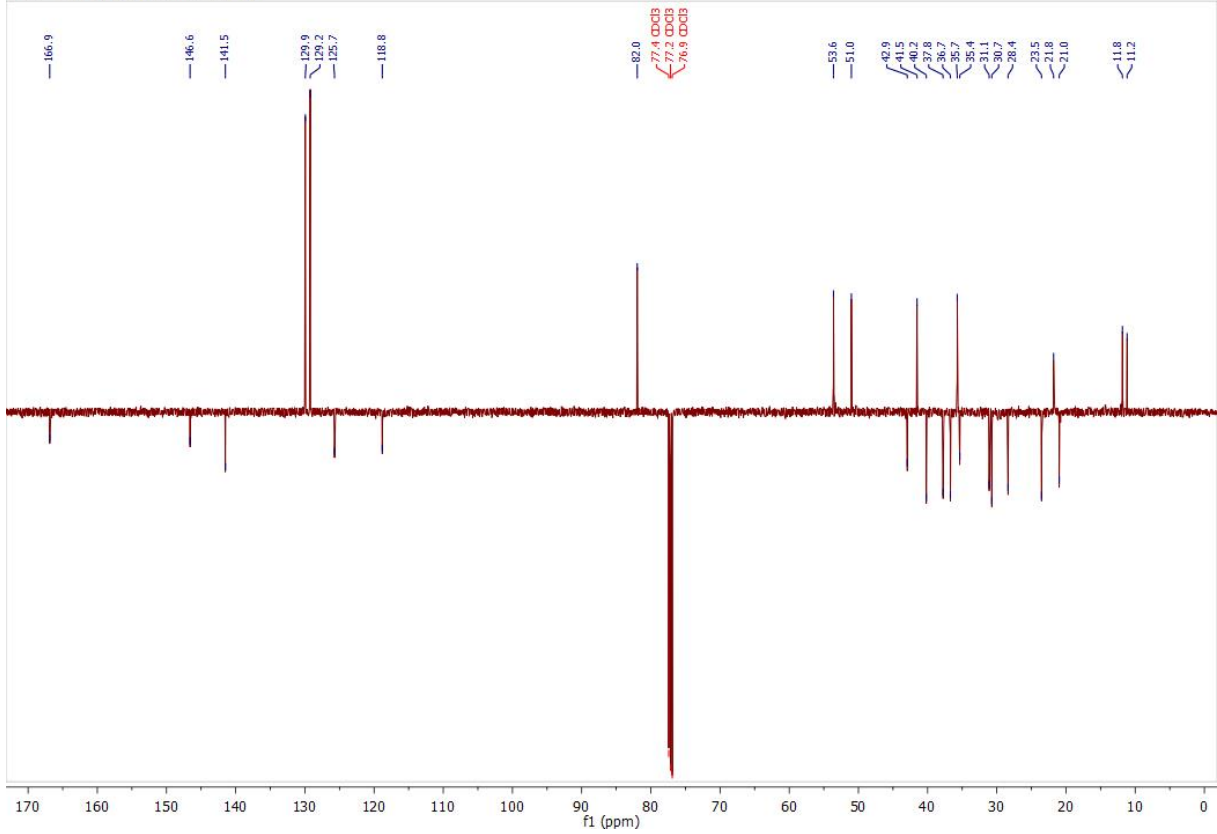
1H — 2020-01-29T03:13:03 — CDCl3



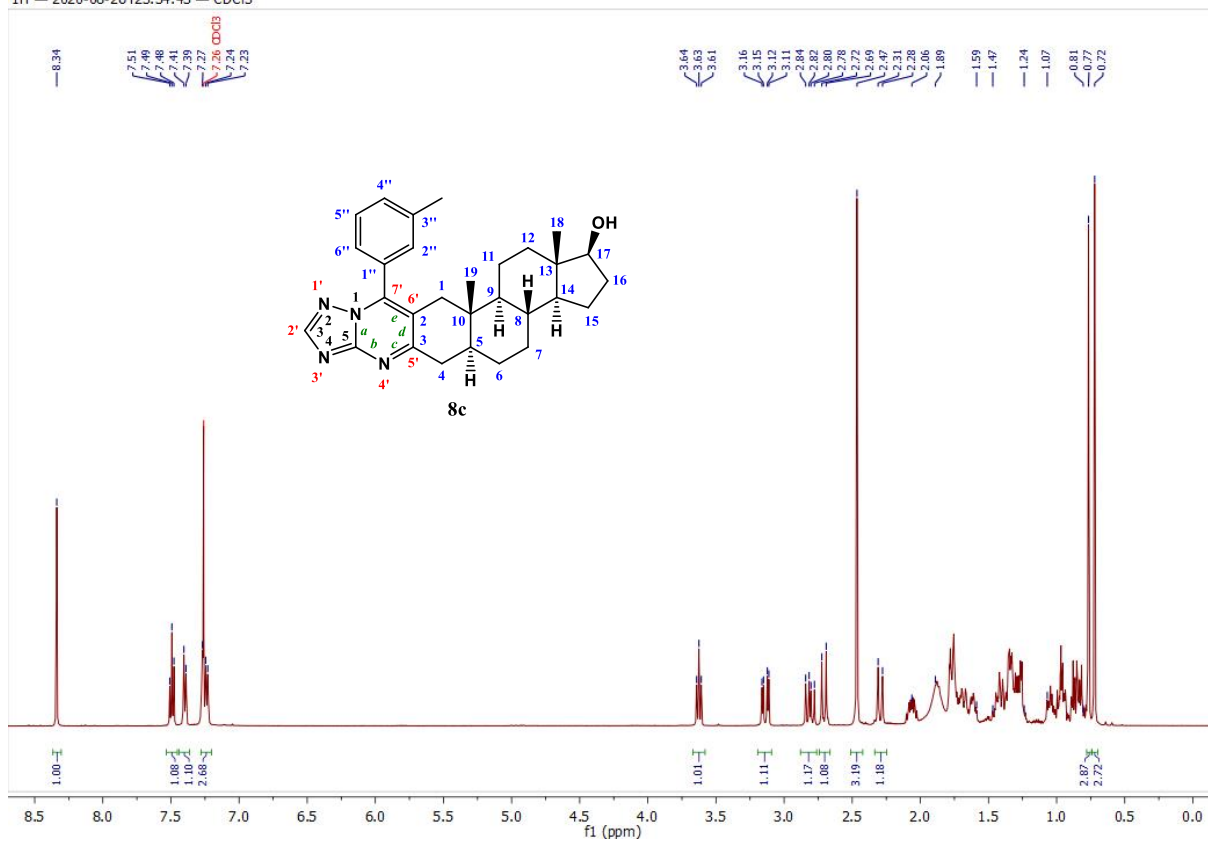
1H — 2020-07-01T03:03:49 — CDCl3



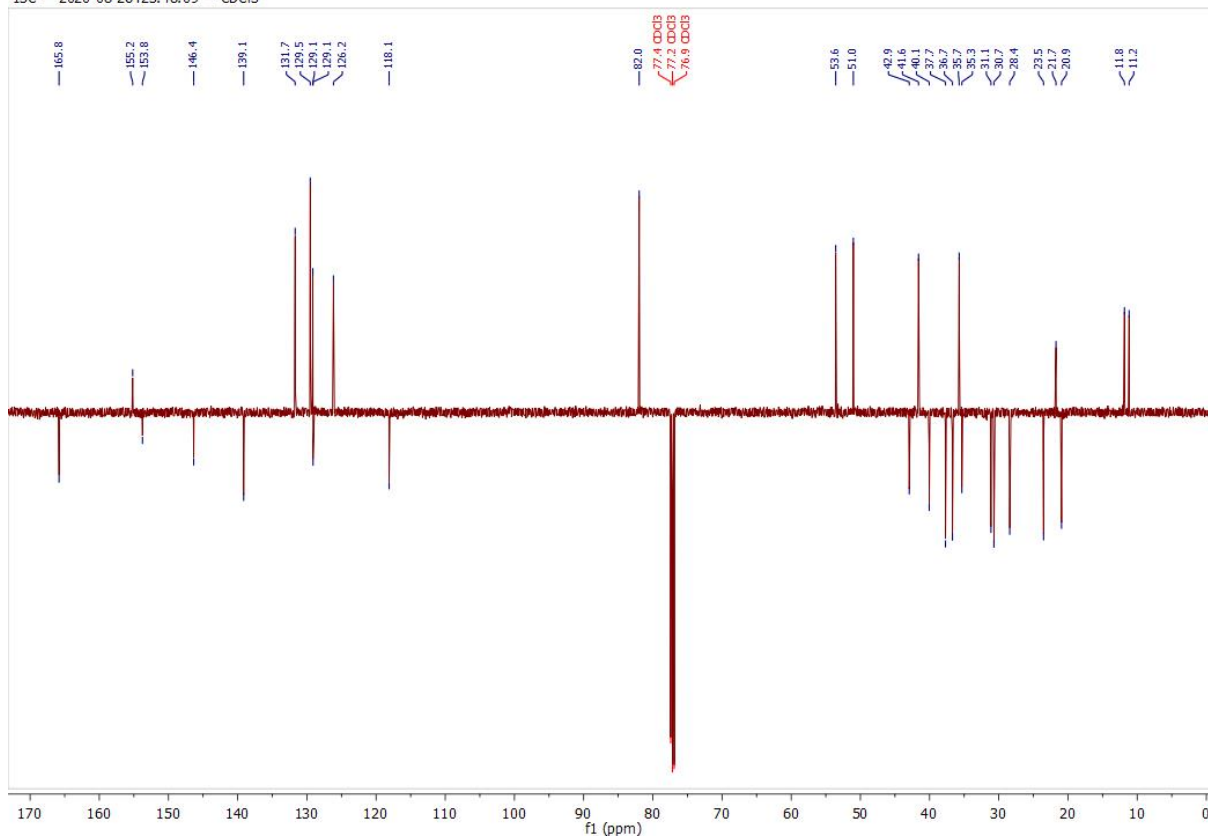
13C — 2020-07-01T03:17:37 — CDCl3



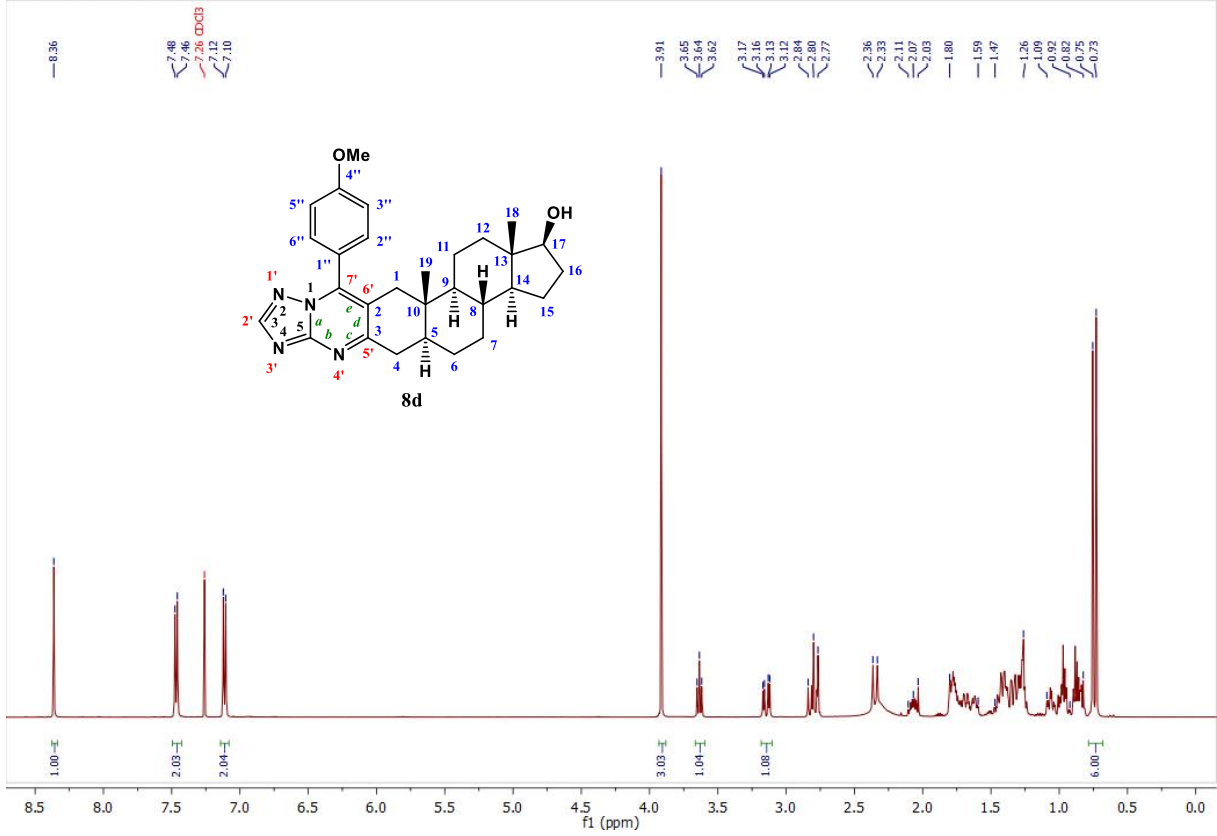
1H — 2020-08-26T23:34:43 — CDCl3



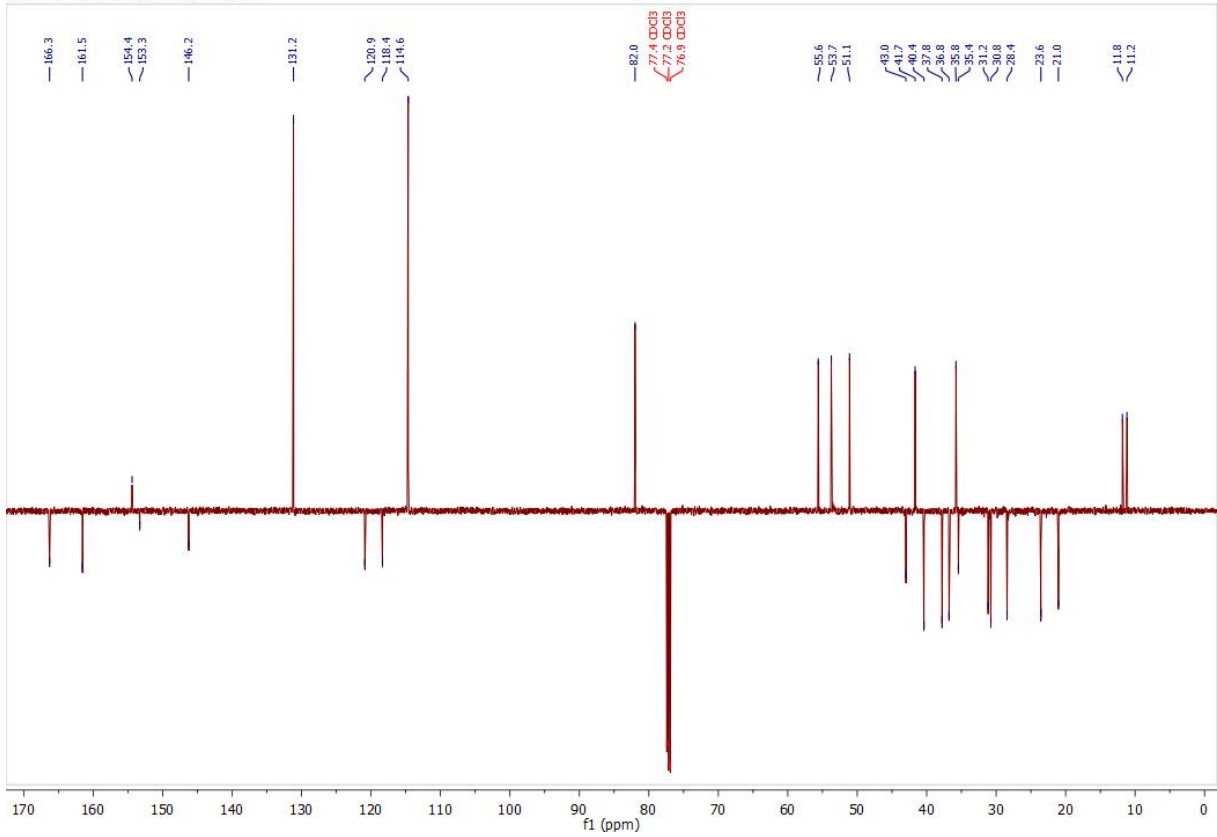
13C — 2020-08-26T23:48:09 — CDCl3



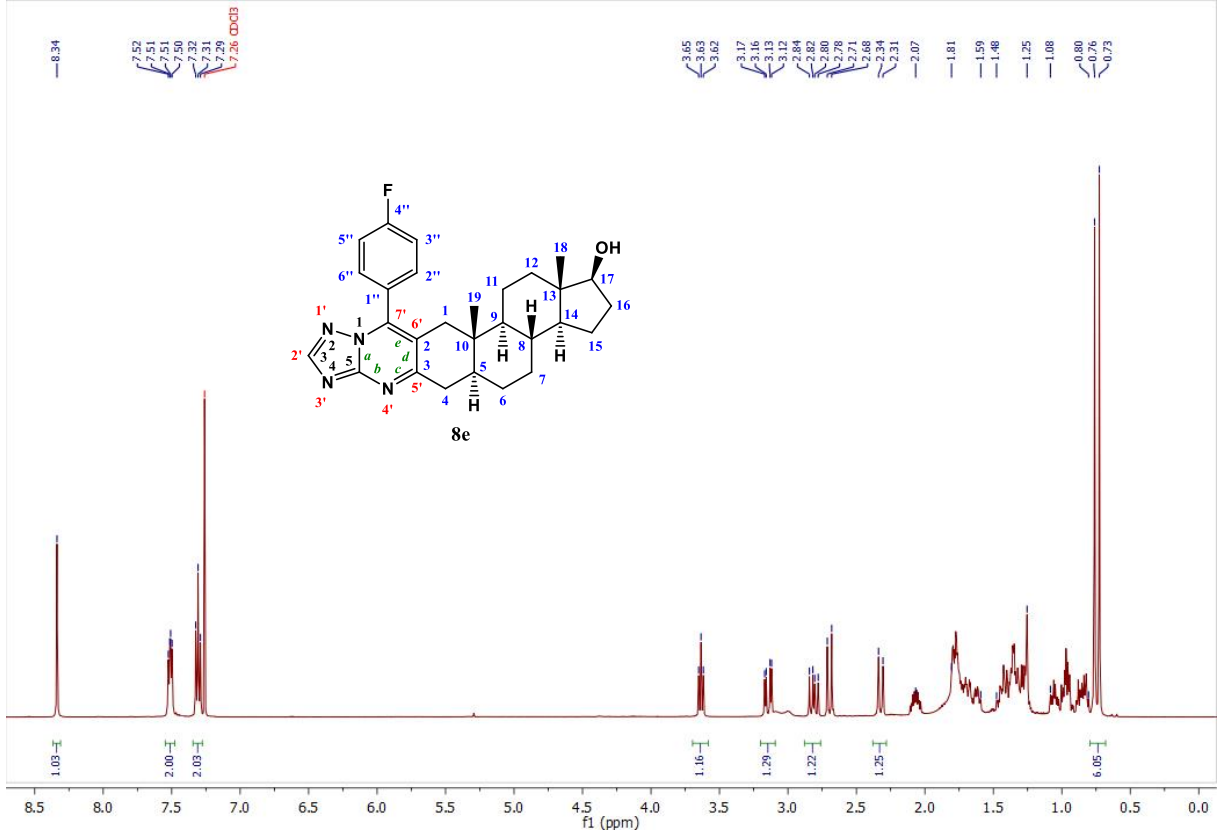
1H — 2020-07-15T21:25:54 — CDCl3



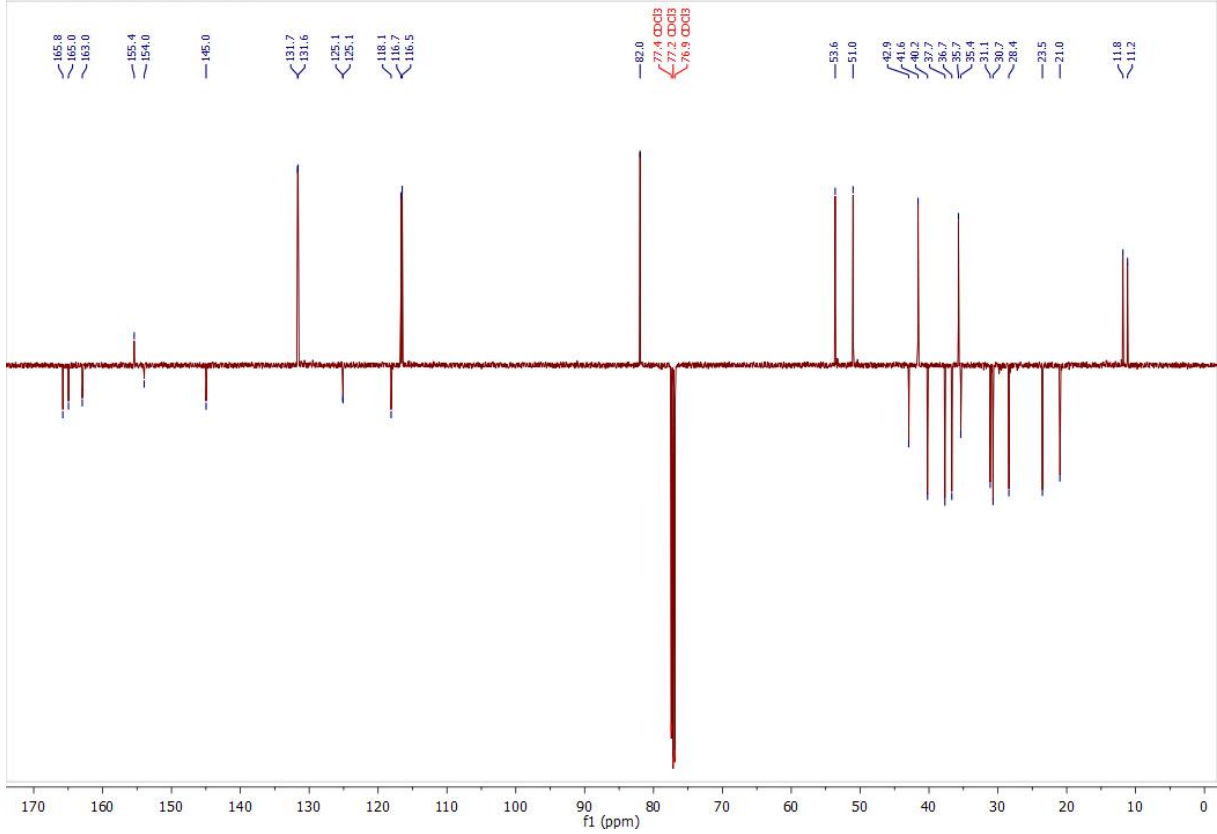
13C — 2020-07-15T21:39:21 — CDCl3



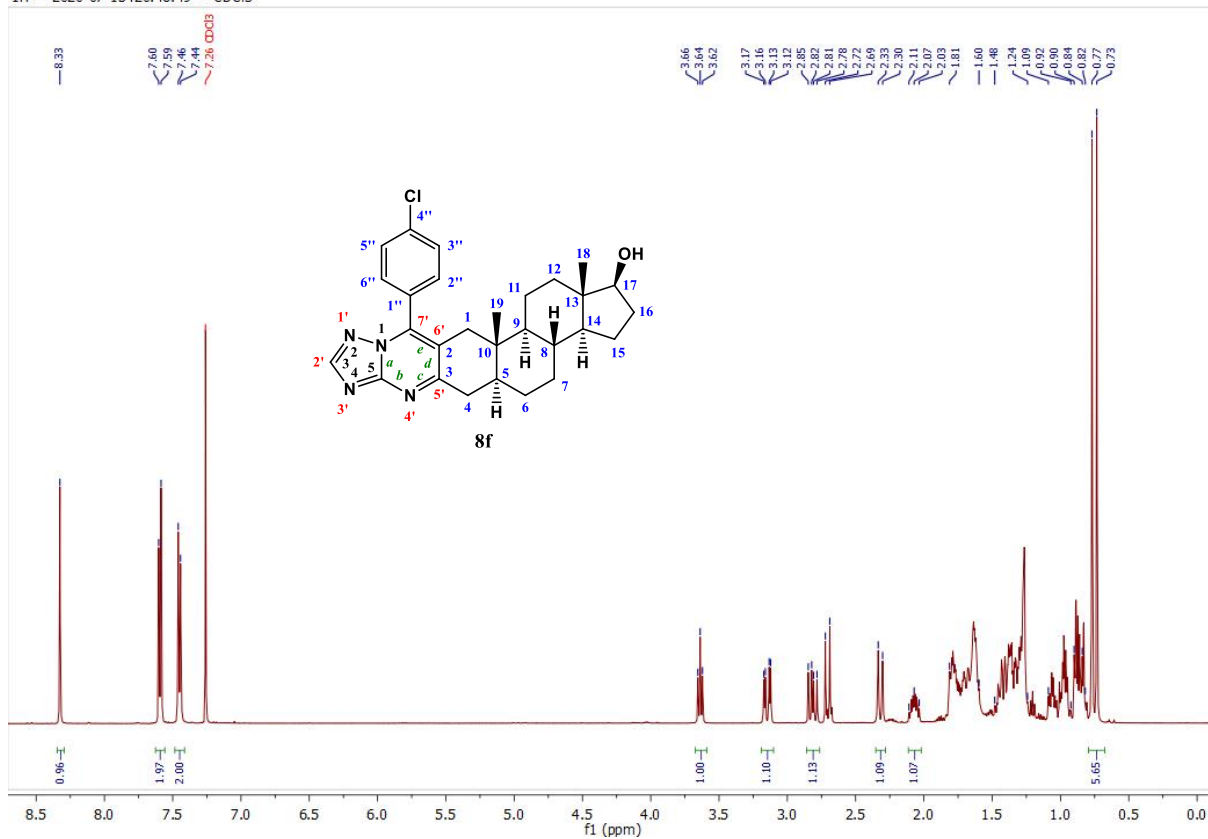
1H — 2020-08-28T13:36:09 — CDCl3



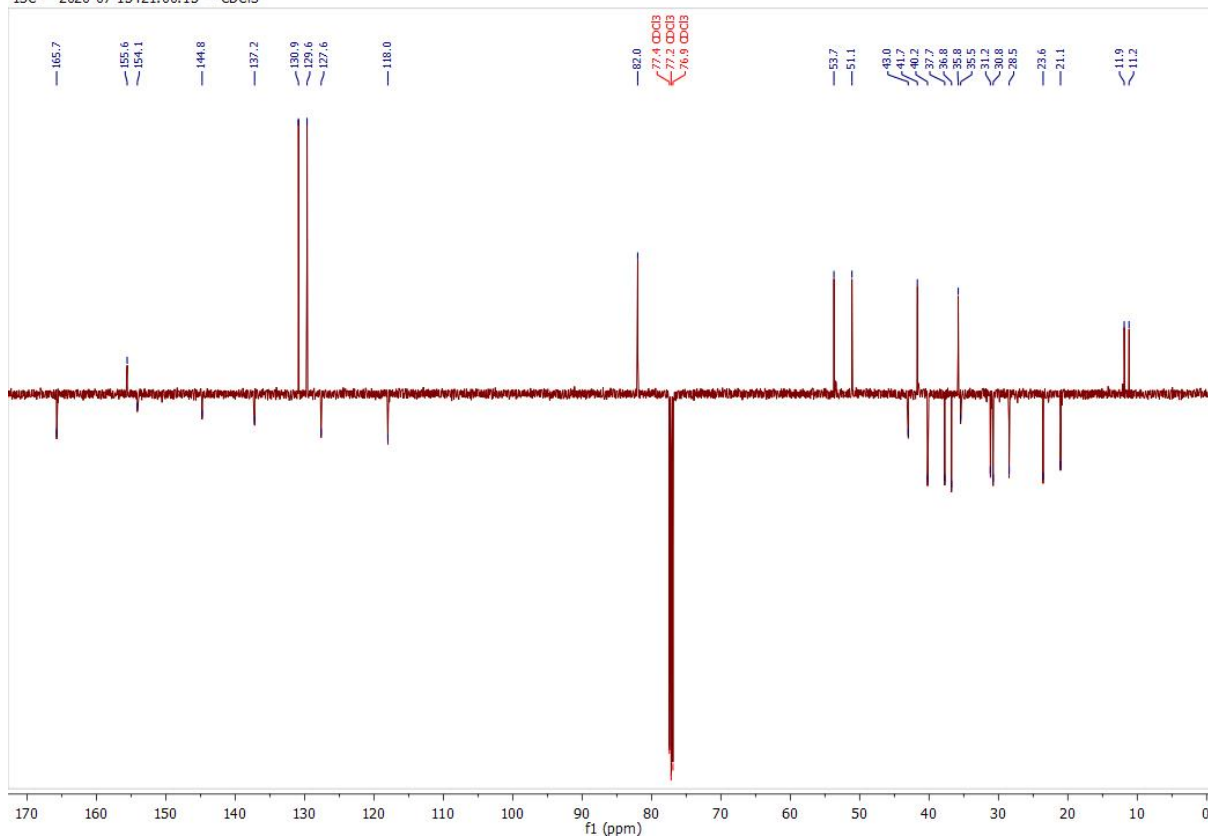
13C — 2020-08-28T14:27:45 — CDCl3

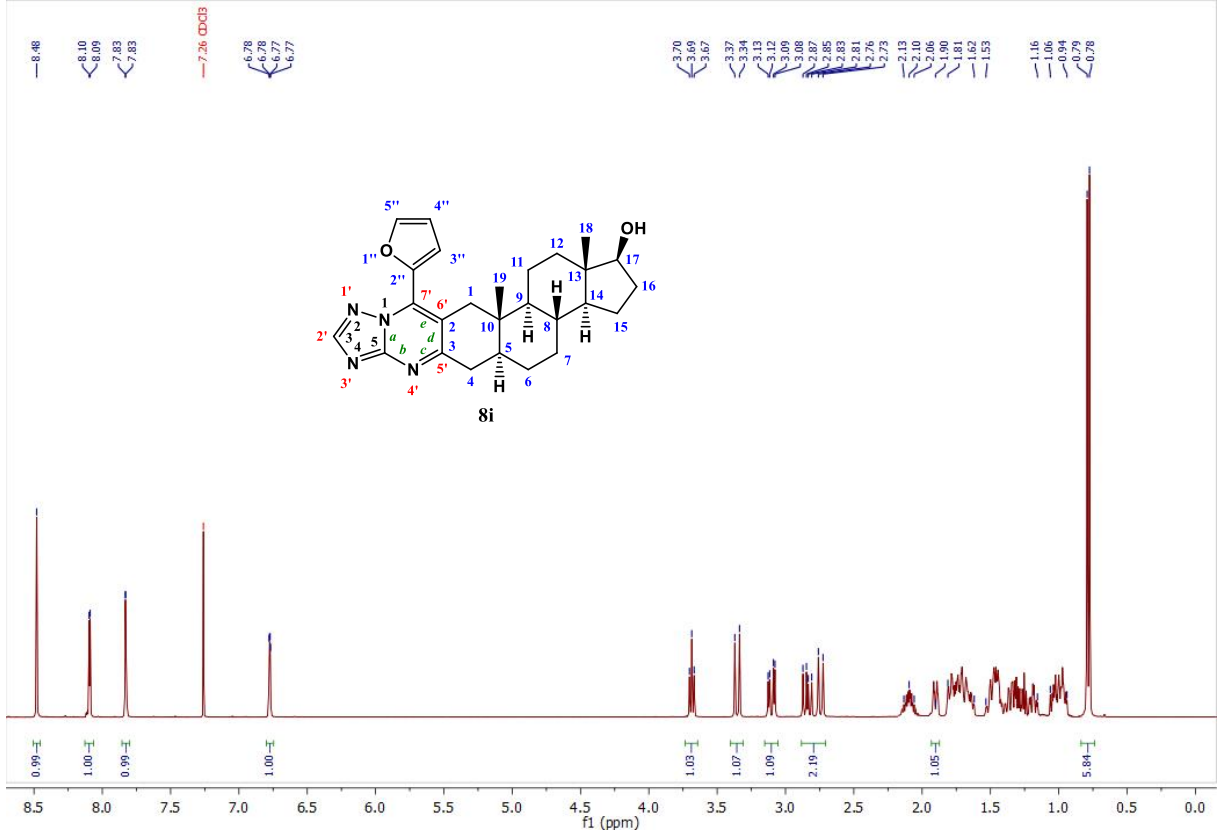
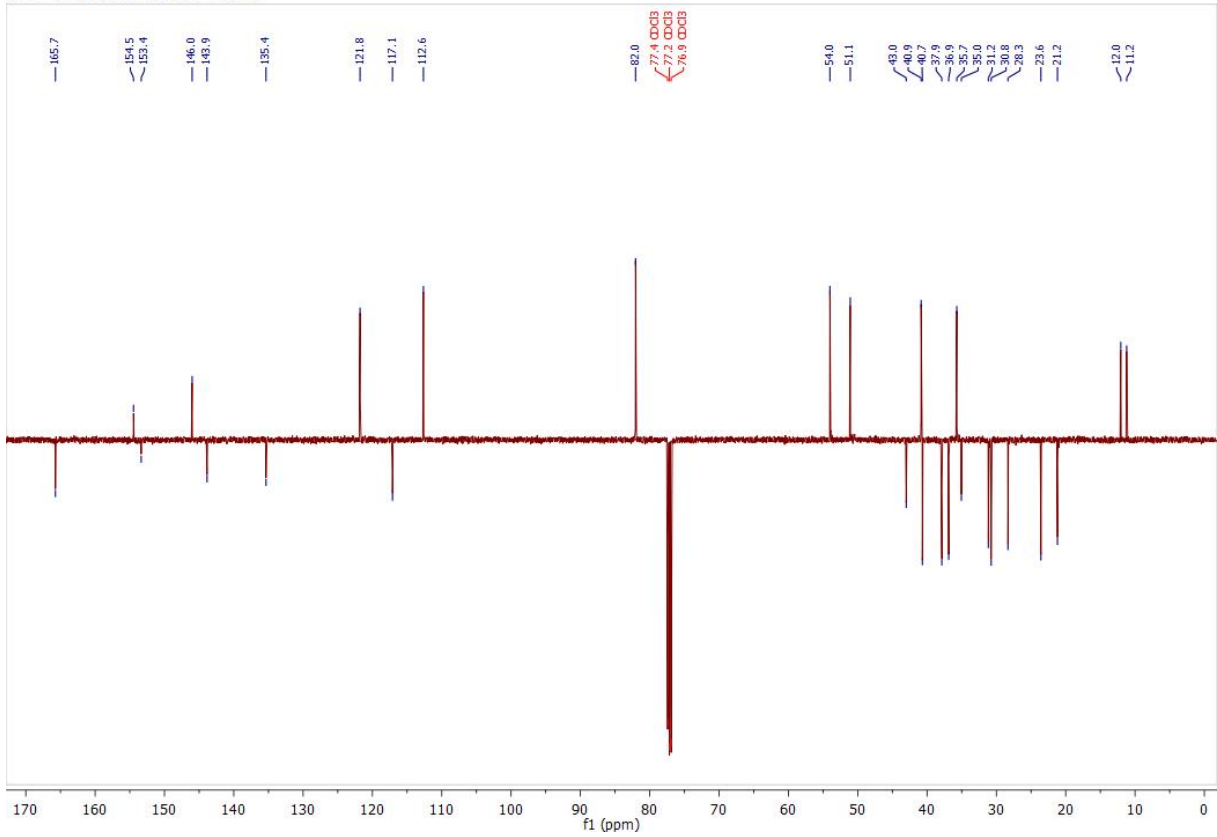


1H — 2020-07-15T20:46:49 — CDCl3

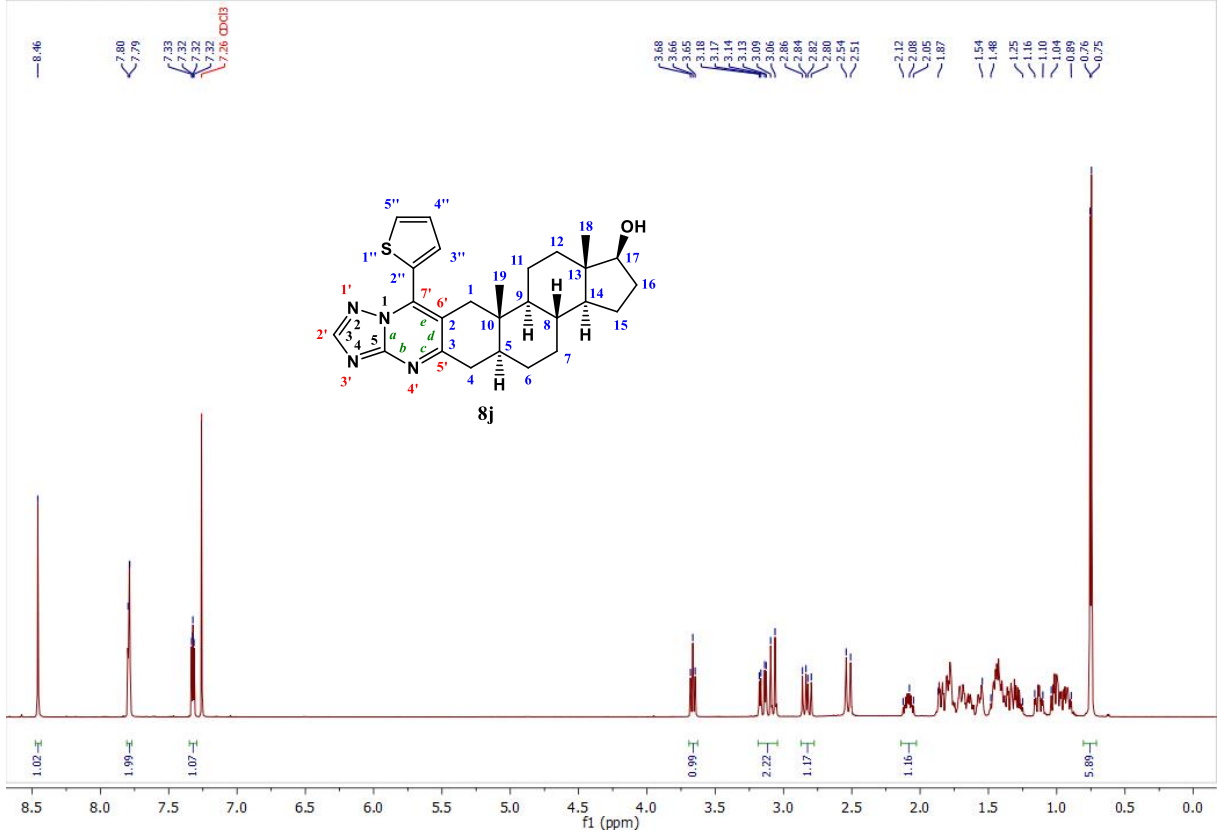


13C — 2020-07-15T21:00:15 — CDCl3

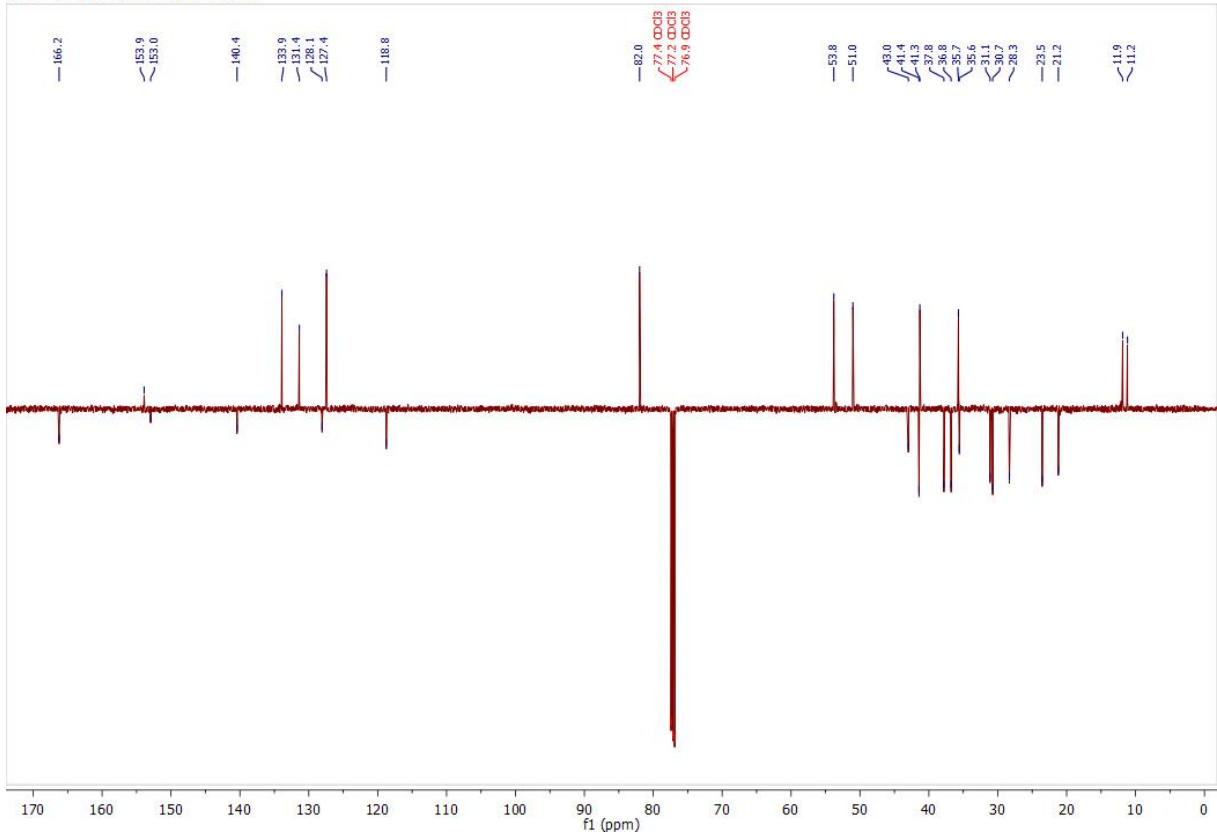


1H — 2020-08-28T12:55:57 — CDCl₃13C — 2020-08-28T13:09:39 — CDCl₃

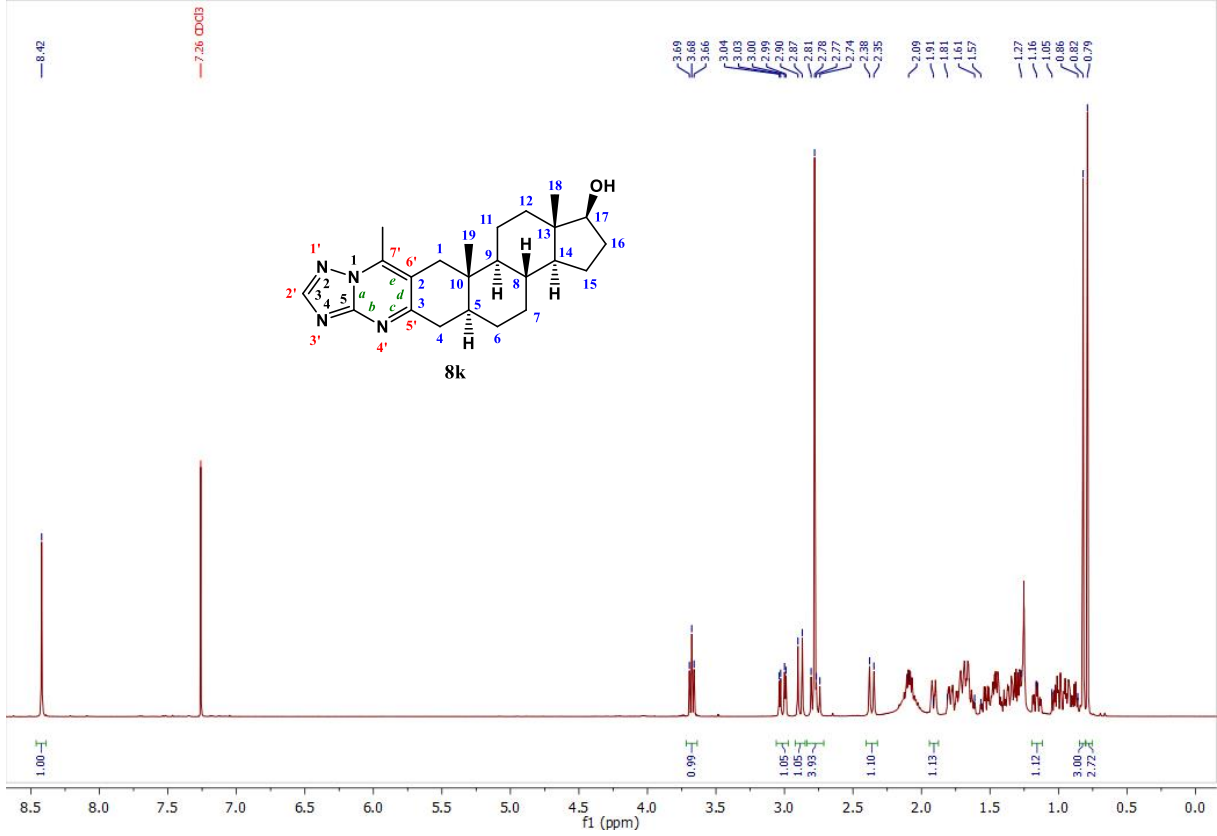
1H — 2020-07-01T04:21:34 — CDCl3



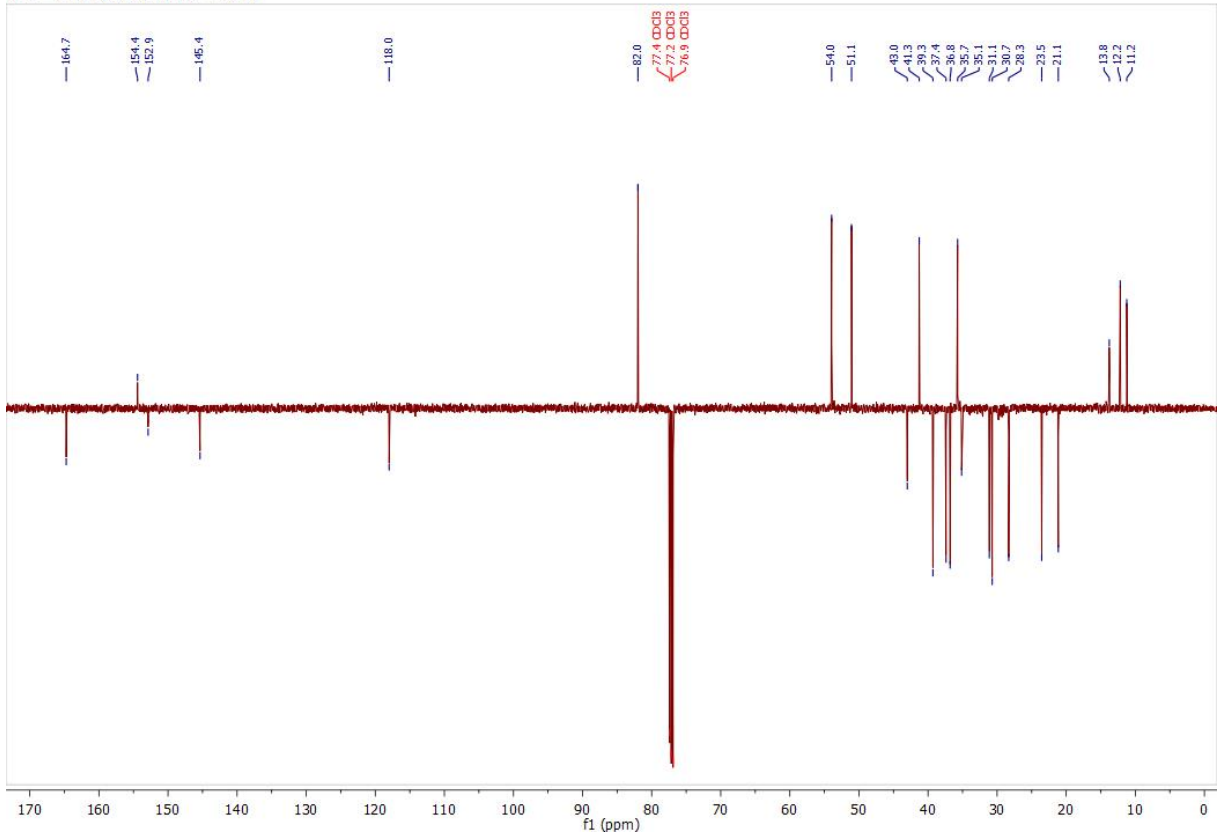
13C — 2020-07-01T04:34:59 — CDCl3



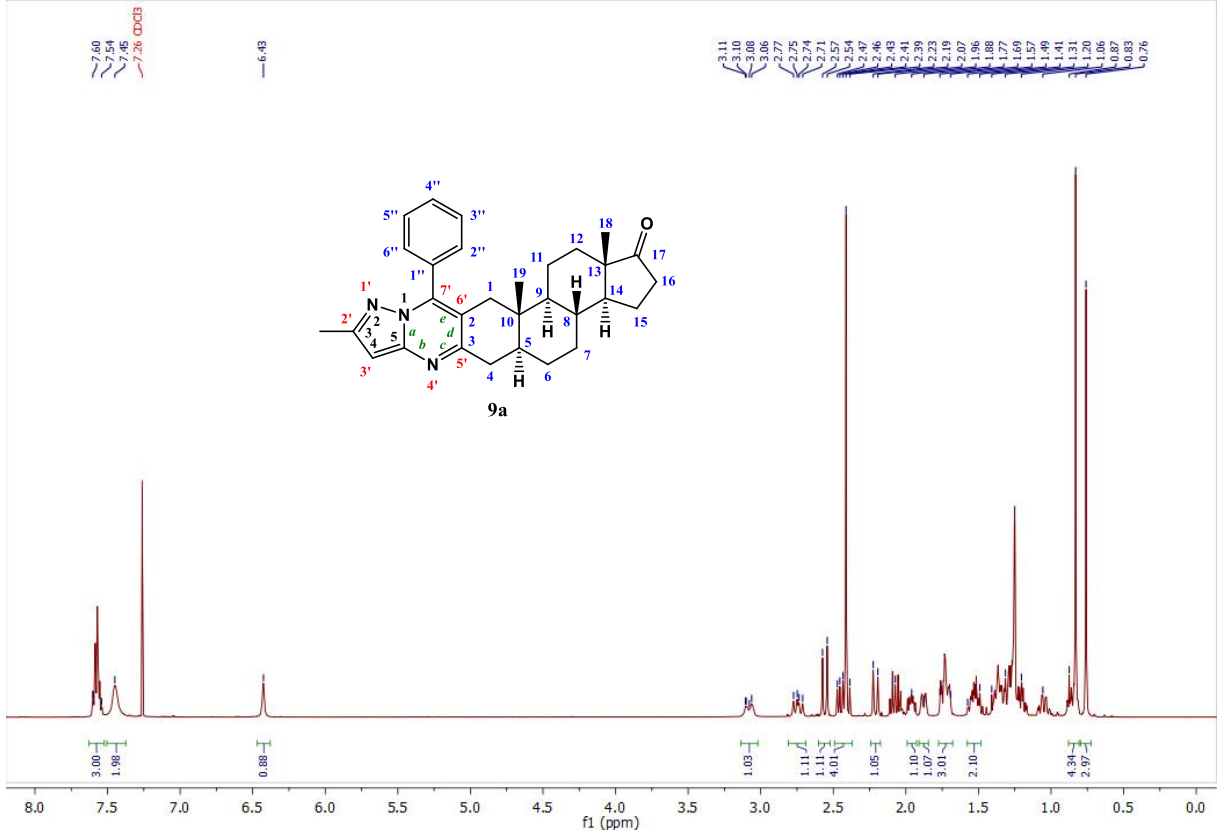
1H — 2020-08-26T22:38:17 — CDCl3



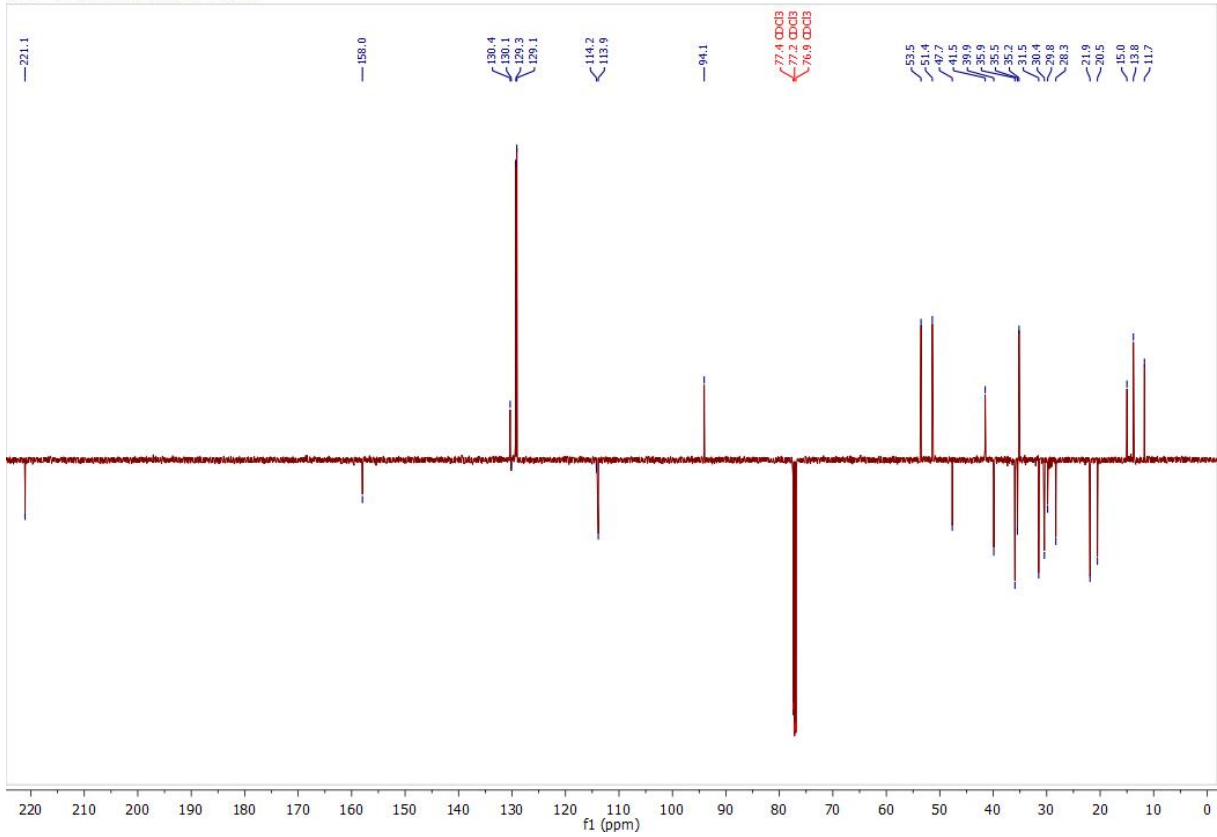
13C — 2020-08-26T22:51:42 — CDCl3



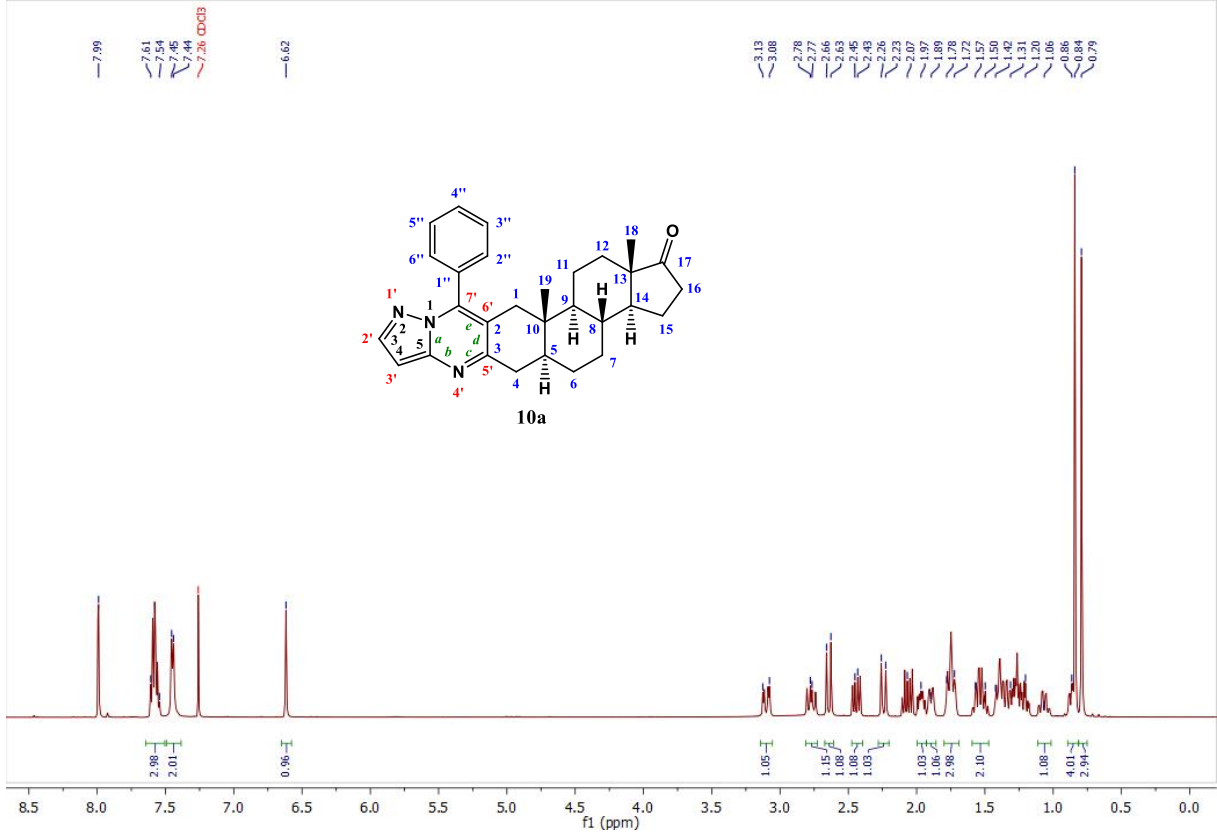
1H — 2020-02-29T00:36:35 — CDCl3



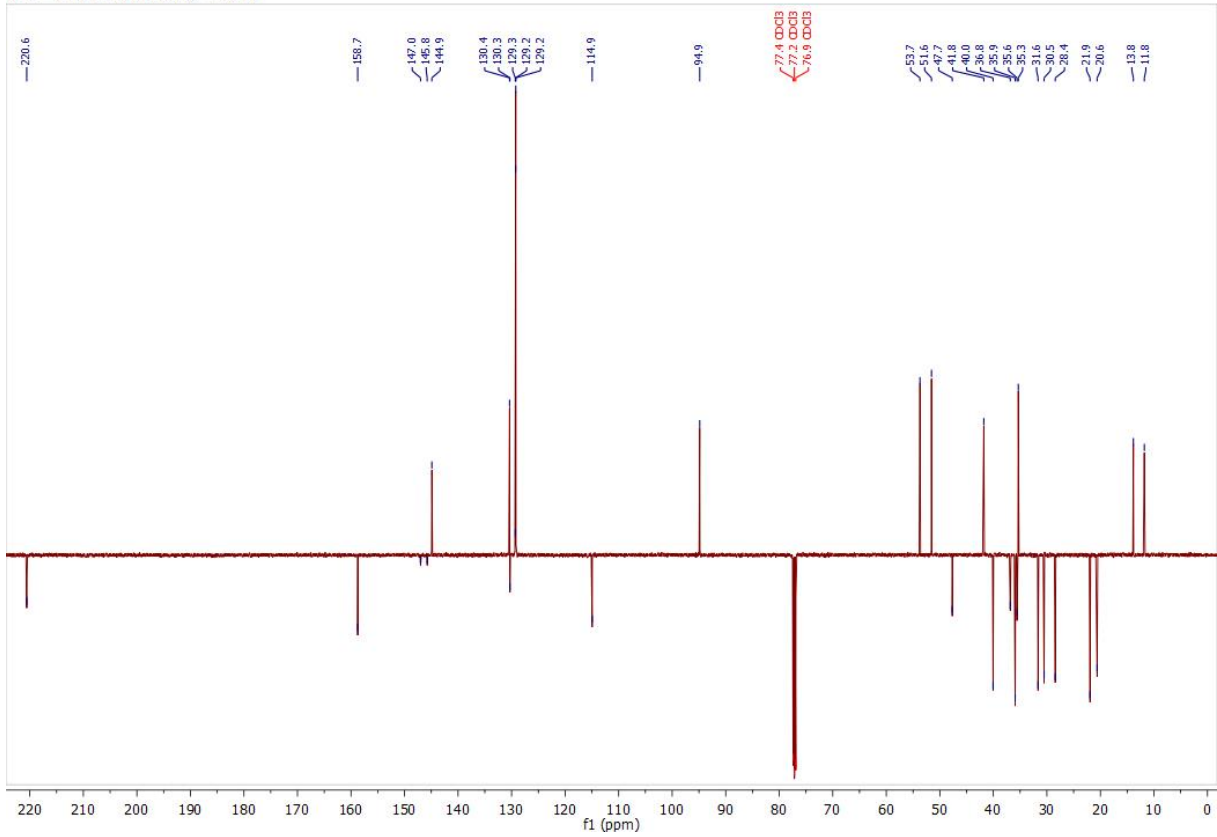
13C — 2020-02-29T00:50:18 — CDCl3



1H — 2020-06-09T08:46:22 — CDCl3

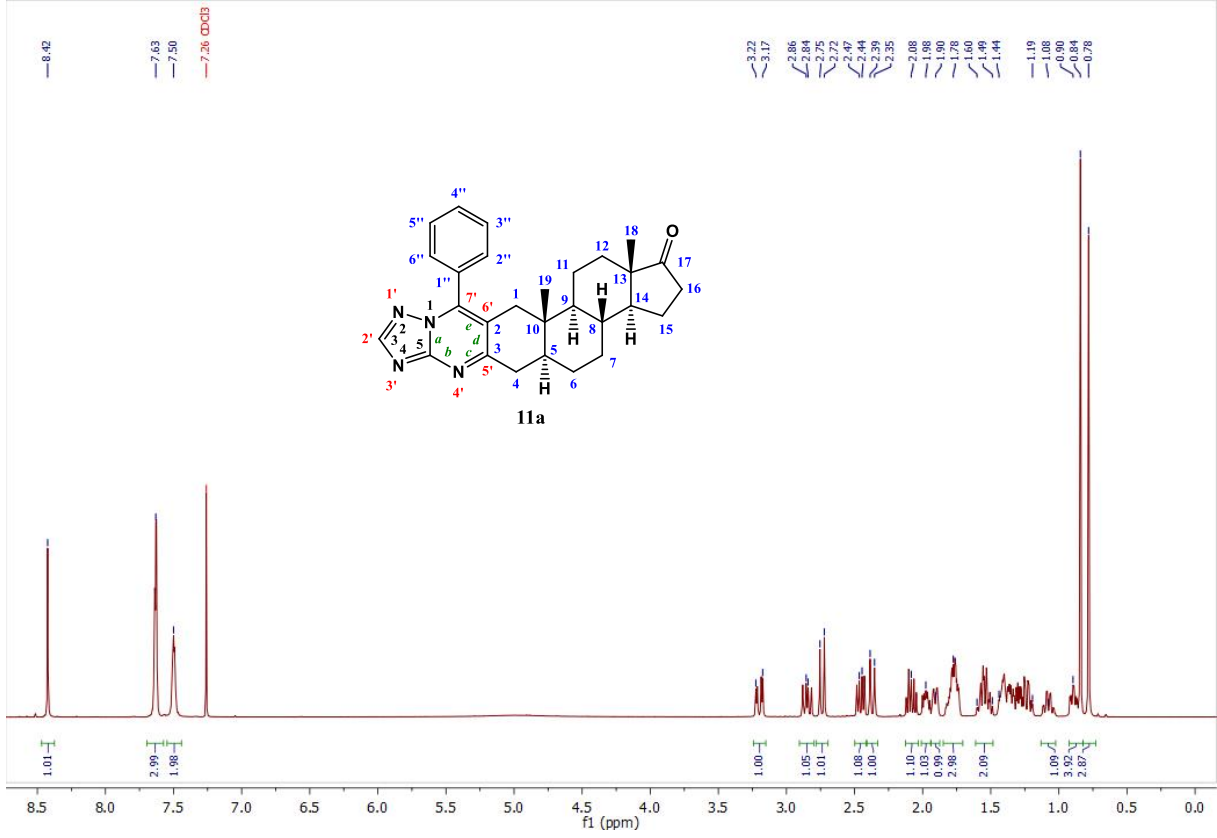


13C — 2020-06-09T09:12:25 — CDCl3

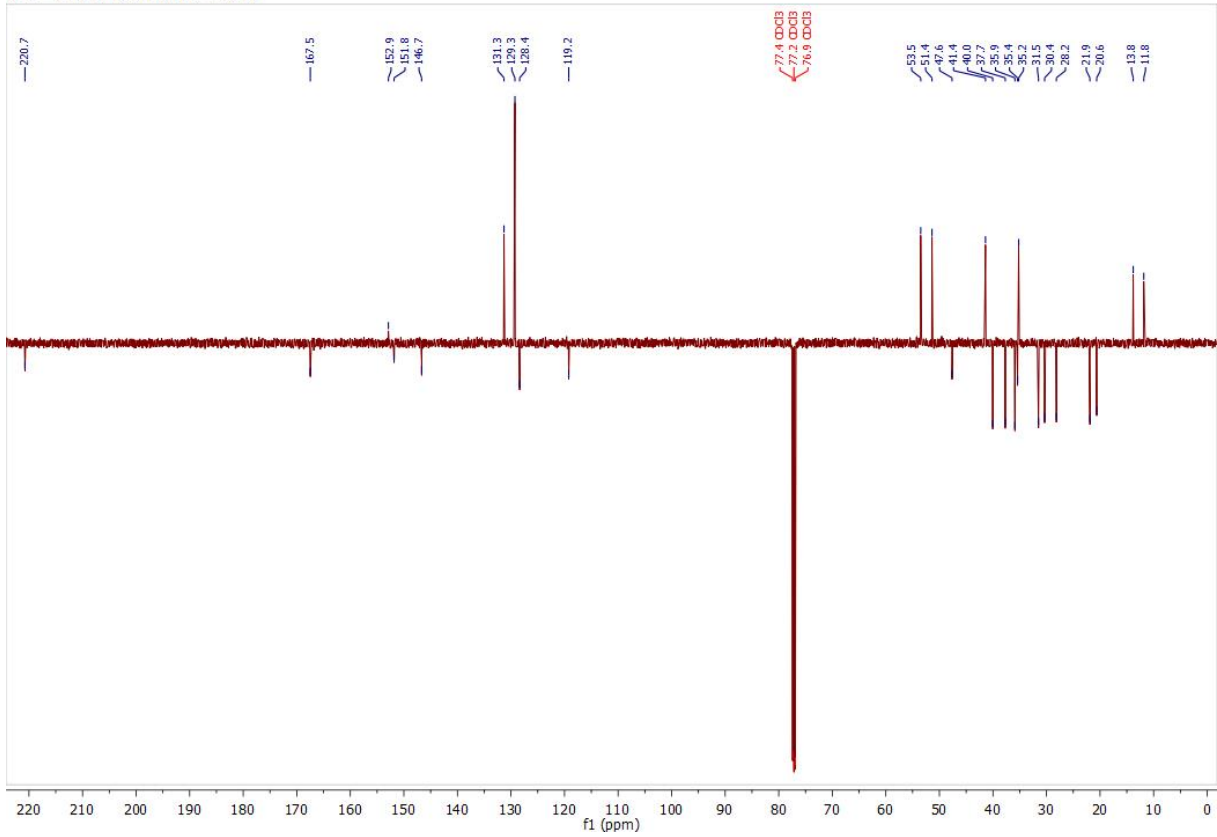


S24

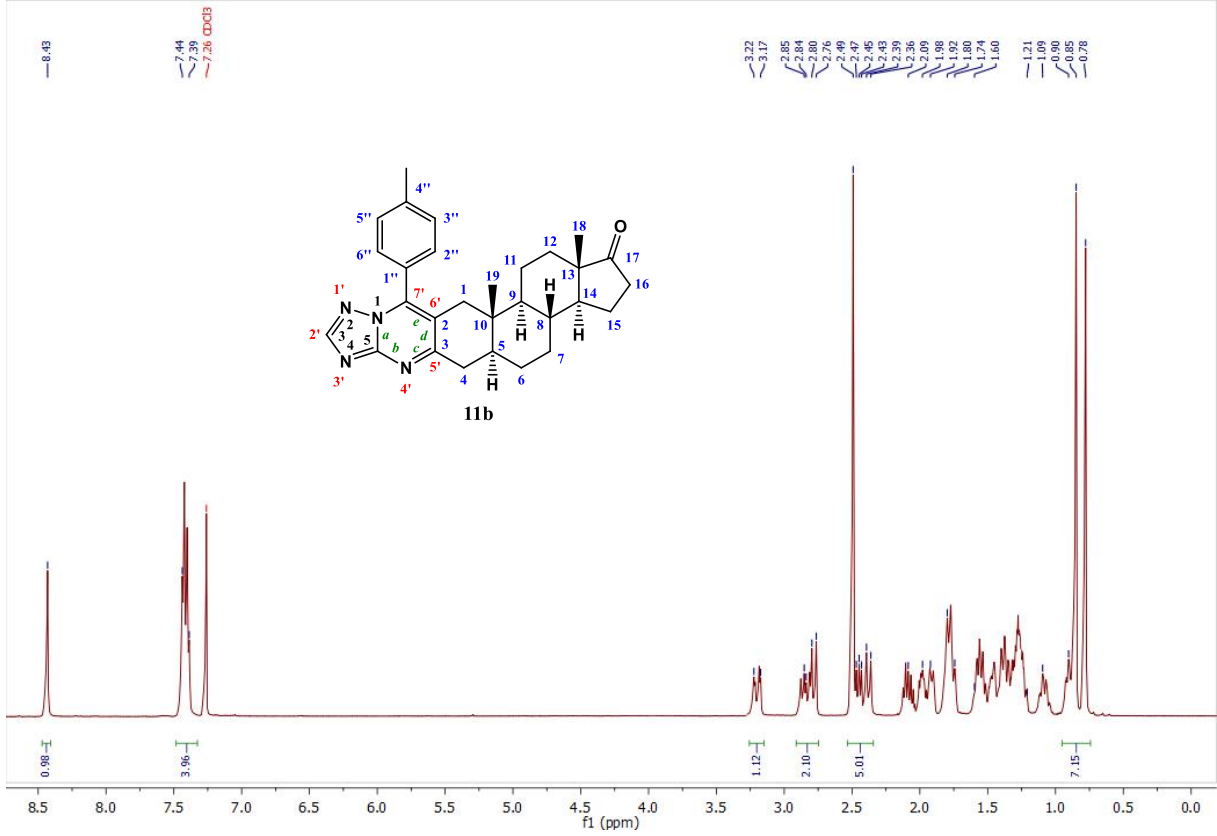
1H — 2020-02-29T01:14:34 — CDCl3



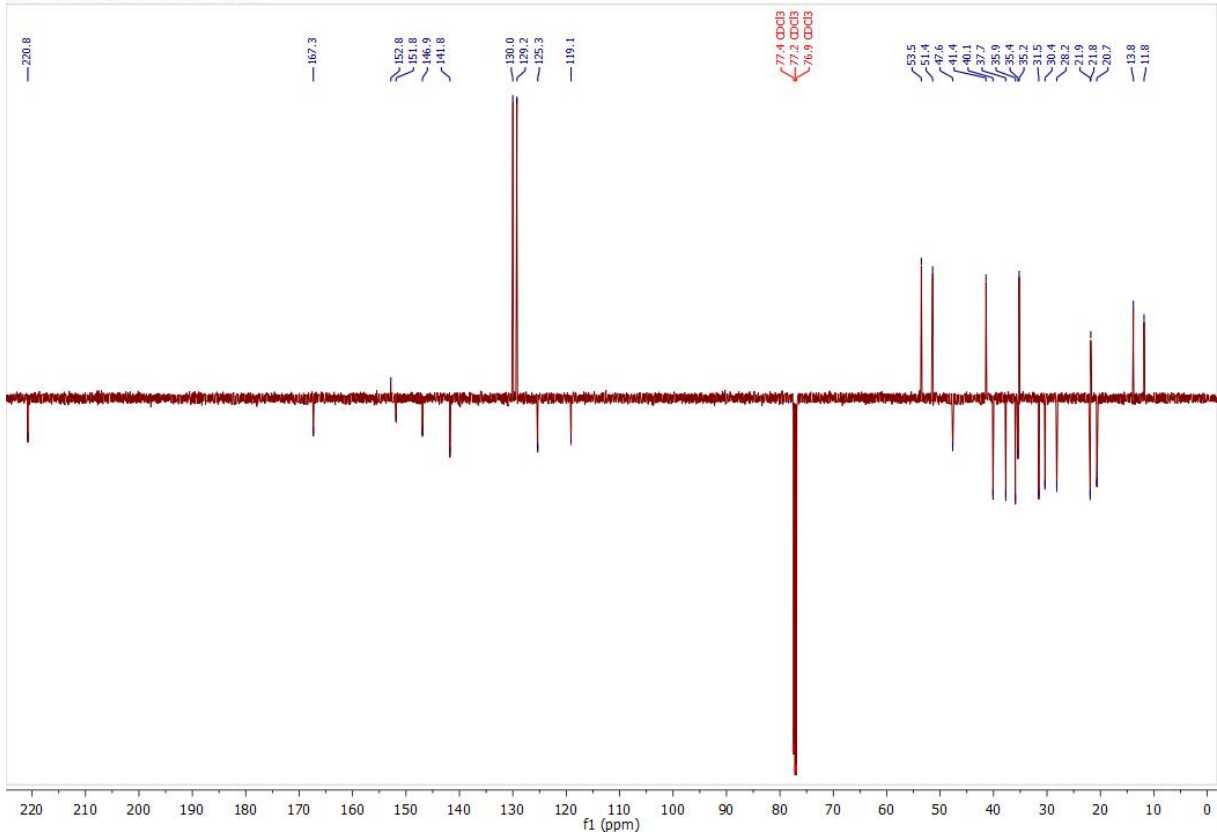
13C — 2020-07-01T02:58:59 — CDCl3



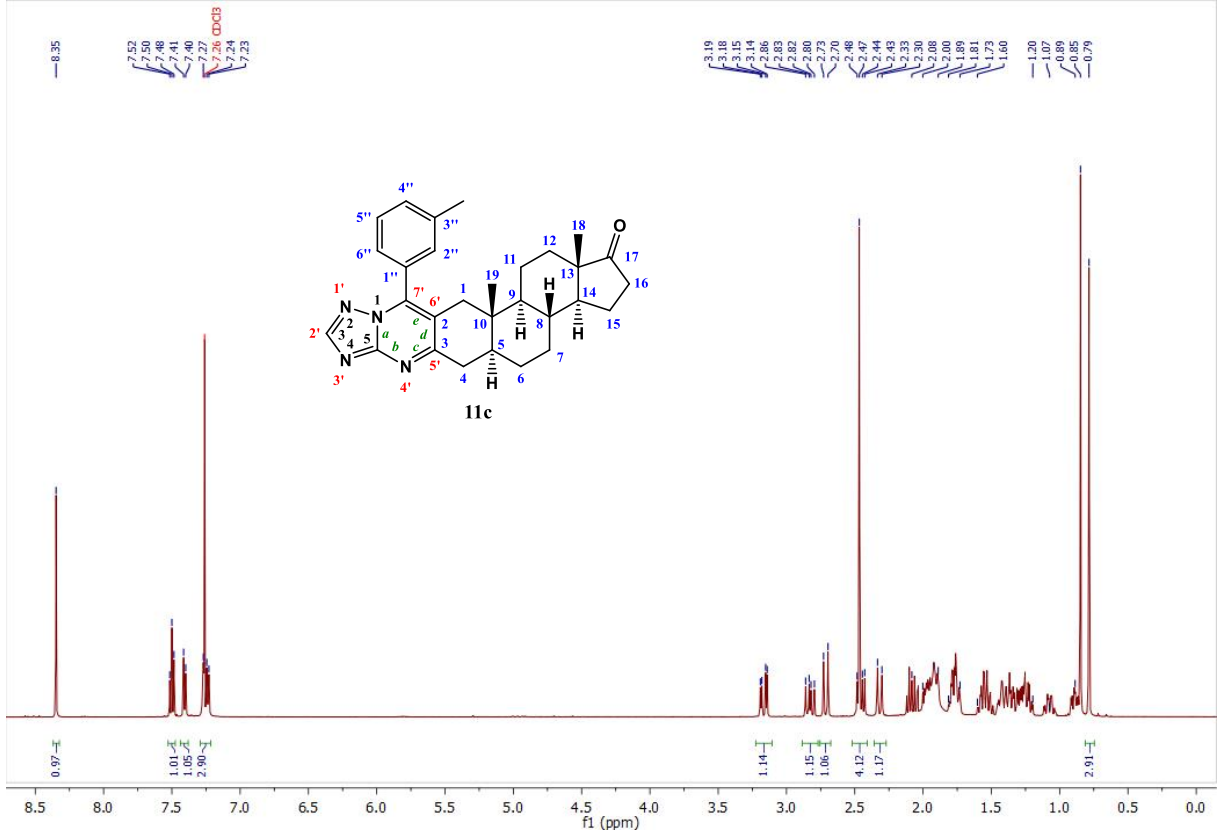
1H — 2020-06-18T23:25:11 — CDCl3



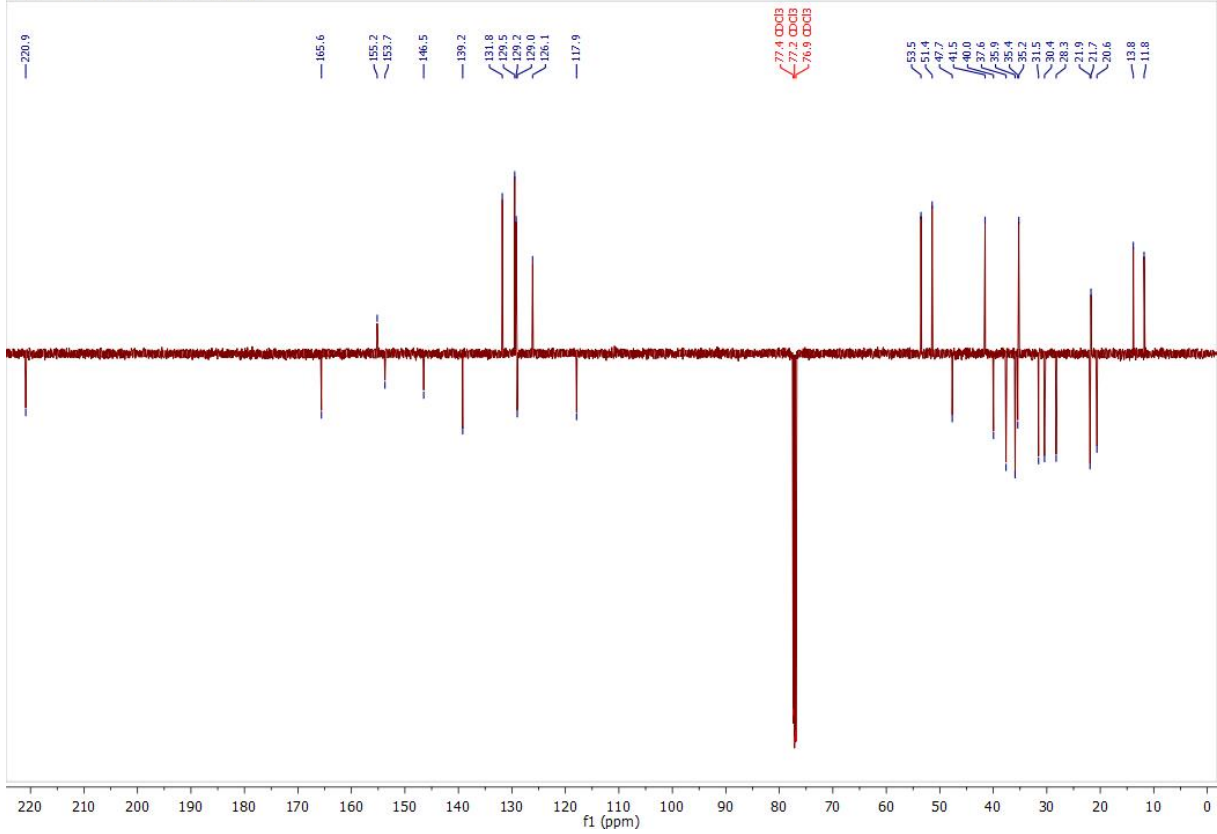
13C — 2020-06-18T23:38:36 — CDCl3



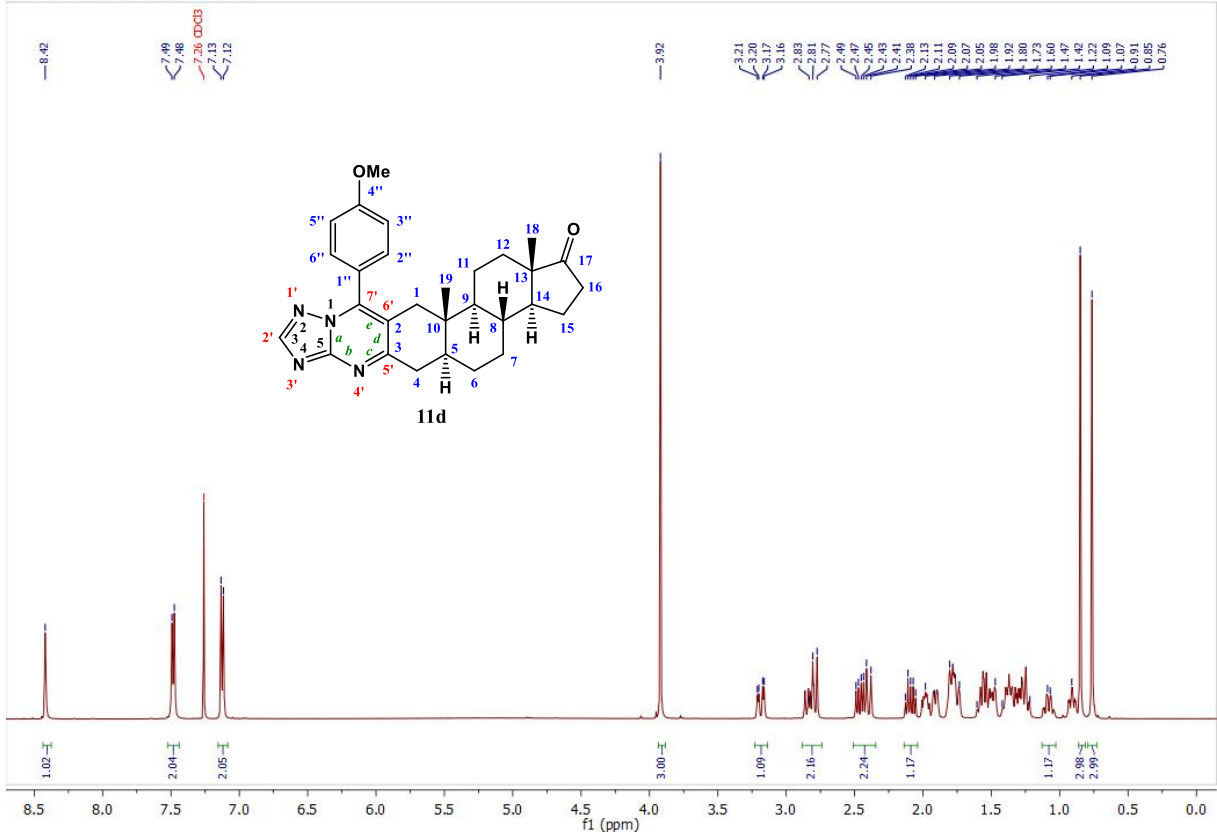
1H — 2020-08-26T23:52:59 — CDCl3



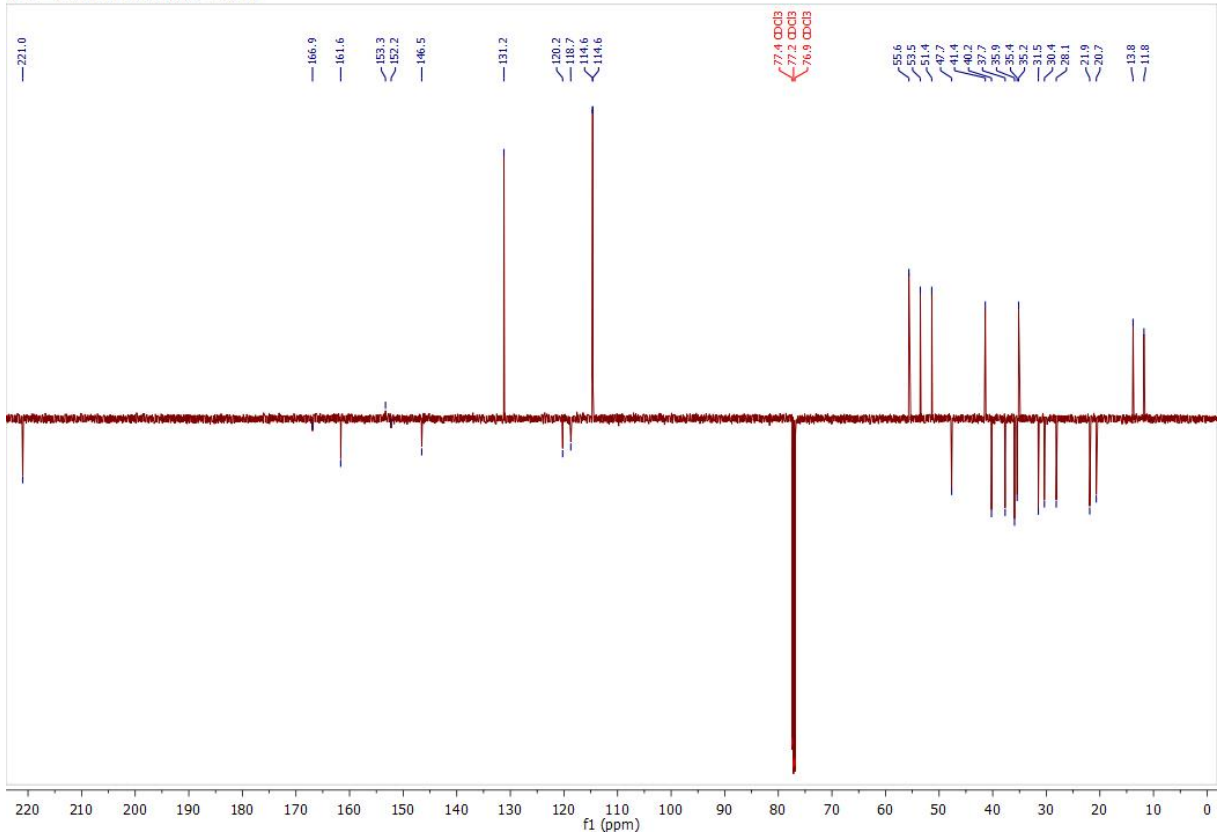
13C — 2020-08-27T00:06:24 — CDCl3



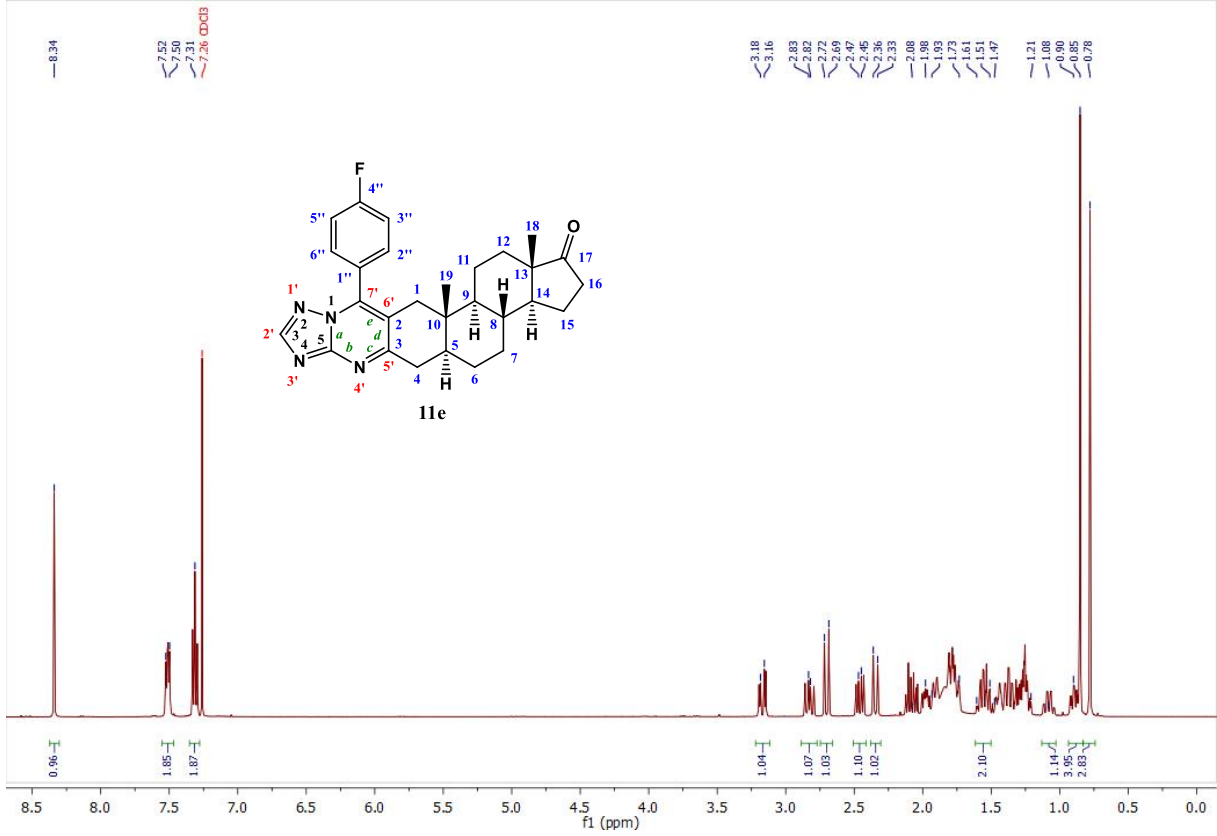
1H — 2018-02-20T06:07:40 — CDCl3



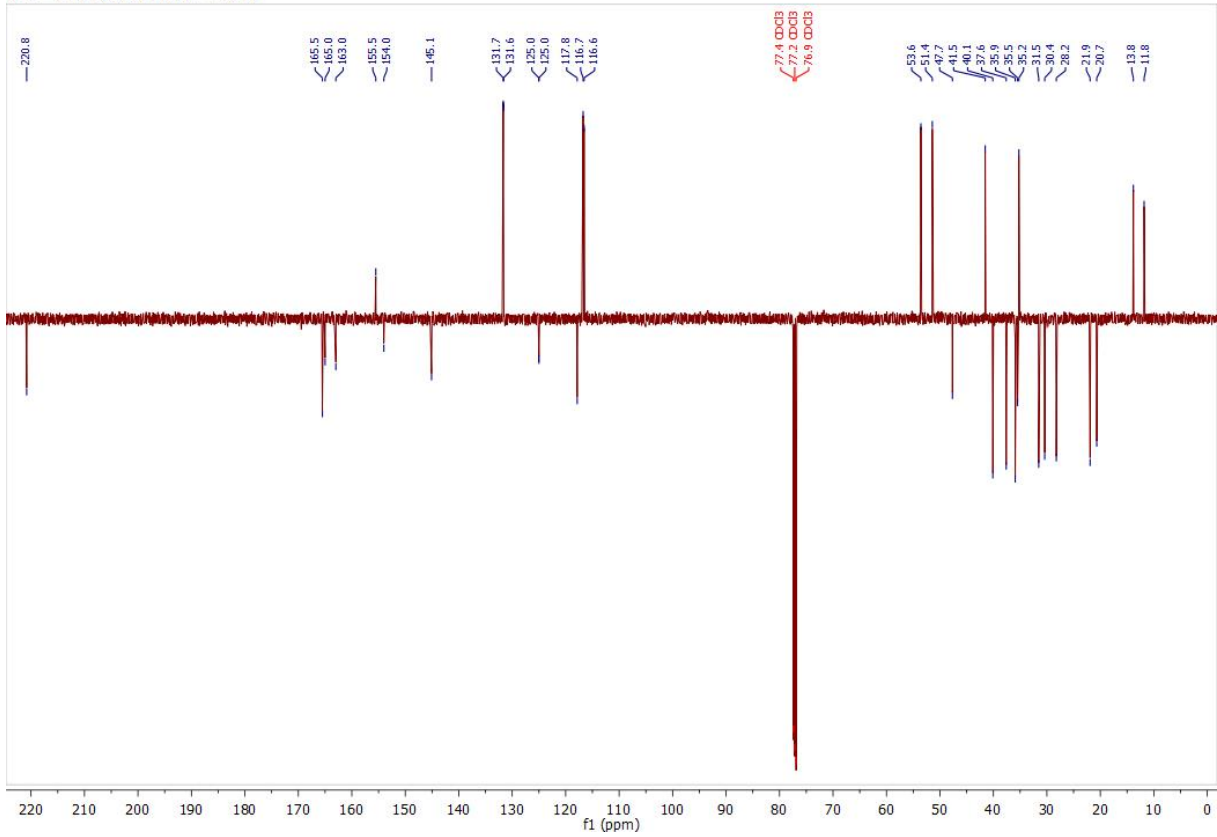
13C — 2018-02-20T06:21:06 — CDCl3



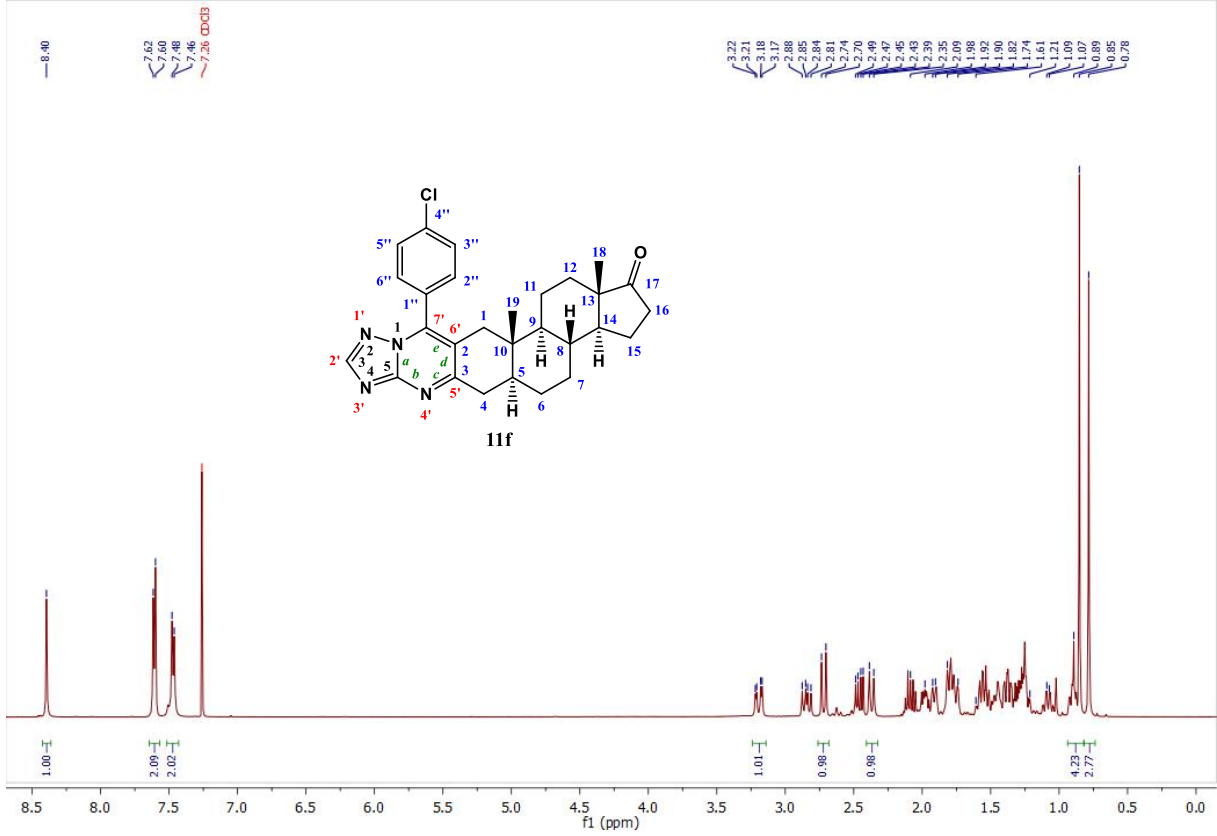
1H — 2020-08-26T23:17:12 — CDCl3



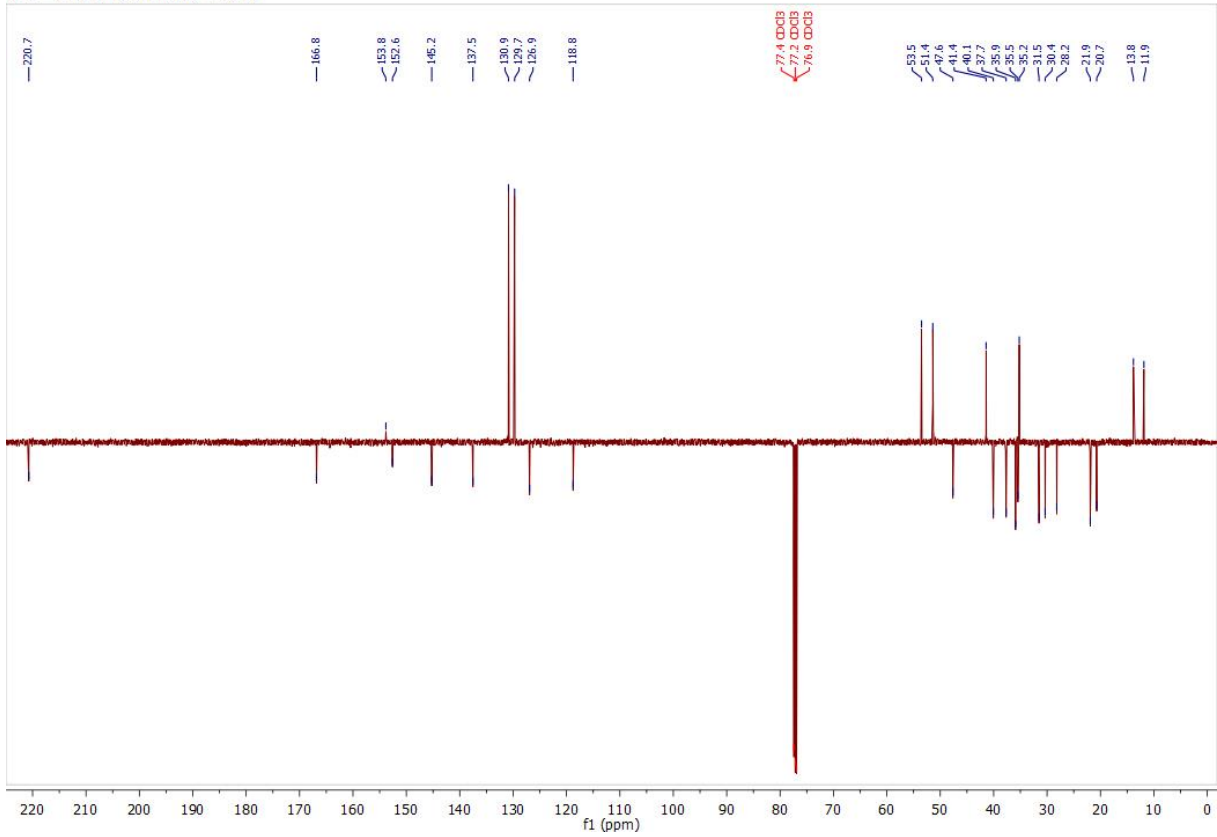
13C — 2020-08-26T23:30:37 — CDCl3



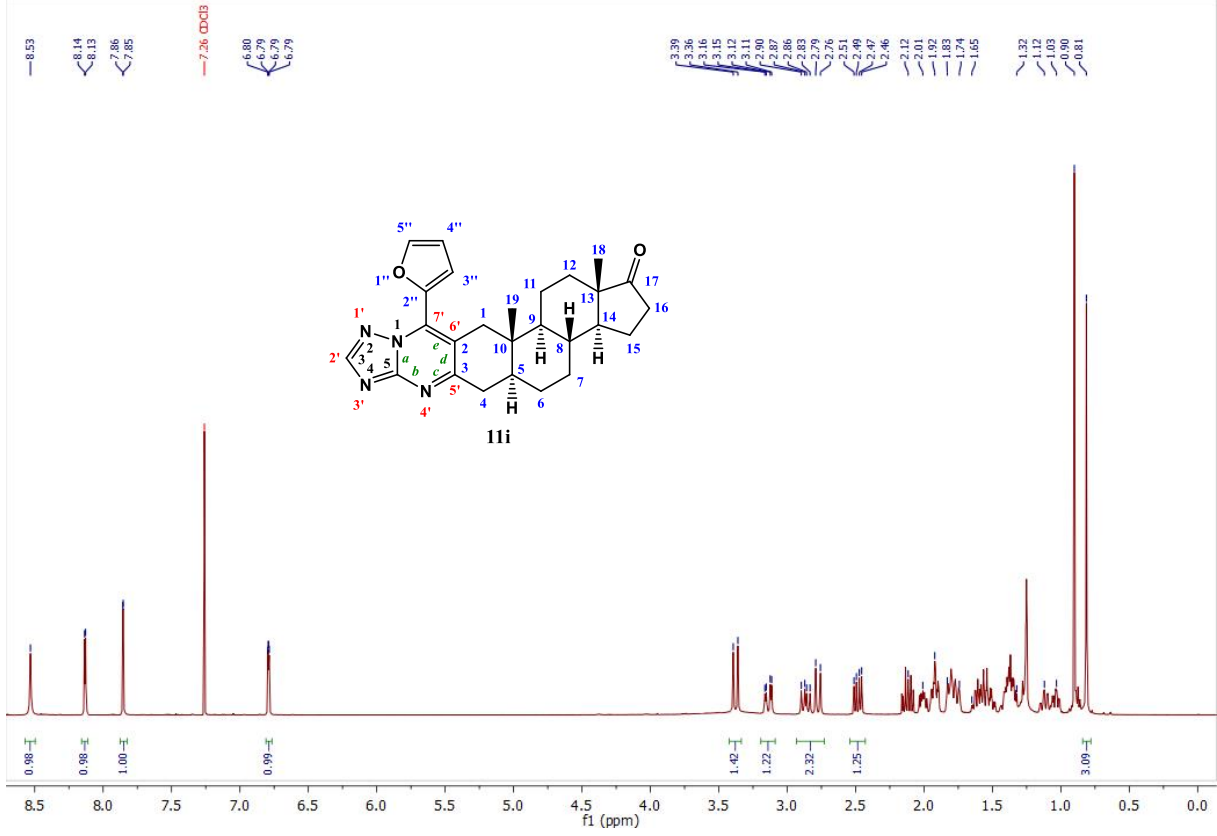
1H — 2020-07-01T02:25:17 — CDCl3



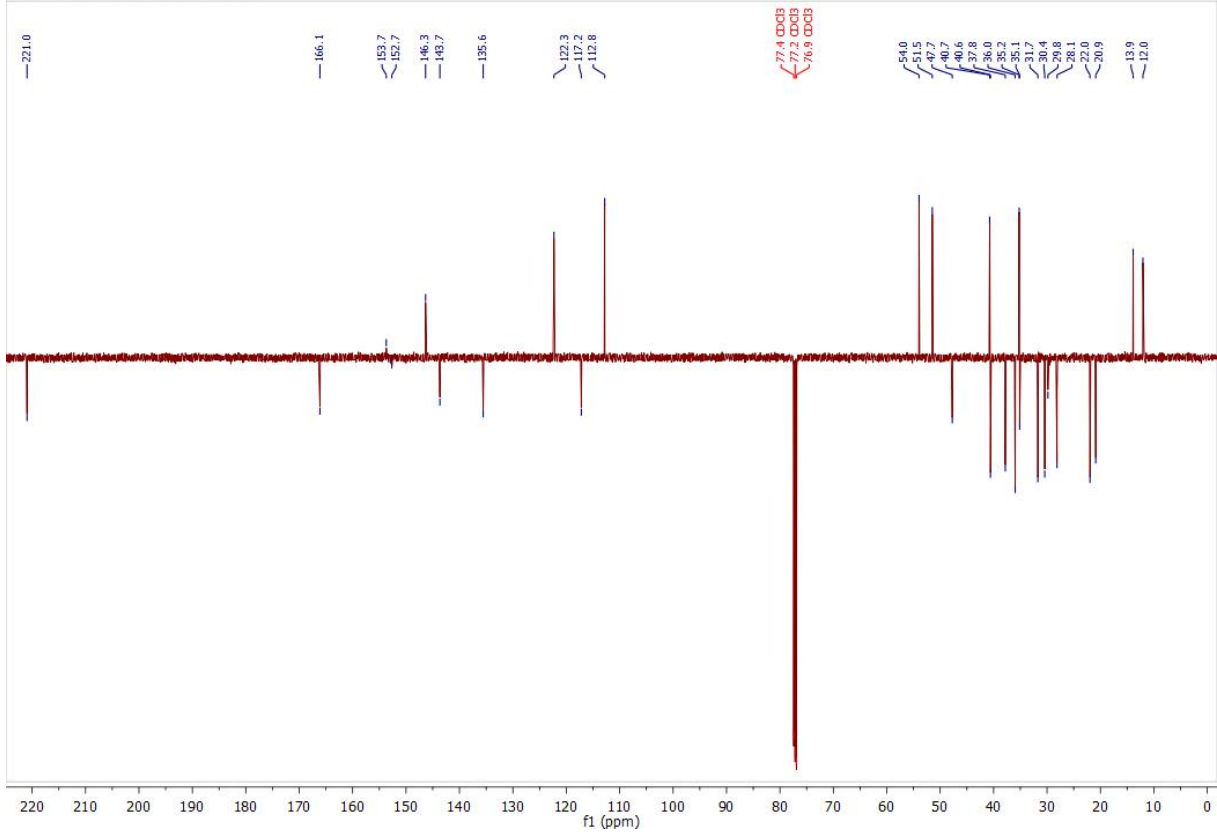
13C — 2020-07-01T02:39:01 — CDCl3



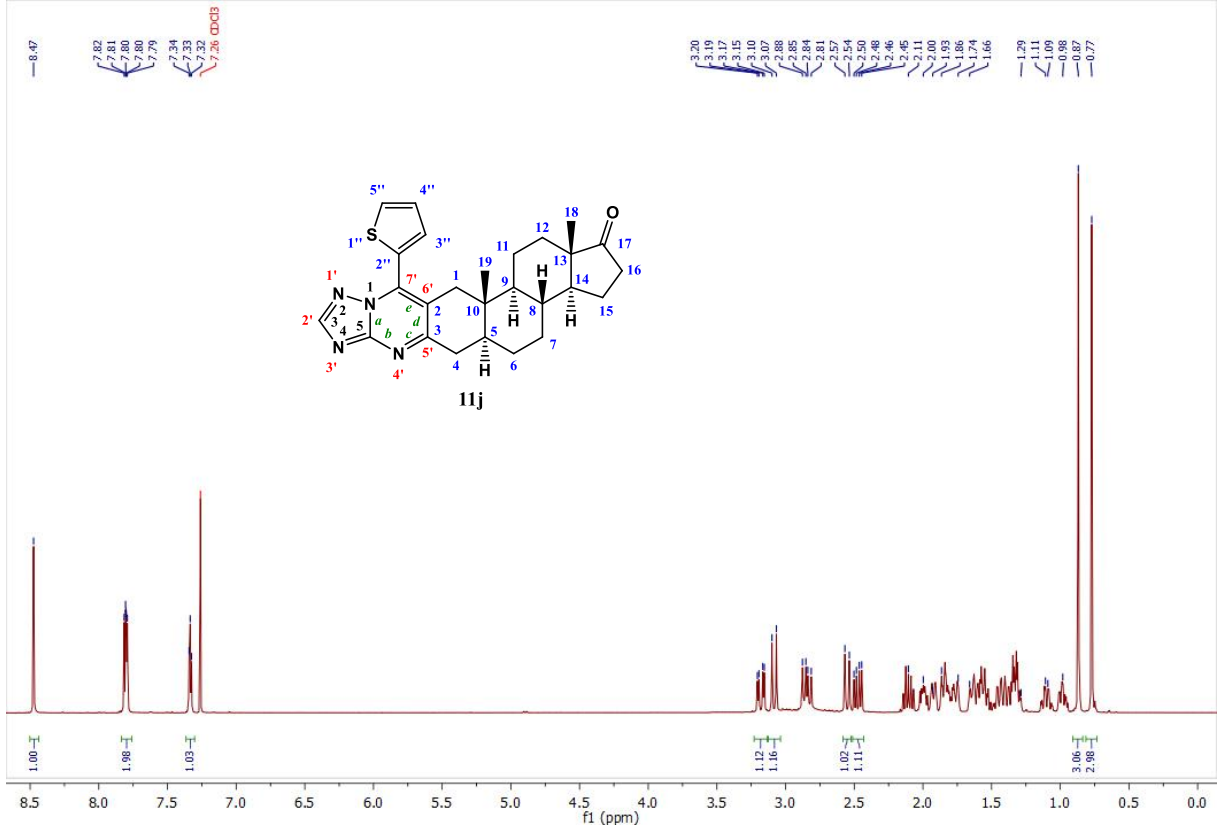
1H — 2020-08-28T13:14:46 — CDCl3



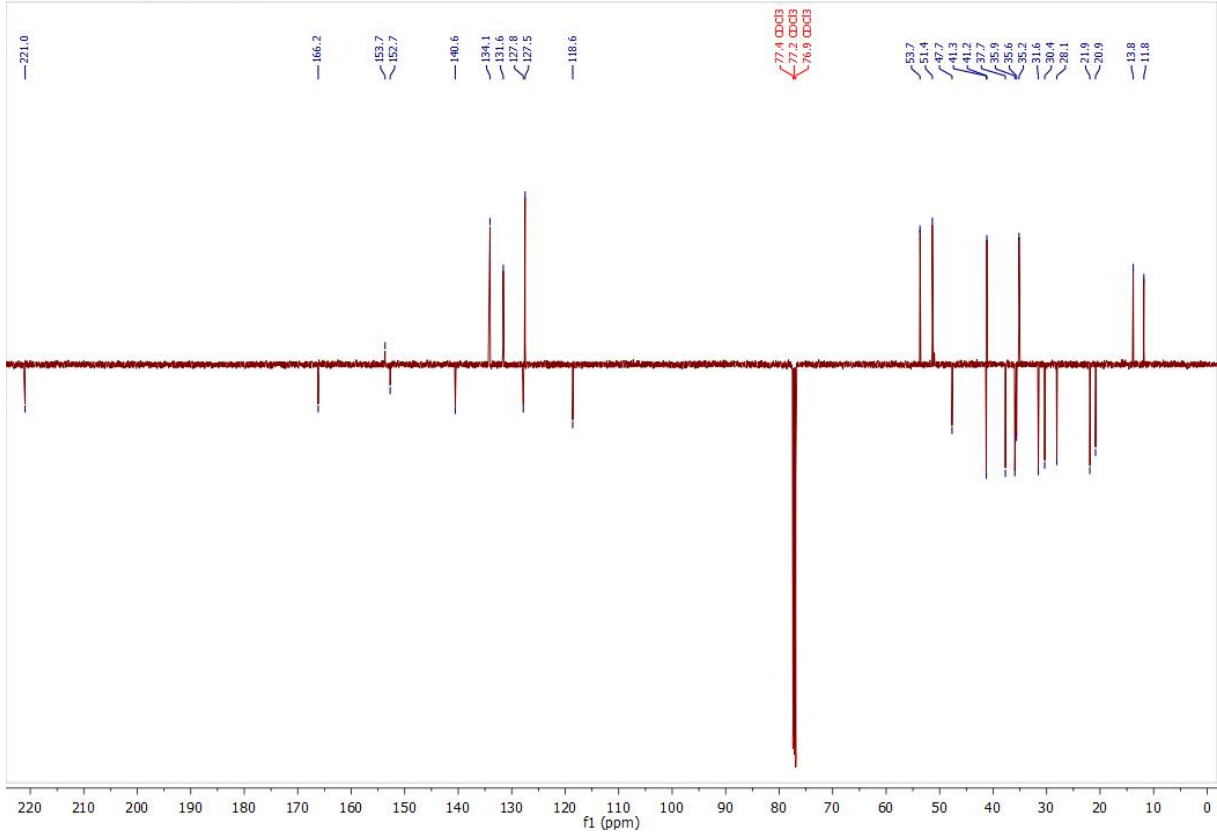
13C — 2020-08-28T13:28:29 — CDCl3



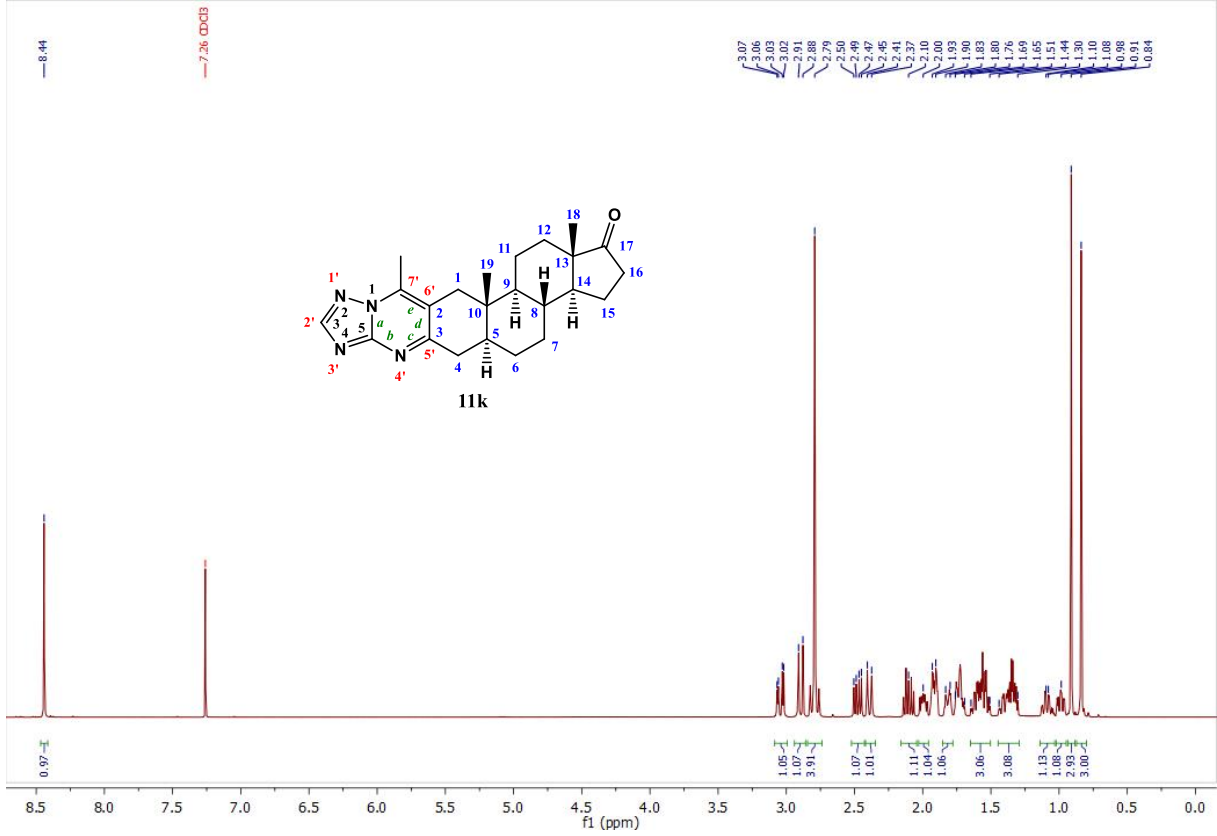
1H — 2020-02-29T01:34:11 — CDCl3



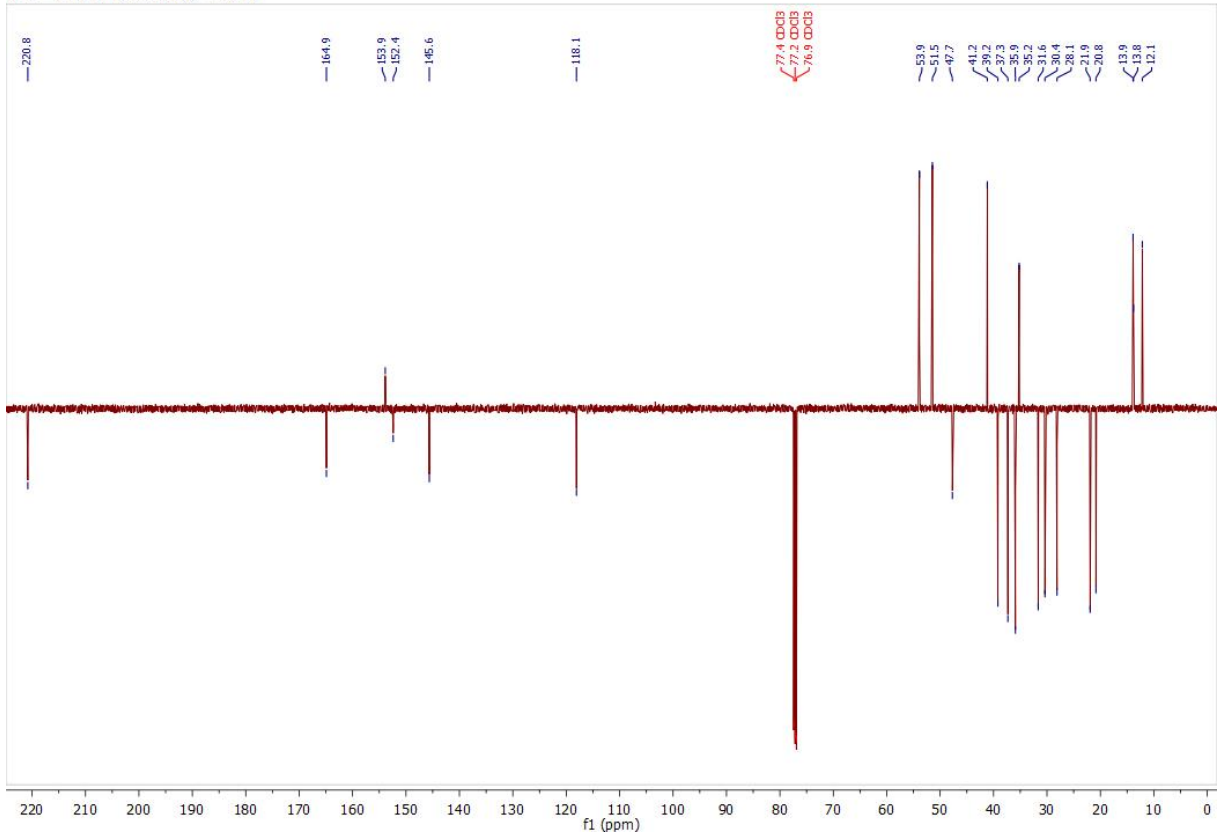
13C — 2020-02-29T01:47:52 — CDCl3



1H — 2020-07-01T04:01:50 — CDCl3



13C — 2020-07-01T04:15:15 — CDCl3



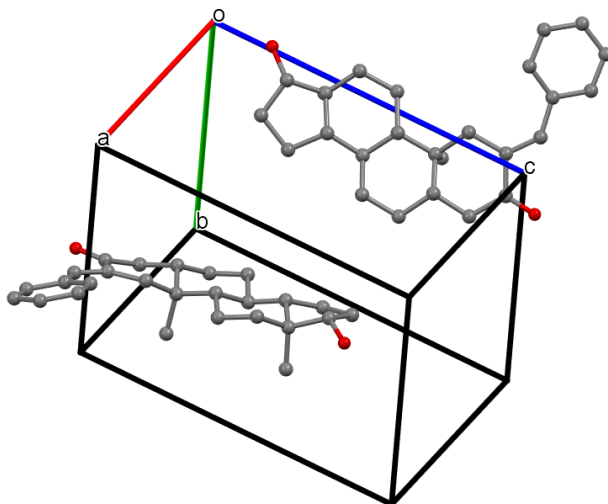


Figure S1. Unit cell containing two molecules in the crystal of **2a**

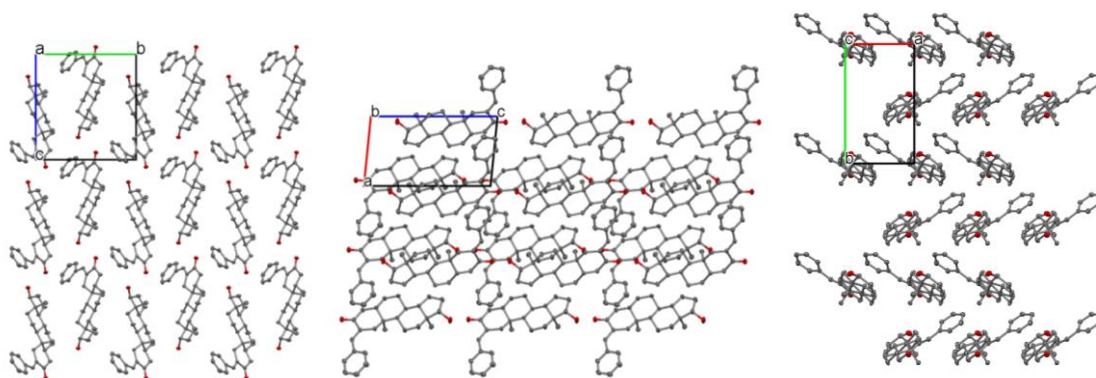


Figure S2. Packing arrangements in crystal **2a** viewed from the crystallographic directions 'a', 'b' and 'c'

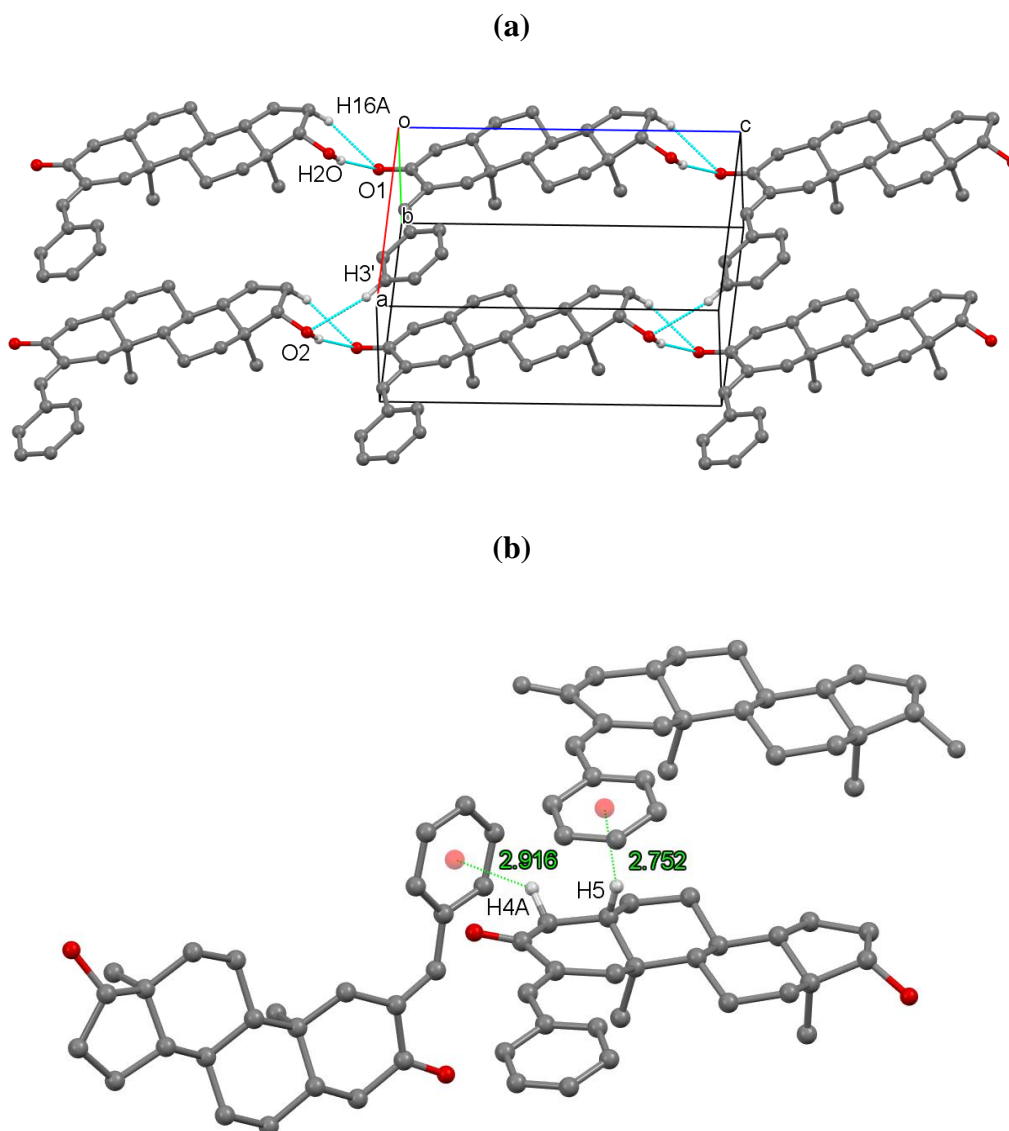


Figure S3. Crystal packing in crystal **2a** showing (a) O-H...O and C-H...O interactions and (b) C-H... π connections of neighbouring molecules in different view points

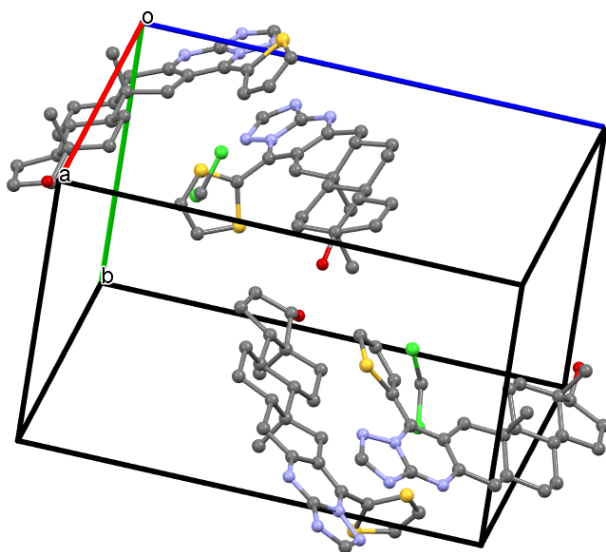


Figure S4. Unit cell containing two molecules in the crystal of **8j**

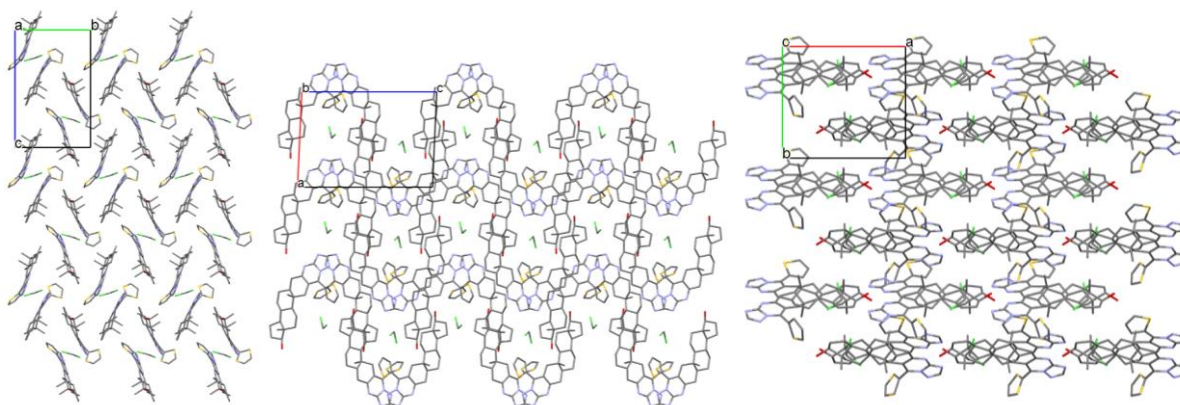


Figure S5. Packing arrangements in crystal **8j** viewed from the crystallographic directions 'a', 'b' and 'c'

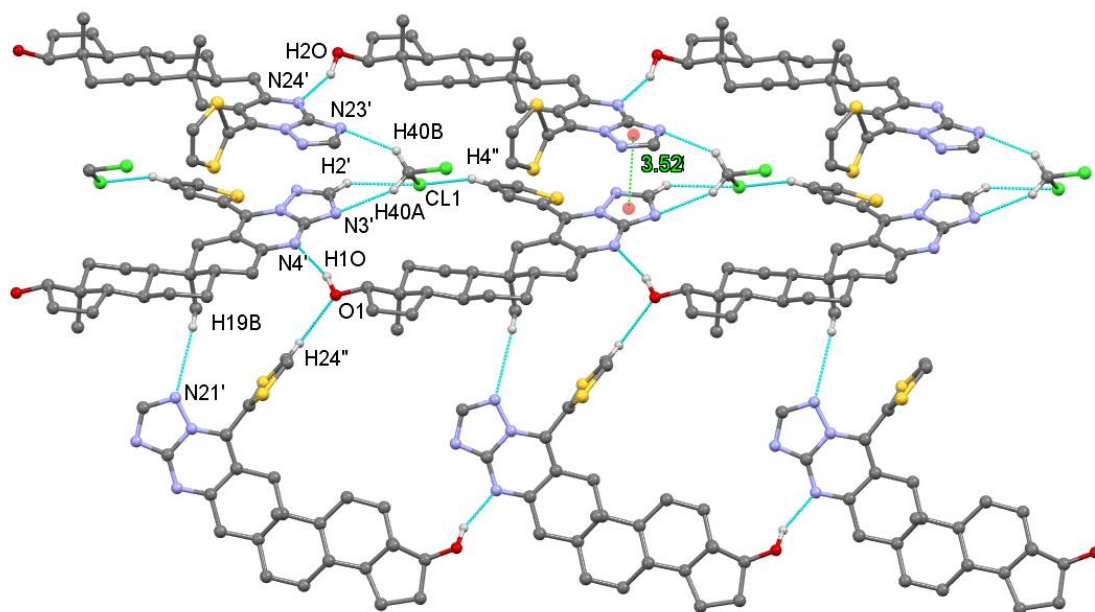


Figure S6. Packing arrangements in crystal **8j** showing the main interactions O/C-H...N and C-H...Cl interactions between neighbouring molecules

Table S1. Bond length obtained for the compound **2a** in crystal I and two molecules of **8j** in crystal II

I		II			
		Molecule 1		Molecule 2	
Bond	Distance (Å)	Bond	Distance (Å)	Bond	Distance (Å)
O1 - C3	1.2279(17)	O1 - C17	1.420(5)	O2 - C37	1.423(5)
O2 - C17	1.4208(19)	C1 - C2	1.522(5)	C21 - C22	1.503(5)
C1 - C2	1.514(2)	C2 - C3	1.432(5)	C22 - C23	1.429(5)
C2 - C3	1.499(2)	C3 - C4	1.492(5)	C23 - C24	1.492(6)
C3 - C4	1.502(2)	C4 - C5	1.518(5)	C24 - C25	1.534(5)
C4 - C5	1.526(2)	C5 - C6	1.519(5)	C25 - C26	1.522(6)
C5 - C6	1.530(2)	C6 - C7	1.519(5)	C26 - C27	1.526(5)
C6 - C7	1.525(2)	C7 - C8	1.528(6)	C27 - C28	1.527(5)
C7 - C8	1.531(2)	C8 - C9	1.556(5)	C28 - C29	1.548(5)
C8 - C9	1.547(2)	C9 - C10	1.545(5)	C29 - C30	1.550(5)
C9 - C10	1.557(2)	C1 - C10	1.533(5)	C21 - C30	1.541(5)
C1 - C10	1.540(2)	C9 - C11	1.534(6)	C29 - C31	1.541(6)
C9 - C11	1.546(2)	C11 - C12	1.529(5)	C31 - C32	1.538(5)
C11 - C12	1.539(2)	C12 - C13	1.518(5)	C32 - C33	1.529(5)
C12 - C13	1.528(2)	C13 - C14	1.536(6)	C33 - C34	1.531(6)
C13 - C14	1.540(2)	C14 - C15	1.538(5)	C34 - C35	1.543(5)
C14 - C15	1.536(2)	C15 - C16	1.548(5)	C35 - C36	1.539(5)
C15 - C16	1.553(2)	C16 - C17	1.534(5)	C36 - C37	1.536(5)
C16 - C17	1.546(3)	C13 - C17	1.536(6)	C33 - C37	1.525(6)
C13 - C17	1.541(2)	C10 - C19	1.542(5)	C30 - C39	1.528(6)
C10 - C19	1.532(2)	C13 - C18	1.537(6)	C33 - C38	1.526(6)
C13 - C18	1.534(2)	C5 - C10	1.539(5)	C25 - C30	1.554(5)
C5 - C10	1.546(2)	C8 - C14	1.523(5)	C28 - C34	1.513(5)
C8 - C14	1.523(2)	S1" - C2"	1.732(4)	S21A - C22"	1.663(5)
C2 - C26	1.352(2)	S1" - C5"	1.687(5)	S21A - C25"	1.649(6)
C1' - C2'	1.407(2)	N1' - C2'	1.320(5)	N21' - C22'	1.318(5)
C2' - C3'	1.387(2)	N4' - C4'	1.336(5)	N24' - C24'	1.346(5)
C3' - C4'	1.385(3)	C2 - C7'	1.385(5)	C22 - C27'	1.369(5)
C4' - C5'	1.392(2)	C3" - C4"	1.412(6)	C23A - C24"	1.453(6)
C5' - C6'	1.389(2)	N1 - C4'	1.371(5)	N21 - C24'	1.381(5)
C1' - C6'	1.403(2)	N3' - C4'	1.328(5)	N23' - C24'	1.330(5)
C1' - C26	1.465(2)	N1 - C7'	1.381(4)	N21 - C27'	1.370(5)
		N4' - C3	1.333(5)	N24' - C23	1.330(5)
		C2" - C7'	1.450(5)	C22" - C27'	1.475(5)
		C4" - C5"	1.343(7)	C24" - C25"	1.301(8)
		N1 - N1'	1.368(5)	N21 - N21'	1.364(5)
		N3' - C2'	1.346(6)	N23' - C22'	1.342(5)
		C2" - C3"	1.367(5)	C22" - C23A	1.483(5)

Table S2. Bond angles obtained for molecules in crystal **2a** and **8j**

Crystal 2a		Crystal 8j			
		Molecule 1		Molecule 2	
Angle	Deg (°)	Angle	Deg (°)	Angle	Deg (°)
C2 - C1 - C10	115.66(12)	C2'' - S1'' - C5''	92.4(2)	C22'' - S21A - C25''	93.8(3)
C6' - C1' - C26	125.78(13)	C4' - N1 - C7'	123.5(3)	N21' - N21 - C27'	127.5(3)
C3 - C2 - C26	115.55(13)	C3 - N4' - C4'	116.9(3)	C22' - N23' - C24'	101.4(3)
O1 - C3 - C4	119.24(14)	C1 - C2 - C7'	121.2(3)	C21 - C22 - C23	121.4(3)
C3 - C4 - C5	115.36(13)	S1'' - C2'' - C3''	109.5(3)	N21' - C22' - N23'	118.9(4)
C4 - C5 - C10	111.25(11)	N4' - C3 - C2	123.6(3)	C22 - C23 - C24	119.7(3)
C5 - C6 - C7	111.57(14)	C2'' - C3'' - C4''	113.2(4)	N21 - C24' - N23'	109.6(3)
C7 - C8 - C9	110.34(12)	N1 - C4' - N4'	121.9(3)	C24 - C25 - C30	111.8(3)
C8 - C9 - C10	112.03(12)	C4 - C5 - C6	111.0(3)	N21 - C27' - C22	117.1(3)
C1 - C10 - C5	108.21(11)	S1'' - C5'' - C4''	112.2(4)	C27 - C28 - C29	109.4(3)
C5 - C10 - C9	107.93(11)	N1 - C7' - C2	115.3(3)	C28 - C29 - C30	111.9(3)
C9 - C11 - C12	113.09(12)	C7 - C8 - C9	110.3(3)	C21 - C30 - C25	106.4(3)
C12 - C13 - C17	115.27(13)	C8 - C9 - C10	112.1(3)	C25 - C30 - C29	107.3(3)
C14 - C13 - C18	113.29(13)	C1 - C10 - C5	108.4(3)	C29 - C31 - C32	113.7(3)
C8 - C14 - C15	119.52(14)	C5 - C10 - C9	108.0(3)	C32 - C33 - C37	115.2(3)
C15 - C16 - C17	106.02(13)	C9 - C11 - C12	113.4(3)	C34 - C33 - C38	112.9(3)
C13 - C17 - C16	104.38(13)	C12 - C13 - C17	115.9(3)	C28 - C34 - C35	119.7(3)
C2' - C1' - C6'	117.80(14)	C14 - C13 - C18	113.4(3)	C35 - C36 - C37	105.8(3)
C1 - C2 - C3	119.37(12)	C8 - C14 - C15	119.3(3)	C33 - C37 - C36	103.3(3)
C1' - C2' - C3'	121.39(15)	C15 - C16 - C17	106.0(3)	C24' - N21 - C27'	122.6(3)
C2 - C3 - C4	118.93(12)	C13 - C17 - C16	104.1(3)	C23 - N24' - C24'	116.4(3)
C3' - C4' - C5'	119.52(15)	N1' - N1 - C4'	109.9(3)	C21 - C22 - C27'	120.9(3)
C6 - C5 - C10	113.03(12)	N1 - N1' - C2'	100.9(3)	S21A - C22'' - 23A	112.1(3)
C1' - C6' - C5'	120.50(14)	C2 - C1 - C10	116.9(3)	N24' - C23 - C22	124.5(3)
C7 - C8 - C14	110.96(12)	C3 - C2 - C7'	118.8(3)	C22'' - C23A - C24''	104.3(3)
C8 - C9 - C11	111.85(12)	S1'' - C2'' - C7'	122.2(3)	N21 - C24' - N24'	121.5(3)
C1 - C10 - C9	109.38(12)	N4' - C3 - C4	115.7(3)	C23A - C24'' - C25''	116.6(5)
C5 - C10 - C19	111.13(12)	C3 - C4 - C5	114.4(3)	C26 - C25 - C30	112.3(3)
C11 - C12 - C13	111.56(14)	N3' - C4' - N4'	128.6(4)	C25 - C26 - C27	112.0(3)
C12 - C13 - C18	111.11(12)	C4 - C5 - C10	111.5(3)	N21 - C27' - C22''	117.8(3)
C17 - C13 - C18	109.46(12)	C5 - C6 - C7	111.9(3)	C27 - C28 - C34	111.6(3)
C13 - C14 - C15	103.70(11)	N1 - C7' - C2''	117.9(3)	C28 - C29 - C31	112.9(3)
O2 - C17 - C13	115.52(12)	C7 - C8 - C14	111.4(4)	C21 - C30 - C29	109.6(3)
C1' - C26 - C2	132.08(14)	C8 - C9 - C11	112.2(3)	C25 - C30 - C39	112.1(3)
C2' - C1' - C26	116.40(14)	C1 - C10 - C9	108.6(3)	C31 - C32 - C33	111.0(3)
C1 - C2 - C26	125.08(13)	C5 - C10 - C19	111.6(3)	C32 - C33 - C38	110.6(3)
O1 - C3 - C2	121.82(13)	C11 - C12 - C13	111.3(3)	C37 - C33 - C38	109.9(3)
C2' - C3' - C4'	120.01(15)	C12 - C13 - C18	110.7(3)	C33 - C34 - C35	103.5(3)
C4 - C5 - C6	109.66(13)	C17 - C13 - C18	109.5(3)	O2 - C37 - C33	116.2(4)
C4' - C5' - C6'	120.73(16)	C13 - C14 - C15	104.5(3)	N21' - N21 - C24'	109.9(3)
C6 - C7 - C8	112.47(12)	O1 - C17 - C13	116.0(4)	N21 - N21' - C22'	100.2(3)
C9 - C8 - C14	109.02(12)	N1' - N1 - C7'	126.7(3)	C22 - C21 - C30	114.6(3)
C10 - C9 - C11	113.82(12)	C2' - N3' - C4'	102.3(3)	C23 - C22 - C27'	117.7(3)
C1 - C10 - C19	108.63(12)	C1 - C2 - C3	120.0(3)	S21A - C22'' - C27'	120.6(3)
C9 - C10 - C19	111.50(12)	N1' - C2' - N3'	117.5(4)	C23A - C22'' - C27'	127.3(4)
C12 - C13 - C14	107.88(12)	C3'' - C2'' - C7'	128.2(3)	N24' - C23 - C24	115.6(3)
C14 - C13 - C17	99.41(11)	C2 - C3 - C4	120.7(3)	C23 - C24 - C25	115.1(4)
C8 - C14 - C13	114.17(12)	N1 - C4' - N3'	109.5(3)	N23' - C24' - N24'	128.9(4)
C14 - C15 - C16	103.55(14)	C3'' - C4'' - C5''	112.7(4)	C24 - C25 - C26	110.3(3)

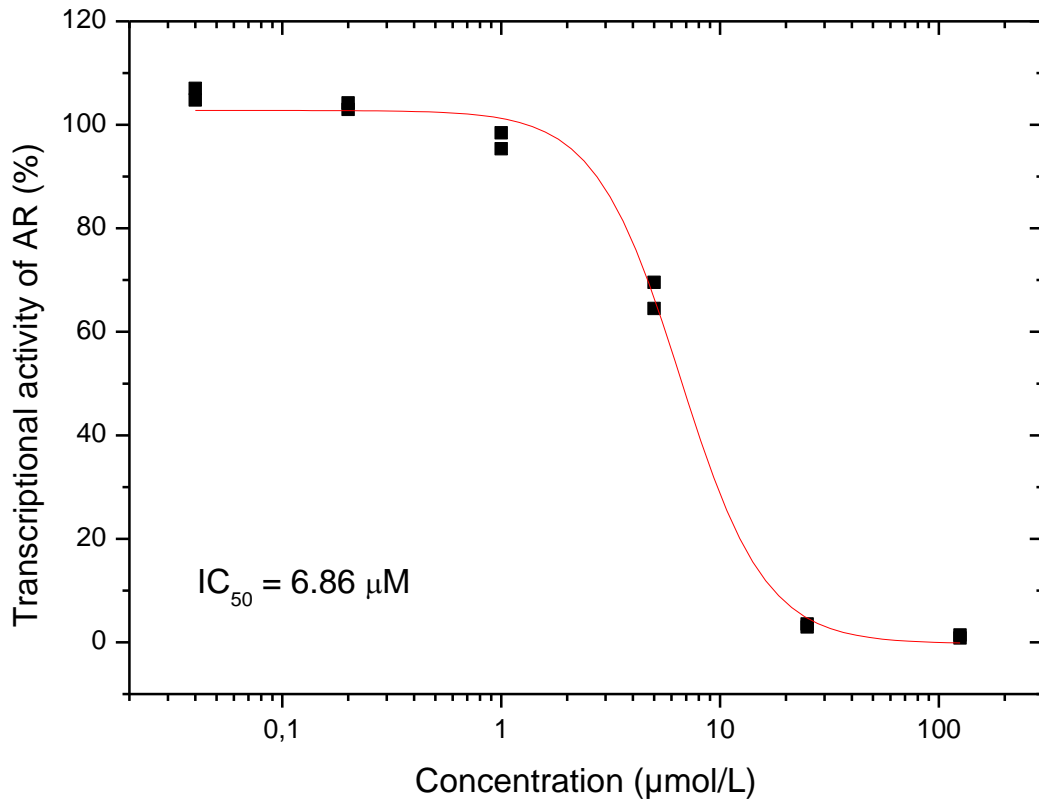
O2 - C17 - C16	114.56(13)	C6 - C5 - C10	112.5(3)	S21A - C25" - 24"	113.2(5)
		C6 - C7 - C8	112.2(3)	C26 - C27 - C28	112.4(3)
		C2 - C7' - C2"	126.8(3)	C22 - C27' - C22"	125.1(3)
		C9 - C8 - C14	108.6(3)	C29 - C28 - C34	109.0(3)
		C10 - C9 - C11	115.0(3)	C30 - C29 - C31	113.7(3)
		C1 - C10 - C19	107.8(3)	C21 - C30 - C39	108.8(3)
		C9 - C10 - C19	112.4(3)	C29 - C30 - C39	112.5(3)
		C12 - C13 - C14	108.0(3)	C32 - C33 - C34	108.1(3)
		C14 - C13 - C17	98.9(3)	C34 - C33 - C37	99.7(3)
		C8 - C14 - C13	114.3(4)	C28 - C34 - C33	114.9(3)
		C14 - C15 - C16	103.6(3)	C34 - C35 - C36	104.3(3)
		O1 - C17 - C16	109.8(3)	O2 - C37 - C36	111.0(3)

Table S3. Hydrogen-bond geometry of crystal **2a** and **8j**

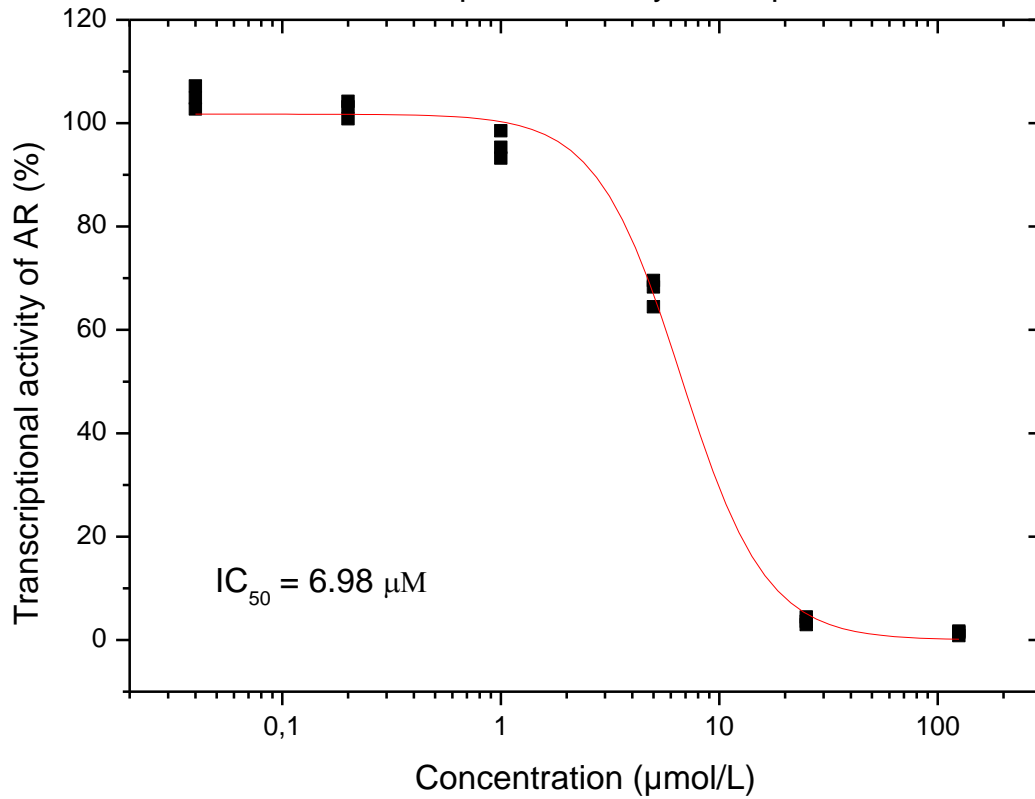
D-H...A	D-H (Å)	H...A(Å)	D...A(Å)	D-H...A (°)	symmetry codes
Crystal 2a					
O2-H2O...O1	0.81(2)	2.00(2)	2.8005(18)	166(2)	x,y,1+z
C4'-H4'...O1	0.95	2.46	3.367(2)	160	1-x,-1/2+y,-z
C3'-H3'...O2	0.95	2.669	3.533(2)	152	
C16-H16A...O1	0.99	2.604	3.424(2)	140	x,y,1+z
Crystal 8j					
O1-H1O...N4'	0.96	1.98	2.911(5)	162	1+x,y,z
O2-H2O...N24'	0.99	2.01	2.923(4)	154	1+x,y,z
C4-H4''...C11	0.93	2.78	3.420(5)	127	
C5''-H5''...O2	0.93	2.27	3.104(6)	149	1-x,-1/2+y,1-z
C40-H40A...N3'	0.97	2.60	3.297(5)	129	1+x,y,z
C40-H40B...N23'	0.97	2.39	3.202(5)	140	1+x,y,z
C19-H19B...N21'	0.96	2.85	3.687(5)	146.8	
C2'-H2'...C11	0.93	2.86	3.538(5)	130.6	

Transcriptional activity (22Rv1-ARE14 gene reporter assay, 24 h)

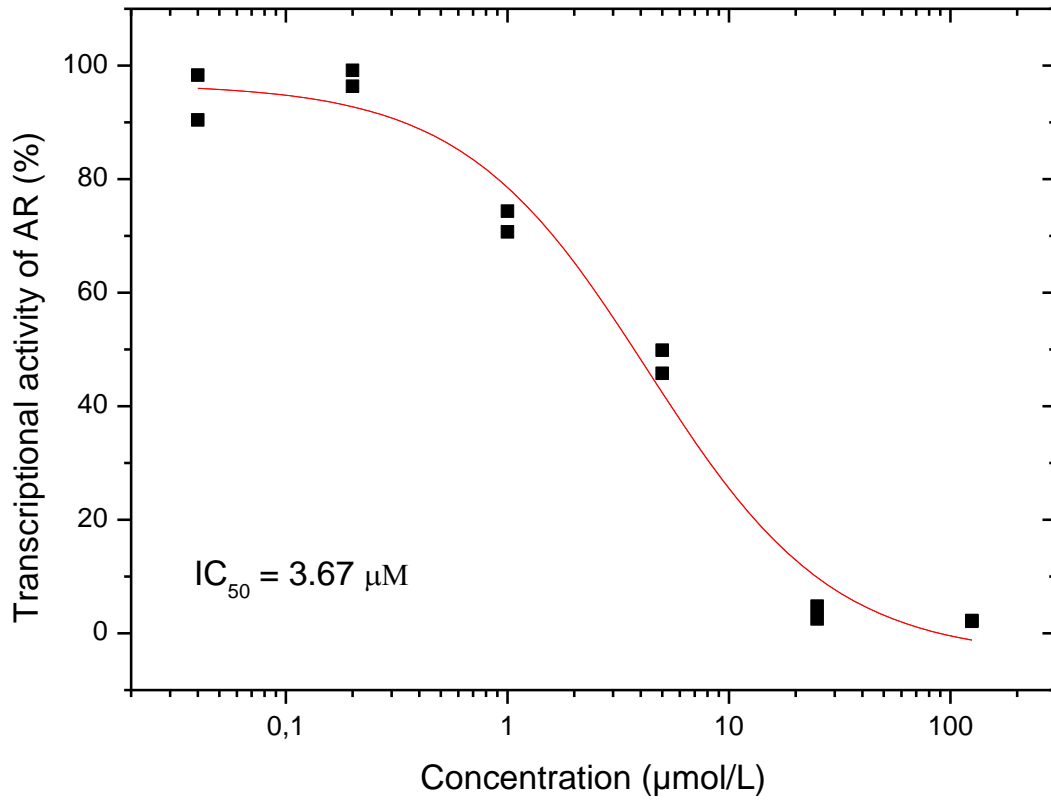
Transcriptional activity 2a



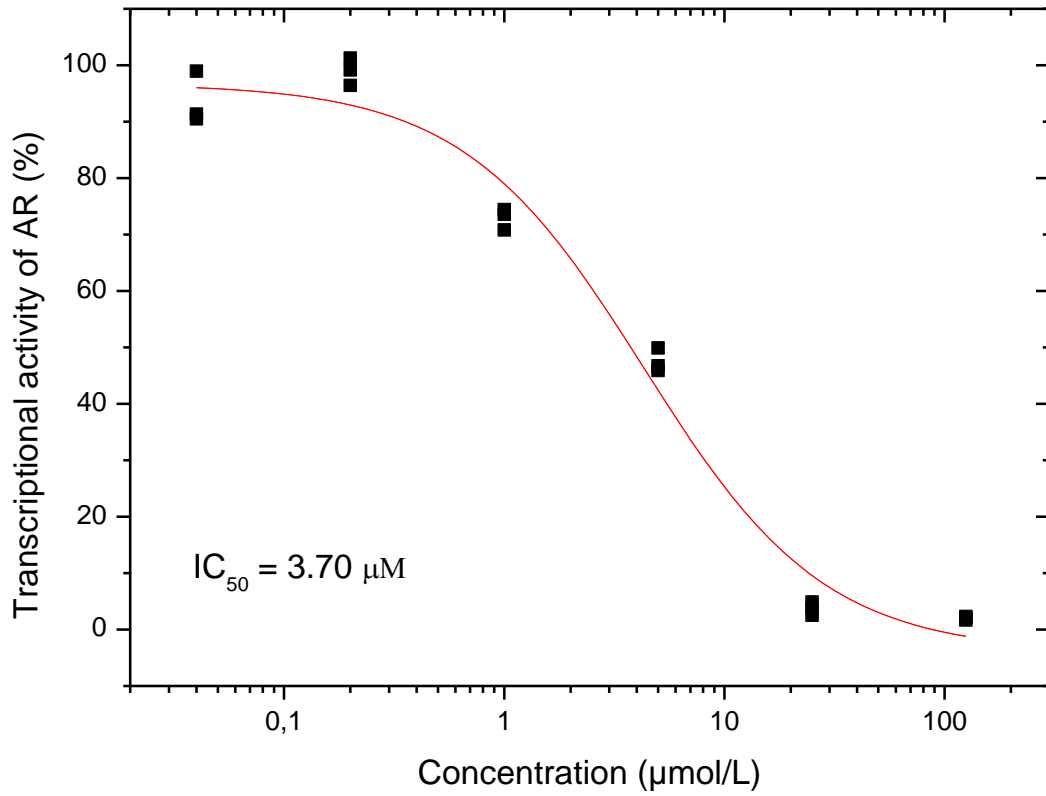
Transcriptional activity 2a, duplicate



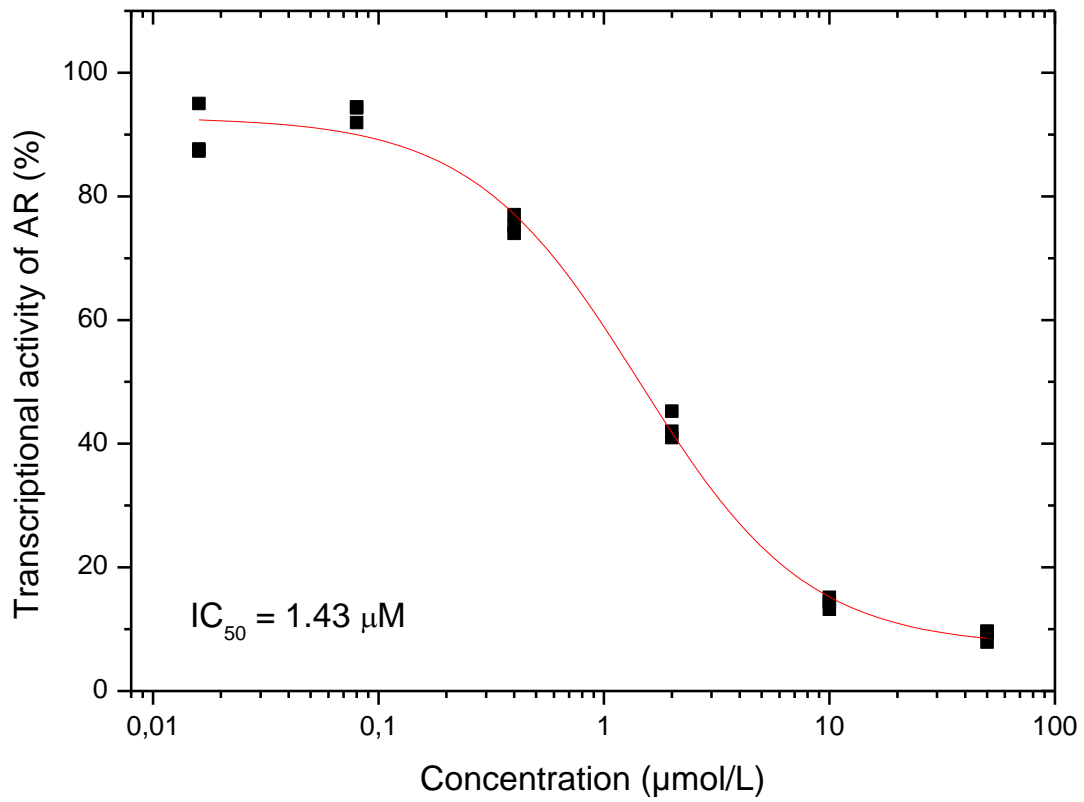
Transcriptional activity 2f



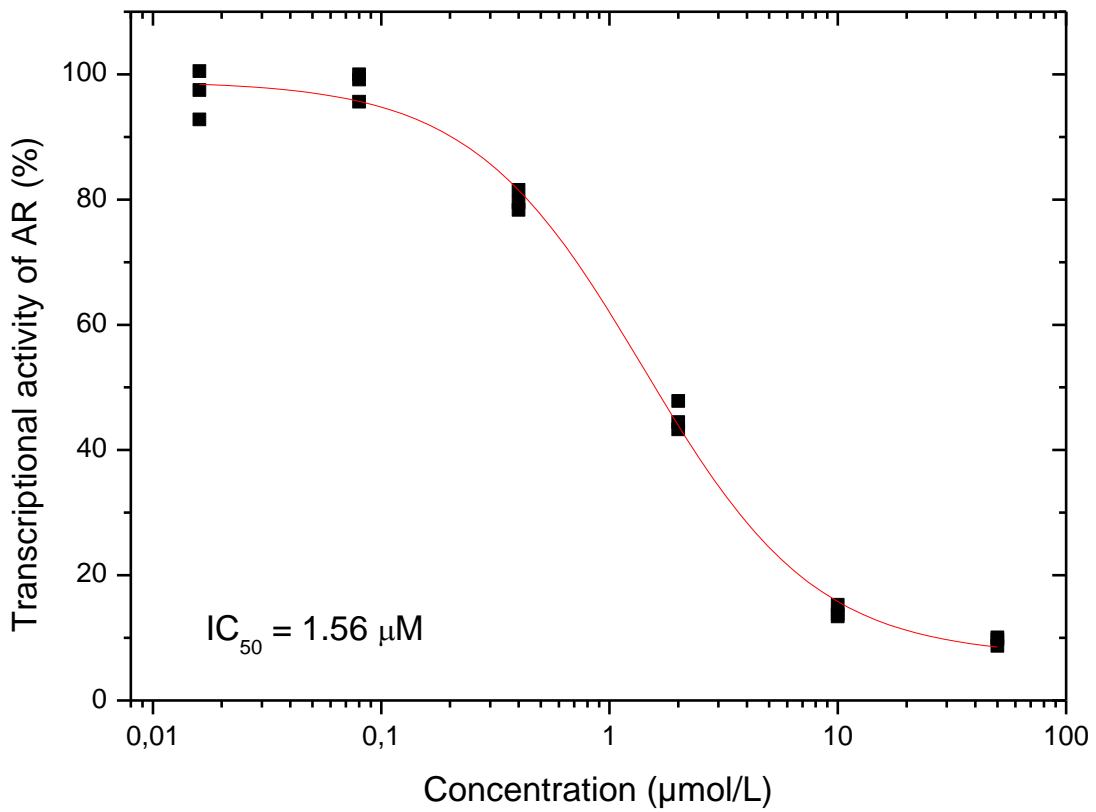
Transcriptional activity 2f, duplicate



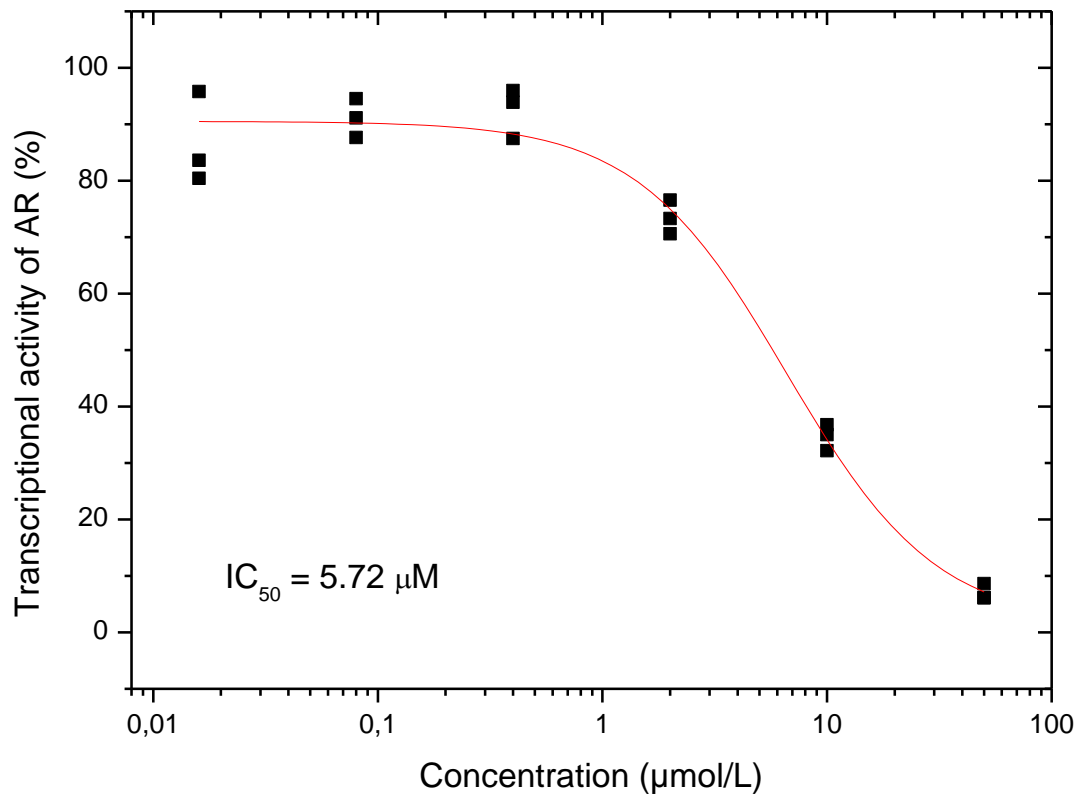
Transcriptional activity Enzalutamide



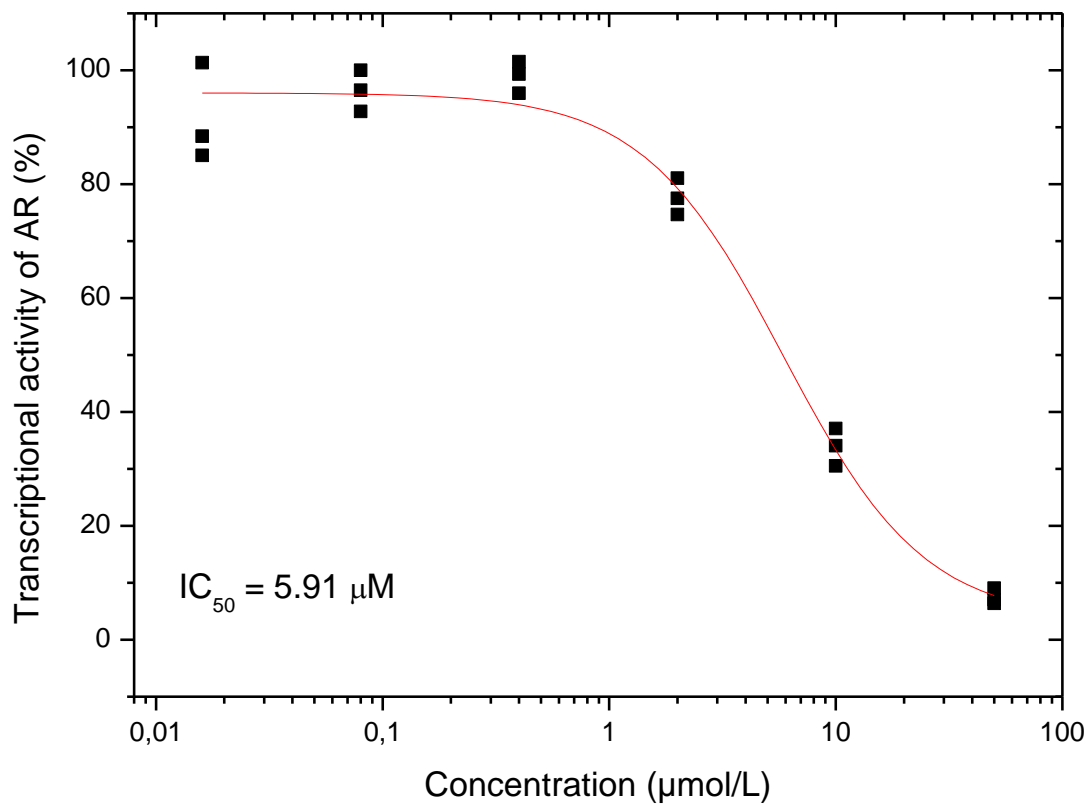
Transcriptional activity Enzalutamide, duplicate



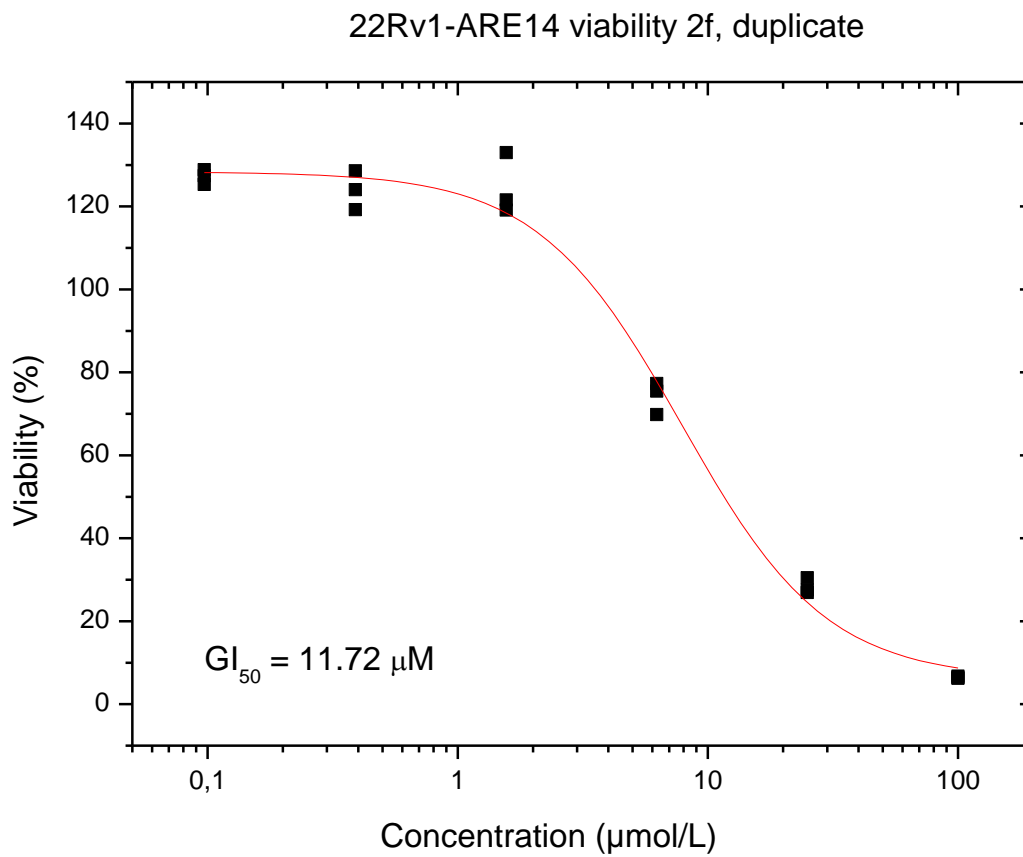
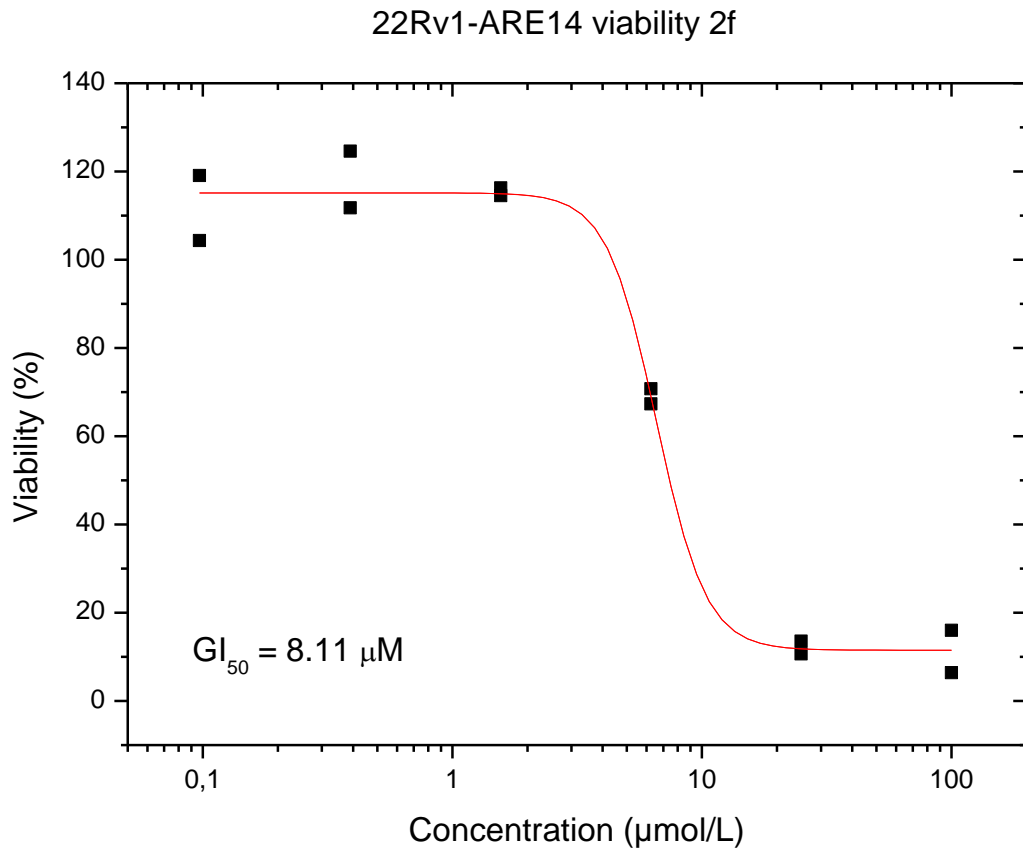
Transcriptional activity Galeterone



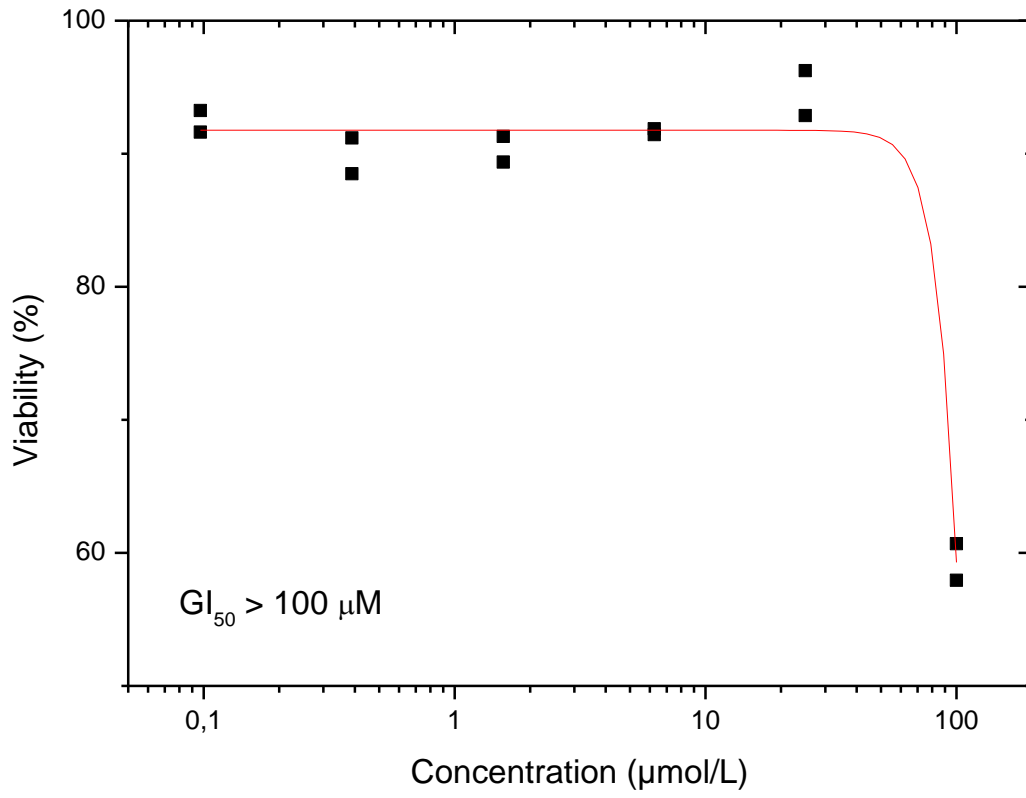
Transcriptional activity Galeterone, duplicate



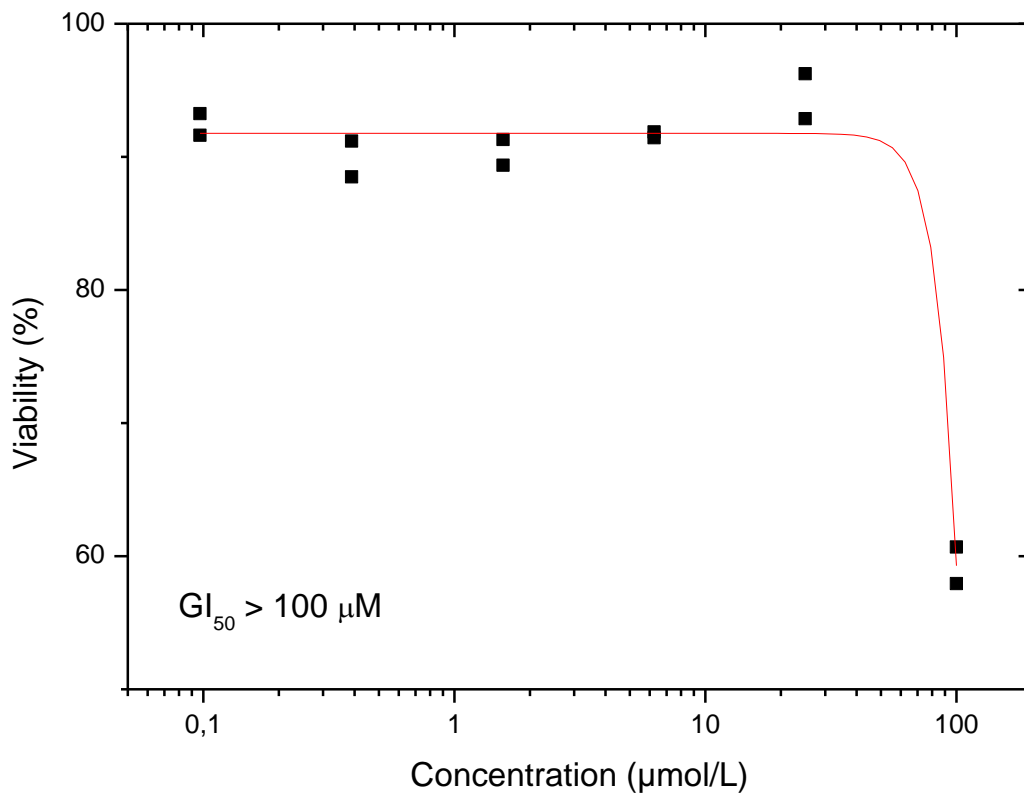
Viability of 22Rv1-ARE14 (72 h)



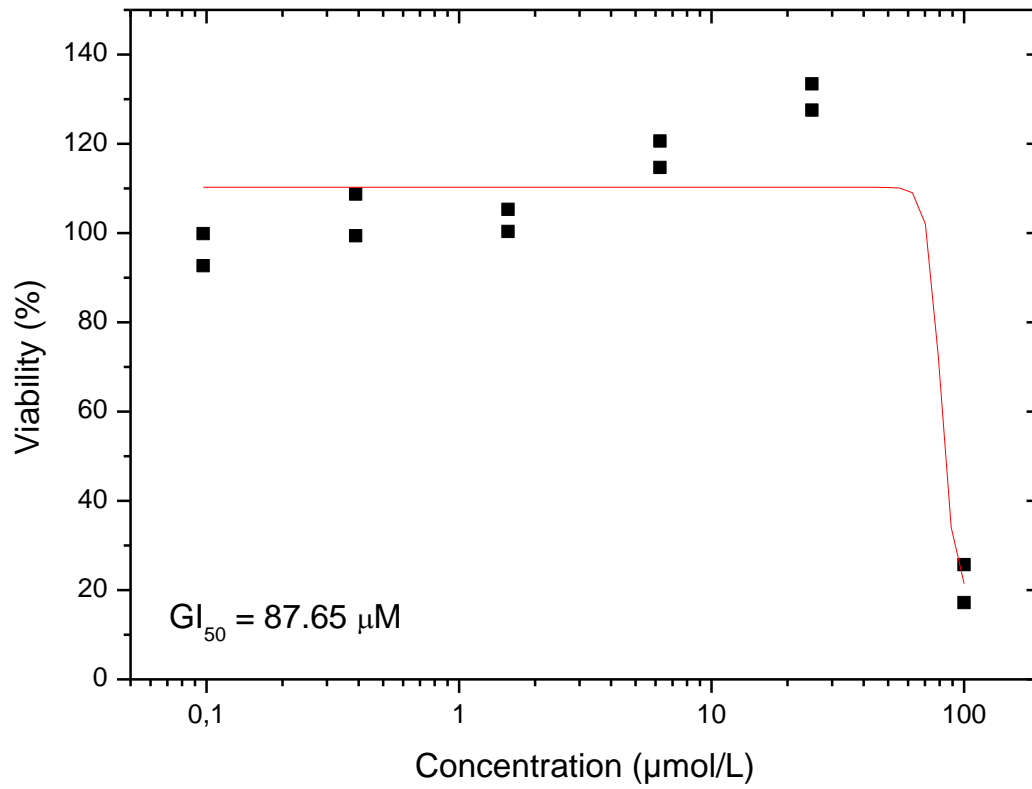
22Rv1-ARE14 viability Enzalutamide



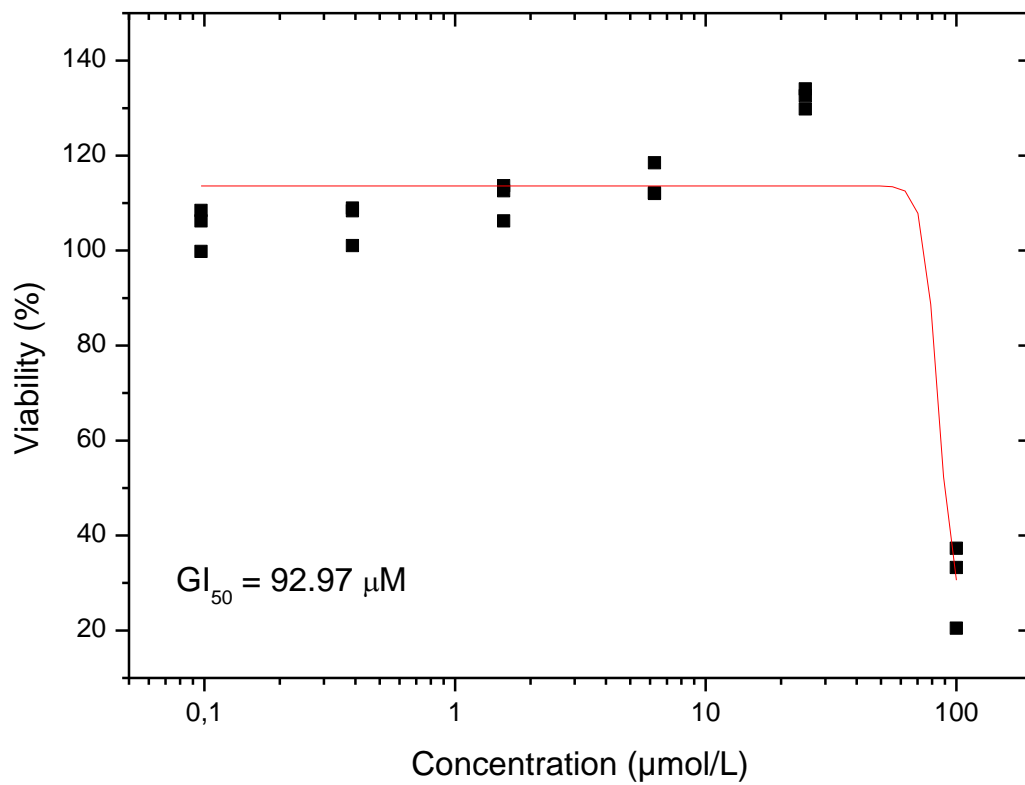
22Rv1-ARE14 viability Enzalutamide, duplicate



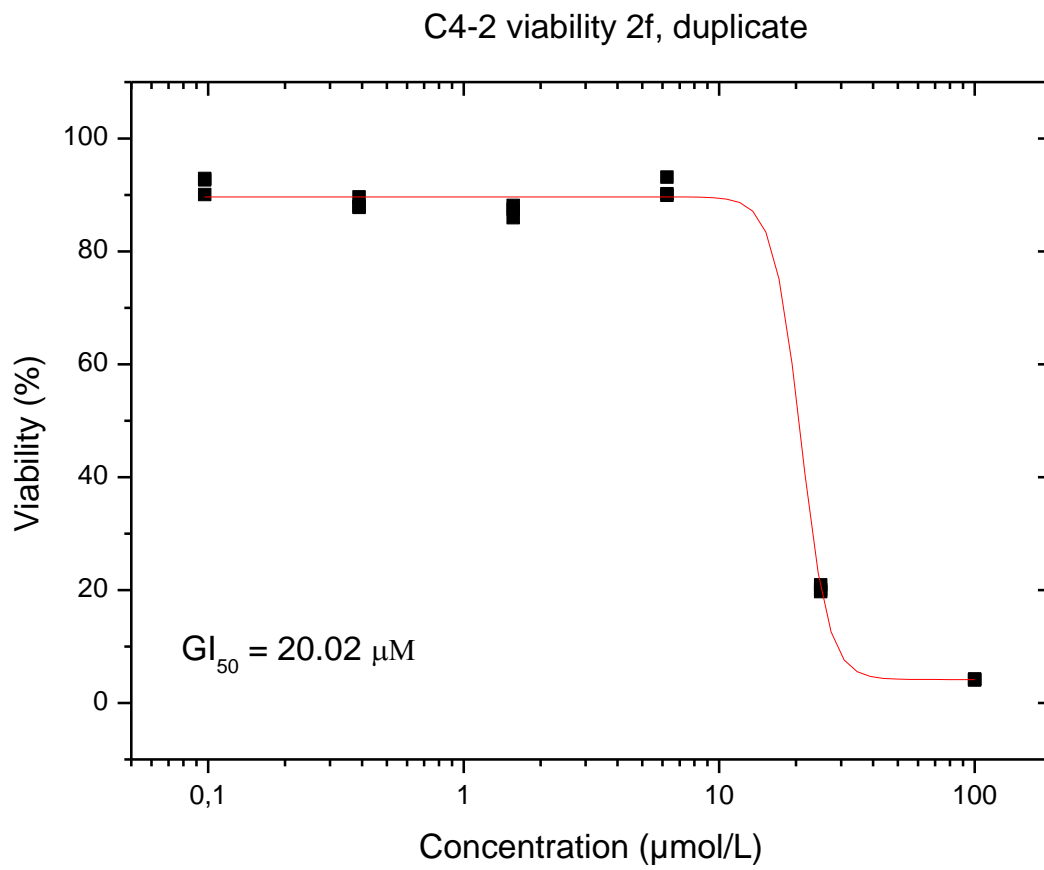
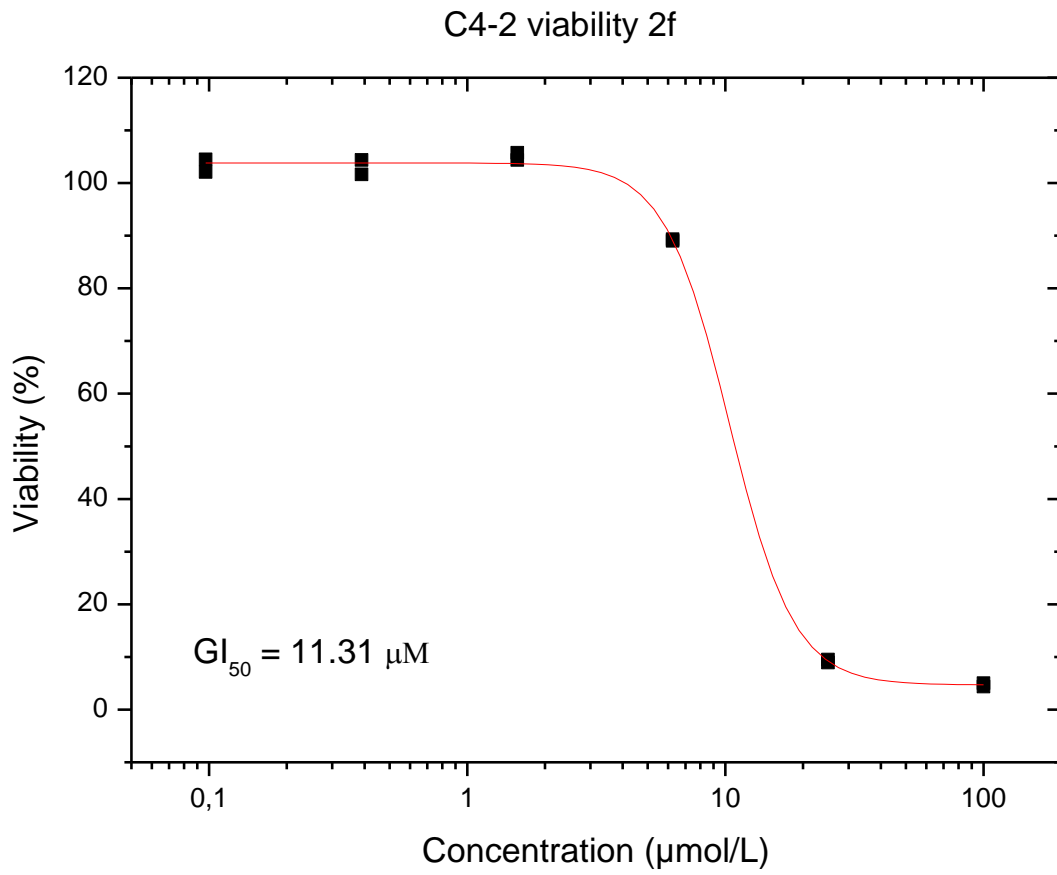
22Rv1-ARE14 viability Galeterone



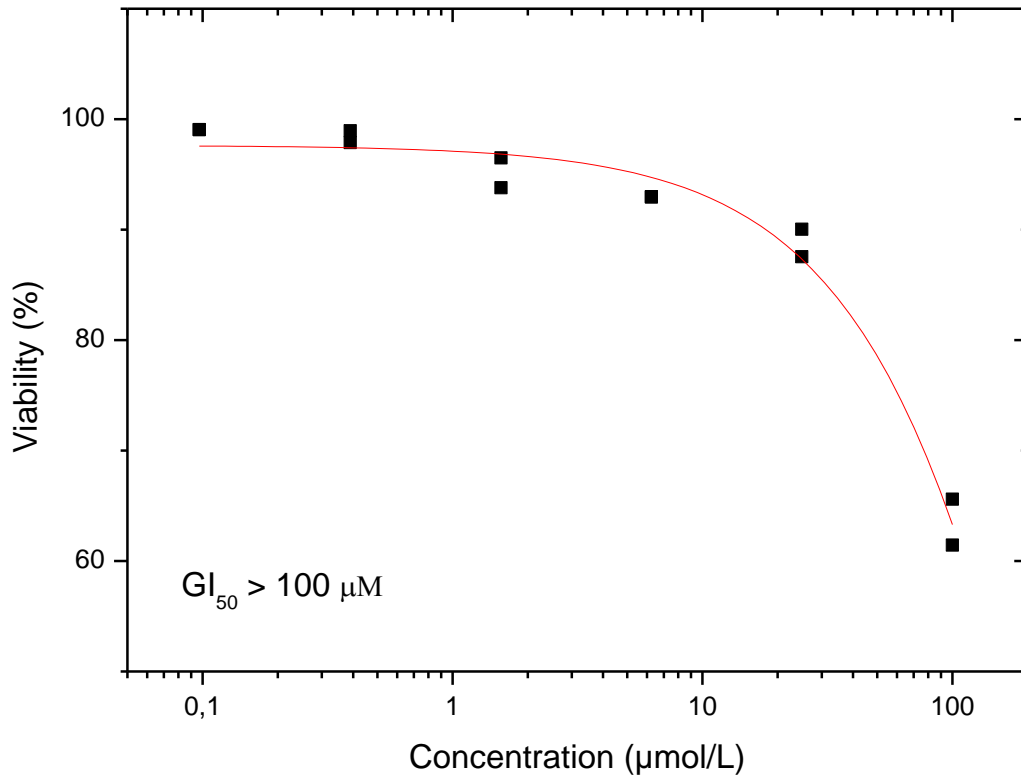
22Rv1-ARE14 viability Galeterone, duplicate



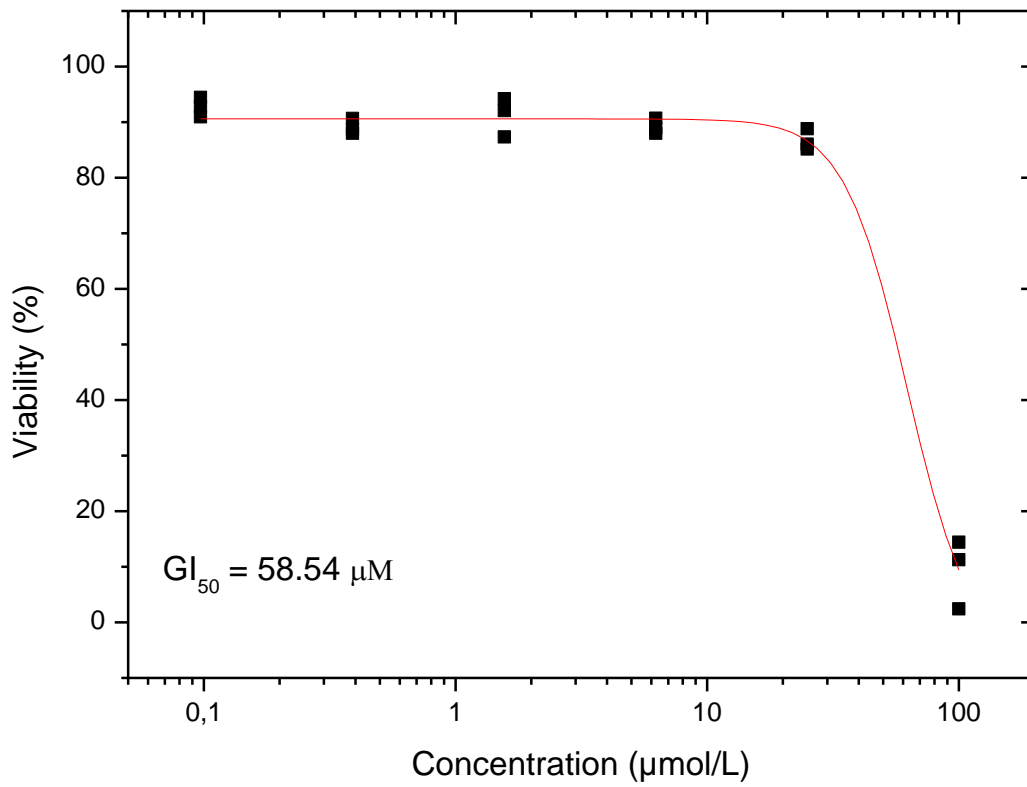
Viability of C4-2 (72 h)



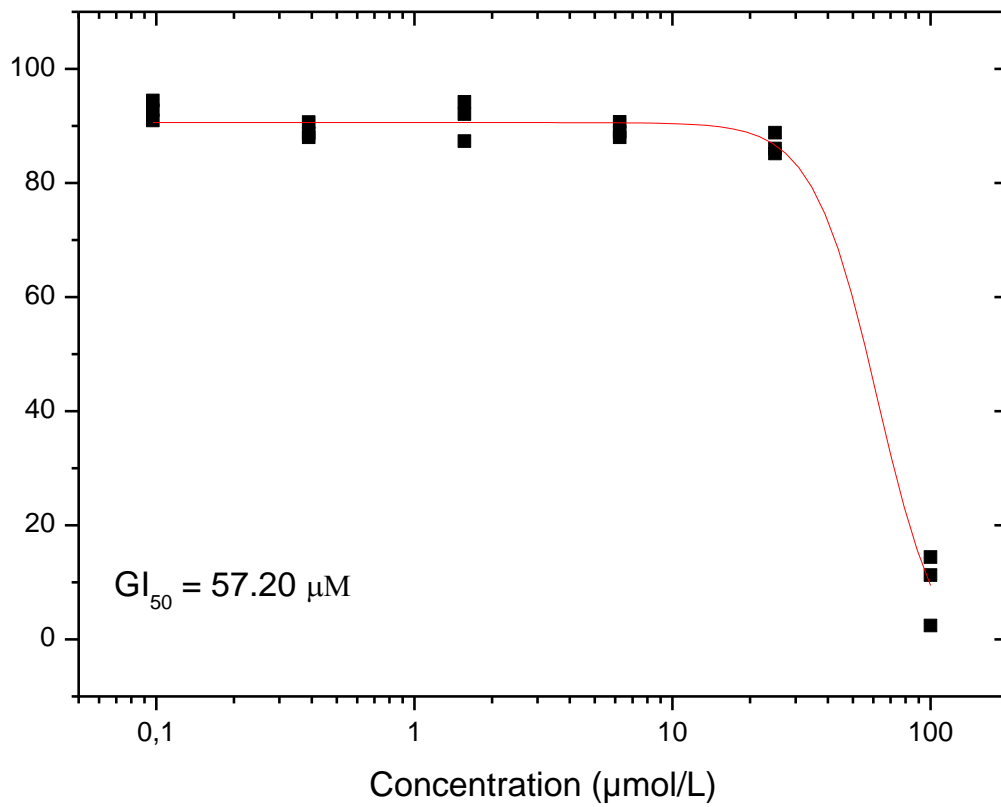
C4-2 viability Enzalutamide



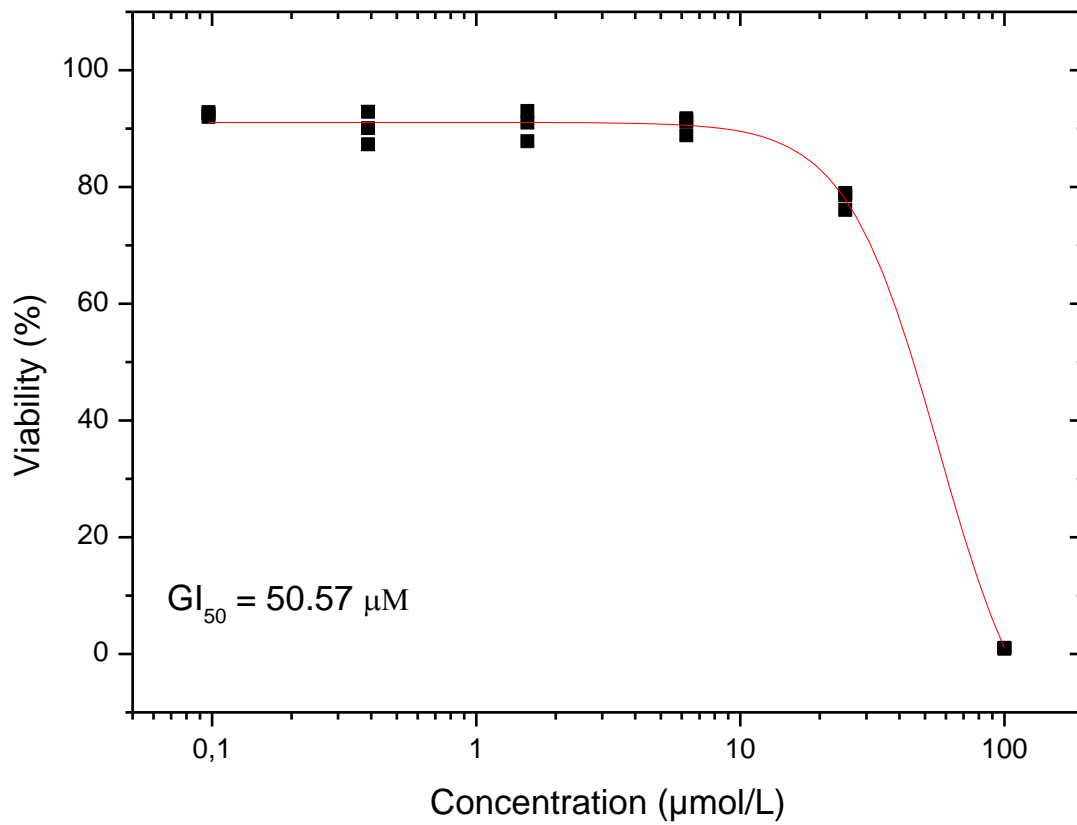
C4-2 viability Enzalutamide, duplicate



C4-2 viability Galeterone



C4-2 viability Galeterone, duplicate



Appendix II.

Peřina M*, Kiss MA*, M6ty6n G, Szczyrbov6 E, Eli6š M, Őtudent V Jr, Kurf6rstov6 D, Kovalov6 M, Mada L, Bouchal J, Frank 6, Jorda R. A-ring-fused pyrazoles of dihydrotestosterone targeting prostate cancer cells via the downregulation of the androgen receptor. *Eur J Med Chem.* 2023a Mar 5;249:115086.

*shared first authorship



Research paper

A-ring-fused pyrazoles of dihydrotestosterone targeting prostate cancer cells via the downregulation of the androgen receptor

Miroslav Peřina^{a,1}, Márton A. Kiss^{b,1}, Gergő Mótyán^b, Eva Szczyrbová^c, Martin Eliáš^c, Vladimír Študent jr.^d, Daniela Kurfürstová^c, Markéta Kovalová^a, Lukáš Mada^a, Jan Bouchal^c, Éva Frank^{b,**}, Radek Jorda^{a,*}

^a Department of Experimental Biology, Faculty of Science, Palacký University Olomouc, Šlechtitelů 27, 78371, Olomouc, Czech Republic

^b Department of Organic Chemistry, University of Szeged, Dóm Tér 8, H-6720, Szeged, Hungary

^c Department of Clinical and Molecular Pathology, Institute of Molecular and Translational Medicine, Palacký University Olomouc and University Hospital Olomouc, Hněvotínská 3, 77515, Olomouc, Czech Republic

^d Department of Urology, Palacký University Olomouc and University Hospital Olomouc, I.P.Pavlova 6, 77900, Olomouc, Czech Republic



ARTICLE INFO

Keywords:

A-ring-fused pyrazoles
Androgen receptor
Prostate cancer
Protein degradation
Transcriptional activity
Structure-activity relationship

ABSTRACT

High expression of the androgen receptor (AR) and the disruption of its regulation are strongly responsible for the development of prostate cancer (PCa). Therapeutically relevant non-steroidal or steroidal antiandrogens are able to block the AR effect by eliminating AR-mediated signalling. Herein we report the synthesis of novel steroidal pyrazoles derived from the natural sex hormone 5 α -dihydrotestosterone (DHT). 2-Ethylidene or 2-(hetero)arylidene derivatives of DHT obtained by regioselective Claisen-Schmidt condensation with acetaldehyde or (hetero)aromatic aldehydes in alkaline ethanol were reacted with monosubstituted hydrazines to give A-ring-fused 1,5-disubstituted pyrazoles as main or exclusive products, depending on the reaction conditions applied. Spontaneous or 2,3-dichloro-5,6-dicyanobenzoquinone (DDQ)-induced oxidation of the primarily formed pyrazolines resulted in the desired products in moderate to good yields, while 17-oxidation also occurred by using the Jones reagent as a strong oxidant. Transcriptional activity of the AR in a reporter cell line was examined for all novel compounds, and several previously synthesized similar DHT-based pyrazoles with differently substituted heteroring were also included to obtain information about the structure-activity relationship. Two specific regioisomeric groups of derivatives significantly diminished the transcriptional activity of the AR in reporter cell line in 10 μ M concentration, and displayed reasonable antiproliferative activity in AR-positive PCa cell lines. Lead compound (**3d**) was found to be a potent AR antagonist (IC₅₀ = 1.18 μ M), it generally suppressed AR signalling in time and dose dependent manner, moreover, it also led to a sharp decrease in wt-AR protein level probably caused by proteasomal degradation. We confirmed the antiproliferative activity of **3d** in AR-positive PCa cell lines (with GI₅₀ in low micromolar ranges), and its cellular, biochemical and in silico binding in AR ligand-binding domain. Moreover, compound **3d** was shown to be potent even *ex vivo* in patient-derived tissues, which highlights the therapeutic potential of A-ring-fused pyrazoles.

1. Introduction

The androgen receptor (AR) is a ligand-activated transcription factor that belongs to the superfamily of steroid and thyroid hormone receptors and plays a crucial role in the normal development of male reproductive tissues. Androgen binding induces conformational changes of the AR

that influences its interactions with other proteins and DNA, as well as its subcellular localization and transcriptional activity. The AR is further regulated by numerous post-translational modifications that affect its physiological role, especially its transcriptional program [1,2].

High expression and/or relaxation of AR regulation is strongly implicated in prostate cancer (PCa). PCa is the second most frequent

* Corresponding author.

** Corresponding author.

E-mail addresses: frank@chem.u-szeged.hu (É. Frank), radek.jorda@upol.cz (R. Jorda).

¹ These authors contributed equally to this work.

cancer in men according to the National Cancer Institute (USA). Primary therapy (androgen deprivation therapy) is based on reduction of the circulating androgens in plasma (by orchiectomy or with luteinizing hormone-releasing hormone agonists), but usually the disease progresses to castration-resistant prostate cancer (CRPC) stage, which is defined by alteration in signalling of AR (high expression, splicing variants) and resistance to standard therapeutics. Therefore, AR has been suggested as an important therapeutic target for PCa, and several anti-AR strategies have been introduced for decades including inhibition of the transcription of the AR gene, inhibition or destabilization of transcript or protein or splicing variants, AR degradation, blocking of AR synthesis, interference with intracellular trafficking of AR, and inhibition of downstream signalling related to AR-V7 activation (Fig. 1) [3,4].

Several steroidal or non-steroidal agents (e.g. abiraterone, enzalutamide, apalutamide, darolutamide) with diverse modes of action (CYP17 hydroxylase/17,20 lyase (CYP17) inhibitors, AR antagonists) have been approved for CRPC, and data have demonstrated an overall survival benefit also in the castration-sensitive stage. On the other hand, several AR-related mechanisms of resistance have been described, and novel strategies to overcome them are an important unmet need. Since recent studies have revealed that several mutations in the AR convert the action of enzalutamide and apalutamide from antagonist to agonist [5, 6], it appears suitable to target AR also indirectly, e.g. by AR-destabilizing agents. Decrease in AR protein stability is accompanied by increased degradation, which is connected with its short half-life (highlighted in the presence of no androgens) and by the presence of PEST sequence responsible for rapid degradation in proteasome. Several compounds with AR degradation activity have been introduced, including hybrid molecules such as PROTACs (proteolysis-targeting chimeras based on the proteasome-mediated degradation of protein of interest) [7–10] or SNIPERs (specific and nongenetic inhibitor of apoptosis protein-dependent protein erasers) [11]. Interestingly, biopharmaceutical company Arvinas developed several AR degraders, and currently ARV-110 (bavdegalutamide) is the first degrader in Phase 2 clinical trial for the treatment of patients with metastatic CRPC [12,13].

Sterane-based D-ring-modified pyrazoles [14,15], structurally related to abiraterone, are known to be potentially effective anti-androgen agents for the treatment of PCa by antagonizing AR, acting as CYP17 enzyme inhibitors and/or having direct cytotoxicity. However, steroids containing a pyrazole moiety in the A-ring were less investigated. We previously described some A-ring-fused arylpyrazoles of DHT and demonstrated their anticancer activity against multiple cancer cell lines including PCa cells [16,17]. Cyclocondensation reactions of 2-hydroxymethylene-DHT led to a mixture of separable pyrazole regioisomers (series 1 and 2) in varying ratio depending on the applied medium and on the electronic character of the substituent of the

phenylhydrazine applied (Fig. 2) [16]. Similar derivatives containing a 1,5-disubstituted pyrazole moiety (series 3 and 4) were also obtained [17].

In the current work, additional 1,5-disubstituted pyrazoles structurally similar to 3 and 4 have been prepared, and a total of 55 compounds including the previously and newly synthesized ones were screened for their ability to affect the transcriptional activity of AR in a reporter cell line. The structure of all novel compounds was determined by 1D and 2D NMR spectroscopy as well as electrospray ionization mass spectrometry (ESI-MS). All compounds were analysed for their agonist and antagonist activity towards the AR, for their ability to decrease AR protein level and to block the formation of LAPC-4 colonies. Based on the obtained results from screening, SAR for compounds was described, and lead compound 3d was further studied in detail. Lead compound exerted reasonable antiproliferative activity towards AR-positive PCa cell lines and inhibited the colony formation. It was demonstrated that 3d dose-dependently diminishes AR transcriptional activity and mRNA expression of PSA (key downstream target). Moreover, lead compound markedly decreased the AR protein level and totally turned off downstream signalling upon longer treatment. Molecular docking proved the possibility of binding 3d into the wt-AR ligand binding domain, but also into frequent Thr877Ala mutant with extensive interactions.

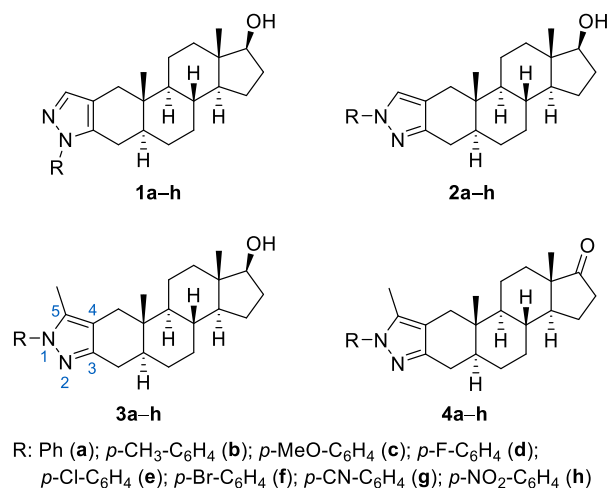


Fig. 2. A-ring-fused pyrazoles of DHT previously synthesized by us [16,17].

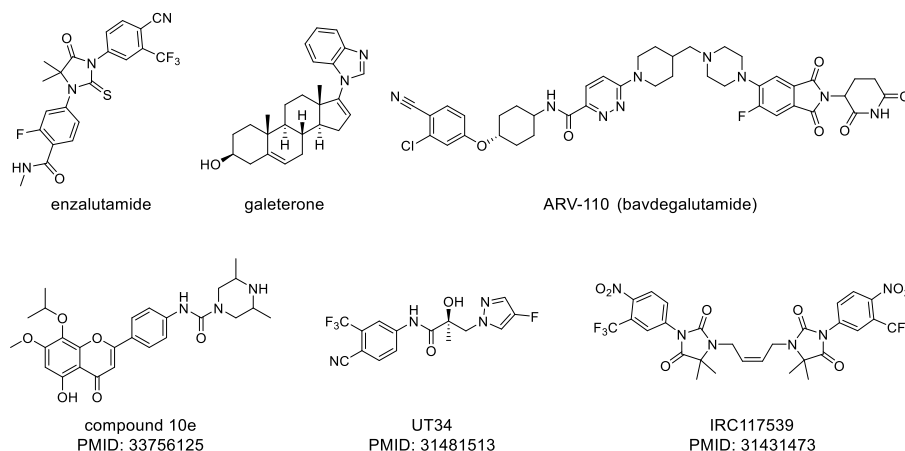


Fig. 1. Examples of AR modulators in clinical trials (upper panel) and compounds with the ability to degrade AR (bottom panel).

2. Results and discussion

2.1. Synthesis and characterization of the target compounds

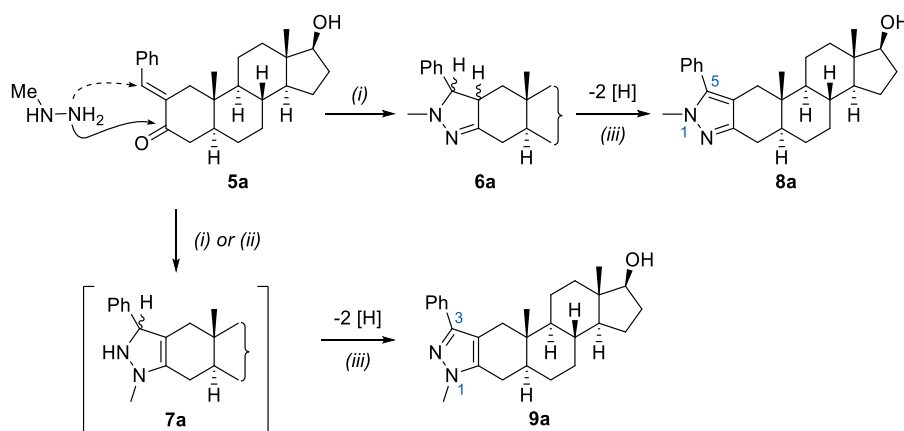
In order to synthesize compounds structurally similar to those from series **3**, arylidene derivatives (**5a–j**) of DHT were first synthesized by Claisen-Schmidt condensation as α,β -enone precursors suitable for heterocyclization (Supporting Information, [Scheme S1](#)). The majority of the compounds were obtained by the method described previously [18], however, two additional molecules (**5f** and **5i**) were also prepared on the basis of preliminary flexible docking into AR and solubility considerations. As a next step, the cyclization of the prepared enones (**5**) with methylhydrazine as binucleophilic reagent was planned to be carried out. Preliminary experiment was performed with **5a** in EtOH using MW irradiation. After an irradiation time of 3 min, complete conversion was observed by thin-layer chromatography (TLC), and four new spots were detected on the silica plate. The products were separated by column chromatography, and their structures were determined by NMR spectroscopy. Two of the four compounds proved to be pyrazole regioisomers **8a** and **9a** formed by heterocyclization and subsequent autooxidation under the reaction conditions, while the other two products were the diastereomeric pairs of the pyrazoline precursor **6a** of the major heteroaromatic product **8a** ([Scheme 1](#)). The order of elution in descending polarity was as follows: **9a** (1,3-pyrazole) > **8a** (1,5-pyrazole) > **6a** (inseparable mixture of two isomers). These results thus showed that a considerable amount of the pyrazolines formed primarily by the ring-closure underwent oxidation under the reaction conditions. The partially saturated precursor **7a** of the 1,3-disubstituted pyrazole **9a** could not be detected.

Since the reaction described above led to the formation of four difficult-to-separate products, an additional oxidation step was introduced before purification to complete the spontaneous oxidation observed partially, and thus reduce the number of products to two. 2,3-Dichloro-5,6-dicyanobenzoquinone (DDQ), which has been successfully used previously for the oxidation of the heteroring without affecting the C17–OH bond [18], was suitable for this purpose. The reaction was first carried out in 1,4-dioxane with conventional heating, which required a relatively large amount of hot solvent to dissolve the starting materials. Although the oxidation was completed within 2 h, the work-up procedure and extraction of the products proved to be difficult. However, when the reaction was carried out in a MW reactor, the higher reaction temperature (120 °C) in a closed vessel allowed the starting materials to dissolve in significantly less solvent (5 mL), and a much shorter time (5 min) was required for the DDQ-induced oxidation. The use of a smaller amount of solvent facilitated the work-up, as a filterable precipitate was observed when the reaction mixture was poured onto water. As

expected, the oxidation resulted in a mixture of the two possible pyrazole regioisomers (**8a** and **9a**) in a ratio of about 2:1, which were easily separable by column chromatography. However, the heterocyclization of **5a** with methylhydrazine sulfate under conventional heating in EtOH for 24 h led to the exclusive formation of the 1,5-pyrazole (**8a**) without the traces of its pyrazoline precursor (**6a**) or the other heteroaromatic regioisomer (**9a**) ([Scheme 1](#)). Since the formation of **9a** by initial 1,4-addition of methylhydrazine to **5a** is under kinetic control, short reaction time under MW heating can lead to the 1,3-disubstituted product in a minor extent by rapid dehydrogenation of the cyclized pyrazoline precursor **7a**. Contrarily, longer reaction time at reflux temperature favoured the exclusive formation of the thermodynamically more stable 1,5-regioisomer (**8a**) by nucleophilic attack of the reagent on the carbonyl-C followed by cyclization and spontaneous oxidation [19].

The structure of the regioisomeric pyrazoles **8a** and **9a** was confirmed by 1D NMR (^1H and ^{13}C NMR, Supporting Information) and 2D NMR measurements (HSQC, HMBC, NOESY). A significant difference between the two spectra can be observed in the range of 2.00–3.00 ppm and above 7.00 ppm in the aromatic region, where the peaks of the protons located at or near to the reaction centre appear. The characteristic signals of the hydrogens at C-1 and C-4 are found at a chemical shift above 2.00 ppm due to the proximity of the heteroaromatic ring. For **8a** and **9a**, the reversed order of the signals indicates a structural difference between the compounds. In order to identify the 1,3- and the 1,5- pyrazoles, their 2D-NMR spectra were also recorded, and after determining the characteristic correlations, we also examined the NOESY spectra of the products, which provided information on the protons with the same spatial arrangement ([Figs. S1 and S2](#)).

As mentioned above, the heterocyclization led to the regioselective formation of the 1,5-regioisomer (**8a**) in good yield under conventional heating without the need for an additional oxidation step ([Scheme 1](#), [Table 1](#), entry 1). As a continuation, further arylidene derivatives (**5b–h**) were subjected to ring-closure, and the corresponding 1,5-regioisomers (**8b–h**) were obtained in moderate to good yields ([Table 1](#), entries 2–8). For compounds bearing a halogen substituent on the benzene ring, the oxidation was completed using DDQ, while spontaneous oxidation occurred in other cases. Treating the crude products with the Jones reagent in acetone, besides the pyrazoline ring, the 17 β -hydroxyl group was also oxidized leading to the corresponding 17-ones (**10b–h**) ([Table 1](#), entries 1–8). Furthermore, the 1,5-dimethyl-substituted pyrazole (**8l**) and its 17-one derivative (**10l**) were also prepared from the previously synthesized ethylidene derivative **5j** [17]. Based on promising preliminary flexible docking studies for diaryl-substituted pyrazoles, oxidative heterocyclization of **5a**, **5e** and **5i** was carried out with phenylhydrazine hydrochloride under MW condition ([Table 1](#), entries 9–11), leading to compounds **8i–k** in high yields. Their D-ring-oxidized



Scheme 1. Synthesis of ring A-fused disubstituted pyrazole regioisomers of DHT. Reagents and conditions: (i) methylhydrazine (2.0 equiv.), EtOH, MW, 100 °C, 3 min; (ii) methylhydrazine sulfate (2.0 equiv.), EtOH, reflux, 24 h; (iii) DDQ, dioxane, 120 °C, 5 min (**8a**: 57%, **9a**: 28%) or spontaneous oxidation (**8a**: 80 %).

Table 1
Synthesis of DHT-derived A-ring-fused 1',5'-pyrazole derivatives.

Entry	Enone ^c	R ¹	R ²	17-OH product	Yield (%) ^c	17=O product	Yield (%) ^c
1	5a	Ph	CH ₃	8a	80	10a	76
2	5b	<i>p</i> -CH ₃ -C ₆ H ₄	CH ₃	8b	81	10b	74
3	5c	<i>p</i> -MeO-C ₆ H ₄	CH ₃	8c	79	10c	74
4	5d ^d	<i>p</i> -F-C ₆ H ₄	CH ₃	8d	66	10d	60
5	5e ^d	<i>p</i> -Cl-C ₆ H ₄	CH ₃	8e	69	10e	64
6	5f ^d	<i>p</i> -Br-C ₆ H ₄	CH ₃	8f	63	10f	57
7	5g	furan-2-yl	CH ₃	8g	52	10g	46
8	5h	thiophen-2-yl	CH ₃	8h	58	10h	53
9	5a	Ph	Ph	8i	84	10i	95
10	5e	<i>p</i> -Cl-C ₆ H ₄	Ph	8j	79	10j	91
11	5i	<i>p</i> -OH-C ₆ H ₄	Ph	8k	90	10k	91
12	5j	CH ₃	CH ₃	8l	60	10l	54

^a CH₃-NH-NH₂·H₂SO₄, EtOH, reflux, 24h (for **8a–h** and **8j**) or Ph-NH-NH₂·HCl, I₂, MW, EtOH, 100 °C, 2 min (for **8i–k**).

^b Jones reagent, acetone, rt, 30 min.

^c Compounds **5j** [17] and **5a–e**, **5g**, **5h** [18] were synthesized as described previously.

^d After the heterocyclization, DDQ was used to oxidize the heteroring.

^e After chromatographic purification.

analogues **10i–k** were also prepared for pharmacological comparison.

2.2. Targeting AR and AR-related processes

We recently described the synthesis of DHT derivatives modified in the A-ring with (hetero)arylidene, pyrazolo[1,5-*a*]pyrimidine and triazolo[1,5-*a*]pyrimidine moieties and their targeting of the AR in PCA cell lines [18].

Currently we introduced novel DHT derivatives, namely A-ring-fused 1,5-disubstituted pyrazoles (**8**) and their C17-oxidized derivatives (**10**). These series were complemented (for better understanding of structure-activity relationship) with previously published A-ring-fused monosubstituted pyrazoles (**1** and **2**) and 1,5-disubstituted pyrazole derivatives of DHT (**3** and **4**) that demonstrated anticancer activity against multiple cancer cell lines including PCA cells, but were not pharmacologically investigated in relation to AR [16,17]. All compounds were investigated for their ability to affect i) the transcriptional activity of the AR using an AR-dependent reporter cell line [20], ii) the formation of cell colonies, and iii) the expression of AR and its well-known AR-regulated genes (Nkx3.1 and PSA) via immunoblotting. All data are presented in Table 2–4, Table S1, Fig. 3 and Figs. S3, S4, S5.

The ability of compounds to diminish the R1881-stimulated transcriptional activity of AR (antagonist mode) or to transactivate AR itself (agonist mode) was examined using an AR-dependent reporter cell line [20]. Compounds from series **1** and **2** displayed only moderate effect on R1881-stimulated AR-transcriptional activity (Table 2). Most of the compounds were not able to reach inhibition values ≤ 50% of control cells stimulated with 1 nM R1881 in 10 μM concentration. Only compounds **1d** and **1e** (2'-*p*-fluorophenyl and 2'-*p*-chlorophenyl-substituted pyrazole derivatives, respectively) showed inhibition values around 39%. Unfortunately, most compounds (except of regioisomers **1f** and **2f**) undesirably activated the AR in agonist mode (Table S1).

Regioisomers of **3** and **8** that bear C-17 hydroxy group and combine methyl and aryl substitution at N1 or C5 position of pyrazole (**3a–3h**,

8a–8h) showed to act as strong antagonists. In total, 12 from 16 compounds were able to decrease the AR-transcriptional activity below 50% of R1881-stimulated control (Tables 3 and 4). Compounds from series **3** were generally more potent antagonists than their regioisomers from series **8**. Importantly, none of the compounds displayed agonist activities except of **8b**. The most potent steroids which were able to decrease the AR-transcriptional activity below 50% already in 2 μM concentration were **3a** bearing 5-methyl-1-phenyl pyrazole moiety, **3d** with 1-fluorophenyl-5-methyl pyrazole moiety and **3g** with 1-cyanoophenyl-5-methyl pyrazole group (Table S1).

Antagonist activities were observed also for series **4** and **10** bearing C-17 keto group (counterparts of **3** and **8**, combining methyl and aryl substitution at N1 or C5 position of the pyrazole ring, respectively). All compounds (**4a–4h**, **10a–10h**) acted predominantly as AR antagonists but were less potent than compounds from series **3** and **8**. Only 5 compounds were capable to decrease the AR-transcriptional activity below 50% of R1881-stimulated control (Tables 3 and 4).

Previous results showed that the combination of a small substituent (Me group) with a bulky one (Ph or modified *para*-substituted Ph moiety) in the 1,5 positions of the pyrazole ring is fundamental to reach strong antagonist activity. This scenario was obvious from the results with derivatives **8l**, **10l** (1,5-dimethyl-substituted) and **8i**, **10i** (1,5-diaryl-substituted) that displayed only agonist activities without any inhibition effect to R1881-stimulated AR transactivation.

Further, we evaluated the protein expression of AR and its transcriptional targets, PSA and Nkx3.1 (Fig. 3, S3) in LAPC-4 cell treated with 10 μM concentration of compounds for 24 h. Results from immunoblot analyses showed that the most significant downregulation of AR-downstream signalling was induced by active compounds from series **3** and **4** (1-aryl-5-methyl substituted pyrazoles) as well as **8** and **10** (5-aryl-1-methyl-substituted pyrazoles). Oppositely, no decrease in analysed proteins was observed upon treatment with compounds from series **2**, **8i–8l** and **10i–10l** that clearly corresponded to the results from AR-transactivation assay. In addition, only three compounds from the

Table 2
Investigated activities for N-monosubstituted pyrazole derivatives of DHT and selected standards.

Cmpd	R ²	R ³	AR transcriptional activity (%)		AR-protein expression (%)	Formation of cell colonies (%)				
			Antagonist mode	Agonist mode						
1a	-	Ph		54		74		≥100		1
1b	-	<i>p</i> -CH ₃ -C ₆ H ₄		51		66		≥100		0
1c	-	<i>p</i> -MeO-C ₆ H ₄		48		77		≥100		0
1d	-	<i>p</i> -F-C ₆ H ₄		38		48		≥100		1
1e	-	<i>p</i> -Cl-C ₆ H ₄		39		44		≥100		0
1f	-	<i>p</i> -Br-C ₆ H ₄		66		18		≥100		1
1g	-	<i>p</i> -CN-C ₆ H ₄		69		84		≥100		12
1h	-	<i>p</i> -NO ₂ -C ₆ H ₄		74		≥100		≥100		15
2a	Ph	-		47		73		≥100		59
2b	<i>p</i> -CH ₃ -C ₆ H ₄	-		93		≥100		≥100		42
2c	<i>p</i> -MeO-C ₆ H ₄	-		67		≥100		≥100		65
2d	<i>p</i> -F-C ₆ H ₄	-		67		89		≥100		66
2e	<i>p</i> -Cl-C ₆ H ₄	-		≥100		87		≥100		98
2f	<i>p</i> -Br-C ₆ H ₄	-		79		35		≥100		24
2g	<i>p</i> -CN-C ₆ H ₄	-		68		48		≥100		76
2h	<i>p</i> -NO ₂ -C ₆ H ₄	-		91		78		≥100		93
Standards										
Enzalutamide				23		20		85		44
Abiraterone				93		13		88		70
Galeterone				45		18		81		30
Bavdegalutamide				16		5		14		7

Transcriptional activity of AR was measured with 10 μM compounds alone (agonist mode) or in the presence of 1 nM R1881 (antagonist mode) in reporter cell line ARE14 for 24 h. Activity was normalised to the signal of R1881 (= 100%). Measured in duplicate and repeated twice, mean plotted in the table. AR protein expression was quantified from immunoblotting results from LAPC-4 treated with 10 μM compounds for 24 h. Data was normalised to untreated control (= 100%). Formation of cell colonies was evaluated in LAPC-4 cultivated with 10 μM compounds during 10 days. Total area of cell colonies was measured in ImageJ and normalised to untreated controls (= 100%).

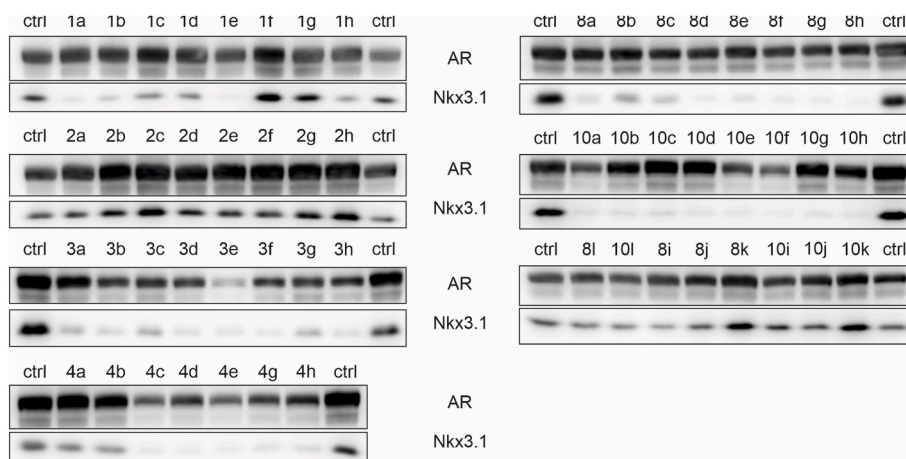
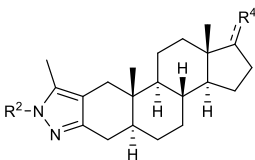


Fig. 3. The LAPC-4 cells were treated with the studied steroids (10 μM, 24 h) in FBS containing medium and lysates were then blotted for detection of appropriate proteins. Representative results are shown; the expression of PSA and α-tubulin (loading control) are included in the Supporting Information, Fig. S3.

Table 3
Investigated activities for 1-aryl-5-methyl pyrazole derivatives of DHT.



Cmpd	R ²	R ⁴	AR transcriptional activity (%)		AR-protein expression (%)	Formation of cell colonies (%)
			Antagonist mode	Agonist mode		
3a	Ph	OH	17	16	91	1
3b	<i>p</i> -CH ₃ -C ₆ H ₄	OH	33	17	61	2
3c	<i>p</i> -MeO-C ₆ H ₄	OH	34	25	63	7
3d	<i>p</i> -F-C ₆ H ₄	OH	14	18	52	3
3e	<i>p</i> -Cl-C ₆ H ₄	OH	22	22	14	4
3f	<i>p</i> -Br-C ₆ H ₄	OH	36	27	49	5
3g	<i>p</i> -CN-C ₆ H ₄	OH	19	21	58	6
3h	<i>p</i> -NO ₂ -C ₆ H ₄	OH	28	25	61	11
4a	Ph	=O	71	31	99	54
4b	<i>p</i> -CH ₃ -C ₆ H ₄	=O	85	20	84	54
4c	<i>p</i> -MeO-C ₆ H ₄	=O	78	26	40	20
4d	<i>p</i> -F-C ₆ H ₄	=O	31	19	50	15
4e	<i>p</i> -Cl-C ₆ H ₄	=O	43	18	35	16
4g	<i>p</i> -CN-C ₆ H ₄	=O	48	26	46	29
4h	<i>p</i> -NO ₂ -C ₆ H ₄	=O	55	27	59	26

Transcriptional activity of AR was measured with 10 μ M compounds alone (agonist mode) or in the presence of 1 nM R1881 (antagonist mode) in reporter cell line ARE14 for 24 h. Activity was normalised to the signal of R1881 (= 100%). Measured in duplicate and repeated twice, mean plotted in the table. AR protein expression was quantified from immunoblotting results from LAPC-4 treated with 10 μ M compounds for 24 h. Data was normalised to untreated control (= 100%). Formation of cell colonies was evaluated in LAPC-4 cultivated with 10 μ M compounds during 10 days. Total area of cell colonies was measured in ImageJ and normalised to untreated controls (= 100%).

monosubstituted pyrazoles, namely, **1a**, **1b**, and **1e** displayed moderate downregulation of the investigated proteins.

More importantly, some compounds from series **3**, **4** and **10** significantly reduced AR protein level (Fig. 3). This process was shown to be important for the prevention of AR re-activation by alternative signaling pathways and by androgens, and provide therapeutic option for CRPC [8,9]. Decrease in AR protein stability, connected with increased degradation was previously published for enzalutamide, bicalutamide, apalutamide and darolutamide [21], but abiraterone and galeterone contributed to enhanced AR protein degradation mainly in cells expressing mutated AR-T878A [22,23].

2.3. Antiproliferative properties of steroid derivatives in different PCa cell lines

Antiproliferative properties of the novel derivatives were screened on the panel of three PCa cell lines, namely LAPC-4 (expressing wild type AR), 22Rv1 (expressing AR-H875Y and splicing variant V-7) and DU145 (no AR expression). Data confirmed the targeting of AR because DU145 has stayed as the most resistant cell line (Table 5). In general, effects corresponded with previous assays showing that compounds from series **3**, **4**, **8**, and **10** belong to the most active ones, while compounds from series **1** and **2** did not exert any effect on viability of PCa cells, consistently with the weak agonist activity of these derivatives. The most potent derivatives in 22Rv1 cells were compounds **3a**, **3d**, **8d-g** (<30% viable cells in 20 μ M concentration), while LAPC4 cells

were the most sensitive to compounds **3d**, **4e** and **10a-h** (<40% viable cells in 20 μ M concentration). Cellular activities of compounds **8i-l**, **10i-l** displaying no AR-antagonist properties were probably related to another mechanism of action.

In the consequence of relatively low antiproliferative potential of novel compounds, we evaluated their effect on the formation of colonies from LAPC-4 cells during the 10 days period.

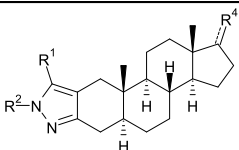
As shown in Table 2–4, Figs. S4 and S5, all compounds from series **3**, **4**, **8** and **10** were potent to block the formation of cell colonies in 5 μ M concentration. Consistently with previous results, compounds from series **2** and **8i-l**, **10i-l** displayed only weak effect comparable to enzalutamide. On the other hand, many compounds from series **1** effectively inhibited colonies growth, but our above-mentioned results indicated the targeting of non-AR related processes in cells.

2.4. Further profiling of candidate compounds

As a next step, we selected 10 hits (compounds **3a**, **3d**, **3g**, **3f**, **4c**, **4e**, **4g**, **8g**, **8h**, and **10f**) from previous assays (potent AR antagonists, AR degraders and inhibitors of formation of LAPC-4 colonies) for further profiling to compare their effect side by side. We excluded all compounds with poor solubility (e.g. **3e**) and those showing agonist or dualist mode of action in reporter assay.

Results from LNCaP cells (AR-Thr877Ala model) treated with 1 nM R1881 along with our hits (Fig. 4A) showed that compounds **3a**, **3d**, **3f** belong to the most potent derivatives, as clearly documented mainly by

Table 4
Investigated activities for 1,5-disubstituted pyrazole derivatives of DHT.



Cmpd	R ¹	R ²	R ⁴	AR transcriptional activity (%)		AR-protein expression (%)	Formation of cell colonies (%)
				Antagonist mode	Agonist mode		
8a	Ph	CH ₃	OH	89	11	93	2
8b	<i>p</i> -CH ₃ -C ₆ H ₄	CH ₃	OH	70	42	96	28
8c	<i>p</i> -MeO-C ₆ H ₄	CH ₃	OH	65	2	85	5
8d	<i>p</i> -F-C ₆ H ₄	CH ₃	OH	64	9	83	16
8e	<i>p</i> -Cl-C ₆ H ₄	CH ₃	OH	45	11	91	26
8f	<i>p</i> -Br-C ₆ H ₄	CH ₃	OH	35	6	79	16
8g	furan-2-yl	CH ₃	OH	13	1	78	2
8h	thiophen-2-yl	CH ₃	OH	37	4	87	1
8i	Ph	Ph	OH	≥100	57	≥100	≥100
8j	<i>p</i> -Cl-C ₆ H ₄	Ph	OH	≥100	68	≥100	47
8k	<i>p</i> -OH-C ₆ H ₄	Ph	OH	≥100	68	≥100	22
8l	CH ₃	CH ₃	OH	≥100	81	98	36
10a	Ph	CH ₃	=O	100	36	65	21
10b	<i>p</i> -CH ₃ -C ₆ H ₄	CH ₃	=O	82	3	92	23
10c	<i>p</i> -MeO-C ₆ H ₄	CH ₃	=O	94	30	≥100	34
10d	<i>p</i> -F-C ₆ H ₄	CH ₃	=O	86	6	100	17
10e	<i>p</i> -Cl-C ₆ H ₄	CH ₃	=O	40	3	67	11
10f	<i>p</i> -Br-C ₆ H ₄	CH ₃	=O	40	3	49	15
10g	furan-2-yl	CH ₃	=O	60	15	97	5
10h	thiophen-2-yl	CH ₃	=O	60	11	92	4
10i	Ph	Ph	=O	≥100	65	≥100	19
10j	<i>p</i> -Cl-C ₆ H ₄	Ph	=O	≥100	68	≥100	91
10k	<i>p</i> -OH-C ₆ H ₄	Ph	=O	≥100	64	≥100	39
10l	CH ₃	CH ₃	=O	≥100	57	86	67

Transcriptional activity of AR was measured with 10 μ M compounds alone (agonist mode) or in the presence of 1 nM R1881 (antagonist mode) in reporter cell line ARE14 for 24 h. Activity was normalised to the signal of R1881 (= 100%). Measured in duplicate and repeated twice, mean plotted in the table. AR protein expression was quantified from immunoblotting results from LAPC-4 treated with 10 μ M compounds for 24 h. Data was normalised to untreated control (= 100%). Formation of cell colonies was evaluated in LAPC-4 cultivated with 10 μ M compounds during 10 days. Total area of cell colonies was measured in ImageJ and normalised to untreated controls (= 100%).

suppression of R1881-stimulated phosphorylation of AR at serine 81, an important marker of AR status in cells [24,25]. Interestingly, the expression of AR was only slightly decreased. The inhibitory effect of the compounds on AR-regulated signalling was further supported by the observation of the Nkx3.1 downregulation (most significantly in the presence of **3a**, **3d**, **4c** and **8g**) contrary to PSA expression.

The same experiment was performed also in LNCaP – Abl cells that were established after long-term cultivation in androgen-depleted medium, which resulted in AR hypersensitivity [5]. As shown in Fig. 4B, most of the compounds are able to block AR activation as documented by monitoring its phosphorylation at S81 and PSA expression. The most profound changes were observed in the cells treated with compounds **3d** and **4g**. Furthermore, sharp decreases in both Nkx3.1 and PSA protein levels were observed upon treatment of LAPC-4 cells, and **3a**, **3d**, **8g**, **8h** and **10f** belonged to the most potent compounds (Fig. 4C). Also, based on the significant decreases in phosphorylation at S81, LAPC-4 cells (AR-wt model) were found to be the most sensitive cell line within our PCA panel.

2.5. Targeting the AR with compound 3d in vitro

We selected compound **3d** for further biological evaluation, mainly due its pronounced effects (PSA and Nkx3.1 decline, diminishing of S81 phosphorylation) in tested PCA cell lines. Preliminary data were obtained from several PCA cell lines treated with 10 μ M concentration in two different conditions, without stimulation by R1881 in FBS containing media or with stimulation by R1881 in CSS containing media. We therefore decided to evaluate the changes in AR and downstream targets precisely in different concentrations and time of treatment in LAPC-4 cells. In the experiment where stimulation of AR signalling is evoked by synthetic androgen R1881, we observed dose-dependent suppression of AR signalling up to 10 μ M concentration of **3d** that was comparable to galeterone's effect in LAPC-4 (Fig. 5A), as well as in 22Rv1 and LNCaP (Fig. S6). Long-term treatment of LAPC-4 showed that the AR expression significantly decreased in tested concentrations after 48 and 72 h (Fig. 5B), as observed for PROTAC-based AR antagonist ARV110 (bavdegalutamide) also. Moreover, the expression of PSA and Nkx3.1 was completely switched off upon 72-h treatment with **3d**. Importantly, the long-term treatment with **3d** caused only proliferation inhibition (still >80% cells alive after 24 h and 48 h treatment; decrease

Table 5
Viability of PCA cells upon treatment with 20 μ M compounds for 72 h^a.

Cmpd	Viability %		
	LAPC-4	22Rv1	DU145
1a	60	36	97
1b	70	97	96
1c	43	75	97
1d	44	57	55
1e	49	80	91
1f	58	62	100
1g	65	65	88
1h	40	97	99
2a	100	≥ 100	≥ 100
2b	≥ 100	≥ 100	100
2c	99	≥ 100	≥ 100
2d	95	≥ 100	≥ 100
2e	82	≥ 100	≥ 100
2f	79	83	≥ 100
2g	93	94	97
2h	96	≥ 100	99
3a	65	24	97
3b	88	37	93
3c	82	54	29
3d	38	26	≥ 100
3e	47	52	107
3f	52	50	89
3g	73	43	50
3h	74	58	85
4a	87	90	100
4b	87	97	≥ 100
4c	57	77	≥ 100
4d	42	75	≥ 100
4e	38	75	≥ 100
4g	78	87	≥ 100
4h	48	57	≥ 100
8a	51	48	100
8b	52	36	98
8c	51	33	≥ 100
8d	44	26	89
8e	41	29	90
8f	42	21	94
8g	50	18	100
8h	46	44	100
8i	72	47	12
8j	30	4	5
8k	63	37	57
8l	52	52	98
10a	36	68	≥ 100
10b	34	73	≥ 100
10c	35	58	97
10d	29	57	90
10e	21	61	98
10f	20	56	96
10g	39	43	100
10h	31	68	100
10i	61	19	19
10j	83	93	98
10k	67	57	94
10l	53	103	≥ 100
Enzalutamide	81	≥ 100	96
Abiraterone	≥ 100	≥ 100	≥ 100
Galeterone	76	95	≥ 100
Bavdegalutamide	5	96	85

^a Measured in duplicate and repeated twice.

in Myc expression) without massive induction of apoptosis as documented by monitoring of PARP-1 and procaspases protein expression including their fragmentation (Fig. S7). We therefore confirmed that the decrease in AR protein level is not directly evoked by cell death.

In rescue experiment, we verified the ability of **3d** to bind to AR cavity. LAPC-4 and LNCaP cells were pre-treated with **3d** for 1 h to saturate the AR LBD domain, and then bavdegalutamide (an effective AR degrader) was added for 4 h. As showed in Fig. 5C, the degradation of AR in the presence of bavdegalutamide was blocked by different doses of **3d** which confirmed targeting the AR.

The binding of the candidate compound **3d** into AR-LBD was evaluated using flexible molecular docking into the LBD of AR (PDB:2P1V) crystallised with natural agonist DHT. Key interaction residues in both extremities of the LBD cavity such as Gln711, Arg752, Thr877, and Asn705 were set as flexible. The flexible docking of compound **3d** revealed extensive binding in AR-LBD with similar positions of interacting residues as in published antagonist model [26]. First two poses of **3d** were characterised by high binding energy ($\Delta G_{\text{Vina}} = -11.8$ kcal/mol and -11.6 kcal/mol, respectively), and similar orientation with nearly identical interactions in the 1'-(4''-fluorophenyl)-5'-methylpyrazolo part of **3d**, where Arg752 and Gly583 create a halogen bond with fluorine on the phenyl ring, which is probably stabilized by hydrophobic interactions with side chains of Gln711, Met749, Val684 and Ala748 (Fig. 6A and B). The methyl group (on the pyrazole ring of **3d**) forms a hydrophobic interaction with Leu707, while the fused pyrazole ring interacts with Phe764 and might also form a hydrogen bond with Met745.

The key difference was observed in the interaction of the 17 β -OH on the D-ring of **3d**. In the first pose the hydroxyl group forms a conserved hydrogen bond with Thr877 (known from the binding of DHT) (Fig. 6A),

while in the second pose the steroid core is positioned in a slightly different angle towards Asn705, where it forms a hydrogen bond with the 17 β -OH group. Further stabilization of the steroidal ring of **3d** is mediated by hydrophobic interactions with neighbouring leucines 701 and 704. Most importantly, the second pose shows a binding pose independent of Thr877 which is mutated in LNCaP cell line by point mutation T877A. Overall, lead compound should bind to the same region with an orientation similar to the known antagonist cyproterone (PDB:2OZ7) [26,27] (Fig. 6C and D). The interaction of our lead compound independent of Thr877 should explain its potency even in PCA bearing mutated AR-LBD.

Next, the binding of **3d** in human recombinant AR-LBD was examined by the micro-scale thermophoresis using the Protein Labeling Kit RED-NHS (Nanotemper). The binding of the **3d** (tested in 25 μ M–0.25 μ M range) induced significant changes in the protein mobility marked by the change of the fluorescence signal (Fig. S8) and confirmed thus binding of **3d** into the AR-LBD.

Further, we evaluated the antiproliferative effect of **3d** in different cell lines in dose dependent manner using colony formation assay and resazurine-based viability assay. We confirmed the increased sensitivity to AR-positive PCA cell lines with GI₅₀ values in low micromole ranges and to wt-AR expressing LAPC-4 cells, being the most sensitive (GI₅₀ = 7.9 \pm 1.6 μ M) (see Fig. S9). Moreover, cell cycle analysis after 48 h of treatment showed a reduced number of cells in S-phase of the cell cycle, which confirmed to us the negative impact of **3d** on proliferation of AR-positive LAPC-4 and 22Rv1 cells, while having no effect on AR-negative DU145 cells (Fig. S10).

Finally, we examined the effect of different doses of **3d** on R1881-stimulated transcriptional activity in reporter cell line, and it was found that IC₅₀ value of **3d** (1.18 μ M) shows higher potency compared to

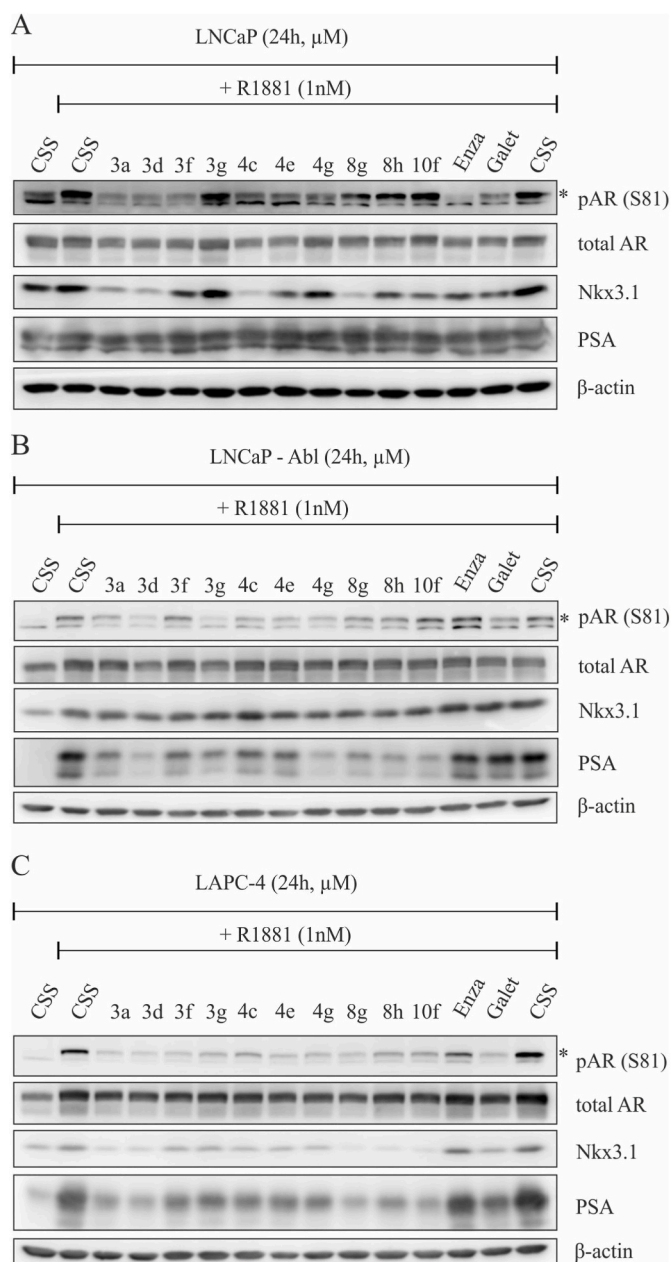


Fig. 4. (A) LNCaP, (B) LNCaP-Abl or (C) LAPC-4 cells were cultivated in CSS containing medium, and then stimulated with 1 nM R1881 in the presence of studied steroids (10 μ M) for 24 h. Lysates were then blotted for detection of appropriate proteins. Stars indicate bands corresponding with phosphorylated AR at S81. β -actin served as protein loading control.

galeterone (7.59 μ M) and enzalutamide (3.32 μ M) assayed as controls (Fig. 7A). We further evaluated the functional consequences of the diminishing of the AR transactivation, and performed qPCR analysis of mRNA expression of AR and PSA, respectively. As showed in Fig. 7B, 3d inhibited PSA mRNA expression in 22Rv1 cells more potently than enzalutamide and galeterone. We also observed comparable results in LAPC-4 cells under similar experimental conditions, where the expression level of AR transcript decreased moderately, as well (Fig. S11).

2.6. Targeting the AR with compound 3d *ex vivo*

Selected compounds 3d and 10f were preliminary tested in a short-term *ex vivo* culture of patient-derived samples. An experienced pathologist provided non-diagnostic tissues (approximately 0.5 cubic centimeter) from five patients undergoing robotic prostatectomy. The tissues were cut with vibratome, and slices were treated for three days with our candidates (10 μ M) along with enzalutamide and bavdegalutamide (1 μ M). Immunohistochemistry results of proliferation marker Ki67 and AR are provided in Fig. 8 and Fig. S12. Samples from one patient were excluded due to missing cancer cells in some tissue slices. Compound 3d caused a mild decrease of the level of Ki67 (marker of proliferation) and heterogenous effect on the AR level, which was slightly decreased in 3 from 4 patients. Tissue slices obtained from patient 1 display the most homogenous morphology and downregulation of AR is clearly visible after treatment with compound 3d, enzalutamide and bavdegalutamide (see Fig. S12). Tissue slices from other patients displayed heterogeneous tissue morphology which hampers direct comparison of the treatments. However, enzalutamide also demonstrated a limited effect only, while bavdegalutamide was shown to be the most potent. Our candidates will be further tested on other patient-derived tissues, as well as organoids which may clarify their therapeutic potential.

3. Conclusion

In summary, our existing compound library of DHT-derived A-ring-fused pyrazoles has been extended to novel derivatives synthesized from α,β -enones with monosubstituted hydrazines. The heterocyclization and subsequent oxidation led to the regioselective formation of the thermodynamically favoured 1,5-disubstituted heterocyclic compounds under conventional heating. A total of 55 differently functionalized derivatives were subjected to the evaluation of their impact on the AR signalling in several PCa models. Lead compound 3d displayed significant potency to disrupt AR signalling in both castration-sensitive and resistant PCa cell lines, with selective antiproliferative potency towards AR-positive cell lines. Treatment with 10 μ M of compound 3d induced massive reduction in AR protein level, slight decrease in AR transcript and total blockage in AR downstream targets (PSA, Nkx3.1), which was associated with the decrease in S-phase cells and proliferation blockage. Moreover, *ex vivo* activity was shown on PCa patient's biopsies with overall encouraging potential as a PCa anticancer agent.

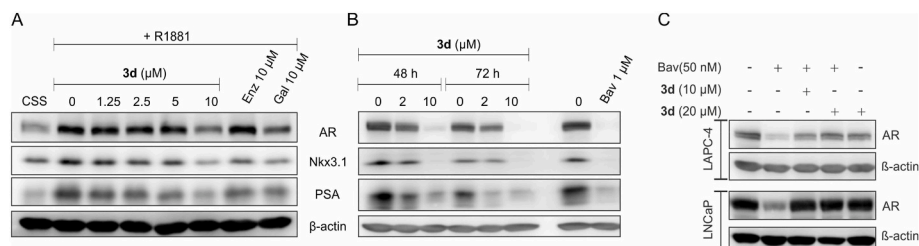


Fig. 5. Effect of 3d on expression of AR and downstream targets PSA and Nkx3.1 in LAPC-4 cells. (A) Cells were cultivated in charcoal-stripped serum medium for 24 h, and then stimulated with 1 nM R1881 alone or with different doses of 3d for additional 24 h. (B) Cells were cultivated in standard media and treated with 3d for indicated time. (C) LAPC-4 and LNCaP cells were pre-treated with 3d for 1 h, and then bavdegalutamide was added for the next 4 h. β -actin level served as protein loading control. Enz, enzalutamide; Gal, galeterone; Bav, bavdegalutamide.

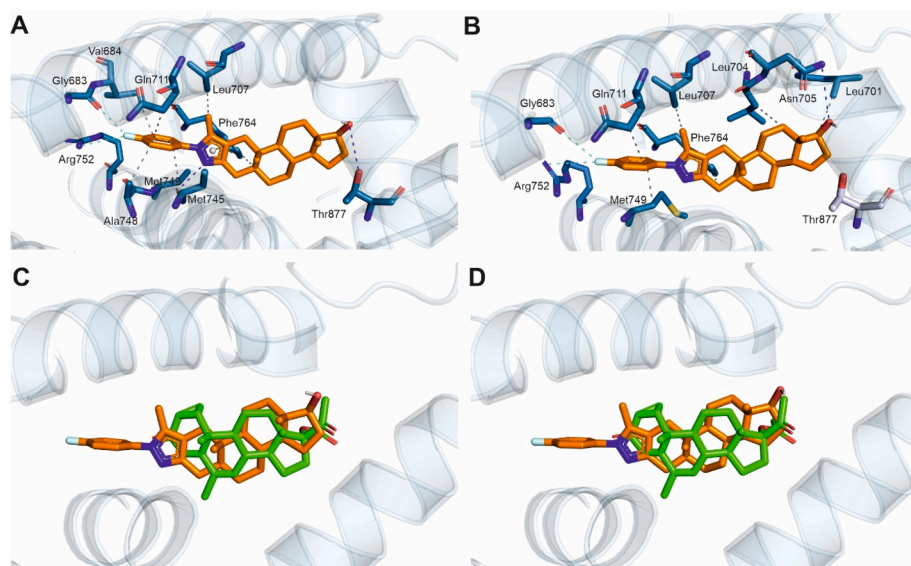


Fig. 6. Binding poses of **3d** in the ligand binding domain of AR (PDB:2PIV) performed by flexible docking. The first pose (A) shows interactions including Thr877, while the second pose (B) shows binding independent of Thr877. Respective alignments with cyproterone is shown as well (C, D). Sticks represent interacting amino acid residues. Nitrogen atoms are shown in blue, oxygen atoms in red, fluorine atom in cyan. Hydrogen bonds are shown with blue dash lines, halogen bonds with cyan dash lines and hydrophobic interactions are shown with grey dash lines.

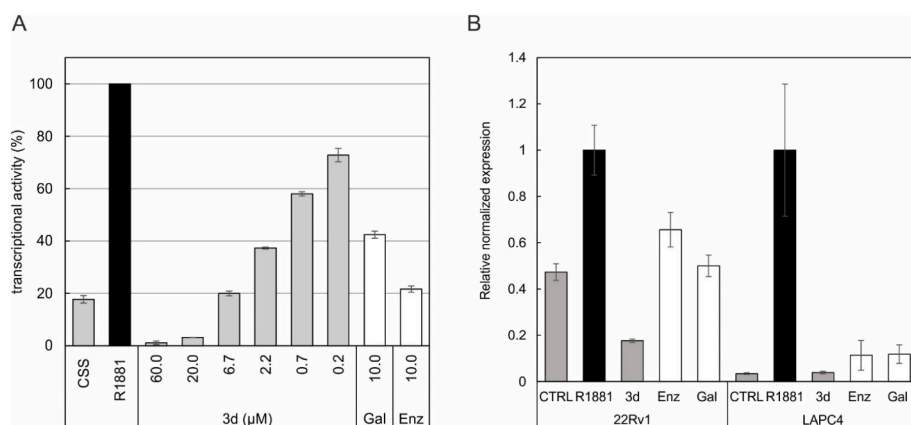


Fig. 7. (A) The effect of **3d** on the AR-mediated transcription in the 22Rv1-ARE14 reporter cell line. Cells were stimulated with 1 nM R1881 (R) alone (black column) or with different doses of **3d** (grey columns) for 24 h in charcoal-stripped serum medium (CSS), and then, the luciferase activity in the cell lysate was measured (B) The effect of compound **3d** and standard AR antagonists on relative normalized mRNA expression of AR-downstream gene KLK3 (PSA). Cells were cultivated in CSS medium overnight, then treated with compounds in 10 μ M concentration in presence of 1 nM R1881 for 24 h. Enz, enzalutamide; Gal, galeterone.

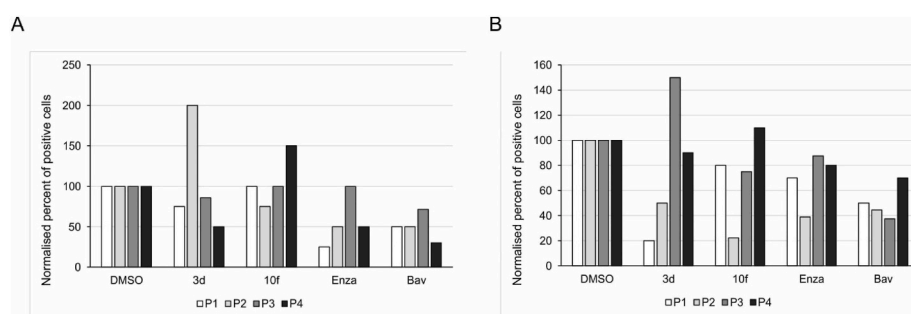


Fig. 8. AR (A) and Ki67 (B) levels from the highest-intensity positive cells assessed by immunostaining of tissue from 4 patients in the explants after 3 days of *ex vivo* culture in the presence of indicated compounds. Candidate compounds **3d** and **10f** were applied in 10 μ M concentrations, while standards enzalutamide (Enz) and bavdegalutamide (Bav) in 1 μ M concentrations. All immunohistochemistry images were evaluated using histoscore method and normalized to DMSO-treated samples (see also Fig. S12).

4. Experimental

4.1. General

Chemicals, reagents and solvents were purchased from commercial suppliers (Sigma-Aldrich, TCI and Alfa Aesar) and used without further purification. Melting points (Mp) were determined on an SRS Optimelt digital apparatus and are uncorrected. For MW-assisted syntheses, a CEM Discover SP laboratory MW reactor was used with a max. power of 200 W (running a dynamic control program). Elementary analysis data were obtained with a PerkinElmer CHN analyzer model 2400. The

transformations were monitored by TLC using 0.25 mm thick Kieselgel-G plates (Si 254 F, Merck). The compound spots were detected by spraying with 5% phosphomolybdic acid in 50% aqueous phosphoric acid. Flash chromatographic purifications were carried out on silica gel 60, 40–63 μ m (Merck). NMR spectra were recorded with a Bruker DRX 500 instrument at room temperature in $CDCl_3$ and DMSO- d_6 using residual solvent signal as an internal reference. Chemical shifts are reported in ppm (δ scale) and coupling constants (J) are given in Hz. Multiplicities of the 1H signals are indicated as a singlet (s), a broad singlet (bs), a doublet (d), a double doublet (dd), a triplet (t), or a multiplet (m). ^{13}C NMR spectra are 1H -decoupled and the J-MOD pulse

sequence was used for multiplicity editing. In this spin-echo type experiment, the signal intensity is modulated by the different coupling constants J of carbons depending on the number of attached protons. Both protonated and unprotonated carbons can be detected (CH_3 and CH carbons appear as positive signals, while CH_2 and C carbons as negative signals). The purified derivatives were dissolved in high purity acetonitrile and introduced with an Agilent 1290 Infinity II liquid chromatography pump to an Agilent 6470 tandem mass spectrometer equipped an electrospray ionization chamber. Flow rate was 0.5 mL min^{-1} , and contained 0.1% formic acid or 0.1% ammonium hydroxide to help facilitate ionization. The instrument operated in MS1 scan mode with 135 V fragmentor voltage, and the spectra were recorded from 200 to 600 m/z , which were corrected with the background.

4.2. Chemistry

4.2.1. Synthesis of the A-ring-modified α,β -enones

Compounds **5a–e**, **5g** and **5h** were synthesized as described previously [18].

4.2.1.1. 17 β -Hydroxy-2-(4-bromo)benzylidene-5 α -androstane-3-one (5f). According to the general method described previously [18], 4-bromobenzaldehyde (666 mg) was used for the reaction. Reaction time: 3 h. White solid. Yield: 1.18 g (86%); Mp 205–207 °C; $^1\text{H NMR}$ (CDCl_3 , 500 MHz): δ_{H} 0.73 (s, 3H, 18-H₃), 0.80 (s, 3H, 19-H₃), 0.85–1.02 (overlapping m, 3H), 1.11 (m, 1H), 1.22–1.65 (overlapping m, 9H), 1.78 (m, 3H), 2.07 (m, 1H), 2.14 (d, 1H, $J = 15.7 \text{ Hz}$, one of 1-H₂), 2.23 (dd, 1H, $J = 18.6 \text{ Hz}$, 13.3 Hz, one of 4-H₂), 2.45 (dd, 1H, $J = 18.6 \text{ Hz}$, $J = 5.2 \text{ Hz}$, the other of 4-H₂), 3.03 (d, 1H, $J = 15.7 \text{ Hz}$, the other of 1-H₂), 3.65 (t, 1H, $J = 8.6 \text{ Hz}$, 17-H), 7.23 (d, 2H, $J = 8.4 \text{ Hz}$, 3'-H and 5'-H), 7.45 (s, 1H, 2a-H), 7.52 (d, 2H, $J = 8.4 \text{ Hz}$, 2'-H and 6'-H); $^{13}\text{C NMR}$ (CDCl_3 , 125 MHz): δ_{C} 11.2 (C-18), 12.0 (C-19), 21.2 (CH_2), 23.5 (CH_2), 28.7 (CH_2), 30.7 (CH_2), 31.2 (CH_2), 35.6 (CH), 36.3 (C-10), 36.8 (CH_2), 42.0 (CH_2), 42.7 (CH), 42.9 (CH_2), 43.0 (C-13), 51.1 (CH), 53.8 (CH), 82.0 (C-17), 122.9 (C-4'), 131.8 (2C, C-2' and C-6'), 131.8 (2C, C-3' and C-5'), 134.7 (C-1'), 136.0 (C-2a), 136.1 (C-2), 201.4 (C-3); ESI-MS 457 [$\text{M}+\text{H}$]⁺; Anal. Calcd. for $\text{C}_{26}\text{H}_{33}\text{BrO}_2$ C 68.27; H 7.27. Found C 68.29; H 7.28.

4.2.1.2. 17 β -Hydroxy-2-(4-hydroxy)benzylidene-5 α -androstane-3-one (5i). According to the general method described previously [18], 4-(methoxymethoxy)benzaldehyde (598 mg) was used for the reaction. The reaction mixture was heated under reflux temperature for 16 h. MOM-protected-5i was obtained as a yellow crystal. Yield: 682 mg (52%). This reaction was repeated to obtain a sufficient amount of protected derivative, then 877 mg (2 mmol) was dissolved in hot MeOH followed by the addition of 6 M HCl solution (0.2 mL) dropwise. The reaction mixture was stirred for 30 min, and then cooled to room temperature. The mixture was poured into water and extracted with EtOAc ($3 \times 10 \text{ mL}$). The combined organic layer was washed with water ($2 \times 20 \text{ mL}$) and brine (20 mL), dried over anhydrous Na_2SO_4 and the solvent was evaporated *in vacuo*. The crude product was purified by column chromatography (silica gel, EtOAc/ $\text{CH}_2\text{Cl}_2 = 10:90$ to EtOAc/ $\text{CH}_2\text{Cl}_2 = 50:50$ using gradient elution). Yield: 554 mg (70%); Mp > 250 °C (decomp.); $^1\text{H NMR}$ ($\text{DMSO-}d_6$, 500 MHz): δ_{H} 0.62 (s, 3H, 18-H₃), 0.71 (s, 3H, 19-H₃), 0.89 (overlapping m, 3H), 1.02 (m, 1H), 1.11–1.42 (overlapping m, 7H), 1.50 (m, 1H), 1.58–1.65 (overlapping m, 2H), 1.77 (m, 1H), 1.84 (m, 1H), 2.11 (dd, 1H, $J = 18.7$, 13.1 Hz, one of 4-H₂), 2.24 (d, 1H, $J = 15.9 \text{ Hz}$, one of 1-H₂), 2.30 (dd, 1H, $J = 18.7$, 5.4 Hz, the other of 4-H₂), 2.94 (d, 1H, $J = 16.0 \text{ Hz}$, the other of 1-H₂), 3.45 (t, 1H, $J = 8.1 \text{ Hz}$, 17-H), 4.42 (bs, 1H, 17-OH), 6.83 (d, 2H, $J = 8.6 \text{ Hz}$, 3'-H and 5'-H), 7.34 (d, 2H, $J = 8.6 \text{ Hz}$, 2'-H and 6'-H), 7.35 (s, 1H, 2a-H), 9.92 (s, 1H, 4'-OH); $^{13}\text{C NMR}$ ($\text{DMSO-}d_6$, 125 MHz): δ_{C} 11.1 (C-18), 11.7 (C-19), 20.5 (CH_2), 23.1 (CH_2), 28.0 (CH_2), 29.9 (CH_2), 30.7 (CH_2), 35.0 (CH), 35.3 (C-10), 36.6 (CH_2), 41.3 (CH), 41.5 (CH_2), 42.1 (CH_2), 42.4 (C-13), 50.4 (CH), 53.0 (CH), 80.0 (C-17), 115.5 (2C, C-3' and C-5'), 126.0

(C-1'), 132.1 (C-2), 132.4 (2C, C-2' and C-6'), 136.5 (C-2a), 158.3 (C-4') 199.3 (C-3); ESI-MS 395 [$\text{M}+\text{H}$]⁺; Anal. Calcd. for $\text{C}_{26}\text{H}_{34}\text{O}_3$ C 79.15; H 8.69. Found C 79.08; H 8.68.

4.2.2. General procedures for the synthesis of DHT-derived A-ring-fused pyrazoles

Method A: 1 mmol arylidene (**5a**) and methylhydrazine (105 μL , 2 equiv.) were dissolved in EtOH (4 mL), and the mixture was irradiated in a closed vessel at 100 °C for 3 min. After completion of the reaction, the mixture was poured into ice water (10 mL), NH_4Cl was added and the white precipitate formed was filtered *in vacuo*, washed with water and dried. The solid thus obtained containing both **6a** and **7a** was oxidized: the crude product was dissolved in 5 mL 1,4-dioxane, and DDQ (250 mg, 1.1 equiv.) was added. The reaction mixture was irradiated in a closed vessel at 120 °C for 5 min. After completion of the reaction, the mixture was poured into ice water, NH_4Cl was added, and the resulting precipitate was filtered and dried. The crude product containing **8a** and **9a** was purified by column chromatography with EtOAc/ $\text{CH}_2\text{Cl}_2 = 10:90$.

Method B: Arylidene (**5a–f**, **5i**), heteroarylidene (**5g**, **5h**) or ethylidene derivative (**5j**) [17] (1.0 mmol) and methylhydrazine sulfate (288 mg, 2 equiv.) were dissolved in absolute EtOH (15 mL) and the mixture was stirred at 78 °C for 24 h, during which in addition to the complete conversion of the starting material, the spontaneous oxidation of the heteroring also occurred in most of the cases. During work-up, the mixture was cooled to room temperature, poured into water and extracted with CH_2Cl_2 ($3 \times 10 \text{ mL}$). The combined organic layer was washed with water ($2 \times 20 \text{ mL}$) and brine (20 mL), dried over anhydrous Na_2SO_4 and the solvent was evaporated *in vacuo*. The crude product was purified by column chromatography except in the reaction of **5d–5f** where oxidation of the heteroring with DDQ was needed. Thus, in this latter case, the residue was dissolved in 1,4-dioxane (10 mL) and DDQ (250 mg, 1.1 equiv.) was added. The mixture was irradiated in a closed vessel at 120 °C for 5 min, then poured into ice-cold water. NH_4Cl was added and the resulting precipitate was filtered and dried. The crude product was purified by column chromatography.

4.2.2.1. 17 β -Hydroxy-1'-methyl-5'-phenylpyrazolo[3',4':3,2]-5 α -androstane (8a). According to Section 4.2.2., Method A or B, 379 mg of **5a** was used. Eluent: EtOAc/ $\text{CH}_2\text{Cl}_2 = 10:90$. Off white solid. Yield: 232 mg (57%, Method A), or 323 mg (80%, Method B); Mp 157–160 °C; $^1\text{H NMR}$ (CDCl_3 , 500 MHz): δ_{H} 0.74 (s, 3H, 18-H₃), 0.76 (s, 3H, 19-H₃), 0.81–1.00 (overlapping m, 3H, 9 α -H, 7 α -H and 14 α -H), 1.05 (m, 1H, 12 α -H), 1.23–1.47 (overlapping m, 5H, 15 β -H, 11 β -H, 6 β -H, 8 β -H and 16 β -H), 1.55–1.65 (overlapping m, 4H, 11 α -H, 5 α -H, 15 α -H and 6 α -H), 1.73 (m, 1H, 7 β -H), 1.79 (m, 1H, 12 β -H), 2.06 (m, 1H, 16 α -H), 2.13 (d, 1H, $J = 15.3 \text{ Hz}$, 1 α -H), 2.33 (dd, 1H, $J = 16.4$, 12.2 Hz, 4 β -H), 2.47 (d, 1H, $J = 15.3 \text{ Hz}$, 1 β -H), 2.67 (dd, 1H, $J = 16.4$, 5.1 Hz, 4 α -H), 3.63 (t, 1H, $J = 8.5 \text{ Hz}$, 17 α -H), 3.77 (s, 3H, N-CH₃), 7.31 (d-like m, 2H, 3'-H and 5'-H), 7.38 (t-like m, 1H, 4''-H), 7.46 (t-like m, 2H, 2''-H and 6''-H); $^{13}\text{C NMR}$ (CDCl_3 , 125 MHz): δ_{C} 11.2 (C-18), 11.8 (C-19), 21.0 (C-11), 23.6 (C-15), 27.9 (C-4), 29.5 (C-6), 30.8 (C-16), 31.6 (C-7), 35.7 (C-1), 36.1 (C-8), 36.6 (C-10), 37.0 (C-12), 37.2 (N-CH₃), 42.8 (C-5), 43.0 (C-13), 51.2 (C-14), 54.3 (C-9), 82.1 (C-17), 114.3 (C-2), 128.1 (C-4''), 128.8 (2C) and 129.3 (2C): C-2'', C-6'', C-3'', C-5'', 131.1 (C-1''), 140.2 (C-5') 147.3 (C-3); ESI-MS 405 [$\text{M}+\text{H}$]⁺; Anal. Calcd. for $\text{C}_{27}\text{H}_{36}\text{N}_2\text{O}$ C 80.15; H 8.97. Found C 80.21; H 8.98.

4.2.2.2. 17 β -Hydroxy-1'-methyl-3'-phenylpyrazolo[4',3':2,3]-5 α -androstane (9a). According to Section 4.2.2., Method A, 379 mg of **5a** was used. Eluent: EtOAc/ $\text{CH}_2\text{Cl}_2 = 10:90$. Off white solid. Yield: 114 mg (28%); Mp 232–236 °C; $^1\text{H NMR}$ (CDCl_3 , 500 MHz): δ_{H} 0.73 (s, 3H, 18-H₃), 0.76 (s, 3H, 19-H₃), 0.86–1.03 (overlapping m, 3H, 9 α -H, 7 α -H and 14 α -H), 1.13 (m, 1H, 12 α -H), 1.28 (m, 1H, 15 β -H), 1.35–1.49 (overlapping m, 4H, 6 β -H, 8 β -H, 11 β -H and 16 β -H), 1.60–1.77 (overlapping m, 5H, 15 α -H, 5 α -H, 6 α -H, 11 α -H, 7 β -H), 1.86 (m, 1H, 12 β -H), 2.07 (m, 1H, 16 α -H),

2.21 (dd, 1H, $J = 16.2, 12.4$ Hz, 4 β -H), 2.32 (d, 1H, $J = 15.1$ Hz, 1 α -H), 2.53 (dd, 1H, $J = 16.2, 4.9$ Hz, 4 α -H), 2.76 (d, 1H, $J = 15.1$ Hz, 1 β -H), 3.66 (t, 1H, $J = 8.5$ Hz, 17 α -H), 3.79 (s, 3H, N-CH₃), 7.29 (t-like m, 1H, 4''-H), 7.40 (t-like m, 2H, 3''-H and 5''-H), 7.70 (d, 2H, $J = 7.3$ Hz, 2''-H and 6''-H); ¹³C NMR (CDCl₃, 125 MHz): δ_c 11.2 (C-18), 11.7 (C-19), 21.0 (C-11), 23.6 (C-15), 26.3 (C-4), 29.2 (C-6), 30.7 (C-16), 31.4 (C-7), 35.7 (N-CH₃), 35.9 (C-8), 36.6 (C-10), 36.8 (C-1), 36.9 (C-12), 41.8 (C-5), 43.0 (C-13), 51.1 (C-14), 54.1 (C-9), 82.0 (C-17), 113.0 (C-2), 126.8 (2C, C-2'' and C-6''), 127.1 (C-4''), 128.6 (2C, C-3'' and C-5''), 134.4 (C-1''), 138.8 (C-5') 147.6 (C-3'); ESI-MS 405 [M+H]⁺; Anal. Calcd. for C₂₇H₃₆N₂O C 80.15; H 8.97. Found C 80.08; H 8.95.

4.2.2.3. 17 β -Hydroxy-1'-methyl-5'-(4''-tolyl)-pyrazolo[3',4':3,2]-5 α -androstane (8b). According to Section 4.2.2., Method B, 393 mg of **5b** was used. Eluent: EtOAc/CH₂Cl₂ = 5:95. Off white solid. Yield: 340 mg (81%); Mp 124–126 °C; ¹H NMR (CDCl₃, 500 MHz): δ_H 0.74 (s, 3H, 18-H₃), 0.75 (s, 3H, 19-H₃), 0.80–0.99 (overlapping m, 3H), 1.06 (m, 1H), 1.23–1.47 (overlapping m, 5H), 1.54–1.64 (overlapping m, 4H), 1.73 (m, 1H), 1.78 (m, 1H), 2.06 (m, 1H), 2.11 (d, 1H, $J = 15.2$ Hz, 1 α -H), 2.31 (dd, 1H, $J = 16.5, 12.1$ Hz, 4 β -H), 2.41 (s, 4''-CH₃), 2.46 (d, 1H, $J = 15.2$ Hz, 1 β -H), 2.66 (dd, 1H, $J = 16.5, 5.0$ Hz, 4 α -H), 3.63 (t, 1H, $J = 8.5$ Hz, 17 α -H), 3.77 (s, 3H, N-CH₃), 7.21 (d, 2H, $J = 8.0$ Hz), 7.26 (d, 2H, $J = 8.0$ Hz); ¹³C NMR (CDCl₃, 125 MHz): δ_c 11.2 (C-18), 11.7 (C-19), 21.0 (C-11), 21.4 (4''-CH₃), 23.6 (C-15), 27.8 (C-4), 29.4 (C-6), 30.7 (C-16), 31.5 (C-7), 35.6 (C-1), 36.0 (C-8), 36.5 (C-10), 36.9 (C-12), 37.1 (N-CH₃), 42.7 (C-5), 43.0 (C-13), 51.2 (C-14), 54.3 (C-9), 82.1 (C-17), 114.1 (C-2), 127.9 (C-4''), 129.2 (2C, C-2'' and C-6''), 129.5 (2C, C-3'' and C-5''), 138.1 (C-1''), 140.2 (C-5'), 147.2 (C-3); ESI-MS 419 [M+H]⁺; Anal. Calcd. for C₂₈H₃₈N₂O C 80.34; H 9.15. Found C 80.11; H 9.16.

4.2.2.4. 17 β -Hydroxy-5'-(4''-methoxyphenyl)-1'-methylpyrazolo[3',4':3,2]-5 α -androstane (8c). According to Section 4.2.2., Method B, 409 mg of **5c** was used. Eluent: EtOAc/CH₂Cl₂ = 5:95. White solid. Yield: 343 mg (79%); Mp 125–128 °C; ¹H NMR (CDCl₃, 500 MHz): δ_H 0.74 (s, 3H, 18-H₃), 0.75 (s, 3H, 19-H₃), 0.80–0.99 (overlapping m, 3H), 1.06 (m, 1H), 1.23–1.47 (overlapping m, 5H), 1.55–1.65 (overlapping m, 4H), 1.73 (m, 1H), 1.79 (m, 1H), 2.05 (m, 1H), 2.10 (d, 1H, $J = 15.2$ Hz, 1 α -H), 2.31 (dd, 1H, $J = 16.4, 12.1$ Hz, 4 β -H), 2.45 (d, 1H, $J = 15.2$ Hz, 1 β -H), 2.65 (dd, 1H, $J = 16.4, 5.0$ Hz, 4 α -H), 3.63 (t, 1H, $J = 8.5$ Hz, 17 α -H), 3.76 (s, 3H, N-CH₃), 3.86 (s, 3H, 4''-OCH₃), 6.99 (d, 2H, $J = 8.7$ Hz, 3''-H and 5''-H), 7.24 (d, 2H, $J = 8.7$ Hz, 2''-H and 6''-H); ¹³C NMR (CDCl₃, 125 MHz): δ_c 11.2 (C-18), 11.7 (C-19), 21.0 (C-11), 23.6 (C-15), 27.8 (C-4), 29.5 (C-6), 30.7 (C-16), 31.5 (C-7), 35.6 (C-1), 36.0 (C-8), 36.5 (C-10), 36.9 (C-12), 37.1 (N-CH₃), 42.7 (C-5), 43.0 (C-13), 51.2 (C-14), 54.3 (C-9), 55.5 (4''-OCH₃), 82.1 (C-17), 114.0 (C-2), 114.3 (2C, C-3'' and C-5''), 123.2 (C-1''), 130.5 (2C, C-2'' and C-6''), 140.0 (C-5'), 147.2 (C-3), 159.5 (C-4''); ESI-MS 435 [M+H]⁺; Anal. Calcd. for C₂₈H₃₈N₂O₂ C 77.38; H 8.81. Found C 77.36; H 8.83.

4.2.2.5. 17 β -Hydroxy-5'-(4''-fluorophenyl)-1'-methylpyrazolo[3',4':3,2]-5 α -androstane (8d). According to Section 4.2.2., Method B, 397 mg of **5d** was used. Eluent: EtOAc/CH₂Cl₂ = 10:90. White solid. Yield: 278 mg (66%); Mp 185–187 °C; ¹H NMR (CDCl₃, 500 MHz): δ_H 0.74 (s, 3H, 18-H₃), 0.75 (s, 3H, 19-H₃), 0.80–0.99 (overlapping m, 3H), 1.06 (m, 1H), 1.23–1.47 (overlapping m, 5H), 1.54–1.64 (overlapping m, 4H), 1.72 (m, 1H), 1.80 (m, 1H), 2.05 (m, 1H), 2.10 (d, 1H, $J = 15.2$ Hz, 1 α -H), 2.30 (dd, 1H, $J = 16.5, 11.9$ Hz, 4 β -H), 2.41 (d, 1H, $J = 15.2$ Hz, 1 β -H), 2.65 (dd, 1H, $J = 16.5, 5.1$ Hz, 4 α -H), 3.63 (t, 1H, $J = 7.6$ Hz, 17 α -H), 3.75 (s, 3H, N-CH₃), 7.15 (t-like m, 2H), 7.28 (overlapping m, 2H); ¹³C NMR (CDCl₃, 125 MHz): δ_c 11.2 (C-18), 11.7 (C-19), 21.0 (C-11), 23.6 (C-15), 27.8 (C-4), 29.4 (C-6), 30.7 (C-16), 31.5 (C-7), 35.5 (C-1), 36.0 (C-8), 36.5 (C-10), 36.9 (C-12), 37.1 (N-CH₃), 42.7 (C-5), 43.0 (C-13), 51.1 (C-14), 54.2 (C-9), 82.1 (C-17), 114.4 (C-2), 115.9 (d, 2C, $J = 21.7$ Hz, C-3'' and C-5''), 127.0 (d, $J = 3.5$ Hz, C-1''), 131.1 (d, 2C, $J = 8.2$ Hz, C-2'' and C-6''), 139.2 (C-5'), 147.3 (C-3), 161.6 (d, $J = 248.4$ Hz, C-4'');

ESI-MS 423 [M+H]⁺; Anal. Calcd. for C₂₇H₃₅FN₂O C 76.74; H 8.35. Found C 76.86; H 8.32.

4.2.2.6. 17 β -Hydroxy-5'-(4''-chlorophenyl)-1'-methylpyrazolo[3',4':3,2]-5 α -androstane (8e). According to Section 4.2.2., Method B, 413 mg of **5e** was used. Eluent: EtOAc/CH₂Cl₂ = 10:90. White solid. Yield: 302 mg (69%); Mp 123–125 °C; ¹H NMR (CDCl₃, 500 MHz): δ_H 0.74 (s, 3H, 18-H₃), 0.75 (s, 3H, 19-H₃), 0.80–1.00 (overlapping m, 3H), 1.07 (m, 1H), 1.23–1.47 (overlapping m, 5H), 1.54–1.66 (overlapping m, 4H), 1.74 (m, 1H), 1.80 (m, 1H), 2.05 (m, 1H), 2.11 (d, 1H, $J = 15.2$ Hz, 1 α -H), 2.32 (dd, 1H, $J = 16.5, 11.9$ Hz, 4 β -H), 2.43 (d, 1H, $J = 15.2$ Hz, 1 β -H), 2.66 (dd, 1H, $J = 16.5, 5.1$ Hz, 4 α -H), 3.63 (t, 1H, $J = 8.5$ Hz, 17 α -H), 3.76 (s, 3H, N-CH₃), 7.24 (d, 2H, $J = 8.5$ Hz, 3''-H and 5''-H), 7.44 (d, 2H, $J = 8.5$ Hz, 2''-H and 6''-H); ¹³C NMR (CDCl₃, 125 MHz): δ_c 11.2 (C-18), 11.8 (C-19), 21.0 (C-11), 23.6 (C-15), 27.8 (C-4), 29.5 (C-6), 30.8 (C-16), 31.6 (C-7), 35.6 (C-1), 36.1 (C-8), 36.6 (C-10), 37.0 (C-12), 37.2 (N-CH₃), 42.8 (C-5), 43.0 (C-13), 51.2 (C-14), 54.3 (C-9), 82.1 (C-17), 114.6 (C-2), 129.1 (2C, C-2'' and C-6''), 129.5 (C-1''), 130.6 (2C, C-3'' and C-5''), 134.3 (C-4''), 139.0 (C-5'), 147.5 (C-3); ESI-MS 439 [M+H]⁺; Anal. Calcd. for C₂₇H₃₅ClN₂O C 73.87; H 8.04. Found C 73.91; H 8.03.

4.2.2.7. 17 β -Hydroxy-5'-(4''-bromophenyl)-1'-methylpyrazolo[3',4':3,2]-5 α -androstane (8f). According to Section 4.2.2., Method B, 457 mg of **5f** was used. Eluent: EtOAc/CH₂Cl₂ = 10:90. White solid. Yield: 304 mg (63%); Mp 143–145 °C; ¹H NMR (CDCl₃, 500 MHz): δ_H 0.74 (s, 3H, 18-H₃), 0.75 (s, 3H, 19-H₃), 0.80–1.00 (overlapping m, 3H), 1.06 (m, 1H), 1.23–1.47 (overlapping m, 5H), 1.54–1.65 (overlapping m, 4H), 1.73 (m, 1H), 1.80 (m, 1H), 2.05 (m, 1H), 2.10 (d, 1H, $J = 15.2$ Hz, 1 α -H), 2.31 (dd, 1H, $J = 16.5, 11.9$ Hz, 4 β -H), 2.43 (d, 1H, $J = 15.2$ Hz, 1 β -H), 2.66 (dd, 1H, $J = 16.5, 5.1$ Hz, 4 α -H), 3.63 (t, 1H, $J = 8.6$ Hz, 17 α -H), 3.76 (s, 3H, N-CH₃), 7.18 (d, 2H, $J = 8.4$ Hz), 7.59 (d, 2H, $J = 8.4$ Hz); ¹³C NMR (CDCl₃, 125 MHz): δ_c 11.2 (C-18), 11.8 (C-19), 21.0 (C-11), 23.6 (C-15), 27.8 (C-4), 29.5 (C-6), 30.8 (C-16), 31.6 (C-7), 35.6 (C-1), 36.1 (C-8), 36.6 (C-10), 37.0 (C-12), 37.2 (N-CH₃), 42.8 (C-5), 43.0 (C-13), 51.2 (C-14), 54.3 (C-9), 82.1 (C-17), 114.6 (C-2), 122.5 (C-4''), 129.9 (C-1''), 130.8 (2C, C-2'' and C-6''), 132.1 (2C, C-3'' and C-5''), 139.0 (C-5'), 147.5 (C-3); ESI-MS 485 [M+H]⁺; Anal. Calcd. for C₂₇H₃₅BrN₂O C 67.07; H 7.30. Found C 66.91; H 7.29.

4.2.2.8. 17 β -Hydroxy-5'-(furan-2''-yl)-1'-methylpyrazolo[3',4':3,2]-5 α -androstane (8g). According to Section 4.2.2., Method B, 369 mg of **5g** was used. Eluent: EtOAc/CH₂Cl₂ = 10:90. Light brown solid. Yield: 207 mg (52%); Mp 112–116 °C; ¹H NMR (CDCl₃, 500 MHz): δ_H 0.76 (s, 3H, 18-H₃), 0.77 (s, 3H, 19-H₃), 0.83–1.01 (overlapping m, 3H), 1.12 (m, 1H), 1.24–1.49 (overlapping m, 5H), 1.53–1.65 (overlapping m, 4H), 1.71 (m, 1H), 1.85 (m, 1H), 2.07 (m, 1H), 2.17 (d, 1H, $J = 15.6$ Hz, 1 α -H), 2.29 (dd, 1H, $J = 16.4, 11.9$ Hz, 4 β -H), 2.62 (overlapping m, 2H, 1 β -H and 4 α -H), 3.65 (t, 1H, $J = 8.6$ Hz, 17 α -H), 3.99 (s, 3H, N-CH₃), 6.44 (d, 1H, $J = 3.4$ Hz, 3''-H), 6.51 (dd, 1H, $J = 3.4, 1.8$ Hz, 4''-H), 7.52 (d, 1H, $J = 1.8$ Hz, 5''-H); ¹³C NMR (CDCl₃, 125 MHz): δ_c 11.2 (C-18), 11.9 (C-19), 21.0 (C-11), 23.6 (C-15), 27.6 (C-4), 29.4 (C-6), 30.7 (C-16), 31.5 (C-7), 36.0 (C-8), 36.1 (C-1), 36.4 (C-10), 37.0 (C-12), 38.6 (N-CH₃), 42.5 (C-5), 43.0 (C-13), 51.1 (C-14), 54.3 (C-9), 82.1 (C-17), 108.5 (C-3''), 111.3 (C-4''), 114.8 (C-2), 130.8 (C-5'), 142.3 (C-5''), 145.5 (C-3), 147.1 (C-2''); ESI-MS 395 [M+H]⁺; Anal. Calcd. for C₂₅H₃₄N₂O₂ C 76.10; H 8.69. Found C 76.31; H 8.71.

4.2.2.9. 17 β -Hydroxy-1'-methyl-5'-(tiophen-2''-yl)-pyrazolo[3',4':3,2]-5 α -androstane (8h). According to Section 4.2.2., Method B, 385 mg of **5h** was used. Eluent: EtOAc/CH₂Cl₂ = 10:90. Light yellow solid. Yield: 237 mg (58%); Mp 124–126 °C; ¹H NMR (CDCl₃, 500 MHz): δ_H 0.75 (s, 3H, 18-H₃), 0.77 (s, 3H, 19-H₃), 0.83–1.01 (overlapping m, 3H), 1.09 (m, 1H), 1.24–1.48 (overlapping m, 5H), 1.55–1.65 (overlapping m, 4H), 1.74 (m, 1H), 1.83 (m, 1H), 2.06 (m, 1H), 2.15 (d, 1H, $J = 15.4$ Hz, 1 α -H), 2.30 (dd, 1H, $J = 16.4, 11.9$ Hz, 4 β -H), 2.58–2.65 (overlapping m,

2H, 1 β -H and 4 α -H), 3.64 (t, 1H, J = 8.5 Hz, 17 α -H), 3.88 (s, 3H, N-CH₃), 7.06 (d, 1H, J = 3.5 Hz, 5''-H), 7.14 (dd, 2H, J = 5.0, 3.7 Hz, 4''-H), 7.41 (d, 1H, J = 5.1 Hz, 3''-H); ¹³C NMR (CDCl₃, 125 MHz): δ_C 11.2 (C-18), 11.8 (C-19), 21.0 (C-11), 23.6 (C-15), 27.8 (C-4), 29.4 (C-6), 30.8 (C-16), 31.6 (C-7), 36.0 (C-1), 36.1 (C-8), 36.6 (C-10), 37.0 (C-12), 37.6 (N-CH₃), 42.7 (C-5), 43.0 (C-13), 51.2 (C-14), 54.3 (C-9), 82.1 (C-17), 115.6 (C-2), 126.5 (C-5''), 127.2 (C-3''), 127.5 (C-4''), 131.6 (C-2''), 133.5 (C-5'), 147.3 (C-3); ESI-MS 411 [M+H]⁺; Anal. Calcd. for C₂₅H₃₄N₂O S C 73.13; H 8.35. Found C 73.09; H 8.38.

4.2.2.10. 17 β -Hydroxy-1',5'-dimethylpyrazolo[3',4':3,2]-5 α -androstane (8l). According to Section 4.2.2., Method B, 316 mg of **5j** was used. Eluent: EtOAc/CH₂Cl₂ = 80:20. White solid. Yield: 207 mg (60%); Mp 240–243 °C; ¹H NMR (CDCl₃, 500 MHz): δ_H 0.74 (s, 3H, 18-H₃), 0.76 (s, 3H, 19-H₃), 0.80–1.00 (overlapping m, 3H), 1.10 (m, 1H), 1.23–1.53 (overlapping m, 5H), 1.56–1.73 (overlapping m, 5H), 1.85 (m, 1H), 1.98 (d, 1H, J = 14.9 Hz, 1 α -H), 2.05 (m, 1H), 2.10 (s, 3H, 5'-CH₃), 2.23 (dd, 1H, J = 16.4, 12.1 Hz, 4 β -H), 2.43 (d, 1H, J = 14.9 Hz, 1 β -H), 2.54 (dd, 1H, J = 16.4, 5.2 Hz, 4 α -H), 3.64 (t, 1H, J = 8.6 Hz, 17 α -H), 3.70 (s, 3H, N-CH₃); ¹³C NMR (CDCl₃, 125 MHz): δ_C 9.6 (5'-CH₃), 11.2 (C-18), 11.8 (C-19), 21.0 (C-11), 23.6 (C-15), 27.7 (C-4), 29.4 (C-6), 30.7 (C-16), 31.5 (C-7), 35.0 (C-1), 35.9 (N-CH₃), 36.0 (C-8), 36.4 (C-10), 37.0 (C-12), 42.8 (C-5), 43.0 (C-13), 51.1 (C-14), 54.3 (C-9), 82.1 (C-17), 113.1 (C-2), 135.0 (C-5') 146.7 (C-3); ESI-MS 343 [M+H]⁺; Anal. Calcd. for C₂₂H₃₄N₂O C 77.14; H 10.01. Found C 77.08; H 9.99.

4.2.3. General procedure for the one-pot synthesis of ring A-condensed pyrazoles

Arylidene derivative (1.0 mmol, **5a**, **5e**, or **5i**) was dissolved in absolute EtOH (5 mL), then I₂ (254 mg, 1 equiv.) and (substituted) phenylhydrazine hydrochloride (2 equiv.) were added, and the mixture was irradiated in a closed vessel at 100 °C for 2 min. After completion of the reaction, the mixture was poured into saturated aqueous solution of Na₂S₂O₃ (10 mL) and extracted with CH₂Cl₂ (3 × 10 mL). The combined organic layers were dried over anhydrous Na₂SO₄ and concentrated *in vacuo*. The crude product was purified by column chromatography.

4.2.3.1. 17 β -Hydroxy-1',5'-diphenylpyrazolo[3',4':3,2]-5 α -androstane (8i). According to Section 4.2.3., 290 mg phenylhydrazine hydrochloride and 379 mg of **5a** was used. Eluent: EtOAc/CH₂Cl₂ = 5:95. White solid. Yield: 394 mg (84%); Mp 224–226 °C; ¹H NMR (CDCl₃, 500 MHz): δ_H 0.75 (s, 3H, 18-H₃), 0.81 (s, 3H, 19-H₃), 0.85–1.02 (overlapping m, 3H, 9 α -H, 7 α -H and 14 α -H), 1.09 (m, 1H, 12 α -H), 1.28 (m, 1H, 15 β -H), 1.35–1.48 (overlapping m, 4H, 6 β -H, 8 β -H, 16 β -H and 11 β -H), 1.64 (overlapping m, 4H, 11 α -H, 5 α -H, 15 α -H and 6 α -H), 1.75 (m, 1H, 7 β -H), 1.82 (m, 1H, 12 β -H), 2.07 (m, 1H, 16 α -H), 2.25 (d, 1H, J = 15.4 Hz, 1 α -H), 2.41 (dd, 1H, J = 16.7, 11.9 Hz, 4 β -H), 2.59 (d, 1H, J = 15.4 Hz, 1 β -H), 2.77 (dd, 1H, J = 16.7, 5.1 Hz, 4 α -H), 3.65 (t, 1H, J = 8.4 Hz, 17 α -H), 7.24 (overlapping m, 10H, aromatic Hs); ¹³C NMR (CDCl₃, 125 MHz): δ_C 11.2 (C-18), 11.9 (C-19), 21.0 (C-11), 23.6 (C-15), 27.9 (C-4), 29.4 (C-6), 30.7 (C-16), 31.5 (C-7), 35.8 (C-1), 36.0 (C-8), 36.6 (C-10), 36.9 (C-12), 42.6 (C-5), 43.0 (C-13), 51.1 (C-14), 54.3 (C-9), 82.1 (C-17), 116.4 (C-2), 124.9 (2C), 126.6 (C-4'''), 127.8 (C-4'''), 128.5 (2C), 128.8 (2C), 129.4 (2C), 131.1 (C-1''), 139.1 (C-1'''), 140.6 (C-5'), 149.4 (C-3); ESI-MS 467 [M+H]⁺; Anal. Calcd. for C₃₂H₃₈N₂O C 82.36; H 8.21. Found C 82.40; H 8.19.

4.2.3.2. 17 β -Hydroxy-5'-(4''-chlorophenyl)-1'-phenylpyrazolo[3',4':3,2]-5 α -androstane (8j). According to Section 4.2.4., 290 mg phenylhydrazine hydrochloride and 413 mg of **5e** was used. Eluent: EtOAc/CH₂Cl₂ = 5:95. White solid. Yield: 397 mg (79%); Mp 185–188 °C; ¹H NMR (CDCl₃, 500 MHz): δ_H 0.75 (s, 3H, 18-H₃), 0.80 (s, 3H, 19-H₃), 0.85–1.02 (overlapping m, 3H, 9 α -H, 7 α -H and 14 α -H), 1.09 (m, 1H, 12 α -H), 1.28 (m, 1H, 15 β -H), 1.35–1.48 (overlapping m, 4H, 6 β -H, 8 β -H, 16 β -H and 11 β -H), 1.59–1.68 (overlapping m, 4H, 11 α -H, 5 α -H, 15 α -H

and 6 α -H), 1.75 (m, 1H, 7 β -H), 1.83 (m, 1H, 12 β -H), 2.07 (m, 1H, 16 α -H), 2.22 (d, 1H, J = 15.4 Hz, 1 α -H), 2.40 (dd, 1H, J = 16.7, 12.1 Hz, 4 β -H), 2.54 (d, 1H, J = 15.4 Hz, 1 β -H), 2.76 (dd, 1H, J = 16.7, 5.1 Hz, 4 α -H), 3.65 (m, 1H, 17 α -H), 7.08 (d, 2H, J = 8.5 Hz, 3''-H and 5''-H), 7.22 (m, 3H), 7.27–7.30 (m, 4H); ¹³C NMR (CDCl₃, 125 MHz): δ_C 11.2 (C-18), 11.9 (C-19), 21.0 (C-11), 23.6 (C-15), 27.8 (C-4), 29.4 (C-6), 30.7 (C-16), 31.5 (C-7), 35.8 (C-1), 36.0 (C-8), 36.5 (C-10), 36.9 (C-12), 42.6 (C-5), 43.0 (C-13), 51.1 (C-14), 54.2 (C-9), 82.1 (C-17), 116.6 (C-2), 124.9 (2C, C-2''' and C-6'''), 126.9 (C-4'''), 128.9 (2C), 129.0 (2C), 129.5 (C-1''), 130.6 (2C), 133.9 (C-4'''), 137.9 (C-1'''), 140.3 (C-5'), 149.6 (C-3); ESI-MS 501 [M+H]⁺; Anal. Calcd. for C₃₂H₃₇ClN₂O C 76.70; H 7.44. Found C 76.62; H 7.46.

4.2.3.3. 17 β -Hydroxy-5'-(4''-hydroxyphenyl)-1'-phenylpyrazolo[3',4':3,2]-5 α -androstane (8k). According to Section 4.2.4., 290 mg phenylhydrazine hydrochloride and 395 mg of **5i** was used. Eluent: EtOAc/CH₂Cl₂ = 20:80. Light brown solid. Yield: 433 mg (90%); Mp 290–292 °C; ¹H NMR (DMSO-*d*₆, 500 MHz): δ_H 0.64 (s, 3H, 18-H₃), 0.71 (s, 3H, 19-H₃), 0.82–1.01 (overlapping m, 4H), 1.18 (m, 1H), 1.28–1.35 (overlapping m, 4H), 1.50–1.60 (overlapping m, 4H), 1.67 (m, 1H), 1.74 (m, 1H), 1.84 (m, 1H), 2.19 (d, 1H, J = 15.4 Hz, 1 α -H), 2.25 (dd, 1H, J = 16.7, 12.4 Hz, 4 β -H), 2.42 (d, 1H, J = 15.4 Hz, 1 β -H), 2.61 (dd, 1H, J = 16.7, 5.1 Hz, 4 α -H), 3.44 (m, 1H, 17 α -H), 4.40 (d, 1H, J = 4.82, 17-OH), 6.73 (d, 2H, J = 8.6 Hz, 3''-H and 5''-H), 6.94 (d, 2H, J = 8.6 Hz, 2''-H and 6''-H), 7.16 (d, 2H, J = 7.5 Hz, 3'''-H and 5'''-H), 7.23 (t-like m, 1H, 4'''-H), 7.31 (t-like m, 2H, 2'''-H and 6'''-H), 9.65 (s, 1H, 4'-OH); ¹³C NMR (DMSO-*d*₆, 125 MHz): δ_C 11.2 (C-18), 11.6 (C-19), 20.4 (C-11), 23.1 (C-15), 27.3 (C-4), 28.8 (C-6), 29.8 (C-16), 31.0 (C-7), 35.0 (C-1), 35.4 (C-8), 35.8 (C-10), 36.5 (C-12), 41.8 (C-5), 42.4 (C-13), 50.5 (C-14), 53.4 (C-9), 80.0 (C-17), 115.1 (C-2), 115.4 (2C, C-3'' and C-5''), 120.8 (C-1''), 124.2 (2C, C-2''' and C-6'''), 126.3 (C-4'''), 128.6 (2C), 130.2 (2C), 138.6 (C-1'''), 140.3 (C-5'), 148.0 (C-3), 157.1 (C-4''); ESI-MS 483 [M+H]⁺; Anal. Calcd. for C₃₂H₃₈N₂O₂ C 79.63; H 7.94. Found C 79.81; H 7.96.

4.2.4. General procedure for the synthesis of heterocyclic 17-keto steroids by jones oxidation

The crude product (**8a-1**) of the heterocyclization (4.2.3.) was dissolved in acetone (10 mL) and Jones reagent (0.2 mL) was added dropwise into the solution, which was then stirred at room temperature for 30 min, after which it was poured into ice-cold water. NH₄Cl was added and the resulting precipitate was filtered off and dried. The crude product was purified by column chromatography.

4.2.4.1. 1'-methyl-5'-phenylpyrazolo[3',4':3,2]-5 α -androstane-17-one (10a). Eluent: EtOAc/CH₂Cl₂ = 10:90. White solid. Yield: 307 mg (76%); Mp 200–203 °C; ¹H NMR (CDCl₃, 500 MHz): δ_H 0.77 (s, 3H, 19-H₃), 0.86 (s, 3H, 18-H₃), 0.89 (m, 1H), 1.04 (m, 1H), 1.22–1.45 (overlapping m, 5H), 1.50–1.71 (overlapping m, 4H), 1.80 (m, 1H), 1.85 (m, 1H), 1.97 (m, 1H), 2.08 (m, 1H, 16 α -H), 2.15 (d, 1H, J = 15.2 Hz, 1 α -H), 2.33 (dd, 1H, J = 16.5, 12.0 Hz, 4 β -H), 2.45 (dd, 1H, J = 19.4, 8.6 Hz, 16 β -H), 2.46 (d, 1H, J = 15.2 Hz, 1 β -H), 2.69 (dd, 1H, J = 16.5, 5.2 Hz, 4 α -H), 3.78 (s, 3H, N-CH₃), 7.31 (d-like m, 2H, 3''-H and 5''-H), 7.39 (t-like m, 1H, 4''-H), 7.46 (t-like m, 2H, 2''-H and 6''-H); ¹³C NMR (CDCl₃, 125 MHz): δ_C 11.7 (C-19), 13.9 (C-18), 20.6 (C-11), 22.0 (C-15), 27.8 (C-4), 29.3 (C-6), 30.8 (C-16), 31.7 (C-7), 35.5 (2C, C-8 and C-1), 36.0 (C-12), 36.6 (C-10), 37.2 (N-CH₃), 42.7 (C-5), 47.8 (C-13), 51.6 (C-14), 54.2 (C-9), 114.1 (C-2), 128.2 (C-4'''), 128.8 (2C, C-3'' and C-5''), 129.3 (2C, C-2'' and C-6''), 130.9 (C-1''), 140.2 (C-5') 147.1 (C-3), 221.4 (C-17); ESI-MS 403 [M+H]⁺; Anal. Calcd. for C₂₇H₃₄N₂O C 80.55; H 8.51. Found C 80.65; H 8.52.

4.2.4.2. 1'-methyl-5'-(4''-tolyl)-pyrazolo[3',4':3,2]-5 α -androstane-17-one (10b). Eluent: EtOAc/CH₂Cl₂ = 10:90. White solid. Yield: 307 mg (74%); Mp 180–183 °C; ¹H NMR (CDCl₃, 500 MHz): δ_H 0.76 (s, 3H, 19-H₃), 0.86 (s, 3H, 18-H₃), 0.88 (m, 1H), 1.03 (m, 1H), 1.21–1.44

(overlapping m, 5H), 1.48–1.71 (overlapping m, 4H), 1.80 (m, 1H), 1.85 (m, 1H), 1.97 (m, 1H), 2.06 (m, 1H, 16 α -H), 2.14 (d, 1H, J = 15.4 Hz, 1 α -H), 2.33 (dd, 1H, J = 16.4, 12.2 Hz, 4 β -H), 2.41 (s, 4''-CH₃), 2.43 (m, 1H, 16 β -H), 2.47 (d, 1H, J = 15.4 Hz, 1 β -H), 2.68 (dd, 1H, J = 16.4, 5.2 Hz, 4 α -H), 3.77 (s, 3H, N-CH₃), 7.20 (d, 2H, J = 8.0 Hz, 2''-H and 6''-H), 7.27 (d, 2H, J = 8.4 Hz, 3''-H and 5''-H); ¹³C NMR (CDCl₃, 125 MHz): δ_C 11.7 (C-19), 13.9 (C-18), 20.6 (C-11), 21.4 (4''-CH₃), 22.0 (C-15), 27.8 (C-4), 29.3 (C-6), 30.8 (C-16), 31.7 (C-7), 35.5 (C-8), 35.6 (C-1), 36.0 (C-12), 36.6 (C-10), 37.2 (N-CH₃), 42.7 (C-5), 47.8 (C-13), 51.6 (C-14), 54.2 (C-9), 113.9 (C-2), 127.9 (C-4''), 129.1 (2C, C-2'' and C-6''), 129.5 (2C, C-3'' and C-5''), 138.1 (C-1''), 140.2 (C-5') 147.0 (C-3), 221.5 (C-17); ESI-MS 417 [M+H]⁺; Anal. Calcd. for C₂₈H₃₆N₂O C 80.73; H 8.71. Found C 80.75; H 8.70.

4.2.4.3. 5'-(4''-methoxyphenyl)-1'-methylpyrazolo[3',4':3,2]-5 α -androstan-17-one (10c). Eluent: EtOAc/CH₂Cl₂ = 20:80. White solid. Yield: 321 mg (74%); Mp 102–105 °C; ¹H NMR (CDCl₃, 500 MHz): δ_H 0.77 (s, 3H, 19-H₃), 0.86 (s, 3H, 18-H₃), 0.88 (m, 1H), 1.04 (m, 1H), 1.22–1.44 (overlapping m, 5H), 1.48–1.70 (overlapping m, 4H), 1.80 (m, 1H), 1.86 (m, 1H), 1.97 (m, 1H), 2.07 (m, 1H, 16 α -H), 2.13 (d, 1H, J = 15.2 Hz, 1 α -H), 2.33 (dd, 1H, J = 16.5, 12.1 Hz, 4 β -H), 2.42–2.48 (overlapping m, 2H, 16 β -H and 1 β -H), 2.68 (dd, 1H, J = 16.5, 5.2 Hz, 4 α -H), 3.76 (s, 3H, N-CH₃), 3.86 (s, 3H, 4''-OCH₃), 6.99 (d, 2H, J = 8.7 Hz, 3''-H and 5''-H), 7.23 (d, 2H, J = 8.7 Hz, 2''-H and 6''-H); ¹³C NMR (CDCl₃, 125 MHz): δ_C 11.7 (C-19), 13.9 (C-18), 20.6 (C-11), 22.0 (C-15), 27.8 (C-4), 29.3 (C-6), 30.8 (C-16), 31.7 (C-7), 35.5 (C-8), 35.6 (C-1), 36.0 (C-12), 36.6 (C-10), 37.1 (N-CH₃), 42.7 (C-5), 47.8 (C-13), 51.6 (C-14), 54.2 (C-9), 55.5 (4''-CH₃), 113.8 (C-2), 114.3 (2C, C-3'' and C-5''), 123.1 (C-1''), 130.5 (2C, C-2'' and C-6''), 140.0 (C-5'), 147.0 (C-3) 159.6 (C-4''), 221.5 (C-17); ESI-MS 433 [M+H]⁺; Anal. Calcd. for C₂₈H₃₆N₂O₂ C 77.74; H 8.39. Found C 77.80; H 8.37.

4.2.4.4. 5'-(4''-fluorophenyl)-1'-methylpyrazolo[3',4':3,2]-5 α -androstan-17-one (10d). Eluent: EtOAc/CH₂Cl₂ = 20:80. White solid. Yield: 251 mg (60%); Mp 185–187 °C; ¹H NMR (CDCl₃, 500 MHz): δ_H 0.77 (s, 3H, 19-H₃), 0.87 (s, 3H, 18-H₃), 0.88 (m, 1H), 1.04 (m, 1H), 1.22–1.44 (overlapping m, 5H), 1.48–1.71 (overlapping m, 4H), 1.80 (m, 1H), 1.86 (m, 1H), 1.97 (m, 1H), 2.07 (m, 1H, 16 α -H), 2.12 (d, 1H, J = 15.4 Hz, 1 α -H), 2.33 (dd, 1H, J = 16.5, 12.1 Hz, 4 β -H), 2.43 (d, 1H, J = 15.4 Hz, 1 β -H), 2.44 (dd, 1H, J = 19.2, 8.8 Hz, 16 β -H), 2.68 (dd, 1H, J = 16.5, 5.2 Hz, 4 α -H), 3.75 (s, 3H, N-CH₃), 7.16 (t-like m, 2H, 2''-H and 6''-H), 7.27 (m, 2H, 3''-H and 5''-H); ¹³C NMR (CDCl₃, 125 MHz): δ_C 11.7 (C-19), 13.8 (C-18), 20.6 (C-11), 22.0 (C-15), 27.8 (C-4), 29.2 (C-6), 30.8 (C-16), 31.7 (C-7), 35.5 (C-1), 35.5 (C-8), 36.0 (C-12), 36.6 (C-10), 37.1 (N-CH₃), 42.6 (C-5), 47.8 (C-13), 51.6 (C-14), 54.2 (C-9), 114.2 (C-2), 115.9 (d, 2C, J = 21.7 Hz, C-3'' and C-5''), 126.9 (d, J = 3.3 Hz, C-1''), 131.1 (d, 2C, J = 8.2 Hz, C-2'' and C-6''), 139.2 (C-5'), 147.2 (C-3), 162.7 (d, J = 248.5 Hz, C-4''), 221.4 (C-17); ESI-MS 421 [M+H]⁺; Anal. Calcd. for C₂₇H₃₃FN₂O C 77.11; H 7.91. Found C 77.05; H 7.90.

4.2.4.5. 5'-(4''-chlorophenyl)-1'-methylpyrazolo[3',4':3,2]-5 α -androstan-17-one (10e). Eluent: EtOAc/CH₂Cl₂ = 20:80. White solid. Yield: 280 mg (64%); Mp 211–215 °C; ¹H NMR (CDCl₃, 500 MHz): δ_H 0.76 (s, 3H, 19-H₃), 0.86 (s, 3H, 18-H₃), 0.88 (m, 1H), 1.04 (m, 1H), 1.23–1.44 (overlapping m, 5H), 1.48–1.73 (overlapping m, 4H), 1.79–1.87 (overlapping m, 2H), 1.97 (m, 1H), 2.06 (m, 1H, 16 α -H), 2.11 (d, 1H, J = 14.7 Hz, 1 α -H), 2.32 (dd, 1H, J = 16.5, 12.4 Hz, 4 β -H), 2.42 (d, 1H, J = 14.7 Hz, 1 β -H), 2.45 (m, 1H, 16 β -H), 2.68 (dd, 1H, J = 16.5, 5.1 Hz, 4 α -H), 3.75 (s, 3H, N-CH₃), 7.23 (d, 2H, J = 8.2 Hz, 3''-H and 5''-H), 7.43 (d, 2H, J = 8.2 Hz, 2''-H and 6''-H); ¹³C NMR (CDCl₃, 125 MHz): δ_C 11.7 (C-19), 13.9 (C-18), 20.7 (C-11), 22.0 (C-15), 27.8 (C-4), 29.3 (C-6), 30.8 (C-16), 31.8 (C-7), 35.6 (C-8), 35.6 (C-1), 36.0 (C-12), 36.7 (C-10), 37.2 (N-CH₃), 42.7 (C-5), 47.8 (C-13), 51.6 (C-14), 54.3 (C-9), 114.4 (C-2), 129.1 (2C, C-2'' and C-6''), 129.3 (C-1''), 130.5 (2C, C-3'' and C-5''), 134.4 (C-4''), 139.1 (C-5') 147.3 (C-3), 221.1 (C-17); ESI-MS 437

[M+H]⁺; Anal. Calcd. for C₂₇H₃₃ClN₂O C 74.21; H 7.61. Found C 77.31; H 7.59.

4.2.4.6. 5'-(4''-bromophenyl)-1'-methylpyrazolo[3',4':3,2]-5 α -androstan-17-one (10f). Eluent: EtOAc/CH₂Cl₂ = 20:80. White solid. Yield: 273 mg (57%); Mp 126–128 °C; ¹H NMR (CDCl₃, 500 MHz): δ_H 0.76 (s, 3H, 19-H₃), 0.87 (s, 3H, 18-H₃), 0.88 (m, 1H), 1.04 (m, 1H), 1.22–1.44 (overlapping m, 5H), 1.48–1.73 (overlapping m, 4H), 1.81 (m, 1H), 1.86 (m, 1H), 1.97 (m, 1H), 2.07 (m, 1H, 16 α -H), 2.13 (d, 1H, J = 15.2 Hz, 1 α -H), 2.33 (dd, 1H, J = 16.5, 12.1 Hz, 4 β -H), 2.42 (d, 1H, J = 15.2 Hz, 1 β -H), 2.45 (dd, 1H, J = 16.5, 5.3 Hz, 16 β -H), 2.68 (dd, 1H, J = 16.5, 5.3 Hz, 4 α -H), 3.76 (s, 3H, N-CH₃), 7.18 (d, 2H, J = 8.4 Hz, 2''-H and 6''-H), 7.60 (d, 2H, J = 8.4 Hz, 3''-H and 5''-H); ¹³C NMR (CDCl₃, 125 MHz): δ_C 11.7 (C-19), 13.9 (C-18), 20.6 (C-11), 22.0 (C-15), 27.7 (C-4), 29.2 (C-6), 30.8 (C-16), 31.7 (C-7), 35.5 (C-8), 35.5 (C-1), 36.0 (C-12), 36.6 (C-10), 37.2 (N-CH₃), 42.6 (C-5), 47.8 (C-13), 51.6 (C-14), 54.2 (C-9), 114.3 (C-2), 122.5 (C-4''), 129.7 (C-1''), 130.8 (2C, C-2'' and C-6''), 132.1 (2C, C-3'' and C-5''), 139.0 (C-5') 147.3 (C-3), 221.4 (C-17); ESI-MS 483 [M+H]⁺; Anal. Calcd. for C₂₇H₃₃BrN₂O C 67.35; H 6.91. Found C 67.37; H 6.93.

4.2.4.7. 5'-(furan-2''-yl)-1'-methylpyrazolo[3',4':3,2]-5 α -androstan-17-one (10g). Eluent: EtOAc/CH₂Cl₂ = 5:95. Light brown solid. Yield: 180 mg (46%); Mp > 80 °C (decomp.); ¹H NMR (CDCl₃, 500 MHz): δ_H 0.78 (s, 3H, 19-H₃), 0.89 (s, 3H, 18-H₃), 0.93 (m, 1H), 1.04 (m, 1H), 1.25–1.70 (overlapping m, 9H), 1.78 (m, 1H), 1.86 (m, 1H), 1.98 (m, 1H), 2.09 (m, 1H, 16 α -H), 2.18 (d, 1H, J = 15.6 Hz, 1 α -H), 2.31 (dd, 1H, J = 16.4, 12.1 Hz, 4 β -H), 2.46 (dd, 1H, J = 19.2, 8.8 Hz, 16 β -H), 2.63 (dd, 1H, J = 16.4, 5.2 Hz, 4 α -H), 2.66 (d, 1H, J = 15.6 Hz, 1 β -H), 3.99 (s, 3H, N-CH₃), 6.44 (d, 1H, J = 3.3 Hz, 3''-H), 6.51 (dd, 1H, J = 3.3, 1.8 Hz, 4''-H), 7.52 (d, 1H, J = 1.3 Hz, 5''-H); ¹³C NMR (CDCl₃, 125 MHz): δ_C 11.9 (C-19), 13.9 (C-18), 20.7 (C-11), 22.0 (C-15), 27.5 (C-4), 29.2 (C-6), 30.8 (C-16), 31.8 (C-7), 35.5 (C-8), 36.0 (C-1), 36.0 (C-12), 36.5 (C-10), 38.6 (N-CH₃), 42.4 (C-5), 47.8 (C-13), 51.6 (C-14), 54.2 (C-9), 108.6 (C-3''), 111.4 (C-4''), 114.6 (C-2), 130.9 (C-5'), 142.3 (C-5''), 145.4 (C-3), 147.0 (C-2''), 221.4 (C-17); ESI-MS 393 [M+H]⁺; Anal. Calcd. for C₂₅H₃₂N₂O₂ C 76.49; H 8.22. Found C 76.37; H 8.20.

4.2.4.8. 1'-methyl-5'-(thiophen-2''-yl)-pyrazolo[3',4':3,2]-5 α -androstan-17-one (10h). Eluent: EtOAc/CH₂Cl₂ = 5:95. Light yellow solid. Yield: 218 mg (53%); Mp 90–92 °C; ¹H NMR (CDCl₃, 500 MHz): δ_H 0.77 (s, 3H, 19-H₃), 0.87 (s, 3H, 18-H₃), 0.91 (m, 1H), 1.04 (m, 1H), 1.25–1.73 (overlapping m, 9H), 1.84 (overlapping m, 2H), 1.97 (m, 1H), 2.08 (m, 1H, 16 α -H), 2.16 (d, 1H, J = 15.4 Hz, 1 α -H), 2.31 (dd, 1H, J = 16.4, 12.1 Hz, 4 β -H), 2.45 (dd, 1H, J = 19.2, 8.8 Hz, 16 β -H), 2.60 (d, 1H, J = 15.3 Hz, 1 β -H), 2.65 (dd, 1H, J = 16.4, 5.2 Hz, 4 α -H), 3.88 (s, 3H, N-CH₃), 7.07 (d, 1H, J = 3.5 Hz, 5''-H), 7.14 (dd, 1H, J = 5.1, 3.6 Hz, 4''-H), 7.43 (d, 1H, J = 5.1 Hz, 3''-H); ¹³C NMR (CDCl₃, 125 MHz): δ_C 11.8 (C-19), 13.9 (C-18), 20.7 (C-11), 22.0 (C-15), 27.7 (C-4), 29.2 (C-6), 30.8 (C-16), 31.7 (C-7), 35.5 (C-8), 35.9 (C-1), 36.0 (C-12), 36.6 (C-10), 37.7 (N-CH₃), 42.5 (C-5), 47.8 (C-13), 51.5 (C-14), 54.2 (C-9), 115.3 (C-2), 126.5 (C-5''), 127.2 (C-3''), 127.6 (C-4''), 131.3 (C-2''), 133.6 (C-5'), 147.1 (C-3), 221.4 (C-17); ESI-MS 409 [M+H]⁺; Anal. Calcd. for C₂₅H₃₂N₂OS C 73.49; H 7.89. Found C 73.53; H 7.88.

4.2.4.9. 1',5'-diphenylpyrazolo[3',4':3,2]-5 α -androstan-17-one (10i). According to Section 4.2.4, 117 mg of **8i** was used. Eluent: EtOAc/CH₂Cl₂ = 2:98. White solid. Yield: 110 mg (95%); Mp 267–270 °C; ¹H NMR (CDCl₃, 500 MHz): δ_H 0.82 (s, 3H, 19-H₃), 0.88 (s, 3H, 18-H₃), 0.94 (m, 1H), 1.07 (m, 1H), 1.25–1.34 (overlapping m, 2H), 1.38–1.61 (overlapping m, 4H), 1.70 (m, 3H), 1.83 (m, 1H), 1.88 (m, 1H), 1.99 (m, 1H), 2.09 (m, 1H, 16 α -H), 2.26 (d, 1H, J = 15.4 Hz, 1 α -H), 2.40–2.49 (overlapping m, 2H, 4 β -H, 16 β -H), 2.59 (d, 1H, J = 15.4 Hz, 1 β -H), 2.80 (dd, 1H, J = 16.7, 5.1 Hz, 4 α -H), 7.15–7.34 (overlapping m, 10H, aromatic Hs); ¹³C NMR (CDCl₃, 125 MHz): δ_C 11.8 (C-19), 13.9 (C-18), 20.7

(C-11), 22.0 (C-15), 27.9 (C-4), 29.3 (C-6), 30.8 (C-16), 31.7 (C-7), 35.5 (C-8), 35.7 (C-1), 36.0 (C-12), 36.6 (C-10), 42.6 (C-5), 47.8 (C-13), 51.6 (C-14), 54.2 (C-9), 116.2 (C-2), 124.9 (2C), 126.7 (C-4''), 127.9 (C-4''), 128.6 (2C), 128.8 (2C), 129.4 (2C), 131.0 (C-1''), 139.2 (C-1'''), 140.6 (C-5'), 149.2 (C-3), 221.4 (C-17); ESI-MS 465 [M+H]⁺; Anal. Calcd. for C₃₂H₃₆N₂O C 82.72; H 7.81. Found C 82.54; H 7.80.

4.2.4.10. 5'-(4''-chlorophenyl)-1'-phenylpyrazolo[3',4':3,2]-5 α -androstan-17-one (10j). According to Section 4.2.5., 125 mg of **8j** was used. Eluent: CH₂Cl₂. White solid. Yield: 114 mg (91%); Mp > 250 °C (decomp.); ¹H NMR (CDCl₃, 500 MHz): δ_{H} 0.81 (s, 3H, 19-H₃), 0.88 (s, 3H, 18-H₃), 0.94 (m, 1H), 1.07 (m, 1H), 1.24–1.34 (overlapping m, 2H), 1.39–1.59 (overlapping m, 4H), 1.70 (m, 3H), 1.82–1.90 (overlapping m, 2H), 1.99 (m, 1H), 2.09 (m, 1H, 16 α -H), 2.24 (d, 1H, *J* = 15.4 Hz, 1 α -H), 2.39–2.49 (overlapping m, 2H, 4 β -H, 16 β -H), 2.55 (d, 1H, *J* = 15.4 Hz, 1 β -H), 2.79 (dd, 1H, *J* = 16.7, 5.1 Hz, 4 α -H), 7.08 (d, 2H, *J* = 8.5 Hz, 3''-H and 5''-H), 7.25 (m, 7H); ¹³C NMR (CDCl₃, 125 MHz): δ_{C} 11.8 (C-19), 13.9 (C-18), 20.7 (C-11), 22.0 (C-15), 27.8 (C-4), 29.2 (C-6), 30.8 (C-16), 31.7 (C-7), 35.5 (C-8), 35.7 (C-1), 36.0 (C-12), 36.6 (C-10), 42.5 (C-5), 47.8 (C-13), 51.5 (C-14), 54.2 (C-9), 116.4 (C-2), 124.9 (2C, C-2'' and C-6'''), 127.0 (C-4'''), 128.9 (2C), 129.0 (2C), 129.4 (C-1''), 130.6 (2C), 134.0 (C-4''), 138.0 (C-1'''), 140.3 (C-5'), 149.4 (C-3), 221.3 (C-17); ESI-MS 499 [M+H]⁺; Anal. Calcd. for C₃₂H₃₅ClN₂O C 77.01; H 7.07. Found C 77.20; H 7.05.

4.2.4.11. 5'-(4''-hydroxyphenyl)-1'-phenylpyrazolo[3',4':3,2]-5 α -androstan-17-one (10k). According to Section 4.2.5., 121 mg of **8k** was used. Eluent: EtOAc/CH₂Cl₂ = 10:90. White solid. Yield: 109 mg (91%); Mp > 250 °C (decomp.); ¹H NMR (CDCl₃, 500 MHz): δ_{H} 0.81 (s, 3H, 19-H₃), 0.89 (s, 3H, 18-H₃), 0.93 (m, 1H), 1.06 (m, 1H), 1.26–1.35 (overlapping m, 2H), 1.39–1.47 (overlapping m, 2H), 1.51–1.61 (overlapping m, 2H), 1.69 (m, 3H), 1.82–1.89 (overlapping m, 2H), 1.99 (m, 1H), 2.10 (m, 1H, 16 α -H), 2.22 (d, 1H, *J* = 15.3 Hz, 1 α -H), 2.38–2.50 (overlapping m, 2H, 4 β -H, 16 β -H), 2.57 (d, 1H, *J* = 15.3 Hz, 1 β -H), 2.77 (dd, 1H, *J* = 16.7, 5.0 Hz, 4 α -H), 6.58 (bs, 1H, 4''-OH), 6.75 (d, 2H, *J* = 8.6 Hz, 3''-H and 5''-H), 6.98 (d, 2H, *J* = 8.6 Hz, 2''-H and 6''-H), 7.22 (m, 5H); ¹³C NMR (CDCl₃, 125 MHz): δ_{C} 11.9 (C-19), 13.9 (C-18), 20.7 (C-11), 22.0 (C-15), 27.7 (C-4), 29.2 (C-6), 30.8 (C-16), 31.7 (C-7), 35.5 (C-8), 35.7 (C-1), 36.1 (C-12), 36.6 (C-10), 42.5 (C-5), 47.9 (C-13), 51.6 (C-14), 54.2 (C-9), 115.6 (C-2), 115.7 (2C, C-3'' and C-5''), 122.7 (C-1''), 125.0 (2C, C-2'' and C-6'''), 126.7 (C-4'''), 128.8 (2C), 130.8 (2C), 139.4 (C-1'''), 140.4 (C-5'), 149.2 (C-3), 156.1 (C-4''), 222.0 (C-17); ESI-MS 481 [M+H]⁺; Anal. Calcd. for C₃₂H₃₆N₂O₂ C 79.96; H 7.55. Found C 79.79; H 7.57.

4.2.4.12. 1',5'-dimethylpyrazolo[3',4':3,2]-5 α -androstan-17-one (10l). Eluent: EtOAc/CH₂Cl₂ = 50:50. Light yellow solid. Yield: 184 mg (54%); Mp 90–92 °C; ¹H NMR (CDCl₃, 500 MHz): δ_{H} 0.76 (s, 3H, 19-H₃), 0.89 (s, 3H, 18-H₃), 0.90 (m, 1H), 1.03 (m, 1H), 1.25–1.78 (overlapping m, 10H), 1.84 (overlapping m, 1H), 1.97 (m, 1H), 1.99 (d, 1H, *J* = 14.8 Hz, 1 α -H), 2.08 (m, 1H, 16 α -H), 2.11 (s, 3H, 5'-CH₃), 2.25 (dd, 1H, *J* = 16.4, 12.1 Hz, 4 β -H), 2.43 (d, 1H, *J* = 14.8 Hz, 1 β -H), 2.45 (dd, 1H, *J* = 19.2, 8.8 Hz, 16 β -H), 2.57 (dd, 1H, *J* = 16.4, 5.2 Hz, 4 α -H), 3.71 (s, 3H, N-CH₃); ¹³C NMR (CDCl₃, 125 MHz): δ_{C} 9.6 (5'-CH₃), 11.8 (C-19), 13.9 (C-18), 20.7 (C-11), 22.0 (C-15), 27.7 (C-4), 29.3 (C-6), 30.8 (C-16), 31.8 (C-7), 35.0 (C-1), 35.5 (C-8), 35.9 (N-CH₃), 36.0 (C-12), 36.5 (C-10), 42.8 (C-5), 47.8 (C-13), 51.6 (C-14), 54.3 (C-9), 112.9 (C-2), 135.1 (C-5'), 146.5 (C-3), 221.5 (C-17); ESI-MS 341 [M+H]⁺; Anal. Calcd. for C₂₂H₃₂N₂O C 77.60; H 9.47. Found C 77.55; H 9.48.

4.3. Cell lines

The ARE14 reporter cell line [20] (kindly gifted by prof. Zdeněk Dvořák from Palacky University Olomouc, Czech Republic) and the LNCaP cells (purchased from ECACC) were grown in RPMI-1640

medium. The 22Rv1, DuCaP, LAPC-4 cell lines (kindly gifted by prof. Zoran Culig, Innsbruck Medical University) and DU145 (purchased from ECACC) were grown in DMEM medium. All media were supplemented with 10% normal or charcoal-stripped fetal bovine serum (steroid-depleted serum), 100 IU/ml penicillin, 100 μ g/ml streptomycin, 4 mM glutamine and 1 mM sodium pyruvate. Cells were cultivated in a humidified incubator at 37 °C and in 5% CO₂ atmosphere.

4.4. AR transcriptional luciferase assay

ARE14 cells were seeded (40 000 cells/well) into the Nunc™ MicroWell™ 96-well optical flat-bottom plate (Thermo Fisher Scientific) for luciferase assay. The second day, the cultivation medium (supplemented with FBS) was discarded, and cells were washed with PBS. Cells were then incubated in presence of analysed compounds dissolved in medium supplemented with CSS (agonist mode) or CSS with 1 nM R1881 (antagonist mode), including CSS and 1 nM R1881 controls. Upon 24 h of incubation, cells were washed with PBS again and lysed for 10 min in a lysis buffer (10 mM Tris pH = 7.4, 2 mM DCTA, 1% nonidet P40, 2 mM DTT) at 37 °C. Next, reaction buffer (20 mM tricine pH = 7.8, 1.07 mM MgSO₄ · 7H₂O, 5 mM ATP, 9.4 μ M luciferin) was added and the luminescence of the samples was measured using a Tecan M200 Pro microplate reader (Biotek).

4.5. Cell viability assay

Cells were seeded into the 96-well tissue culture plates, the other day, solutions of compounds were added in different concentrations in duplicate for 72 h. Upon treatment, the resazurin solution (Sigma Aldrich) was added for 4 h, and then the fluorescence of resorufin was measured at 544 nm/590 nm (excitation/emission) using a Fluoroskan Ascent microplate reader (Labsystems). Percentual viability was calculated and in the separate experiment, GI₅₀ value was calculated from the dose response curves that resulted from the measurements using GraphPad Prism 5.

4.6. Colony formation assay

PCa cells 22Rv1 and DU-145 (5000 cells per well), LAPC-4 and PC-3 (10 000 cells per well) were seeded into 6-well plates. After two days of cultivation, the medium was replaced with fresh medium containing different concentrations of the compounds. Cells were cultivated for 10 days at the presence of compounds. After the treatment, the medium was discarded and colonies were fixed with 70% ethanol for 15 min, washed with PBS and stained with crystal violet (1% solution in 96% ethanol) for 1 h. Finally, wells were washed with PBS and colonies' photograph was captured.

4.7. Immunoblotting

After all treatments, cells were harvested by centrifugation, washed twice with PBS, pelleted and kept frozen at –80 °C. Pellets were thawed, resuspended in ice-cold RIPA lysis buffer supplemented with phosphatase and protease inhibitors. Ultrasound sonication (10 s with 30% amplitude) of cells was performed on ice and soluble proteins in supernatants we obtained by centrifugation at 14.000g for 30 min. Protein concentration in supernatants was measured and balanced within samples. Proteins were denatured by addition of SDS-loading buffer, separated by SDS-PAGE and electroblotted onto nitrocellulose membranes. Immunodetection of proteins was performed as usual, membranes were blocked in BSA solution, incubated overnight with primary antibodies, washed and incubated with secondary antibodies conjugated with peroxidase. Then, peroxidase activity was detected by SuperSignal West Pico reagents (Thermo Scientific) using a CCD camera LAS-4000 (Fuji-film). Primary antibodies purchased from Merck (anti- α -tubulin, clone DM1A; anti-phosphorylated AR (S81)). Primary antibodies purchased

from Santa Cruz Biotechnology (anti- β -actin, clone C4). Specific antibodies purchased from Cell Signalling Technology (anti-AR, clone D6F11; anti-PSA/KLK3, clone D6B1; anti-Nkx3.1, clone D2Y1A); anti-rabbit secondary antibody (porcine anti-rabbit immunoglobulin serum); anti-mouse secondary antibody (rabbit anti-mouse IgG, clone D3V2A)). All antibodies were diluted in 4% BSA and 0.1% Tween 20 in TBS.

4.8. Analyses of mRNA expression

Cells were treated and harvested into lysis buffer and total RNA was isolated using RNeasy plus mini kit (QIAGEN) based on the manufacturer's instruction. RNA concentration and purity was evaluated using DeNovix DS-11 spectrophotometer, while quality of RNA was determined by gel electrophoresis (high-quality samples displayed intact ribosomal RNA). The RNA (0.5–1 μ g) of those samples was used for reverse transcription into first-strand cDNA which was carried out by SensiFast cDNA Synthesis Kit (Bioline). RNA Spike I template (TATAA) was used as a transcriptional inhibition control. Quantitative RT-PCR was performed on CFX96 Real-Time PCR Detection System (Biorad) with a SensiFAST SYBR No-Rox Kit (Bioline). The suitable primers were designed using Primer-BLAST [28] and synthesized by Generi Biotech. Primary data were analysed using Bio-rad CFX Maestro 2.2. Relative gene expression levels were determined using $\Delta\Delta$ Ct method [29]. Expressions were normalized per *ACTB* and *SDHA* genes which were selected as the most stable by Bio-rad CFX Maestro 2.2.

Used primers:

ACTB (F: GCACCACACCTTCTACAAT; R: GTCTCAAACATGATCTGGT);

AR-FL (F: TTCGCCCTGATCTGGTTTT; R: TGCCTCATTCGGACACACTG);

KLK3 (F: CCACACCCGCTCTACGATATG; R: GGAGGTCCACACACTGAAGTT);

SDHA (F: TACAAGGTGCGGATTGATGA; R: GTTTTGTGCGATCAGGGTCT).

4.9. Molecular docking

Molecular docking was performed with the crystal structure of AR-antagonist model. The 3D structures of all compounds were obtained and their energy was minimized by molecular mechanics with Avogadro 1.90.0, a software used for the drawing and characterization of chemical structures. Polar hydrogens were added to ligands and proteins with the AutoDock Tools program [30] and docking studies were performed using AutoDock Vina 1.05 [31]. Interaction between ligand and amino acid residues were modelled in PLIP software [32]. Figures were generated in Pymol ver. 2.0.4 (Schrödinger, LLC).

4.10. Ex vivo tissue culture

This pilot study was approved by the Ethical Committee of the University Hospital Olomouc (Ref. No. 127/14) and all five patients signed an informed consent. Prostate tissue from radical prostatectomy was examined by a pathologist and a small piece of PCa lesion was selected for a short time *ex vivo* culture according to the recently optimized protocol [33]. Briefly, PCa tissue was cut into 300 μ m slices on vibratome Leica VT1200S (Leica Biosystems). One slice was fixed in 10% formaldehyde at time 0 (T0) as a control. Two slices for each treatment were put on 70 μ m pores strainer (MACS SmartStrainer, Miltenyi Biotec) in a tissue culture plate with 1.5 ml of 10% DMEM medium supplemented with 10% fetal bovine serum, 4 mM glutamine, 100 IU/ml penicillin, 100 μ g/ml streptomycin, and 1 mM sodium pyruvate, 5 μ g/ml insulin, 0.5 μ g/ml hydrocortisone, 0.05 μ g/ml EGF and enriched with tested compounds or DMSO as vehicle. *Ex vivo* cultures were incubated in standard conditions (37 °C, 5% CO₂) on a 3D Mini-Shaker (BioSan) that provided continuous mixing for 72 h. The slices were then fixed in 10% formalin and FFPE blocks were prepared.

Standard hematoxylin-eosin staining and immunohistochemistry for AR (antibody clone AR441, Dako, dilution 1:25), and Ki-67 (antibody clone MIB1, Dako, dilution 1:200) were performed. Protein expression was assessed semiquantitatively by a pathologist using the histoscore method where the percentage of positive cells (0–100%) was multiplied by staining intensity (0–3), which resulted in a final histoscore between 0 and 300. Ki67 staining at the end-point confirmed the proliferation of cancer cells in the slice.

4.11. AR-LBD preparation and micro-scale thermophoresis (MST) measurements

AR-LBD (with His₆-tag) was expressed using recombinant plasmid pET-15b-hAR-663-919, which was a generous gift from Elizabeth Wilson (Addgene plasmid # 89083) and expression bacteria BL21(DE3) pLysS similar to the original protocol [34]. Cells were grown in LB medium, the expression was induced by 0.1 mM isopropyl thiogalactopyranoside and suspension was further cultivated overnight at 18 °C. Cells were resuspended in lysis buffer (25 mM Tris, 300 mM NaCl, pH 8.0, 5 mM DTT, supplemented with protease inhibitors and 1% Nonidet P-40), lysed using a sonicator and lysate was clarified by centrifugation at 19 000 g for 30 min at 4 °C. The purification was performed on Ni²⁺-metal affinity-Sepharose column (His-Bind, Merck), pre-equilibrated with 25 mM Tris, 300 mM NaCl, pH 8.0, 5 mM DTT and 50 mM imidazole. Column was thoroughly washed with the equilibration buffer and with 100 mM imidazole in the equilibration buffer, subsequently. Elution was performed by 500 mM imidazole in 25 mM Tris, 300 mM NaCl, pH 8.0, 5 mM DTT. The buffer from elution fraction was exchanged to storage buffer (25 mM Tris, 300 mM NaCl, pH 8.0, 5 mM DTT) without imidazole and concentrated up to 0.5 mg/ml using centrifugal filter unit with 10 kDa cutoff (Merck). MST method was used to prove binding of **3d** in the AR-LBD, which was labelled with the His-Tag Labeling Kit RED-tris-NTA (NanoTemper) (100 nM dye + 800 nM His-tagged protein) for 30 min. The labelled protein was used for MST measurements with or without **3d** in final concentration of 400 nM His-tagged protein in the storage buffer, supplemented with 0.1% Tween. Measurements were done on a Monolith NT.115 instrument (NanoTemper Technologies).

Funding

The publication was funded by the University of Szeged Open Access Fund (FundRef, Grant No. 5950). The authors gratefully acknowledge financial support from the Palacký University Olomouc (IGA_PrF_2022_007 and LF_2022_004), from the Czech Ministry of Education, Youth and Sports via the project National Institute for Cancer Research (Programme EXCELES, ID Project No. LX22NPO5102 funded by the European Union – Next Generation EU), and from the Czech Ministry of Health (grants NU20-03-00201 and DRO (FNOL, 00098892)).

Declaration of competing interest

The authors declare that they have no known competing financial interests or personal relationships that could have appeared to influence the work reported in this paper.

Data availability

Data will be made available on request.

Acknowledgement

We would like to thank Jakub Bělíček and Veronika Vojáčková for their technical assistance.

Appendix A. Supplementary data

Supplementary data to this article can be found online at <https://doi.org/10.1016/j.ejmech.2023.115086>.

References

- [1] K. Coffey, C.N. Robson, Regulation of the androgen receptor by post-translational modifications, *J. Endocrinol.* 215 (2012) 221–237.
- [2] T. van der Steen, D.J. Tindall, H. Huang, Posttranslational modification of the androgen receptor in prostate cancer, *Int. J. Mol. Sci.* 14 (2013) 14833–14859.
- [3] S. Saranyutanon, S.K. Srivastava, S. Pai, S. Singh, A.P. Singh, Therapies targeted to androgen receptor signaling axis in prostate cancer: progress, challenges, and hope, *Cancers* 12 (2019).
- [4] T. Uo, S.R. Plymate, C.C. Sprenger, The potential of AR-V7 as a therapeutic target, *Expert Opin. Ther. Targets* 22 (2018) 201–216.
- [5] Z. Culig, J. Hoffmann, M. Erdel, I.E. Eder, A. Hobisch, A. Hittmair, G. Bartsch, G. Utermann, M.R. Schneider, K. Parczyk, H. Klocker, Switch from antagonist to agonist of the androgen receptor bicalutamide is associated with prostate tumour progression in a new model system, *Br. J. Cancer* 81 (1999) 242–251.
- [6] E. Jernberg, A. Bergh, P. Wikstrom, Clinical relevance of androgen receptor alterations in prostate cancer, *Endocr. Connect.* 6 (2017) R146–R161.
- [7] X. Han, L. Zhao, W. Xiang, C. Qin, B. Miao, T. Xu, M. Wang, C.Y. Yang, K. Chinnaswamy, J. Stuckey, S. Wang, Discovery of highly potent and efficient PROTAC degraders of androgen receptor (AR) by employing weak binding affinity VHL E3 ligase ligands, *J. Med. Chem.* 62 (2019) 11218–11231.
- [8] S. Kregel, C. Wang, X. Han, L. Xiao, E. Fernandez-Salas, P. Bawa, B.L. McCollum, K. Wilder-Romans, I.J. Apel, X. Cao, C. Speers, S. Wang, A.M. Chinnaiyan, Androgen receptor degraders overcome common resistance mechanisms developed during prostate cancer treatment, *Neoplasia* 22 (2020) 111–119.
- [9] J. Salami, S. Alabi, R.R. Willard, N.J. Vitale, J. Wang, H. Dong, M. Jin, D. P. McDonnell, A.P. Crew, T.K. Neklesa, C.M. Crews, Androgen receptor degradation by the proteolysis-targeting chimera ARCC-4 outperforms enzalutamide in cellular models of prostate cancer drug resistance, *Commun. Biol.* 1 (2018) 100.
- [10] W. Xiang, L. Zhao, X. Han, C. Qin, B. Miao, D. McEachern, Y. Wang, H. Metwally, P. D. Kirchhoff, L. Wang, A. Matvekas, M. He, B. Wen, D. Sun, S. Wang, Discovery of ARD-2585 as an exceptionally potent and orally active PROTAC degrader of androgen receptor for the treatment of advanced prostate cancer, *J. Med. Chem.* 64 (2021) 13487–13509.
- [11] N. Shibata, K. Nagai, Y. Morita, O. Ujikawa, N. Ohoka, T. Hattori, R. Koyama, O. Sano, Y. Imaeda, H. Nara, N. Cho, M. Naito, Development of protein degradation inducers of androgen receptor by conjugation of androgen receptor ligands and inhibitor of apoptosis protein ligands, *J. Med. Chem.* 61 (2018) 543–575.
- [12] B. Dale, M. Cheng, K.S. Park, H.U. Kaniskan, Y. Xiong, J. Jin, Advancing targeted protein degradation for cancer therapy, *Nat. Rev. Cancer* 21 (2021) 638–654.
- [13] H. Xie, J. Liu, D.M. Alem Glison, J.B. Fleming, The clinical advances of proteolysis targeting chimeras in oncology, *Explor. Target Antitumor. Ther.* 2 (2021) 511–521.
- [14] D. Kovacs, J. Wolfling, N. Szabo, M. Szecsi, Z. Schelz, I. Zupko, E. Frank, Synthesis of novel 17-(4'-formyl)pyrazolylandrosta-5,16-dienes and their derivatives as potent 17 α -hydroxylase/C17,20-lyase inhibitors or antiproliferative agents depending on the substitution pattern of the heteroring, *Eur. J. Med. Chem.* 120 (2016) 284–295.
- [15] Y.Z. Ling, J.S. Li, Y. Liu, K. Kato, G.T. Klus, A. Brodie, 17-Imidazolyl, pyrazolyl, and isoxazolyl androstene derivatives. Novel steroidal inhibitors of human cytochrome C17,20-lyase (P450(17 α)), *J. Med. Chem.* 40 (1997) 3297–3304.
- [16] A. Bajji, F. Kovacs, G. Motyan, G. Schneider, J. Wolfling, I. Sinka, I. Zupko, I. Ocsovszki, E. Frank, Investigation of pH and substituent effects on the distribution ratio of novel steroidal ring D- and A-fused arylpyrazole regioisomers and evaluation of their cell-growth inhibitory effects in vitro, *Steroids* 126 (2017) 35–49.
- [17] G. Motyan, M.K. Gopisetty, R.E. Kiss-Faludy, A. Kulmany, I. Zupko, E. Frank, M. Kiricsi, Anti-cancer activity of novel dihydrotestosterone-derived ring A-condensed pyrazoles on androgen non-responsive prostate cancer cell lines, *Int. J. Mol. Sci.* 20 (2019) 2170.
- [18] M.A. Kiss, M. Perina, V. Bazgier, N.V. May, A. Bajji, R. Jorda, E. Frank, Synthesis of dihydrotestosterone derivatives modified in the A-ring with (hetero)arylidene, pyrazolo[1,5-a]pyrimidine and triazolo[1,5-a]pyrimidine moieties and their targeting of the androgen receptor in prostate cancer, *J. Steroid Biochem. Mol. Biol.* 211 (2021), 105904.
- [19] A. Nakhai, J. Bergman, Synthesis of hydrogenated indazole derivatives starting with α,β -unsaturated ketones and hydrazine derivatives, *Tetrahedron* 65 (2009) 2298–2306.
- [20] I. Bartonkova, A. Novotna, Z. Dvorak, Novel stably transfected human reporter cell line AIZ-AR as a tool for an assessment of human androgen receptor transcriptional activity, *PLoS One* 10 (2015), e0121316.
- [21] T. Siciliano, I.H. Simons, A.K. Beier, C. Ebersbach, C. Aksoy, R.I. Seed, M.B. Stope, C. Thomas, H.H.H. Erb, A systematic comparison of antiandrogens identifies androgen receptor protein stability as an indicator for treatment response, *Life* 11 (2021).
- [22] A.K. Kwegyir-Afful, S. Ramalingam, P. Purushottamachar, V.P. Ramamurthy, V. C. Njar, Galeterone and VNPT55 induce proteasomal degradation of AR/AR-V7, induce significant apoptosis via cytochrome c release and suppress growth of castration resistant prostate cancer xenografts in vivo, *Oncotarget* 6 (2015) 27440–27460.
- [23] H.S. Soifer, N. Souleimanian, S. Wu, A.M. Voskresenskiy, F.K. Collak, B. Cinar, C. A. Stein, Direct regulation of androgen receptor activity by potent CYP17 inhibitors in prostate cancer cells, *J. Biol. Chem.* 287 (2012) 3777–3787.
- [24] S. Chen, S. Gulla, C. Cai, S.P. Balk, Androgen receptor serine 81 phosphorylation mediates chromatin binding and transcriptional activation, *J. Biol. Chem.* 287 (2012) 8571–8583.
- [25] J.W. Russo, X. Liu, H. Ye, C. Calagua, S. Chen, O. Voznesensky, J. Condulis, F. Ma, M.E. Taplin, D.J. Einstein, S.P. Balk, S. Chen, Phosphorylation of androgen receptor serine 81 is associated with its reactivation in castration-resistant prostate cancer, *Cancer Lett.* 438 (2018) 97–104.
- [26] J. Wahl, M. Smiesko, Endocrine disruption at the androgen receptor: employing molecular dynamics and docking for improved virtual screening and toxicity prediction, *Int. J. Mol. Sci.* 19 (2018).
- [27] C.E. Bohl, Z. Wu, D.D. Miller, C.E. Bell, J.T. Dalton, Crystal structure of the T877A human androgen receptor ligand-binding domain complexed to cyproterone acetate provides insight for ligand-induced conformational changes and structure-based drug design, *J. Biol. Chem.* 282 (2007) 13648–13655.
- [28] J. Ye, G. Coulouris, I. Zaretskaya, I. Cutcutache, S. Rozen, T.L. Madden, Primer-BLAST: a tool to design target-specific primers for polymerase chain reaction, *BMC Bioinf.* 13 (2012) 134.
- [29] K.J. Livak, T.D. Schmittgen, Analysis of relative gene expression data using real-time quantitative PCR and the 2(-Delta Delta C(T)) Method, *Methods* 25 (2001) 402–408.
- [30] G.M. Morris, R. Huey, W. Lindstrom, M.F. Sanner, R.K. Belew, D.S. Goodsell, A. J. Olson, AutoDock4 and AutoDockTools4: automated docking with selective receptor flexibility, *J. Comput. Chem.* 30 (2009) 2785–2791.
- [31] O. Trott, A.J. Olson, AutoDock Vina, Improving the speed and accuracy of docking with a new scoring function, efficient optimization, and multithreading, *J. Comput. Chem.* 31 (2010) 455–461.
- [32] M.F. Adasme, K.L. Linnemann, S.N. Bolz, F. Kaiser, S. Salentin, V.J. Haupt, M. Schroeder, PLIP 2021: expanding the scope of the protein-ligand interaction profiler to DNA and RNA, *Nucleic Acids Res.* 49 (2021) W530–W534.
- [33] W. Zhang, W.M. van Weerden, C.M.A. de Ridder, S. Erkens-Schulze, E. Schonfeld, T.G. Meijer, R. Kanaar, D.C. van Gent, J. Nonnekens, Ex vivo treatment of prostate tumor tissue recapitulates in vivo therapy response, *Prostate* 79 (2019) 390–402.
- [34] E.B. Askew, R.T. Gampe Jr., T.B. Stanley, J.L. Faggart, E.M. Wilson, Modulation of androgen receptor activation function 2 by testosterone and dihydrotestosterone, *J. Biol. Chem.* 282 (2007) 25801–25816, <https://doi.org/10.1074/jbc.M703268200>.

SUPPLEMENTARY INFORMATION

A-ring-fused pyrazoles of dihydrotestosterone targeting prostate cancer cells via the downregulation of the androgen receptor.

Miroslav Peřina^{1,‡}, Márton A. Kiss^{2,‡}, Gergő Mótyán², Eva Szczyrbová³, Martin Eliáš³, Vladimír Študent jr.⁴, Daniela Kurfurstová³, Markéta Kovalová¹, Lukáš Mada¹, Jan Bouchal³, Éva Frank^{2,*}
Radek Jorda^{1,*}

¹*Department of Experimental Biology, Faculty of Science, Palacký University Olomouc, Šlechtitelů 27, 78371 Olomouc, Czech Republic*

²*Department of Organic Chemistry, University of Szeged, Dóm tér 8, H-6720 Szeged, Hungary*

³*Department of Clinical and Molecular Pathology, Institute of Molecular and Translational Medicine, Palacký University Olomouc and University Hospital Olomouc, Hněvotínská 3, 77515 Olomouc, Czech Republic*

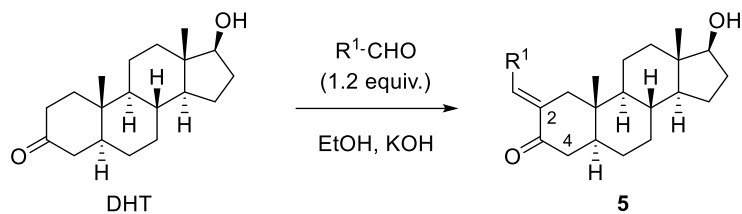
⁴*Department of Urology, Palacký University Olomouc and University Hospital Olomouc, I.P.Pavlova 6, 77900 Olomouc, Czech Republic*

[‡]These authors contributed equally to this work.

*Corresponding authors: radek.jorda@upol.cz; Tel.: +420 585 634 854;
frank@chem.u-szeged.hu; Tel.: +36 62 544 275

Table of contents

Scheme S1 Synthesis of 2-(hetero)arylidene derivatives of DHT	3
Figure S1 Partial 2D-NOESY spectrum of compound 8a	4
Figure S2 Partial 2D-NOESY spectrum of compound 9a	4
¹ H and ¹³ C NMR spectra of the synthesized compounds	5-31
Table S1 AR transcriptional activity in antagonist and agonist mode	32
Figure S3 Western blot of AR-regulated proteins in LAPC-4 upon treatment with compounds	34
Figure S4 Colony formation assay of LAPC-4 treated by series 1, 2, 8i-8k, 10i-10k , standards	35
Figure S5 Colony formation assay of LAPC-4 treated by series 3, 4, 8a-8h, 10a-10h	36
Figure S6 Dose dependent effect of 3d on AR-signalling in 22Rv1 and LNCaP	37
Figure S7 Antiproliferative activity of 3d in LAPC-4 (long time treatment, protein levels)	38
Figure S8 MST measurement of binding of 3d in AR-LBD	39
Figure S9 Antiproliferative activity of 3d on cell lines' panel	40
Figure S10 Cell cytometry of 22Rv1 cells after 48h treatment with 3d or bavdegalutamide	41
Figure S11 Relative normalized expression of AR in LAPC-4 cells	42
Figure S12 Images of Ki67 and AR immunostaining of tumor slices after 72 h <i>ex vivo</i> treatment	43



R¹: Ph (**a**); *p*-CH₃-C₆H₄ (**b**); *p*-MeO-C₆H₄ (**c**); *p*-F-C₆H₄ (**d**); *p*-Cl-C₆H₄ (**e**);
p-Br-C₆H₄ (**f**); furan-2-yl (**g**); thiophen-2-yl (**h**); *p*-OH-C₆H₄ (**i**); CH₃ (**j**)

Scheme S1. Synthesis of 2-(hetero)arylidene derivatives of DHT. *Reagents and conditions: ref. [18] for 5a–e, 5g and 5h; 0 °C, 3 h for 5f (86%); reflux, 16 h (with MOM-protected *p*-OH-phenol), then dil. HCl, MeOH (36% after two steps) for 5i; ref [17] for 5j.*

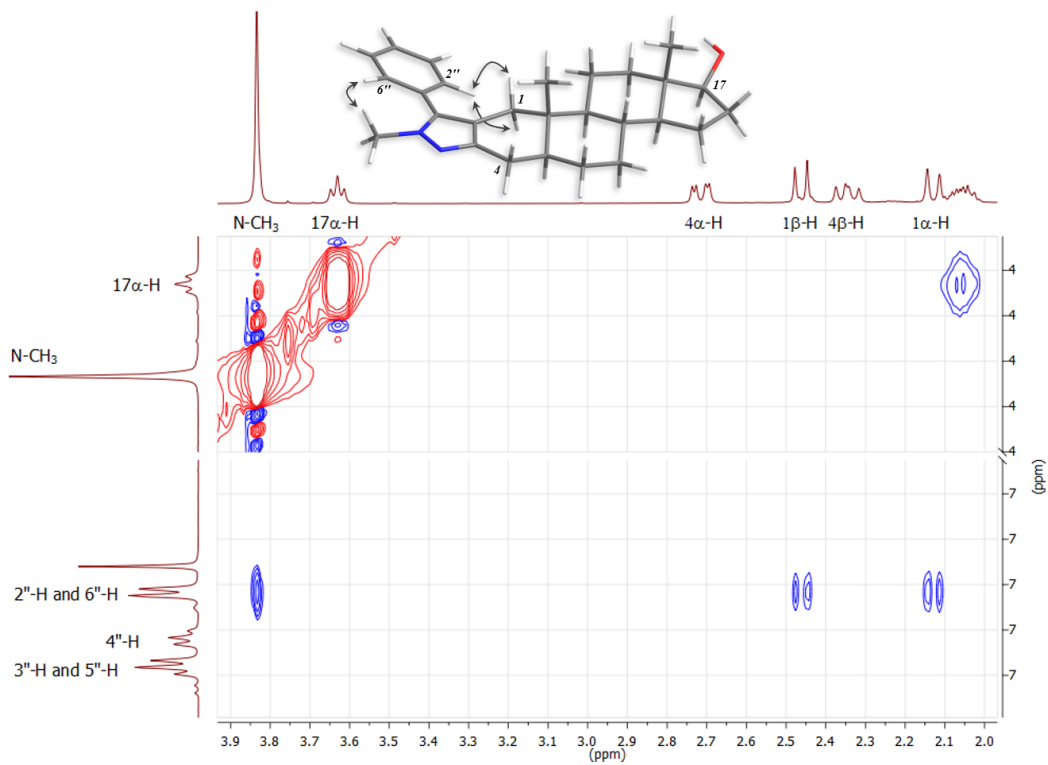


Figure S1. Partial 2D-NOESY spectrum of compound **8a** and the correlations between protons observed.

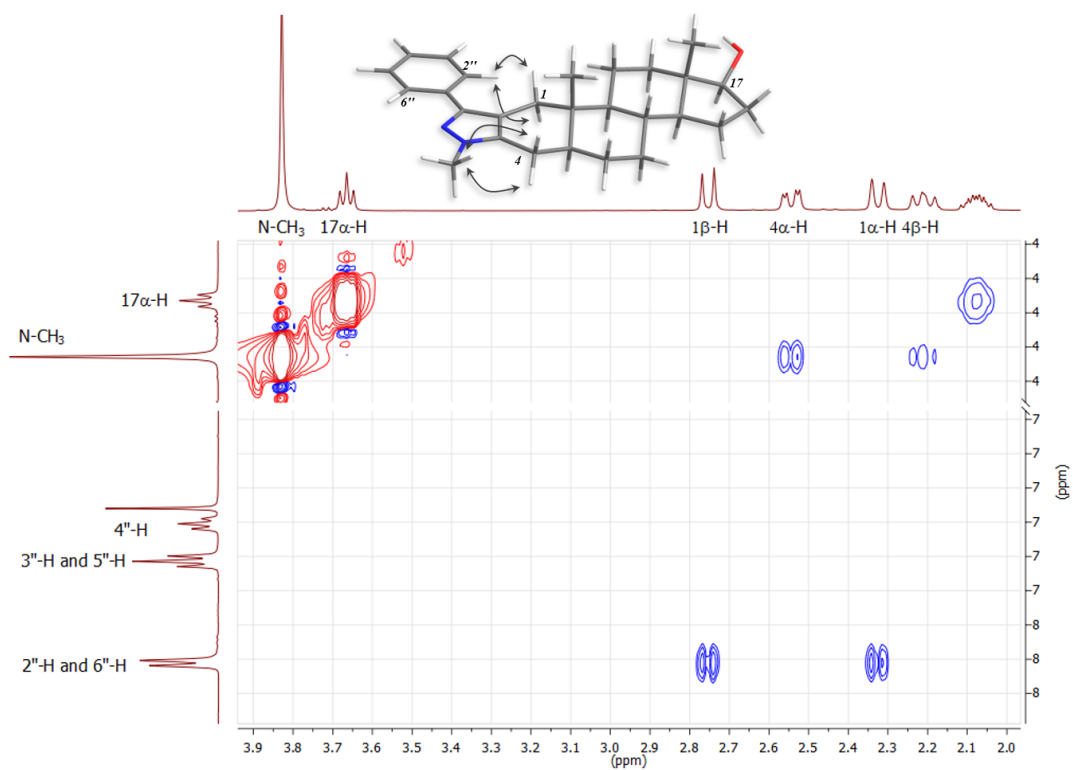
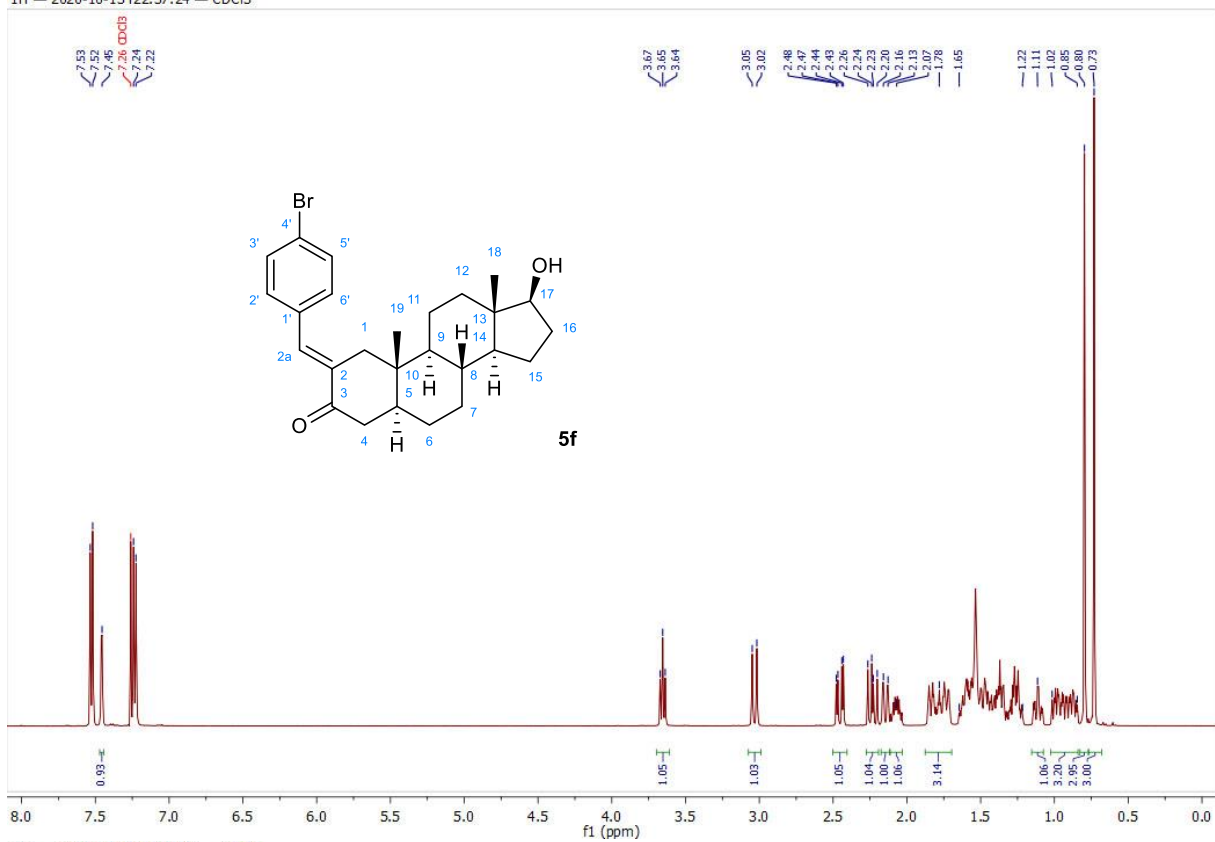


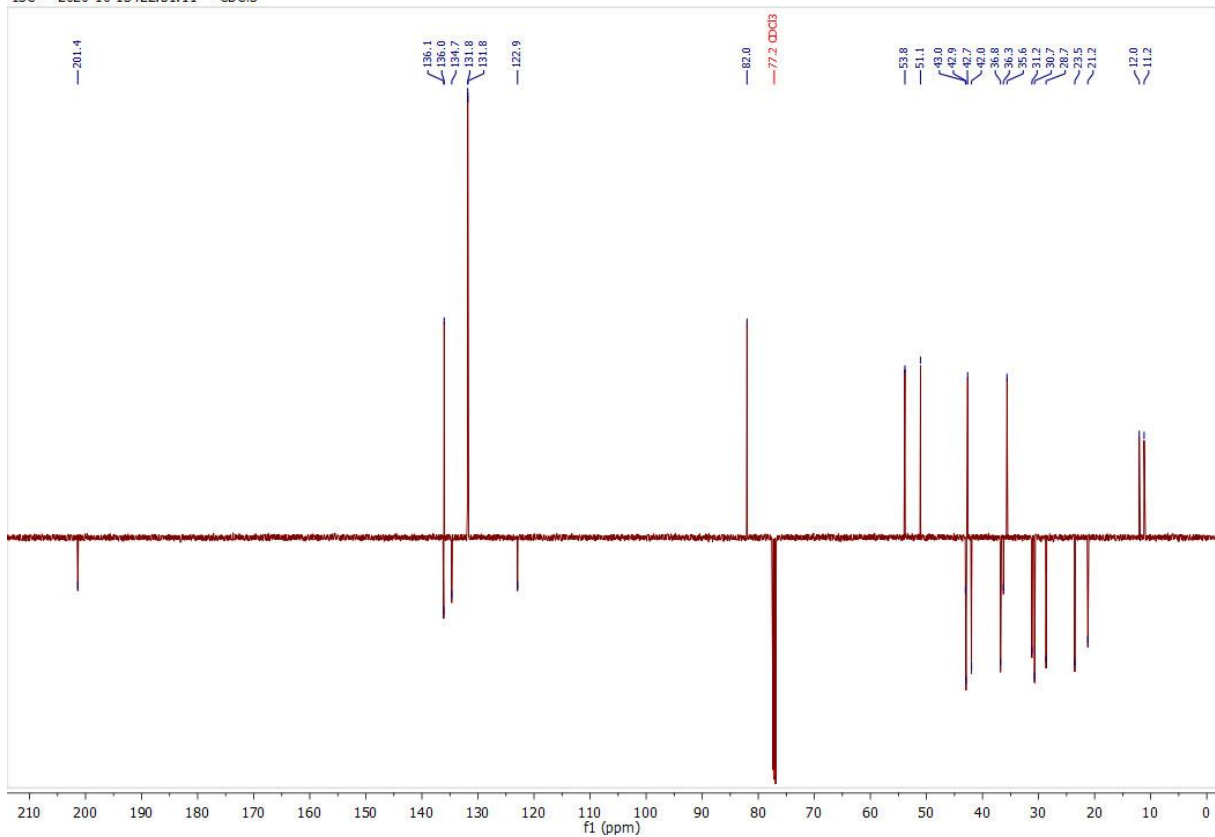
Figure S2. Partial 2D-NOESY spectrum of compound **9a** and the correlations between protons observed.

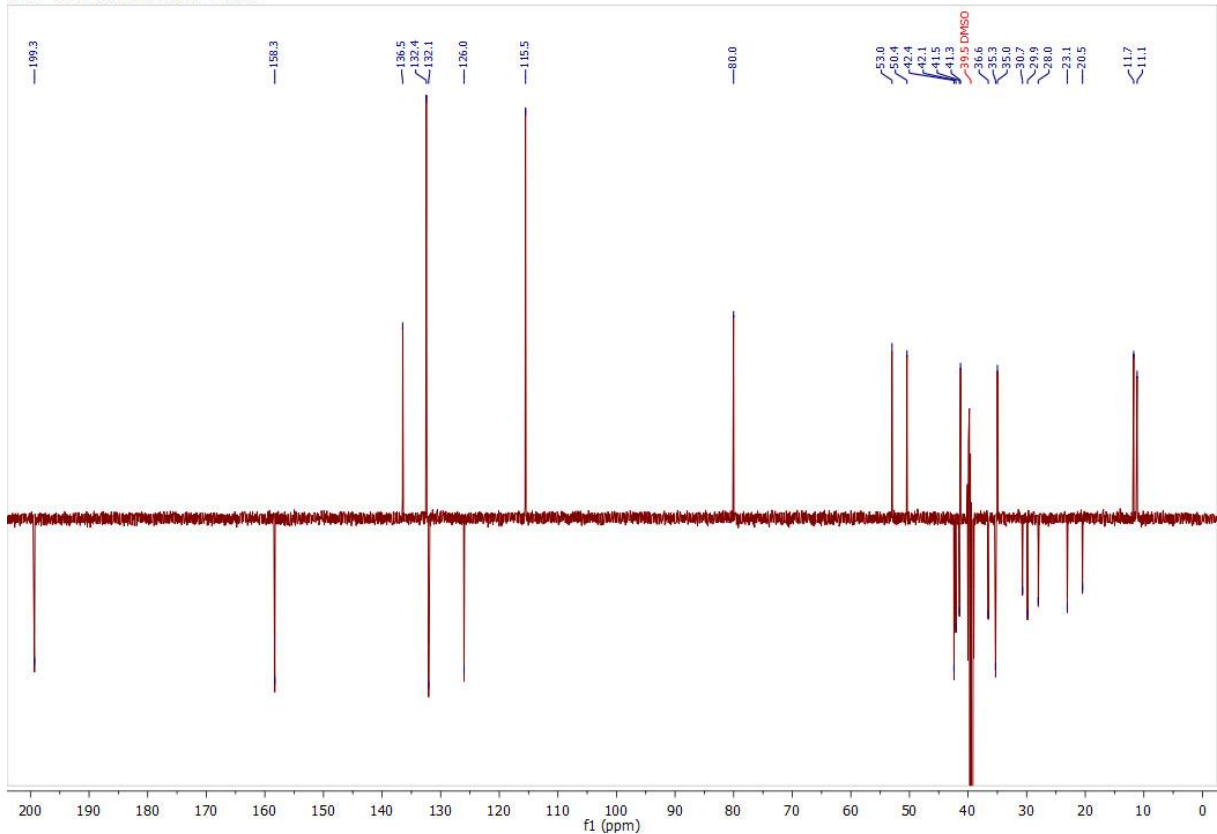
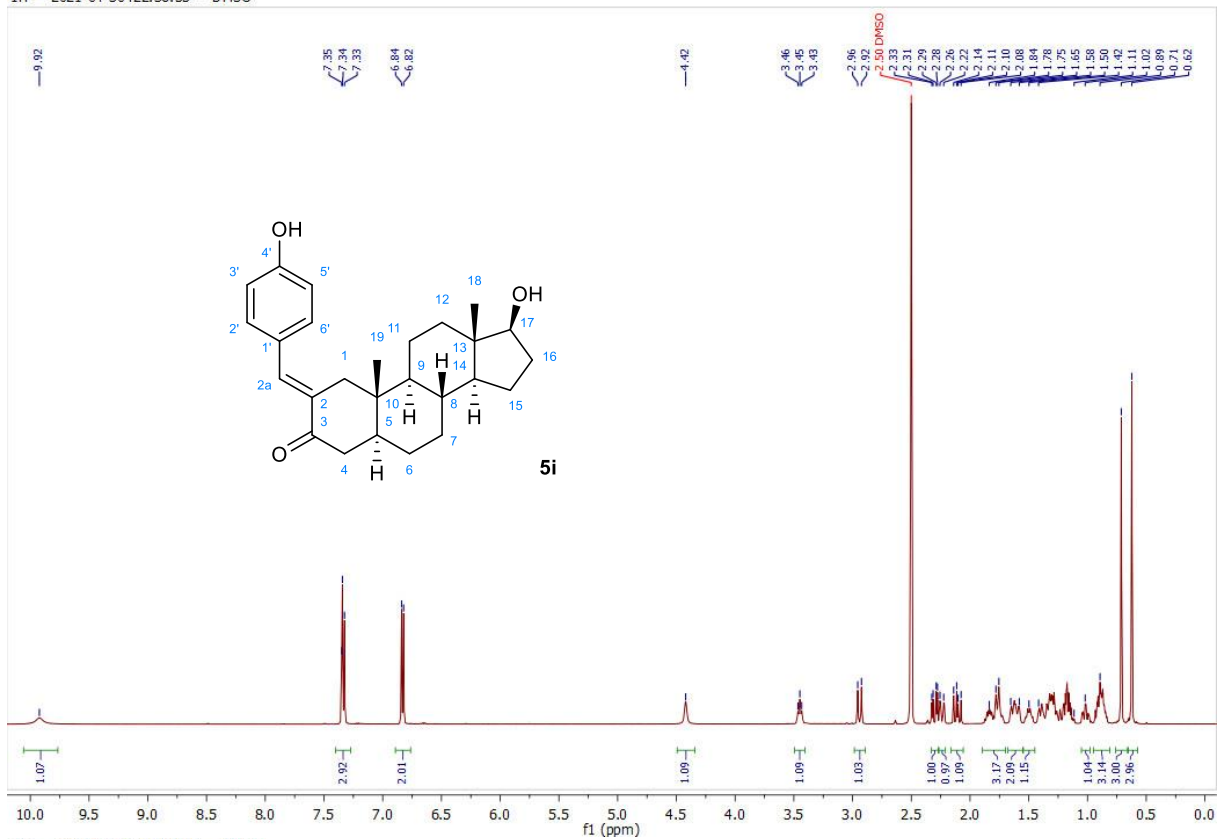
¹H and ¹³C NMR spectra of the synthesized compounds

¹H — 2020-10-13T22:37:24 — CDCl₃

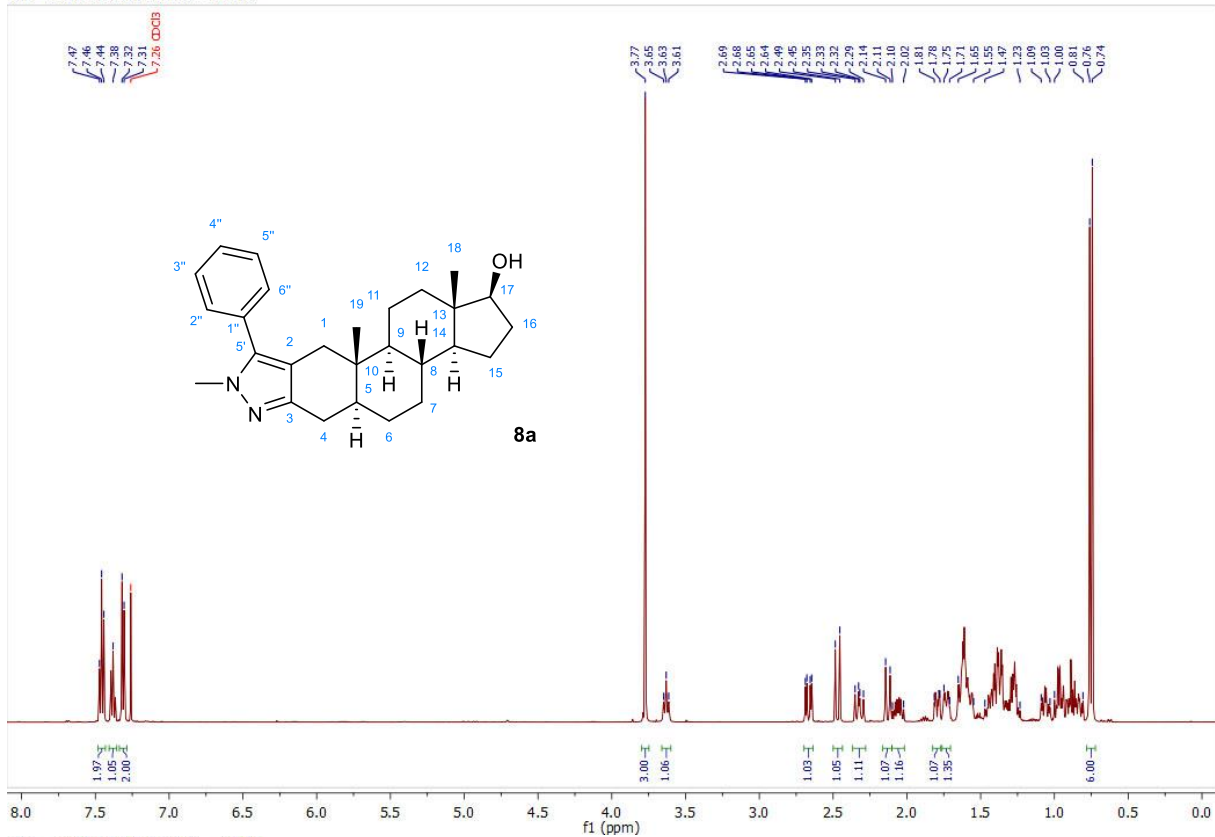


¹³C — 2020-10-13T22:51:11 — CDCl₃

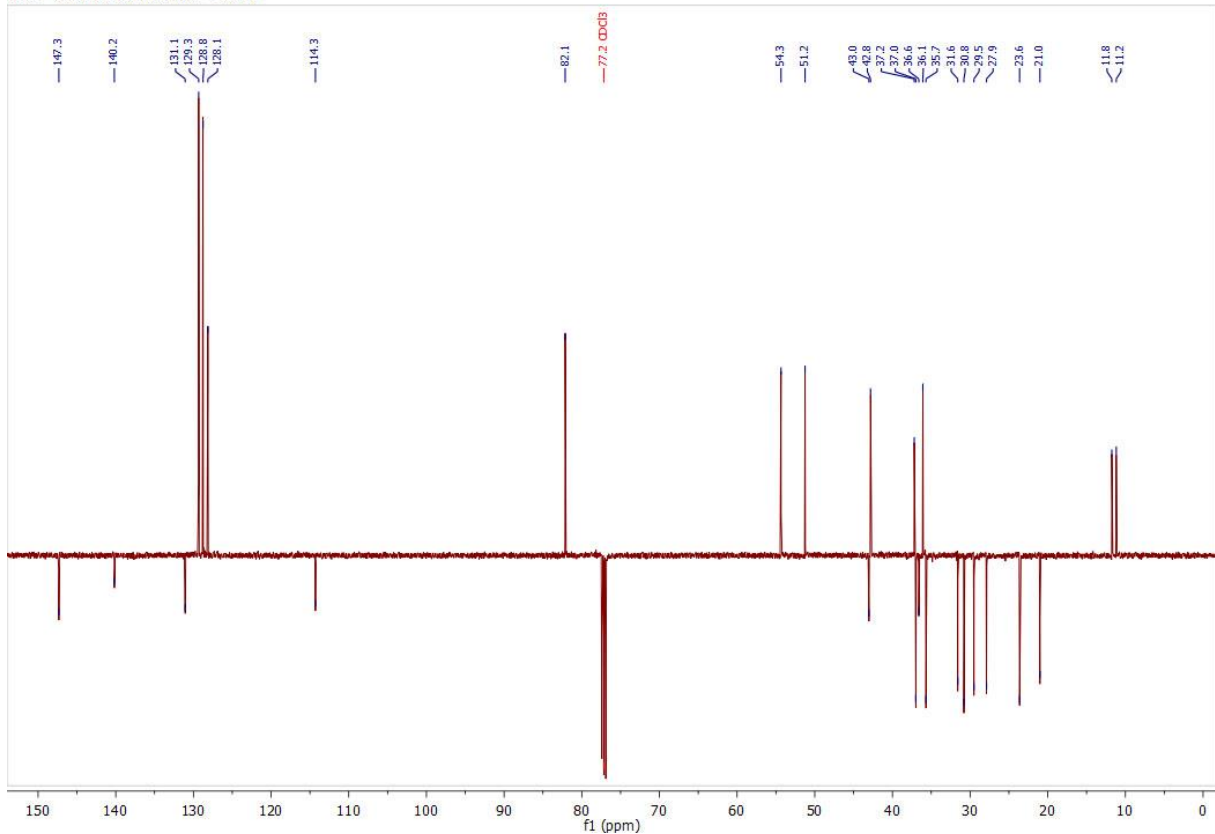




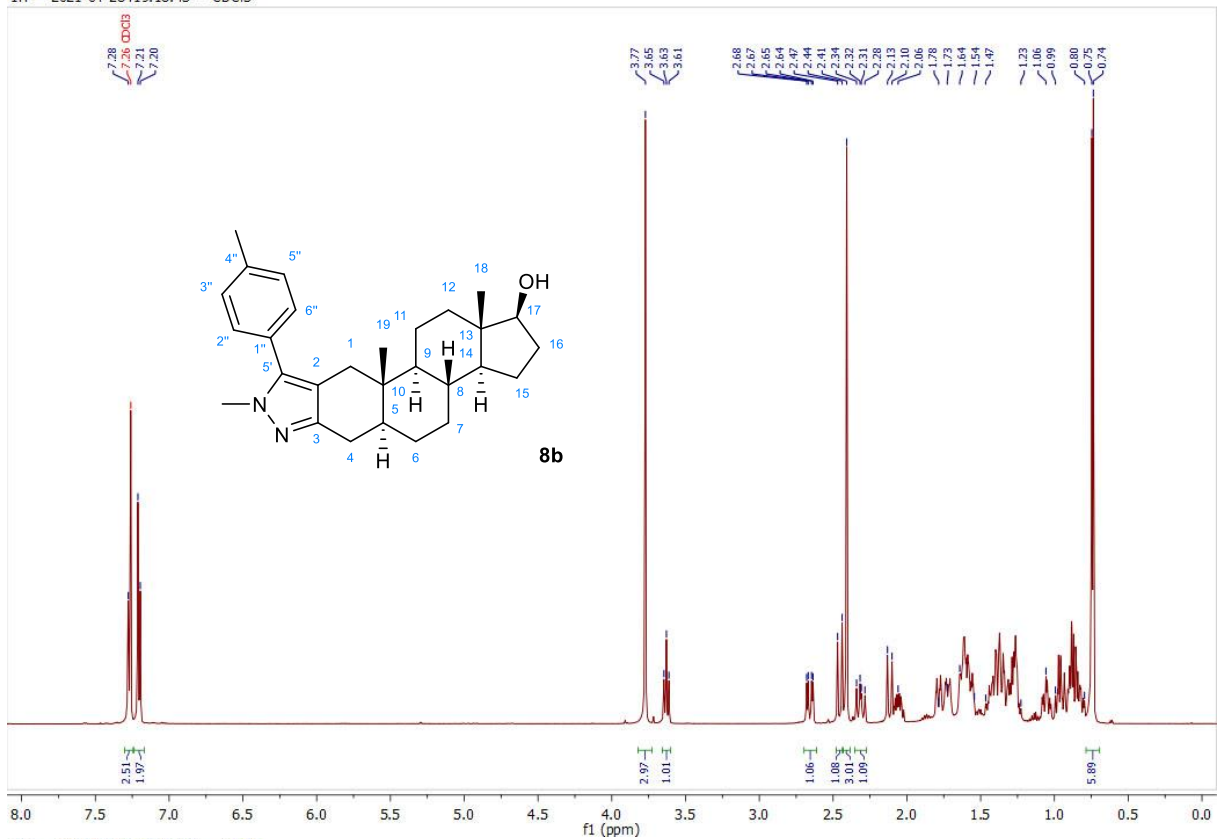
1H — 2020-11-14T13:00:19 — CDCl3



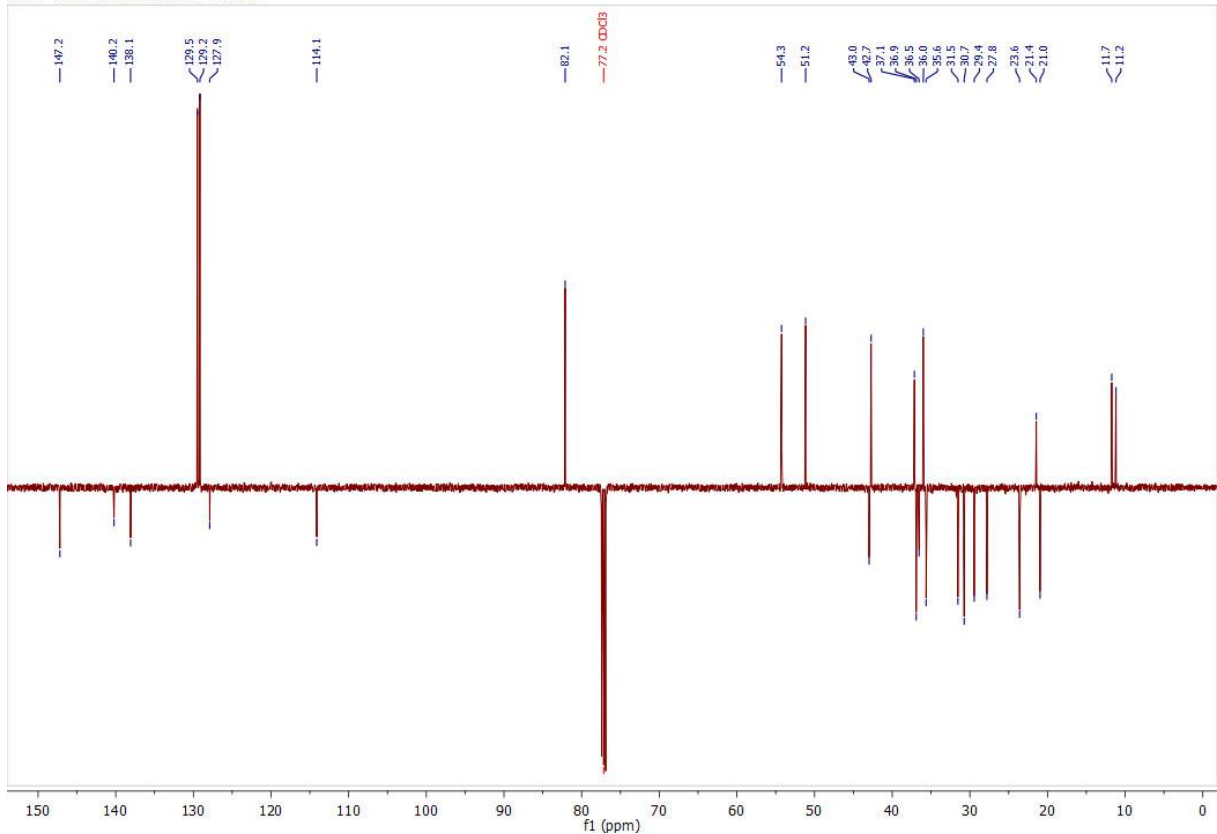
13C — 2020-11-14T13:13:57 — CDCl3



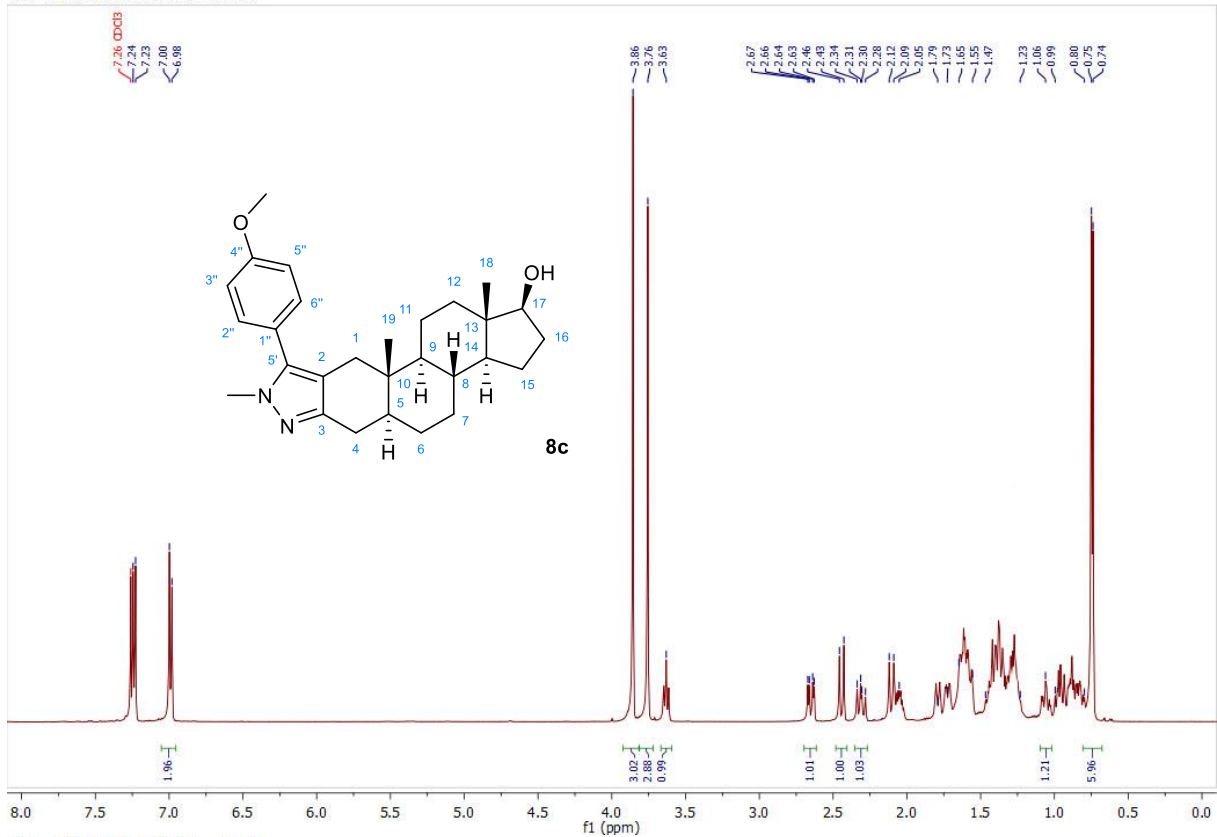
1H — 2021-04-28T19:18:43 — CDCl3



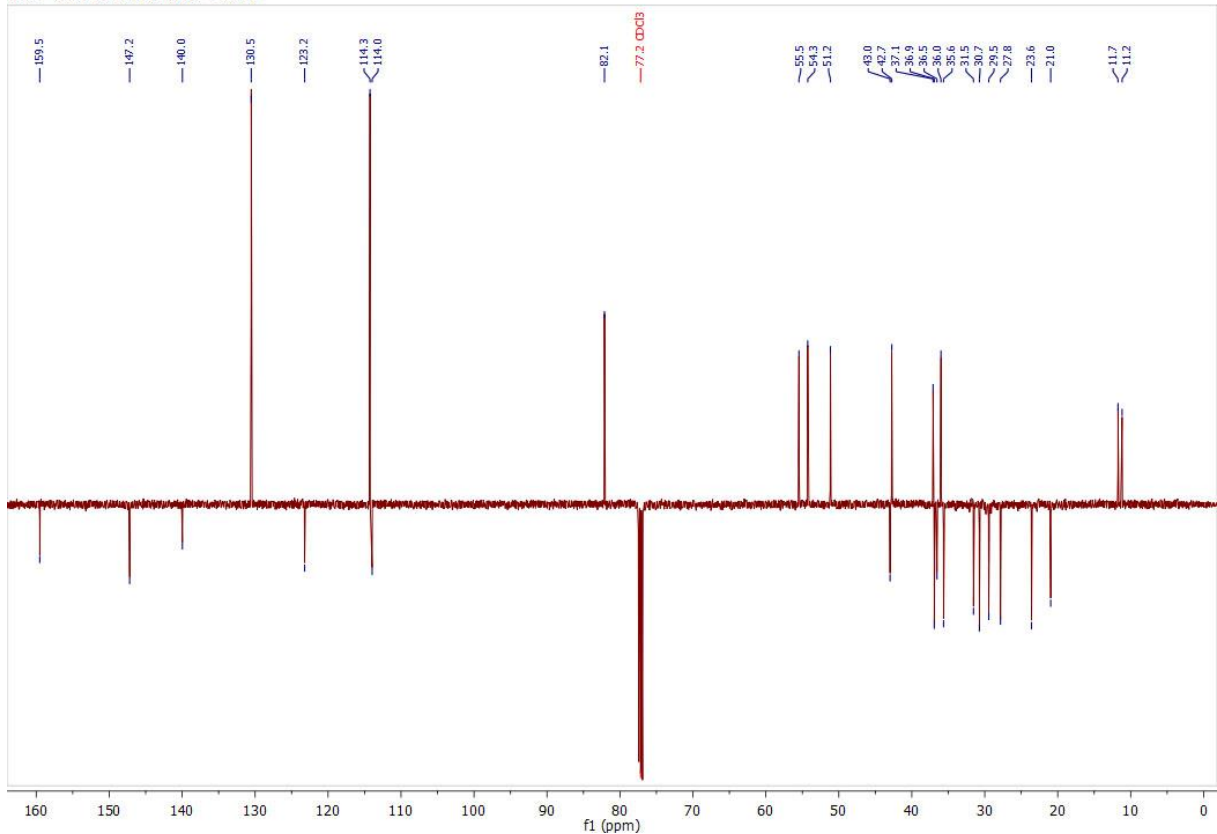
13C — 2021-04-28T19:32:20 — CDCl3



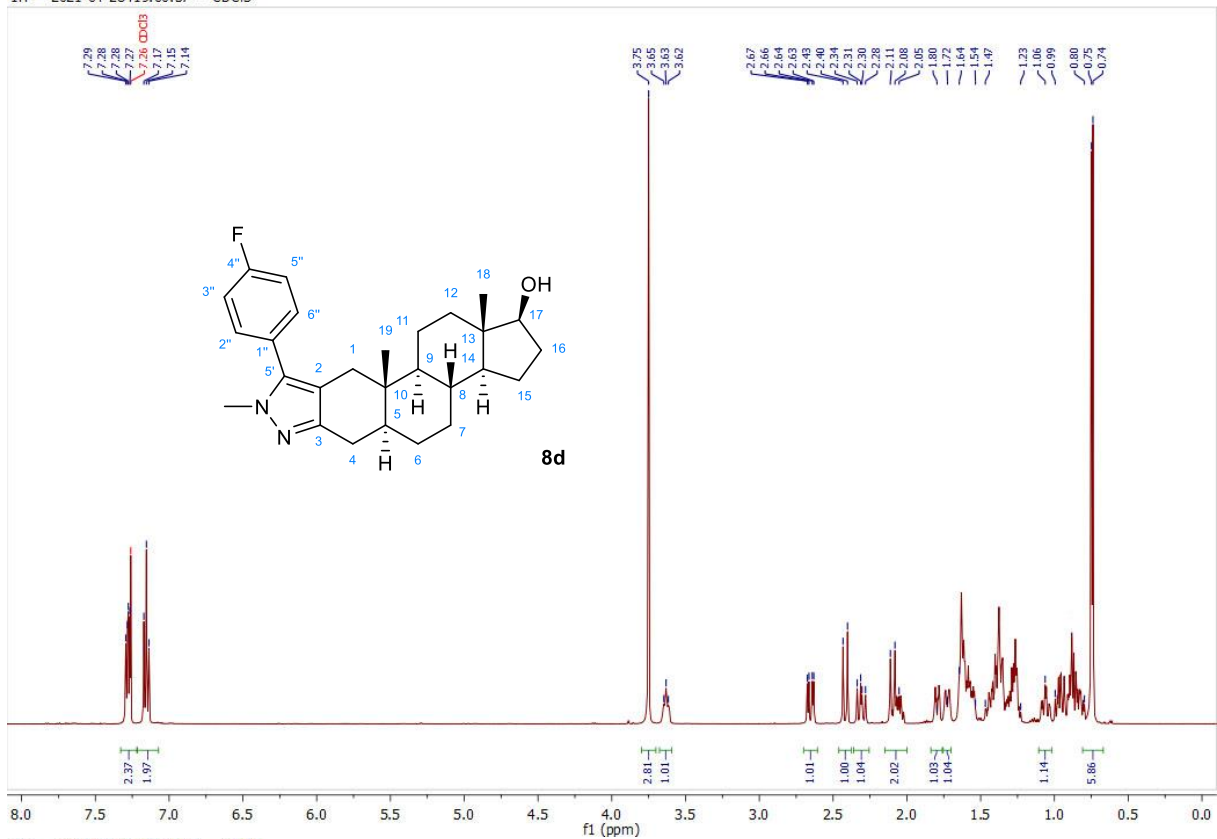
1H — 2021-04-28T21:25:25 — CDCl3



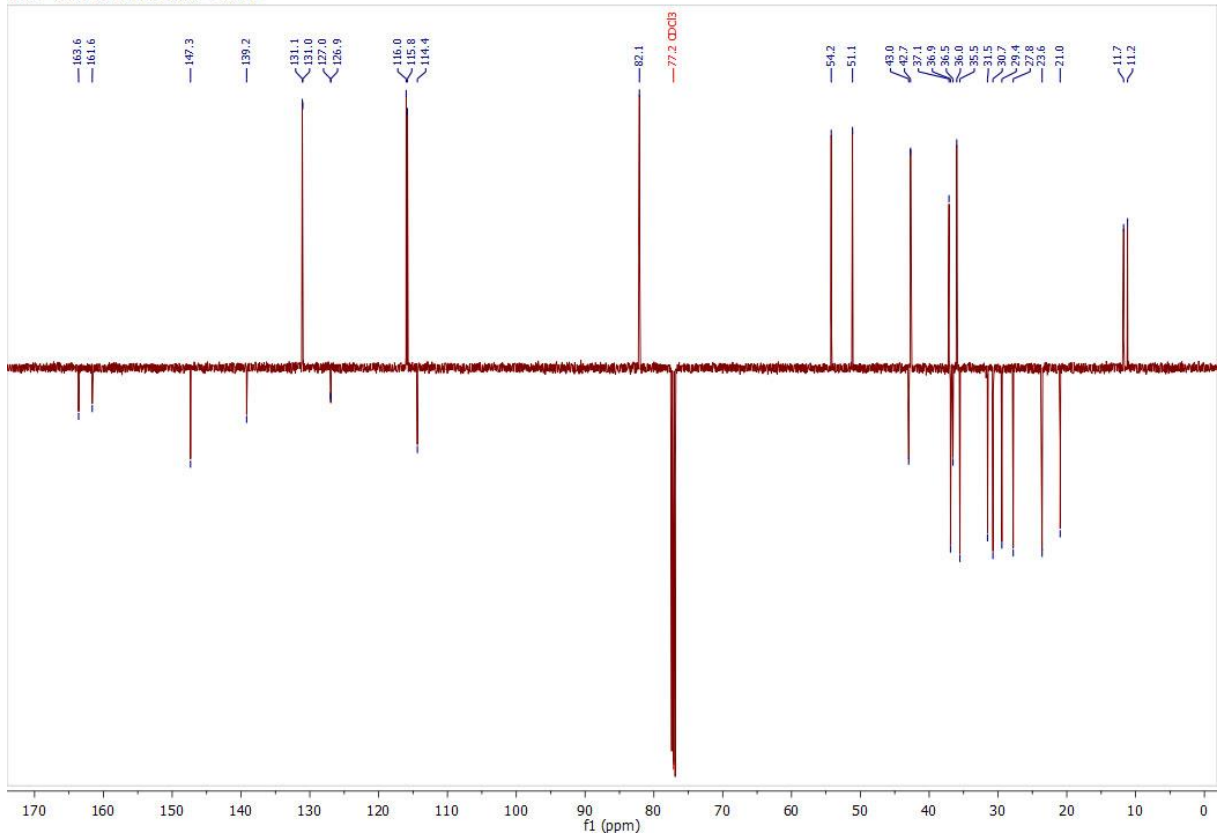
13C — 2021-04-28T21:39:02 — CDCl3

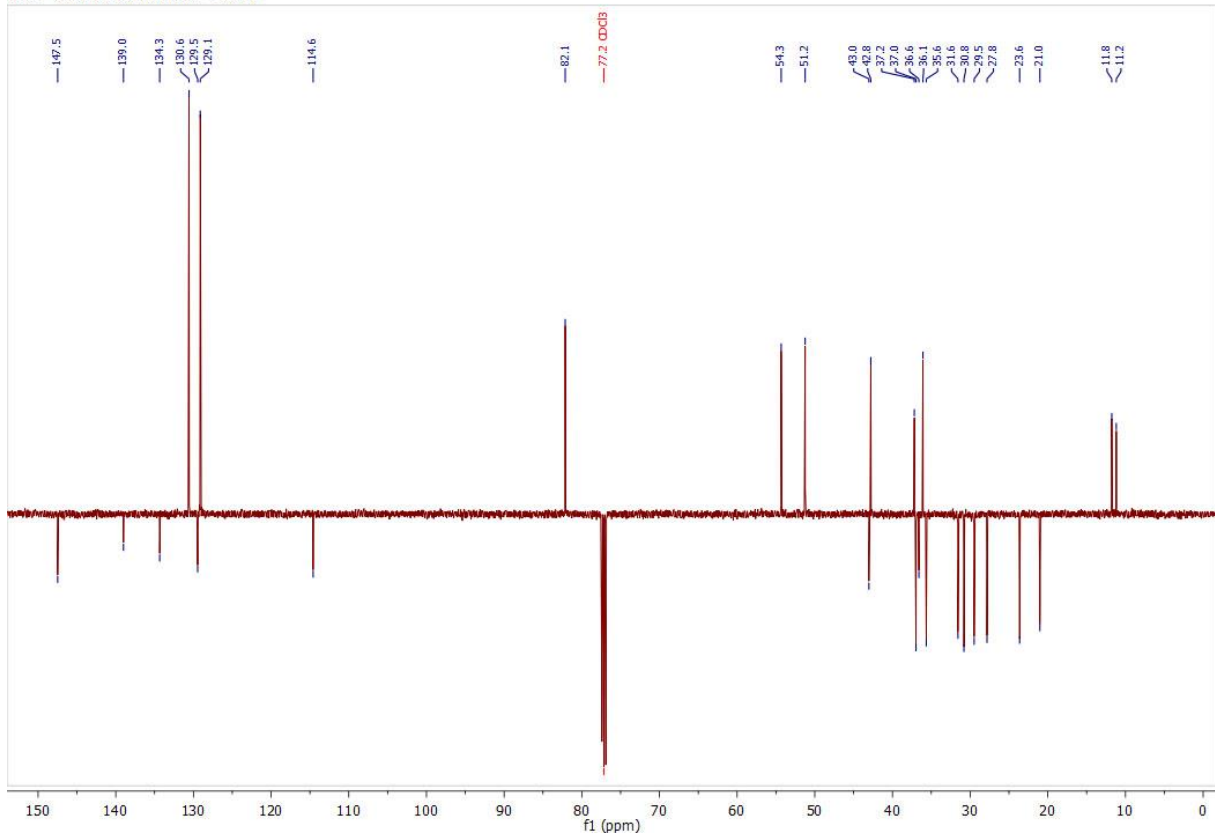
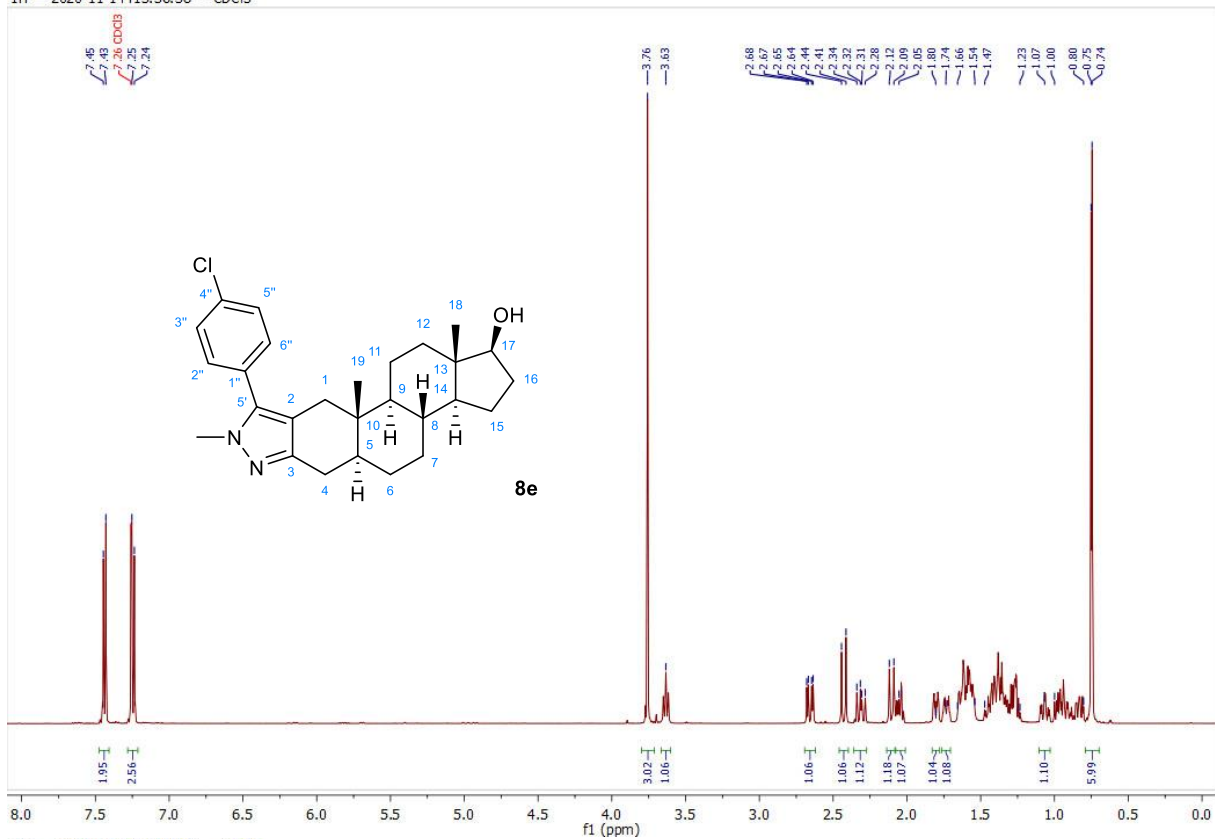


1H — 2021-04-28T19:00:57 — CDCl3

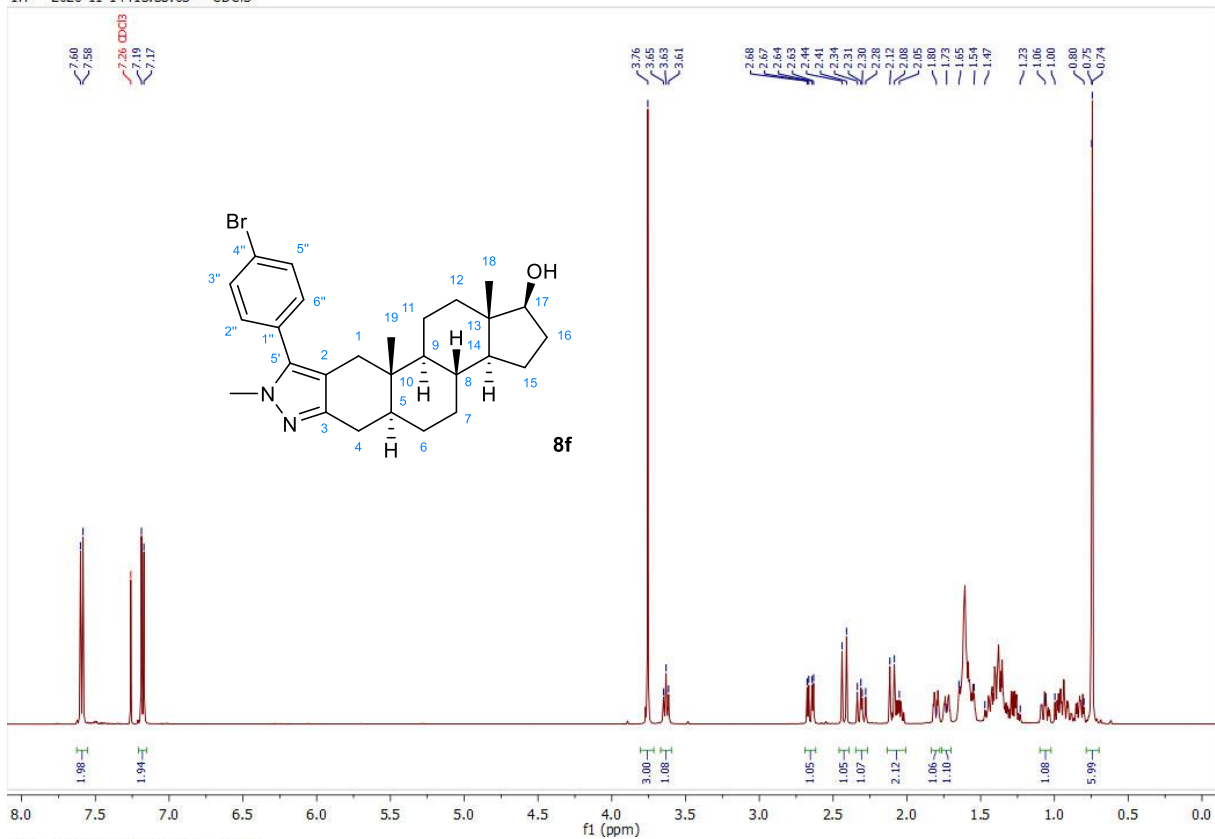


13C — 2021-04-28T19:14:35 — CDCl3

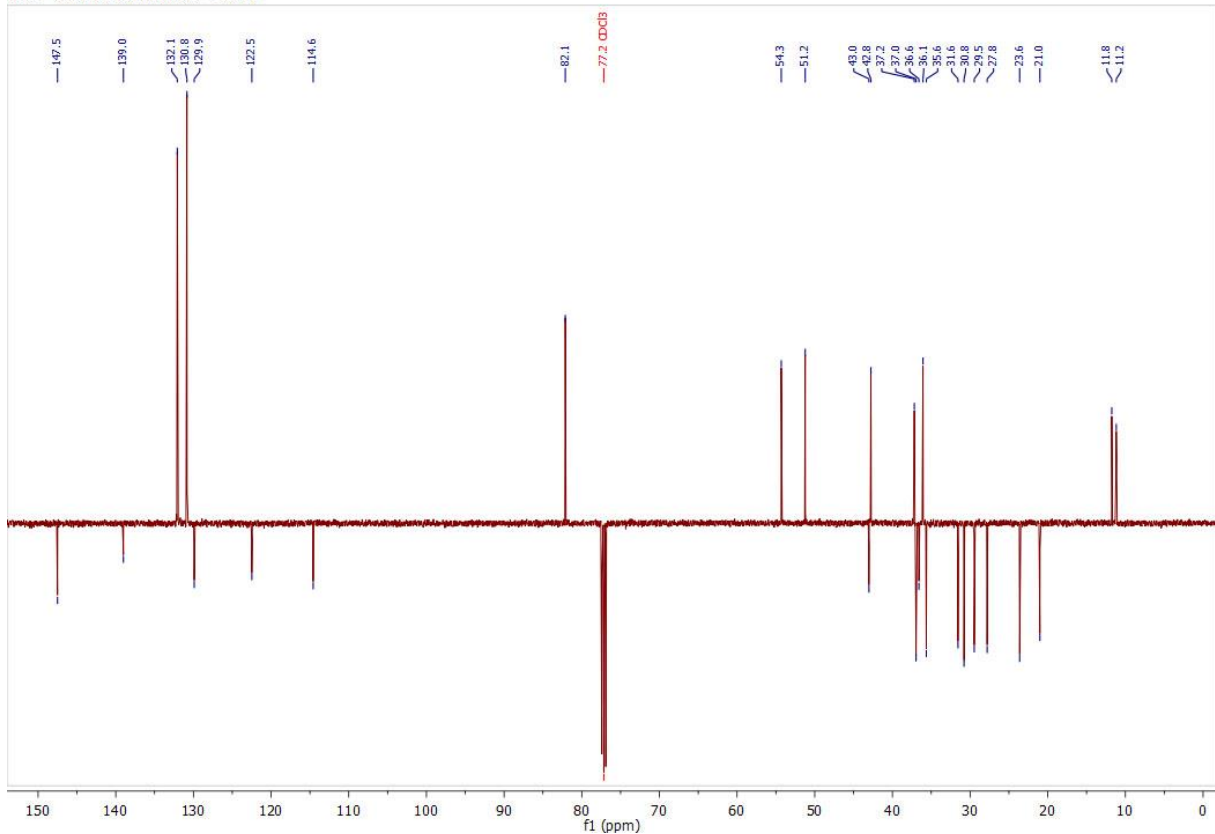




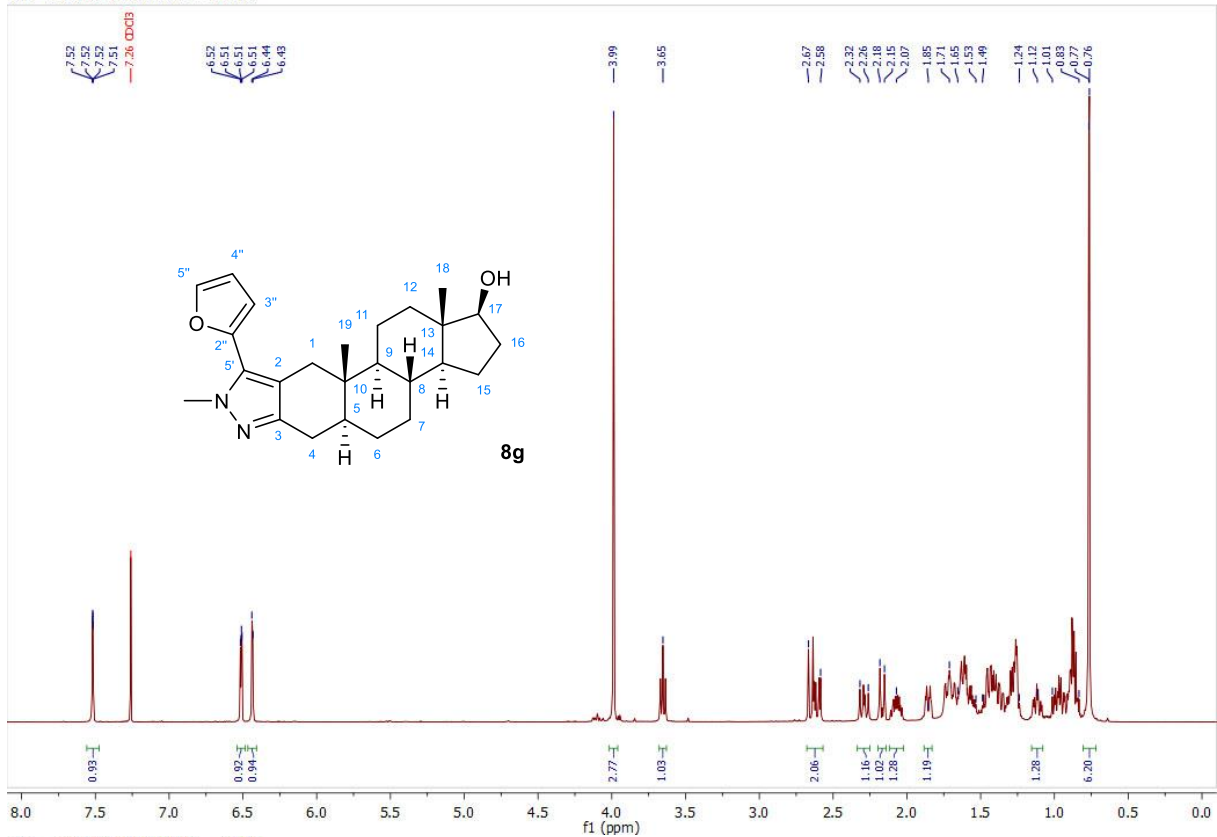
1H — 2020-11-14T13:55:03 — CDCl3



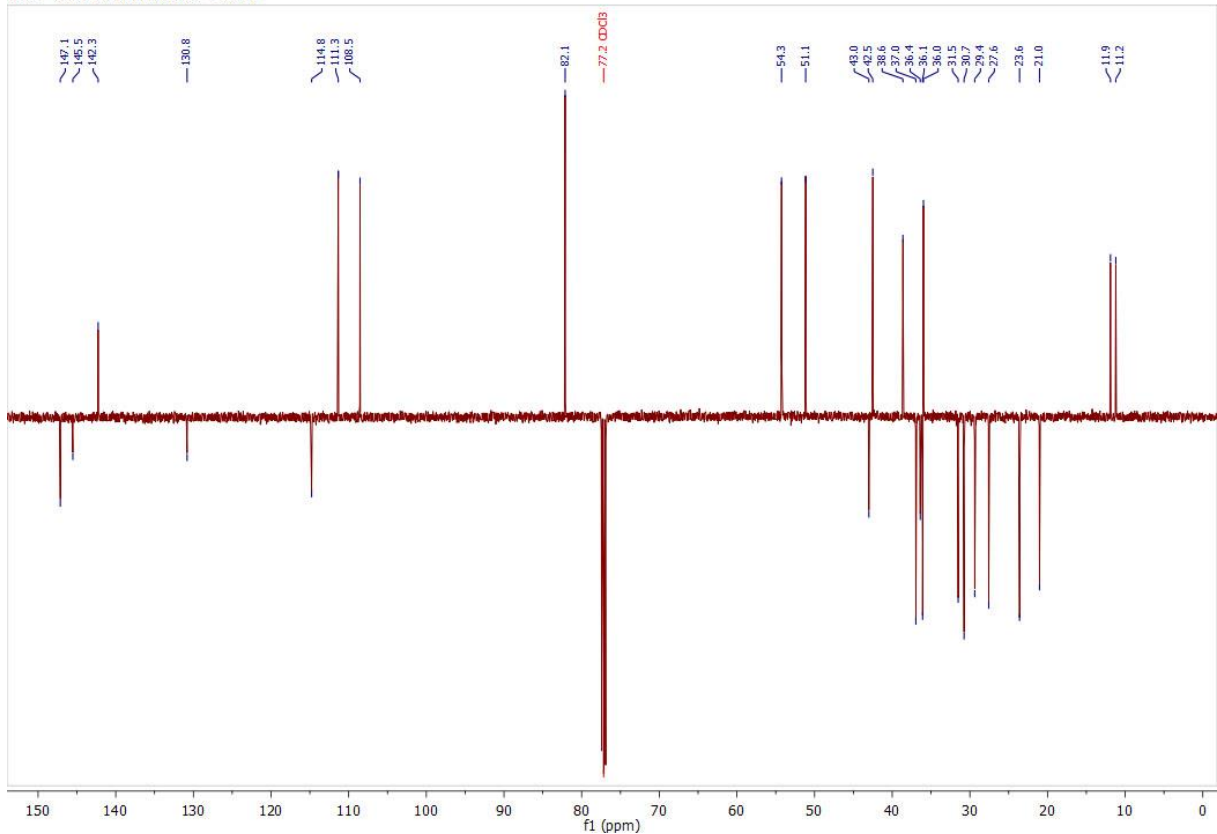
13C — 2020-11-14T14:08:53 — CDCl3



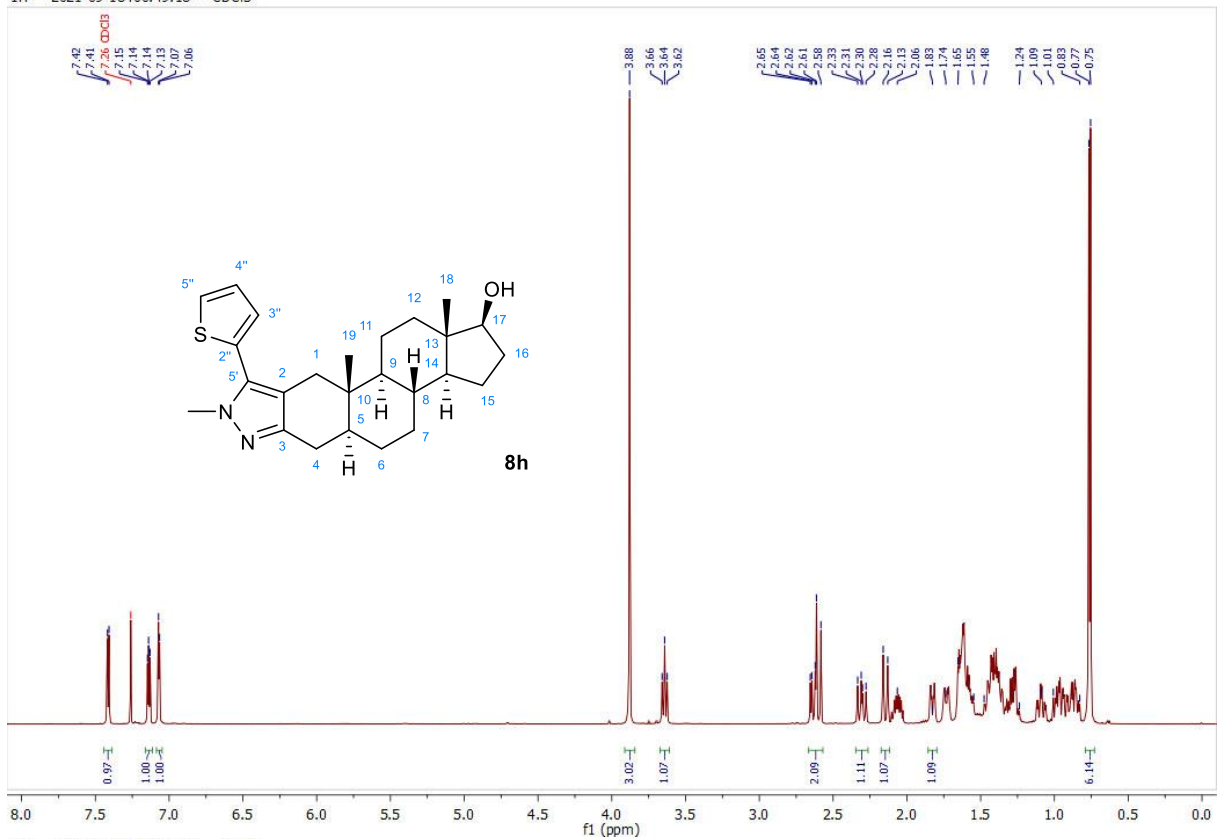
1H — 2021-02-13T18:06:57 — CDCl3



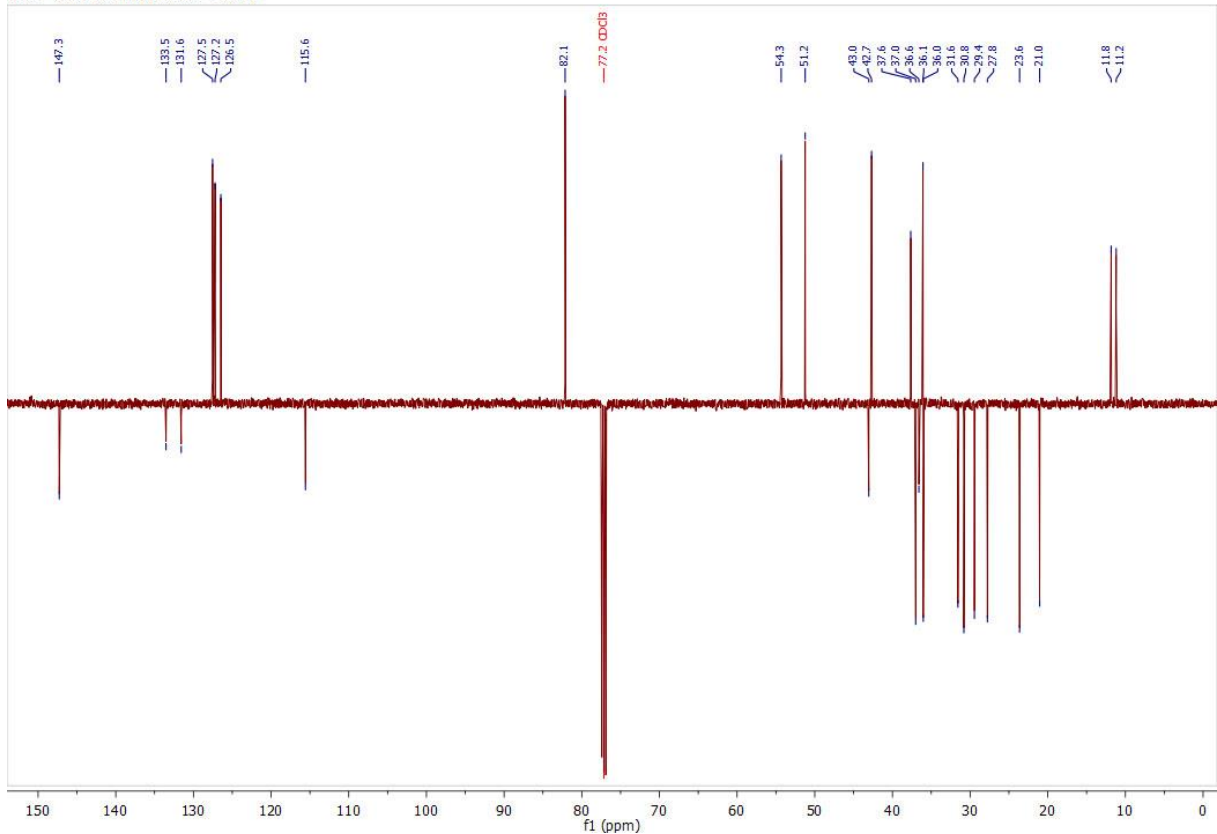
13C — 2021-02-13T18:20:32 — CDCl3



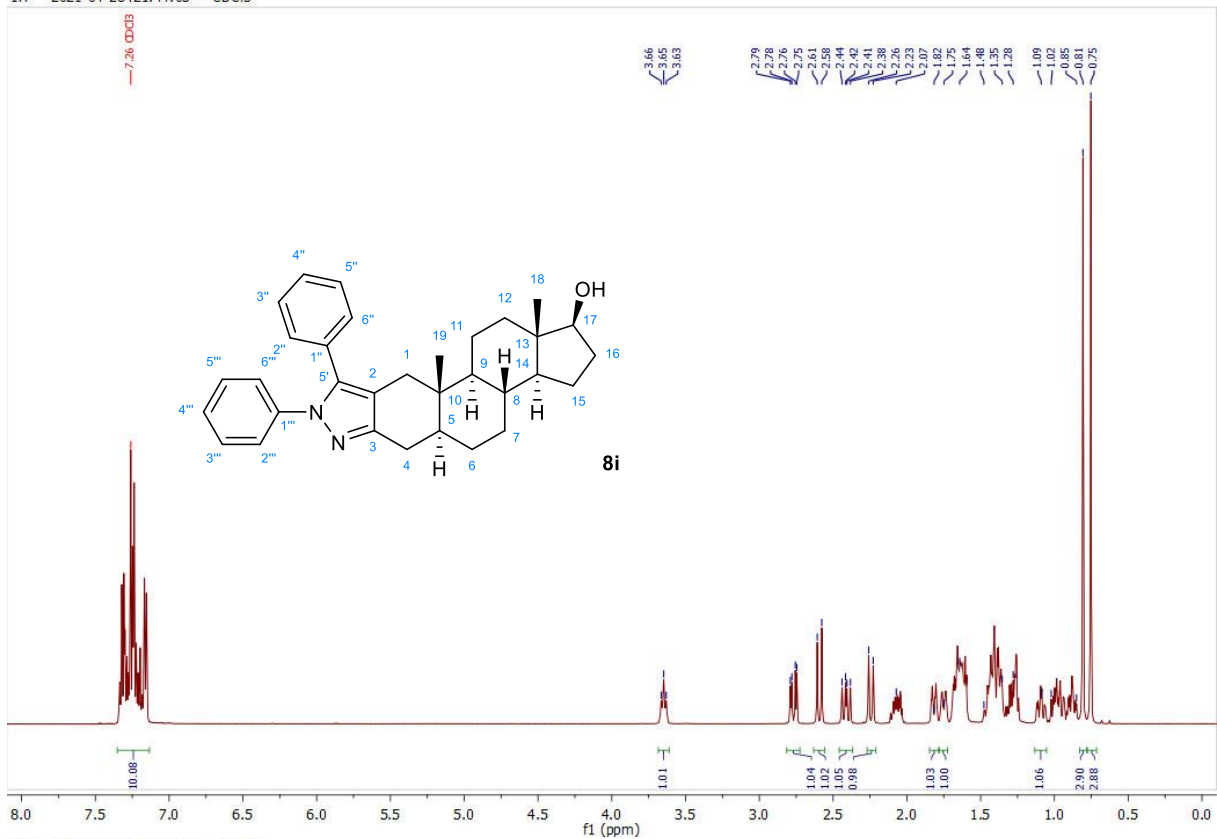
1H — 2021-09-18T00:49:18 — CDCl3



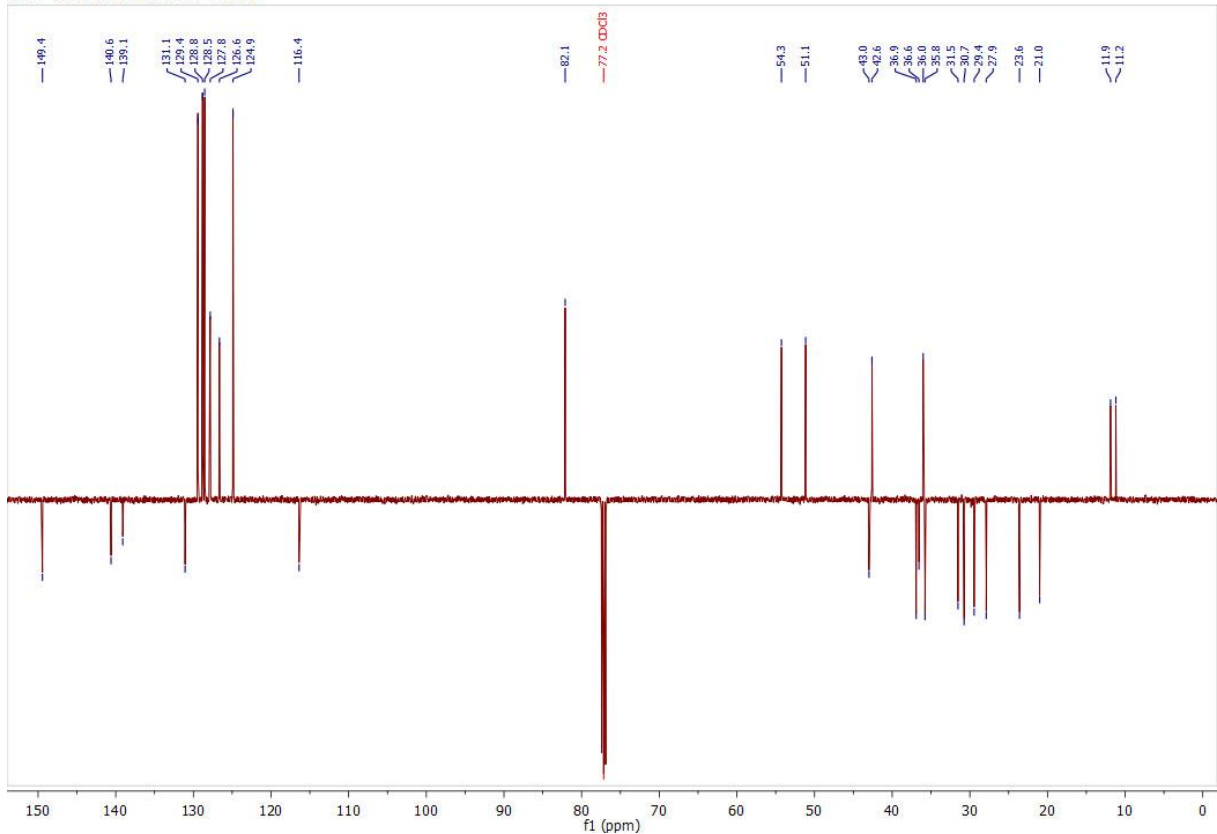
13C — 2021-09-18T01:03:06 — CDCl3



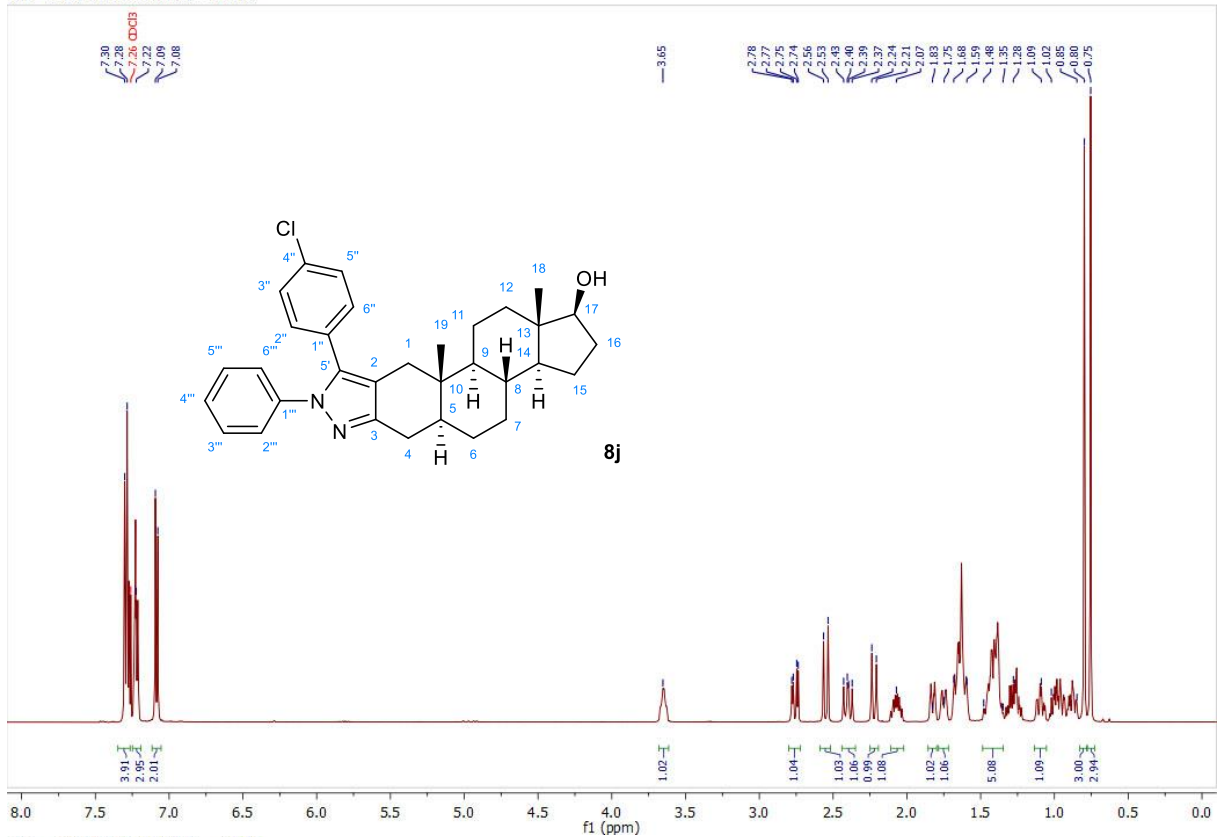
1H — 2021-04-28T21:44:05 — CDCl3



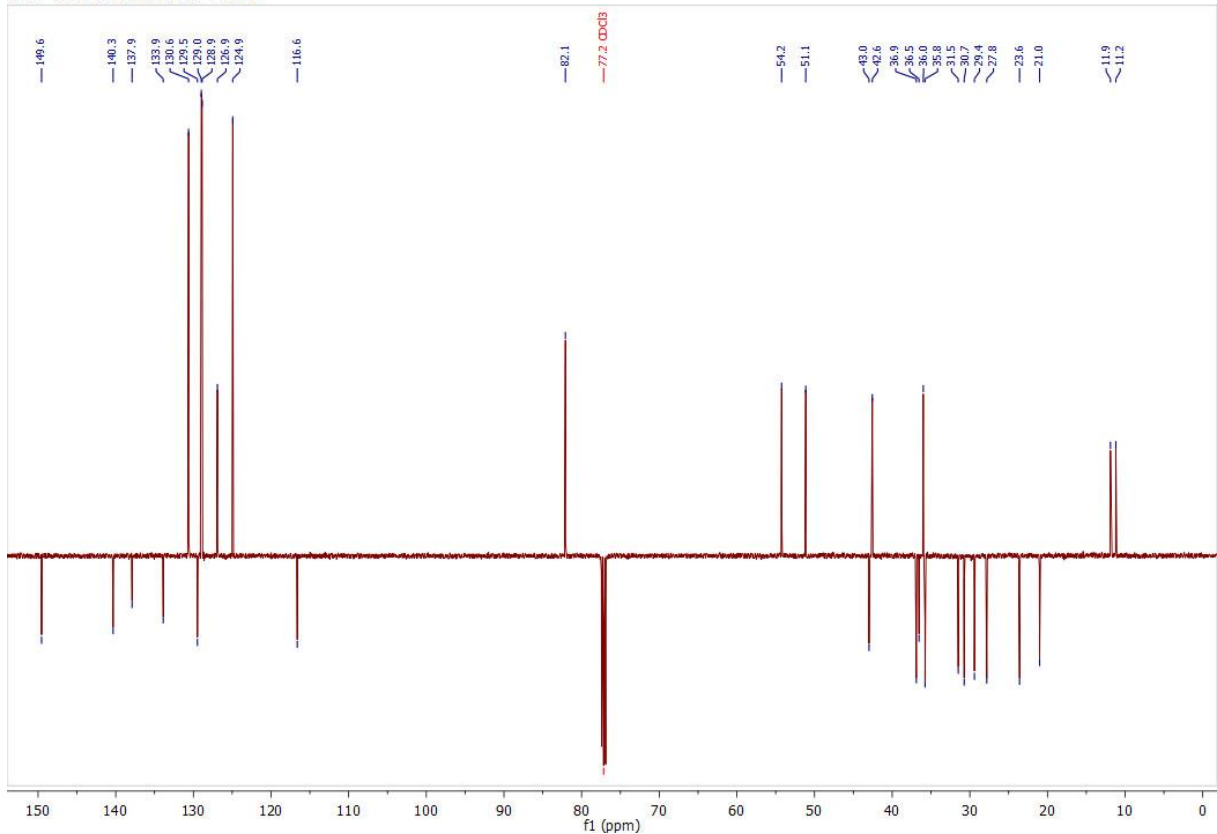
13C — 2021-04-28T21:57:43 — CDCl3



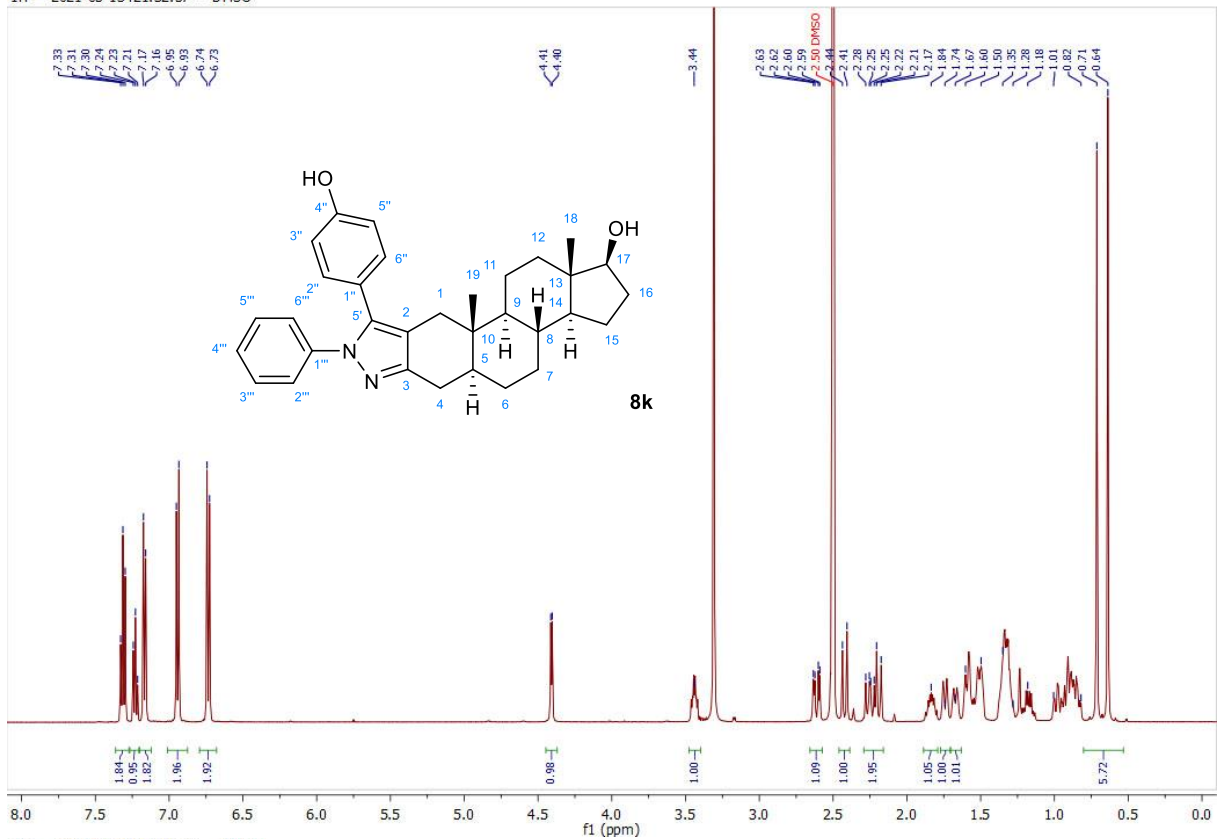
1H — 2021-04-28T22:20:05 — CDCl3



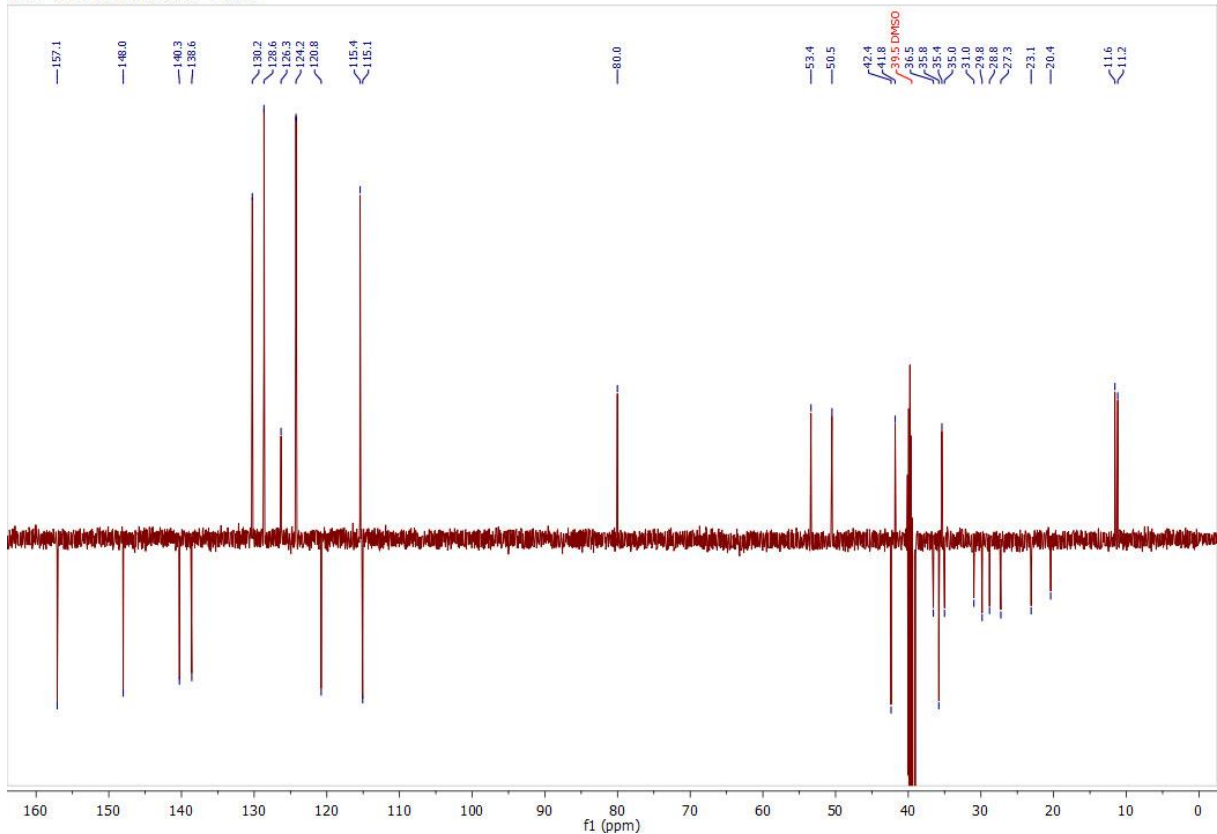
13C — 2021-04-28T22:33:42 — CDCl3



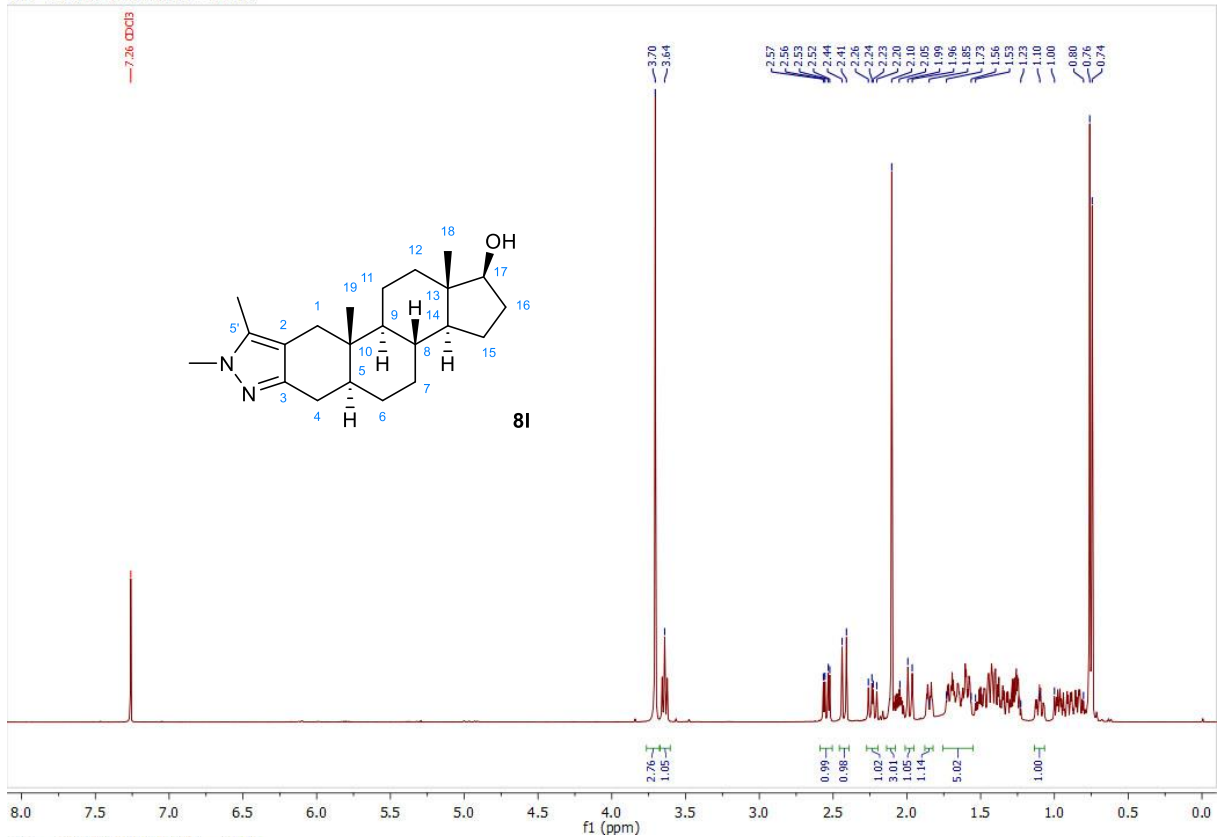
1H — 2021-05-13T21:32:57 — DMSO



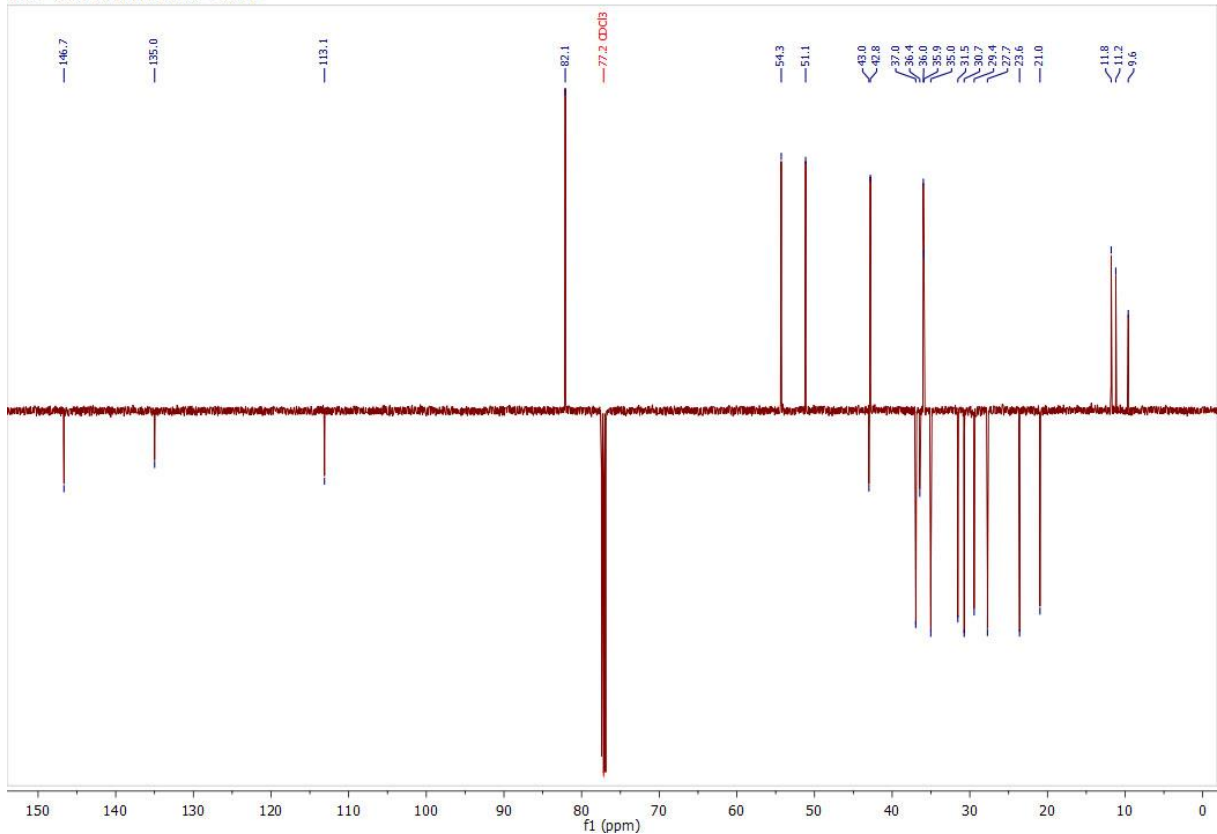
13C — 2021-05-13T21:46:51 — DMSO



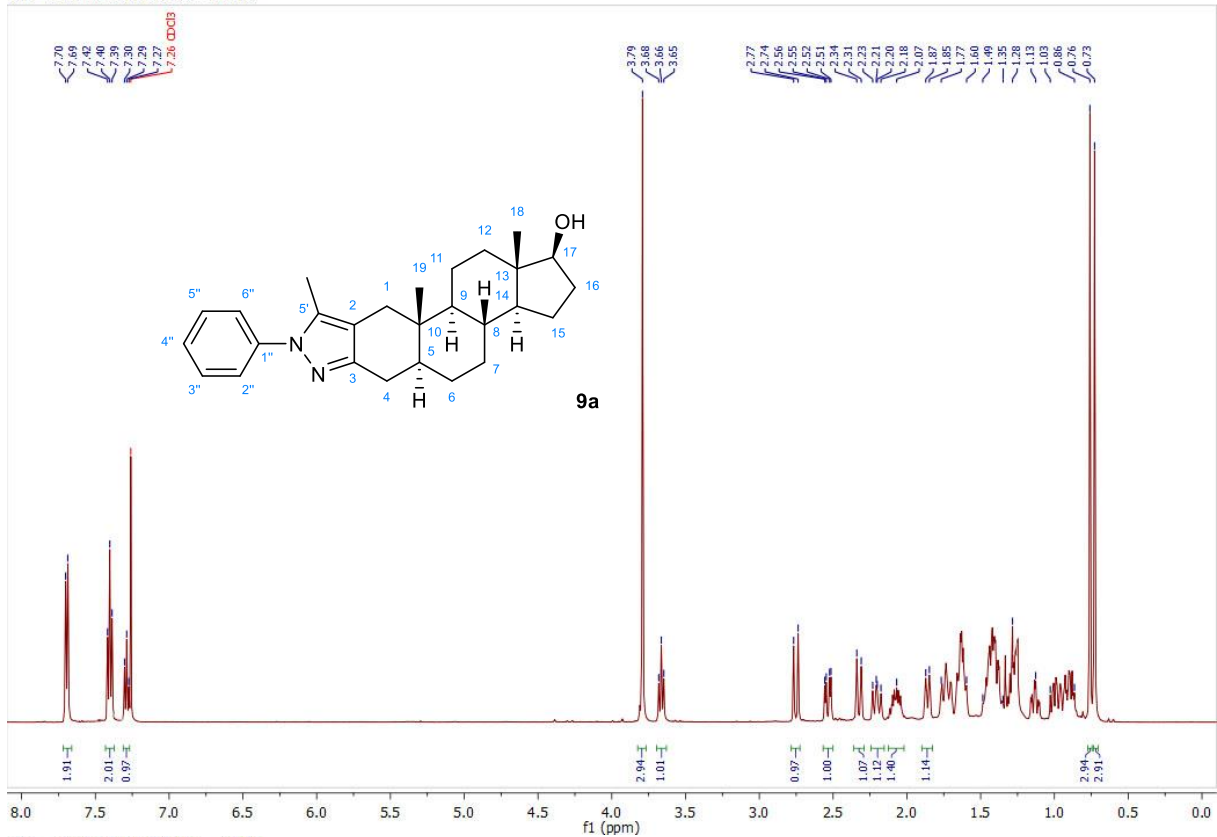
1H — 2021-02-13T17:49:18 — CDCl3



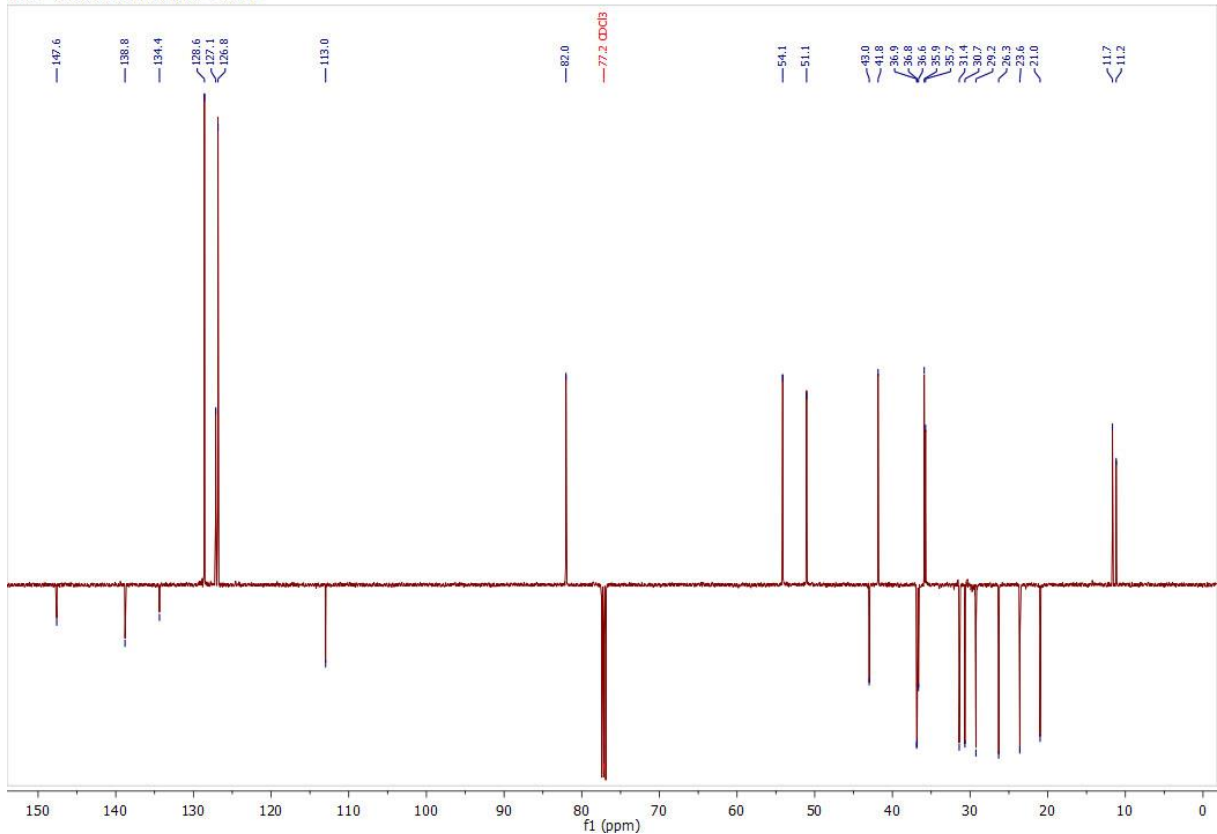
13C — 2021-02-13T18:02:55 — CDCl3



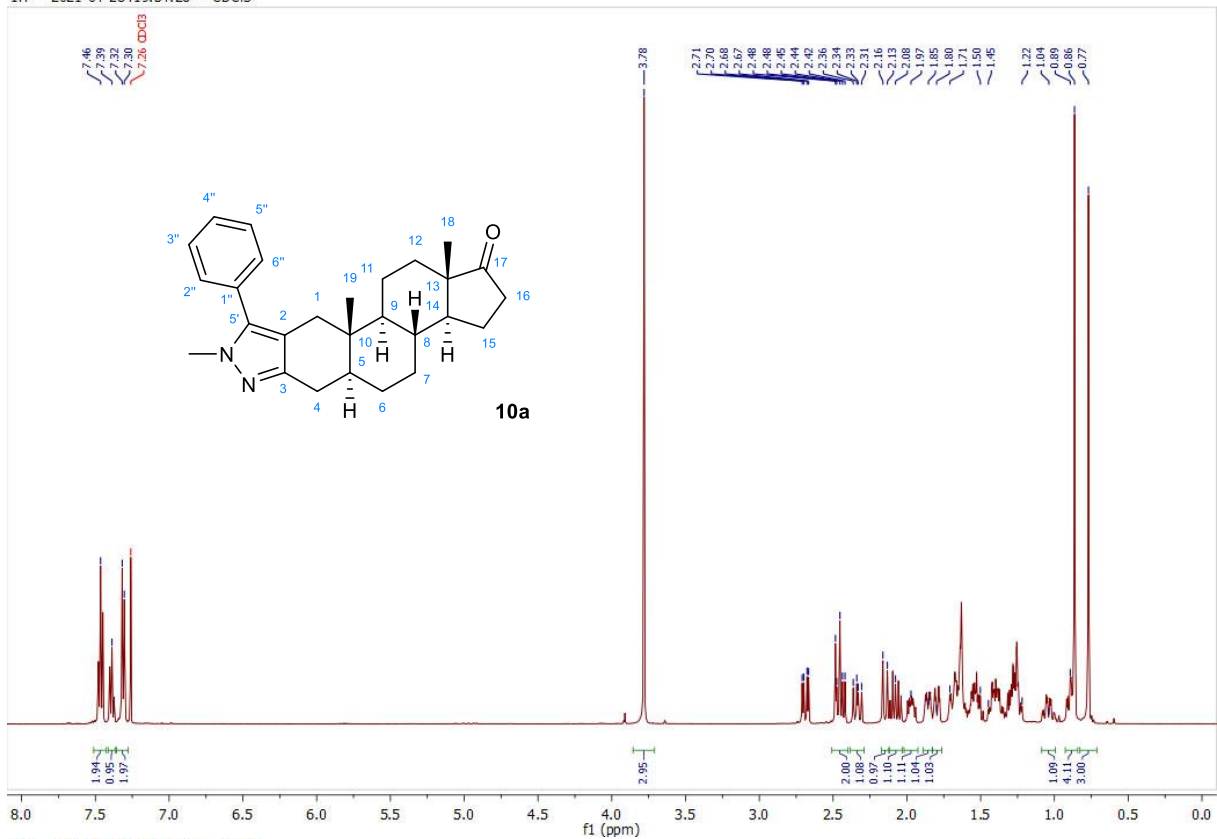
1H — 2017-12-06T11:17:44 — CDCl3



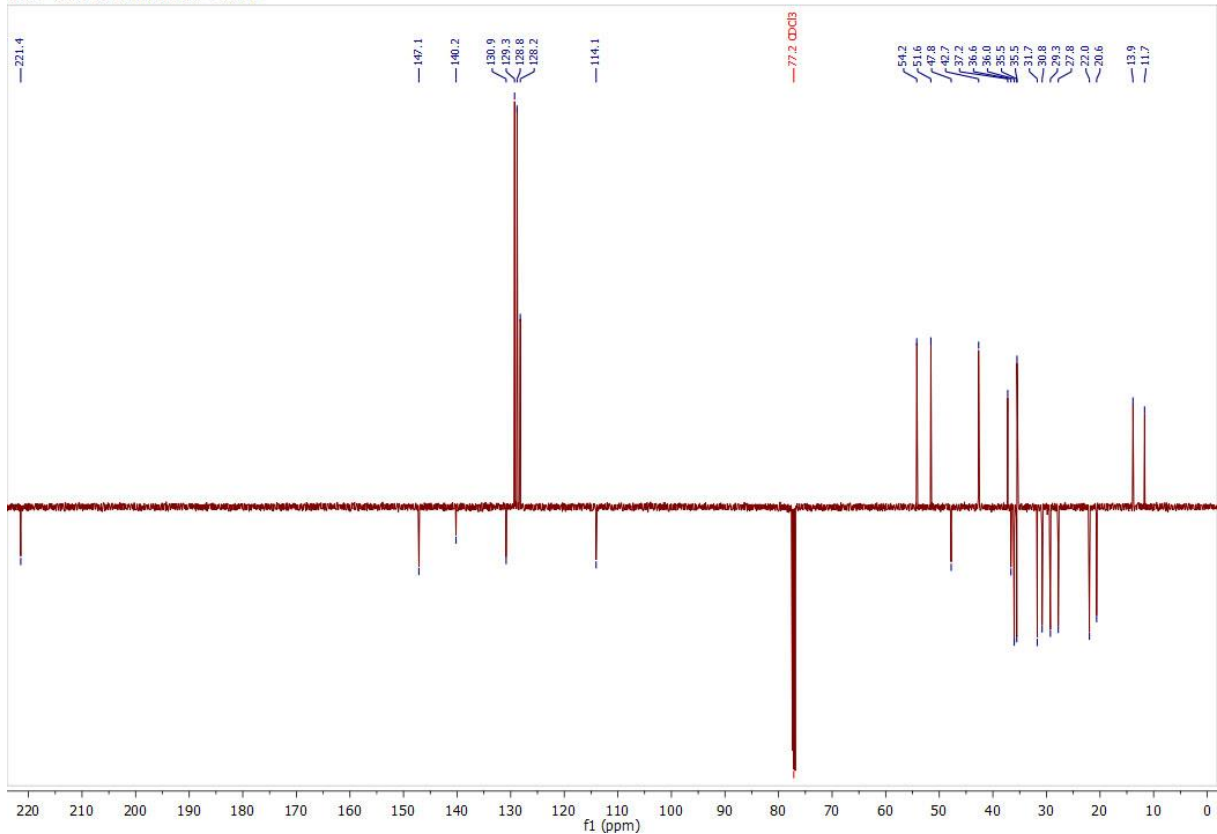
13C — 2017-11-11T13:24:44 — CDCl3



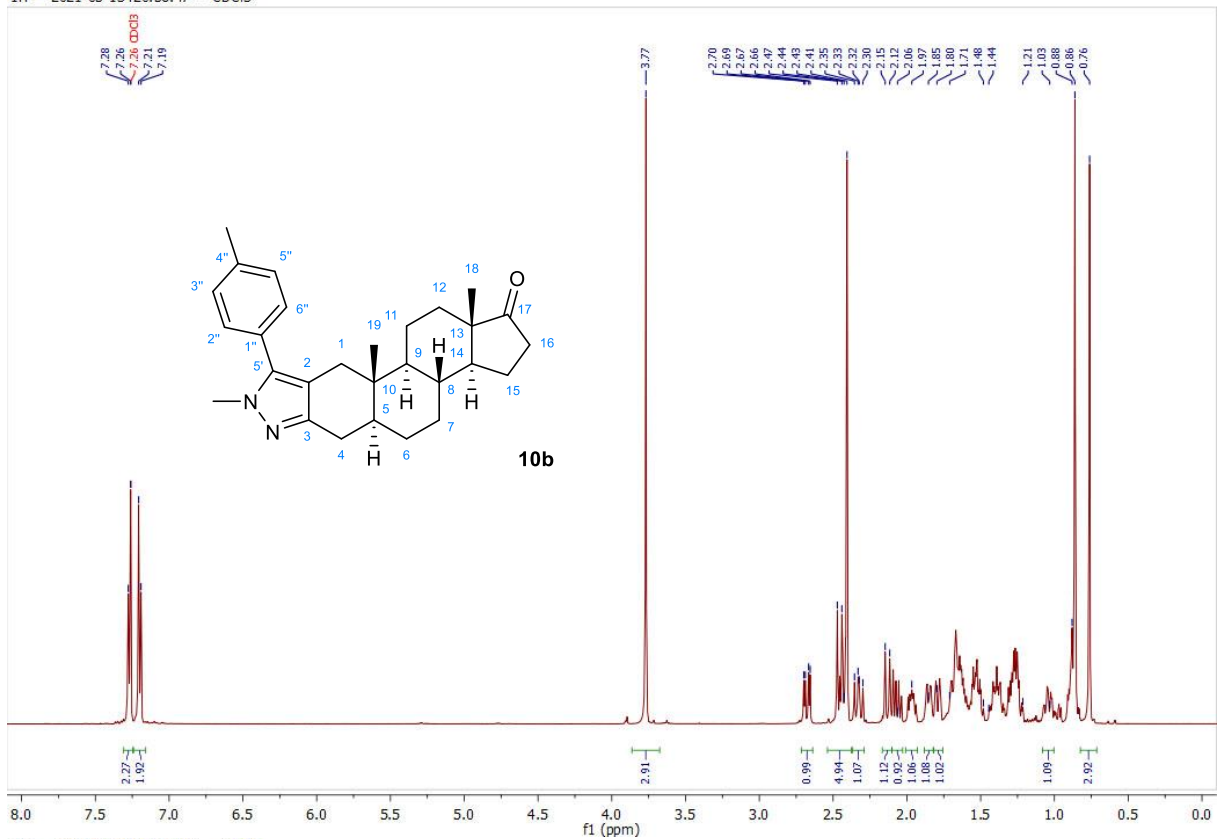
1H — 2021-04-28T19:54:26 — CDCl3



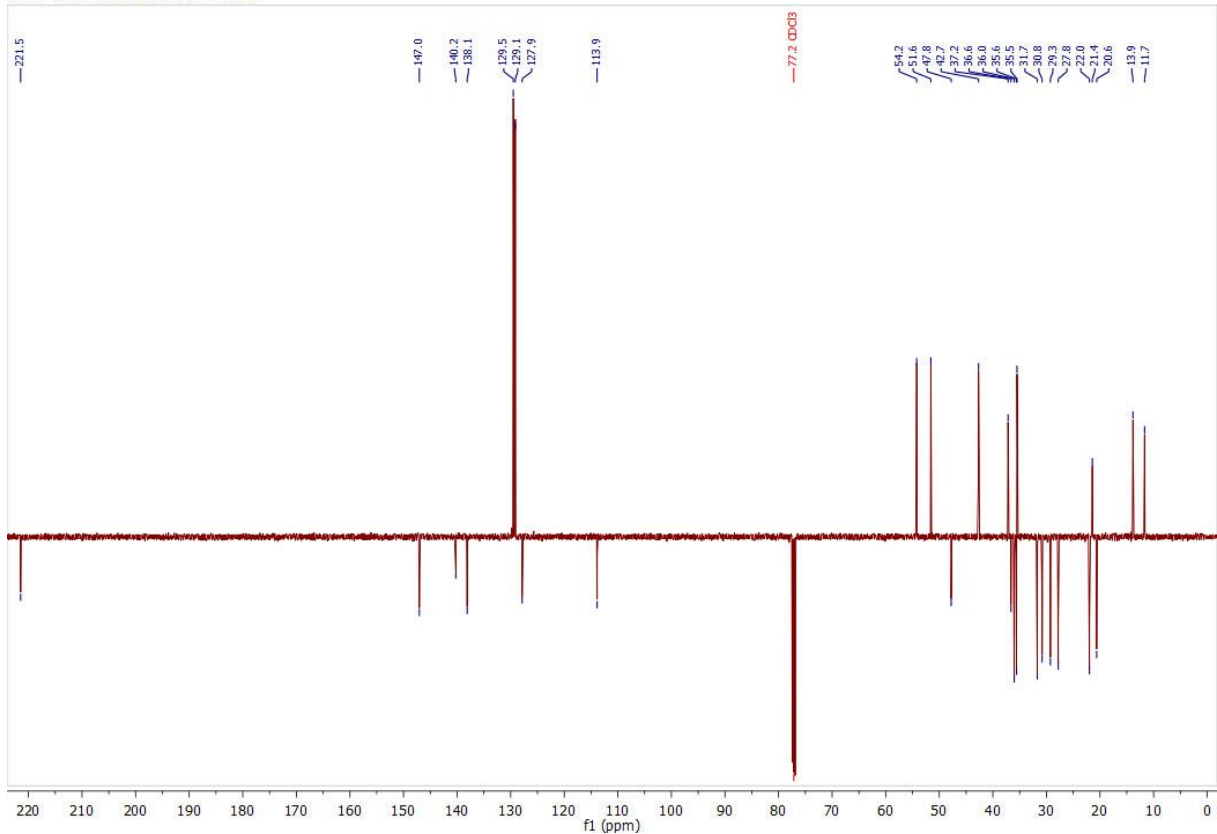
13C — 2021-04-28T20:08:04 — CDCl3



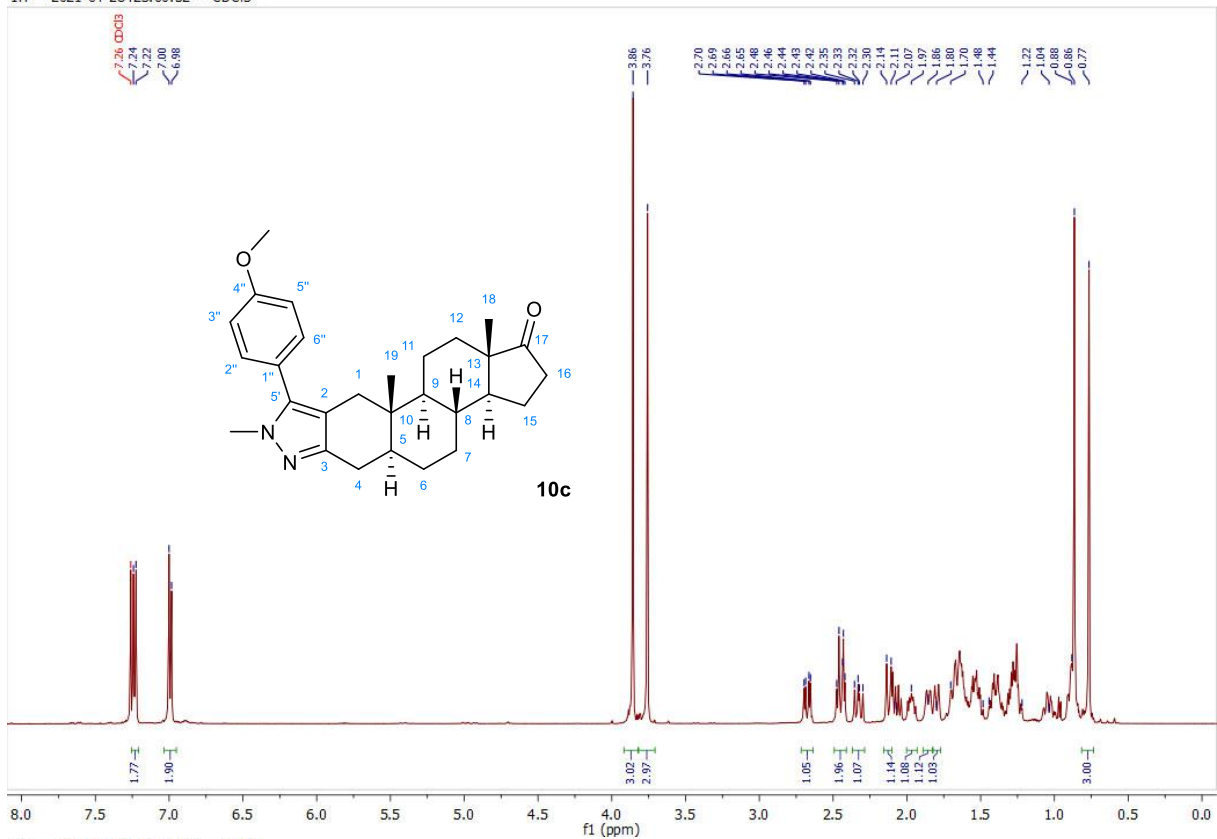
1H — 2021-05-13T20:56:47 — CDCl3



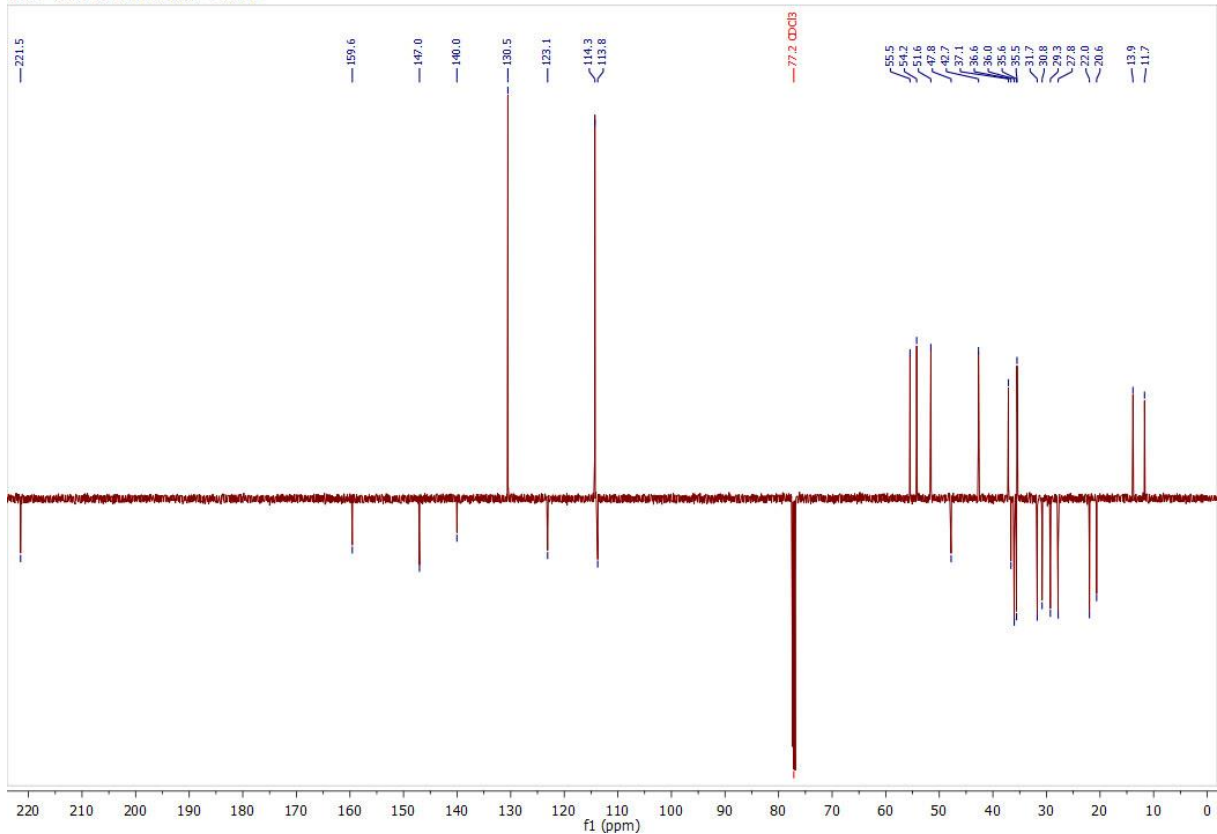
13C — 2021-05-13T21:10:27 — CDCl3



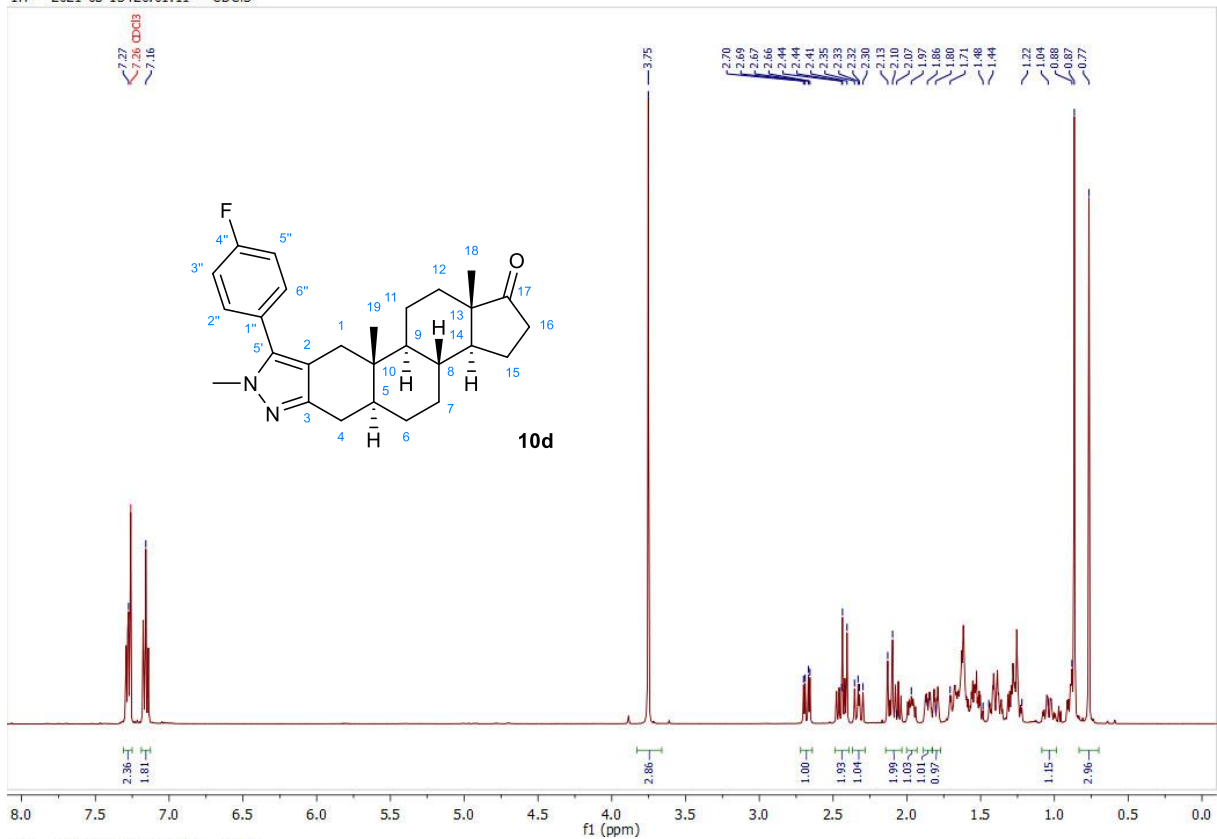
1H — 2021-04-28T23:00:52 — CDCl3



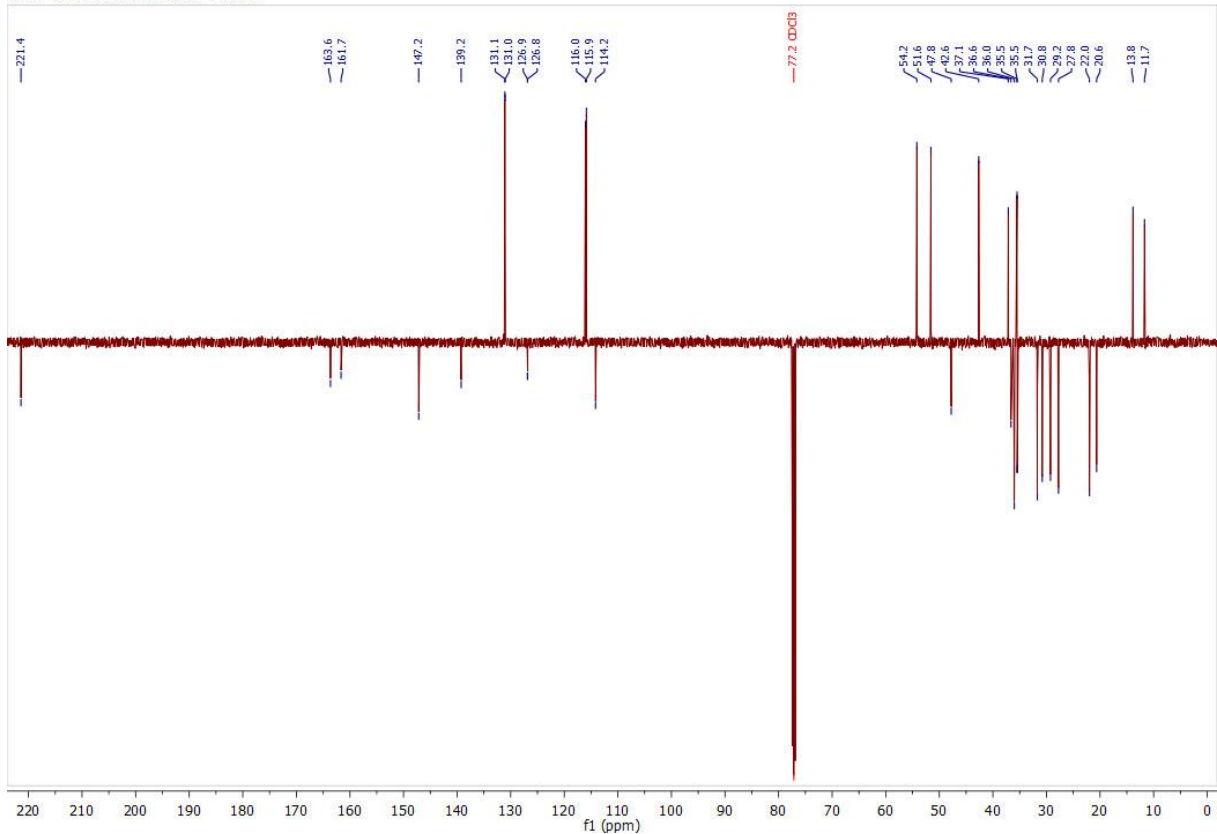
13C — 2021-04-28T23:14:29 — CDCl3



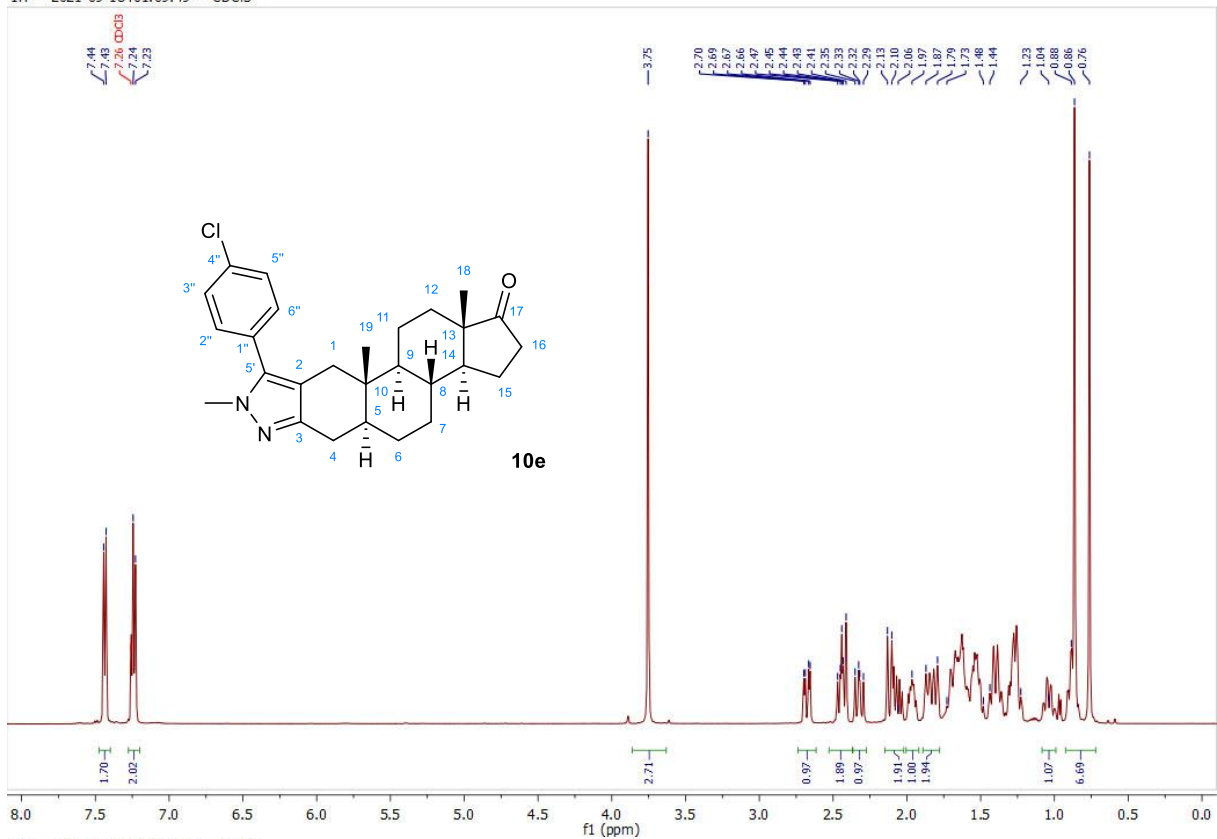
1H — 2021-05-13T20:01:11 — CDCl3



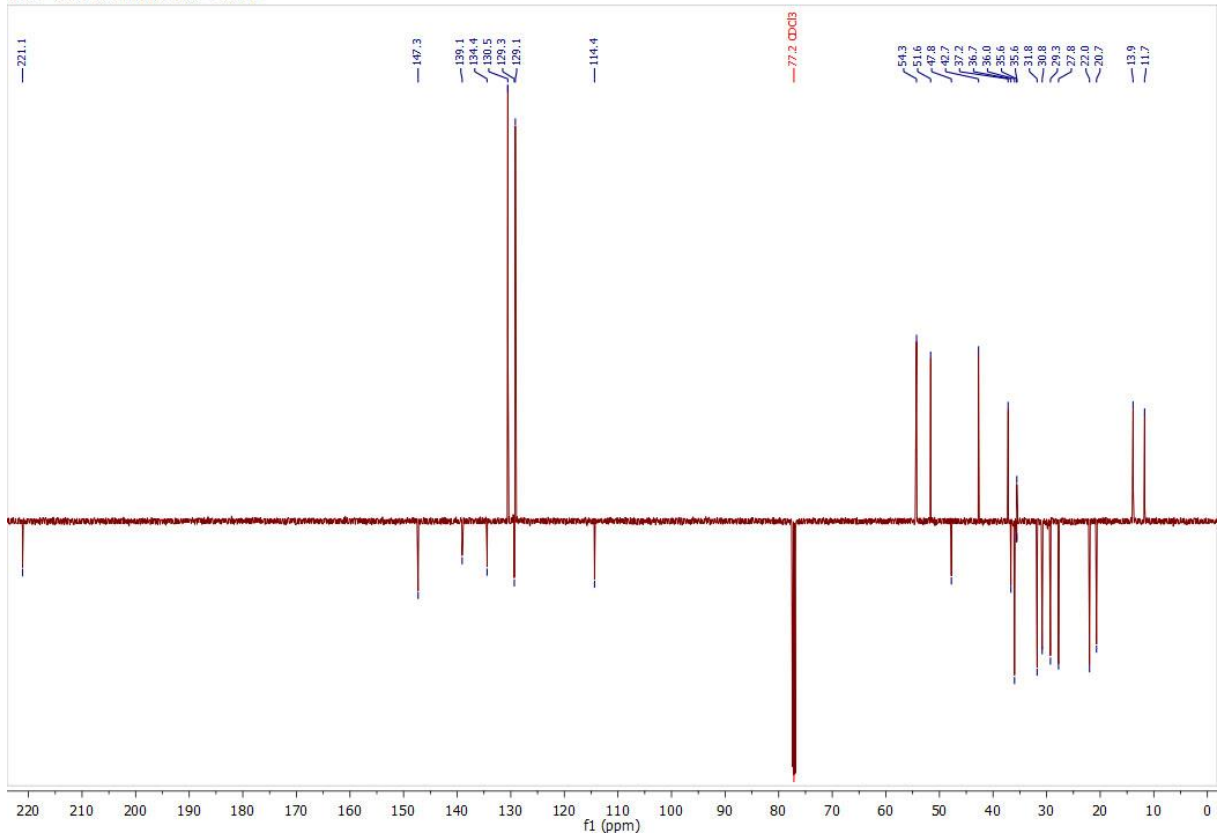
13C — 2021-05-13T20:14:50 — CDCl3



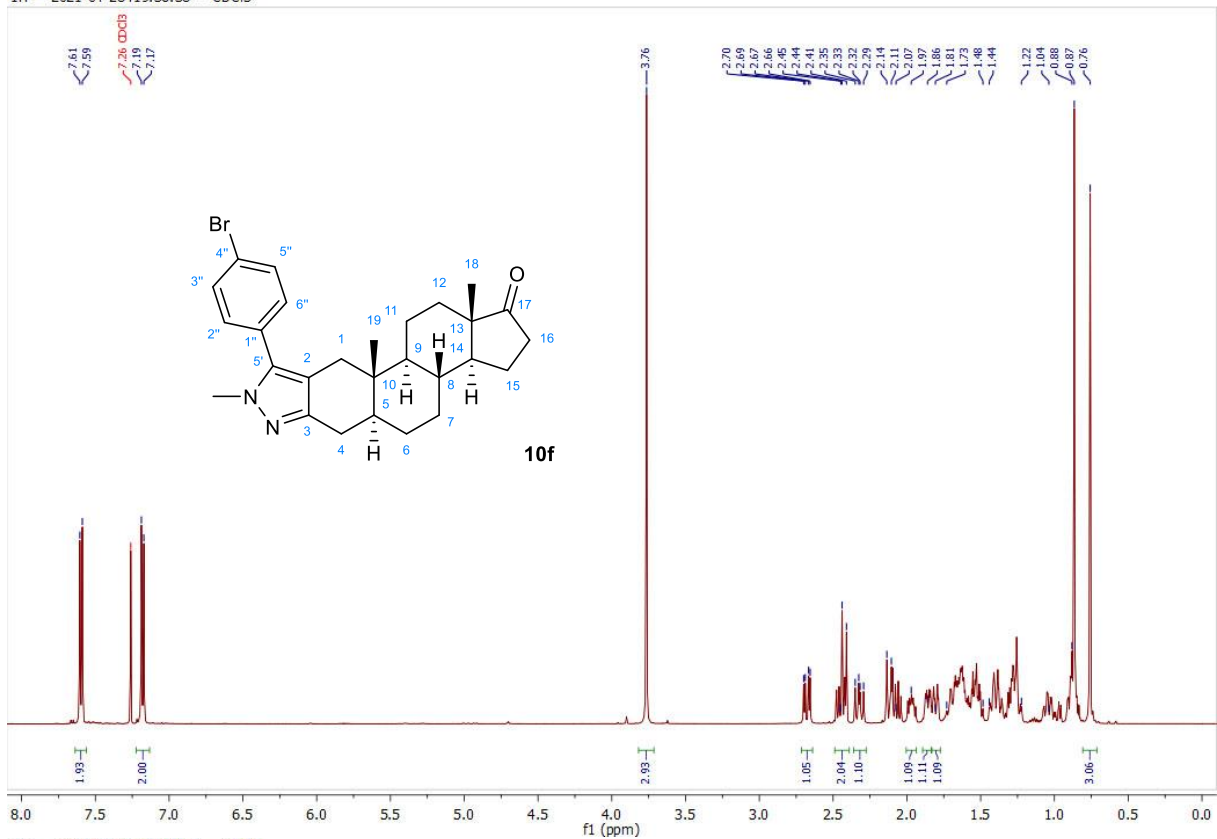
1H — 2021-09-18T01:09:49 — CDCl3



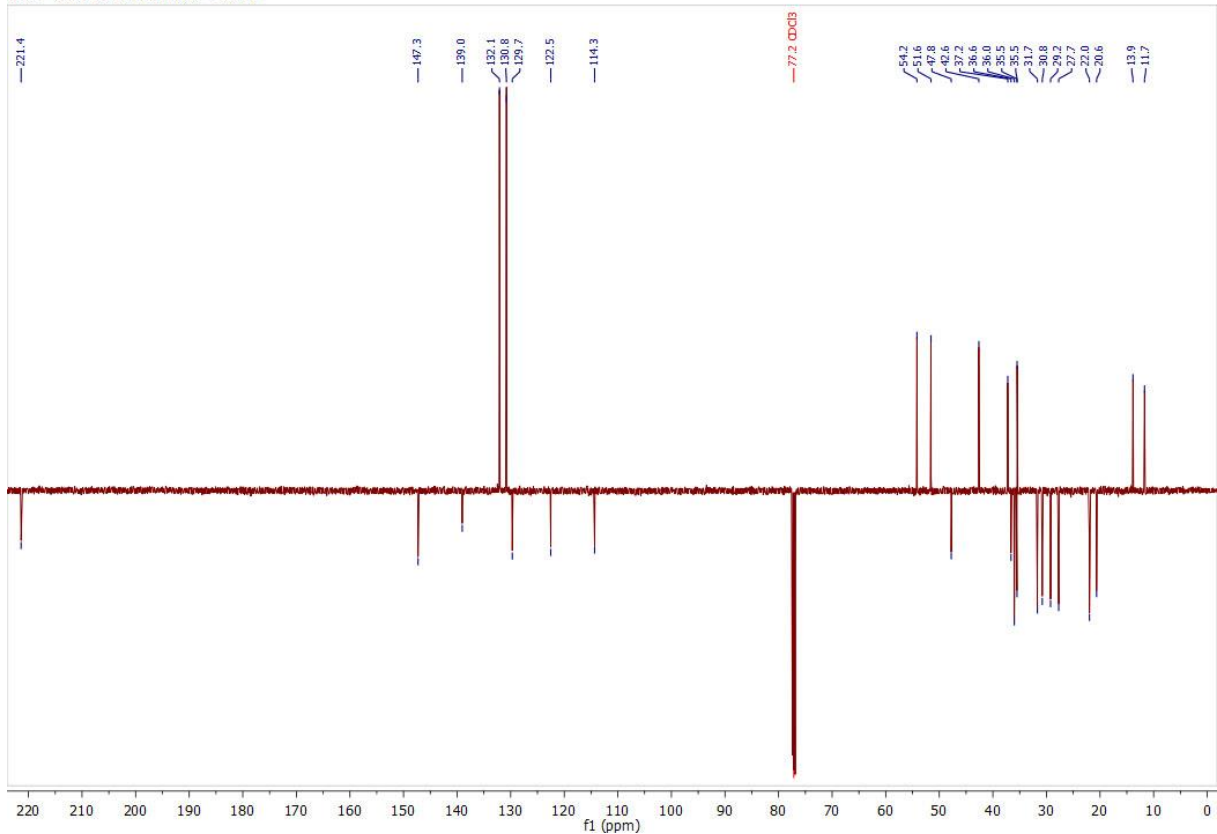
13C — 2021-09-18T01:23:25 — CDCl3



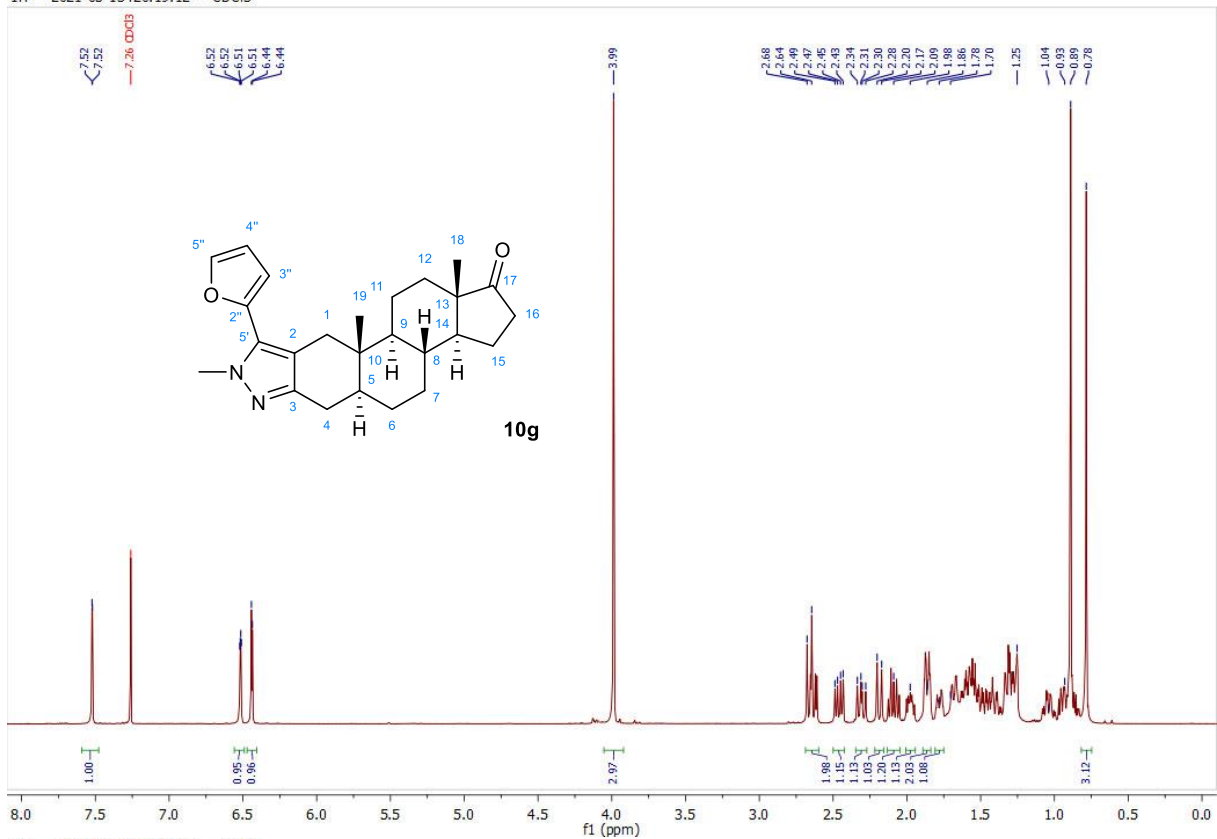
1H — 2021-04-28T19:36:38 — CDCl3



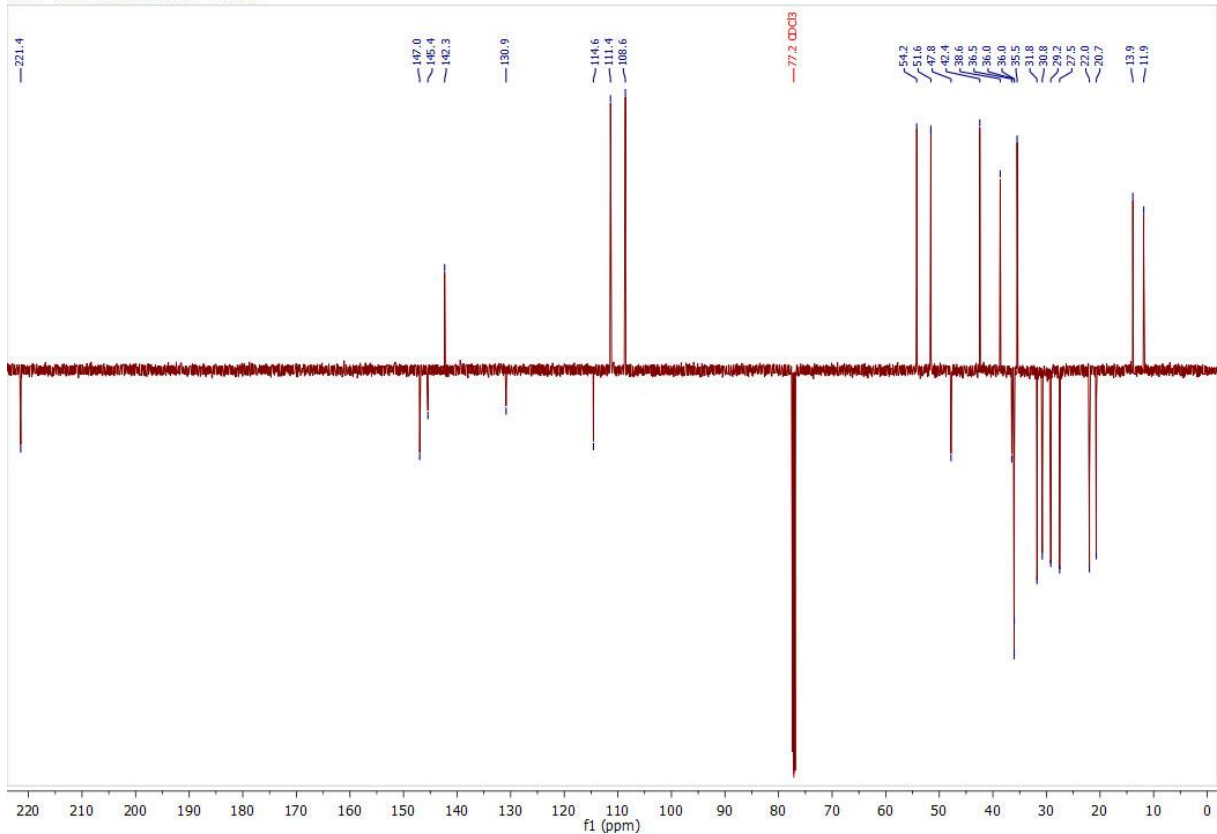
13C — 2021-04-28T19:50:15 — CDCl3



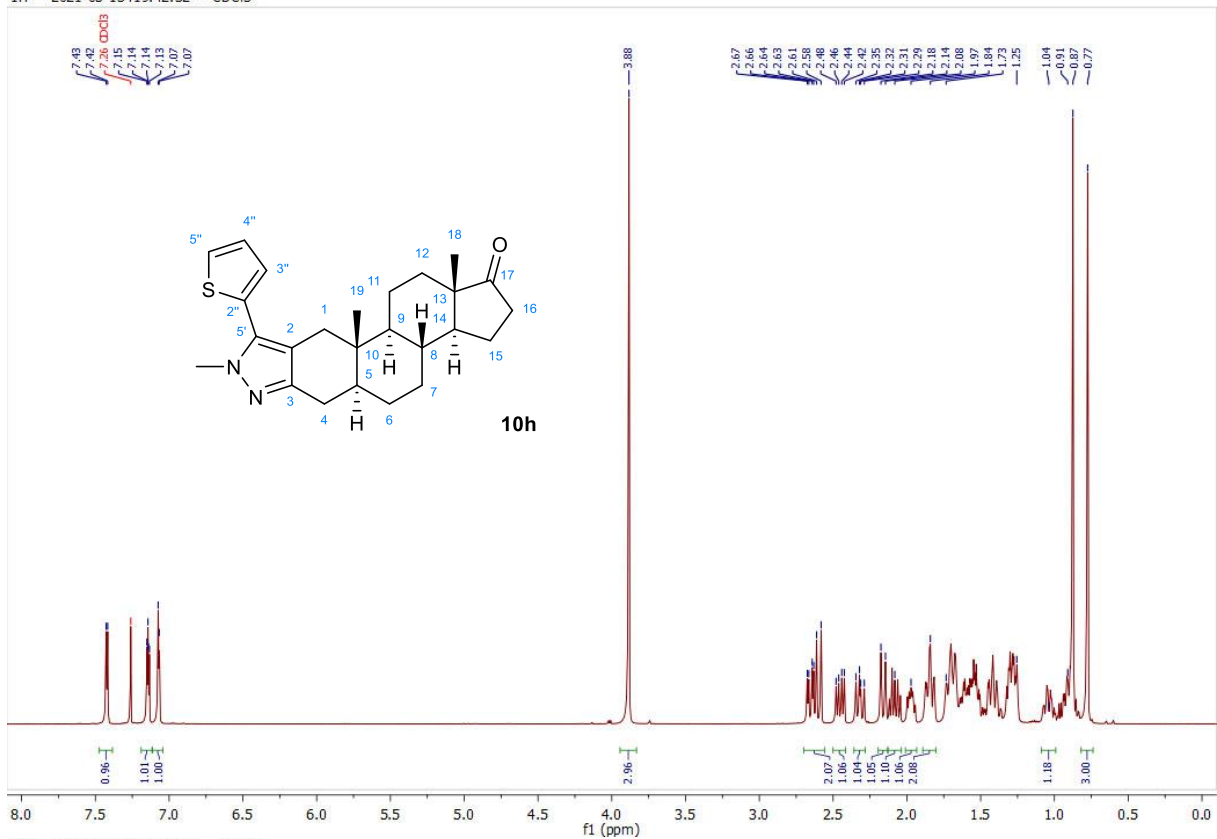
1H — 2021-05-13T20:19:12 — CDCl3



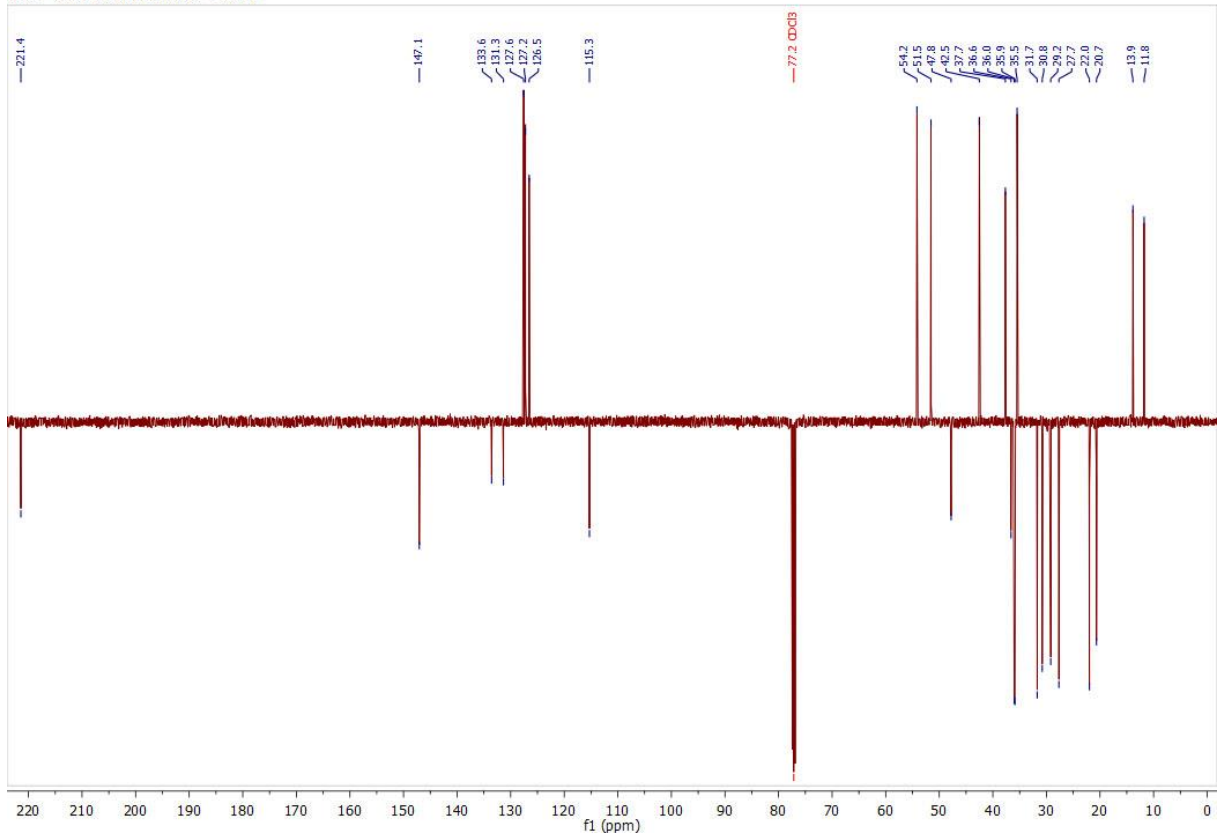
13C — 2021-05-13T20:32:53 — CDCl3



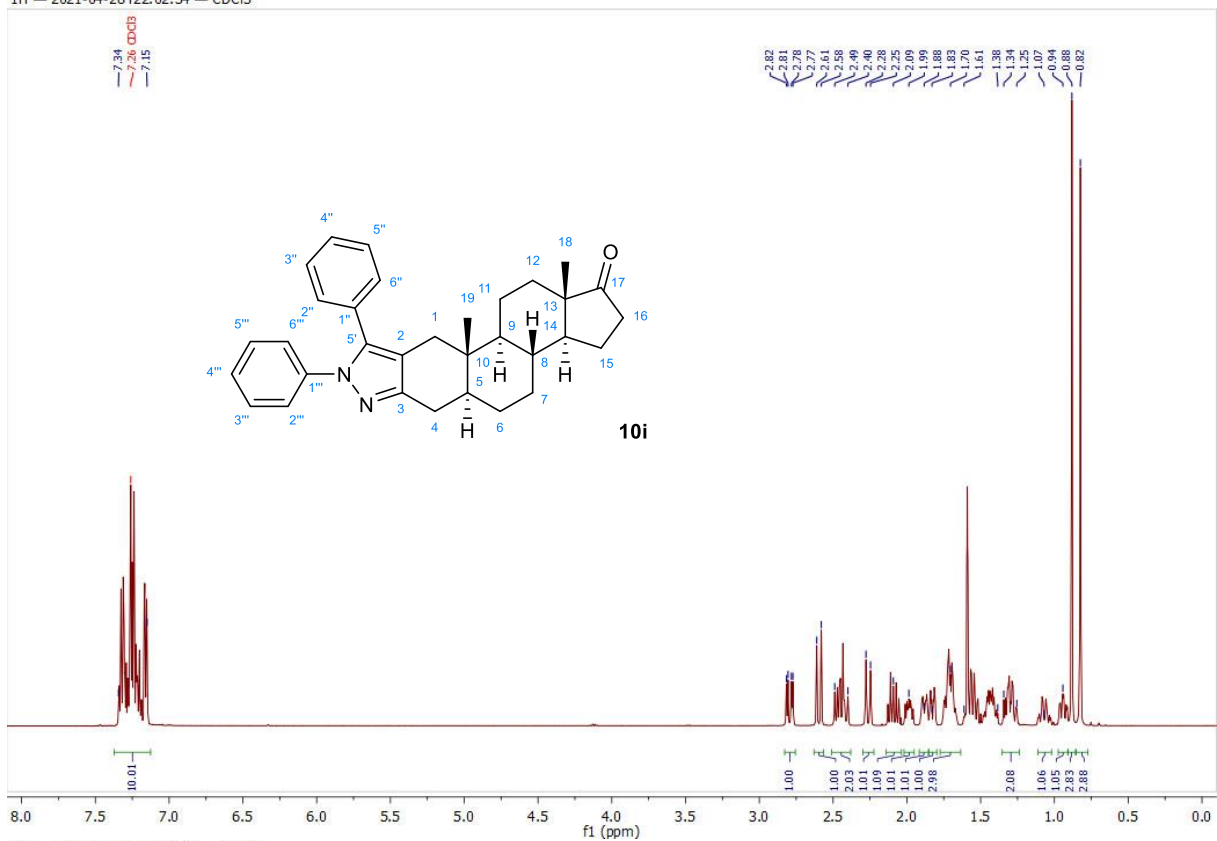
1H — 2021-05-13T19:42:32 — CDCl3



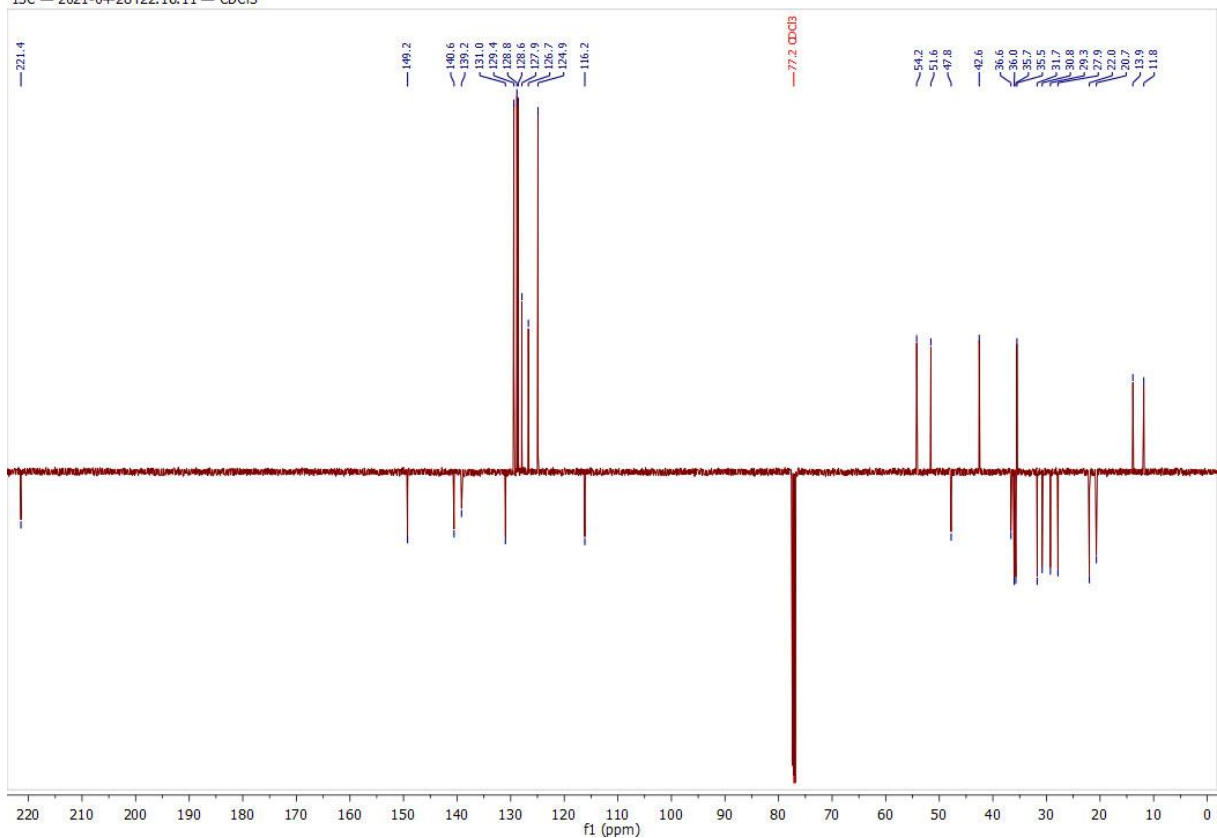
13C — 2021-05-13T19:56:12 — CDCl3



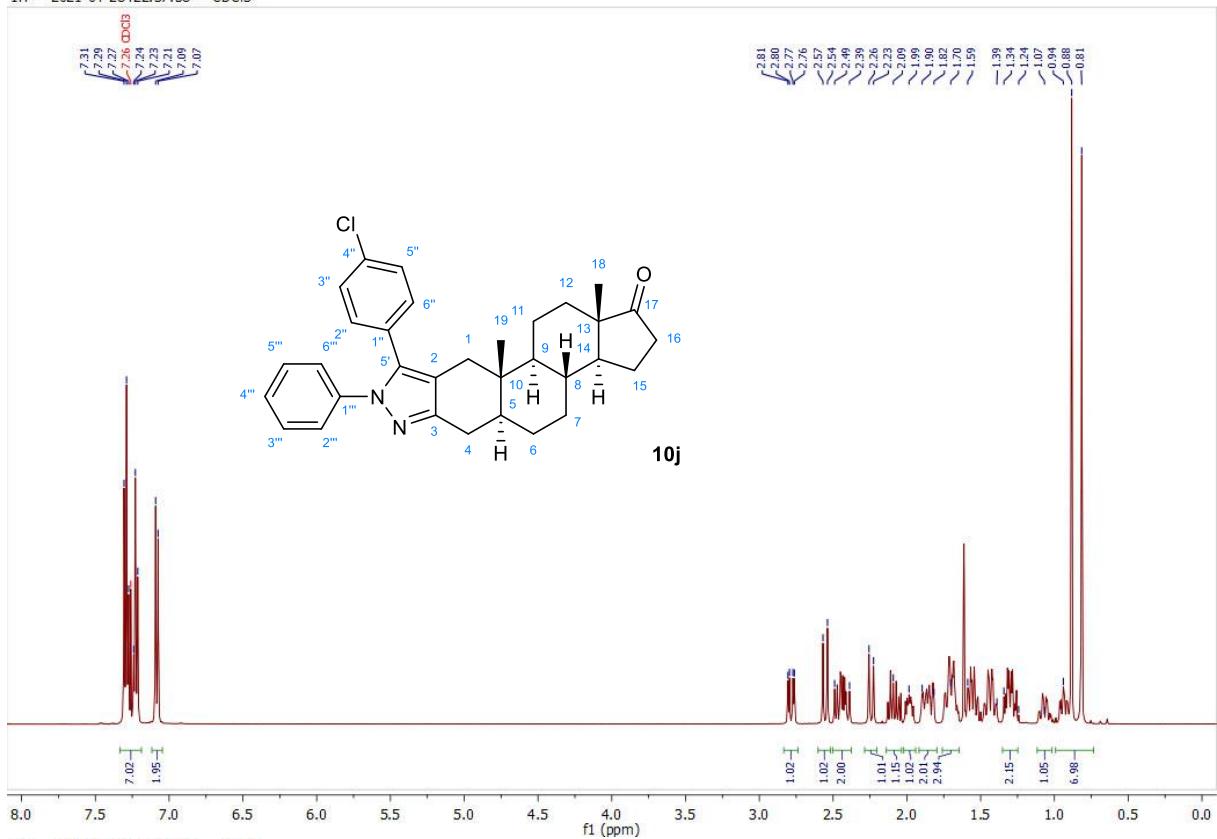
1H — 2021-04-28T22:02:34 — CDCl3



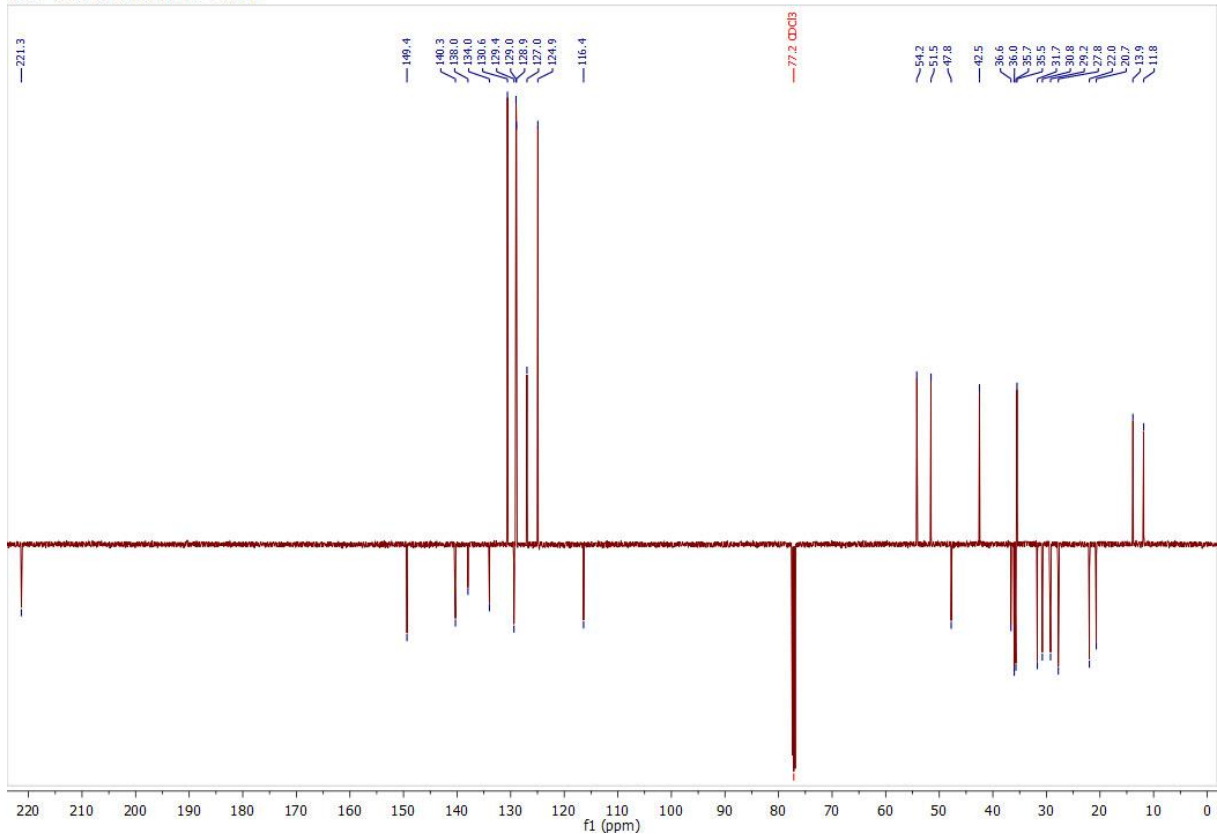
13C — 2021-04-28T22:16:11 — CDCl3



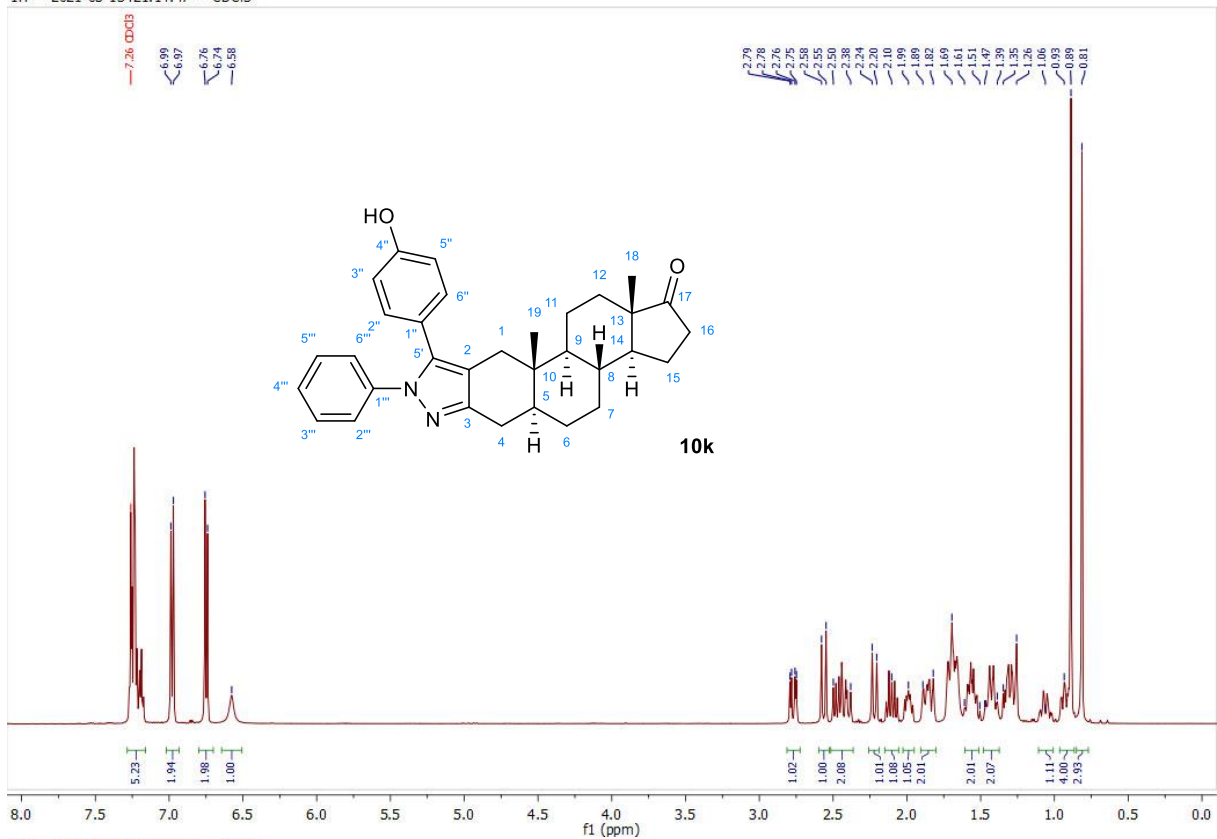
1H — 2021-04-28T22:37:58 — CDCl3



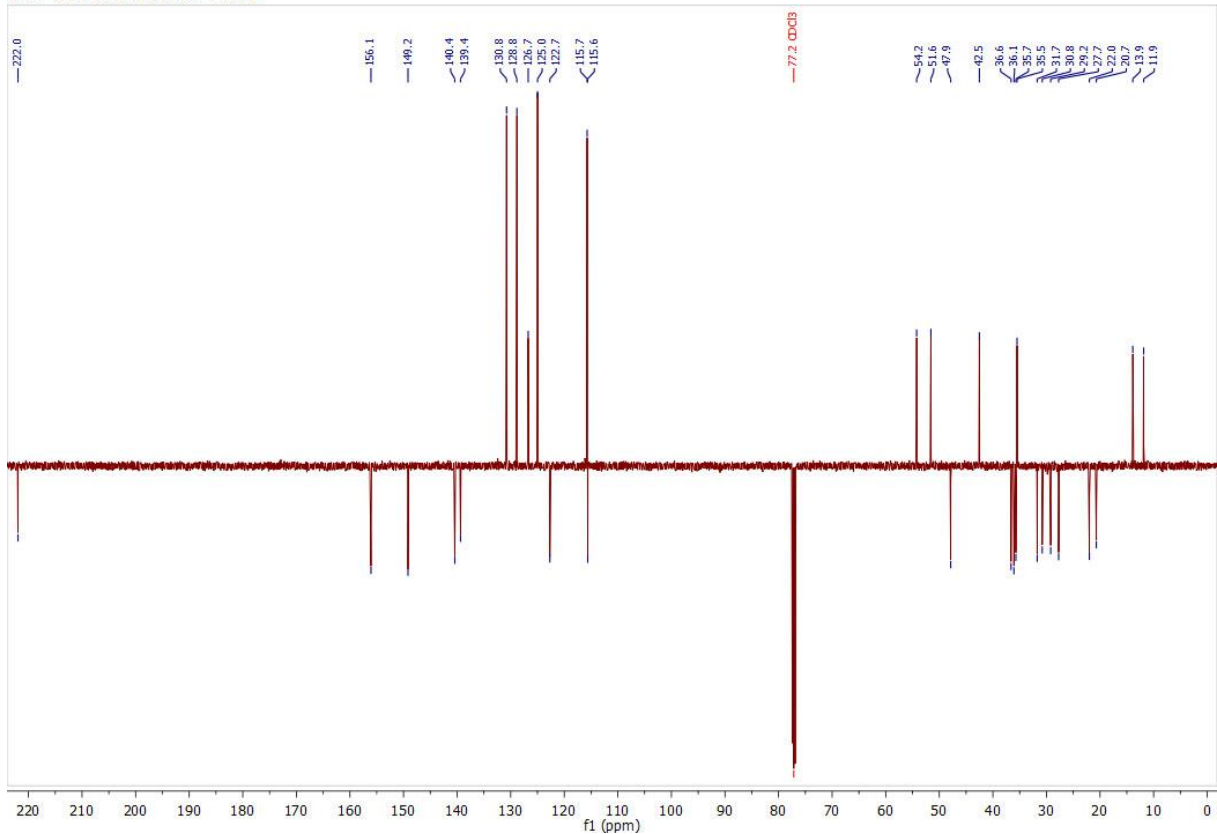
13C — 2021-04-28T22:51:36 — CDCl3



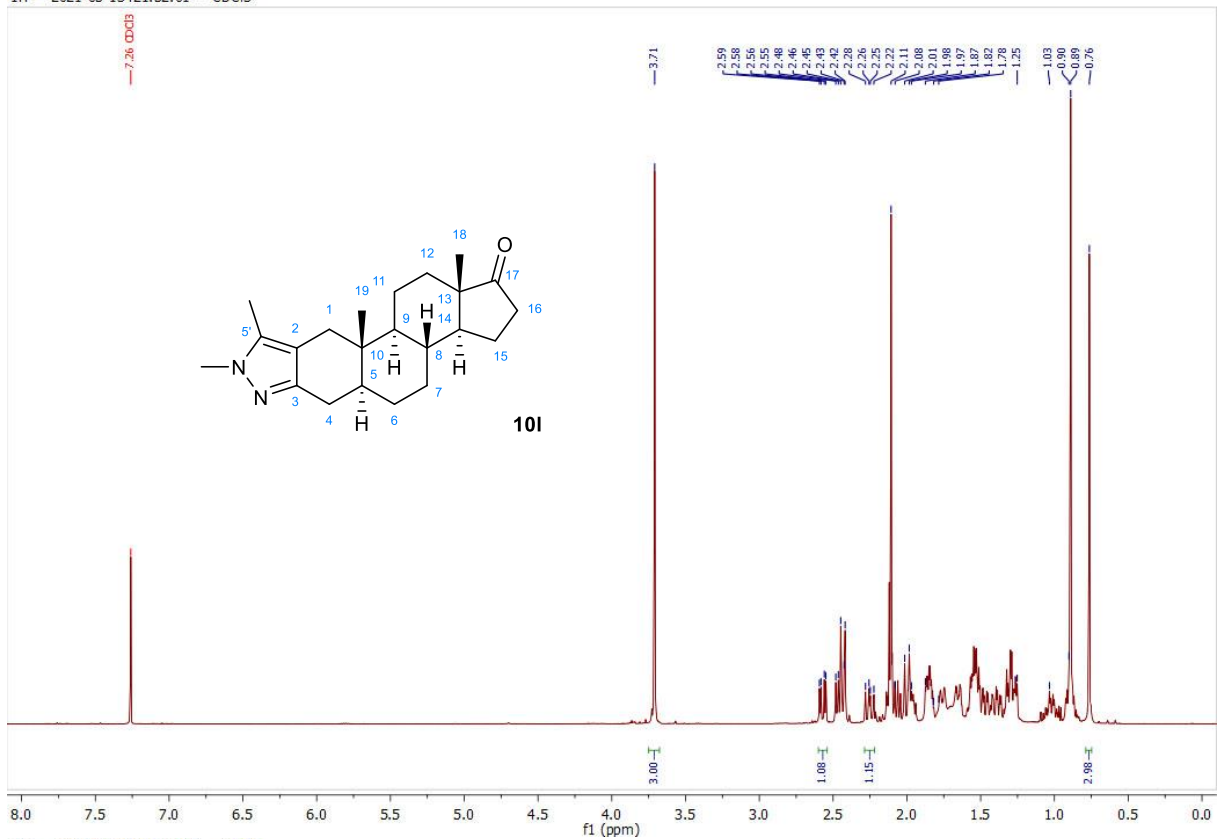
1H — 2021-05-13T21:14:47 — CDCl3



13C — 2021-05-13T21:28:26 — CDCl3



1H — 2021-05-13T21:52:01 — CDCl3



13C — 2021-05-13T22:05:58 — CDCl3

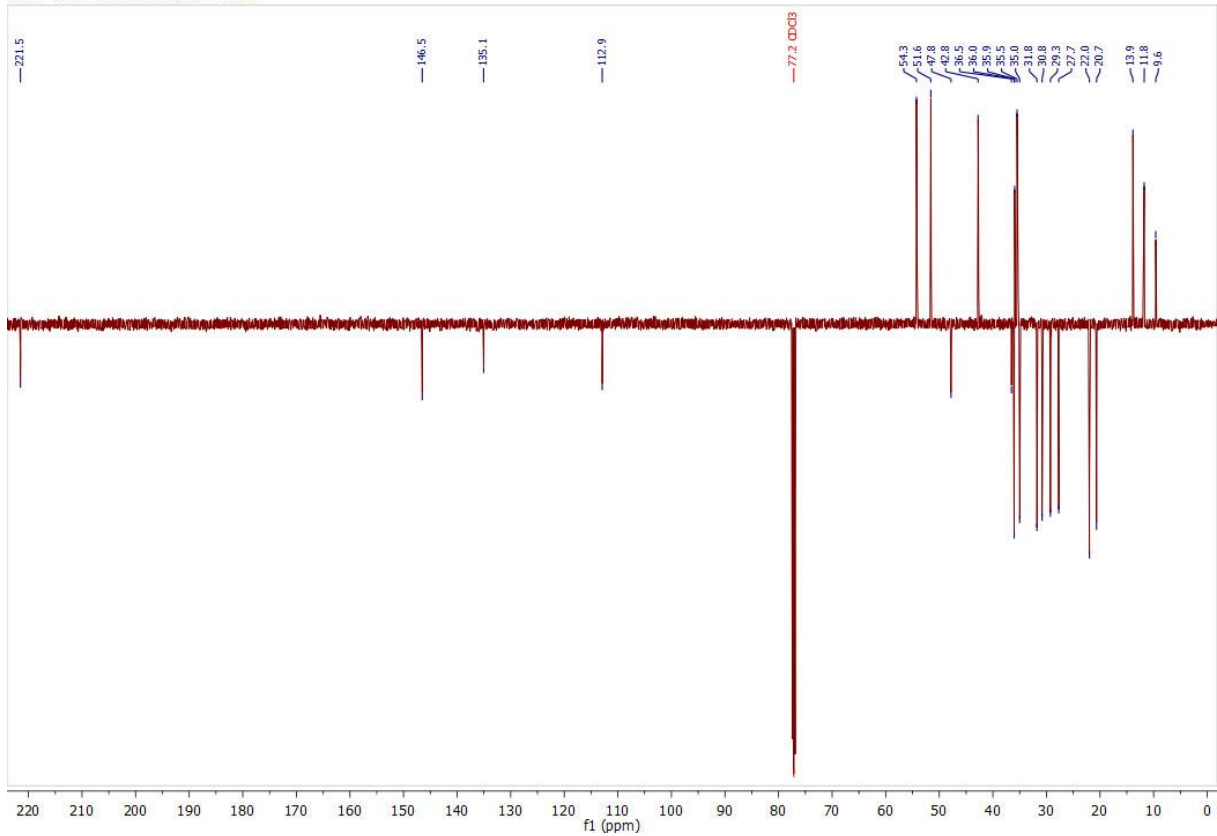


Table S1. AR transcriptional activity in antagonist and agonist mode upon treatment with displayed concentrations of compounds.

Cmp	AR transcriptional activity (% of control stimulated with 1 nM metribolone) ANTAGONIST			AR transcriptional activity (% of control stimulated with 1 nM metribolone) AGONIST		
	10 μ M	2 μ M	0.4 μ M	10 μ M	2 μ M	0.4 μ M
1a	53.7	90.2	96.7	73.8	69.3	63.1
1b	51.1	72.4	97.0	66.1	69.4	58.9
1c	48.5	73.4	92.8	77.4	83.2	83.9
1d	37.9	65.9	92.5	48.5	38.1	32.1
1e	39.2	64.6	84.2	43.8	48.3	42.9
1f	66.1	73.2	80.2	17.7	28.6	26.2
1g	69.4	76.9	78.9	84.1	72.7	65.4
1h	73.6	68.0	84.9	102.9	91.8	67.1
2a	47.5	75.2	94.5	72.6	59.2	56.2
2b	93.1	103.3	109.4	103.7	87.4	78.2
2c	67.3	83.8	96.8	108.0	84.3	67.9
2d	67.1	83.9	110.3	89.2	64.0	41.7
2e	107.0	120.9	100.7	87.1	72.2	46.6
2f	78.7	86.8	77.1	35.0	21.6	8.0
2g	67.7	81.6	86.2	48.5	57.6	54.0
2h	90.8	83.0	91.4	78.5	66.4	55.7
3a	16.6	46.7	84.5	16.4	26.7	26.4
3b	33.1	64.4	92.4	17.3	21.0	26.4
3c	34.0	53.1	80.7	25.2	29.1	33.8
3d	13.7	42.8	88.0	17.8	25.4	27.7
3e	21.7	53.9	93.2	21.7	25.4	26.1
3f	35.7	61.6	82.4	27.2	28.9	27.1
3g	18.7	36.8	72.8	20.7	23.8	26.1
3h	28.3	63.4	91.8	25.2	34.9	31.1
4a	71.2	82.1	98.3	31.4	27.9	23.9
4b	85.3	89.4	87.1	20.1	25.3	26.4
4c	78.3	108.6	119.6	25.7	31.2	32.7
4d	30.6	64.7	88.0	18.9	22.4	26.7
4e	43.3	97.2	108.2	17.7	25.8	26.4
4g	47.9	66.5	79.8	26.1	33.8	29.9
4h	54.6	87.6	98.0	27.3	33.5	32.7
8a	88.7	90.5	92.2	11.4	17.0	18.5
8b	70.4	99.5	89.1	41.7	42.3	25.9
8c	65.5	89.3	92.9	1.7	7.4	7.3
8d	63.7	85.0	92.8	9.0	16.3	20.1
8e	44.6	79.9	95.5	10.9	30.4	23.5
8f	34.5	80.6	95.5	6.3	18.0	15.9

8g	13.0	67.4	81.5	0.9	15.2	14.4
8h	37.4	75.6	89.9	4.1	24.6	25.8
8i	139.1	113.4	95.3	57.0	43.9	22.6
8j	121.6	108.5	111.9	67.6	46.9	27.9
8k	156.8	106.4	100.6	67.6	49.7	25.2
8l	138.5	94.9	89.7	80.8	66.1	37.5
10a	100.1	105.5	105.9	36.3	21.6	8.1
10b	82.2	94.5	95.5	2.8	4.6	8.4
10c	93.5	98.4	103.7	29.6	20.3	13.0
10d	86.2	99.3	109.7	6.4	6.9	10.7
10e	40.4	84.1	92.1	2.6	4.3	7.7
10f	40.1	88.5	95.1	3.2	5.0	6.4
10g	59.6	99.7	100.9	14.5	24.7	22.7
10h	59.5	94.1	96.3	11.1	16.7	18.9
10i	136.3	115.8	97.5	65.4	42.6	25.1
10j	168.8	124.1	114.9	67.7	43.3	24.5
10k	165.0	131.5	119.0	64.1	41.0	23.2
10l	149.3	104.1	99.0	56.7	47.6	26.0

Transcriptional activity of AR was measured with compounds alone (agonist mode) or in the presence of 1 nM R1881 (antagonist mode) in reporter cell line ARE14 for 24 h. Activity was normalised to the signal of R1881 (= 100%). Measured in duplicate and repeated twice, mean plotted in the table.

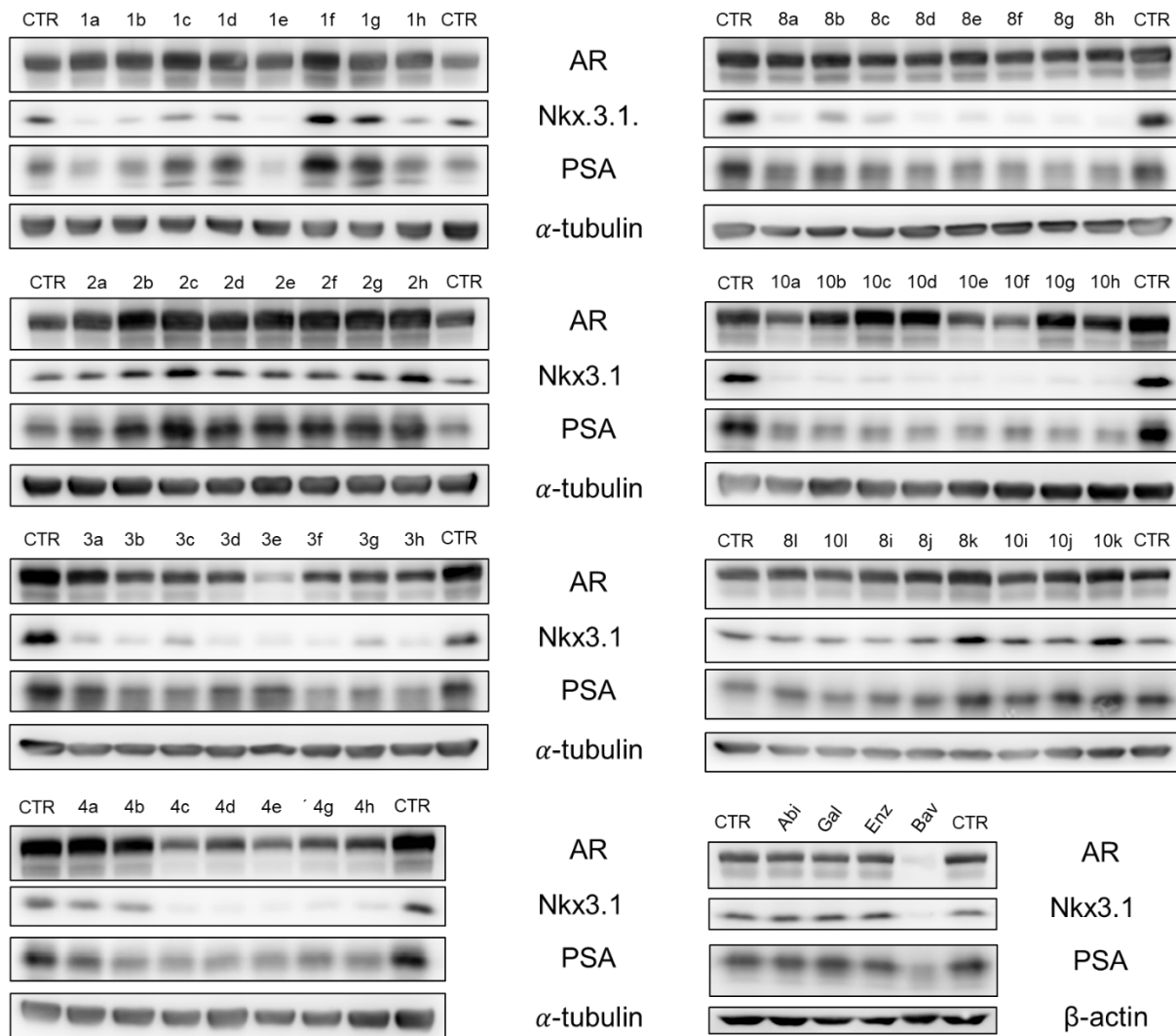


Figure S3. (10 μ M, 24 h) in FBS containing medium and lysates were then blotted for detection of appropriate Immunoblotting analysis of important signaling proteins from the LAPC-4 cells, which were treated with studied compounds proteins. Level of α -tubulin or β -actin served as loading control. Abi, abiraterone; Gal, galeterone; Enz, enzalutamide; Bav, bavdegalutamide.

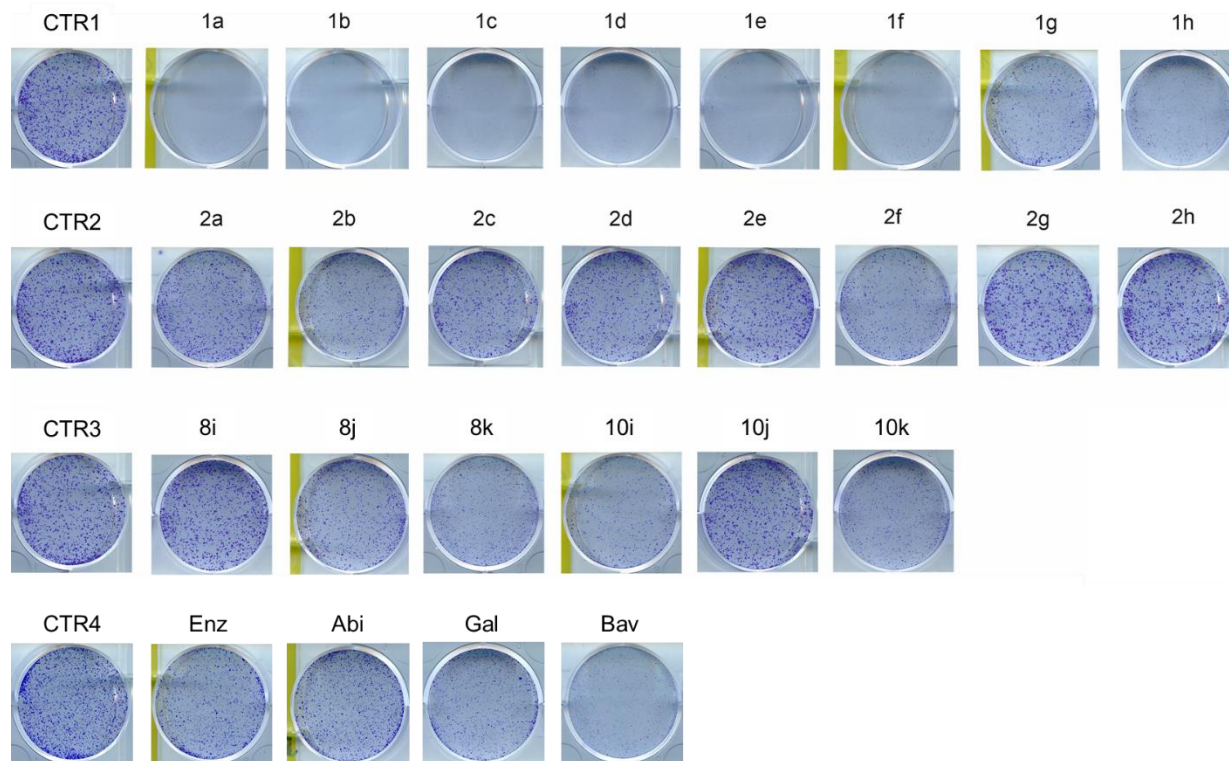


Figure S4. Antiproliferative activity of compounds determined by colony formation assay with LAPC-4 cell line. Cells were seeded, treated with 5 μ M concentration of compounds and cultivated for 10 days in the presence of compounds. Colonies were fixed and stained as described in experimental part.

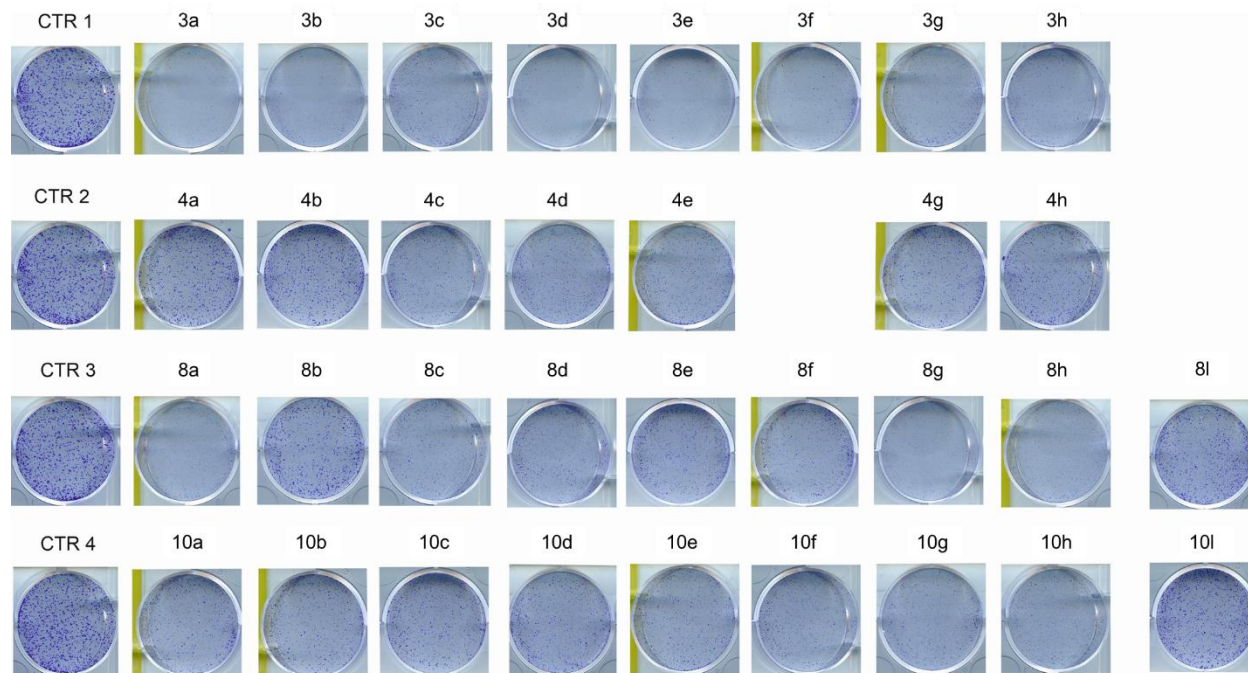


Figure S5. Antiproliferative activity of compounds determined by colony formation assay with LAPC-4 cell line. Cells were seeded, treated with 5 μ M concentration of compounds and cultivated for 10 days in the presence of compounds. Colonies were fixed and stained as described in experimental part.

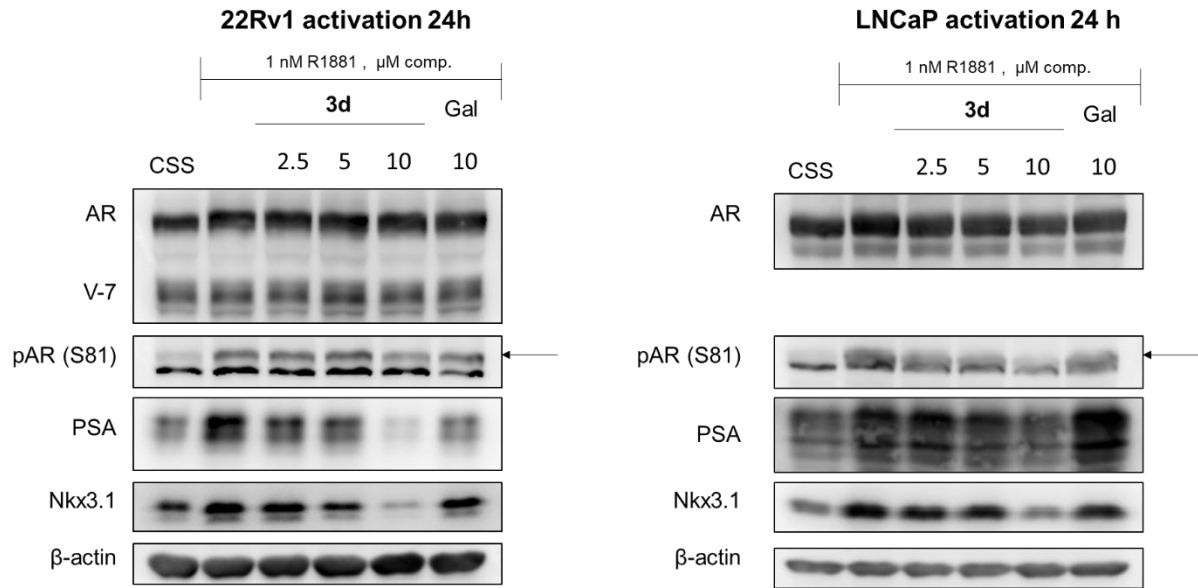


Figure S6. Dose dependent effect of **3d** on AR- signalling in 22Rv1, LNCaP. Level of β -actin served as loading control. Gal, galeterone.

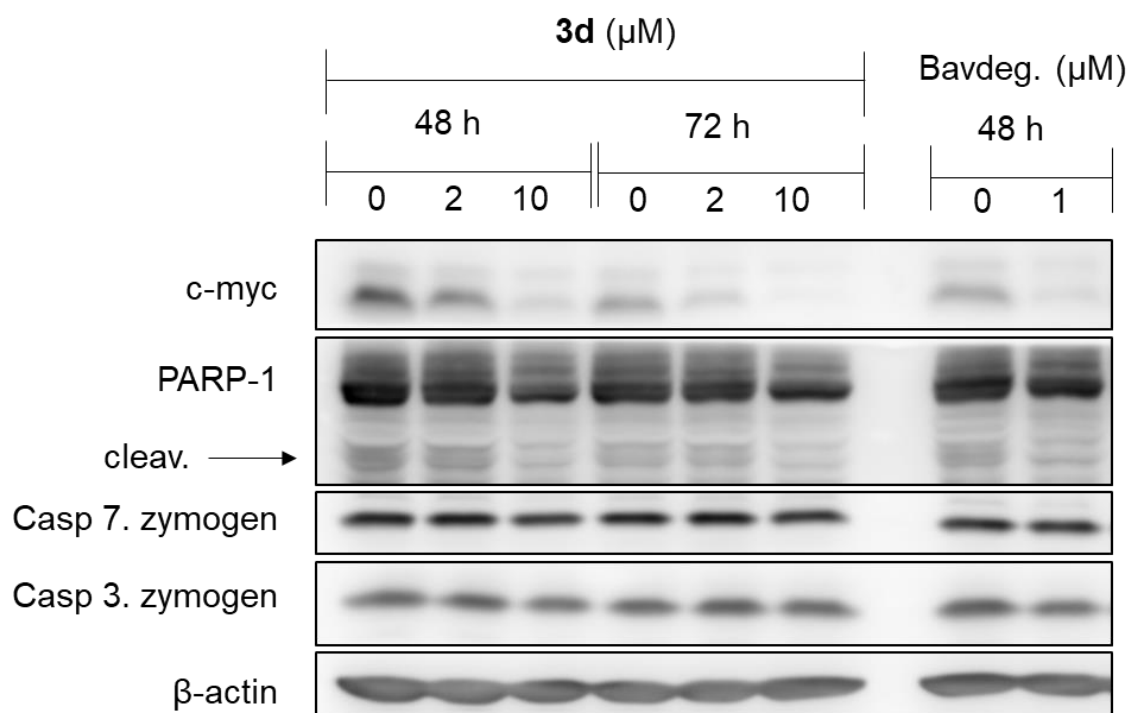
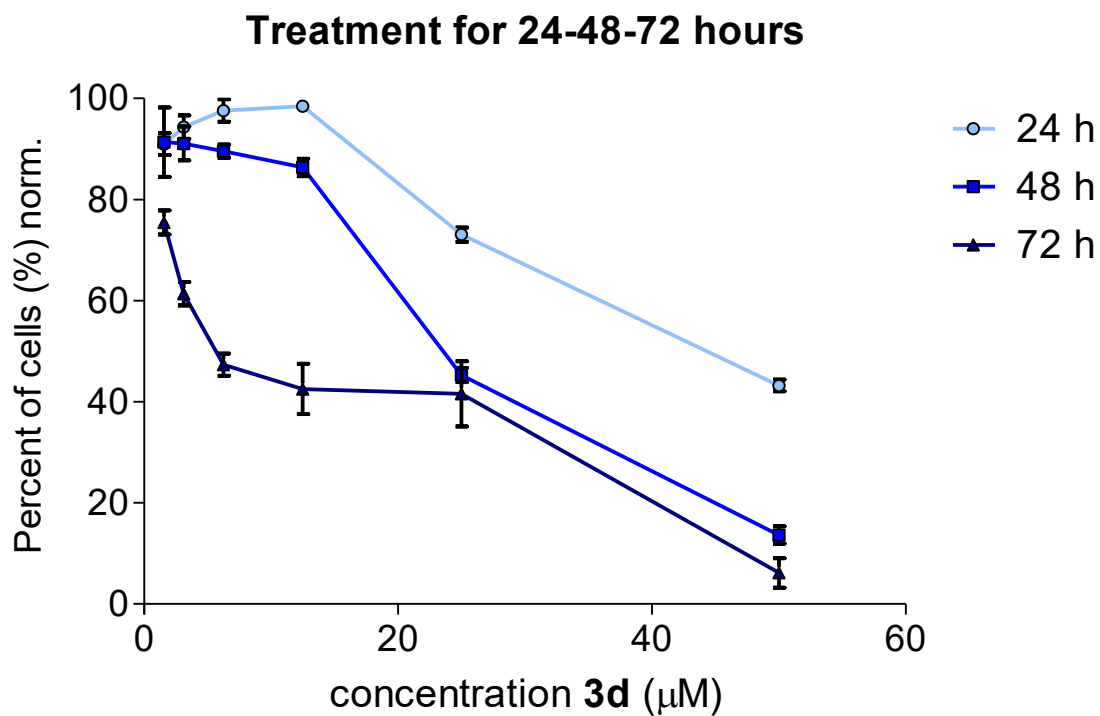


Figure S7. Antiproliferative activity of **3d** in LAPC-4 cell line after 24 h, 48 h and 72 h measured by resazurin-based viability assay. Protein levels of important proteins connected with proliferation and apoptosis in LAPC-4 treated by **3d** or bavdegalutamide for 48 h or 72, analogously to the treatment displayed in **Figure 5**. Level of β -actin served as loading control.

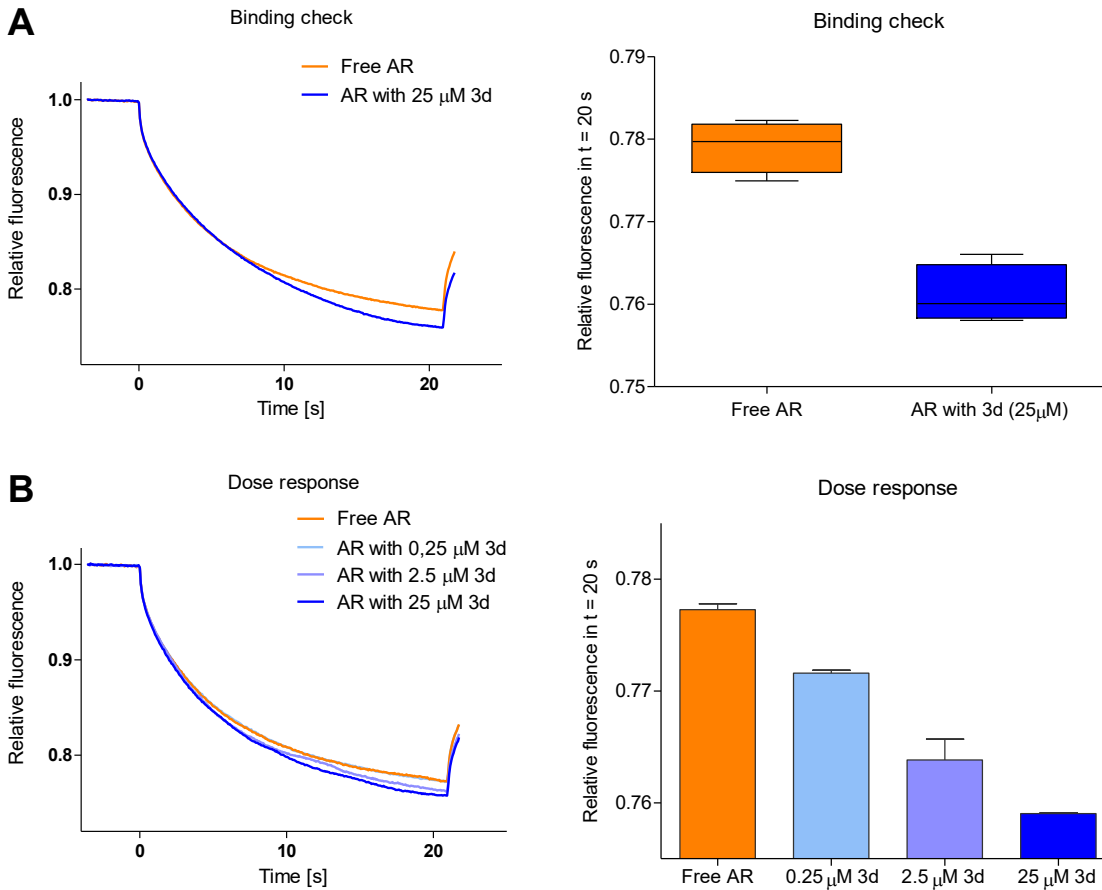
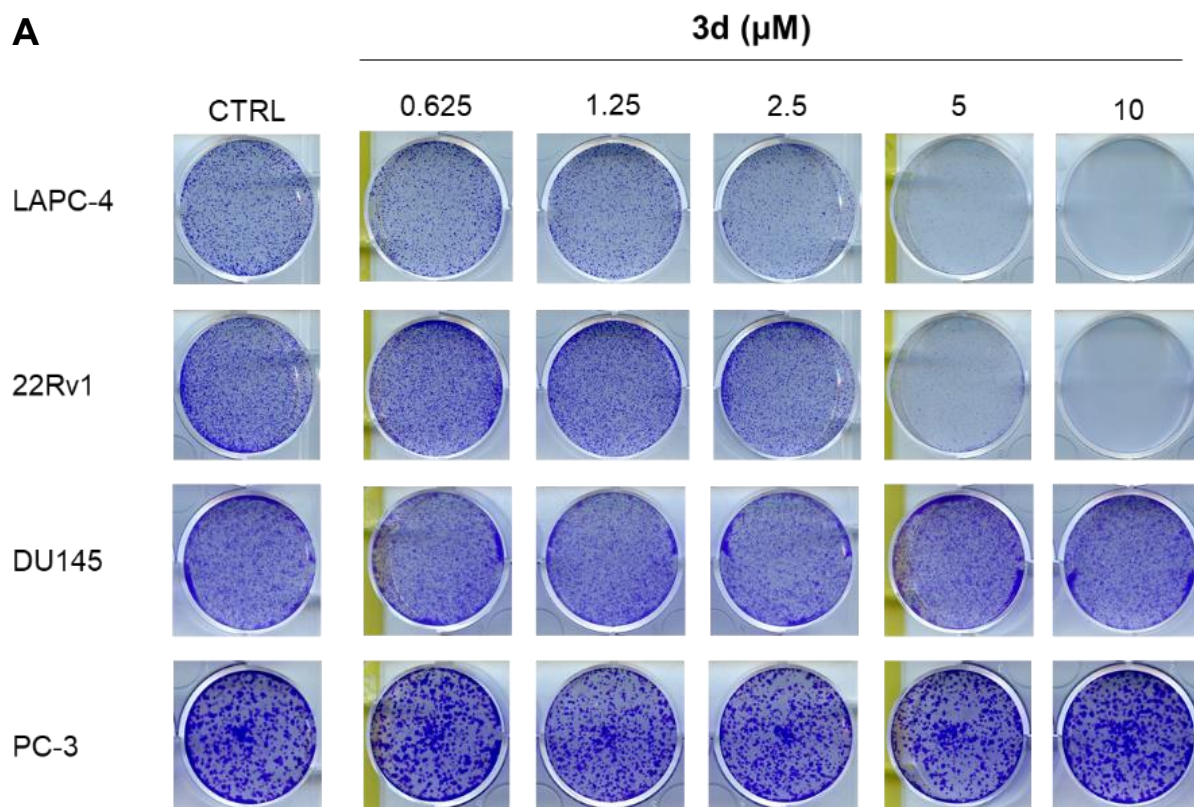
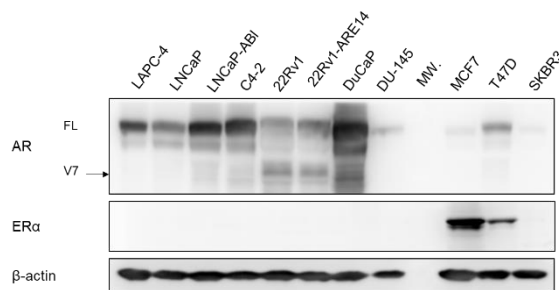


Figure S8. MST Measurement. Measured with recombinantly expressed and purified human AR-LBD, stained with NanoRed-NHS (Nanotemper). (A) Binding check measured with free AR and AR with 25 μM **3d**. Curves display the mean from ($n=4$), while box plot display the mean and min. and max. value from ($n=4$). (B) Dose response measurement was performed analogously, with free AR and 0.25 μM , 2.5 μM and 25 μM **3d**. Curves display the mean from ($n=2$), while bar plot display the mean \pm SD ($n=2$).



B

Type	AR status*	Cell line	GI ₅₀ ± SD
Prostate	positive	LAPC-4	7.9 ± 1.6
Prostate	positive	22Rv1	18.3 ± 0.6
Prostate	positive	LNCaP	16.6 ± 0.8
Prostate	positive	DuCaP	22.9 ± 1.8
Prostate	negative	DU145	>50
Prostate	negative	PC-3	>50
Breast	positive	T47D	18.2 ± 0.3
Breast	positive	SKBR3	25.5 ± 5.2
Breast	positive	MCF7	38.0 ± 6.1



* based on literature and determined from the protein expression

Figure S9. Antiproliferative activity of **3d** determined by colony formation assay (A) or resazurin-based viability assay (B). In the table in panel B, protein levels of AR and ER α are shown, based on western blotting. Level of β -actin served as loading control. See experimental part for assay's detail.

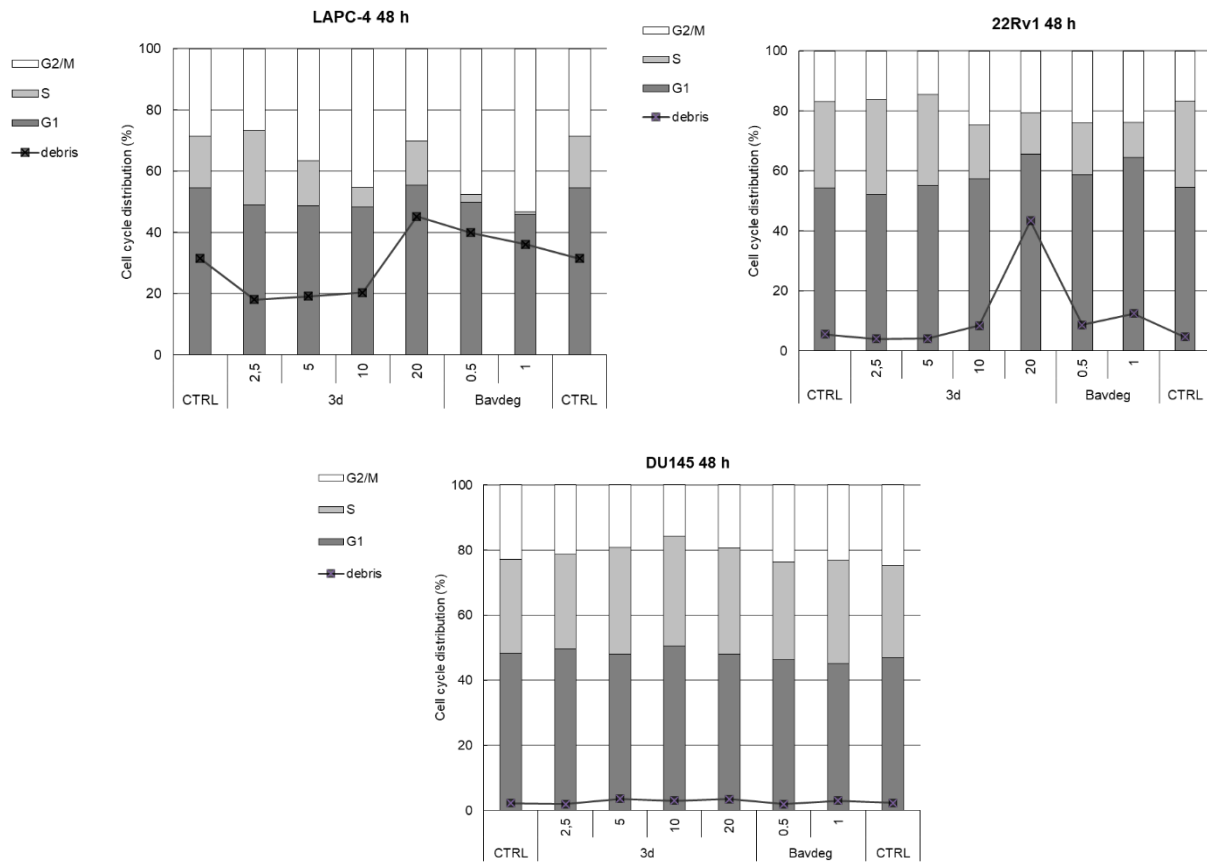


Figure S10. Cell cycle analysis of LAPC-4, 22Rv1 and DU145 after 48h treatment with 3d or bavdegalutamide.

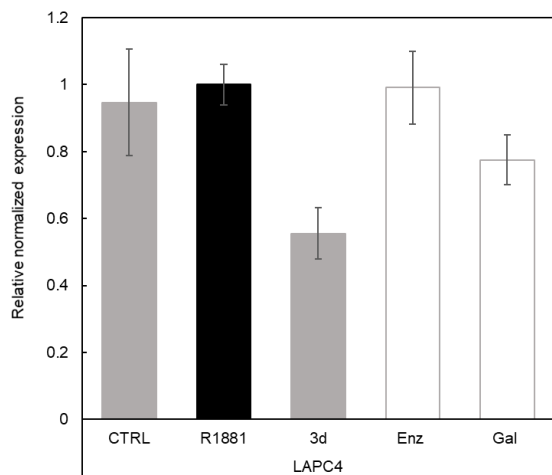


Figure S11. The effect of compound **3d** and standard AR antagonists on relative normalized expression of AR (full-length) in LAPC-4 cells. Cells were cultivated in CSS medium overnight, then treated with compounds in 10 μ M concentration in presence of 1 nM R1881 for 24 h. Enz, enzalutamide; Gal, galeterone.

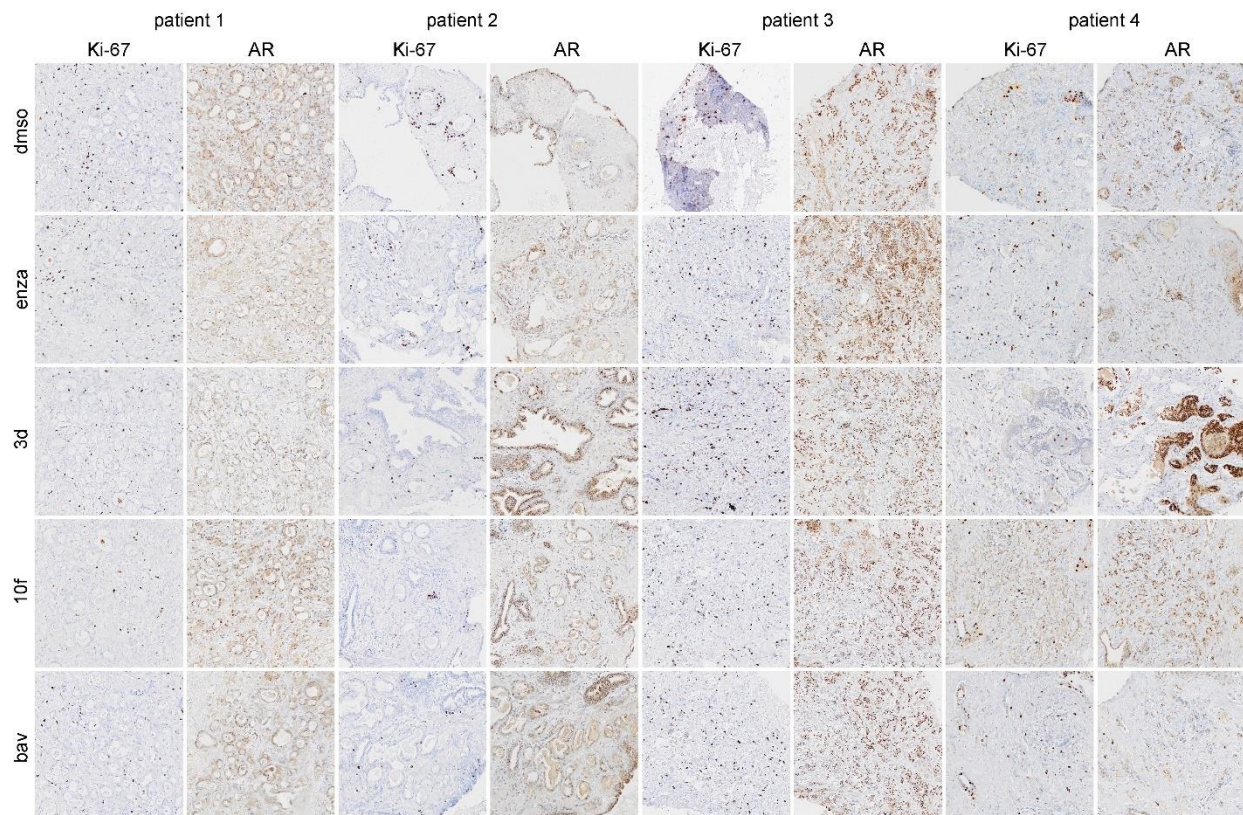


Figure S12. Immunohistochemistry analysis of Ki67 and AR in the *ex vivo* tissue culture experiment. The prostatectomy tissues were cut with vibratome, and slices were treated for three days with our candidates **3d** and **10f** (both 10 μ M) along with enzalutamide and bavdegalutamide (both 1 μ M). The tissues were then formalin-fixed, paraffin-embedded and processed for standard immunohistochemistry.

Appendix III.

Kiss MA, **Peřina M**, Bereczki L, Baji Á, Bělíček J, Jorda R, Frank É.
Dihydrotestosterone-based A-ring-fused pyridines: Microwave-assisted
synthesis and biological evaluation in prostate cancer cells compared to
structurally related quinolines. **J Steroid Biochem Mol Biol.** 2023
Jul;231:106315.



Dihydrotestosterone-based A-ring-fused pyridines: Microwave-assisted synthesis and biological evaluation in prostate cancer cells compared to structurally related quinolines

Márton A. Kiss^a, Miroslav Peřina^b, Laura Bereczki^{c,d}, Ádám Baji^a, Jakub Bělčiček^b, Radek Jorda^{b,*}, Éva Frank^{a,*}

^a Department of Organic Chemistry, University of Szeged, Dóm tér 8, H-6720 Szeged, Hungary

^b Department of Experimental Biology, Faculty of Science, Palacký University Olomouc, Šlechtitelů 27, 78371 Olomouc, Czech Republic

^c Structural Research Centre, Research Centre for Natural Sciences, Magyar tudósok körútja 2, H-1117 Budapest, Hungary

^d Institute of Materials and Environmental Chemistry, Research Centre for Natural Sciences, Magyar tudósok körútja 2, H-1117 Budapest, Hungary

ARTICLE INFO

Keywords:

Dihydrotestosterone
Pyridines
Androgen receptor
Crystal structure
Transcriptional activity

ABSTRACT

Dysfunction of the androgen receptor (AR) signalling axis plays a pivotal role in the development and progression of prostate cancer (PCa). Steroidal and non-steroidal AR antagonists can significantly improve the survival of PCa patients by blocking the action of the endogenous ligand through binding to the hormone receptor and preventing its activation. Herein, we report two synthetic strategies, each utilizing the advantages of microwave irradiation, to modify the A-ring of natural androgen 5 α -dihydrotestosterone (DHT) with pyridine scaffolds. Treatment of DHT with appropriate Mannich salts led to 1,5-diketones, which were then converted with hydroxylamine to A-ring-fused 6'-substituted pyridines. To extend the compound library with 4',6'-disubstituted analogues, 2-arylidene derivatives of DHT were subjected to ring closure reactions according to the Kröhnke's pyridine synthesis. The crystal structure of a monosubstituted pyridine product was determined by single crystal X-ray diffraction. AR transcriptional activity in a reporter cell line was investigated for all novel A-ring-fused pyridines and a number of previously synthesized DHT-based quinolines were included to the biological study to obtain information about the structure-activity relationship. It was shown that several A-ring-fused quinolines acted as AR antagonists, in comparison with the dual or agonist character of the majority of A-ring-fused pyridines. Derivative **1d** (A-ring-fused 6'-methoxyquinoline) was studied in detail and showed to be a low-micromolar AR antagonist (IC₅₀ = 10.5 μ M), and it suppressed the viability and proliferation of AR-positive PCa cell lines. Moreover, the candidate compound blocked the AR downstream signalling, induced moderate cell-cycle arrest and showed to bind recombinant AR and to target AR in cells. The binding mode and crucial interactions were described using molecular modelling.

1. Introduction

The androgen receptor is a ligand-activated transcription factor from the family of steroid hormone receptors, which plays a fundamental role in the normal development and physiology of male tissues. Upon binding of androgens, AR undergoes substantial conformational changes, various post-translation modifications, and is imported into nucleus where it interacts with co-regulators and DNA and modulates its transcriptional program [1].

Overexpression of AR, which might be accompanied by the

relaxation of its regulation is strongly connected with the development of prostate cancer (PCa), which is the second most common cancer in men (USA). First-line therapy targets androgen biosynthesis to decrease the level of plasma-circulating androgens (by orchiectomy, modulation of the luteinizing hormone release or CYP17A1 inhibitors). Androgen-deprivation therapy is usually combined with the AR antagonists, to block the pro-oncogenic signalling. Several steroidal (abiraterone, galeterone) or non-steroidal antagonists (e.g., enzalutamide, apalutamide, darolutamide, rezvilutamide) (Fig. 1) have entered clinical trials or were successfully approved as drugs [2]. Despite being very effective

* Corresponding authors.

E-mail addresses: radek.jorda@upol.cz (R. Jorda), frank@chem.u-szeged.hu (É. Frank).

<https://doi.org/10.1016/j.jsbmb.2023.106315>

Received 7 March 2023; Received in revised form 19 April 2023; Accepted 20 April 2023

Available online 21 April 2023

0960-0760/© 2023 The Author(s). Published by Elsevier Ltd. This is an open access article under the CC BY license (<http://creativecommons.org/licenses/by/4.0/>).

and demonstrating an overall survival benefit in the castration-sensitive state, the treatment frequently progresses into the castration-resistant PCa (CRPC) stage characterized by further alterations in AR signalling and undruggable splicing variants. Although various anti-AR strategies have been introduced (targeting the transcription of the AR gene, stability of transcript or protein, intracellular trafficking of AR or its downstream signalling [3–5]), still a number of AR-related mechanisms of resistance exist and novel strategies are needed to overcome them.

Pyridine-based ring systems, including quinolines comprising benzene-fused pyridines, are among the most prevalent structural motifs in drug design, with numerous bioactive representatives already identified [6–9]. The best-known steroidal pyridine derivative, abiraterone (Fig. 1), used as its acetate prodrug in the treatment of castration-resistant PCa, inhibits the CYP17A1 enzyme involved in androgen biosynthesis, thus preventing testosterone production in the adrenal glands and intratumorally [10]. Besides reduced hormone levels, abiraterone is also able to bind directly to the AR and block its activity as a ligand-dependent transcription factor [11]. Other D-ring-modified steroidal pyridines, structurally similar to abiraterone, were also investigated and found to be effective *in vitro* against androgen-sensitive and -insensitive prostate cancer cell lines (LNCaP and PC-3) [12]. Moreover, some D-ring-condensed [13] and D-secosteroid-connected quinolines [14] were also found to be effective anticancer agents. In contrast, steroids fused with a pyridine or quinoline moiety in the A-ring are less studied and only a few examples have been reported but without biological supplementation [15].

We have previously demonstrated that introducing different N-containing heterocycles to the A-ring of DHT can result in compounds that reduce the transcriptional activity of AR and exhibit antiproliferative activity in AR-positive PCa cell lines [16,17]. As our goal – in the absence of an AR crystal structure in antagonistic conformation [18] – is to investigate systematically the effect of additional heterocycles condensed to the A-ring of DHT on biological activity, in this article we report the synthesis and biological evaluation of novel mono- and disubstituted pyridine-fused derivatives (series 2 and 3, Fig. 2). All new compounds were structurally characterized by ^1H and ^{13}C NMR spectroscopy and electrospray ionization mass spectrometry (ESI-MS), and in the case of a representative novel pyridine derivative, by single crystal X-ray diffraction. A number of steroidal A-ring-fused quinolines (1a–i, Fig. 2) that have displayed modest antiproliferative activity against a panel of human gynaecological malignant cell lines [19], but have not previously been investigated for their effects on AR signalling, were also included in the current biological study due to structural similarity. Accordingly, the DHT-based quinolines and the newly prepared

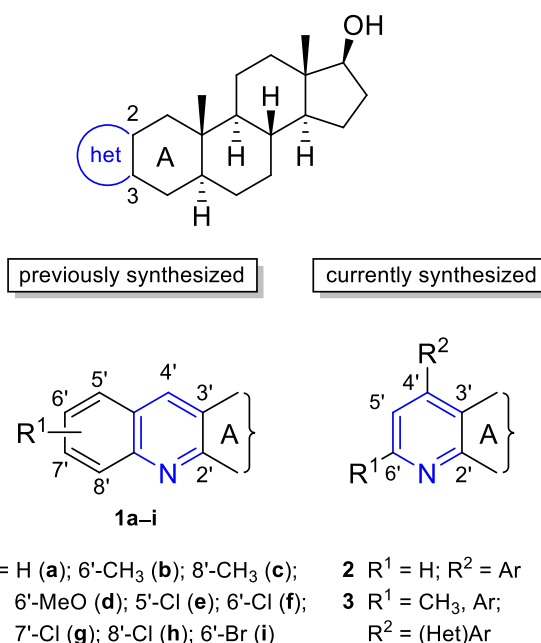


Fig. 2. Steroidal A-ring-fused quinolines [19] and pyridines investigated in this study.

pyridines were primarily screened for their ability to affect the transcriptional activity of AR in a reporter cell line. Candidate compound 1d was further studied and showed to be a low-micromolar AR antagonist, it suppressed the viability and proliferation of AR-positive PCa cell lines. Moreover, the candidate compound blocked the AR downstream signalling, mainly in wild-type AR model, induced moderate G1 arrest and was proven to bind the AR in cells and the recombinant AR protein as well. The binding mode and interaction was described using molecular modelling.

2. Results and discussion

2.1. Synthesis and characterization of DHT-based pyridine derivatives

As a first synthetic step, the regioselective modification of the A-ring of DHT was planned to be carried out using 3-(dimethylamino)propio-phenone hydrochloride (4a) leading to a 1,5-diketone moiety at C-2 position. By amine elimination, β -amino ketone hydrochloride salts are

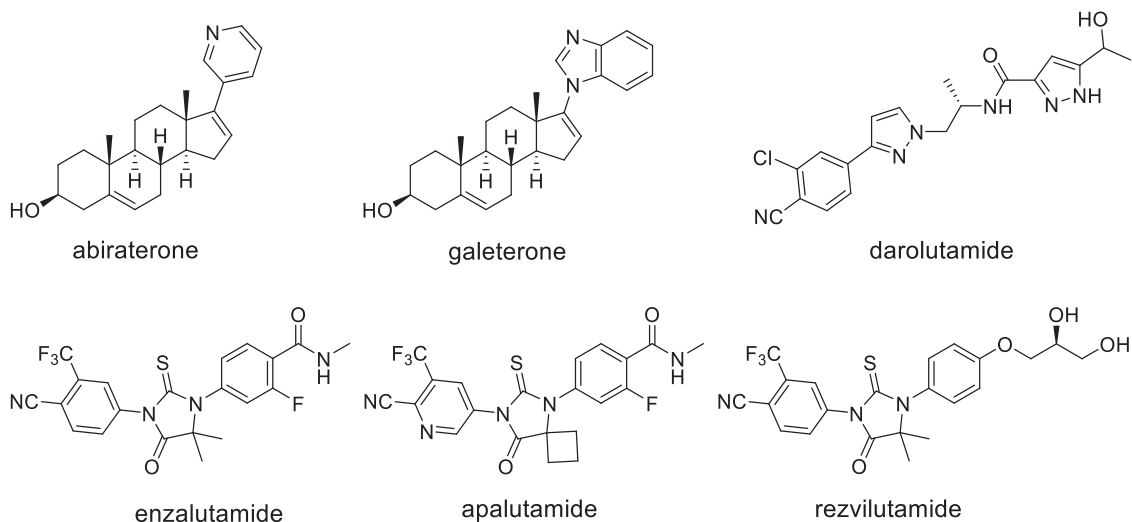
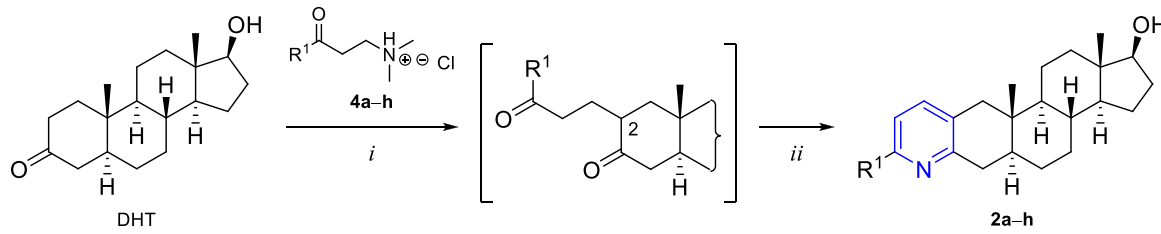


Fig. 1. Examples of different types of antiandrogens.

Table 1
Synthesis of DHT-derived A-ring-fused 6'-substituted pyridine derivatives.



Entry	R ¹	Product ^a	Yield (%) ^b
1	Ph	2a	81
2	<i>p</i> -CH ₃ -C ₆ H ₄	2b	70
3	<i>p</i> -MeO-C ₆ H ₄	2c	79
4	<i>p</i> -NO ₂ -C ₆ H ₄	2d	72
5	<i>p</i> -F-C ₆ H ₄	2e	80
6	<i>p</i> -Cl-C ₆ H ₄	2f	72
7	<i>p</i> -Br-C ₆ H ₄	2g	78
8	<i>o</i> -OH-C ₆ H ₄	2h	67

Reagents and conditions: i) pyrrolidine, 1,4-dioxane, 120 °C, 20 min, MW; ii) HONH₂·HCl, EtOH, 90 °C, 10 min, MW.

^a Heterocyclization was performed with the crude diketone intermediate.

^b Calculated for two steps from DHT after column chromatography.

able to form α,β -unsaturated ketones *in situ* [20], which can act as Michael acceptors in the reaction with DHT. Preliminary experiments under conventional heating in absolute EtOH, using triethylamine (TEA) as a base, showed the formation of a new product, but complete conversion was not achieved even after 24 h. In order to facilitate the alkylation reaction, pyrrolidine was applied instead of TEA in 1,4-dioxane to generate the corresponding enamine *in situ* from DHT, which then readily reacted as a more efficient Michael donor under microwave (MW) conditions with **4a** according to the Stork enamine alkylation [21]. After 20 min of irradiation, only a small amount of residual starting material and a spot of a newly formed compound with a similar retention factor were detected by thin-layer chromatography (TLC). The crude product was used in the heterocyclization reaction without further purification (Table 1, entry 1).

Our initial attempts for a tandem-like cyclization of the dicarbonyl intermediate with hydroxylamine hydrochloride as an ammonia surrogate [22] in the previously used 1,4-dioxane led to incomplete conversion and the formation of a dioxime product verified by ESI-MS. In contrast, the desired 6'-phenylpyridine derivative **2a** was successfully obtained when the dioxane was evaporated and the residue was redissolved in absolute EtOH. Compound **2a** was purified by column chromatography on silica gel, but high yields were only obtained when dichloromethane containing 1 v/v% TEA was used as eluent. To extend the compound library, Mannich salts **4b–h** from various substituted aryl-methyl-ketones were synthesized according to methods described previously [23,24]. These were then all subjected to 1,5-diketone formation from DHT, followed by cyclization to obtain the corresponding 6'-monosubstituted A-ring-condensed pyridines (**2b–h**) in moderate to good yields, regardless of the electronic nature of the R¹ substituent (Table 1, entries 2–8).

The solid phase structure of a colourless prism of **2a** was determined by single crystal X-ray diffraction (Fig. 3). The molecule crystallized in the monoclinic crystal system, in *P2*₁ space group. The asymmetric unit contains two molecules in the opposite position and the unit cell contains four molecules.

The configuration of **2a** is established based on the known absolute configuration of the utilized natural starting compound, R at C8 and C8 * and S at C5, C5 *, C9, C9 *, C10, C10 *, C13, C13 *, C14, C14 *, C17, C17 * (Fig. S1). Molecules of **2a** are arranged parallel to each other in columns running along the *b* crystallographic axis (Fig. 4). C-H... π interactions stabilize the packing (Fig. S2). In the molecule of **2a**, only one acceptor (N1, N1') and one donor atom are present (O1, O1') and a hydrogen bond is formed between them that connects the columns formed by the stacking of the molecules. Additionally, the O1 oxygen accepts a hydrogen from a carbon donor (Table S1).

As a continuation, similar analogues substituted at both C-4' and C-6' positions of the pyridine moiety were aimed to be synthesized. For this, steroidal arylidene derivatives **5a–e**, previously obtained from DHT [16, 17,25] were used as starting materials, since these α,β -enones can be reacted with α -pyridinium methyl ketone salts in Kröhnke pyridine cyclization reactions. Thus, 1-(2-oxo-phenylethyl)pyridinium iodide (**6a**) and its analogues (**6b**, **6c**) were first prepared in an Ortoleva-King reaction by heating acetophenone, 2'-hydroxyacetophenone or 2-acetylpyridine with elemental iodine in pyridine according to the method described in the literature [26,27]. The resulting precipitates were washed with cold pyridine and diethyl ether several times, and the crude products were used in the following cyclization of **5a–e** with ammonium acetate under Kröhnke conditions (Table 2). Systematic combination of **5a–e** with **6a–c** in the pyridine formation reactions resulted in 15 differently substituted heterocyclic products **3a–o** in moderate to good yields (51–82%) after chromatographic purification.

The structure of all novel products was confirmed by NMR spectroscopy and ESI-MS measurements. The characteristic splitting of 1-H₂ (two doublets) and 4-H₂ (two double doublets) in the ¹H NMR spectra is indicative for the 2,3-fused heteroring. The signals of protons at C4' and C5' of the pyridine ring in **2a–g** can be detected as doublets with the same coupling constant of around 8 Hz. However, only a singlet proton peak (5'-H) can be noticed for the highly substituted pyridine ring of **3a–o**.

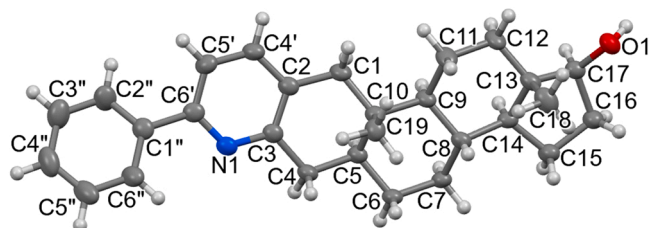


Fig. 3. Molecular model and atom labelling of **2a**. Ellipsoid representation, displacement parameters are drawn at the 50% probability level.

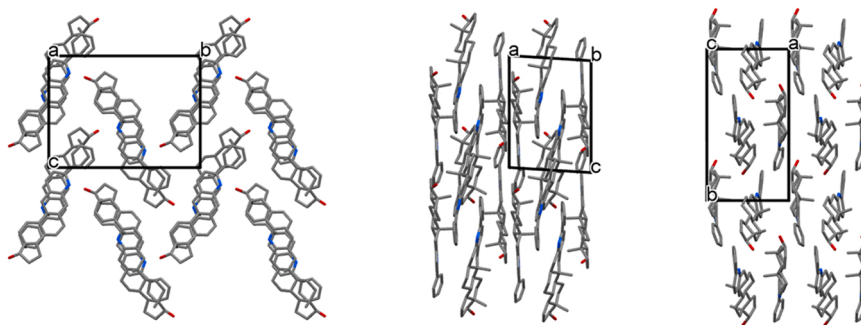


Fig. 4. Crystal packing of **2a** shown in the *a*, *b* and *c* crystallographic directions. Molecules are drawn by stick representation, hydrogens are omitted for clarity.

Table 2

Synthesis of DHT-derived A-ring-fused 4',6'-disubstituted pyridine derivatives.

Entry	Enone	R ²	R ¹	Product	Yield (%)
1	5a	CH ₃	Ph	3a	72
2			<i>o</i> -OH-C ₆ H ₄	3b	65
3			pyridin-2-yl	3c	71
4	5b	Ph	Ph	3d	77
5			<i>o</i> -OH-C ₆ H ₄	3e	76
6			pyridin-2-yl	3f	82
7	5c	<i>p</i> -F-C ₆ H ₄	Ph	3g	67
8			<i>o</i> -OH-C ₆ H ₄	3h	59
9			pyridin-2-yl	3i	68
10	5d	<i>p</i> -Cl-C ₆ H ₄	Ph	3j	73
11			<i>o</i> -OH-C ₆ H ₄	3k	70
12			pyridin-2-yl	3l	77
13	5e	<i>p</i> -Br-C ₆ H ₄	Ph	3m	52
14			<i>o</i> -OH-C ₆ H ₄	3n	51
15			pyridin-2-yl	3o	54

Reagents and conditions: i) NH₄OAc, EtOH, MW, 90 °C, 20 min.

2.2. Screening of compounds for their activity towards AR and PCa cells' viability

We recently reported several DHT-based A-ring-fused (hetero)arylidenes, azolo[1,5-*a*]pyrimidines, and differently substituted pyrazoles and their targeting of the AR in PCa cell lines [16,17].

In this study, novel DHT derivatives by modifying the A-ring with mono- and disubstituted pyridines (**2a–h** and **3a–o**) are introduced. These series were extended with some structurally similar quinolines (**1a–i**, Fig. 2), which were previously published but were not pharmacologically investigated in relation to AR.

Transcription of AR-regulated genes is tightly connected to its activity, as AR is a direct transcription factor. Therefore, inhibition of transcriptional activity was evaluated at first using AR-dependent reporter cell line (22Rv1-ARE14), expressing the inserted luciferase gene under the control of AR-response element [28]. All compounds were screened to their effect on AR transcriptional activity at three concentrations (2 – 10 – 50 μM) in both agonist (evaluation of the ability to induce the AR activation in comparison to the synthetic agonist R1881) and antagonist mode (evaluation of the ability to suppress the AR activation in the presence of synthetic agonist R1881).

The analysed library comprised 9 already published steroidal A-ring-fused quinolines (**1a–1i**) [19], 8 novel A-ring-fused 6'-substituted pyridine derivatives (**2a–2h**) and 15 A-ring-fused 4',6'-disubstituted

pyridine derivatives (**3a–3o**). From the 32 evaluated compounds, 14 were able to decrease the AR-transcriptional activity in the antagonist scheme of the experiment in 50 μM. Overall, A-ring-fused quinoline derivatives were the most potent derivatives (Table 3), from which 3 compounds (**1a**, **1d**, **1i**) were able to diminish the R1881-activated AR transcriptional activity to approx. 50% at 10 μM concentration. Based on the structure comparison, the potent derivatives were unsubstituted A-ring fused quinoline (**1a**) or 6'-substituted quinoline derivatives bearing methoxy- or bromo-moiety (**1d**, **1i**, respectively). All these 3 compounds reached similar activity as steroidal standard galeterone, but did not outperform the non-steroidal standard enzalutamide, which decreased the AR transcriptional activity below 25%.

Analysing the agonist activities of the studied compounds towards the AR, we have observed that 2 of 8 A-ring-fused quinolines displayed dose dependent agonist activity (**1b** and **1g** in correspondence with the antagonist mode). Two other A-ring fused quinolines exerted moderate agonist activities in 10 μM and 2 μM (**1c**, **1i**), while the rest of this group was found to be no AR agonist, including **1a** and **1d**, which belong to the most potent antagonists and were selected for further experiments.

Despite the fact that there is no generally clear SAR within series 2 and 3, several characteristics can be pointed out. The monosubstitution at C-6' position of the A-ring fused pyridine by an aromatic moiety clearly led to compounds exerting strong agonist activities in series 2, except for compounds **2f** and **2g** (bearing a *p*-Cl-phenyl or *p*-Br-phenyl

Table 3

AR transcriptional activity in antagonist and agonist modes.

cmpd.	AR transcriptional activity antagonist mode ^a			AR transcriptional activity agonist mode ^a				
	50 μ M	10 μ M	2 μ M	50 μ M	10 μ M	2 μ M		
A-ring-fused quinolines	1a	4	50	85	3	17	20	
	1b	142	121	108	41	30	24	
	1c	11	98	104	16	59	43	
	1d	16	53	96	5	10	16	
	1e	46	96	103	8	14	16	
	1f	7	103	114	3	18	19	
	1g	110	106	106	93	65	56	
	1h	96	67	92	10	10	14	
	1i	18	52	102	5	49	53	
	2a	115	90	94	121	67	66	
A-ring-fused 6'-substituted pyridines	2b	196	116	107	190	110	83	
	2c	183	136	123	194	133	122	
	2d	124	83	93	73	43	30	
	2e	151	110	110	146	56	34	
	2f	36	85	89	51	69	69	
	2g	70	105	105	69	68	53	
	2h	116	88	89	19	13	15	
	A-ring-fused 4',6'-disubstituted pyridines	3a	71	105	105	58	43	23
		3b	26	100	102	24	62	34
		3c	4	92	103	5	94	100
3d		78	100	99	31	23	17	
3e		113	114	111	94	77	57	
3f		99	92	104	85	88	63	
3g		70	111	111	47	40	21	
3h		84	106	113	63	72	64	
3i		113	130	120	89	117	120	
3j		135	129	114	16	16	16	
3k	109	113	110	55	23	16		
3l	167	148	127	143	127	116		
3m	129	111	111	31	19	16		
3n	115	114	112	55	24	16		
3o	163	123	106	120	70	32		
galeterone	8	48	84	3	12	14		
enzalutamide	20	24	46	12	14	14		

^a Transcriptional activity of AR upon 24 h treatment of 22Rv1-ARE14 with analysed compounds in antagonist (competition with standard agonist, 1 nM R1881) and agonist (compound alone) modes, normalised to the signal of 1 nM R1881. Measured in duplicate and repeated twice, mean is presented.

substituent, respectively), which displayed moderate antagonist activity. In series 3, the combination of a methyl moiety at 4'-position with an aryl substitution in C-6' position of the A-ring fused pyridine yielded compounds with weak to moderate antagonist properties (**3a–3c**). Similar beneficial effect was recently observed in very potent disubstituted A-ring fused pyrazoles [17]. In contrast, substitutions by aryl groups in both C-4' and C-6' positions of the pyridine moiety yielded compounds with moderate to strong agonist activities, where the combination of *p*-halophenyl with pyridin-2-yl functionalities at these positions led to the most potent agonists from the series 3. This observation also correlates with our previous research, where biaryl derivatives of A-ring fused pyrazoles were found to be potent AR agonists [17].

Next, all compounds were evaluated in 20 μ M concentration for their effect on PCa cell lines' proliferation using the resazurine-based cell viability assay after 72 h treatment. The collection of PCa cell lines represented LAPC-4 (wild type AR), 22Rv1 (LBD mutation AR-H875Y and splicing variant V-7), LNCaP (LBD mutation T877A) and DU145 (AR negative). It is known that AR antagonists induce only moderate

cytotoxicity, since the blockage of AR-mediated signalling leads rather to cytostatic effect. Our results confirmed those studies, because the majority of compounds decreased the viability only to 70–80% of the vehicle-treated cells. Generally, the viability of DU145 was not influenced by most of the compounds, which, in our hypotheses, supports the targeting of the AR (Table 4).

In the 3 most potent antagonists from the A-ring-fused quinoline derivatives (**1a**, **1d**, **1i**), we expected to observe the antiproliferative activity against AR-positive PCa cells. Corresponding with the AR-antagonist activity, compounds **1d** and **1i** indeed displayed reasonable antiproliferative activity predominantly in 22Rv1 (decreasing the viability to approx. 20% of the control treated by vehicle), but also in LAPC-4 and LNCaP. Compound **1d** outperformed the standard antagonist galeterone in 22Rv1 and displayed similar potency to this standard in LNCaP and LAPC-4. There was a clear difference between the sensitivity of the AR-positive cell lines and the AR-negative DU145 (Table 4). Based on the structure of compounds, the unsubstituted A-ring fused quinoline (**1a**) displayed weaker antiproliferative activity compared

Table 4Viability of PCa cells after 72 h treatment with 20 μ M compounds.

Cmpd.	Viability of Pca cell lines after treatment with 20 μ M for 72 h (mean) ^a				
	LNCaP	LAPC-4	22Rv1	DU145	
A-ring-fused quinolines	1a	80	84	77	98
	1b	85	98	114	88
	1c	83	74	99	104
	1d	56	80	24	89
	1e	92	86	111	103
	1f	80	71	66	92
	1g	84	90	122	106
	1h	94	82	44	97
	1i	81	59	19	84
A-ring-fused 6'-substituted pyridines	2a	85	61	91	112
	2b	84	90	113	107
	2c	85	98	75	103
	2d	87	79	82	99
	2e	88	79	106	102
	2f	80	33	67	112
	2g	84	73	73	107
	2h	85	89	87	97
	3a	83	66	124	111
A-ring-fused 4',6'-disubstituted pyridines	3b	78	61	98	112
	3c	70	59	49	108
	3d	79	80	69	113
	3e	74	62	70	100
	3f	63	78	70	114
	3g	70	64	56	106
	3h	65	16	67	98
	3i	60	69	81	103
	3j	89	109	86	103
	3k	87	107	84	105
	3l	68	89	96	106
3m	86	100	85	108	
3n	90	106	89	101	
3o	79	106	113	103	
galeterone	58	76	95	109	
enzalutamide	99	81	102	96	

^a Cytotoxic effect of compounds was evaluated by resazurine-based viability assay (72-hour treatment) with a single dose of 20 μ M compounds. Measured in duplicate and repeated twice.

with the 6'-methoxy- or bromo-substituted analogues (**1d**, **1i**, respectively). Interestingly, the most sensitive cell line to these two derivatives was 22Rv1, with less but still notable sensitivity to **1h** (8'-chloroquinoline derivative) and **1f** (6'-chloroquinoline derivative).

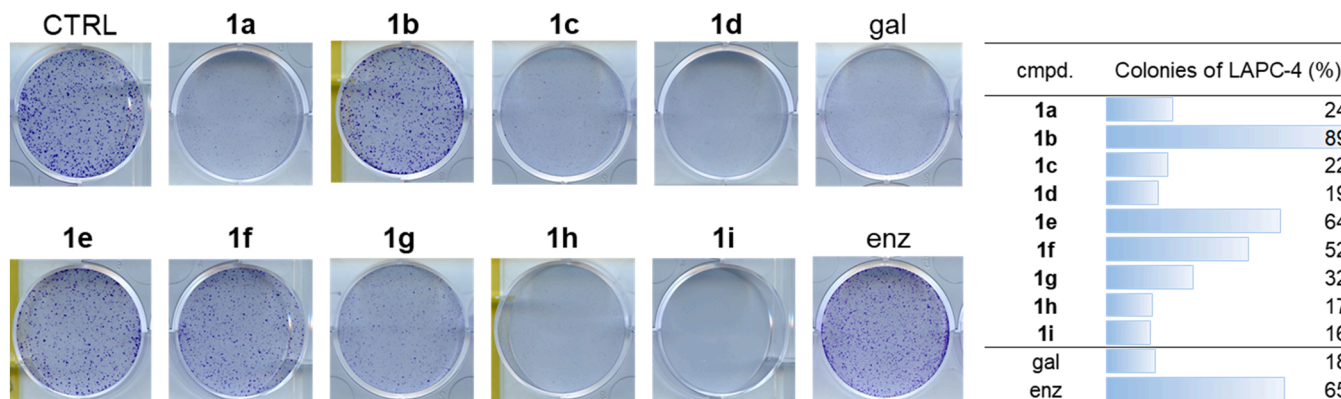


Fig. 5. A-ring fused quinolines reduce LAPC-4 derived colony formation. Antiproliferative activity of compounds from series 1 was evaluated in 10 μ M concentration using colony-formation assay (10 days treatment). Gal, galeterone; Enz, enzalutamide.

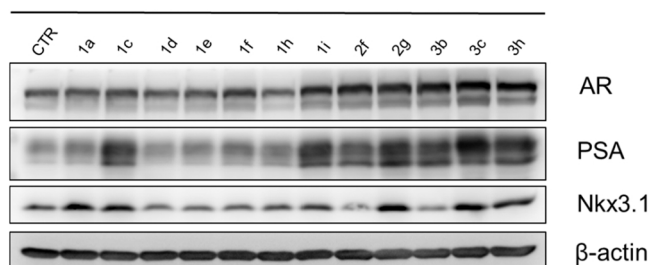
LAPC-4

Fig. 6. Several A-ring fused quinolines display agonist mode of action. Effect on AR-signalling was evaluated using immunoblotting in LAPC-4 cells treated with 10 μ M concentration of selected compounds for 48 h.

Since the most promising compounds were found within series 1, we have evaluated the antiproliferative activity of these derivatives in 10 μ M towards the LAPC-4 cell line using the colony-formation assay (CFA) for 10 days. Compounds **1a**, **1c**, **1d**, **1g**, **1h** and **1i** decreased the colony-formation to 16–30% of control treated by vehicle, while **1b**, **1e**, and **1f** did not have such effect (Fig. 5).

The perspective members of series 1 (except for **1b** and **1g**) were further tested for their effect on the AR protein level and AR-regulated proteins in LAPC-4 at 10 μ M concentration, upon 48-h treatment. We did not observe any profound decreases in AR and AR-regulated proteins. On the other hand, compounds **1c** and **1i** increased the level of PSA. Selected compounds from series 2 (**2f**, **2g**) and 3 (**3b**, **3c** and **3h**) increased the AR and PSA protein level that confirmed their agonist mode of action (Fig. 6). Within analogous experiment in LNCaP, we observed a marked decrease in Nkx3.1 and PSA level upon 48-h treatment with 10 μ M of **1d** (Fig. S3). On the other hand, compounds **1a**, **1e**, **1f**, **1h** affected only the Nkx3.1 protein level, by significant decrease in case of **1f** and moderate decrease for the rest (Fig. S3).

Based on all the above-mentioned results, we have evaluated that compound **1d** displayed the highest potency towards the AR transcriptional activity, AR-positive PCa cell lines' viability and beneficial effects on AR signalling, therefore we further evaluated other characteristics of this lead compound.

2.3. Detailed effect of 1d on AR signalling, PCa cells' viability, proliferation, and the cell cycle

We have evaluated the effect of **1d** on the AR-transcriptional activity using the reporter cell line 22Rv1-ARE14 again, in wide concentration range, both in agonist and antagonist modes. It was found that IC₅₀ value of **1d** antagonism (10.5 μ M) (Fig. 7A) shows weaker, but comparable potency to galeterone (7.6 μ M), a known standard antagonist. After

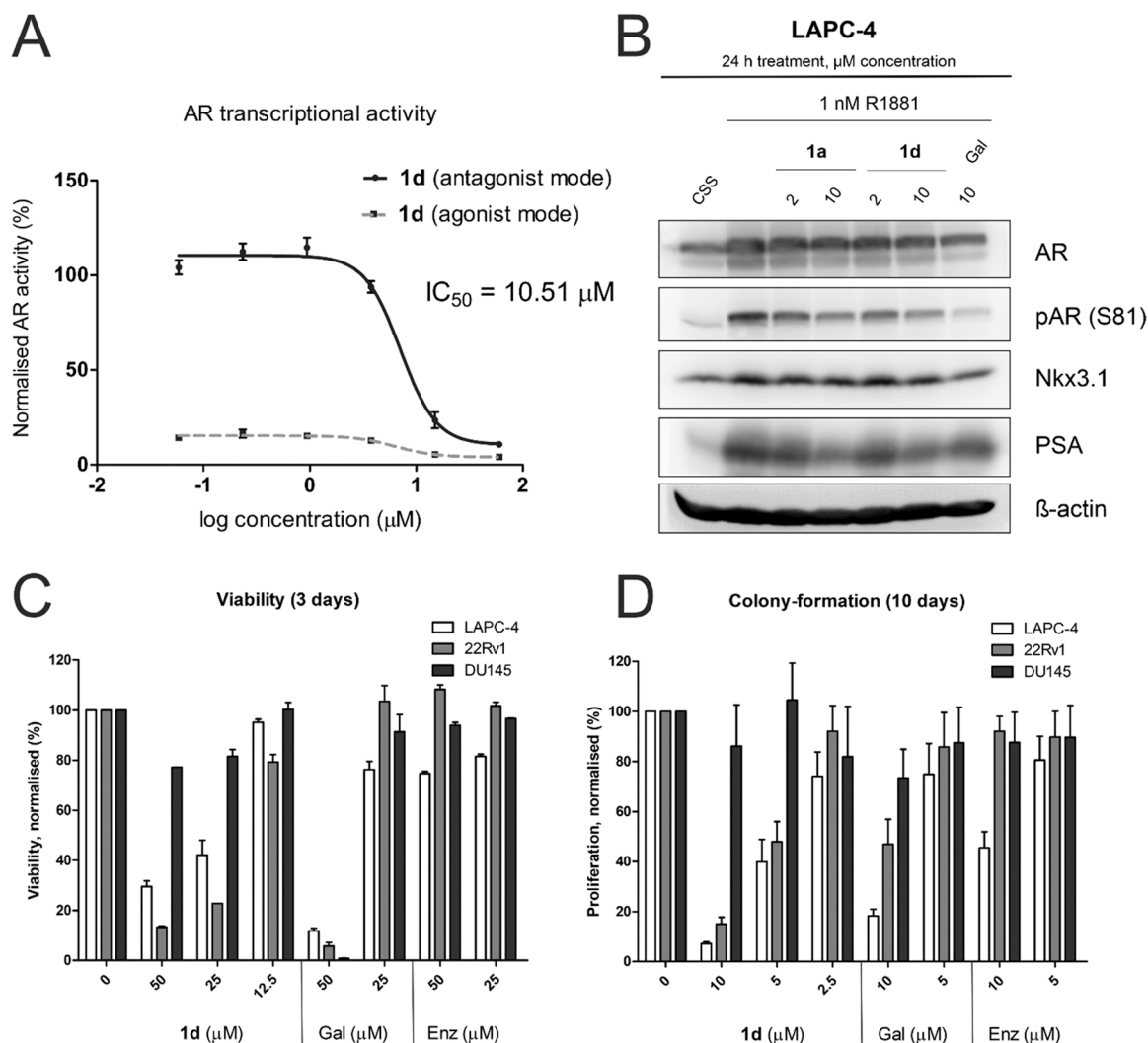


Fig. 7. Compound **1d** acts as a pure antagonist, interferes with AR-downstream signalling and displays selective antiproliferative activity towards AR-positive PCa cell lines. **(A)** Transcriptional activity of AR upon treatment with **1d** in antagonist (competition with standard agonist, 1 nM R1881) and agonist (compound alone) modes, normalised to the signal of 1 nM R1881. Curves were plotted via non-linear curve fit in GraphPad Prism 5 from 4 independent experiments, error bars represent SD. **(B)** Effect of **1a** and **1d** on expression of AR and its downstream targets using immunoblotting. The cells were deprived of androgens (in CSS) for 24 h and stimulated with 1 nM of R1881 alone or with analysed compounds for additional 24 h. **(C)** Cytotoxic effect of **1d** and standards was evaluated by resazurine-based viability assay (3-days treatment), measured in duplicate and repeated twice. **(D)** Antiproliferative activity of **1d** and standards was evaluated using colony-formation assay (10-days treatment) in duplicate and repeated twice. Gal, galeterone; Enz, enzalutamide.

steroid withdrawal and subsequent stimulation of AR signalling by synthetic androgen R1881, we observed the ability of **1d** and **1a** to diminish the AR activating phosphorylation on S81 and suppression of AR signalling in 10 μM concentration (decrease of the PSA protein level), similar to the effect of galeterone (Fig. 7B). We observed similar activity of the lead compound mainly on the PSA level even in LNCaP and 22Rv1 (Fig. S4).

The antiproliferative effect of **1d** was further evaluated in PCa cell lines in dose dependent manner, using both the resazurine-based viability assay upon 3 days of treatment (Fig. 7C) and colony formation assay upon 10 days of treatment (Fig. 7D). We clearly confirmed that **1d** targets preferentially the AR-positive PCa cell lines. Upon 3 days of treatment, compound **1d** was able to decrease the viability of LAPC-4 and 22Rv1 below the 50% of control treated by vehicle at 50 μM and 25 μM , with 22Rv1 being slightly more sensitive. The lead compound outperformed the standard galeterone, which displayed an antiproliferative activity only at 50 μM after 3 days, and enzalutamide, which exerted moderate antiproliferative effect only in LAPC-4. In contrast with galeterone, which markedly affected also the AR-negative

DU145 at 50 μM , we did not observe significant effect of **1d** towards the DU145 cell line (Fig. 7C). In agreement with previous findings, the antiproliferative activity of the lead compound was enhanced after 10 days of treatment, which was assessed by the colony-formation analysis. The lead compound preferentially blocked the formation of LAPC-4 and 22Rv1 cell colonies in dose dependent manner and showed to be more effective than galeterone and enzalutamide (Fig. 7D).

Cell cycle analysis after 24 h of treatment showed an increased number of cells in G1 phase with reduced S-phase cells' percentage, which reflected the proliferation blockage of LAPC-4 and LNCaP, mainly at 10 μM concentration of the lead compound. The effect of **1d** was more profound, in comparison with galeterone or enzalutamide (Fig. S5).

2.4. Interaction of 1d with the AR-LBD and molecular modelling

To verify the ability of **1d** to bind to the AR cavity in cells, we performed "the rescue experiment" in LAPC-4 cells. The cells were treated with **1d** for 2 h to saturate the AR-ligand-binding domain (LBD) and then bavdegalutamide (ARV-110, an effective AR degrader) was added

for additional 6 h. As presented in Fig. 8A, the degradation of AR induced by bavdegalutamide was attenuated by 20 μM of **1d** and confirmed its cellular interaction with the AR cavity.

Next, the interaction of **1d** was also confirmed by the microscale thermophoresis (MST) using His6-tagged human AR-LBD [29]. Binding of **1d** in 12.5 μM and 25 μM concentrations led to an extensive change of the labelling dye-fluorescence (Fig. 8B). Moreover, the change was consistent with the effect of 25 μM galeterone (Fig. 8B).

We recruited the flexible molecular docking of the candidate compound **1d** into AR-LBD co-crystal structure with natural agonist DHT (PDB: 2PIV). The key residues in extremities of the cavity (Asn705, Gln711, Arg752, and Thr877) were set flexible, which allowed rearrangement of the cavity to fit **1d**. The best pose displayed high binding energy ($\Delta G_{\text{vina}} = -10.2$ kcal/mol) and similar orientation as was observed for steroidal antagonists cyproterone [30] or galeterone [31]. Overall, the A-ring fused 6'-methoxyquinoline part was sandwiched between the helix 2 and 3 and the methoxy moiety was oriented towards the Val 684, with possible hydrogen bonds between the oxygen and Arg752 and Gln711. The fused quinoline moiety was stabilised by

hydrophobic bonds with Leu707, Met749 and Phe764. Further hydrophobic interactions were formed between the steroid ring and side chains of Leu704, Met780 and Leu873. The 17 β -OH on the D-ring formed a conserved bond with Thr877, with a possible interaction with Asn705 as well (Fig. 8C).

3. Conclusions

In conclusion, we reported the efficient syntheses of A-ring-fused mono- and disubstituted pyridine derivatives of DHT in two different synthetic pathways, using microwave irradiation as an energy source. 1,5-Diketones were prepared using Mannich salts, which were then converted to A-ring-fused 6'-substituted pyridines with hydroxylamine. The compound library was extended with 4',6'-disubstituted analogues by the Kröhnke's pyridine synthesis. Single crystal X-ray diffraction confirmed the exact structure of a representative monosubstituted pyridine derivative. Pharmacological investigations were performed in prostate cancer cells in comparison with previously prepared, structurally similar quinolines. It was shown that several A-ring-fused quinolines

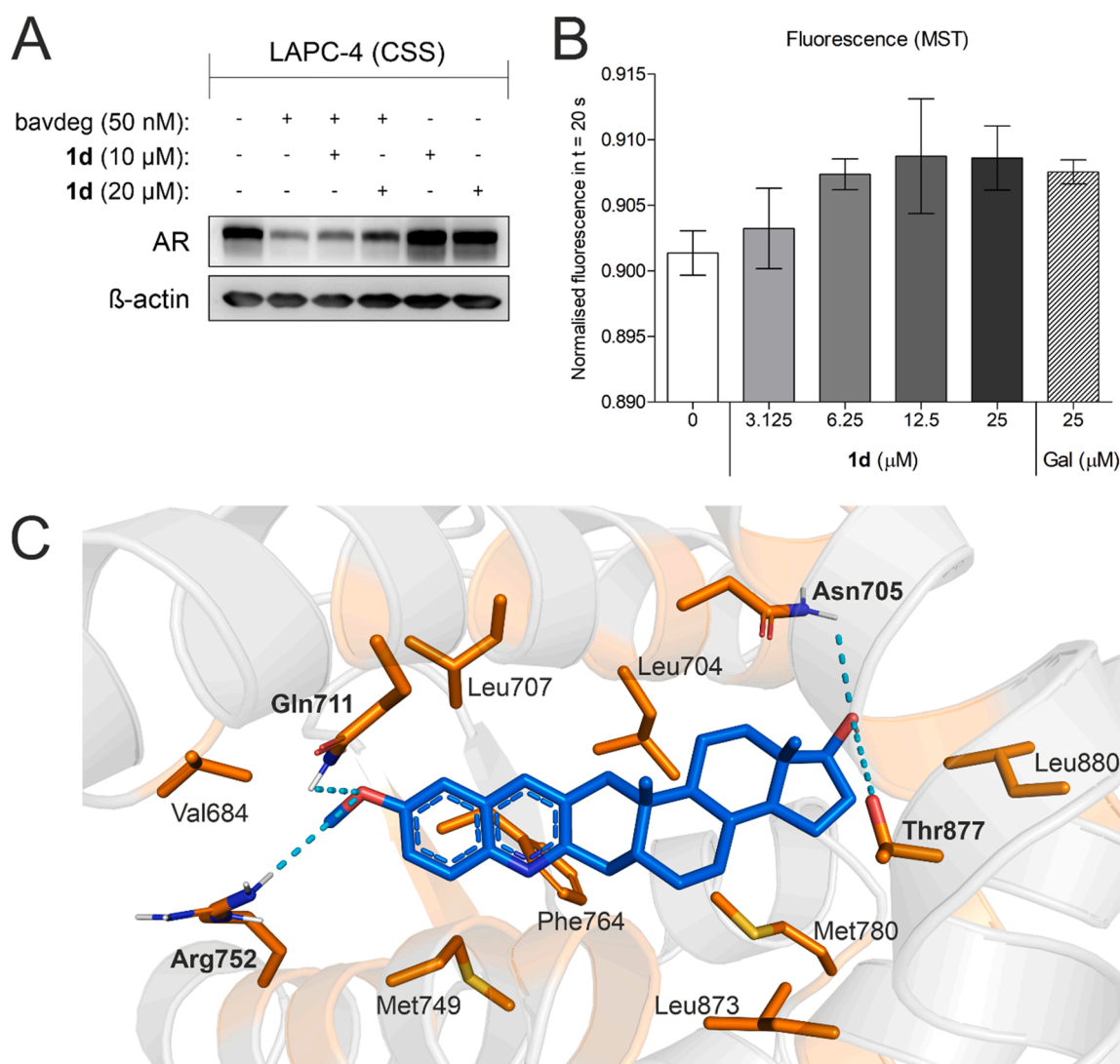


Fig. 8. Compound **1d** binds the AR protein *in vitro* and *in silico*. (A) Compound **1d** suppresses bavdegalutamide-induced AR-degradation. LAPC-4 cells were cultivated in CSS-supplemented medium, pre-treated with **1d** for 2 h and then bavdegalutamide was added for the next 6 h. Level of β -actin served as protein loading control. Bavdeg, bavdegalutamide. (B) Binding of **1d** to recombinant AR was evaluated by MST measurement with His6-tagged human AR-LBD. Bar chart displays the mean \pm SD ($n = 2$). Gal, galeterone. (C) Binding pose of **1d** in the LBD of AR (PDB: 2PIV) performed by flexible docking. AR protein is shown in grey, orange sticks represent interacting amino acid residues, labelled in bold are residues displaying hydrogen bonds. Nitrogen atoms are shown in blue, oxygen atoms in red, hydrogens in white. Hydrogen bonds are shown as cyan dash lines.

acted as AR antagonists, in comparison with the dual or agonist character of the majority of A-ring-fused pyridines. Based on the antagonist and antiproliferative activity of the whole set of compounds, the best derivative **1d** (6'-methoxy-substituted A-ring fused quinoline) was chosen as the lead compound. It was further studied and showed to be a low-micromolar AR antagonist ($IC_{50} = 10.5 \mu\text{M}$), it suppressed the viability and proliferation of AR-positive PCa cell lines. Moreover, the candidate compound blocked the AR downstream signalling, induced moderate cell-cycle arrest and was proven to bind the AR in cells and the recombinant AR protein as well. The binding mode and interaction was described using molecular modelling.

4. Experimental

4.1. General

Chemicals, reagents and solvents were purchased from commercial suppliers (Sigma-Aldrich, TCI and Alfa Aesar) and used without further purification. For MW-assisted syntheses, a CEM Discover SP laboratory MW reactor was used with a max. power of 200 W (running a dynamic control program). Elementary analysis data were obtained with a PerkinElmer CHN analyzer model 2400. The transformations were monitored by TLC using 0.25 mm thick Kieselgel-G plates (Si 254 F, Merck). The compound spots were detected by spraying with 5% phosphomolybdic acid in 50% aqueous phosphoric acid. Column chromatography (CC) was carried out on silica gel 60, 40–63 μm (Merck). Melting points (Mp) were determined on an SRS Optimelt digital apparatus and are uncorrected. NMR spectra were recorded with a Bruker DRX 500 instrument at room temperature in CDCl_3 using residual solvent signal as an internal reference. Chemical shifts are reported in ppm (δ scale) and coupling constants (J) are given in Hz. Multiplicities of the ^1H signals are indicated as a singlet (s), a doublet (d), a doublet (dd), a triplet (t), or a multiplet (m). ^{13}C NMR spectra are ^1H -decoupled and the J-MOD pulse sequence was used for multiplicity editing. In this spin-echo type experiment, the signal intensity is modulated by the different coupling constants J of carbons depending on the number of attached protons. Both protonated and unprotonated carbons can be detected (CH_3 and CH carbons appear as positive signals, while CH_2 and C carbons as negative signals). The purified derivatives were dissolved in high purity acetonitrile and introduced with an Agilent 1290 Infinity II liquid chromatography pump to an Agilent 6470 tandem mass spectrometer equipped an electrospray ionization chamber. Flow rate was 0.5 mL·min⁻¹ and contained 0.1% formic acid or 0.1% ammonium hydroxide to help facilitate ionization. The instrument operated in MS1 scan mode with 135 V fragmentor voltage, and the spectra were recorded from 300 to 500 m/z , which were corrected with the background.

4.2. Chemistry

4.2.1. General procedure for the synthesis of A-ring-fused 6'-substituted pyridine derivatives of DHT (2a-h)

DHT (290 mg, 1 mmol) and the corresponding Mannich salt (**4a-h**, 2 equiv.) were dissolved in 1,4-dioxane (5 mL), and pyrrolidine (246 μL , 3 equiv.) was added. The mixture was irradiated in a closed vessel at 120 °C for 20 min. After completion of the reaction, the mixture was cooled to room temperature, and the solvent was evaporated under reduced pressure. The brown oil thus obtained was dissolved in absolute EtOH (10 mL), then hydroxylamine hydrochloride (83 mg, 1.2 equiv.) was added and the mixture was irradiated in a closed vessel at 90 °C for 10 min. During work-up, the mixture was cooled to room temperature, poured into water (20 mL) and saturated NaHCO_3 solution was added to neutralize the reaction mixture. The water phase was extracted with CH_2Cl_2 ($2 \times 10 \text{ mL}$). The combined organic layer was washed with water ($2 \times 10 \text{ mL}$) and brine (20 mL), dried over anhydrous Na_2SO_4 and the solvent was evaporated under reduced pressure to yield a brown oil, which was then purified by CC with a pure solvent or solvent mixture as

described in each subchapter containing 1 v/v% TEA.

4.2.1.1. 6'-Phenylpyridino[2',3':3,2]-5 α -androstan-17 β -ole (**2a**). According to Section 4.2.1., **4a** (427 mg) was used. The crude product was purified by CC (CH_2Cl_2). Yield: 326 mg (81%, off white solid). Mp 213–216 °C; ^1H NMR (CDCl_3 , 500 MHz): δ_{H} 0.77 (s, 3 H, 18-H₃), 0.81 (s, 3 H, 19-H₃), 0.81–1.02 (overlapping m, 3 H, 9 α -H, 7 α -H and 14 α -H), 1.13 (m, 1 H, 12 α -H), 1.24–1.52 (overlapping m, 5 H, 15 β -H, 11 β -H, 6 β -H, 8 β -H and 16 β -H), 1.60–1.70 (overlapping m, 4 H, 11 α -H, 5 α -H, 15 α -H and 6 α -H), 1.77 (m, 1 H, 7 β -H), 1.88 (m, 1 H, 12 β -H), 2.07 (m, 1 H, 16 α -H), 2.51 (d, 1 H, $J = 16.3 \text{ Hz}$, 1 α -H), 2.76–2.83 (overlapping dd and d, 2 H, 4 β -H and 1 β -H), 3.25 (m, 1 H, 4 α -H), 3.66 (m, 1 H, 17 α -H), 7.42 (t-like m, 1 H, 4''-H), 7.48 (t-like m, 2 H, 3''-H and 5''-H), 7.52 (d, 1 H, $J = 7.9 \text{ Hz}$) and 7.56 (d, 1 H, $J = 7.9 \text{ Hz}$): 4'-H and 5'-H, 7.99 (d, 2 H, $J = 7.2 \text{ Hz}$, 2''-H and 6''-H); ^{13}C NMR (CDCl_3 , 125 MHz): δ_{C} 11.2 (C-18), 11.9 (C-19), 21.1 (C-11), 23.6 (C-15), 28.7 (C-6), 30.8 (C-16), 31.4 (C-7), 35.4 (C-10), 35.9 (C-8), 37.0 (C-4), 37.1 (C-12), 42.4 (C-5), 43.1 (C-13), 43.3 (C-1), 51.2 (C-14), 54.1 (C-9), 82.1 (C-17), 118.1 (C-5'), 127.0 (2 C, C-2'' and C-6''), 128.5 (C-4''), 128.7 (2 C, C-3'' and C-5''), 129.9 (C-2), 138.1 (C-4'), 140.0 (C-1''), 154.9 (C-6'), 156.4 (C-3); ESI-MS 402 $[\text{M}+\text{H}]^+$; Anal. Calcd. for $\text{C}_{28}\text{H}_{35}\text{NO}$ C 83.74; H 8.78. Found C 83.63; H 8.76.

4.2.1.2. 6'-(*p*-Tolyl)pyridino[2',3':3,2]-5 α -androstan-17 β -ole (**2b**). According to Section 4.2.1., **4b** (455 mg) was used. The crude product was purified by CC (CH_2Cl_2). Yield: 290 mg (70%, off white solid). Mp 251–254 °C; ^1H NMR (CDCl_3 , 500 MHz): δ_{H} 0.78 (s, 3 H, 18-H₃), 0.81 (s, 3 H, 19-H₃), 0.83–1.03 (overlapping m, 3 H), 1.12 (m, 1 H), 1.25–1.52 (overlapping m, 5 H), 1.62–1.72 (overlapping m, 4 H), 1.76 (m, 1 H), 1.88 (m, 1 H), 2.07 (m, 1 H, 16 α -H), 2.39 (s, 3 H, 4''-CH₃), 2.47 (d, 1 H, $J = 16.2 \text{ Hz}$, 1 α -H), 2.67 (dd, 1 H, $J = 18.0 \text{ Hz}$, $J = 12.6 \text{ Hz}$, 4 β -H), 2.75 (d, 1 H, $J = 16.2 \text{ Hz}$, 1 β -H), 2.93 (dd, 1 H, $J = 18.0 \text{ Hz}$, $J = 5.2 \text{ Hz}$, 4 α -H), 3.66 (t, 1 H, $J = 8.3 \text{ Hz}$, 17 α -H), 7.24 (d, 2 H, $J = 7.9 \text{ Hz}$, 3''-H and 5''-H), 7.36 (d, 1 H, $J = 7.9 \text{ Hz}$, 4'-H), 7.43 (d, 1 H, $J = 7.9 \text{ Hz}$, 5'-H), 7.85 (d, 2 H, $J = 7.9 \text{ Hz}$, 2''-H and 6''-H); ^{13}C NMR (CDCl_3 , 125 MHz): δ_{C} 11.2 (C-18), 11.9 (C-19), 21.1 (C-11), 21.4 (4''-CH₃), 23.6 (C-15), 28.8 (C-6), 30.8 (C-16), 31.4 (C-7), 35.4 (C-10), 35.9 (C-8), 37.0 (C-4), 37.1 (C-12), 42.4 (C-5), 43.1 (C-13), 43.3 (C-1), 51.2 (C-14), 54.1 (C-9), 82.1 (C-17), 117.8 (C-5'), 126.8 (2 C, C-2'' and C-6''), 129.5 (2 C, C-3'' and C-5''), 129.5 (C-4''), 137.3 (C-2), 138.0 (C-4'), 138.4 (C-1''), 154.9 (C-6'), 156.3 (C-3); ESI-MS 416 $[\text{M}+\text{H}]^+$; Anal. Calcd. for $\text{C}_{29}\text{H}_{37}\text{NO}$ C 83.81; H 8.97. Found C 83.95; H 8.99.

4.2.1.3. 6'-(*p*-Methoxyphenyl)pyridino[2',3':3,2]-5 α -androstan-17 β -ole (**2c**). According to Section 4.2.1., **4c** (487 mg) was used. The crude product was purified by CC (CH_2Cl_2). Yield: 342 mg (79%, off white solid). Mp 230–233 °C; ^1H NMR (CDCl_3 , 500 MHz): δ_{H} 0.78 (s, 3 H, 18-H₃), 0.81 (s, 3 H, 19-H₃), 0.85 (m, 1 H), 0.93–1.02 (overlapping m, 2 H), 1.12 (m, 1 H), 1.24–1.52 (overlapping m, 5 H), 1.60–1.77 (overlapping m, 5 H), 1.87 (m, 1 H), 2.07 (m, 1 H, 16 α -H), 2.46 (d, 1 H, $J = 16.2 \text{ Hz}$, 1 α -H), 2.67 (dd, 1 H, $J = 18.0 \text{ Hz}$, $J = 12.5 \text{ Hz}$, 4 β -H), 2.75 (d, 1 H, $J = 16.2 \text{ Hz}$, 1 β -H), 2.91 (dd, 1 H, $J = 18.0 \text{ Hz}$, $J = 5.3 \text{ Hz}$, 4 α -H), 3.66 (t, 1 H, $J = 8.6 \text{ Hz}$, 17 α -H), 3.85 (s, 3 H, 4''-OMe), 6.97 (d, 2 H, $J = 8.8 \text{ Hz}$, 3''-H and 5''-H), 7.35 (d, 1 H, $J = 8.0 \text{ Hz}$, 4'-H), 7.40 (d, 1 H, $J = 8.0 \text{ Hz}$, 5'-H), 7.90 (d, 2 H, $J = 8.8 \text{ Hz}$, 2''-H and 6''-H); ^{13}C NMR (CDCl_3 , 125 MHz): δ_{C} 11.2 (C-18), 11.9 (C-19), 21.1 (C-11), 23.6 (C-15), 28.7 (C-6), 30.7 (C-16), 31.4 (C-7), 35.4 (C-10), 35.8 (C-8), 36.9 (C-4), 37.1 (C-12), 42.3 (C-5), 43.0 (C-13), 43.2 (C-1), 51.1 (C-14), 54.0 (C-9), 55.5 (4''-OMe), 82.1 (C-17), 114.1 (2 C, C-3'' and C-5''), 117.4 (C-5'), 128.1 (2 C, C-2'' and C-6''), 129.1 (C-1''), 132.7 (C-2), 138.1 (C-4'), 154.5 (C-6'), 156.2 (C-3), 160.2 (C-4''); ESI-MS 432 $[\text{M}+\text{H}]^+$; Anal. Calcd. for $\text{C}_{29}\text{H}_{37}\text{NO}_2$ C 80.70; H 8.64. Found C 80.88; H 8.67.

4.2.1.4. 6'-(*p*-Nitrophenyl)pyridino[2',3':3,2]-5 α -androstan-17 β -ole (**2d**). According to Section 4.2.1., **4d** (517 mg) was used. The crude product was purified by CC ($\text{EtOAc}/\text{CH}_2\text{Cl}_2 = 2:98$). Yield: 321 mg (72%, light yellow solid). Mp > 250 °C decomposes; ^1H NMR (CDCl_3 , 500 MHz): δ_{H} 0.78 (s, 3 H, 18-H₃), 0.82 (s, 3 H, 19-H₃), 0.88 (m, 1 H), 0.95–1.04 (overlapping m, 2 H), 1.13 (m, 1 H), 1.28–1.53 (overlapping m, 5 H), 1.60–1.72 (overlapping m, 4 H), 1.77 (m, 1 H), 1.88 (m, 1 H),

2.08 (m, 1 H, 16 α -H), 2.51 (d, 1 H, J = 16.4 Hz, 1 α -H), 2.69 (dd, 1 H, J = 18.2 Hz, J = 12.4 Hz, 4 β -H), 2.82 (d, 1 H, J = 16.4 Hz, 1 β -H), 2.95 (dd, 1 H, J = 18.2 Hz, J = 5.3 Hz, 4 α -H), 3.67 (t, 1 H, J = 8.3 Hz, 17 α -H), 7.46 (d, 1 H, J = 8.0 Hz, 4'-H), 7.54 (d, 1 H, J = 8.0 Hz, 5'-H), 8.14 (d, 2 H, J = 8.7 Hz, 2''-H and 6''-H), 8.29 (d, 2 H, J = 8.7 Hz, 3''-H and 5''-H); ^{13}C NMR (CDCl₃, 125 MHz): δ_{C} 11.2 (C-18), 11.9 (C-19), 21.1 (C-11), 23.6 (C-15), 28.7 (C-6), 30.7 (C-16), 31.3 (C-7), 35.4 (C-10), 35.8 (C-8), 36.9 (C-4), 37.0 (C-12), 42.3 (C-5), 43.0 (C-13), 43.3 (C-1), 51.1 (C-14), 53.9 (C-9), 82.1 (C-17), 118.7 (C-5'), 124.1 (2 C, C-3'' and C-5''), 127.6 (2 C, C-2'' and C-6''), 131.9 (C-2), 138.4 (C-4'), 145.9 (C-1''), 147.9 (C-4''), 152.0 (C-6'), 157.2 (C-3); ESI-MS 447 [M+H]⁺; Anal. Calcd. for C₂₈H₃₄N₂O₃ C 75.31; H 7.67. Found C 75.08; H 7.66.

4.2.1.5. 6'-(*p*-Fluorophenyl)pyridino[2',3':3,2]-5 α -androstan-17 β -ole (**2e**). According to Section 4.2.1., **4e** (463 mg) was used. The crude product was purified by CC (EtOAc/CH₂Cl₂ = 2:98). Yield: 337 mg (80%, off white solid). Mp > 200 °C decomposes; ^1H NMR (CDCl₃, 500 MHz): δ_{H} 0.78 (s, 3 H, 18-H₃), 0.81 (s, 3 H, 19-H₃), 0.87–1.03 (overlapping m, 3 H), 1.13 (m, 1 H), 1.25–1.53 (overlapping m, 5 H), 1.61–1.72 (overlapping m, 4 H), 1.76 (m, 1 H), 1.88 (m, 1 H), 2.07 (m, 1 H, 16 α -H), 2.48 (d, 1 H, J = 16.2 Hz, 1 α -H), 2.67 (dd, 1 H, J = 18.1 Hz, J = 12.6 Hz, 4 β -H), 2.77 (d, 1 H, J = 16.2 Hz, 1 β -H), 2.92 (dd, 1 H, J = 18.1 Hz, J = 5.2 Hz, 4 α -H), 3.66 (t, 1 H, J = 8.5 Hz, 17 α -H), 7.11 (t, 2 H, J = 8.0 Hz, 3''-H and 5''-H), 7.38 (d, 1 H, J = 8.0 Hz, 4'-H), 7.41 (d, 1 H, J = 8.0 Hz, 5'-H), 7.94 (dd, 2 H, J = 8.7 Hz, J = 5.5 Hz, 2''-H and 6''-H); ^{13}C NMR (CDCl₃, 125 MHz): δ_{C} 11.2 (C-18), 11.9 (C-19), 21.1 (C-11), 23.6 (C-15), 28.7 (C-6), 30.8 (C-16), 31.4 (C-7), 35.4 (C-10), 35.9 (C-8), 37.0 (C-4), 37.1 (C-12), 42.4 (C-5), 43.1 (C-13), 43.2 (C-1), 51.2 (C-14), 54.1 (C-9), 82.1 (C-17), 115.6 (2 C, J = 21.4 Hz, C-3'' and C-5''), 117.7 (C-5'), 128.7 (2 C, J = 8.2 Hz, C-2'' and C-6''), 129.9 (C-2), 136.2 (J = 2.9 Hz, C-1''), 138.2 (C-4'), 153.8 (C-6'), 156.5 (C-3), 163.5 (J = 247.5 Hz, C-4''); ESI-MS 420 [M+H]⁺; Anal. Calcd. for C₂₈H₃₄FNO C 80.15; H 8.17. Found C 79.94; H 8.15.

4.2.1.6. 6'-(*p*-Chlorophenyl)pyridino[2',3':3,2]-5 α -androstan-17 β -ole (**2f**). According to Section 4.2.1., **4f** (496 mg) was used. The crude product was purified by CC (EtOAc/CH₂Cl₂ = 5:95). Yield: 313 mg (72%, off white solid). Mp > 200 °C decomposes; ^1H NMR (CDCl₃, 500 MHz): δ_{H} 0.78 (s, 3 H, 18-H₃), 0.81 (s, 3 H, 19-H₃), 0.86 (m, 1 H), 0.91–1.03 (overlapping m, 2 H), 1.13 (m, 1 H), 1.23–1.52 (overlapping m, 5 H), 1.59–1.72 (overlapping m, 4 H), 1.76 (m, 1 H), 1.87 (m, 1 H), 2.08 (m, 1 H, 16 α -H), 2.47 (d, 1 H, J = 16.3 Hz, 1 α -H), 2.67 (dd, 1 H, J = 18.0 Hz, J = 12.7 Hz, 4 β -H), 2.77 (d, 1 H, J = 16.3 Hz, 1 β -H), 2.92 (dd, 1 H, J = 18.0 Hz, J = 5.1 Hz, 4 α -H), 3.66 (t, 1 H, J = 8.3 Hz, 17 α -H), 7.38–7.44 (overlapping m, 4 H, 4'-H, 5'-H, 3''-H and 5''-H), 7.90 (d, 2 H, J = 8.2 Hz, 2''-H and 6''-H); ^{13}C NMR (CDCl₃, 125 MHz): δ_{C} 11.2 (C-18), 11.9 (C-19), 21.1 (C-11), 23.6 (C-15), 28.7 (C-6), 30.7 (C-16), 31.4 (C-7), 35.4 (C-10), 35.8 (C-8), 36.9 (C-4), 37.1 (C-12), 42.3 (C-5), 43.0 (C-13), 43.2 (C-1), 51.1 (C-14), 54.0 (C-9), 82.1 (C-17), 117.9 (C-5'), 128.5 (2 C, C-3'' and C-5''), 131.9 (2 C, C-2'' and C-6''), 130.3 (C-2), 134.6 (C-4''), 138.2 (C-4'), 138.4 (C-1''), 153.5 (C-6'), 156.6 (C-3); ESI-MS 436 [M+H]⁺; Anal. Calcd. for C₂₈H₃₄ClNO C 77.13; H 7.86. Found C 77.23; H 7.88.

4.2.1.7. 6'-(*p*-Bromophenyl)pyridino[2',3':3,2]-5 α -androstan-17 β -ole (**2g**). According to Section 4.2.1., **4g** (585 mg) was used. The crude product was purified by CC (EtOAc/CH₂Cl₂ = 5:95). Yield: 374 mg (78%, off white solid). Mp 223–226 °C; ^1H NMR (CDCl₃, 500 MHz): δ_{H} 0.78 (s, 3 H, 18-H₃), 0.81 (s, 3 H, 19-H₃), 0.86 (m, 1 H), 0.92–1.03 (overlapping m, 2 H), 1.13 (m, 1 H), 1.25–1.53 (overlapping m, 5 H), 1.60–1.72 (overlapping m, 4 H), 1.77 (m, 1 H), 1.88 (m, 1 H), 2.08 (m, 1 H, 16 α -H), 2.47 (d, 1 H, J = 16.3 Hz, 1 α -H), 2.67 (dd, 1 H, J = 18.1 Hz, J = 12.5 Hz, 4 β -H), 2.77 (d, 1 H, J = 16.3 Hz, 1 β -H), 2.92 (dd, 1 H, J = 18.1 Hz, J = 5.3 Hz, 4 α -H), 3.66 (m, 1 H, 17 α -H), 7.38 (d, 1 H, J = 8.0 Hz, 4'-H), 7.43 (d, 1 H, J = 8.0 Hz, 5'-H), 7.56 (d, 2 H, J = 8.4 Hz, 3''-H and 5''-H), 7.84 (d, 2 H, J = 8.4 Hz, 2''-H and 6''-H); ^{13}C NMR (CDCl₃, 125 MHz): δ_{C} 11.2 (C-18), 11.9 (C-19), 21.1 (C-11), 23.6 (C-15), 28.7 (C-6), 30.8 (C-16), 31.4 (C-7), 35.4 (C-10), 35.9 (C-8), 37.0 (C-4), 37.1 (C-12), 42.4 (C-5), 43.1 (C-13), 43.3 (C-1), 51.2 (C-14), 54.1 (C-9),

82.1 (C-17), 117.8 (C-5'), 122.9 (C-4''), 128.5 (2 C, C-2'' and C-6''), 130.4 (C-2), 131.9 (2 C, C-3'' and C-5''), 138.2 (C-4'), 138.9 (C-1''), 153.6 (C-6'), 156.6 (C-3); ESI-MS 480 [M+H]⁺; Anal. Calcd. for C₂₈H₃₄BrNO C 69.99; H 7.13. Found C 70.12; H 7.14.

4.2.1.8. 6'-(*o*-Hydroxyphenyl)pyridino[2',3':3,2]-5 α -androstan-17 β -ole (**2h**). According to Section 4.2.1., **4h** (459 mg) was used. The crude product was purified by CC (CH₂Cl₂). Yield: 278 mg (67%, white solid). Mp 298–300 °C; ^1H NMR (CDCl₃, 500 MHz): δ_{H} 0.78 (s, 3 H, 18-H₃), 0.80 (s, 3 H, 19-H₃), 0.86 (m, 1 H), 0.94–1.02 (overlapping m, 2 H), 1.13 (m, 1 H), 1.26–1.52 (overlapping m, 5 H), 1.60–1.70 (overlapping m, 4 H), 1.76 (m, 1 H), 1.88 (m, 1 H), 2.08 (m, 1 H, 16 α -H), 2.47 (d, 1 H, J = 16.3 Hz, 1 α -H), 2.65 (dd, 1 H, J = 18.0 Hz, 12.5 Hz, 4 β -H), 2.77 (d, 1 H, J = 16.3 Hz, 1 β -H), 2.86 (dd, 1 H, J = 18.0 Hz, J = 5.1 Hz, 4 α -H), 3.66 (m, 1 H, 17 α -H), 6.88 (t-like m, 1 H, 4''-H), 7.00 (d, 1 H, J = 8.2 Hz, 6''-H), 7.26 (t-like m, 1 H, 5''-H), 7.48 (d, 1 H, J = 8.3 Hz, 4'-H), 7.66 (d, 1 H, J = 8.3 Hz, 5'-H), 7.77 (d, 1 H, J = 8.0 Hz, 3''-H), 14.78 (s, 1 H, Ph-OH); ^{13}C NMR (CDCl₃, 125 MHz): δ_{C} 11.2 (C-18), 11.9 (C-19), 21.1 (C-11), 23.6 (C-15), 28.5 (C-6), 30.7 (C-16), 31.3 (C-7), 35.5 (C-10), 35.7 (C-8), 36.0 (C-4), 36.9 (C-12), 42.0 (C-1), 42.9 (C-5), 43.0 (C-13), 51.1 (C-14), 53.9 (C-9), 82.1 (C-17), 116.5 (C-6''), 118.6 and 118.7 (C-5' and C-5''), 119.2 (C-2''), 126.0 (C-4''), 129.7 (C-2), 131.0 (C-3''), 139.2 (C-4'), 153.0 (C-6'), 155.1 (C-1''), 160.3 (C-3); ESI-MS 418 [M+H]⁺; Anal. Calcd. for C₂₈H₃₅NO₂ C 80.53; H 8.45. Found C 80.49; H 8.42.

4.2.2. General procedure for the synthesis of A-ring-fused 4',6'-disubstituted pyridine derivatives of DHT (3a–o)

2-Ethylidene (**5a**) or 2-arylidene (**5b–e**) derivative (1.0 mmol), appropriate pyridinium iodide salt (**6a–c**, 1.4 equiv.) and ammonium acetate (771 mg, 10.0 equiv.) were suspended in absolute EtOH (5 mL), and the mixture was irradiated in a closed vessel at 90 °C for 20 min. After completion of the reaction, the mixture was cooled to room temperature, poured into water (20 mL) and extracted with CH₂Cl₂ (2 \times 10 mL). The combined organic layer was washed with water (2 \times 10 mL) and brine (20 mL), dried over anhydrous Na₂SO₄ and the solvent was evaporated under reduced pressure. The crude product thus obtained was purified by CC with a pure solvent or solvent mixture as described in each subchapter containing 1 v/v% TEA.

4.2.2.1. 4'-Methyl-6'-phenylpyridino[2',3':3,2]-5 α -androstan-17 β -ole (**3a**). According to Section 4.2.2., **5a** (316 mg) and **6a** (455 mg) were used. The crude product was purified by CC (EtOAc/hexane = 30:70). Yield: 298 mg (72%, white solid). Mp 263–265 °C; ^1H NMR (CDCl₃, 500 MHz): δ_{H} 0.79 (s, 3 H, 18-H₃), 0.82 (s, 3 H, 19-H₃), 0.86–1.04 (overlapping m, 3 H), 1.15 (m, 1 H), 1.25–1.55 (overlapping m, 5 H), 1.61–1.66 (overlapping m, 3 H), 1.75 (overlapping m, 2 H), 1.89 (m, 1 H), 2.08 (m, 1 H, 16 α -H), 2.23 (d, 1 H, J = 16.6 Hz, 1 α -H), 2.27 (s, 3 H, 4'-CH₃), 2.69–2.77 (overlapping dd and d, 2 H, 4 β -H and 1 β -H), 2.90 (dd, 1 H, J = 17.9 Hz, J = 5.0 Hz, 4 α -H), 3.67 (m, 1 H, 17 α -H), 7.36 (overlapping m, 2 H, 5'-H and 4''-H), 7.43 (t, 2 H, J = 7.6 Hz, 3''-H and 5''-H), 7.94 (d, 2 H, J = 7.4 Hz, 2''-H and 6''-H); ^{13}C NMR (CDCl₃, 125 MHz): δ_{C} 11.2 (C-18), 12.3 (C-19), 19.6 (4'-CH₃), 21.1 (C-11), 23.6 (C-15), 28.6 (C-6), 30.8 (C-16), 31.4 (C-7), 35.2 (C-10), 35.8 (C-8), 36.9 (C-4), 37.2 (C-12), 40.3 (C-1), 41.9 (C-5), 43.0 (C-13), 51.2 (C-14), 54.3 (C-9), 82.1 (C-17), 119.9 (C-5'), 127.0 (2 C, C-2'' and C-6''), 128.4 (C-4''), 128.7 (2 C, C-3'' and C-5''), 128.8 (C-2), 140.1 (C-1''), 146.7 (C-4'), 154.3 (C-6'), 155.8 (C-3); ESI-MS 416 [M+H]⁺; Anal. Calcd. for C₂₉H₃₇NO C 83.81; H 8.97. Found C 83.99; H 8.99.

4.2.2.2. 6'-(*o*-Hydroxyphenyl)-4'-methylpyridino[2',3':3,2]-5 α -androstan-17 β -ole (**3b**). According to Section 4.2.2., **5a** (316 mg) and **6b** (478 mg) were used. The crude product was purified by CC (CH₂Cl₂). Yield: 281 mg (65%, off white solid); Mp 265–267 °C; ^1H NMR (CDCl₃, 500 MHz): δ_{H} 0.78 (s, 3 H, 18-H₃), 0.80 (s, 3 H, 19-H₃), 0.84–1.02 (overlapping m, 3 H), 1.14 (m, 1 H), 1.26–1.54 (overlapping m, 5 H), 1.57–1.67 (overlapping m, 3 H), 1.74 (overlapping m, 2 H), 1.89 (m, 1 H), 2.08 (m, 1 H, 16 α -H), 2.21 (d, 1 H, J = 16.7 Hz, 1 α -H), 2.30 (s, 3 H, 4'-CH₃), 2.67 (dd, 1 H, J = 18.2 Hz, 12.5 Hz, 4 β -H), 2.73 (d, 1 H, J =

16.7 Hz, 1 β -H), 2.81 (dd, 1 H, $J = 18.2$ Hz, $J = 5.1$ Hz, 4 α -H), 3.67 (m, 1 H, 17 α -H), 6.86 (t, 1 H, $J = 7.6$ Hz, 4''-H), 7.00 (d, 1 H, $J = 8.2$ Hz, 6''-H), 7.25 (t-like m, 1 H, 5''-H), 7.52 (s, 1 H, 5'-H), 7.77 (d, 1 H, $J = 8.0$ Hz, 3''-H), 15.0 (s, 1 H, Ph-OH); ^{13}C NMR (CDCl₃, 125 MHz): δ_{C} 11.2 (C-18), 12.3 (C-19), 19.9 (4'-CH₃), 21.1 (C-11), 23.6 (C-15), 28.4 (C-6), 30.7 (C-16), 31.3 (C-7), 35.3 (C-10), 35.7 (C-8), 36.1 (C-4), 36.9 (C-12), 40.1 (C-1), 41.6 (C-5), 43.0 (C-13), 51.1 (C-14), 54.2 (C-9), 82.1 (C-17), 117.9 (C-6''), 118.5 (2 C, C-4'' and C-5''), 119.1 (C-2''), 125.9 (C-5''), 128.7 (C-2), 130.8 (C-3''), 148.2 (C-4'), 152.2 (C-6'), 154.4 (C-1''), 160.3 (C-3); ESI-MS 432 [M+H]⁺; Anal. Calcd. for C₂₉H₃₇NO₂ C 80.70; H 8.64. Found C 80.51; H 8.61.

4.2.2.3. 4'-Methyl-6'-(pyridin-2''-yl)pyridino[2',3':3,2]-5 α -androstan-17 β -ole (3c). According to Section 4.2.2., 5a (316 mg) and 6c (457 mg) were used. The crude product was purified by CC (EtOAc/hexane = 40:60). Yield: 294 mg (71%, off white solid). Mp 226–229 °C; ^1H NMR (CDCl₃, 500 MHz): δ_{H} 0.78 (s, 3 H, 18-H₃), 0.81 (s, 3 H, 19-H₃), 0.86–1.03 (overlapping m, 3 H), 1.14 (m, 1 H), 1.25–1.55 (overlapping m, 5 H), 1.60–1.67 (overlapping m, 3 H), 1.76 (overlapping m, 2 H), 1.89 (m, 1 H), 2.08 (m, 1 H, 16 α -H), 2.24 (d, 1 H, $J = 16.7$ Hz, 1 α -H), 2.29 (s, 3 H, 4'-CH₃), 2.69–2.79 (overlapping dd and d, 2 H, 4 β -H and 1 β -H), 2.90 (dd, 1 H, $J = 17.8$ Hz, $J = 4.8$ Hz, 4 α -H), 3.67 (t, 1 H, $J = 8.5$ Hz, 17 α -H), 7.25 (t-like m, 1 H, 5''-H), 7.77 (t, 1 H, $J = 7.7$ Hz, 4''-H), 7.97 (s, 1 H, 5'-H), 8.35 (d, 1 H, $J = 8.0$ Hz, 3''-H), 8.65 (d, 1 H, $J = 4.9$ Hz, 6''-H); ^{13}C NMR (CDCl₃, 125 MHz): δ_{C} 11.2 (C-18), 12.3 (C-19), 19.5 (C-4'), 21.1 (C-11), 23.6 (C-15), 28.6 (C-6), 30.7 (C-16), 31.4 (C-7), 35.2 (C-10), 35.8 (C-8), 36.9 (C-4), 37.2 (C-12), 40.5 (C-1), 41.9 (C-5), 43.0 (C-13), 51.2 (C-14), 54.3 (C-9), 82.1 (C-17), 120.2 (C-5'), 121.1 (C-3''), 123.3 (C-5''), 130.7 (C-2), 136.9 (C-4''), 147.1 (C-4'), 149.2 (C-6''), 152.8 (C-6'), 155.5 and 157.0: C-2'' and C-3; ESI-MS 417 [M+H]⁺; Anal. Calcd. for C₂₈H₃₆N₂O C 80.73; H 8.71. Found C 80.95; H 8.74.

4.2.2.4. 4',6'-Diphenylpyridino[2',3':3,2]-5 α -androstan-17 β -ole (3d). According to Section 4.2.2., 5b (379 mg) and 6a (455 mg) were used. The crude product was purified by CC (EtOAc/hexane = 20:80). Yield: 368 mg (77%, white solid). Mp 139–142 °C; ^1H NMR (CDCl₃, 500 MHz): δ_{H} 0.72 (s, 3 H, 18-H₃), 0.75 (s, 3 H, 19-H₃), 0.81 (m, 1 H), 0.91–1.07 (overlapping m, 3 H), 1.23–1.46 (overlapping m, 5 H), 1.59–1.76 (overlapping m, 6 H), 2.06 (m, 1 H, 16 α -H), 2.32 (d, 1 H, $J = 16.5$ Hz, 1 α -H), 2.68–2.79 (overlapping dd and d, 2 H, 4 β -H and 1 β -H), 3.05 (dd, 1 H, $J = 18.1$ Hz, $J = 5.4$ Hz, 4 α -H), 3.63 (t, 1 H, $J = 8.4$ Hz, 17 α -H), 7.33–7.48 (overlapping m, 9 H, Ph-H⁴, Ph-H³, Ph-H⁵, Ph-H², Ph-H⁶, 4''-H, 3''-H, 5''-H and 5'-H), 7.98 (d, 2 H, $J = 7.7$ Hz, 2''-H and 6''-H); ^{13}C NMR (CDCl₃, 125 MHz): δ_{C} 11.2 (C-18), 11.8 (C-19), 21.0 (C-11), 23.6 (C-15), 28.6 (C-6), 30.7 (C-16), 31.4 (C-7), 35.5 (C-10), 35.8 (C-8), 36.8 (C-4), 37.6 (C-12), 41.4 (C-1), 42.1 (C-5), 43.0 (C-13), 51.1 (C-14), 54.0 (C-9), 82.1 (C-17), 119.5 (C-5'), 127.0 (2 C, C-2'' and C-6''), 127.4 (C-2), 127.9 (Ph-C⁴), 128.5 (2 C, Ph-C² and Ph-C⁶), 128.6 (C-4''), 128.7 (2 C, Ph-C³ and Ph-C⁵), 128.8 (2 C, C-3'' and C-5''), 139.9 and 140.0: Ph-C¹ and C-1'', 150.9 (C-4'), 154.4 (C-6'), 156.9 (C-3); ESI-MS 478 [M+H]⁺; Anal. Calcd. for C₃₄H₃₉NO C 85.49; H 8.23. Found C 85.19; H 8.20.

4.2.2.5. 6'-(*o*-Hydroxyphenyl)-4'-phenylpyridino[2',3':3,2]-5 α -androstan-17 β -ole (3e). According to Section 4.2.2., 5b (379 mg) and 6b (478 mg) was used. The crude product was purified by CC (EtOAc/CH₂Cl₂ = 2:98). Yield: 377 mg (76%, off white solid). Mp 146–149 °C; ^1H NMR (CDCl₃, 500 MHz): δ_{H} 0.71 (s, 3 H, 18-H₃), 0.74 (s, 3 H, 19-H₃), 0.80 (m, 1 H), 0.87–1.06 (overlapping m, 3 H), 1.22–1.46 (overlapping m, 6 H), 1.57–1.76 (overlapping m, 5 H), 2.06 (m, 1 H, 16 α -H), 2.30 (d, 1 H, $J = 16.5$ Hz, 1 α -H), 2.66 (d, 1 H, $J = 16.5$ Hz, 1 β -H), 2.71 (dd, 1 H, $J = 18.0$ Hz, 12.4 Hz, 4 β -H), 3.05 (dd, 1 H, $J = 18.1$ Hz, $J = 5.5$ Hz, 4 α -H), 3.62 (m, 1 H, 17 α -H), 6.85 (t, 1 H, $J = 7.5$ Hz, 4''-H), 7.00 (d, 1 H, $J = 8.2$ Hz, 6''-H), 7.27 (t-like m, 1 H, 5''-H), 7.32 (d, 2 H, $J = 7.1$ Hz, Ph-H² and Ph-H⁶), 7.44 (t-like m, 1 H, Ph-H⁴), 7.48 (t-like m, 2 H, Ph-H³ and Ph-H⁵), 7.58 (s, 1 H, 5'-H), 7.76 (d, 1 H, $J = 7.9$ Hz, 3''-H), 14.82 (s, 1 H, Ph-OH); ^{13}C NMR (CDCl₃, 125 MHz): δ_{C} 11.2 (C-18), 11.8 (C-19), 20.9 (C-11), 23.5 (C-15), 28.5 (C-6), 30.7 (C-16), 31.3 (C-7), 35.5 (C-

10), 35.7 (C-8), 36.5 (C-4), 36.8 (C-12), 41.2 (C-1), 41.8 (C-5), 42.9 (C-13), 51.1 (C-14), 53.9 (C-9), 82.1 (C-17), 117.8 (C-6''), 118.6 and 118.7 (C-4'' and C-5'), 119.1 (C-2''), 126.1 (C-5''), 127.3 (C-2), 128.3 (Ph-C⁴), 128.6 (2 C, Ph-C² and Ph-C⁶), 128.7 (2 C, Ph-C³ and Ph-C⁵), 131.1 (C-3''), 139.4 (Ph-C¹), 152.2 (C-4'), 153.4 (C-6'), 154.6 (C-1''), 160.3 (C-3); ESI-MS 494 [M+H]⁺; Anal. Calcd. for C₃₄H₃₉NO₂ C 82.72; H 7.96. Found C 82.98; H 7.97.

4.2.2.6. 4'-Phenyl-6'-(pyridin-2''-yl)pyridino[2',3':3,2]-5 α -androstan-17 β -ole (3f). According to Section 4.2.2., 5b (379 mg) and 6c (457 mg) were used. The crude product was purified by CC (EtOAc/hexane = 40:60). Yield: 391 mg (82%, white solid). Mp 156–159 °C; ^1H NMR (CDCl₃, 500 MHz): δ_{H} 0.72 (s, 3 H, 18-H₃), 0.75 (s, 3 H, 19-H₃), 0.81 (m, 1 H), 0.91–1.06 (overlapping m, 3 H), 1.22–1.46 (overlapping m, 5 H), 1.60–1.76 (overlapping m, 6 H), 2.06 (m, 1 H, 16 α -H), 2.34 (d, 1 H, $J = 16.7$ Hz, 1 α -H), 2.72–2.80 (overlapping dd and d, 2 H, 4 β -H and 1 β -H), 3.05 (dd, 1 H, $J = 18.1$ Hz, $J = 5.5$ Hz, 4 α -H), 3.62 (t-like m, 1 H, 17 α -H), 7.26 (t-like m, 1 H, 5''-H), 7.35 (d, 2 H, $J = 7.7$ Hz, Ph-H² and Ph-H⁶), 7.39 (t-like m, 1 H, Ph-H⁴), 7.44 (t-like m, 2 H, Ph-H³ and Ph-H⁵), 7.79 (t, 1 H, $J = 7.7$ Hz, 4''-H), 8.04 (s, 1 H, 5'-H), 8.39 (d, 1 H, $J = 8.0$ Hz, 3''-H), 8.64 (d, 1 H, $J = 4.3$ Hz, 6''-H); ^{13}C NMR (CDCl₃, 125 MHz): δ_{C} 11.2 (C-18), 11.8 (C-19), 21.0 (C-11), 23.6 (C-15), 28.7 (C-6), 30.7 (C-16), 31.4 (C-7), 35.5 (C-10), 35.8 (C-8), 36.8 (C-4), 37.6 (C-12), 41.6 (C-1), 42.1 (C-5), 43.0 (C-13), 51.2 (C-14), 54.0 (C-9), 82.1 (C-17), 119.9 (C-5'), 121.2 (C-3''), 123.4 (C-5''), 127.8 (Ph-C⁴), 128.4 (2 C, Ph-C² and Ph-C⁶), 128.8 (2 C, Ph-C³ and Ph-C⁵), 129.1 (C-2), 136.9 (C-4''), 139.8 (Ph-C¹), 149.3 (C-6''), 151.2 (C-4'), 153.1 (C-6'), 156.5 and 156.8: C-2'' and C-3; ESI-MS 479 [M+H]⁺; Anal. Calcd. for C₃₃H₃₈N₂O C 82.80; H 8.00. Found C 82.58; H 7.98.

4.2.2.7. 4'-(*p*-Fluorophenyl)-6'-penylpyridino[2',3':3,2]-5 α -androstan-17 β -ole (3g). According to Section 4.2.2., 5c (397 mg) and 6a (455 mg) were used. The crude product was purified by CC (EtOAc/hexane = 20:80). Yield: 334 mg (67%, white solid). Mp 209–211 °C; ^1H NMR (CDCl₃, 500 MHz): δ_{H} 0.72 (s, 3 H, 18-H₃), 0.75 (s, 3 H, 19-H₃), 0.81 (m, 1 H), 0.92–1.08 (overlapping m, 3 H), 1.23–1.47 (overlapping m, 6 H), 1.59–1.78 (overlapping m, 5 H), 2.06 (m, 1 H, 16 α -H), 2.30 (d, 1 H, $J = 16.5$ Hz, 1 α -H), 2.65 (d, 1 H, $J = 16.5$ Hz, 1 β -H), 2.75 (dd, 1 H, $J = 18.0$ Hz, $J = 12.5$ Hz, 4 β -H), 3.05 (dd, 1 H, $J = 18.1$ Hz, $J = 5.3$ Hz, 4 α -H), 3.64 (m, 1 H, 17 α -H), 7.16 (t, 2 H, $J = 8.4$ Hz, Ph-H³ and Ph-H⁵), 7.30 (t-like m, 2 H, Ph-H² and Ph-H⁶), 7.38 (overlapping m, 2 H, 4''-H and 5''-H), 7.45 (t, 2 H, $J = 7.4$ Hz, 3''-H and 5''-H), 7.97 (d, 2 H, $J = 7.7$ Hz, 2''-H and 6''-H); ^{13}C NMR (CDCl₃, 125 MHz): δ_{C} 11.2 (C-18), 11.8 (C-19), 21.0 (C-11), 23.6 (C-15), 28.6 (C-6), 30.7 (C-16), 31.4 (C-7), 35.5 (C-10), 35.8 (C-8), 36.8 (C-4), 37.6 (C-12), 41.4 (C-1), 42.1 (C-5), 43.0 (C-13), 51.1 (C-14), 54.0 (C-9), 82.1 (C-17), 115.6 (d, $J = 21.3$, Ph-C³ and Ph-C⁵), 119.4 (C-5'), 127.0 (2 C, C-2'' and C-6''), 127.4 (C-2), 128.7 (C-4''), 128.8 (2 C, C-3'' and C-5''), 130.5 (d, 2 C, $J = 8.1$ Hz, Ph-C² and Ph-C⁶), 135.9 (d, $J = 3.4$ Hz, Ph-C¹), 139.7 (C-1''), 149.9 (C-4'), 154.5 (C-6'), 157.0 (C-3), 162.6 (d, $J = 247.2$ Hz, Ph-C⁴); ESI-MS 496 [M+H]⁺; Anal. Calcd. for C₃₄H₃₈FNO C 82.39; H 7.73. Found C 82.57; H 7.75.

4.2.2.8. 4'-(*p*-Fluorophenyl)-6'-(*o*-hydroxyphenyl)-pyridino[2',3':3,2]-5 α -androstan-17 β -ole (3h). According to Section 4.2.2., 5c (397 mg) and 6b (478 mg) were used. The crude product was purified by CC (EtOAc/CH₂Cl₂ = 2:98). Yield: 301 mg (59%; off white solid). Mp > 110 °C decomposes; ^1H NMR (CDCl₃, 500 MHz): δ_{H} 0.72 (s, 3 H, 18-H₃), 0.73 (s, 3 H, 19-H₃), 0.81 (m, 1 H), 0.87–1.08 (overlapping m, 3 H), 1.23–1.47 (overlapping m, 6 H), 1.57–1.79 (overlapping m, 5 H), 2.07 (m, 1 H, 16 α -H), 2.29 (d, 1 H, $J = 16.6$ Hz, 1 α -H), 2.63 (d, 1 H, $J = 16.5$ Hz, 1 β -H), 2.71 (dd, 1 H, $J = 18.1$ Hz, 12.3 Hz, 4 β -H), 2.96 (dd, 1 H, $J = 18.2$ Hz, $J = 5.2$ Hz, 4 α -H), 3.63 (t, 1 H, $J = 8.3$ Hz, 17 α -H), 6.86 (t, 1 H, $J = 7.5$ Hz, 4''-H), 7.01 (d, 1 H, $J = 8.2$ Hz, 6''-H), 7.18 (t, 2 H, $J = 7.9$ Hz, Ph-H³ and Ph-H⁵), 7.29 (overlapping m, 3 H, 5''-H, Ph-H² and Ph-H⁶), 7.56 (s, 1 H, 5'-H), 7.76 (d, 1 H, $J = 7.9$ Hz, 3''-H), 14.73 (s, 1 H, Ph-OH); ^{13}C NMR (CDCl₃, 125 MHz): δ_{C} 11.2 (C-18), 11.8 (C-19), 21.0 (C-11), 23.5 (C-15), 28.5 (C-6), 30.7 (C-16), 31.3 (C-7), 35.6 (C-10),

35.7 (C-8), 36.5 (C-4), 36.8 (C-12), 41.3 (C-1), 41.8 (C-5), 43.0 (C-13), 51.1 (C-14), 53.9 (C-9), 82.1 (C-17), 115.8 (d, $J = 21.4$, Ph-C³ and Ph-C⁵), 117.8 (C-6''), 118.6 and 118.7 (C-4'' and C-5'), 118.9 (C-2''), 126.1 (C-5''), 127.3 (C-2), 130.4 (d, 2 C, $J = 8.1$ Hz, Ph-C² and Ph-C⁶), 131.2 (C-3''), 135.3 (d, $J = 3.4$ Hz, Ph-C¹), 151.2 (C-4'), 153.6 (C-6'), 154.7 (C-1''), 160.3 (C-3), 162.7 (d, $J = 247.8$ Hz, Ph-C⁴); ESI-MS 512 [M+H]⁺; Anal. Calcd. for C₃₄H₃₈FNO₂ C 79.81; H 7.49. Found C 79.57; H 7.47.

4.2.2.9. 4'-(*p*-Fluorophenyl)-6'-(pyridin-2''-yl)pyridino[2',3':3,2]-5 α -androstan-17 β -ole (**3i**). According to Section 4.2.2., **5c** (397 mg) and **6c** (457 mg) were used. The crude product was purified by CC (EtOAc/hexane = 40:60). Yield: 339 mg (68%, off white solid). Mp 148–151 °C; ¹H NMR (CDCl₃, 500 MHz): δ_{H} 0.72 (s, 3 H, 18-H₃), 0.74 (s, 3 H, 19-H₃), 0.81 (m, 1 H), 0.92–1.07 (overlapping m, 3 H), 1.22–1.46 (overlapping m, 6 H), 1.58–1.78 (overlapping m, 5 H), 2.06 (m, 1 H, 16 α -H), 2.32 (d, 1 H, $J = 16.6$ Hz, 1 α -H), 2.69 (d, 1 H, $J = 16.6$ Hz, 1 β -H), 2.75 (dd, 1 H, $J = 18.0$ Hz, 12.5 Hz, 4 β -H), 3.05 (dd, 1 H, $J = 18.2$ Hz, $J = 5.2$ Hz, 4 α -H), 3.63 (t, 1 H, $J = 8.5$ Hz, 17 α -H), 7.13 (t, 2 H, $J = 8.5$ Hz, Ph-H³ and Ph-H⁵), 7.27 (m, 1 H, 5''-H), 7.32 (t-like m, 2 H, Ph-H² and Ph-H⁶), 7.79 (t, 1 H, $J = 7.7$ Hz, 4''-H), 8.03 (s, 1 H, 5'-H), 8.40 (d, 1 H, $J = 8.0$ Hz, 3''-H), 8.64 (d, 1 H, $J = 4.5$ Hz, 6''-H); ¹³C NMR (CDCl₃, 125 MHz): δ_{C} 11.2 (C-18), 11.8 (C-19), 21.0 (C-11), 23.6 (C-15), 28.6 (C-6), 30.7 (C-16), 31.3 (C-7), 35.5 (C-10), 35.8 (C-8), 36.8 (C-4), 37.5 (C-12), 41.6 (C-1), 42.1 (C-5), 43.0 (C-13), 51.1 (C-14), 54.0 (C-9), 82.1 (C-17), 115.5 (d, $J = 21.4$, Ph-C³ and Ph-C⁵), 119.8 (C-5''), 121.2 (C-3''), 123.5 (C-5''), 129.2 (C-2), 130.5 (d, 2 C, $J = 7.9$ Hz, Ph-C² and Ph-C⁶), 135.7 (d, $J = 3.3$ Hz, Ph-C¹), 137.0 (C-4''), 149.3 (C-6''), 150.2 (C-4'), 153.1 (C-6'), 156.6 and 156.7: C-2'' and C-3, 162.6 (d, $J = 246.9$ Hz, Ph-C⁴); ESI-MS 497 [M+H]⁺; Anal. Calcd. for C₃₃H₃₇FN₂O C 79.80; H 7.51. Found C 79.91; H 7.52.

4.2.2.10. 4'-(*p*-Chlorophenyl)-6'-penylpyridino[2',3':3,2]-5 α -androstan-17 β -ole (**3j**). According to Section 4.2.2., **5d** (413 mg) and **6a** (455 mg) were used. The crude product was purified by CC (EtOAc/hexane = 20:80). Yield: 374 mg (73%, white solid). Mp 164–167 °C; ¹H NMR (CDCl₃, 500 MHz): δ_{H} 0.72 (s, 3 H, 18-H₃), 0.74 (s, 3 H, 19-H₃), 0.81 (m, 1 H), 0.91–1.08 (overlapping m, 3 H), 1.23–1.47 (overlapping m, 6 H), 1.59–1.79 (overlapping m, 5 H), 2.06 (m, 1 H, 16 α -H), 2.30 (d, 1 H, $J = 16.5$ Hz, 1 α -H), 2.65 (d, 1 H, $J = 16.5$ Hz, 1 β -H), 2.75 (dd, 1 H, $J = 18.1$ Hz, $J = 12.5$ Hz, 4 β -H), 3.05 (dd, 1 H, $J = 18.2$ Hz, $J = 5.3$ Hz, 4 α -H), 3.64 (t-like m, 1 H, 17 α -H), 7.27 (m, 2 H, Ph-H³ and Ph-H⁵), 7.38 (overlapping m, 2 H, 5'-H and 4''-H), 7.44 (overlapping m, 4 H, Ph-H², Ph-H⁶, 3''-H and 5''-H), 7.97 (d, 2 H, $J = 7.9$ Hz, 2''-H and 6''-H); ¹³C NMR (CDCl₃, 125 MHz): δ_{C} 11.2 (C-18), 11.8 (C-19), 21.0 (C-11), 23.6 (C-15), 28.6 (C-6), 30.7 (C-16), 31.3 (C-7), 35.5 (C-10), 35.8 (C-8), 36.8 (C-4), 37.6 (C-12), 41.4 (C-1), 42.1 (C-5), 43.0 (C-13), 51.1 (C-14), 54.0 (C-9), 82.1 (C-17), 119.3 (C-5''), 127.0 (2 C, C-2'' and C-6''), 127.2 (C-2), 128.7 (C-4''), 128.8 (4 C, C-3'', C-5'', Ph-C³ and Ph-C⁵), 130.1 (2 C, Ph-C² and Ph-C⁶), 134.0 (Ph-C⁴), 138.3 (Ph-C¹), 139.7 (C-1''), 149.7 (C-4'), 154.5 (C-6'), 157.1 (C-3); ESI-MS 512 [M+H]⁺; Anal. Calcd. for C₃₄H₃₈ClNO C 79.74; H 7.48. Found C 79.56; H 7.45.

4.2.2.11. 4'-(*p*-Chlorophenyl)-6'-(*o*-hydroxyphenyl)-pyridino[2',3':3,2]-5 α -androstan-17 β -ole (**3k**). According to Section 4.2.2., **5d** (413 mg) and **6b** (478 mg) were used. The crude product was purified by CC (EtOAc/CH₂Cl₂ = 2:98). Yield: 379 mg (70%, light yellow solid). Mp 260–263 °C; ¹H NMR (CDCl₃, 500 MHz): δ_{H} 0.73 (s, 3 H, 18-H₃), 0.74 (s, 3 H, 19-H₃), 0.81 (m, 1 H), 0.91–1.00 (overlapping m, 2 H), 1.06 (m, 1 H), 1.23–1.47 (overlapping m, 6 H), 1.59–1.79 (overlapping m, 5 H), 2.07 (m, 1 H, 16 α -H), 2.29 (d, 1 H, $J = 16.6$ Hz, 1 α -H), 2.62 (d, 1 H, $J = 16.6$ Hz, 1 β -H), 2.71 (dd, 1 H, $J = 18.1$ Hz, 12.5 Hz, 4 β -H), 2.97 (dd, 1 H, $J = 18.2$ Hz, $J = 5.3$ Hz, 4 α -H), 3.64 (t-like m, 1 H, 17 α -H), 6.86 (t, 1 H, $J = 7.5$ Hz, 4''-H), 7.01 (d, 1 H, $J = 8.2$ Hz, 6''-H), 7.27 (overlapping m, 3 H, 5''-H, Ph-H³ and Ph-H⁵), 7.47 (d, 2 H, $J = 7.7$ Hz, Ph-H² and Ph-H⁶), 7.55 (s, 1 H, 5'-H), 7.75 (d, 1 H, $J = 8.0$ Hz, 3''-H), 14.69 (s, 1 H, Ph-OH); ¹³C NMR (CDCl₃, 125 MHz): δ_{C} 11.2 (C-18), 11.8 (C-19), 21.0 (C-11), 23.5 (C-15), 28.5 (C-6), 30.7 (C-16), 31.3 (C-7), 35.6 (C-10), 35.7 (C-8), 36.5 (C-4), 36.8 (C-12), 41.2 (C-1), 41.7 (C-

10), 35.7 (C-8), 36.5 (C-4), 36.8 (C-12), 41.2 (C-1), 41.8 (C-5), 43.0 (C-13), 51.1 (C-14), 53.9 (C-9), 82.1 (C-17), 117.6 (C-6''), 118.6 and 118.7 (C-4'' and C-5'), 118.9 (C-2''), 126.1 (C-5''), 127.2 (C-2), 129.0 (2 C, Ph-C³ and Ph-C⁵), 130.0 (2 C, Ph-C² and Ph-C⁶), 131.2 (C-3''), 134.5 (Ph-C⁴), 137.8 (Ph-C¹), 150.9 (C-4'), 153.7 (C-6'), 154.8 (C-1''), 160.3 (C-3); ESI-MS 528 [M+H]⁺; Anal. Calcd. for C₃₄H₃₈ClNO₂ C 77.32; H 7.25. Found C 77.08; H 7.22.

4.2.2.12. 4'-(*p*-Chlorophenyl)-6'-(pyridin-2''-yl)pyridino[2',3':3,2]-5 α -androstan-17 β -ole (**3l**). According to Section 4.2.2., **5d** (413 mg) and **6c** (457 mg) were used. The crude product was purified by CC (EtOAc/hexane = 40:60). Yield: 394 mg (77%, off white solid). Mp 142–145 °C; ¹H NMR (CDCl₃, 500 MHz): δ_{H} 0.72 (s, 3 H, 18-H₃), 0.74 (s, 3 H, 19-H₃), 0.81 (m, 1 H), 0.93–1.07 (overlapping m, 3 H), 1.22–1.46 (overlapping m, 6 H), 1.59–1.78 (overlapping m, 5 H), 2.05 (m, 1 H, 16 α -H), 2.32 (d, 1 H, $J = 16.6$ Hz, 1 α -H), 2.68 (d, 1 H, $J = 16.6$ Hz, 1 β -H), 2.75 (dd, 1 H, $J = 18.0$ Hz, 12.5 Hz, 4 β -H), 3.05 (dd, 1 H, $J = 18.1$ Hz, $J = 5.3$ Hz, 4 α -H), 3.63 (t, 1 H, $J = 8.5$ Hz, 17 α -H), 7.27 (m, 1 H, 5''-H), 7.29 (d, 2 H, $J = 7.9$ Hz, Ph-H³ and Ph-H⁵), 7.42 (d, 2 H, $J = 7.9$ Hz, Ph-H² and Ph-H⁶), 7.79 (t, 1 H, $J = 7.7$ Hz, 4''-H), 8.02 (s, 1 H, 5'-H), 8.40 (d, 1 H, $J = 8.0$ Hz, 3''-H), 8.64 (d, 1 H, $J = 4.6$ Hz, 6''-H); ¹³C NMR (CDCl₃, 125 MHz): δ_{C} 11.2 (C-18), 11.8 (C-19), 21.0 (C-11), 23.6 (C-15), 28.6 (C-6), 30.7 (C-16), 31.3 (C-7), 35.5 (C-10), 35.8 (C-8), 36.8 (C-4), 37.5 (C-12), 41.6 (C-1), 42.1 (C-5), 43.0 (C-13), 51.1 (C-14), 54.0 (C-9), 82.1 (C-17), 119.7 (C-5''), 121.2 (C-3''), 123.5 (C-5''), 128.7 (2 C, Ph-C³ and Ph-C⁵), 129.0 (C-2), 130.2 (2 C, Ph-C² and Ph-C⁶), 133.9 (Ph-C⁴), 137.0 (C-4''), 138.2 (Ph-C¹), 149.3 (C-6''), 150.0 (C-4'), 153.2 (C-6'), 156.5 and 156.7: C-2'' and C-3; ESI-MS 513 [M+H]⁺; Anal. Calcd. for C₃₃H₃₇ClN₂O C 77.25; H 7.27. Found C 76.98; H 7.24.

4.2.2.13. 4'-(*p*-Bromophenyl)-6'-penylpyridino[2',3':3,2]-5 α -androstan-17 β -ole (**3m**). According to Section 4.2.2., **5e** (457 mg) and **6a** (455 mg) were used. The crude product was purified by CC (EtOAc/hexane = 20:80). Yield: 292 (52%, white solid). Mp 163–166 °C; ¹H NMR (CDCl₃, 500 MHz): δ_{H} 0.73 (s, 3 H, 18-H₃), 0.74 (s, 3 H, 19-H₃), 0.81 (m, 1 H), 0.91–1.08 (overlapping m, 3 H), 1.23–1.47 (overlapping m, 6 H), 1.60–1.79 (overlapping m, 5 H), 2.06 (m, 1 H, 16 α -H), 2.30 (d, 1 H, $J = 16.5$ Hz, 1 α -H), 2.65 (d, 1 H, $J = 16.5$ Hz, 1 β -H), 2.75 (dd, 1 H, $J = 18.0$ Hz, $J = 12.5$ Hz, 4 β -H), 3.05 (dd, 1 H, $J = 18.2$ Hz, $J = 5.2$ Hz, 4 α -H), 3.64 (m, 1 H, 17 α -H), 7.21 (d, 2 H, $J = 7.8$ Hz, Ph-H² and Ph-H⁶), 7.38 (overlapping m, 2 H, 5'-H and 4''-H), 7.44 (t, 2 H, $J = 7.4$ Hz, 3''-H and 5''-H), 7.60 (d, 2 H, $J = 7.8$ Hz, Ph-H³ and Ph-H⁵), 7.97 (d, 2 H, $J = 7.6$ Hz, 2''-H and 6''-H); ¹³C NMR (CDCl₃, 125 MHz): δ_{C} 11.2 (C-18), 11.8 (C-19), 21.0 (C-11), 23.6 (C-15), 28.6 (C-6), 30.7 (C-16), 31.3 (C-7), 35.5 (C-10), 35.8 (C-8), 36.8 (C-4), 37.6 (C-12), 41.4 (C-1), 42.1 (C-5), 43.0 (C-13), 51.1 (C-14), 54.0 (C-9), 82.1 (C-17), 119.2 (C-5''), 122.2 (Ph-C⁴), 127.0 (2 C, C-2'' and C-6''), 127.2 (C-2), 128.7 (C-4''), 128.8 (2 C, C-3'' and C-5''), 130.4 (2 C, Ph-C² and Ph-C⁶), 131.8 (2 C, Ph-C³ and Ph-C⁵), 138.8 (Ph-C¹), 139.6 (C-1''), 149.7 (C-4'), 154.6 (C-6'), 157.1 (C-3); ESI-MS 558 [M+H]⁺; Anal. Calcd. for C₃₄H₃₈BrNO C 73.37; H 6.88. Found C 73.51; H 6.90.

4.2.2.14. 4'-(*p*-Bromophenyl)-6'-(*o*-hydroxyphenyl)-pyridino[2',3':3,2]-5 α -androstan-17 β -ole (**3n**). According to Section 4.2.2., **5e** (457 mg) and **6b** (478 mg) were used. The crude product was purified by CC (EtOAc/CH₂Cl₂ = 2:98). Yield: 293 mg (51%, light yellow solid). Mp 269–271 °C; ¹H NMR (CDCl₃, 500 MHz): δ_{H} 0.73 (s, 3 H, 18-H₃), 0.73 (s, 3 H, 19-H₃), 0.80 (m, 1 H), 0.91–1.00 (overlapping m, 2 H), 1.05 (m, 1 H), 1.23–1.47 (overlapping m, 6 H), 1.59–1.80 (overlapping m, 5 H), 2.07 (m, 1 H, 16 α -H), 2.28 (d, 1 H, $J = 16.6$ Hz, 1 α -H), 2.62 (d, 1 H, $J = 16.6$ Hz, 1 β -H), 2.71 (dd, 1 H, $J = 18.2$ Hz, 12.3 Hz, 4 β -H), 2.96 (dd, 1 H, $J = 18.2$ Hz, $J = 5.3$ Hz, 4 α -H), 3.64 (m, 1 H, 17 α -H), 6.86 (t, 1 H, $J = 7.5$ Hz, 4''-H), 7.00 (d, 1 H, $J = 8.2$ Hz, 6''-H), 7.21 (d, 2 H, $J = 7.8$ Hz, Ph-H² and Ph-H⁶), 7.27 (t-like m, 1 H, 5''-H), 7.54 (s, 1 H, 5'-H), 7.62 (d, 2 H, $J = 7.8$ Hz, Ph-H³ and Ph-H⁵), 7.74 (d, 1 H, $J = 8.0$ Hz, 3''-H), 14.68 (s, 1 H, Ph-OH); ¹³C NMR (CDCl₃, 125 MHz): δ_{C} 11.2 (C-18), 11.8 (C-19), 21.0 (C-11), 23.5 (C-15), 28.5 (C-6), 30.7 (C-16), 31.3 (C-7), 35.6 (C-10), 35.7 (C-8), 36.5 (C-4), 36.8 (C-12), 41.2 (C-1), 41.7 (C-

5), 43.0 (C-13), 51.1 (C-14), 53.9 (C-9), 82.1 (C-17), 117.5 (C-6''), 118.6 and 118.8 (C-4'' and C-5'), 118.9 (C-2''), 122.6 (Ph-C⁴), 126.0 (C-5''), 127.1 (C-2), 130.3 (2 C, Ph-C² and Ph-C⁶), 131.2 (C-3''), 131.9 (2 C, Ph-C³ and Ph-C⁵), 138.3 (Ph-C¹), 150.9 (C-4'), 153.7 (C-6'), 154.8 (C-1''), 160.3 (C-3); ESI-MS 574 [M+H]⁺; Anal. Calcd. for C₃₄H₃₈BrNO₂ C 71.32; H 6.69. Found C 71.06; H 6.67.

4.2.2.15. 4'-(*p*-Bromophenyl)-6'-(pyridin-2''-yl)pyridino[2',3':3,2]-5 α -androstan-17 β -ole (3o). According to Section 4.2.2., 5e (457 mg) and 6c (457 mg) were used. The crude product was purified by CC (EtOAc/hexane = 40:60). Yield: 303 mg (54%, off white solid). Mp 146–148 °C; ¹H NMR (CDCl₃, 500 MHz): δ_{H} 0.73 (s, 3 H, 18-H₃), 0.74 (s, 3 H, 19-H₃), 0.81 (m, 1 H), 0.91–1.00 (overlapping m, 2 H), 1.05 (m, 1 H), 1.23–1.47 (overlapping m, 6 H), 1.59–1.79 (overlapping m, 5 H), 2.06 (m, 1 H, 16 α -H), 2.32 (d, 1 H, *J* = 16.6 Hz, 1 α -H), 2.69 (d, 1 H, *J* = 16.6 Hz, 1 β -H), 2.75 (dd, 1 H, *J* = 18.0 Hz, 12.4 Hz, 4 β -H), 3.05 (dd, 1 H, *J* = 18.1 Hz, *J* = 5.3 Hz, 4 α -H), 3.64 (t, 1 H, *J* = 8.4 Hz, 17 α -H), 7.23 (d, 2 H, *J* = 7.8 Hz, Ph-H² and Ph-H⁶), 7.27 (m, 1 H, 5''-H), 7.58 (d, 2 H, *J* = 7.8 Hz, Ph-H³ and Ph-H⁵), 7.79 (t, 1 H, *J* = 7.7 Hz, 4''-H), 8.02 (s, 1 H, 5''-H), 8.39 (d, 1 H, *J* = 8.0 Hz, 3''-H), 8.64 (d, 1 H, *J* = 4.6 Hz, 6''-H); ¹³C NMR (CDCl₃, 125 MHz): δ_{C} 11.2 (C-18), 11.8 (C-19), 21.0 (C-11), 23.6 (C-15), 28.6 (C-6), 30.7 (C-16), 31.3 (C-7), 35.5 (C-10), 35.8 (C-8), 36.8 (C-4), 37.5 (C-12), 41.6 (C-1), 42.1 (C-5), 43.0 (C-13), 51.1 (C-14), 54.0 (C-9), 82.1 (C-17), 119.6 (C-5'), 121.1 (C-3''), 122.1 (Ph-C⁴), 123.5 (C-5''), 128.9 (C-2), 130.5 (2 C, Ph-C² and Ph-C⁶), 131.6 (2 C, Ph-C³ and Ph-C⁵), 137.0 (C-4''), 138.7 (Ph-C¹), 149.3 (C-6''), 149.9 (C-4'), 153.2 (C-6'), 156.6 and 156.8: C-2'' and C-3; ESI-MS 559 [M+H]⁺; Anal. Calcd. for C₃₃H₃₇BrN₂O C 71.09; H 6.69. Found C 71.38; H 6.72.

4.3. X-ray data collection, structure solution and refinement for compound 2a

A colourless prism of **2a** was mounted on a loop and measured by single crystal X-ray diffraction. Intensity data were collected on a Rigaku R-Axis Rapid diffractometer (graphite monochromator; Mo-K α radiation, λ = 0.71073 Å) at 103(2) K. A numerical absorption correction was applied to the data using NUMABS [32] and CrystalClear [33] software. The structure was solved by direct methods by SIR [34] software and was refined using SHELX [35] program package under WinGX [36] software. The structure was visualized using Mercury [37] software. Selected bond lengths and angles were calculated by PLATON [38] software. The ratio of anomalous scattering centres is low in **2a** and the absolute structure could not be determined on the basis of the diffraction data. The absolute structure parameter is 0.6(16). The handedness of the crystal structure was set on the basis of the known absolute configuration of the molecule. (Friedel coverage: 0.936, Friedel fraction max.: 0.994, Friedel fraction full: 0.998). The weighting scheme applied was $w = 1/[\sigma^2(F_o^2) + (0.04460.4073 P)^2 + 0.4073 P]$ where $P = (F_o^2 + 2F_c^2)/3$. Hydrogen atomic positions were calculated from assumed geometries. Hydrogen atoms were included in structure factor calculations, but they were not refined. The isotropic displacement parameters of the hydrogen atoms were approximated from the *U*(eq) value of the atom they were bonded to. Crystal data and details of the structure determination and refinement are listed in Table 5. Bond lengths and angles respectively are listed in Tables S2 and S3. The crystallographic data file for compound **2a** has been deposited with the Cambridge Crystallographic Database as CCDC 2247232.

4.4. Cell lines

The 22Rv1-ARE14 reporter cell line [28] (kind gift from prof. Zdeněk Dvořák from Palacký University Olomouc, Czech Republic), the LNCaP and DU145 cells (purchased from ECACC) were grown in RPMI-1640 medium. The LAPC-4 (kind gift from doc. Jan Bouchal, Palacký University Olomouc and University Hospital Olomouc, Czech Republic) cell line was grown in DMEM medium. All media were supplemented with 10% fetal bovine serum or charcoal-stripped serum (steroid-depleted),

Table 5

Crystal data and details of structure refinement.

Empirical formula	C28 H35 N O
Formula weight	401.57
Temperature	103(2)
Radiation and wavelength	Mo-K α , λ = 0.71073 Å
Crystal system	monoclinic
Space group	<i>P</i> 21
Unit cell dimensions	<i>a</i> = 9.6396(4) Å <i>b</i> = 17.8123(6) Å <i>c</i> = 13.1637(5) Å α = 90° β = 93.553(7)° γ = 90°
Volume	2255.91(15) Å ³
Z	4
Density (calculated)	1.182 Mg/m ³
Absorption coefficient, μ	0.070 mm ⁻¹
<i>F</i> (000)	872
Crystal colour	colourless
Crystal description	prism
Crystal size	0.65 × 0.57 × 0.47 mm
Absorption correction	numerical
Max. and min. transmission	0.9920.995
θ – range for data collection	3.101 ≤ θ ≤ 27.471°
Index ranges	-12 ≤ <i>h</i> ≤ 12; -23 ≤ <i>k</i> ≤ 23; -17 ≤ <i>l</i> ≤ 17
Reflections collected	66,337
Completeness to 2 θ	0.998
Absolute structure parameter	0.6(16)
Friedel coverage	0.936
Friedel fraction max.	0.994
Friedel fraction full	0.998
Independent reflections	10,343 [R(int) = 0.0698]
Reflections <i>I</i> > 2 σ (<i>I</i>)	8680
Refinement method	full-matrix least-squares on <i>F</i> ²
Data / restraints / parameters	10,286 / 1 / 548
Goodness-of-fit on <i>F</i> ²	1.062
Final <i>R</i> indices [<i>I</i> > 2 σ (<i>I</i>)]	<i>R</i> 1 = 0.0567, <i>wR</i> 2 = 0.1013
<i>R</i> indices (all data)	<i>R</i> 1 = 0.0715, <i>wR</i> 2 = 0.1059
Max. and mean shift/esd	0.000;0.000
Largest diff. peak and hole	0.304; -0.190 e.Å ⁻³

100 IU/mL penicillin, 100 μ g/mL streptomycin, 4 mM glutamine and 1 mM sodium pyruvate. Cells were cultivated in a humidified incubator, in 5% CO₂ atmosphere, at 37 °C.

4.5. AR transcriptional luciferase assay

AR-transcriptional luciferase assay was performed using the 22Rv1-ARE14 cells based on the published protocol [17]. The Nunc™ MicroWell™ 96-well optical flat-bottom plate (Thermo Fisher Scientific) were used for luciferase assay and the luminescence of the samples was measured using a Tecan M200 Pro microplate reader (Biotek).

4.6. Cell viability assay

Cells were seeded into the 96-well tissue culture plates. The following day, solutions of compounds were added for 72 h. Upon treatment, the resazurin solution (Sigma Aldrich) was added for 4 h, and then the fluorescence of resorufin was measured at 544 nm/590 nm (excitation/emission) using a Fluoroskan Ascent microplate reader (Labsystems). Percentual viability or GI₅₀ value were calculated using GraphPad Prism 5.

4.7. Colony formation assay

Cells were seeded in low density into 6-well plates. After two days, the medium was replaced with fresh medium containing different concentrations of the compounds. Cells were cultivated for 10 days. Then, the medium was discarded, and colonies were fixed with 70% ethanol for 15 min, washed with PBS and stained with crystal violet (1% solution

in 96% ethanol). Finally, wells were washed with PBS and photograph was captured. After drying, cell colonies were dissolved in 1% SDS, collected from the plate and the absorbance of the crystal violet was measured in 570 nm.

4.8. Immunoblotting

Cell pellets were obtained after treatments, washed with PBS and kept frozen at -80 °C. Lysis of the cell material was performed in ice-cold RIPA (radioimmunoprecipitation assay) buffer supplemented with protease and phosphatase inhibitors. After the ultrasound sonication (10 s with 30% amplitude), supernatants were obtained by centrifugation at 14,000 g for 30 min. Protein concentration in supernatants was measured and balanced, proteins were denatured in SDS-loading buffer with heating at 95 °C. After the separation by SDS-PAGE, proteins were electroblotted onto nitrocellulose membranes. For immunodetection, membranes were blocked in 4% BSA and 0.1% Tween 20 in TBS solution and incubated overnight with primary antibodies, subsequently washed and incubated with secondary antibodies conjugated with peroxidase. Peroxidase activity was detected by SuperSignal West Pico reagents (Thermo Scientific) using a CCD camera LAS-4000 (Fujifilm). Primary antibodies were purchased from Santa Cruz Biotechnology (anti- β -actin, clone C4). Primary antibodies were purchased from Merck (anti- α -tubulin, clone DM1A; anti-phosphorylated AR (S81)). Specific antibodies were purchased from Cell Signaling Technology (anti-AR, clone D6F11; anti-PSA/KLK3, clone D6B1; anti-Nkx3.1, clone D2Y1A); anti-rabbit secondary antibody (porcine anti-rabbit immunoglobulin serum); anti-mouse secondary antibody (rabbit anti-mouse IgG, clone D3V2A)). All antibodies were diluted in 4% BSA and 0.1% Tween 20 in TBS.

4.9. Cell-cycle analysis

Cells were treated with test compounds for 24 h, they were harvested by trypsinisation, washed with PBS and fixed with 70% ethanol. After rehydration, cells were permeabilised by 2 M HCl, 0.5% Triton X-100. Following neutralization and wash with PBS, the cells were stained with propidium iodide and analyzed by flow cytometry with a 488 nm laser (BD FACS Verse with BD FACSuite software, version 1.0.6.). Cell cycle distribution was analyzed using ModFit LT (Verity Software House, version 5.0).

4.10. Molecular docking

The flexible molecular docking was recruited to model the binding of the candidate compound **1d** into AR-LBD co-crystal structure with natural agonist DHT (PDB: 2PIV). The key residues in extremities of the cavity (Asn705, Gln711, Arg752, and Thr877) were set flexible. The 3D-structures of compound **1d** was obtained and its energy was minimized by molecular mechanics with Avogadro 1.90.0. Polar hydrogens were added to ligands and proteins using the AutoDock Tools program [39] and docking studies were performed using AutoDock Vina 1.05 [40]. Interactions of the candidate compound with the protein and the figure were generated in Pymol ver. 2.0.4 (Schrödinger, LLC).

4.11. Preparation and micro-scale thermophoresis (MST) of AR-LBD

AR-LBD (with His₆-tag) was expressed using recombinant plasmid pET-15b-hAR-663–919, which was a generous gift from Elizabeth Wilson (Addgene plasmid # 89083) in expression bacteria BL21(DE3) pLysS similar to the original protocol [29]. Cells were homogenized in lysis buffer (50 mM Tris, 300 mM KCl, pH 8.0, 5 mM dithiothreitol (DTT), 1 mM mono-thioglycerol (MTG) supplemented with protease inhibitors and 1% Nonidet P-40), using an ultrasound sonicator. Supernatant was clarified by centrifugation at 19,000 g for 30 min at 4 °C. The purification was performed using the NGC chromatographic system (Bio-Rad) on Ni²⁺- metal affinity-Sepharose column (His-Trap, Cytiva),

equilibrated with 50 mM Tris, 300 mM KCl, pH 8.0, 5 mM DTT, 1 mM MTG and 50 mM imidazole. After loading, the column was washed with the equilibration buffer, followed by a wash with 100 mM imidazole in the equilibration buffer. Elution was performed by 500 mM imidazole in storage buffer (50 mM Tris, 300 mM KCl, pH 8.0, 5 mM DTT, 1 mM MTG). The imidazole was washed out and the protein was concentrated in the storage buffer up to 0.5 mg/mL using centrifugal filter unit with 10 kDa cutoff (Merck). MST method was used to prove interaction of **1d** with the AR-LBD, which was labelled with the Red-Tris-NTA 2nd generation labelling dye (NanoTemper Technologies) (100 nM dye + 800 nM His-tagged protein) for 30 min on ice. The labelled protein underwent the MST measurements with or without **1d** in final concentration of 400 nM His-tagged protein in the storage buffer, supplemented with 0.1% Tween. Measurements were done on a Monolith NT.115 instrument (NanoTemper Technologies) at 37 °C. Obtained results were evaluated and normalised fluorescence in $t = 20$ s was used to create a bar chart in GraphPad Prism 5.

Funding

The publication was funded by the University of Szeged Open Access Fund (FundRef, Grant No. 6143).

CRediT authorship contribution statement

Éva Frank, Radek Jorda: Conceptualization, Methodology, Resources, Supervision, Writing – review & editing. **Márton A. Kiss, Ádám Baji:** Chemical synthesis and optimization experiments. **Miroslav Perina, Jakub Bělíček:** Pharmacological studies. **Laura Bereczki:** Single crystal X-ray analysis. **Miroslav Perina:** Flexible docking. **Márton A. Kiss:** Structural analysis. **Ádám Baji, Miroslav Perina, Jakub Bělíček:** Formal analysis and interpretation of data. **Miroslav Perina, Laura Bereczki, Márton A. Kiss:** Writing – original draft preparation. All authors have read and agreed to the published version of the manuscript.

Declaration of Competing Interest

The authors declare that they have no known competing financial interests or personal relationships that could have appeared to influence the work reported in this paper.

Data availability

Data will be made available on request.

Acknowledgement

The authors gratefully acknowledge financial support from the Palacký University Olomouc (IGA_PrF_2023_012).

Appendix A. Supporting information

Supplementary data associated with this article can be found in the online version at [doi:10.1016/j.jsbmb.2023.106315](https://doi.org/10.1016/j.jsbmb.2023.106315).

References

- [1] D. Li, W. Zhou, J. Pang, Q. Tang, B. Zhong, C. Shen, L. Xiao, T. Hou, A magic drug target: Androgen receptor, *Med Res Rev.* 39 (2019) 1485–1514, <https://doi.org/10.1002/med.21558>.
- [2] A. Paschalis, J.S. de Bono, Prostate Cancer 2020: “The Times They Are a’Changing.”, *Cancer Cell.* 38 (2020) 25–27, <https://doi.org/10.1016/j.ccell.2020.06.008>.
- [3] T. Uo, S.R. Plymate, C.C. Sprenger, The potential of AR-V7 as a therapeutic target, *Expert Opin. Ther. Targets* 22 (2018) 201–216, <https://doi.org/10.1080/14728222.2018.1439016>.

- [4] S. Saranyutanon, S.K. Srivastava, S. Pai, S. Singh, A.P. Singh, Therapies targeted to androgen receptor signaling axis in prostate cancer: progress, challenges, and hope, *Cancers (Basel)* 12 (2019) 51, <https://doi.org/10.3390/cancers12010051>.
- [5] X. Jia, X. Han, Targeting androgen receptor degradation with PROTACs from bench to bedside, *Biomed. Pharmacother.* 158 (2023), 114112, <https://doi.org/10.1016/j.biopha.2022.114112>.
- [6] S. De, A. Kumar S K, S.K. Shah, S. Kazi, N. Sarkar, S. Banerjee, S. Dey, Pyridine: the scaffolds with significant clinical diversity, *RSC Adv.* 12 (2022) 15385–15406, <https://doi.org/10.1039/D2RA01571D>.
- [7] D. Wang, L. Désaubry, G. Li, M. Huang, S. Zheng, Recent Advances in the Synthesis of C2-Functionalized Pyridines and Quinolines Using N-Oxide Chemistry, *Adv. Synth. Catal.* 363 (2021) 2–39, <https://doi.org/10.1002/adsc.202000910>.
- [8] A. Dorababu, Quinoline: a promising scaffold in recent antiprotazoal drug discovery, *ChemistrySelect* 6 (2021) 2164–2177, <https://doi.org/10.1002/slct.202100115>.
- [9] O.O. Ajani, K.T. Iyaye, O.T. Ademosun, Recent advances in chemistry and therapeutic potential of functionalized quinoline motifs – a review, *RSC Adv.* 12 (2022) 18594–18614, <https://doi.org/10.1039/D2RA02896D>.
- [10] T.S. Vasaitis, R.D. Bruno, V.C.O. Njar, CYP17 inhibitors for prostate cancer therapy, *J. Steroid Biochem Mol. Biol.* 125 (2011) 23–31, <https://doi.org/10.1016/J.JSBMB.2010.11.005>.
- [11] J. Richards, A.C. Lim, C.W. Hay, A.E. Taylor, A. Nowakowska, C. Pezaro, S. Carreira, J. Goodall, W. Arlt, I.J. McEwan, J.S. de Bono, G. Attard, Interactions of Abiraterone, Eplerenone, and Prednisolone with Wild-type and Mutant Androgen Receptor: A Rationale for Increasing Abiraterone Exposure or Combining with MDV3100, *Cancer Res* 72 (2012) 2176–2182, <https://doi.org/10.1158/0008-5472.CAN-11-3980>.
- [12] Y.K. Shi, B. Wang, X.L. Shi, Y. di Zhao, B. Yu, H.M. Liu, Synthesis and biological evaluation of new steroidal pyridines as potential anti-prostate cancer agents, *Eur. J. Med Chem.* 145 (2018) 11–22, <https://doi.org/10.1016/J.EJMECH.2017.12.094>.
- [13] Y.T. Yang, S. Du, S. Wang, X. Jia, X. Wang, X. Zhang, Synthesis of new steroidal quinolines with antitumor properties, *Steroids* 151 (2019), 108465, <https://doi.org/10.1016/J.STEROIDS.2019.108465>.
- [14] A.I. Ilovaisky, A.M. Scherbakov, V.M. Merkulova, E.I. Chernoburova, M. A. Shchetinina, O.E. Andreeva, D.I. Salmikova, I. v Zavarzin, A.O. Terent'ev, Secosteroid–quinoline hybrids as new anticancer agents, *J. Steroid Biochem Mol. Biol.* 228 (2023), 106245, <https://doi.org/10.1016/J.JSBMB.2022.106245>.
- [15] M.G. Barthakur, M. Borthakur, R.C. Boruah, Convenient preparation of A-ring fused pyridines from steroidal enamides, *Steroids* 73 (2008) 1137–1142, <https://doi.org/10.1016/J.STEROIDS.2008.04.016>.
- [16] M.A. Kiss, M. Peřina, V. Bazgier, N. v May, Á. Baji, R. Jorda, É. Frank, Synthesis of dihydrotestosterone derivatives modified in the A-ring with (hetero)arylidene, pyrazolo[1,5-a]pyrimidine and triazolo[1,5-a]pyrimidine moieties and their targeting of the androgen receptor in prostate cancer, *J. Steroid Biochem Mol. Biol.* 211 (2021), 105904, <https://doi.org/10.1016/J.JSBMB.2021.105904>.
- [17] M. Peřina, M.A. Kiss, G. Mótýán, E. Szczyrbóvá, M. Eliáš, V. Študent, D. Kurfürstová, M. Kovalová, L. Mada, J. Bouchal, É. Frank, R. Jorda, A-ring-fused pyrazoles of dihydrotestosterone targeting prostate cancer cells via the downregulation of the androgen receptor, *Eur. J. Med Chem.* 249 (2023), 115086, <https://doi.org/10.1016/J.EJMECH.2023.115086>.
- [18] M. Radaeva, H. Li, E. LeBlanc, K. Dalal, F. Ban, F. Ciesielski, B. Chow, H. Morin, S. Awrey, K. Singh, P.S. Rennie, N. Lalous, A. Cherkasov, Structure-Based Study to Overcome Cross-Reactivity of Novel Androgen Receptor Inhibitors, *Cells* 11 (2022) 2785, <https://doi.org/10.3390/cells11182785>.
- [19] Á. Baji, A. Gyovai, J. Wölfling, R. Minorics, I. Ocsvoszki, I. Zupkó, É. Frank, Microwave-assisted one-pot synthesis of steroid–quinoline hybrids and an evaluation of their antiproliferative activities on gynecological cancer cell lines, *RSC Adv.* 6 (2016) 27501–27516, <https://doi.org/10.1039/C6RA03910C>.
- [20] H.S.P. Rao, E. Poonguzhali, S.P. Senthilkumar, Microwave-Mediated Facile Synthesis of Steroid-like 1,5-Diketones from Mannich Salts, *Synth. Commun.* 38 (2008) 937–942, <https://doi.org/10.1080/00397910701845514>.
- [21] D. Sielemann, R. Keuper, N. Risch, Efficient preparation of substituted 5,6,7,8-tetrahydroquinolines and octahydroacridine derivatives, *J. Für Prakt. Chem.* 341 (1999) 487–491, [https://doi.org/10.1002/\(SICI\)1521-3897\(199907\)341:5<487::AID-PRAC487>3.0.CO;2-J](https://doi.org/10.1002/(SICI)1521-3897(199907)341:5<487::AID-PRAC487>3.0.CO;2-J).
- [22] T. Miyakoshi, H. Konno, Improved synthesis of 2,4,6-trialkylpyridines from 1,5-diketoalkanes: the total synthesis of Anibamine, *Org. Biomol. Chem.* 17 (2019) 2896–2905, <https://doi.org/10.1039/C8OB02723D>.
- [23] G. Roman, M. Mareš, V. Nástasá, A. Novel Antifungal, Agent with Broad Spectrum: 1-(4-Biphenyl)-3-(1-H-imidazol-1-yl)-1-propanone, *Arch. Pharm. (Weinh.)* 346 (2013) 110–118, <https://doi.org/10.1002/ardp.201200287>.
- [24] S.H. Yoon, E. Lee, D.Y. Cho, H.M. Ko, H.Y. Baek, D.K. Choi, E. Kim, J.Y. Park, Synthesis of 4-(3-oxo-3-phenylpropyl)morpholin-4-ium chloride analogues and their inhibitory activities of nitric oxide production in lipopolysaccharide-induced BV2 cells, *Bioorg. Med Chem. Lett.* 36 (2021), 127780, <https://doi.org/10.1016/J.BMCL.2021.127780>.
- [25] G. Mótýán, M.K. Gopisetty, R.E. Kiss-Faludy, Á. Kulmány, I. Zupkó, É. Frank, M. Kiricsi, Anti-cancer activity of novel dihydrotestosterone-derived ring A-condensed pyrazoles on androgen non-responsive prostate cancer cell lines, *Int J. Mol. Sci.* 20 (2019) 2170, <https://doi.org/10.3390/ijms20092170>.
- [26] P. Thapa, R. Karki, M. Yun, T.M. Kadayat, E. Lee, H.B. Kwon, Y. Na, W.J. Cho, N. D. Kim, B.S. Jeong, Y. Kwon, E.S. Lee, Design, synthesis, and antitumor evaluation of 2,4,6-triaryl pyridines containing chlorophenyl and phenolic moiety, *Eur. J. Med Chem.* 52 (2012) 123–136, <https://doi.org/10.1016/J.EJMECH.2012.03.010>.
- [27] G. Bist, S. Park, C. Song, T.B. Thapa Magar, A. Shrestha, Y. Kwon, E.S. Lee, Dihydroxylated 2,6-diphenyl-4-chlorophenylpyridines: Topoisomerase I and II dual inhibitors with DNA non-intercalative catalytic activity, *Eur. J. Med Chem.* 133 (2017) 69–84, <https://doi.org/10.1016/J.EJMECH.2017.03.048>.
- [28] I. Bartonkova, A. Novotna, Z. Dvorak, Novel Stably Transfected Human Reporter Cell Line AIZ-AR as a Tool for an Assessment of Human Androgen Receptor Transcriptional Activity, *PLoS One* 10 (2015), e0121316, <https://doi.org/10.1371/journal.pone.0121316>.
- [29] E.B. Askew, R.T. Gampe, T.B. Stanley, J.L. Faggart, E.M. Wilson, Modulation of androgen receptor activation function 2) by testosterone and dihydrotestosterone, *J. Biol. Chem.* 282 (2007) 25801–25816, <https://doi.org/10.1074/JBC.M703268200>.
- [30] C.E. Bohl, Z. Wu, D.D. Miller, C.E. Bell, J.T. Dalton, Crystal Structure of the T877A Human Androgen Receptor Ligand-binding Domain Complexed to Cyproterone Acetate Provides Insight for Ligand-induced Conformational Changes and Structure-based Drug Design, *J. Biol. Chem.* 282 (2007) 13648–13655, <https://doi.org/10.1074/JBC.M611711200>.
- [31] V.C.O. Njar, A.M.H. Brodie, Discovery and Development of Galeterone (TOK-001 or VN-124-1) for the Treatment of All Stages of Prostate Cancer, *J. Med Chem.* 58 (2015) 2077–2087, <https://doi.org/10.1021/jm501239f>.
- [32] N.U.M.A.B.S.: Higashi, T, 1998, rev. 2002. (Rigaku/MSF Inc.).
- [33] CrystalClear: SM 1.4.0 (Rigaku/MSF Inc., 2008), (n.d.).
- [34] M.C. Burla, R. Caliandro, M. Camalli, B. Carrozzini, G.L. Cascarano, L. de Caro, C. Giacovazzo, G. Polidori, R. Spagna, *SIR2004*: an improved tool for crystal structure determination and refinement, *J. Appl. Crystallogr* 38 (2005) 381–388, <https://doi.org/10.1107/S002188980403225X>.
- [35] S.H.E.L.X.L.: Sheldrick, G.M, 2013, SHELXL-2013 Program for Crystal Structure Solution, University of Göttingen, Germany.
- [36] L.J. Farrugia, *WinGX* suite for small-molecule single-crystal crystallography, *J. Appl. Crystallogr* 32 (1999) 837–838, <https://doi.org/10.1107/S0021889899006020>.
- [37] C.F. Macrae, P.R. Edgington, P. McCabe, E. Pidcock, G.P. Shields, R. Taylor, M. Towler, J. van de Streek, *Mercury*: visualization and analysis of crystal structures, *J. Appl. Crystallogr* 39 (2006) 453–457, <https://doi.org/10.1107/S002188980600731X>.
- [38] A.L. Spek, Single-crystal structure validation with the program *PLATON*, *J. Appl. Crystallogr* 36 (2003) 7–13, <https://doi.org/10.1107/S0021889802022112>.
- [39] G.M. Morris, R. Huey, W. Lindstrom, M.F. Sanner, R.K. Belew, D.S. Goodsell, A. J. Olson, AutoDock4 and AutoDockTools4: Automated docking with selective receptor flexibility, *J. Comput. Chem.* 30 (2009) 2785–2791, <https://doi.org/10.1002/jcc.21256>.
- [40] O. Trott, A.J. Olson, AutoDock Vina: Improving the speed and accuracy of docking with a new scoring function, efficient optimization, and multithreading, *J. Comput. Chem.* (2009), <https://doi.org/10.1002/jcc.21334>.

SUPPLEMENTARY INFORMATION

Dihydrotestosterone-based A-ring-fused pyridines: microwave-assisted synthesis and biological evaluation in prostate cancer cells compared to structurally related quinolines

Márton A. Kiss¹, Miroslav Peřina², Laura Bereczki^{3,4}, Ádám Baji¹, Jakub Bělíček², Radek Jorda^{2,*}, Éva Frank^{1,*}

¹*Department of Organic Chemistry, University of Szeged, Dóm tér 8, H-6720 Szeged, Hungary*

²*Department of Experimental Biology, Faculty of Science, Palacký University Olomouc, Šlechtitelů 27, 78371 Olomouc, Czech Republic*

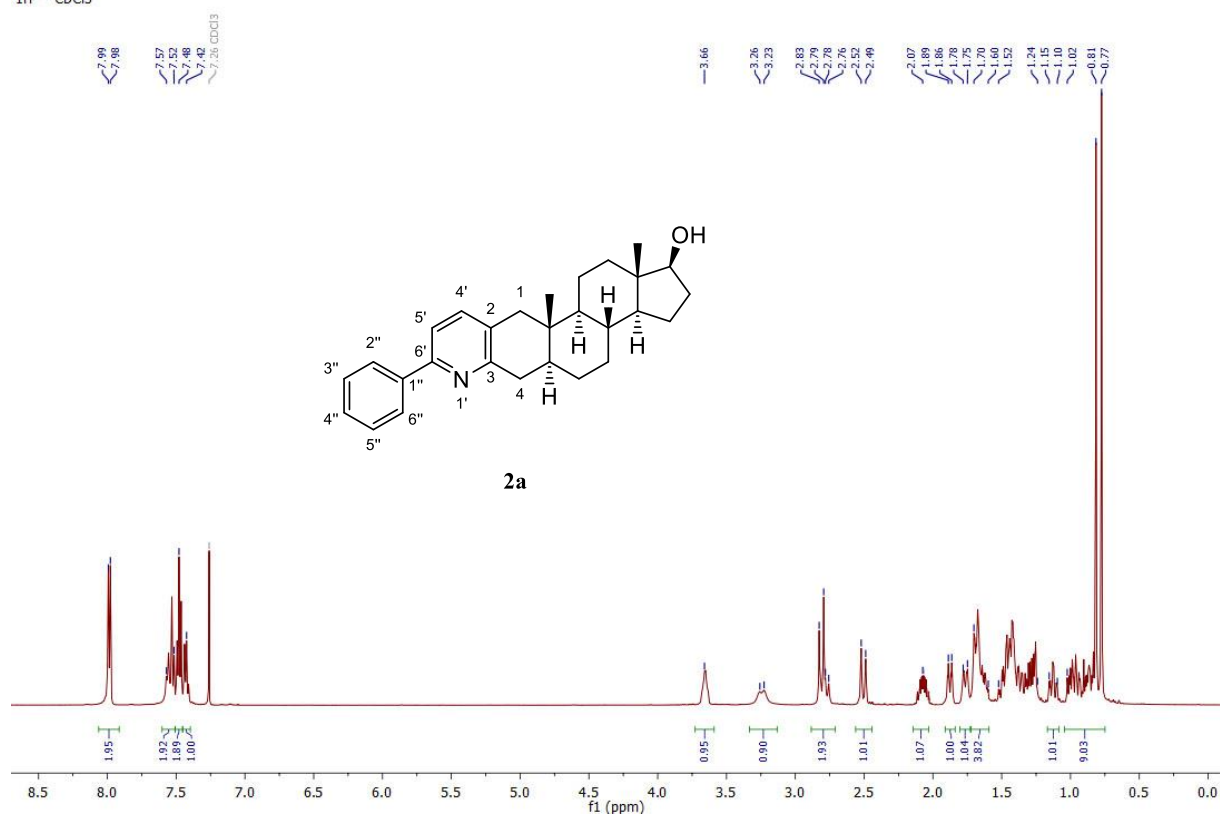
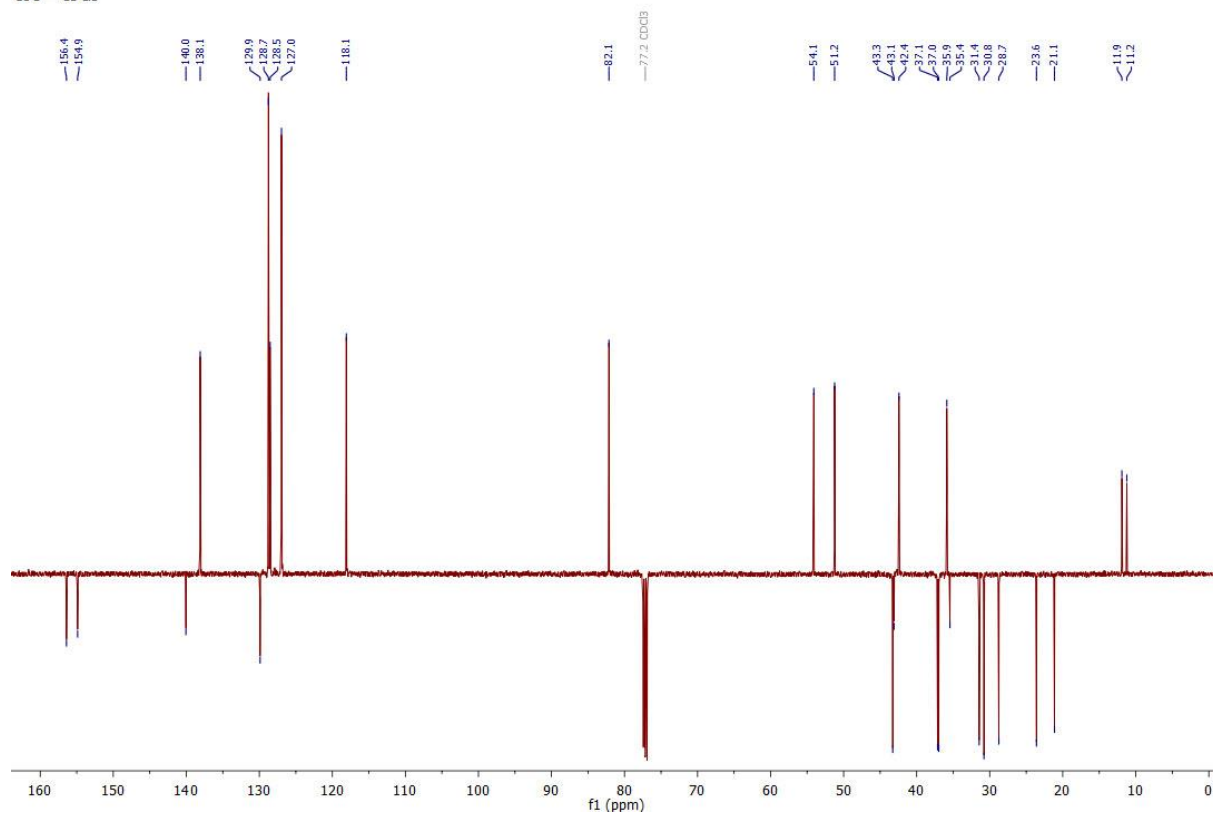
³*Structural Research Centre, Research Centre for Natural Sciences, Magyar tudósok körútja 2, H-1117 Budapest, Hungary*

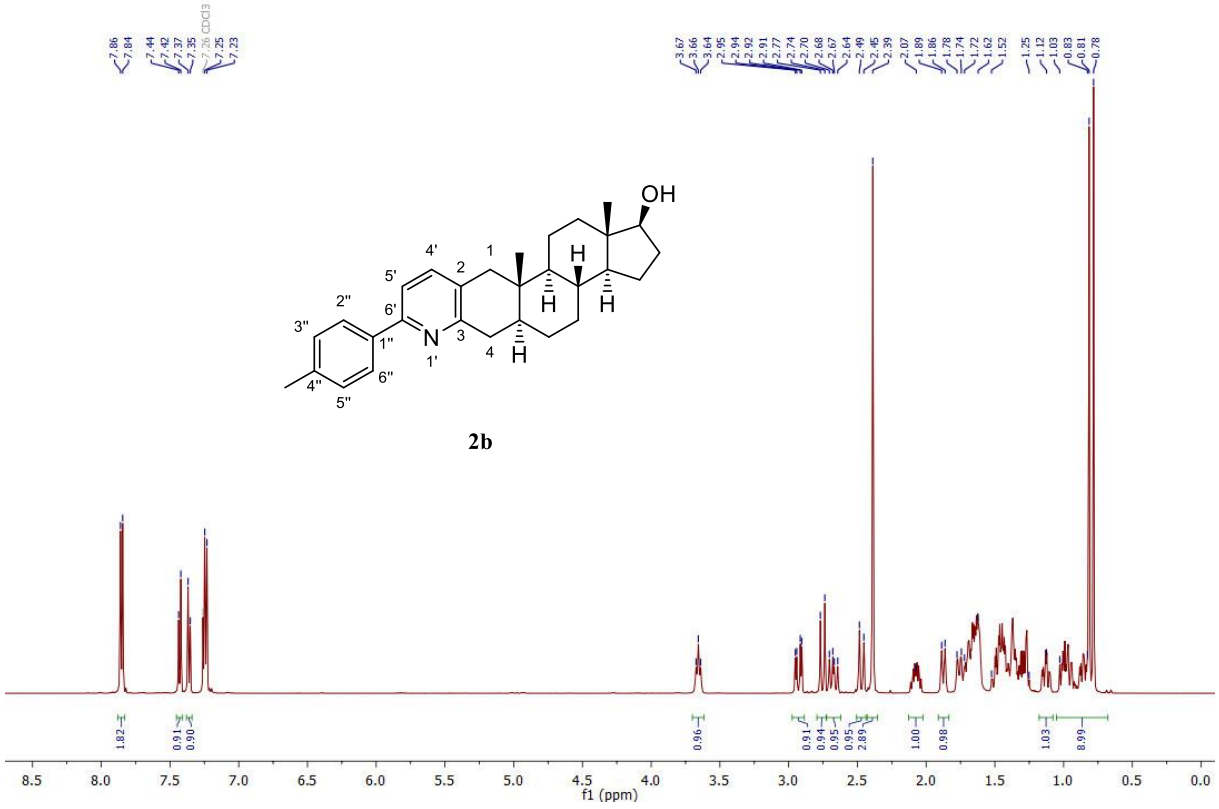
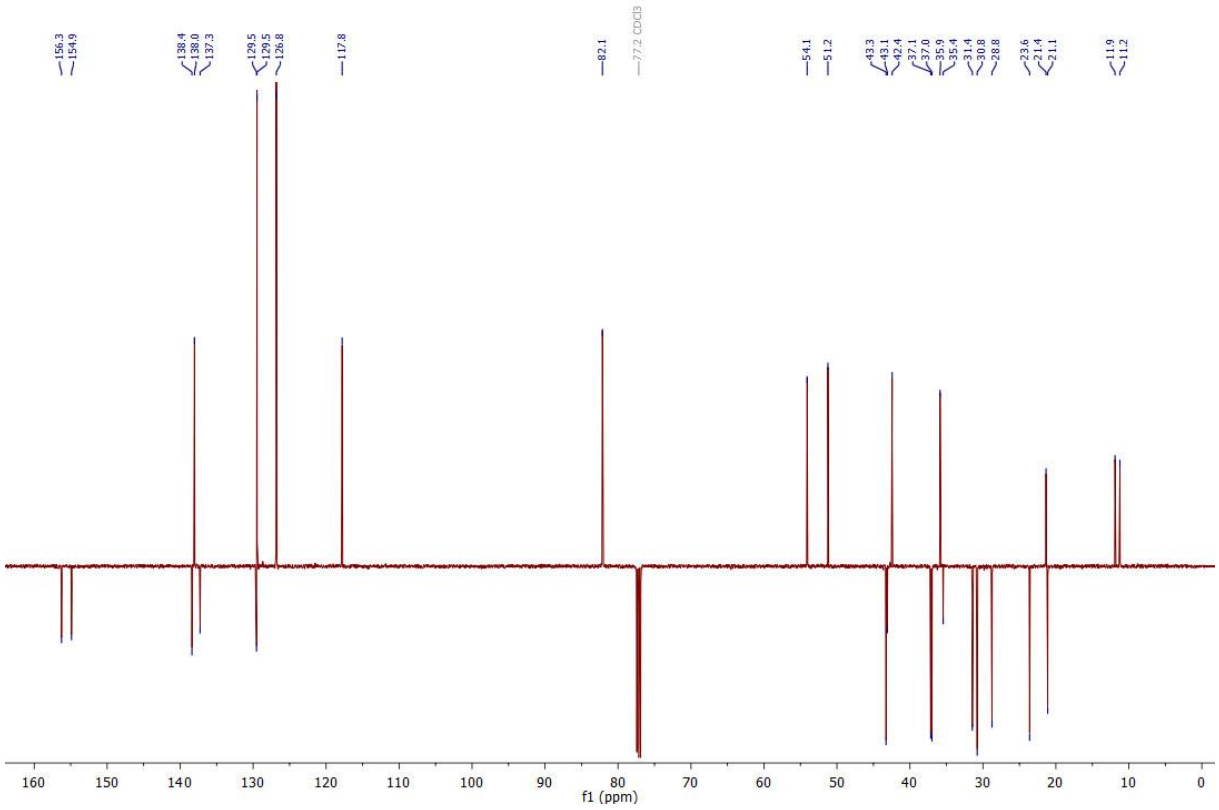
⁴*Institute of Materials and Environmental Chemistry, Research Centre for Natural Sciences, Magyar tudósok körútja 2, H-1117 Budapest, Hungary*

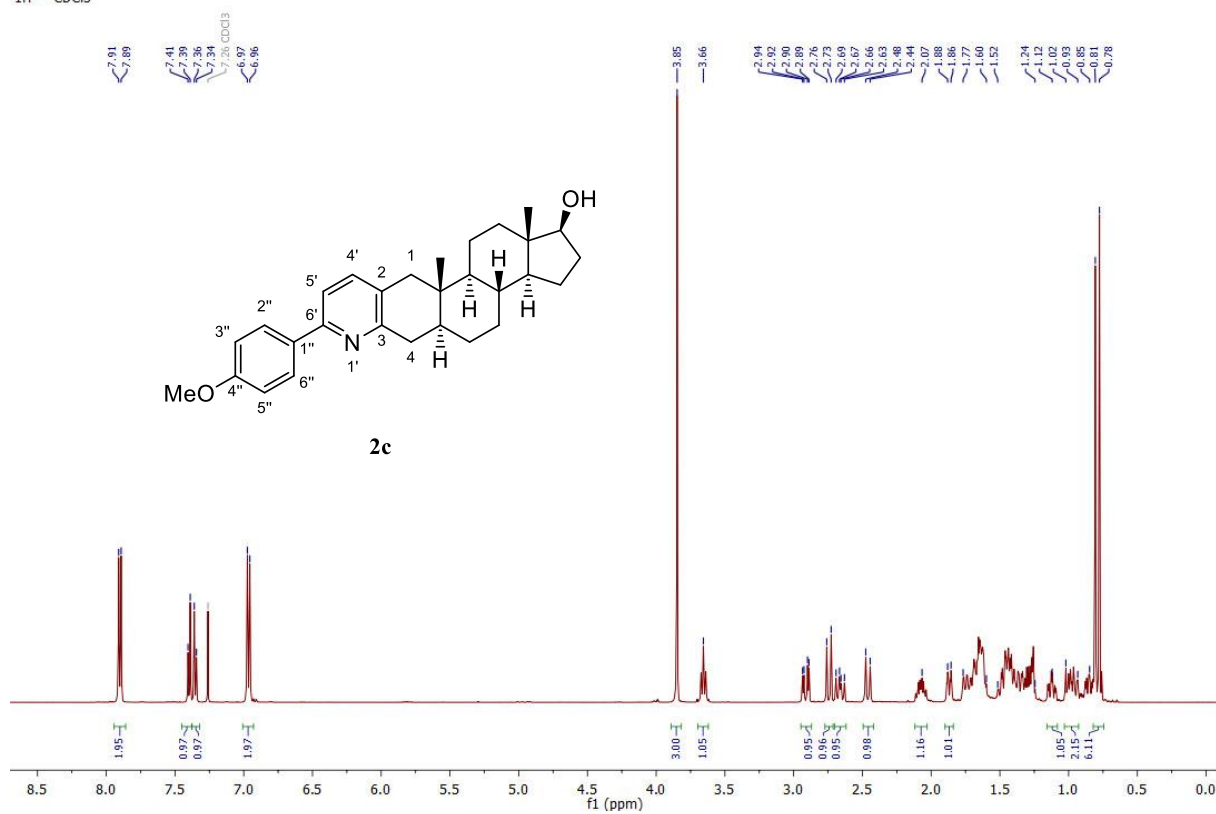
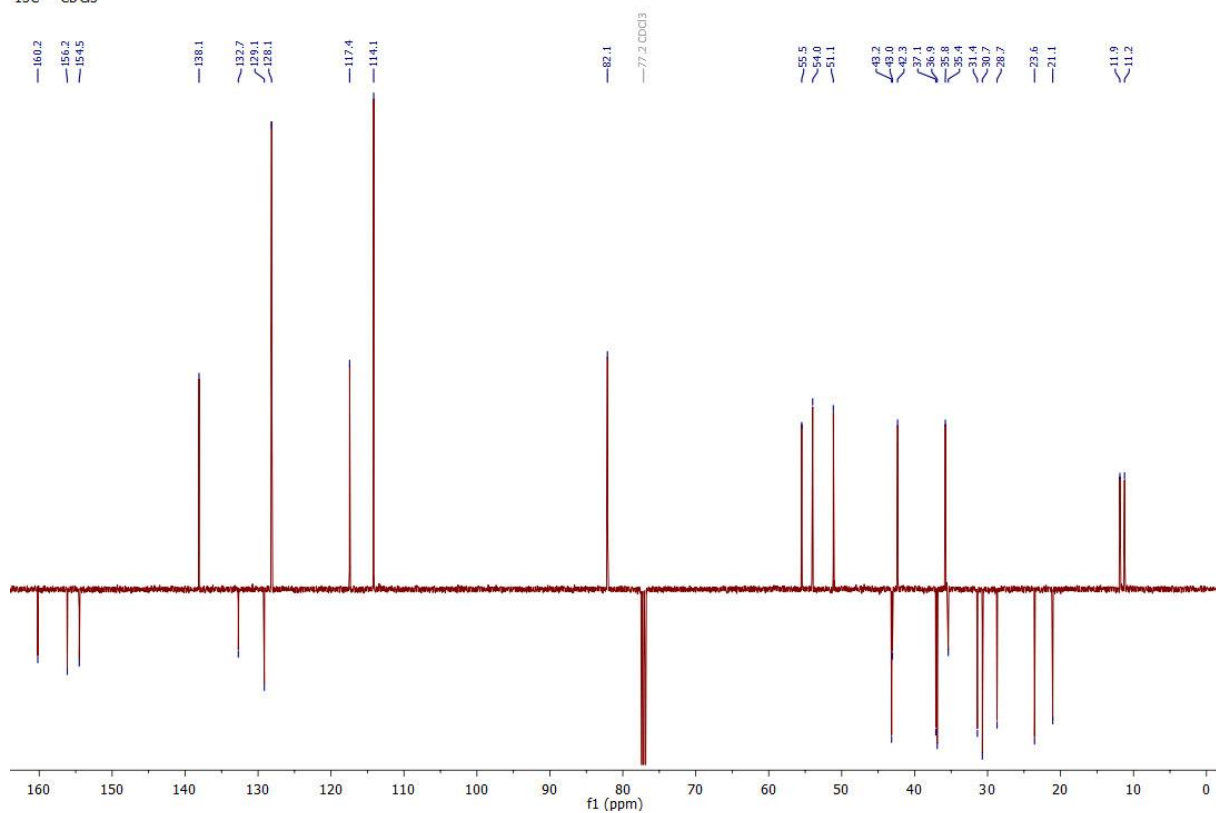
*Corresponding authors: frank@chem.u-szeged.hu; Tel.: +36 62 544 275;
radek.jorda@upol.cz; Tel.: +420 585 634 854

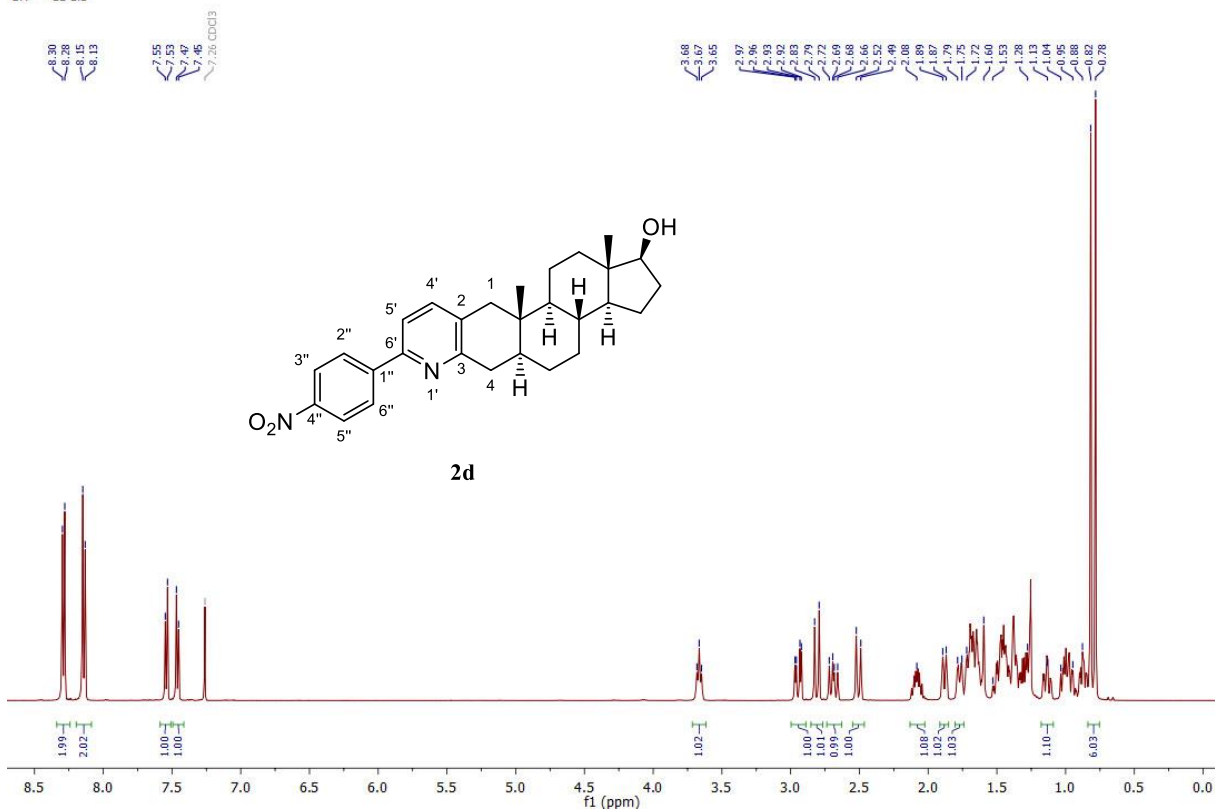
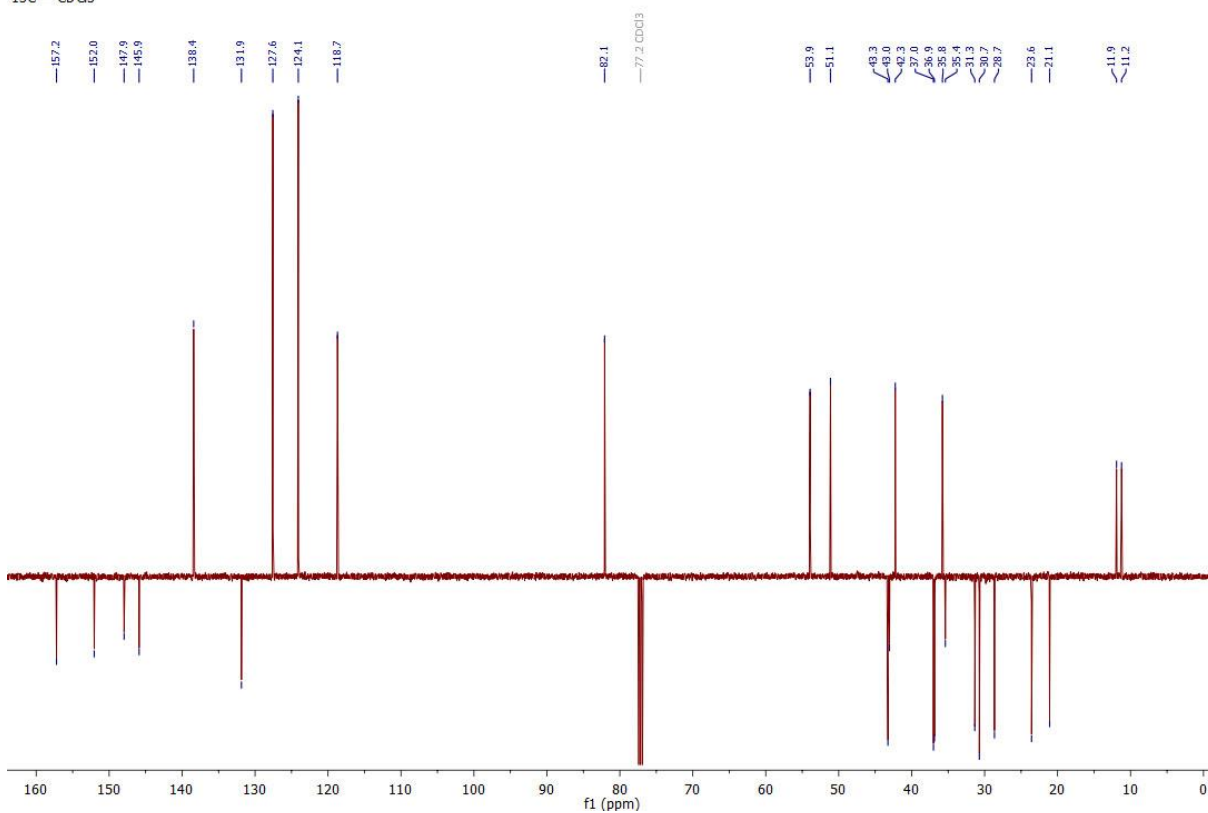
Table of Contents

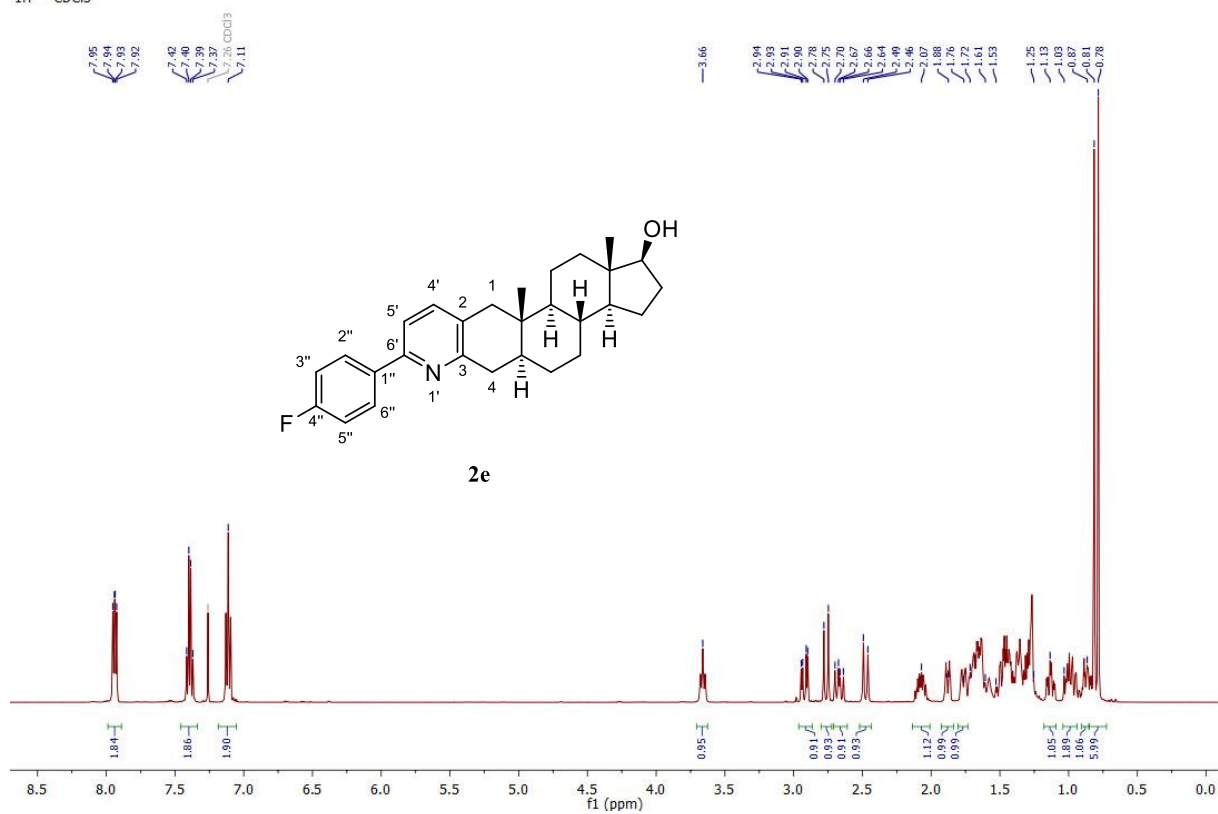
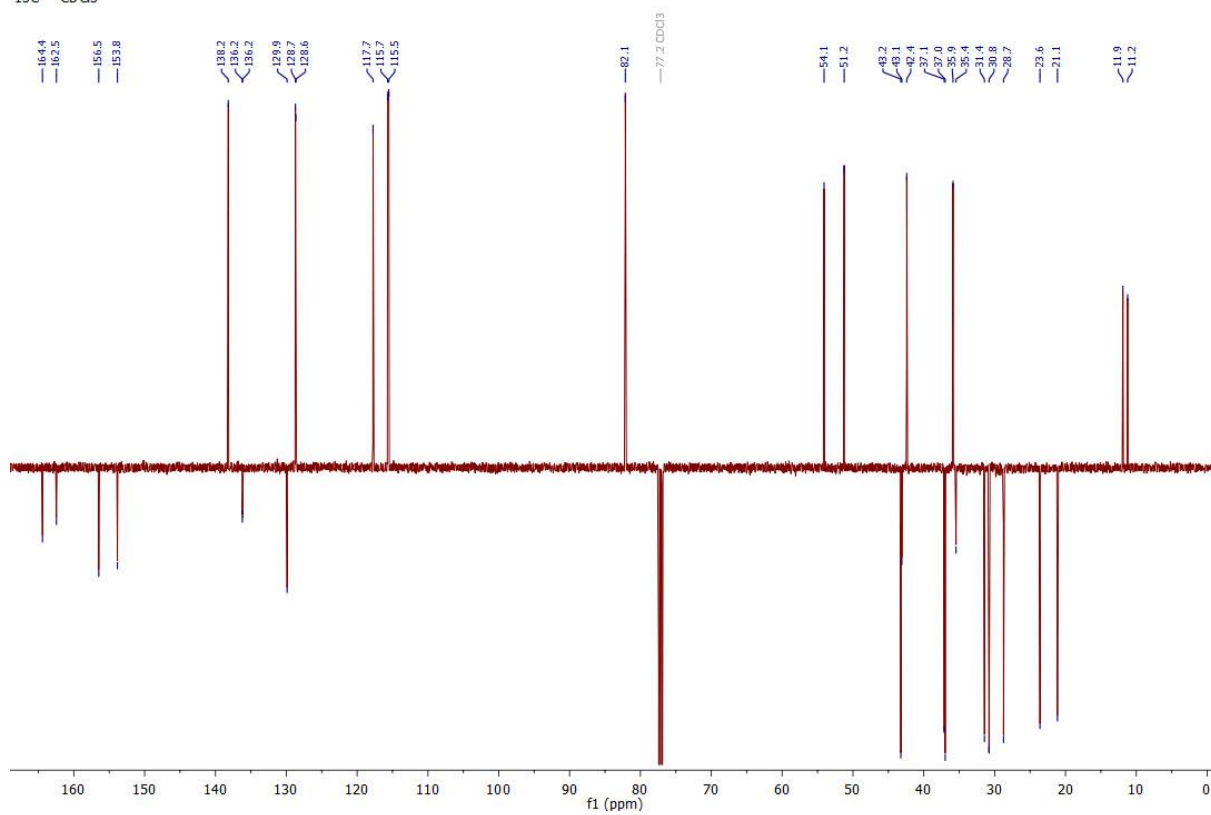
¹ H and ¹³ C NMR spectra of the synthesized compounds	1–23
Figure S1. The two molecules in the asymmetric unit of 2a	24
Figure S2. Packing of 2a molecules	24
Table S1. Analysis of Potential Hydrogen Bonds and Schemes	24
Table S2. Bond lengths (Å) in 2a	25
Table S3. Bond angles (°) in 2a	26
Figure S3. AR and AR-regulated proteins in LNCaP after 48-h treatment with selected compounds.	27
Figure S4. Dose dependent effect of 1a and 1d on AR-signalling in LNCaP and 22Rv1 .	27
Figure S5. Cell cycle analysis of the LAPC-4 and LNCaP cell lines	28

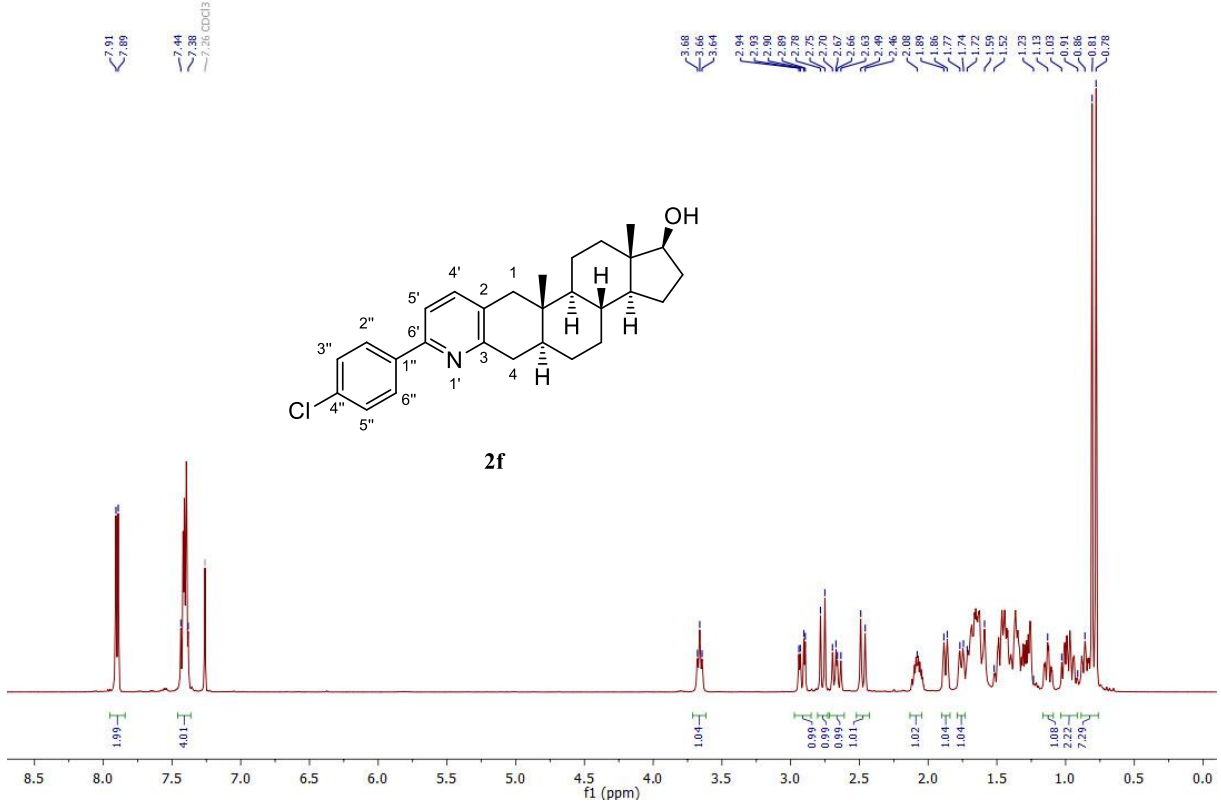
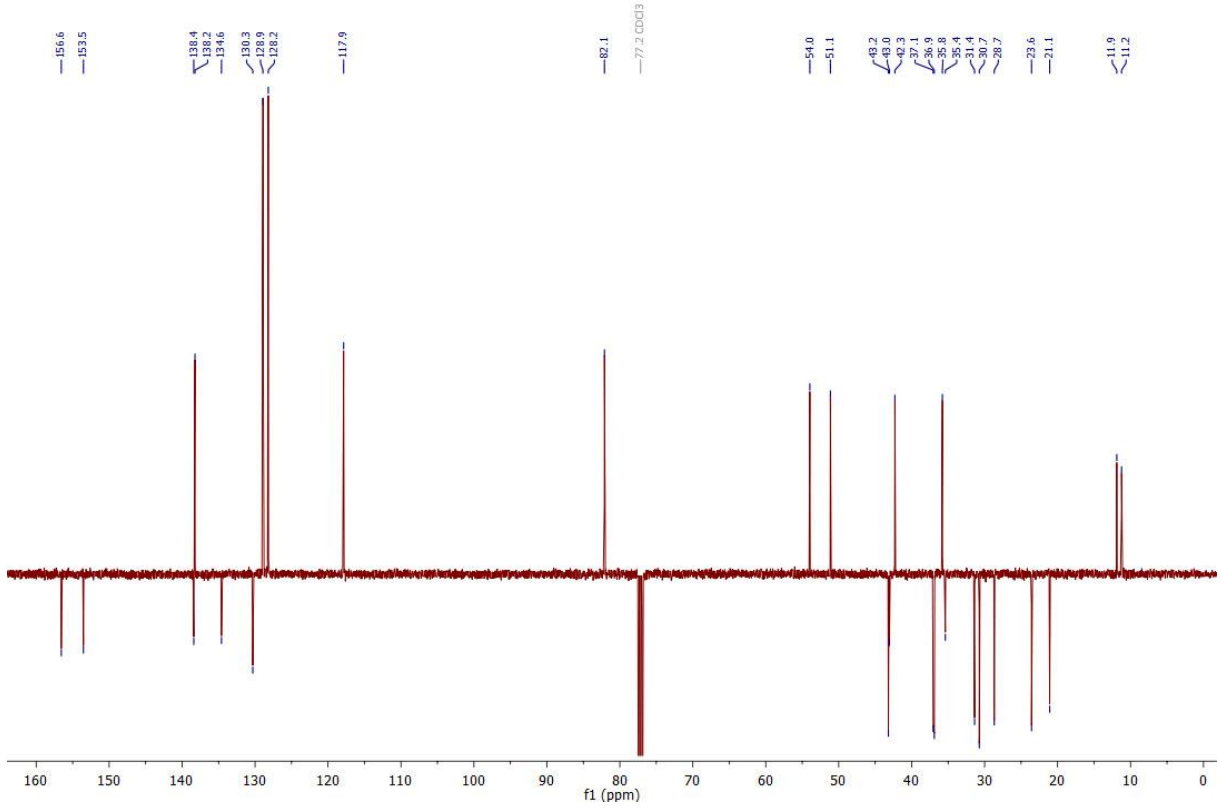
^1H and ^{13}C NMR spectra of the synthesized compounds ^1H — CDCl_3  ^{13}C — CDCl_3 

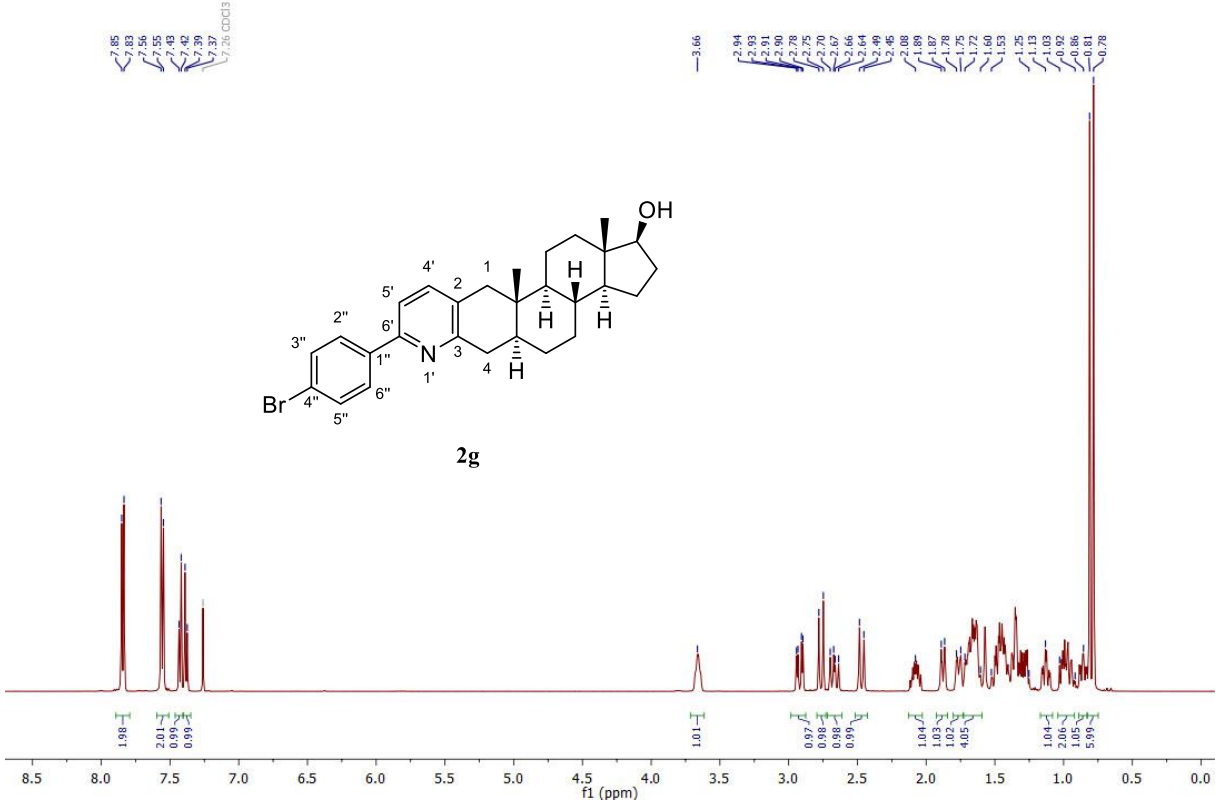
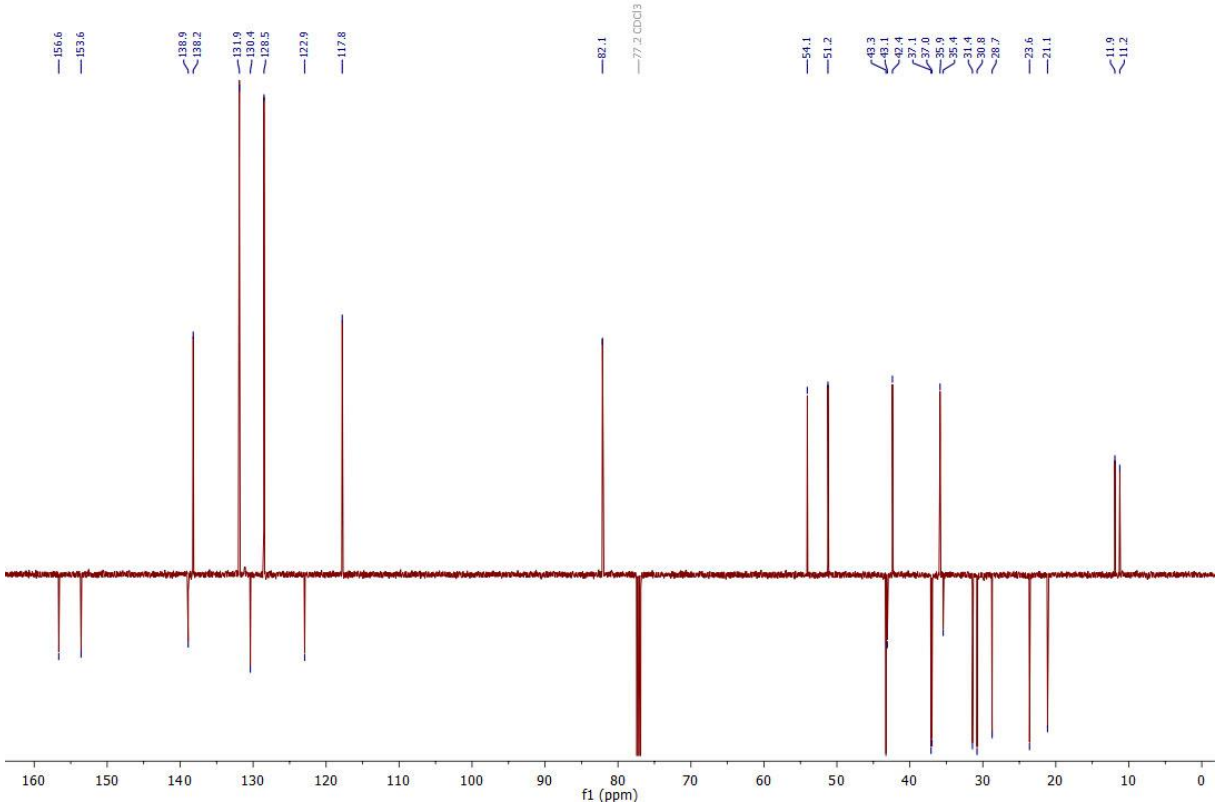
¹H — CDCl₃¹³C — CDCl₃

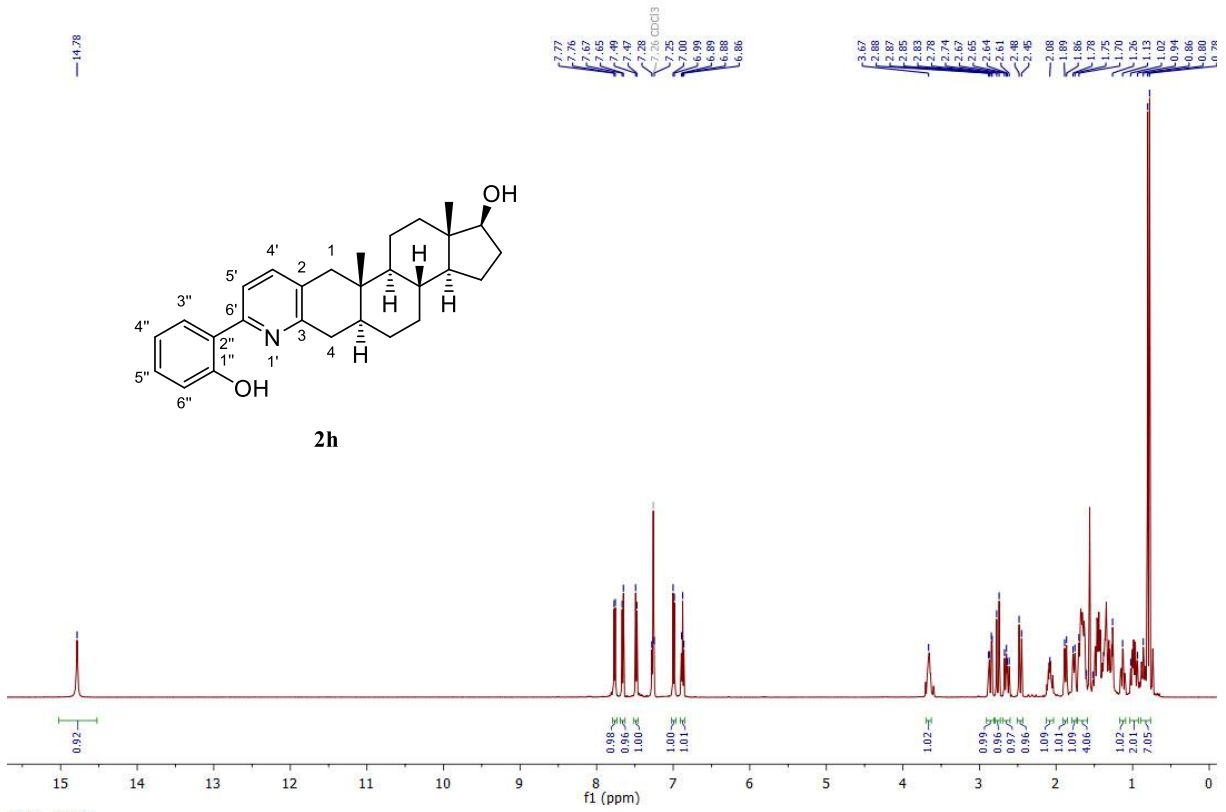
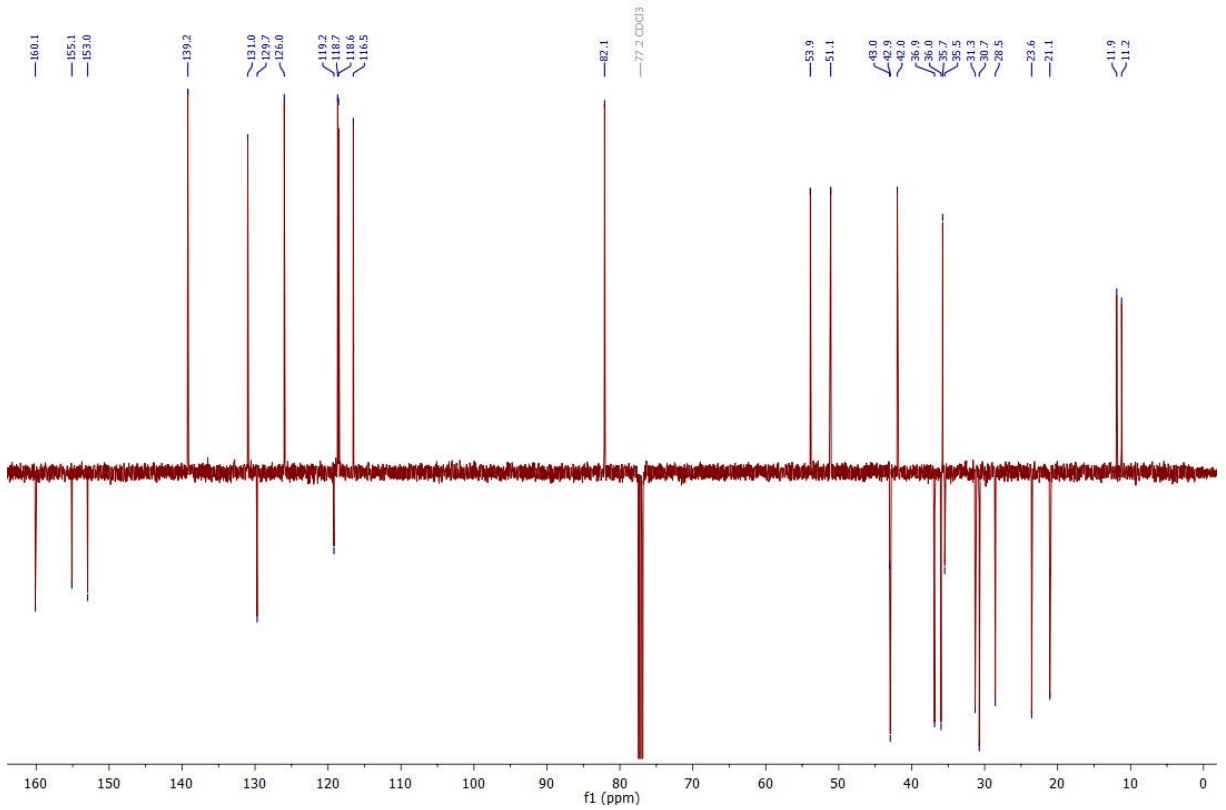
¹H — CDCl₃¹³C — CDCl₃

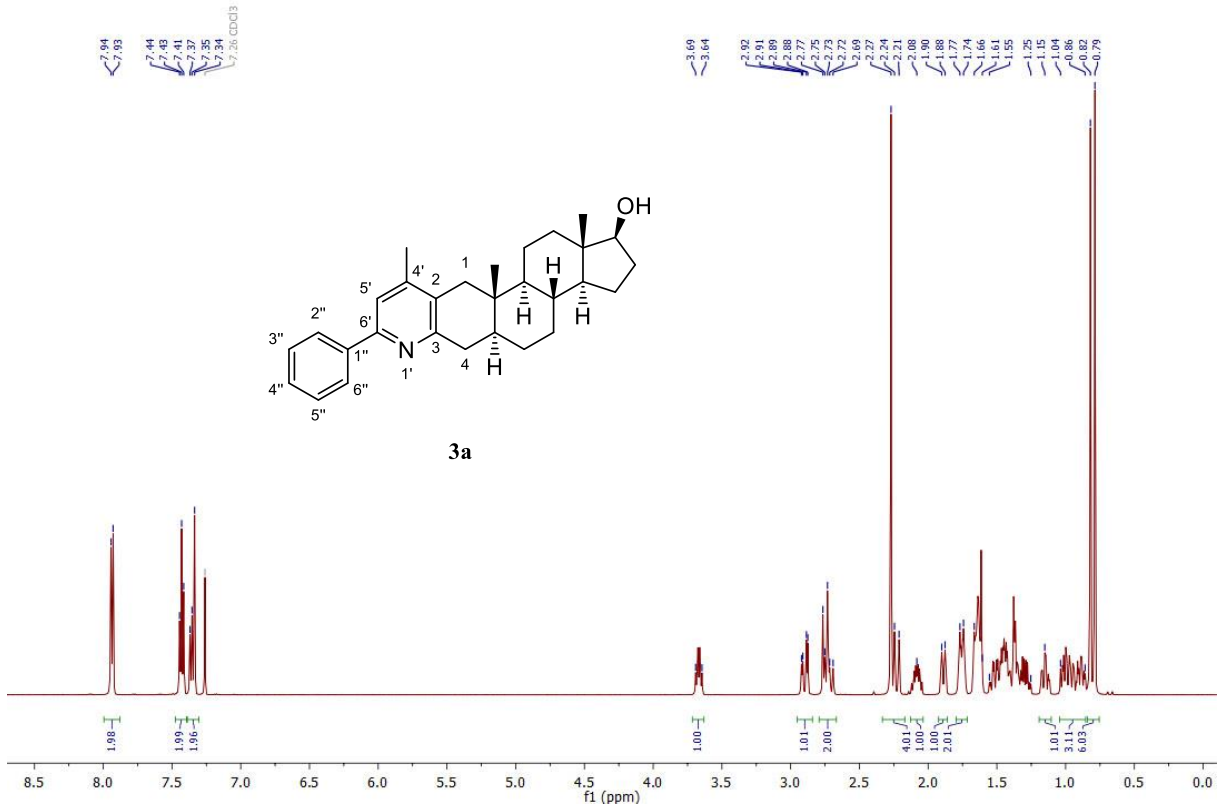
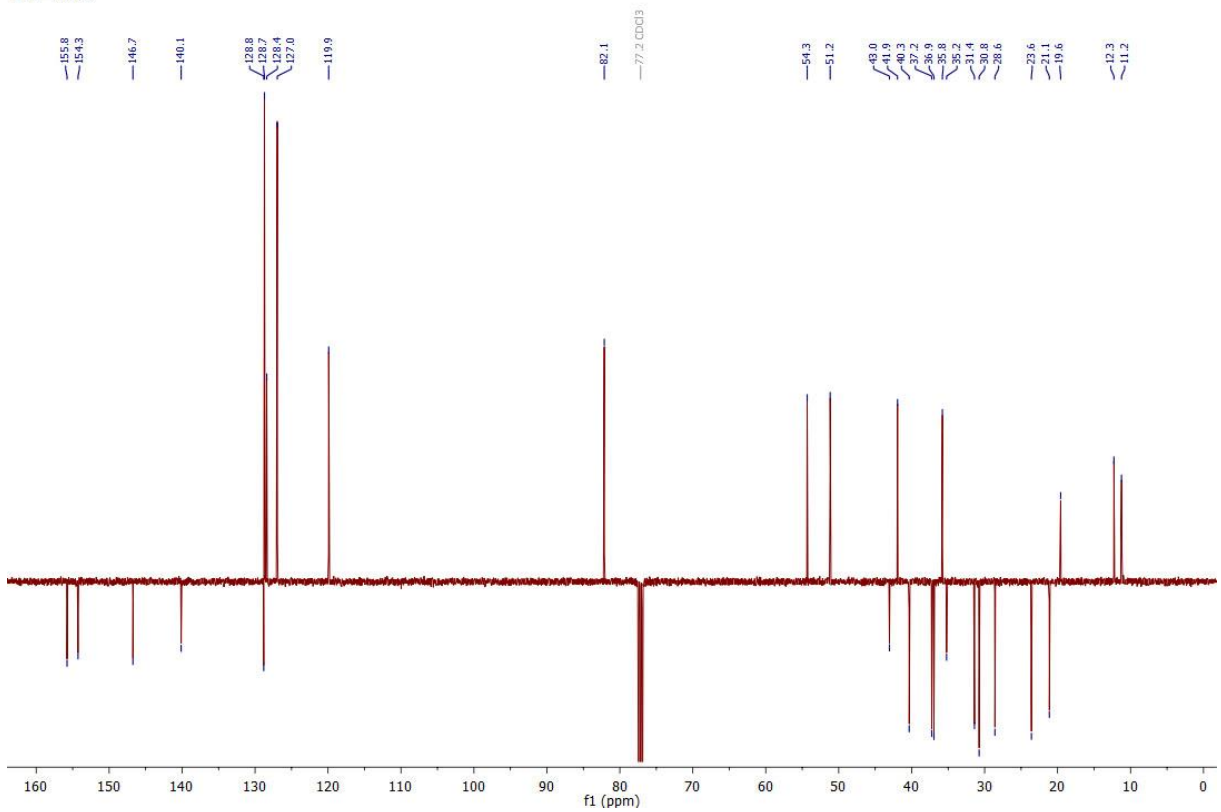
¹H — CDCl₃¹³C — CDCl₃

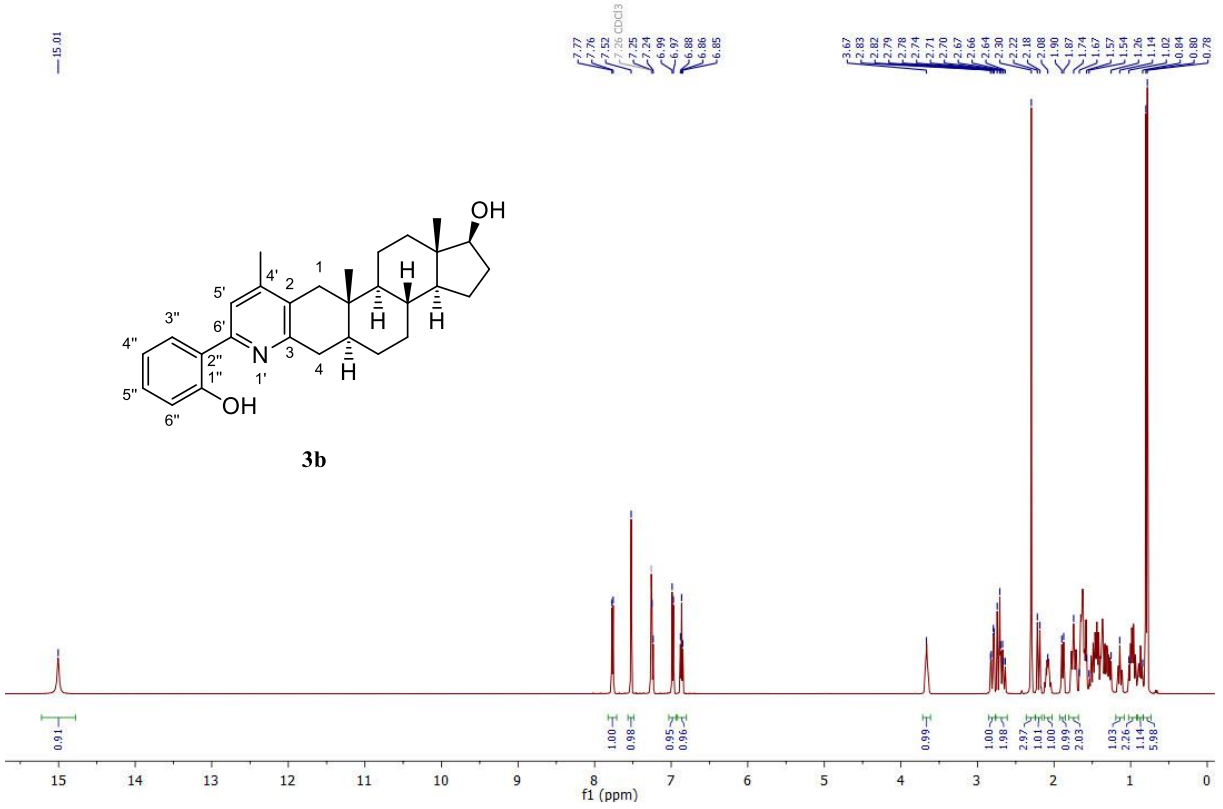
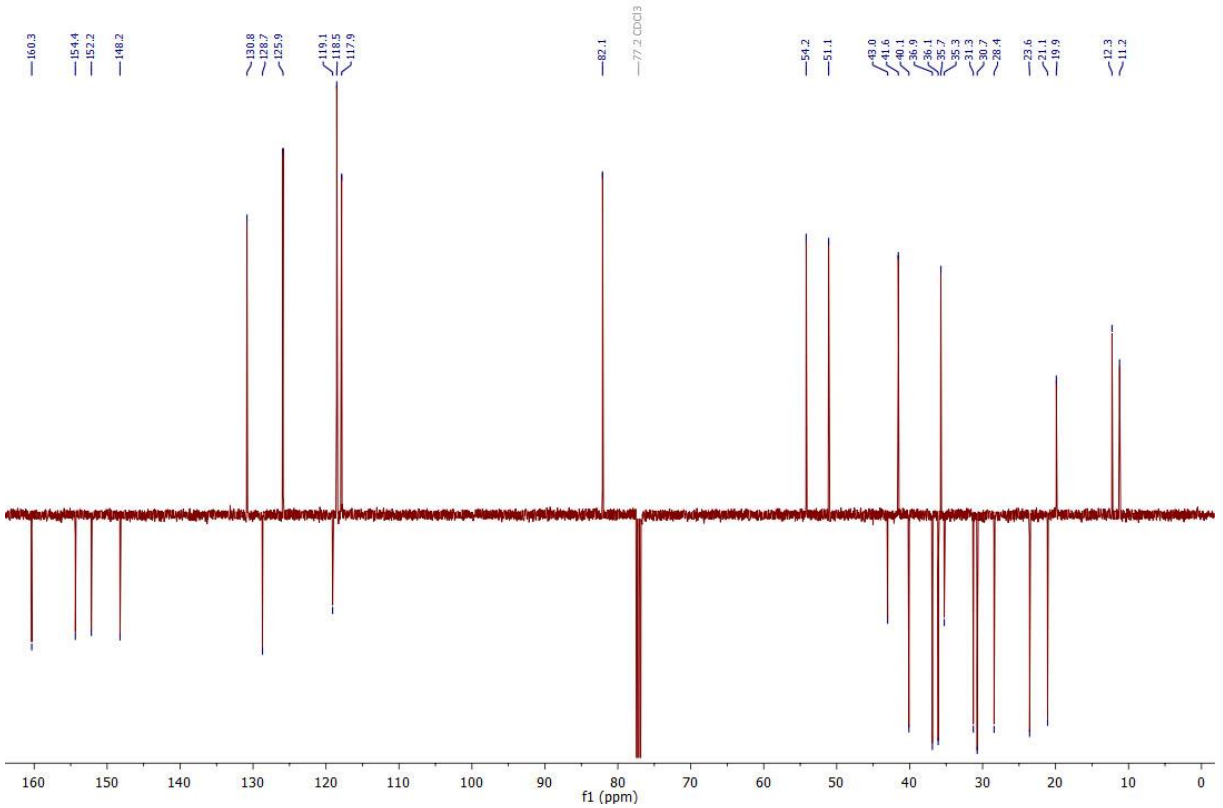
¹H — CDCl₃¹³C — CDCl₃

¹H — CDCl₃¹³C — CDCl₃

¹H — CDCl₃¹³C — CDCl₃

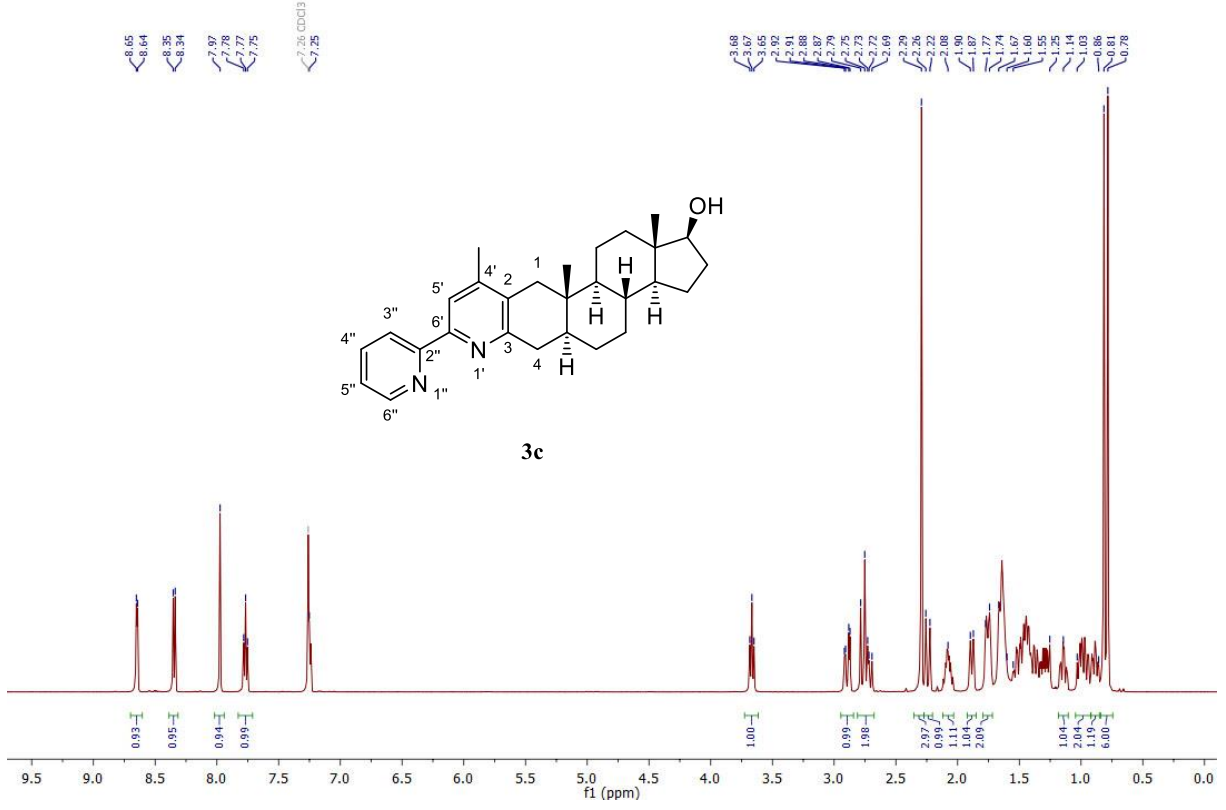
¹H — CDCl₃¹³C — CDCl₃

¹H — CDCl₃¹³C — CDCl₃

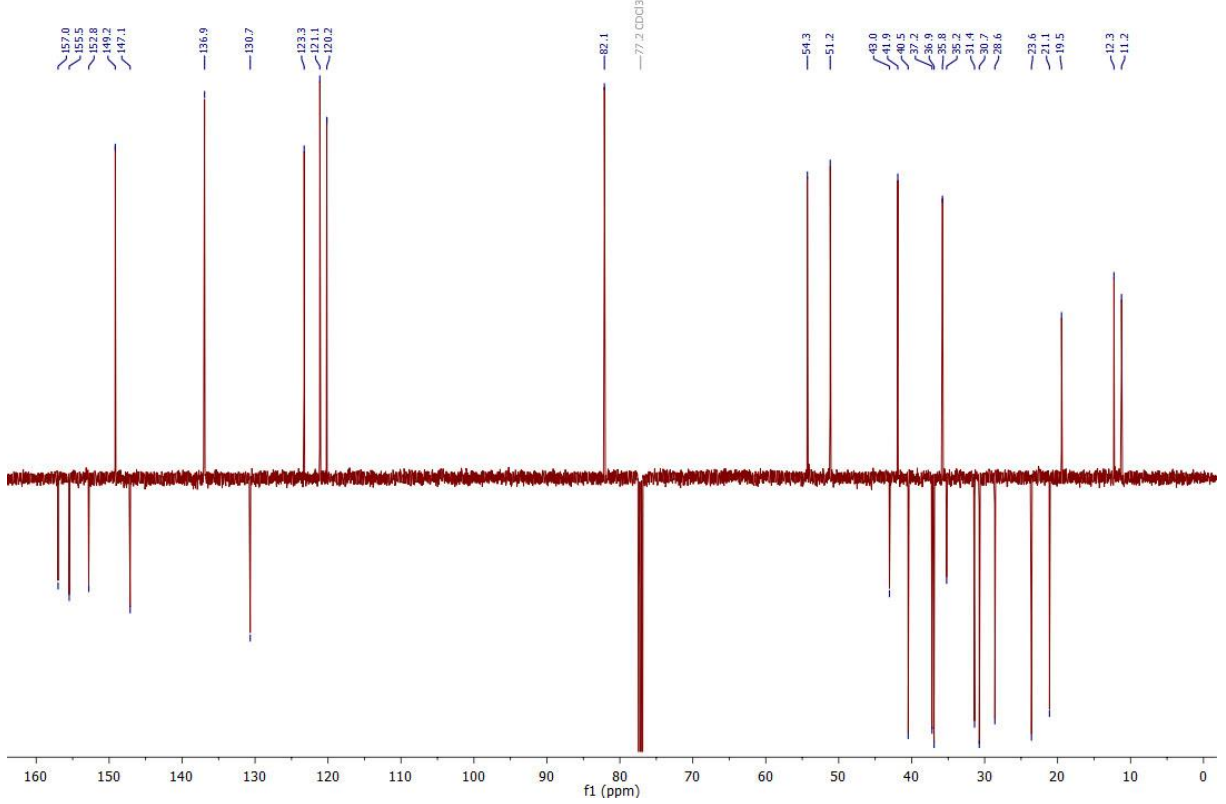
¹H — CDCl₃¹³C — CDCl₃

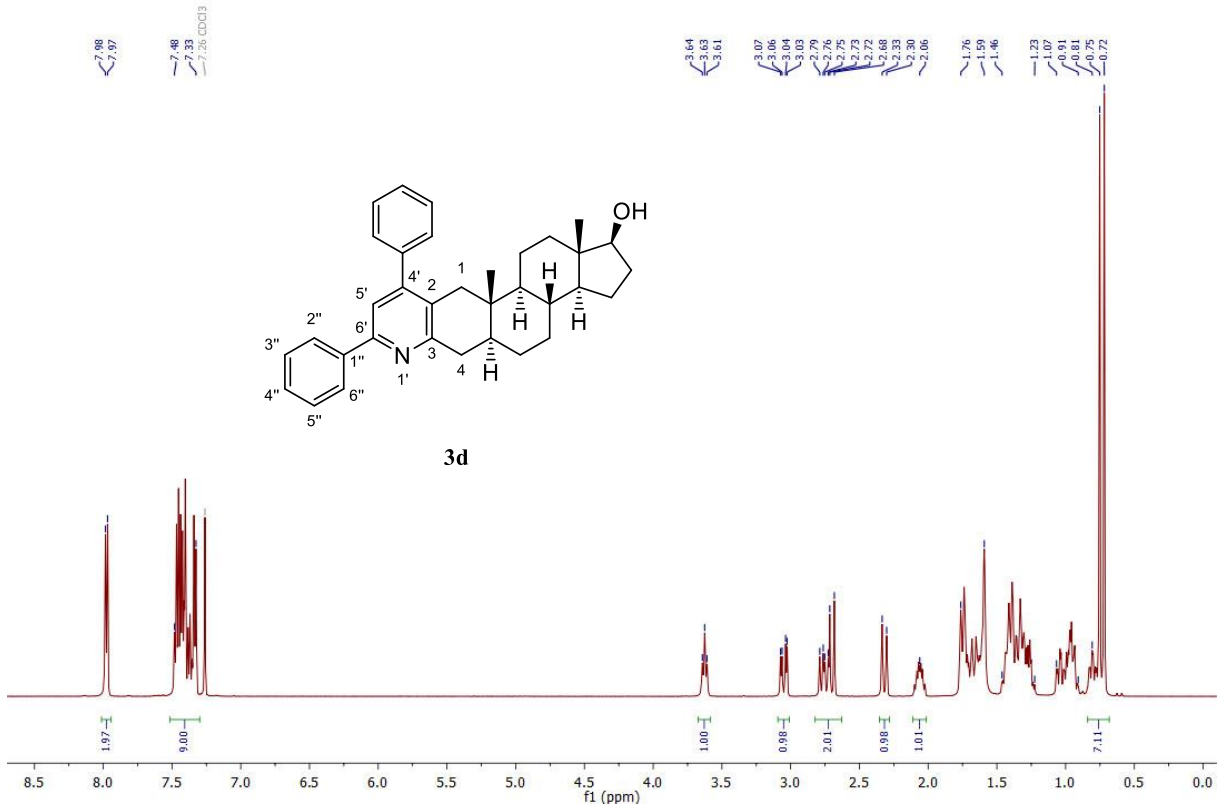
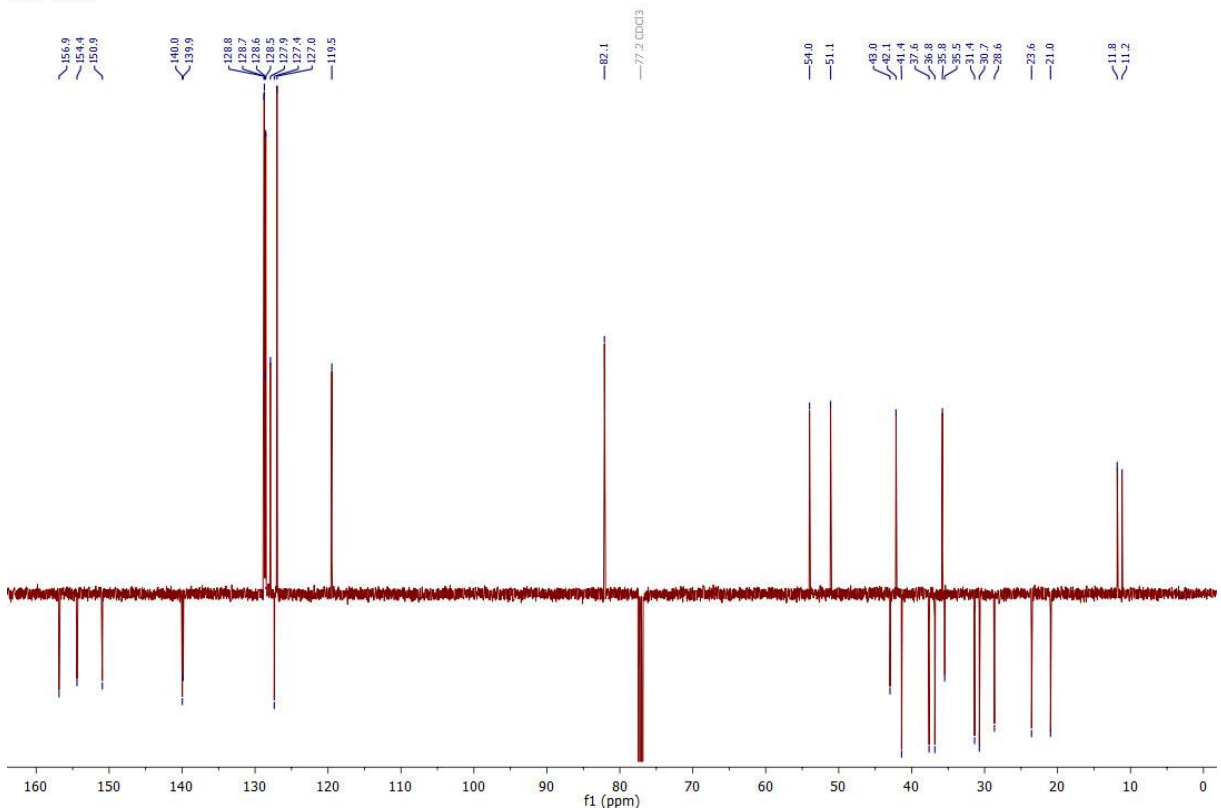
S11

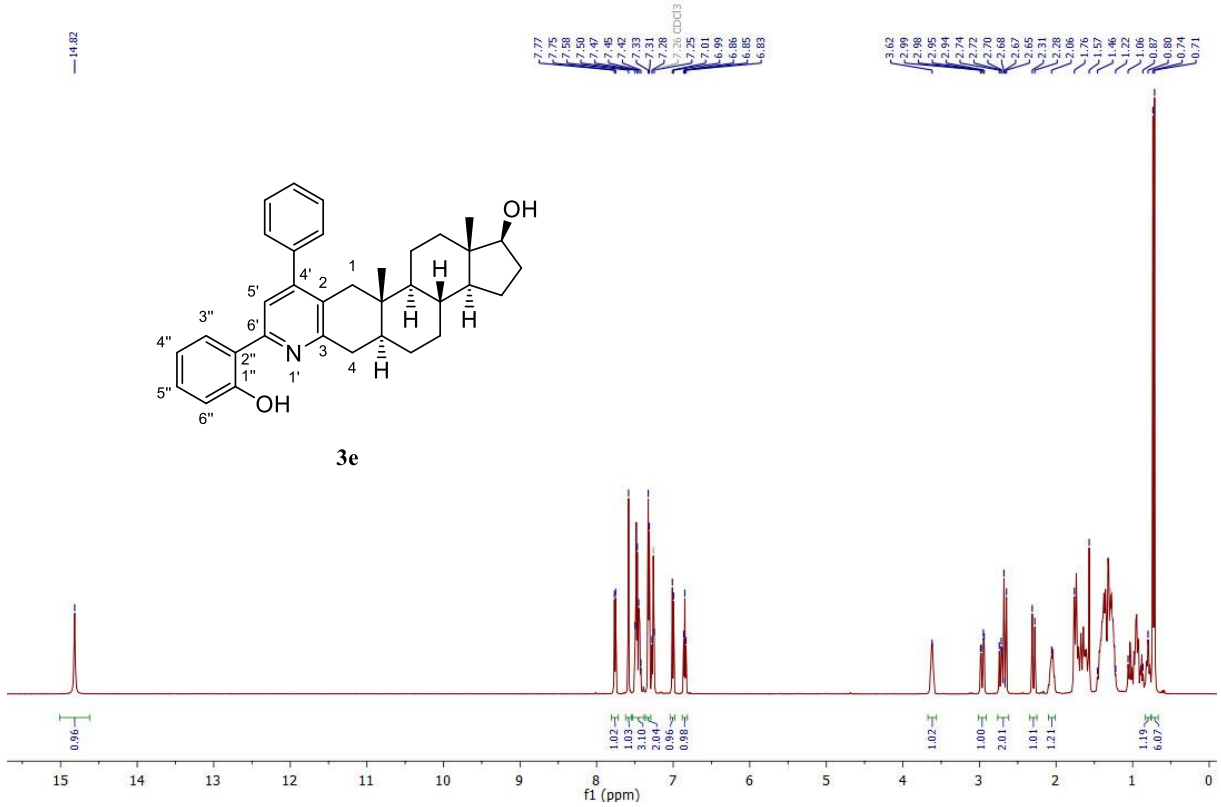
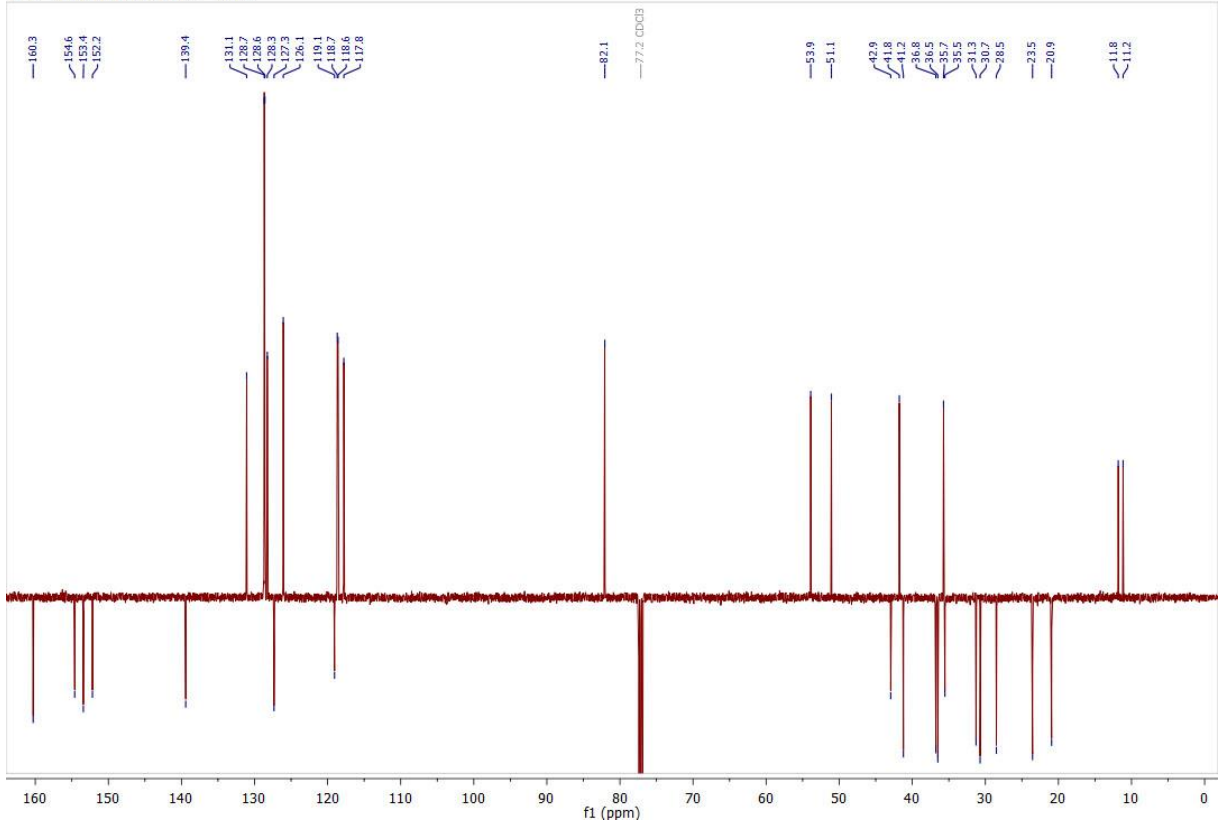
¹H — CDCl₃



¹³C — CDCl₃

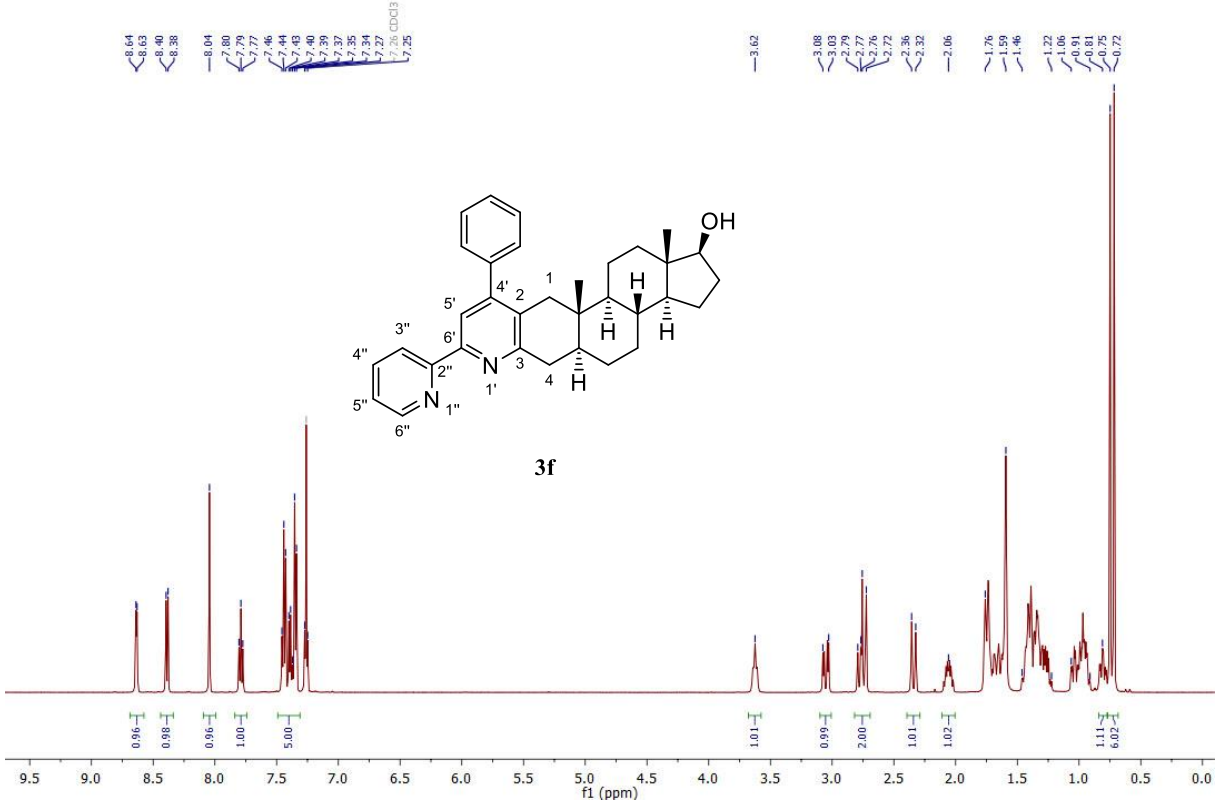


¹H — CDCl₃¹³C — CDCl₃

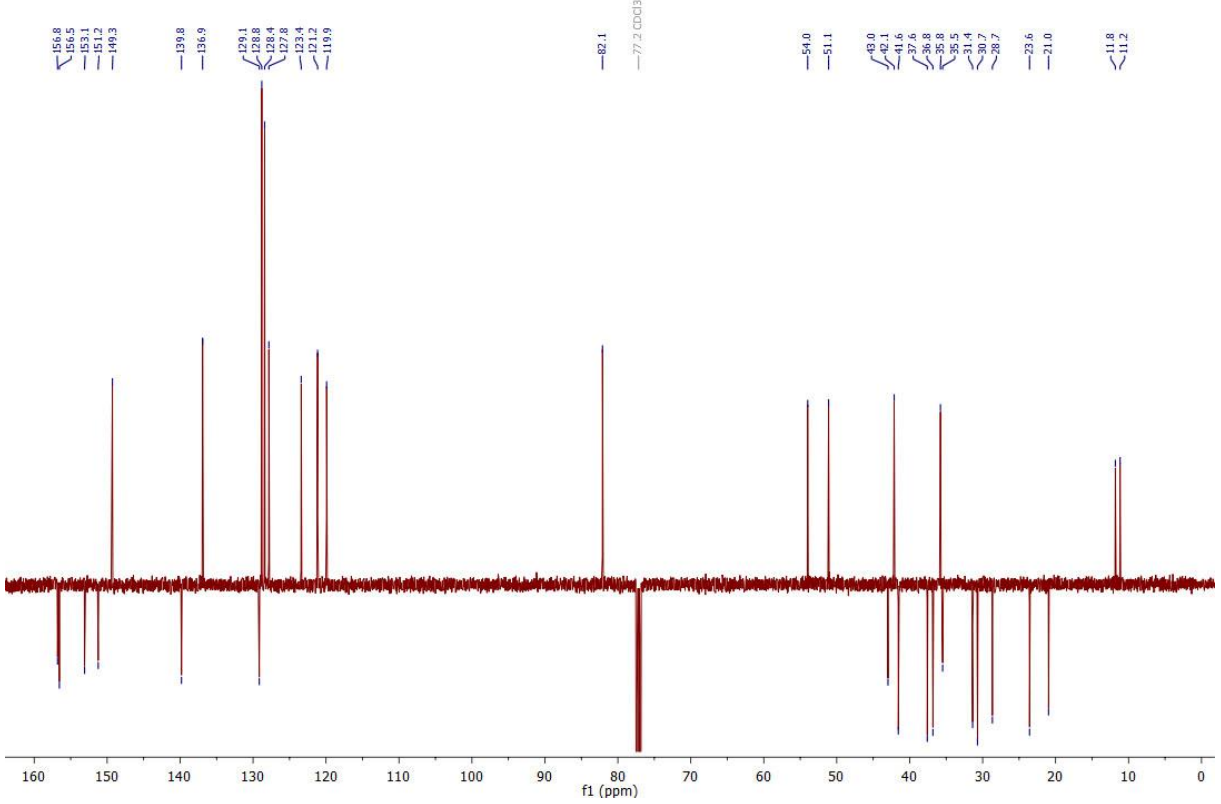
¹H — CDCl₃¹³C — 2022-02-01T21:38:55 — CDCl₃

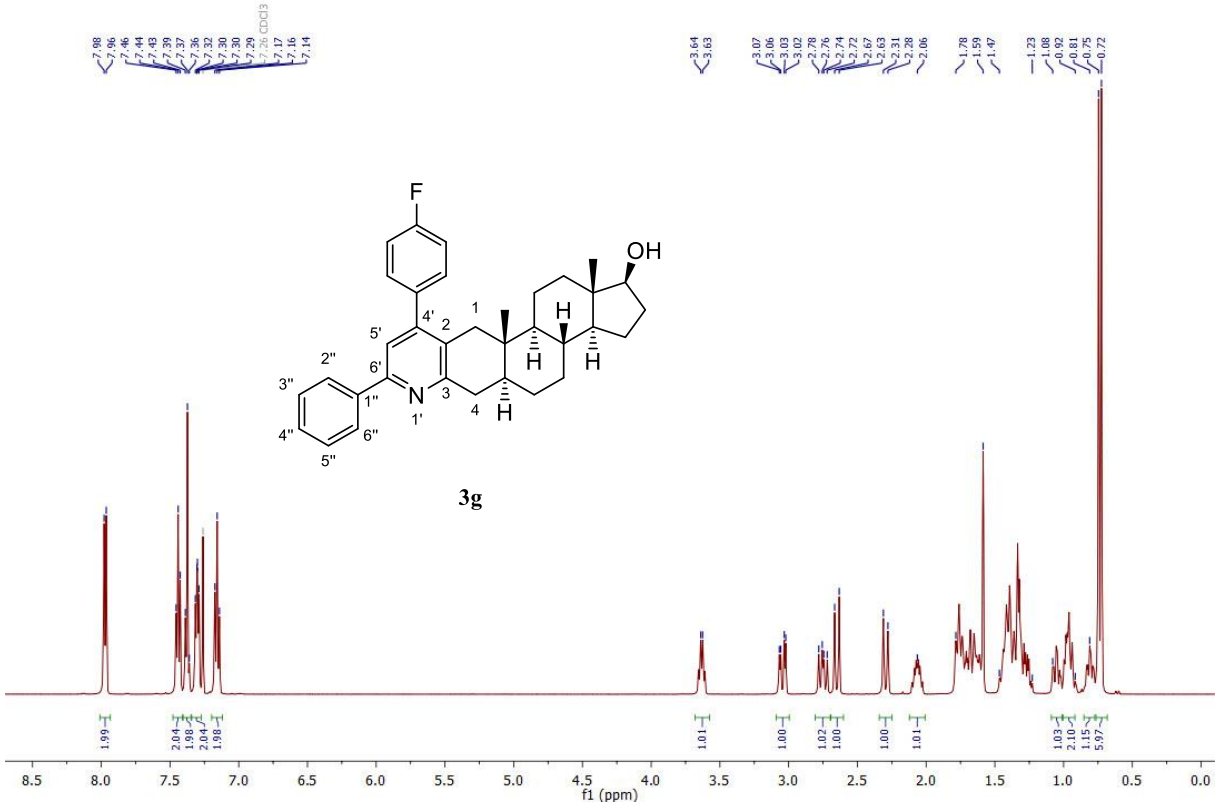
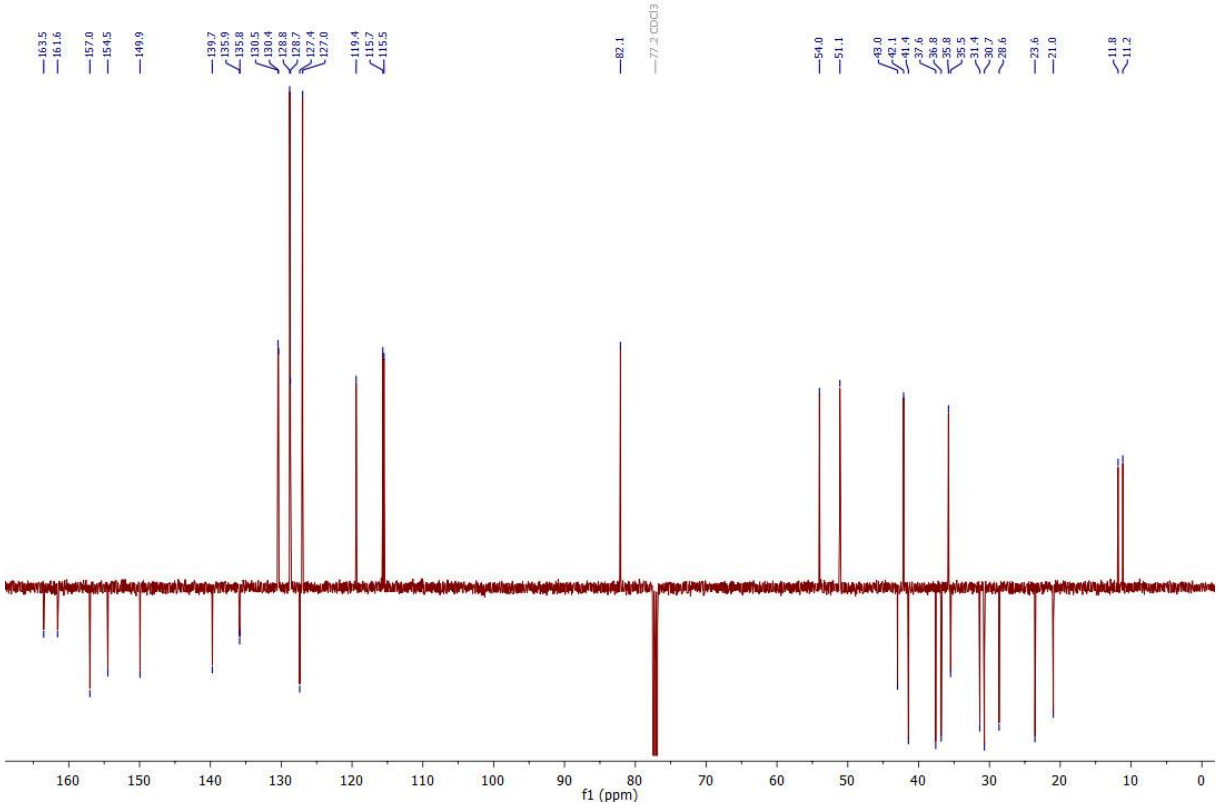
S14

¹H — CDCl₃



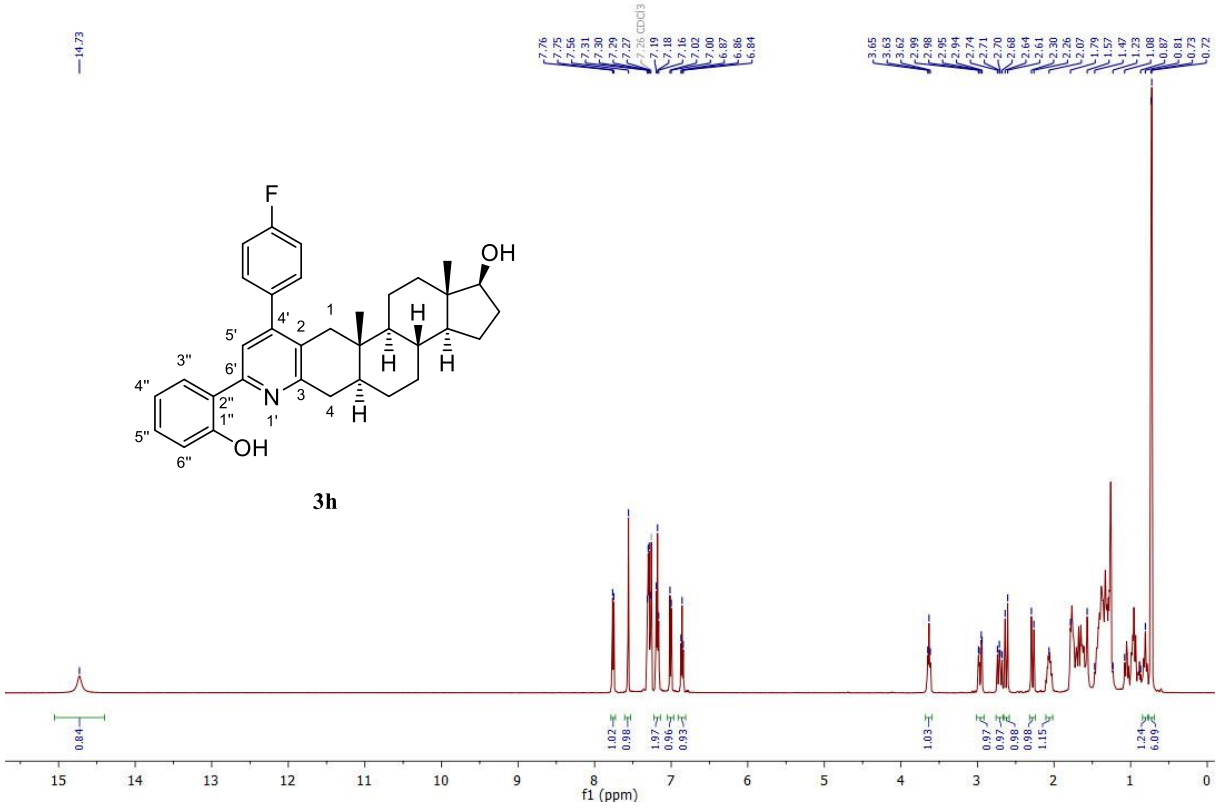
¹³C — CDCl₃



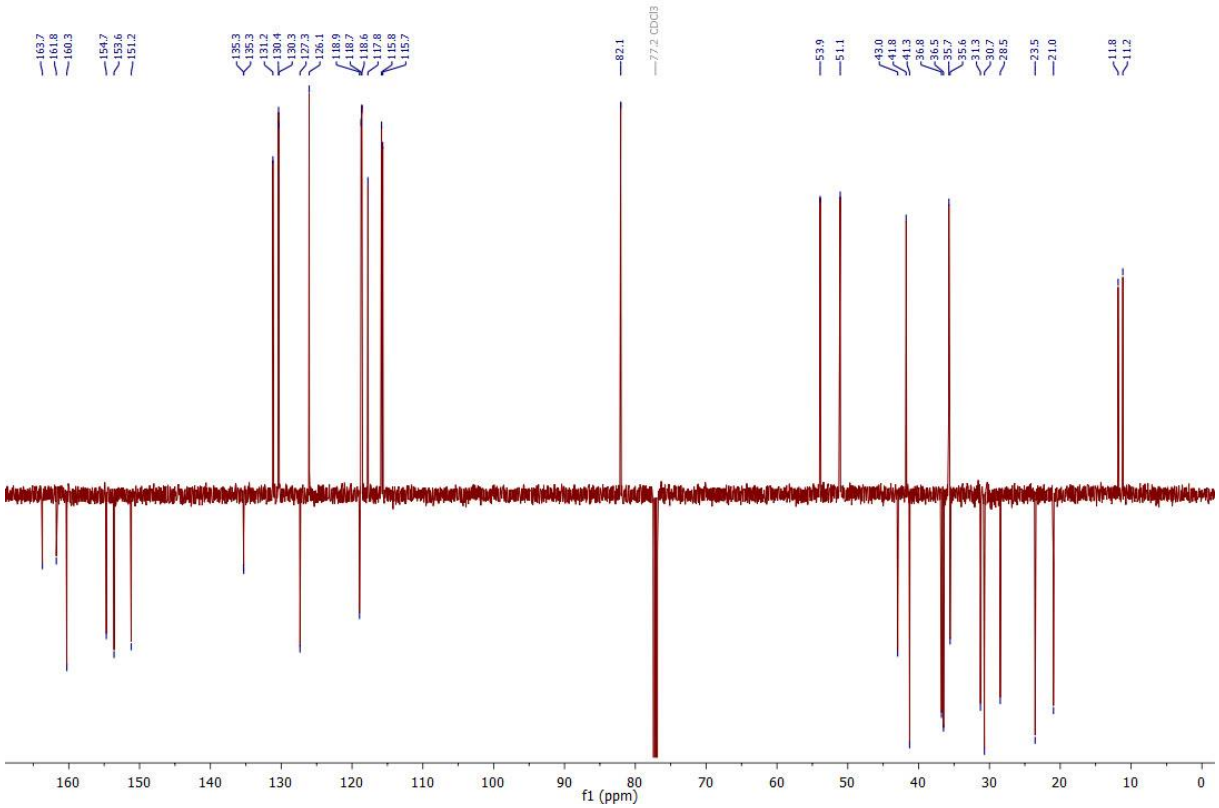
¹H — CDCl₃¹³C — CDCl₃

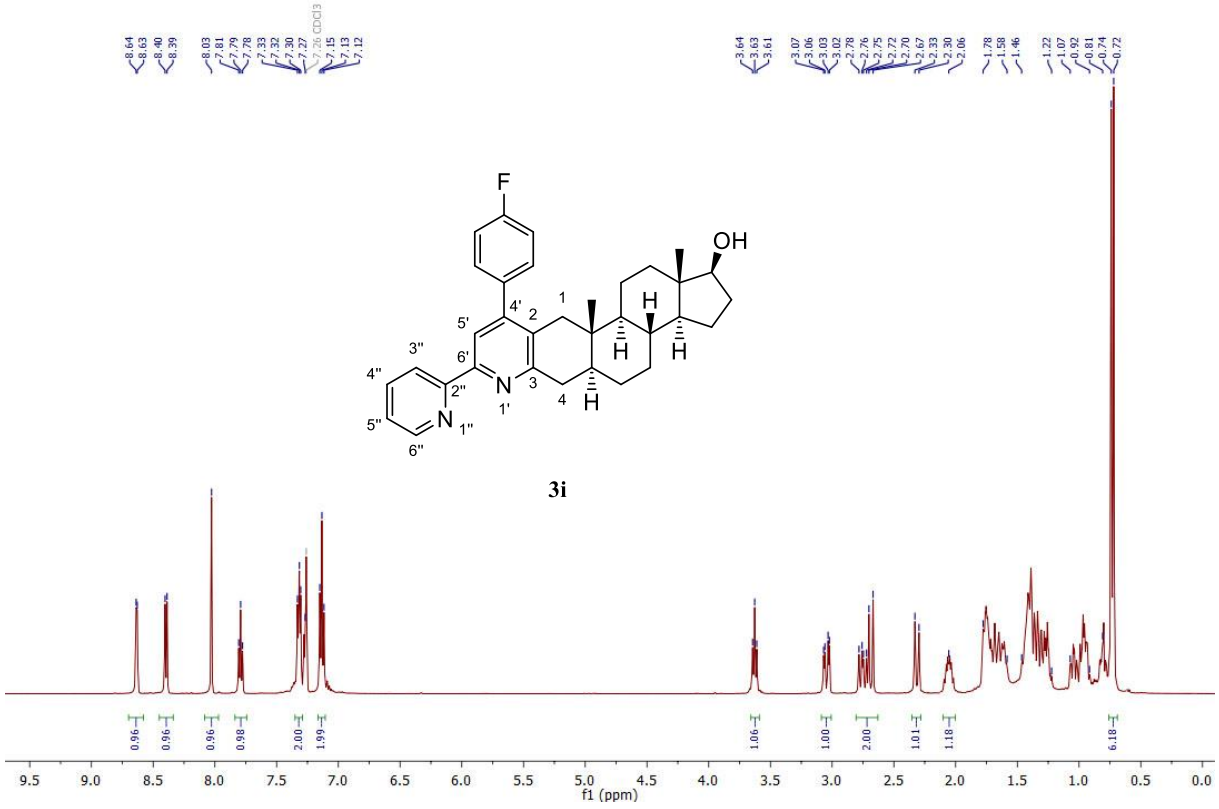
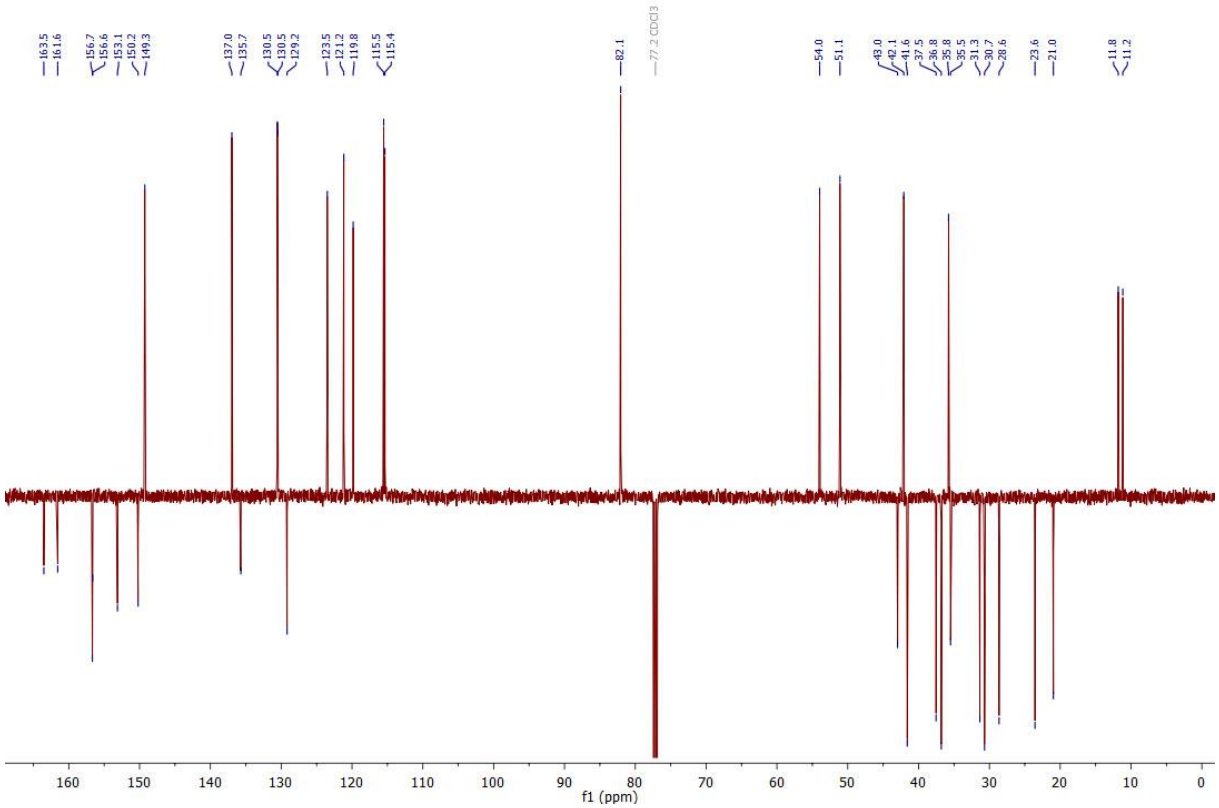
S16

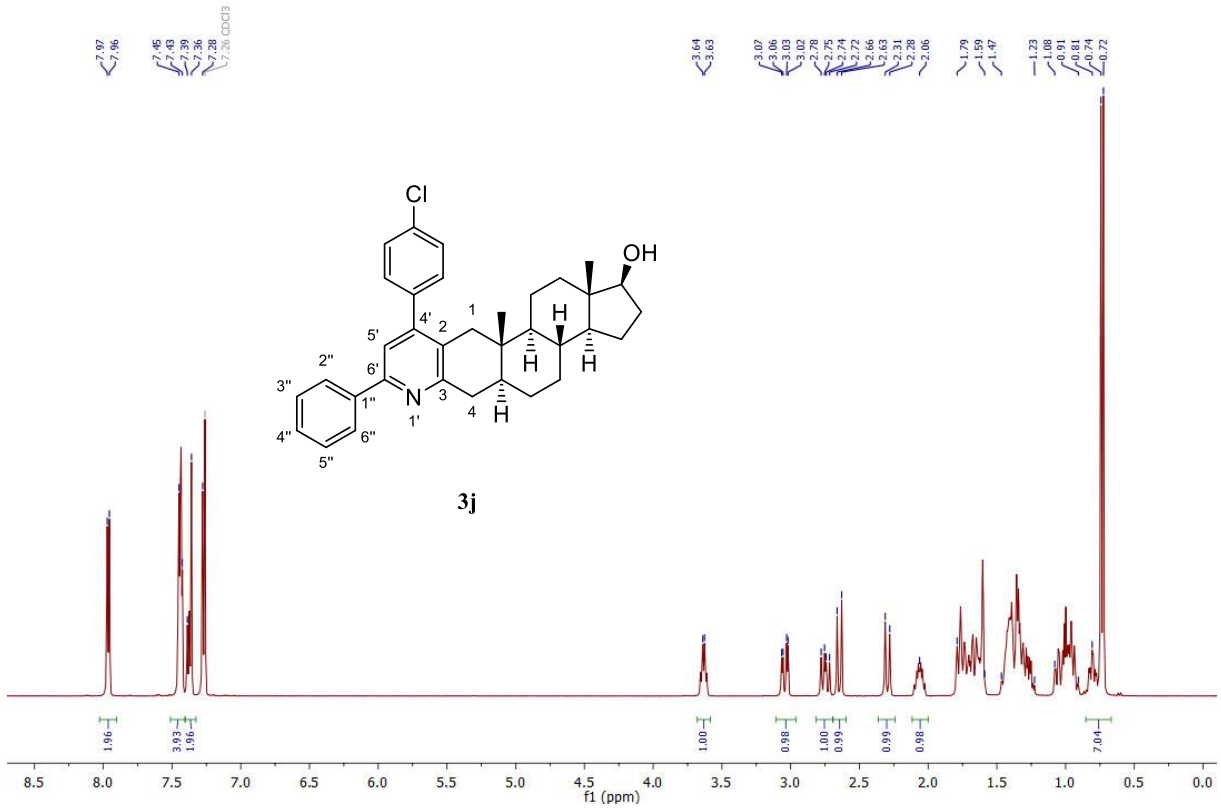
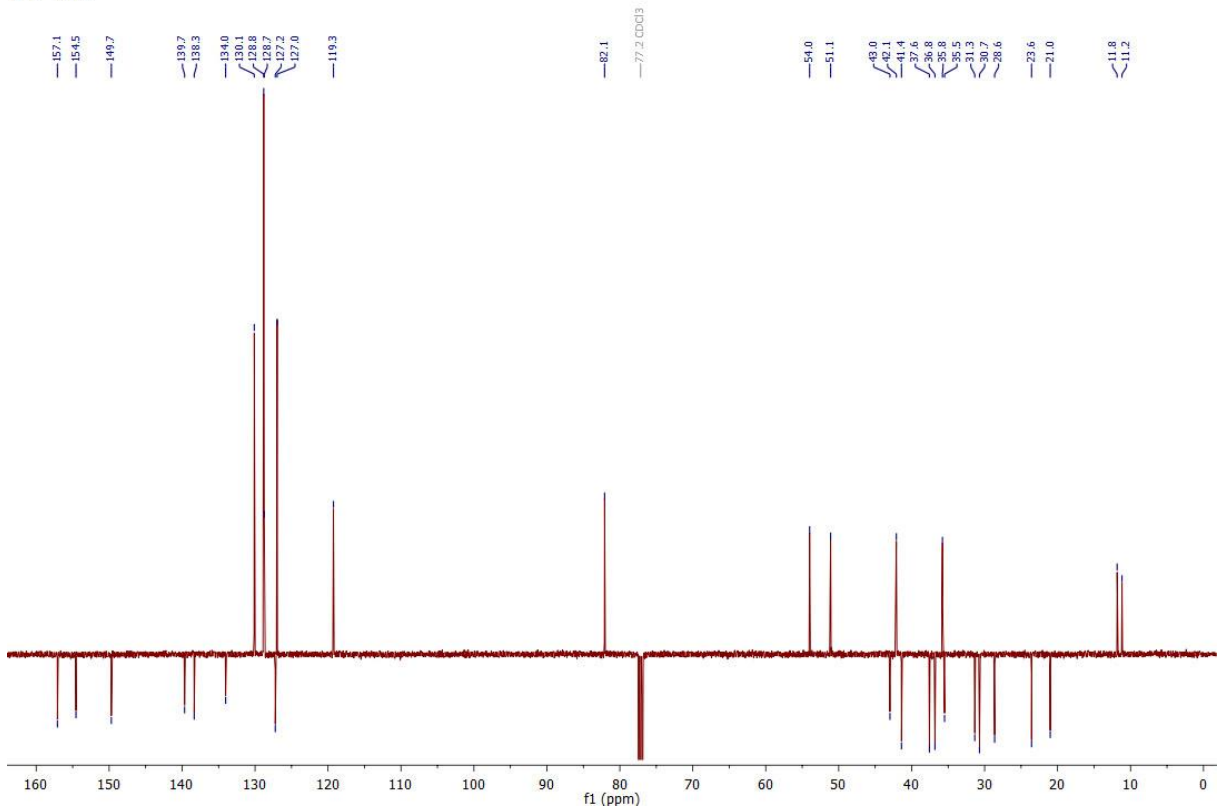
¹H — CDCl₃



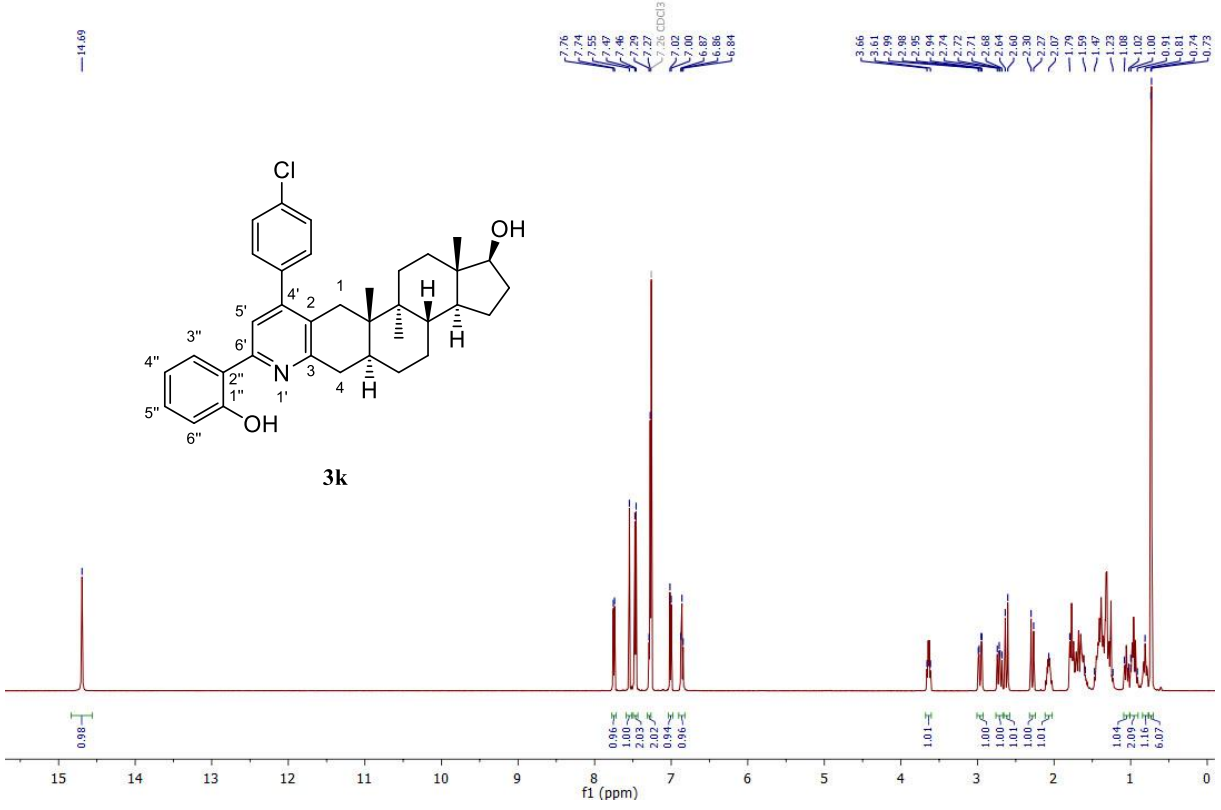
¹³C — CDCl₃



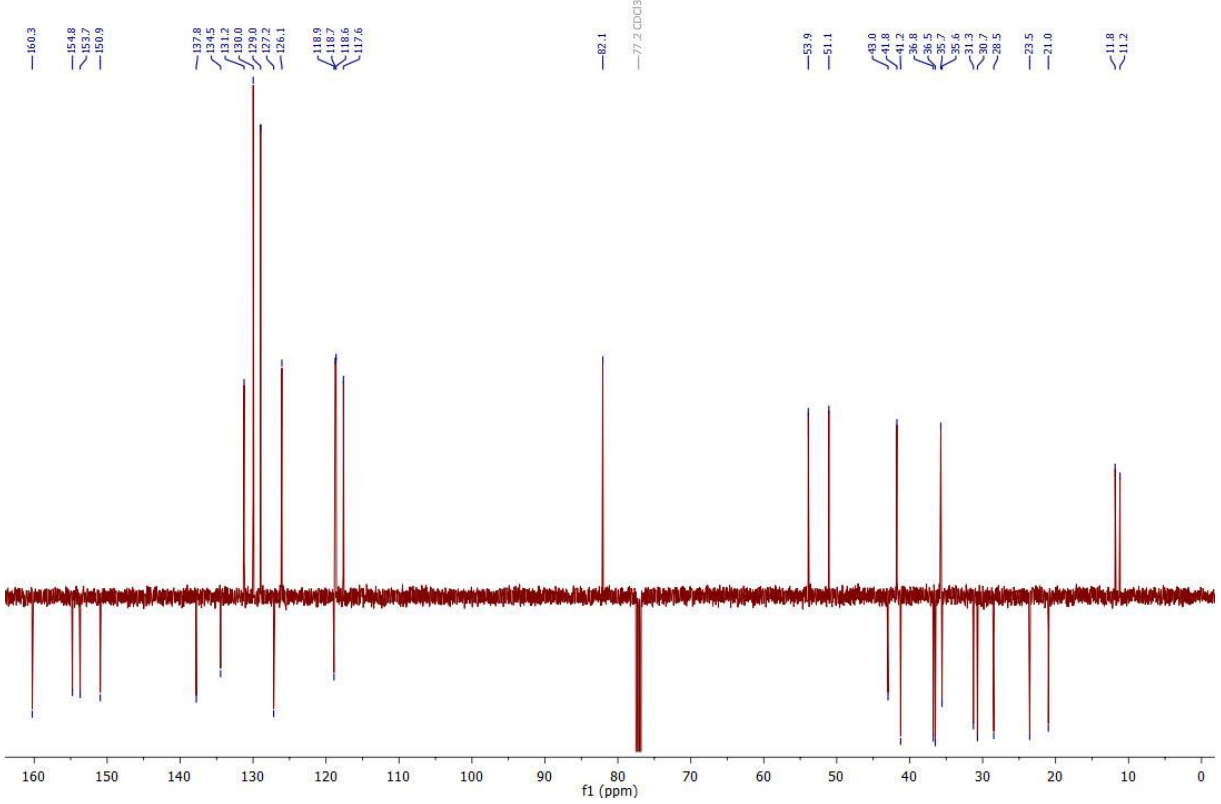
¹H — CDCl₃¹³C — CDCl₃

¹H — CDCl₃¹³C — CDCl₃

¹H — CDCl₃

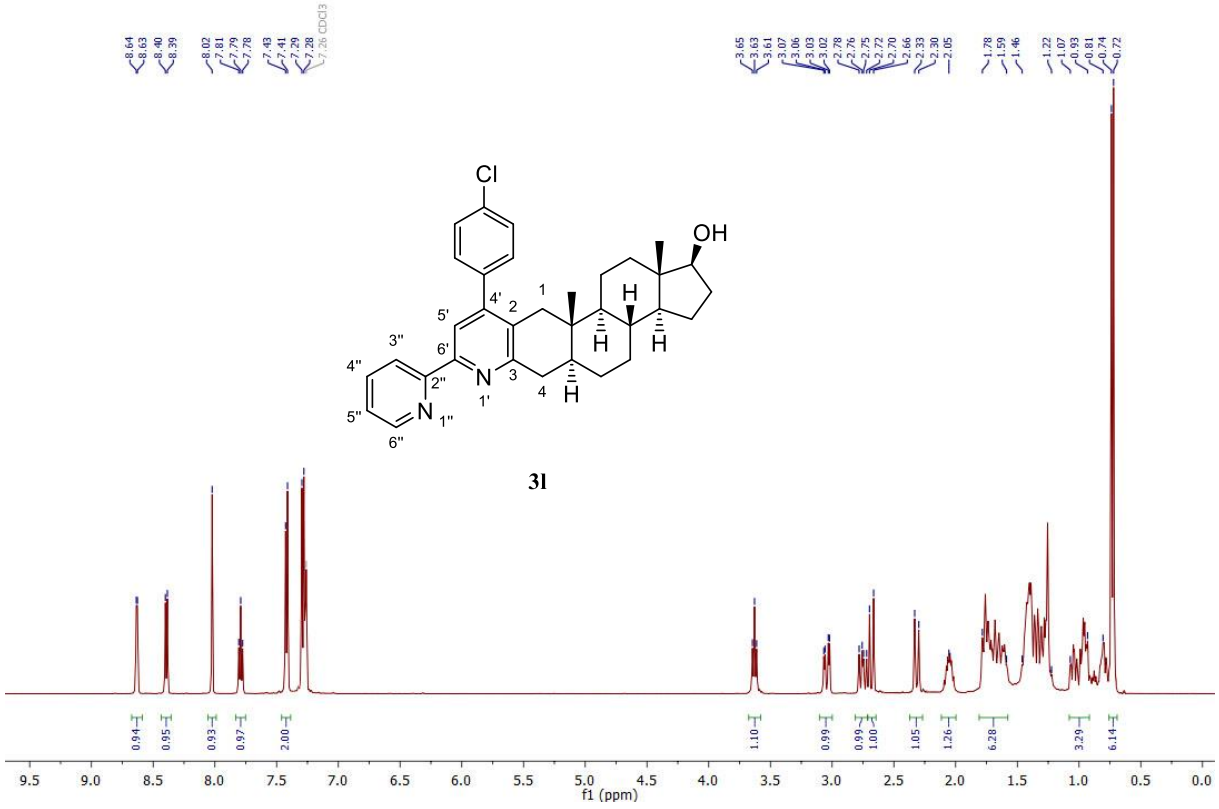


¹³C — CDCl₃

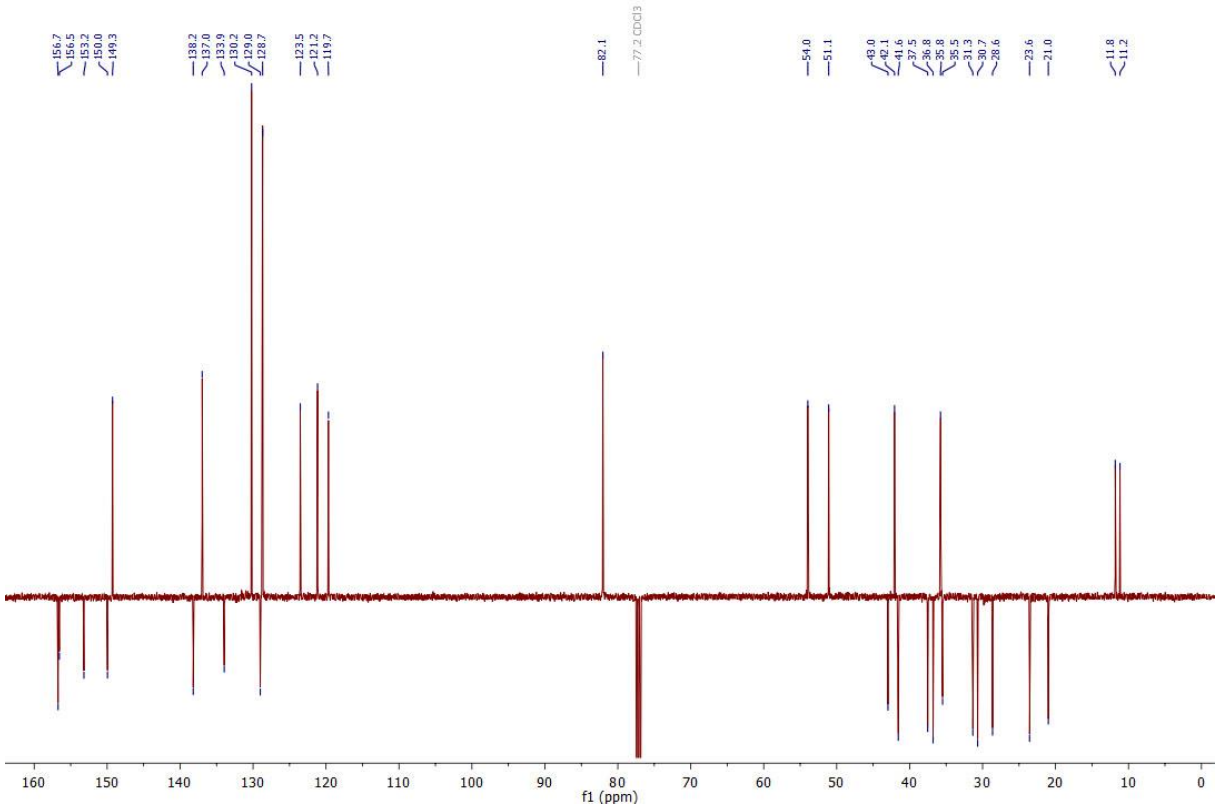


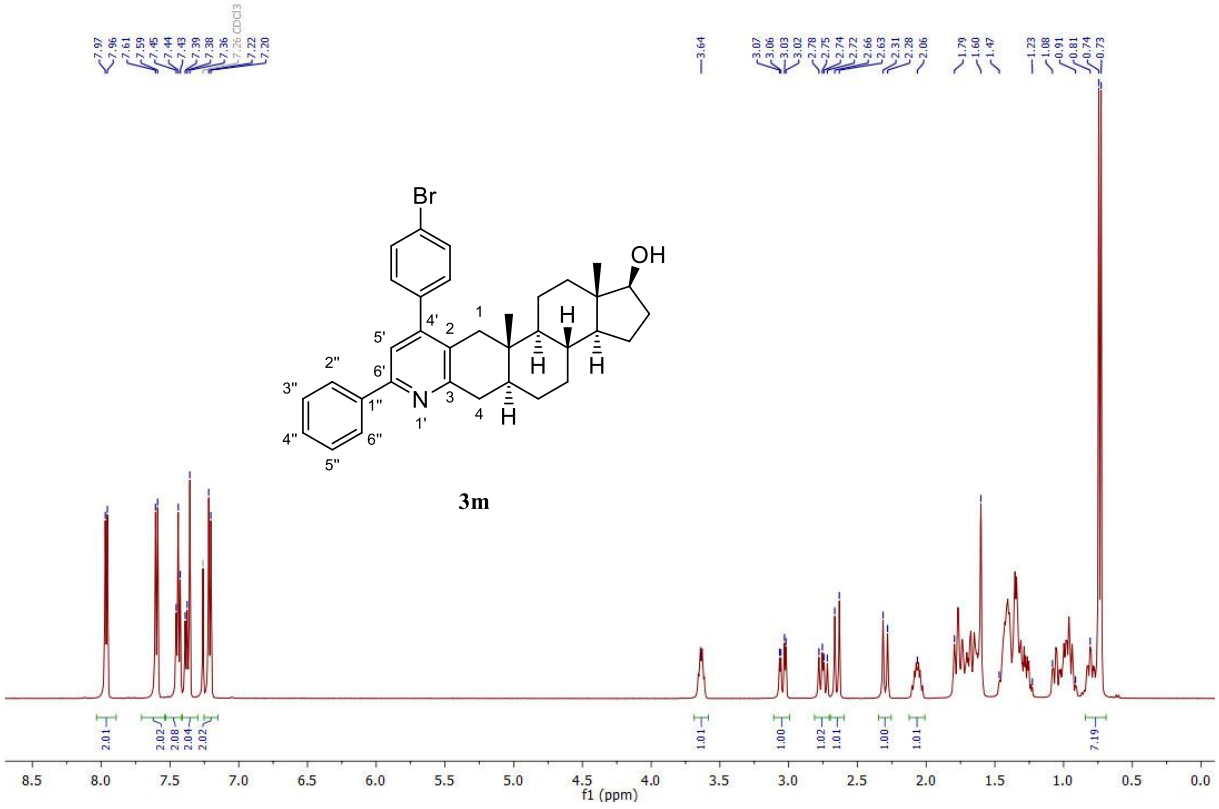
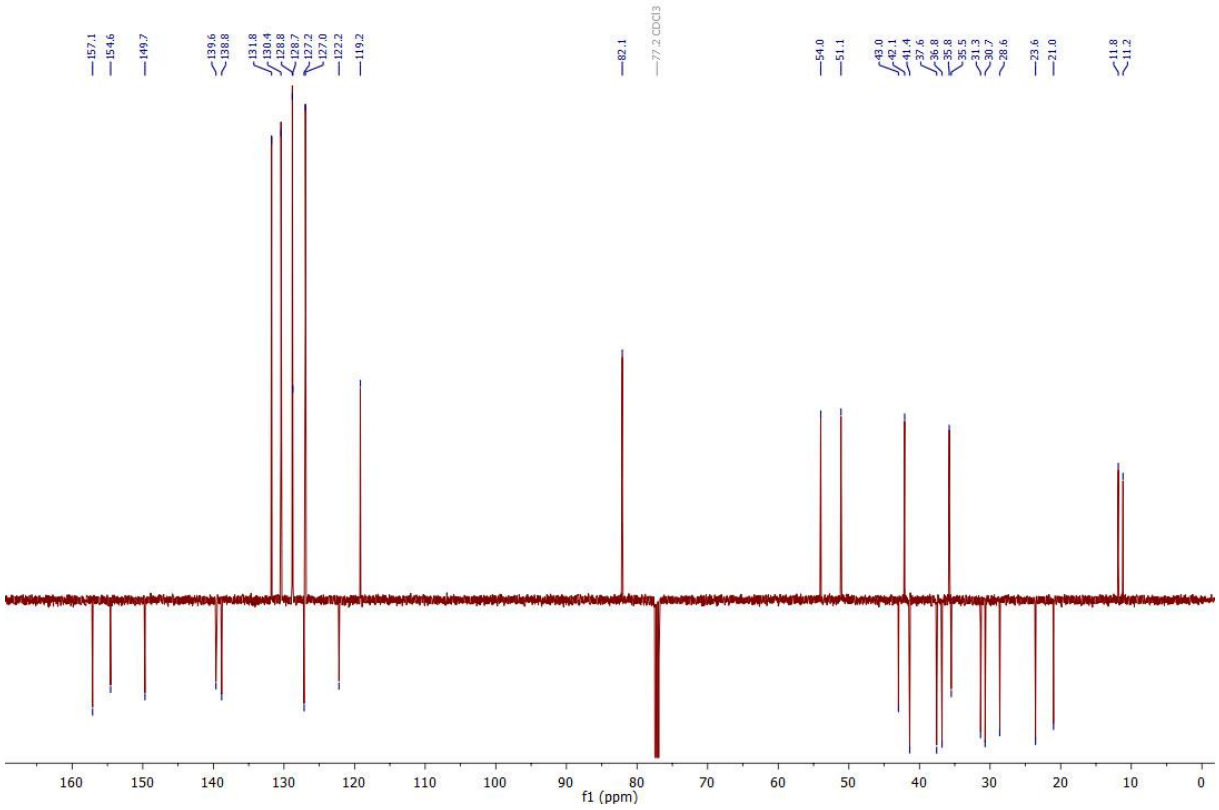
S20

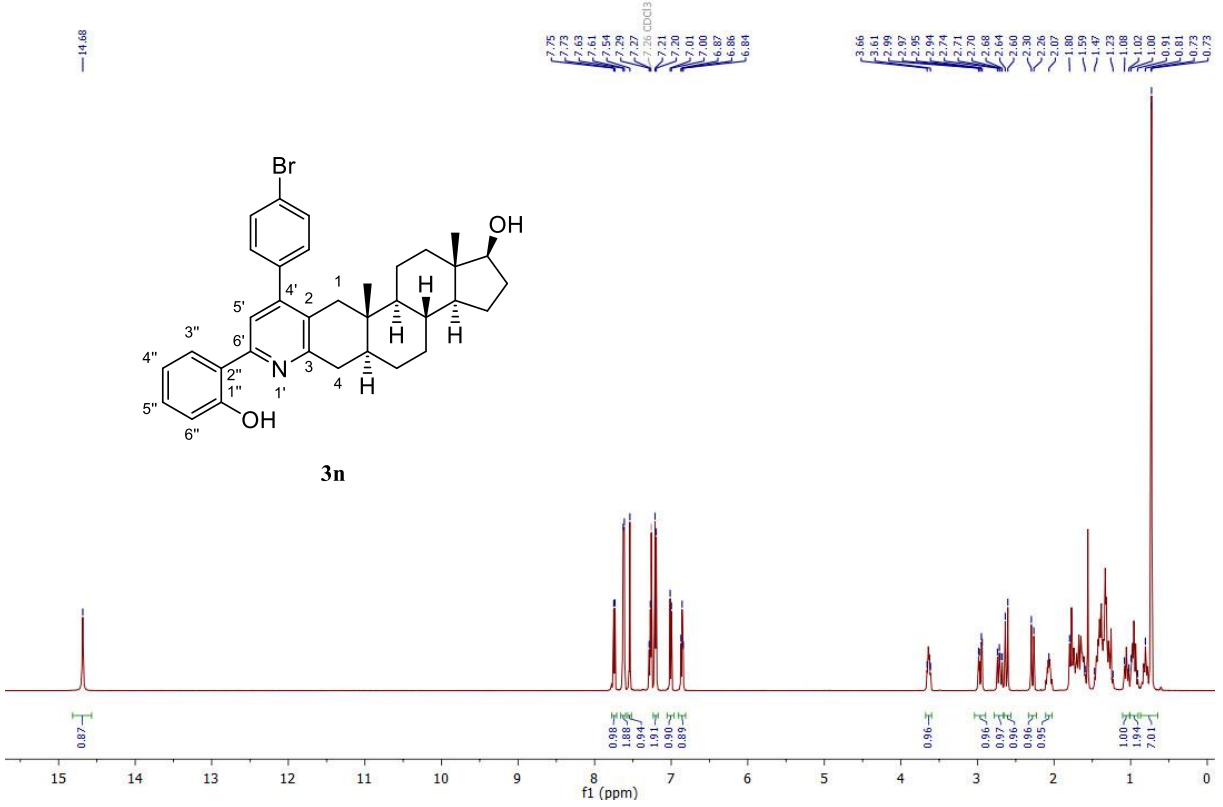
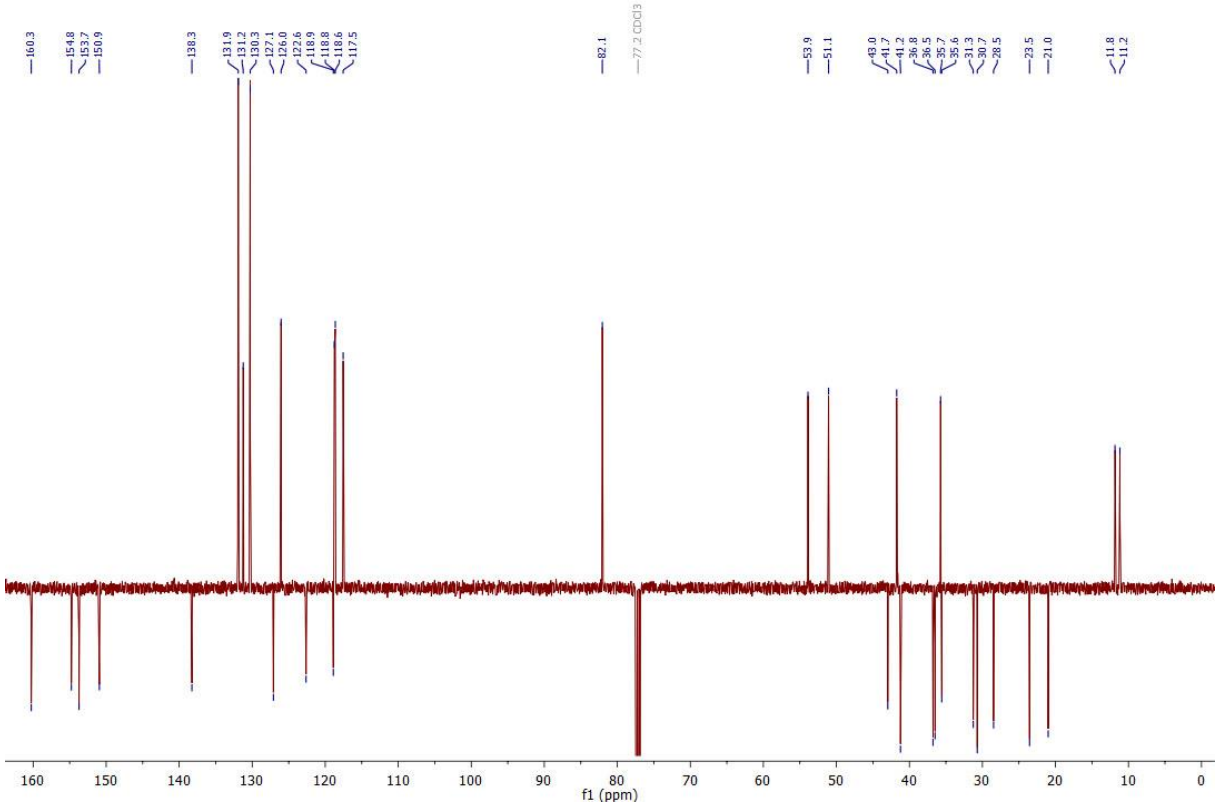
¹H — CDCl₃

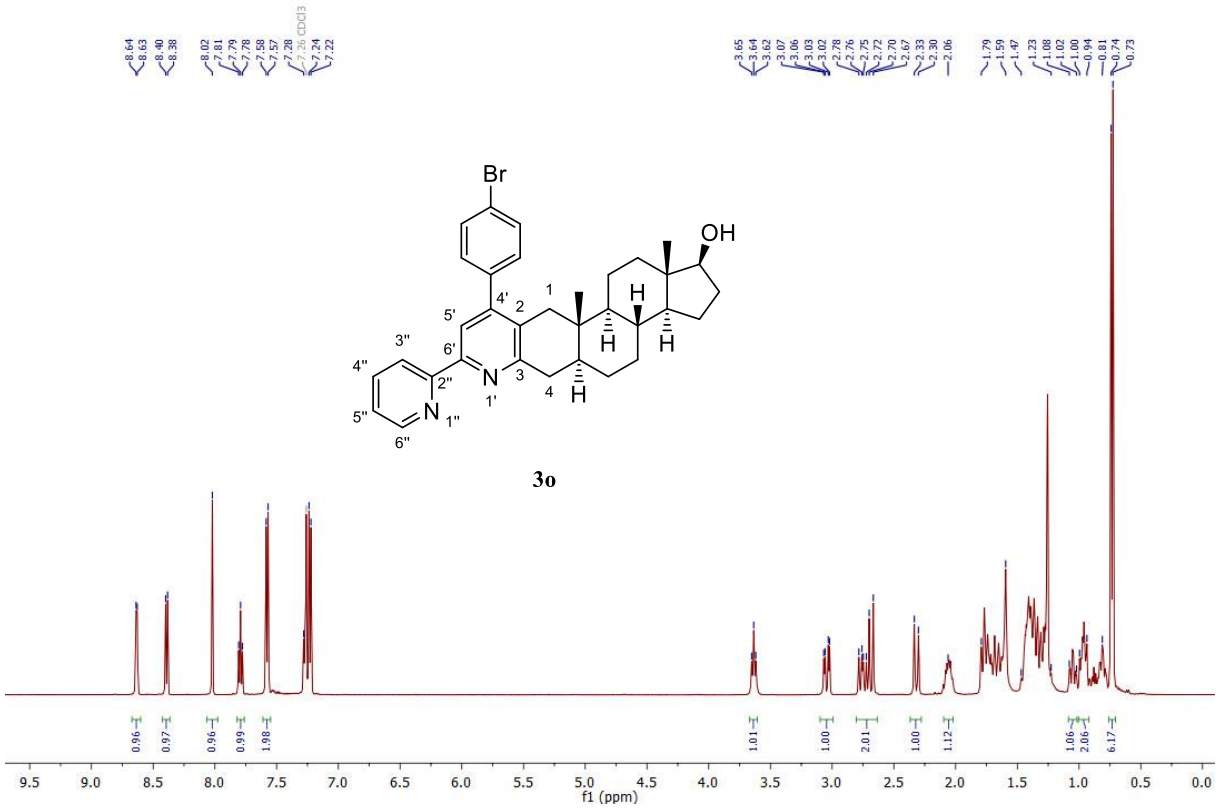
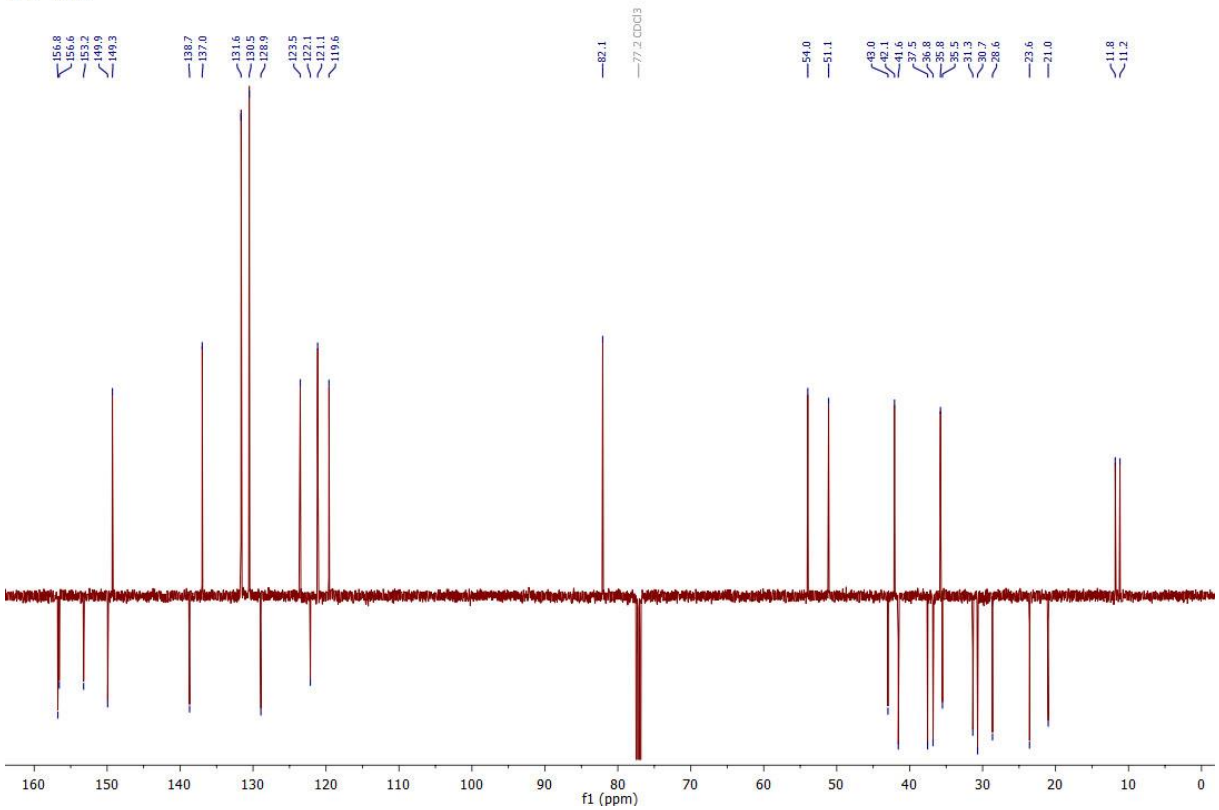


¹³C — CDCl₃



¹H — CDCl₃¹³C — CDCl₃

¹H — CDCl₃¹³C — CDCl₃

¹H — CDCl₃¹³C — CDCl₃

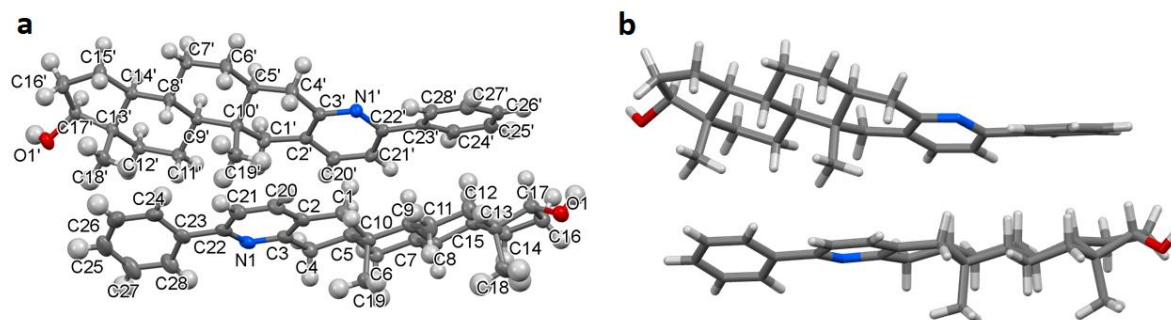


Figure S1. The two molecules in the asymmetric unit of **2a**, (a) ellipsoid representation, displacement parameters are drawn at 50% probability level, (b) stick representation. The numbering of the second molecule in the asymmetric unit is identical to the first one but with an asterisk added to each atom number.

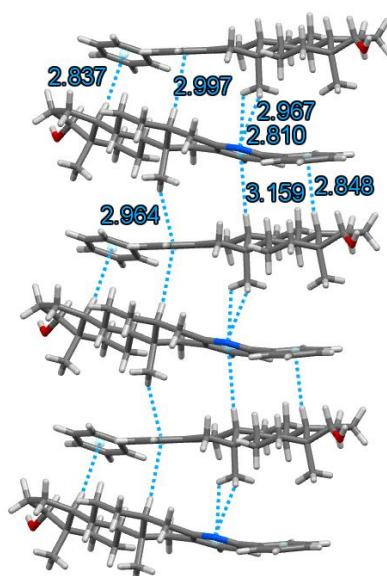


Figure S2. Packing of **2a** molecules, C-H... π interactions are drawn by blue dotted lines, interaction lengths are given in Ångströms.

Table S1. Analysis of Potential Hydrogen Bonds and Schemes with $d(D...A) < R(D)+R(A)+0.50$, $d(H...A) < R(H)+R(A)-0.12$ Ang., $D-H...A > 100.0$ Deg

Res	Donor	H...	Acceptor	Symm. op.	D-H (Å)	H...A (Å)	D...A (Å)	D - H...A (°)
1	O1	--H1	..N1	$1/2+y, 2-z$	0.84	2.10	2.921(3)	166
2	O1'	--H1'	..N1'	$-1/2+y, 1-z$	0.84	2.05	2.888(3)	175
1	C1	--H1A	..O1'	$1/2+y, 1-z$	0.99	2.42	3.396(4)	170

Table S2. Bond lengths (Å) in **2a**

O1*-C17*	1.429(3)	N1*-C3*	1.336(4)
N1*-C6'*	1.343(4)	C2*-C4'*	1.388(4)
C2*-C3*	1.398(4)	C2*-C1*	1.515(4)
C10*-C19*	1.532(4)	C10*-C1*	1.544(4)
C10*-C5*	1.547(4)	C10*-C9*	1.555(4)
C9*-C11*	1.544(4)	C9*-C8*	1.548(4)
C3*-C4*	1.501(4)	C13*-C12*	1.527(4)
C13*-C17*	1.533(4)	C13*-C18*	1.535(4)
C13*-C14*	1.536(4)	C8*-C14*	1.518(4)
C8*-C7*	1.526(4)	C5*-C4*	1.521(4)
C5*-C6*	1.527(4)	C6'*-C5'*	1.395(4)
C6'*-C1''*	1.494(4)	C14*-C15*	1.531(4)
C4'*-C5'*	1.379(4)	C12*-C11*	1.536(4)
C1''*-C2''*	1.388(4)	C1''*-C6''*	1.390(4)
C17*-C16*	1.542(4)	C2''*-C3''*	1.389(4)
C6*-C7*	1.520(4)	C3''*-C4''*	1.383(5)
C4''*-C5''*	1.375(5)	C15*-C16*	1.548(4)
C6''*-C5''*	1.388(4)	O1-C17	1.422(4)
N1-C3	1.343(4)	N1-C6'	1.343(4)
C6'-C5'	1.394(4)	C6'-C1''	1.493(4)
C10-C19	1.533(4)	C10-C1	1.536(4)
C10-C5	1.541(4)	C10-C9	1.558(4)
C2-C4'	1.394(4)	C2-C3	1.398(4)
C2-C1	1.515(4)	C9-C8	1.536(4)
C9-C11	1.545(4)	C13-C12	1.524(4)
C13-C17	1.534(4)	C13-C14	1.536(4)
C13-C18	1.537(4)	C1''-C6''	1.387(4)
C1''-C2''	1.389(5)	C5-C6	1.532(4)
C5-C4	1.534(4)	C4'-C5'	1.371(4)
C8-C7	1.522(4)	C8-C14	1.535(4)
C4-C3	1.507(4)	C6-C7	1.528(4)
C17-C16	1.552(4)	C14-C15	1.529(4)
C2''-C3''	1.378(5)	C6''-C5''	1.380(5)
C4''-C5''	1.375(6)	C4''-C3''	1.376(6)
C11-C12	1.547(4)	C16-C15	1.555(4)

Table S3. Bond angles (°) in **2a**

C3*-N1*-C6*	119.6(2)	C4''*-C2*-C3*	116.6(3)
C4''*-C2*-C1*	121.4(2)	C3*-C2*-C1*	121.9(3)
C19*-C10*-C1*	109.2(2)	C19*-C10*-C5*	111.8(2)
C1*-C10*-C5*	107.1(2)	C19*-C10*-C9*	111.3(2)
C1*-C10*-C9*	109.2(2)	C5*-C10*-C9*	108.2(2)
C11*-C9*-C8*	112.2(2)	C11*-C9*-C10*	114.2(2)
C8*-C9*-C10*	111.7(2)	N1*-C3*-C2*	123.3(3)
N1*-C3*-C4*	115.7(2)	C2*-C3*-C4*	121.0(3)
C12*-C13*-C17*	115.8(2)	C12*-C13*-C18*	111.0(2)
C17*-C13*-C18*	109.7(2)	C12*-C13*-C14*	107.6(2)
C17*-C13*-C14*	98.8(2)	C18*-C13*-C14*	113.5(2)
C14*-C8*-C7*	110.6(2)	C14*-C8*-C9*	108.6(2)
C7*-C8*-C9*	110.6(2)	C4*-C5*-C6*	109.8(2)
C4*-C5*-C10*	111.8(2)	C6*-C5*-C10*	113.3(2)
N1*-C6''*-C5''*	120.7(3)	N1*-C6''*-C1''*	115.7(2)
C5''*-C6''*-C1''*	123.6(3)	C8*-C14*-C15*	118.6(2)
C8*-C14*-C13*	113.8(2)	C15*-C14*-C13*	104.5(2)
C5''*-C4''*-C2''*	120.5(3)	C4''*-C5''*-C6''*	119.3(3)
C13*-C12*-C11*	111.5(2)	C3*-C4''*-C5''*	113.8(2)
C2*-C1*-C10*	114.1(2)	C12*-C11*-C9*	113.1(2)
C2''*-C1''*-C6''*	118.1(3)	C2''*-C1''*-C6''*	122.0(3)
C6''*-C1''*-C6''*	119.9(3)	O1*-C17*-C13*	112.7(2)
O1*-C17*-C16*	113.2(2)	C13*-C17*-C16*	104.3(2)
C1''*-C2''*-C3''*	121.0(3)	C7*-C6''*-C5''*	111.5(2)
C6*-C7*-C8*	112.2(2)	C4''*-C3''*-C2''*	119.9(3)
C5''*-C4''*-C3''*	119.9(3)	C14*-C15*-C16*	104.1(2)
C5''*-C6''*-C1''*	121.1(3)	C4''*-C5''*-C6''*	120.0(3)
C17*-C16*-C15*	105.3(2)	C3-N1-C6'	119.5(3)
N1-C6'-C5'	121.0(3)	N1-C6'-C1''	116.6(3)
C5'-C6'-C1''	122.3(3)	C19-C10-C1	109.1(2)
C19-C10-C5	111.8(2)	C1-C10-C5	106.6(2)
C19-C10-C9	111.4(3)	C1-C10-C9	109.0(2)
C5-C10-C9	108.9(2)	C4'-C2-C3	116.7(3)
C4'-C2-C1	121.2(3)	C3-C2-C1	122.1(3)
C2-C1-C10	114.0(2)	C8-C9-C11	111.7(3)
C8-C9-C10	113.7(2)	C11-C9-C10	113.0(2)
C12-C13-C17	114.9(2)	C12-C13-C14	108.3(3)
C17-C13-C14	100.0(2)	C12-C13-C18	111.6(3)
C17-C13-C18	108.5(3)	C14-C13-C18	113.1(3)
C6''-C1''-C2''	117.5(3)	C6''-C1''-C6'	120.3(3)
C2''-C1''-C6'	122.3(3)	C6-C5-C4	110.6(2)
C6-C5-C10	113.2(2)	C4-C5-C10	112.0(2)
C5'-C4'-C2	120.8(3)	C7-C8-C14	111.2(2)
C7-C8-C9	111.4(2)	C14-C8-C9	107.4(2)
C3-C4-C5	114.1(2)	C7-C6-C5	111.2(2)
O1-C17-C13	112.6(2)	O1-C17-C16	113.9(3)
C13-C17-C16	104.5(2)	C15-C14-C8	120.5(2)
C15-C14-C13	104.9(2)	C8-C14-C13	113.6(2)
C4'-C5'-C6'	119.1(3)	C8-C7-C6	112.2(2)
C3''-C2''-C1''	121.6(3)	C5''-C6''-C1''	120.8(4)
C5''-C4''-C3''	119.0(4)	C9-C11-C12	112.3(2)
C17-C16-C15	105.8(2)	C13-C12-C11	111.3(3)
C4''-C5''-C6''	121.0(4)	C4''-C3''-C2''	120.2(4)
C14-C15-C16	104.0(2)	N1-C3-C2	122.8(3)
N1-C3-C4	116.5(2)	C2-C3-C4	120.6(3)

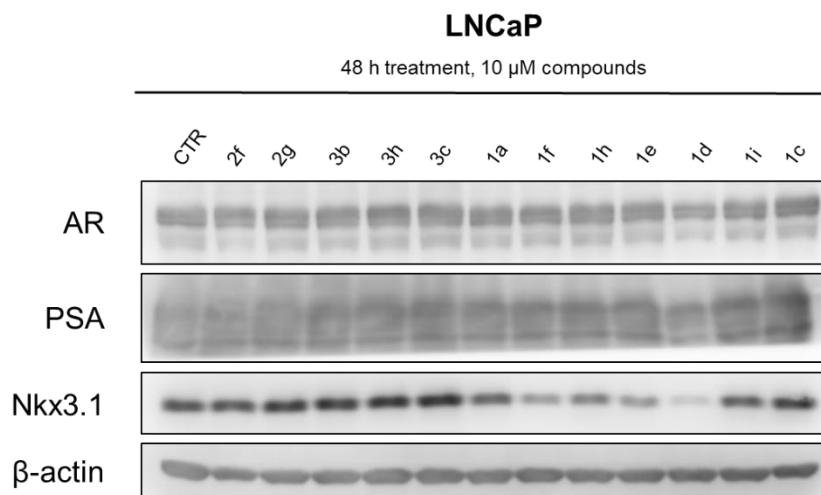


Figure S3. AR and AR-regulated proteins in LNCaP after 48-h treatment with selected compounds.

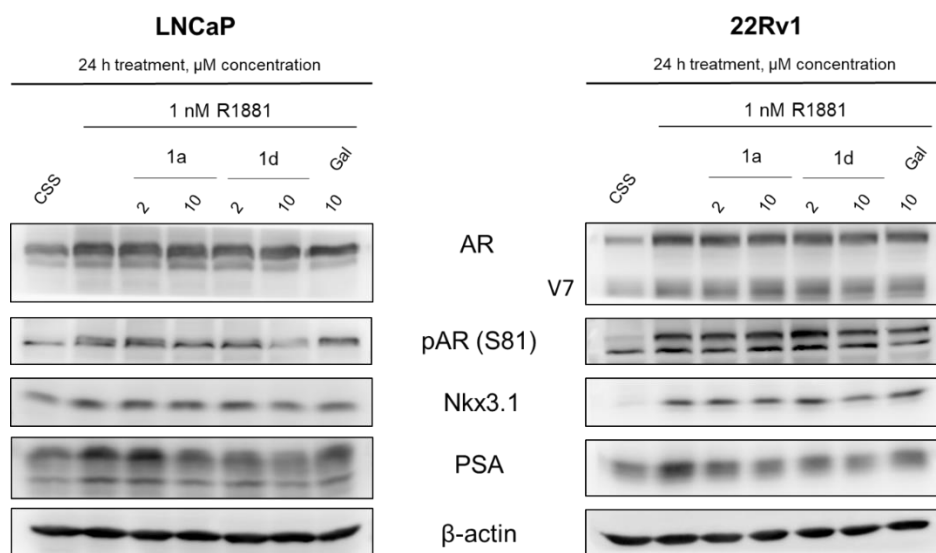


Figure S4. Dose dependent effect of **1a** and **1d** on AR- signalling in LNCaP, 22Rv1. Level of β -actin served as loading control. Gal, galeterone.

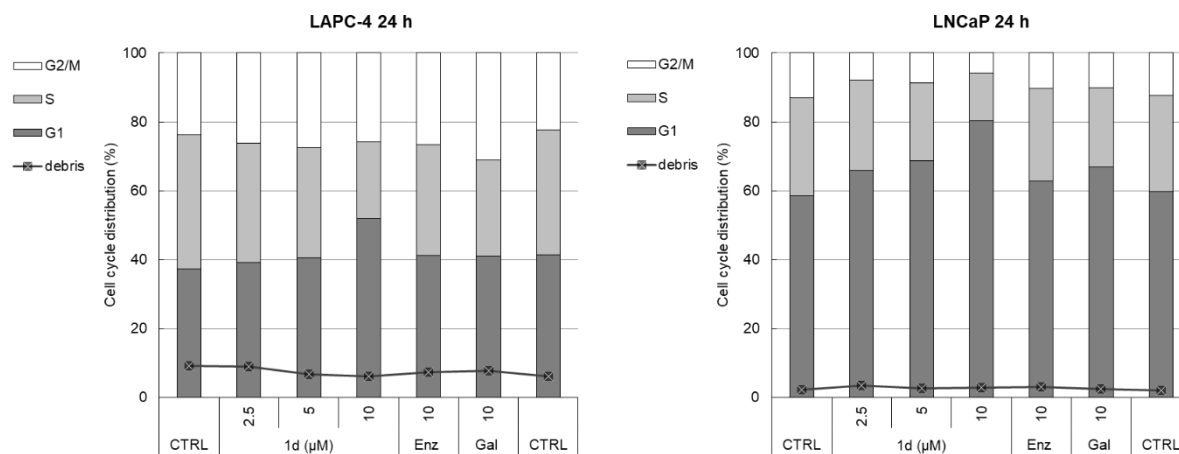


Figure S5. Cell cycle analysis of the LAPC-4 and LNCaP cell lines analysed after 24 h treatment with **1d** or standards enzalutamide, galeterone.

Appendix IV.

Peřina M, Kiss A, Mernyák E, Mada L, Schneider G, Jorda R. Synthesis of hydrocortisone esters targeting androgen and glucocorticoid receptors in prostate cancer in vitro. **J Steroid Biochem Mol Biol.** 2023b May;229:106269.



Contents lists available at ScienceDirect

Journal of Steroid Biochemistry and Molecular Biology

journal homepage: www.elsevier.com/locate/jsbmb

Synthesis of hydrocortisone esters targeting androgen and glucocorticoid receptors in prostate cancer *in vitro*

Miroslav Peřina^a, Anita Kiss^b, Erzsébet Mernyák^b, Lukáš Mada^a, Gyula Schneider^{b,*},
Radek Jorda^{a,*}

^a Department of Experimental Biology, Faculty of Science, Palacký University Olomouc, Štechtitelů 27, 78371 Olomouc, Czech Republic

^b Department of Organic Chemistry, University of Szeged, Dóm tér 8, 17720 Szeged, Hungary

ARTICLE INFO

Keywords:

Hydrocortisone derivatives
Androgen receptor
Glucocorticoid receptor
Prostate cancer
Castration resistant prostate cancer
Transcriptional activity

ABSTRACT

Androgen and glucocorticoid receptors have been recently described as key players in processes related to prostate cancer and mainly androgen receptor's inactivation was shown as an effective way for the prostate cancer treatment. Unfortunately, androgen deprivation therapy usually loses its effectivity and the disease frequently progresses into castration-resistant prostate cancer with poor prognosis. The role of the glucocorticoid receptor is associated with the mechanism of resistance; therefore, pharmacological targeting of glucocorticoid receptor in combination with antiandrogen treatment was shown as an alternative approach in the prostate cancer treatment. We introduce here the synthesis of novel 17 α - and/or 21-ester or carbamate derivatives of hydrocortisone and evaluation of their biological activity towards androgen and glucocorticoid receptors in different prostate cancer cell lines. A 17 α -butyryloxy-21-(alkyl)carbamoyloxy derivative **14** was found to diminish the transcriptional activity of both receptors (in single-digit micromolar range), with comparable potency to enzalutamide towards the androgen receptor, but weaker potency compared to mifepristone towards the glucocorticoid receptor. Lead compound inhibited proliferation and the formation of cell colonies in both androgen and glucocorticoid receptors-positive prostate cancer cell lines in low micromolar concentrations. Candidate compound **14** showed to interact with both receptors in cells and inhibited the translocation of receptors to nucleus and their activation phosphorylation. Moreover, binding to receptor's ligand binding domains was assessed by molecular modelling. Lead compound also induced the accumulation of cells in G1 phase and its combination with enzalutamide was shown to be more effective than enzalutamide alone.

1. Introduction

Nuclear receptors are suitable and promising pharmacologic targets for various diseases, including cancer. Androgen receptor (AR) is a key oncogene which drives the progression of prostate cancer (PCa) [1]. Given the AR-signalling its crucial role, androgen deprivation therapy combined with antiandrogens (e.g. using abiraterone and enzalutamide) is a standard first-line therapy of PCa [2]. While the treatment is often effective at the beginning, disease frequently progresses into

castration-resistant prostate cancer (CRPC) with reactivated AR signalling, characterised by AR overexpression, expression of splicing variants independent of androgens and mutations in ligand-binding domain [3, 4].

Number of studies have shown that another receptor, glucocorticoid (GR), is able to activate similar transcription programme to AR and bypass AR blockade and thus GR activity could be a possible mechanism of resistance to therapy in CRPC [5,6]. In addition, long-term androgen deprivation, AR inhibition or resistance to docetaxel chemotherapy

Abbreviations: ATP, adenosine triphosphate; AR, androgen receptor; ARE, androgen response element; CETSAs, cellular-thermal shift assay; CSS, charcoal stripped serum; CRPC, castration-resistant prostate cancer; DCTA, *trans*-1,2-diaminocyclohexane-*N,N,N',N'*-tetraacetic acid; DMF, *N,N*-dimethylformamide; DTT, dithiothreitol; FBS, foetal bovine serum; Gal, galeterone; GR, glucocorticoid receptor; LBD, ligand-binding domain; Mif, mifepristone; Mp, melting point; NMR, nuclear magnetic resonance; PBS, phosphate-buffered saline; PCa, prostate cancer; PCR, polymerase chain reaction; PPTS, pyridinium *p*-toluenesulfonate; PSA, prostate-specific antigen; RIPA, radioimmunoprecipitation assay buffer; SDS-PAGE, sodium dodecyl sulphate-polyacrylamide gel electrophoresis; TLC, thin layer chromatography.

* Corresponding authors.

E-mail addresses: bobe@chem.u-szeged.hu (G. Schneider), radek.jorda@upol.cz (R. Jorda).

¹ Deceased.

<https://doi.org/10.1016/j.jsbmb.2023.106269>

Received 17 October 2022; Received in revised form 29 January 2023; Accepted 7 February 2023

Available online 10 February 2023

0960-0760/© 2023 Elsevier Ltd. All rights reserved.

leads to significantly increased GR expression *in vitro* and also in samples from relapsed patients [5,7,8]. Concerning that glucocorticoids are frequently used in primary or metastatic PCa patients [9] and the newly unravelled role of GR in PCa progression, there is an urgent need to establish novel therapeutic schedules, concerning GR expression. Importantly, recent research has shown that targeting GR pathway in combination with antiandrogen therapy may further improve PCa therapy [6,10] and novel compounds acting as AR/GR antagonists are under development [11].

Glucocorticoids (e.g. the 17-esters of corticosteroids) are among the most effective therapeutics available for the treatment of chronic inflammatory disease [12,13], but the antiandrogenic activity of a series of 17 α -esters of cortisolone has been reported [14–17] as well. Recently described dual and selective antagonists of AR/GR, cortisolone 17 α -valerate-21-propionate (CB-03–10) and cortisolone 17 α -valerate (CB-03–05), displayed high antitumor activity across a panel of human prostate and triple negative breast cancers, as well as *in vivo* murine LNCaP xenograft models [18]. This study supported further development of similar compounds acting as dual AR/GR antagonists instead of combining the AR antagonists with non-selective (e.g. cyproterone acetate and mifepristone) or selective GR antagonists (e.g. ORIC-101 or OP-3633) (Fig. 1) [19–21].

Here, we report the synthesis and characterisation of 17 α - and/or 21-ester or carbamate derivatives of hydrocortisone. Compounds were analysed for their agonist or antagonist activity in the AR and GR reporter cell lines. Potent AR and GR antagonists were found within prepared compounds, which were further studied and lead compound 14 showed to interact with AR and GR and suppress the signalling of both receptors in several prostate cell lines differing in AR/GR expression. Antiproliferative assay showed only mild cytotoxicity in PCa cell lines, however candidate compounds showed to markedly inhibit colony formation of PCa cells. Molecular modelling suggested that candidate compound binds to both receptor's ligand binding domains with extensive interactions.

2. Results

2.1. Synthesis and characterisation of the target compounds

The 17 α -monoesters (8–10) of hydrocortisone were prepared via transesterification reaction, using the appropriate short chain alkyl orthoesters as reagents. Without isolation of the cyclic 17 α ,21-orthoesters, their decomposition under controlled conditions at pH= 3 led to the corresponding 17 α -monoesters (8–10, Scheme 1) [22,23].

Ester moieties at the C-21 position (in compounds 12 and 13) were established *via* acylation with the corresponding acyl chloride in pyridine. 21-*O*-Carbamoyl derivatives (11, 15–17) were prepared with a variety of commercially available isocyanates, or with *N,N*-diethyl carbamoyl chloride (in compound 14) (Schemes 1 and 2).

2.2. The effect of compounds on AR and GR transcriptional activity

To evaluate the effect of compounds on both nuclear receptors, we examined the dexamethasone-stimulated transcriptional activity of GR and metribolone (R1881)-stimulated transcriptional activity of AR after 24 h treatment with novel hydrocortisone-derivatives. Transcriptional activity of AR and GR was analysed in reporter cell lines, 22Rv1-ARE14 [24] and AZ-GR [25] respectively, where inserted luciferase gene is under control of adequate hormone response element.

Characterised set of novel hydrocortisone-derivatives 8–17 comprised three 17 α -monoesters (8–10), two C-21 carbamates (16, 17), three 17 α -monoesters-21 carbamates (11, 14, 15) and two 17 α -monoesters-21-octyl-thiocarbonates (12, 13). As shown in Table 1. and Figs. S1–S4, derivatives significantly differed in their ability to modulate AR and GR transcriptional activity.

Hydrocortisone and its 17 α -monoesters displayed agonist properties to both AR and GR and were able to induce transcriptional activity of studied nuclear receptors to at least 50% of standard agonist in concentrations that were analysed (Figs. S1 and S3). In the antagonist mode (in the presence of known concentration of synthetic agonist), compounds 7–10 increased transcriptional activity of AR above the level of 1 nM R1881, on the other hand, decreased transcriptional activity of GR below the level of 100 nM dexamethasone (Table 1, Figs. S2 and S4), suggesting dual activity of these compounds. Significant correlation

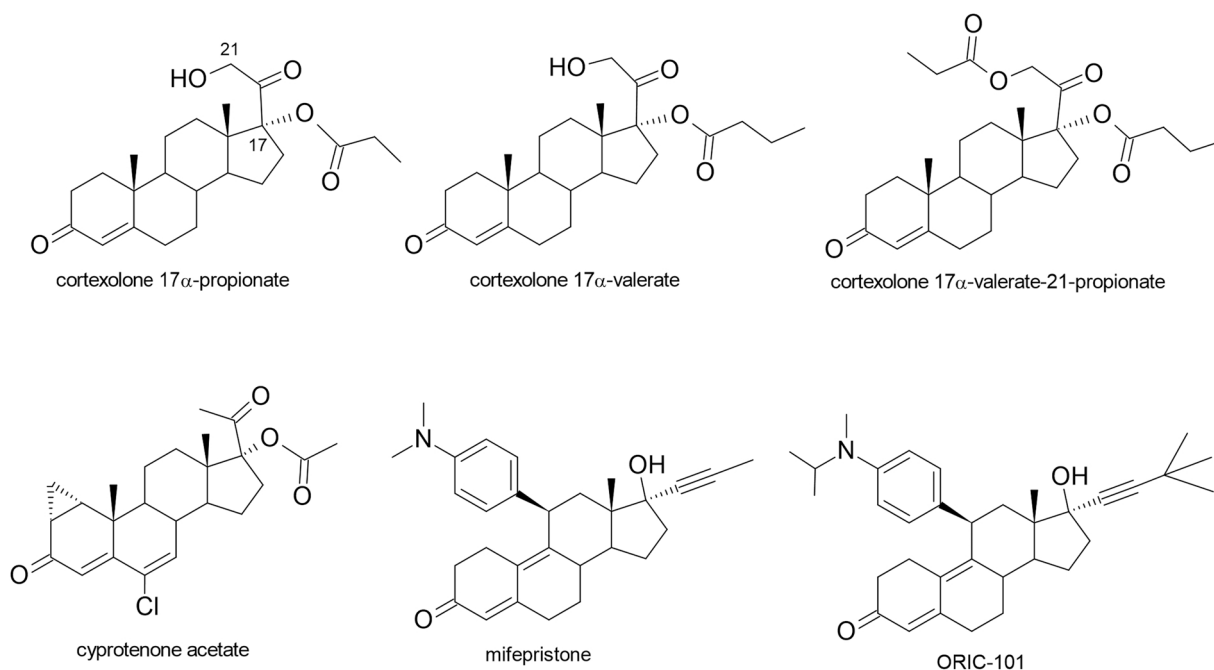
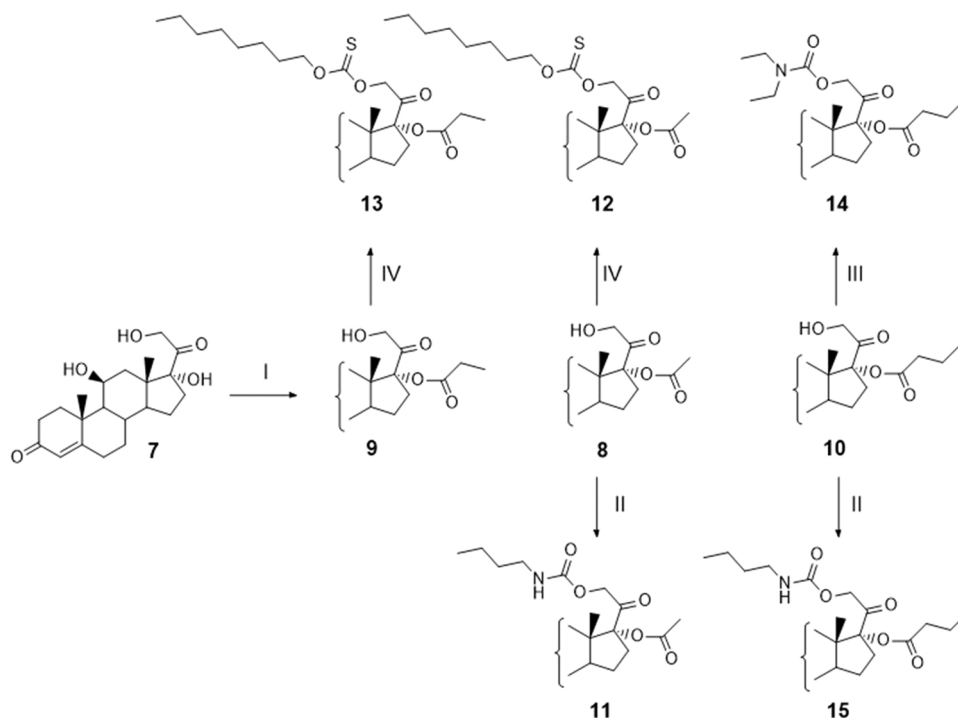
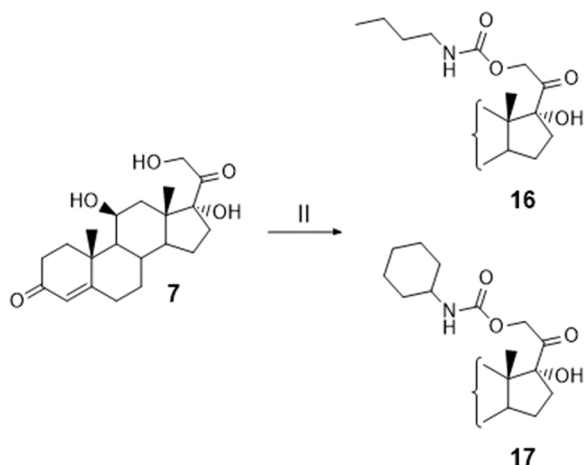


Fig. 1. Representatives of steroidal dual GR/AR antagonists (1–4) and selective GR antagonists (5, 6).



Scheme 1. Synthesis of 17 α -monoesters (8-10), 17 α - and 21-diester (12 and 13) and carbamates (11, 14-15). I: Corresponding alkyl orthoesters, pyridinium *p*-toluenesulfonate (PPTS), toluene, 30 min; reflux. II: Corresponding isocyanate, toluene, 2 h; reflux. III: *N,N*-diethylcarbamoyl chloride, triethylamine, 6 h; reflux. IV: *O*-(*n*-octyl) chlorotioformate, pyridine, 0 °C, 30 min, 6 h; rt.



Scheme 2. Synthesis of carbamates 16 and 17. II: Corresponding isocyanate, toluene, 2 h; reflux.

between the length of carbon chain of the ester and activity was not found.

C-21 carbamates (16 and 17) exerted weak GR and almost no AR agonist activities (Figs. S1 and S3). On the other hand, these compounds acted as GR and AR antagonists, being able to decrease transcriptional activity at least below 40% and 80% of stimulated control, respectively (Table 1, Figs. S2 and S4).

Combination of moieties at positions C-17 and C-21 was found crucial for the rest of the compounds. Compounds bearing long unsaturated chain (12 and 13) acted as both GR agonists and antagonists and weak AR agonists (Figs. S1-S4). Combination of shorter C-21 butylcarbamate chain with 17 α -acetate substituent yielded in compound 11 (with similar AR and GR antagonist activity as was observed in 16 and 17 (C-21 carbamates)). On the other hand, compounds 14 (17 α -butyrate-

21-diethylcarbamate) and 15 (17 α -butyrate-21-butylcarbamate) with longer 17 α -ester carbon chain were potent AR and GR antagonists (Table 1, Figs. S2 and S4), with similar activities compared to standards.

Antagonist activities of compounds towards AR reached up low micromolar values (IC_{50} = 3.96 μ M and 11.38 μ M for 14 and 15, respectively), comparable to values obtained for standards, i.e. enzalutamide (IC_{50} = 3.32 μ M) and galeterone (IC_{50} = 7.59 μ M). Moreover, antagonist activities of compounds towards GR reached up single-digit micromolar values (IC_{50} = 4.44 μ M and 8.11 μ M for 14 and 15, respectively), weaker than for standard mifepristone (IC_{50} = 0.59 μ M) (Fig. 2). No clear agonist activity with dose-dependent manner was observed for compounds 14 and 15 neither towards the AR, nor the GR (Figs. S1 and S2).

2.3. The effect of compounds on proliferation and colony formation of PCa cells

Antiproliferative properties of all novel derivatives (Table 2) were tested in four PCa cell lines, namely LAPC-4 (expressing both AR and GR) and C4-2 (expressing only AR) originated from lymph node metastatic lesions, 22Rv1 (expressing both AR and GR) from sample of primary PCa and DU145 (AR-negative and GR overexpressing) originated from brain metastatic lesion. (see expression pattern of receptors in Fig. S5).

Hydrocortisone and its 17 α -monoesters (7-10) did not exhibit any antiproliferative activities, which is consistent with AR and GR agonist potency of these compounds [24,25]. Similarly, compounds 12 and 13, which acted as both GR and AR weak agonists, did not decrease the proliferation potential, except of the derivative 12 in LAPC-4, which was not probably connected with AR or GR. Derivatives which were found to be weak AR antagonists and GR dualist (16, 17 and 11) did not exert similar antiproliferative activities, only 17 decreased the viability below 90% in all AR-positive PCa cell lines. Antiproliferative activities of the most potent derivatives 14 and 15 displayed mid-micromolar values (GI_{50} 25 μ M - 40 μ M upon treatment for 72 h, curves shown in Fig. S6) in

Table 1

The ability of compounds to effect the transcriptional activities of AR and GR receptors in the presence of 1 nM R1881 and 100 nM dexamethasone, respectively (antagonist mode).^a

Compound	Transcriptional activity (% ± SD)					
	Androgen receptor			Glucocorticoid receptor		
	30 μM	10 μM	3.33 μM	30 μM	10 μM	3.33 μM
7	> 100	> 100	> 100	68.1 ± 6.7	79.8 ± 0.1	77.6 ± 2.1
8	> 100	> 100	> 100	75.7 ± 4.8	78.1 ± 0.6	78.9 ± 1.9
9	> 100	> 100	> 100	76.4 ± 0.4	85.4 ± 3.5	93.1 ± 0.5
10	> 100	> 100	> 100	87.2 ± 1.8	78.4 ± 8.5	91.4 ± 3.5
11	79.2 ± 10.4	88.9 ± 7.3	90.8 ± 11.3	39.0 ± 0.3	46.8 ± 2.3	53.9 ± 0.6
12	89.0 ± 7.8	> 100	> 100	50.7 ± 2.0	57.4 ± 1.0	67.8 ± 9.8
13	> 100	> 100	> 100	54.7 ± 0.8	69.4 ± 2.3	77.2 ± 1.1
14	20.5 ± 1.2	32.7 ± 2.6	52.5 ± 4.9	16.9 ± 1.5	27.6 ± 1.4	59.4 ± 6.7
15	17.6 ± 1.7	55.9 ± 0.7	87.3 ± 3.8	22.7 ± 0.1	42.9 ± 2.2	77.4 ± 0.7
16	63.6 ± 4.8	80.8 ± 1.2	89.3 ± 1.9	33.2 ± 3.9	42.8 ± 2.6	65.7 ± 8.3
17	75.8 ± 3.3	88.5 ± 4.4	89.3 ± 4.0	31.4 ± 4.3	37.0 ± 1.8	55.5 ± 1.7
galeterone	18.7 ± 3.7	37.6 ± 5.9	64.6 ± 7.3	56.3 ± 5.5	67.9 ± 1.2	82.8 ± 1.5
enzalutamide	18.7 ± 1.8	28.6 ± 5.4	47.6 ± 1.5	70.4 ± 0.9	83.1 ± 8.1	87.9 ± 1.2
mifepristone	12.6 ± 2.0	26.1 ± 0.1	41.2 ± 2.9	n.t.	n.t.	19.1 ± 3.7

n.t. not tested.

^a Tested compounds were competing with standard agonists. In case of AR, 22Rv1-ARE14 cells were treated by 1 nM R1881 and concentration doses of studied compounds in CSS medium (without other steroids). In case of GR, AZ-GR cells were treated by 100 nM dexamethasone and concentration doses of studied compounds in CSS medium. Transcriptional activity of AR and GR was normalised to 1 nM R1881 and 100 nM dexamethasone, respectively. Measured in duplicate and repeated at least twice.

all AR-positive PCa cells, comparable with standards galeterone (AR antagonist) and mifepristone (GR antagonist). Compound 14 was the only one which reached measurable $GI_{50} = 80 \mu\text{M}$ in AR-negative DU145 cells (Fig. S6).

Considering the mild antiproliferative activity of compounds, connected with low acute toxicity, we performed colony formation assay (CFA) to assess the prolonged antiproliferative potency of compounds 14 and 15 in 22Rv1, LAPC-4 and DU145.

As shown in Fig. 3, both compounds were able to significantly inhibit formation of cell colonies in a dose dependent manner after 10 days of treatment in AR-positive cell lines 22Rv1 and LAPC-4. In these cell lines, galeterone exhibited stronger effect than mifepristone, which corresponds with the antiproliferative activity in 72 h treatment. On the other hand, candidate compounds displayed weaker effect on colony formation inhibition in AR-negative DU145, in which mifepristone was slightly more potent than galeterone. Generally, compound 14 exhibited strong colony-formation inhibition in AR-positive PCa cell lines, comparable with standard galeterone, but weaker colony-formation inhibition in AR-negative and GR-overexpressing PCa cell line, compared to both galeterone and mifepristone.

It has been proposed and shown that GR upregulation and transcriptional activity could be a possible mechanism of resistance to anti-AR therapy in CRPC, bypassing AR blockade [28]. Possible explanation

is related with the observation that long-term androgen deprivation and/or androgen receptor inhibition (by abiraterone or enzalutamide) leads to significantly increased GR expression [5–7]. Therefore, we

Table 2

Viability of PCa cells upon treatment with 40 μM compounds for 72 h assessed by resazurin viability assay.^a

Compound	Viable cells (% ± SD)			
	22Rv1	C4-2	LAPC-4	DU145
7	96.3 ± 3.5	93.4 ± 3.7	99.4 ± 2.9	89.1 ± 11.7
8	97.2 ± 2.8	91.1 ± 2.4	99.9 ± 3.1	89.2 ± 13.1
9	95.5 ± 4.2	91.0 ± 3.0	98.6 ± 2.1	88.9 ± 11.8
10	96.4 ± 4.7	88.5 ± 2.3	95.4 ± 2.3	89.3 ± 12.0
11	91.7 ± 1.2	81.8 ± 2.1	91.9 ± 1.9	98.3 ± 4.9
12	85.1 ± 1.9	81.9 ± 7.9	38.6 ± 2.8	94.5 ± 7.4
13	97.6 ± 1.7	91.0 ± 7.8	64.9 ± 4.1	91.3 ± 7.4
14	34.8 ± 6.6	32.8 ± 6.2	29.0 ± 3.4	94.8 ± 3.1
15	54.9 ± 4.0	52.6 ± 1.7	52.4 ± 1.4	90.6 ± 9.5
16	93.4 ± 3.2	71.9 ± 5.4	86.5 ± 0.4	96.4 ± 6.9
17	79.6 ± 3.4	65.0 ± 3.8	85.3 ± 2.1	93.2 ± 9.9
galeterone	52.7 ± 7.4	10.5 ± 6.5	35.9 ± 4.6	84.2 ± 7.8
mifepristone	45.5 ± 6.8	77.8 ± 1.5	97.1 ± 5.3	15.7 ± 2.0
enzalutamide	> 100	98.7 ± 0.8	73.9 ± 1.0	92.8 ± 1.5

^a Measured in duplicate and repeated at least twice.

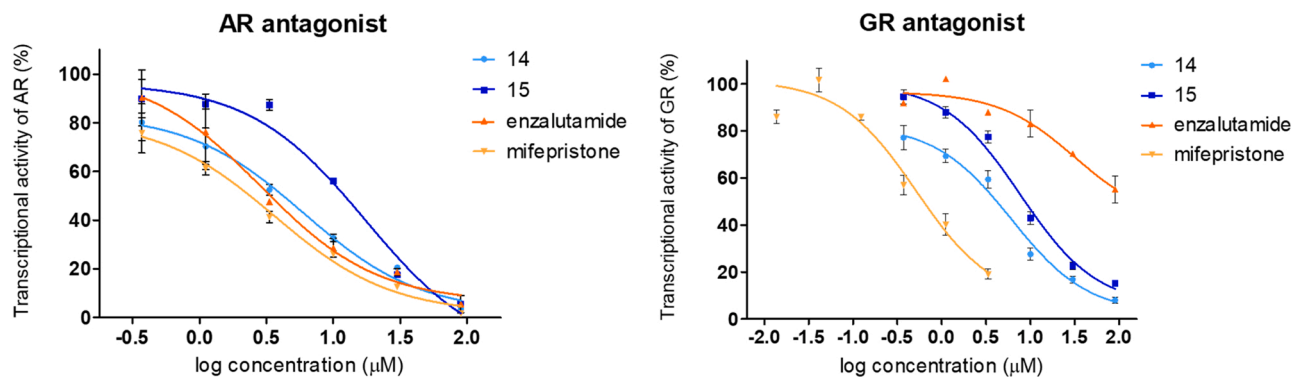


Fig. 2. Transcriptional activity of AR and GR upon treatment with compounds 14 and 15 along with standards enzalutamide and mifepristone in antagonist mode (competition with standard agonists 1 nM R1881 (AR) or 100 nM dexamethasone (GR)). Curves were plotted via non-linear curve fit in GraphPad Prism 5 from $n = 4$, error bars represent SD.

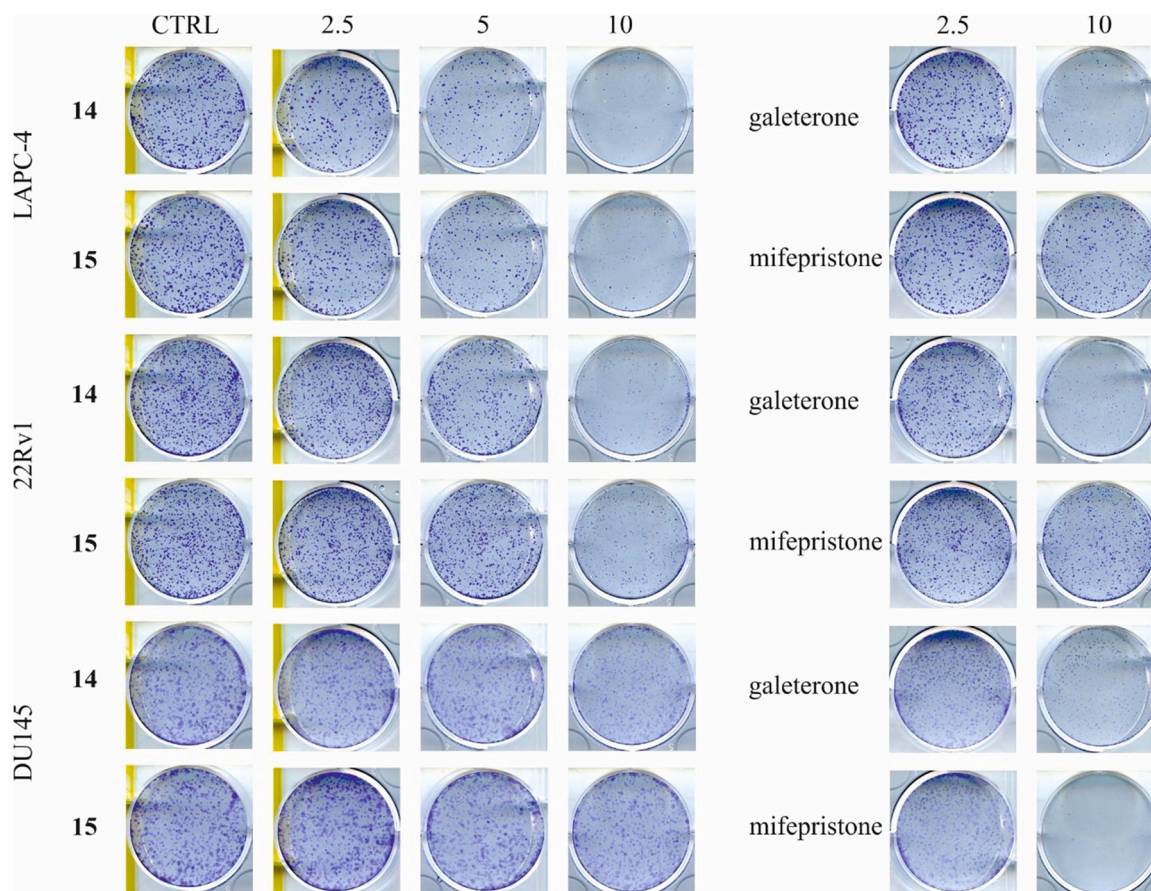


Fig. 3. Colony formation assay of PCa cells. Cells were treated with indicated concentrations of novel compounds or standards (μM) for 10 days. Medium was replaced by fresh medium with compound after 5 days. Upon treatment, cells were fixed, stained with crystal violet and photograph was captured. Representative result from two replicates is shown.

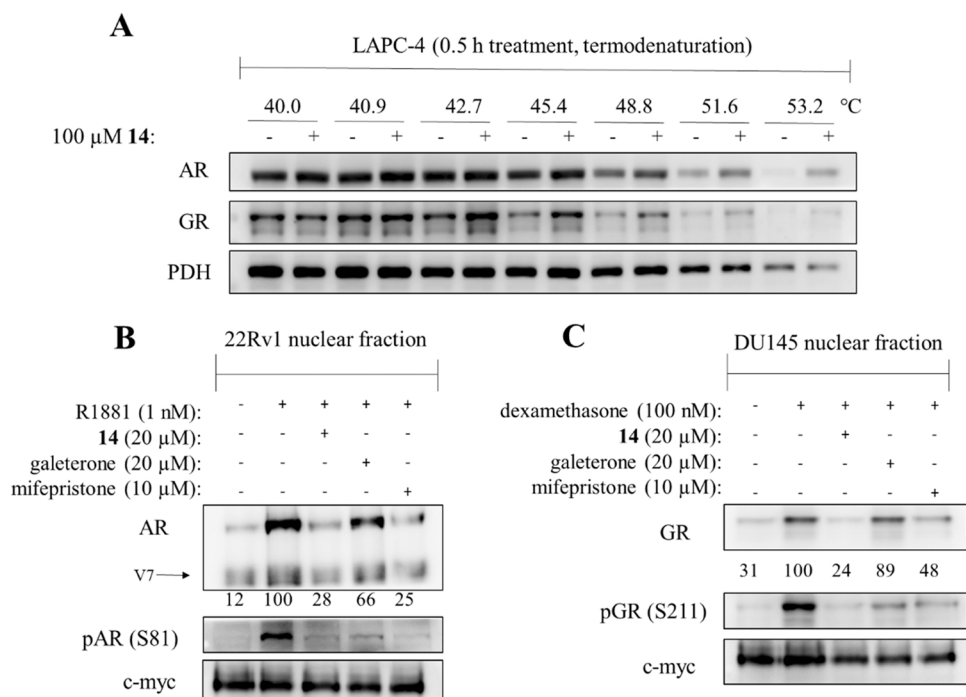


Fig. 4. (A) Western blotting analysis showing the level of soluble AR, GR and PDH after indicated heating of LAPC-4 cells without (-) or upon treatment (+) with 100 μM 14. PDH level was used as a control of equal protein loading. (B) AR, its phosphorylated form on S81 and GR distribution in 22Rv1 cells and (C) GR and its phosphorylated form in S211 distribution in DU145 cells. The cells were deprived of steroids by cultivation in charcoal stripped serum (CSS) medium for 24 h and then treated with (B) 1 nM R1881 and (C) with 100 nM dexamethasone alone or in combination with 20 μM 14, 20 μM galeterone or 10 μM mifepristone for additional 24 h. Cellular fractions were isolated using the incubation with different detergents in buffers and subjected for immunoblot analysis of appropriate proteins. Nuclear protein c-myc was used as control of equal protein loading. Quantification was performed using Multigauge 3.0 software. Representative result from two replicates is shown.

examined the effect of candidate compounds **14** and **15** in the same cell lines after 3 days and 7 days of treatment, but we did not observe significant increase in GR or AR levels in those periods (Fig. S7). Moreover, the treatment with enzalutamide clearly lead to the increase in GR protein level, already upon 3 and 7 days, while combination with lead compound **14** reduced this increase. There was no clear activation of apoptosis observed after 3 or 7 days of treatment (Fig. S7).

Since the lead compound did not display high toxicity upon 72 h treatment, we analogously evaluated the antiproliferative effects of compound **14** alone and in combination with enzalutamide using CFA for 7 days in LAPC-4 and 22Rv1. The lead compound displayed higher antiproliferative effect than standard enzalutamide and both these compounds were more potent in LAPC-4, compared with 22Rv1. The combination of **14** with enzalutamide displayed slightly higher antiproliferative activity in LAPC-4 but profound decrease in viability of 22Rv1, mainly in 10 μ M concentrations (Fig. S8).

2.4. The effect of **14** on thermal stability and localisation of AR and GR

Further, the thermal stability of AR and GR was analysed in LAPC-4 (expressing both AR and GR) PCa cells. Compound **14** was proven to increase the thermal stability of both AR and GR in 100 μ M concentration (high concentration according to the short treatment, corresponding with literature ([29–31]), which should be connected with extensive interaction with both nuclear receptors (Fig. 4A). There was no obvious thermal stabilisation of pyruvate dehydrogenase (PDH), which can serve as loading control.

Further, we investigated the ability of **14** to block the transport, accumulation and phosphorylation of AR or GR in nucleus in R1881-stimulated 22Rv1 cells and in dexamethasone-stimulated DU145 cells, respectively. As shown in Fig. 4B,C candidate compound **14** significantly decreased translocation of both receptors to nucleus and their activating phosphorylation level in comparison to hormone activated cells, as well as standards galeterone and mifepristone did [32–34].

2.5. The effect of **14** on the downstream signalling of AR and GR and on the cell cycle

We showed that compounds **14** and **15** are able to reduce AR a GR transcriptional activity in a dose-dependent manner and to inhibit colony formation of investigated PCa cell lines. We further analysed whether candidate compounds can affect the protein expression of well-known AR transcriptional targets, namely PSA and Nkx3.1 and GR transcriptional targets SGK-1 and 11- β -HSD2. Immunoblotting analysis in LAPC-4 (Fig. 5A) revealed that while the expression of AR on protein level was markedly stimulated by R1881, both compounds diminished the R1881-stimulated AR activation (monitored as phosphorylation on S81 and PSA and Nkx3.1 activation). Interestingly we observed slight decrease in the expression of total AR in 20 μ M concentration, whereas

GR level remained unchanged. All trends are in agreement with AR-transcriptional assay and are comparable with results observed for galeterone. The effect of the two investigated compounds was nearly identical in 22Rv1 (Fig. S9). Analysis of DU145 (Fig. 5B) revealed that activating phosphorylation of GR on S211 was blocked by 20 μ M **14**, comparable with mifepristone while the expression of GR did not change significantly. The most pronounced decrease in the protein levels of 11- β -HSD2 and SGK-1 (known GR substrates) was observed upon treatment with 20 μ M **14** and corresponded with results with mifepristone.

Next, we have evaluated whether the effect of the lead compound **14** on the cell cycle is consistent with the blockage of AR signalling [35,36]. Evaluation of the cell cycle distribution upon 48 h treatment with compound **14** was performed in 22Rv1 and LAPC-4 cell lines. The effect of compound **14** observed after 24 h was negligible (not shown) and consistent to enzalutamide and mifepristone treatment. However, prolonged 48 h treatment revealed decrease in S-phase population of treated cells that was compensated by increased number of cells in the G1-phase of the cell cycle (Fig. S10).

2.6. Molecular docking of compound **14** into the ligand-binding domain (LBD) of GR and AR

To prove the binding of the candidate compound, we recruited molecular docking into the LBD of antagonistic model of studied nuclear receptors. For GR, an X-ray structure with antagonist mifepristone (PDB ID: 1NHZ) [37] was used to model and compare the interaction with candidate compound. In the best binding pose **14** is bound in the similar way as mifepristone but showed stronger binding energy ($\Delta G_{\text{vina}} = -11.5$ kcal/mol and -10.8 kcal/mol, respectively) (Fig. 6A, B). The steroid core of candidate compound is held in place by interaction with hydrophobic residues that outline the cavity (Leu566, Leu608, Phe623, Leu733, Phe737). Conserved direct hydrogen bonds from the 3-carbonyl oxygen in the A-ring of the steroid core to Gln570 and Arg611 orient the steroid. At the other side, the C20-keto group (in comparison with 17 β -hydroxyl group of mifepristone) makes a hydrogen bond to Gln-642. Additional hydrogen bonds are formed between the 11 β -hydroxy group of the steroid core and the backbone carbonyl group of Leu-563 and between keto group of C21-carbamoyl moiety and Asn-564 (Fig. 6A) (analogous with interactions of hydrocortisone). Interestingly, the 21-(*N,N*-diethylcarbamoyloxy) chain forms extensive hydrophobic bonds and is orientated in the same direction as dimethylaniline side chain of mifepristone (Fig. 6A, B).

In case of AR, there is no antagonist-bound wild type-crystal structure yet available, which complicates the modelling or screening for antagonists. Recently, molecular dynamics simulations led to generation of antagonist AR models based on X-ray structures of T877A and W741L mutants with bound antagonists and agonists [38]. To compare the binding of candidate compound **14**, wild type-antagonist model with expanded binding cavity based on the structure of cyproterone acetate

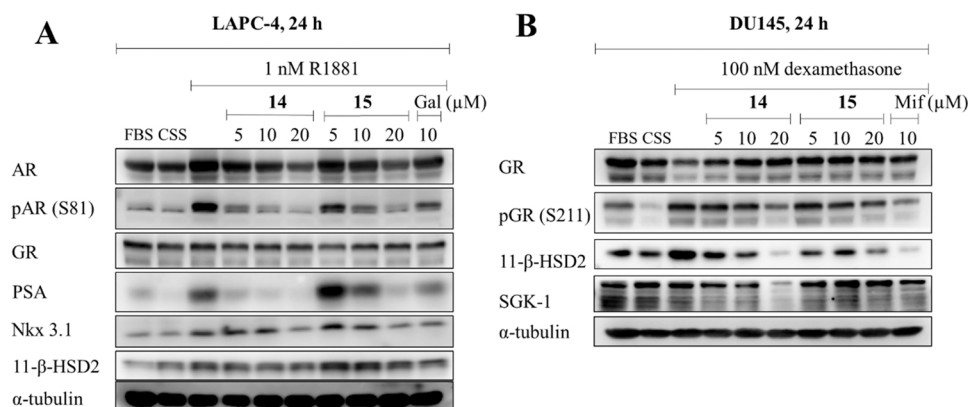


Fig. 5. Western blotting analysis of AR- and GR-regulated proteins in treated LAPC-4 (A) and DU145 (B). The cells were deprived of steroids (cultivated in CSS medium) for 24 h and then treated with 1 nM R1881 (A, LAPC-4) or 100 nM dexamethasone (B, DU-145) alone or in combination with different concentrations of candidate compounds **14** and **15** or 10 μ M standards galeterone (Gal) or mifepristone (Mif) for 24 h. Alpha-tubulin was control of equal protein loading. Representative result from two replicates is shown. FBS, foetal bovine serum; CSS, charcoal stripped serum (no androgens).

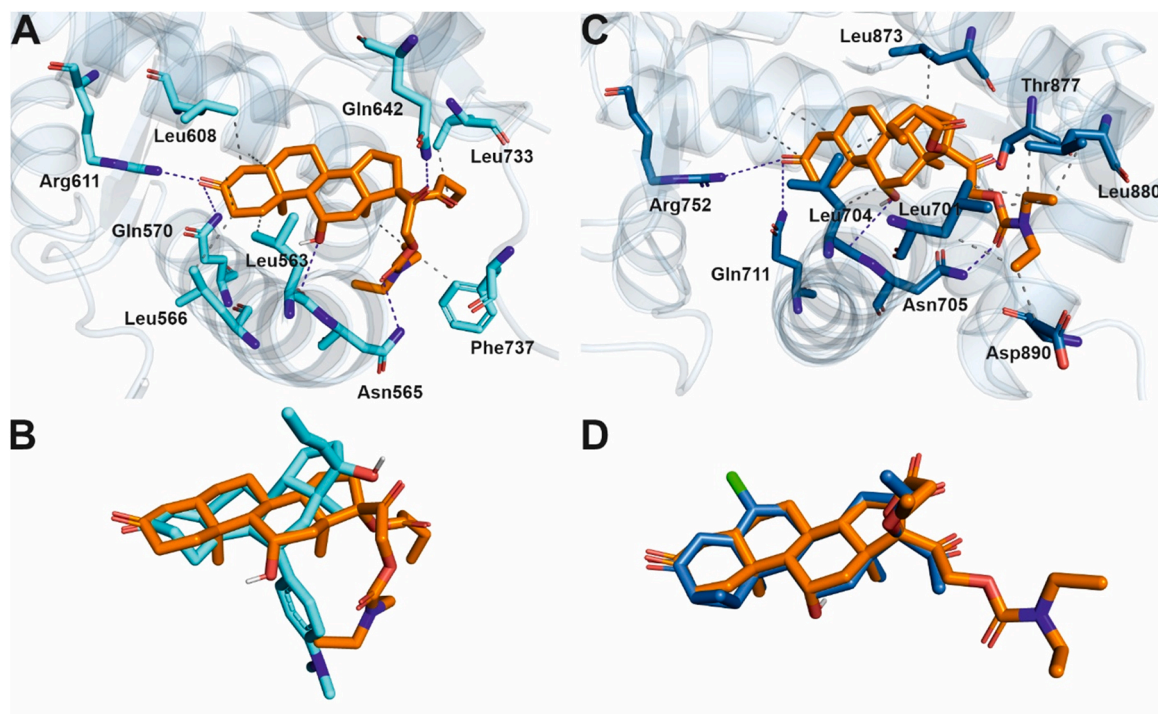


Fig. 6. (A) Model of the binding pose of compound **14** (orange) in GR-LBD and (B) alignment of binding pose with mifepristone (cyan) in PDB:1NHZ. (C) Model of the binding pose of compound **14** (orange) in AR-LBD and (D) alignment of binding pose with cyproterone acetate (blue) in AR-antagonist model [39]. Binding poses of the lead compound **14** was modelled based on rigid docking into appropriate crystal structures. Sticks represent interacting amino acid residues of nuclear receptors. Nitrogen heteroatoms are shown in blue, oxygen atoms in red, chloride atom in green. Hydrophobic interactions are shown with grey dash lines and hydrogen bonds are shown with blue dash lines.

bound to AR-T877A (PDB ID: 2OZ7) [39] was used.

Molecular docking of compound **14** into the AR-antagonist model revealed the same binding as cyproterone (Fig. 6C, D) with similar binding energy ($\Delta G_{\text{vina}} = -12.5$ kcal/mol and -12.1 kcal/mol, respectively) and the same position of steroid core as in docking to GR. Key interaction residues in the AR LBD (Arg752 and Gln711) create a conserved hydrogen bonds with C3-keto group of steroid ligand and at the other extremity of the binding site, Thr877 and Asn705 form hydrogen bonds with keto groups on side chains. Compared to cyproterone, **14** forms an additional hydrogen bond with backbone carbonyl of Leu704 by 11β -hydroxy group of the steroid core (analogous with interaction in GR). In comparison to the binding pose in GR, flexible C-17 and C-21 side chains point out to the edge of LBD creating extensive hydrophobic interactions with Leu701, Leu880, Asp890 (Fig. 6C).

3. Discussion and conclusion

Both AR and GR showed to play pivotal role in pro-oncogenic processes in prostate cancer cells. GR agonists are often included in standard therapeutic regimens for their anti-inflammatory properties and for the ability to reduce toxic effects of cytostatic drugs during chemotherapy. A few studies described beneficial outcomes of glucocorticoid monotherapy in treatment of PCa accompanied by PSA decline and improved quality of life [9,40,41]. On the other hand, several clinical studies revealed their harmful, tumorigenic effect [6,42]. This emerging data are related with the observation of long-term androgen ablation or AR inhibition that leads to significantly increased GR expression [5,6,28]. Moreover, AR and GR share the same chromatin binding sites thus compensatory GR upregulation is considered as the way for long-lasting activation of AR specific pathways [32,33]. Based on studies on resistant PCa cell lines [6–8], it is evident that use of GR or dual AR/GR antagonist might have potential in AR-driven cancers, mainly in CRPC subtypes and in tumours resistant after AR-targeted therapy.

Recently, the initial outcome of a phase I/II trial combining enzalutamide and mifepristone in metastatic CRPC (NCT02012296) was published. The combination was safe and tolerable, however, showed no clinical benefit (indicated by time to PSA progression) [43]. On the other hand, there are two clinical trials ongoing, evaluating the combination of more selective GR antagonist relacorilant (CORT125281) in the combination with enzalutamide (NCT03674814, NCT03437941), which could uncover better clinical significance of dual AR/GR blockage.

Here, we described novel 17α - and/or 21 -ester or carbamate derivatives of hydrocortisone, a known GR agonist, that were evaluated for their biological activity towards androgen and glucocorticoid receptors in different prostate cancer cell lines. Within prepared compounds, some AR agonists were described, in agreement with previous publications, which showed that hydrocortisone alone is able to activate AR [24] and generally, that glucocorticoids can act as AR agonists depending on mutations in AR-ligand binding domain [26]. However, we focused on two 17α -butyryloxy, 21 -(alkyl)carbamoyloxy derivatives **14** and **15** that displayed strong antagonist properties towards both AR and GR confirmed using the transcriptional cell-based activity assay. Interaction with both nuclear receptors was confirmed by cellular-thermal shift assay and followed the previous studies showing thermal stabilisation of AR in the presence of AR modulators.

Antagonist's effect on cellular distribution of both receptors was reported as a common phenomenon in the evaluation of ligand efficacy, novel agents were capable to eliminate the AR translocation to nucleus and thus enhance AR degradation. We showed decreased translocation of AR to nucleus in the presence of studied compounds, as well as was for galeterone, which confirmed published data [32]. Compound **14** also markedly blocked the translocation of GR into nucleus, similarly to mifepristone [33,34].

Molecular docking analysis confirmed the binding of compound **14** in the GR in a manner similar to mifepristone, but with stronger binding energy. It was shown that the 21 -(*N,N*-diethylcarbamoyloxy) can form

extensive hydrophobic bonds and can be orientated in the same direction as dimethylaniline side chain of mifepristone (Fig. S7A, B), which is responsible of active antagonism, disrupting helix-12 position, thus preventing the receptor from recruiting a co-activator [37].

Antiproliferative activities of studied compounds displayed mid-micromolar values comparable with standards galeterone (AR antagonist) and mifepristone (GR antagonist) which both exerted presumed effects on corresponding cell lines. Enzalutamide had only slight effect on the proliferation of 22Rv1 and moderately decreased proliferation of LAPC-4, which is in agreement with modulation of AR-wild type and AR-H875Y by enzalutamide [27]. However, the combination of enzalutamide with **14** displayed increased antiproliferative activity in 22Rv1 and partly also in LAPC-4.

Development of enzalutamide-resistant cell lines leads to slightly increased GR expression in 22Rv1 and markedly increased GR expression in LAPC-4 *in vitro* [5]. More importantly, first changes leading to the resistance could be observed just in 7 days after the treatment with sub-lethal concentration of enzalutamide *in vitro* [5,7]. Our results showed that candidate compounds **14** and **15** did not cause significant increase in GR or AR levels during the same periods. Importantly, compound **14** was able to reduce the enzalutamide-induced GR upregulation upon 3 and 7 days treatment.

Further, biologically active glucocorticoids possess an 11 β -OH moiety, which normally undergoes an oxidation by 11 β -HSD2 (11 β -OH \rightarrow 11-keto), an enzyme responsible for its inactivation and subsequent storage in the endoplasmic reticulum. Resistant tumours frequently lose the 11 β -HSD2 [44] (observed also upon enzalutamide treatment [45]), which allows upregulated glucocorticoids to activate the GR and drive the resistance. We speculate that simultaneous blockage of AR and GR would prevent the GR overexpression and 11 β -HSD2 loss. Based on the importance of active glucocorticoids in resistance it would be plausible to evaluate the effect of novel derivatives on the glucocorticoids' metabolism.

In summary, the understanding and mechanism, which leads to the PCa tumour growth and resistance to AR antagonists is crucial for further CRPC treatment. Many different mechanisms of resistance have been described, and e.g. the GR signalling has been recognised as an endocrine-mediated way to turn on the pro-survival signalling after AR-antagonism treatment. Overall, our findings support the development and deep characterisation of dual AR and GR antagonists as anticancer agents in PCa cases with upregulation of GR activity. Therefore, described derivatives will be evaluated in PCa cell lines models resistant to the second-generation AR antagonists, further, in *ex vivo* model of tissue slices of PCa tumours along with the organoids from PCa biopsies.

4. Experimental

4.1. General chemistry

Melting points (Mp) were determined on a Kofler block and are uncorrected. Specific rotations were measured in CHCl₃ (c 1) at 20 °C with a POLAMAT-A (Zeiss-Jena) polarimeter and are given in units of 10⁻¹ deg cm² g⁻¹. Reactions were monitored by thin-layer chromatography (TLC) on Kieselgel-G (Si 254 F, Merck KGaA, Darmstadt, Germany) layers (0.25 mm thick); solvent systems (ss): (A) isopropyl ether, (B) acetone/toluene/hexane (30:35:35 v/v). The spots were detected by spraying with 5% phosphomolybdic acid in 50% aqueous phosphoric acid. The R_f values were determined for the spots observed by illumination at 254 and 365 nm. Flash chromatography: Merck silica gel 60, 40–63 μ m (Merck KGaA, Darmstadt, Germany). Elementary analysis data were determined with a PerkinElmer CHN analyser model 2400 (PerkinElmer Inc, Waltham, MA, USA). All solvents were distilled prior to use. NMR spectra were recorded on a Bruker DRX 500 instrument at 500 (¹H NMR) or 125 MHz (¹³C NMR) and these are included in [Supplementary Information](#). Chemical shifts are reported in ppm (δ scale), and coupling constants (*J*) are given in Hertz. For the determination of

multiplicities, the *J*-MOD pulse sequence was used. The purity of all synthesised compounds was determined by HPLC (Acquity UPLC® H-Class System, Waters; Symmetry C18 column; 5 μ m, 150 \times 2.1 mm) coupled to Acquity QDa mass spectrometry detector (Waters).

4.2. General method for synthesis of hydrocortisone 17 α -esters (8–10)

A solution of hydrocortisone (**7**) (3.62 g, 10 mmol) in benzene (200 ml), containing pyridinium-*p*-toluenesulfonate (125 mg, 0.5 mmol) was heated to boiling point for a few minutes. To the hot reaction mixture, the corresponding short chain alkyl orthoester (two equivalent) was added. After a brief distillation of benzene (50 ml), the reaction was monitored by TLC (ss A). After 30 min the starting compound disappeared and the formation of 17 α ,21-orthoester of hydrocortisone was complete. After addition of pyridine (1 ml), the solvents were evaporated *in vacuo*. The residual oil was dissolved in methanol (150 ml), and 0.1 N acetic acid (50 ml) and 0.1 N NaOAc solution (5 ml) were added. The reaction mixture was refluxed for 20 min and then was diluted with water and extracted with CH₂Cl₂. The CH₂Cl₂ solution was washed with NaHCO₃ solution and then with water, dried and evaporated. The residual oil was purified by column chromatography on silica gel with ethyl acetate/CH₂Cl₂ (2:98 v/v%) as eluent.

4.2.1. 17 α -Acetoxy-11 β ,21-dihydroxypregn-4-ene-3,20-dione (**8**)

Compound **7** (3.62 g, 10 mmol) and triethyl orthoacetate (3.24 g, 20 mmol) were used for the synthesis as described in [Section 4.2](#). The crude product was chromatographed on silica gel with ethyl acetate/CH₂Cl₂ (2:98 v/v%) to yield pure **8** (3.58 g, 88%). Mp.: 232–234 °C, (234–237 °C [12]), R_f = 0.45 (ss B), [α]_D²⁰ + 62 (c 1 in CHCl₃). Found: C, 68.46; H, 8.06. C₂₃H₃₂O₆ (404.50) requires: C, 68.29; H, 7.97%. ¹H NMR (CDCl₃, 500 MHz): δ 0.94 (s, 3 H, 18-H₃), 1.44 (s, 3 H, 19-H₃), 2.06 (s, 3 H, Ac-H₃), 3.07 (brs, 1 H, OH), 4.25 (d, 1 H, *J* = 18.5 Hz, 21-H₂), 4.29 (d, 1 H, *J* = 18.0 Hz, 21-H₂), 4.49 (d, 1 H, *J* = 3.5 Hz, 11-H), 5.69 (s, 1 H, 4-H). ¹³C NMR (CDCl₃, 125 MHz): δ 16.9 (C-18), 21.2 (C-19), 24.1 (C-15), 30.5, 31.5 (C-8 and Ac-Me), 32.1, 32.7, 34.0, 35.1, 39.3, 40.2, 47.1 (C-13), 52.4 (C-14), 56.0 (C-9), 67.4 (C-21), 68.3 (C-11), 93.5 (C-17), 122.7 (C-4), 170.7 (Ac-C=O), 171.7 (C-5), 199.5 (C-3), 206.5 (C-20). HPLC/MS purity – 94.9%.

Continued elution with ethyl acetate/CH₂Cl₂ (10:90 v/v%) resulted the starting compound **7** (250 mg, 7%). ¹H NMR (DMSO-d₆, 500 MHz): δ 0.75 (s, 3 H, 18-H₃), 1.36 (s, 3 H, 19-H₃), 4.08 (dd, 1 H, *J* = 5.5 Hz, *J* = 19.0 Hz, 21-H₂), 4.25 (brs, 2 H, 17 α -OH and 21-OH), 4.50 (dd, 1 H, *J* = 6.0 Hz, *J* = 19.0 Hz, 21-H₂), 4.60 (t, 1 H, *J* = 6.0 Hz, 11-H), 5.15 (brs, 1 H, 11-OH), 5.56 (s, 1 H, 4-H). ¹³C NMR (DMSO-d₆, 125 MHz): δ 16.9 (C-18), 20.4 (C-19), 23.3 (C-15), 31.2 (C-8), 31.4, 32.8, 32.9, 33.4 (C-16), 34.0, 38.8, 39.0, 46.3 (C-13), 51.5 (C-14), 55.5 (C-9), 65.8 (C-21), 66.4 (C-11), 88.4 (C-17), 121.4 (C-4), 172.3 (C-5), 198.0 (C-3), 211.5 (C-20). HPLC/MS purity – 97.2%.

4.2.2. 11 β ,21-Dihydroxy-17 α -propionyloxy-pregn-4-ene-3,20-dione (**9**)

Compound **7** (3.62 g, 10 mmol) and triethyl orthopropionate (3.52 g, 20 mmol) were used for the synthesis as described in [Section 4.2](#). The crude product was crystallised from a mixture of acetone/hexane to afford **9** (2.96 g, 70%). Mp.: 203–205 °C, (201–203 °C [13]), R_f = 0.42 (ss B), [α]_D²⁰ + 55 (c 1 in CHCl₃). Found: C, 68.46; H, 7.98. C₂₄H₃₆O₆ (418.53) requires: C, 68.88; H, 8.19%. ¹H NMR (CDCl₃, 500 MHz): δ 0.94 (s, 3 H, 18-H₃), 1.12 (t, 3 H, *J* = 7.5 Hz, ω -H₃), 1.44 (s, 3 H, 19-H₃), 4.24 (d, 1 H, *J* = 18.5 Hz, 21-H₂), 4.34 (d, 1 H, *J* = 18.5 Hz, 21-H₂), 4.49 (s, 1 H, 11-H), 5.69 (s, 1 H, 4-H). ¹³C NMR (CDCl₃, 125 MHz): δ 9.0 (ω -Me), 17.0 (C-18), 21.2 (C-19), 24.1 (C-15), 27.8, 30.6, 31.5 (C-8), 32.1, 32.8, 34.0, 35.2, 39.4, 40.3, 47.2 (C-13), 52.5 (C-14), 56.0 (C-9), 67.3 (C-21), 68.3 (C-11), 93.2 (C-17), 122.7 (C-4), 171.7 (C-5), 174.1 (Ac-C=O), 199.5 (C-3), 206.5 (C-20). HPLC/MS purity – 96.8%.

4.2.3. 17 α -Butyryloxy-11 β ,21-dihydroxypregn-4-ene-3,20-dione (10)

Compound **7** (3.62 g, 10 mmol) and triethyl orthobutyrate (3.80 g, 20 mmol) were used for the synthesis as described in Section 4.2. The crude product was crystallised from a mixture of acetone/hexane to afford **10** (3.95 g, 91%). Mp.: 210–212 °C, (204–207 °C [14]), R_f = 0.40 (ss B), $[\alpha]_D^{20}$ + 43 (c 1 in CHCl₃). Found: C, 69.55; H, 8.12. C₂₅H₃₆O₆ (432.55) requires: C, 69.42; H 8.39%. ¹H NMR (CDCl₃, 500 MHz): δ 0.95 (t, 6 H, J = 5.0 Hz, 18-H₃ and ω -H₃), 1.44 (s, 3 H, 19-H₃), 4.24 (d, 1 H, J = 18.0 Hz, 21-H₂), 4.34 (d, 1 H, J = 18.0 Hz, 21-H₂), 4.49 (s, 1 H, 11-H), 5.69 (s, 1 H, 4-H). ¹³C NMR (CDCl₃, 125 MHz): δ 13.7 (ω -Me), 16.9 (C-18), 18.4 (CH₂-Me), 21.2 (C-19), 24.1 (C-15), 30.6, 31.5 (C-8), 32.1, 32.8, 34.0, 35.2, 36.3, 39.4, 40.3, 47.2 (C-13), 52.5 (C-14), 56.1 (C-9), 67.4 (C-21), 68.3 (C-11), 93.2 (C-17), 122.7 (C-4), 171.7 (C-5), 173.4 (Ac-C=O), 199.5 (C-3), 206.5 (C-20). HPLC/MS purity – 97.6%.

4.3. 21-(*N*-Butylcarbamoyloxy)-11 β ,17 α -dihydroxypregn-4-ene-3,20-dione (16)

Compound **7** (362 mg, 1 mmol) was dissolved in toluene (15 ml) and the solution was refluxed with butyl isocyanate (990 mg, 10 mmol) for 2 h. It was then diluted with hexane (100 ml) and the crystals that separated were filtered and washed with hexane. Recrystallisation from a mixture of acetone/hexane yielded **16** (390 mg, 84%). Mp.: 158–160 °C, R_f = 0.80 (ss B), $[\alpha]_D^{20}$ + 159 (c 1 in CHCl₃). Found: C, 67.82; H, 8.37. C₂₆H₃₉NO₆ (461.60) requires: C, 67.65; H, 8.52%. ¹H NMR (CDCl₃, 500 MHz): δ 0.93 (t, 3 H, J = 7.5 Hz, ω -H₃), 0.97 (s, 3 H, 18-H₃), 1.44 (s, 3 H, 19-H₃), 3.18 (dd, 2 H, J = 7.0 Hz, J = 13.5 Hz, N-H₂), 4.46 (s, 1 H, 11-H), 4.77 (d, 1 H, J = 17.5 Hz, 21-H₂), 4.92 (brs, 1 H, NH), 5.00 (d, 1 H, J = 17.5 Hz, 21-H₂), 5.68 (s, 1 H, 4-H). ¹³C NMR (CDCl₃, 125 MHz): δ 13.9 (ω -Me), 17.3 (C-18), 20.0 (N-CH₂), 21.2 (C-19), 23.8 (C-15), 31.6 (C-8), 32.0, 32.2, 32.9, 34.0, 34.6, 35.2, 39.4, 40.0, 41.1, 47.6 (C-13), 52.1 (C-14), 56.2 (C-9), 67.9 (C-21), 68.5 (C-11), 89.8 (C-17), 122.5 (C-4), 156.1 (amide C=O), 172.2 (C-5), 199.9 (C-3), 206.6 (C-20). HPLC/MS purity – 100%.

4.4. 21-(*N*-Cyclohexylcarbamoyloxy)-11 β ,17 α -dihydroxypregn-4-ene-3,20-dione (17)

Compound **7** (362 mg, 1 mmol) was dissolved in toluene (15 ml) and the solution was refluxed with cyclohexyl isocyanate (1.25 mg, 10 mmol) for 6 h. It was then diluted with hexane (100 ml) and the precipitate that separated was filtered and washed with hexane. The crude product was subjected to chromatographic separation on silica gel with CH₂Cl₂. Compound **17** eluted first (230 mg, 47%). Mp.: 198–201 °C, R_f = 0.75 (ss B), $[\alpha]_D^{20}$ + 98 (c 1, in CHCl₃). Found: C, 68.72; H, 8.66. C₂₈H₄₁NO₆ (487.63) requires: C, 68.97; H, 8.47%. ¹H NMR (CDCl₃, 500 MHz): δ 1.02 (s, 3 H, 18-H₃), 1.44 (s, 3 H, 19-H₃), 3.47 (m, 1 H, N-CH), 4.48 (s, 1 H, 11-H), 4.62 (d, 1 H, J = 15.0 Hz, 21-H₂), 4.87 (d, 2 H, J = 15.0 Hz, 21-H₂ and NH), 5.69 (s, 1 H, 4-H). ¹³C NMR (CDCl₃, 125 MHz): δ 16.5 (C-18), 21.2 (C-19), 24.0 (C-15), 24.9, 25.6, 30.7 (2 C), 31.5 (C-8), 32.1, 32.8, 33.3, 33.4, 34.0, 35.1, 39.4, 40.1, 47.1 (C-13), 50.3 (cyclohexyl CH), 52.3 (C-14), 56.0 (C-9), 67.5 (C-21), 68.3 (C-11), 94.5 (C-17), 122.6 (C-4), 155.0 (amide C=O), 172.0 (C-5), 200.0 (C-3), 200.5 (C-20). HPLC/MS purity – 100%.

Continued elution with CH₂Cl₂/ethyl acetate (98:2 v/v%) resulted in **7** (85 mg, 23%).

4.5. 17 α -Acetoxy-21-(*N*-butylcarbamoyloxy)-11 β -hydroxypregn-4-ene-3,20-dione (11)

Compound **8** (405 mg, 1 mmol) was solved in toluene (15 ml) and the solution was refluxed with butyl isocyanate (990 mg, 10 mmol) for 2 h. The solution was diluted with hexane (100 ml). The precipitate was collected by filtration and recrystallised from a mixture of acetone/hexane to obtain **11** (380 mg, 75%). Mp.: 115–118 °C, R_f = 0.80 (ss A), $[\alpha]_D^{20}$ + 79 (c 1 in CHCl₃). Found: C, 66.52; H, 8.37. C₂₈H₄₁NO₇ (503.64)

requires: C, 66.78; H, 8.21%. ¹H NMR (CDCl₃, 500 MHz): δ 0.91 (t, 3 H, J = 7.5 Hz, ω -H₃), 1.02 (s, 3 H, 18-H₃), 1.44 (s, 3 H, 19-H₃), 2.07 (s, 3 H, Ac-H₃), 3.19 (dd, 2 H, J = 6.5 Hz, J = 13.0 Hz, N-H₂), 4.48 (d, 1 H, J = 3.5 Hz, 11-H), 4.62 (d, 1 H, J = 17.0 Hz, 21-H₂), 4.90 (d, 1 H, J = 17.0 Hz, 21-H₂), 4.94 (brs, 1 H, NH), 5.69 (s, 1 H, 4-H). ¹³C NMR (CDCl₃, 125 MHz): δ 13.9 (ω -Me), 16.5 (C-18), 20.0 (N-CH₂), 21.2 (C-19), 21.4 (Ac-Me), 24.0 (C-15), 30.7, 31.5 (C-8), 32.0, 32.1, 32.8, 34.0, 35.1, 39.4, 40.1, 41.1, 47.1 (C-13), 52.5 (C-14), 56.0 (C-9), 67.6 (C-21), 68.3 (C-11), 94.6 (C-17), 122.6 (C-4), 155.8 (amide C=O), 171.0 (Ac-C=O), 172.0 (C-5), 199.6 (C-3), 200.4 (C-20). HPLC/MS purity – 98.6%.

4.6. 17 α -Acetoxy-11 β -hydroxy-21-((octyloxycarbonothioyl)oxy)pregn-4-ene-3,20-dione (12)

Compound **8** (405 mg, 1 mmol) was dissolved in anhydrous pyridine (5 ml) and chloro-thiocarbonic acid-octylester (312 mg, 1.5 mmol) was added dropwise cooling with ice. The reaction mixture was allowed to stand at room temperature for 6 h, and then was poured onto a mixture of ice (150 g) and H₂SO₄ (2 ml), and extracted with CH₂Cl₂. The CH₂Cl₂ solution was washed with NaHCO₃ solution and then with water, dried and evaporated. The residual oil was chromatographed on silica gel with CH₂Cl₂, yielding pure **12** (430 mg, 74%). Mp.: 140–141 °C, R_f = 0.80 (ss A), $[\alpha]_D^{20}$ + 93 (c 1, in CHCl₃). Found: C, 66.42; H, 8.14. C₃₂H₄₈O₇S (576.80) requires: C, 66.64; H, 8.39%. ¹H NMR (CDCl₃, 500 MHz): δ 0.88 (t, 3 H, J = 7.0 Hz, ω -H₃), 1.01 (s, 3 H, 18-H₃), 1.45 (s, 3 H, 19-H₃), 2.07 (s, 3 H, Ac-H₃), 2.84 (m, 2 H, O-H₂), 4.49 (s, 1 H, 11-H), 4.79 (d, 1 H, J = 16.5 Hz, 21-H₂), 4.98 (d, 1 H, J = 16.5 Hz, 21-H₂), 5.69 (s, 1 H, 4-H). ¹³C NMR (CDCl₃, 125 MHz): δ 14.2 (ω -Me), 16.6 (C-18), 21.2 (C-19), 21.3 (Ac-Me), 22.8 (CH₂-Me), 24.0 (C-15), 28.8, 29.2, 29.3, 29.7, 30.8, 31.4, 31.5 (C-8), 31.9, 32.1, 32.8, 34.0, 35.2, 39.4, 40.2, 47.2 (C-13), 52.4 (C-14), 56.0 (C-9), 68.3 (C-11), 69.4 (C-21), 94.3 (C-17), 122.6 (C-4), 170.9 (Ac-C=O), 171.6 (C=S), 171.8 (C-5), 198.5 (C-3), 199.5 (C-20). HPLC/MS purity – 98.3%.

4.7. 11 β -Hydroxy-21-((octyloxycarbonothioyl)oxy)-17 α -propionyloxy-4-ene-3,20-dione (13)

Compound **9** (418 mg, 1 mmol) was dissolved in anhydrous pyridine (5 ml) and chloro-thiocarbonic acid-octylester (312 mg, 1.5 mmol) was added dropwise cooling with ice. The reaction mixture was allowed to stand at room temperature for 6 h, and then was poured onto a mixture of ice (150 g) and H₂SO₄ (2 ml), and extracted with CH₂Cl₂. The CH₂Cl₂ solution was washed with NaHCO₃ solution and then with water, dried and evaporated. The residue was chromatographed on silica gel with CH₂Cl₂, yielding pure **13** (445 mg, 75%). Mp.: 139–141 °C, R_f = 0.82 (ss A), $[\alpha]_D^{20}$ + 90 (c 1, in CHCl₃). Found: 66.95; H, 8.32. C₃₃H₅₀O₇S (590.81) requires: C, 67.09; H, 8.53%. ¹H NMR (CDCl₃, 500 MHz): δ 0.88 (t, 3 H, J = 7.0 Hz, octyl ω -H₃), 1.01 (s, 3 H, 18-H₃), 1.45 (s, 3 H, 19-H₃), 2.84 (m, 2 H, O-H₂), 4.49 (d, 1 H, J = 3.0 Hz, 11-H), 4.77 (d, 1 H, J = 16.5 Hz, 21-H₂), 4.98 (d, 1 H, J = 16.5 Hz, 21-H₂), 5.69 (s, 1 H, 4-H). ¹³C NMR (CDCl₃, 125 MHz): δ 9.03 (Ac-Me), 14.2 (octyl ω -Me), 16.6 (C-18), 21.2 (C-19), 22.8 (CH₂-Me), 24.0 (C-15), 27.9, 28.8, 29.2, 29.3, 29.7, 30.8, 31.4, 31.5 (C-8), 31.9, 32.1, 32.8, 34.0, 35.2, 39.4, 40.3, 47.3 (C-13), 52.5 (C-14), 56.1 (C-9), 68.3 (C-11), 69.3 (C-21), 94.1 (C-17), 122.6 (C-4), 171.6 (Ac-C=O), 171.8 (C-5), 174.2 (C=S), 198.5 (C-3), 199.5 (C-20). HPLC/MS purity – 100%.

4.8. 17 α -Butyryloxy-21-(*N,N*-diethylcarbamoyloxy)-11 β -hydroxypregn-4-ene-3,20-dione (14)

Compound **10** (432 mg, 1 mmol) was dissolved in anhydrous triethyl amine (5 ml) and *N,N*-diethylcarbamoyl chloride (205 mg, 1.5 mmol) was added dropwise cooling with ice. The reaction mixture was allowed to stand at room temperature for 6 h, and then was poured onto a mixture of ice (150 g) and H₂SO₄ (2 ml), and extracted with CH₂Cl₂. The CH₂Cl₂ solution was washed with NaHCO₃ solution and then with water,

dried and evaporated. The residue was chromatographed on silica gel with CH₂Cl₂, yielding pure **14** (470 mg, 88%). Mp.: 159–160 °C, *R_f* = 0.75 (ss A), [α]_D²⁰ + 78 (c 1 in CHCl₃). Found: C, 67.52; H, 8.75. C₃₀H₄₅NO₇ (531.70) requires: C, 67.77; H, 8.53%. ¹H NMR (CDCl₃, 500 MHz): δ 0.96 (t, 3 H, *J* = 7.5 Hz, butyryl ω-H₃), 1.02 (s, 3 H, 18-H₃), 1.44 (s, 3 H, 19-H₃), 3.31 (m, 4 H, 2 x N-H₂), 4.48 (d, 1 H, *J* = 3.0 Hz, 11-H), 4.59 (d, 1 H, *J* = 16.5 Hz, 21-H₂), 4.93 (d, 1 H, *J* = 16.5 Hz, 21-H₂), 5.69 (s, 1 H, 4-H). ¹³C NMR (CDCl₃, 125 MHz): δ 13.6 (N-Me), 13.8 (butyryl ω-Me), 14.1 (N-Me), 16.4 (C-18), 18.5 (butyryl CH₂-Me), 21.1 (C-19), 23.9 (C-15), 30.7, 31.5 (C-8), 32.9, 34.0, 35.1, 36.6 (2 x N-CH₂), 39.4, 40.2, 41.8, 42.3, 47.2 (C-13), 52.7 (C-14), 56.1 (C-9), 67.8 (C-21), 68.3 (C-11), 94.7 (C-17), 122.6 (C-4), 155.4 (amide C=O), 173.5 (butyryl C=O), 172.1 (C-5), 199.6 (C-3), 200.2 (C-20). HPLC/MS purity – 100%.

4.9. 17α-Butyryloxy-21-(*N*-buthylcarbamoyloxy)-11β-hydroxypregn-4-ene-3,20-dione (**15**)

Compound **10** (432 mg, 1 mmol) was dissolved in toluene (15 ml) and the solution was refluxed with butyl isocyanate (990 mg, 10 mmol) for 2 h. The solution was diluted with hexane (100 ml). The precipitate was collected by filtration and recrystallised from a mixture of acetone/hexane to obtain **15** (410 mg, 77%). Mp.: 99–102 °C, *R_f* = 0.65 (ss A), [α]_D²⁰ + 86 (c 1 in CHCl₃). Found: C, 67.31; H, 8.65. C₃₀H₄₅NO₇ (531.69) requires: C, 67.77; H, 8.53%. ¹H NMR (CDCl₃, 500 MHz): δ 0.93 (m, 6 H, 2 x ω-H₃), 1.02 (s, 3 H, 18-H₃), 1.44 (s, 3 H, 19-H₃), 3.19 (m, 2 H, N-H₂), 4.48 (d, 1 H, *J* = 3.0 Hz, 11-H), 4.60 (d, 1 H, *J* = 17.0 Hz, 21-H₂), 4.80 (d, 1 H, *J* = 17.0 Hz, 21-H₂), 4.94 (brs, 1 H, NH), 5.69 (s, 1 H, 4-H). ¹³C NMR (CDCl₃, 125 MHz): δ 13.8 (2 x ω-Me), 16.5 (C-18), 18.5 (N-CH₂), 20.0 (butyryl CH₂-Me), 21.1 (C-19), 24.0 (C-15), 30.7, 31.5 (C-8), 32.0, 32.1, 32.9, 34.0, 35.1, 36.5, 39.4, 40.1, 41.1, 47.2 (C-13), 52.6 (C-14), 56.1, 67.6, 68.3, 94.3, 122.6, 155.9, 172.0, 173.5 (butyryl C=O), 199.6 (C-3), 200.4 (C-20). HPLC/MS purity – 100%.

4.10. Cell lines

The 22Rv1-ARE14 and AZ-GR reporter cell lines [24,25] were a kind gift from prof. Zdeněk Dvořák (Palacky University Olomouc, Czech Republic). 22Rv1, C4–2 and DU145 cell lines (all kindly gifted by dr. Jan Bouchal from Palacky University and University Hospital, Olomouc, Czech Republic) and 22Rv1-ARE14 were grown in RPMI-1640 medium. AZ-GR and LAPC-4 cells were grown in DMEM medium. All media were supplemented with 10% normal or charcoal-stripped foetal bovine serum (steroid-depleted serum), 100 IU/ml penicillin, 100 mg/ml streptomycin, 4 mM glutamine and 1 mM sodium pyruvate. Cells were cultivated in a humidified incubator at 37 °C and in 5% CO₂ atmosphere.

4.11. AR and GR-transcriptional luciferase assay

The Nunc™ MicroWell™ 96-well optical flat-bottom plate (Thermo Fisher Scientific) was used for luciferase assays, in which 22Rv1-ARE14 or AZ-GR cells were seeded (40,000 or 20,000 cells/well, respectively). The second day, the cultivation medium (supplemented with FBS) was discarded and cells were washed with PBS. Cells were then incubated in the absence or presence of analysed compounds dissolved in medium supplemented with CSS and 1 nM R1881 or 100 nM dexamethasone in case of 22Rv1-ARE14 or AZ-GR, respectively. Upon 24 h of incubation, cells were washed with PBS again and lysed for 10 min in a lysis buffer (10 mM Tris pH = 7.4, 2 mM DCTA, 1% nonidet P40, 2 mM DTT) at 37 °C. Next, reaction buffer (20 mM tricine pH = 7.8, 1.07 mM MgSO₄·7H₂O, 5 mM ATP, 9.4 mM luciferin) was added and the luminescence of the samples was measured using a Tecan M200 Pro microplate reader (Biotek). Assays were performed in duplicate.

4.12. Cell viability assay

In the viability assays, cells were seeded into the 96-well tissue culture plates. The other day, solutions of analysed compounds were added in different concentrations in duplicate for 72 h. Upon treatment, the resazurin solution (Sigma Aldrich) was added for 4 h, and then the fluorescence of resorufin was measured at 544 nm/590 nm (excitation/emission) using a Fluoroskan Ascent microplate reader (Labsystems). Percentual viability was calculated and in the separate experiment, GI₅₀ value was calculated from the dose response curves that resulted from the measurements using GraphPad Prism 5.

4.13. Colony formation assay

Prostate cancer cells 22Rv1 and DU-145 (2000 cells per well) or LAPC-4 (5000 cells per well) were seeded into 6-well plates. The other day, the medium was replaced with fresh medium containing different concentrations of the compounds. Media containing compounds were replaced once within 10 days. After the treatment, the medium was discarded and colonies were fixed with 70% ethanol for 15 min, washed with PBS and stained with crystal violet (1% solution in 96% ethanol) for 1 h. Finally, wells were washed with PBS and colonies' photograph was captured.

4.14. Cellular thermal shift assay

CETSA experiments were performed according to the general protocol [29]. LAPC-4 cells deprived of androgens (24 h in CSS-supplemented media) were harvested, washed twice with PBS and treated with **14** for 1 h at 37 °C in PBS with 5 mM glucose. After that, treated cells were washed with PBS, resuspended in fresh PBS with protease inhibitors and the suspension was aliquoted into PCR strips. Samples were heated at temperatures ranging from 40° to 53.2 °C for 3 min in CFX96 Touch Real-time PCR detection system (BioRad), before they were snap-frozen in liquid nitrogen. All samples were lysed by freeze-thaw using liquid nitrogen. Supernatants containing soluble proteins were obtained by centrifugation at 14,000 g for 30 min, and mixed with SDS-loading buffer, separated by SDS-PAGE and immunoblotted as described below.

4.15. Immunoblotting

After all treatments, cells were harvested by centrifugation, washed twice with PBS, pelleted and kept frozen at – 80 °C. Pellets were thawed, resuspended in ice-cold RIPA lysis buffer supplemented with phosphatase and protease inhibitors. Ultrasound sonication (10 s with 30% amplitude) of cells was performed on ice and soluble proteins in supernatants were obtained by centrifugation at 14,000 g for 30 min. Cellular fractionation experiments were performed using the Qproteome Cell Compartment Kit (Qiagen). Protein concentration in supernatants was measured and balanced within samples. Proteins were denatured by addition of SDS-loading buffer, separated by SDS-PAGE and electroblotted onto nitrocellulose membranes. Immunodetection of proteins was performed as usual, membranes were blocked in BSA solution, incubated overnight with primary antibodies, washed and incubated with secondary antibodies conjugated with peroxidase. Then, peroxidase activity was detected by SuperSignal West Pico reagents (Thermo Scientific) using a CCD camera LAS-4000 (Fujifilm). Primary antibodies purchased from Merck (anti-α-tubulin, clone DM1A; anti-phosphorylated AR (S81)). Primary antibodies purchased from Santa Cruz Biotechnology (anti-GR, clone G-5; anti-SGK-1, clone H-4; anti-11-β-HSD, clone C-9). Specific antibodies purchased from Cell Signalling Technology (anti-AR, clone D6F11; anti-PSA/KLK3, clone D6B1; anti-Nkx3.1, clone D2Y1A; anti-phosphorylated GR (S211); anti-c-myc, clone D3N8F; anti-PDH, clone C54G1; anti-caspase 9; anti-caspase 7; anti-rabbit secondary antibody (porcine anti-rabbit immunoglobulin

serum); anti-mouse secondary antibody (rabbit anti-mouse IgG, clone D3V2A)). All antibodies were diluted in 4% BSA and 0.1% Tween 20 in TBS.

4.16. Molecular docking

Molecular docking was performed with the crystal structure of GR-LBD with mifepristone (PDB ID:1NHZ) and AR-antagonist model [39]. The 3D structures of all compounds were obtained and their energy was minimised by molecular mechanics with Avogadro 1.90.0, a software used for the drawing and characterisation of chemical structures. Polar hydrogens were added to ligands and proteins with the AutoDock Tools program [46] and docking studies were performed using AutoDock Vina 1.05 [47]. Interaction between ligand and amino acid residues were modelled in PLIP software [48]. Figures were generated in Pymol ver. 2.0.4 (Schrödinger, LLC).

CRedit authorship contribution statement

Miroslav Peřina: Conceptualization, Investigation, Writing – original draft. **Anita Kiss:** Investigation, Visualization. **Erzsébet Mernyák:** Writing – review & editing. **Lukás Mada:** Validation. **Gyula Schneider:** Supervision. **Radek Jorda:** Conceptualization, Writing – review & editing, Supervision.

Declaration of Competing Interest

The authors declare that they have no known competing financial interests or personal relationships that could have appeared to influence the work reported in this paper.

Data availability

Data will be made available on request.

Acknowledgements

The authors gratefully acknowledge financial support from the Palacky University Olomouc (IGA_PrF_2022_007).

Appendix A. Supplementary material

Supplementary data associated with this article can be found in the online version at [doi:10.1016/j.jsmb.2023.106269](https://doi.org/10.1016/j.jsmb.2023.106269).

References

- [1] V. Dhiman, M. Bolt, K. White, Nuclear receptors in cancer — uncovering new and evolving roles through genomic analysis, *Nat. Rev. Genet.* 19 (2018) 160–174, <https://doi.org/10.1038/nrg.2017.102>.
- [2] M.T. Schweizer, E.Y. Yu, Persistent androgen receptor addiction in castration-resistant prostate cancer, *J. Hematol. Oncol.* 8 (2015) 128, <https://doi.org/10.1186/s13045-015-0225-2>.
- [3] N.G.R.D. Elshan, M.B. Rettig, M.E. Jung, Molecules targeting the androgen receptor (AR) signaling axis beyond the AR-Ligand binding domain, *Med. Res. Rev.* 39 (3) (2019) 910–960, <https://doi.org/10.1002/med.21548>.
- [4] D. Li, W. Zhou, J. Pang, Q. Tang, B. Zhong, C. Shen, L. Xiao, T. Hou, A magic drug target: androgen receptor, *Med. Res. Rev.* 39 (5) (2019) 1485–1514, <https://doi.org/10.1002/med.21558>.
- [5] M. Isikbay, K. Otto, S. Kregel, J. Kach, Y. Cai, D.J. Vander Griend, S.D. Conzen, R. Z. Szmulewitz, Glucocorticoid receptor activity contributes to resistance to androgen-targeted therapy in prostate cancer, *Horm. Cancer* 5 (2) (2014) 72–89, <https://doi.org/10.1007/s12672-014-0173-2>.
- [6] M. Pühr, J. Hoefler, A. Eigentler, C. Ploner, F. Handle, G. Schaefer, J. Kroon, A. Leo, I. Heidegger, I. Eder, Z. Culig, G. Van der Pluijm, H. Klocker, The glucocorticoid receptor is a key player for prostate cancer cell survival and a target for improved antiandrogen therapy, *Clin. Cancer Res.* 24 (4) (2018) 927–938, <https://doi.org/10.1158/1078-0432.CCR-17-0989>.
- [7] Z. Culig, Molecular mechanisms of enzalutamide resistance in prostate cancer, *Curr. Mol. Biol. Rep.* 3 (4) (2017) 230–235, <https://doi.org/10.1007/s40610-017-0079-1>.
- [8] J. Kroon, M. Pühr, J.T. Buijs, et al., Glucocorticoid receptor antagonism reverts docetaxel resistance in human prostate cancer, *Endocr. Relat. Cancer* 23 (1) (2016) 35–45, <https://doi.org/10.1530/ERC-15-0343>.
- [9] S. Sideris, F. Aoun, C.N. Martinez, S. Latifyan, A. Awada, G. Costante, T. Gil, Role of corticosteroids in prostate cancer progression: implications for treatment strategy in metastatic castration-resistant patients, *J. Endocrinol. Investig.* 39 (7) (2016) 729–738, <https://doi.org/10.1007/s40618-016-0430-z>.
- [10] S. Narayanan, S. Srinivas, D. Feldman, Androgen-glucocorticoid interactions in the era of novel prostate cancer therapy, *Nat. Rev. Urol.* 13 (1) (2016) 47–60, <https://doi.org/10.1038/nrurol.2015.254>.
- [11] M. Wu, Y. Xie, X. Cui, C. Huang, R. Zhang, Y. He, X. Li, M. Liu, S. Cen, J. Zhou, Rational drug design for androgen receptor and glucocorticoids receptor dual antagonist, *Eur. J. Med. Chem.* 166 (2019) 232–242, <https://doi.org/10.1016/j.ejmech.2019.01.036>.
- [12] L.W. Moreland, J.R. O'Dell, Glucocorticoids and rheumatic arthritis; back to the future? *Arthritis Rheum* 46 (2002) 2553–2563, <https://doi.org/10.1002/art.10567>.
- [13] H.J. Kooreman, A.F. Marx, D. vd Sijde, The synthesis of 17-ester of corticosteroids protection of 11 β -hydroxyl by the trimethylsilyl group, *Synth. Commun. Int. J. Rapid Commun. Synth. Org. Chem.* 1–2 (2013) 81–87, <https://doi.org/10.1080/00397917108081620>.
- [14] G. Celasco, L. Moro, R. Bozzella, P. Ferraboschi, L. Bartorelli, C. Quattrocchi, F. Nicoletti, Biological profile of corticosterone 17 α -propionate (CB-03-01), a new topical and peripherally selective androgen antagonist, *Arzneim. Forsch.* 54 (2004) 881–886, <https://doi.org/10.1055/s-0031-1297043>.
- [15] G. Celasco, L. Moro, R. Bozzella, P. Ferraboschi, L. Bartorelli, R. Di Marco, C. Quattrocchi, F. Nicoletti, Pharmacological profile of 9,11-dehydrocorticosterone 17 α -butyrate (CB-03-04), a new androgen antagonist with antagonistic activity, *Arzneim. Forsch.* 55 (2005) 581–587, <https://doi.org/10.1055/s-0031-1296908>.
- [16] M. Gold, Clascoterone cream (1%) topical androgen receptor inhibitor for the treatment of acne in patients 12 years and older, *Expert Rev. Clin. Immunol.* 17 (4) (2021) 301–308, <https://doi.org/10.1080/1744666X.2021.1894131>.
- [17] C. Rosette, N. Rosette, A. Mazzetti, L. Moro, M. Gerloni, Corticosterone 17 α -propionate (clascoterone) is an androgen receptor antagonist in dermal papilla cells in vitro, *J. Drugs Dermatol.* 18 (2) (2019) 197–201.
- [18] C. Rosette, F.J. Agan, N. Rosette, A. Mazzetti, L. Moro, M. Gerloni, The dual androgen receptor and glucocorticoid receptor antagonist CB-03-10 as potential treatment for tumors that have acquired GR-mediated resistance to AR blockade, *Mol. Cancer Ther.* (2020), <https://doi.org/10.1158/1535-7163.MCT-19-1137>.
- [19] Y. Rew, X. Du, J. Eksterowicz, H. Zhou, N. Jahchan, L. Zhu, X. Yan, H. Kawai, L. R. McGee, J.C. Medina, T. Huang, C. Chen, T. Zavorotinskaya, D. Sutimantanapi, J. Waszczuk, E. Jackson, E. Huang, Q. Ye, V.R. Fantin, D. Sun, Discovery of a potent and selective steroidal glucocorticoid receptor antagonist (ORIC-101), *J. Med. Chem.* 61 (17) (2018) 7767–7784, <https://doi.org/10.1021/acs.jmedchem.8b00743>.
- [20] X. Du, J. Eksterowicz, H. Zhou, Y. Rew, L. Zhu, X. Yan, J.C. Medina, T. Huang, X. Chen, D. Sutimantanapi, N. Jahchan, W. Kong, J. Sun, T. Zavorotinskaya, Q. Ye, V.R. Fantin, D. Sun, Discovery of a potent steroidal glucocorticoid receptor antagonist with enhanced selectivity against the progesterone and androgen receptors (OP-3633), *J. Med. Chem.* 62 (14) (2019) 6751–6764, <https://doi.org/10.1021/acs.jmedchem.9b00711>.
- [21] C. Honer, K. Nam, C. Fink, P. Marshall, G. Ksander, R. Chatelain, W. Cornell, R. Steele, R. Schweitzer, C. Schumacher, Glucocorticoid receptor antagonist by cyproterone acetate and RU486, *Mol. Pharmacol.* 63 (5) (2003) 1012–1020, <https://doi.org/10.1124/mol.63.5.1012>.
- [22] K. Sota, M. Mitsukuchi, J. Nakagami, Y. Tachi, J. Sawada, S. Otomo, M. Ohzeki, Synthesis and antiinflammatory activity of hydrocortisone 17,21-diester, *Yakugaku Zasshi* 102 (1982) 365–370, <https://doi.org/10.1248/yakushi1947.102.4.365>.
- [23] H.J. Kooreman, A.F. Marx, vd D. Sijde, The synthesis of 17-ester of corticosteroids protection of 11 β -hydroxyl by trimethylsilyl group, *Synth. Comm.* 1 (2) (2013) 81–87, <https://doi.org/10.1080/00397917108081620>.
- [24] I. Bartonkova, A. Novotna, Z. Dvorak, Novel stably transfected human reporter cell line AIZ-AR as a tool for an assessment of human androgen receptor transcriptional activity, *PLoS One* 10 (2015), e0121316, <https://doi.org/10.1371/journal.pone.0121316>.
- [25] A. Novotna, P. Pavek, Z. Dvorak, Construction and characterization of a reporter gene cell line for assessment of human glucocorticoid receptor activation, *Eur. J. Pharm. Sci.* 47 (5) (2012) 842–847, <https://doi.org/10.1016/j.ejps.2012.10.003>.
- [26] X.Y. Zhao, P.J. Malloy, A.V. Krishnan, S. Swami, N.M. Navone, D.M. Peehl, D. Feldman, Glucocorticoids can promote androgen-independent growth of prostate cancer cells through a mutated androgen receptor, *Nat. Med.* 6 (6) (2000) 703–706, <https://doi.org/10.1038/76287>. Erratum in: *Nat Med* 2000 Aug;6(8): 939.
- [27] E. Jernberg, A. Bergh, P. Wikström, Clinical relevance of androgen receptor alterations in prostate cancer, *Endocr. Connect.* 6 (8) (2017) R146–R161, <https://doi.org/10.1530/EC-17-0118>.
- [28] V.K. Arora, E. Schenkein, R. Murali, S.K. Subudhi, J. Wongvipat, M.D. Balbas, N. Shah, L. Cai, E. Efstathiou, C. Logothetis, D. Zheng, C.L. Sawyers, Glucocorticoid receptor confers resistance to antiandrogens by bypassing androgen receptor blockade, *Cell* 155 (6) (2013) 1309–1322, <https://doi.org/10.1016/j.cell.2013.11.012>.
- [29] J. Shaw, M. Leveridge, C. Norling, J. Karén, D.M. Molina, D. O'Neill, J.E. Dowling, P. Davey, S. Cowan, M. Dabrowski, M. Main, D. Gianni, Determining direct binders

- of the androgen receptor using a high-throughput cellular thermal shift assay, *Sci. Rep.* 8 (2018) 163, <https://doi.org/10.1038/s41598-017-18650-x>.
- [30] M.A. Kiss, M. Peřina, V. Bazgier, N.V. May, A. Baji, R. Jorda, E. Frank, Synthesis of dihydrotestosterone derivatives modified in the A-ring with (hetero)arylidene, pyrazolo[1,5-a]pyrimidine and triazolo[1,5-a]pyrimidine moieties and their targeting of the androgen receptor in prostate cancer, *J. Steroid Biochem. Mol. Biol.* 211 (2021), <https://doi.org/10.1016/j.jsmb.2021.105904>.
- [31] S. Lv, Q. Song, G. Chen, E. Cheng, W. Chen, R. Cole, Z. Wu, L.E. Pascal, K. Wang, P. Wipf, J.B. Nelson, Q. Wei, W. Huang, Z. Wang, Regulation and targeting of androgen receptor nuclear localization in castration-resistant prostate cancer, *J. Clin. Investig.* (2020), <https://doi.org/10.1172/JCI141335>.
- [32] Z. Yu, C. Cai, S. Gao, N.I. Simon, H.C. Shen, S.P. Balk, Galeterone prevents androgen receptor binding to chromatin and enhances degradation of mutant androgen receptor, *Clin. Cancer Res.* 20 (2014) 4075–4085, <https://doi.org/10.1158/1078-0432.CCR-14-0292>.
- [33] Jun Yang, Jimin Liu, Donald B. DeFranco, Subnuclear trafficking of glucocorticoid receptors in vitro: chromatin recycling and nuclear export, *J. Cell Biol.* 5 (3) (1997) 523–538, <https://doi.org/10.1083/jcb.137.3.523>.
- [34] B.W. Peeters, G.S. Ruigt, M. Craighead, P. Kitchener, Differential effects of the new glucocorticoid receptor antagonist ORG 34517 and RU486 (mifepristone) on glucocorticoid receptor nuclear translocation in the AT20 cell line, *Ann. N. Y. Acad. Sci.* 1148 (2008) 536–541, <https://doi.org/10.1196/annals.1410.072>.
- [35] C.W. Gregory, R.T. Johnson Jr., S.C. Presnell, J.L. Mohler, F.S. French, Androgen receptor regulation of G1 cyclin and cyclin-dependent kinase function in the CWR22 human prostate cancer xenograft, *J. Androl.* 22 (4) (2001) 537–548, <https://doi.org/10.1002/j.1939-4640.2001.tb02213.x>.
- [36] Y. Koryakina, K.E. Knudsen, D. Gioeli, Cell-cycle-dependent regulation of androgen receptor function, *Endocr. Relat. Cancer* 22 (2) (2015) 249–264, <https://doi.org/10.1530/ERC-14-0549>.
- [37] B. Kauppi, C. Jakob, M. Färnegårdh, J. Yang, H. Ahola, M. Alarcon, K. Calles, O. Engström, J. Harlan, S. Muchmore, A.K. Ramqvist, S. Thorell, L. Ohman, J. Greer, J.A. Gustafsson, J. Carlstedt-Duke, M. Carlquist, The three-dimensional structures of antagonistic and agonistic forms of the glucocorticoid receptor ligand-binding domain: RU-486 induces a transconformation that leads to active antagonism, *J. Biol. Chem.* 278 (25) (2003) 22748–22754, <https://doi.org/10.1074/jbc.M212711200>.
- [38] J. Wahl, M. Smiesko, Endocrine disruption at the androgen receptor: employing molecular dynamics and docking for improved virtual screening and toxicity prediction, *Published 2018 Jun 15, Int. J. Mol. Sci.* 19 (6) (2018) 1784, <https://doi.org/10.3390/ijms19061784>.
- [39] C.E. Bohl, Z. Wu, D.D. Miller, C.E. Bell, J.T. Dalton, Crystal structure of the T877A human androgen receptor ligand-binding domain complexed to cyproterone acetate provides insight for ligand-induced conformational changes and structure-based drug design, *J. Biol. Chem.* 282 (18) (2007) 13648–13655, <https://doi.org/10.1074/jbc.M611711200>.
- [40] S.L. Holder, J. Drabick, J. Zhu, M. Joshi, Dexamethasone may be the most efficacious corticosteroid for use as monotherapy in castration-resistant prostate cancer, *Cancer Biol. Ther.* 16 (2) (2015) 207–209, <https://doi.org/10.1080/15384047.2014.1002687>.
- [41] N. Romero-Laorden, R. Lozano, A. Jayaram, F. López-Campos, M.I. Saez, A. Montesa, A. Gutierrez-Pecharoman, R. Villatoro, B. Herrera, R. Correa, A. Rosero, M.I. Pacheco, T. Garcés, Y. Cendón, M.P. Nombela, F. Van de Poll, G. Grau, L. Rivera, P.P. López, J.J. Cruz, D. Lorente, G. Attard, E. Castro, D. Olmos, Phase II pilot study of the prednisone to dexamethasone switch in metastatic castration-resistant prostate cancer (mCRPC) patients with limited progression on abiraterone plus prednisone (SWITCH study), *Br. J. Cancer* 119 (9) (2018) 1052–1059, <https://doi.org/10.1038/s41416-018-0123-9>.
- [42] S. Narayanan, S. Srinivas, D. Feldman, Androgen-glucocorticoid interactions in the era of novel prostate cancer therapy, *Nat. Rev. Urol.* 13 (1) (2016) 47–60, <https://doi.org/10.1038/nrurol.2015.254>.
- [43] A.V. Serritella, D. Shevrin, E.I. Heath, J.L. Wade, E. Martinez, A. Anderson, J. Schonhoff, Y.L. Chu, T. Karrison, W.M. Stadler, R.Z. Szmulewitz, Phase I/II trial of enzalutamide and mifepristone, a glucocorticoid receptor antagonist, for metastatic castration-resistant prostate cancer, *Clin. Cancer Res.* 28 (8) (2022) 1549–1559, <https://doi.org/10.1158/1078-0432.CCR-21-4049>.
- [44] J. Li, M. Berk, M. Alyamani, N. Sabharwal, C. Goins, J. Alvarado, M. Baratchian, Z. Zhu, S. Stauffer, E.A. Klein, N. Sharifi, Hexose-6-phosphate dehydrogenase blockade reverses prostate cancer drug resistance in xenograft models by glucocorticoid inactivation, *Sci. Transl. Med.* 13 (595) (2021) eabe8226, <https://doi.org/10.1126/scitranslmed.abe8226>.
- [45] J. Li, M. Alyamani, A. Zhang, K.H. Chang, M. Berk, Z. Li, Z. Zhu, M. Petro, C. Magi-Galluzzi, M.E. Taplin, J.A. Garcia, K. Courtney, E.A. Klein, N. Sharifi, Aberrant corticosteroid metabolism in tumor cells enables GR takeover in enzalutamide resistant prostate cancer, *eLife* 6 (2017), <https://doi.org/10.7554/eLife.20183>.
- [46] G.M. Morris, R. Huey, W. Lindstrom, et al., AutoDock4 and AutoDockTools4: automated docking with selective receptor flexibility, *J. Comput. Chem.* 30 (16) (2009) 2785–2791, <https://doi.org/10.1002/jcc.21256>.
- [47] O. Trott, A.J. Olson, AutoDock Vina: Improving the speed and accuracy of docking with a new scoring function, efficient optimization, and multithreading (NA-NA), *J. Comput. Chem.* 31 (2) (2009), <https://doi.org/10.1002/jcc.21334>.
- [48] Melissa F. Adasme, Katja L. Linnemann, Sarah Naomi Bolz, Florian Kaiser, Sebastian Salentin, V. Joachim Haupt, Michael Schroeder, PLIP 2021: expanding the scope of the protein–ligand interaction profiler to DNA and RNA, *Nucleic Acids Res.* 49 (W1) (2021) W530–W534, <https://doi.org/10.1093/nar/gkab294>.

SUPPLEMENTARY INFORMATION

Synthesis of hydrocortisone esters targeting androgen and glucocorticoid receptors in prostate cancer *in vitro*

Miroslav Peřina^a, Anita Kiss^b, Erzsébet Mernyák^b, Lukáš Mada^a, Gyula Schneider^{b, †, *} Radek Jorda^{a, *}

^a Department of Experimental Biology, Faculty of Science, Palacký University Olomouc, Šlechtitelů 27, 78371 Olomouc, Czech Republic

^b Department of Organic Chemistry, University of Szeged, Dóm tér 8. 17720 Szeged, Hungary

[†] Deceased

*Corresponding authors:

Radek Jorda, radek.jorda@upol.cz; Tel.: +420 585 634 854

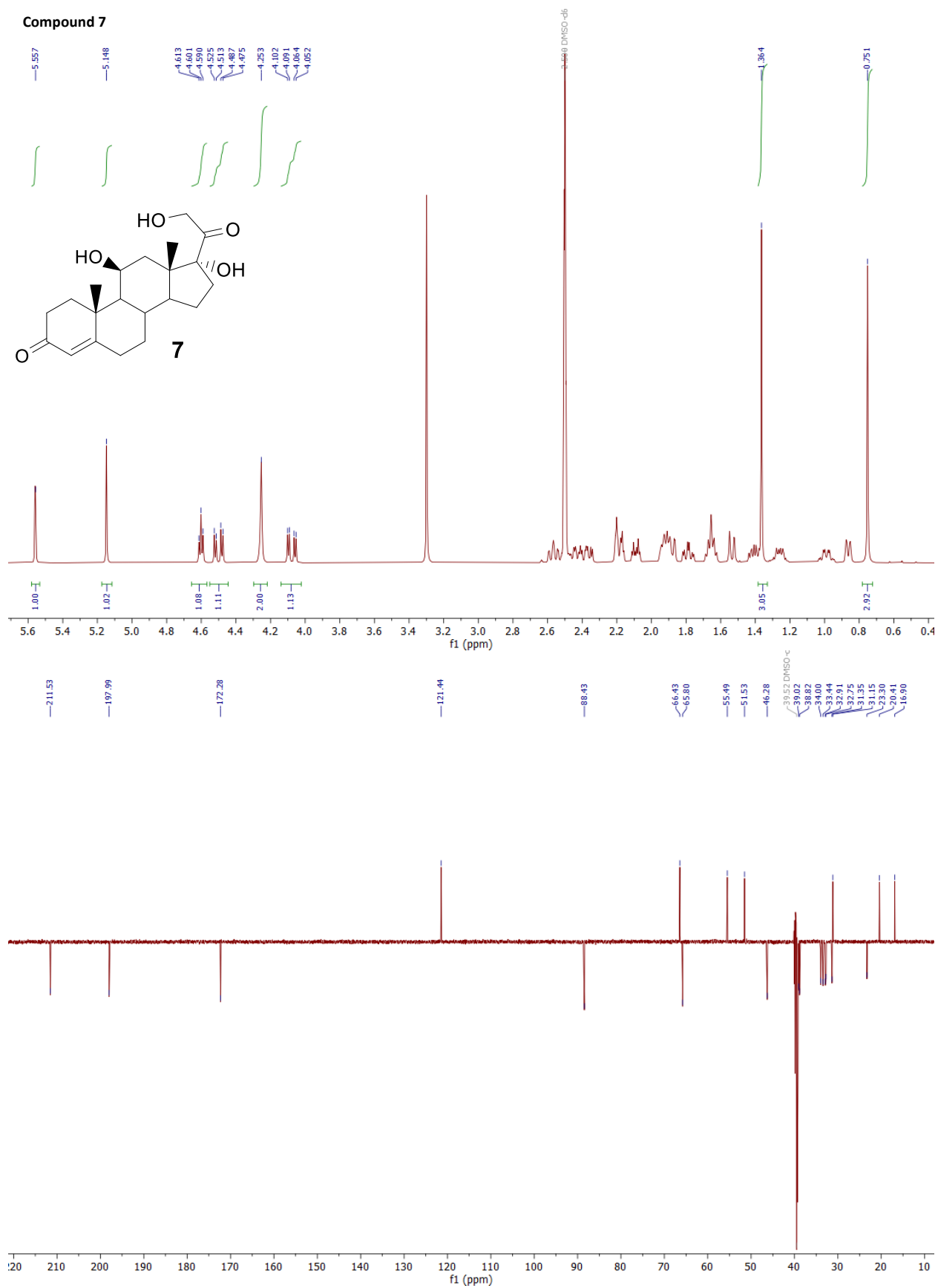
Gyula Schneider, bobbe@chem.u-szeged.hu

Keywords: hydrocortisone derivatives, androgen receptor, glucocorticoid receptor, prostate cancer, castration resistant prostate cancer, transcriptional activity

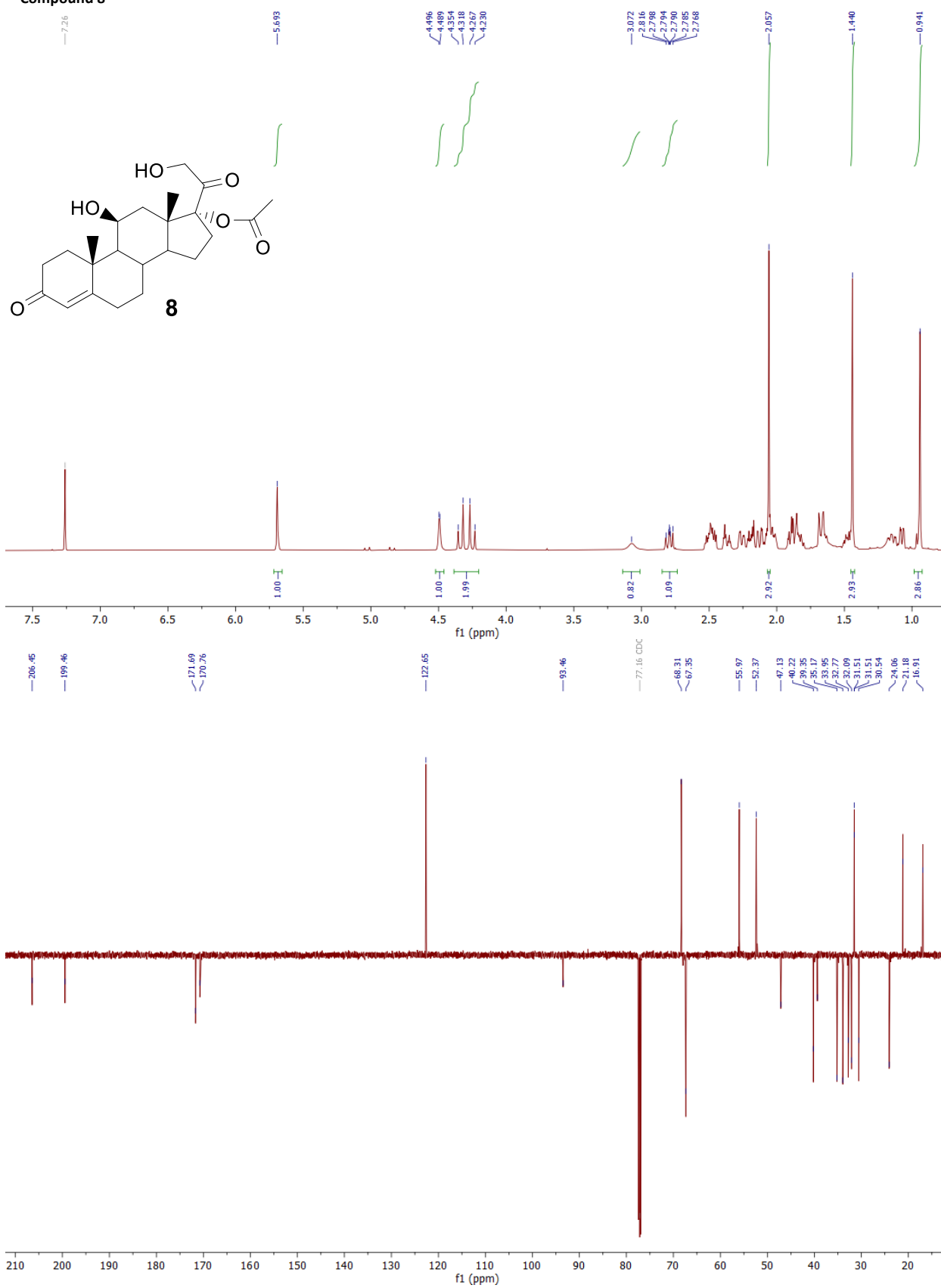
Table of contents

¹H and ¹³C NMR spectra of studied compounds (7–16)	3–13
Figure S1 Effect of compounds on transcriptional activity of AR in agonist or antagonist mode	14
Figure S2 Effect of compounds on transcriptional activity of GR in agonist or antagonist mode	15
Figure S3 Effect of compounds on transcriptional activity of GR in agonist or antagonist mode	16
Figure S4 Effect of compounds on transcriptional activity of GR in agonist or antagonist mode	17
Figure S5 Expression pattern of AR, GR	18
Figure S6 Viability of PCa cell lines	19
Figure S7 AR and GR levels upon 3 days and 7 days treatment	20
Figure S8 Viability of LAPC-4 and 22Rv1 treated by 14 , enzalutamide and combination	21
Figure S9 Downstream signaling of AR in 22Rv1 treated by 14 , 15 and galeterone	22
Figure S10 Cell cycle analysis of LAPC-4 and 22Rv1 treated by 14 and standards for 48 h	22

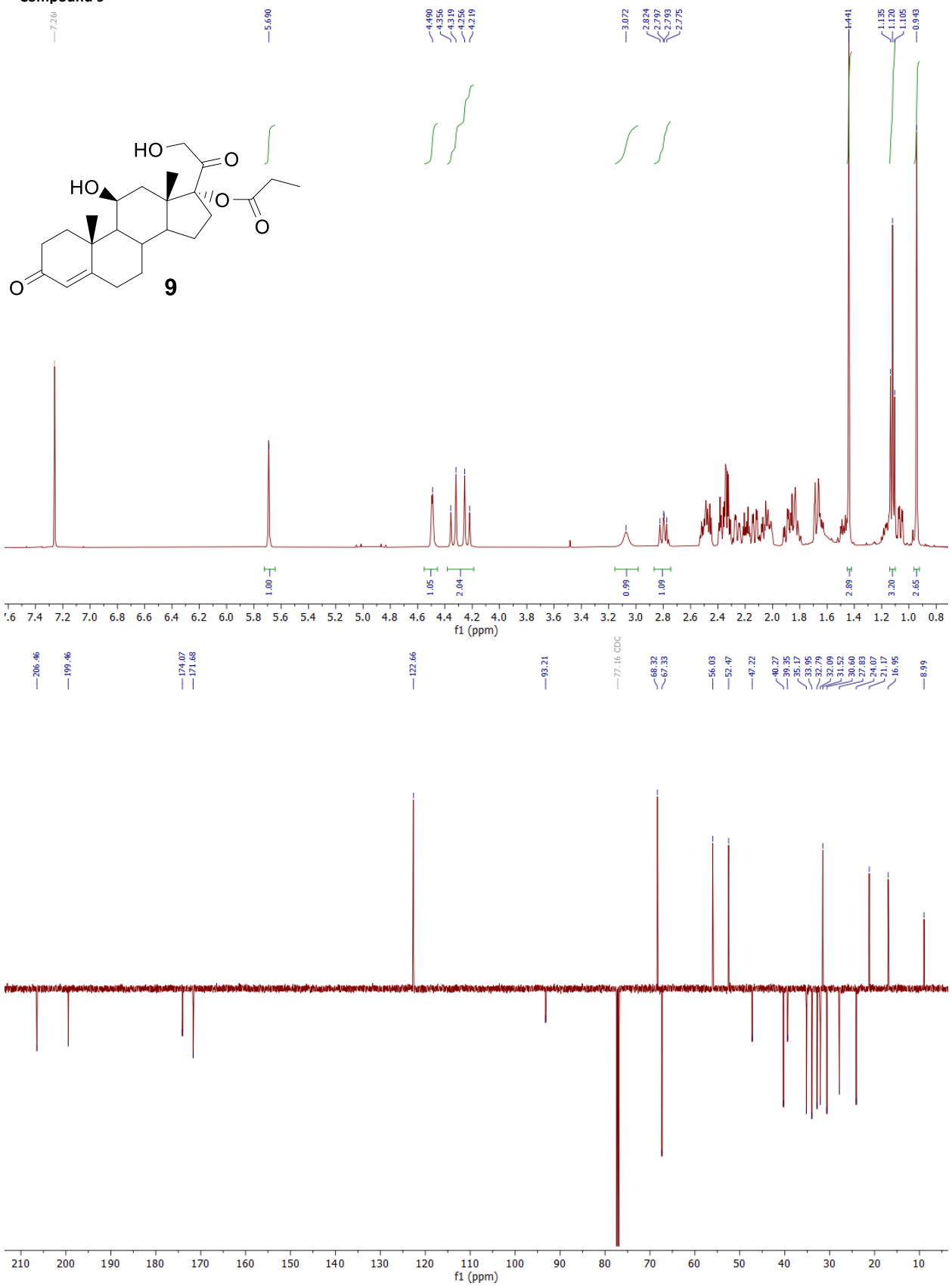
Compound 7



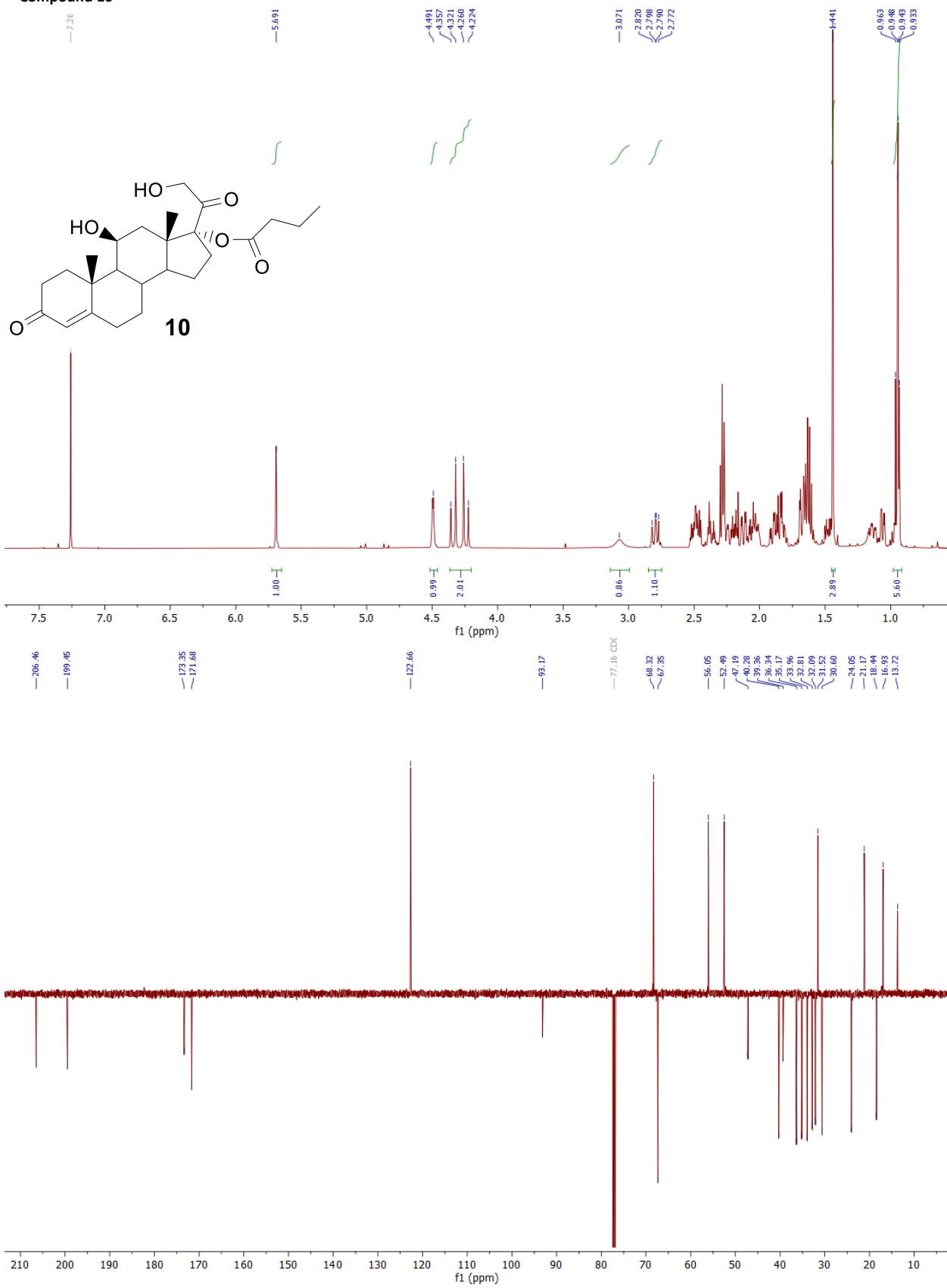
Compound 8



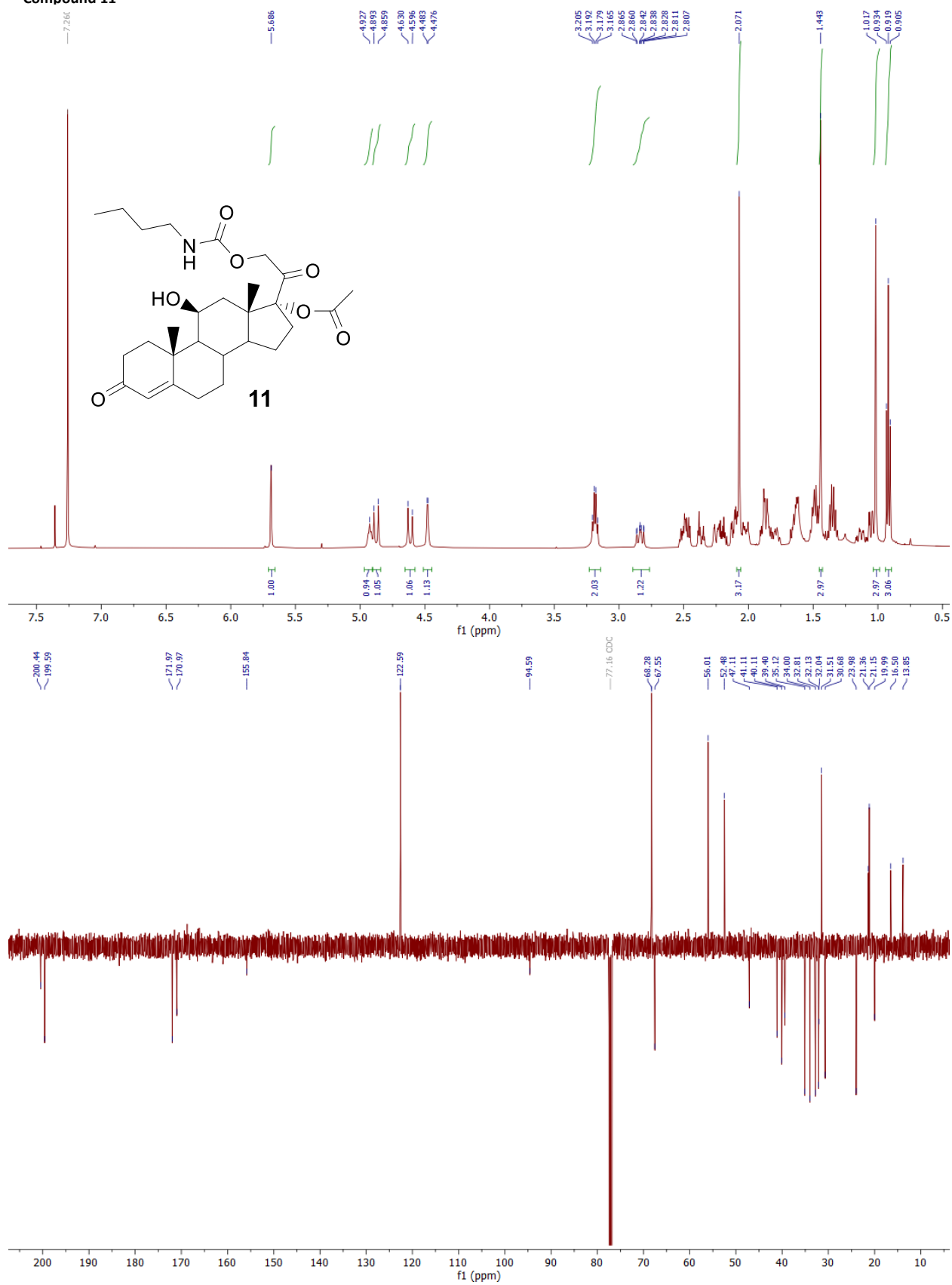
Compound 9



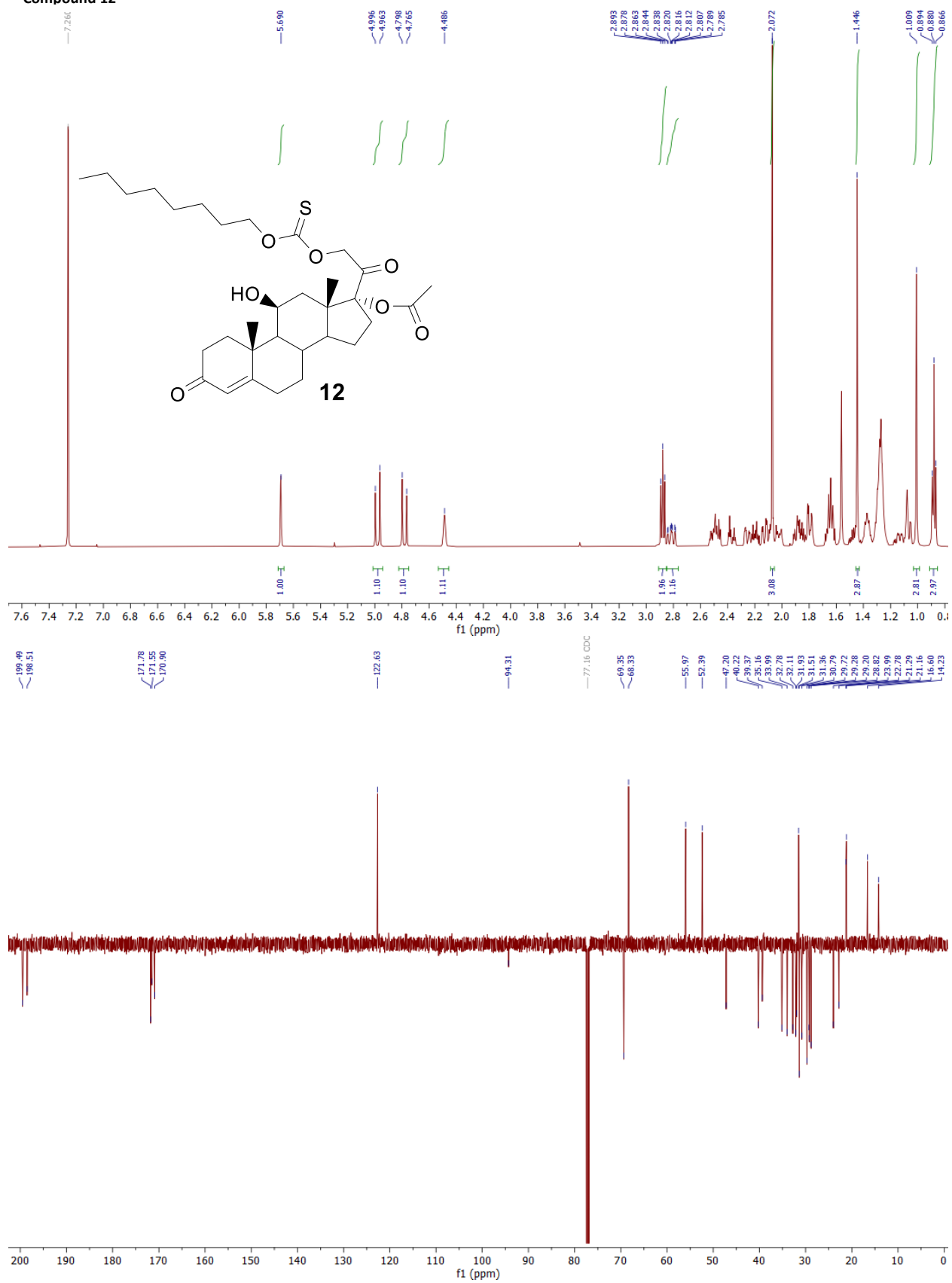
Compound 10



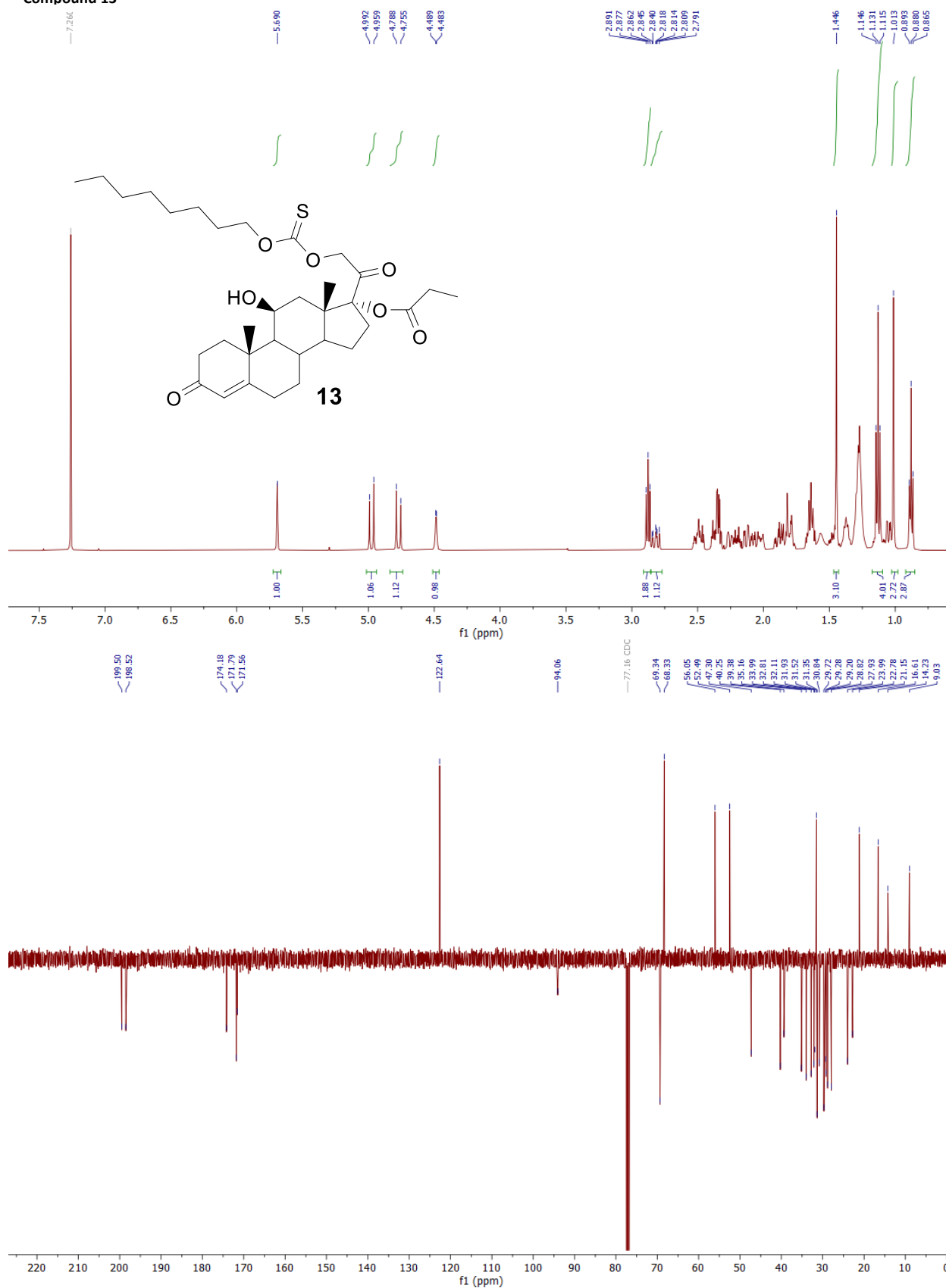
Compound 11



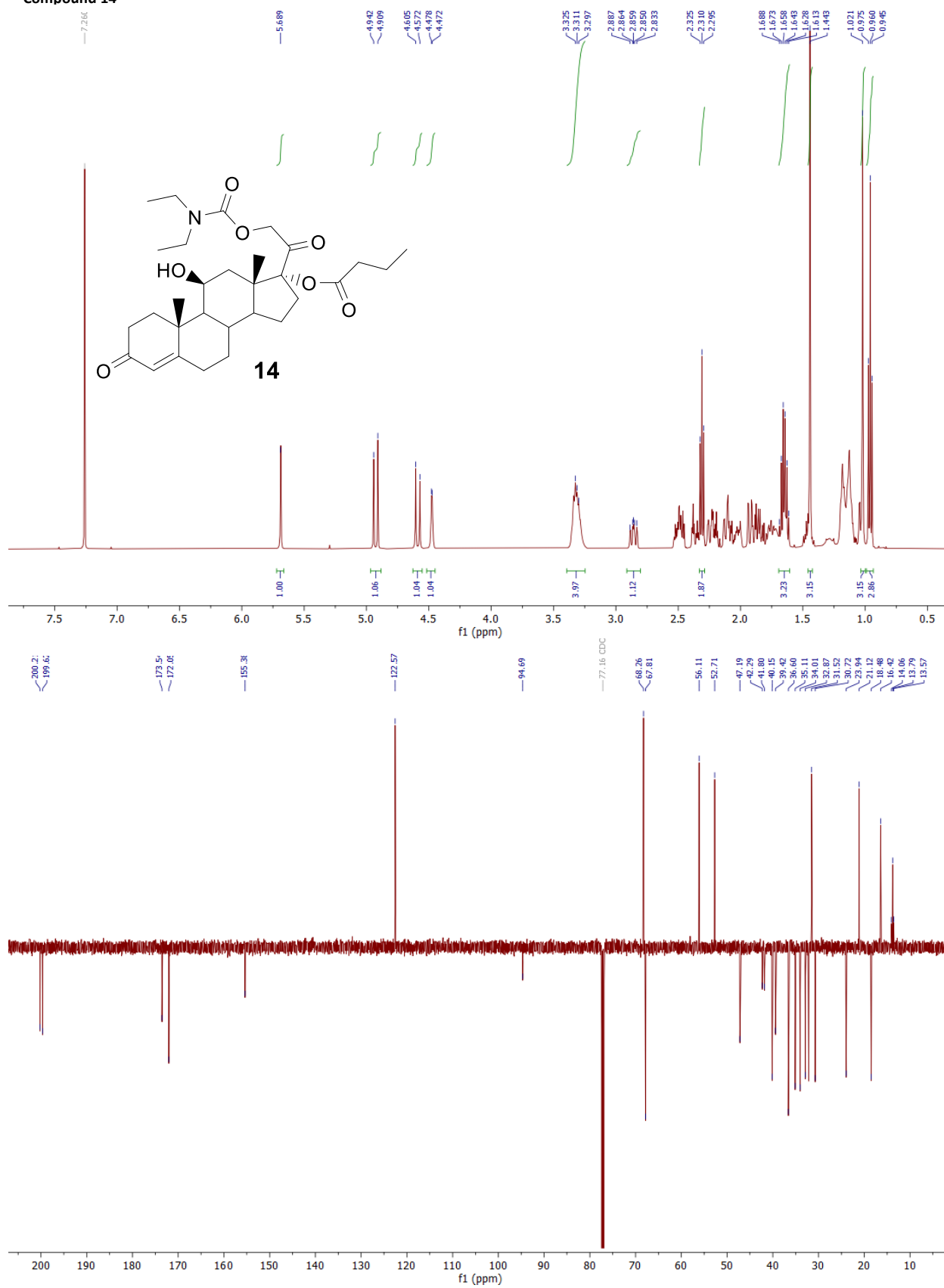
Compound 12



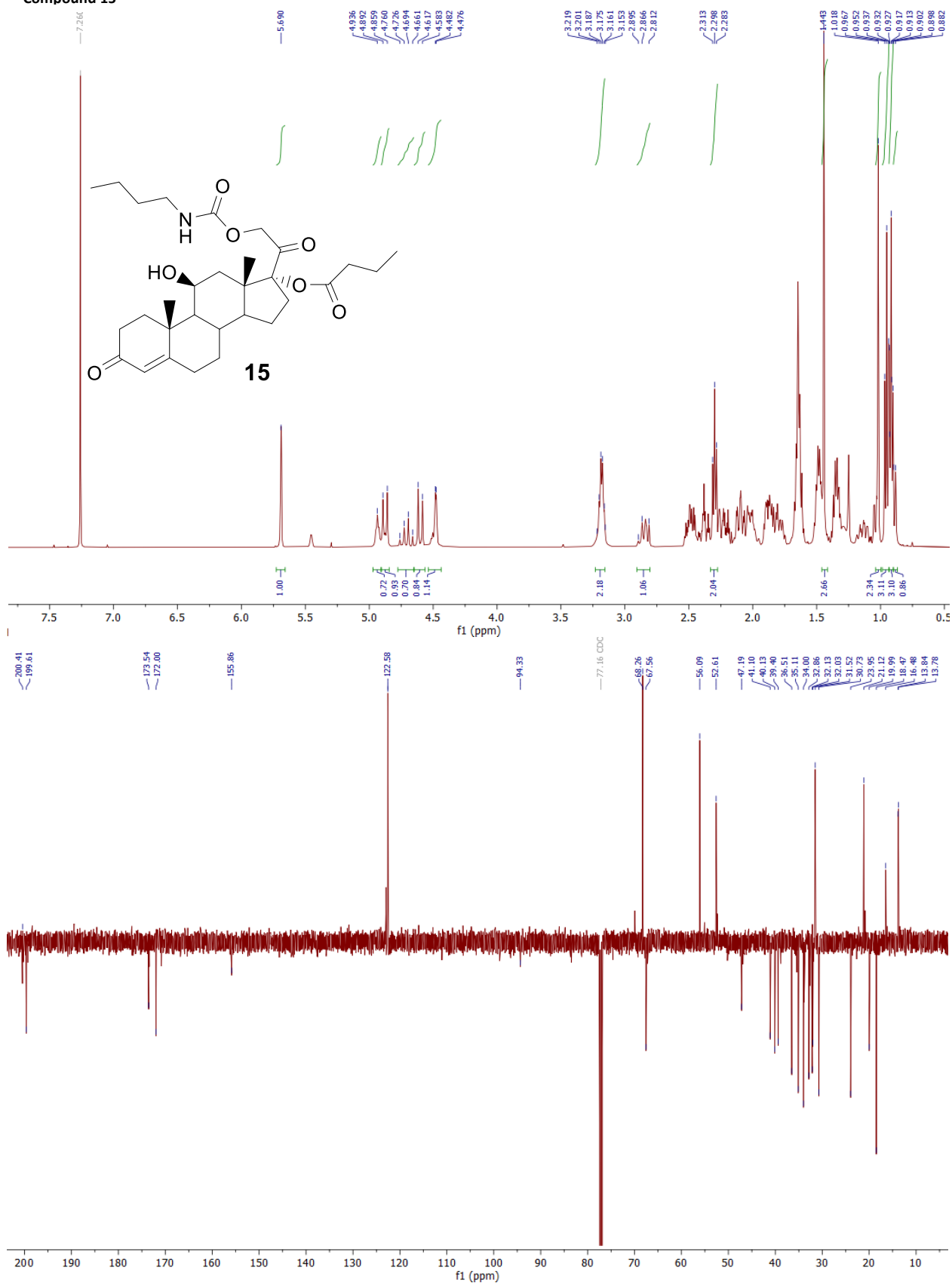
Compound 13



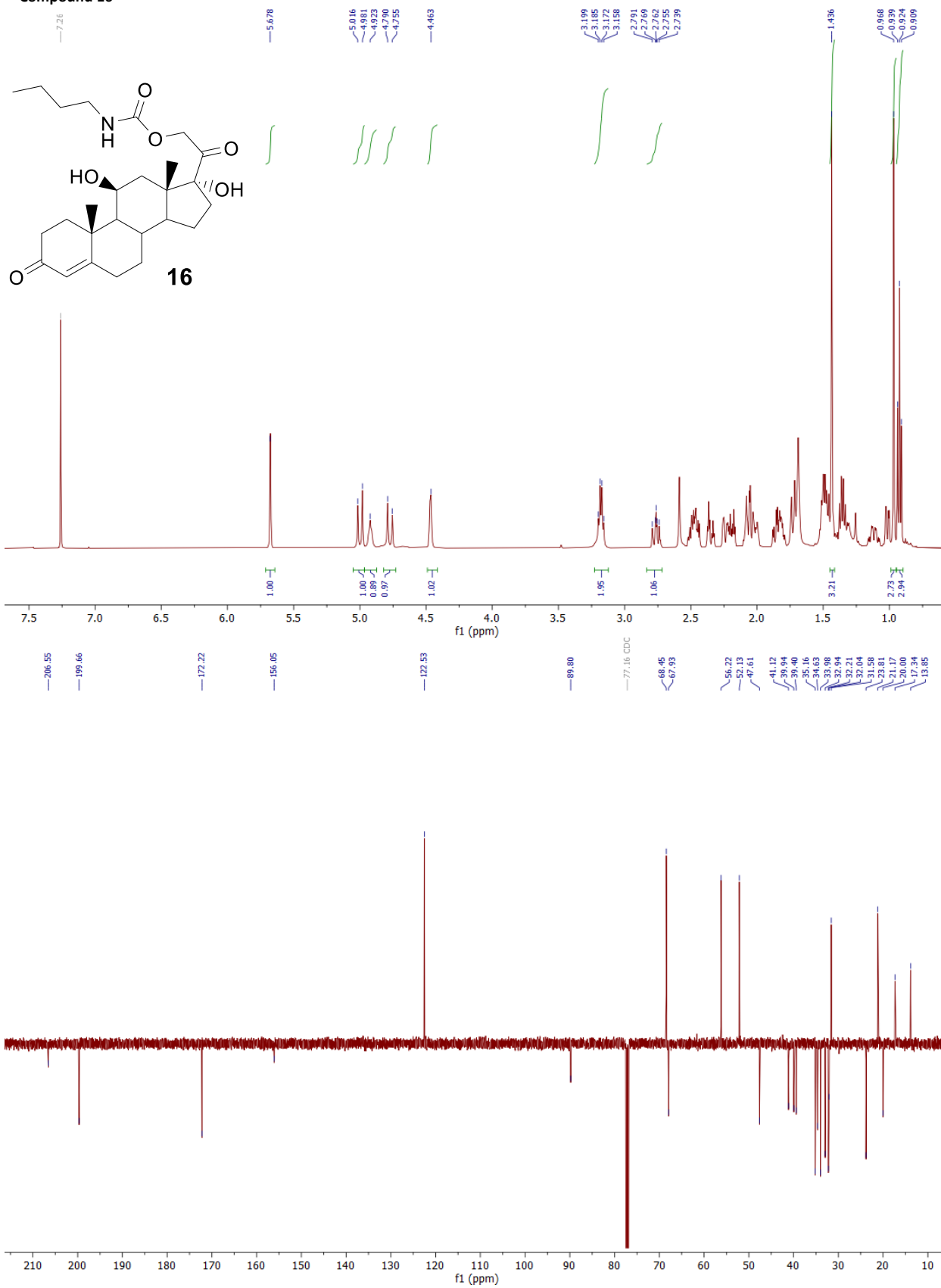
Compound 14



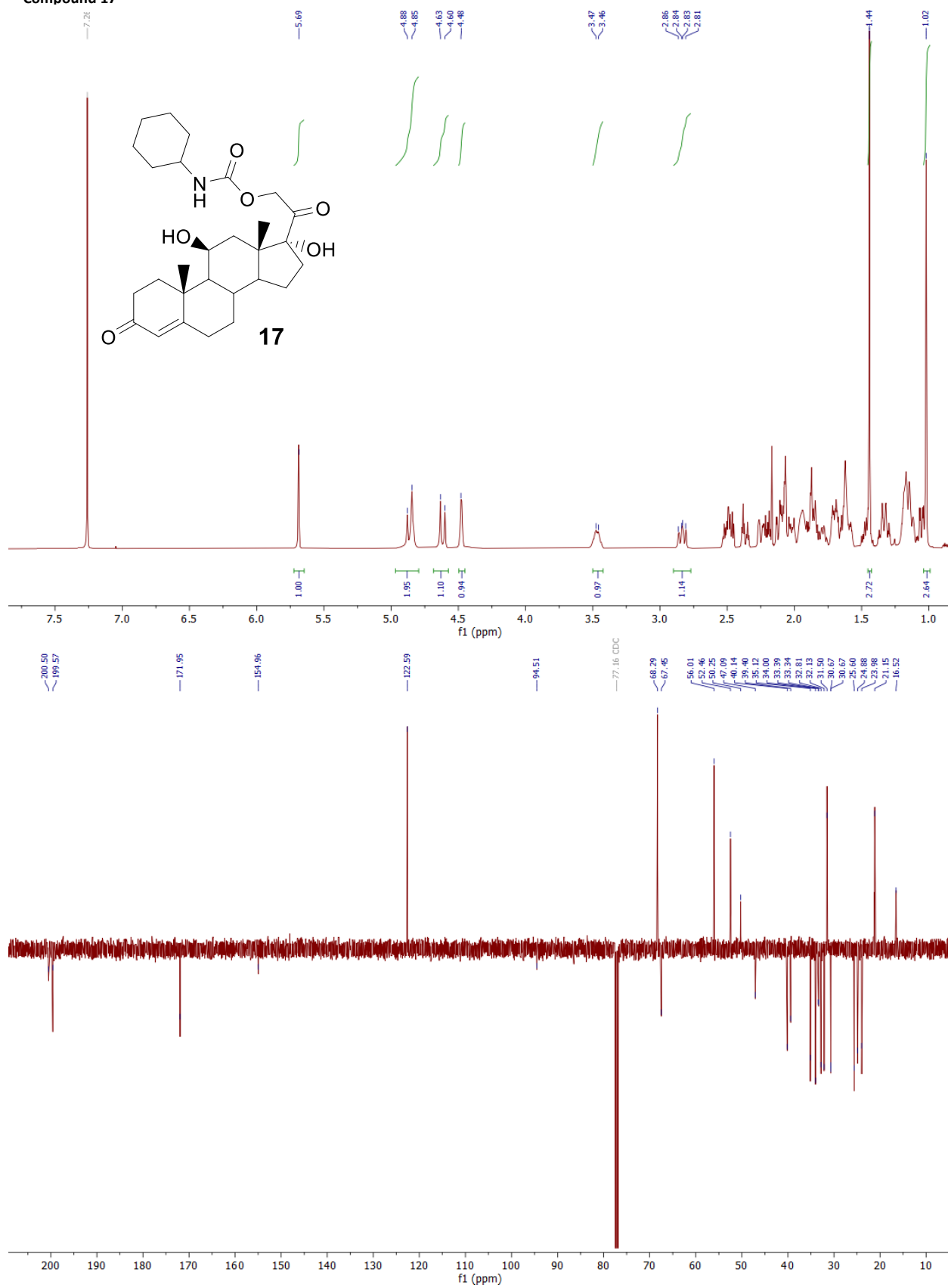
Compound 15



Compound 16



Compound 17



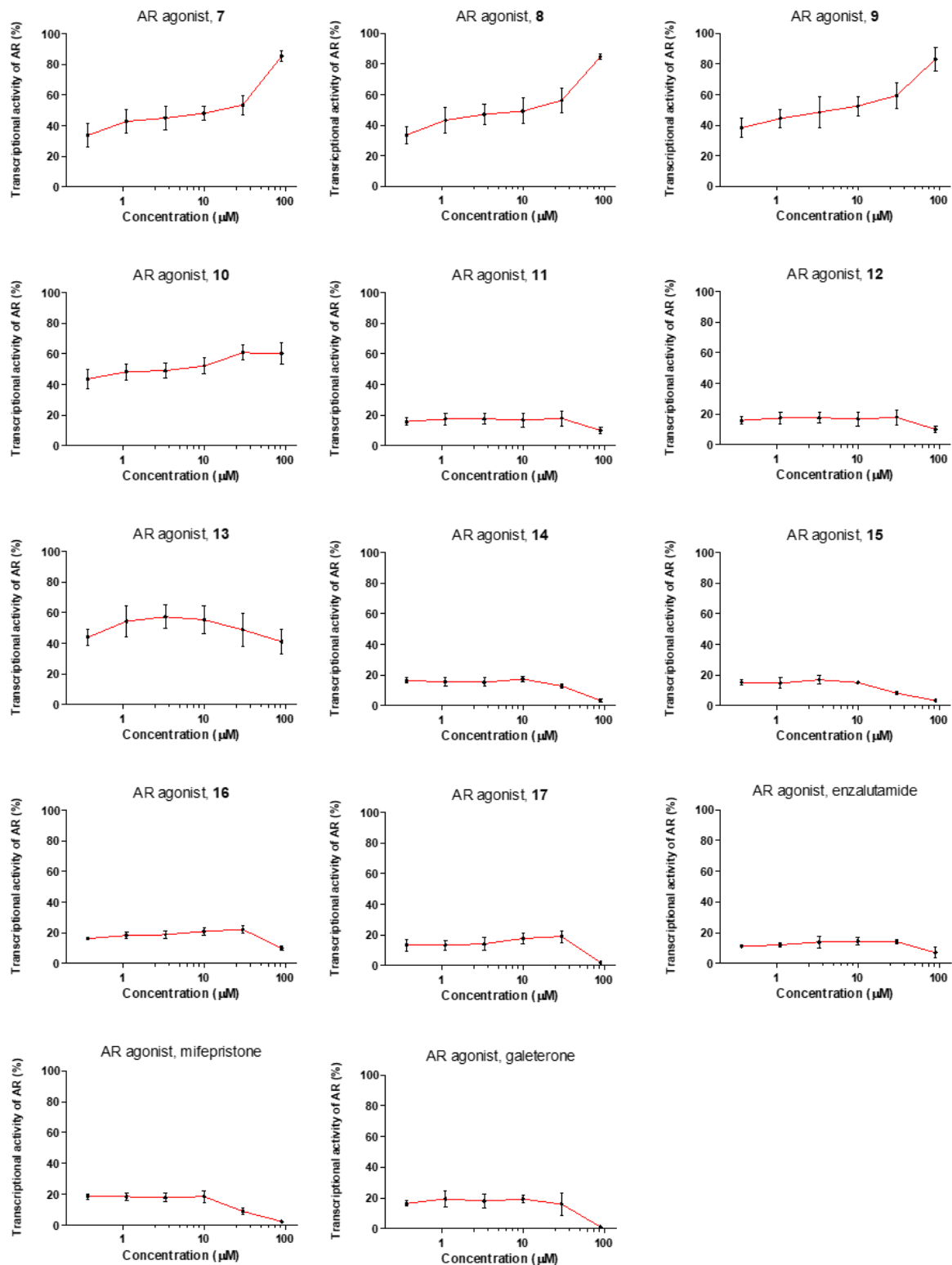


Figure S1. Transcriptional activity of AR after treatment with compounds in agonist mode (tested compounds alone) in CSS media (no androgens). The signal was normalised to the transcriptional activity of AR upon treatment with standard agonist, 1 nM R1881 (100 %). Measured in duplicate and repeated at least twice.

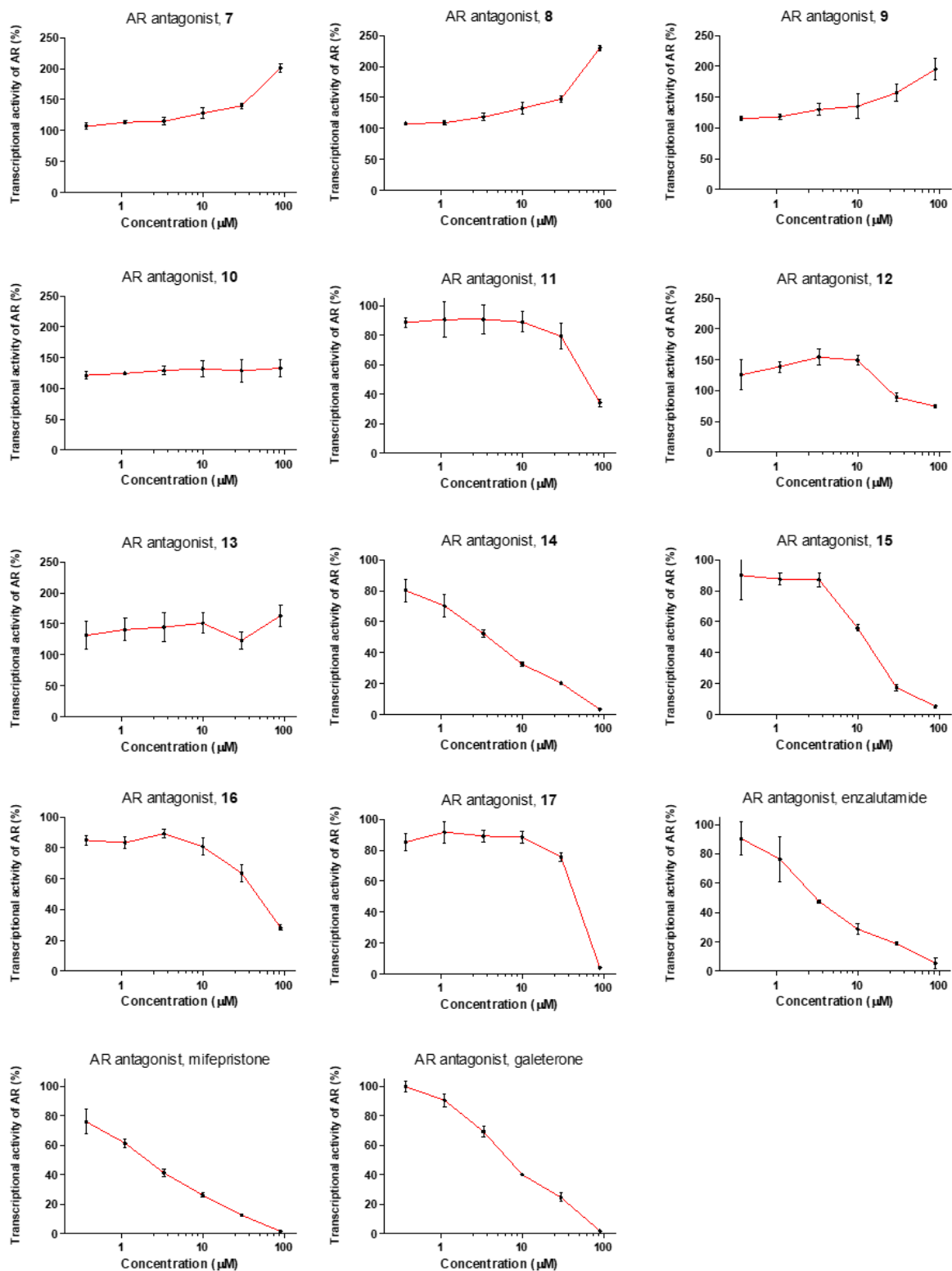


Figure S2. Transcriptional activity of AR after treatment with compounds in antagonist mode (tested compounds competing with 1 nM R1881) in CSS media. The signal was normalised to the transcriptional activity of AR upon treatment with standard agonist, 1 nM R1881 (100 %). Measured in duplicate and repeated at least twice.

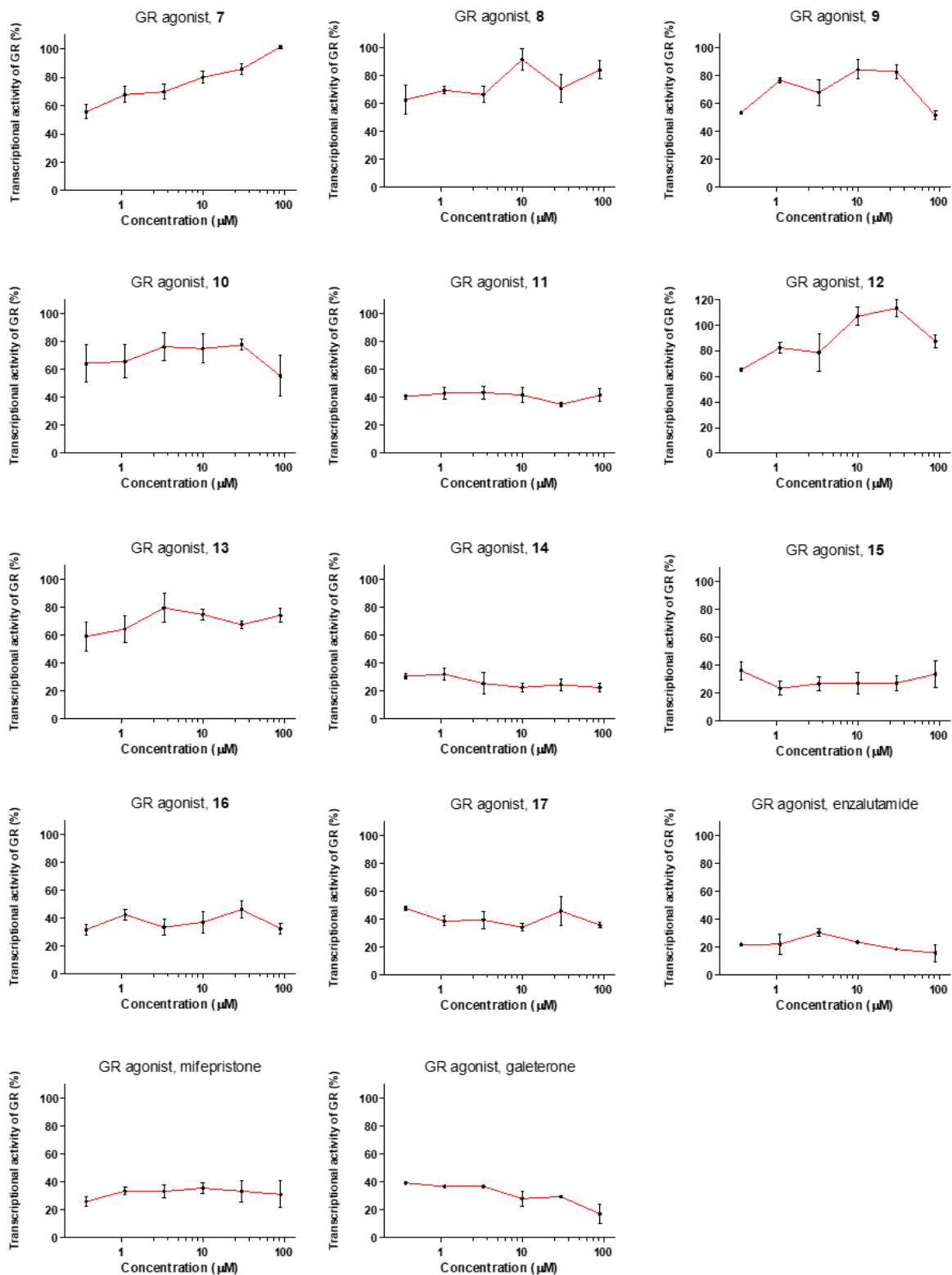


Figure S3. Transcriptional activity of GR after treatment with compounds in agonist mode (tested compounds alone) in CSS media. The signal was normalised to the transcriptional activity of GR upon treatment with standard agonist, 100 nM dexamethasone (100 %). Measured in duplicate and repeated at least twice.

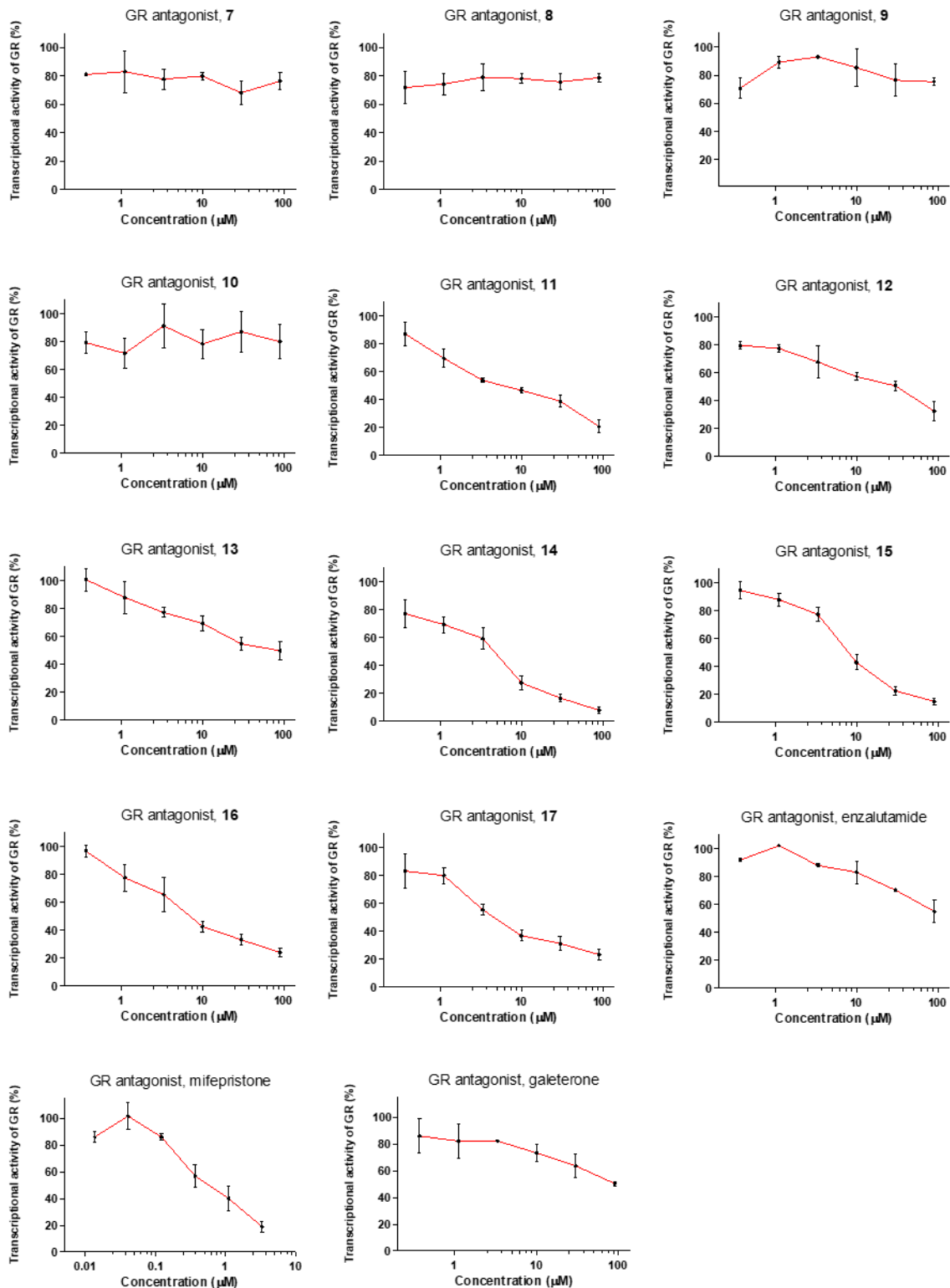


Figure S4. Transcriptional activity of GR after treatment with compounds in antagonist mode (tested compounds competing with 100 nM dexamethasone) in CSS media. The signal was normalised to the transcriptional activity of GR upon treatment with standard agonist, 100 nM dexamethasone (100 %). Measured in duplicate and repeated at least twice.

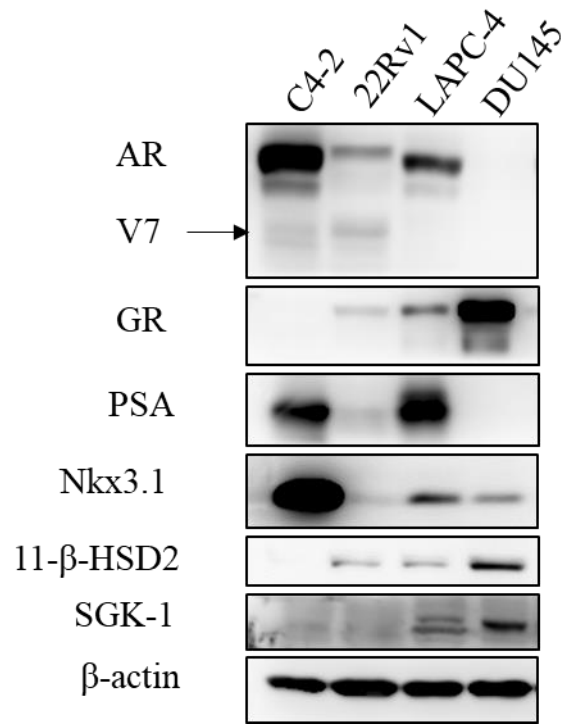
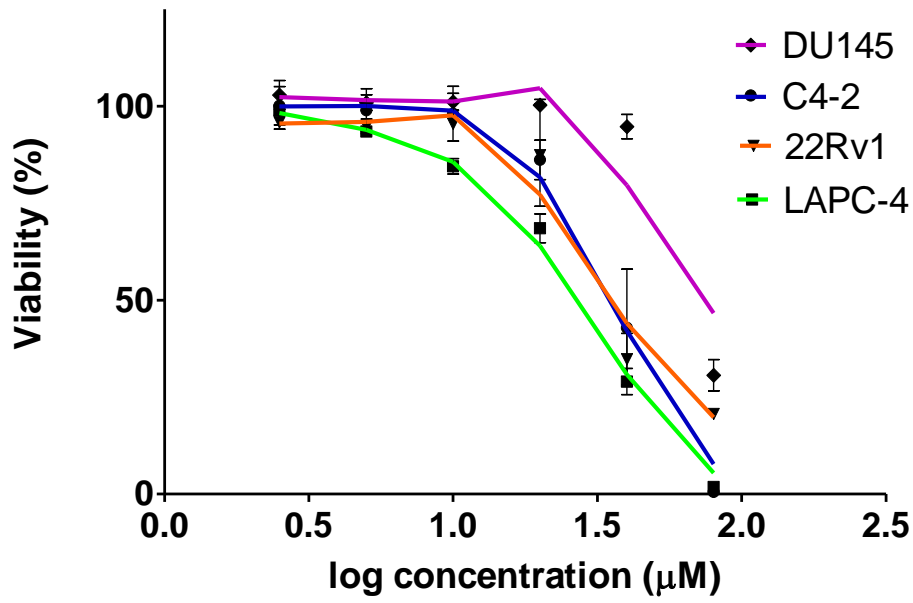


Figure S5. Expression pattern of AR, GR and their downstream proteins in PCa cell lines used for cellular experiments.

Viability of cell lines - compound 14



Viability of cell lines - compound 15

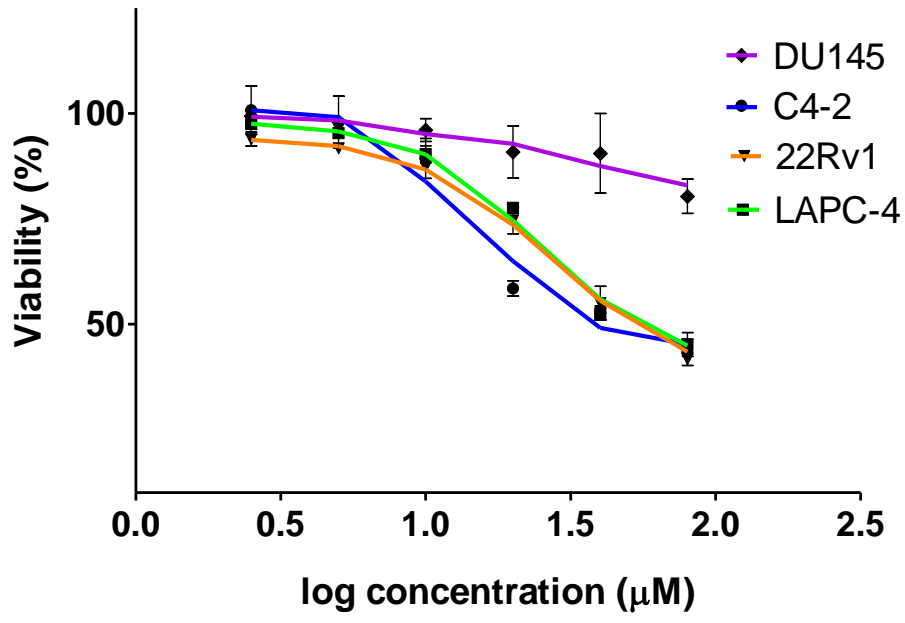


Figure S6. Viability of PCa cells upon treatment with two candidate compounds. Curves plotted from $n=4$, error bars represent SD.

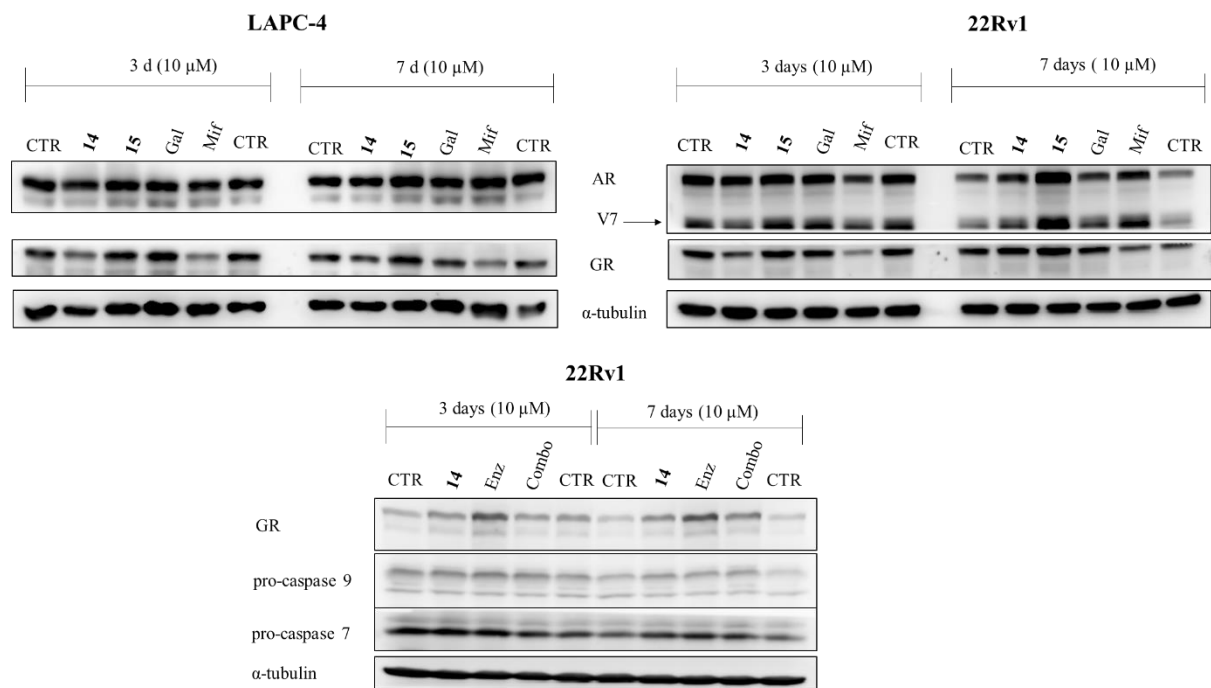


Figure S7. Upper: Western blotting analysis of AR and GR levels in LAPC-4 and 22Rv1 cells after 3 days or 7 days of treatment. Cells were cultivated in presence of 10 μM compounds and standards. The level of α-tubulin served as a control of equal protein loading. Representative result from two replicates is shown. **Lower:** Western blotting analysis of AR and GR levels and pro-caspases (related to apoptosis) in 22Rv1 cells after 3 days or 7 days of treatment with 10 μM **14** or enzalutamide or their combination.

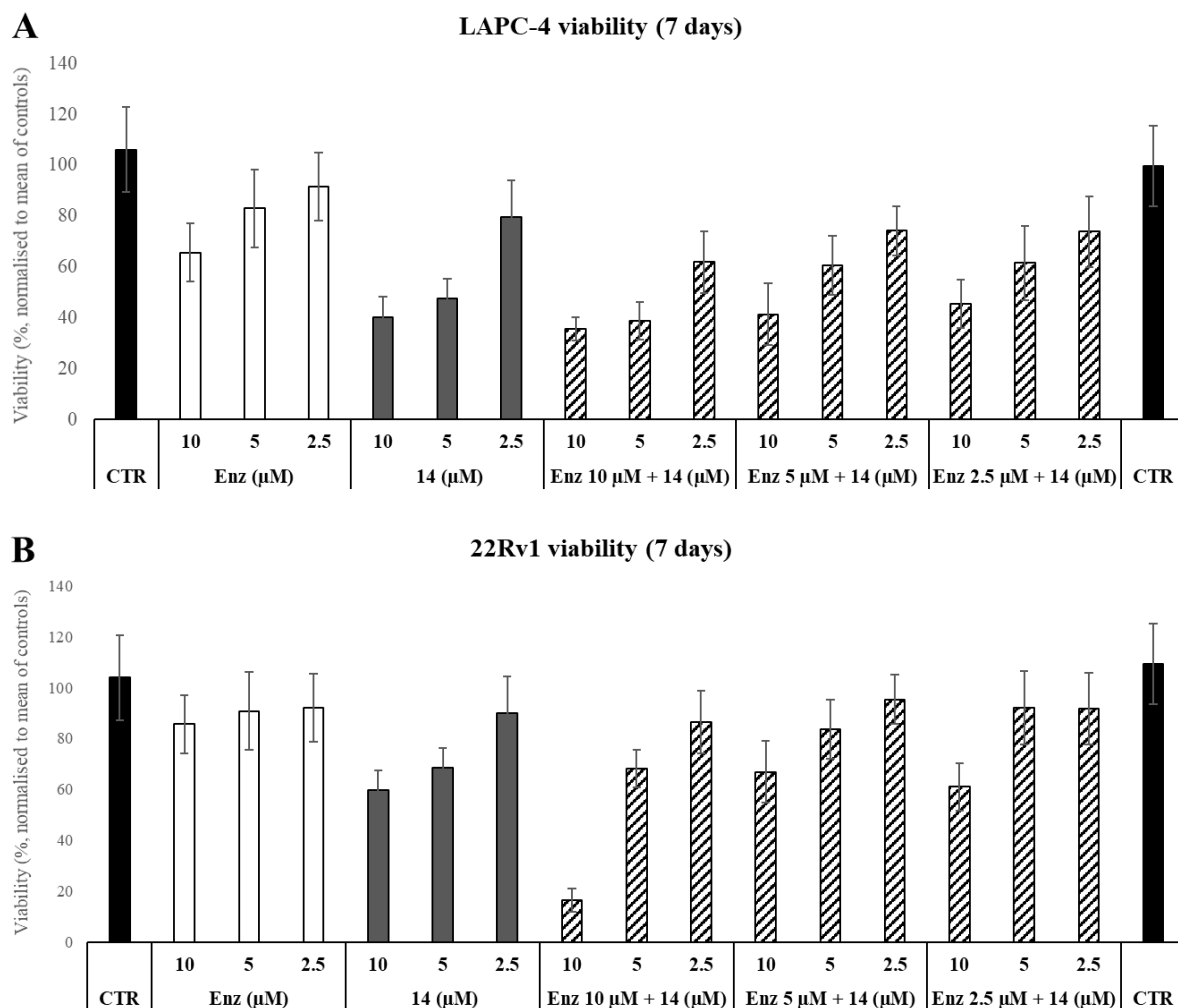


Figure S8. Analysis of viability based on the CFA assay upon treatment with the lead compound **14** alone, enzalutamide alone and combination of both. Cells (**A**: LAPC-4, **B**: 22Rv1) were seeded in 12-well plate in low density and treated by compounds for 7 days to grow colonies. Then they were fixed and stained by crystal violet. Photograph of the plate was captured and colonies were dissolved in 1% SDS and the absorbance of the crystal violet was measured at 570 nm. Measured in hexaplicate and repeated twice.

22Rv1, 24 h

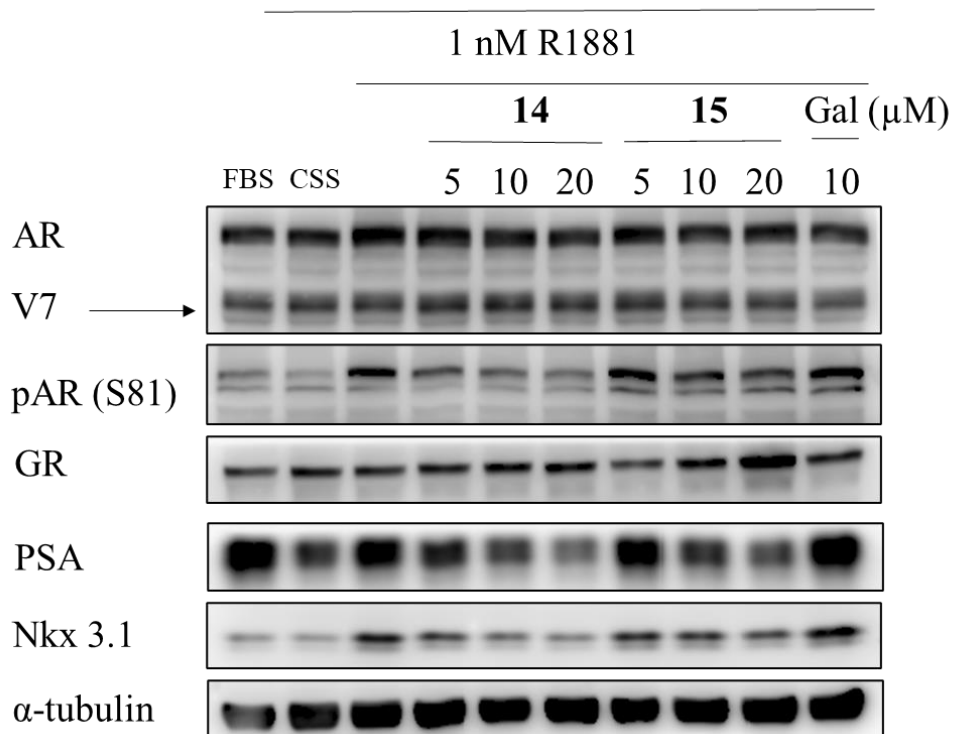


Figure S9. Western blotting analysis of AR-regulated proteins in treated 22Rv1. The cells were deprived of androgens (cultivated in CSS medium) for 24 h and then treated with 1 nM R1881 alone or in combination with different concentrations of candidate compounds **14** and **15** or standards galeterone (Gal) or mifepristone (Mif) for 24 h. The level of α -tubulin was control of equal protein loading. Representative result from two replicates is shown. FBS, fetal bovine serum; CSS, charcoal stripped serum (no steroids).

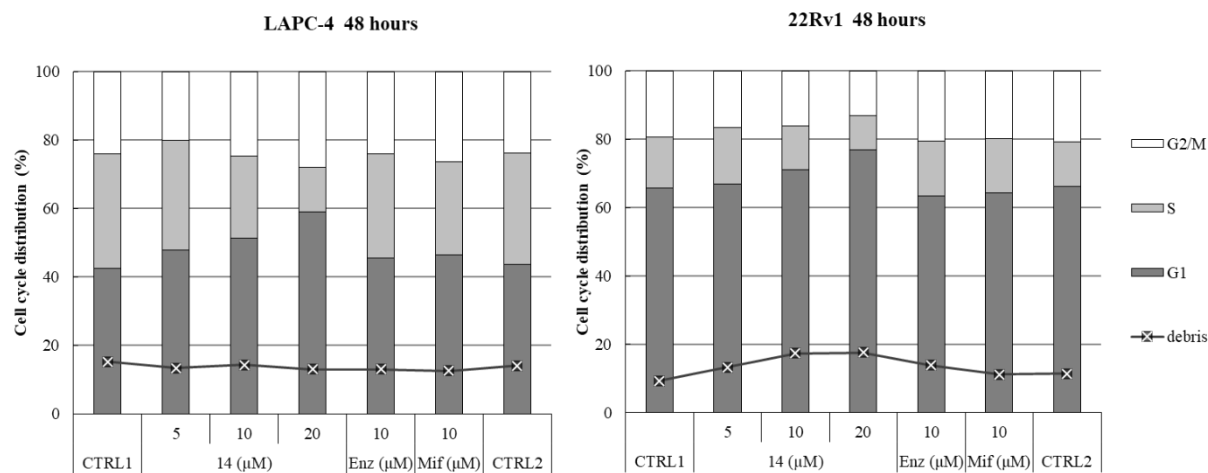


Figure S10. Cell cycle analysis of LAPC-4 and 22Rv1 upon treatment with **14** or standards enzalutamide (Enz) and mifepristone (Mif) for 48 h.

Appendix V.

Rudovich AS, **Peřina M**, Krech AV, Novozhilova MY, Tumilovich AM, Shkel TV, Grabovec IP, Kvasnica M, Mada L, Zavialova MG, Mekhtiev AR, Jorda R, Zhabinskii VN, Khripach VA. Synthesis and Biological Evaluation of New Isoxazolyl Steroids as Anti-Prostate Cancer Agents. **Int J Mol Sci.** 2022 Nov 4;23(21):13534.



Article

Synthesis and Biological Evaluation of New Isoxazolyl Steroids as Anti-Prostate Cancer Agents

Anton S. Rudovich ¹, Miroslav Peřina ², Anastasiya V. Krech ¹, Maria Y. Novozhilova ¹,
Anastasia M. Tumulovich ¹, Tatyana V. Shkel ¹, Irina P. Grabovec ¹, Miroslav Kvasnica ², Lukáš Mada ²,
Maria G. Zavialova ³, Arif R. Mekhtiev ³, Radek Jorda ^{2,4}, Vladimir N. Zhabinskii ^{1,*},
and Vladimir A. Khripach ¹

- ¹ Institute of Bioorganic Chemistry, National Academy of Sciences of Belarus, Kuprevich Str., 5/2, 220141 Minsk, Belarus
- ² Department of Experimental Biology, Faculty of Science, Palacký University Olomouc, Šlechtitelů 27, 78371 Olomouc, Czech Republic
- ³ Institute of Biomedical Chemistry, 10 Building 8, Pogodinskaya Str., 119121 Moscow, Russia
- ⁴ Institute of Molecular and Translational Medicine, Faculty of Medicine and Dentistry, Palacký University Olomouc, Hněvotínská 5, 77900 Olomouc, Czech Republic
- * Correspondence: vz@iboch.by; Tel.: +375-297-579-811

Abstract: Steroids with a nitrogen-containing heterocycle in the side chain are known as effective inhibitors of androgen signaling and/or testosterone biosynthesis, thus showing beneficial effects for the treatment of prostate cancer. In this work, a series of 3 β -hydroxy-5-ene steroids, containing an isoxazole fragment in their side chain, was synthesized. The key steps included the preparation of Weinreb amide, its conversion to acetylenic ketones, and the 1,2- or 1,4-addition of hydroxylamine, depending on the solvent used. The biological activity of the obtained compounds was studied in a number of tests, including their effects on 17 α -hydroxylase and 17,20-lyase activity of human CYP17A1 and the ability of selected compounds to affect the downstream androgen receptor signaling. Three derivatives diminished the transcriptional activity of androgen receptor and displayed reasonable antiproliferative activity. The candidate compound, **24j** (17*R*)-17-((3-(2-hydroxypropan-2-yl)isoxazol-5-yl)methyl)-androst-5-en-3 β -ol, suppressed the androgen receptor signaling and decreased its protein level in two prostate cancer cell lines, LNCaP and LAPC-4. Interaction of compounds with CYP17A1 and the androgen receptor was confirmed and described by molecular docking.

Keywords: prostate cancer; androgen signaling; androgen receptor; CYP17A1; isoxazoles; Weinreb amide; LNCaP; LAPC-4; molecular docking



Citation: Rudovich, A.S.; Peřina, M.; Krech, A.V.; Novozhilova, M.Y.; Tumulovich, A.M.; Shkel, T.V.; Grabovec, I.P.; Kvasnica, M.; Mada, L.; Zavialova, M.G.; et al. Synthesis and Biological Evaluation of New Isoxazolyl Steroids as Anti-Prostate Cancer Agents. *Int. J. Mol. Sci.* **2022**, *23*, 13534. <https://doi.org/10.3390/ijms232113534>

Academic Editor: Stefano Fais

Received: 19 October 2022

Accepted: 2 November 2022

Published: 4 November 2022

Publisher's Note: MDPI stays neutral with regard to jurisdictional claims in published maps and institutional affiliations.



Copyright: © 2022 by the authors. Licensee MDPI, Basel, Switzerland. This article is an open access article distributed under the terms and conditions of the Creative Commons Attribution (CC BY) license (<https://creativecommons.org/licenses/by/4.0/>).

1. Introduction

Prostate cancer (PCa) is the most common cancer in men in developed countries. More than 80 years have passed since Charles Huggins showed that a decrease in androgen levels in patients with PCa causes tumor regression [1]. The androgenic pathway remains the main target of prostate cancer therapies—it plays a major role in the formation and progression of this type of cancer [2]. Therapy has aimed at reducing the content of testosterone in the blood, which can significantly slow down the process of tumor development and alleviate the patient's condition. Therefore, a number of drugs are used to block the synthesis of androgens in the testes or adrenal cortex as an accepted alternative to surgical intervention (orchiectomy).

The most important step in the biosynthesis of androgens is the conversion of pregnenolone to 17 α -OH-pregnenolone, and then to dehydroepiandrosterone (DHEA), secreted by the testes and adrenal cortex [3]. Both reactions proceed with the participation of cytochrome P450 CYP17A1, which combines the functions of 17 α -hydroxylase and 17,20-lyase.

In 2011, a new CYP17A1 inhibitor, abiraterone, was approved, effective for the treatment of prostate cancer, insensitive to hormone therapy, and reducing the level of testosterone in the blood [4]. Thus, abiraterone (Figure 1), which is a pyridine derivative of DHEA, inhibits two key reactions in the androgen synthesis pathway. The optimal CYP17A1 inhibitor should have significant effect on 17,20-lyase activity, with moderate or no effect towards 17 α -hydroxylase activity of the enzyme, to modulate sex steroid biosynthesis with minimal effect on glucocorticoid hormones biosynthesis [5].

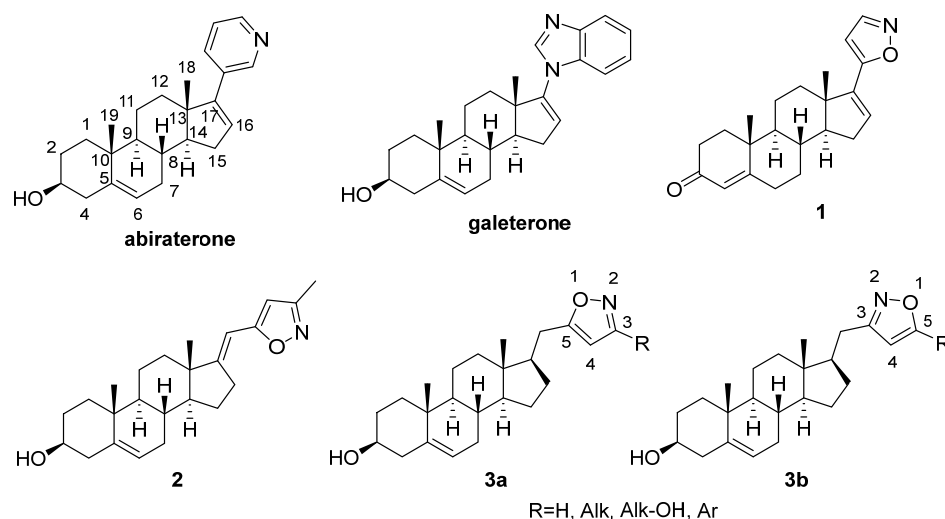


Figure 1. Structures of some heterocyclic steroids with anti-prostate cancer effects and target compounds **3a** and **3b**.

During the development of new inhibitors of CYP17A1, a large number of androstane and pregnane derivatives have been introduced containing pyridyl-, picolidine-, pyrazolyl-, imidazolyl-, triazolyl-, isoxazolyl-, dihydrooxazolyl-, tetrahydrooxazolyl-, benzimidazolyl-, and carbamoyl- substituents, mainly in positions 16, 17, and 22 [6–18]. Galeterone, the most advanced among them and having a multiple mechanism of action, has reached phase III clinical trials [19].

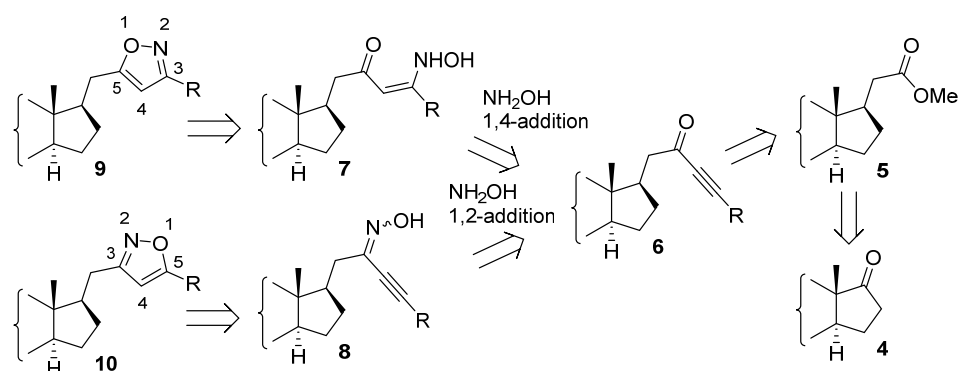
To date, previous studies have shown that steroids with 5-membered rings containing one nitrogen and one oxygen (oxazole or isoxazole) are of great interest in the development of drugs for the treatment of prostate cancer [6,11,12,14,20–25]. Thus, isoxazole **2** showed potent and non-competitive inhibition of human microsomal 17 β -hydroxylase/C17,20-lyase, with an IC₅₀ value of 59 nM, and demonstrated potent and competitive inhibition of 5 α -reductase in human prostate microsomes with an IC₅₀ value of 33 nM [21]. It was also shown that **1**, at a concentration of 5 μ M, exhibits antiandrogenic activity in human prostate cancer cell lines (e.g., LNCaP), preventing the binding of labeled synthetic androgen R1881 (5 nM) to the androgen receptor (AR). Compound **2** had a significant effect on the growth of LNCaP and PC-3 cells, commensurate with that of galeterone [11]. It should be noted that **2** showed no inhibitory potency towards CYP17A1, thus confirming that inhibition of this enzyme is not the only mechanism of anticancer action of such steroids.

Obviously, further studies of new nitrogen-containing steroids, in particular the investigation of their effect on various signaling pathways involved in the pathological processes of tumor development, are relevant and of great interest. In this regard, the present paper aims (i) to develop synthesis of a series of novel steroidal isoxazoles **3a,b** and (ii) to carry out studies of their effects on the 17 α -hydroxylase and 17,20-lyase activity of human CYP17A1 and the ability of selected compounds to affect the downstream androgen receptor signaling.

2. Results and Discussion

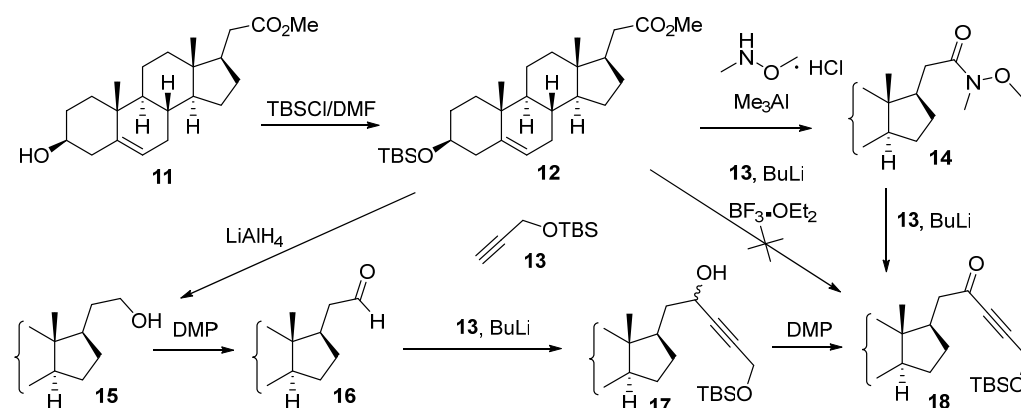
2.1. Chemistry

One of the tasks of the present study was to develop an efficient route to regioisomeric isoxazoles **9** and **10** (Scheme 1). We envisaged that both isoxazoles could be derived from the same α,β -acetylenic ketones **6** via 1,4- or 1,2-cycloaddition of hydroxylamine followed by the cyclization of intermediates **7** or **8**. The regioselectivity of the addition of hydroxylamine to acetylenic ketones can be controlled by the choice of solvent: in a mixture of tetrahydrofuran-water, the reaction proceeds in a 1,4-manner [26], while in aqueous methanol, 1,2-addition products are formed [27,28]. Ynones in **6** could be made available from the known esters in **5**, which in turn can be prepared from commercial 17-ketones in **4**.



Scheme 1. Retrosynthetic analysis for the synthesis of isoxazoles **9**, **10**.

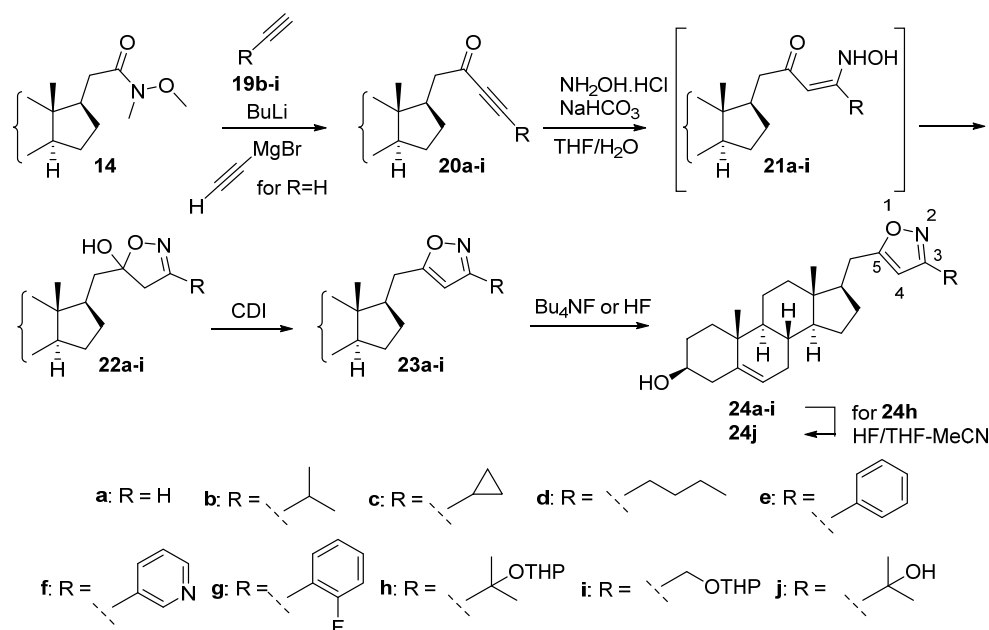
The synthesis of target compounds was initiated with ester **11**, obtained in two steps from androstenedione [29]. Initially, the possibility of a one-step conversion of **12** into **18**, described for fluoroketones [26] and consisting in the addition of lithium acetylenides to esters in the presence of boron trifluoride etherate, was studied (Scheme 2). However, the reaction of **12** with a lithium salt of **13** resulted in the formation of a complex mixture of products.



Scheme 2. Attempted approaches to the synthesis of ynone **18**.

Next, an attempt was made to obtain ynone **18** using an approach based on the conversion of ester **12** to aldehyde **16**. Its reaction with the lithium salt of **13** gave a mixture of isomeric alcohols in **17**, which was oxidized in the last stage to give the target ynone **18**. The obvious disadvantage of this method was the necessity to accomplish a multistep reaction procedure. In this connection, the possibility of using Weinreb amides was studied. This approach showed good results for the preparation of ynone **18** via amide **14** and was further used for the synthesis of all other α,β -acetylenic ketones.

Ynone **20b–i** was prepared in a 78–90% yield by the addition of lithium salts obtained in situ from BuLi and the corresponding acetylene **19b–i** to the Weinreb amide **14** (Scheme 3). The unsubstituted ynone **20a** was synthesized by using commercially available ethynylmagnesium bromide as an organometallic reagent.

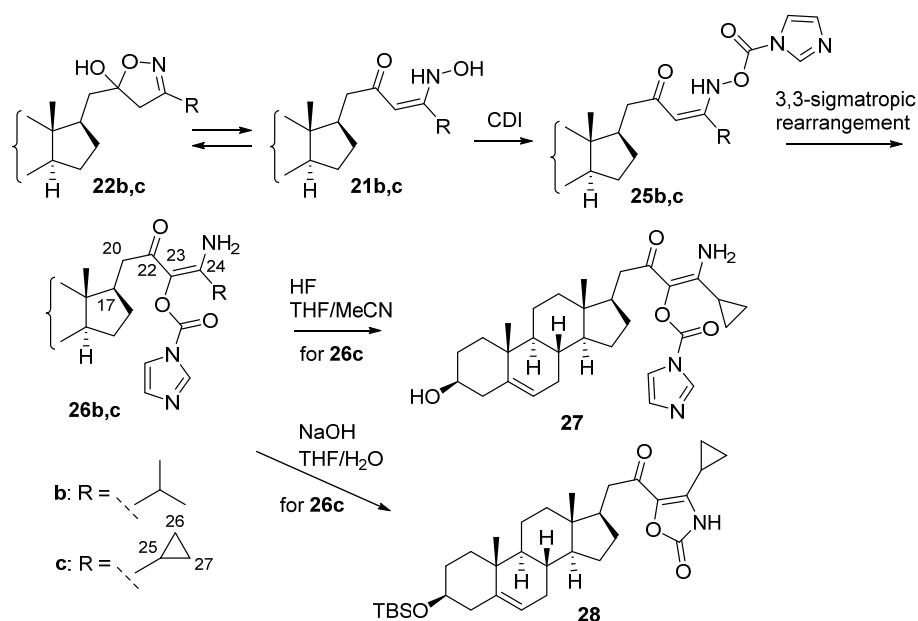


Scheme 3. Synthesis of the isoxazoles in **24**.

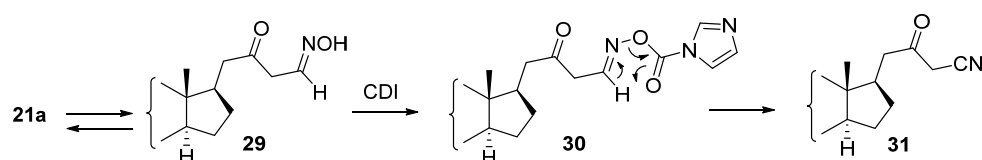
The regioselectivity of hydroxylamine addition to α,β -acetylenic ketones is highly dependent on the reaction conditions. The optimal conditions for the conjugated 1,4-addition were found using a mixture of organic solvents with water [28]. The enamine, formed as a result of conjugated addition, undergoes intramolecular cyclization to form 5-hydroxy-4,5-dihydroisoxazoles. We used the reaction conditions (water–THF, NaHCO_3 as a base) proposed in [26]; in this case, the hydroxyisoxazoline **22a–i** was obtained in a 56–88% yield.

The next stage involved the dehydration of **22a–i** to form the corresponding isoxazole **23a–i**. The reaction proceeded relatively smoothly in the case of the derivative **22d–i**; however, isoxazoles **23b,c** were obtained only in 9 and 45% yields, respectively. Simultaneously, compounds **26b,c** (44–50%) were isolated from the reaction mixture (Scheme 4). The possible mechanism of their formation can be explained as follows. 5-Hydroxy-4,5-dihydroisoxazoles **22b,c** are expected to exist in equilibrium with enehydroxylamines **21b,c**. The latter, as a result of reaction with CDI, can give derivatives **25b,c**. It is known that such derivatives can undergo 3,3-sigmatropic rearrangement [30,31]. In the case of **25b,c**, such a rearrangement resulted in the formation of substituted enaminketones (**26b,c**). Their structures were determined by spectral methods, including two-dimensional NMR experiments. Signals at δ 197.1, 134.2, and 157.2 in the ^{13}C NMR spectrum of **26c** were assigned to C-22, C-23, and C-24, respectively. The connectivity of the side chain was established by the key HMBC correlations: H-20 and H-17 correlated to C-22; H-25, H-26, and H-27 correlated to C-24; and H-20 correlated to C-23.

Another direction of the reaction of 5-hydroxy-4,5-dihydroisoxazoles with CDI was found in the case of compound **22a**. In addition to the target isoxazole **23a** (51%), β -oxonitrile **31** was also isolated in 40% yield. A possible mechanism of its formation is shown in Scheme 5. It is assumed that the enehydroxylamine **21a** is converted to β -ketoxime **29**, which then reacts with CDI to form the imidazole derivative **30**. The latter loses imidazole carboxylic acid in a six-membered transition state [32] to form β -oxonitrile **31**.



Scheme 4. Synthetic transformations of hydroxyisoxazolines **22b,c**.



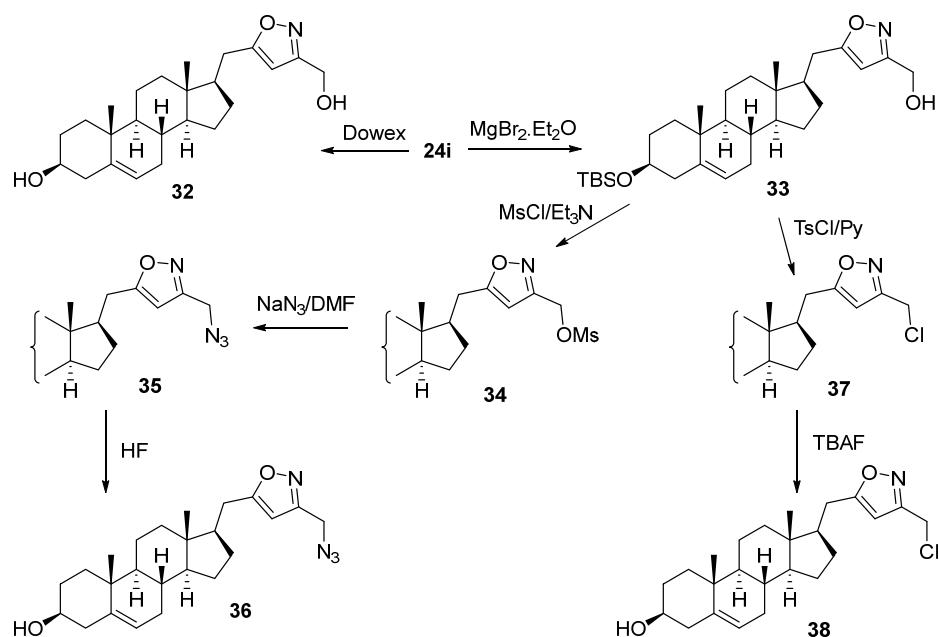
Scheme 5. Possible mechanism for the formation of ketonitrile **31**.

The removal of protective groups completed the synthesis of target isoxazoles **24** containing a steroid at C-5 of the isoxazole heterocycle. The reaction was carried out by treating the esters **23a–i** with TBAF or HF. The latter option is preferred for compound **24h**, additionally containing tetrahydropyranyl protection.

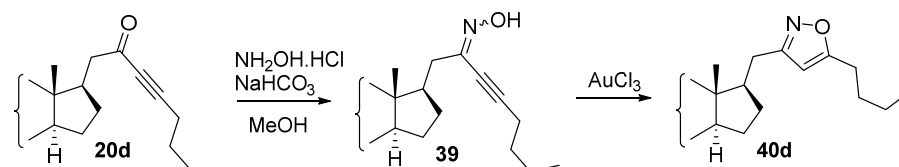
Attempts were made to carry out some transformations of the sigmatropic rearrangement product **26c** in order to obtain compounds suitable for biological testing (Scheme 4). Removal of the silyl protective group proceeded smoothly, without affecting the functional groups in the side chain, to form alcohol **27**. Removal of the imidazole-carboxylic fragment was expected to be achieved under alkaline hydrolysis conditions. However, the reaction led to compound **28**, containing an oxazolone heterocycle. An attempt to remove the silyl group in **28** ($\text{Bu}_4\text{NF}/\text{THF}$) gave a complex mixture of products.

Simultaneous removal of both protecting groups in **24i** gave the diol **32** (Scheme 6). Compound **24i** contains a functional group in the isoxazole core that can be used for the synthesis of other derivatives, which was demonstrated in the synthesis of azide **36**. Selective removal of the tetrahydropyranyl protecting group was achieved by reaction of **24i** with magnesium bromide diethyl etherate [33]. The tosylation reaction of **33** gave chloride **37** instead of the expected tosylate. The desired product **35** was obtained via $\text{S}_{\text{N}}2$ displacement of primary mesylate **34** with the azide group.

Ynone **20d** was used as a model compound to study suitable conditions for the preparation of isoxazoles **40**. Its reaction with hydroxylamine in aqueous methanol in the presence of NaHCO_3 [27,28] gave oxime **39** as a mixture (1:1) of *E/Z*-isomers (Scheme 7). The next step in the synthesis of isoxazole **40** was the gold-catalyzed cycloisomerization of acetylenic oximes [34]. The desired product **40d** was obtained from **39**, but in a moderate 46% yield, as only the *Z*-isomer underwent the cyclization under these conditions. At the same time, it was found that prolonged heating of the reaction mixture at the stage of hydroxylamine addition led directly to the formation of isoxazoles without any catalysis.

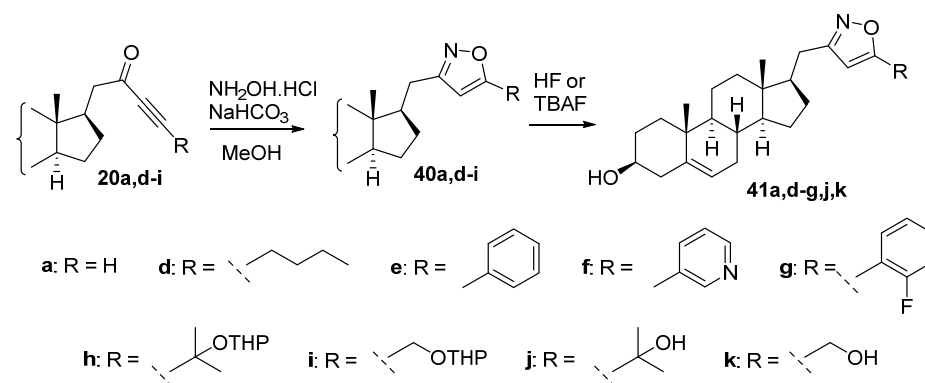


Scheme 6. Synthesis of the isoxazoles 32, 36, and 38.



Scheme 7. Synthesis of the isoxazole 40d.

For this reason, the transformation of the remaining yrones **20a,e–i** was carried out in one step without the isolation of the intermediate acetylenic oximes (Scheme 8). The yield of isoxazoles **40a,e–i** was 40–82%, depending on the substituent R. Removal of the silyl protective group was performed out by treatment with Bu_4NF or, in the case of compounds **40h,i**, containing additionally tetrahydropyranyl ether, with HF in a mixture of THF-MeCN.

Scheme 8. Synthesis of the isoxazoles **41a,d–g,j,k**.

2.2. Biology

Biological studies included analysis of the interaction of the prepared compounds with the CYP17A1 active site, testing their effect towards the AR-transcriptional activity and evaluation of their ability to influence the downstream AR signaling. Compounds used in one or more biological tests are shown in Table 1.

Table 1. Compounds used for biological studies.

N	Structure	N	Structure	N	Structure
24a		24j		41a	
24b		27		41e	
24c		32		41f	
24d		36		41g	
24e		38		41j	
24g				41k	

2.2.1. Effect of Compounds on 17 α -hydroxylase and 17,20-lyase Activity of Human CYP17A1

As the first step in the analysis of the interaction of compounds with the CYP17A1 active site, we performed spectrophotometric titration of selected compounds. Progesterone with $K_{d,app} < 1 \mu\text{M}$ was used as a positive control for the substrate-like ligand (type I). As a positive control for an inhibitor-like ligand (type II), abiraterone with a $K_{d,app} < 1 \mu\text{M}$ was used. DMSO or ethanol was used as a negative control. For the negative controls, no type I or type II spectral responses were observed. Analysis of binding of series of compounds (**24a,d,g,j**, **32**, **36**, **38**) with human CYP17A1 showed that only four compounds were able to bind to the active site of human CYP17A1 (**32** with $K_{d,app}$ -13.41 \pm 2.38 μM , **24j** with $K_{d,app}$ -1.90 \pm 0.23 μM , **24d** with $K_{d,app}$ -1.50 \pm 0.21 μM , and **24a** with $K_{d,app}$ -0.13 \pm 0.02 μM). However, all these compounds show type I (substrate-like) spectral response, which indicates their potentially low inhibitory ability against this enzyme.

To evaluate the effect of isoxazoles on a potential molecular target, CYP17A1, we performed an inhibitory assay using an in vitro reconstituted system containing recombinant human CYP17A1. We analyzed the inhibitory effect of the compounds (50 μM —final

concentration) on two types of reactions catalyzed by CYP17A1: 17 α -hydroxylase activity and 17,20-lyase activity. There was almost no inhibition of 17,20-lyase activity of human CYP17A1 with the compound **24j** (11% of enzyme inhibition at 50 μ M of compound **24j**). Most isoxazoles were shown to have a moderate inhibitory effect on human CYP17A1 activity (Table 2). The maximum inhibition of 17,20-lyase activity was found for isoxazole **41a** containing no substituent at C-5 of the heterocyclic ring. A similar inhibitory effect was observed for pyridine derivative **41f**. It should be noted that compound **41a** showed a minimal inhibitory capacity for 17 α -hydroxylase activity, being the most 17,20 lyase selective, which is important for the development of the next generation CYP17 targeted drugs [35].

Table 2. Inhibitory effect of compounds on human CYP17A1-catalyzed reaction.

Compound	17 α -Hydroxylase Activity		17,20-Lyase Activity	
	Activity, min ⁻¹	Inhibition, %	Activity, min ⁻¹	Inhibition, %
Control	1.95 \pm 0.10	-	1.98 \pm 0.10	-
24b	1.07 \pm 0.19	45.0	1.64 \pm 0.08	17.4
24c	1.06 \pm 0.10	45.7	1.86 \pm 0.08	6.3
41a	1.89 \pm 0.05	3.1	1.14 \pm 0.10	42.3
41e	1.30 \pm 0.16	33.3	1.30 \pm 0.16	34.4
41k	1.84 \pm 0.03	5.5	1.58 \pm 0.07	20.4
41g	1.68 \pm 0.36	13.6	1.46 \pm 0.33	26.4
41j	1.73 \pm 0.24	10.9	1.39 \pm 0.47	29.7
41f	1.43 \pm 0.17	26.5	1.17 \pm 0.13	41.1

2.2.2. The Effect of Derivatives on AR Transcriptional Activity and Viability of PCa Cells

Based on the structural similarity of novel derivatives with galeterone and other published compounds (abiraterone, **3**, and [6]), we tested the effect of our compounds towards the AR-transcriptional activity. Compounds were evaluated using an AR-dependent reporter cell line (ARE14) with a firefly-luciferase gene under the control of an androgen response element [36].

As shown in Table 3, within the studied isoxazoles, three AR antagonists with moderate activity were found (reduced R1881-stimulated AR transcriptional activity to \leq 50% at 50 μ M concentration), namely **24j**, **32**, and **41a**. Despite that, these derivatives acted as AR-antagonists in dose-dependent manner, and none of them were able to overcome the activity of the standard steroidal antagonist galeterone (\approx 35% of activity at 10 μ M concentration). Based on the obtained results, it is evident that derivatives bearing only unsubstituted isoxazole (**41a**), or isoxazoles substituted with small polar substituent (-CH₃-OH in **32**, t-butyl in **24j**), were able to decrease the AR-transcriptional activity, while isoxazoles bearing longer unsaturated (**24d**), or bulky aromatic substituents (**24e**, **24g**), were inactive. Importantly, none of novel derivatives displayed AR-agonist activity in the chosen concentrations (Table 3).

Antiproliferative properties of all novel steroids were tested in two AR-positive prostate cancer cell lines (LNCaP and LAPC-4) and one AR-negative cell line (DU145) using the Alamar-blue assay after 72 h treatment. Antiproliferative activities of the most potent derivatives **24j** and **32** displayed mid-micromolar values (in agreement to AR-antagonist assay) in both AR-positive PCa cell lines, while no targeting of the AR-negative DU145 cells was observed. Compound **36** displayed reasonable antiproliferative activity only in LAPC-4 cell line.

We further evaluated the potency of the most active derivative **24j**. We analyzed its effect on AR transcriptional activity in a broad concentration range and found the IC₅₀ value = 21.11 \pm 1.07 μ M (Figure 2A) while IC₅₀ = 7.59 μ M for galeterone. On the other hand, galeterone displayed worse antiproliferative activities and effects related to AR signaling. Importantly, no clear agonist activity was observed for **24j** in tested concentrations (Figure 2A).

Table 3. AR transcriptional and antiproliferative activities of novel derivatives ^a.

Cmp.	AR Transcriptional Activity (%)						Viability after 72 h (GI ₅₀) ^d		
	ANTAGONIST MODE ^b			AGONIST MODE ^c			LNCaP	LAPC-4	DU145
	50 μM	10 μM	2 μM	50 μM	10 μM	2 μM			
24d	103.6	112.8	109.0	18.6	21.1	17.8	>50	>50	>50
24e	125.3	101.1	101.3	12.8	14.2	14.7	>50	>50	>50
24g	111.6	112.5	112.9	19.7	17.5	15.6	>50	>50	>50
24j	21.6	84.8	100.2	6.1	12.6	14.4	25.8	18.2	>50
27	63.5	62.0	89.7	20.4	20.9	17.4	>50	>50	>50
32	31.1	87.8	99.7	14.6	12.1	14.0	19.5	18.9	>50
36	67.4	72.5	101.1	16.3	12.0	14.7	>50	19.0	>50
38	78.2	92.6	96.1	7.3	13.0	14.6	>50	>50	>50
41a	50.8	73.7	98.2	12.1	14.7	14.5	>50	>50	>50
Gal	3.0	35.1	65.2	2.4	10.8	15.4	46.8	28.6	47.6

^a raw data from all assays and standard errors are included in the Supplementary Materials, Table S1. ^b Measured in the presence of compound and 1 nM R1881 and normalized to a signal of 1 nM R1881 = 100%, determined in duplicate and repeated twice. ^c Measured in the presence of compound only, normalized to signal of 1 nM R1881 = 100% and measured in duplicate and repeated twice. ^d Measured at least in duplicate.

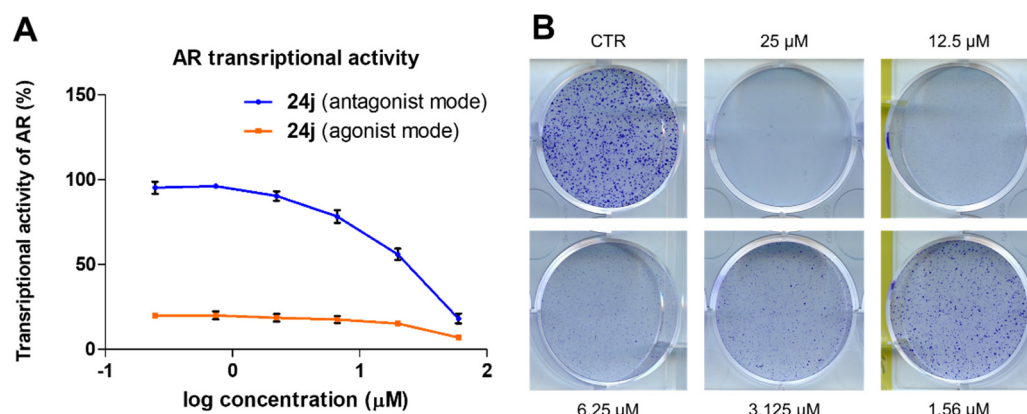


Figure 2. (A) Transcriptional activity of AR measured in reporter cell line in both antagonist (competition with 1 nM R1881) and agonist (presence of compound alone) mode upon treatment with different concentration of **24j**. Mean and SD was plotted from $n = 4$. Raw data are available in the Supplementary Materials, Table S2. (B) Colony formation assay of PCa cells LAPC-4 after treatment with **24j** for 10 days. The raw picture and comparison with the activity of standards abiraterone and galeterone is presented in Supplementary Materials, Figures S1 and S2.

We also performed colony formation assay (CFA) within 10 days to evaluate the prolonged antiproliferative potency of **24j** in the LAPC-4 cell line. CFA is frequently used for the validation of PCa cell lines growth because of their high doubling time in culture. Our compound, **24j**, significantly inhibited the formation of cell colonies in a dose-dependent manner after 10 days in LAPC-4, already from a 1.56 μM concentration (Figure 2B).

2.2.3. Targeting the AR Signaling Pathway

Further, we evaluated the ability of compounds **24j**, **32**, and **41a** to influence the downstream AR signaling (levels of known transcriptional targets PSA and Nkx3.1) in LAPC-4 and LNCaP cell lines after R1881 stimulation. Western blot analysis (Figure 3) showed that **24j** and **32** were able to markedly suppress R1881 stimulated S81-phosphorylation in both LAPC-4 and LNCaP cell lines after 24 h. Observed effects were accompanied by a profound decrease in Nkx3.1 and PSA protein levels in LAPC-4, while were only limited in LNCaP cells (Figure 3).

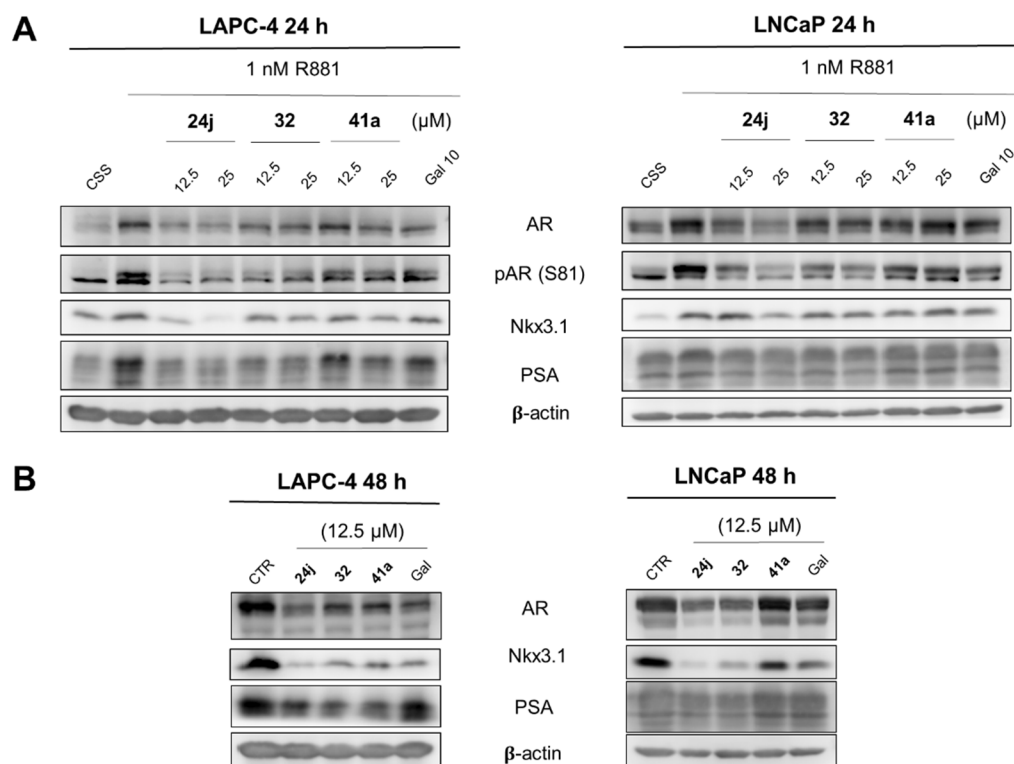


Figure 3. Western blotting analysis of AR and AR-regulated proteins after being treated with LAPC-4 and LNCaP. **(A)** PCa cells were deprived of androgens (cultivated in CSS-supplemented medium) for 24 h and then treated with different concentrations of candidate compounds or standard galeterone (Gal), combined with 1 nM R1881 for 24 h. **(B)** PCa cells were cultivated in FBS-supplemented media and treated with candidate compounds or galeterone (Gal) for 48 h. The level of β -actin serves as a control for equal protein loading. Raw pictures are presented in Supplementary Materials Figures S3 and S4.

Candidate compounds were further tested in the same PCa cell lines (without R1881 activation) for a longer period to monitor the effects on AR stability. Compounds **24j** and **32** (12.5 μ M) induced a significant decrease in Nkx3.1 and PSA levels in both LAPC-4 and LNCaP after 48 h. Moreover, they both induced a significant decrease in AR protein level that was comparable to galeterone's effect.

2.2.4. Molecular Docking into the Active Site of CYP17A1 and into the AR-LBD

The binding of candidate compounds into their cellular targets was evaluated by rigid molecular docking into the crystal structure of human CYP17A1 co-crystallized with abiraterone and heme (PDB:3RUK) and by flexible docking into the AR ligand-binding domain (LBD) from the crystal structure with DHT (PDB:2PIV).

The best binding pose of **41a** in the active site of CYP17A1 was oriented in nearly the same pose as abiraterone and showed similar binding energy ($\Delta G_{\text{Vina}} = -12.6$ kcal/mol and -13.0 kcal/mol, respectively) (Figure 4A,B). The isoxazole ring is oriented towards the Fe^{2+} central ion of heme, similar to the pyridine ring in abiraterone. The most promising compound, **24j**, was modelled into the CYP17A1 as well, with a similar pose as abiraterone and **41a**, but with lower binding energy ($\Delta G_{\text{Vina}} = -10.1$ kcal/mol, picture not shown).

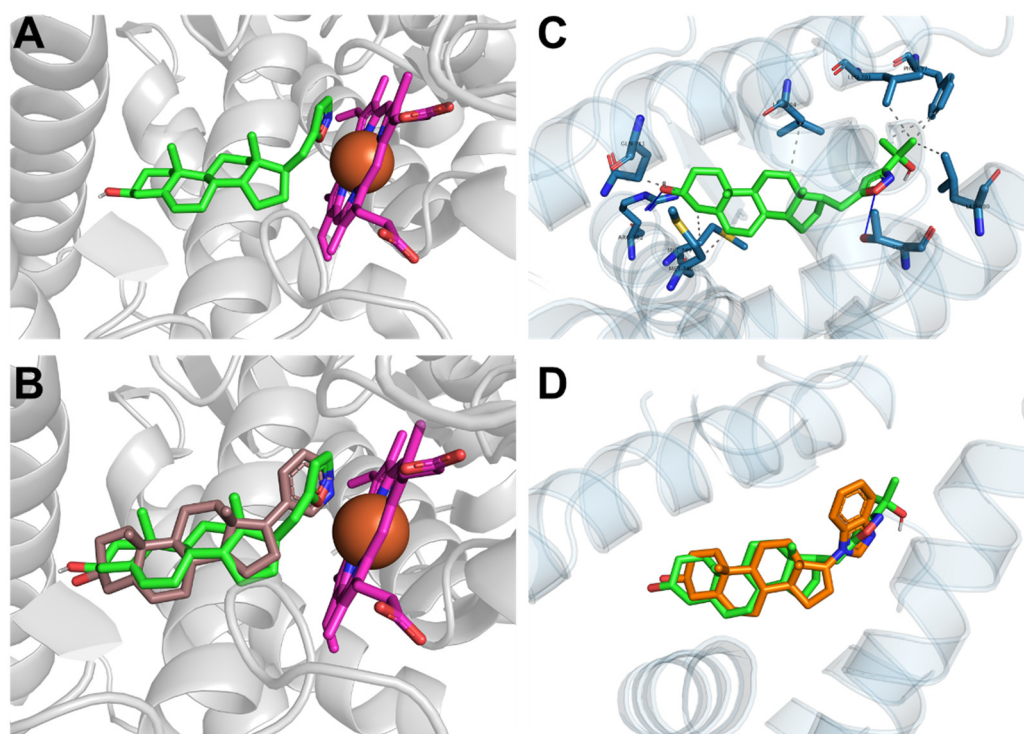


Figure 4. (A) Model of the binding pose of **41a** (green) in CYP17A1 (rigid docking into the PDB:3RUK) and (B) alignment of the binding pose with abiraterone (brown) from the original crystal structure. Heme is shown in magenta. (C) Model of the binding pose of **24j** (green) in AR-LBD (flexible docking into the PDB:2PIV) with the interacting amino acid residues. Hydrogen bonds are shown as blue lines, and hydrophobic bonds are shown by gray dashed lines. (D) Alignment of binding pose of **24j** with the galeterone (orange) binding pose from flexible docking.

In the case of the AR-LBD structure, two key amino acid residues in both extremities of the cavity (Arg752 and Thr877) were set as flexible. The docking of **24j** revealed a pose with extensive binding in AR-LBD, with binding energy comparable to galeterone ($\Delta G_{\text{Vina}} = -10.5$ kcal/mol and -10.8 kcal/mol, respectively (Figure 4C,D)). The position of the steroid core is conserved. C3-OH on the A-ring forms a typical hydrogen bond with Arg752, while the oxygen atom of the isoxazole ring forms a hydrogen bond with Thr877 at the other extremity of the LBD-cavity. The steroid core is further positioned by hydrophobic interactions with Gln711, Met745, Met746, and Leu 704. The tert-butyl substituent could be hydrophobically bound with Leu701, Phe647, and Leu880, which could be a key for the activity and selectivity of **24j** (Figure 4C).

3. Materials and Methods

3.1. Chemistry

Commercially available reagents were used without further purification. If necessary, solvents were distilled and dried before use by standard methods. Column chromatography was performed through silica gel (200–300 mesh). Thin layer chromatography (TLC) was performed using Silica gel 60 F₂₅₄ plates and visualized using UV light or phosphomolybdic acid. ¹H and ¹³C NMR spectra were recorded in CDCl₃, on a Bruker AVANCE 500 spectrometer. Chemical shifts in ¹H NMR spectra are reported in parts per million (ppm) on the δ scale from an internal standard of residual non-deuterated solvent in CDCl₃ (7.26 ppm). Data for ¹H NMR are reported as follows: chemical shift, multiplicity (s = singlet, d = doublet, t = triplet, q = quartet, m = multiplet, br = broad), coupling constant in Hertz (Hz), and integration. Data for ¹³C NMR spectra are reported in terms of chemical shift in ppm from the central peak of CDCl₃ (77.16 ppm). High resolution mass

spectrometry (HRMS) analysis was performed using a Q Exactive HFX (Thermo Scientific) mass spectrometer in ESI ionization mode.

3.1.1. Methyl 2-(3 β -((*tert*-butyldimethylsilyl)oxy)-androst-5-en-17-yl)acetate (**12**)

A solution of alcohol **11** (prepared from androstenolone in two steps according to [29]) (1.92 g, 5.55 mmol), TBSCl (1.25 g, 8.29 mmol), and imidazole (838 mg, 12.3 mmol) in dry DMF (8 mL) was stirred at 90 °C for 12 h. After the reaction was completed, the mixture was diluted with water, the organic layer was separated, and the reaction product was extracted from the aqueous layer with PE. The combined organic extracts were dried with sodium sulfate. Then, the solvent was removed under reduced pressure, and the resulting residue was purified by column chromatography on SiO₂ (PE/EtOAc, 20:1) to yield ether **12** (2.35 g, 92%) as an oil. ¹H NMR (500 MHz, CDCl₃) δ 5.31 (dt, *J* = 5.4, 2.1 Hz, 1H), 3.65 (s, 3H), 3.47 (tt, *J* = 11.0, 4.7 Hz, 1H), 2.37 (dd, *J* = 14.7, 5.1 Hz, 1H), 2.26 (ddd, *J* = 13.5, 10.6, 2.7 Hz, 1H), 2.20–2.13 (m, 1H), 2.12 (dd, *J* = 14.7, 9.8 Hz, 1H), 1.00 (s, 3H), 0.88 (s, 9H), 0.60 (s, 3H), 0.05 (s, 6H). ¹³C NMR (126 MHz, CDCl₃) δ 174.5, 141.8, 121.2, 72.7, 55.8, 51.6, 50.6, 47.0, 43.0, 42.1, 37.6, 37.4, 36.8, 35.1, 32.2, 32.1, 32.1, 28.3, 26.1 (x3), 24.7, 20.9, 19.6, 18.4, 12.5, –4.4 (x2).

3.1.2. 3 β -((*tert*-Butyldimethylsilyl)oxy)-pregn-5-en-21-ol (**15**)

A mixture of ester **12** (95 mg, 0.27 mmol), LiAlH₄ (20 mg, 0.53 mmol), and THF (2 mL) was stirred at 0 °C for 30 min. Then saturated Na₂SO₄ (1 mL) and PE (3 mL) were added, and the precipitate was filtered off and washed with PE. The organic layer was evaporated to give alcohol **15** (89 mg, 99%) as an oil. ¹H NMR (500 MHz, CDCl₃) δ 5.31 (dt, *J* = 5.0, 2.0 Hz, 1H), 3.68 (ddd, *J* = 10.4, 8.3, 4.6 Hz, 1H), 3.60 (dt, *J* = 10.3, 6.9 Hz, 1H), 3.48 (tt, *J* = 11.1, 4.8 Hz, 1H), 2.26 (tq, *J* = 11.0, 2.7 Hz, 1H), 2.16 (ddd, *J* = 13.3, 5.0, 2.3 Hz, 1H), 1.98 (dtd, *J* = 17.1, 5.1, 2.7 Hz, 1H), 1.00 (s, 3H), 0.88 (s, 9H), 0.60 (s, 3H), 0.05 (s, 6H). ¹³C NMR (126 MHz, CDCl₃) δ 141.8, 121.2, 72.8, 62.8, 56.1, 50.8, 47.2, 43.0, 42.1, 37.8, 37.6, 36.8, 33.7, 32.2, 32.2, 32.1, 28.5, 26.1 (x3), 25.0, 21.0, 19.6, 18.4, 12.6, –4.4 (x2).

3.1.3. 3 β -((*tert*-Butyldimethylsilyl)oxy)-pregn-5-en-21-al (**16**)

A mixture of alcohol **15** (100 mg, 0.23 mmol), Dess-Martin reagent (850 mg, 2.0 mmol), and DCM (4.6 mL) was stirred under argon at 0 °C for 30 min. Then it was diluted with water and extracted with a mixture of PE/EtOAc (3:1). The residue after evaporation of the solvents was chromatographed on SiO₂ (PE/EtOAc, 90:1→70:30) to afford aldehyde **16** (64 mg, 65%) as an oil. ¹H NMR (500 MHz, CDCl₃) δ 9.76 (t, *J* = 2.4 Hz, 1H), 5.31 (dd, *J* = 5.0, 2.5 Hz, 1H), 3.47 (tt, *J* = 11.1, 4.7 Hz, 1H), 1.00 (s, 3H), 0.88 (s, 9H), 0.61 (s, 3H), 0.05 (s, 6H).

3.1.4. 5-((*tert*-Butyldimethylsilyl)oxy)-1-((17*R*)-3 β -((*tert*-butyldimethylsilyl)oxy)-androst-5-en-17-yl)pent-3-yn-2-one (**18**)

A 2M solution of BuLi in hexanes (0.7 mL, 1.4 mmol) was added to a cooled –70 °C solution of *tert*-butyldimethyl(prop-2-yn-1-yloxy)silane (**13**) (prepared according to [37], 211 mg, 1.24 mmol) in THF (4 mL). After 15 min, a solution of aldehyde **16** (380 mg, 0.88 mmol) in THF (2.5 mL) was added to the reaction mixture. It was stirred for 20 min at –70 °C, then the cooling bath was removed, and the mixture was allowed to get ambient temperature. NH₄Cl (150 mg) was added, then the mixture was diluted with water and extracted with EtOAc. The organic layers were dried over Na₂SO₄, then evaporated, and the residue was chromatographed on SiO₂ to give a mixture of isomeric at C-22 alcohol **17** (467 mg), which was used in the next step without further purification.

A mixture of alcohol **17** (467 mg, 0.78 mmol), Dess-Martin reagent (2.30 g, 5.42 mmol), and DCM (15 mL) was stirred under argon at 0 °C for 3 h. Then it was diluted with water and extracted with DCM. The residue after evaporation of the extracts was chromatographed on SiO₂ (PE/EtOAc, 98:2) to give ketone **18** (388 mg, 73% from **16**) as an oil. ¹H NMR (500 MHz, CDCl₃) δ 5.32 (dt, *J* = 5.3, 2.1 Hz, 1H), 4.47 (s, 1H), 3.48 (tt, *J* = 11.1, 4.7 Hz, 1H), 2.63 (dd, *J* = 15.2, 4.0 Hz, 1H), 2.43–2.33 (m, 1H), 2.26 (ddd, *J* = 13.8, 10.8, 2.8 Hz,

1H), 2.17 (ddd, $J = 13.3, 5.1, 2.3$ Hz, 1H), 2.04–1.87 (m, 1H), 1.81 (dt, $J = 13.3, 3.6$ Hz, 1H), 1.00 (s, 3H), 0.92 (s, 9H), 0.89 (s, 9H), 0.61 (s, 3H), 0.14 (s, 6H), 0.05 (s, 6H). ^{13}C NMR (126 MHz, CDCl_3) δ 188.1, 141.8, 121.1, 90.3, 84.3, 72.7, 55.7, 51.7, 50.6, 46.7, 46.2, 43.0, 42.3, 37.6, 37.5, 36.8, 32.2, 32.1, 32.1, 28.2, 26.1 (x3), 25.9 (x3), 24.8, 20.9, 19.6, 18.4, 12.7, -4.4 (x2), -5.0 (x2).

3.1.5. 2-(3 β -((*tert*-Butyldimethylsilyloxy)-androst-5-en-17-yl)-N-methoxy-N-methylacetamide (**14**)

To a stirred suspension of Weinreb salt (555 mg, 5.72 mmol) in dry toluene (10 mL), a 1M solution of Me_3Al in heptane (5.7 mL, 5.7 mmol) was added dropwise at 0 °C. After stirring for 40 min at this temperature, a solution of ester **12** (1.00 g, 2.17 mmol) in toluene (10 mL) was added dropwise. The cooling bath was removed, and the reaction mixture was allowed to stir overnight at room temperature. A 2N solution of HCl was added on cooling until pH 2 was reached. The mixture was diluted with water and extracted with EtOAc. The combined organic extracts were washed with saturated aqueous NaHCO_3 , saturated NaCl, dried over anhydrous Na_2SO_4 , and evaporated to dryness. The residue was purified by silica gel column chromatography (PE/EtOAc, 100:0→70:30) to give the Weinreb amide **14** (650 mg, 61%) as an off-white solid. ^1H NMR (500 MHz, CDCl_3) δ 5.31 (dt, $J = 5.3, 2.0$ Hz, 1H), 3.68 (s, 3H), 3.47 (tt, $J = 10.9, 4.7$ Hz, 1H), 3.16 (s, 3H), 2.48 (dd, $J = 15.1, 4.2$ Hz, 1H), 2.25 (qd, $J = 13.3, 6.4$ Hz, 2H), 2.16 (ddd, $J = 13.3, 5.0, 2.3$ Hz, 1H), 1.00 (s, 3H), 0.88 (s, 9H), 0.63 (s, 3H), 0.05 (s, 6H). ^{13}C NMR (126 MHz, CDCl_3) δ 174.9, 141.7, 121.2, 61.3, 55.7, 50.6, 46.4, 43.0, 42.1, 37.6, 37.4, 36.8, 32.6, 32.2, 32.1, 32.1, 28.5, 26.1 (x3), 24.8, 20.9, 19.6, 18.4, 12.7, -4.4 (x2).

3.1.6. 1-(((17*R*)-3 β -((*tert*-Butyldimethylsilyloxy)-androst-5-en-17-yl)but-3-yn-2-one (**20a**)

To a solution of **14** (300 mg, 0.61 mmol) in THF (0.6 mL), a 0.5M THF solution of ethynylmagnesium bromide (2.8 mL, 1.4 mmol) was added at 0 °C. The reaction mixture was left to warm to room temperature for 1 h, then quenched with saturated NH_4Cl , and extracted with EtOAc. Combined organics were washed with water, brine, dried over Na_2SO_4 , and concentrated in vacuo. The crude product was purified by silica gel chromatography (PE:EtOAc, 100:0 to 85:15) to give ynone **20a** (221 mg, 79%) as a white solid. ^1H NMR (500 MHz, CDCl_3) δ 5.31 (dt, $J = 5.1, 2.1$ Hz, 1H), 3.48 (tt, $J = 11.0, 4.8$ Hz, 1H), 3.20 (s, 1H), 2.66 (dd, $J = 15.4, 4.1$ Hz, 1H), 2.45–2.33 (m, 1H), 2.26 (ddd, $J = 13.6, 10.9, 2.7$ Hz, 1H), 2.17 (ddd, $J = 13.3, 5.0, 2.3$ Hz, 1H), 2.03–1.86 (m, 2H), 1.81 (dt, $J = 13.3, 3.6$ Hz, 1H), 1.00 (s, 3H), 0.88 (s, 9H), 0.61 (s, 3H), 0.05 (s, 6H). ^{13}C NMR (126 MHz, CDCl_3) δ 187.9, 141.8, 121.1, 81.9, 78.4, 72.7, 55.7, 50.6, 46.9, 46.1, 43.0, 42.3, 37.6, 37.5, 36.8, 32.2, 32.1, 32.1, 28.2, 26.1 (x3), 24.8, 20.9, 19.6, 12.7, -4.4 (x2). HRMS (ESI): m/z calcd for $\text{C}_{29}\text{H}_{47}\text{O}_2\text{Si}$ $[\text{M}+\text{H}]^+$: 455.3340, found 455.3350.

3.1.7. General Procedure for the Synthesis of Yrones (**20b–i**)

To a solution of an appropriate terminal alkyne **19b–i** (2.5 eq) in dry THF (1.5M), $n\text{-BuLi}$ (2.3M in hexane, 2.5 eq) was added dropwise at -78 °C. The resulting solution was stirred at -50 °C for 40 min, then a 2M solution of the Weinreb amide **14** (1 eq) in THF was added dropwise at -78 °C. The reaction mixture was slowly warmed to room temperature over 0.5 h and stirred for additional 1–1.5 h (monitored by TLC). Upon completion of the reaction, the mixture was quenched with saturated aq. NH_4Cl and extracted with EtOAc. The organic layers were washed with water and saturated NaCl, dried over Na_2SO_4 , and concentrated and purified by silica gel chromatography (PE:EtOAc), thus affording yrones (**20b–i**).

1-(((17*R*)-3 β -((*tert*-Butyldimethylsilyloxy)-androst-5-en-17-yl)-5-methylhex-3-yn-2-one (**20b**)

The title compound **20b** (130 mg) was prepared as a white solid in 85% yield using 3-methylbut-1-yne (**19b**) as an alkyne. ^1H NMR (500 MHz, CDCl_3) δ 5.31 (dt, $J = 5.5, 2.1$ Hz, 1H), 3.47 (tt, $J = 11.0, 4.7$ Hz, 1H), 2.71 (hept, $J = 7.0$ Hz, 1H), 2.60 (dd, $J = 15.3, 4.3$ Hz, 1H), 2.35 (dd, $J = 15.3, 9.7$ Hz, 1H), 2.26 (tq, $J = 11.1, 2.8$ Hz, 1H), 2.17 (ddd, $J = 13.3, 5.0, 2.4$ Hz,

1H), 1.24 (s, 3H), 1.22 (s, 3H), 1.00 (s, 3H), 0.88 (s, 9H), 0.60 (s, 3H), 0.05 (s, 3H). ¹³C NMR (126 MHz, CDCl₃) δ 189.0, 141.8, 121.2, 98.8, 80.5, 72.7, 55.7, 50.6, 47.0, 46.4, 43.0, 42.3, 37.6, 37.5, 36.8, 32.2, 32.1, 32.1, 28.3, 26.1 (x3), 24.9, 22.1 (x2), 20.9, 20.9, 19.6, 18.4, 12.7, −4.4 (x2).

1-((17R)-3β-((*tert*-Butyldimethylsilyloxy)-androst-5-en-17-yl)-4-cyclopropylbut-3-yn-2-one (20c)

The title compound **20c** (235 mg) was prepared as a white solid in 78% yield using ethynylcyclopropane (**19c**) as an alkyne. ¹H NMR (500 MHz, CDCl₃) δ 5.32 (dd, *J* = 4.9, 2.5 Hz, 1H), 3.48 (tt, *J* = 11.0, 4.7 Hz, 1H), 2.58 (dd, *J* = 15.2, 4.3 Hz, 1H), 2.37–2.21 (m, 2H), 2.17 (ddd, *J* = 13.4, 5.1, 2.3 Hz, 1H), 1.00 (s, 3H), 0.89 (s, 9H), 0.60 (s, 3H), 0.05 (s, 6H). ¹³C NMR (126 MHz, CDCl₃) δ 188.6, 141.8, 121.2, 98.5, 72.7, 55.7, 50.6, 46.7, 46.4, 43.0, 42.3, 37.6, 37.5, 36.8, 32.2, 32.2, 32.1, 28.3, 26.1 (x3), 24.9, 20.9, 19.6, 18.4, 12.7, 9.8 (x2), −0.1, −4.4 (x2). HRMS (ESI): *m/z* calcd for C₃₂H₅₁O₂Si [M+H]⁺: 495.3653, found 495.3665.

1-((17R)-3β-((*tert*-Butyldimethylsilyloxy)-androst-5-en-17-yl)oct-3-yn-2-one (20d)

The title compound **20d** (290 mg) was prepared as a white solid in 89% yield using hex-1-yne **3-2c** as an alkyne. ¹H NMR (500 MHz, CDCl₃) δ 5.31 (dt, *J* = 4.9, 2.0 Hz, 1H), 3.48 (tt, *J* = 11.0, 4.7 Hz, 1H), 2.60 (dd, *J* = 15.2, 4.2 Hz, 1H), 2.39–2.31 (m, 3H), 2.26 (tq, *J* = 11.2, 2.8 Hz, 1H), 2.17 (ddd, *J* = 13.3, 5.0, 2.3 Hz, 1H), 1.00 (s, 3H), 0.93 (t, *J* = 7.4 Hz, 3H), 0.88 (s, 9H), 0.60 (s, 3H), 0.05 (s, 6H). ¹³C NMR (126 MHz, CDCl₃) δ 188.8, 141.7, 121.1, 94.2, 81.3, 72.6, 55.6, 50.5, 46.8, 46.3, 42.9, 42.1, 37.5, 37.4, 36.7, 32.1, 32.0, 32.0, 29.8, 28.1, 26.0 (x3), 24.7, 22.0, 20.8, 19.5, 18.7, 18.3, 13.5, 12.6, −4.5 (x2). HRMS (ESI): *m/z* calcd for C₃₃H₅₅O₂Si [M+H]⁺: 511.3966, found 511.3979.

1-((17R)-3β-((*tert*-Butyldimethylsilyloxy)-androst-5-en-17-yl)-4-phenylbut-3-yn-2-one (20e)

The title compound **20e** (850 mg) was prepared as a white solid in 89% yield using ethynylbenzene (**19e**) as an alkyne. ¹H NMR (500 MHz, CDCl₃) δ 7.57 (dt, *J* = 6.9, 1.4 Hz, 2H), 7.49–7.42 (m, 1H), 7.42–7.34 (m, 2H), 5.32 (dd, *J* = 4.8, 2.4 Hz, 1H), 3.48 (tt, *J* = 11.0, 4.7 Hz, 1H), 2.75 (dd, *J* = 15.2, 4.0 Hz, 1H), 2.49 (dd, *J* = 15.1, 9.4 Hz, 1H), 2.27 (ddt, *J* = 13.5, 11.0, 2.7 Hz, 1H), 2.17 (ddd, *J* = 13.3, 5.0, 2.3 Hz, 1H), 1.01 (s, 3H), 0.89 (s, 9H), 0.65 (s, 3H), 0.06 (s, 6H). ¹³C NMR (126 MHz, CDCl₃) δ 188.6, 141.8, 133.2 (x2), 130.8, 128.8 (x2), 121.2, 120.3, 90.6, 88.4, 72.7, 55.7, 50.6, 47.0, 46.5, 43.0, 42.4, 37.6 (x2), 36.8, 32.2, 32.2, 32.1, 28.3, 26.1 (x3), 24.9, 21.0, 19.6, 18.4, 12.8, −4.4 (x2).

1-((17R)-3β-((*tert*-Butyldimethylsilyloxy)-androst-5-en-17-yl)-4-(pyridin-3-yl)but-3-yn-2-one (20f)

The title compound **20f** (360 mg) was prepared as a white solid in 90% yield using 3-ethynylpyridine (**19f**) as an alkyne. ¹H NMR (500 MHz, CDCl₃) δ 8.82–8.76 (m, 1H), 8.66 (dd, *J* = 5.0, 1.6 Hz, 1H), 7.85 (dt, *J* = 7.9, 1.9 Hz, 1H), 7.33 (ddd, *J* = 7.9, 5.0, 0.9 Hz, 1H), 5.32 (dt, *J* = 4.5, 2.0 Hz, 1H), 3.48 (tt, *J* = 11.0, 4.7 Hz, 1H), 2.76 (dd, *J* = 15.4, 4.1 Hz, 1H), 2.51 (dd, *J* = 15.4, 9.4 Hz, 1H), 2.26 (tq, *J* = 11.2, 2.6 Hz, 1H), 2.17 (ddd, *J* = 13.3, 5.0, 2.3 Hz, 1H), 2.05–1.92 (m, 3H), 1.81 (dt, *J* = 13.3, 3.5 Hz, 1H), 1.01 (s, 3H), 0.88 (s, 8H), 0.65 (s, 3H), 0.05 (s, 6H). ¹³C NMR (126 MHz, CDCl₃) δ 188.1, 153.4, 150.8, 141.8, 139.9, 123.4, 121.1, 117.6, 90.8, 86.5, 72.7, 55.7, 50.6, 47.0, 46.4, 43.0, 42.4, 37.6 (x2), 36.8, 32.2, 32.2, 32.1, 28.3, 26.1 (x3), 24.9, 20.9, 19.6, 18.4, 12.8, −4.4 (x2).

1-((17R)-3β-((*tert*-Butyldimethylsilyloxy)-androst-5-en-17-yl)-4-(2-fluorophenyl)but-3-yn-2-one (20g)

The title compound **20g** (160 mg) was prepared as a white solid in 85% yield using 1-ethynyl-2-fluorobenzene (**19g**) as an alkyne. ¹H NMR (500 MHz, CDCl₃) δ 7.55 (ddd, *J* = 7.7, 6.8, 1.8 Hz, 1H), 7.44 (dddd, *J* = 8.4, 7.3, 5.3, 1.8 Hz, 1H), 7.20–7.10 (m, 2H), 5.32 (dt, *J* = 5.5, 2.1 Hz, 1H), 3.48 (tt, *J* = 10.9, 4.7 Hz, 1H), 2.76 (dd, *J* = 15.1, 3.9 Hz, 1H), 2.50 (dd, *J* = 15.3, 9.1 Hz, 1H), 2.32–2.22 (m, 1H), 2.17 (ddd, *J* = 13.3, 5.0, 2.3 Hz, 1H), 2.07–1.95 (m, 3H), 1.81 (dt, *J* = 13.3, 3.6 Hz, 1H), 1.77–1.64 (m, 3H), 1.01 (s, 3H), 0.89 (s, 9H), 0.65 (s, 3H), 0.06 (s, 6H). ¹³C NMR (126 MHz, CDCl₃) δ 188.4, 163.7 (d, *J* = 255.3 Hz), 141.8, 134.8, 132.8

(d, $J = 8.0$ Hz), 124.5 (d, $J = 3.6$ Hz), 121.2, 116.0 (d, $J = 20.4$ Hz), 92.7, 83.9, 72.8, 55.7, 50.6, 47.1, 46.5, 43.0, 42.4, 37.6, 37.5, 36.9, 32.2, 32.2, 32.1, 28.3, 26.1 (x3), 24.9, 21.0, 19.6, 18.4, 12.8, -4.4 (x2).

1-((17R)-3 β -((*tert*-Butyldimethylsilyl)oxy)-androst-5-en-17-yl)-5-methyl-5-((tetrahydro-2H-pyran-2-yl)oxy)hex-3-yn-2-one (**20h**)

The title compound **20h** (570 mg) was prepared as a white solid in 83% yield using 2-((2-methylbut-3-yn-2-yl)oxy)tetrahydro-2H-pyran (**19h**) as an alkyne. ^1H NMR (500 MHz, CDCl_3) δ 5.31 (dt, $J = 4.4, 2.0$ Hz, 1H), 5.04–4.96 (m, 1H), 4.00–3.90 (m, 1H), 3.54–3.43 (m, 2H), 2.62 (dd, $J = 15.3, 4.3$ Hz, 1H), 2.38 (dd, $J = 9.7, 2.3$ Hz, 1H), 2.35 (dd, $J = 9.6, 2.3$ Hz, 0H), 2.26 (tq, $J = 11.2, 2.8$ Hz, 1H), 2.16 (ddd, $J = 13.4, 5.0, 2.3$ Hz, 1H), 1.58 (s, 3H), 1.54 (s, 6H), 1.00 (s, 3H), 0.88 (s, 9H), 0.61 (s, 3H), 0.05 (s, 6H). ^{13}C NMR (126 MHz, CDCl_3) δ 188.4, 141.8, 121.1, 96.5, 94.1, 83.3, 72.7, 70.8, 63.5, 55.7, 50.6, 47.0, 46.4, 43.0, 42.3, 37.6, 36.8, 32.2, 32.1, 32.1, 32.0, 29.8, 29.4, 28.2, 26.1, 25.4, 24.8, 20.9, 20.4, 19.6, 18.4, 12.7, -4.4 .

1-((17R)-3 β -((*tert*-Butyldimethylsilyl)oxy)-androst-5-en-17-yl)-5-((tetrahydro-2H-pyran-2-yl)oxy)pent-3-yn-2-one (**20i**)

The title compound **20i** (540 mg) was prepared as a white solid in 84% yield using 2-(prop-2-yn-1-yloxy)tetrahydro-2H-pyran (**19i**) as an alkyne. ^1H NMR (500 MHz, CDCl_3) δ 5.31 (dt, $J = 4.8, 2.0$ Hz, 1H), 4.81 (t, $J = 3.4$ Hz, 1H), 4.42 (s, 2H), 3.83 (ddd, $J = 11.9, 9.3, 3.0$ Hz, 1H), 3.55 (dtd, $J = 11.3, 4.3, 1.5$ Hz, 1H), 3.48 (tt, $J = 11.0, 4.7$ Hz, 1H), 2.64 (dd, $J = 15.4, 4.2$ Hz, 1H), 2.39 (dd, $J = 15.4, 9.6$ Hz, 1H), 2.26 (tq, $J = 11.1, 2.8$ Hz, 1H), 2.17 (ddd, $J = 13.3, 5.0, 2.3$ Hz, 1H), 1.00 (s, 3H), 0.88 (s, 9H), 0.60 (s, 3H), 0.05 (s, 6H). ^{13}C NMR (126 MHz, CDCl_3) δ 188.0, 141.8, 121.1, 97.3, 87.9, 85.3, 72.7, 62.2, 55.7, 54.0, 50.6, 46.8, 46.2, 43.0, 42.3, 37.6, 37.5, 36.8, 32.2, 32.1, 32.1, 30.3, 28.2, 26.1 (x3), 25.4, 24.8, 20.9, 19.6, 19.0, 18.4, 12.8, -4.4 (x2). HRMS (ESI): m/z calcd for $\text{C}_{35}\text{H}_{57}\text{O}_4\text{Si}$ [$\text{M}+\text{H}$] $^+$: 569.4021, found 569.4028.

3.1.8. General Procedure for the Synthesis of Hydroxyisoxazolines (**22a–i**)

An aqueous 4M solution of hydroxylamine hydrochloride (2 equiv.) and NaHCO_3 (2 equiv.) was stirred at room temperature until gas evolution ceased (30 min). Then, a 0.4M THF solution of an appropriate ynone, **20a–i** (1 eq.), was added. The biphasic mixture was stirred overnight at room temperature, then partitioned between a saturated aqueous NaCl and EtOAc. The aqueous phase was further extracted with EtOAc. The combined organic washings were dried over Na_2SO_4 , and the solvent was concentrated under reduced pressure. The residue was purified by silica gel chromatography (PE:EtOAc) to give hydroxyisoxazolines **22a–i**.

5-(((17R)-3 β -((*tert*-Butyldimethylsilyl)oxy)-androst-5-en-17-yl)-4,5-dihydroisoxazol-5-ol (**22a**)

The title compound **22a** (325 mg) was prepared as a white solid in 88% yield from ynone **20a**. ^1H NMR (500 MHz, CDCl_3) δ 7.22 (d, $J = 5.6$ Hz, 1H), 5.32 (dd, $J = 5.1, 2.6$ Hz, 1H), 3.49 (ddq, $J = 15.7, 10.7, 4.7$ Hz, 1H), 2.97–2.83 (m, 2H), 2.31–2.22 (m, 1H), 2.17 (ddd, $J = 13.3, 5.1, 2.3$ Hz, 1H), 1.01 (s, 3H), 0.89 (s, 9H), 0.60 (s, 3H), 0.05 (s, 6H). ^{13}C NMR (126 MHz, CDCl_3) δ 147.5, 147.1, 141.8, 121.2, 107.2, 106.8, 72.7, 55.6, 55.5, 50.7, 46.9, 46.6, 46.0, 45.7, 43.0, 38.9, 38.5, 37.6, 37.3, 36.8, 32.2, 32.1, 32.1, 29.8, 29.2, 26.1 (x3), 25.2, 20.9, 19.6, 18.4, 12.5, 12.4, -4.4 (x2). HRMS (ESI): m/z calcd for $\text{C}_{29}\text{H}_{50}\text{NO}_3\text{Si}$ [$\text{M}-\text{H}_2\text{O}+\text{H}$] $^+$: 488.3554, found 488.3564.

5-(((17R)-3 β -((*tert*-Butyldimethylsilyl)oxy)-androst-5-en-17-yl)-3-isopropyl-4,5-dihydroisoxazol-5-ol (**22b**)

The title compound **22b** (170 mg) was prepared as a white solid in 84% yield from ynone **20b**. ^1H NMR (500 MHz, CDCl_3) δ 5.31 (d, $J = 5.4$ Hz, 1H), 3.47 (tt, $J = 10.7, 4.7$ Hz, 1H), 2.89–2.66 (m, 3H), 2.26 (ddd, $J = 13.8, 10.9, 2.8$ Hz, 1H), 2.17 (ddd, $J = 13.3, 5.0, 2.3$ Hz, 1H), 1.18 (s, 3H), 1.17 (s, 3H), 1.00 (s, 3H), 0.88 (s, 9H), 0.59 (s, 3H), 0.05 (s, 6H). ^{13}C NMR (126 MHz, CDCl_3) δ 165.1, 164.7, 141.8, 121.2, 121.2, 108.4, 107.9, 72.7, 55.6, 55.5, 50.7, 47.1,

46.6, 45.5, 45.3, 43.0, 42.7, 42.6, 39.1, 38.7, 37.6, 37.3, 36.8, 32.2, 32.1, 32.1, 29.8, 29.2, 28.4, 26.1 (x3), 25.3, 25.2, 20.9, 20.3, 20.0, 19.6, 18.4, 12.5, 12.4, -4.4 (x2).

5-(((17R)-3 β -((*tert*-Butyldimethylsilyloxy)-androst-5-en-17-yl)-3-cyclopropyl-4,5-dihydroisoxazol-5-ol (**22c**))

The title compound **22c** (130 mg) was prepared as a white solid in 55% yield from ynone **20c**. ^1H NMR (500 MHz, CDCl_3) δ 5.32 (dd, $J = 5.3, 2.5$ Hz, 1H), 3.48 (tt, $J = 10.5, 4.7$ Hz, 1H), 2.74 (dd, $J = 17.2, 9.0$ Hz, 1H), 2.61 (dd, $J = 28.2, 17.2$ Hz, 1H), 2.26 (tq, $J = 11.2, 2.8$ Hz, 1H), 2.17 (ddd, $J = 13.3, 5.0, 2.2$ Hz, 1H), 1.00 (s, 3H), 0.88 (s, 9H), 0.77–0.74 (m, 2H), 0.58 (s, 3H), 0.05 (s, 6H). ^{13}C NMR (126 MHz, CDCl_3) δ 162.5, 162.1, 141.8, 121.2, 108.3, 107.9, 72.7, 55.6, 55.5, 50.7, 47.0, 46.6, 45.6, 45.3, 43.0, 42.7, 42.6, 39.0, 38.6, 37.6, 37.3, 37.3, 36.8, 32.2, 32.1, 32.1, 29.8, 29.2, 26.1 (x3), 25.3, 25.2, 20.9, 19.6, 18.4, 12.5, 12.4, 9.5, 6.8, 6.8, 6.0, -4.4 (x2). HRMS (ESI): m/z calcd for $\text{C}_{32}\text{H}_{52}\text{NO}_2\text{Si}$ [$\text{M}-\text{H}_2\text{O}+\text{H}$] $^+$: 510.3762, found 510.3776.

3-Butyl-5-(((17R)-3 β -((*tert*-butyldimethylsilyloxy)-androst-5-en-17-yl)methyl)-4,5-dihydroisoxazol-5-ol (**22d**))

The title compound **22d** (203 mg) was prepared as a white solid in 68% yield from ynone **20d**. ^1H NMR (500 MHz, CDCl_3) δ 5.31 (dt, $J = 4.9, 2.2$ Hz, 1H), 3.48 (tt, $J = 10.9, 4.7$ Hz, 1H), 2.90–2.72 (m, 2H), 2.36 (ddd, $J = 11.5, 6.6, 3.0$ Hz, 2H), 2.26 (tq, $J = 11.1, 2.7$ Hz, 1H), 2.17 (ddd, $J = 13.3, 5.0, 2.2$ Hz, 1H), 1.00 (s, 3H), 0.93 (t, $J = 7.4$ Hz, 3H), 0.88 (s, 9H), 0.59 (s, 3H), 0.05 (s, 6H). ^{13}C NMR (126 MHz, CDCl_3) δ 160.7, 160.3, 141.8, 121.2, 121.2, 108.4, 107.9, 72.7, 55.6, 55.6, 50.7, 47.5, 47.2, 47.1, 46.6, 43.0, 42.7, 42.6, 39.1, 38.7, 37.6, 37.3, 36.8, 32.2, 32.1, 32.1, 29.9, 29.2, 28.6, 27.9, 26.1 (x3), 25.3, 25.2, 22.5, 20.9, 19.6, 18.4, 13.9, 12.5, 12.4, -4.4 (x2).

5-(((17R)-3 β -((*tert*-Butyldimethylsilyloxy)-androst-5-en-17-yl)methyl)-3-phenyl-4,5-dihydroisoxazol-5-ol (**22e**))

The title compound **22e** (220 mg) was prepared as a white solid in 61% yield from ynone **20e**. ^1H NMR (500 MHz, CDCl_3) δ 7.65 (ddd, $J = 6.0, 3.1, 1.4$ Hz, 2H), 7.45–7.29 (m, 3H), 5.36–5.26 (m, 1H), 3.49 (tt, $J = 10.9, 4.6$ Hz, 1H), 1.01 (s, 3H), 0.89 (d, $J = 1.4$ Hz, 9H), 0.61 (s, 3H), 0.06 (s, 6H). ^{13}C NMR (126 MHz, CDCl_3) δ 157.8, 157.4, 141.8, 132.2, 132.0, 130.3, 129.8, 128.8, 128.5, 128.5, 126.8, 126.8, 121.2, 109.6, 109.2, 72.7, 55.6, 55.5, 50.7, 50.6, 46.9, 46.6, 45.4, 45.1, 42.9, 42.7, 42.6, 39.2, 38.7, 37.6, 37.3, 36.8, 32.2, 32.2, 32.1, 32.1, 29.9, 29.8, 29.3, 26.1 (x3), 25.3, 25.2, 20.9, 19.6, 18.4, 12.5, 12.4, -4.4 (x2). HRMS (ESI): m/z calcd for $\text{C}_{35}\text{H}_{52}\text{NO}_2\text{Si}$ [$\text{M}-\text{H}_2\text{O}+\text{H}$] $^+$: 546.3762, found 546.3773.

5-(((17R)-3 β -((*tert*-Butyldimethylsilyloxy)-androst-5-en-17-yl)-3-(pyridin-3-yl)-4,5-dihydroisoxazol-5-ol (**22f**))

The title compound **22f** (200 mg) was prepared as a white solid in 56% yield from ynone **20f**. ^1H NMR (500 MHz, CDCl_3) δ 8.76 (t, $J = 2.8$ Hz, 1H), 8.61 (dd, $J = 5.0, 1.6$ Hz, 1H), 8.06–7.99 (m, 1H), 7.36–7.30 (m, 1H), 5.32 (dt, $J = 5.2, 1.7$ Hz, 1H), 3.89 (s, 1H), 3.48 (tt, $J = 10.6, 4.7$ Hz, 1H), 3.31–3.19 (m, 2H), 2.27 (tq, $J = 11.2, 2.7$ Hz, 1H), 2.17 (ddd, $J = 15.1, 6.0, 1.9$ Hz, 2H), 2.04–1.92 (m, 1H), 1.01 (s, 3H), 0.88 (s, 9H), 0.62 (s, 3H), 0.05 (s, 6H). ^{13}C NMR (126 MHz, CDCl_3) δ 155.2, 154.8, 151.0, 147.7, 141.8, 133.9, 133.8, 126.2, 123.8, 121.2, 110.1, 109.7, 72.7, 55.6, 55.5, 50.7, 46.9, 46.6, 44.8, 44.4, 43.0, 42.8, 42.7, 39.2, 38.7, 37.6, 37.4, 36.8, 32.2, 32.1, 29.9, 29.3, 26.1 (x3), 25.3, 25.2, 20.9, 19.6, 18.4, 12.5, 12.5, -4.4 (x2).

5-(((17R)-3 β -((*tert*-Butyldimethylsilyloxy)-androst-5-en-17-yl)-3-(2-fluorophenyl)-4,5-dihydroisoxazol-5-ol (**22g**))

The title compound **22g** (60 mg) was prepared as a white solid in 68% yield from ynone **20g**. ^1H NMR (500 MHz, CDCl_3) δ 7.88 (tt, $J = 7.6, 1.6$ Hz, 1H), 7.39 (dddd, $J = 8.6, 7.1, 5.1, 1.8$ Hz, 1H), 7.18 (td, $J = 7.6, 1.2$ Hz, 1H), 7.15–7.06 (m, 1H), 5.32 (dt, $J = 5.4, 1.9$ Hz, 1H), 3.48 (td, $J = 10.9, 5.1$ Hz, 1H), 3.42–3.27 (m, 2H), 2.27 (tq, $J = 11.0, 2.7$ Hz, 1H), 1.01 (s, 3H), 0.89 (s, 9H), 0.63–0.61 (m, 3H), 0.06 (s, 6H). ^{13}C NMR (126 MHz, CDCl_3) δ 160.5 (d, $J = 252.3$ Hz), 154.2 (d, $J = 48.4$ Hz), 141.8, 132.0 (d, $J = 8.8$ Hz), 129.0, 124.6, 121.2, 117.9

(d, $J = 11.6$ Hz), 116.5 (d, $J = 21.9$ Hz), 109.4 (d, $J = 52.4$ Hz), 72.8, 55.6, 55.5, 50.7, 47.3, 47.0, 46.9, 46.6, 43.0, 42.8, 42.7, 39.1, 38.7, 37.6, 37.3, 36.9, 32.2, 32.1, 30.2, 29.9, 29.3, 26.1 (x3), 25.6, 25.3, 25.2, 20.9, 19.6, 18.4, 12.5, 12.5, -4.4 (x2). HRMS (ESI): m/z calcd for $C_{35}H_{51}FNO_2Si$ $[M-H_2O+H]^+$: 564.3668, found 564.3680.

5-(((17R)-3 β -((*tert*-Butyldimethylsilyl)oxy)-androst-5-en-17-yl)-3-(2-((tetrahydro-2H-pyran-2-yl)oxy)propan-2-yl)-4,5-dihydroisoxazol-5-ol (**22h**))

The title compound **22h** (520 mg) was prepared as a white solid in 83% yield from ynone **20h**. 1H NMR (500 MHz, $CDCl_3$) δ 5.33–5.30 (m, 1H), 5.29 (s, 1H), 5.25 (s, 0.5H), 5.20 (s, 0.5H), 4.83 (dt, $J = 5.9, 3.0$ Hz, 1H), 3.89 (ddd, $J = 11.2, 7.4, 3.0$ Hz, 1H), 3.48 (ddt, $J = 15.7, 10.9, 4.6$ Hz, 2H), 2.91–2.74 (m, 2H), 2.26 (tq, $J = 11.0, 2.7$ Hz, 1H), 2.21–2.10 (m, 2H), 1.38 (s, 3H), 1.00 (s, 3H), 0.88 (m, 12H), 0.59 (s, 3H), 0.05 (s, 6H). ^{13}C NMR (126 MHz, $CDCl_3$) δ 162.6, 162.2, 141.8, 141.8, 121.3, 121.2, 109.5, 109.2, 94.3, 94.2, 73.8, 73.8, 72.8, 63.4, 63.2, 55.7, 55.6, 50.8, 47.0, 46.6, 43.9, 43.5, 43.0, 42.6, 42.5, 37.6, 37.4, 37.3, 36.9, 36.9, 36.6, 32.2, 32.2, 32.1, 32.0, 31.9, 29.6, 29.1, 26.9, 26.1 (x3), 25.3, 25.2, 22.7, 20.9, 19.9, 19.8, 19.6, 18.4, 12.5, 12.5, -4.4 (x2). HRMS (ESI): m/z calcd for $C_{32}H_{54}NO_3Si$ $[M-OTHP]^+$: 528.3867, found 528.3856.

5-(((17R)-3 β -((*tert*-Butyldimethylsilyl)oxy)-androst-5-en-17-yl)methyl)-3-(((tetrahydro-2H-pyran-2-yl)oxy)methyl)-4,5-dihydroisoxazol-5-ol (**22i**)

The title compound **22i** (630 mg) was prepared as a white solid in 86% yield from ynone **20i**. 1H NMR (500 MHz, $CDCl_3$) δ 5.32 (dt, $J = 5.0, 2.1$ Hz, 1H), 4.65 (ddt, $J = 7.3, 5.0, 2.7$ Hz, 1H), 4.51–4.40 (m, 1H), 4.33 (ddd, $J = 12.7, 8.5, 3.8$ Hz, 1H), 3.93–3.79 (m, 1H), 3.58–3.43 (m, 2H), 3.03–2.76 (m, 2H), 2.27 (tq, $J = 11.3, 2.8$ Hz, 1H), 1.00 (s, 3H), 0.88 (s, 9H), 0.60 (s, 3H), 0.05 (s, 6H). ^{13}C NMR (126 MHz, $CDCl_3$) δ 158.3, 141.8, 121.2, 109.4, 109.3, 109.0, 108.8, 99.8, 99.6, 98.8, 63.4, 63.3, 63.3, 63.1, 62.7, 62.2, 55.6, 50.7, 46.9, 46.6, 45.9, 45.6, 45.5, 45.2, 43.0, 42.6, 39.1, 38.6, 38.3, 37.8, 37.6, 37.3, 36.8, 32.2, 32.1, 32.1, 30.8, 30.5, 29.8, 29.2, 26.1, 25.4, 25.3, 20.9, 19.8, 19.7, 19.6, 19.5, 18.4, 12.5, 12.4, -4.4 . HRMS (ESI): m/z calcd for $C_{35}H_{60}NO_5Si$ $[M+H]^+$: 602.4235, found 602.4242; calcd for $C_{35}H_{58}NO_4Si$ $[M-H_2O+H]^+$: 584.4130, found 584.4136.

3.1.9. General Procedure for the Synthesis of Isoxazoles (**23a–i**)

CDI (1.7 eq.) was added to a 0.4M solution of dihydroisoxazololes **22a–i** (1 eq.) in dry CH_2Cl_2 , and the mixture was stirred at room temperature for 16 h. Upon completion of the reaction, the mixture was concentrated under reduced pressure, and the residue was chromatographed on silica gel (PE:EtOAc) to afford isoxazoles **23a–i**.

5-(((17R)-3 β -((*tert*-butyldimethylsilyl)oxy)-androst-5-en-17-yl)methyl)isoxazole (**23a**)

The title compound **23a** (110 mg) was prepared as a white solid in 51% yield from hydroxyisoxazoline **22a** together with 4-(3 β -((*tert*-butyldimethylsilyl)oxy)-androst-5-en-17-yl)-3-oxobutanenitrile (**31**) (85 mg, 40%) isolated as a slightly yellow solid.

Isoxazole **23a**: 1H NMR (500 MHz, $CDCl_3$) δ 8.12 (d, $J = 1.7$ Hz, 1H), 5.96 (d, $J = 1.7$ Hz, 1H), 5.31 (dt, $J = 5.5, 2.0$ Hz, 1H), 3.48 (tt, $J = 10.9, 4.7$ Hz, 1H), 2.85 (dd, $J = 15.0, 5.0$ Hz, 1H), 2.59 (dd, $J = 15.0, 9.7$ Hz, 1H), 2.26 (ddd, $J = 13.6, 10.8, 2.7$ Hz, 1H), 2.17 (ddd, $J = 13.3, 5.0, 2.4$ Hz, 1H), 1.99 (dtd, $J = 16.9, 5.0, 2.6$ Hz, 1H), 1.00 (s, 3H), 0.89 (s, 9H), 0.69 (s, 3H), 0.05 (s, 6H). ^{13}C NMR (126 MHz, $CDCl_3$) δ 173.0, 150.3, 141.8, 121.1, 100.3, 72.7, 55.9, 50.6, 49.1, 43.0, 42.3, 37.6, 37.5, 36.8, 32.2, 32.1, 32.1, 28.6, 27.6, 26.1 (x3), 24.7, 20.9, 19.6, 18.4, 12.4, -4.4 (x2). HRMS (ESI): m/z calcd for $C_{29}H_{48}NO_2Si$ $[M+H]^+$: 470.3449, found 470.3460.

β -Oxonitrile **31**: 1H NMR (500 MHz, $CDCl_3$) δ 5.31 (dq, $J = 5.5, 3.3, 2.7$ Hz, 1H), 3.52–3.41 (m, 3H), 2.69 (dd, $J = 16.4, 3.9$ Hz, 1H), 2.41 (dd, $J = 16.5, 10.1$ Hz, 1H), 2.26 (tq, $J = 11.1, 2.8$ Hz, 1H), 2.17 (ddd, $J = 13.3, 5.0, 2.3$ Hz, 1H), 1.00 (s, 3H), 0.89 (s, 9H), 0.61 (s, 3H), 0.05 (s, 6H). ^{13}C NMR (126 MHz, $CDCl_3$) δ 197.8, 141.7, 121.1, 114.0, 72.7, 55.6, 50.5, 45.6, 43.4, 42.9, 42.2, 37.6, 37.4, 36.8, 32.3, 32.2, 32.1, 32.0, 28.4, 26.1, 24.8, 20.9, 19.6, 18.4, 12.8, -4.4 .

5-(((17R)-3 β -((*tert*-Butyldimethylsilyloxy)-androst-5-en-17-yl)methyl)-3-isopropylisoxazole (**23b**)

The title compound **23b** (45 mg) was prepared as a white solid in 27% yield from hydroxyisoxazoline **22b** together with (*E*)-4-amino-1-(((17R)-3 β -((*tert*-butyldimethylsilyloxy)-androst-5-en-17-yl)-5-methyl-2-oxohex-3-en-3-yl 1*H*-imidazole-1-carboxylate (**26b**) (103 mg, 50%) isolated as a white solid.

Isioxazole **23b**: ^1H NMR (500 MHz, CDCl_3) δ 5.81 (s, 1H), 5.31 (dt, $J = 5.5, 2.0$ Hz, 1H), 3.00 (hept, $J = 6.9$ Hz, 1H), 2.78 (dd, $J = 15.1, 4.9$ Hz, 1H), 2.50 (dd, $J = 15.1, 10.0$ Hz, 1H), 2.26 (tq, $J = 11.1, 2.7$ Hz, 1H), 2.16 (ddd, $J = 13.4, 5.0, 2.3$ Hz, 1H), 1.26 (s, 3H), 1.25 (s, 3H), 1.00 (s, 3H), 0.88 (s, 9H), 0.67 (s, 3H), 0.05 (s, 6H). ^{13}C NMR (126 MHz, CDCl_3) δ 173.2, 169.4, 141.8, 121.1, 99.0, 56.0, 50.6, 49.1, 43.0, 42.3, 37.6, 37.5, 36.8, 32.2, 32.1, 32.1, 28.6, 27.7, 26.6, 26.1 (x3), 24.7, 21.9 (x2), 20.9, 19.6, 18.4, 12.4, -4.4 (x2).

Imidazolecarboxylate **26b**: ^1H NMR (500 MHz, CDCl_3) δ 8.21 (d, $J = 1.1$ Hz, 1H), 7.56 (t, $J = 1.4$ Hz, 1H), 7.20 (t, $J = 1.2$ Hz, 1H), 5.31 (dt, $J = 5.6, 2.0$ Hz, 1H), 3.82 (hept, $J = 7.0$ Hz, 1H), 3.47 (tt, $J = 10.9, 4.7$ Hz, 1H), 3.01 (dd, $J = 15.7, 3.6$ Hz, 1H), 2.72 (dd, $J = 15.7, 9.1$ Hz, 1H), 2.26 (ddd, $J = 13.7, 10.8, 2.8$ Hz, 2H), 2.17 (ddd, $J = 13.3, 5.0, 2.3$ Hz, 1H), 1.32 (d, $J = 2.1$ Hz, 3H), 1.31 (d, $J = 2.2$ Hz, 3H), 1.01 (s, 3H), 0.88 (s, 9H), 0.69 (s, 3H), 0.05 (s, 6H). ^{13}C NMR (126 MHz, CDCl_3) δ 197.4, 160.4, 147.7, 141.8, 135.3, 132.7, 131.0, 121.2, 116.6, 72.7, 55.8, 50.6, 46.1, 43.0, 42.3, 41.4, 37.6, 37.5, 36.8, 32.2, 32.2, 32.1, 28.4, 26.3, 26.1 (x3), 24.9, 21.0, 20.6, 20.5, 19.6, 18.4, 12.8, -4.4 (x2).

5-(((17R)-3 β -((*tert*-Butyldimethylsilyloxy)-androst-5-en-17-yl)methyl)-3-cyclopropylisoxazole (**23c**)

The title compound **23c** (11 mg) was prepared as a white solid in 9% yield from hydroxyisoxazoline **22c** together with (*E*)-1-amino-4-(((17R)-3 β -((*tert*-butyldimethylsilyloxy)-androst-5-en-17-yl)-1-cyclopropyl-3-oxobut-1-en-2-yl 1*H*-imidazole-1-carboxylate **26c** (35 mg, 44%) isolated as a white solid.

Isioxazole **23c**: ^1H NMR (500 MHz, CDCl_3) δ 5.60 (s, 1H), 5.31 (dt, $J = 5.0, 2.0$ Hz, 1H), 3.47 (tt, $J = 11.0, 4.7$ Hz, 1H), 2.75 (dd, $J = 15.0, 5.0$ Hz, 1H), 2.47 (dd, $J = 15.0, 10.0$ Hz, 1H), 2.31–2.22 (m, 1H), 2.16 (ddd, $J = 13.4, 5.1, 2.3$ Hz, 1H), 1.00 (s, 3H), 0.88 (s, 9H), 0.66 (s, 3H), 0.05 (s, 6H). ^{13}C NMR (126 MHz, CDCl_3) δ 173.3, 166.4, 141.8, 121.1, 98.4, 72.7, 55.9, 50.6, 49.0, 43.0, 42.3, 37.6, 37.5, 36.8, 32.2, 32.1, 32.1, 28.6, 27.7, 26.1 (x3), 24.7, 20.9, 19.6, 18.4, 12.4, 8.0 (x2), 7.5, -4.4 (x2).

Imidazolecarboxylate **26c**: ^1H NMR (500 MHz, CDCl_3) δ 8.10 (s, Im-2, 1H), 7.46 (t, $J = 1.5, 1\text{H}$), 7.14 (s, Im-4, 1H), 5.29 (dt, H-6, $J = 5.6, 2.0$ Hz, 1H), 3.45 (tt, H-3, $J = 10.9, 4.7, 1\text{H}$), 2.98 (dd, H-20, $J = 15.6, 3.4$ Hz, 1H), 2.83 (tt, H-25, $J = 8.5, 5.2$ Hz, 1H), 2.70 (dd, H-20, $J = 15.6, 9.1$ Hz, 1H), 2.24 (tq, H-4, $J = 11.0, 2.6$ Hz, 1H), 2.14 (ddd, H-4, $J = 13.4, 5.1, 2.3$ Hz, 1H), 1.96 (m, H-2, 1H), 1.93 (m, H-17, 1H), 1.93 (m, H-16, 1H), 1.80 (m, H-1, 1H), 1.74 (m, H-12, 1H), 1.74 (m, H-1, 1H), 1.67 (m, H-7, 1H), 1.63 (m, H-15, 1H), 1.50 (m, H-2, 1H), 1.44 (m, H-8, 1H), 1.43 (m, H-11, 1H), 1.30 (m, H-16, 1H), 1.18 (m, H-26 and H-27, 2H), 1.15 (m, H-15, 1H), 1.08 (m, H-26 and H-27, 2H), 1.06 (m, H-12, 1H), 1.01 (m, H-14, 1H), 0.98 (s, H-19, 3H), 0.93 (m, H-9, 1H), 0.85 (s, SiCMe₃, 9H), 0.67 (s, H-18, 3H), 0.02 (s, SiMe₂, 6H). ^{13}C NMR (126 MHz, CDCl_3) δ 197.1 (s, C-22), 157.2 (s, C-24), 146.4 (s, >C=O), 141.6 (s, C-5), 135.1 (s, Im-2), 134.2 (s, C-23), 130.9 (s, Im-4), 121.1 (d, C-6), 116.5 (s, Im-5), 72.6 (d, C-3), 55.7 (d, C-14), 50.6 (d, C-9), 46.0 (d, C-17), 42.9 (t, C-4), 42.3 (s, C-13), 41.1 (d, C-20), 37.5 (t, C-12), 37.4 (t, C-1), 36.8 (s, C-10), 32.2 (t, C-7), 32.1 (d, C-8), 32.0 (t, C-2), 28.4 (t, C-16), 26.0 (s, SiCMe₃, x3), 24.8 (t, C-15), 20.9 (t, C-11), 19.5 (s, C-19), 18.3 (s, SiCMe₃), 12.8 (s, C-18), 9.5 (t, C-26 and C-27, x2), 8.2 (d, C-25), -4.5 (s, SiMe₂, x2). Selected HMBC correlations are between δ 2.98, 2.70 (H-20), 1.93 (H-17) and 197.1 (C-22), between δ 2.83 (H-25), 1.18, 1.08 (H-26, H-27) and 157.2 (C-24), between δ 2.70 (H-20) and 134.2 (C-23).

3-Butyl-5-(((17R)-3 β -((*tert*-butyldimethylsilyl)oxy)-androst-5-en-17-yl)methyl)isoxazole (23d)

The title compound **23d** (100 mg) was prepared as a white solid in 58% yield from hydroxyisoxazoline **22d**. ^1H NMR (500 MHz, CDCl_3) δ 5.79 (s, 1H), 5.31 (dt, $J = 4.8, 2.1$ Hz, 1H), 3.47 (tt, $J = 11.1, 4.7$ Hz, 1H), 2.78 (dd, $J = 15.0, 5.1$ Hz, 1H), 2.61 (t, $J = 7.7$ Hz, 2H), 2.51 (dd, $J = 15.0, 9.9$ Hz, 1H), 2.26 (ddd, $J = 13.6, 10.9, 2.7$ Hz, 1H), 2.17 (ddd, $J = 13.4, 5.1, 2.3$ Hz, 1H), 1.98 (dtd, $J = 16.9, 5.0, 2.6$ Hz, 1H), 1.00 (s, 3H), 0.93 (t, $J = 7.3$ Hz, 4H), 0.88 (s, 9H), 0.67 (s, 3H), 0.05 (s, 6H). ^{13}C NMR (126 MHz, CDCl_3) δ 173.2, 164.1, 141.8, 121.1, 100.7, 72.7, 56.0, 50.6, 49.1, 43.0, 42.3, 37.6, 37.5, 36.8, 32.2, 32.1, 32.1, 30.6, 28.6, 27.7, 26.1 (x3), 25.9, 24.7, 22.4, 20.9, 19.6, 18.4, 13.9, 12.4, -4.4 (x2).

5-(((17R)-3 β -((*tert*-Butyldimethylsilyl)oxy)-androst-5-en-17-yl)methyl)-3-phenylisoxazole (23e)

The title compound **23e** (105 mg) was prepared as a white solid in 61% yield from hydroxyisoxazoline **22e**. ^1H NMR (500 MHz, CDCl_3) δ 7.83–7.75 (m, 2H), 7.48–7.38 (m, 3H), 6.28 (s, 1H), 5.32 (dt, $J = 5.5, 2.0$ Hz, 1H), 3.48 (tt, $J = 11.0, 4.7$ Hz, 1H), 2.87 (dd, $J = 15.0, 5.1$ Hz, 1H), 2.61 (dd, $J = 15.0, 9.7$ Hz, 1H), 2.32–2.23 (m, 1H), 2.18 (ddd, $J = 13.3, 5.0, 2.3$ Hz, 1H), 1.01 (s, 3H), 0.89 (s, 9H), 0.71 (s, 3H), 0.06 (s, 6H). ^{13}C NMR (126 MHz, CDCl_3) δ 174.2, 162.4, 141.7, 129.9, 129.6, 128.9 (x2), 126.9 (x2), 121.1, 99.2, 72.7, 55.9, 50.6, 49.1, 43.0, 42.3, 37.5, 37.5, 36.8, 32.2, 32.1, 32.1, 28.6, 27.8, 26.1 (x3), 24.7, 20.9, 19.6, 18.4, 12.4, -4.4 (x2). HRMS (ESI): m/z calcd for $\text{C}_{35}\text{H}_{52}\text{NO}_2\text{Si}$ [$\text{M}+\text{H}$] $^+$: 546.3762, found 546.3767.

5-(((17R)-3 β -((*tert*-Butyldimethylsilyl)oxy)-androst-5-en-17-yl)methyl)-3-(pyridin-3-yl)isoxazole (23f)

The title compound **23f** (54 mg) was prepared as a white solid in 60% yield from hydroxyisoxazoline **22f**. ^1H NMR (500 MHz, CDCl_3) δ 8.98 (d, $J = 2.3$ Hz, 1H), 8.66 (dd, $J = 4.8, 1.7$ Hz, 1H), 8.13 (dt, $J = 7.9, 2.0$ Hz, 1H), 7.38 (dd, $J = 7.9, 4.8$ Hz, 1H), 6.33 (s, 1H), 5.32 (dd, $J = 4.8, 2.4$ Hz, 1H), 3.48 (tt, $J = 11.0, 4.7$ Hz, 1H), 2.90 (dd, $J = 15.1, 5.0$ Hz, 1H), 2.63 (dd, $J = 15.1, 9.7$ Hz, 1H), 2.27 (ddd, $J = 13.6, 11.0, 3.0$ Hz, 1H), 2.17 (ddd, $J = 13.4, 5.1, 2.3$ Hz, 1H), 1.01 (s, 3H), 0.88 (s, 9H), 0.71 (s, 2H), 0.05 (s, 6H). ^{13}C NMR (126 MHz, CDCl_3) δ 175.0, 159.9, 150.9, 148.1, 141.8, 134.1, 125.8, 123.9, 121.1, 98.9, 72.7, 56.0, 50.6, 49.1, 43.0, 42.4, 37.6 (x2), 36.8, 32.2, 32.1, 32.1, 28.6, 27.9, 26.1 (x3), 24.7, 20.9, 19.6, 18.4, 12.5, -4.4 (x2). HRMS (ESI): m/z calcd for $\text{C}_{34}\text{H}_{51}\text{N}_2\text{O}_2\text{Si}$ [$\text{M}+\text{H}$] $^+$: 547.3714, found 547.3717.

5-(((17R)-3 β -((*tert*-Butyldimethylsilyl)oxy)-androst-5-en-17-yl)methyl)-3-(2-fluorophenyl)isoxazole (23g)

The title compound **23g** (20 mg) was prepared as a white solid in 71% yield from hydroxyisoxazoline **22g**. ^1H NMR (500 MHz, CDCl_3) δ 7.98 (td, $J = 7.6, 1.8$ Hz, 1H), 7.40 (dddd, $J = 8.4, 7.1, 5.2, 1.8$ Hz, 1H), 7.22 (td, $J = 7.6, 1.2$ Hz, 1H), 7.16 (ddd, $J = 11.1, 8.3, 1.2$ Hz, 1H), 6.43 (d, $J = 3.7$ Hz, 1H), 5.32 (dt, $J = 5.5, 2.0$ Hz, 1H), 3.48 (tt, $J = 11.0, 4.7$ Hz, 1H), 2.89 (dd, $J = 15.1, 5.0$ Hz, 1H), 2.63 (dd, $J = 15.1, 9.7$ Hz, 1H), 2.27 (ddd, $J = 13.6, 10.8, 2.7$ Hz, 1H), 2.17 (ddd, $J = 13.3, 5.0, 2.3$ Hz, 1H), 1.99 (dtd, $J = 16.9, 5.0, 2.6$ Hz, 1H), 1.01 (s, 3H), 0.89 (s, 9H), 0.71 (s, 3H), 0.06 (s, 6H). ^{13}C NMR (126 MHz, CDCl_3) δ 174.1, 160.4 (d, $J = 251.3$ Hz), 157.8, 141.8, 131.5 (d, $J = 8.6$ Hz), 129.2 (d, $J = 3.0$ Hz), 124.7 (d, $J = 3.5$ Hz), 121.1, 117.7 (d, $J = 12.0$ Hz), 116.4 (d, $J = 22.0$ Hz), 101.8 (d, $J = 9.0$ Hz), 56.0, 50.6, 49.1, 43.0, 42.3, 37.6, 37.5, 36.8, 32.2, 32.1, 32.1, 28.6, 27.8, 26.1 (x3), 24.7, 20.9, 19.6, 18.4, 12.5, 1.2, -4.4 (x2).

5-(((17R)-3 β -((*tert*-Butyldimethylsilyl)oxy)-androst-5-en-17-yl)-3-(2-((tetrahydro-2H-pyran-2-yl)oxy)propan-2-yl)isoxazole (23h)

The title compound **23h** (384 mg) was prepared as a white solid in 78% yield from hydroxyisoxazoline **22h**. ^1H NMR (500 MHz, CDCl_3) δ 5.97 (s, 1H), 5.31 (dt, $J = 5.1, 2.1$ Hz, 1H), 4.50 (dt, $J = 6.1, 2.8$ Hz, 1H), 3.91 (dd, $J = 11.0, 4.9$ Hz, 1H), 3.47 (tt, $J = 8.4, 3.5$ Hz, 1H), 3.39 (dddd, $J = 9.4, 7.0, 4.2, 2.2$ Hz, 1H), 2.82–2.76 (m, 1H), 2.54 (ddd, $J = 15.0, 9.5, 3.6$ Hz, 1H), 2.26 (tt, $J = 14.0, 2.9$ Hz, 1H), 2.16 (ddd, $J = 13.4, 5.0, 2.2$ Hz, 1H), 1.98 (dtd, $J = 16.7, 5.0, 2.5$ Hz, 1H), 1.65 (s, 2H), 1.54 (s, 4H), 1.00 (s, 4H), 0.88 (s, 9H), 0.68, 0.67 (s, 3H), 0.05 (s, 6H).

^{13}C NMR (126 MHz, CDCl_3) δ 173.5, 173.4, 168.9, 168.8, 141.8, 121.1, 99.5, 99.4, 95.8, 95.7, 74.4, 72.7, 63.9, 63.9, 56.0, 50.6, 49.2, 48.9, 43.0, 42.3, 37.6, 37.5, 36.8, 32.3, 32.2, 32.1, 32.1, 29.2, 29.1, 28.6, 28.6, 27.8, 27.7, 26.1 (x3), 25.9, 25.8, 25.4, 24.7, 20.9, 19.6, 18.4, 12.4, -4.4 (x2).

5-(((17R)-3 β -((*tert*-Butyldimethylsilyl)oxy)-androst-5-en-17-yl)-3-(((tetrahydro-2H-pyran-2-yl)oxy)methyl)isoxazole (**23i**)

The title compound **23i** (530 mg) was prepared as a white solid in 87% yield from hydroxyisoxazoline **22i**. ^1H NMR (500 MHz, CDCl_3) δ 6.03 (s, 1H), 5.31 (dt, J = 5.5, 2.0 Hz, 1H), 4.73 (d, J = 12.8 Hz, 1H), 4.70 (t, J = 3.6 Hz, 1H), 4.57 (d, J = 12.8 Hz, 1H), 3.88 (ddd, J = 11.4, 8.3, 2.9 Hz, 1H), 3.58–3.52 (m, 2H), 3.47 (tt, J = 11.0, 4.7 Hz, 1H), 2.81 (dd, J = 15.0, 4.9 Hz, 1H), 2.54 (dd, J = 15.1, 10.0 Hz, 1H), 2.26 (tq, J = 11.0, 2.7 Hz, 1H), 2.16 (ddd, J = 13.3, 5.0, 2.3 Hz, 1H), 1.98 (dtd, J = 16.8, 5.0, 2.6 Hz, 1H), 1.00 (s, 3H), 0.88 (s, 9H), 0.68 (s, 3H), 0.05 (s, 6H). ^{13}C NMR (126 MHz, CDCl_3) δ 173.9, 161.6, 141.8, 121.1, 100.6, 100.6, 98.4, 72.7, 62.4, 60.7, 55.9, 50.6, 49.0, 43.0, 42.3, 37.6, 37.5, 36.8, 32.2, 32.1, 32.1, 30.5, 28.6, 27.7, 26.1 (x3), 25.5, 24.7, 20.9, 19.6, 19.4, 18.4, 12.4, -4.4 (x2). HRMS (ESI): m/z calcd for $\text{C}_{35}\text{H}_{58}\text{NO}_4\text{Si}$ [$\text{M}+\text{H}$] $^+$: 584.4130, found 584.4143.

3.1.10. (E)-1-Amino-4-((17R)-3 β -hydroxy-androst-5-en-17-yl)-1-cyclopropyl-3-oxobut-1-en-2-yl 1H-imidazole-1-carboxylate (**27**)

The title compound **27** (35 mg) was obtained from **26c** in a similar manner for the preparation of **24j** as a white solid in 87% yield. ^1H NMR (500 MHz, CDCl_3) δ 8.13 (s, 1H), 7.52–7.45 (m, 1H), 7.17 (s, 1H), 5.35 (dt, J = 4.7, 2.0 Hz, 1H), 3.52 (tt, J = 11.1, 4.7 Hz, 1H), 3.00 (dd, J = 15.6, 3.4 Hz, 1H), 2.85 (tt, J = 8.4, 5.2 Hz, 1H), 2.72 (dd, J = 15.6, 9.0 Hz, 1H), 2.34–2.18 (m, 2H), 1.02 (s, 3H), 0.70 (s, 3H). ^{13}C NMR (126 MHz, CDCl_3) δ 197.2, 157.3, 146.5, 141.0, 135.2, 134.3, 131.0, 121.7, 116.6, 71.8, 55.7, 50.6, 46.1, 42.4, 42.3, 41.2, 37.5, 37.4, 36.7, 32.1, 32.1, 31.8, 28.4, 24.9, 21.0, 19.6, 12.8, 9.6 (x2), 8.2.

3.1.11. 5-(2-((17R)-3 β -((*tert*-Butyldimethylsilyl)oxy)-androst-5-en-17-yl)acetyl)-4-cyclopropyloxazol-2(3H)-one (**28**)

A mixture of **26c** (20 mg, 31 μmol), THF (500 μL), water (200 μL), and NaOH (6.4 mg, 160 μmol) was heated at 70 $^\circ\text{C}$ for 36 h. Then, it was neutralized with saturated NH_4Cl and extracted with EtOAc. The combined organic layers were washed with brine, dried over Na_2SO_4 , and concentrated under reduced pressure. The crude product was purified by silica gel chromatography (PE:EtOAc, 90:10 \rightarrow 70:30) to afford oxazolone **28** (12 mg, 66%) as a white solid. ^1H NMR (500 MHz, CDCl_3) δ 8.30 (s, 1H), 5.31 (dt, J = 5.0, 2.1 Hz, 1H), 3.48 (tt, J = 10.9, 4.7 Hz, 1H), 2.92 (dd, J = 14.7, 4.9 Hz, 1H), 2.68 (dd, J = 14.8, 9.1 Hz, 1H), 2.26 (ddd, J = 13.6, 11.0, 2.7 Hz, 1H), 2.18 (tt, J = 7.9, 4.7 Hz, 2H), 2.03–1.94 (m, 1H), 1.00 (s, 3H), 0.89 (s, 9H), 0.69 (s, 3H), 0.05 (s, 6H). ^{13}C NMR (126 MHz, CDCl_3) δ 189.2, 153.3, 149.5, 141.8, 123.2, 121.1, 72.7, 55.8, 50.5, 49.3, 43.0, 42.4, 37.6, 37.4, 36.8, 32.2, 32.1, 32.0, 28.2, 27.7, 26.1 (x3), 24.6, 20.9, 19.6, 18.9, 18.4, 12.5, 11.74, 11.70, -4.4 (x2).

3.1.12. General Procedure for the Synthesis of Alcohols (**24a–i**)

A 1M solution of silyl ethers **23a–i** (1 eq.) and TBAF (1.2 eq.) in THF was kept at room temperature for 24 h. On completion of the reaction, the mixture was diluted with saturated NH_4Cl and extracted with EtOAc. The combined organic layers were washed with water, brine, dried over Na_2SO_4 and concentrated under reduced pressure. The residue was purified by silica gel chromatography (PE:EtOAc) to give alcohols **24a–i**.

(17R)-(Isoxazol-5-ylmethyl)-androst-5-en-3 β -ol (**24a**)

The title compound **24a** (70 mg) was prepared as a white solid in 73% yield from silyl ether **23a**. ^1H NMR (500 MHz, CDCl_3) δ 8.12 (d, J = 1.7 Hz, 1H), 5.96 (d, J = 1.7 Hz, 1H), 5.35 (dt, J = 5.5, 2.0 Hz, 1H), 3.52 (tt, J = 11.2, 4.6 Hz, 1H), 2.85 (dd, J = 15.0, 5.1 Hz, 1H), 2.59 (dd, J = 15.0, 9.7 Hz, 1H), 2.30 (ddd, J = 13.1, 5.1, 2.1 Hz, 1H), 2.23 (ddq, J = 13.4, 11.0, 2.7 Hz, 1H), 1.99 (dtd, J = 16.9, 4.9, 2.6 Hz, 1H), 1.01 (s, 3H), 0.69 (s, 3H). ^{13}C NMR (126 MHz,

CDCl₃) δ 173.0, 150.3, 141.0, 121.7, 100.3, 71.9, 55.9, 50.5, 49.1, 42.4, 42.3, 37.5, 37.4, 36.7, 32.1, 32.0, 31.8, 28.5, 27.6, 24.7, 20.9, 19.6, 12.4.

(17*R*)-17-((3-isopropylisoxazol-5-yl)methyl)-androst-5-en-3 β -ol (**24b**)

The title compound **24b** (31 mg) was prepared as a white solid in 85% yield from silyl ether **23b**. ¹H NMR (500 MHz, CDCl₃) δ 5.81 (s, 1H), 5.34 (dt, J = 4.9, 2.0 Hz, 1H), 3.51 (tt, J = 11.2, 4.5 Hz, 1H), 3.00 (hept, J = 6.9 Hz, 1H), 2.78 (dd, J = 15.1, 5.0 Hz, 1H), 2.50 (dd, J = 15.0, 10.0 Hz, 1H), 2.35–2.18 (m, 2H), 1.98 (dtd, J = 17.0, 5.0, 2.6 Hz, 1H), 1.25 (d, J = 7.0 Hz, 6H), 1.01 (s, 3H), 0.67 (s, 3H). ¹³C NMR (126 MHz, CDCl₃) δ 173.2, 169.4, 141.0, 121.6, 99.1, 71.8, 55.9, 50.5, 49.0, 42.4, 42.3, 37.4 (x2), 36.7, 32.1, 32.0, 31.8, 28.6, 27.7, 26.6, 24.7, 21.9 (x2), 20.9, 19.5, 12.4. HRMS (ESI): m/z calcd for C₂₆H₄₀NO₂ [M+H]⁺: 398.3054, found 398.3064.

(17*R*)-17-((3-Cyclopropylisoxazol-5-yl)methyl)-androst-5-en-3 β -ol (**24c**)

The title compound **24c** (27 mg) was prepared as a white solid in 70% yield from silyl ether **23c**. ¹H NMR (500 MHz, CDCl₃) δ 5.60 (s, 1H), 5.34 (dt, J = 5.3, 2.0 Hz, 1H), 3.51 (tt, J = 11.2, 4.6 Hz, 1H), 2.75 (dd, J = 15.0, 5.0 Hz, 1H), 2.47 (dd, J = 15.0, 10.0 Hz, 1H), 2.29 (ddd, J = 13.1, 5.1, 2.2 Hz, 1H), 2.22 (ddq, J = 13.4, 11.1, 2.6 Hz, 1H), 1.01 (s, 3H), 1.00–0.96 (m, 2H), 0.76 (dt, J = 6.8, 4.6 Hz, 2H), 0.66 (s, 3H). ¹³C NMR (126 MHz, CDCl₃) δ 173.3, 166.4, 141.0, 121.6, 98.4, 71.8, 55.9, 50.5, 49.0, 42.4, 42.3, 37.4 (x2), 36.7, 32.1, 32.0, 31.8, 28.6, 27.7, 24.7, 20.9, 19.6, 12.4, 8.0 (x2), 7.5. HRMS (ESI): m/z calcd for C₂₆H₃₈NO₂ [M+H]⁺: 396.2897, found 396.2908.

17 β -((3-Butylisoxazol-5-yl)methyl)-androst-5-en-3 β -ol (**24d**)

The title compound **24d** (53 mg) was prepared as a white solid in 70% yield from silyl ether **23d**. ¹H NMR (500 MHz, CDCl₃) δ 5.79 (s, 1H), 5.34 (dt, J = 5.4, 2.0 Hz, 1H), 3.52 (tt, J = 11.2, 4.6 Hz, 1H), 2.78 (dd, J = 15.0, 5.1 Hz, 1H), 2.65–2.55 (m, 2H), 2.51 (dd, J = 15.1, 9.9 Hz, 1H), 2.32–2.19 (m, 2H), 1.99 (dtd, J = 16.9, 5.0, 2.5 Hz, 1H), 1.01 (s, 3H), 0.92 (t, J = 7.4 Hz, 3H), 0.67 (s, 3H). ¹³C NMR (126 MHz, CDCl₃) δ 173.2, 164.2, 141.0, 121.6, 100.7, 71.9, 55.9, 50.5, 49.0, 42.4, 42.3, 37.5, 37.4, 36.7, 32.1, 32.0, 31.8, 30.6, 28.6, 27.7, 25.9, 24.7, 22.4, 20.9, 19.6, 13.9, 12.4.

(17*R*)-17-((3-(Pyridin-3-yl)isoxazol-5-yl)methyl)-androst-5-en-3 β -ol (**24f**)

The title compound **24f** (15 mg) was prepared as a white solid in 64% yield from silyl ether **23f**. ¹H NMR (500 MHz, CDCl₃) δ 9.01 (s, 1H), 8.69 (s, 1H), 8.14 (d, J = 7.9 Hz, 1H), 7.40 (s, 1H), 6.33 (s, 1H), 5.35 (dd, J = 5.0, 2.4 Hz, 1H), 3.52 (tt, J = 11.2, 4.4 Hz, 1H), 2.90 (dd, J = 15.1, 5.1 Hz, 1H), 2.63 (dd, J = 15.1, 9.8 Hz, 1H), 2.34–2.27 (m, 1H), 2.23 (ddd, J = 13.5, 11.0, 2.8 Hz, 1H), 1.02 (s, 3H), 0.72 (s, 3H). ¹³C NMR (126 MHz, CDCl₃) δ 175.0, 159.9, 150.9, 148.0, 141.0, 134.1, 121.6, 99.0, 77.4, 77.2, 76.9, 71.9, 55.9, 50.5, 49.1, 42.4, 42.4, 37.5, 37.4, 36.7, 32.1, 32.0, 31.8, 28.6, 27.9, 24.7, 21.0, 19.6, 12.5. HRMS (ESI): m/z calcd for C₂₈H₃₇N₂O₂ [M+H]⁺: 433.2850, found 433.2862.

17 β -((3-(2-Fluorophenyl)isoxazol-5-yl)methyl)-androst-5-en-3 β -ol (**24g**)

The title compound **24g** (9 mg) was prepared as a white solid in 82% yield from silyl ether **23g**. ¹H NMR (500 MHz, CDCl₃) δ 7.97 (td, J = 7.6, 1.9 Hz, 1H), 7.45–7.36 (m, 1H), 7.22 (td, J = 7.6, 1.2 Hz, 1H), 7.19–7.13 (m, 1H), 6.43 (d, J = 3.7 Hz, 1H), 5.36 (dd, J = 4.9, 2.3 Hz, 1H), 3.52 (dq, J = 11.3, 5.7, 5.0 Hz, 1H), 2.89 (dd, J = 15.1, 5.1 Hz, 1H), 2.63 (dd, J = 15.1, 9.7 Hz, 1H), 2.30 (ddd, J = 13.1, 5.1, 2.1 Hz, 1H), 2.23 (ddd, J = 13.6, 10.6, 2.6 Hz, 1H), 2.00 (dtd, J = 16.9, 4.9, 2.5 Hz, 1H), 1.02 (s, 3H), 0.72 (s, 3H). ¹³C NMR (126 MHz, CDCl₃) δ 174.1, 160.4 (d, J = 251.4 Hz), 157.8, 141.0, 131.5 (d, J = 8.6 Hz), 129.2 (d, J = 3.1 Hz), 124.7 (d, J = 3.5 Hz), 121.7, 117.6 (d, J = 12.1 Hz), 116.4 (d, J = 21.9 Hz), 101.8 (d, J = 9.1 Hz), 71.9, 55.9, 50.5, 49.1, 42.4, 42.3, 37.5, 37.4, 36.7, 32.1, 32.0, 31.8, 28.6, 27.8, 24.7, 21.0, 19.6, 12.5.

3.1.13. (17R)-17-((3-(2-Hydroxypropan-2-yl)isoxazol-5-yl)methyl)-androst-5-en-3 β -ol (**24j**)

A mixture of silyl ether **23h** (270 mg, 0.44 mmol), THF (1 mL), MeCN (4 mL), and 40% aq. HF (100 μ L, 2 mmol) in a Teflon vial was stirred at room temperature for 16 h. Then, it was neutralized with saturated NaHCO₃ and extracted with EtOAc. The combined organic layers were washed with water, brine, dried over Na₂SO₄, and concentrated under reduced pressure. The residue was purified by silica gel chromatography (CHCl₃: MeOH, 100:0 \rightarrow 80:20) to give diol **24j** (128 mg, 70%) as a white solid. ¹H NMR (500 MHz, CDCl₃) δ 5.97 (s, 1H), 5.35 (dd, *J* = 4.8, 2.3 Hz, 1H), 3.52 (tt, *J* = 11.1, 4.6 Hz, 1H), 2.80 (dd, *J* = 15.1, 4.9 Hz, 1H), 2.53 (dd, *J* = 15.1, 10.1 Hz, 1H), 2.30 (ddd, *J* = 13.1, 5.1, 2.0 Hz, 1H), 2.23 (ddd, *J* = 13.2, 10.7, 2.6 Hz, 1H), 1.58 (s, 6H), 1.01 (s, 3H), 0.68 (s, 3H). ¹³C NMR (126 MHz, CDCl₃) δ 174.0, 170.5, 141.0, 121.6, 98.6, 71.9, 69.4, 55.9, 50.5, 49.1, 42.4, 42.3, 37.5, 37.4, 36.7, 32.1, 32.0, 31.8, 30.0 (x2), 28.6, 27.8, 24.7, 21.0, 19.6, 12.4. HRMS (ESI): *m/z* calcd for C₂₆H₄₀NO₃ [M+H]⁺: 414.3003, found 414.3014.

3.1.14. (17R)-17-((3-Phenylisoxazol-5-yl)methyl)-androst-5-en-3 β -ol (**24e**)

The title compound **24e** (30 mg) was obtained from **23e** in a similar manner for the preparation of **24j** as a white solid in 88% yield. ¹H NMR (500 MHz, CDCl₃) δ 7.83–7.73 (m, 2H), 7.44 (d, *J* = 6.8 Hz, 3H), 6.28 (s, 1H), 5.40–5.30 (m, 1H), 3.52 (ddd, *J* = 18.6, 12.0, 5.9 Hz, 1H), 2.88 (dd, *J* = 15.1, 5.1 Hz, 1H), 2.61 (dd, *J* = 15.1, 9.7 Hz, 1H), 2.36–2.18 (m, 2H), 1.02 (s, 3H), 0.71 (s, 3H). ¹³C NMR (126 MHz, CDCl₃) δ 174.2, 162.4, 141.0, 129.9, 129.6, 129.0 (x2), 126.9 (x2), 121.7, 99.2, 71.9, 55.9, 50.5, 49.1, 42.4, 42.3, 37.5, 37.4, 36.7, 32.1, 32.0, 31.8, 28.6, 27.8, 24.7, 20.9, 19.6, 12.5. HRMS (ESI): *m/z* calcd for C₂₉H₃₈NO₂ [M+H]⁺: 432.2897, found 432.2910.

3.1.15. (17R)-17-((3-(Hydroxymethyl)isoxazol-5-yl)methyl)-androst-5-en-3 β -ol (**32**)

Dowex 50 W (H⁺-form) ion-exchanger (2 mg) was added to a solution of **24i** (40 mg, 6.8 μ mol) in THF (340 μ L) and MeOH (800 μ L). The suspension was stirred at room temperature for 48 h. Solids were filtered off and washed with EtOAc. The filtrate was evaporated under reduced pressure, and the crude material was purified by silica gel chromatography (CHCl₃:MeOH, 100:0 \rightarrow 80:20) to give diol **32** (23 mg, 87%) as a white solid. ¹H NMR (500 MHz, CDCl₃) δ 6.02 (s, 1H), 5.35 (dt, *J* = 4.7, 2.0 Hz, 1H), 4.71 (s, 2H), 3.51 (tt, *J* = 11.2, 4.6 Hz, 1H), 2.82 (dd, *J* = 15.1, 5.1 Hz, 1H), 2.55 (dd, *J* = 15.1, 9.9 Hz, 1H), 2.29 (ddd, *J* = 13.0, 5.1, 2.1 Hz, 1H), 2.26–2.18 (m, 4H), 1.99 (dtd, *J* = 16.8, 5.0, 2.6 Hz, 1H), 1.01 (s, 3H), 0.68 (s, 3H). ¹³C NMR (126 MHz, CDCl₃) δ 174.2, 163.5, 141.0, 121.6, 99.9, 71.9, 57.3, 55.9, 50.5, 49.1, 42.4, 42.3, 37.5, 37.4, 36.7, 32.1, 32.0, 31.8, 28.6, 27.8, 24.7, 20.9, 19.6, 12.4. HRMS (ESI): *m/z* calcd for C₂₄H₃₆NO₃ [M+H]⁺: 386.2690, found 386.2690.

3.1.16. 5-(((17R)-3 β -((*tert*-Butyldimethylsilyloxy)-androst-5-en-17-yl)methyl)isoxazole-3-yl)methanol (**33**)

A mixture of magnesium bromide diethyl etherate (prepared from Mg (63.4 mg, 2.61 mmol) by dropwise addition of 1,2-dibromoethane (222 μ L, 2.56 mmol) in anhydrous Et₂O (3 mL) and subsequent reflux until gas evolution subsides) and ether **24i** (440 mg, 0.75 mmol) was vigorously stirred at room temperature for 16 h. The mixture was quenched with saturated NH₄Cl and extracted with EtOAc. Organic extracts were washed with brine, dried over Na₂SO₄, and rotoevaporated. The residue was purified by silica gel chromatography (PE:EtOAc, 95:5 \rightarrow 70:30) to afford alcohol **33** as a white solid (323 mg, 85%), in addition to the unreacted starting material **24i** (43 mg, 9.8%). ¹H NMR (500 MHz, CDCl₃) δ 6.01 (s, 1H), 5.31 (dt, *J* = 5.1, 2.1 Hz, 1H), 4.69 (s, 2H), 3.47 (tt, *J* = 11.0, 4.7 Hz, 1H), 2.81 (dd, *J* = 15.1, 5.0 Hz, 1H), 2.54 (dd, *J* = 15.1, 9.9 Hz, 1H), 2.48–2.35 (m, 1H), 2.26 (tq, *J* = 11.1, 2.7 Hz, 1H), 2.16 (ddd, *J* = 13.3, 5.1, 2.3 Hz, 1H), 1.98 (dtd, *J* = 16.8, 5.0, 2.6 Hz, 1H), 1.00 (s, 3H), 0.88 (s, 9H), 0.67 (s, 3H), 0.05 (s, 6H). ¹³C NMR (126 MHz, CDCl₃) δ 174.2, 163.6, 141.7, 121.1, 99.9, 72.7, 57.2, 55.9, 50.5, 49.0, 42.9, 42.3, 37.5, 37.5, 36.8, 32.2, 32.1, 32.0, 28.5, 27.7, 26.1 (x3), 24.7, 20.9, 19.6, 18.4, 12.4, –4.5 (x2).

3.1.17. 5-(((17R)-3 β -((*tert*-Butyldimethylsilyloxy)-androst-5-en-17-yl)methyl)-3-(chloromethyl)isoxazole (37)

To a solution of alcohol **33** (212 mg, 0.42 mmol) in pyridine (0.5 mL), TsCl (122, 0.64 mmol) was added at 0 °C. The cooling bath was removed, and the reaction mixture was kept at room temperature for 16 h. On completion of the reaction, the mixture was diluted with water and extracted with EtOAc. The combined organics were washed with brine, dried over Na₂SO₄, and rotoevaporated. The residue was purified by silica gel chromatography (PE:EtOAc, 95:5→85:15) to give chloride **37** (43 mg, 20%) as a white solid. ¹H NMR (500 MHz, CDCl₃) δ 6.08 (s, 1H), 5.31 (dt, *J* = 5.5, 2.0 Hz, 1H), 4.55 (s, 2H), 3.48 (tt, *J* = 11.0, 4.7 Hz, 1H), 2.82 (dd, *J* = 15.2, 5.0 Hz, 1H), 2.55 (dd, *J* = 15.1, 9.9 Hz, 1H), 2.26 (ddd, *J* = 13.7, 10.9, 2.7 Hz, 1H), 2.17 (ddd, *J* = 13.4, 5.0, 2.3 Hz, 1H), 1.00 (s, 3H), 0.89 (s, 9H), 0.68 (s, 3H), 0.05 (s, 6H). ¹³C NMR (126 MHz, CDCl₃) δ 174.8, 160.8, 141.8, 129.6, 121.1, 100.8, 72.7, 55.9, 50.6, 49.0, 43.0, 42.3, 37.6, 37.5, 36.8, 36.0, 32.2, 32.1, 32.1, 28.6, 27.8, 26.1 (x3), 24.7, 20.9, 19.6, 18.4, 12.4, -4.4 (x2). HRMS (ESI): *m/z* calcd for C₃₀H₄₉ClNO₂Si [M+H]⁺: 518.3216, found 518.3226.

3.1.18. 5-((3 β -((*tert*-Butyldimethylsilyloxy)-androst-5-en-17-yl)methyl)isoxazol-3-yl)methyl methanesulfonate (34)

To a solution of alcohol **33** (250 mg, 0.5 mmol) in DCM (2 mL) and Et₃N (120 μ L, 0.86 mmol), MsCl (55 μ L, 0.71 mmol) was added at -15 °C. The mixture was stirred at this temperature for 15 min, then quenched with saturated NaHCO₃. The organic layer was separated, the water phase was extracted with CH₂Cl₂. The combined organics were washed with brine, dried over Na₂SO₄, and evaporated under reduced pressure. The residue was purified by silica gel chromatography (PE:EtOAc, 95:5→80:20) to give mesylate **34** (266 mg, 92%) as a white solid. ¹H NMR (500 MHz, CDCl₃) δ 6.13 (s, 1H), 5.31 (dt, *J* = 5.5, 2.0 Hz, 1H), 5.26 (s, 2H), 3.47 (tt, *J* = 10.7, 4.7 Hz, 1H), 3.05 (s, 3H), 2.84 (dd, *J* = 15.2, 5.0 Hz, 1H), 2.57 (dd, *J* = 15.2, 9.9 Hz, 1H), 2.26 (ddd, *J* = 13.7, 10.9, 2.7 Hz, 1H), 2.17 (ddd, *J* = 13.3, 5.0, 2.3 Hz, 1H), 1.99 (dtd, *J* = 16.8, 5.0, 2.5 Hz, 1H), 1.00 (s, 3H), 0.88 (s, 9H), 0.68 (s, 3H), 0.05 (s, 6H). ¹³C NMR (126 MHz, CDCl₃) δ 175.4, 158.1, 141.8, 121.1, 100.8, 72.7, 62.3, 55.9, 50.5, 49.0, 43.0, 42.3, 38.3, 37.6, 37.5, 36.8, 32.2, 32.1, 32.0, 28.5, 27.8, 26.1 (x3), 24.7, 20.9, 19.6, 18.4, 12.4, -4.4 (x2). HRMS (ESI): *m/z* calcd for C₃₁H₅₂NO₅SSi [M+H]⁺: 578.3330, found 578.3333.

3.1.19. 3-(Azidomethyl)-5-(((17R)-3 β -((*tert*-butyldimethylsilyloxy)-androst-5-en-17-yl)methyl)isoxazole (35)

A mixture of mesylate **34** (260 mg, 0.45 mmol), NaN₃ (88 mg, 1.35 mmol), and DMF (2 mL) was stirred at 70 °C for 3 h. On completion of the reaction, the mixture was diluted with water and extracted with EtOAc. The organic layers were washed with water, brine, dried over Na₂SO₄, and concentrated under reduced pressure. The resulting product was purified by silica gel chromatography (PE:EtOAc, 100:0→85:15) to afford azide **35** (220 mg, 93%) as a white solid. ¹H NMR (500 MHz, CDCl₃) δ 6.02 (s, 1H), 5.31 (dt, *J* = 5.5, 2.0 Hz, 1H), 4.37 (s, 2H), 3.47 (tt, *J* = 11.1, 4.7 Hz, 1H), 2.84 (dd, *J* = 15.1, 5.1 Hz, 1H), 2.57 (dd, *J* = 15.1, 9.8 Hz, 1H), 2.31–2.22 (m, 1H), 2.17 (ddd, *J* = 13.4, 5.0, 2.3 Hz, 1H), 1.99 (dtd, *J* = 16.8, 4.9, 2.6 Hz, 1H), 1.00 (s, 3H), 0.88 (s, 9H), 0.68 (s, 3H), 0.05 (s, 6H). ¹³C NMR (126 MHz, CDCl₃) δ 175.0, 159.1, 141.8, 121.1, 100.3, 72.7, 55.9, 50.5, 49.0, 45.9, 43.0, 42.3, 37.6, 37.5, 36.8, 32.2, 32.1, 32.1, 28.5, 27.8, 26.1 (x3), 24.7, 20.9, 19.6, 18.4, 12.4, -4.4 (x2).

3.1.20. (17R)-17-((3-(Azidomethyl)isoxazol-5-yl)methyl)-androst-5-en-3 β -ol (36)

The title compound **36** (25 mg) was obtained from **35** in a similar manner for the preparation of **24j** as a white solid in 81% yield. ¹H NMR (500 MHz, CDCl₃) δ 6.02 (s, 1H), 5.34 (dt, *J* = 4.8, 2.1 Hz, 1H), 4.36 (s, 2H), 3.52 (tt, *J* = 11.2, 4.5 Hz, 1H), 2.83 (dd, *J* = 15.1, 5.1 Hz, 1H), 2.57 (dd, *J* = 15.1, 9.8 Hz, 1H), 2.29 (ddd, *J* = 13.1, 5.2, 2.1 Hz, 1H), 2.23 (tq, *J* = 13.5, 2.6 Hz, 1H), 1.99 (dtd, *J* = 16.9, 5.0, 2.5 Hz, 1H), 1.01 (s, 3H), 0.69 (s, 3H). ¹³C NMR (126 MHz, CDCl₃) δ 175.0, 159.1, 141.0, 121.6, 100.3, 71.8, 55.9, 50.4, 49.0, 45.9, 42.4, 42.3, 37.5, 37.4, 36.7, 32.1, 32.0, 31.8, 28.5, 27.8, 24.7, 20.9, 19.5, 12.4.

3.1.21. (17R)-17-((3-(Chloromethyl)isoxazol-5-yl)methyl)-androst-5-en-3 β -ol (**38**)

The title compound **38** (26 mg) was obtained from **37** in a similar manner for the preparation of **24a** as a white solid in 85% yield. ^1H NMR (500 MHz, CDCl_3) δ 6.08 (s, 1H), 5.39–5.32 (m, 1H), 4.54 (s, 1H), 3.52 (tt, $J = 11.2, 4.6$ Hz, 1H), 2.82 (dd, $J = 15.1, 5.0$ Hz, 1H), 2.55 (dd, $J = 15.1, 10.2$ Hz, 1H), 2.30 (ddd, $J = 13.1, 5.1, 2.1$ Hz, 1H), 2.26–2.19 (m, 1H), 1.01 (s, 3H), 0.68 (s, 3H). ^{13}C NMR (126 MHz, CDCl_3) δ 174.8, 160.8, 141.0, 121.6, 100.8, 71.9, 55.9, 50.5, 49.0, 42.4, 42.3, 37.4, 37.4, 36.7, 36.0, 32.1, 32.0, 31.8, 28.5, 27.8, 24.7, 20.9, 19.6, 12.4. HRMS (ESI): m/z calcd for $\text{C}_{24}\text{H}_{35}\text{ClNO}_2$ $[\text{M}+\text{H}]^+$: 404.2351, found 404.2358.

3.1.22. 1-((17R)-3 β -((*tert*-Butyldimethylsilyl)oxy)-androst-5-en-17-yl)oct-3-yn-2-one oxime (**39**)

A mixture of ynone **20d** (100 mg, 0.20 mmol), $\text{NH}_2\text{OH}\cdot\text{HCl}$ (42 mg, 0.60 mmol), NaHCO_3 (50 mg, 0.60 mmol), and methanol (1.5 mL) was stirred at 60 $^\circ\text{C}$ for 40 min, then evaporated to dryness at reduced pressure and purified by silica gel chromatography (PE:EtOAc, 100:0 \rightarrow 80:20), affording oxime **39** as an oil. ^1H NMR (500 MHz, CDCl_3) δ 5.31 (dt, $J = 5.6, 2.0$ Hz, 1H), 3.47 (td, $J = 11.0, 5.3$ Hz, 1H), 1.01, 1.00 (s, 3H), 0.89 (s, 9H), 0.66 (s, 3H), 0.63, 0.62 (s, 3H), 0.06 (s, 6H). ^{13}C NMR (126 MHz, CDCl_3) δ 162.3, 148.4, 144.0, 141.8, 121.2, 103.6, 92.7, 72.8, 56.1, 55.9, 55.9, 50.7, 48.1, 47.6, 47.5, 47.5, 43.0, 42.6, 42.4, 42.3, 37.7, 37.6, 37.5, 37.5, 36.9, 35.6, 34.7, 34.0, 32.2, 32.2, 32.1, 30.5, 30.4, 29.7, 28.7, 28.5, 28.3, 28.1, 28.0, 27.3, 26.1, 24.8, 24.8, 23.1, 22.6, 22.1, 21.0, 19.6, 19.5, 19.1, 18.4, 14.0, 13.7, 12.5, 12.4, 12.4, 12.3, -4.4 .

3.1.23. 5-Butyl-3-(((17R)-3 β -((*tert*-butyldimethylsilyl)oxy)-androst-5-en-17-yl)methyl)isoxazole (**40d**)

A mixture of oxime **39** (93 mg, 0.18 mmol), AuCl_3 (1.5 mg, 0.005 mmol), and DCM (0.7 mL) was stirred at room temperature for 30 min. The solvent was evaporated, and the residue was purified by silica gel chromatography (PE:EtOAc, 100:0 \rightarrow 85:15) to give isoxazole **40d** (43 mg, 46%) as an oil. ^1H NMR (500 MHz, CDCl_3) δ 5.79 (d, $J = 0.9$ Hz, 1H), 5.31 (dt, $J = 5.6, 1.9$ Hz, 1H), 3.52–3.43 (m, 1H), 2.75–2.65 (m, 2H), 2.48–2.37 (m, 1H), 1.01 (s, 3H), 0.93 (t, $J = 7.4$ Hz, 3H), 0.89 (s, 9H), 0.69 (s, 3H), 0.05 (s, 6H). ^{13}C NMR (126 MHz, CDCl_3) δ 173.3, 163.9, 141.8, 121.2, 100.7, 72.8, 56.1, 50.7, 49.8, 43.0, 42.4, 37.7, 37.6, 36.8, 32.2, 32.1, 29.7, 28.6, 26.9, 26.6, 26.1 (x3), 24.7, 22.3, 21.0, 19.6, 18.4, 13.8, 12.4, -4.4 (x2).

3.1.24. General Procedure for the Synthesis of Isoxazoles **40a,e-i**

A 0.1M methanol solution of ynones **20a,e-i** (1 eq) was added to $\text{NH}_2\text{OH}\cdot\text{HCl}$ (3 eq) and NaHCO_3 (3 eq). The resulting mixture was stirred at 60 $^\circ\text{C}$ for 16 h, then the solvent was evaporated at reduced pressure and the residue was purified by silica gel chromatography (PE:EtOAc) to afford isoxazoles **40a,e-i**.

3-(((17R)-3 β -((*tert*-Butyldimethylsilyl)oxy)-androst-5-en-17-yl)methyl)isoxazole (**40a**)

The title compound **40a** (47 mg) was prepared as a white solid in 61% yield from ynone **20a**. ^1H NMR (500 MHz, CDCl_3) δ 8.28 (s, 1H), 6.18 (s, 1H), 5.31 (d, $J = 5.0$ Hz, 1H), 3.52–3.43 (m, 1H), 2.81 (dd, $J = 14.6, 4.9$ Hz, 1H), 2.54–2.46 (m, 1H), 2.27 (t, $J = 12.2$ Hz, 1H), 2.21–2.13 (m, 1H), 1.99 (d, $J = 16.8$ Hz, 1H), 1.00 (s, 3H), 0.88 (s, 9H), 0.70 (s, 3H), 0.05 (s, 6H). ^{13}C NMR (126 MHz, CDCl_3) δ 162.9, 158.0, 141.8, 121.2, 104.4, 72.8, 56.1, 50.6, 49.8, 43.0, 42.4, 37.7, 37.6, 36.8, 32.2, 32.1, 29.9, 28.6, 26.7, 26.1 (x3), 24.7, 21.0, 19.6, 18.4, 12.5, -4.4 (x2).

3-(((17R)-3 β -((*tert*-Butyldimethylsilyl)oxy)-androst-5-en-17-yl)methyl)-5-phenylisoxazole (**40e**)

The title compound **40e** (140 mg) was prepared as a white solid in 82% yield from ynone **20e**. ^1H NMR (500 MHz, CDCl_3) δ 7.80–7.73 (m, 2H), 7.49–7.38 (m, 3H), 6.37 (s, 1H), 5.32 (dd, $J = 4.8, 2.7$ Hz, 1H), 3.48 (tt, $J = 11.0, 4.7$ Hz, 1H), 2.81 (dd, $J = 14.3, 4.9$ Hz, 1H), 2.51 (dd, $J = 14.3, 10.1$ Hz, 1H), 2.26 (ddt, $J = 13.7, 5.5, 2.8$ Hz, 1H), 2.17 (ddd, $J = 13.3, 5.0, 2.2$ Hz, 1H), 2.04–1.95 (m, 1H), 1.01 (s, 3H), 0.89 (s, 9H), 0.73 (s, 3H), 0.06 (s, 6H). ^{13}C NMR (126 MHz, CDCl_3) δ 169.5, 164.6, 141.8, 130.1, 129.1 (x2), 127.9, 125.9 (x2), 121.2, 99.6, 72.8,

56.1, 50.7, 49.8, 43.0, 42.5, 37.8, 37.6, 36.8, 32.2, 32.1 (x2), 28.6, 27.0, 26.1 (x3), 24.8, 21.0, 19.6, 18.4, 12.5, -4.4 (x2). HRMS (ESI): m/z calcd for $C_{35}H_{52}NO_2Si$ $[M+H]^+$: 546.3762, found 546.3772.

3-(((17R)-3 β -((*tert*-Butyldimethylsilyl)oxy)-androst-5-en-17-yl)methyl)-5-(pyridin-3-yl)isoxazole (**40f**)

The title compound **40f** (40 mg) was prepared as a white solid in 40% yield from ynone **20f**. 1H NMR (500 MHz, $CDCl_3$) δ 8.99 (d, J = 2.3 Hz, 1H), 8.65 (dd, J = 4.9, 1.7 Hz, 1H), 8.07 (dt, J = 8.0, 2.0 Hz, 1H), 7.40 (ddd, J = 8.0, 4.8, 0.9 Hz, 1H), 6.47 (s, 1H), 5.31 (dt, J = 5.7, 1.9 Hz, 1H), 3.47 (tt, J = 11.0, 4.7 Hz, 1H), 2.83 (dd, J = 14.3, 4.9 Hz, 1H), 2.53 (dd, J = 14.3, 10.1 Hz, 1H), 2.26 (ddd, J = 13.7, 10.9, 2.7 Hz, 1H), 2.17 (ddd, J = 13.3, 5.0, 2.3 Hz, 1H), 1.01 (s, 3H), 0.88 (s, 9H), 0.72 (s, 3H), 0.05 (s, 6H). ^{13}C NMR (126 MHz, $CDCl_3$) δ 166.6, 164.8, 150.8, 147.1, 141.8, 133.0, 124.1, 123.9, 121.1, 100.6, 72.7, 56.1, 50.6, 49.8, 43.0, 42.5, 37.7, 37.6, 36.8, 32.2, 32.1, 28.6, 27.0, 26.1 (x2), 24.7, 20.9, 19.6, 18.4, 12.5, -4.4 (x2).

3-(((17R)-3 β -((*tert*-Butyldimethylsilyl)oxy)-androst-5-en-17-yl)methyl)-5-(2-fluorophenyl)isoxazole (**40g**)

The title compound **40g** (97 mg) was prepared as a white solid in 69% yield from ynone **20g**. 1H NMR (500 MHz, $CDCl_3$) δ 7.95 (td, J = 7.6, 1.7 Hz, 1H), 7.40 (tdd, J = 7.4, 5.0, 1.8 Hz, 1H), 7.29–7.22 (m, 1H), 7.18 (dd, J = 11.0, 8.2 Hz, 1H), 6.56 (d, J = 3.9 Hz, 1H), 5.32 (d, J = 5.2 Hz, 1H), 3.48 (tt, J = 10.9, 4.7 Hz, 1H), 2.83 (dd, J = 14.3, 4.9 Hz, 1H), 2.54 (dd, J = 14.3, 10.0 Hz, 1H), 2.27 (ddd, J = 13.9, 10.9, 2.8 Hz, 1H), 2.17 (ddd, J = 13.3, 5.1, 2.3 Hz, 1H), 1.02 (s, 3H), 0.89 (s, 9H), 0.73 (s, 3H), 0.06 (s, 6H). ^{13}C NMR (126 MHz, $CDCl_3$) δ 164.9, 163.2, 159.2 (d, J = 252.8 Hz), 141.8, 131.4 (d, J = 8.6 Hz), 127.8, 124.8, 124.8, 121.2, 116.3 (d, J = 21.3 Hz), 116.2, 103.8 (d, J = 10.9 Hz), 72.7, 56.1, 50.6, 49.7, 43.0, 42.5, 37.7, 37.6, 36.8, 32.2, 32.1, 28.6, 27.0, 26.1 (x3), 24.8, 21.0, 19.6, 18.4, 12.5, -4.4 (x2). HRMS (ESI): m/z calcd for $C_{35}H_{51}FNO_2Si$ $[M+H]^+$: 564.3668, found 564.3678.

3-(((17R)-3 β -((*tert*-Butyldimethylsilyl)oxy)-androst-5-en-17-yl)methyl)-5-(2-((tetrahydro-2H-pyran-2-yl)oxy)propan-2-yl)isoxazole (**40h**)

The title compound **40h** (60 mg) was prepared as a white solid in 73% yield from ynone **20h**. 1H NMR (500 MHz, $CDCl_3$) δ 5.99 (d, J = 1.0 Hz, 1H), 5.31 (dd, J = 4.7, 2.3 Hz, 1H), 4.59 (dt, J = 5.4, 2.5 Hz, 1H), 3.90 (dt, J = 11.3, 5.0 Hz, 1H), 3.47 (ddt, J = 15.7, 10.9, 4.7 Hz, 1H), 3.39 (dt, J = 11.1, 5.1 Hz, 1H), 2.74 (ddd, J = 14.3, 5.0, 2.2 Hz, 1H), 2.44 (dd, J = 14.3, 10.0 Hz, 1H), 2.26 (ddd, J = 13.7, 11.1, 2.9 Hz, 1H), 2.16 (ddd, J = 13.3, 5.0, 2.3 Hz, 1H), 1.64 (s, 3H), 1.58 (s, 3H), 1.00 (s, 3H), 0.88 (s, 9H), 0.69 (s, 3H), 0.05 (s, 6H). ^{13}C NMR (126 MHz, $CDCl_3$) δ 175.7, 175.6, 163.8, 163.7, 141.8, 121.1, 101.1, 101.0, 95.4, 95.3, 73.7, 73.6, 72.7, 63.3, 63.3, 56.1, 50.6, 49.7, 43.0, 42.4, 37.7, 37.6, 36.8, 32.2, 32.1, 32.0, 28.6, 28.6, 28.3, 28.2, 26.9, 26.2, 26.1, 25.4, 24.7, 21.0, 20.4, 20.4, 19.6, 18.4, 12.4, -4.4.

3-(((17R)-3 β -((*tert*-Butyldimethylsilyl)oxy)-androst-5-en-17-yl)methyl)-5-(((tetrahydro-2H-pyran-2-yl)oxy)methyl)isoxazole (**40i**)

The title compound **40i** (86 mg) was prepared as a white solid in 45% yield from ynone **20i**. 1H NMR (500 MHz, $CDCl_3$) δ 6.09 (s, 1H), 5.31 (dt, J = 5.7, 1.9 Hz, 1H), 4.77–4.70 (m, 2H), 4.59 (d, J = 13.6 Hz, 1H), 3.86 (ddd, J = 11.6, 8.9, 2.9 Hz, 1H), 3.58–3.51 (m, 1H), 3.47 (tt, J = 10.9, 4.6 Hz, 1H), 2.75 (dd, J = 14.3, 4.7 Hz, 1H), 2.45 (dd, J = 14.3, 10.2 Hz, 1H), 2.26 (ddt, J = 13.8, 5.5, 3.0 Hz, 1H), 2.16 (ddd, J = 13.3, 5.0, 2.3 Hz, 1H), 1.00 (s, 3H), 0.88 (s, 9H), 0.69 (s, 3H), 0.05 (s, 6H). ^{13}C NMR (126 MHz, $CDCl_3$) δ 168.9, 163.9, 141.8, 121.2, 121.1, 103.0, 98.1, 72.7, 62.2, 59.8, 56.1, 50.6, 49.7, 43.0, 42.4, 37.7, 37.6, 36.8, 32.2, 32.1, 30.4, 28.6, 26.9, 26.1, 25.4, 24.7, 20.9, 19.6, 19.1, 18.4, 12.4, -4.4.

3.1.25. (17R)-17-(Isoxazol-3-ylmethyl)-androst-5-en-3 β -ol (**41a**)

The title compound **41a** (20 mg) was obtained from **40a** in a similar manner for the preparation of **24a** as a white solid in 87% yield. 1H NMR (500 MHz, $CDCl_3$) δ 8.28 (d, J = 1.6 Hz, 1H), 6.18 (d, J = 1.7 Hz, 1H), 5.35 (dt, J = 5.5, 2.0 Hz, 1H), 3.52 (tt, J = 11.2, 4.6 Hz,

1H), 2.81 (dd, $J = 14.3, 5.0$ Hz, 1H), 2.50 (dd, $J = 14.3, 10.0$ Hz, 1H), 2.30 (ddd, $J = 13.1, 5.1, 2.2$ Hz, 1H), 2.23 (ddq, $J = 13.3, 11.0, 2.5$ Hz, 1H), 1.01 (s, 3H), 0.71 (s, 3H). ^{13}C NMR (126 MHz, CDCl_3) δ 162.9, 158.0, 141.0, 121.7, 104.4, 71.9, 56.0, 50.5, 49.8, 42.4, 37.7, 37.4, 36.7, 32.1, 32.1, 31.8, 28.5, 26.7, 24.7, 21.0, 19.6, 12.5. HRMS (ESI): m/z calcd for $\text{C}_{23}\text{H}_{34}\text{NO}_2$ $[\text{M}+\text{H}]^+$: 356.2584, found 356.2592.

3.1.26. (17R)-17-((5-Butylisoxazol-3-yl)methyl)-androst-5-en-3 β -ol (41d)

The title compound **41d** (63 mg) was obtained from **40d** in a similar manner for the preparation of **24a** as a white solid in 80% yield. ^1H NMR (500 MHz, CDCl_3) δ 5.79 (s, 1H), 5.34 (dt, $J = 5.5, 2.0$ Hz, 1H), 3.51 (tt, $J = 11.1, 4.5$ Hz, 1H), 2.76–2.65 (m, 3H), 2.40 (dd, $J = 14.2, 10.2$ Hz, 1H), 2.29 (ddd, $J = 13.0, 5.1, 2.2$ Hz, 1H), 2.22 (ddd, $J = 13.4, 11.0, 2.8$ Hz, 1H), 1.98 (dtd, $J = 16.7, 4.7, 2.4$ Hz, 1H), 1.01 (s, 3H), 0.92 (t, $J = 7.4$ Hz, 3H), 0.68 (s, 3H). ^{13}C NMR (126 MHz, CDCl_3) δ 173.3, 163.9, 141.0, 121.6, 100.7, 71.8, 56.0, 50.5, 49.7, 42.4, 42.4, 37.6, 37.4, 36.7, 32.1 (x2), 31.8, 29.7, 28.5, 26.9, 26.5, 24.7, 22.3, 20.9, 19.5, 13.8, 12.4. HRMS (ESI): m/z calcd for $\text{C}_{27}\text{H}_{42}\text{NO}_2$ $[\text{M}+\text{H}]^+$: 412.3210, found 412.3221.

3.1.27. (17R)-17-((5-Phenylisoxazol-3-yl)methyl)-androst-5-en-3 β -ol (41e)

The title compound **41e** (46 mg) was obtained from **40e** in a similar manner for the preparation of **24a** as a white solid in 85% yield. ^1H NMR (500 MHz, CDCl_3) δ 7.80–7.70 (m, 2H), 7.43 (dt, $J = 11.4, 6.7$ Hz, 3H), 6.37 (s, 1H), 5.35 (d, $J = 5.1$ Hz, 1H), 3.58–3.45 (m, 2H), 2.81 (dd, $J = 14.2, 5.0$ Hz, 1H), 2.51 (dd, $J = 14.3, 10.0$ Hz, 1H), 2.36–2.17 (m, 2H), 2.04–1.95 (m, 1H), 1.02 (s, 3H), 0.72 (s, 3H). ^{13}C NMR (126 MHz, CDCl_3) δ 169.5, 164.6, 141.0, 130.1, 129.0 (x2), 127.8, 125.9 (x2), 121.7, 99.5, 71.9, 56.0, 50.5, 49.8, 42.4 (x2), 37.7, 37.4, 36.7, 32.1, 32.1, 31.8, 28.6, 27.0, 24.7, 21.0, 19.6, 12.5. HRMS (ESI): m/z calcd for $\text{C}_{29}\text{H}_{38}\text{NO}_2$ $[\text{M}+\text{H}]^+$: 432.2897, found 432.2903.

3.1.28. (17R)-17-((5-(Pyridin-3-yl)isoxazol-3-yl)methyl)-androst-5-en-3 β -ol (41f)

The title compound **41f** (27 mg) was obtained from **40f** in a similar manner for the preparation of **24a** as a white solid in 62% yield. ^1H NMR (500 MHz, CDCl_3) δ 8.99 (s, 1H), 8.69–8.59 (m, 1H), 8.07 (dt, $J = 8.0, 1.9$ Hz, 1H), 7.41 (dd, $J = 8.0, 4.8$ Hz, 1H), 6.48 (s, 1H), 5.35 (dt, $J = 5.5, 1.9$ Hz, 1H), 3.52 (tt, $J = 11.1, 4.5$ Hz, 1H), 2.83 (dd, $J = 14.3, 4.9$ Hz, 1H), 2.54 (dd, $J = 14.3, 10.1$ Hz, 1H), 2.30 (ddd, $J = 13.0, 5.1, 2.1$ Hz, 1H), 2.24 (ddd, $J = 13.2, 10.8, 2.6$ Hz, 1H), 2.00 (dtd, $J = 16.5, 4.7, 2.4$ Hz, 1H), 1.02 (s, 3H), 0.73 (s, 3H). ^{13}C NMR (126 MHz, CDCl_3) δ 166.7, 164.8, 150.8, 147.1, 141.0, 133.0, 129.9, 123.9, 121.7, 100.6, 71.9, 56.1, 50.6, 49.8, 42.5, 42.4, 37.7, 37.4, 36.8, 32.1, 32.1, 31.8, 28.6, 27.0, 24.7, 21.0, 19.6, 12.5. HRMS (ESI): m/z calcd for $\text{C}_{28}\text{H}_{37}\text{N}_2\text{O}_2$ $[\text{M}+\text{H}]^+$: 433.2850, found 433.2858.

3.1.29. (17R)-17-((5-(2-Fluorophenyl)isoxazol-3-yl)methyl)-androst-5-en-3 β -ol (41g)

The title compound **41g** (53 mg) was obtained from **40g** in a similar manner for the preparation of **24a** as a white solid in 90% yield. ^1H NMR (500 MHz, CDCl_3) δ 7.95 (td, $J = 7.6, 1.8$ Hz, 1H), 7.40 (tdd, $J = 7.4, 5.0, 1.8$ Hz, 1H), 7.26 (dq, $J = 7.4, 3.9, 2.9$ Hz, 2H), 7.18 (dd, $J = 11.4, 8.0$ Hz, 2H), 6.56 (d, $J = 3.9$ Hz, 1H), 5.35 (d, $J = 5.1$ Hz, 1H), 3.57–3.47 (m, 1H), 2.83 (dd, $J = 14.3, 5.0$ Hz, 1H), 2.54 (dd, $J = 14.3, 10.0$ Hz, 1H), 2.30 (ddd, $J = 13.2, 5.2, 2.0$ Hz, 1H), 2.24 (dt, $J = 15.5, 7.7$ Hz, 1H), 1.02 (s, 3H), 0.73 (s, 3H). ^{13}C NMR (126 MHz, CDCl_3) δ 164.9, 163.2, 159.2 (d, $J = 252.8$ Hz), 131.4 (d, $J = 8.5$ Hz), 131.4, 128.8 (d, $J = 101.8$ Hz), 124.8 (d, $J = 3.5$ Hz), 121.7, 116.3 (d, $J = 21.7$ Hz), 103.8 (d, $J = 10.9$ Hz), 71.9, 56.0, 50.5, 49.7, 42.4 (x2), 37.7, 37.4, 36.7, 32.1, 32.1, 31.8, 28.5, 27.0, 24.7, 21.0, 19.6, 12.5. HRMS (ESI): m/z calcd for $\text{C}_{29}\text{H}_{37}\text{FNO}_2$ $[\text{M}+\text{H}]^+$: 450.2803, found 450.2813.

3.1.30. (17R)-17-((5-(2-Hydroxypropan-2-yl)isoxazol-3-yl)methyl)-androst-5-en-3 β -ol (41j)

The title compound **41j** (182 mg) was obtained from **40h** in a similar manner for the preparation of **24j** as a white solid in 70% yield. ^1H NMR (500 MHz, $\text{C}_5\text{D}_5\text{N}$) δ 6.42 (s, 1H), 5.43 (d, $J = 4.9$ Hz, 1H), 3.86 (td, $J = 10.4, 5.7$ Hz, 1H), 2.86 (dd, $J = 14.2, 4.8$ Hz, 1H), 2.68–2.59 (m, 2H), 2.55 (dd, $J = 14.2, 9.6$ Hz, 1H), 2.15–2.06 (m, 1H), 1.96 (dtd, $J = 17.1, 5.2,$

2.2 Hz, 1H), 1.83 (s, 6H), 1.06 (s, 3H), 0.66 (s, 3H). ^{13}C NMR (126 MHz, $\text{C}_5\text{D}_5\text{N}$) δ 180.1, 164.2, 142.4, 121.5, 100.1, 71.6, 68.7, 56.4, 51.1, 50.2, 43.9, 42.7, 38.3, 38.0, 37.4, 33.0, 32.6, 32.5, 30.2, 30.1, 29.1, 27.5, 25.1, 21.5, 20.0, 12.7. HRMS (ESI): m/z calcd for $\text{C}_{26}\text{H}_{40}\text{NO}_3$ $[\text{M}+\text{H}]^+$: 414.3003, found 414.3013.

3.1.30.1. (17R)-17-((5-(Hydroxymethyl)isoxazol-3-yl)methyl)-androst-5-en-3 β -ol (**41k**)

The title compound **41k** (23 mg) was obtained from **40i** in a similar manner for the preparation of **24j** as a white solid in 90% yield. ^1H NMR (500 MHz, $\text{C}_5\text{D}_5\text{N}$) δ 6.45 (s, 1H), 5.43 (d, $J = 4.9$ Hz, 1H), 5.04 (s, 2H), 3.87 (tt, $J = 10.3, 5.4$ Hz, 1H), 2.86 (dd, $J = 14.2, 5.0$ Hz, 1H), 2.65 (qd, $J = 8.0, 2.3$ Hz, 2H), 2.54 (dd, $J = 14.2, 9.6$ Hz, 1H), 2.15–2.07 (m, 1H), 1.06 (s, 3H), 0.66 (s, 3H). ^{13}C NMR (126 MHz, $\text{C}_5\text{D}_5\text{N}$) δ 174.1, 164.5, 142.5, 121.6, 102.4, 71.7, 56.7, 56.5, 51.2, 50.3, 44.0, 42.8, 38.3, 38.2, 37.4, 33.1, 32.7, 32.6, 29.2, 27.5, 25.2, 21.5, 20.1, 12.8. HRMS (ESI): m/z calcd for $\text{C}_{24}\text{H}_{36}\text{NO}_3$ $[\text{M}+\text{H}]^+$: 386.2690, found 386.2694.

3.2. Biology

3.2.1. CYP17A1 Inhibitory Assay

Recombinant human CYP17A1 was purified according to [38]. Recombinant rat NADPH-cytochrome P450 reductase (CPR) was purified according to [39]. Recombinant human cytochrome b_5 was purified according to [40].

To determine ligand binding constants ($K_{d_{app}}$ values) of the CYP17A1, spectrophotometric titration was performed using a Cary 5000 UV–Vis NIR dual-beam spectrophotometer (Agilent Technologies, Santa Clara, CA) in 1 cm quartz cuvettes. Stock solutions of the steroids were prepared at concentration 10 mM in DMSO. The titration was repeated at least three times, and $K_{d_{app}}$ was calculated as described previously [41].

CYP17A1 activity was measured in the reconstituted system at 37 °C in 25 mM Hepes buffer (pH 7.2) according to early developed method [38]. Aliquots of concentrated recombinant proteins were mixed and pre-incubated for 5 min at RT. Progesterone or 17 α -hydroxypregnenolone were added to the reaction mixture at the final concentration of 50 μM . Selected compounds were added to the reaction mixture at the final concentration of 50 μM . To measure the activity, the final concentrations of CYP17A1 and CPR were 1.0 and 2.0 μM , respectively. For analysis of 17,20-lyase activity, 1.0 μM cytochrome b_5 was used. After 10 min of pre-incubation at 37 °C, the reaction was started by adding NADPH at the final concentration 0.25 mM. Aliquots (0.5 mL) were taken from the incubation mixture after 30 min of reaction. Steroids were extracted with 5 mL of methylene chloride. The organic layer was carefully removed and dried under argon flow. 100 μL of methanol was added to the pellet, and steroids were analyzed on a computerized HPLC system.

3.2.2. Cultivation of Cell Lines

The reporter cell line ARE14 derived from 22Rv1 [36] was a kind gift from prof. Zdeněk Dvořák (Palacký University Olomouc, Czech Republic). LNCaP were purchased from ECACC, while LAPC-4 and DU145 cells were kindly gifted by prof. Jan Bouchal (Palacký University Olomouc and University Hospital, Olomouc, Czech Republic). ARE14, LNCaP, and DU145 were cultivated in RPMI-1640 medium, and LAPC-4 was cultivated in DMEM medium. All media were supplemented with 10% standard or charcoal-stripped fetal bovine serum (steroid-depleted serum), 100 IU/mL penicillin, 100 $\mu\text{g}/\text{mL}$ streptomycin, 4 mM glutamine, and 1 mM sodium pyruvate. Cells were cultivated in a humidified incubator at 37 °C and in 5% CO_2 atmosphere.

3.2.3. AR-Transcriptional Activity Assay

ARE14 cells were seeded (40,000 cells/well) into the Nunc™ MicroWell™ 96-well optical plate (Thermo Fisher Scientific, Waltham, MA, USA) on the second day. The cultivation medium was discarded, and the cells were washed with PBS. Analyzed compounds were dissolved in medium supplemented with CSS (agonist mode) or CSS with 1 nM R1881 (antagonist mode) and added to cells, including CSS and 1 nM R1881 controls. Upon 24 h

of incubation, cells were washed with PBS and lysed for 10 min in a lysis buffer (10 mM Tris pH = 7.4, 2 mM DCTA, 1% nonidet P40, 2 mM DTT) at 37 °C. Next, a reaction buffer (20 mM tricine pH = 7.8, 1.07 mM MgSO₄·7H₂O, 5 mM ATP, 9.4 mM luciferin) was added, and the luminescence was measured using a Tecan M200 Pro microplate reader (Biotek, Winooski, VT, USA).

3.2.4. Cell Viability Assay

Cells were seeded into the 96-well tissue culture plates and, on the other day, compounds were added in different concentrations in duplicate for 72 h. Upon treatment, the resazurin solution (Sigma Aldrich, St. Louis, MI, USA) was added for 4 h, and then the fluorescence of resorufin was measured at 544 nm/590 nm (excitation/emission) using a Fluoroskan Ascent microplate reader (Labsystems, Budapest, Hungary). The GI₅₀ value was calculated from the dose–response curves that resulted from the measurements using GraphPad Prism 5.

3.2.5. Colony Formation Assay

LAPC-4 (10,000 cells per well) were seeded into 6 well plates and cultivated for 2 days. Next, the medium was removed and replaced with fresh medium containing different concentrations of the compound. Cells were cultivated with the compounds for 10 days. After that, the medium was discarded, colonies were fixed with 70% ethanol, washed with PBS, and stained with crystal violet (1% solution in 96% ethanol). Finally, wells were washed with PBS until the bottom was clear and colonies were visible and the photograph was captured.

3.2.6. Immunoblotting

After the treatment, cells were washed twice with PBS, pelleted, and kept frozen in –80 °C. Cells were lysed, as usual, in ice-cold RIPA lysis buffer supplemented with protease and phosphatase inhibitors. Cells were disrupted by ultrasound sonication on ice and clarified by centrifugation at 14,000× *g* for 30 min. Protein concentration was measured and balanced within samples. Protein solutions were denatured in SDS-loading buffer, and proteins were separated by SDS-PAGE and electroblotted onto nitrocellulose membranes. Membranes were blocked in 4% BSA and incubated overnight with primary antibodies. On the next day, membranes were washed and incubated with secondary antibodies conjugated with peroxidase. Peroxidase activity was detected by SuperSignal West Pico reagents (Thermo Fisher Scientific, Waltham, MA, USA) using a CCD camera LAS-4000 (Fujifilm, Minato, Japan). Primary antibodies purchased from Merck (Darmstadt, Germany): (anti-β-actin, clone C4; anti-phosphorylated AR (S81)) and from Cell Signaling Technology (Danvers, MA, USA) (anti-AR, clone D6F11; anti-PSA/KLK3, clone D6B1; anti-Nkx3.1, clone D2Y1A; anti-rabbit secondary antibody (porcine anti-rabbit immunoglobulin serum)). All antibodies were diluted in 4% BSA and 0.1% Tween 20 in TBS.

3.2.7. Molecular Docking

Molecular docking of compounds **3–7j** and **6–4z** was performed into the crystal structure of CYP17A1 co-crystalised with heme and abiraterone (PDB:3RUK). The abiraterone molecule was extracted from the protein target before docking, for which the protein was set rigid. For molecular docking into the AR-LBD structure, its crystal structure with DHT was used (PDB:2PIV), and two key amino-acid residues in both extremities of the cavity (Arg752 and Thr877) were set flexible. Accuracy of the docking was assured by re-docking of abiraterone and galeterone into the protein targets and comparison with crystal structure or previously published docking poses. The 3D structures of all compounds were prepared, and their energy was minimized by molecular mechanics with Avogadro 1.90.0. Polar hydrogens were added to molecules with the AutoDock Tools program [42], and docking was performed using AutoDock Vina 1.05 [43]. Figures were generated in Pymol ver. 2.0.4 (Schrödinger, LLC, Cambridge, UK).

4. Conclusions

In summary, in this paper, we present the synthesis and biological studies of steroids containing an isoxazole fragment on their side chain. The presented synthetic approach allowed the preparation of regioisomeric isoxazole derivatives bearing a steroid moiety at both C-3 and C-5 of the heterocycle using common intermediates. Biological studies of the obtained compounds included an examination of their effects on 17 α -hydroxylase and 17,20-lyase activity of human CYP17A1 and the ability of selected compounds to influence the downstream AR signaling.

Most of the compounds have a moderate inhibitory effect on the activity of human CYP17A1. The most promising results (predominant inhibitory effect on 17/20-lyase reaction over effect on 17 α -hydroxylase activity of CYP17A1) were obtained for the compounds **41a** and **41k**. These molecules are the most perspective for further optimization. Compounds **41f,g,j** also had a predominant effect on the 17,20-lyase reaction of CYP17A1. Moreover, binding and interactions of **41a** in CYP17A1 was described using molecular docking and was found nearly identical, compared to abiraterone. Several compounds were further evaluated for their ability to affect the AR transactivation and the viability of several PCa cell lines. Within prepared compounds, three AR antagonists were found to abolish the AR transcriptional activity and the viability of AR-positive PCa cell lines in mid-micromolar concentrations. Candidate compound **24j** decreased the AR protein level and blocked its downstream signaling and significantly inhibited colony formation of LAPC-4 cells. Binding of **24j** in AR-LBD was described to be similar to galeterone. Overall, the results support the development of novel steroidal derivatives targeting CYP17A1 and AR as anticancer agents in PCa therapy.

Supplementary Materials: The supporting information can be downloaded at: <https://www.mdpi.com/article/10.3390/ijms232113534/s1>.

Author Contributions: Conceptualization, V.N.Z. and R.J.; methodology, V.N.Z., M.P. and R.J.; synthesis, A.S.R., A.V.K. and M.Y.N.; biological activity evaluations, M.P., L.M., A.M.T., T.V.S. and I.P.G.; HRMS, M.G.Z. and A.R.M.; writing—original draft preparation, V.N.Z., M.P. and R.J.; writing—review and editing, V.N.Z., V.A.K., R.J. and M.K.; supervision, V.A.K.; project administration, V.A.K. and R.J.; funding acquisition, V.N.Z. and R.J. All authors have read and agreed to the published version of the manuscript.

Funding: This research was funded by the Belarusian Foundation for Fundamental Research, grant number X22Mldg-001. The authors gratefully acknowledge financial support from the Palacky University Olomouc (IGA_PrF_2022_007), from the Czech Ministry of Education, Youth and Sports via the project National Institute for Cancer Research (Programme EXCELES, ID Project No. LX22NPO5102 funded by the European Union—Next Generation EU). This work was also financed by the Ministry of Science and Higher Education of the Russian Federation within the framework of state support for the creation and development of World-Class Research Centers' 'Digital Biodesign and Personalized Healthcare' (No 075-15-2022-305).

Institutional Review Board Statement: Not applicable.

Informed Consent Statement: Not applicable.

Data Availability Statement: Not applicable.

Acknowledgments: We acknowledge the International Journal of Molecular Sciences for providing the APC waiver.

Conflicts of Interest: The authors declare no conflict of interest.

Abbreviations

AR	androgen receptor
CCS	charcoal stripped serum
CDI	<i>N,N</i> -carbonyldiimidazole
CFA	colony formation assay
CPR	NADPH-cytochrome P450 reductase
DCM	dichloromethane
DHT	dihydrotestosterone
DMF	dimethylformamide
DMP	Dess-Martin periodinane
ESI	electrospray ionization
FBS	fetal bovine serum
Gal	galeterone
HRMS	high resolution mass spectrometry
LBD	ligand-binding domain
PC	prostate cancer
PE	petroleum ether
TBAF	tetra- <i>n</i> -butylammonium fluoride
TBS	<i>tert</i> -butyldimethylsilyl
THF	tetrahydrofuran

References

- Huggins, C.; Stevens, R.E., Jr.; Hodges, C.V. Studies on prostatic cancer: II. The effects of castration on advanced carcinoma of the prostate gland. *Arch. Surg.* **1941**, *43*, 209–223. [[CrossRef](#)]
- Saylor, P.J. The androgen receptor remains front and centre. *Nat. Rev. Clin. Oncol.* **2013**, *10*, 126–128. [[CrossRef](#)]
- Sharifi, N.; McPhaul, M.J.; Auchus, R.J. “Getting from here to there”—Mechanisms and limitations to the activation of the androgen receptor in castration-resistant prostate cancer. *J. Invest. Med.* **2010**, *58*, 938–944. [[CrossRef](#)]
- Fizazi, K.; Scher, H.I.; Molina, A.; Logothetis, C.J.; Chi, K.N.; Jones, R.J.; Staffurth, J.N.; North, S.; Vogelzang, N.J.; Saad, F.; et al. Abiraterone acetate for treatment of metastatic castration-resistant prostate cancer: Final overall survival analysis of the COU-AA-301 randomised, double-blind, placebo-controlled phase 3 study. *Lancet Oncol.* **2012**, *13*, 983–992. [[CrossRef](#)]
- Sushko, T.A.; Gilep, A.A.; Usanov, S.A. Genetics, structure, function, mode of actions and role in cancer development of CYP17. *Anticancer Agents Med. Chem.* **2014**, *14*, 66–76. [[CrossRef](#)]
- Latysheva, A.S.; Zolottsev, V.A.; Veselovsky, A.V.; Scherbakov, K.A.; Morozovich, G.E.; Pokrovsky, V.S.; Novikov, R.A.; Timofeev, V.P.; Tkachev, Y.V.; Misharin, A.Y. New steroidal oxazolines, benzoxazoles and benzimidazoles related to abiraterone and galeterone. *Steroids* **2020**, *153*, 108534. [[CrossRef](#)]
- Zhao, J.-W.; Guo, J.-W.; Huang, M.-J.; You, Y.-Z.; Wu, Z.-H.; Liu, H.-M.; Huang, L.-H. Design, synthesis and biological evaluation of new steroidal β -triazolonyl enones as potent antiproliferative agents. *Steroids* **2019**, *150*, 108431. [[CrossRef](#)]
- Jorda, R.; Řezníčková, E.; Kielczewska, U.; Maj, J.; Morzycki, J.W.; Siergiejczyk, L.; Bazgier, V.; Berka, K.; Rárová, L.; Wojtkielewicz, A. Synthesis of novel galeterone derivatives and evaluation of their in vitro activity against prostate cancer cell lines. *Eur. J. Med. Chem.* **2019**, *179*, 483–492. [[CrossRef](#)]
- Jorda, R.; Lopes, S.M.M.; Řezníčková, E.; Ajani, H.; Pereira, A.V.; Gomes, C.S.B.; Pinho E Melo, T.M.V.D. Tetrahydropyrazolo [1,5-*a*]pyridine-fused steroids and their in vitro biological evaluation in prostate cancer. *Eur. J. Med. Chem.* **2019**, *178*, 168–176. [[CrossRef](#)]
- Hou, Q.; He, C.; Lao, K.; Luo, G.; You, Q.; Xiang, H. Design and synthesis of novel steroidal imidazoles as dual inhibitors of AR/CYP17 for the treatment of prostate cancer. *Steroids* **2019**, *150*, 108384. [[CrossRef](#)]
- Dalidovich, T.S.; Hurski, A.L.; Morozovich, G.E.; Latysheva, A.S.; Sushko, T.A.; Strushkevich, N.V.; Gilep, A.A.; Misharin, A.Y.; Zhabinskii, V.N.; Khripach, V.A. Newazole derivatives of [17(20)*E*]-21-norpregnane: Synthesis and inhibition of prostate carcinoma cell growth. *Steroids* **2019**, *147*, 10–18. [[CrossRef](#)]
- Zolottsev, V.A.; Tkachev, Y.V.; Latysheva, A.S.; Kostin, V.A.; Novikov, R.A.; Timofeev, V.P.; Morozovich, G.E.; Kuzikov, A.V.; Shumyantseva, V.V.; Misharin, A.Y. Comparison of [17(20)*E*]-21-norpregnane oxazolonyl and benzoxazolonyl derivatives as inhibitors of CYP17A1 activity and prostate carcinoma cells growth. *Steroids* **2018**, *129*, 24–34. [[CrossRef](#)]
- Tantawy, M.A.; Nafie, M.S.; Elmegeed, G.A.; Ali, I.A.I. Auspicious role of the steroidal heterocyclic derivatives as a platform for anti-cancer drugs. *Bioorg. Chem.* **2017**, *73*, 128–146. [[CrossRef](#)]
- Kostin, V.A.; Zolottsev, V.A.; Kuzikov, A.V.; Masamrekh, R.A.; Shumyantseva, V.V.; Veselovsky, A.V.; Stulov, S.V.; Novikov, R.A.; Timofeev, V.P.; Misharin, A.Y. Oxazolonyl derivatives of [17(20)*E*]-21-norpregnane differing in the structure of A and B rings. Facile synthesis and inhibition of CYP17A1 catalytic activity. *Steroids* **2016**, *115*, 114–122. [[CrossRef](#)]

15. Szabo, N.; Ajdukovic, J.J.; Djurendic, E.A.; Sakac, M.N.; Ignath, I.; Gardi, J.; Mahmoud, G.; Klisuric, O.R.; Jovanovic-Santa, S.; Penov Gasi, K.M.; et al. Determination of 17 α -hydroxylase-C_{17,20}-lyase (P450_{17 α}) enzyme activities and their inhibition by selected steroidal picolyl and picolinylidene compounds. *Acta Biol. Hung.* **2015**, *66*, 41–51. [[CrossRef](#)]
16. Stulov, S.V.; Dugin, N.O.; Zharkova, M.S.; Shcherbinin, D.S.; Kuzikov, A.V.; Shumantseva, V.V.; Misharin, A.Y.; Veselovsky, A.V. Interaction of novel oxazoline derivatives of 17(20)E-pregna-5,17(20)-diene with cytochrome P450 17A1. *Biochem. Suppl. Ser. B Biomed. Chem.* **2015**, *9*, 114–120. [[CrossRef](#)]
17. Kostin, V.A.; Latysheva, A.S.; Zolotsev, V.A.; Tkachev, Y.V.; Timofeev, V.P.; Kuzikov, A.V.; Shumyantseva, V.V.; Morozovich, G.E.; Misharin, A.Y. Oxazoline derivatives of [17(20)E]-21-norpregnene—Inhibitors of CYP17A1 activity and proliferation of prostate carcinoma cells. *Russ. Chem. Bull.* **2018**, *67*, 682–687. [[CrossRef](#)]
18. Hu, Q.; Hartmann, R.W. Chapter 11—The Renaissance of CYP17 Inhibitors for the Treatment of Prostate Cancer. In *Cancer Drug Design and Discovery*, 2nd ed.; Neidle, S., Ed.; Academic Press: San Diego, CA, USA, 2014; pp. 319–356. [[CrossRef](#)]
19. Njar, V.C.O.; Brodie, A.M.H. Discovery and development of galeterone (TOK-001 or VN/124-1) for the treatment of all stages of prostate cancer. *J. Med. Chem.* **2015**, *58*, 2077–2087. [[CrossRef](#)]
20. Ling, Y.Z.; Li, J.S.; Liu, Y.; Kato, K.; Klus, G.T.; Brodie, A. 17-Imidazolyl, pyrazolyl, and isoxazolyl androstene derivatives. Novel steroidal inhibitors of human cytochrome C_{17,20}-lyase (P450_{17 α}). *J. Med. Chem.* **1997**, *40*, 3297–3304. [[CrossRef](#)]
21. Nnane, I.P.; Long, B.J.; Ling, Y.Z.; Grigoryev, D.N.; Brodie, A.M. Anti-tumour effects and pharmacokinetic profile of 17-(5'-isoxazolyl)androst-4,16-dien-3-one (L-39) in mice: An inhibitor of androgen synthesis. *Br. J. Cancer* **2000**, *83*, 74–82. [[CrossRef](#)]
22. Nnane, I.P.; Kato, K.; Liu, Y.; Long, B.J.; Lu, Q.; Wang, X.; Ling, Y.-Z.; Brodie, A. Inhibition of androgen synthesis in human testicular and prostatic microsomes and in male rats by novel steroidal compounds. *Endocrinology* **1999**, *140*, 2891–2897. [[CrossRef](#)] [[PubMed](#)]
23. Banday, A.H.; Giri, A.K.; Parveen, R.; Bashir, N. Design and synthesis of D-ring steroidal isoxazolines and oxazolines as potential antiproliferative agents against LNCaP, PC-3 and DU-145 cells. *Steroids* **2014**, *87*, 93–98. [[CrossRef](#)] [[PubMed](#)]
24. Banday, A.H.; Singh, S.; Alam, M.S.; Reddy, D.M.; Gupta, B.D.; Sampath Kumar, H.M. Synthesis of novel steroidal D-ring substituted isoxazoline derivatives of 17-oxoandrostanes. *Steroids* **2008**, *73*, 370–374. [[CrossRef](#)] [[PubMed](#)]
25. Kuzikov, A.V.; Dugin, N.O.; Stulov, S.V.; Shcherbinin, D.S.; Zharkova, M.S.; Tkachev, Y.V.; Timofeev, V.P.; Veselovsky, A.V.; Shumyantseva, V.V.; Misharin, A.Y. Novel oxazoliny derivatives of prena-5,17(20)-diene as 17 α -hydroxylase/17,20-lyase (CYP17A1) inhibitors. *Steroids* **2014**, *88*, 66–71. [[CrossRef](#)] [[PubMed](#)]
26. Chalyk, B.A.; Khutorianskyi, A.; Lysenko, A.; Fil, Y.; Kuchkovska, Y.O.; Gavrilenko, K.S.; Bakanovych, I.; Moroz, Y.S.; Gorlova, A.O.; Grygorenko, O.O. Regioselective synthesis of functionalized 3- or 5-fluoroalkyl isoxazoles and pyrazoles from fluoroalkyl ynones and binucleophiles. *J. Org. Chem.* **2019**, *84*, 15212–15225. [[CrossRef](#)] [[PubMed](#)]
27. Jeyaveeran, J.C.; Praveen, C.; Arun, Y.; Prince, A.A.M.; Perumal, P.T. Cycloisomerization of acetylenic oximes and hydrazones under gold catalysis: Synthesis and cytotoxic evaluation of isoxazoles and pyrazoles. *J. Chem. Sci.* **2016**, *128*, 73–83. [[CrossRef](#)]
28. Xie, M.; Li, M.; Liu, C.; Zhang, J.; Feng, C. Facile regioselective synthesis of 5-hydroxy-4,5-dihydroisoxazoles from acetylenic ketones. *J. Heterocycl. Chem.* **2012**, *49*, 1462–1465. [[CrossRef](#)]
29. Zarecki, A.; Wicha, J. Magnesium in methanol selective reduction of a conjugate double bond in an α,β -unsaturated ester related to pregnadiene. *Synthesis* **1996**, *1996*, 455–456. [[CrossRef](#)]
30. Reis, L.V.; Lobo, A.M.; Prabhakar, S. Enehydroxylamines as versatile compounds in 3,3-sigmatropic rearrangements. *Tetrahedron Lett.* **1994**, *35*, 2747–2750. [[CrossRef](#)]
31. Reis, L.V.; Lobo, A.M.; Prabhakar, S.; Duarte, M.P. 3,3-Sigmatropic rearrangements involving N–O bond-cleavage of enehydroxylamine derivatives. *Eur. J. Org. Chem.* **2003**, *2003*, 190–208. [[CrossRef](#)]
32. Al-Awadi, N.A.; Abdelkhalik, M.M.; Abdelhamid, I.A.; Elnagdi, M.H. Pyrolytic methods in organic synthesis: Novel routes for the synthesis of 3-oxoalkanenitriles, 2-acyl anilines, and 2-aroil anilines. *Synlett* **2007**, *2007*, 2979–2982. [[CrossRef](#)]
33. Kim, S.; Park, J.H. Selective removal of tetrahydropyranyl ethers in the presence of tert-butyl dimethylsilyl ethers with magnesium bromide in ether. *Tetrahedron Lett.* **1987**, *28*, 439–440. [[CrossRef](#)]
34. Praveen, C.; Kalyanasundaram, A.; Perumal, P.T. Gold(III)-catalyzed synthesis of isoxazoles by cycloisomerization of α,β -acetylenic oximes. *Synlett* **2010**, *2010*, 777–781. [[CrossRef](#)]
35. Bird, I.M.; Abbott, D.H. The hunt for a selective 17,20 lyase inhibitor; learning lessons from nature. *J. Steroid Biochem. Mol. Biol.* **2016**, *163*, 136–146. [[CrossRef](#)]
36. Bartonkova, I.; Novotna, A.; Dvorak, Z. Novel stably transfected human reporter cell line AIZ-AR as a tool for an assessment of human androgen receptor transcriptional activity. *PLoS ONE* **2015**, *10*, e0121316. [[CrossRef](#)]
37. Goggins, S.; Apsey, E.A.; Mahon, M.F.; Frost, C.G. Ratiometric electrochemical detection of hydrogen peroxide and glucose. *Org. Biomol. Chem.* **2017**, *15*, 2459–2466. [[CrossRef](#)]
38. Pechurskaya, T.A.; Lukashevich, O.P.; Gilep, A.A.; Usanov, S.A. Engineering, expression, and purification of “soluble” human cytochrome P450_{17 α} and its functional characterization. *Biochem. Biokhimiia* **2008**, *73*, 806–811. [[CrossRef](#)]
39. Bonina, T.A.; Gilep, A.A.; Estabrook, R.W.; Usanov, S.A. Engineering of proteolytically stable NADPH-cytochrome P450 reductase. *Biochem. Biokhimiia* **2005**, *70*, 357–365. [[CrossRef](#)]
40. Yablokov, E.; Florinskaya, A.; Medvedev, A.; Sergeev, G.; Strushkevich, N.; Luschik, A.; Shkel, T.; Haidukevich, I.; Gilep, A.; Usanov, S.; et al. Thermodynamics of interactions between mammalian cytochromes P450 and b5. *Arch. Biochem. Biophys.* **2017**, *619*, 10–15. [[CrossRef](#)]

41. Guryev, O.L.; Gilep, A.A.; Usanov, S.A.; Estabrook, R.W. Interaction of apo-cytochrome b5 with cytochromes P4503A4 and P45017A: Relevance of heme transfer reactions. *Biochemistry* **2001**, *40*, 5018–5031. [[CrossRef](#)]
42. Morris, G.M.; Huey, R.; Lindstrom, W.; Sanner, M.F.; Belew, R.K.; Goodsell, D.S.; Olson, A.J. AutoDock4 and AutoDockTools4: Automated docking with selective receptor flexibility. *J. Comput. Chem.* **2009**, *30*, 2785–2791. [[CrossRef](#)] [[PubMed](#)]
43. Trott, O.; Olson, A.J. AutoDock Vina: Improving the speed and accuracy of docking with a new scoring function, efficient optimization, and multithreading. *J. Comput. Chem.* **2010**, *31*, 455–461. [[CrossRef](#)] [[PubMed](#)]

Supporting information to:

Rudovich, A. S.; Peřina, M.; Krech, A. V.; Novozhilova, M. Y.;
Tumilovich, A. M.; Shkel, T. V.; Grabovec, I. P.; Kvasnica, M.; Mada, L.;
Zavialova, M. G.; Mekhtiev, A. R.; Jorda, R.; Zhabinskii, V. N.;
Khripach, V. A.

**Synthesis and Biological Evaluation of New Isoxazolyl Steroids as
Anti-Prostate Cancer Agents**

Table S1. AR transcriptional and antiproliferative activities of novel derivatives.

Cmp.	AR transcriptional activity (%)						Viability after 72 h (GI ₅₀) ^c		
	ANTAGONIST MODE ^a			AGONIST MODE ^b			LNCaP	LAPC-4	DU145
	50 μ M	10 μ M	2 μ M	50 μ M	10 μ M	2 μ M			
24d	103.6 \pm 42.6	112.8 \pm 21.1	109.0 \pm 12.1	18.6 \pm 3.6	21.1 \pm 1.6	17.8 \pm 0.1	> 50	> 50	> 50
24e	125.3 \pm 27.4	101.1 \pm 13.6	101.3 \pm 9.5	12.8 \pm 0.2	14.2 \pm 1.4	14.7 \pm 0.5	> 50	> 50	> 50
24g	111.6 \pm 19.9	112.5 \pm 14.5	112.9 \pm 10.9	19.7 \pm 1.6	17.5 \pm 0.5	15.6 \pm 0.6	> 50	> 50	> 50
24j	21.6 \pm 7.8	84.8 \pm 17.4	100.2 \pm 13.5	6.1 \pm 1.5	12.6 \pm 0.1	14.4 \pm 2.8	25.8 \pm 0.6	18.2 \pm 1.2	> 50
27	63.5 \pm 8.0	62.0 \pm 14.8	89.7 \pm 9.9	20.4 \pm 4.2	20.9 \pm 2.9	17.4 \pm 0.5	> 50	> 50	> 50
32	31.1 \pm 13.3	87.8 \pm 20.9	99.7 \pm 17.4	14.6 \pm 0.5	12.1 \pm 2.7	14.0 \pm 1.1	19.5 \pm 0.1	18.9 \pm 7.2	> 50
36	67.4 \pm 21.9	72.5 \pm 15.7	101.1 \pm 18.1	16.3 \pm 1.7	12.0 \pm 0.5	14.7 \pm 0.2	> 50	19.0 \pm 7.8	> 50
38	78.2 \pm 24.9	92.6 \pm 20.5	96.1 \pm 11.2	7.3 \pm 1.1	13.0 \pm 0.4	14.6 \pm 1.0	> 50	> 50	> 50
41a	50.8 \pm 18.8	73.7 \pm 14.9	98.2 \pm 17.5	12.1 \pm 1.3	14.7 \pm 0.1	14.5 \pm 1.5	> 50	> 50	> 50
Gal	3.0 \pm 1.8	35.1 \pm 3.3	65.2 \pm 6.1	2.4 \pm 1.1	10.8 \pm 3.1	15.4 \pm 0.4	46.8 \pm 0.1	28.6 \pm 0.6	47.6 \pm 0.2

^a measured in the presence of compound and 1 nM R1881 and normalized to signal of 1 nM R1881 = 100%, determined in duplicate and repeated twice, mean \pm SD is presented.

^b measured in the presence of compound only, normalized to signal of 1 nM R1881 = 100%, measured in duplicate and repeated twice, mean \pm SD is presented.

^c measured at least in duplicate, mean \pm SD is presented.

Table S2. Raw data for **Figure 2. (A)** Transcriptional activity of AR measured in reporter cell line in both antagonist (competition with 1 nM R1881) and agonist (presence of compound alone) mode upon treatment with different concentration of **24j**.

Concentration (μ M)	AR transcriptional activity (%) after treatment with 24 j (antagonist mode)					AR transcriptional activity (%) after treatment with 24 j (agonist mode)			
60.00	20.55	20.45	15.39	15.98		6.48	8.33	7.15	5.97
20.00	55.89	57.74	58.97	51.32		14.35	16.25	14.56	15.38
6.67	78.82	77.07	74.29	83.26		16.97	15.48	17.44	20.21
2.22	88.25	93.78	91.50	88.12		15.89	17.90	21.24	19.34
0.74	95.70	97.95	95.17	95.70		17.18	19.44	20.73	22.58
0.25	98.38	91.23	93.41	98.15		18.16	19.80	20.78	20.68

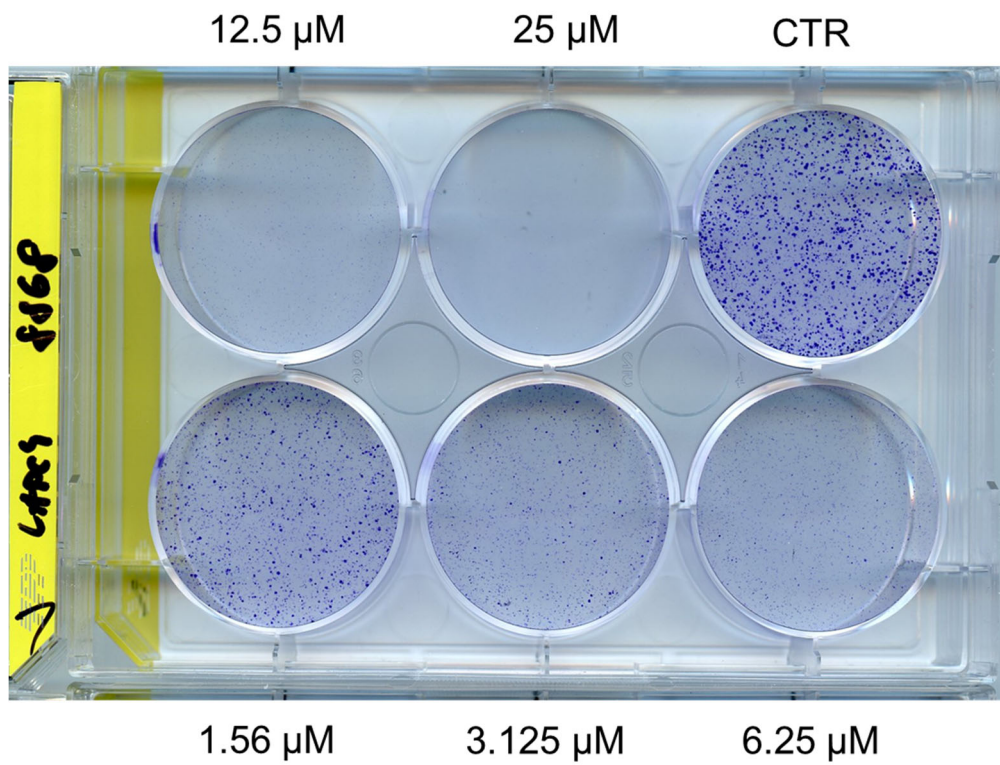


Figure S1. Raw picture for **Figure 2. (B)** Colony formation assay of PCa cells LAPC-4 after treatment with **24j** for 10 days.

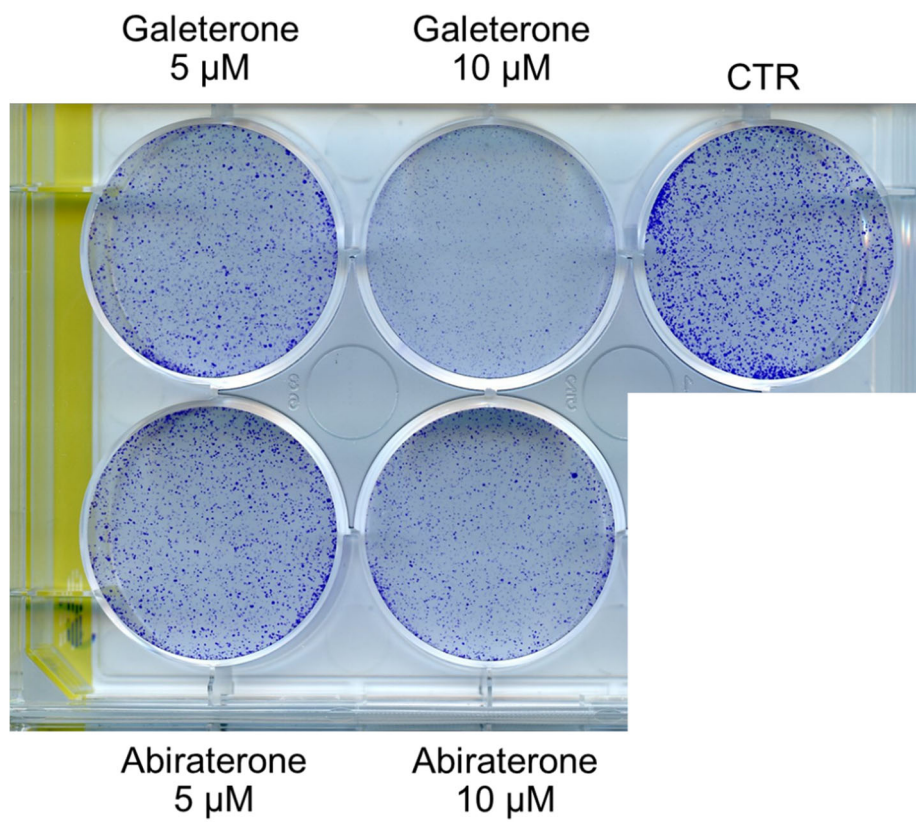


Figure S2. Colony formation assay of PCa cells LAPC-4 after treatment with standards for 10 days.

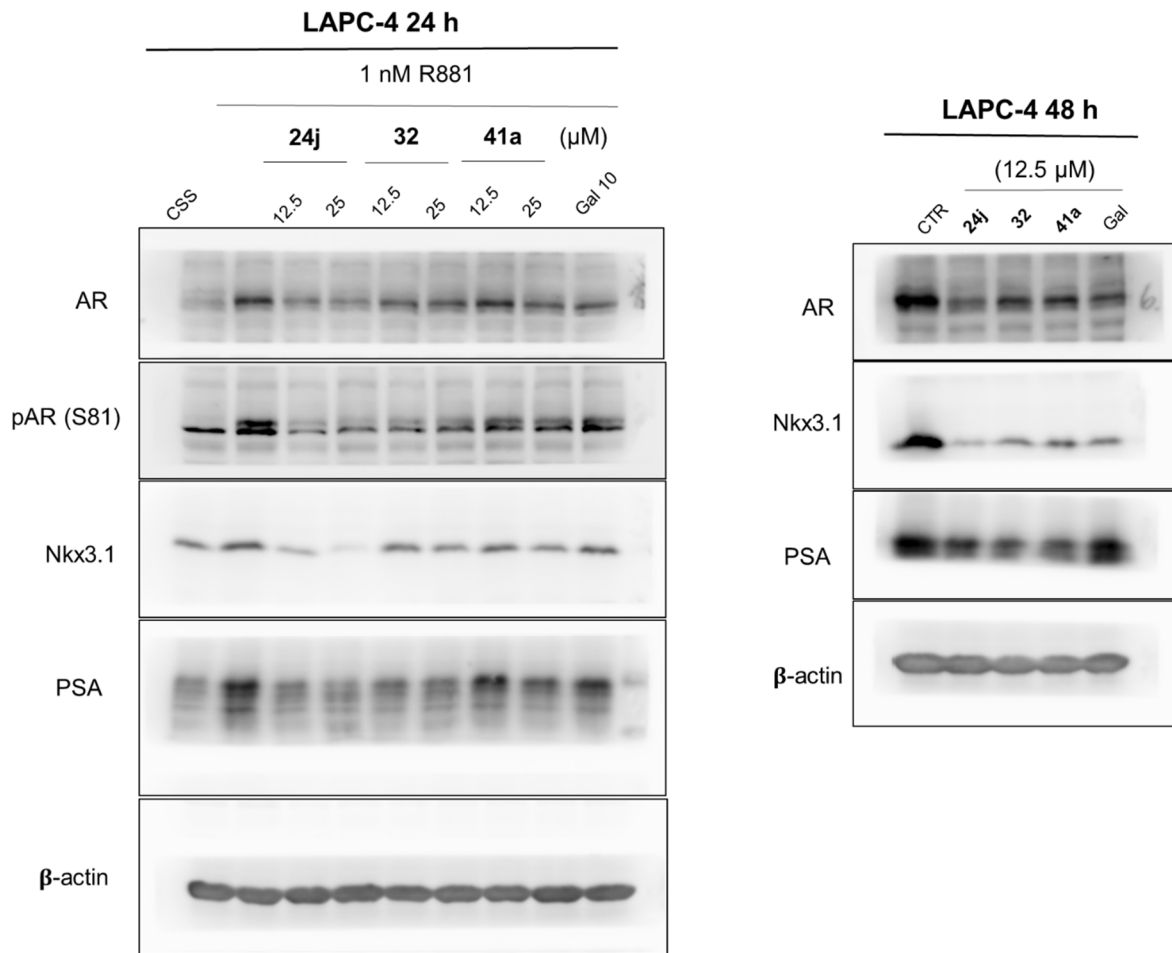


Figure S3. Raw picture for **Figure 3.** Western blotting analysis of AR and AR-regulated proteins in treated LAPC-4 cells.

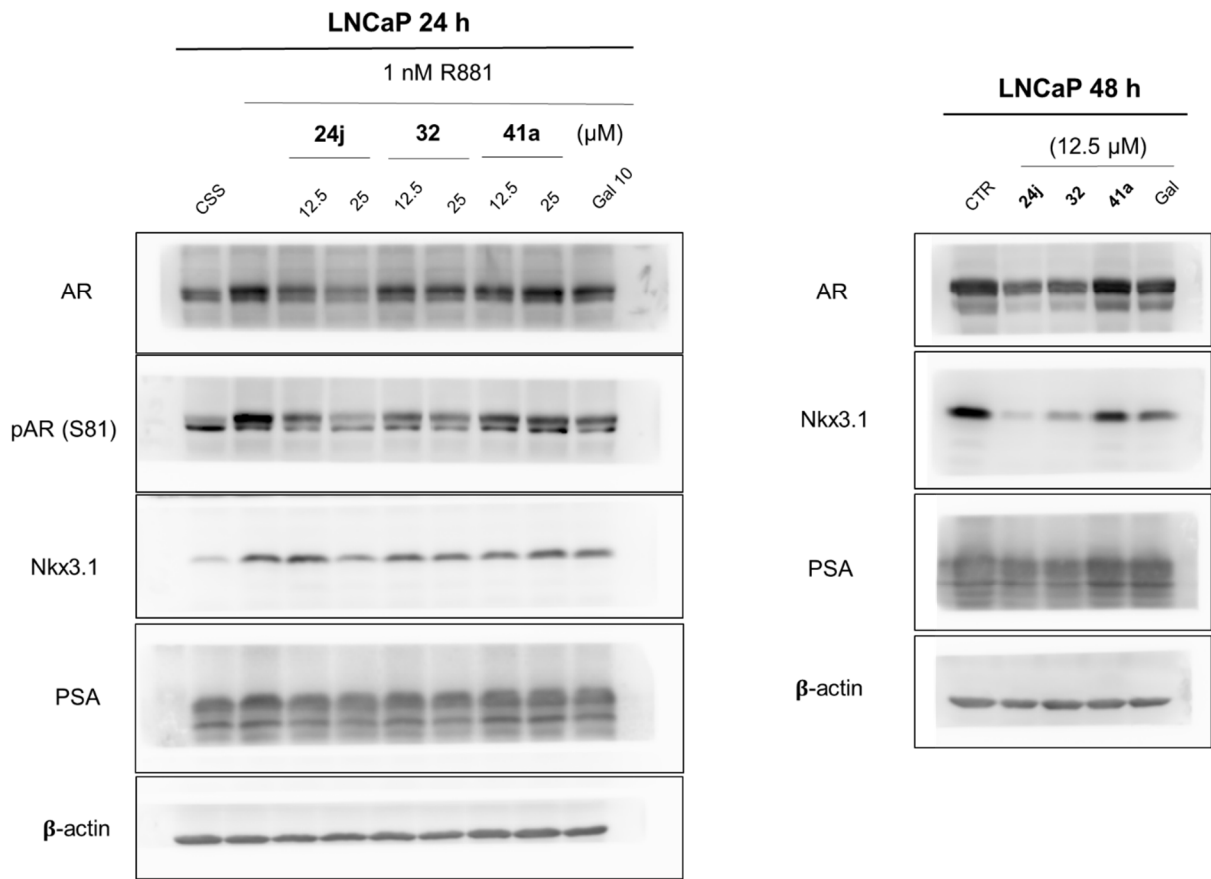
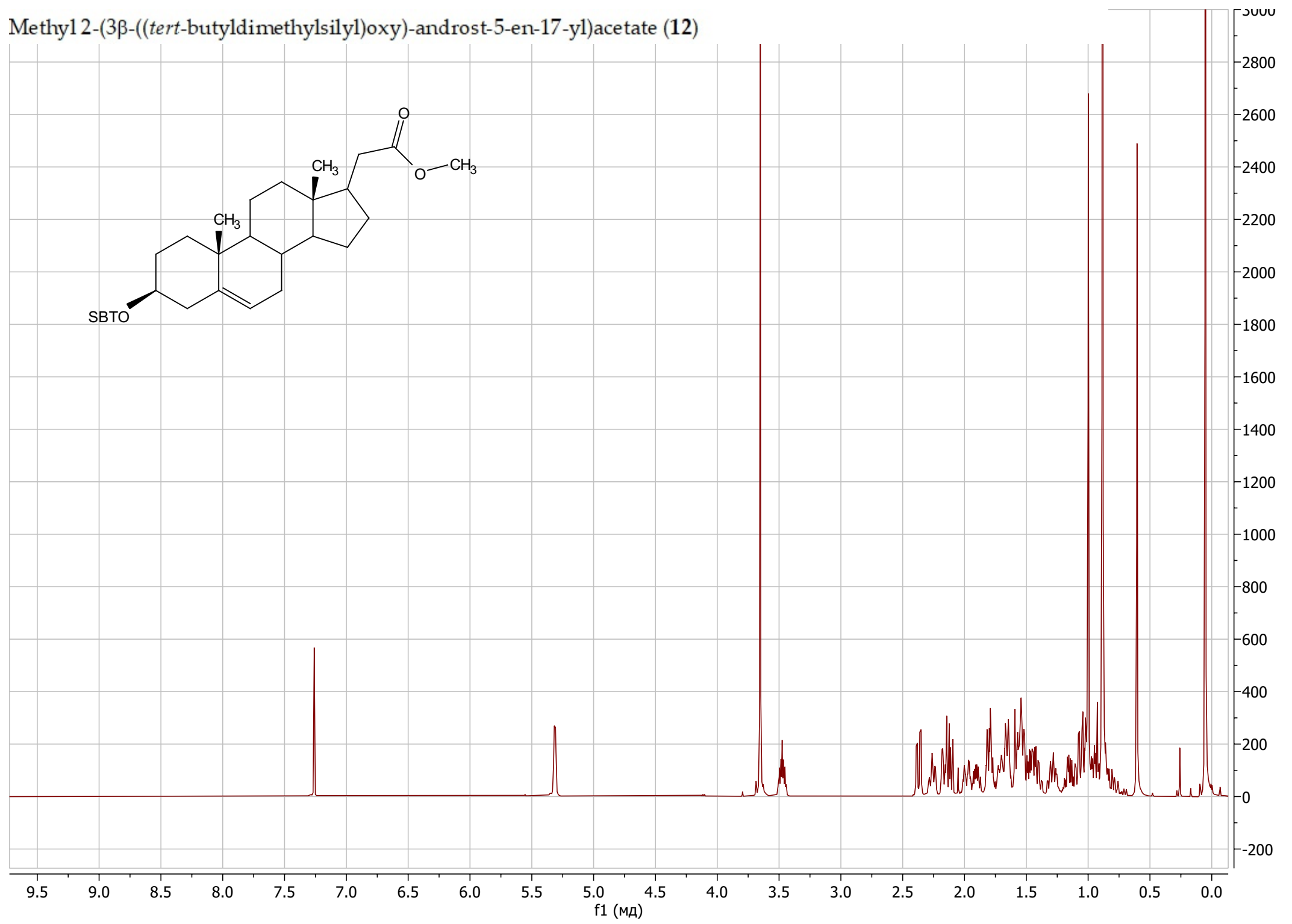
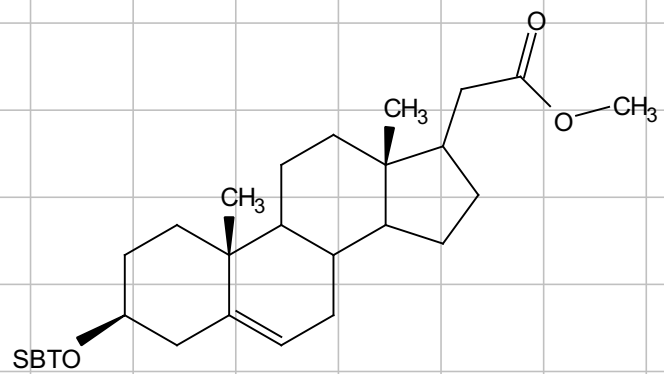


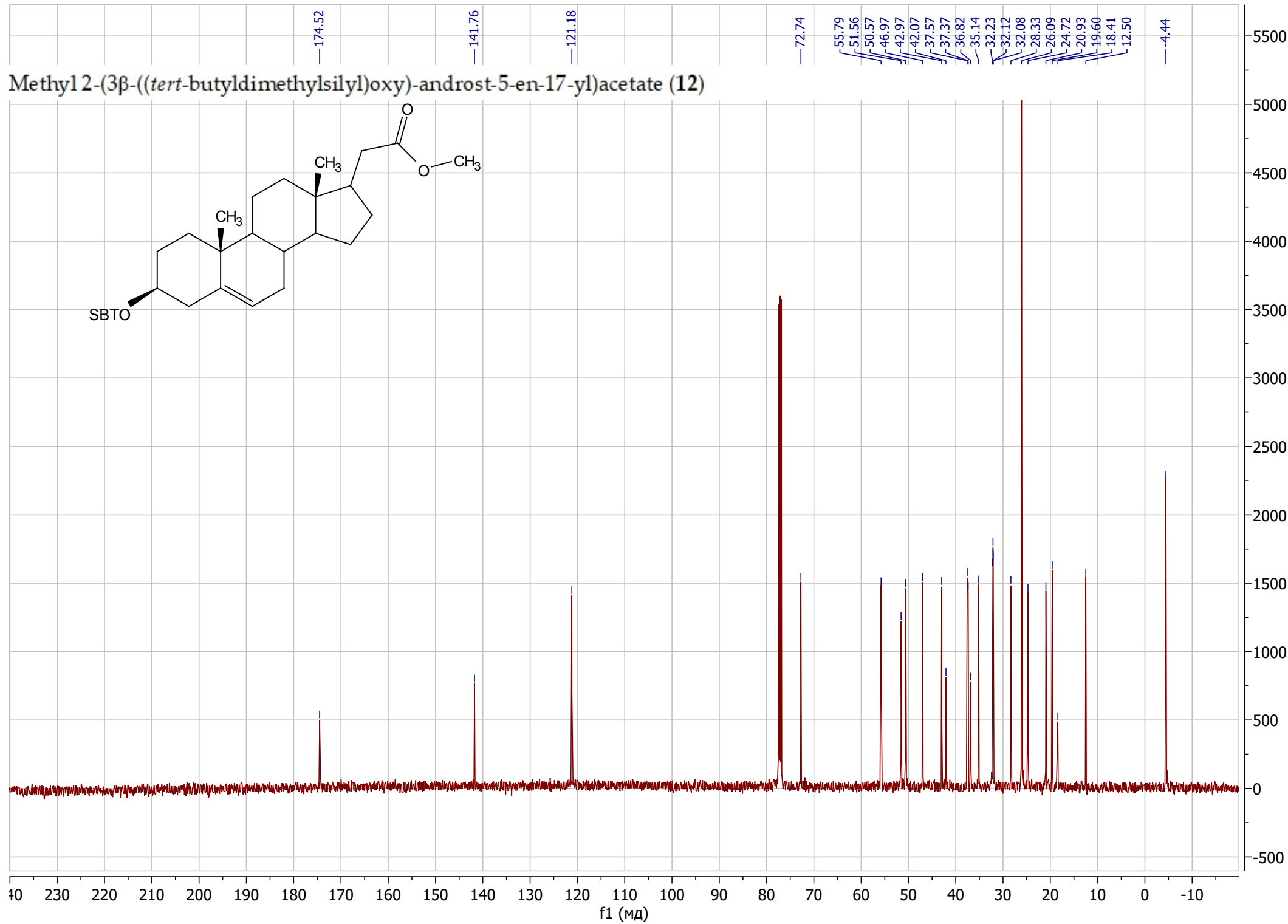
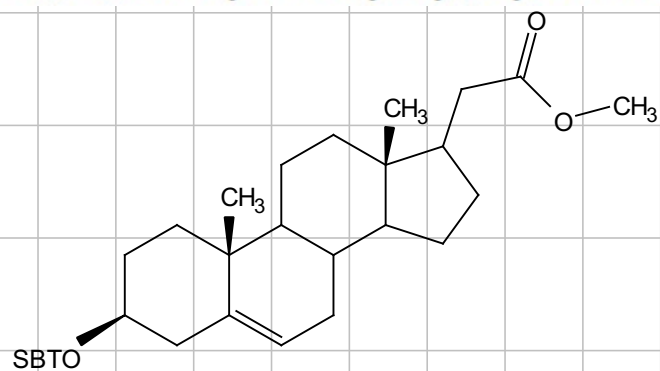
Figure S4. Raw picture for **Figure 3.** Western blotting analysis of AR and AR-regulated proteins in treated LAPC-4 cells.

^1H and ^{13}C NMR spectra

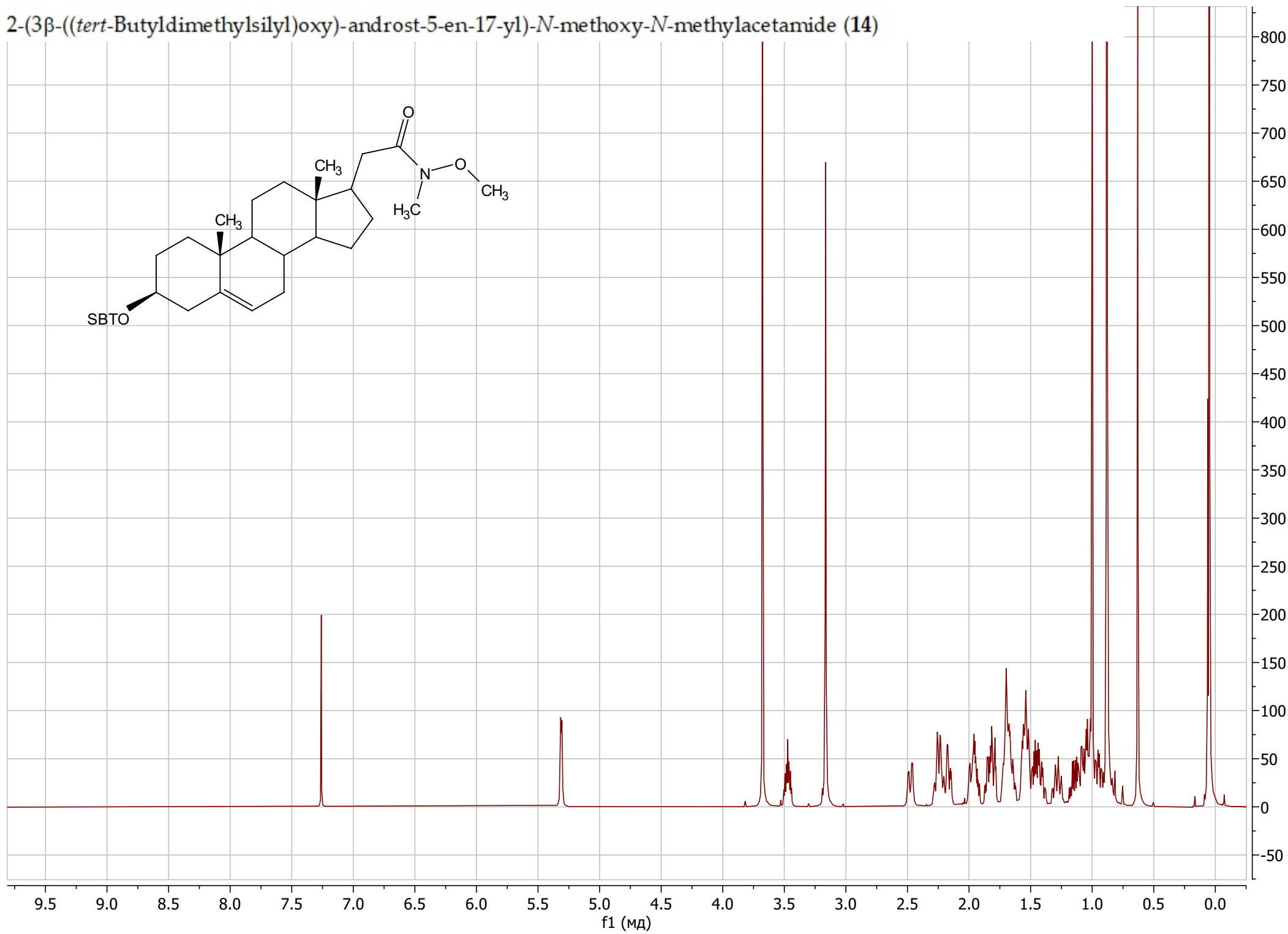
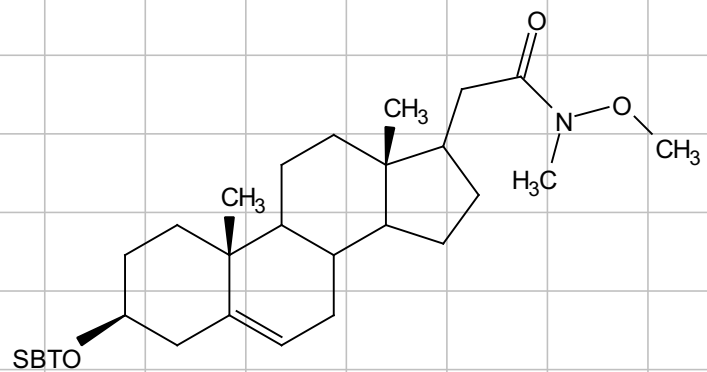
Methyl 2-(3 β -((*tert*-butyldimethylsilyl)oxy)-androst-5-en-17-yl)acetate (12)



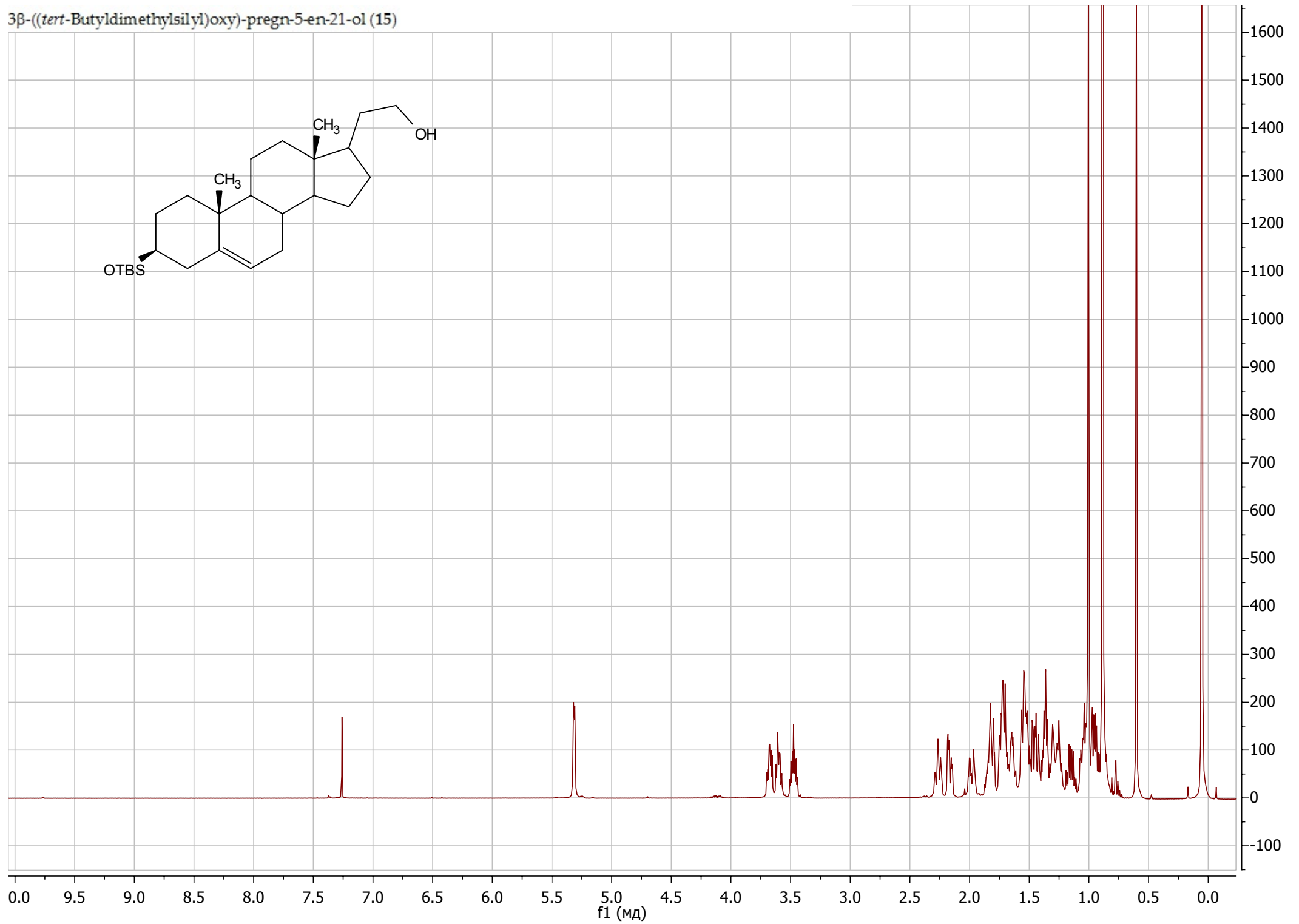
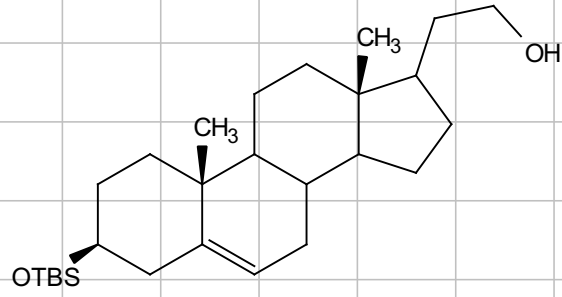
Methyl 2-(3 β -((*tert*-butyldimethylsilyl)oxy)-androst-5-en-17-yl)acetate (12)



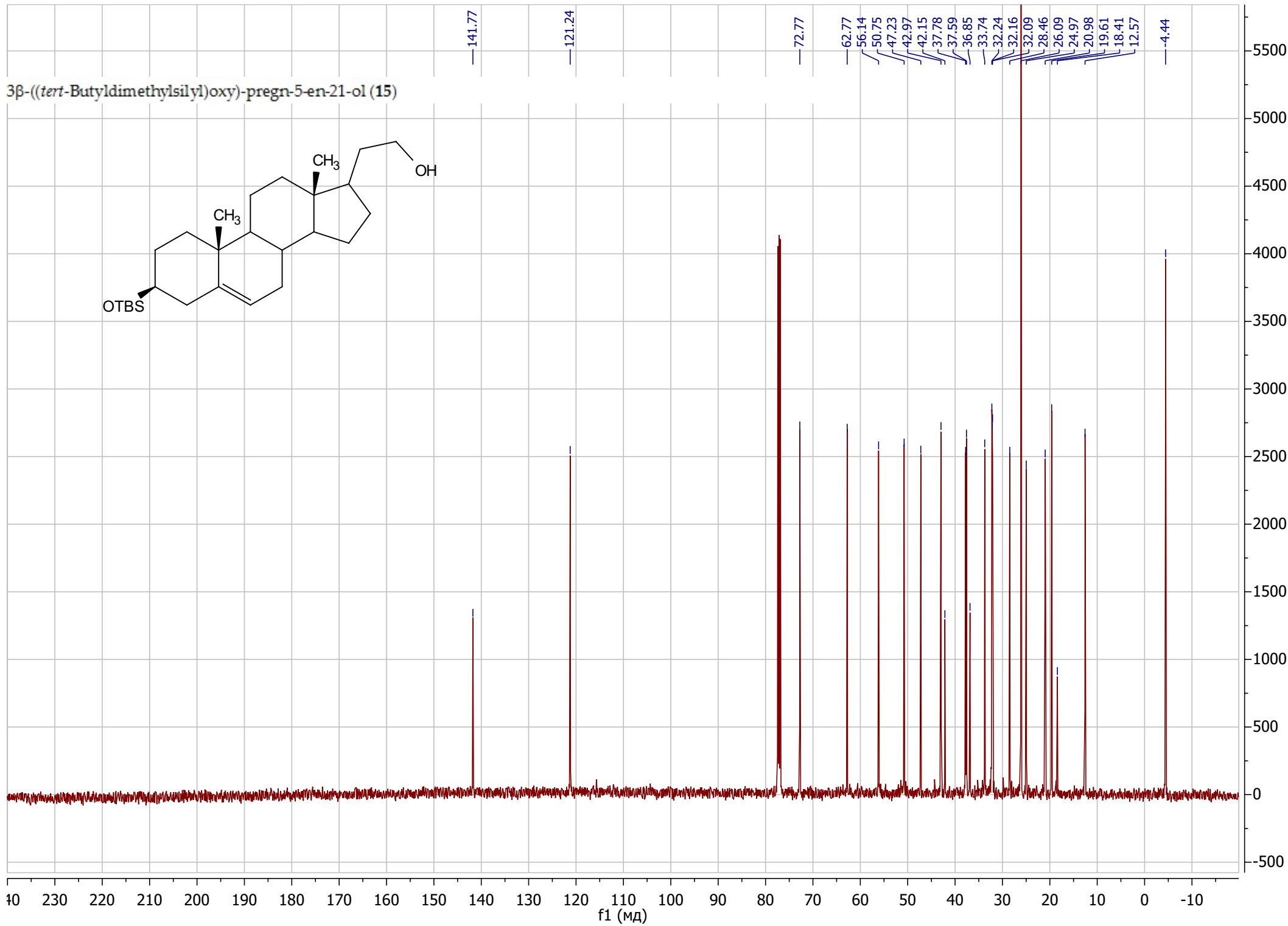
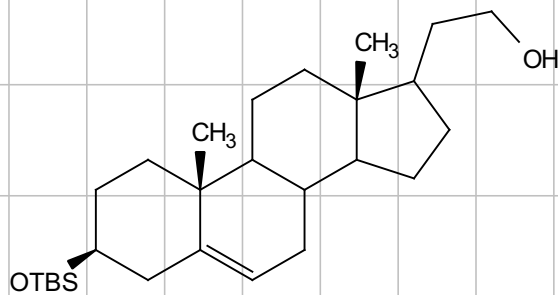
2-(3 β -((*tert*-Butyldimethylsilyl)oxy)-androst-5-en-17-yl)-*N*-methoxy-*N*-methylacetamide (14)



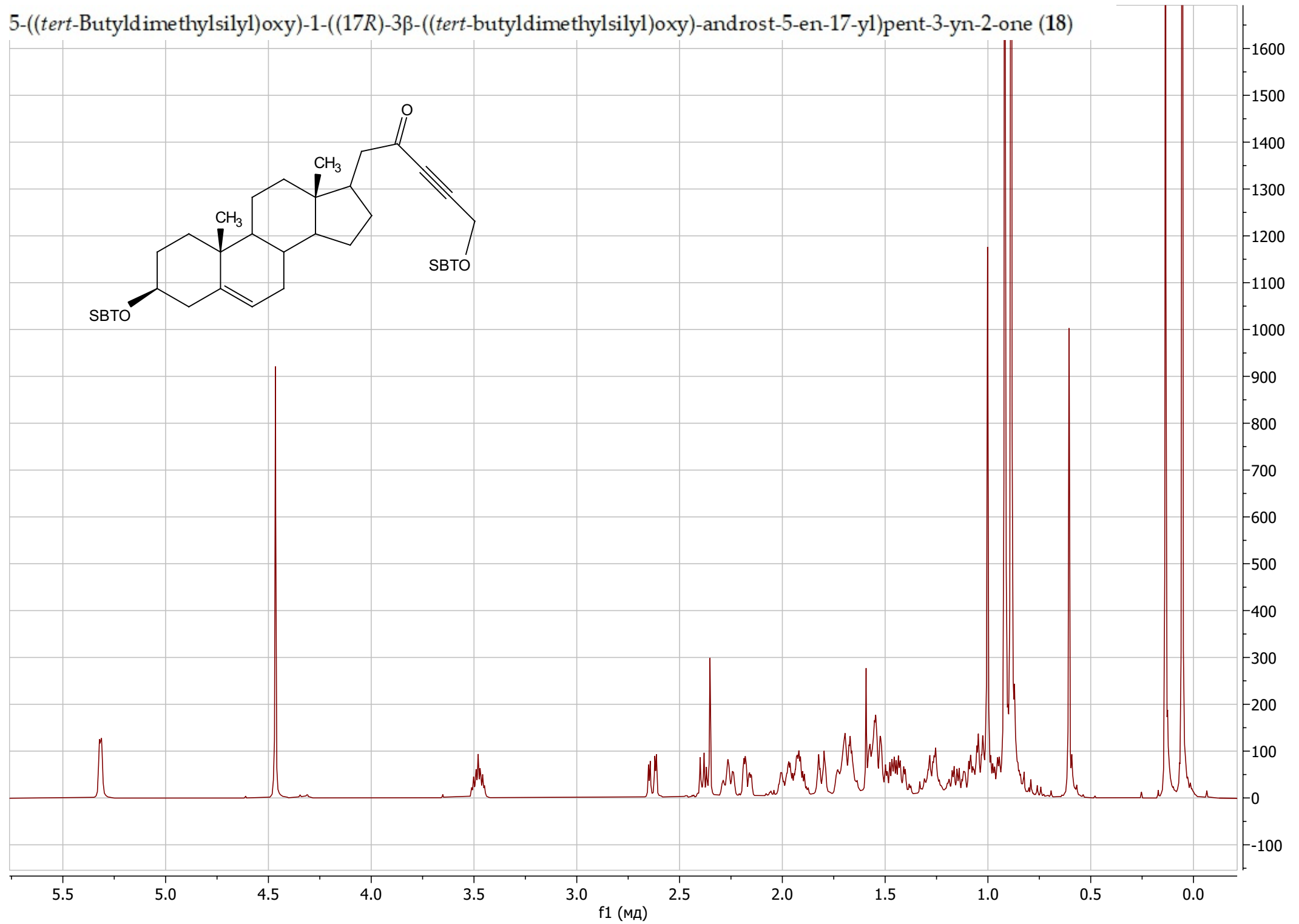
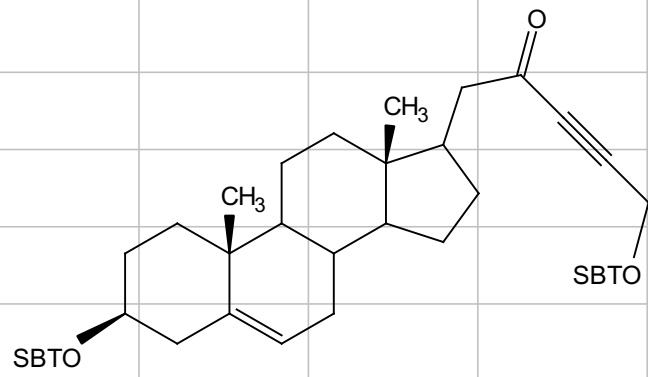
3 β -((*tert*-Butyldimethylsilyl)oxy)-pregn-5-en-21-ol (15)

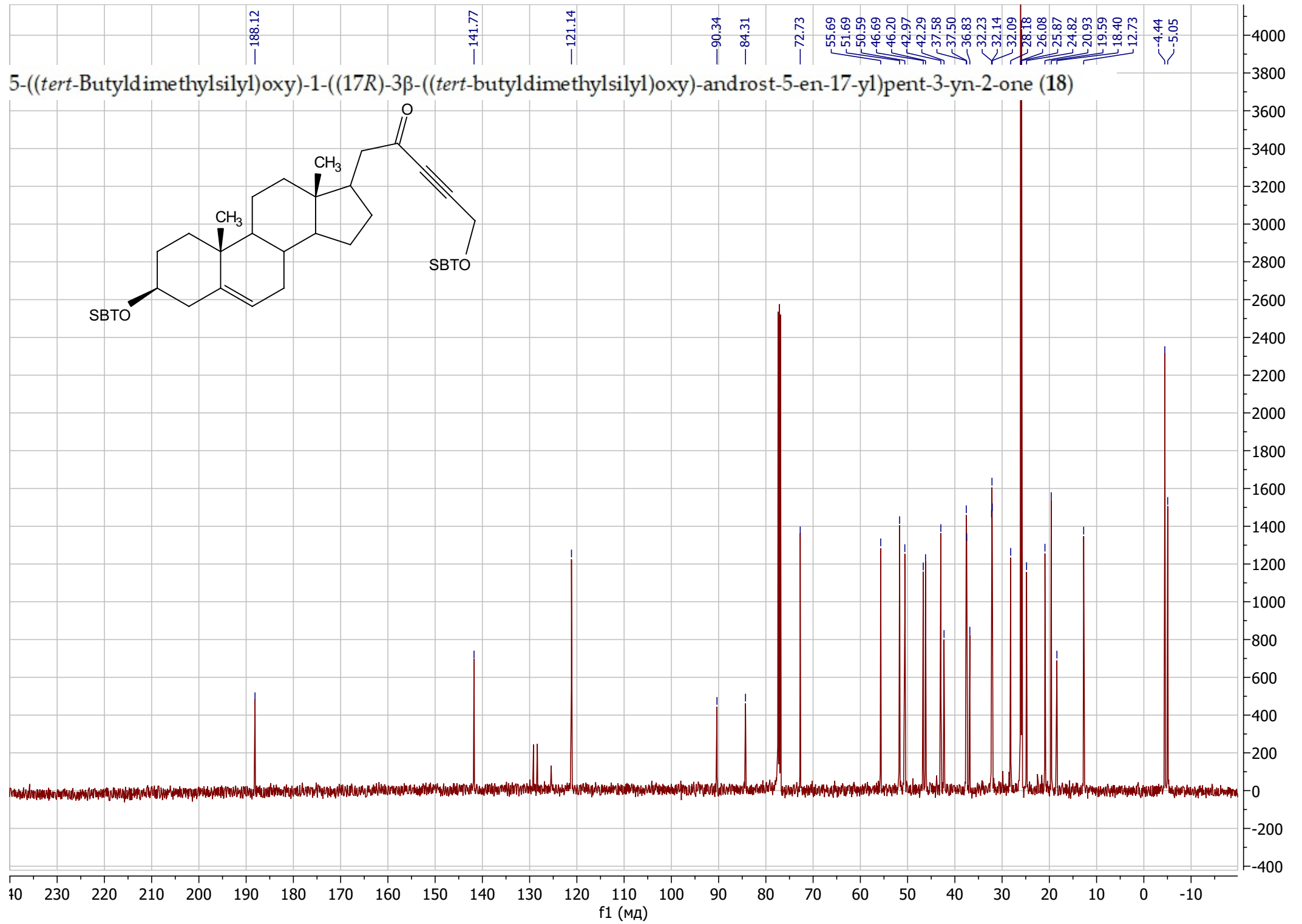


3 β -((*tert*-Butyldimethylsilyl)oxy)-pregn-5-en-21-ol (15)

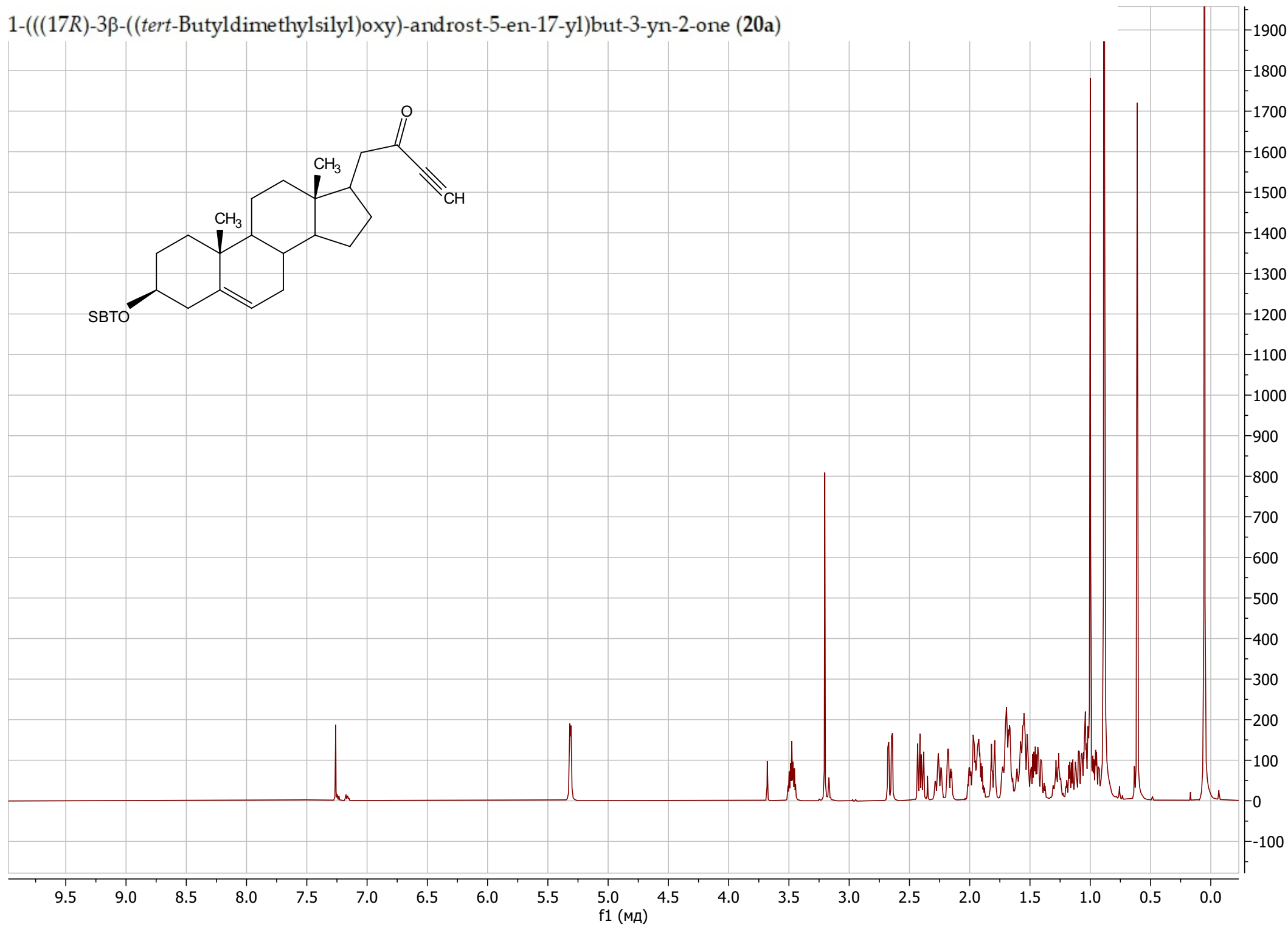
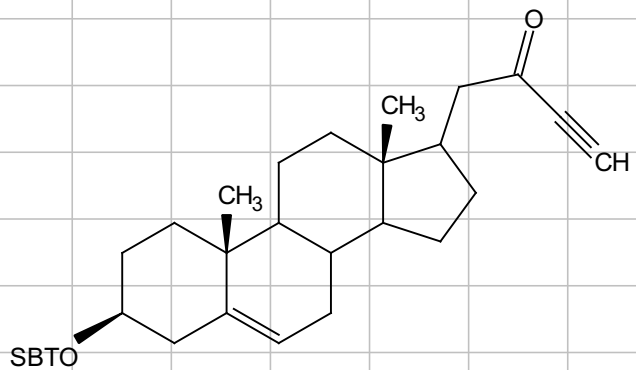


5-((*tert*-Butyldimethylsilyl)oxy)-1-((17*R*)-3β-((*tert*-butyldimethylsilyl)oxy)-androst-5-en-17-yl)pent-3-yn-2-one (18)

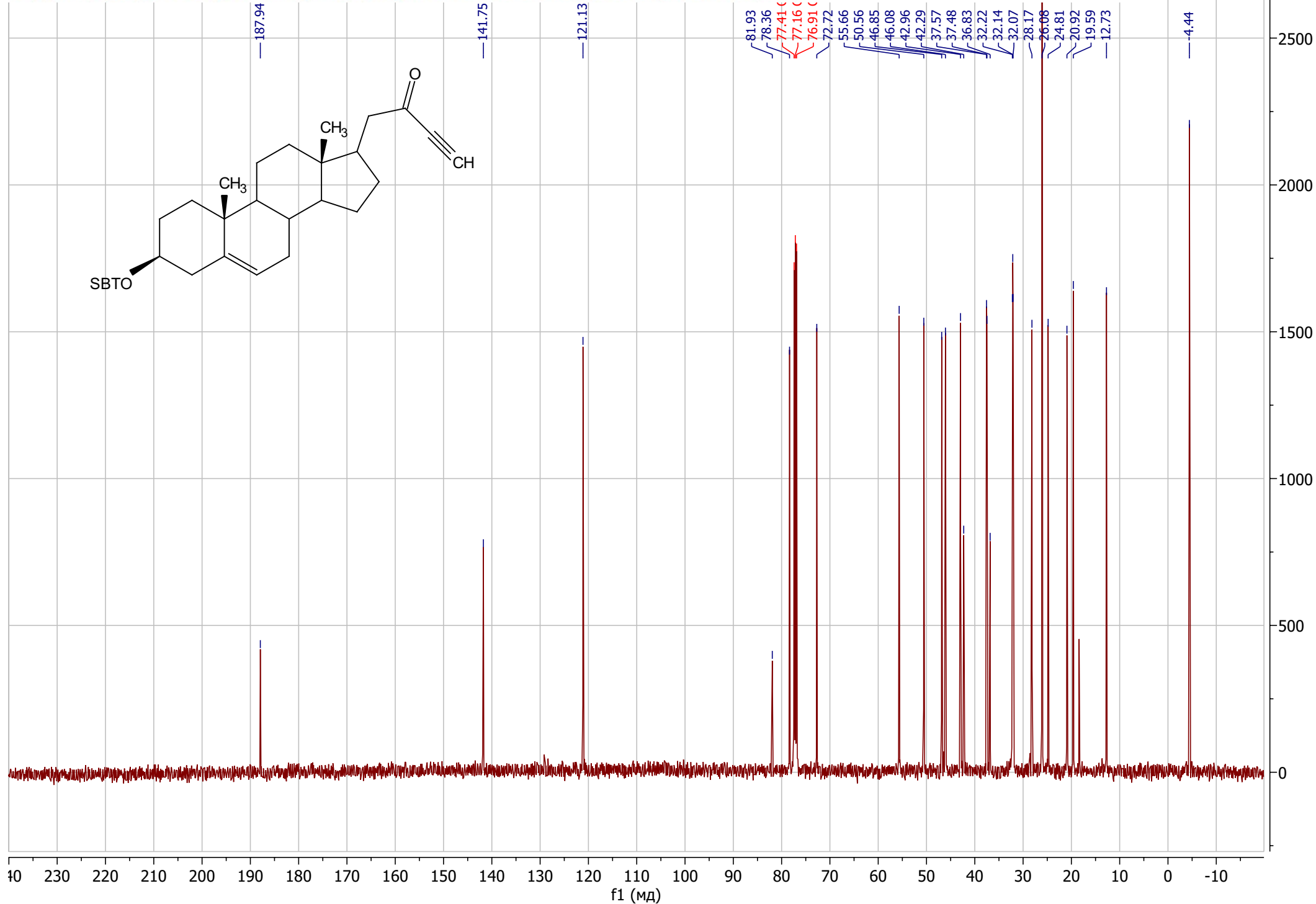




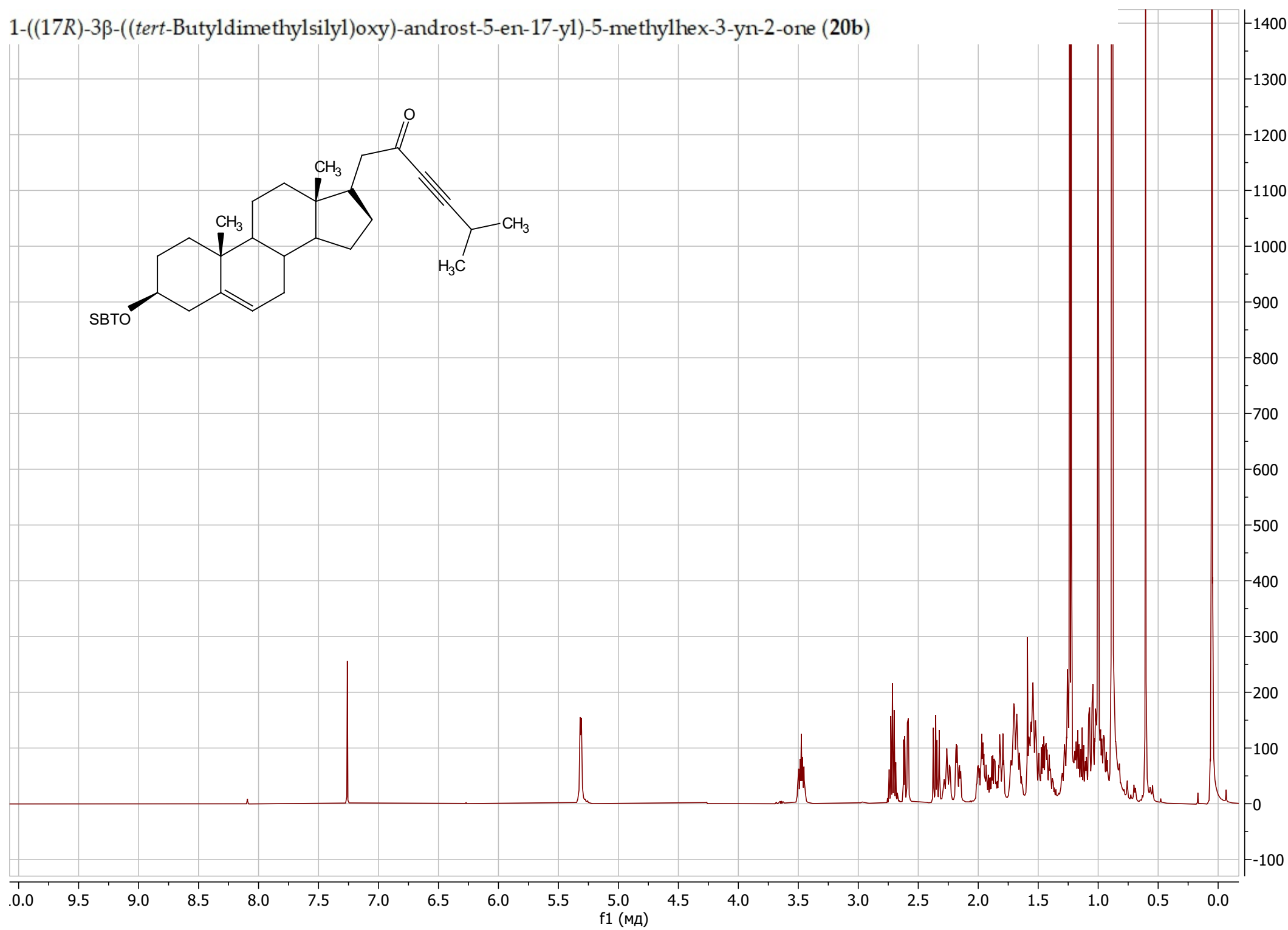
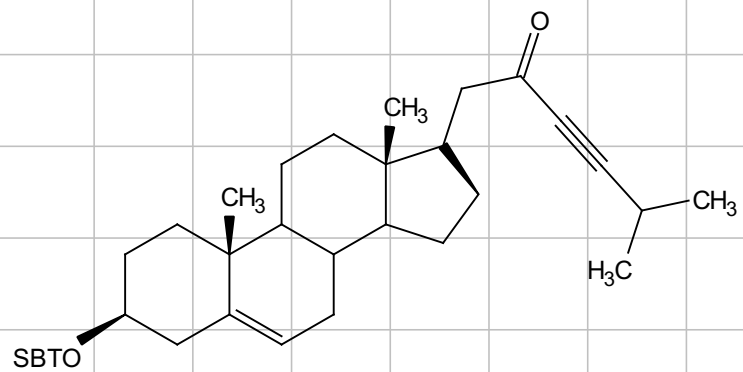
1-(((17R)-3 β -((*tert*-Butyldimethylsilyl)oxy)-androst-5-en-17-yl)but-3-yn-2-one (20a)



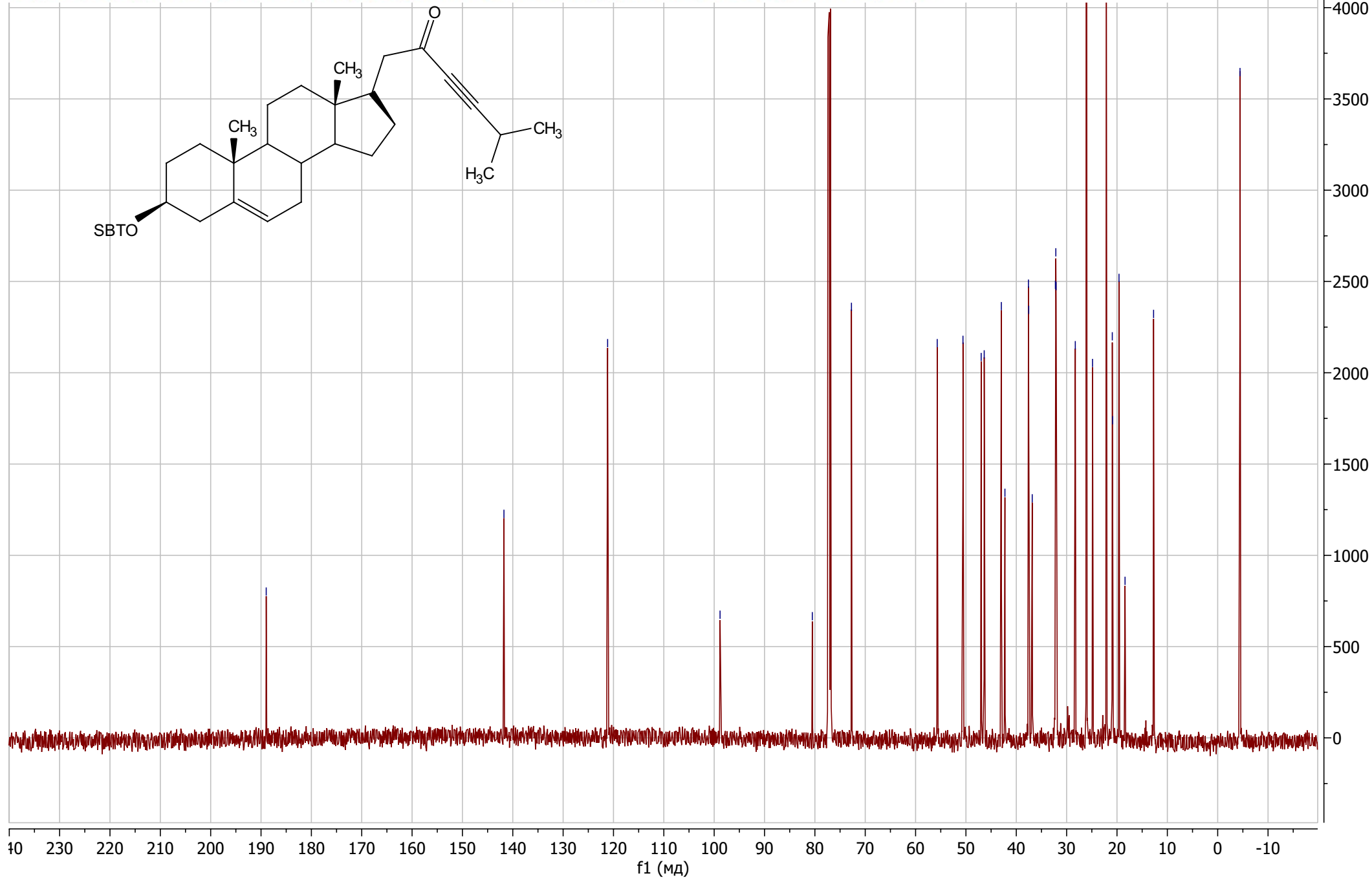
1-(((17R)-3 β -((*tert*-Butyldimethylsilyl)oxy)-androst-5-en-17-yl)but-3-yn-2-one (20a)



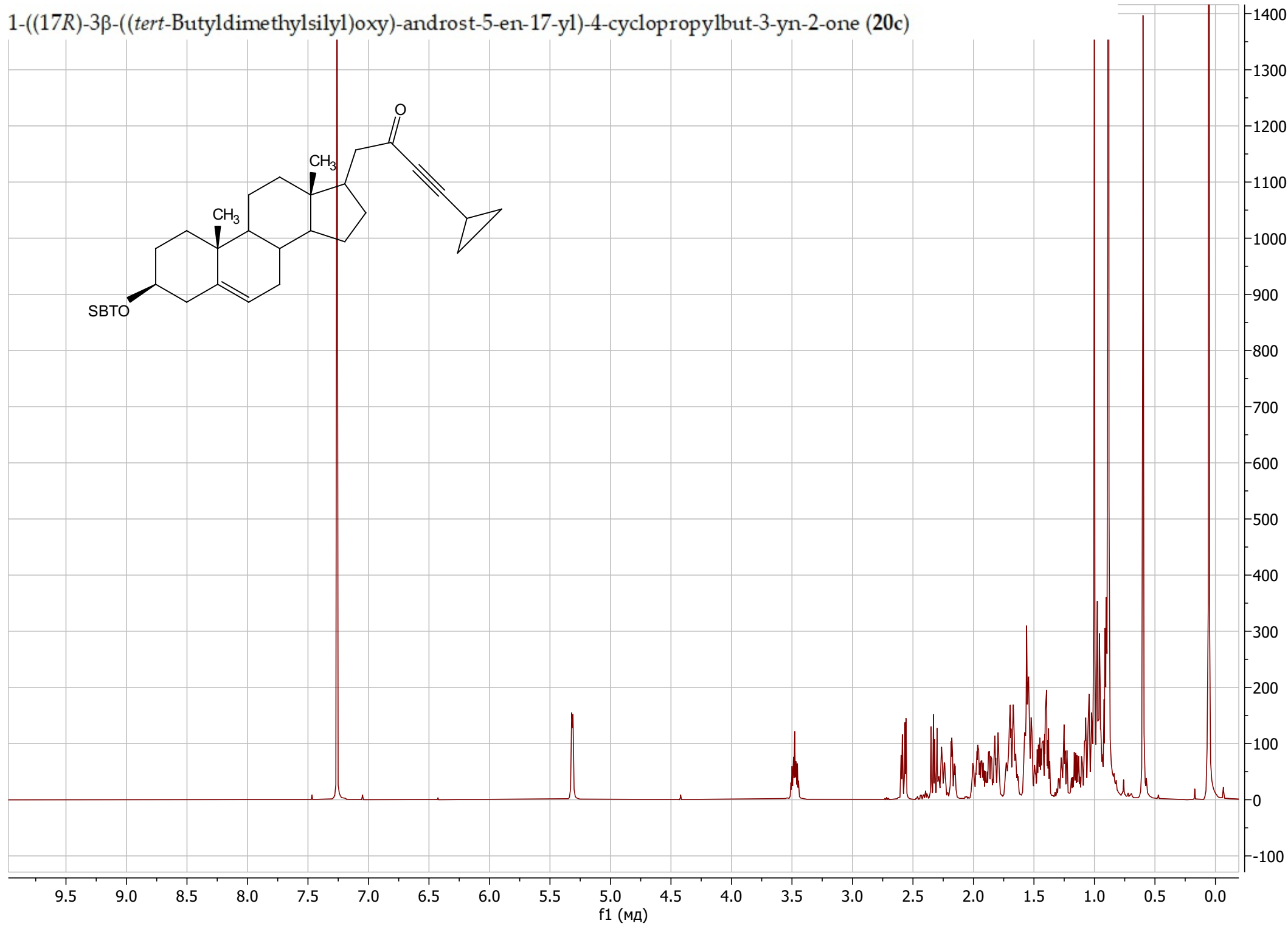
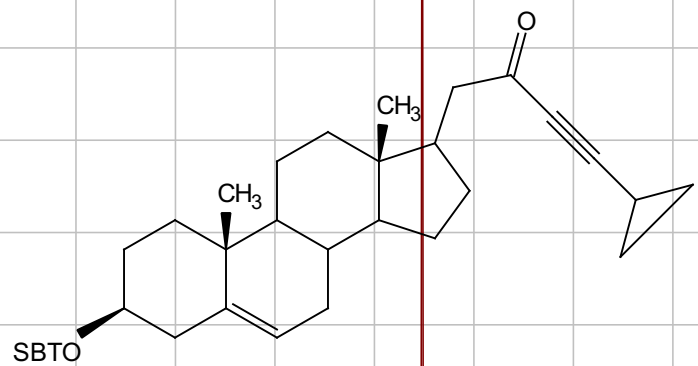
1-((17R)-3β-((*tert*-Butyldimethylsilyl)oxy)-androst-5-en-17-yl)-5-methylhex-3-yn-2-one (20b)

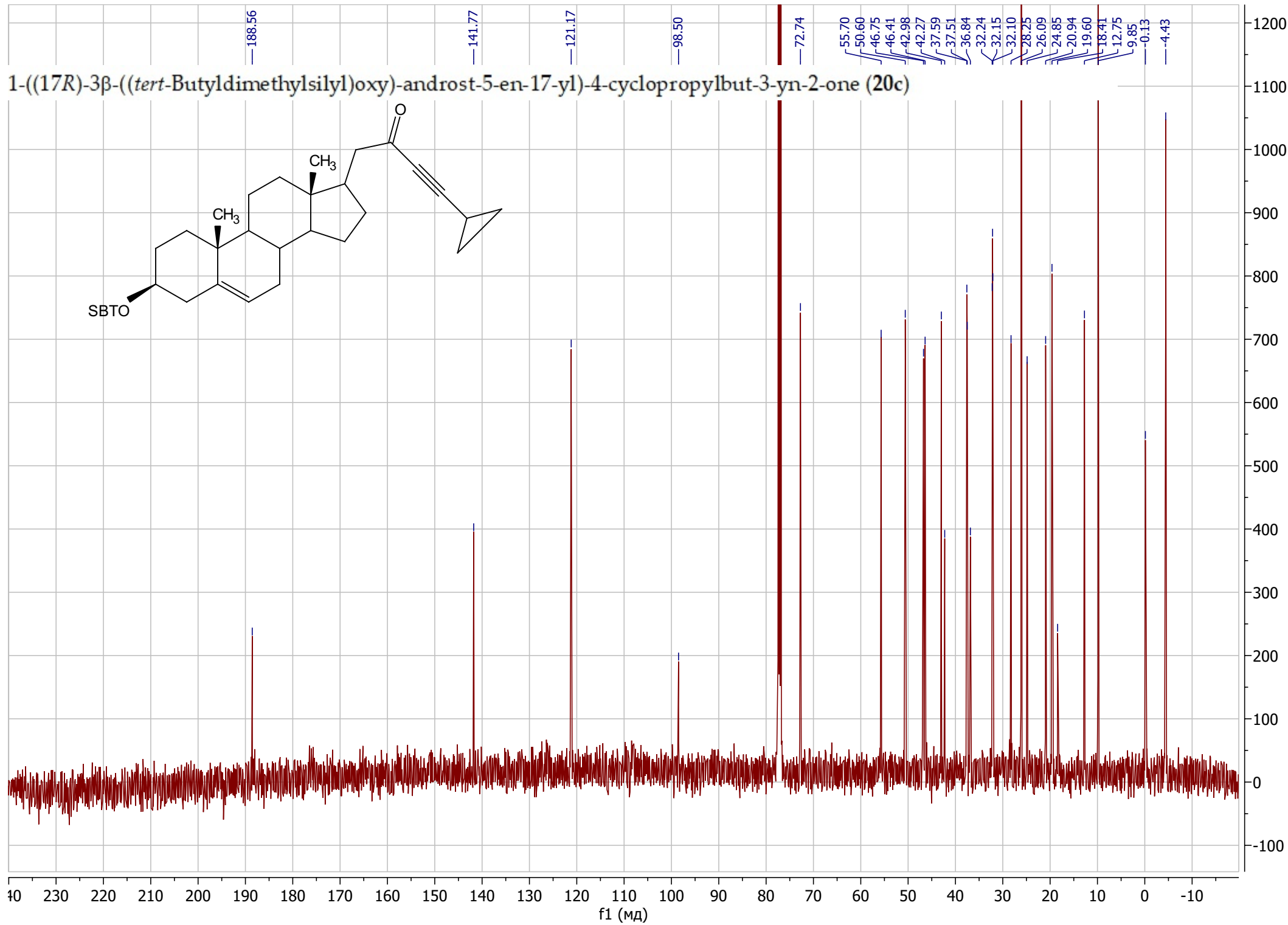


1-((17R)-3 β -((*tert*-Butyldimethylsilyl)oxy)-androst-5-en-17-yl)-5-methylhex-3-yn-2-one (20b)

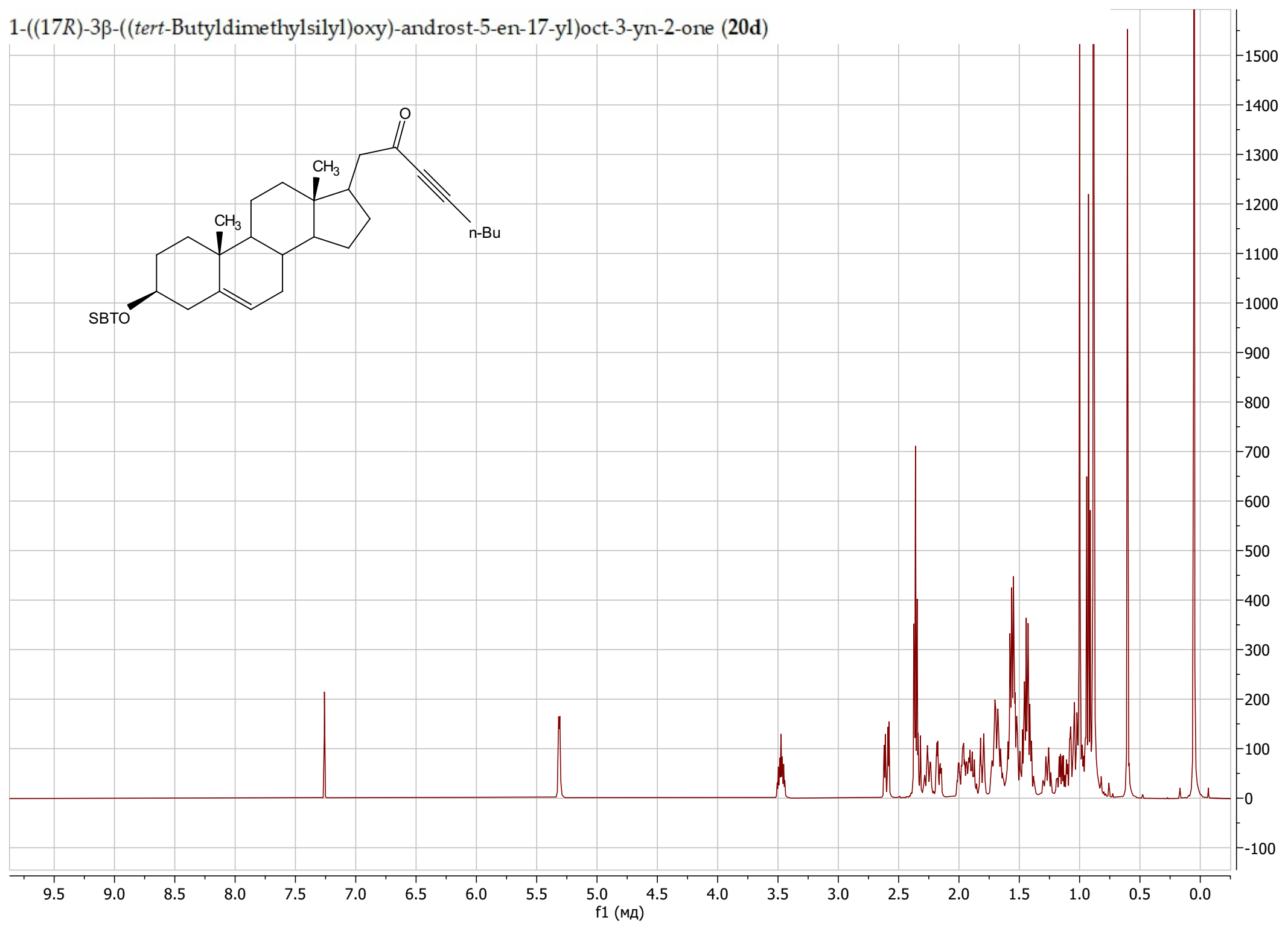
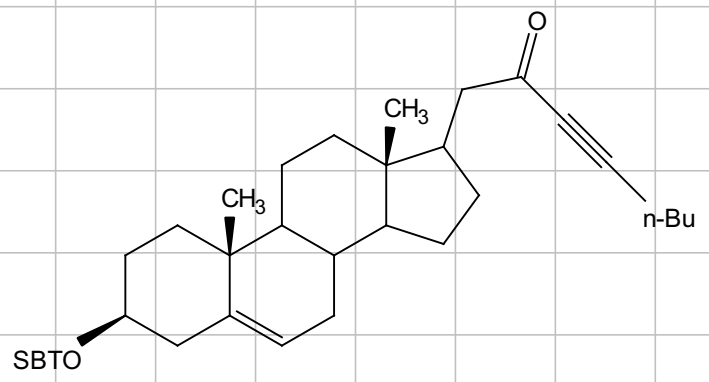


1-((17R)-3β-((*tert*-Butyldimethylsilyloxy)-androst-5-en-17-yl)-4-cyclopropylbut-3-yn-2-one (20c)

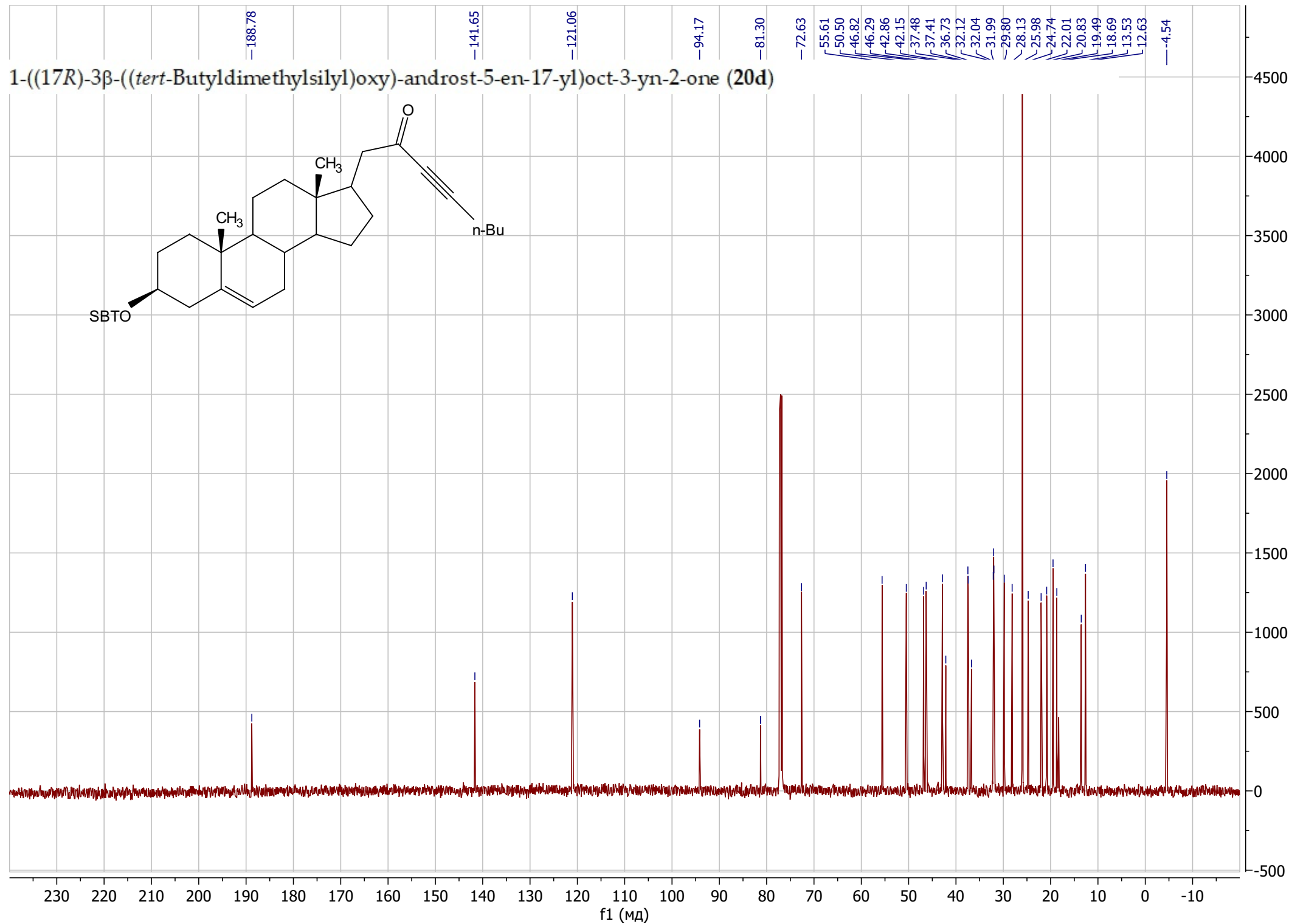
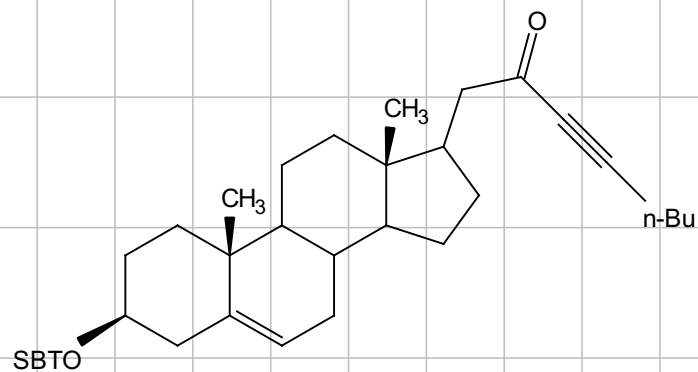




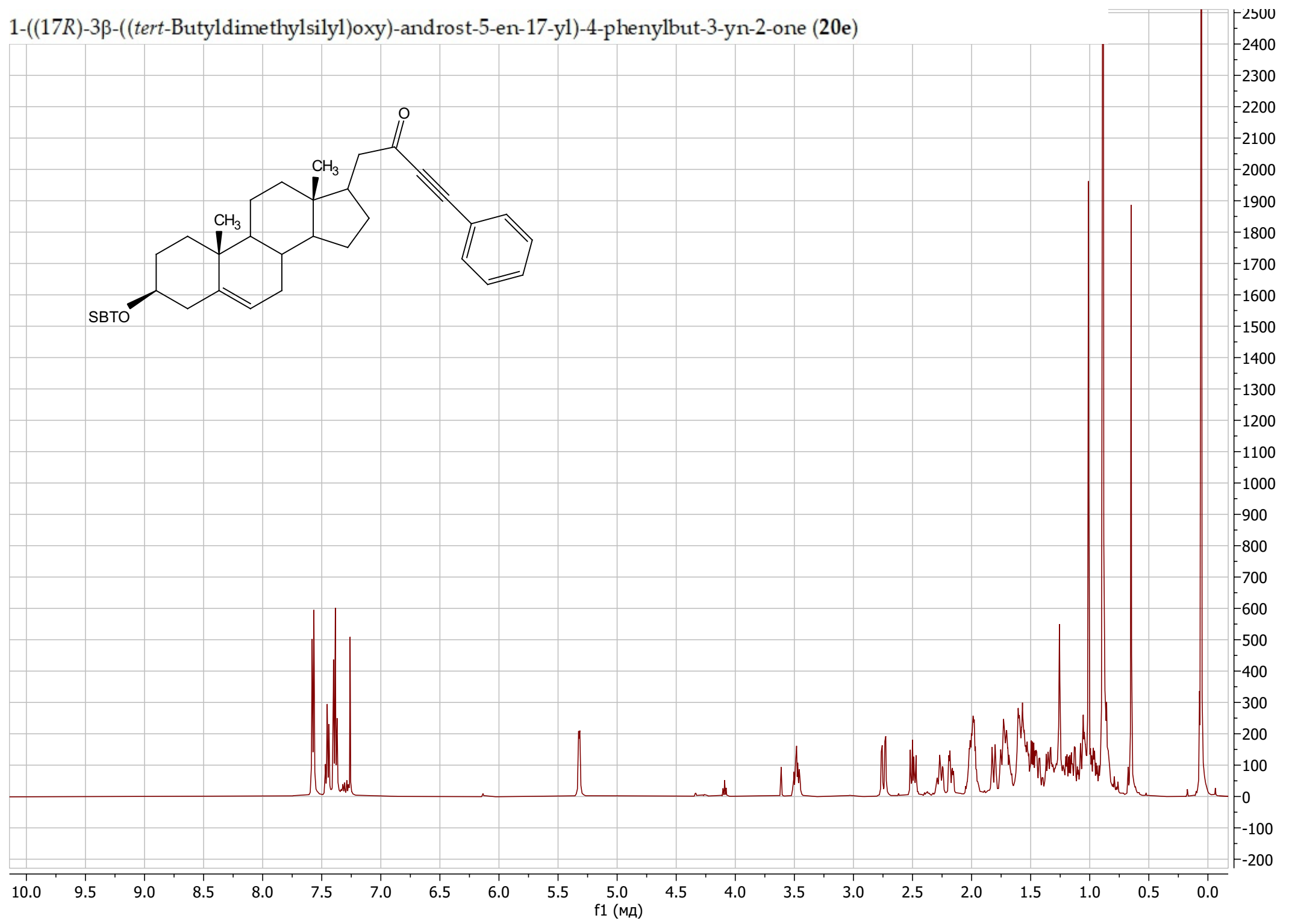
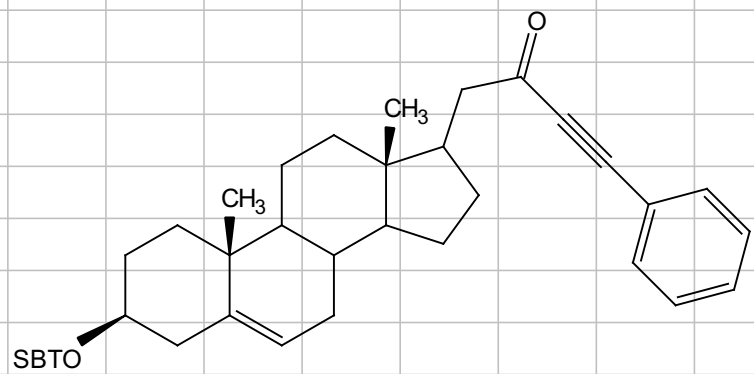
1-((17R)-3 β -((*tert*-Butyldimethylsilyl)oxy)-androst-5-en-17-yl)oct-3-yn-2-one (20d)



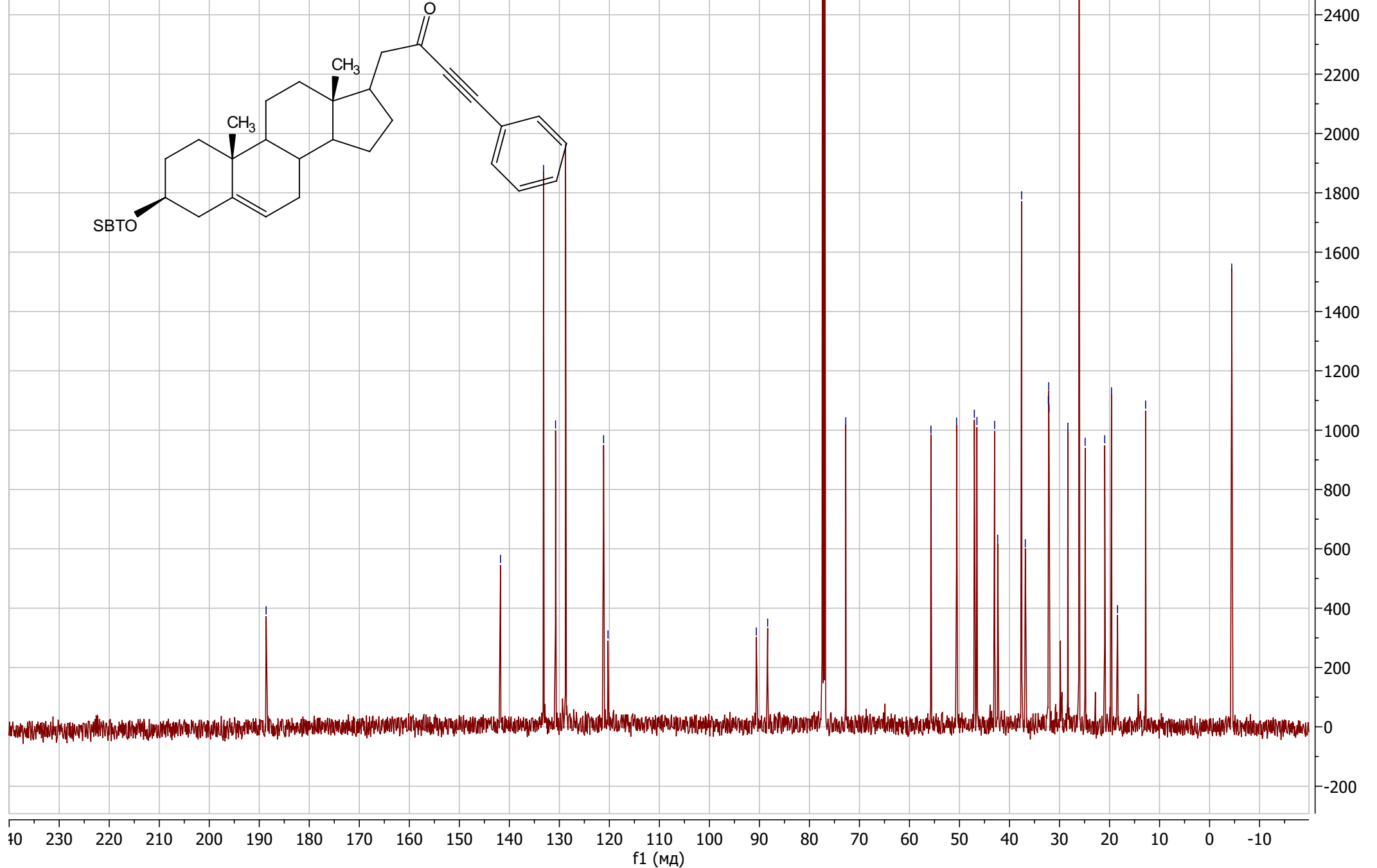
1-((17R)-3 β -((*tert*-Butyldimethylsilyl)oxy)-androst-5-en-17-yl)oct-3-yn-2-one (20d)



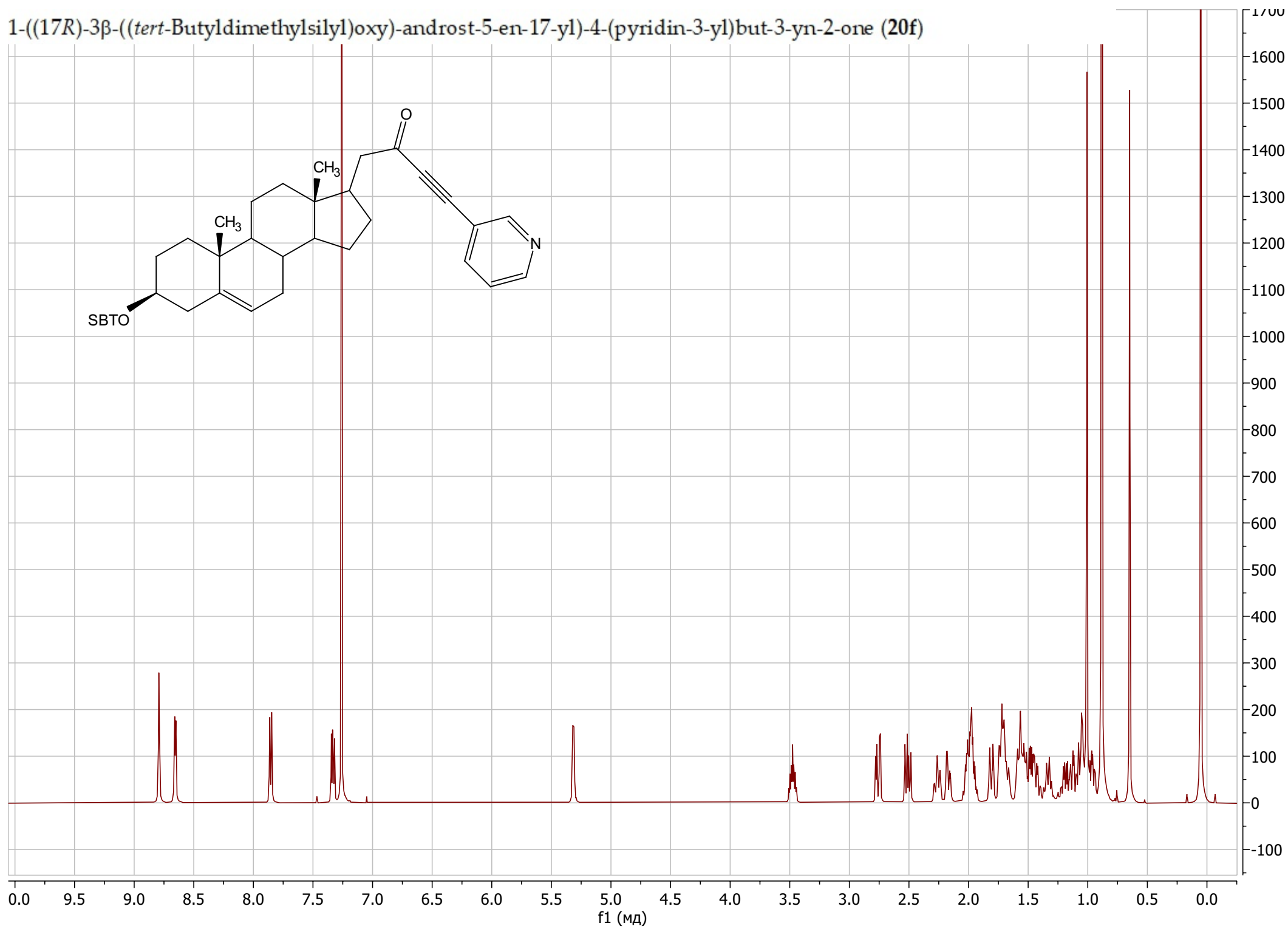
1-((17R)-3β-((*tert*-Butyldimethylsilyloxy)-androst-5-en-17-yl)-4-phenylbut-3-yn-2-one (20e)



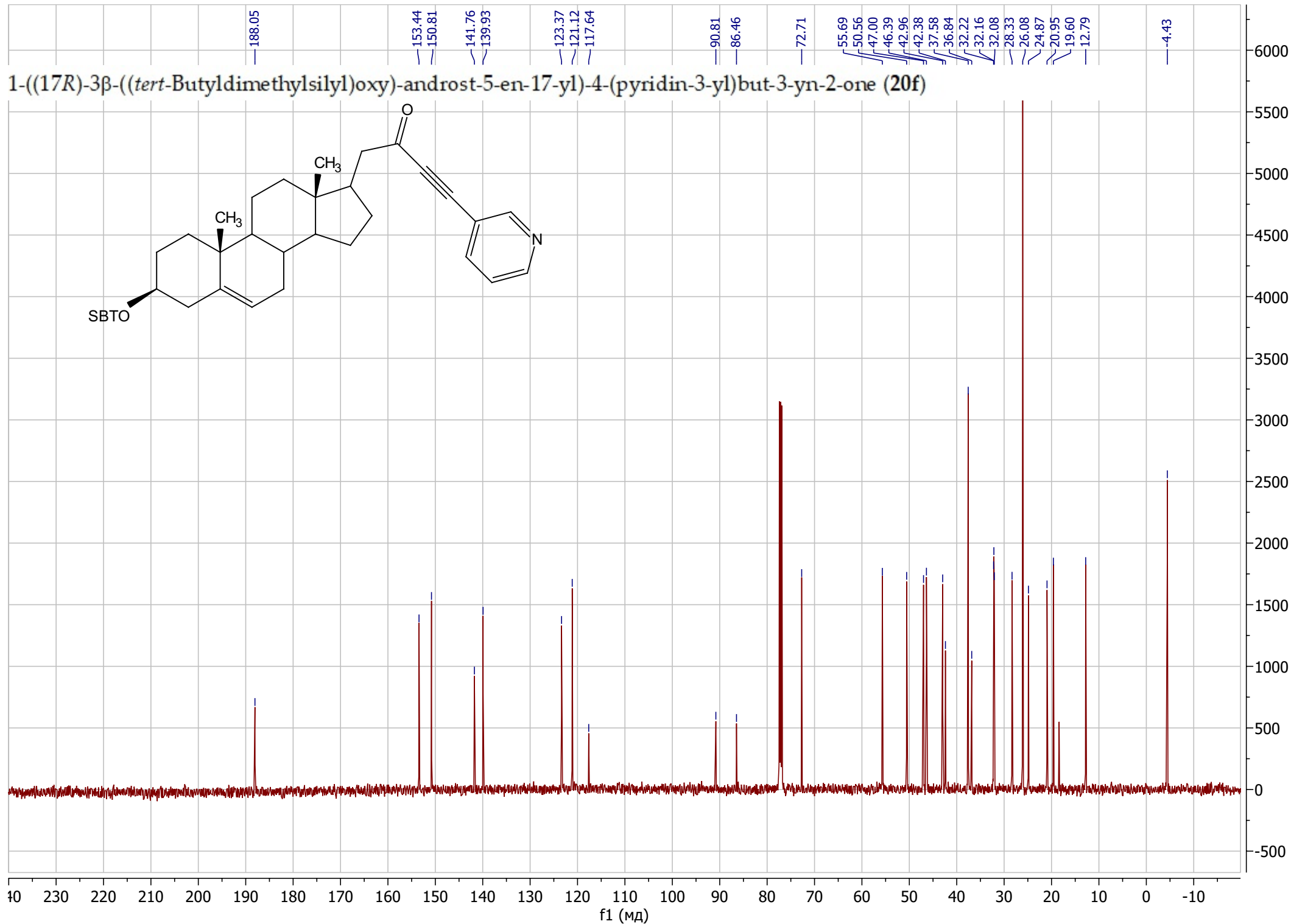
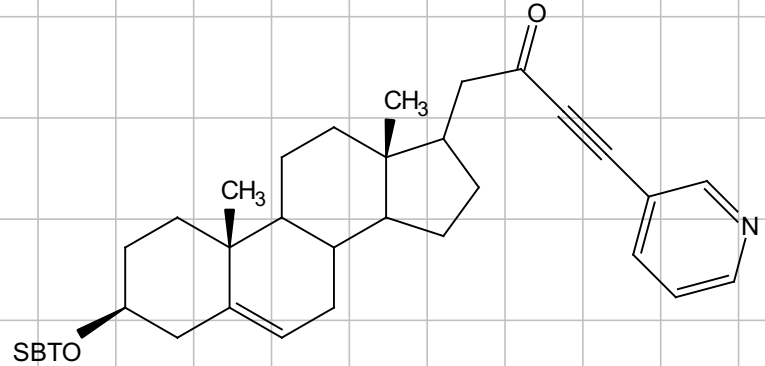
1-((17R)-3β-((*tert*-Butyldimethylsilyl)oxy)-androst-5-en-17-yl)-4-phenylbut-3-yn-2-one (20e)



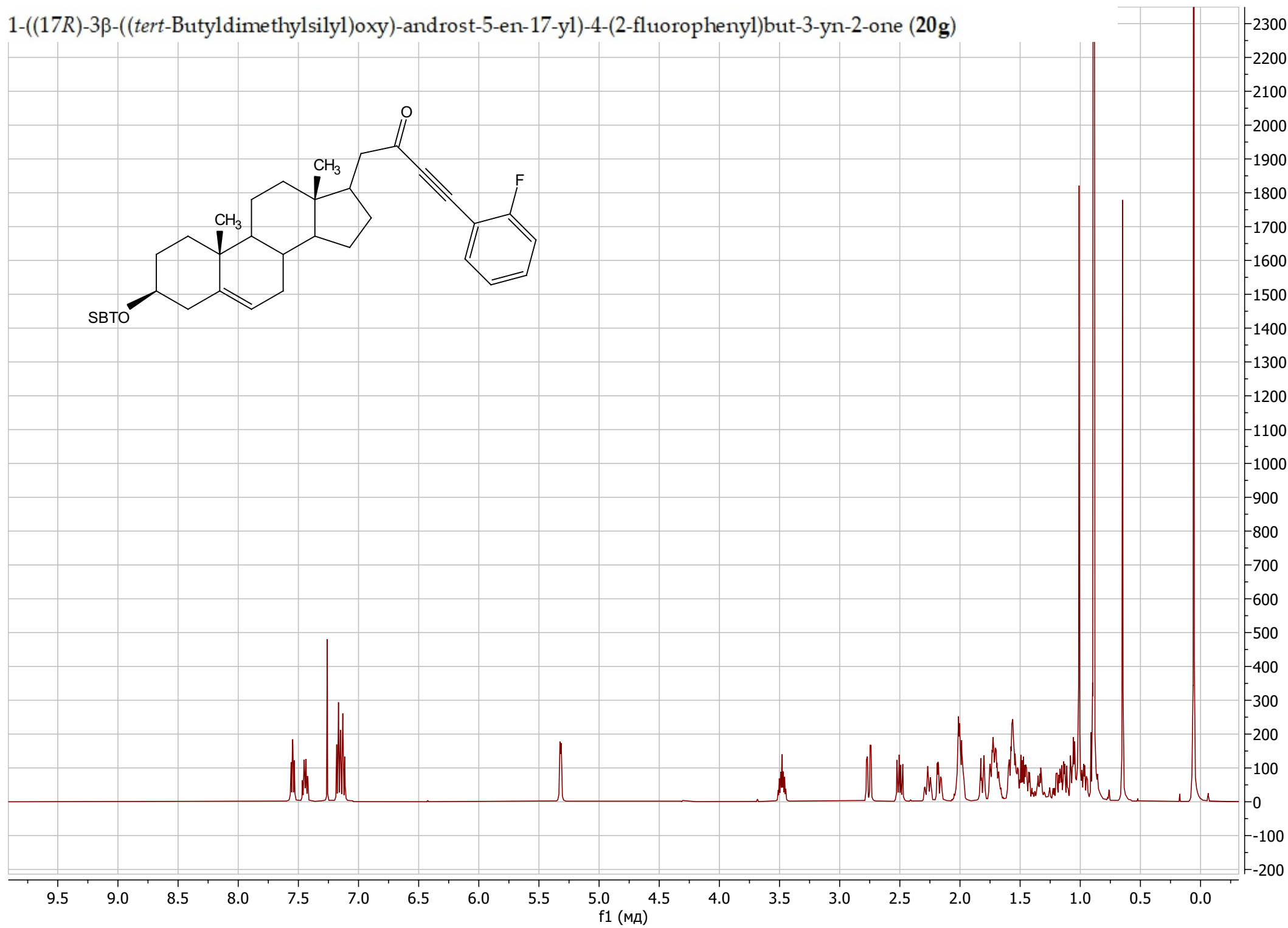
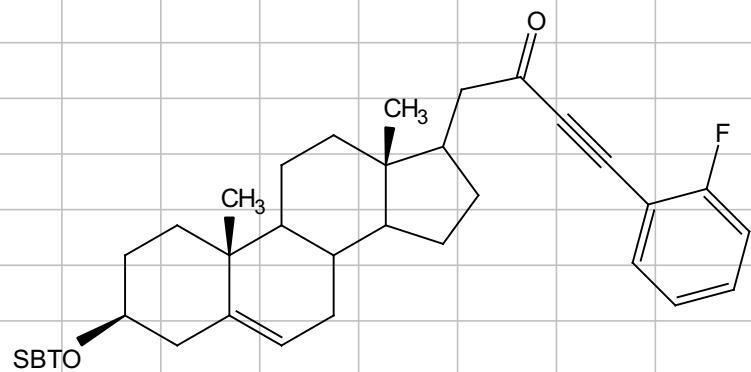
1-((17R)-3β-((tert-Butyldimethylsilyloxy)-androst-5-en-17-yl)-4-(pyridin-3-yl)but-3-yn-2-one (20f)

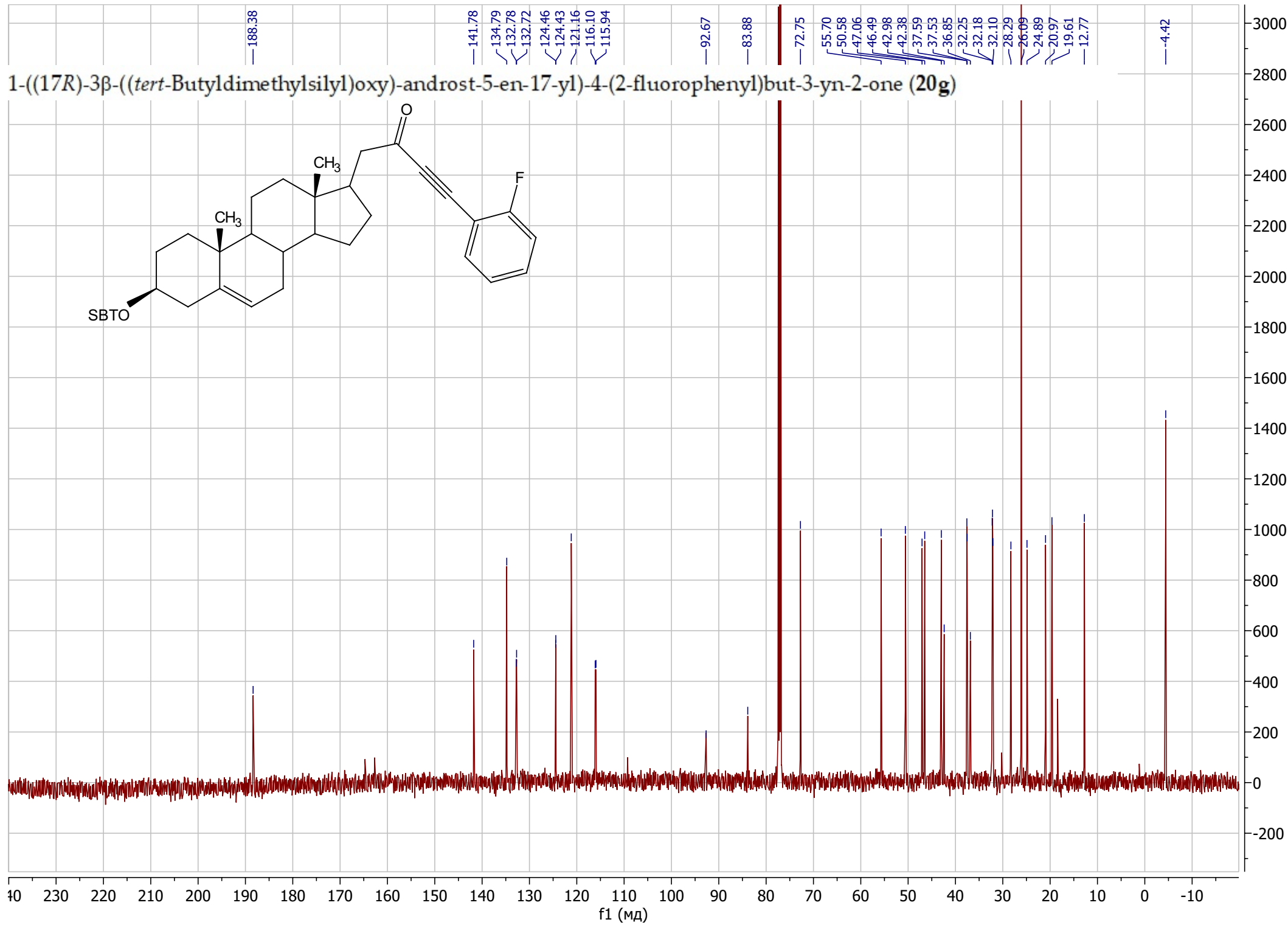


1-((17R)-3β-((*tert*-Butyldimethylsilyl)oxy)-androst-5-en-17-yl)-4-(pyridin-3-yl)but-3-yn-2-one (20f)

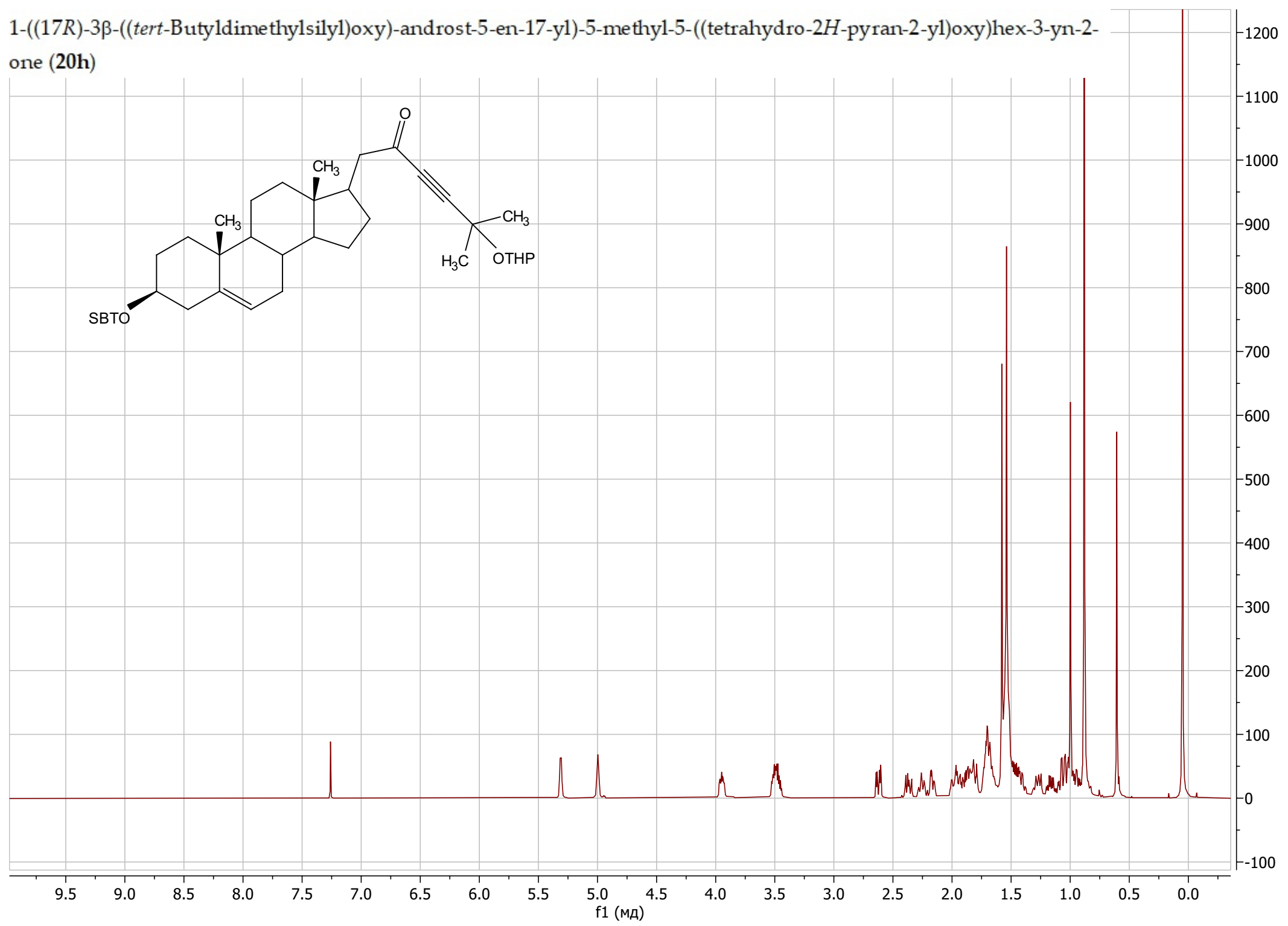
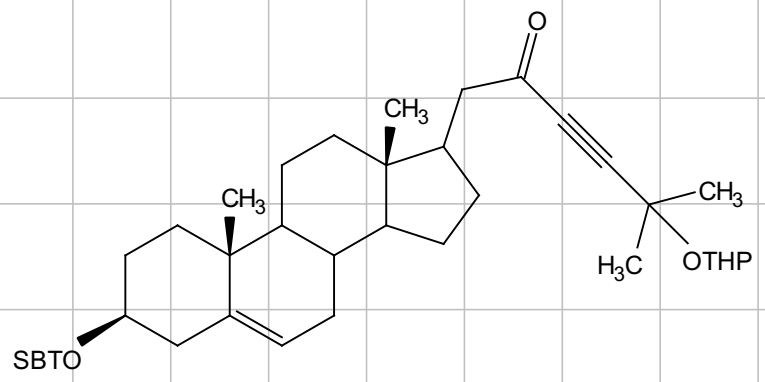


1-((17R)-3β-((*tert*-Butyldimethylsilyloxy)-androst-5-en-17-yl)-4-(2-fluorophenyl)but-3-yn-2-one (20g)

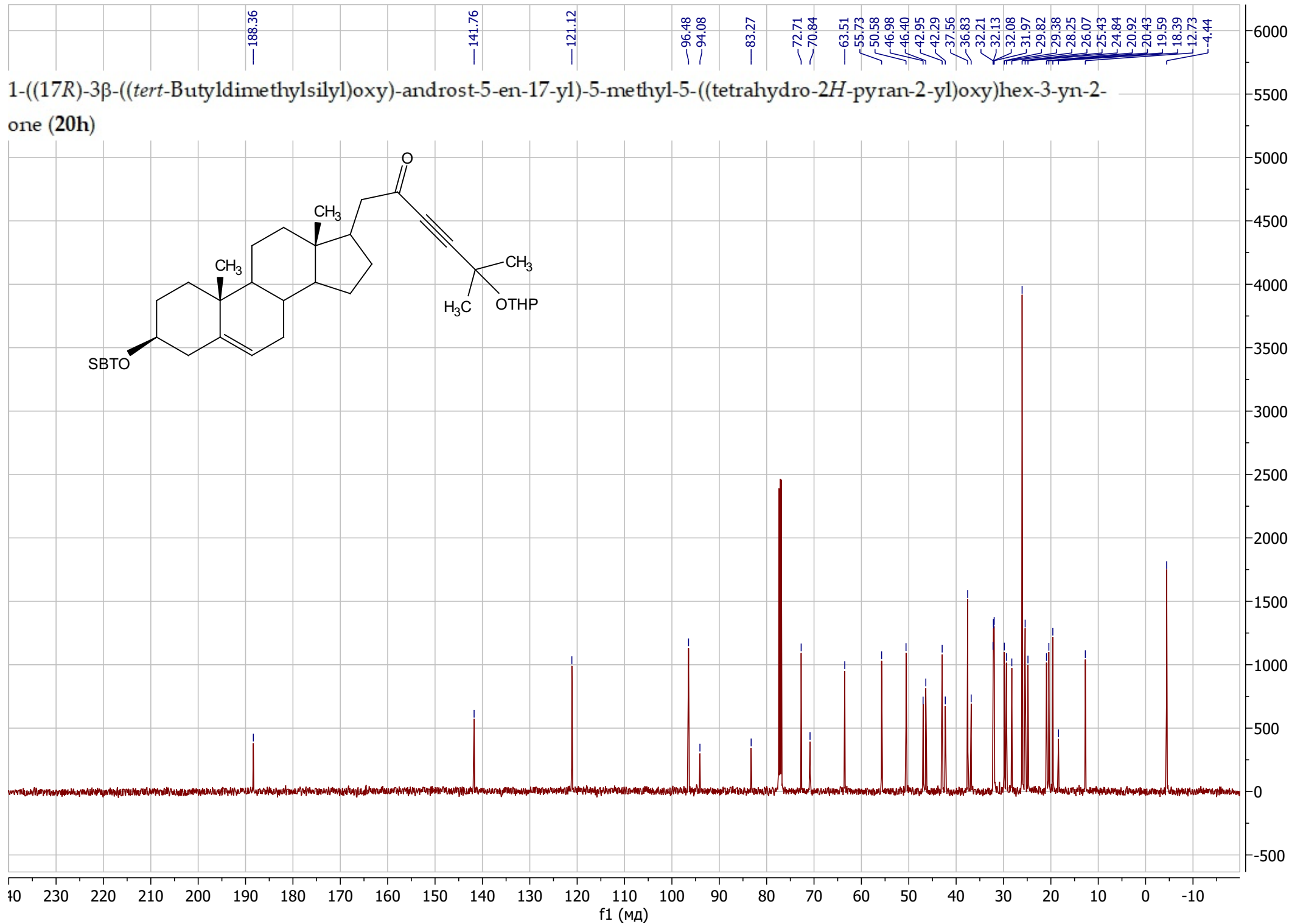
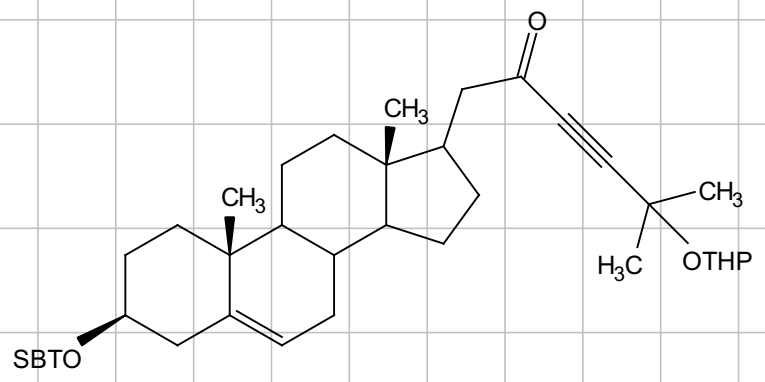




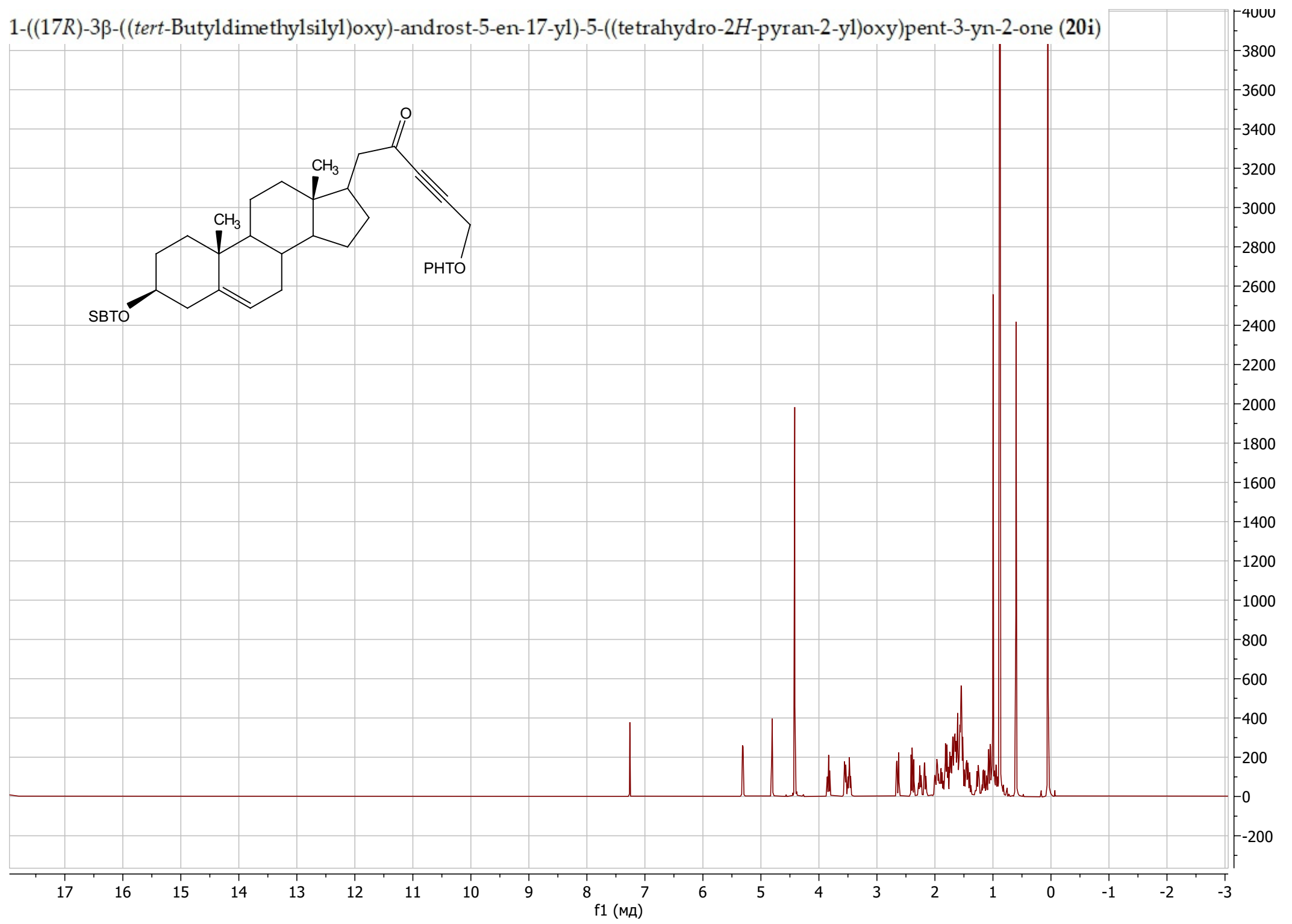
1-((17R)-3β-((*tert*-Butyldimethylsilyl)oxy)-androst-5-en-17-yl)-5-methyl-5-((tetrahydro-2H-pyran-2-yl)oxy)hex-3-yn-2-one (20h)



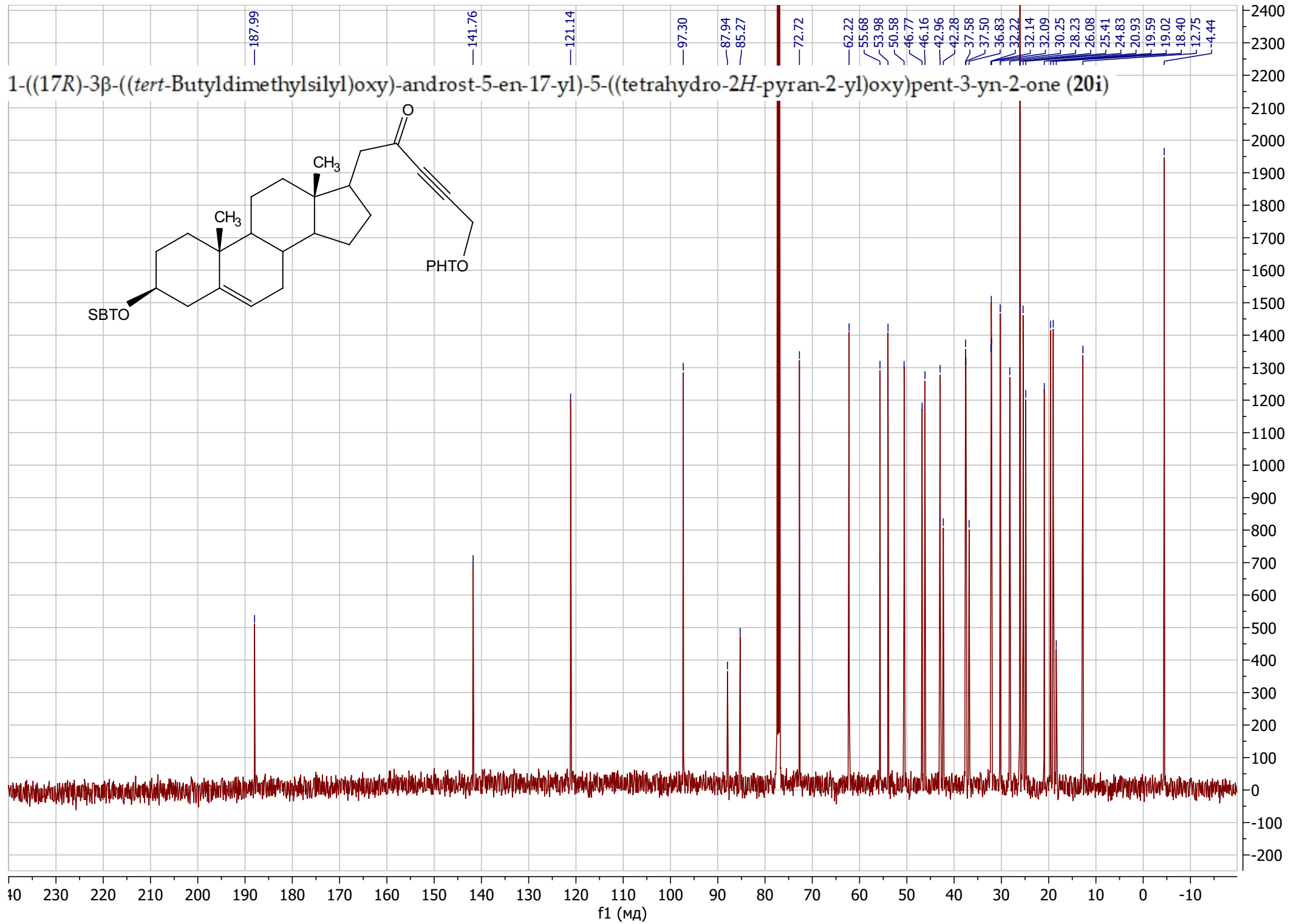
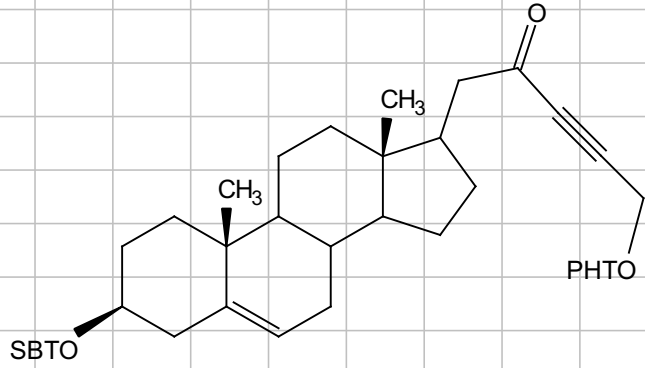
1-((17R)-3β-((*tert*-Butyldimethylsilyl)oxy)-androst-5-en-17-yl)-5-methyl-5-((tetrahydro-2H-pyran-2-yl)oxy)hex-3-yn-2-one (20h)



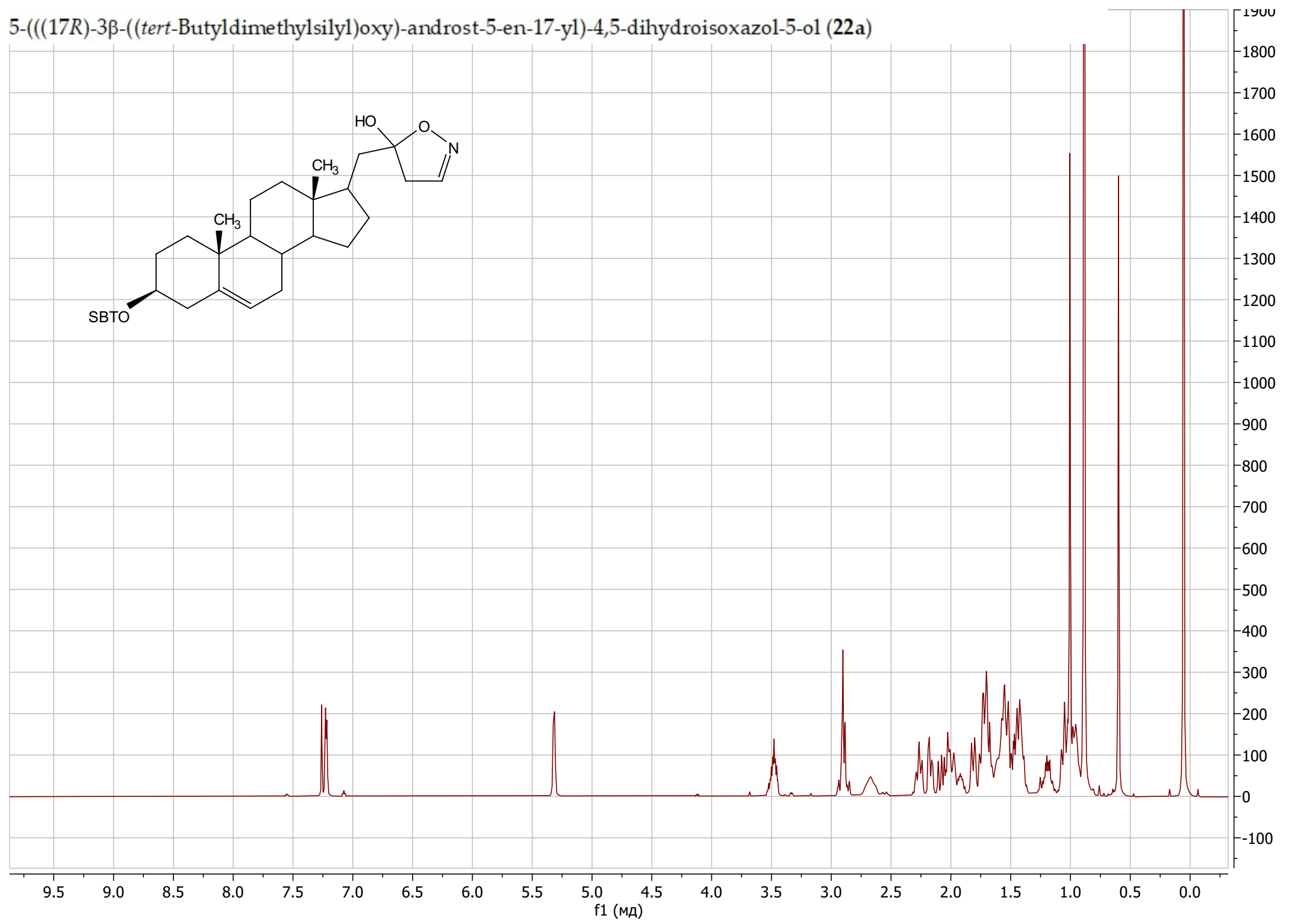
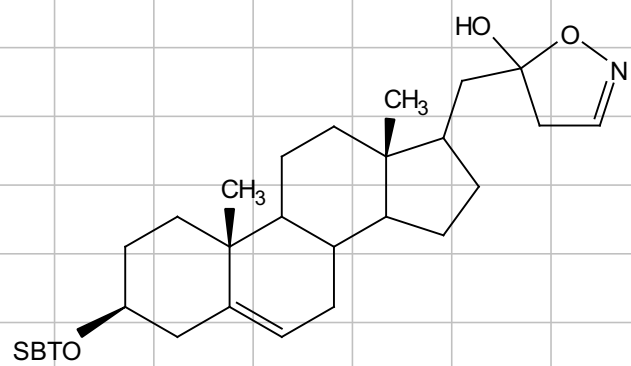
1-((17R)-3 β -((*tert*-Butyldimethylsilyl)oxy)-androst-5-en-17-yl)-5-((tetrahydro-2H-pyran-2-yl)oxy)pent-3-yn-2-one (20i)



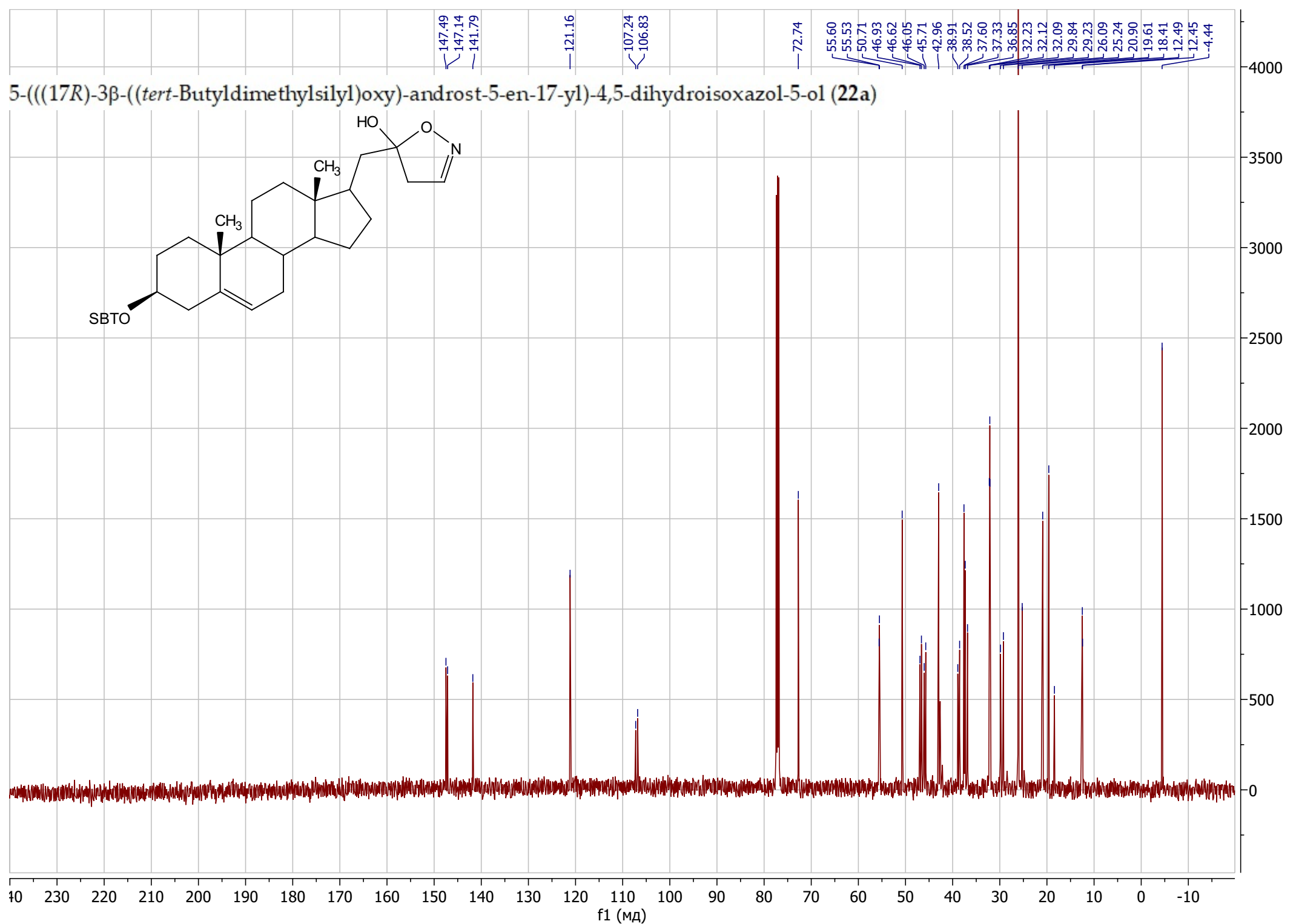
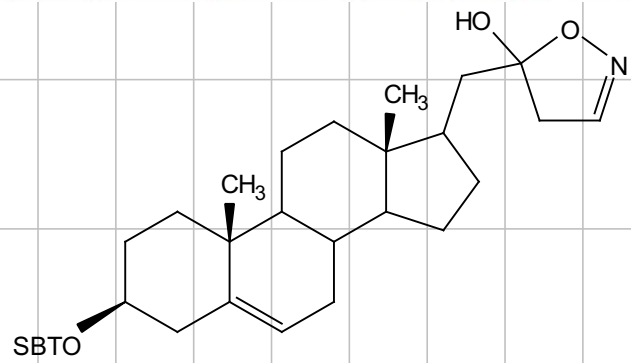
1-((17R)-3 β -((*tert*-Butyldimethylsilyl)oxy)-androst-5-en-17-yl)-5-((tetrahydro-2H-pyran-2-yl)oxy)pent-3-yn-2-one (20i)



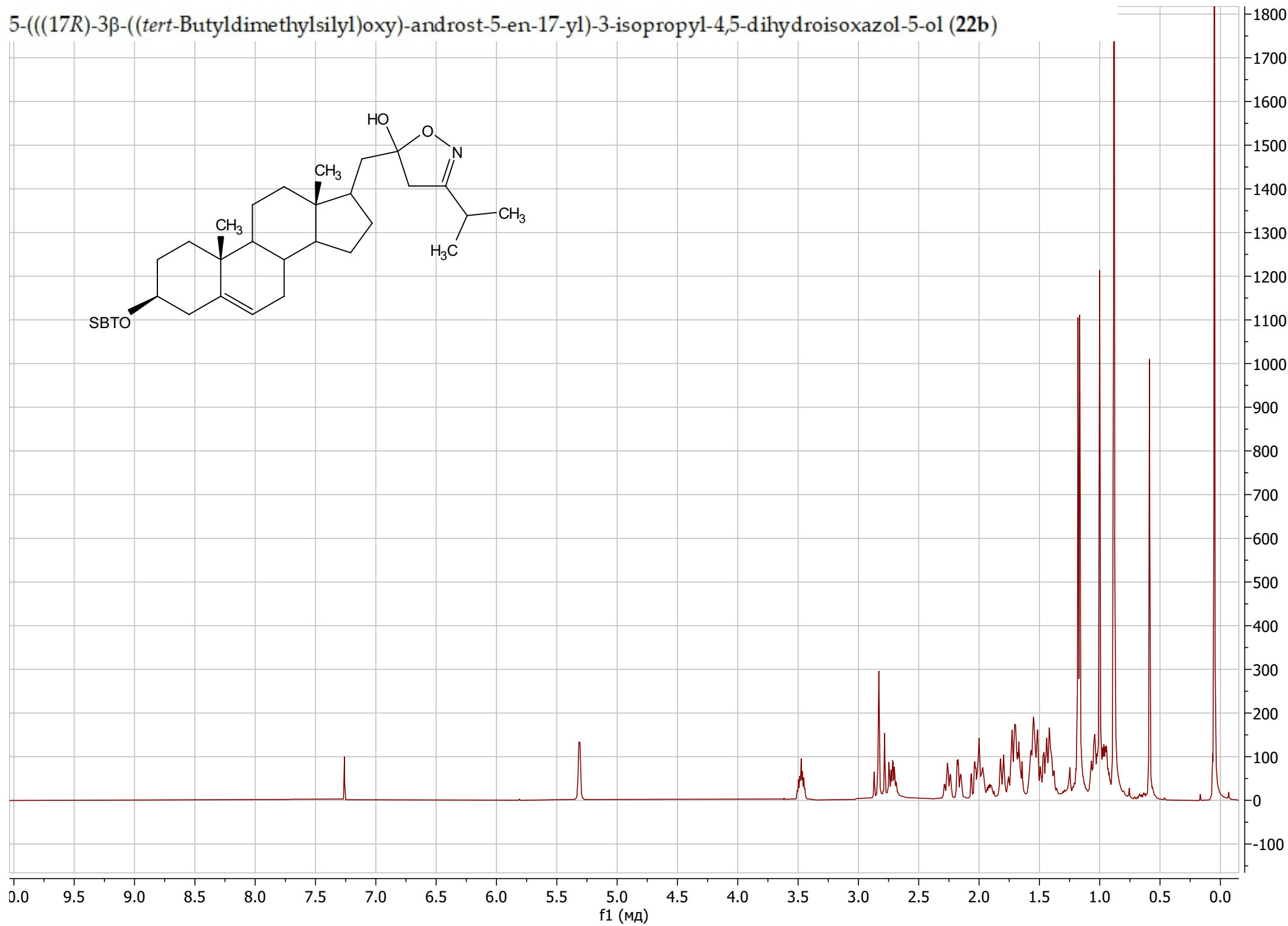
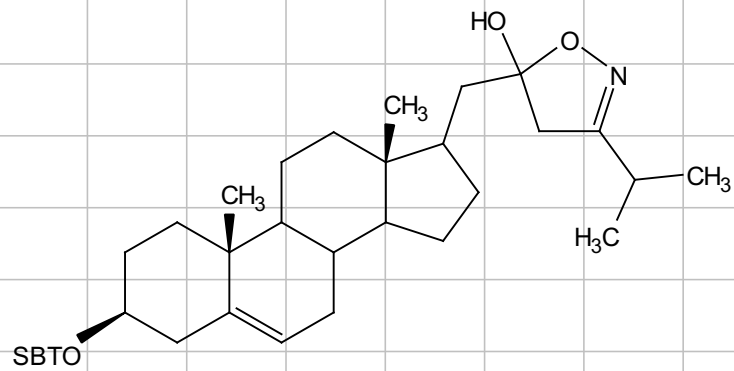
5-(((17R)-3 β -((*tert*-Butyldimethylsilyl)oxy)-androst-5-en-17-yl)-4,5-dihydroisoxazol-5-ol (22a)



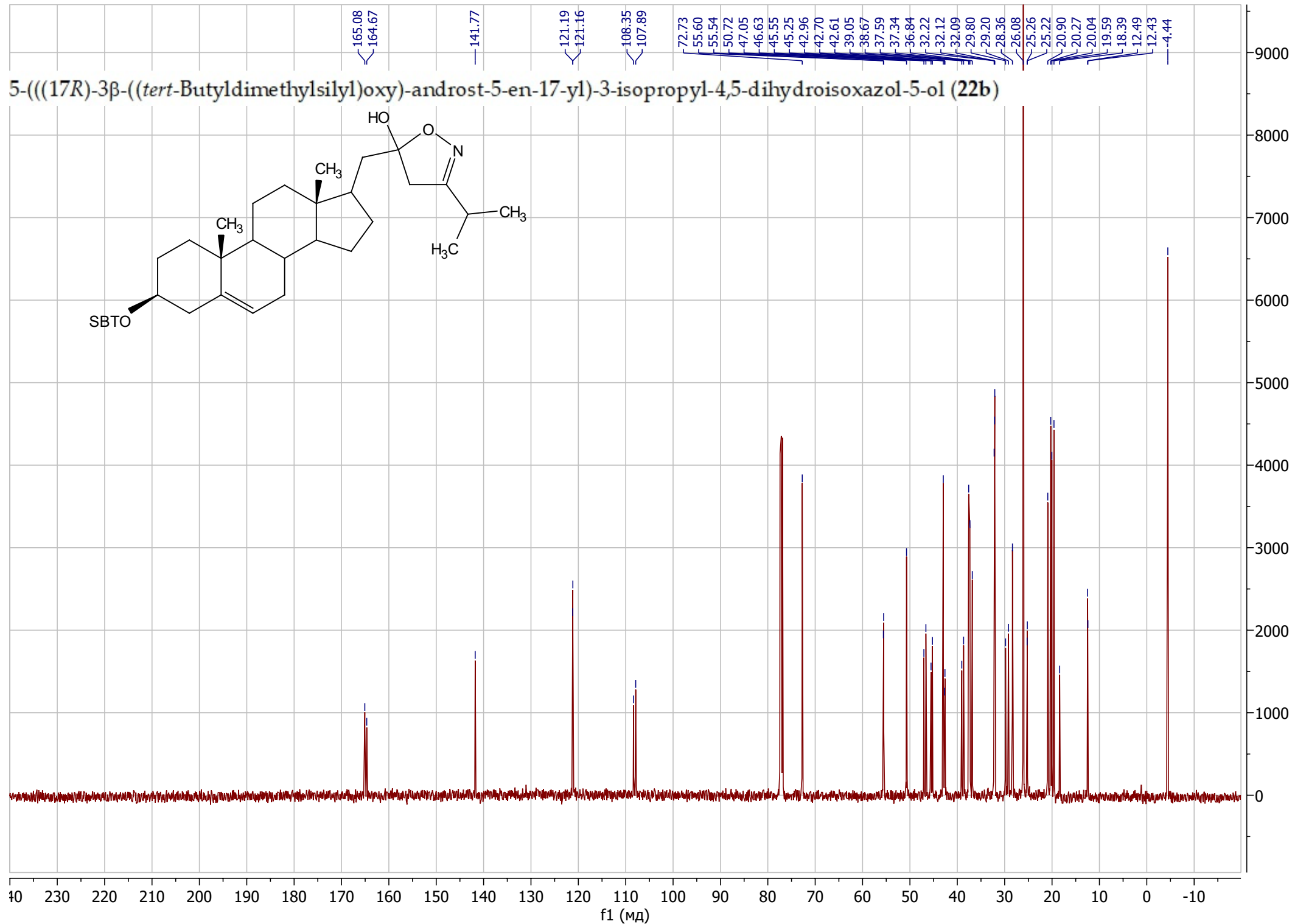
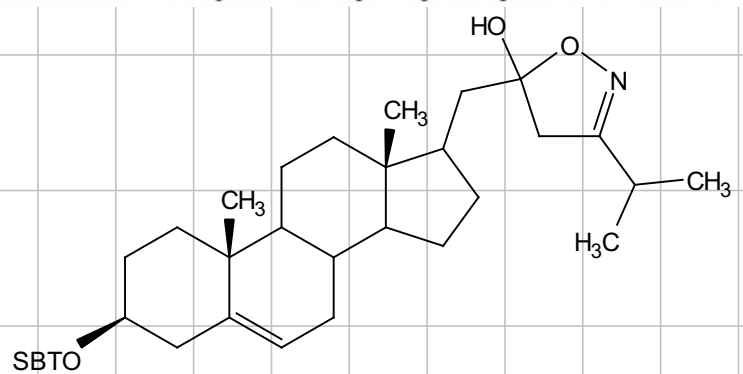
5-(((17R)-3 β -((*tert*-Butyldimethylsilyl)oxy)-androst-5-en-17-yl)-4,5-dihydroisoxazol-5-ol (22a)



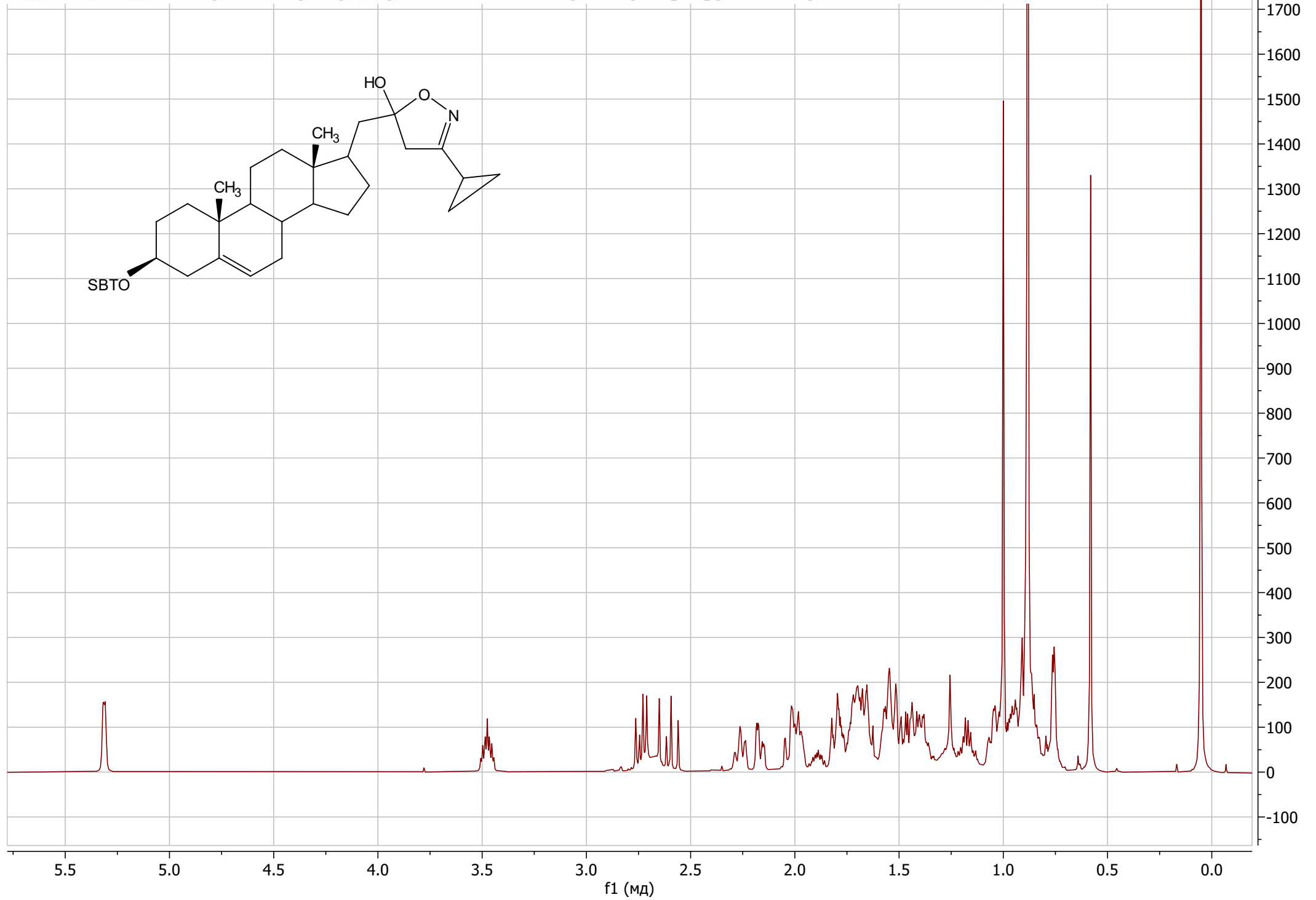
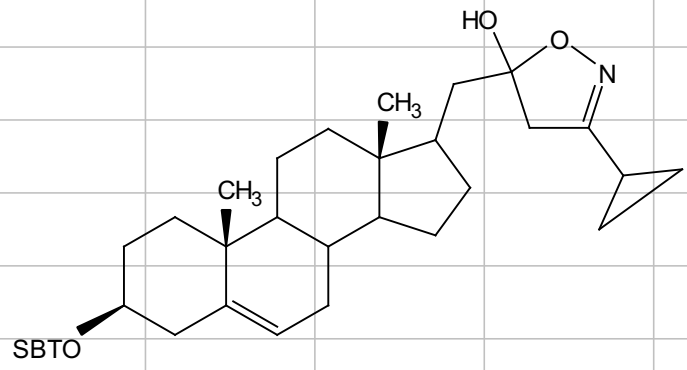
5-(((17R)-3 β -((*tert*-Butyldimethylsilyl)oxy)-androst-5-en-17-yl)-3-isopropyl-4,5-dihydroisoxazol-5-ol (22b)



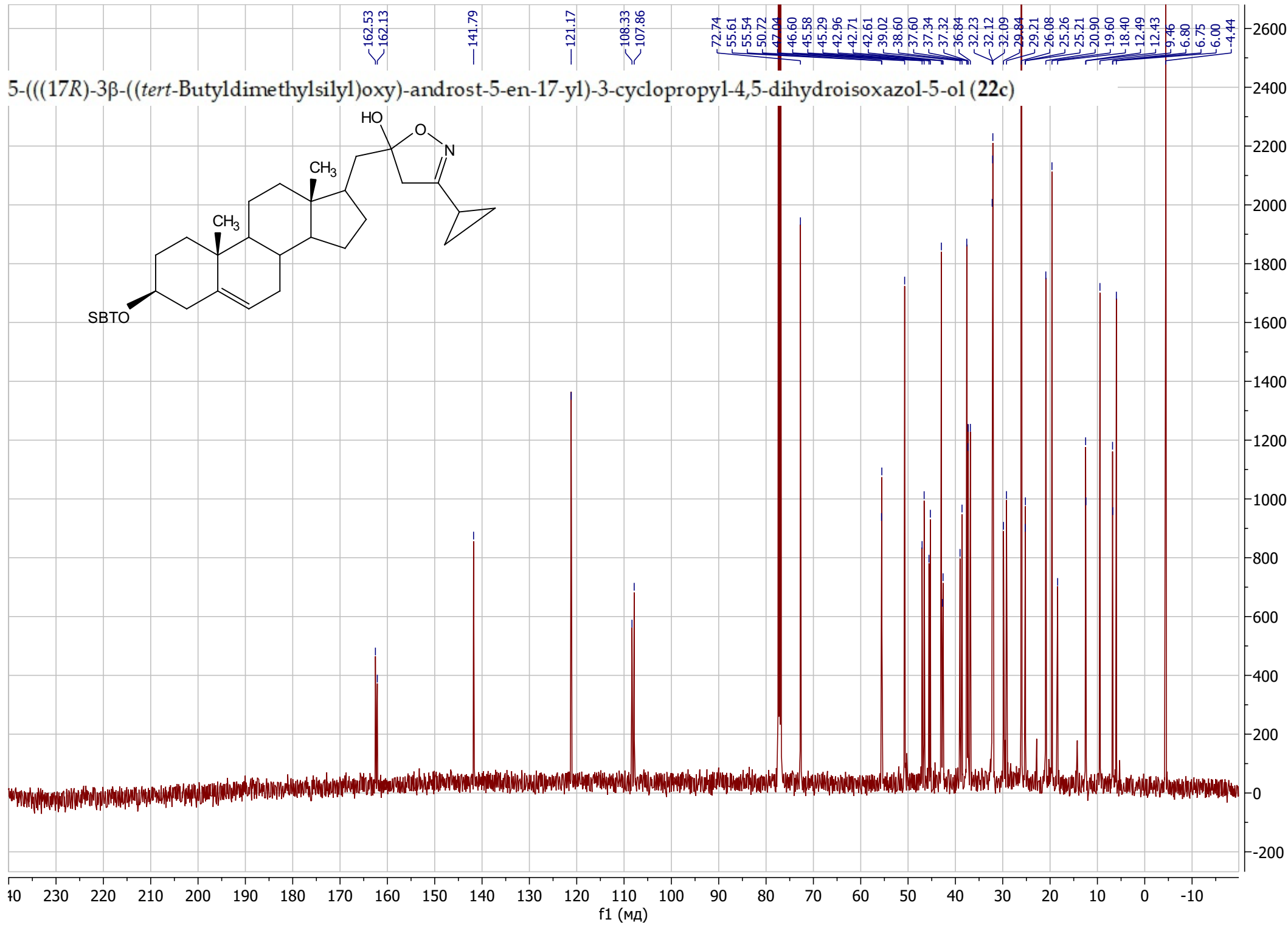
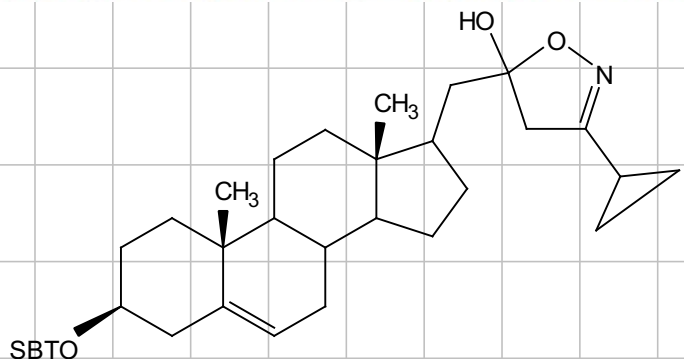
5-(((17R)-3β-(*tert*-Butyldimethylsilyl)oxy)-androst-5-en-17-yl)-3-isopropyl-4,5-dihydroisoxazol-5-ol (22b)



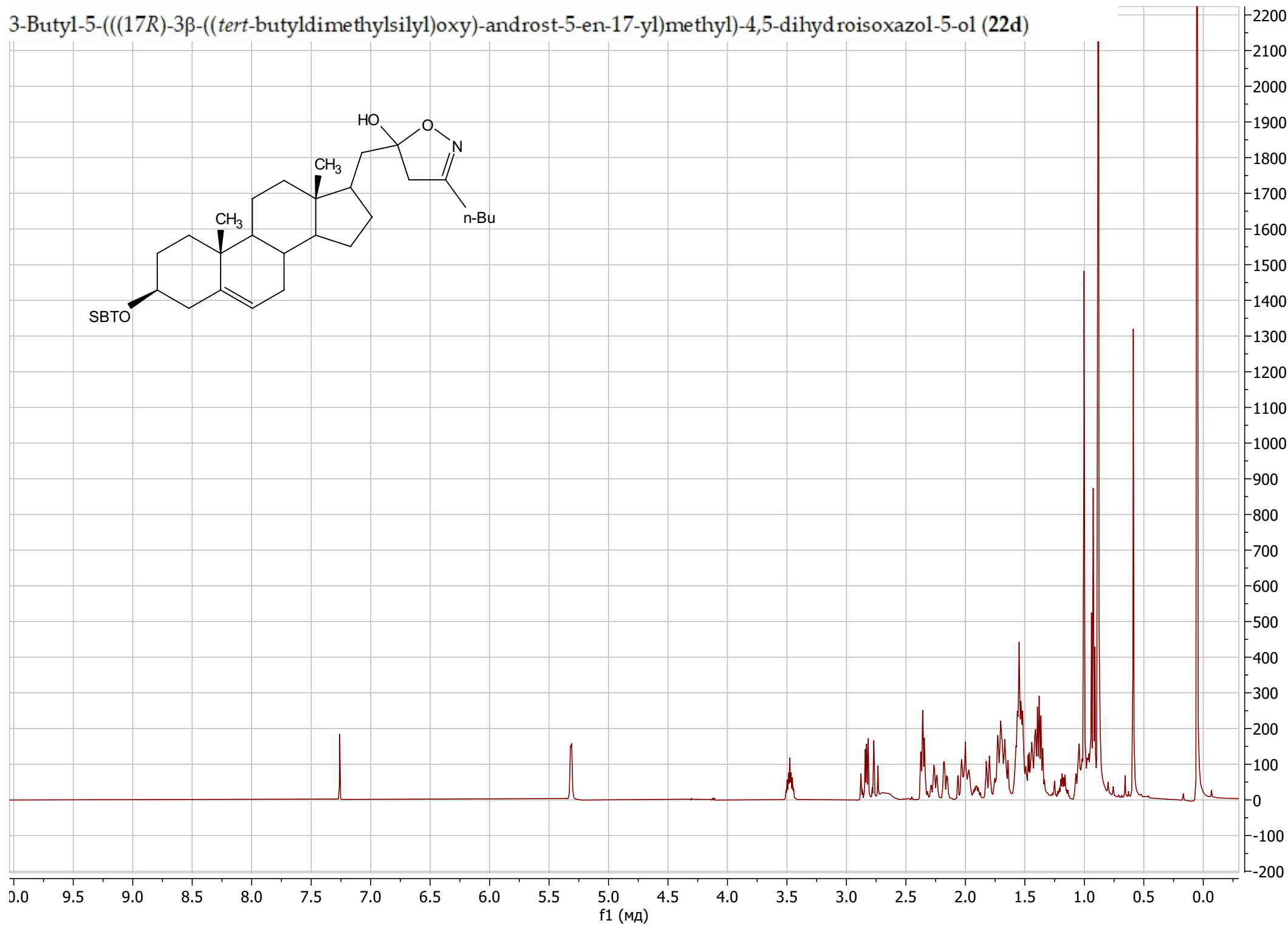
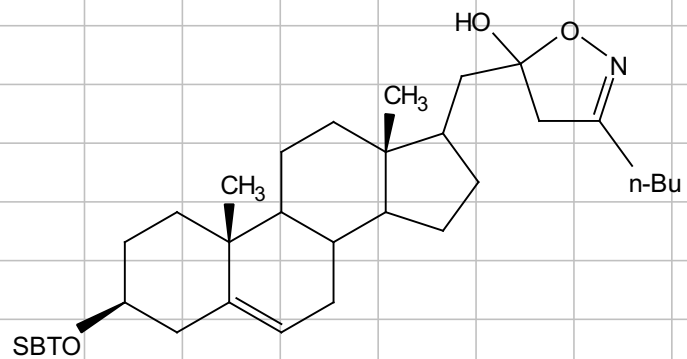
5-(((17R)-3 β -((*tert*-Butyldimethylsilyl)oxy)-androst-5-en-17-yl)-3-cyclopropyl-4,5-dihydroisoxazol-5-ol (22c)



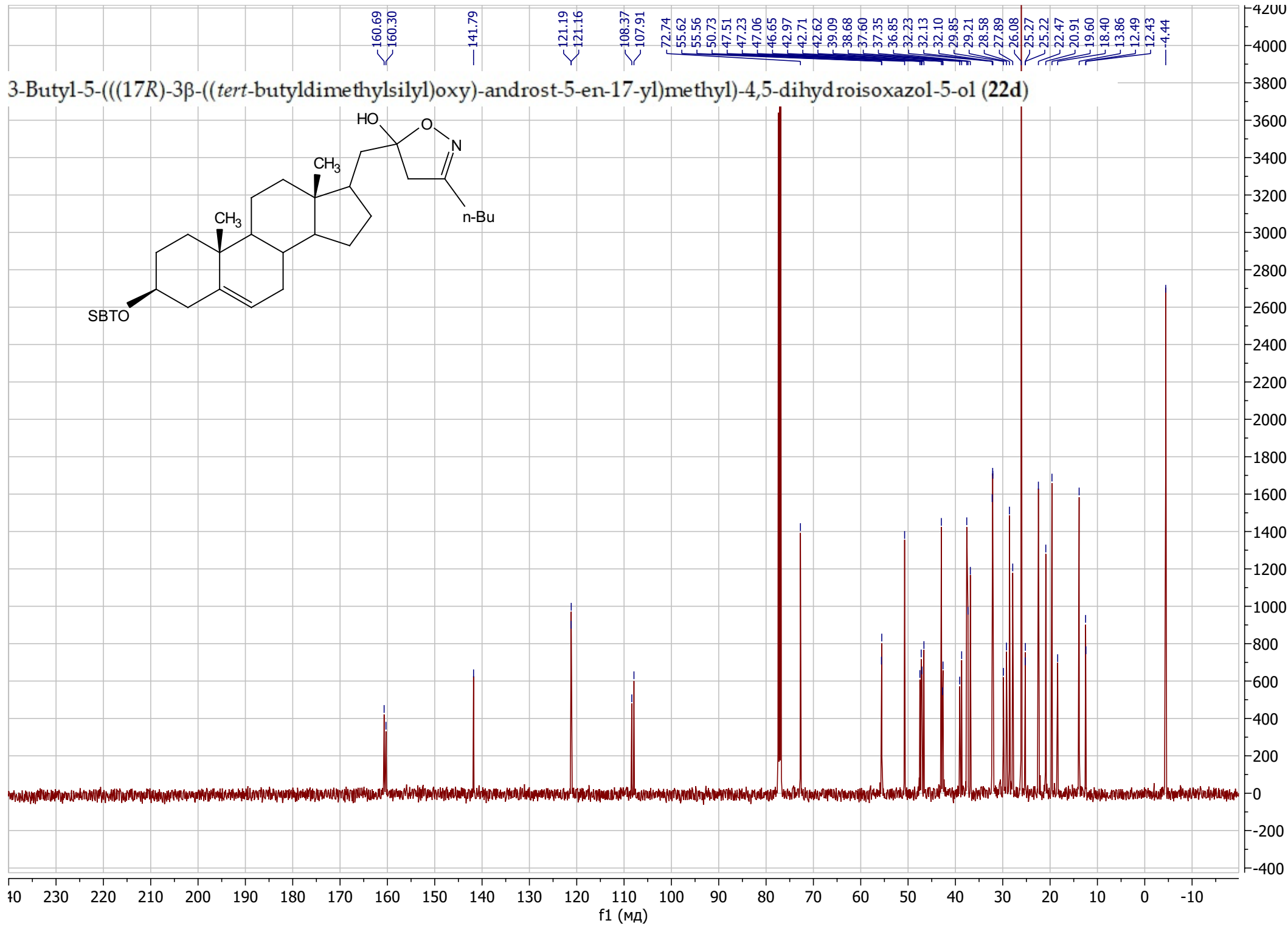
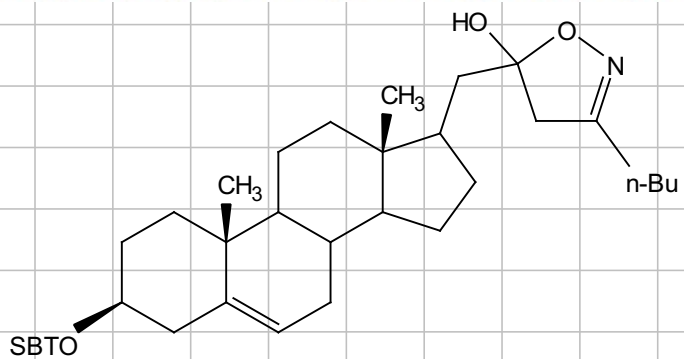
5-(((17R)-3 β -((*tert*-Butyldimethylsilyl)oxy)-androst-5-en-17-yl)-3-cyclopropyl-4,5-dihydroisoxazol-5-ol (22c)



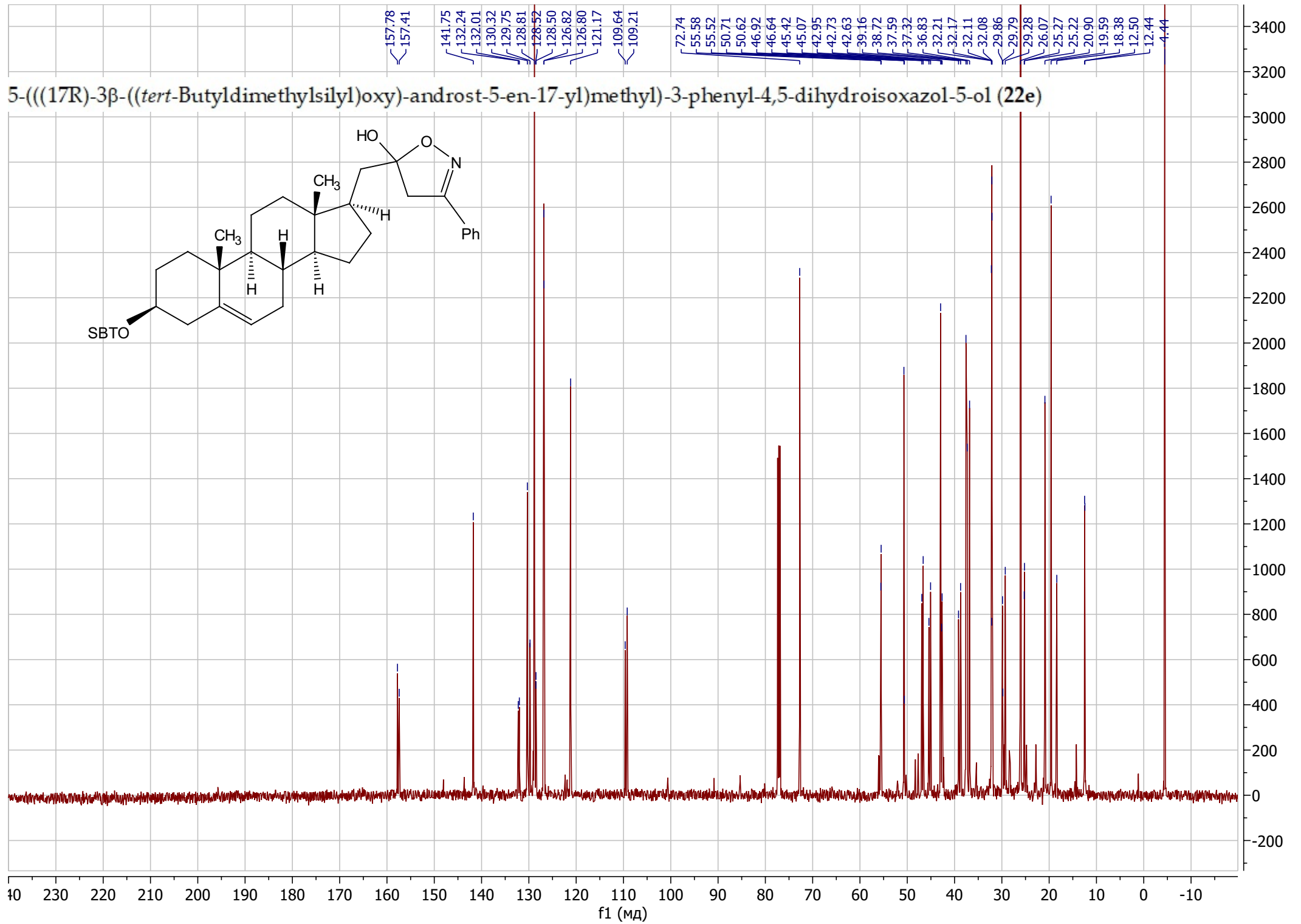
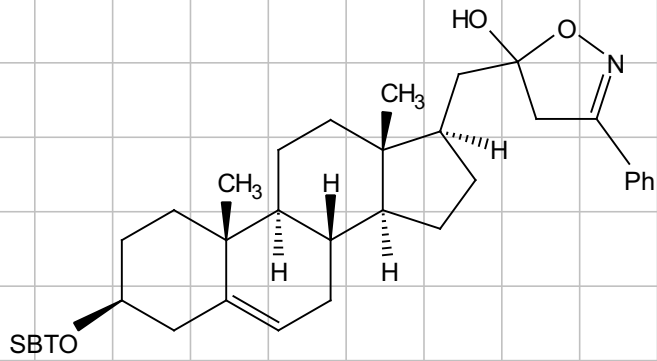
3-Butyl-5-(((17R)-3β-((*tert*-butyldimethylsilyl)oxy)-androst-5-en-17-yl)methyl)-4,5-dihydroisoxazol-5-ol (22d)



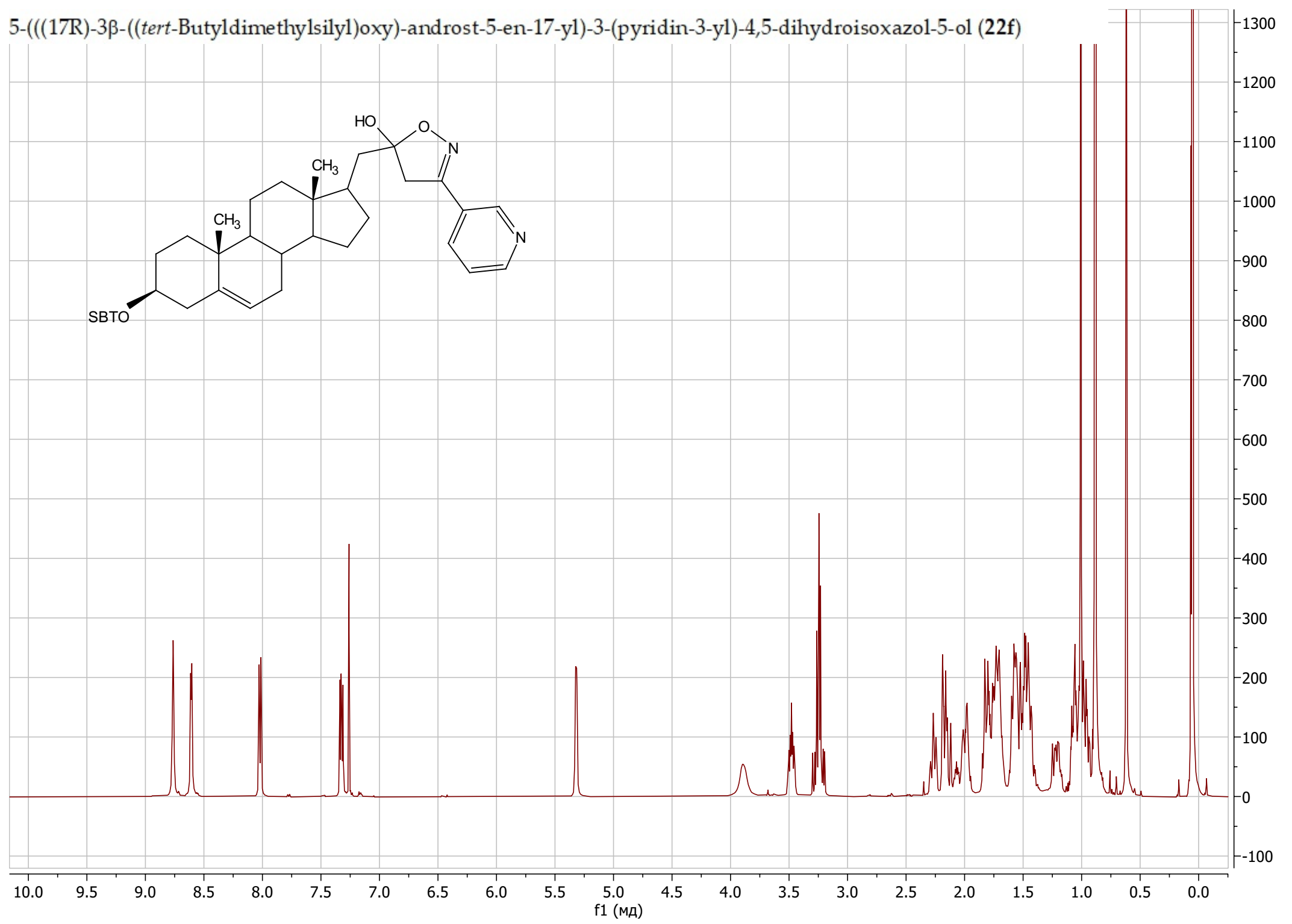
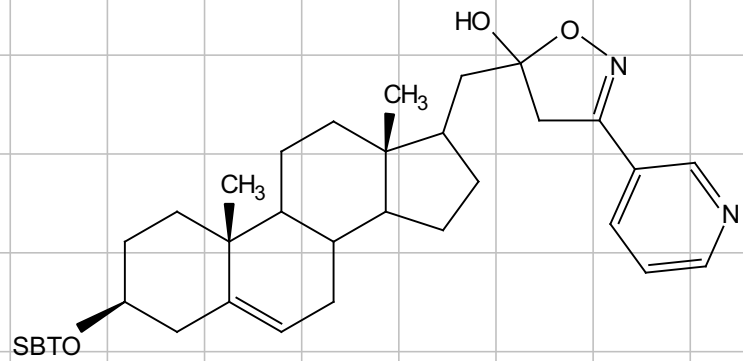
3-Butyl-5-(((17R)-3 β -((*tert*-butyldimethylsilyl)oxy)androst-5-en-17-yl)methyl)-4,5-dihydroisoxazol-5-ol (22d)



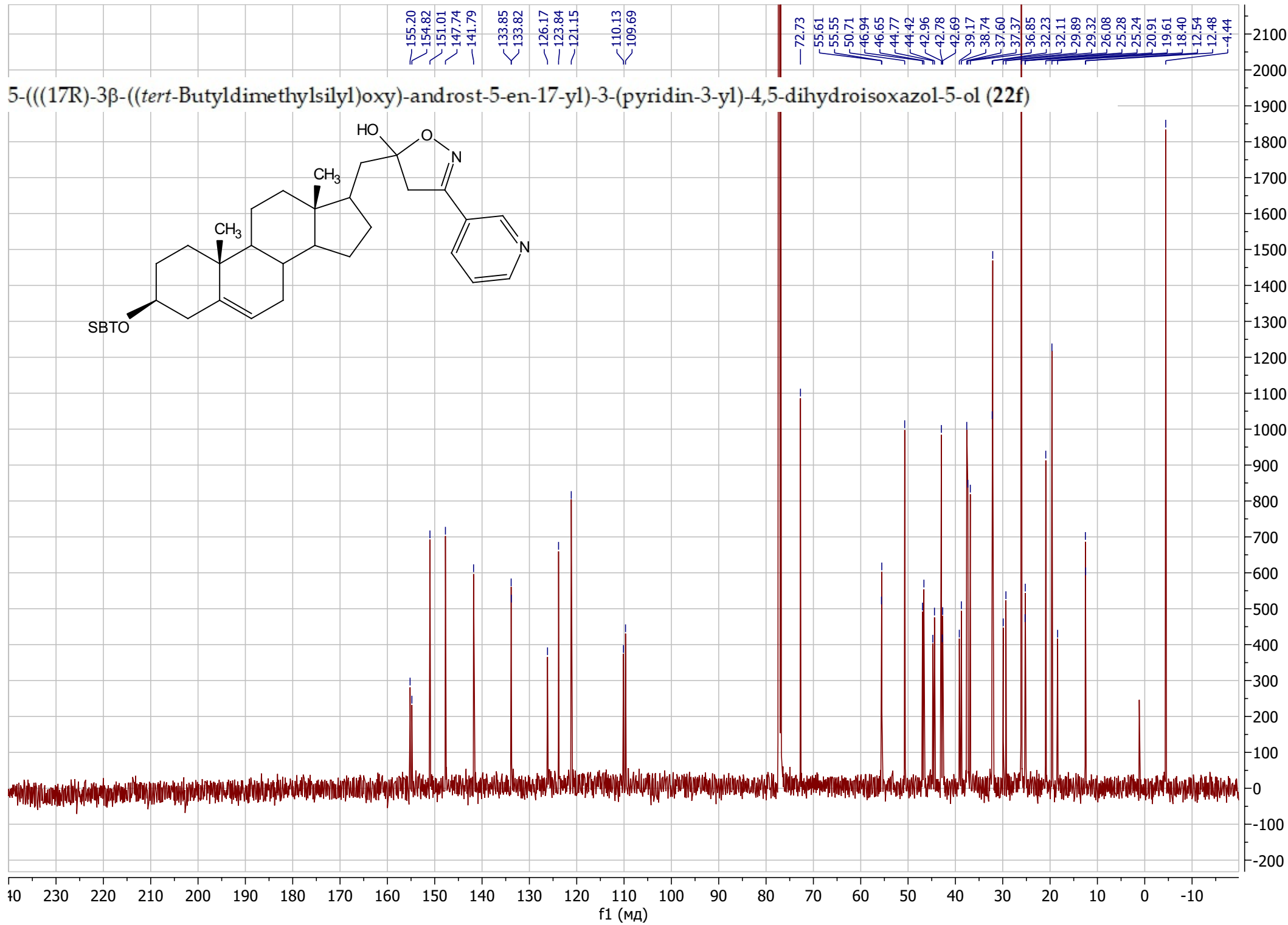
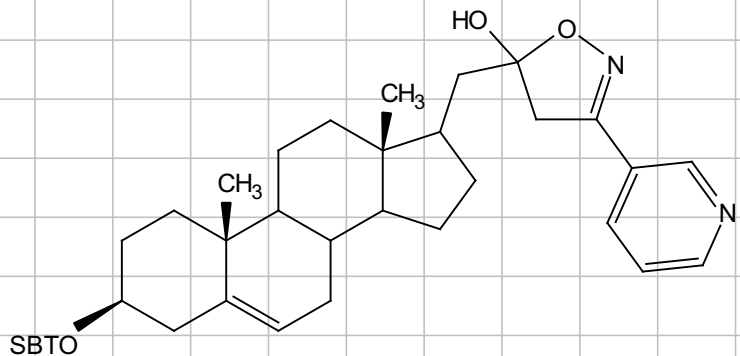
5-(((17R)-3 β -((*tert*-Butyldimethylsilyl)oxy)-androst-5-en-17-yl)methyl)-3-phenyl-4,5-dihydroisoxazol-5-ol (22e)



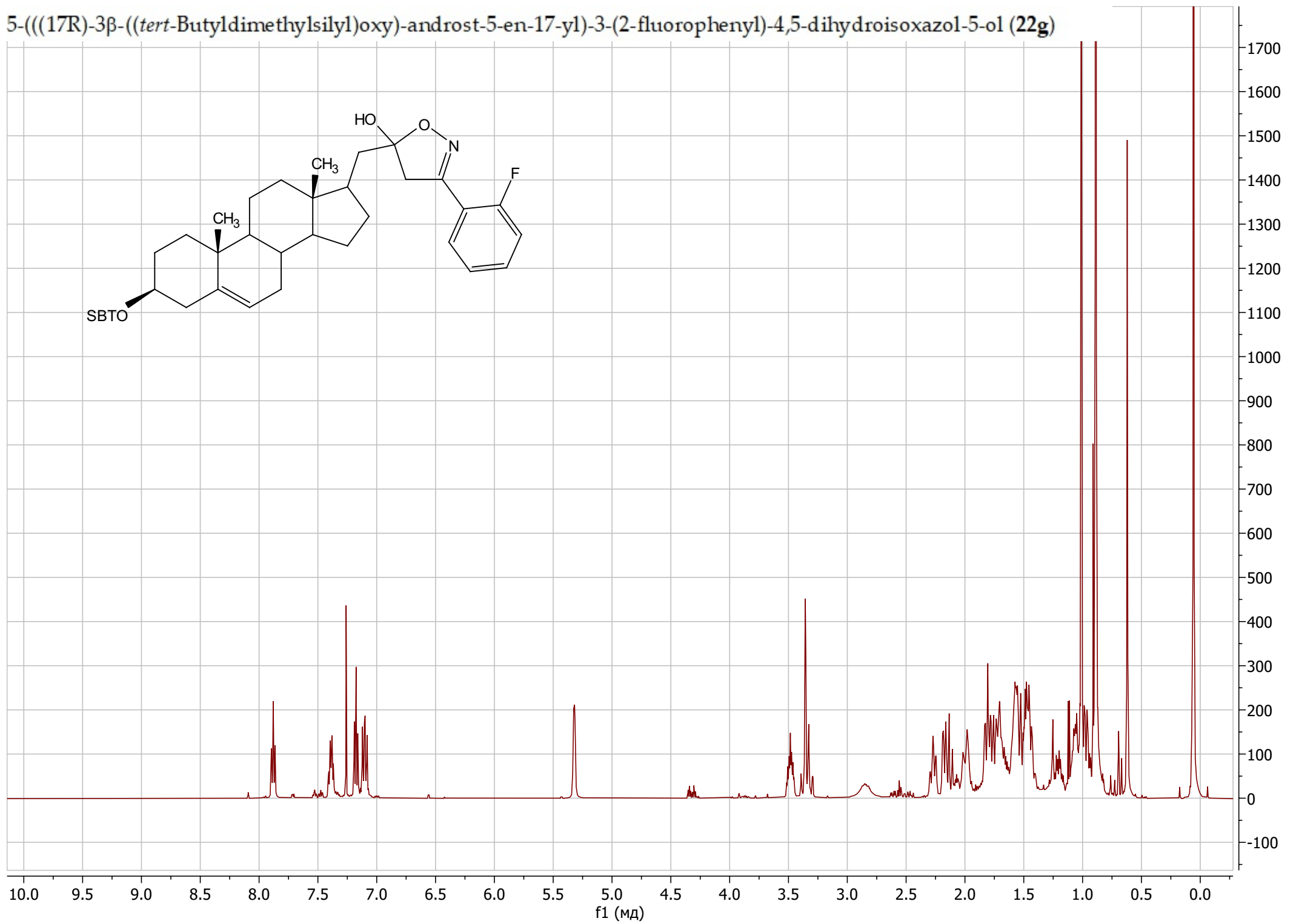
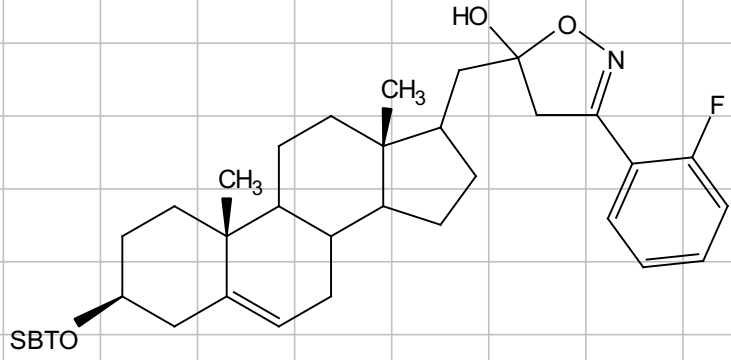
5-(((17R)-3 β -((*tert*-Butyldimethylsilyl)oxy)-androst-5-en-17-yl)-3-(pyridin-3-yl)-4,5-dihydroisoxazol-5-ol (22f)

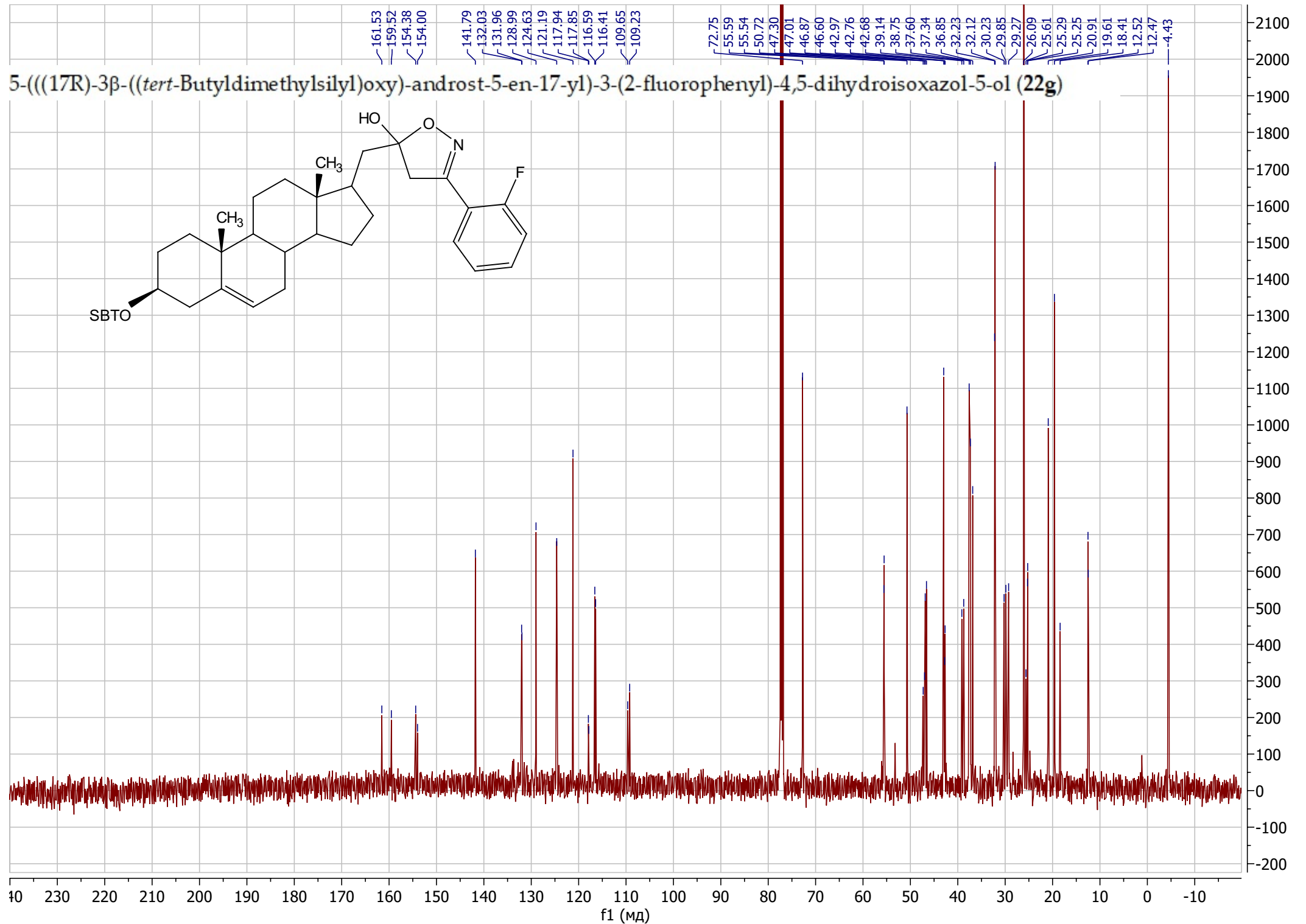


5-(((17R)-3 β -((*tert*-Butyldimethylsilyl)oxy)-androst-5-en-17-yl)-3-(pyridin-3-yl)-4,5-dihydroisoxazol-5-ol (22f)

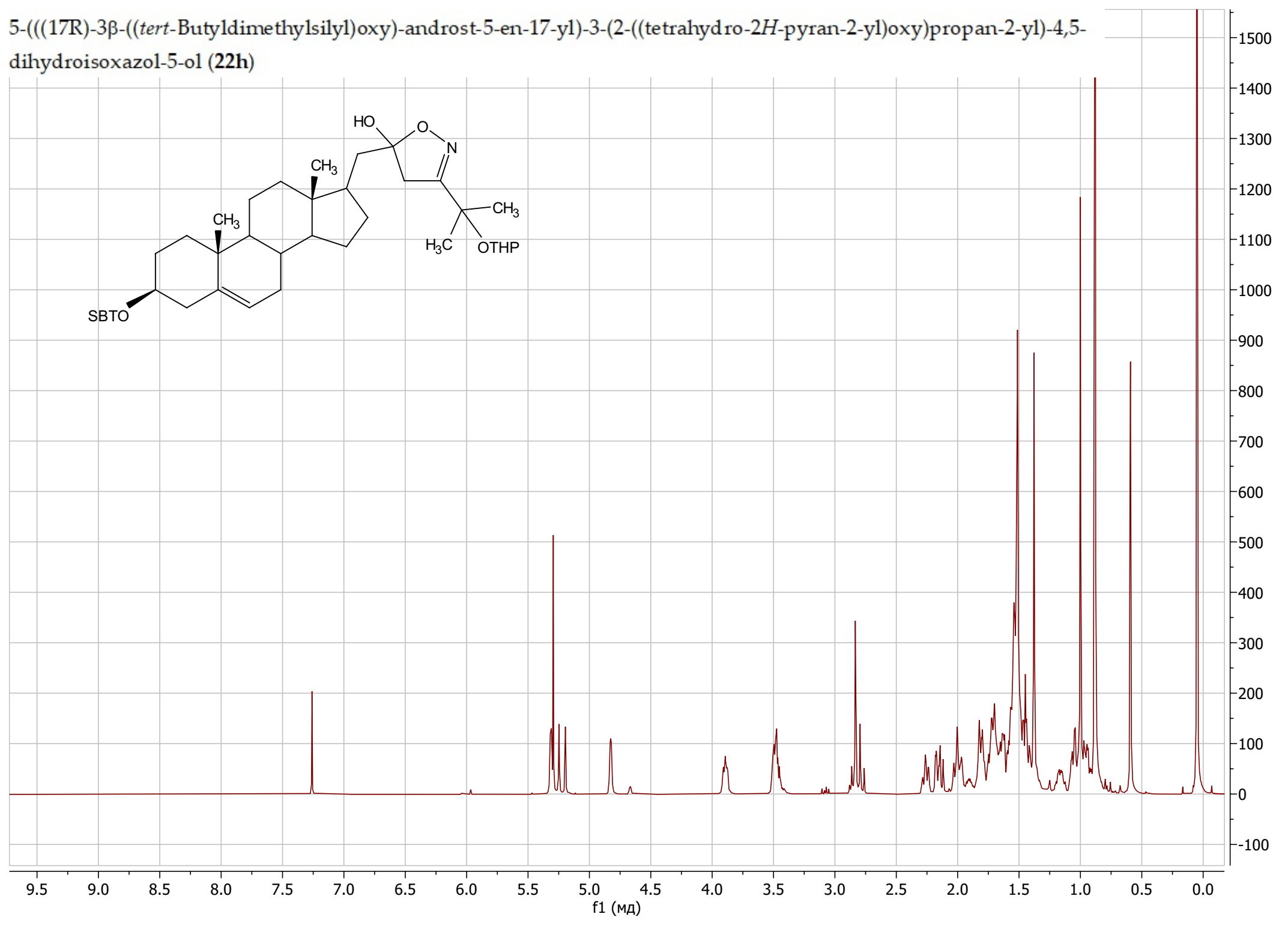
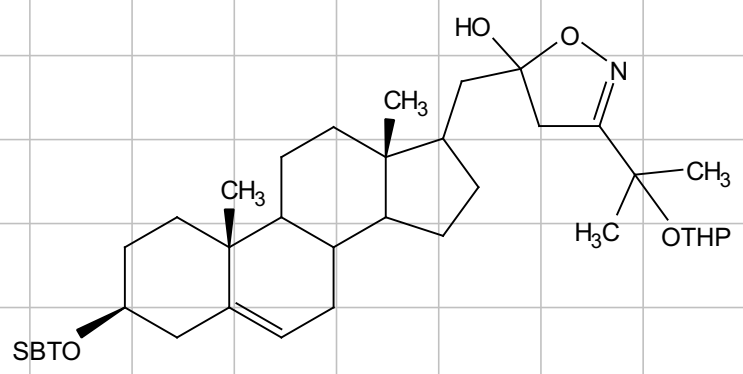


5-(((17R)-3 β -((*tert*-Butyldimethylsilyl)oxy)-androst-5-en-17-yl)-3-(2-fluorophenyl)-4,5-dihydroisoxazol-5-ol (22g)

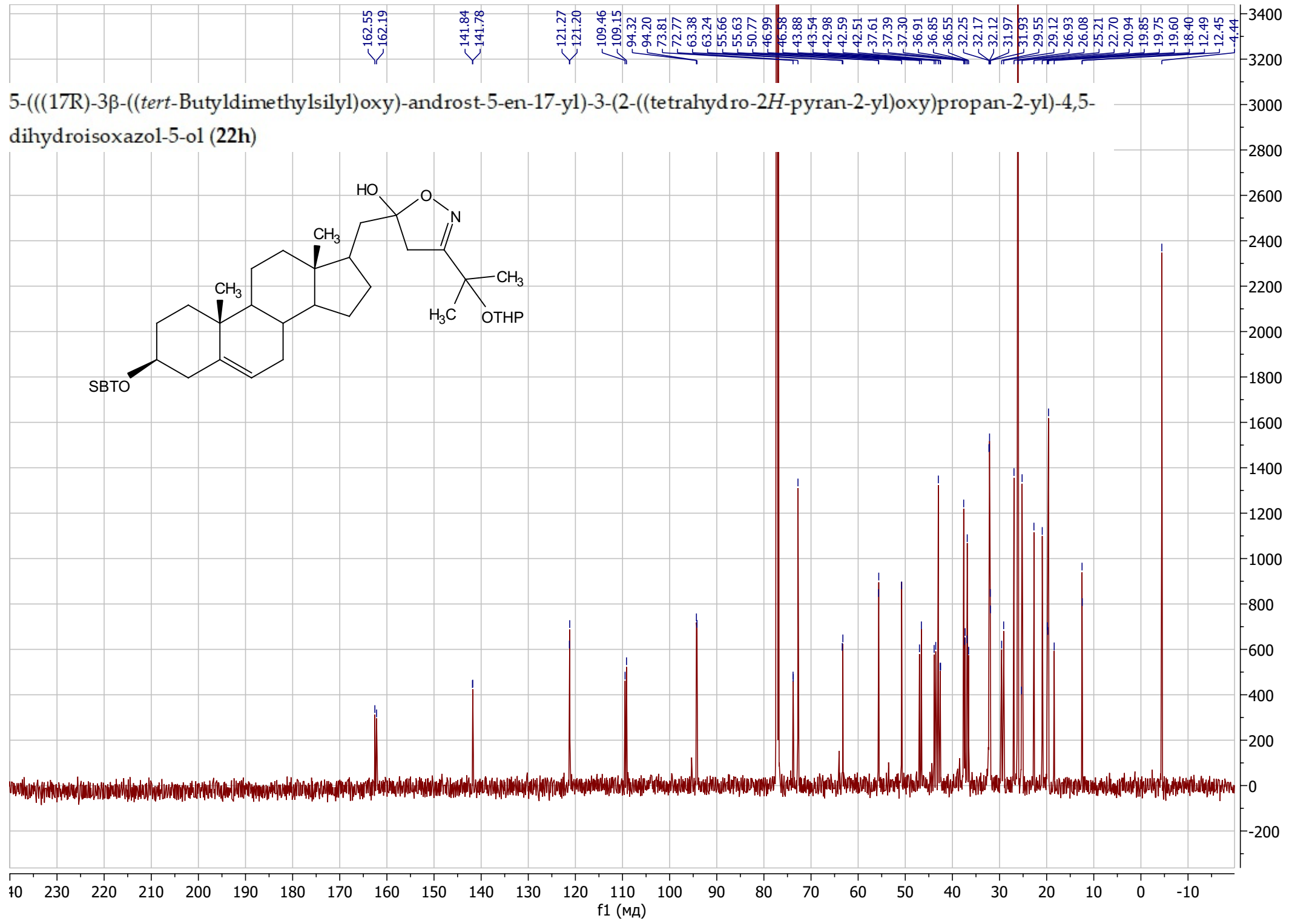
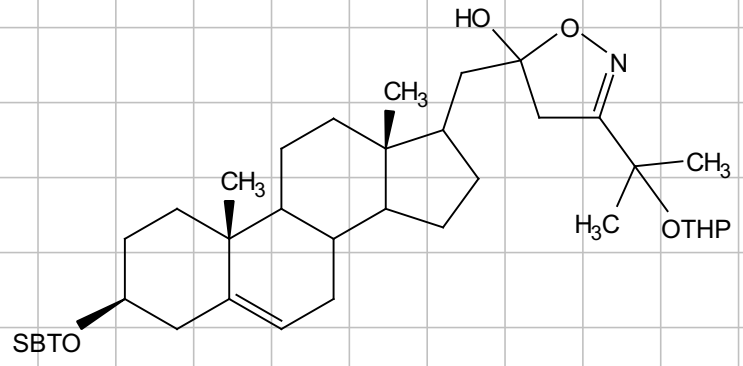




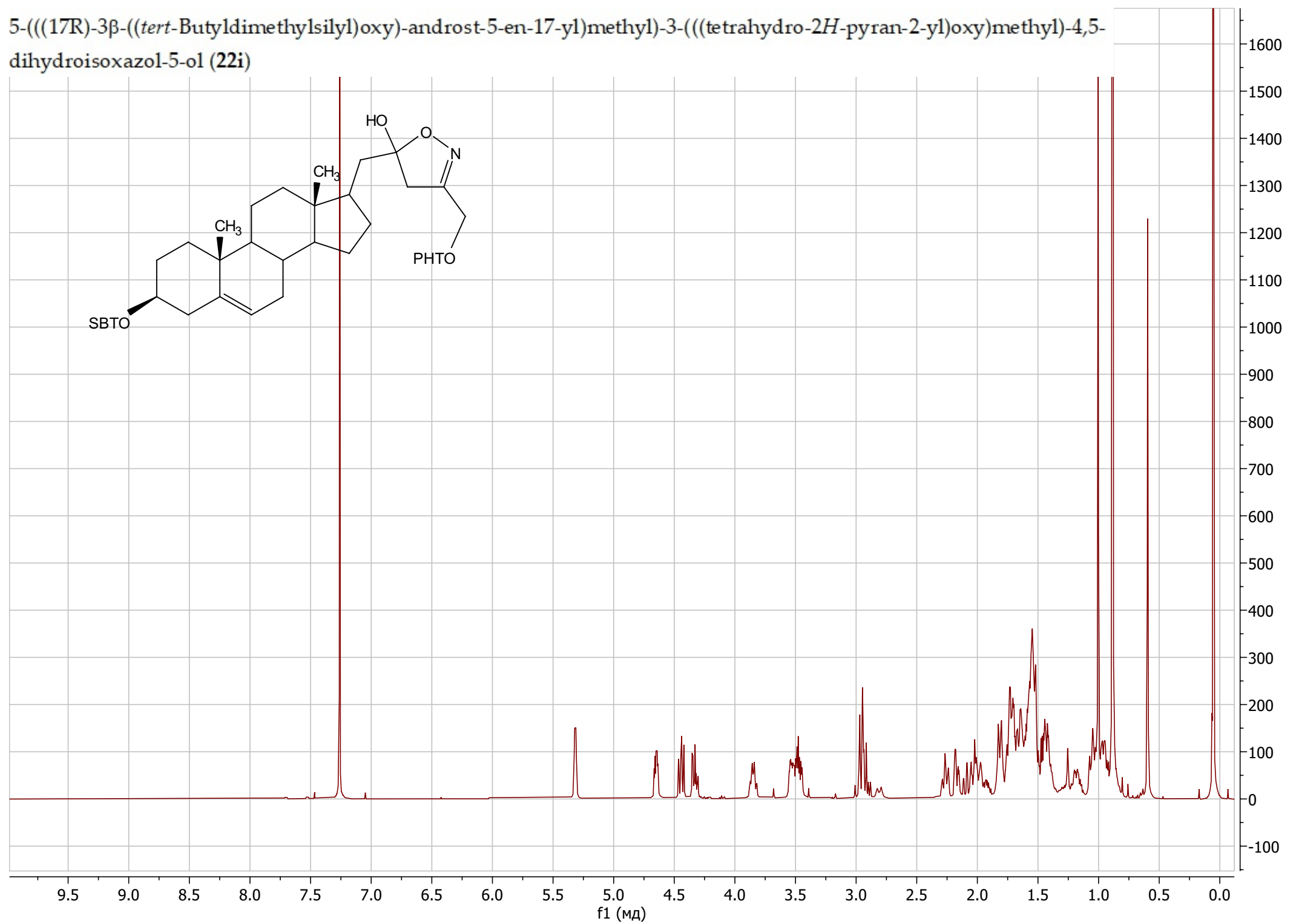
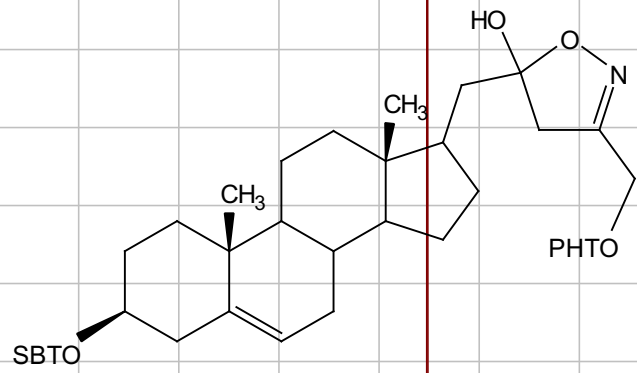
5-(((17R)-3 β -((*tert*-Butyldimethylsilyl)oxy)-androst-5-en-17-yl)-3-(2-(((tetrahydro-2*H*-pyran-2-yl)oxy)propan-2-yl)-4,5-dihydroisoxazol-5-ol (22h)



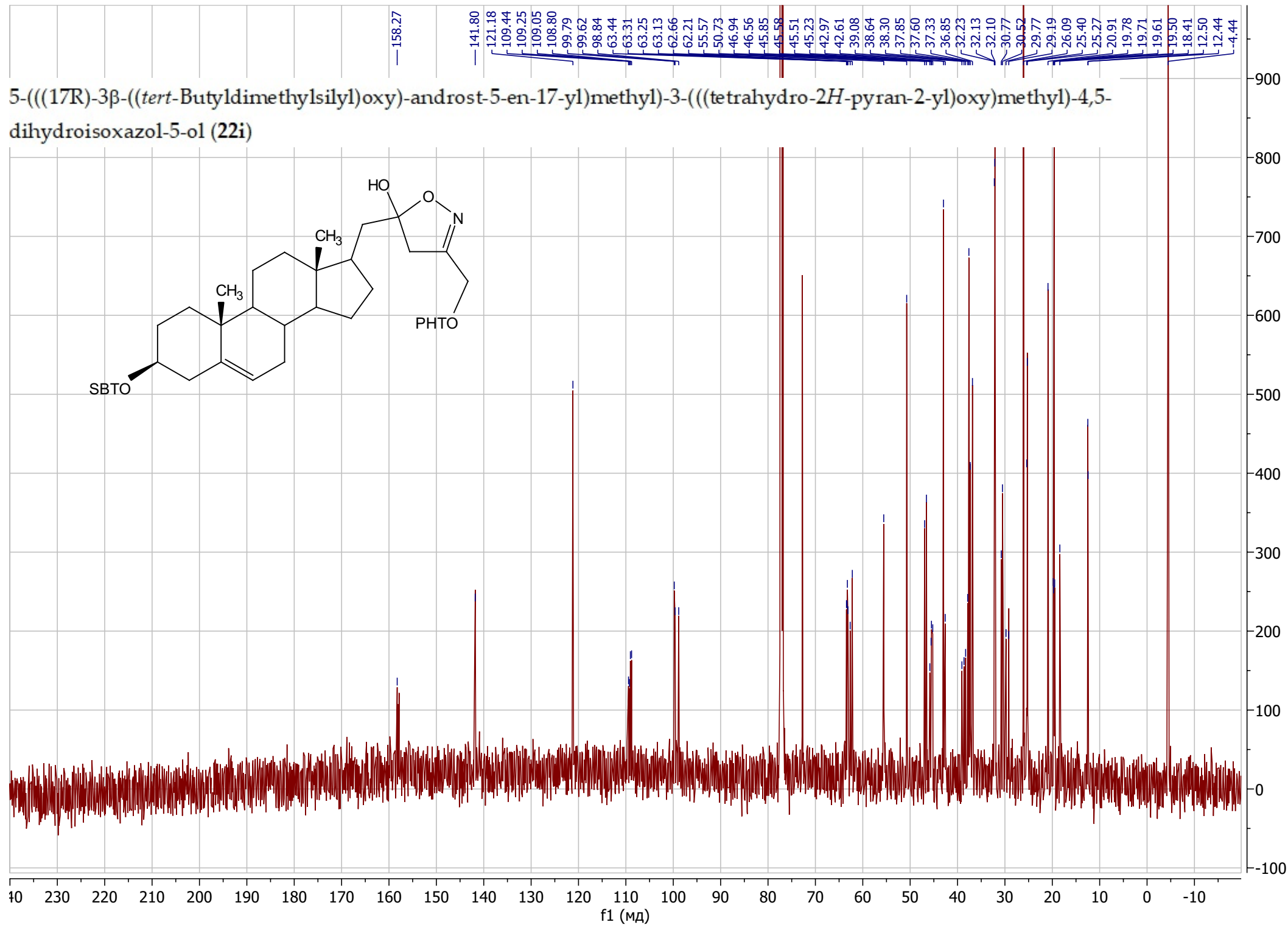
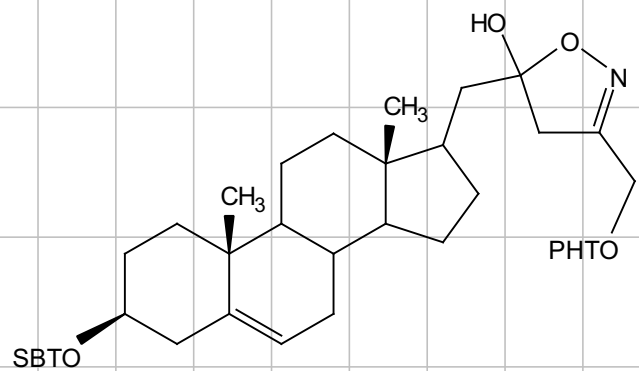
5-(((17R)-3 β -((*tert*-Butyldimethylsilyl)oxy)-androst-5-en-17-yl)-3-(2-(((tetrahydro-2*H*-pyran-2-yl)oxy)propan-2-yl)-4,5-dihydroisoxazol-5-ol (22h)



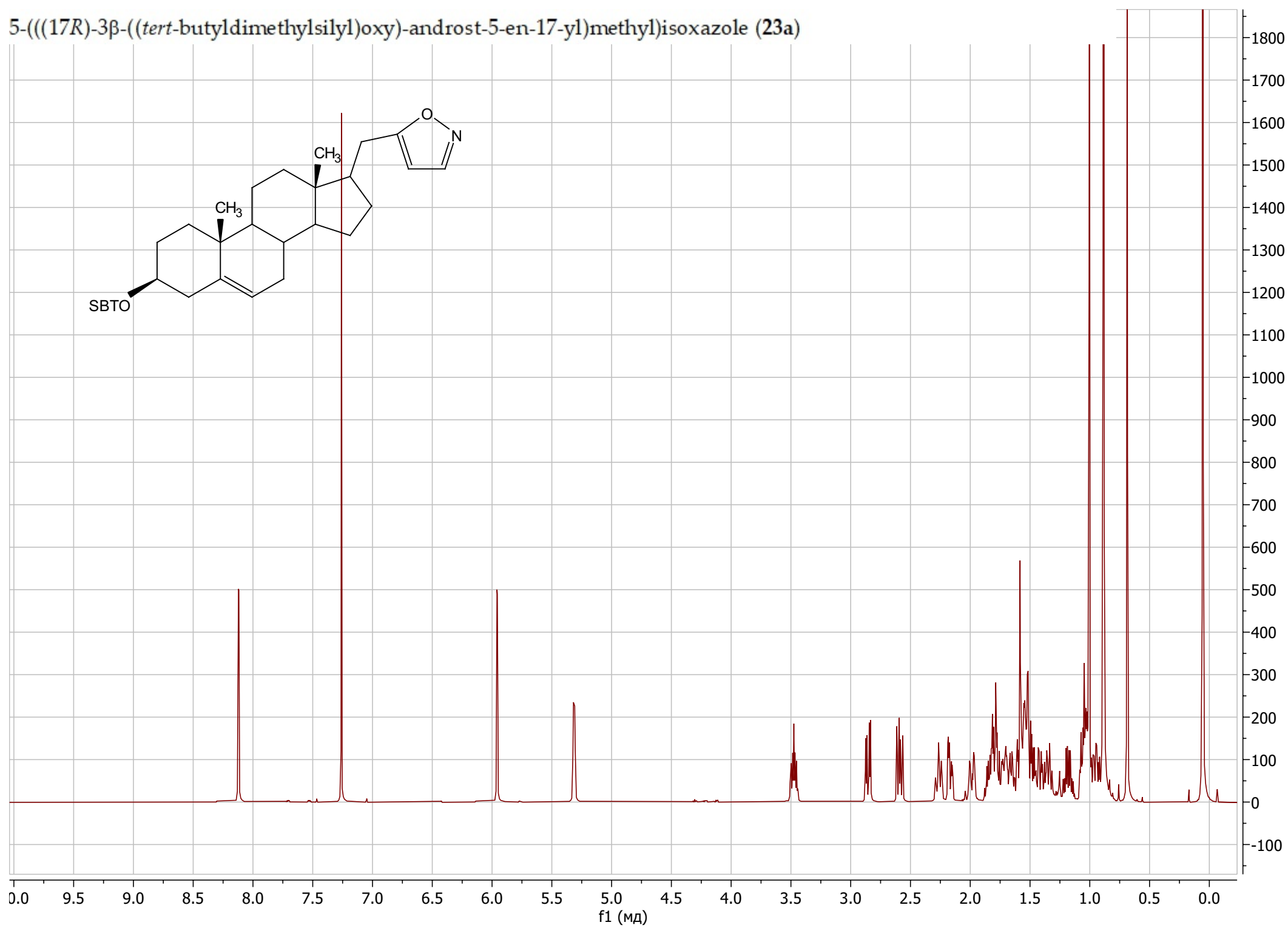
5-(((17R)-3 β -((*tert*-Butyldimethylsilyl)oxy)-androst-5-en-17-yl)methyl)-3-(((tetrahydro-2*H*-pyran-2-yl)oxy)methyl)-4,5-dihydroisoxazol-5-ol (**22i**)



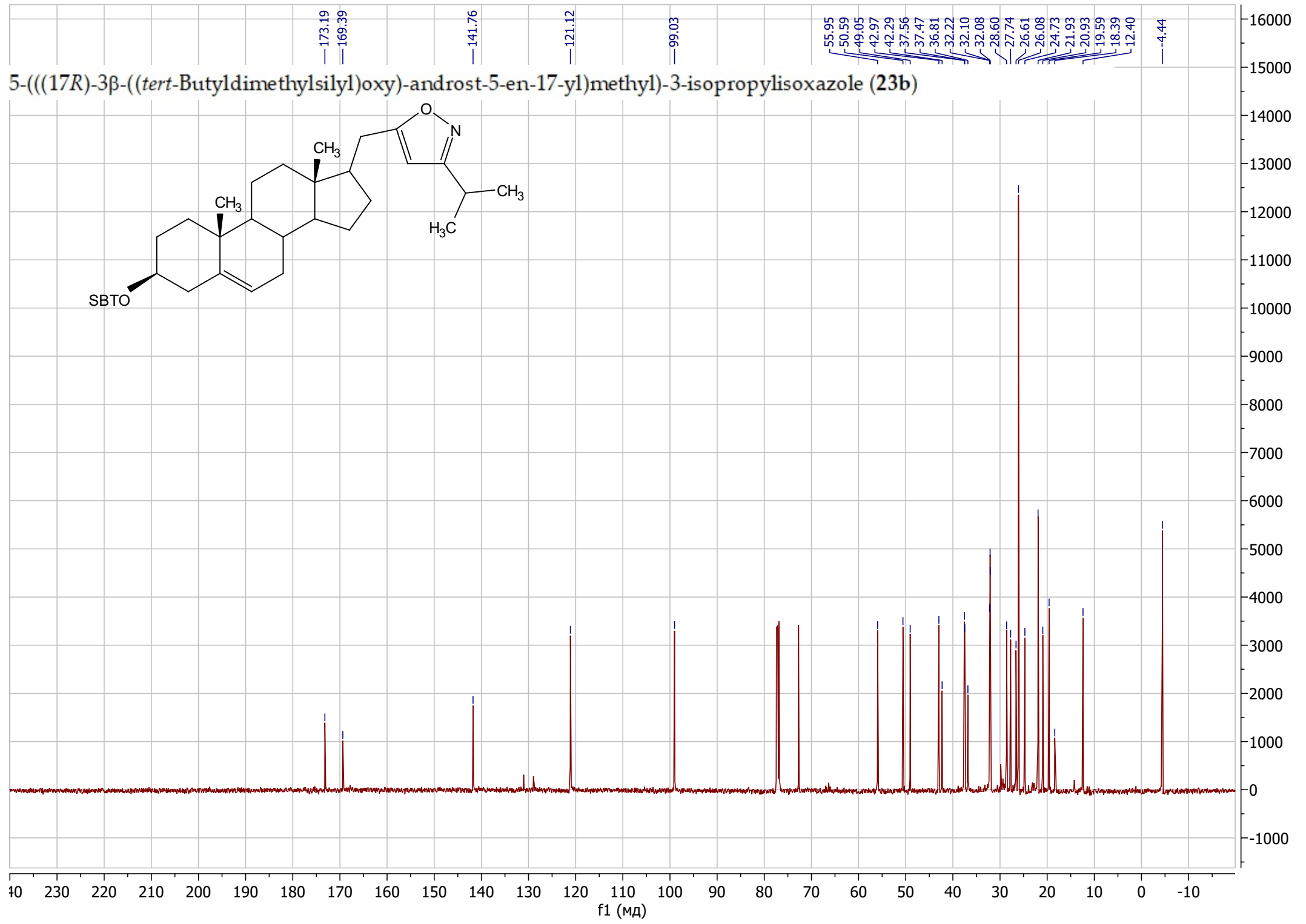
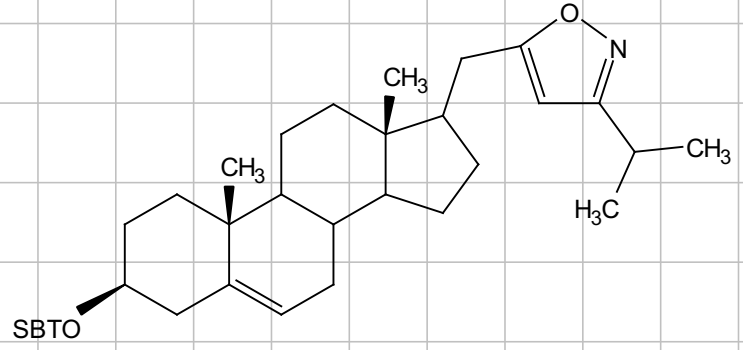
5-(((17R)-3 β -((*tert*-Butyldimethylsilyl)oxy)-androst-5-en-17-yl)methyl)-3-(((tetrahydro-2*H*-pyran-2-yl)oxy)methyl)-4,5-dihydroisoxazol-5-ol (**22i**)



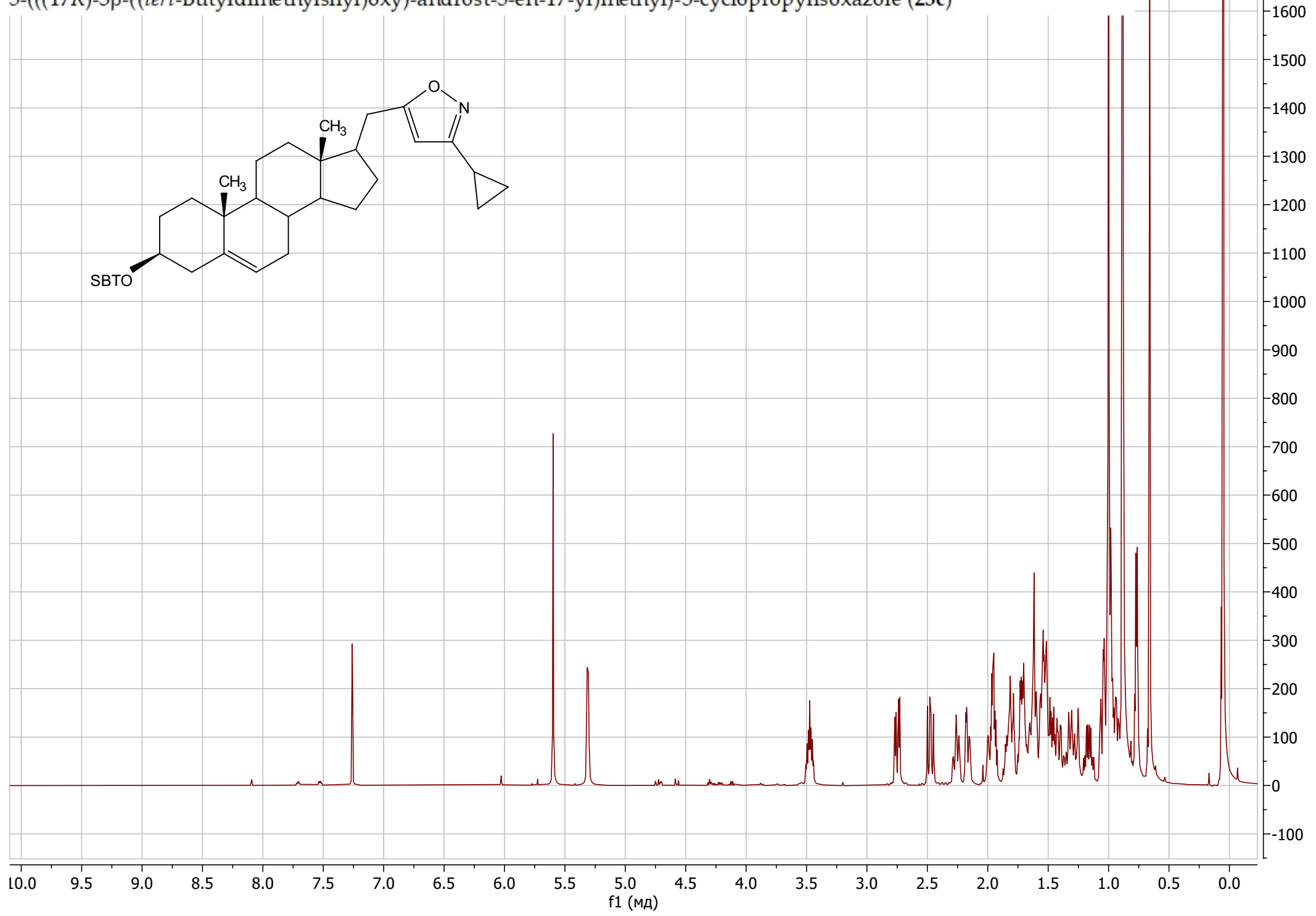
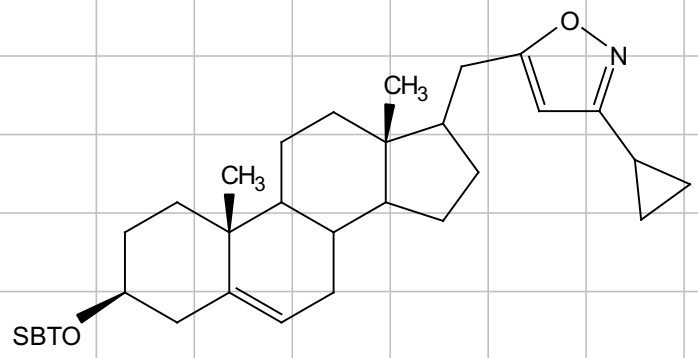
5-(((17R)-3 β -((*tert*-butyldimethylsilyl)oxy)-androst-5-en-17-yl)methyl)isoxazole (23a)



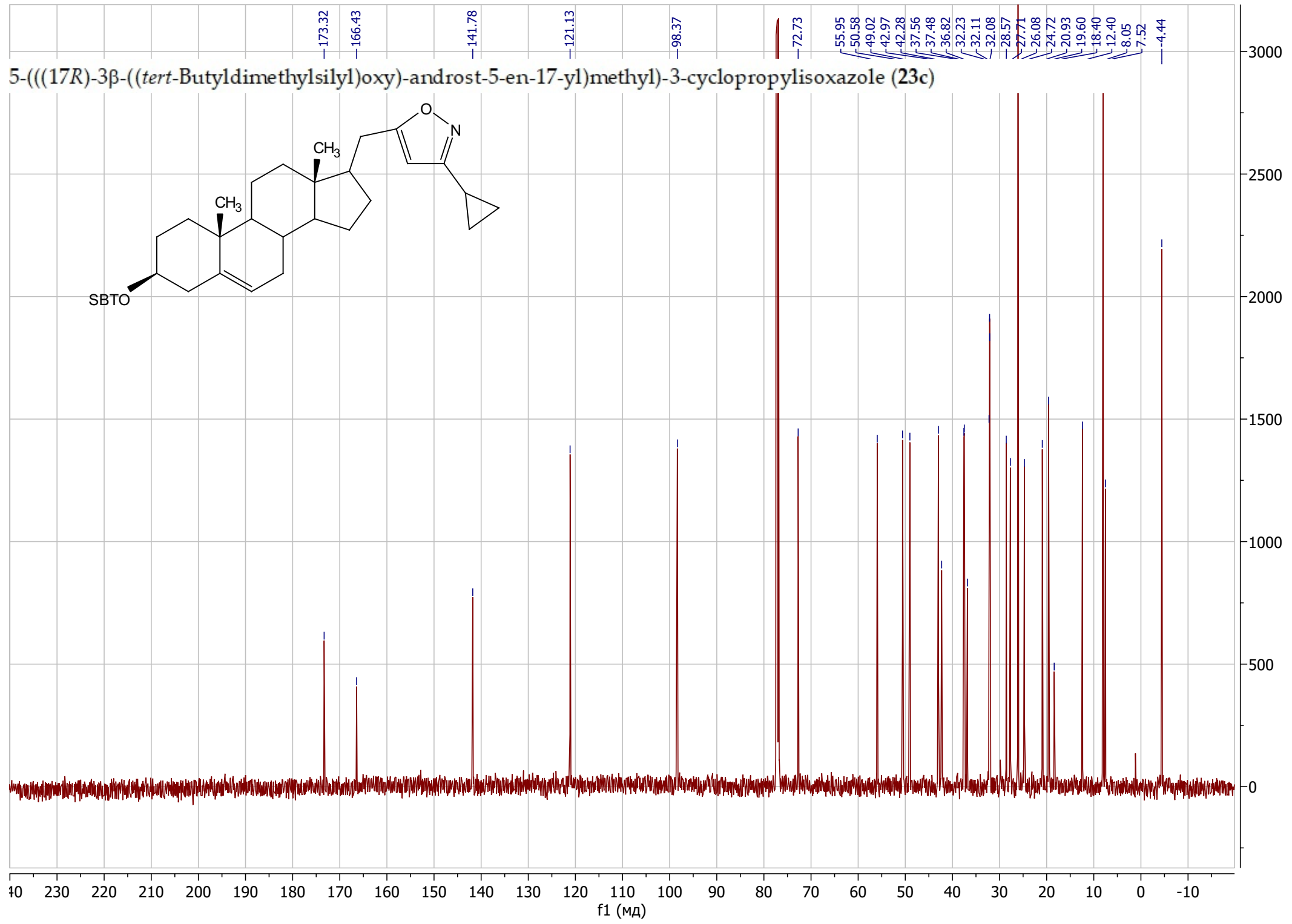
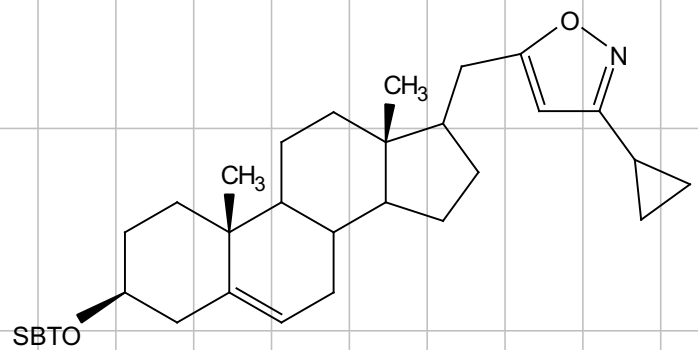
5-(((17R)-3 β -((*tert*-Butyldimethylsilyl)oxy)-androst-5-en-17-yl)methyl)-3-isopropylisoxazole (23b)



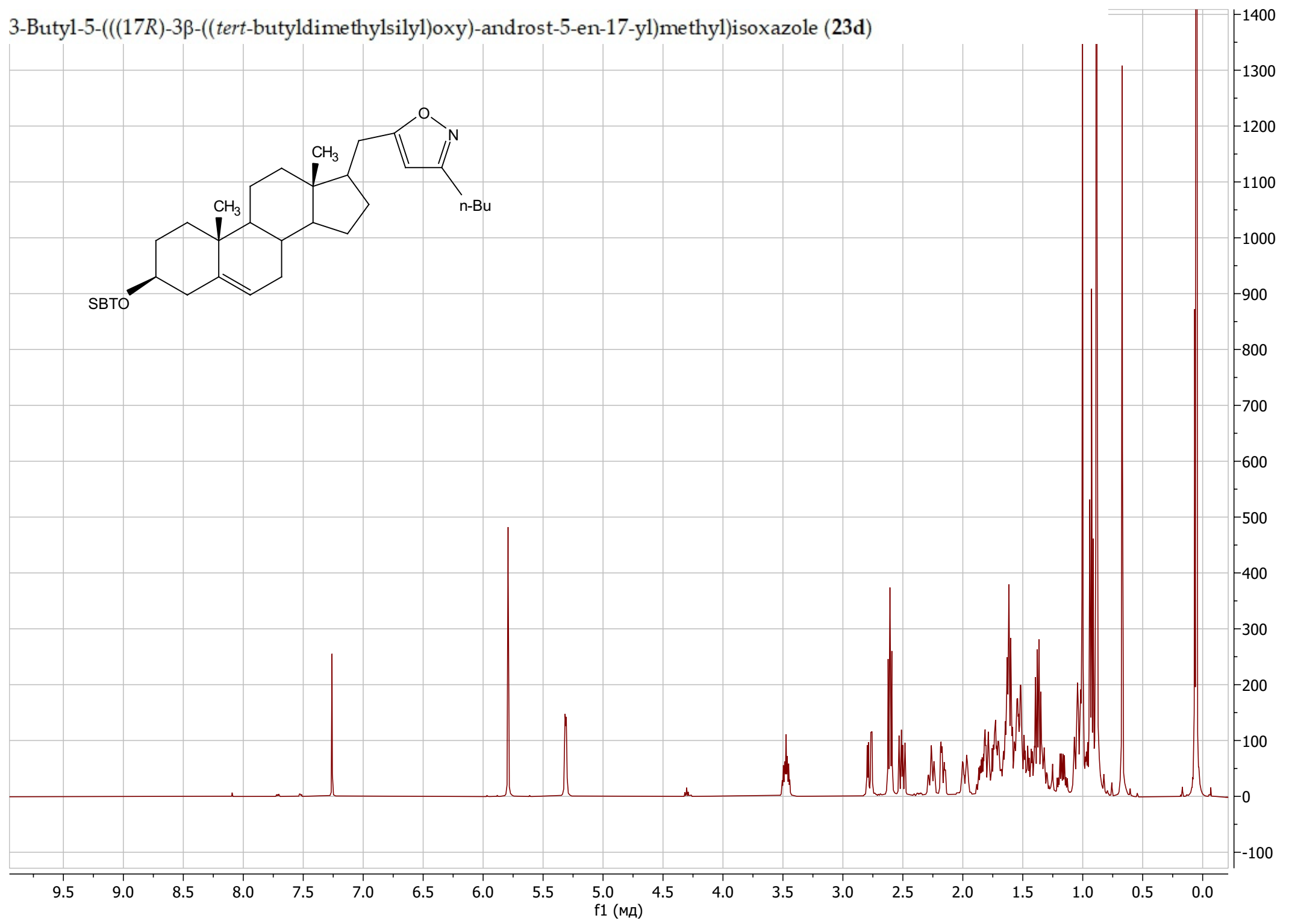
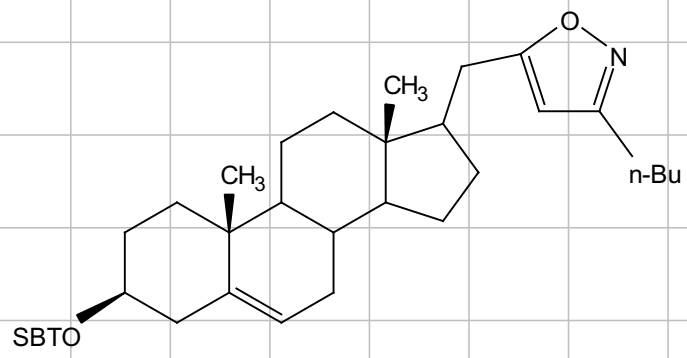
5-(((17R)-3 β -((*tert*-Butyldimethylsilyloxy)-androst-5-en-17-yl)methyl)-3-cyclopropylisoxazole (23c)



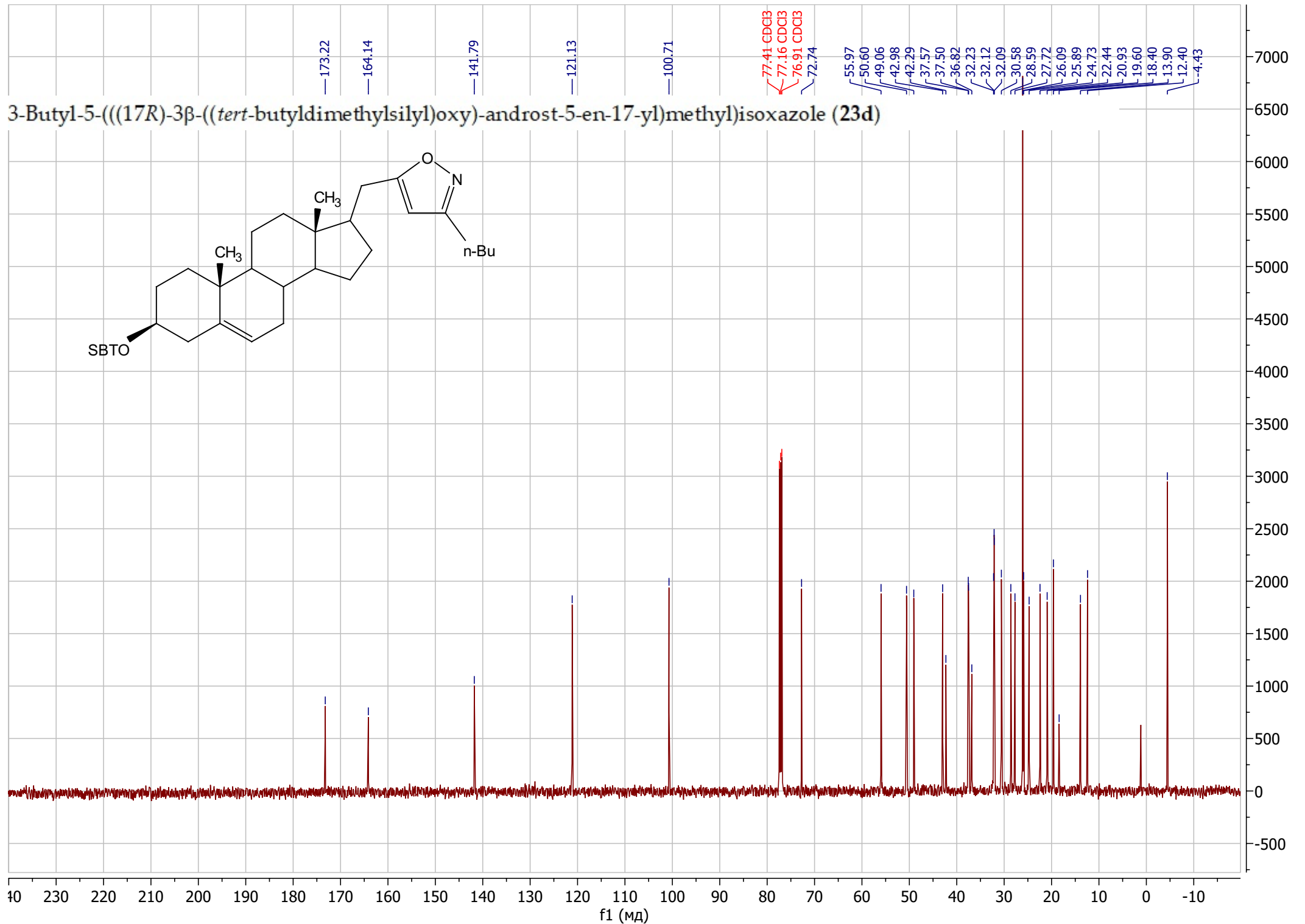
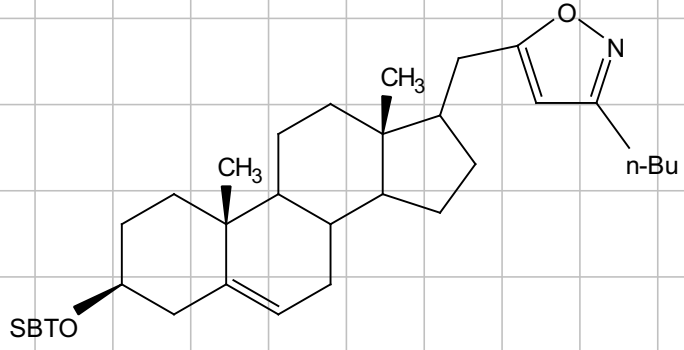
5-(((17R)-3 β -((*tert*-Butyldimethylsilyl)oxy)-androst-5-en-17-yl)methyl)-3-cyclopropylisoxazole (23c)



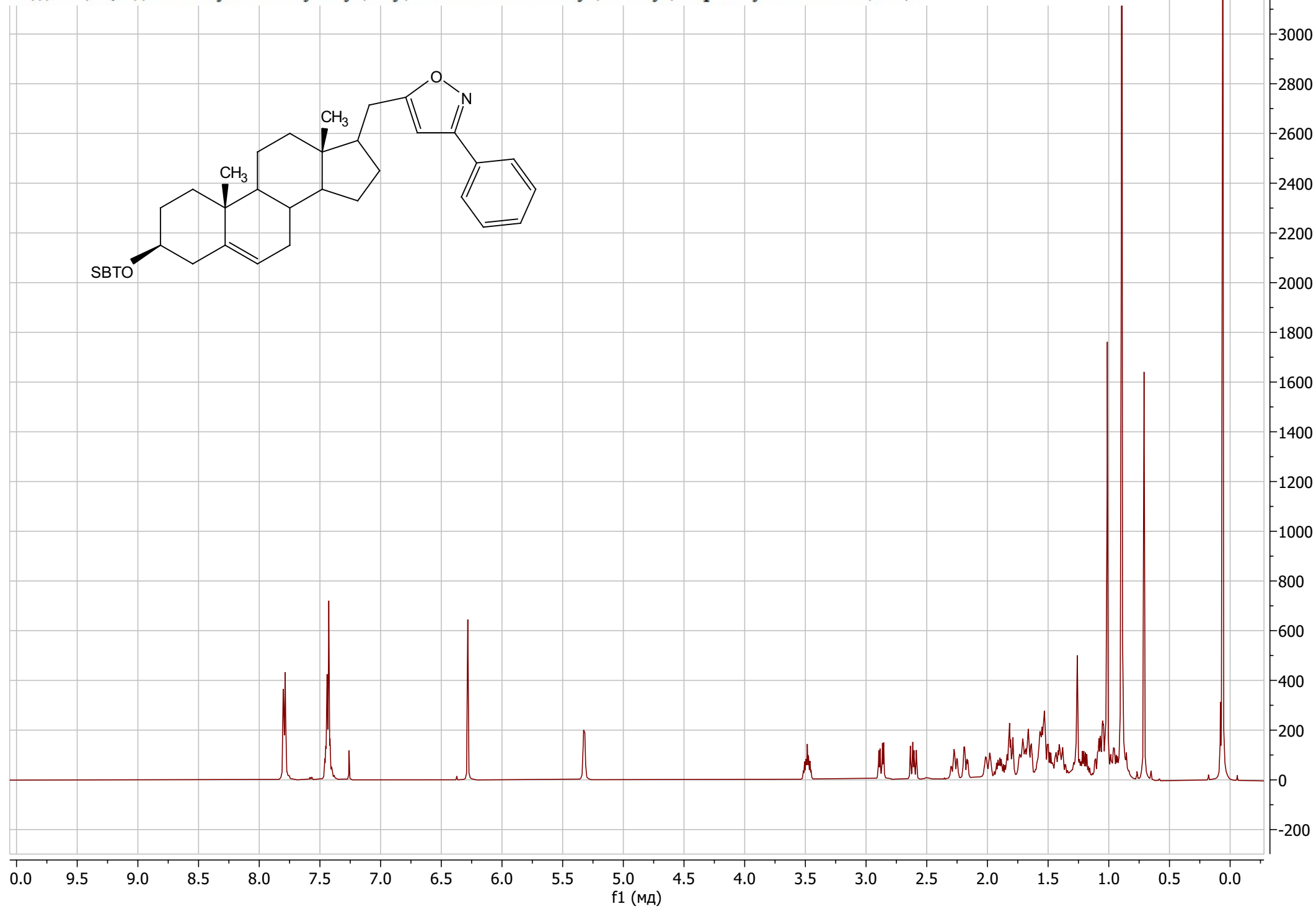
3-Butyl-5-(((17R)-3 β -((*tert*-butyldimethylsilyl)oxy)-androst-5-en-17-yl)methyl)isoxazole (23d)



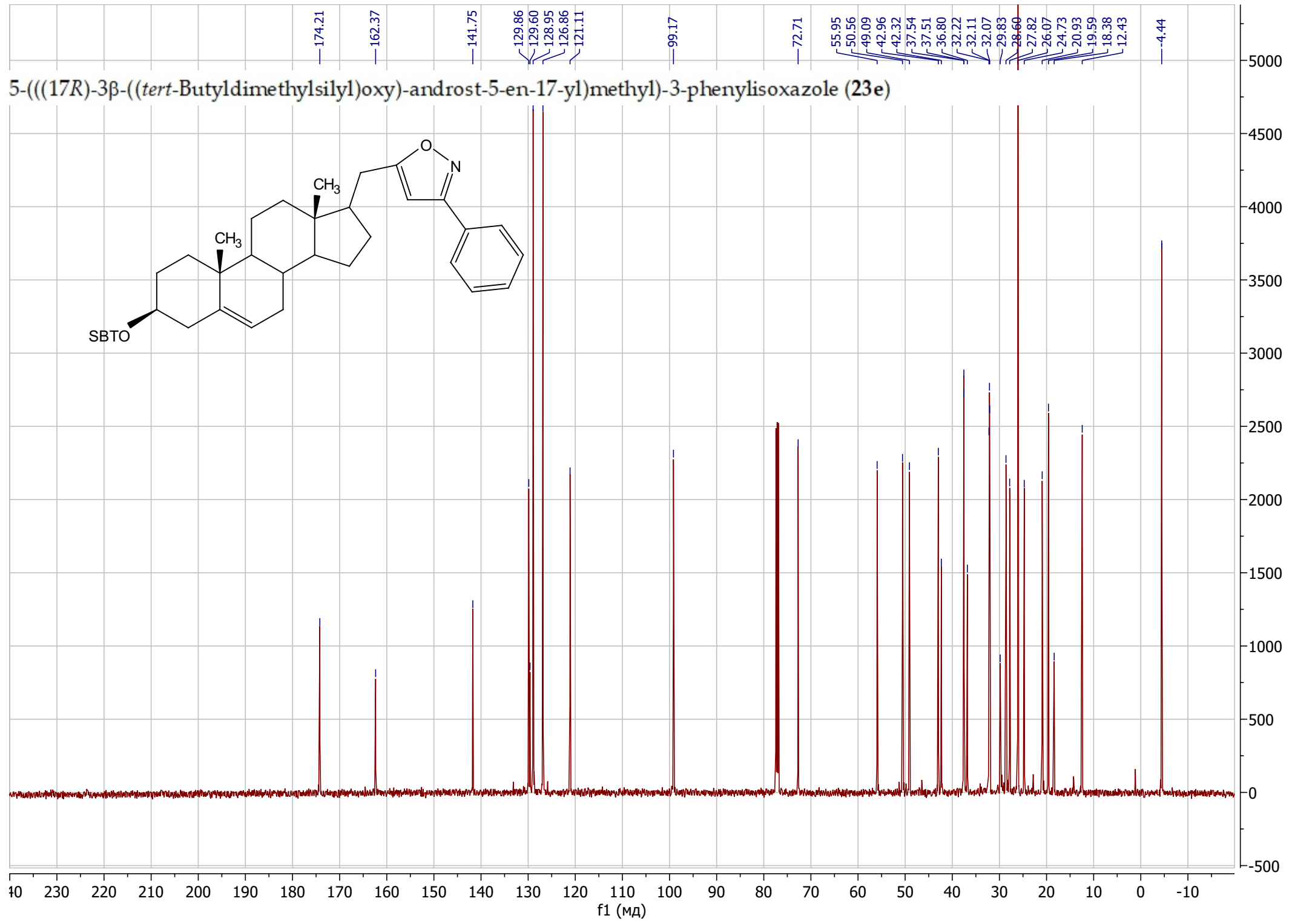
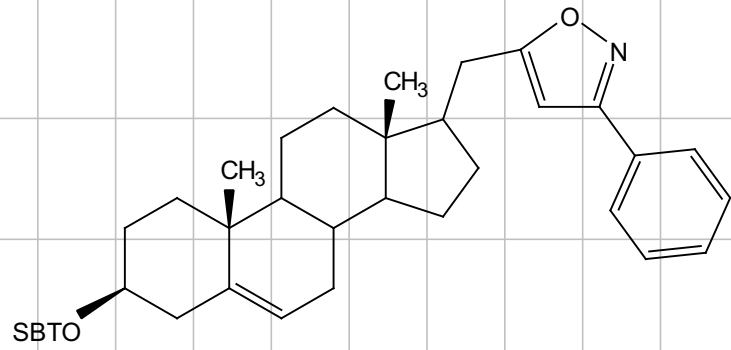
3-Butyl-5-(((17R)-3β-((*tert*-butyldimethylsilyl)oxy)-androst-5-en-17-yl)methyl)isoxazole (23d)



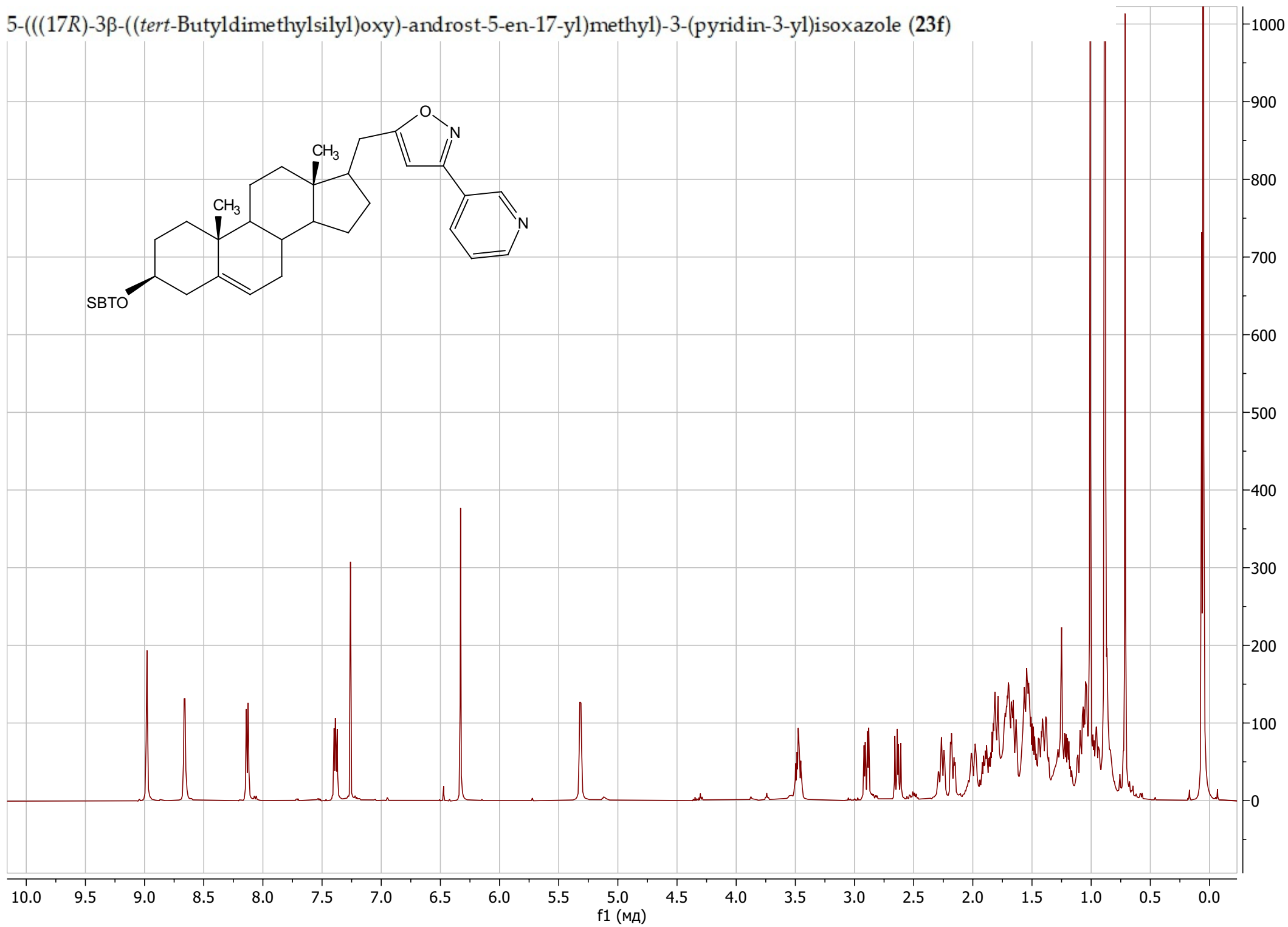
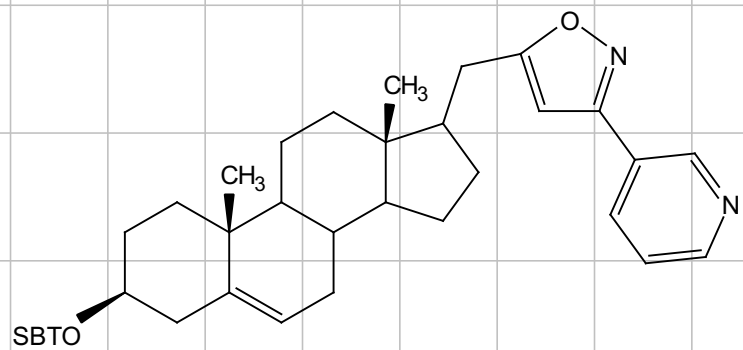
5-(((17R)-3 β -((*tert*-Butyldimethylsilyloxy)-androst-5-en-17-yl)methyl)-3-phenylisoxazole (23e)



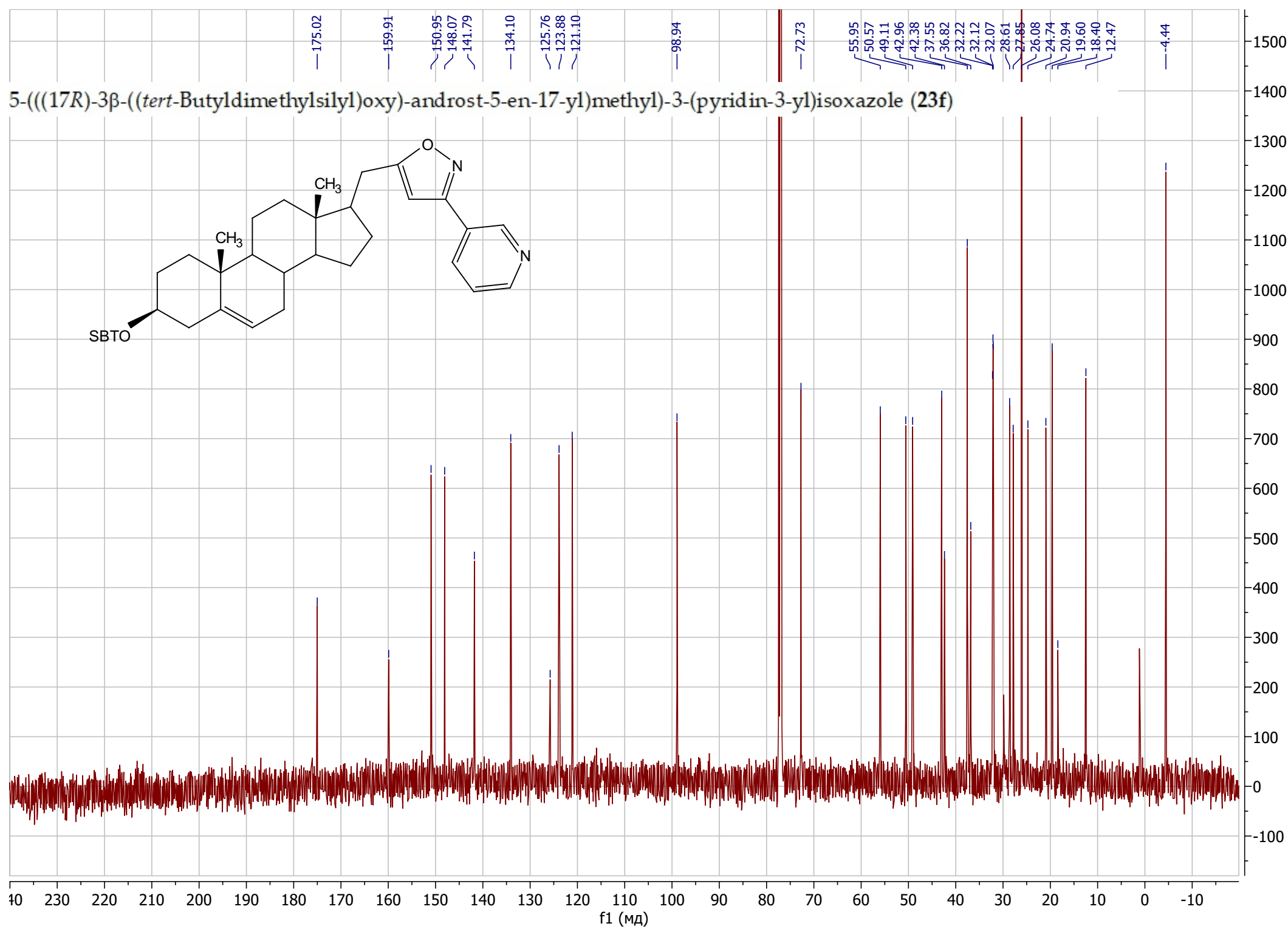
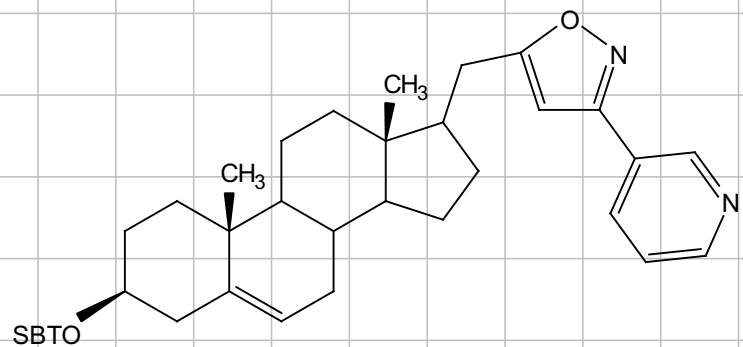
5-(((17R)-3 β -((*tert*-Butyldimethylsilyl)oxy)-androst-5-en-17-yl)methyl)-3-phenylisoxazole (23e)



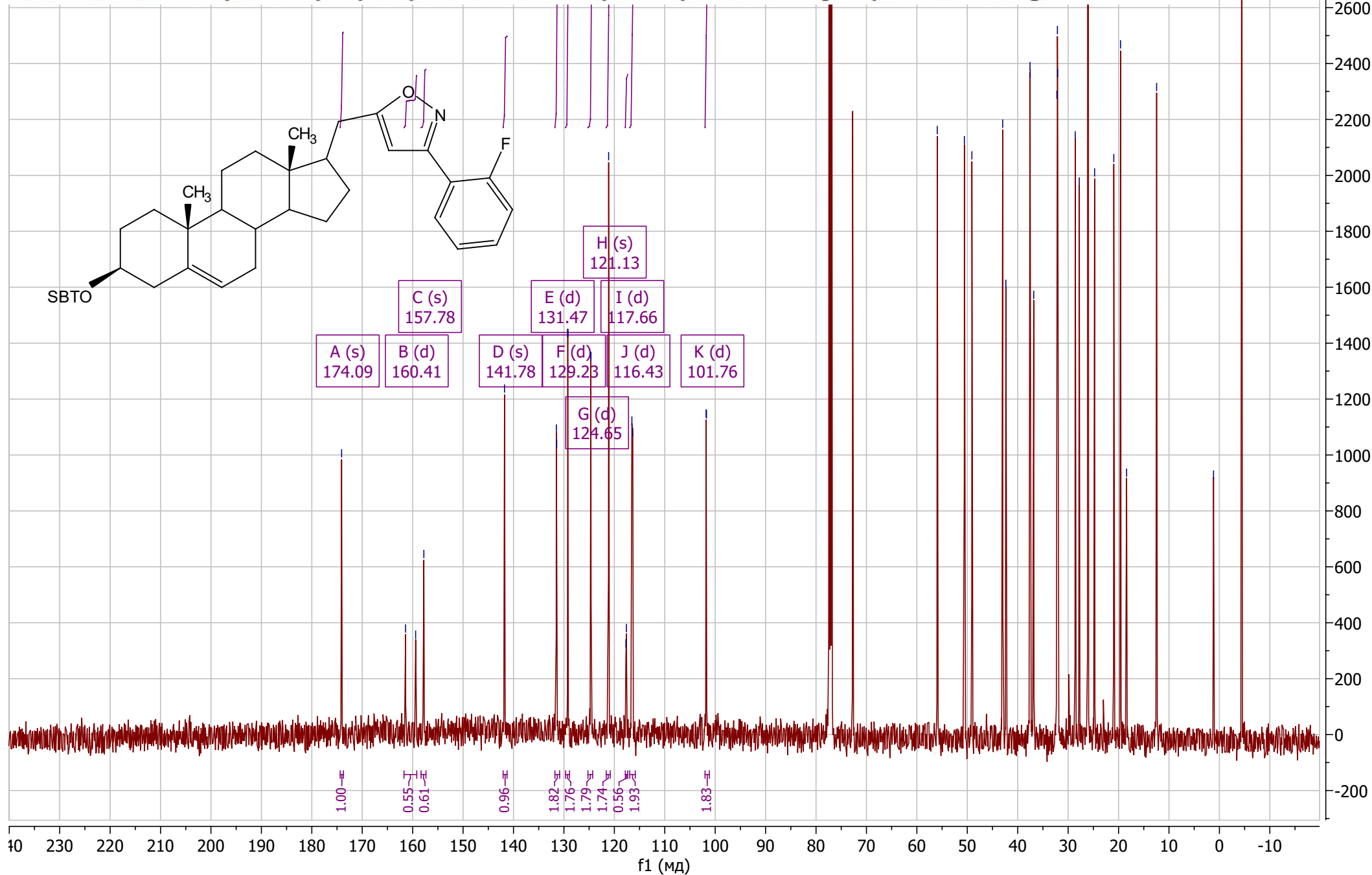
5-(((17R)-3 β -((*tert*-Butyldimethylsilyloxy)-androst-5-en-17-yl)methyl)-3-(pyridin-3-yl)isoxazole (23f)



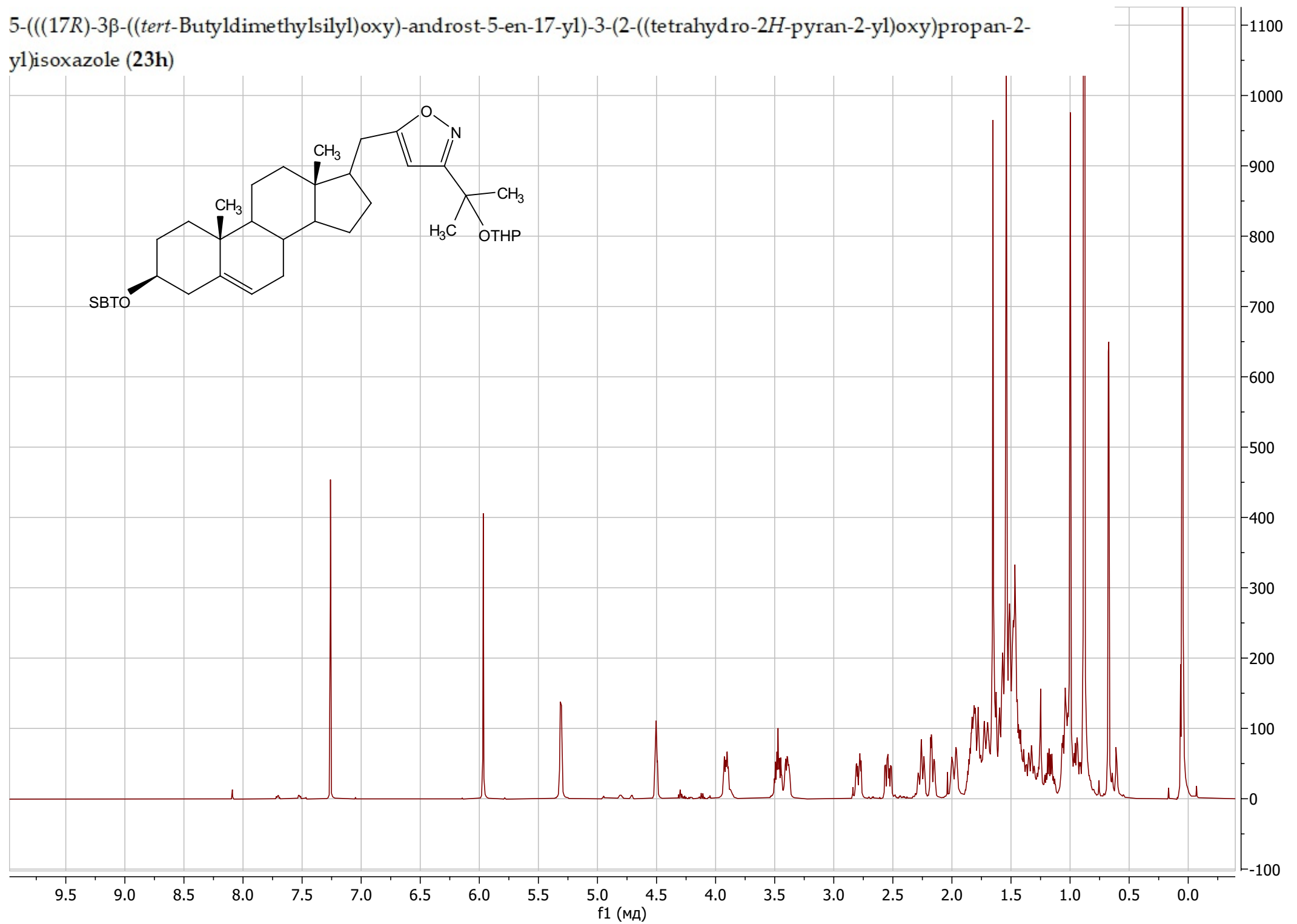
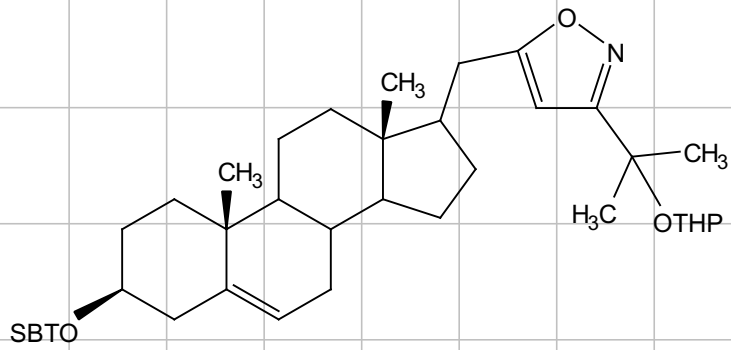
5-(((17R)-3β-((*tert*-Butyldimethylsilyl)oxy)-androst-5-en-17-yl)methyl)-3-(pyridin-3-yl)isoxazole (23f)



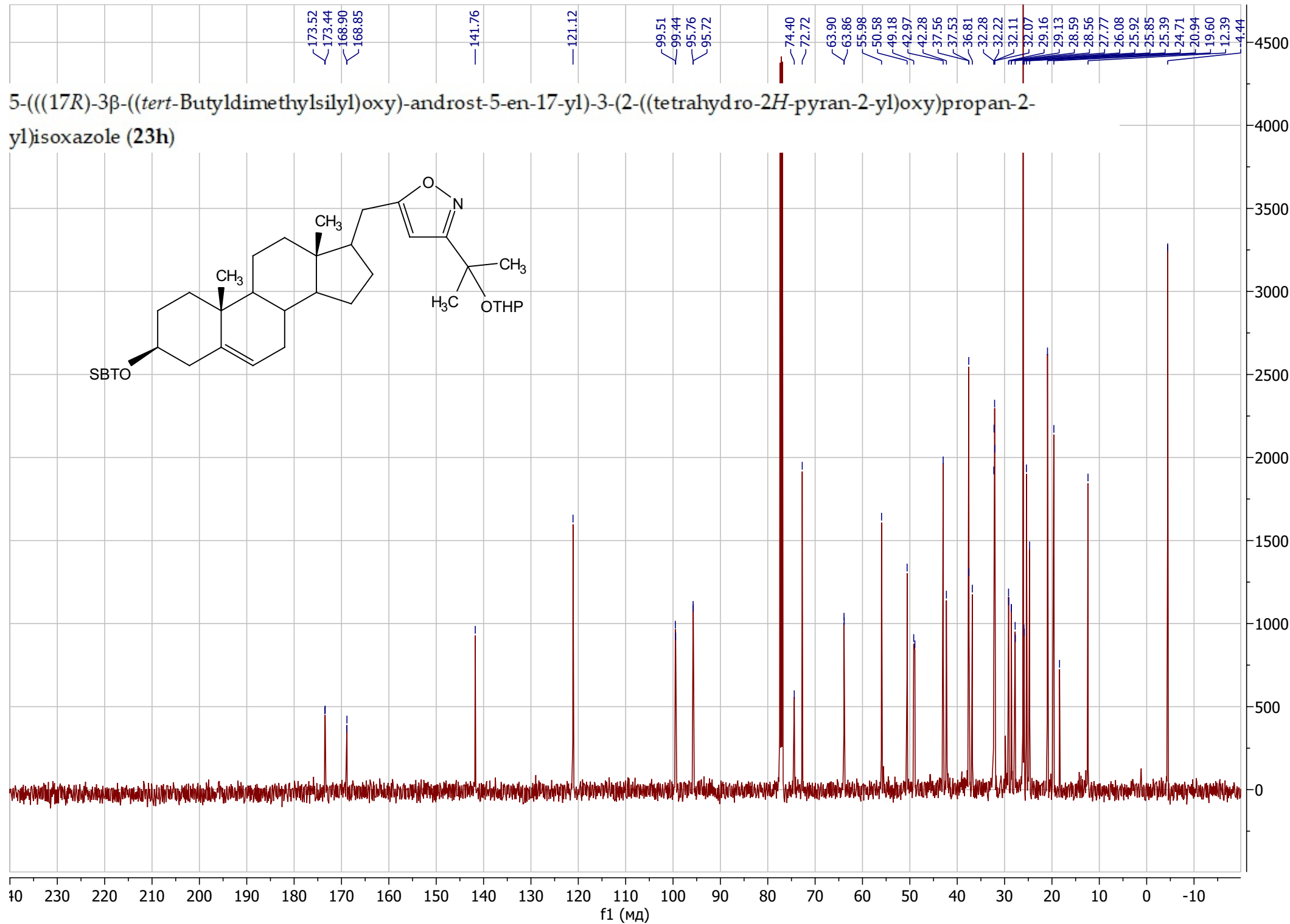
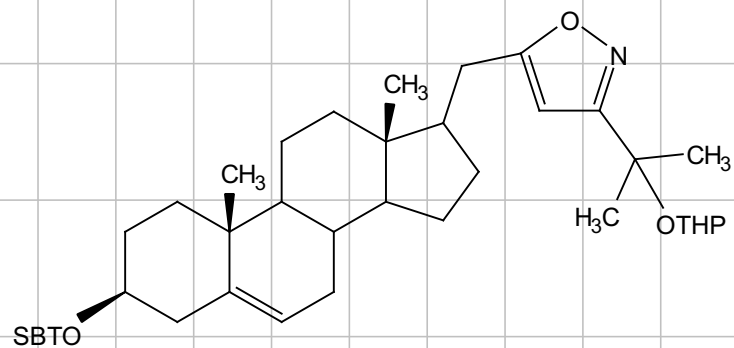
5-(((17R)-3 β -((*tert*-Butyldimethylsilyl)oxy)-androst-5-en-17-yl)methyl)-3-(2-fluorophenyl)isoxazole (23 g)



5-(((17R)-3 β -((*tert*-Butyldimethylsilyl)oxy)-androst-5-en-17-yl)-3-(2-((tetrahydro-2H-pyran-2-yl)oxy)propan-2-yl)isoxazole (23h)

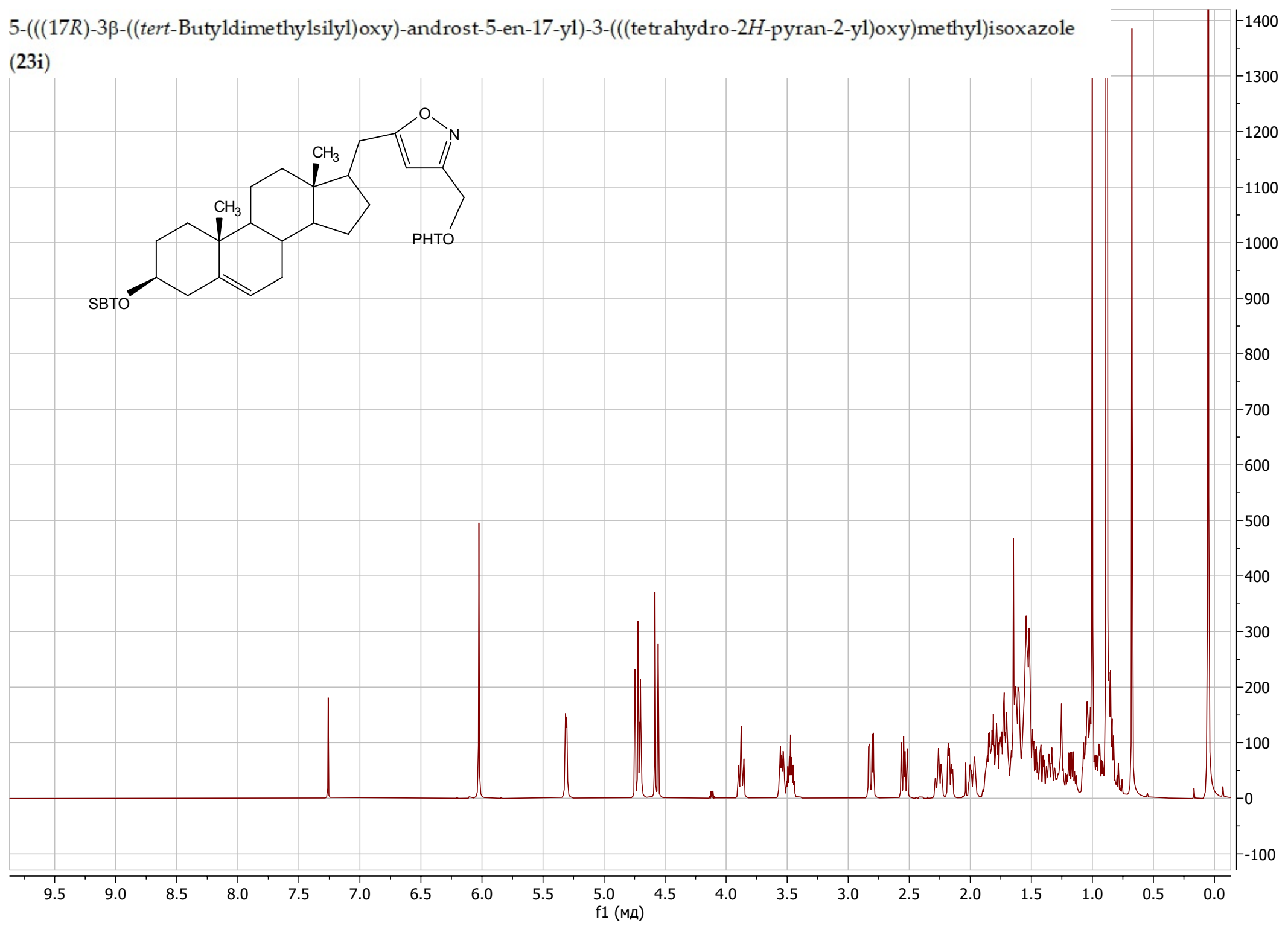
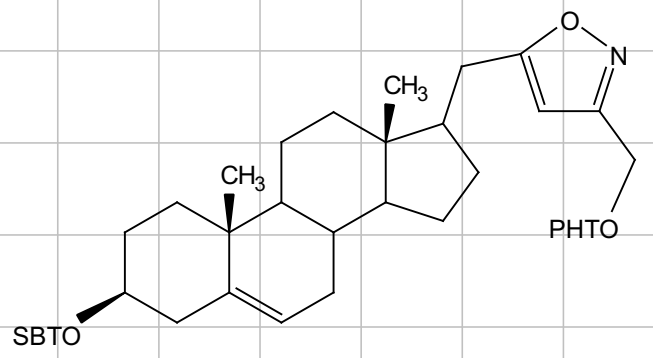


5-(((17R)-3 β -((*tert*-Butyldimethylsilyl)oxy)-androst-5-en-17-yl)-3-(2-((tetrahydro-2H-pyran-2-yl)oxy)propan-2-yl)isoxazole (23h)

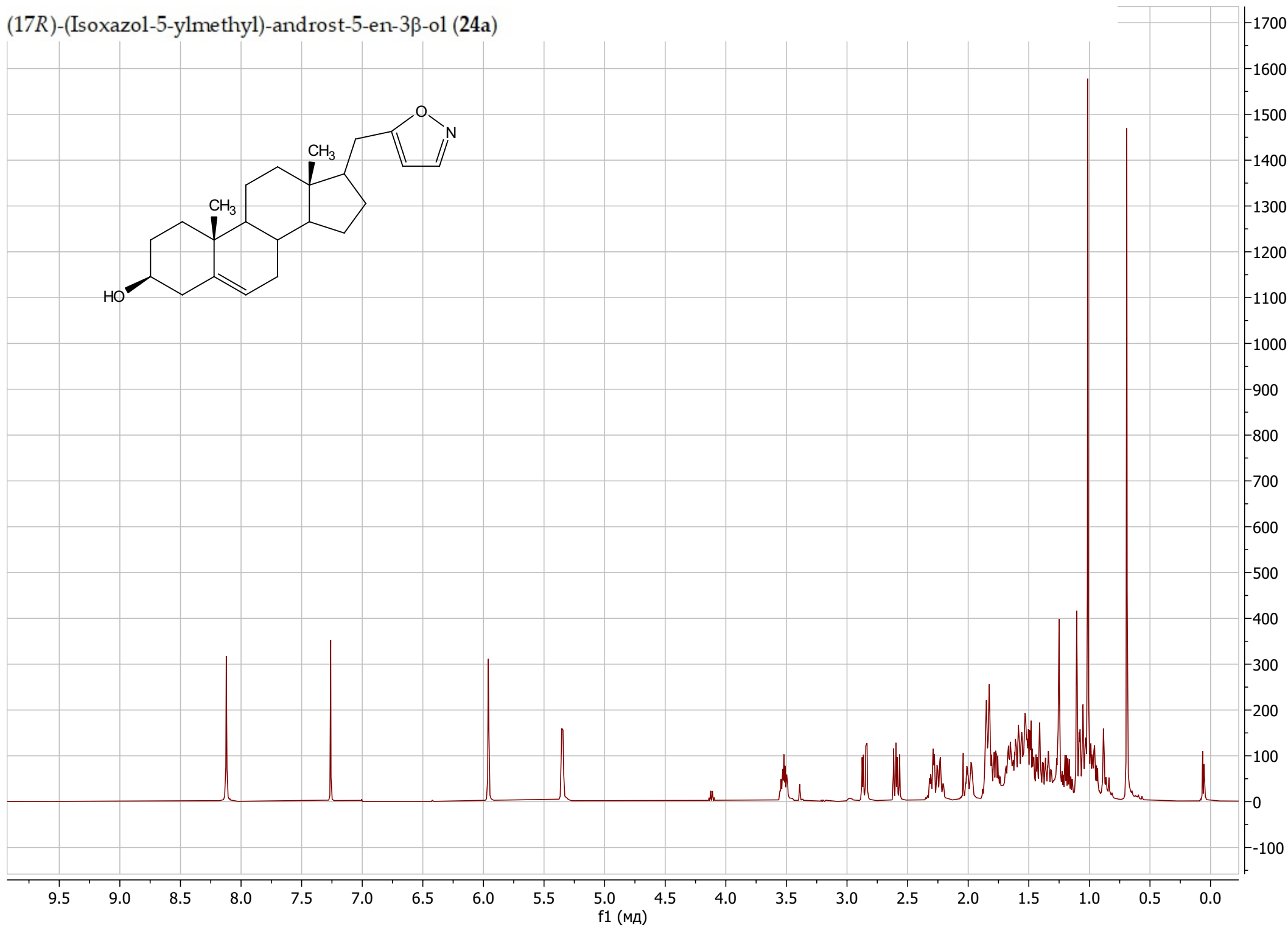
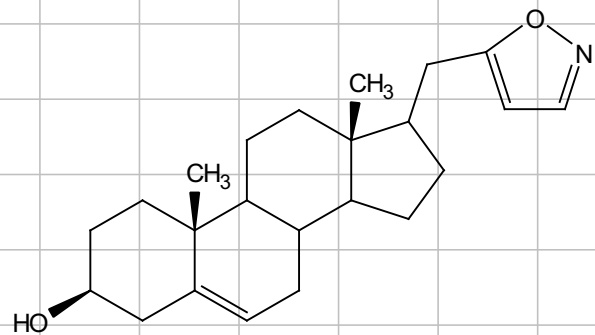


5-(((17R)-3 β -((*tert*-Butyldimethylsilyl)oxy)-androst-5-en-17-yl)-3-(((tetrahydro-2H-pyran-2-yl)oxy)methyl)isoxazole

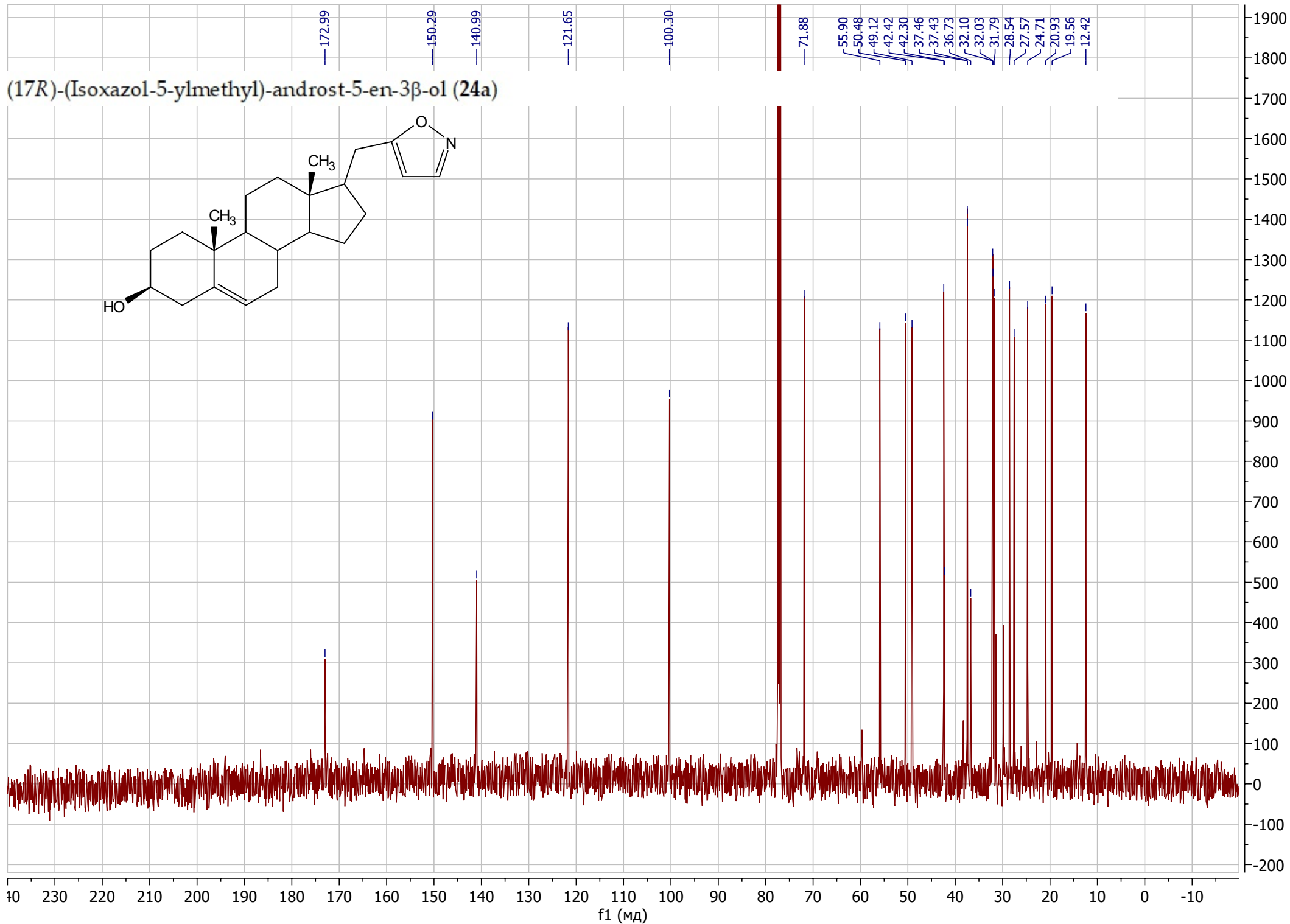
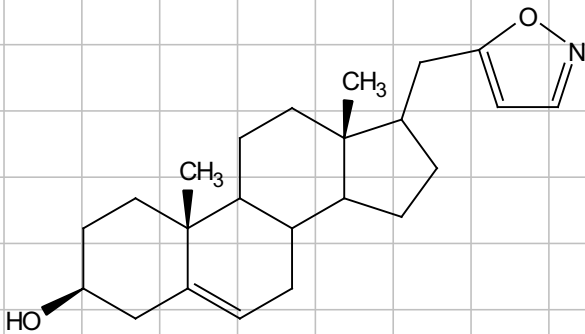
(23i)



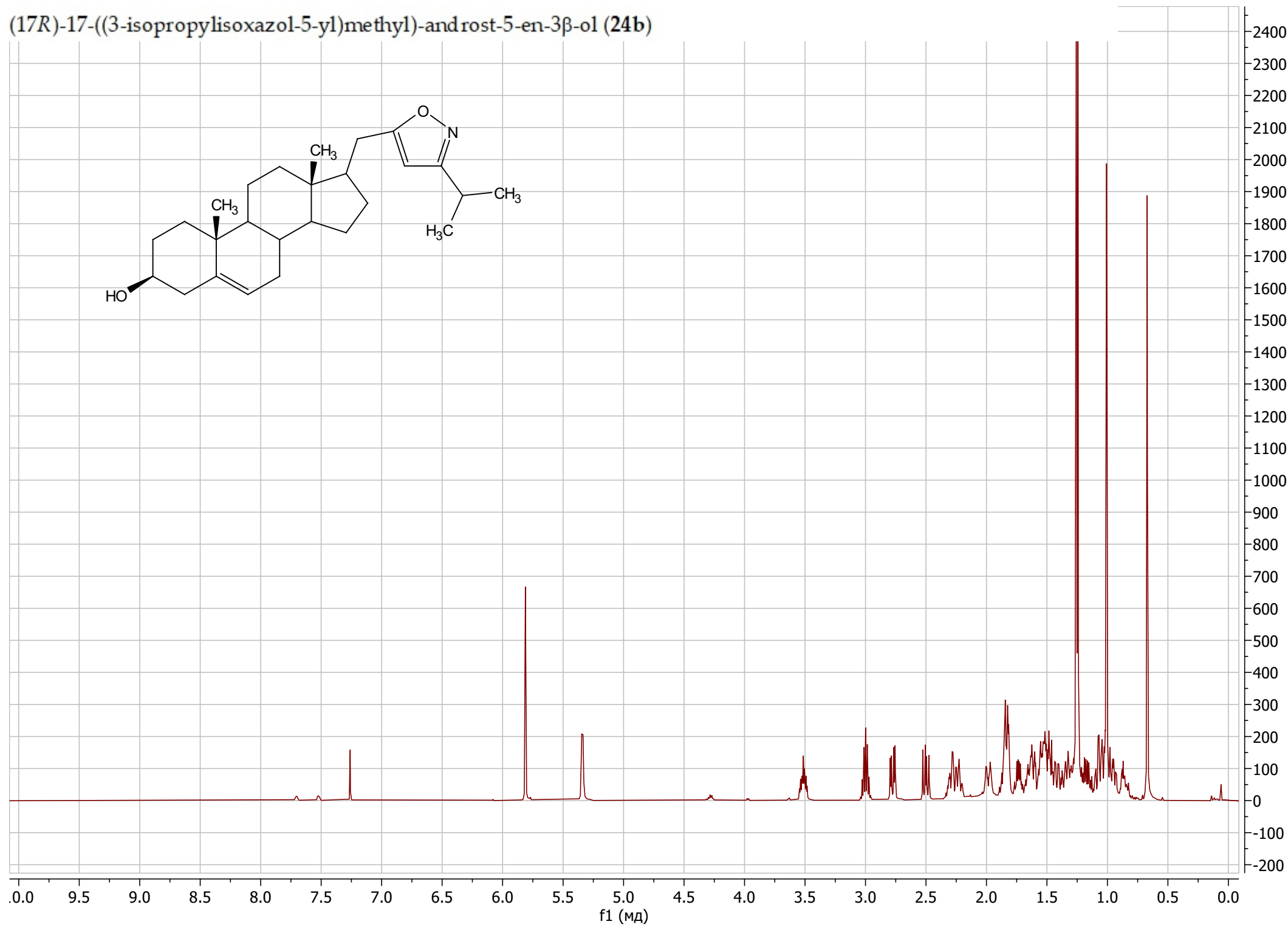
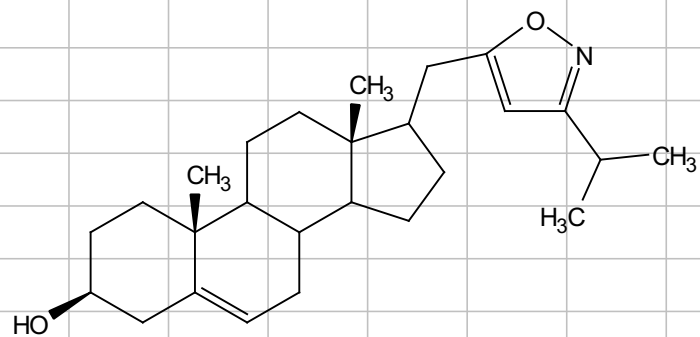
(17R)-(Isoxazol-5-ylmethyl)-androst-5-en-3 β -ol (24a)



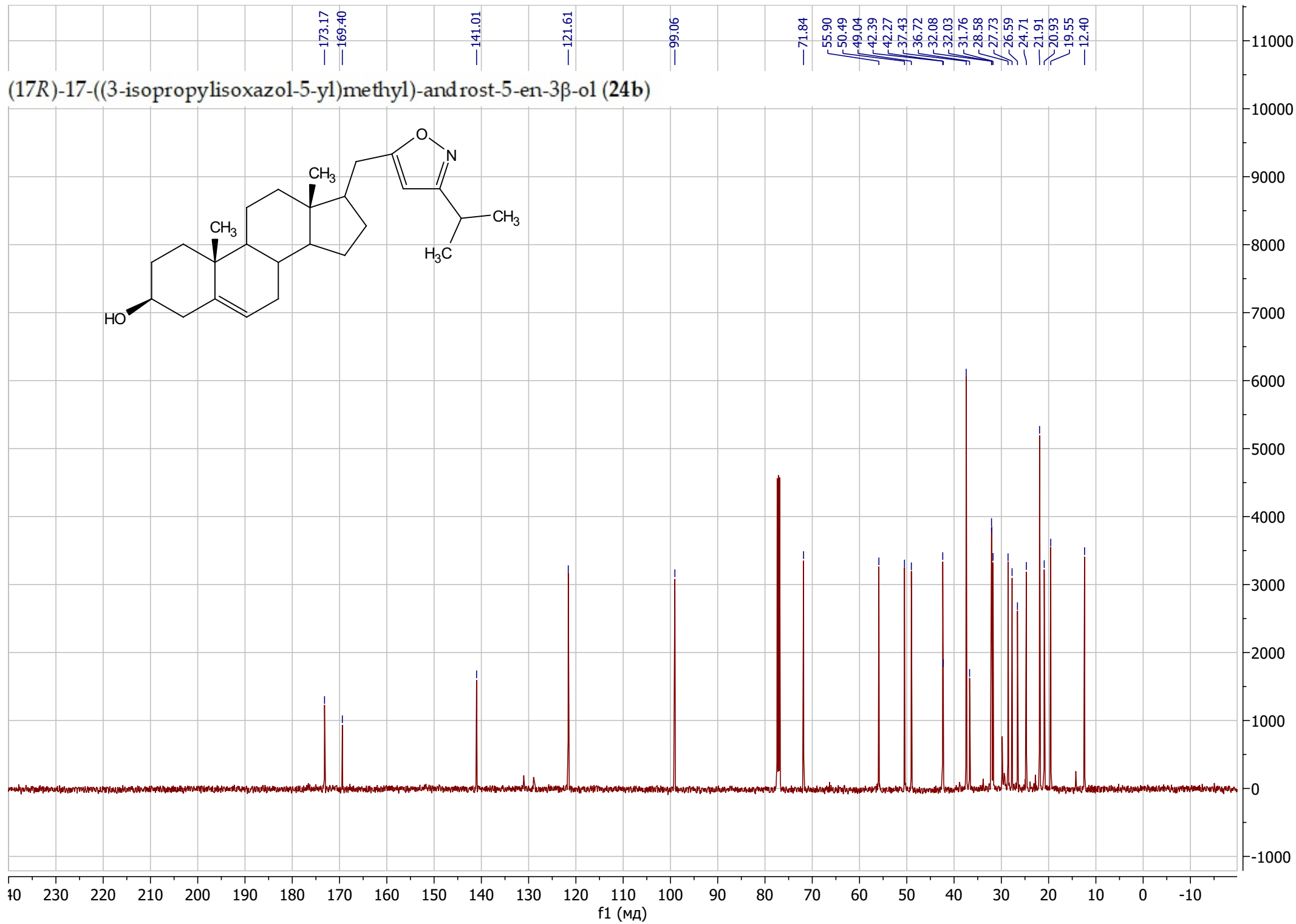
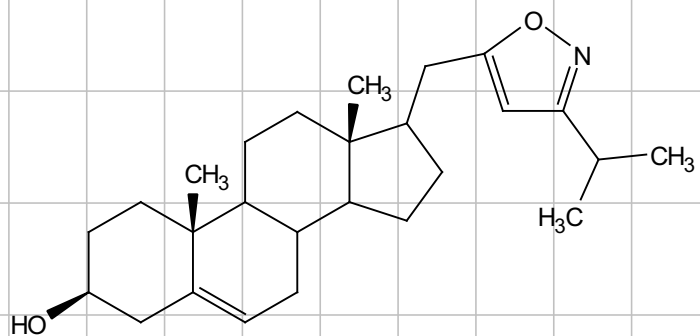
(17R)-(Isoxazol-5-ylmethyl)-androst-5-en-3 β -ol (24a)



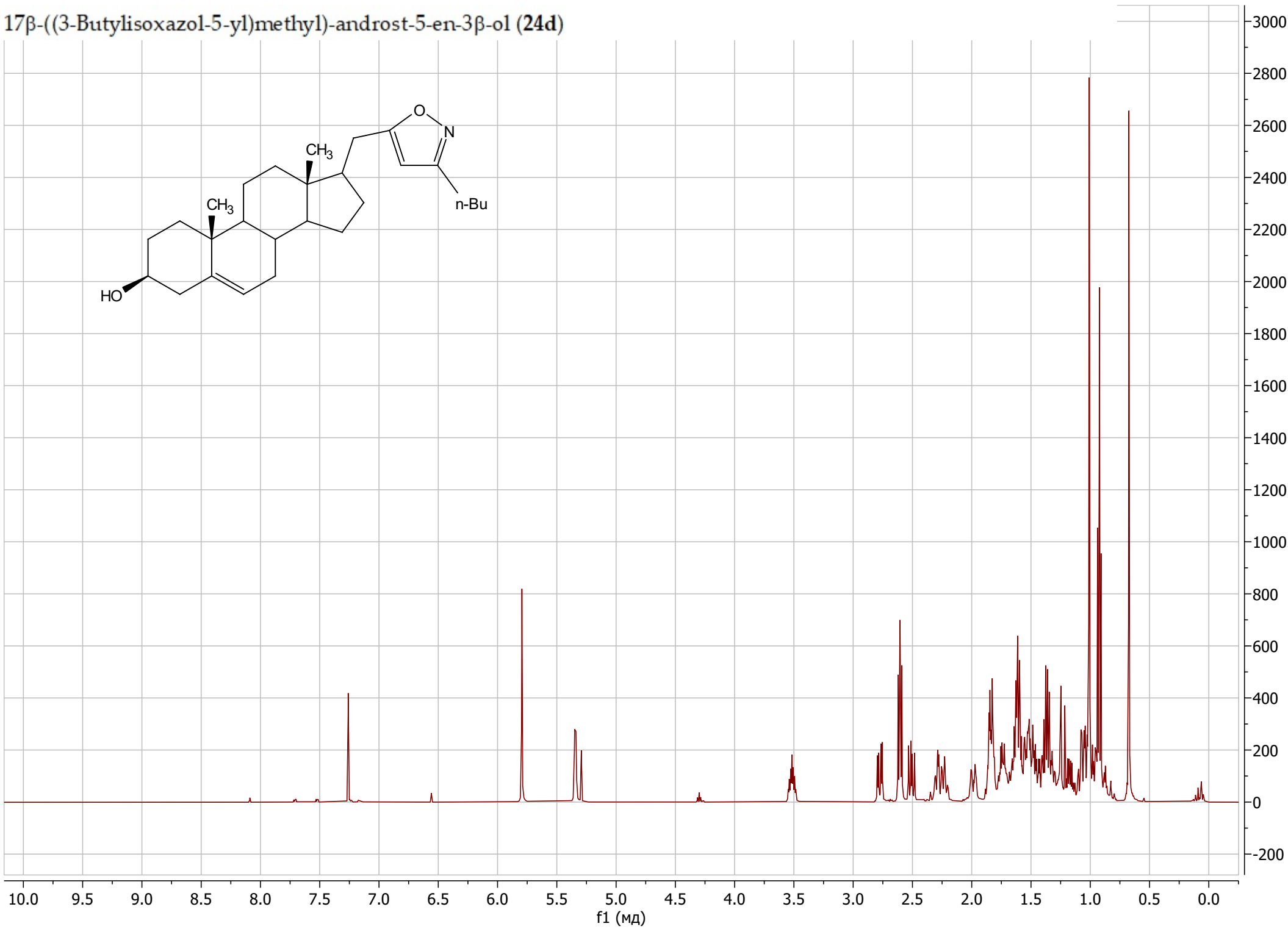
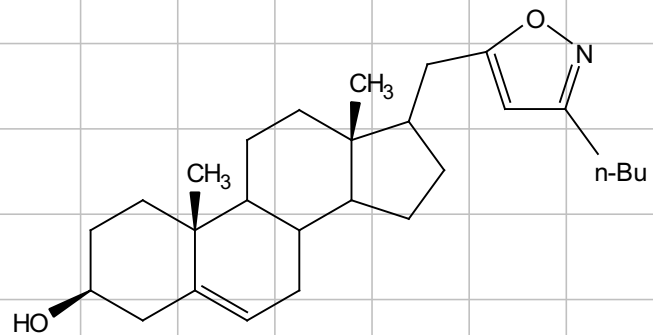
(17R)-17-((3-isopropylisoxazol-5-yl)methyl)-androst-5-en-3 β -ol (24b)



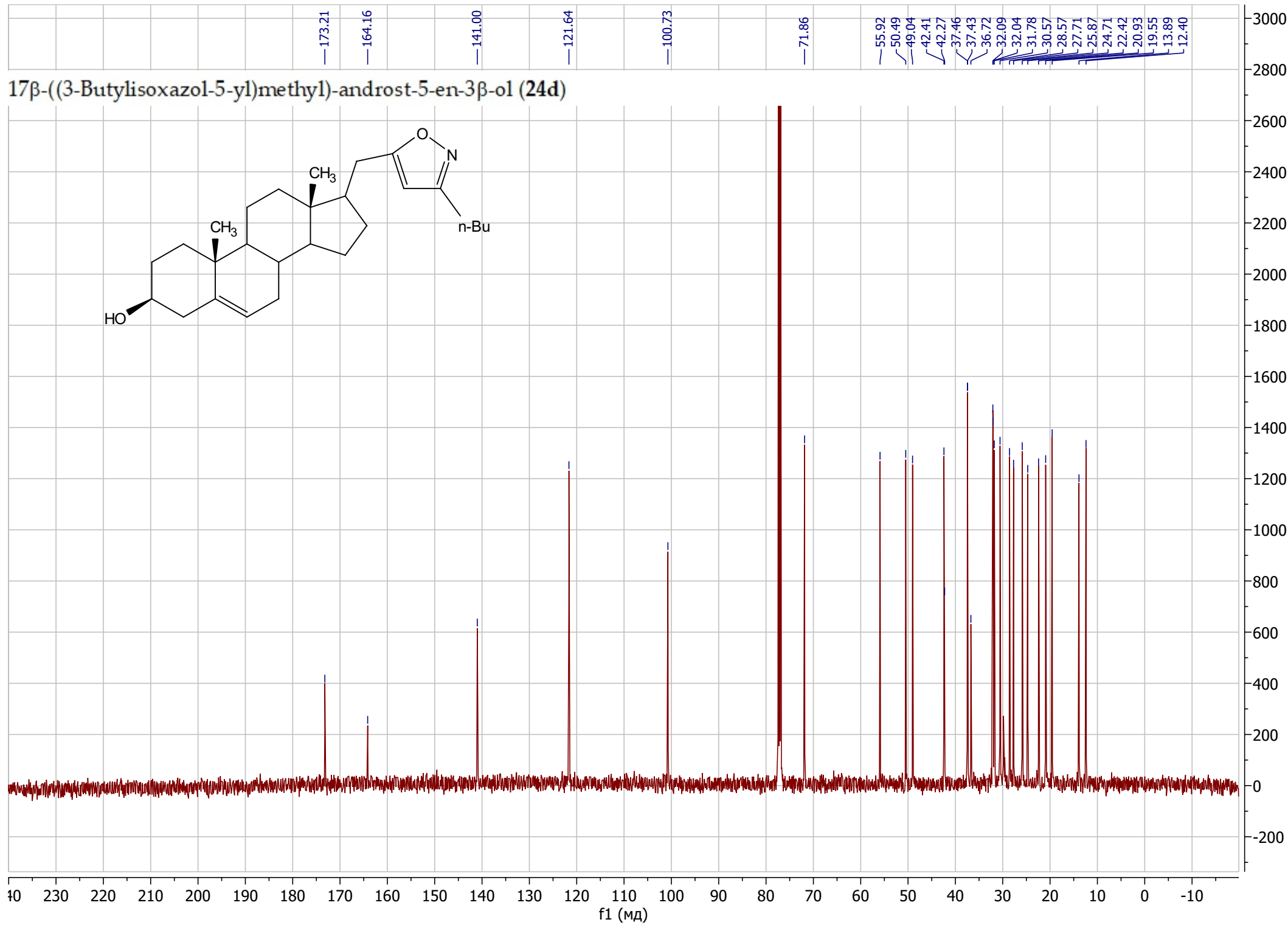
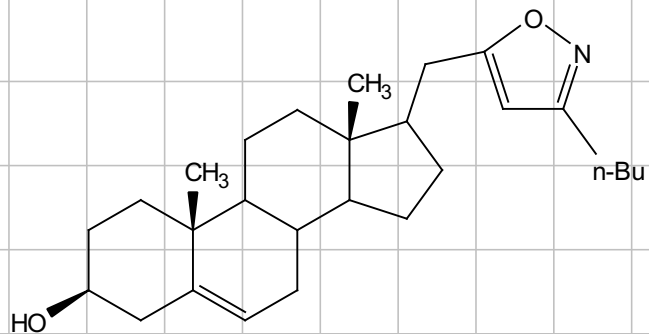
(17R)-17-((3-isopropylisoxazol-5-yl)methyl)-androst-5-en-3 β -ol (24b)



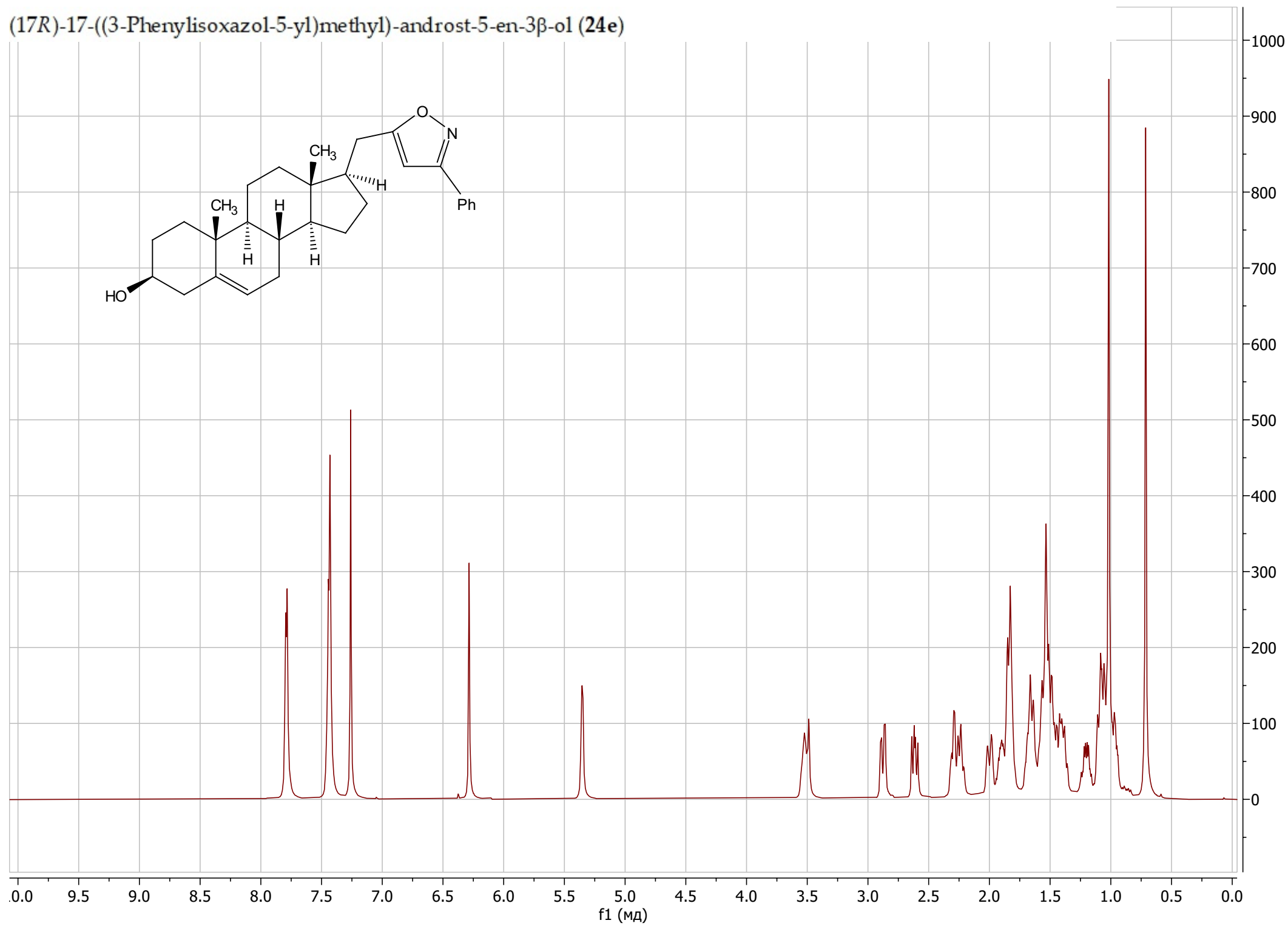
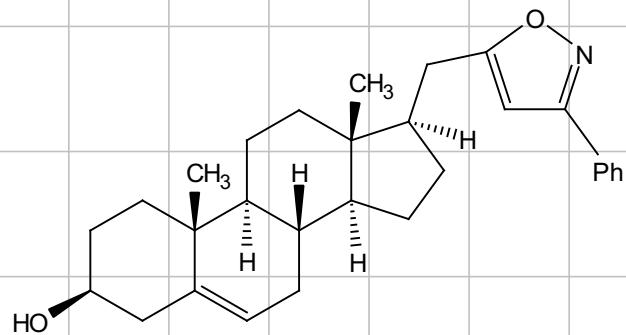
17 β -((3-Butylisoxazol-5-yl)methyl)-androst-5-en-3 β -ol (24d)



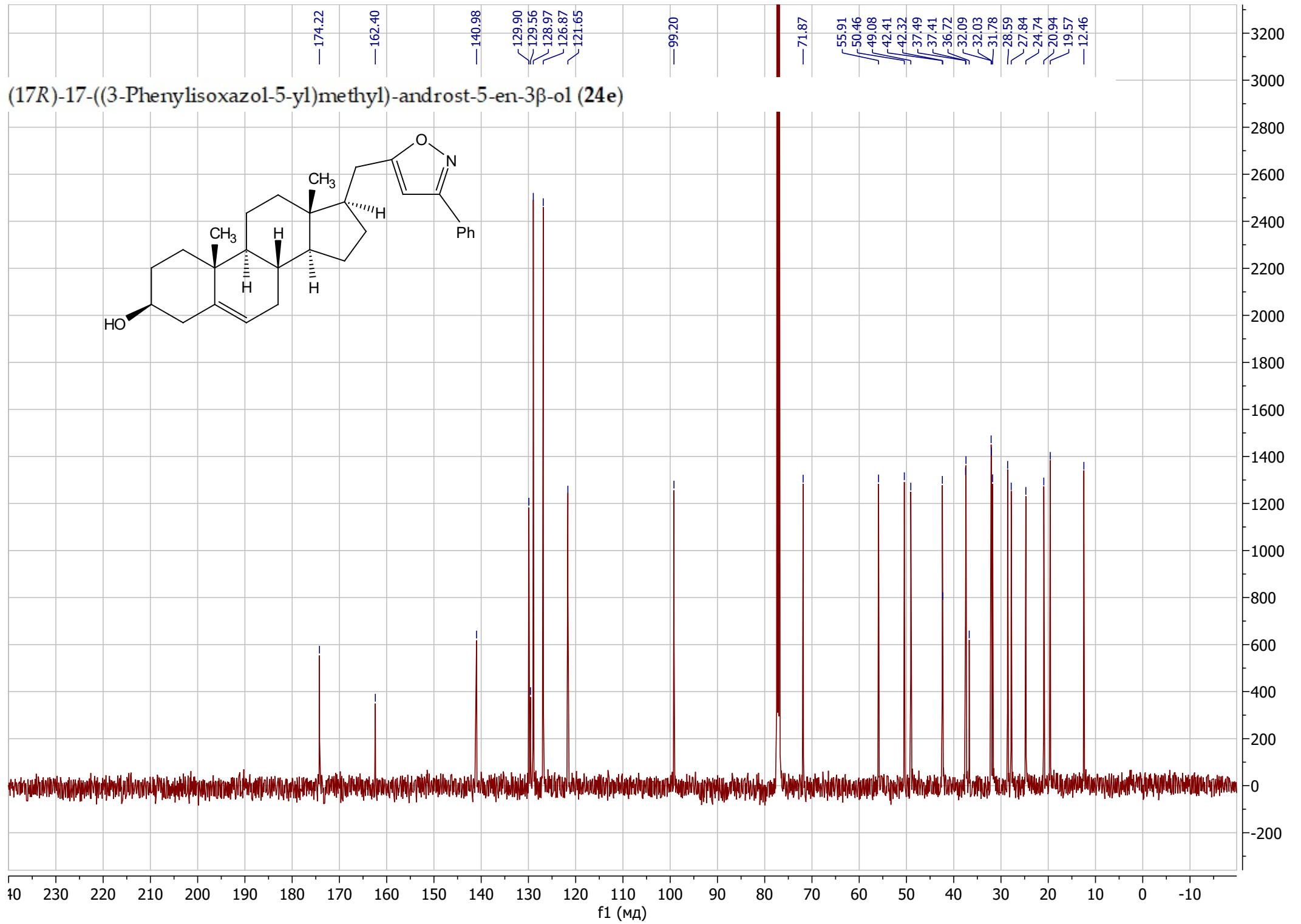
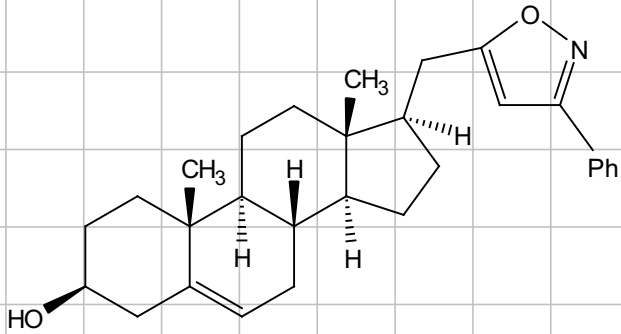
17β-((3-Butylisoxazol-5-yl)methyl)-androst-5-en-3β-ol (24d)



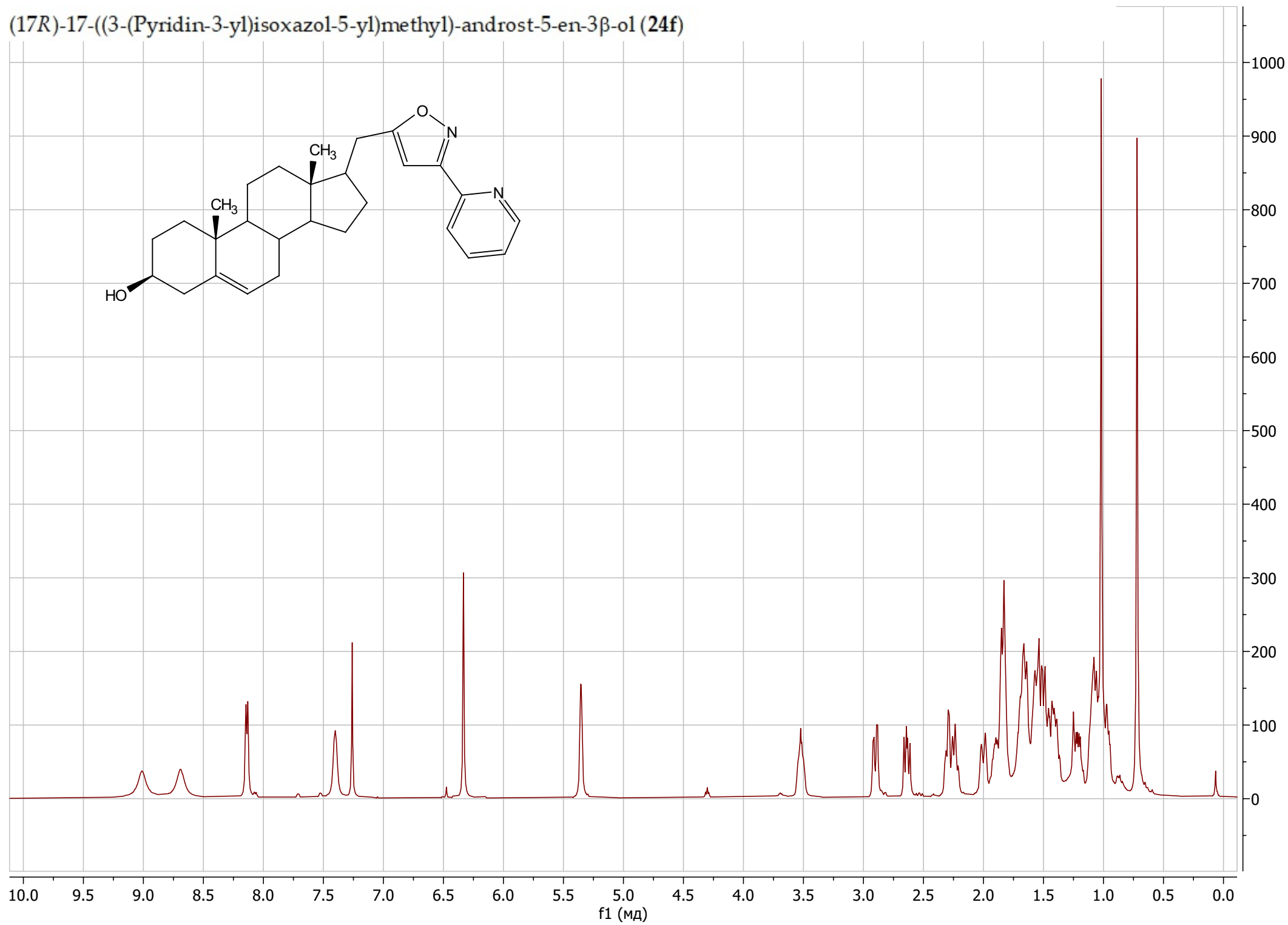
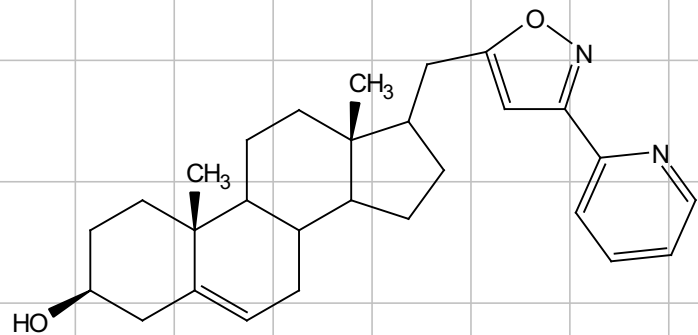
(17R)-17-((3-Phenylisoxazol-5-yl)methyl)-androst-5-en-3 β -ol (24e)



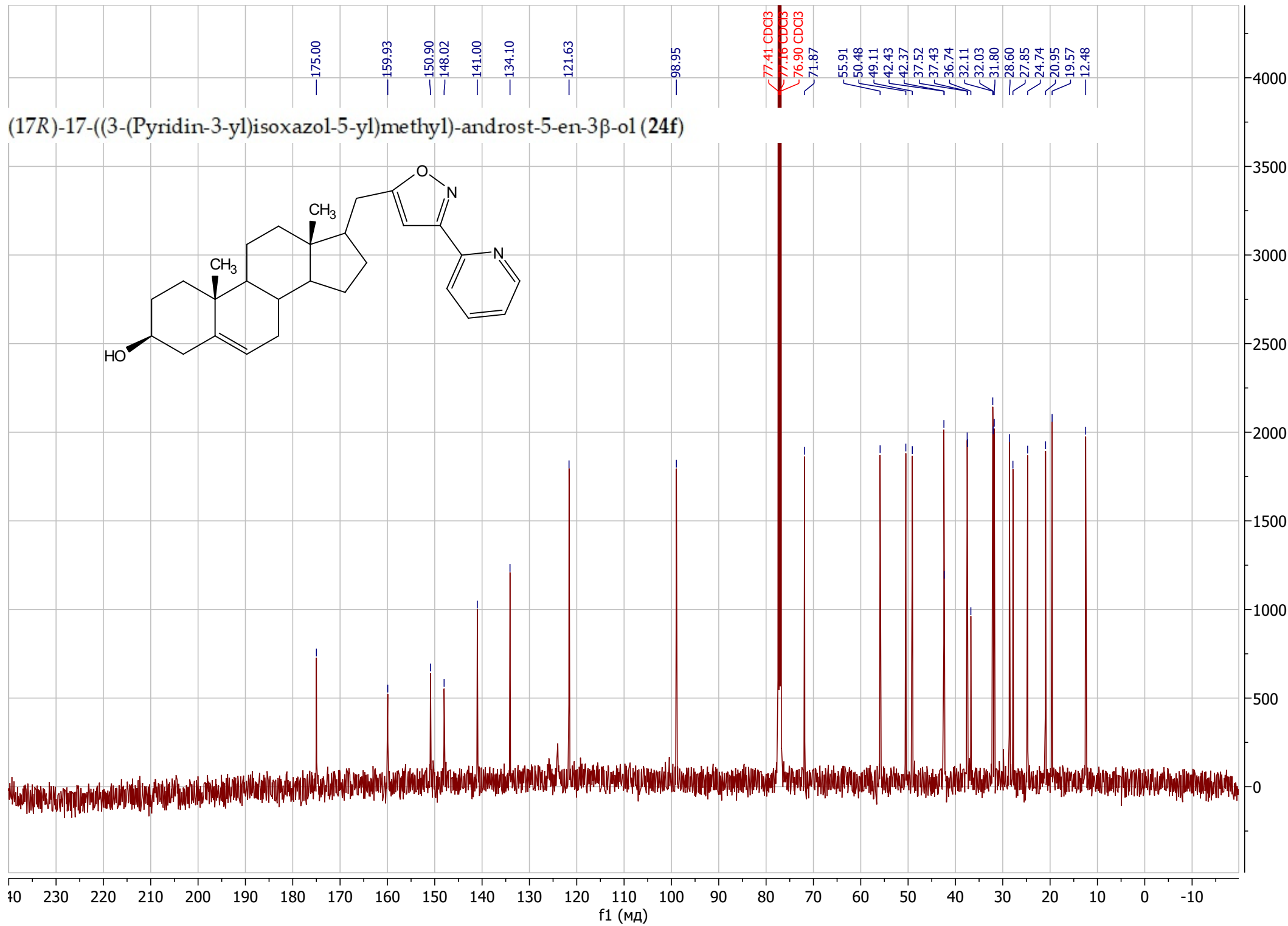
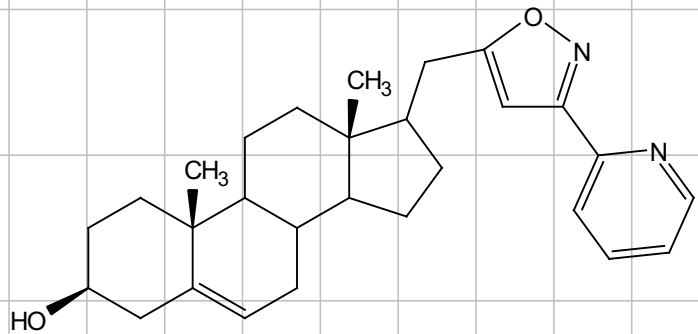
(17R)-17-((3-Phenylisoxazol-5-yl)methyl)-androst-5-en-3 β -ol (24e)



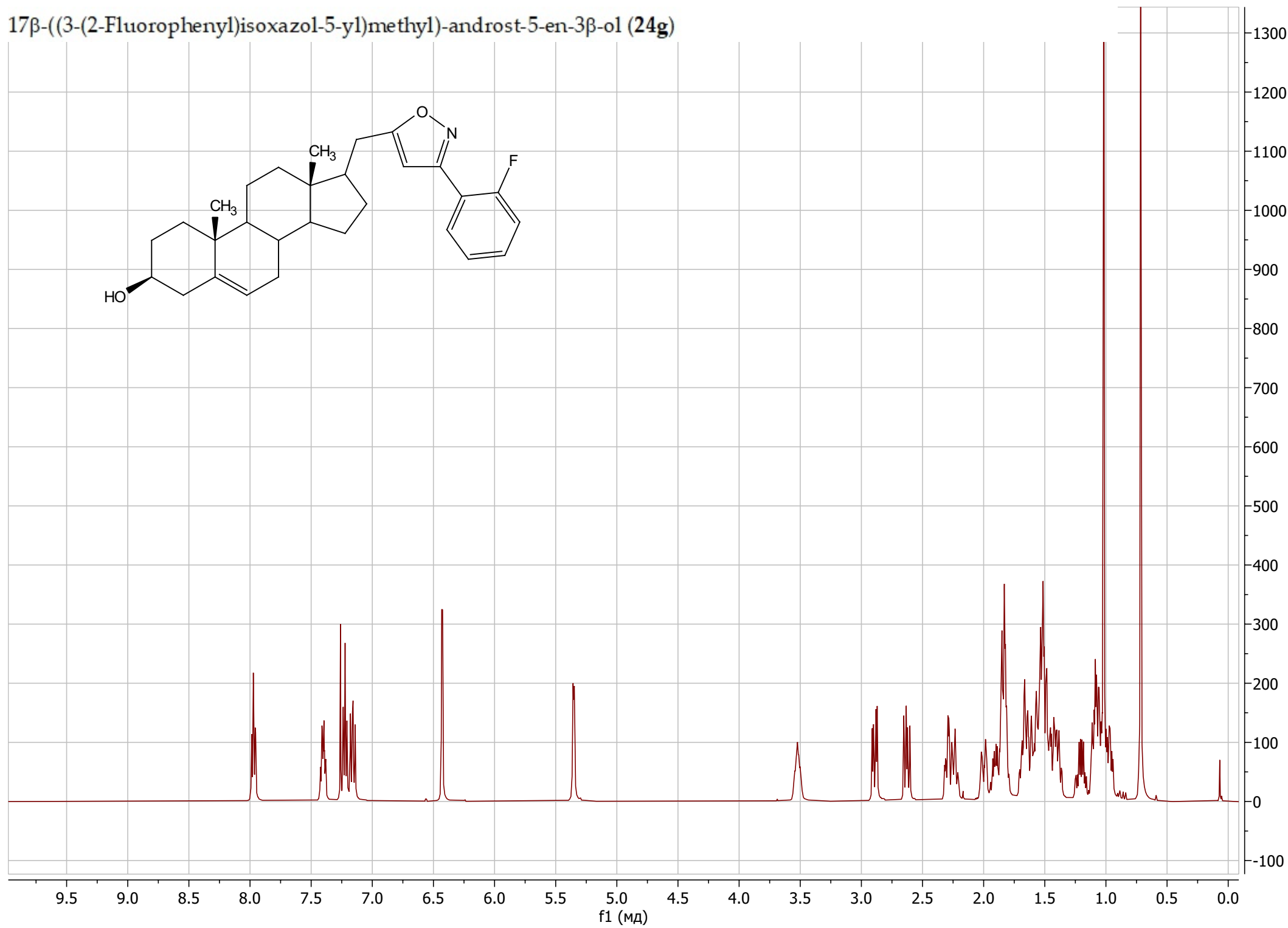
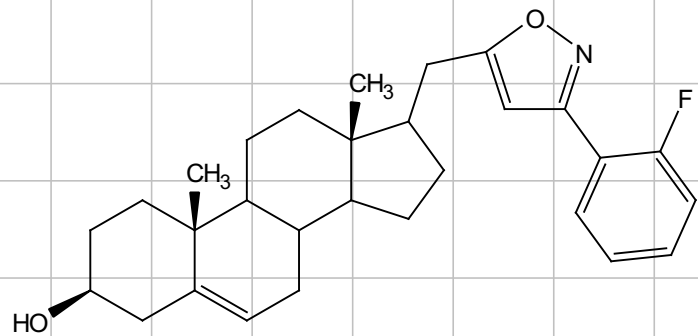
(17R)-17-((3-(Pyridin-3-yl)isoxazol-5-yl)methyl)-androst-5-en-3 β -ol (24f)



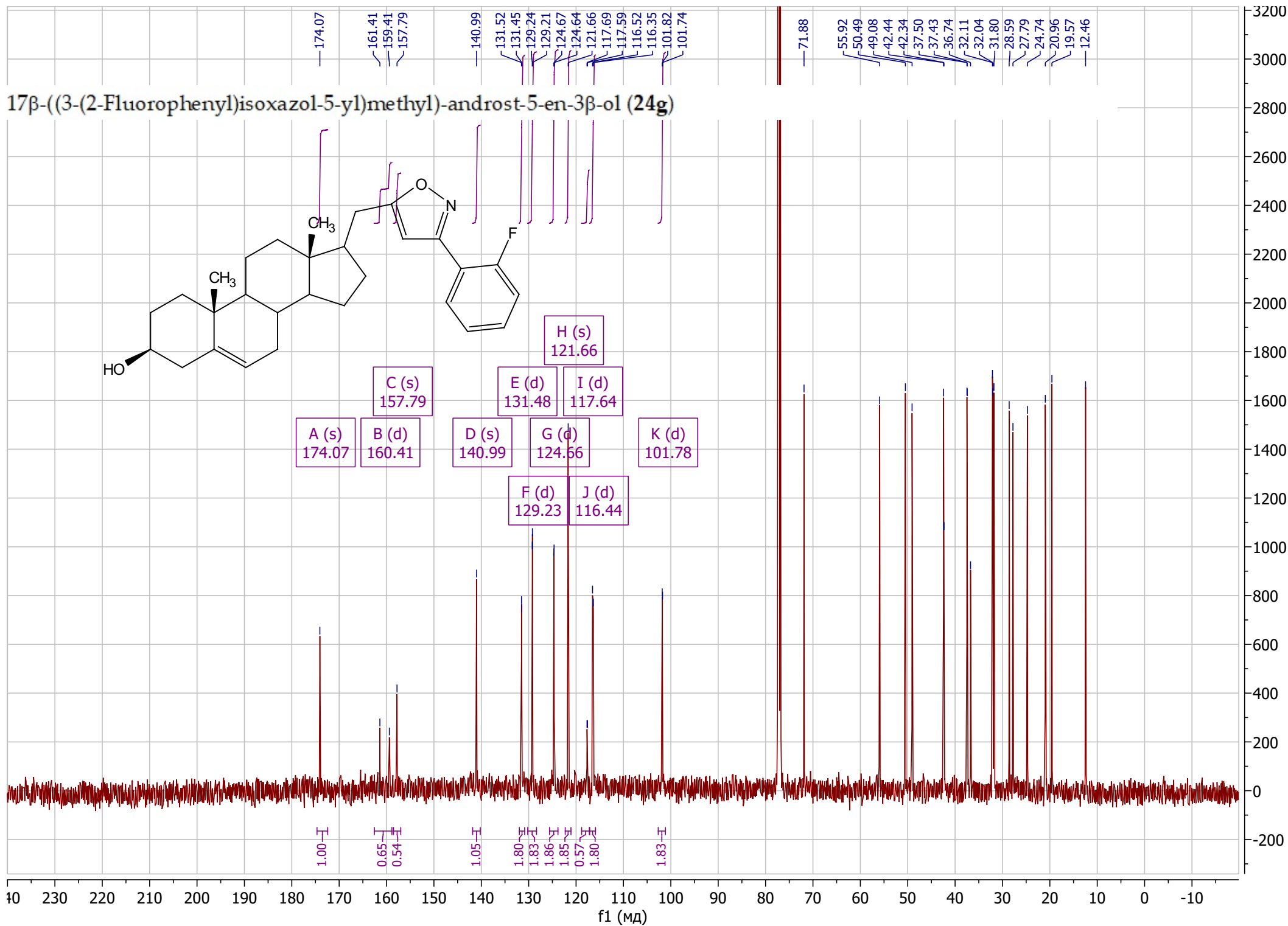
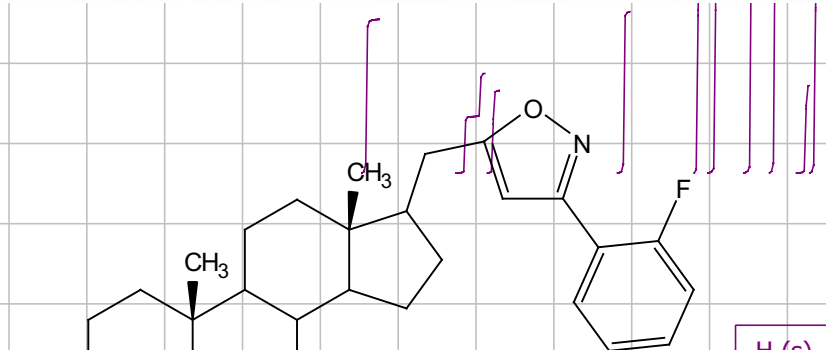
(17R)-17-((3-(Pyridin-3-yl)isoxazol-5-yl)methyl)-androst-5-en-3 β -ol (24f)



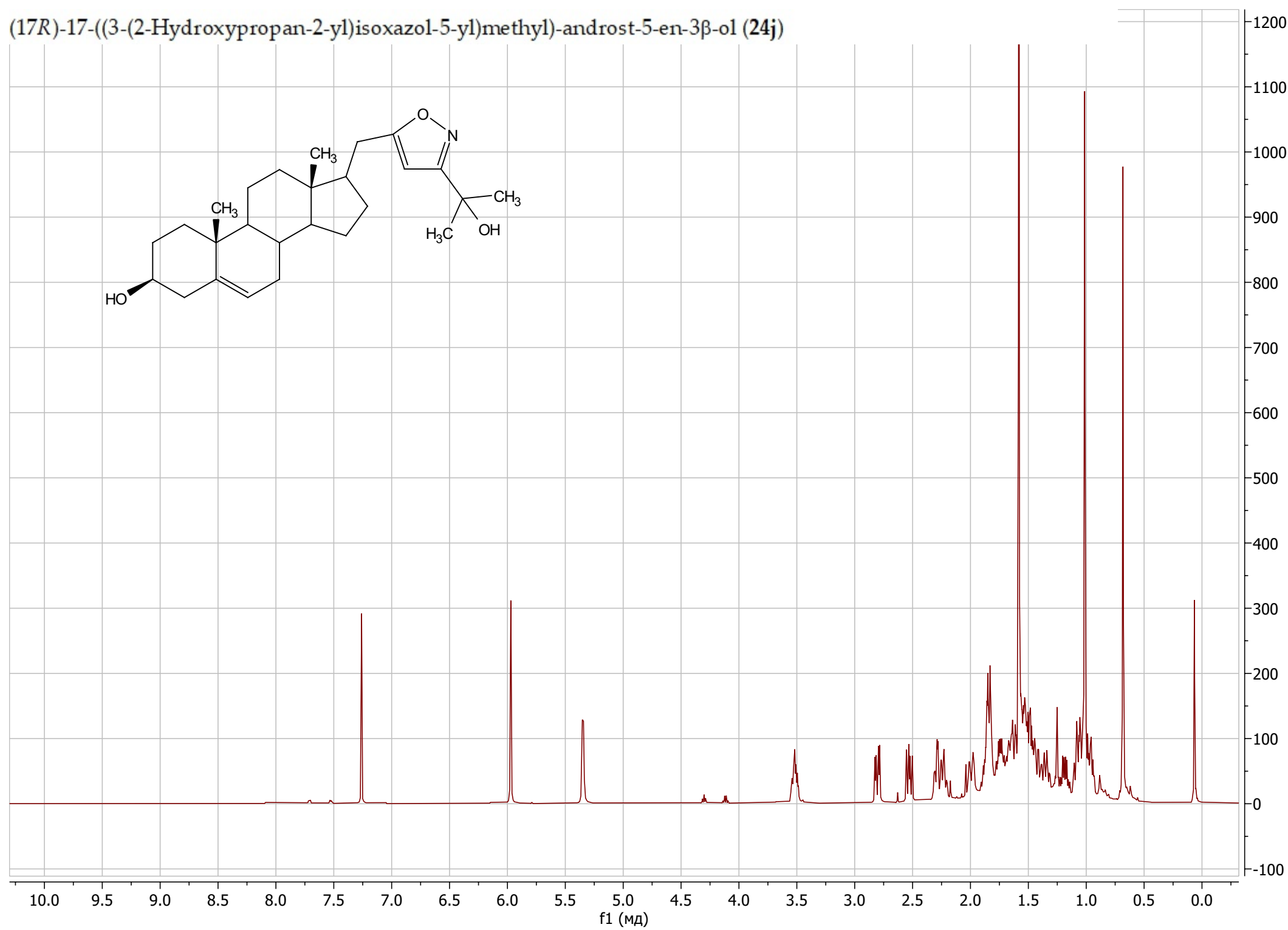
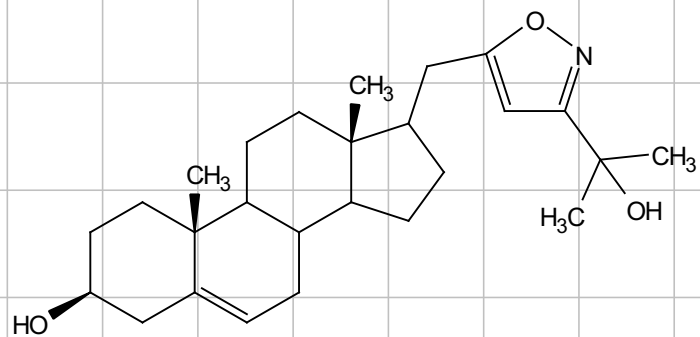
17 β -((3-(2-Fluorophenyl)isoxazol-5-yl)methyl)-androst-5-en-3 β -ol (24g)



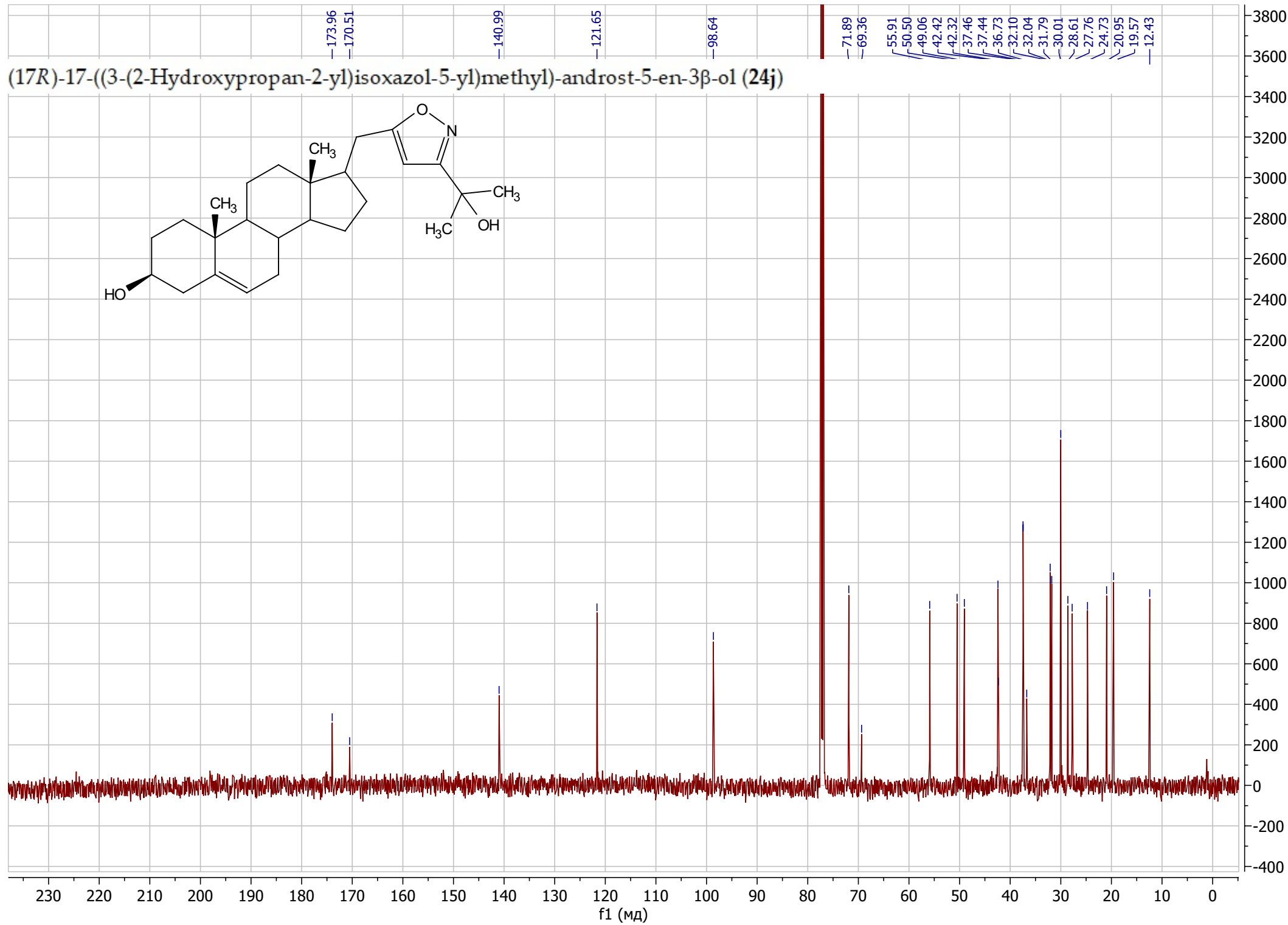
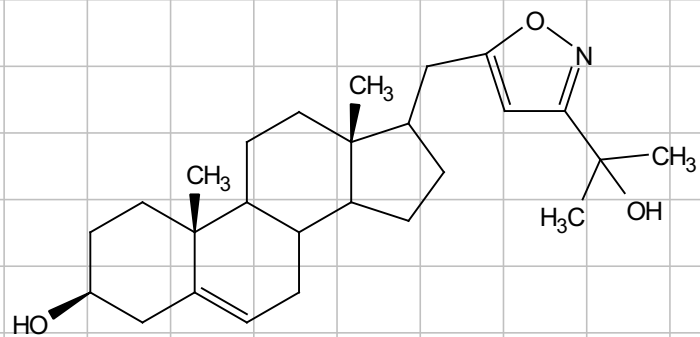
17β-(3-(2-Fluorophenyl)isoxazol-5-yl)methyl)-androst-5-en-3β-ol (24g)



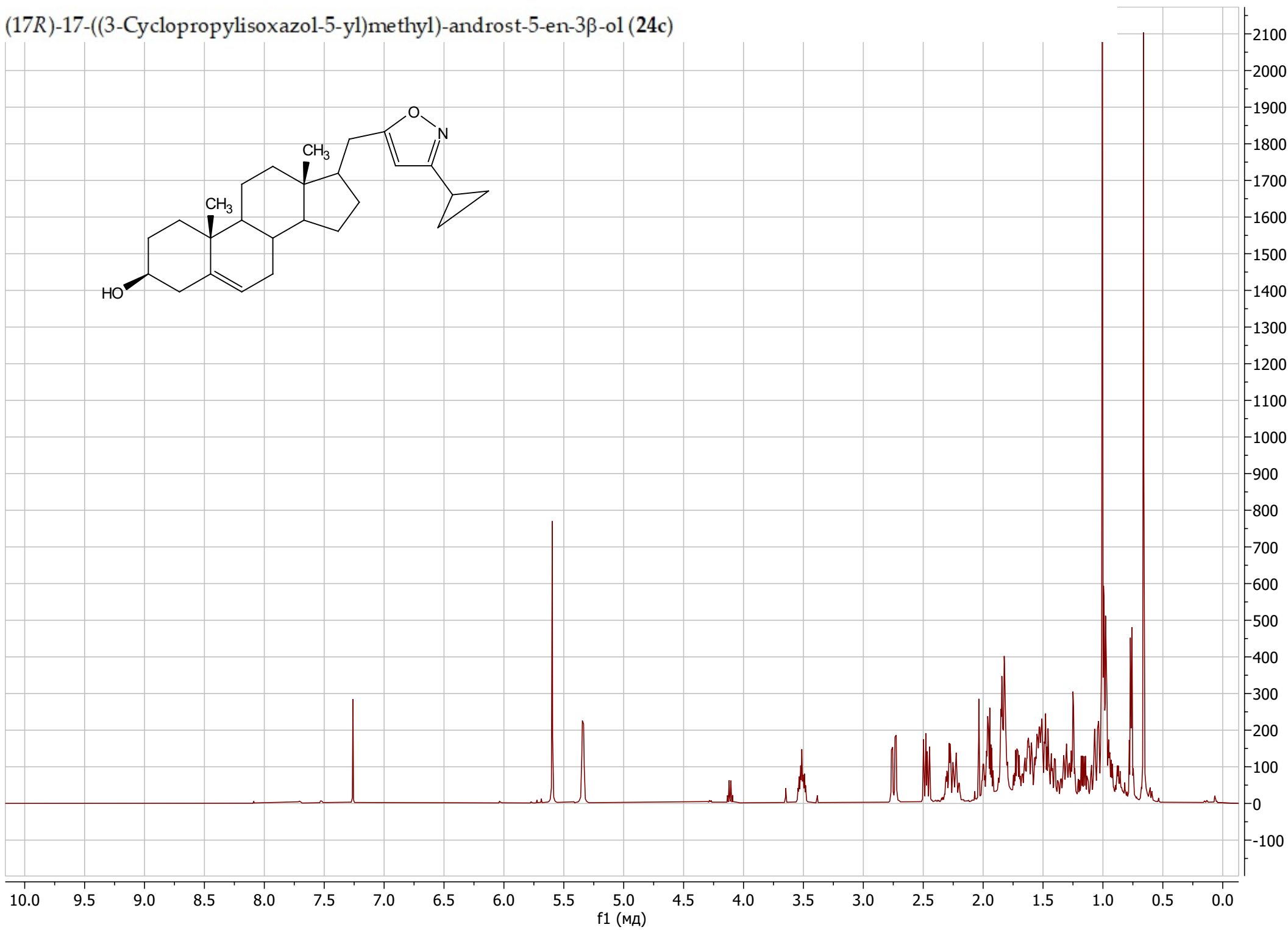
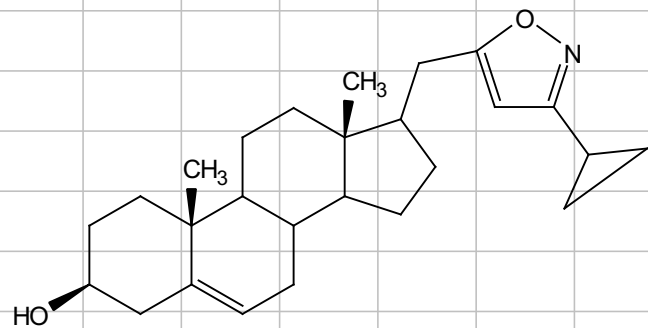
(17R)-17-((3-(2-Hydroxypropan-2-yl)isoxazol-5-yl)methyl)-androst-5-en-3 β -ol (24j)



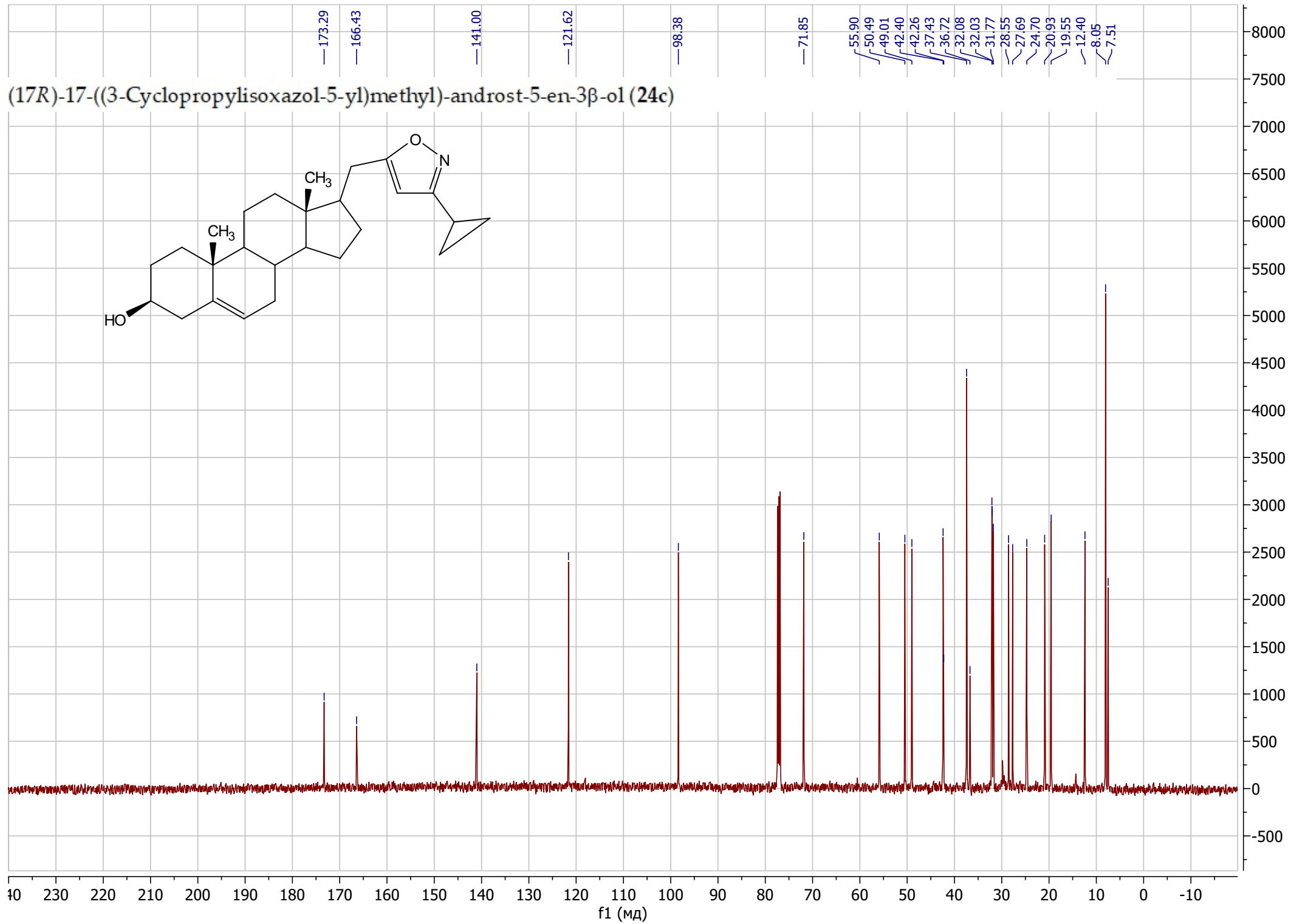
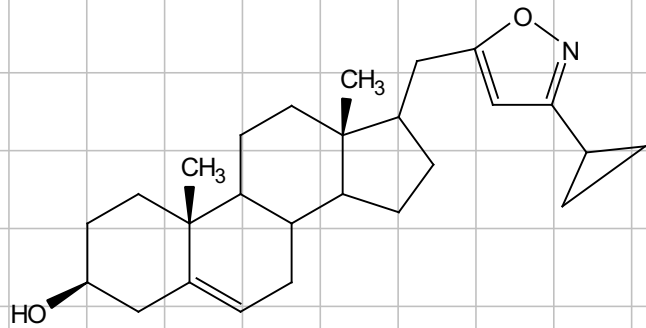
(17R)-17-((3-(2-Hydroxypropan-2-yl)isoxazol-5-yl)methyl)-androst-5-en-3 β -ol (24j)



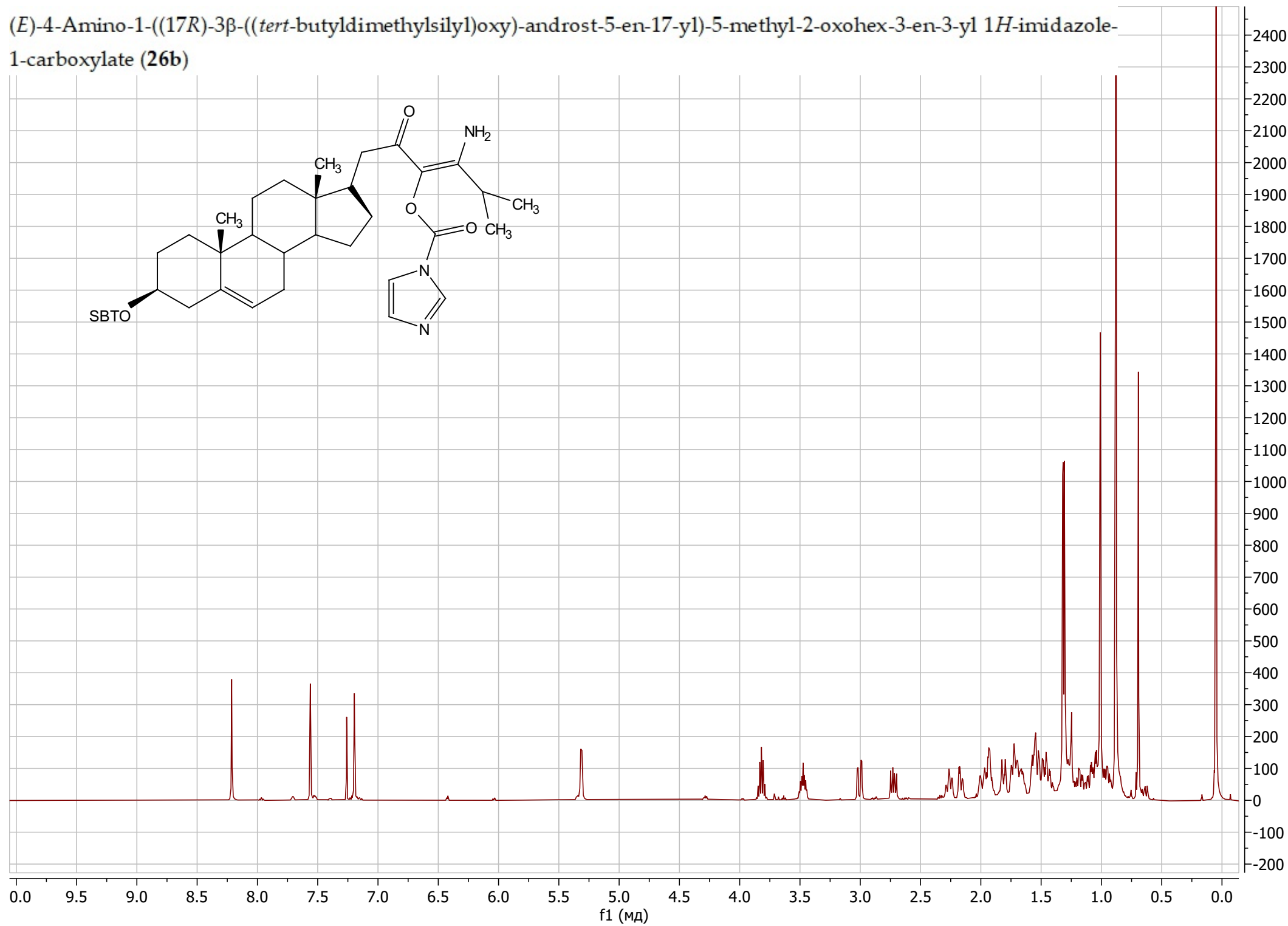
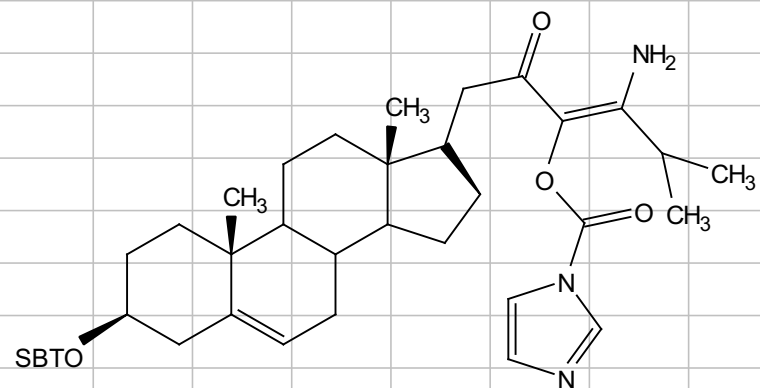
(17R)-17-((3-Cyclopropylisoxazol-5-yl)methyl)-androst-5-en-3 β -ol (24c)



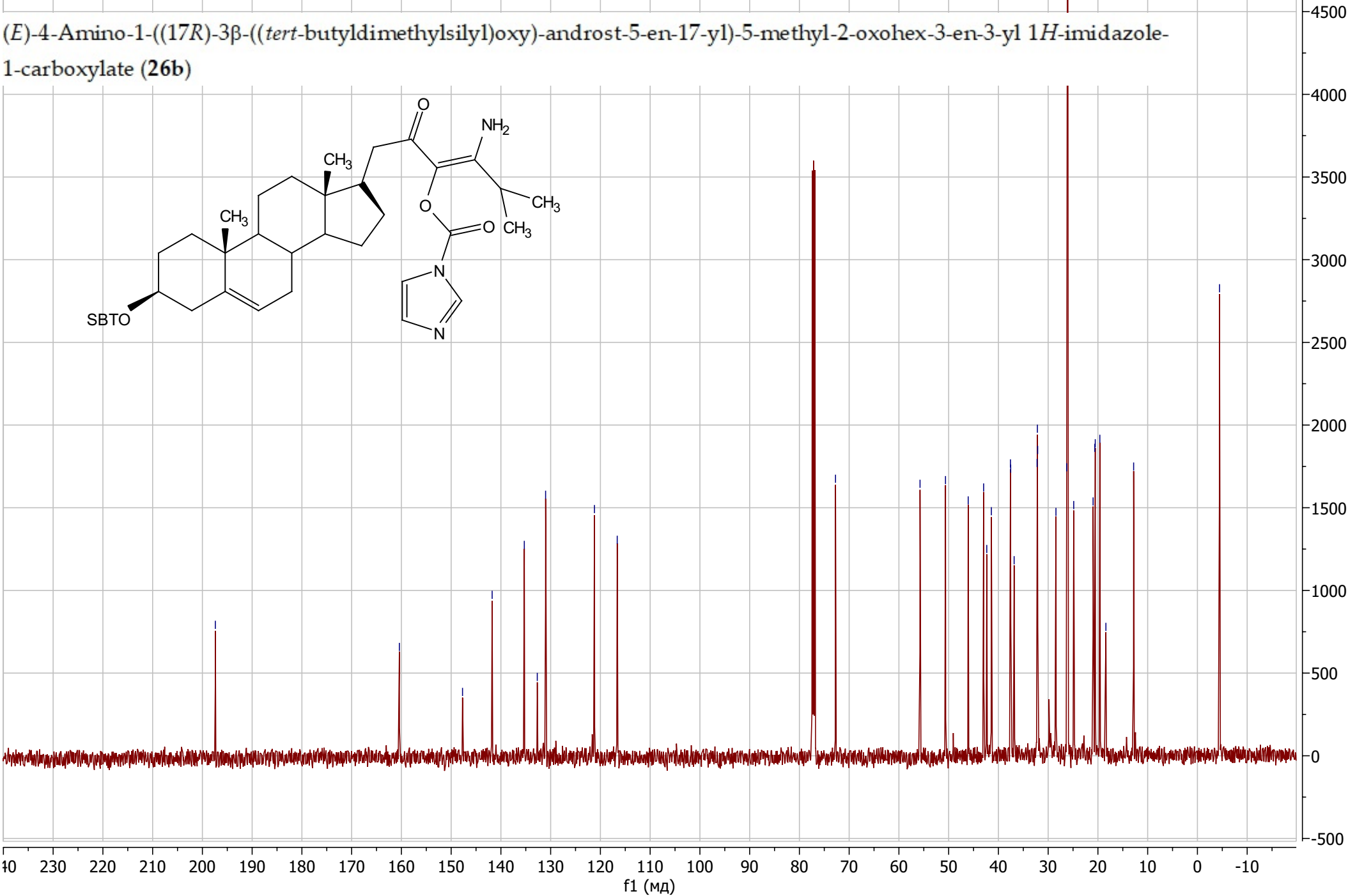
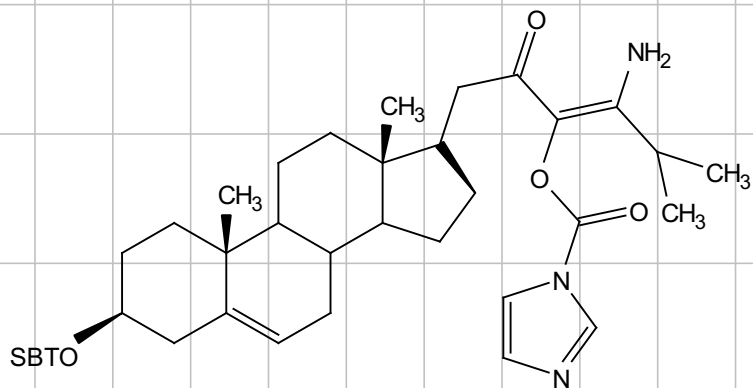
(17R)-17-((3-Cyclopropylisoxazol-5-yl)methyl)-androst-5-en-3 β -ol (24c)



(E)-4-Amino-1-((17R)-3β-((tert-butyl dimethylsilyl)oxy)-androst-5-en-17-yl)-5-methyl-2-oxohex-3-en-3-yl 1H-imidazole-1-carboxylate (26b)

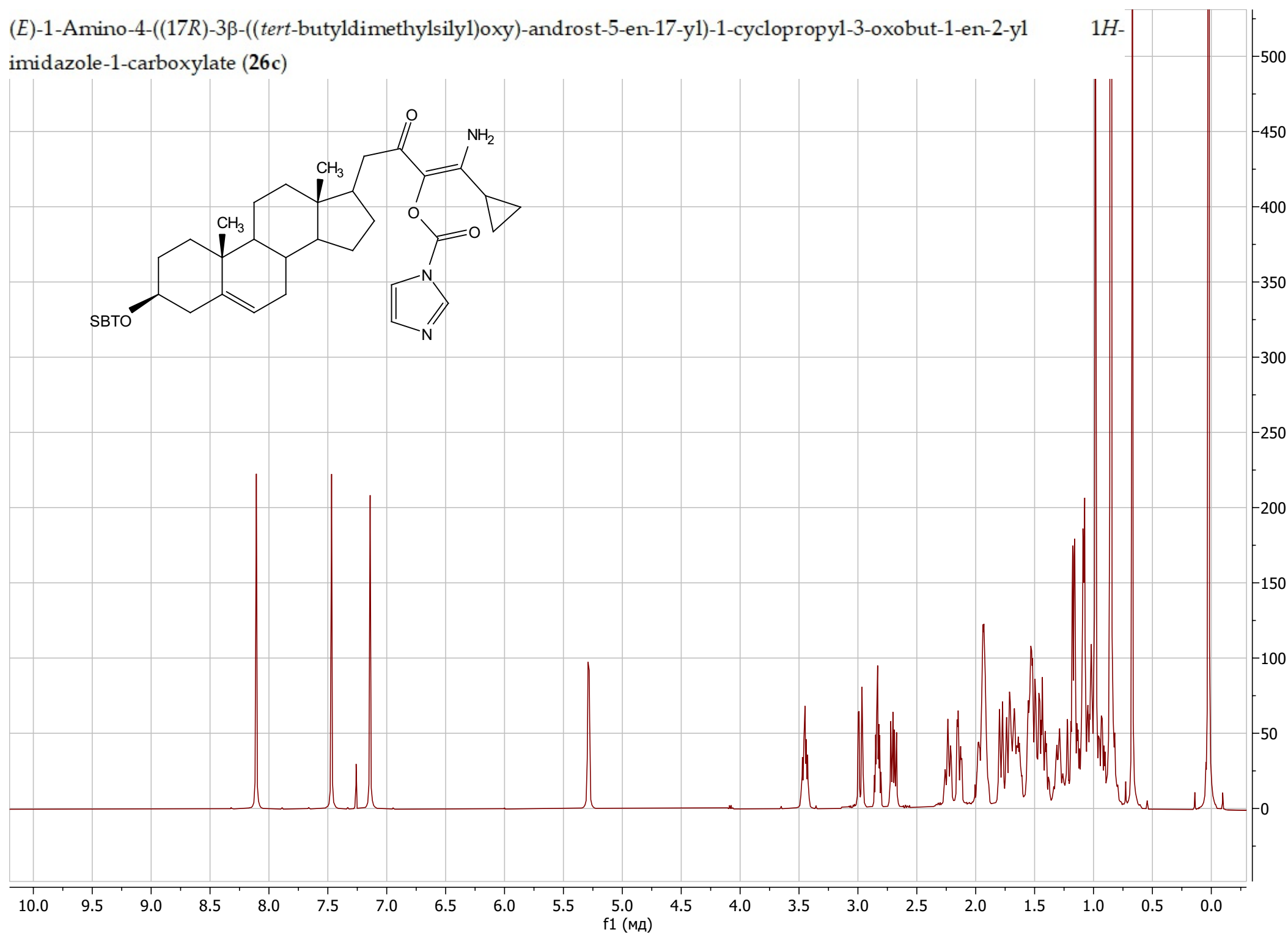


(E)-4-Amino-1-((17R)-3β-((tert-butyl dimethylsilyl)oxy)-androst-5-en-17-yl)-5-methyl-2-oxohex-3-en-3-yl 1H-imidazole-1-carboxylate (26b)

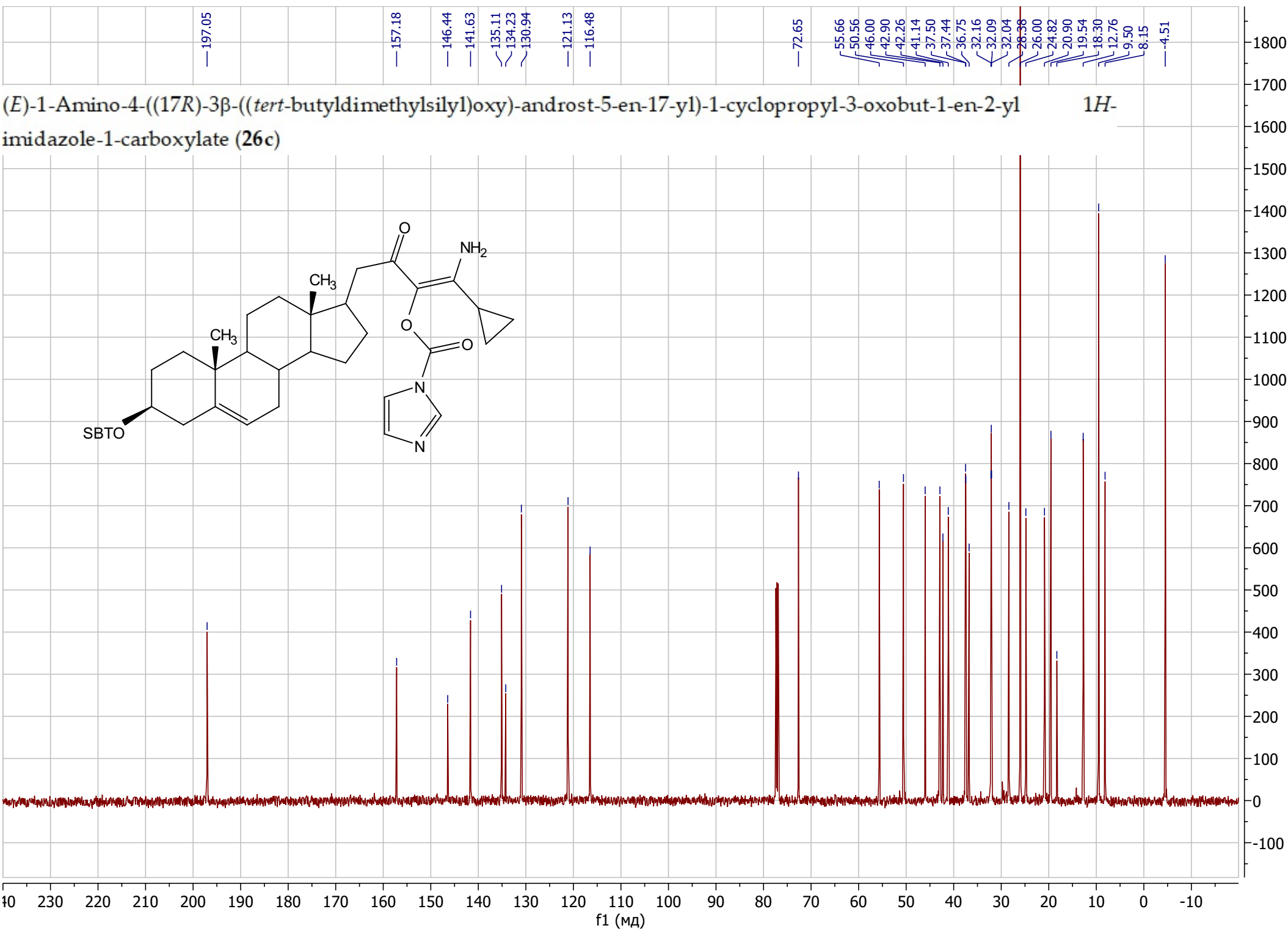
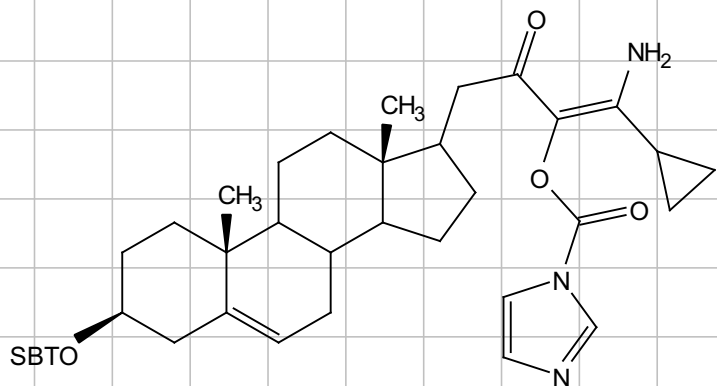


(*E*)-1-Amino-4-((17*R*)-3 β -((*tert*-butyldimethylsilyl)oxy)-androst-5-en-17-yl)-1-cyclopropyl-3-oxobut-1-en-2-yl imidazole-1-carboxylate (**26c**)

¹H-

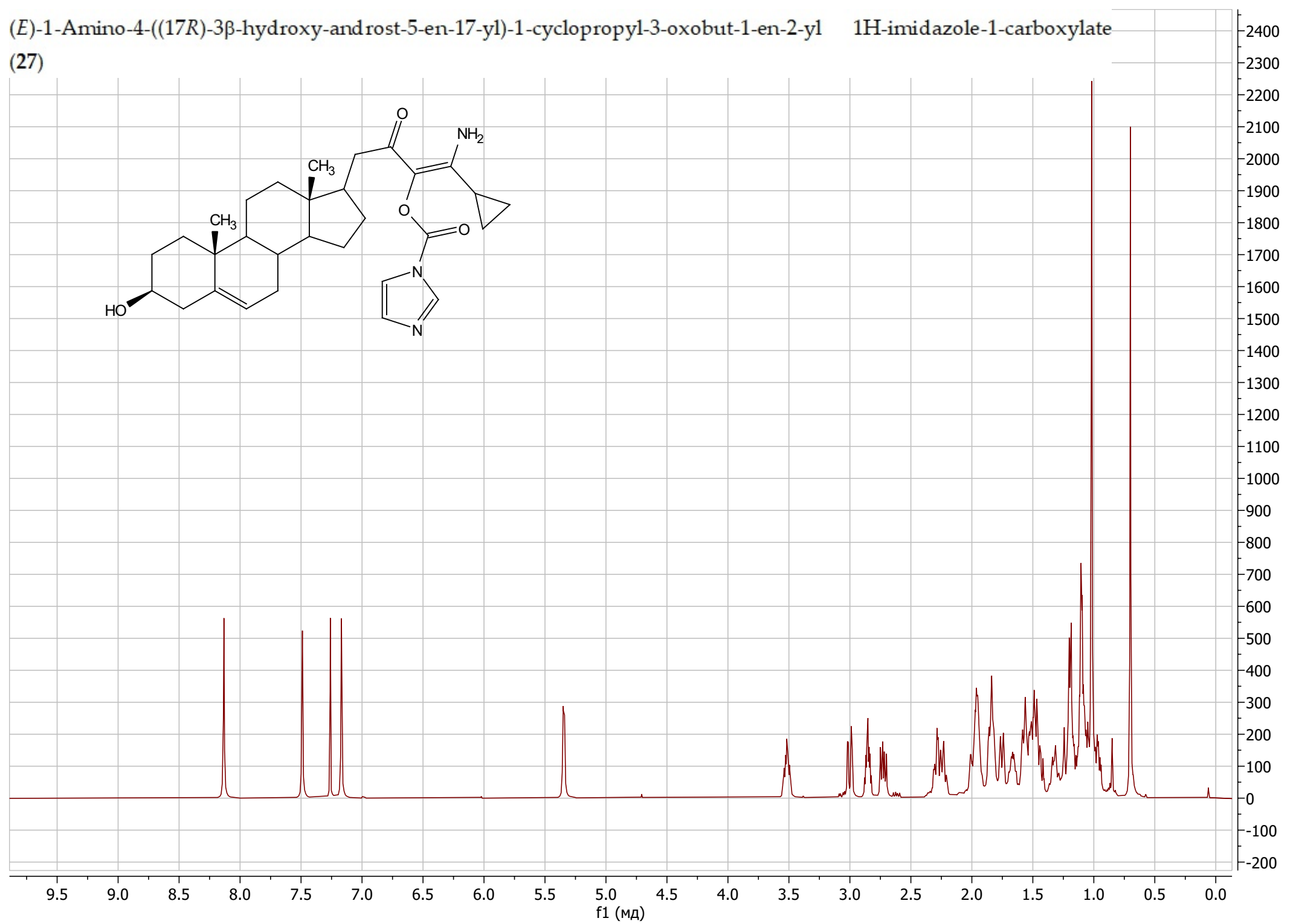
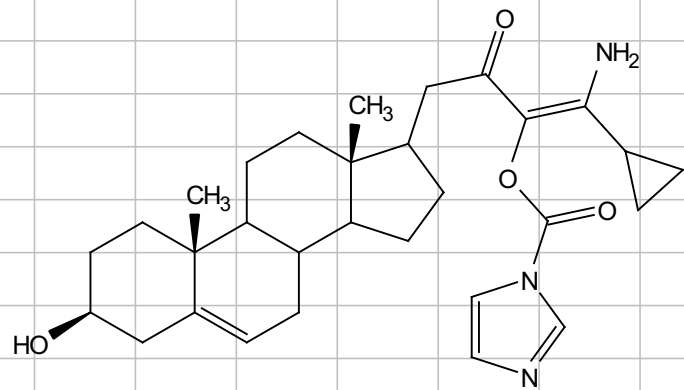


(E)-1-Amino-4-((17*R*)-3β-((*tert*-butyldimethylsilyl)oxy)-androst-5-en-17-yl)-1-cyclopropyl-3-oxobut-1-en-2-yl imidazole-1-carboxylate (**26c**)



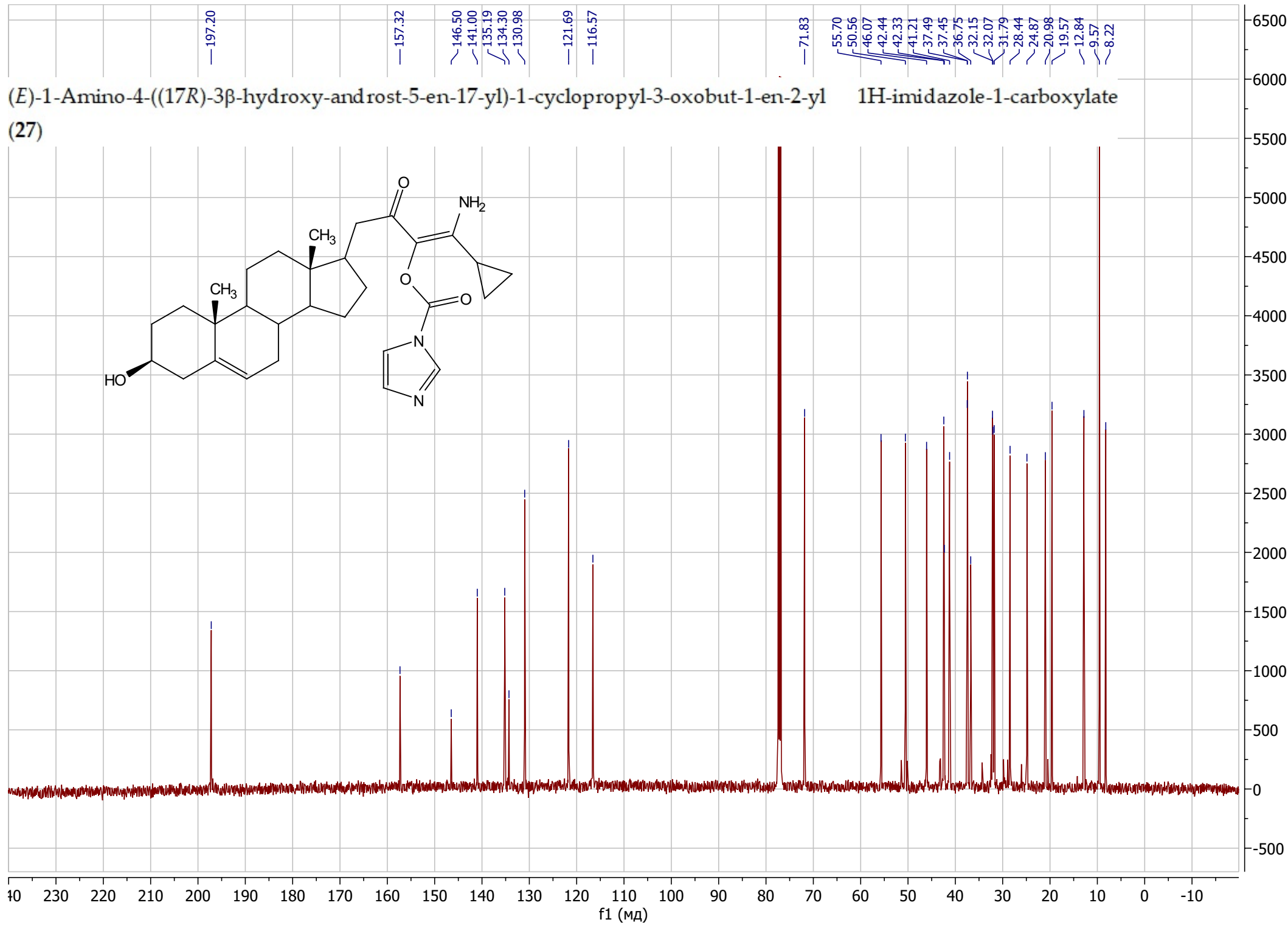
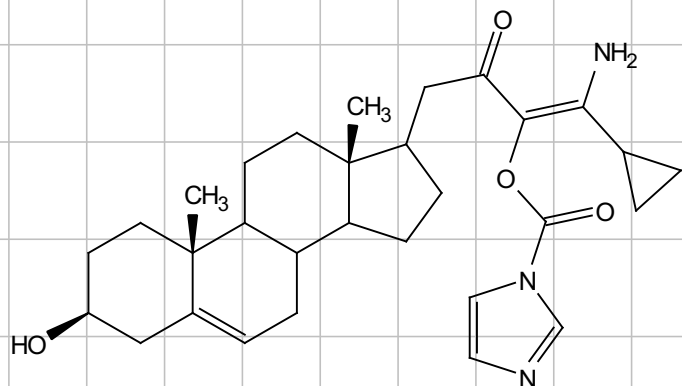
(E)-1-Amino-4-((17R)-3β-hydroxy-androst-5-en-17-yl)-1-cyclopropyl-3-oxobut-1-en-2-yl 1H-imidazole-1-carboxylate

(27)

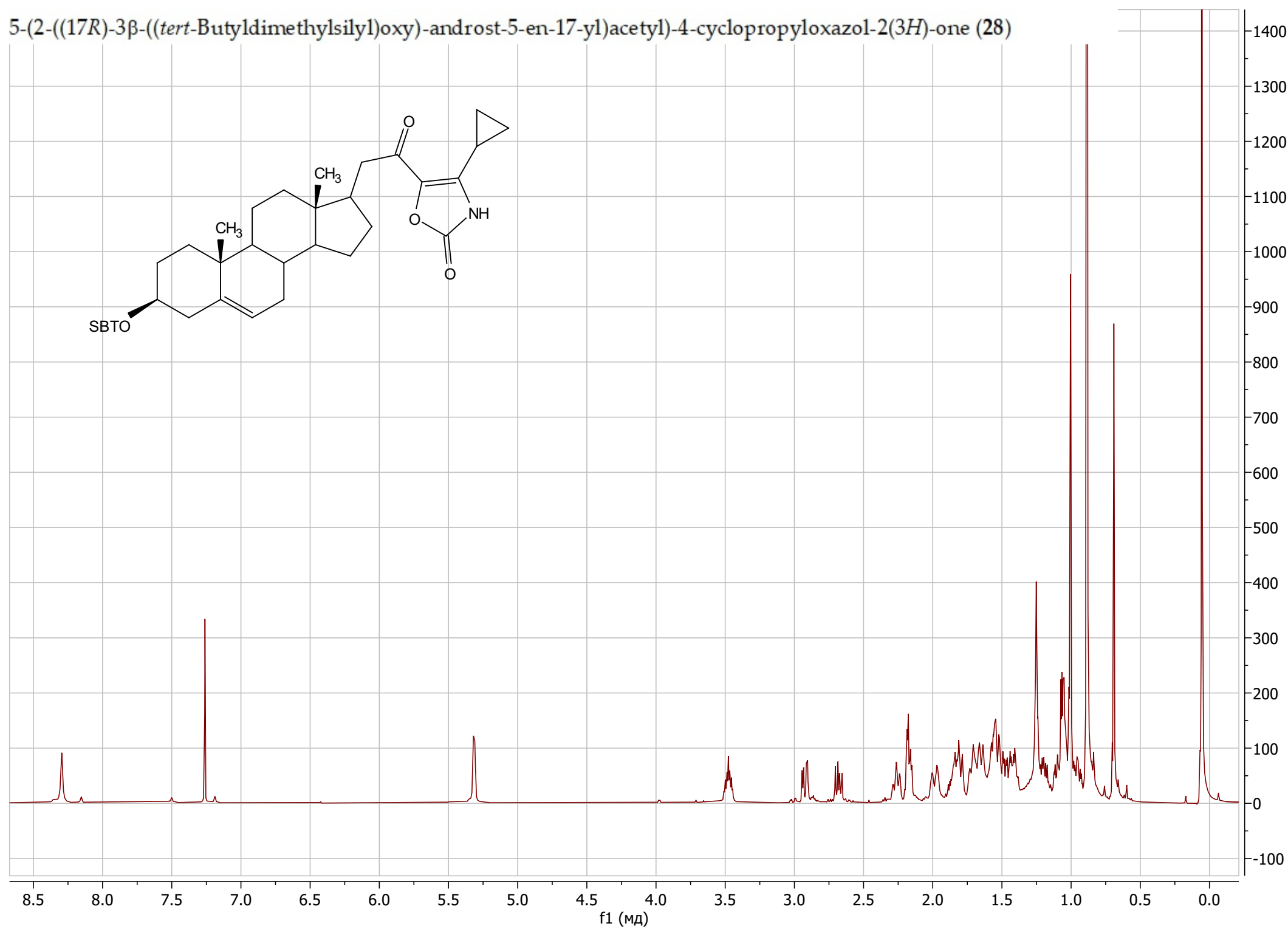
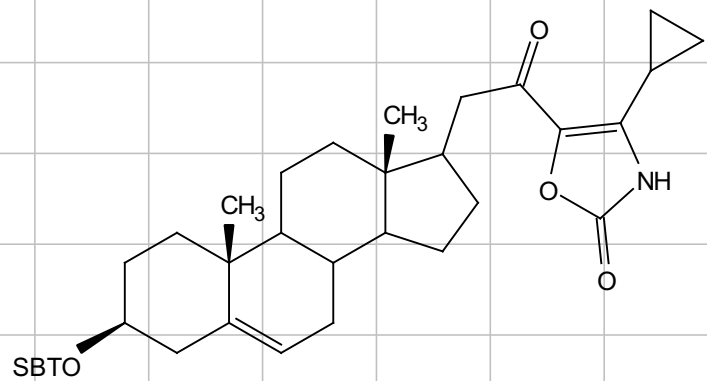


(E)-1-Amino-4-((17R)-3 β -hydroxy-androst-5-en-17-yl)-1-cyclopropyl-3-oxobut-1-en-2-yl 1H-imidazole-1-carboxylate

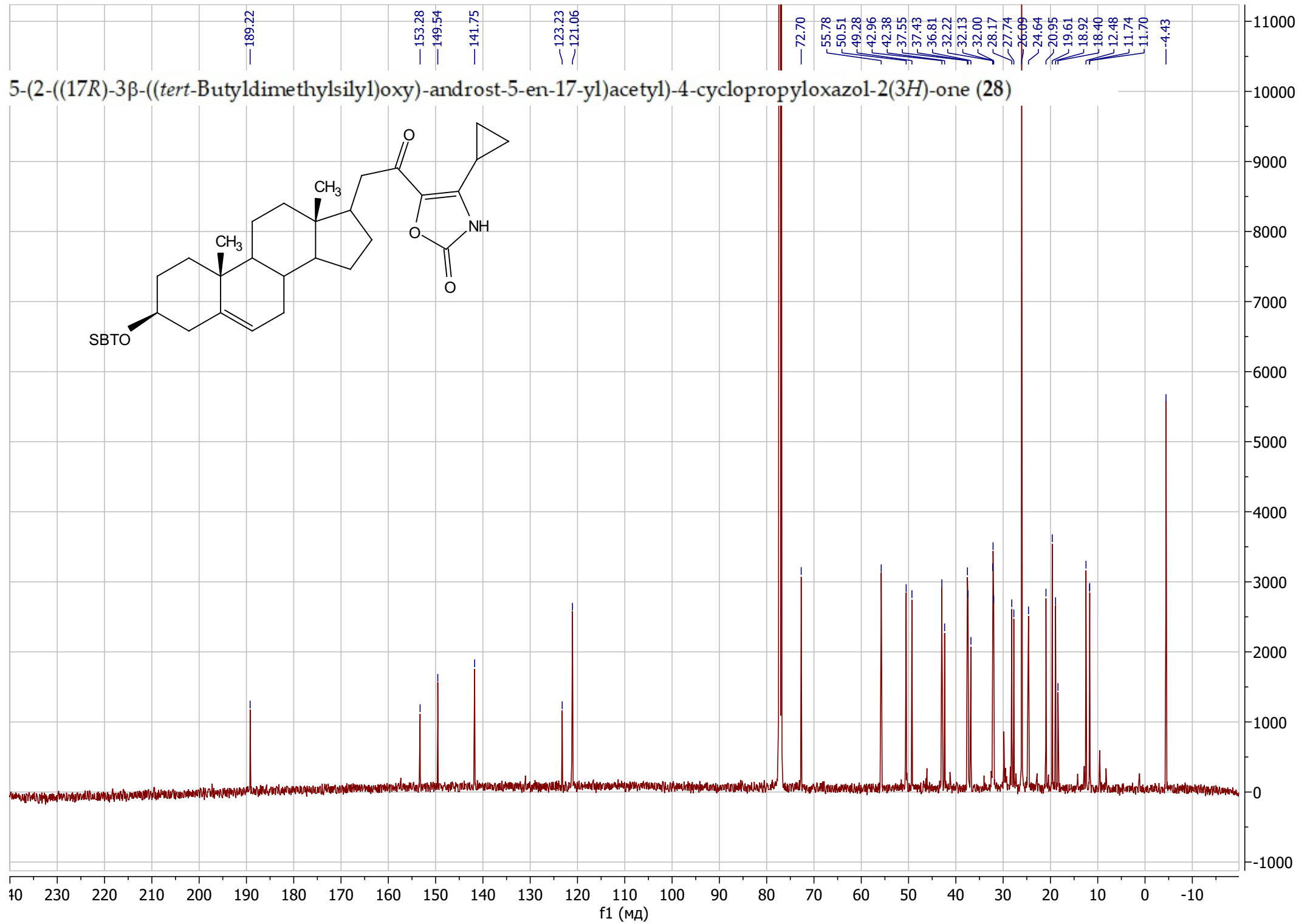
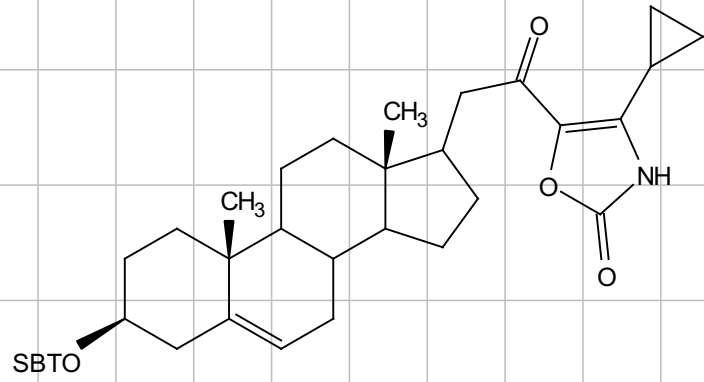
(27)



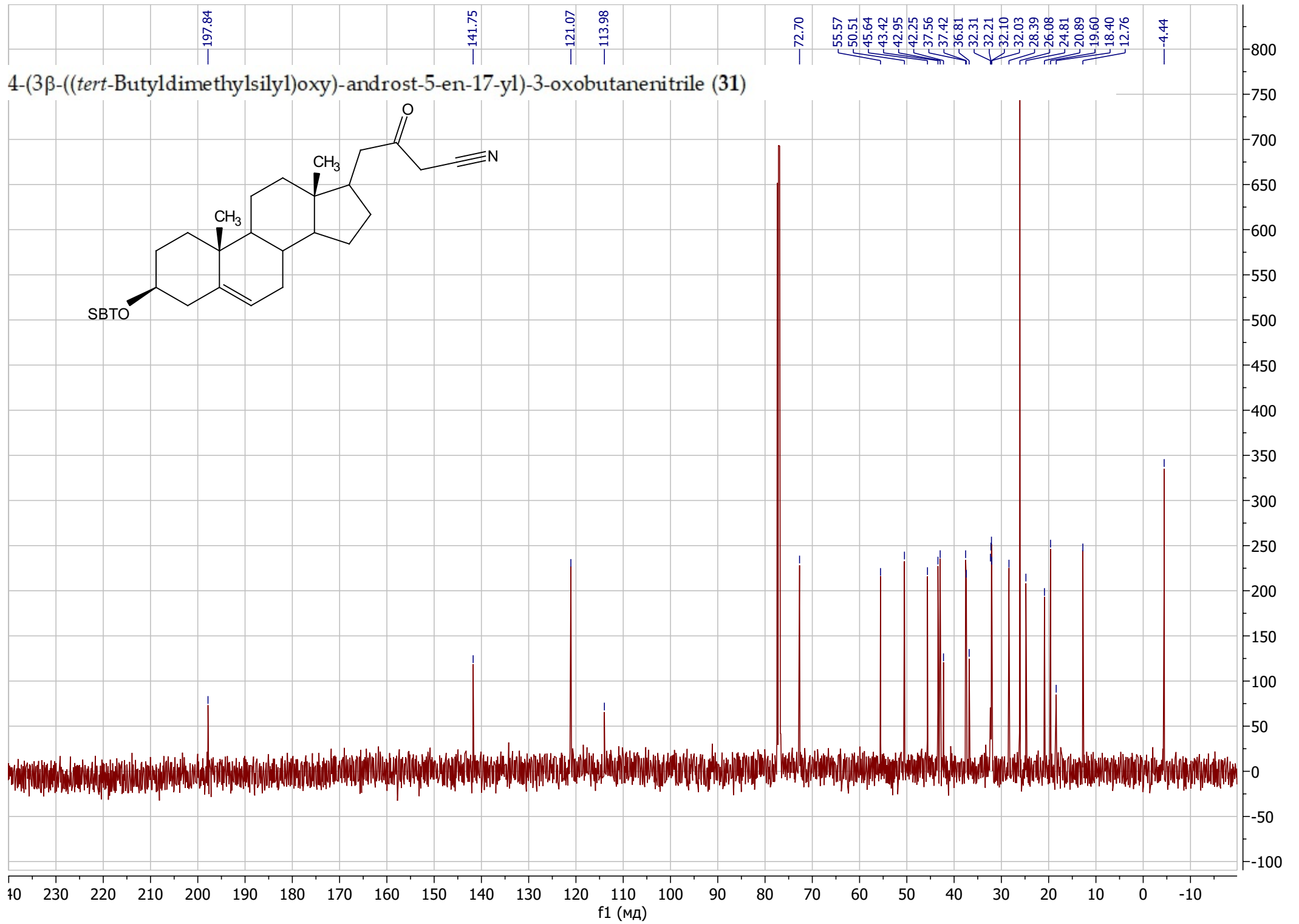
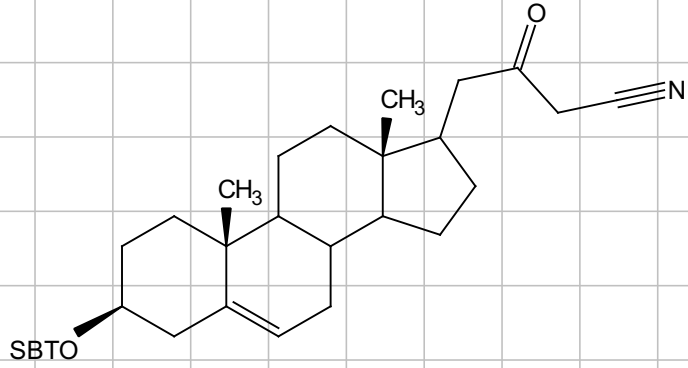
5-(2-((17R)-3β-((*tert*-Butyldimethylsilyl)oxy)-androst-5-en-17-yl)acetyl)-4-cyclopropyloxazol-2(3H)-one (28)



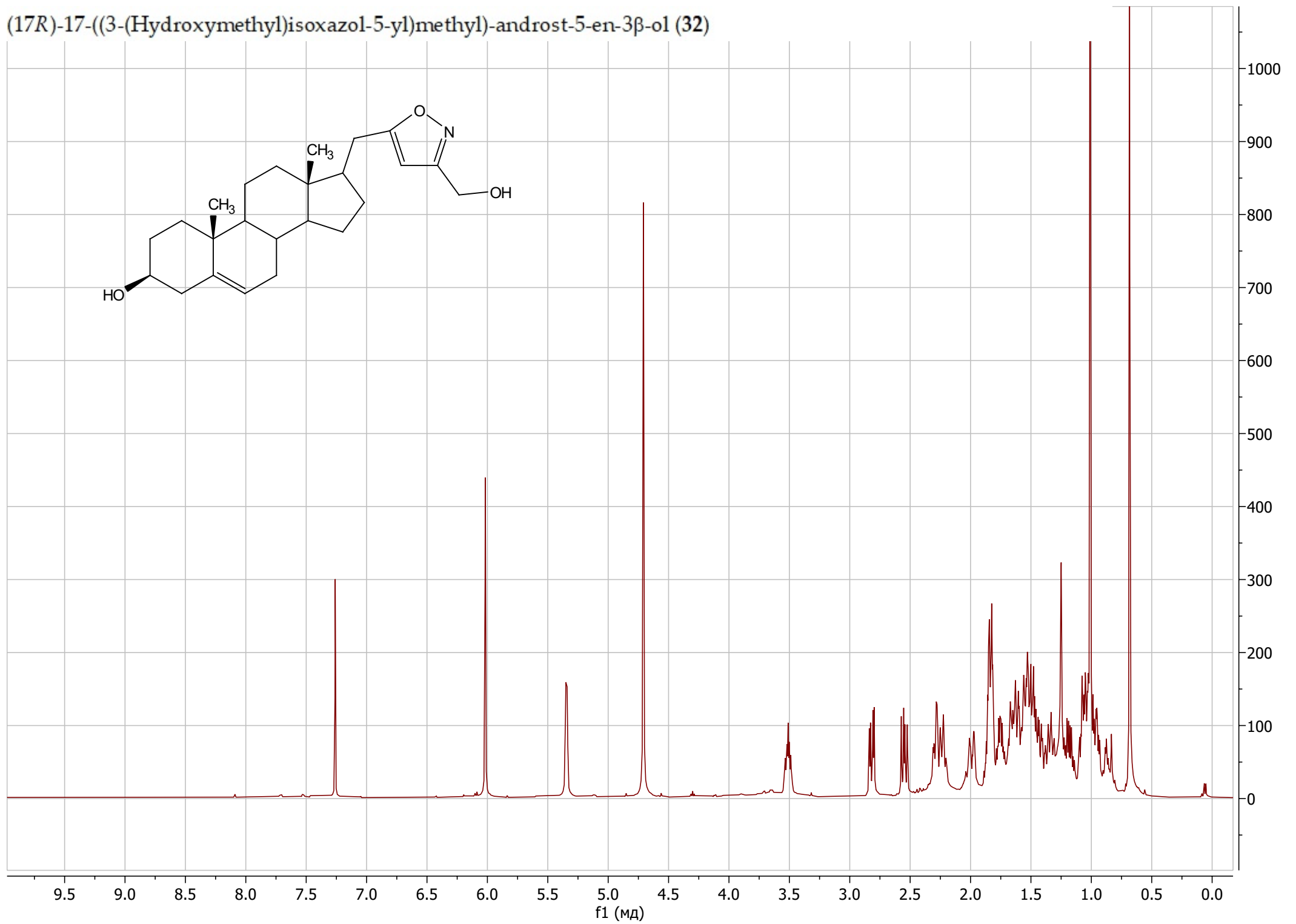
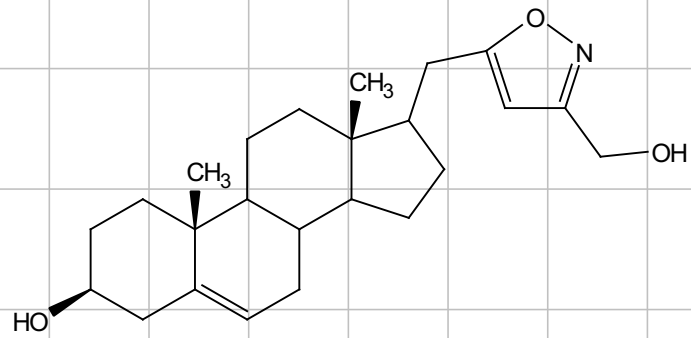
5-(2-((17R)-3β-((*tert*-Butyldimethylsilyl)oxy)-androst-5-en-17-yl)acetyl)-4-cyclopropyloxazol-2(3H)-one (28)



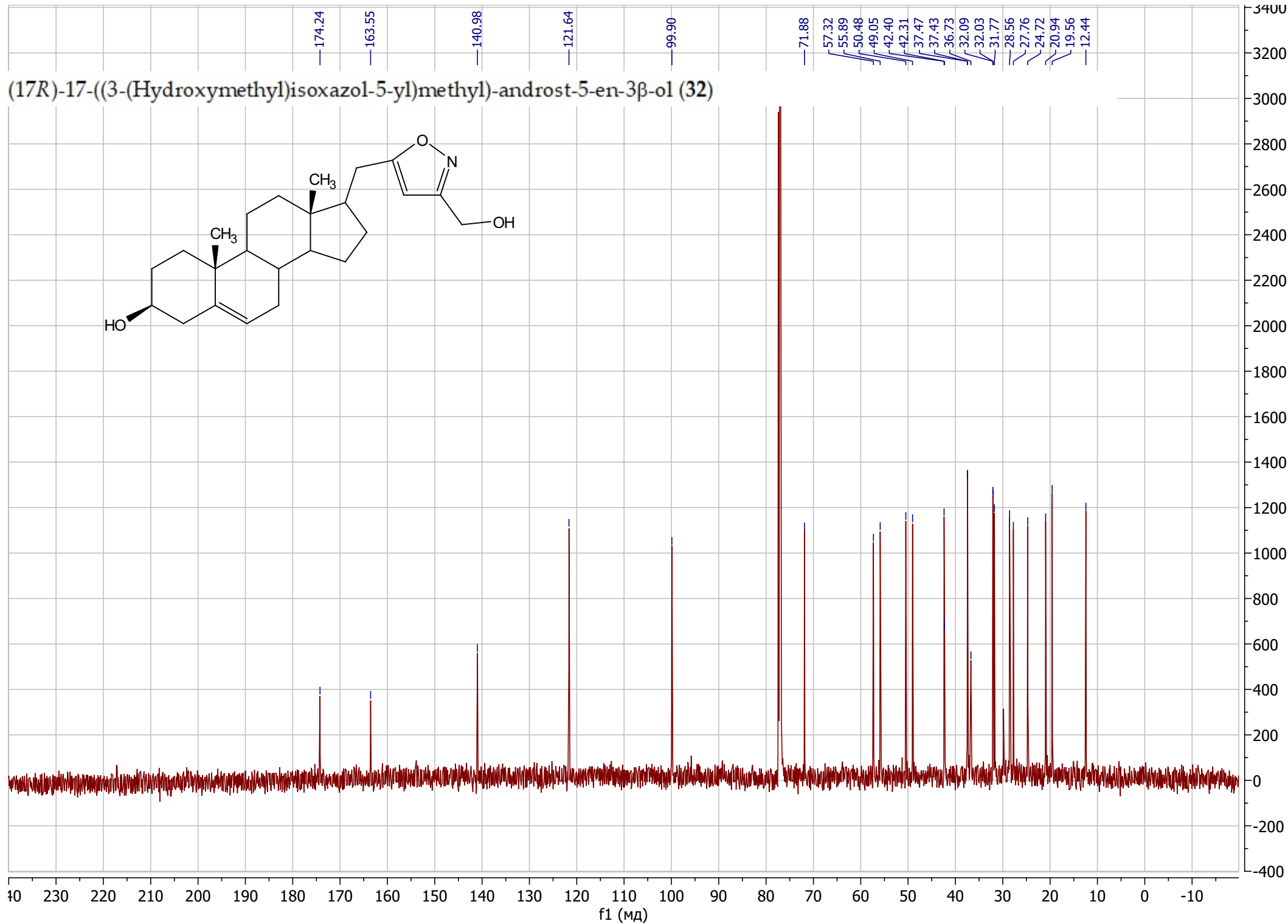
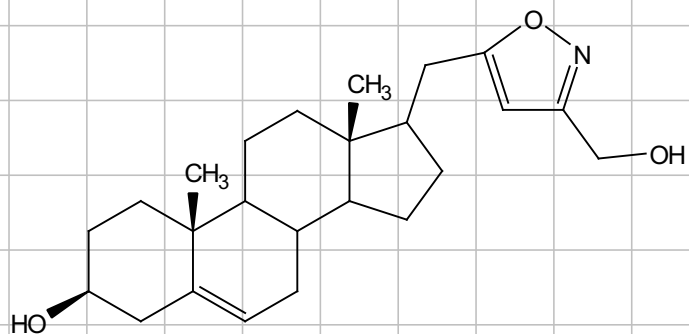
4-(3 β -((*tert*-Butyldimethylsilyl)oxy)-androst-5-en-17-yl)-3-oxobutanenitrile (31)



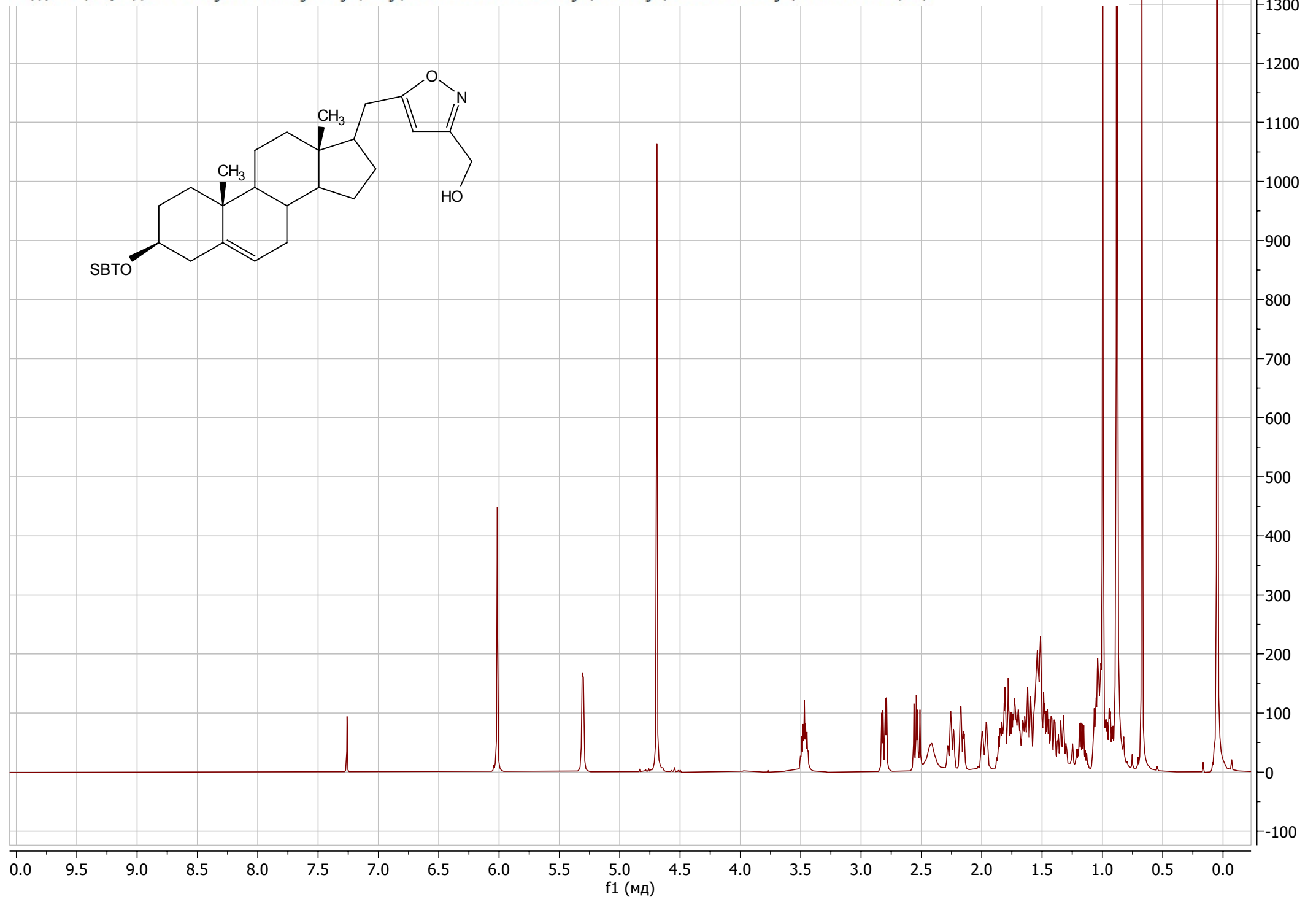
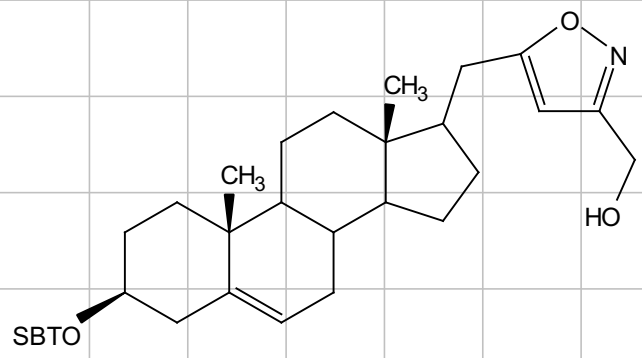
(17R)-17-((3-(Hydroxymethyl)isoxazol-5-yl)methyl)-androst-5-en-3 β -ol (32)



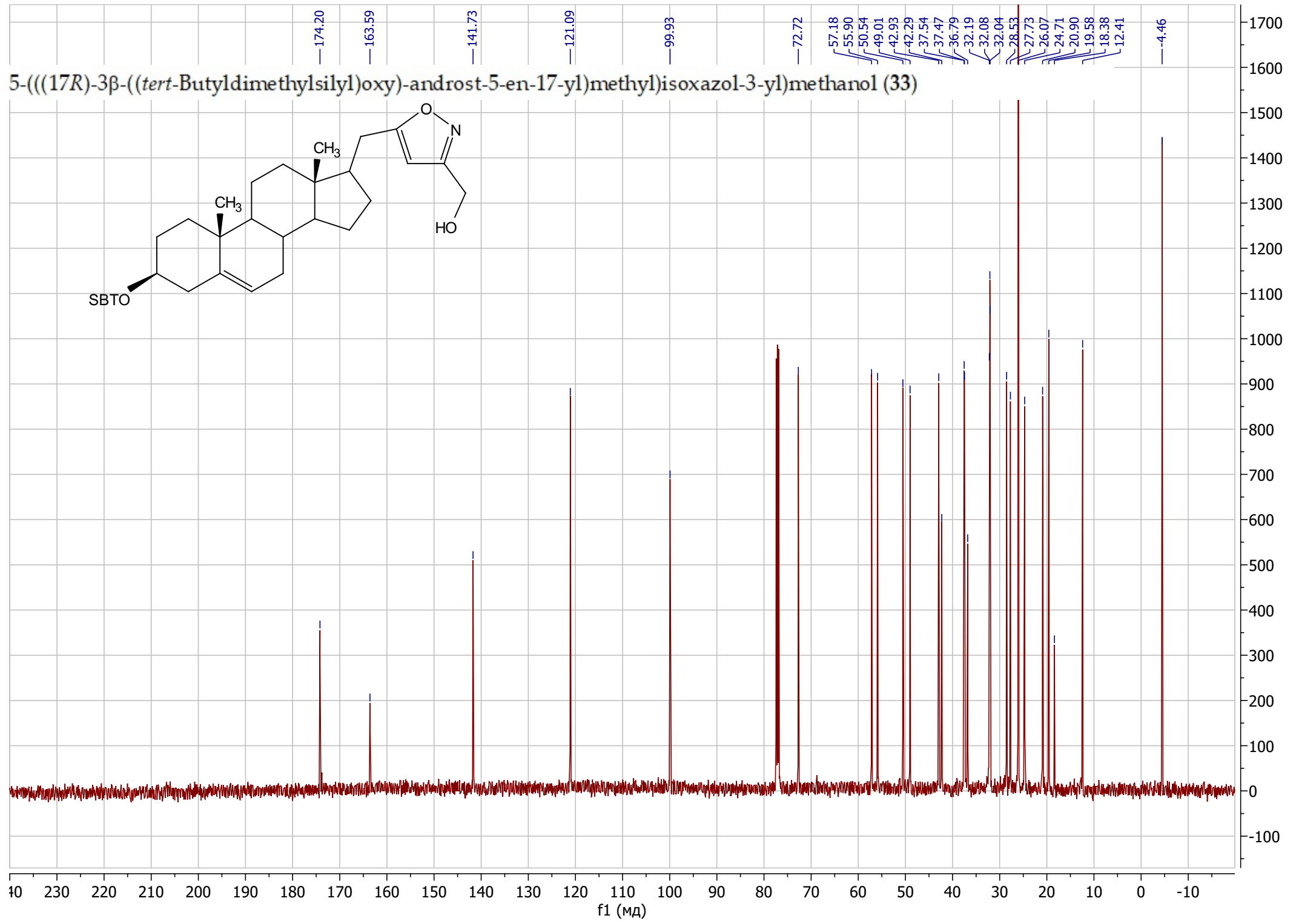
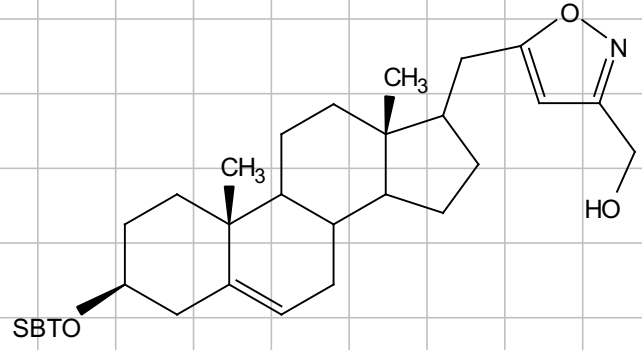
(17R)-17-((3-(Hydroxymethyl)isoxazol-5-yl)methyl)-androst-5-en-3 β -ol (32)



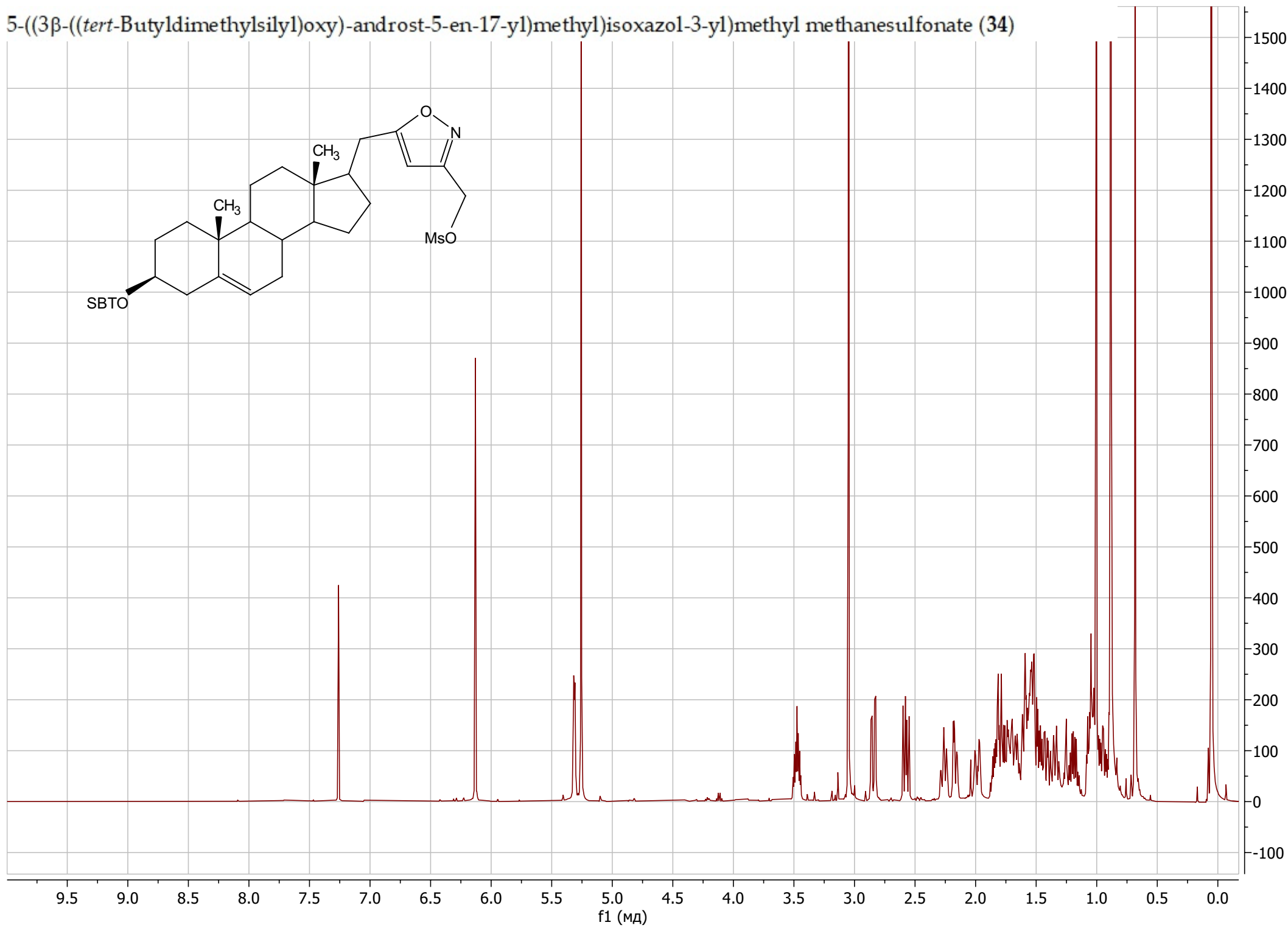
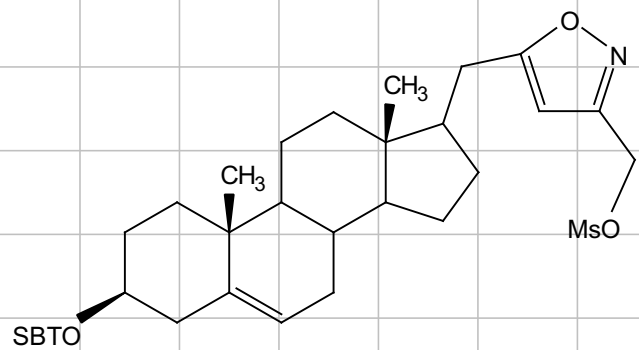
5-(((17R)-3 β -((*tert*-Butyldimethylsilyloxy)-androst-5-en-17-yl)methyl)isoxazol-3-yl)methanol (33)



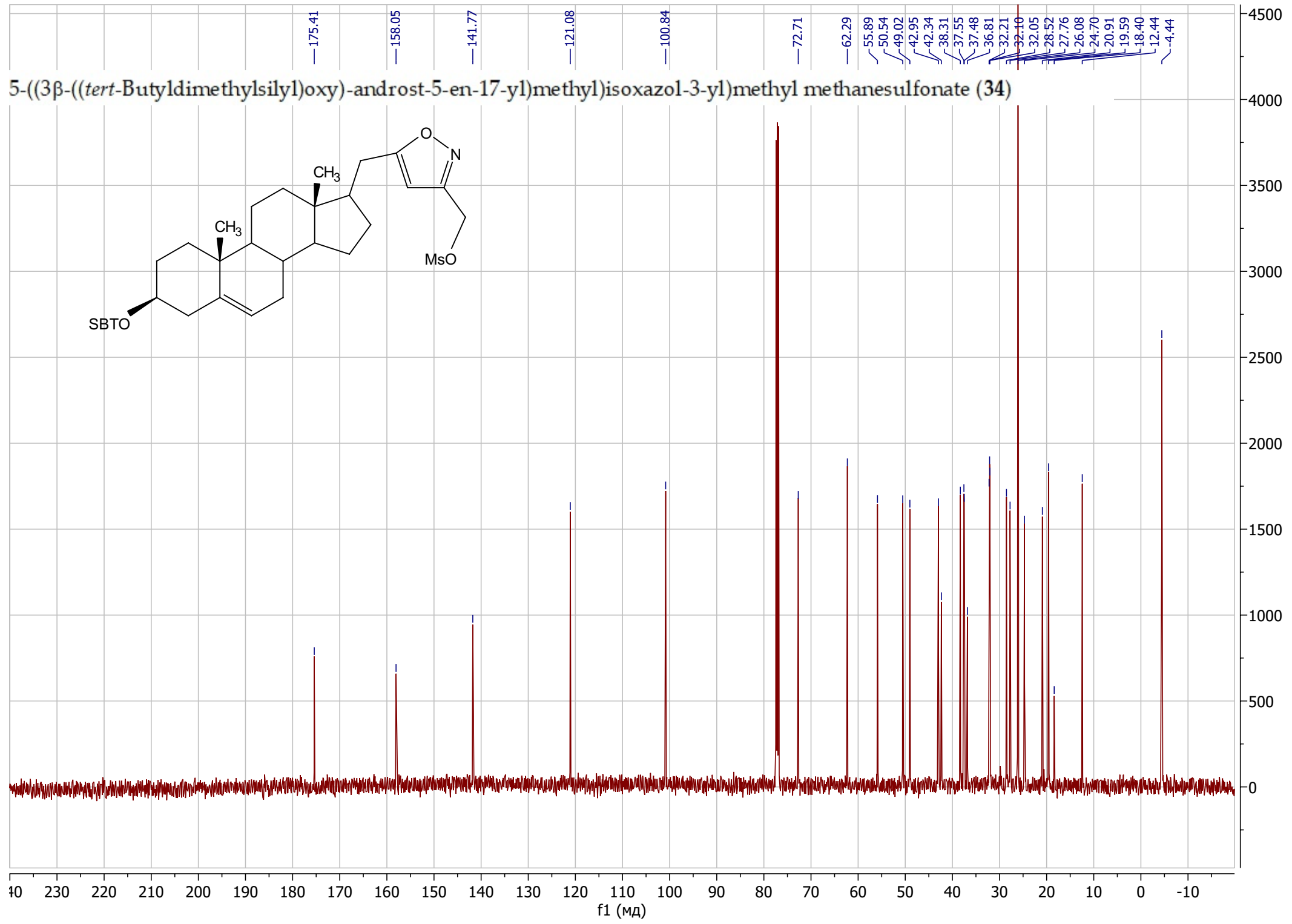
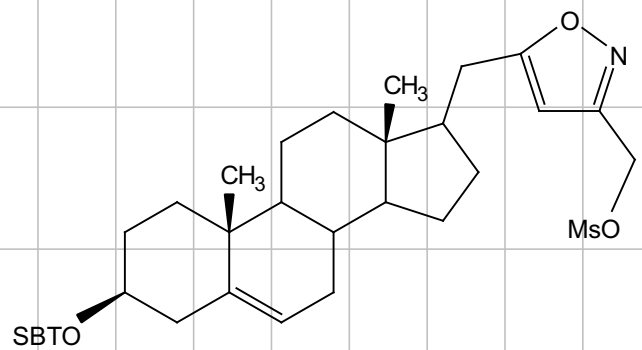
5-(((17R)-3β-((*tert*-Butyldimethylsilyl)oxy)-androst-5-en-17-yl)methyl)isoxazol-3-yl)methanol (33)



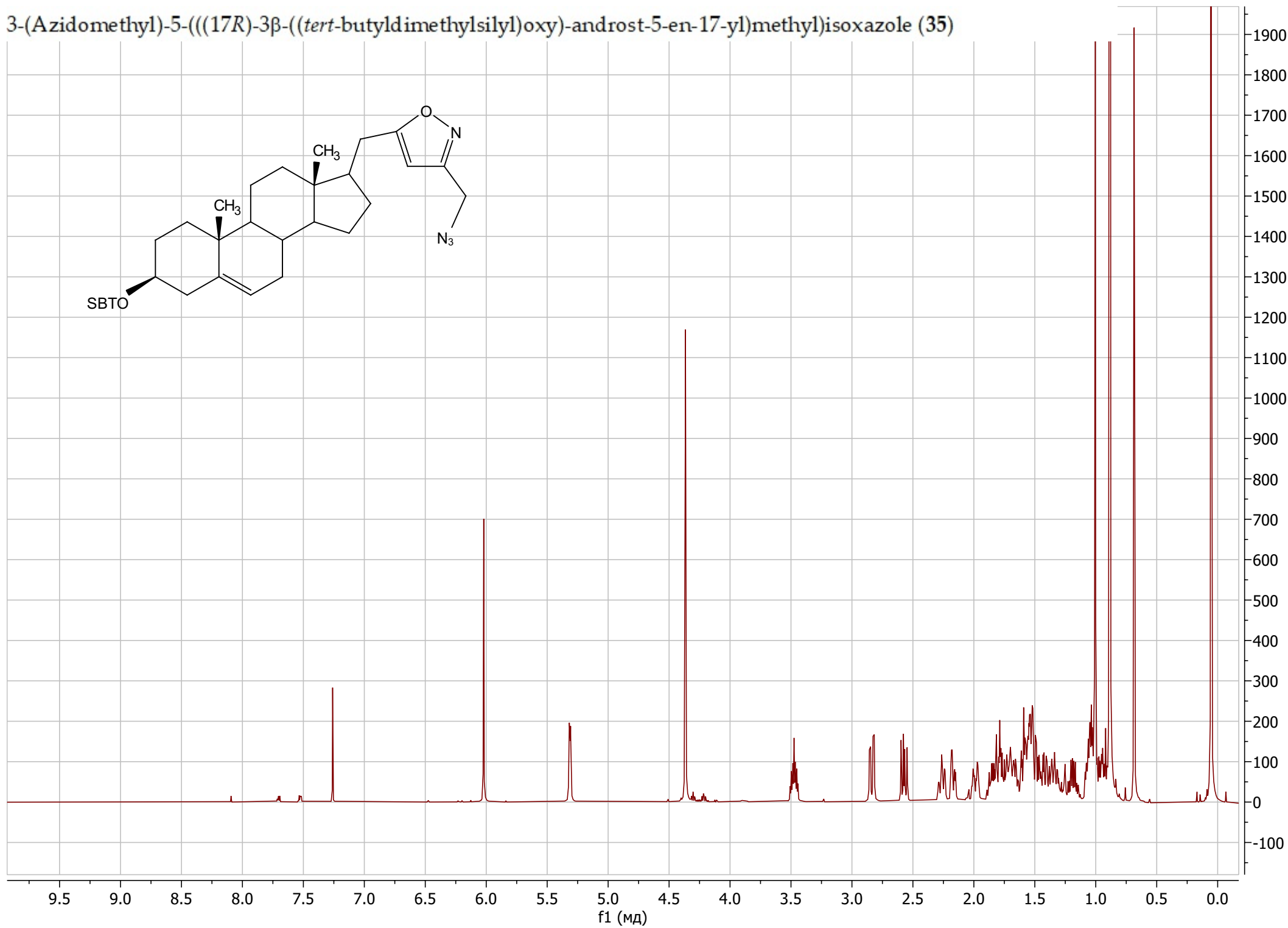
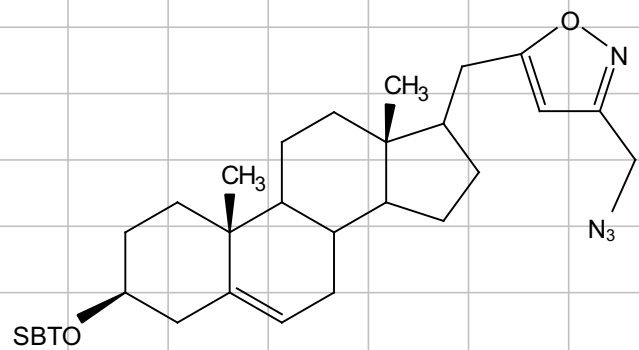
5-((3β-((*tert*-Butyldimethylsilyl)oxy)-androst-5-en-17-yl)methyl)isoxazol-3-yl)methyl methanesulfonate (34)



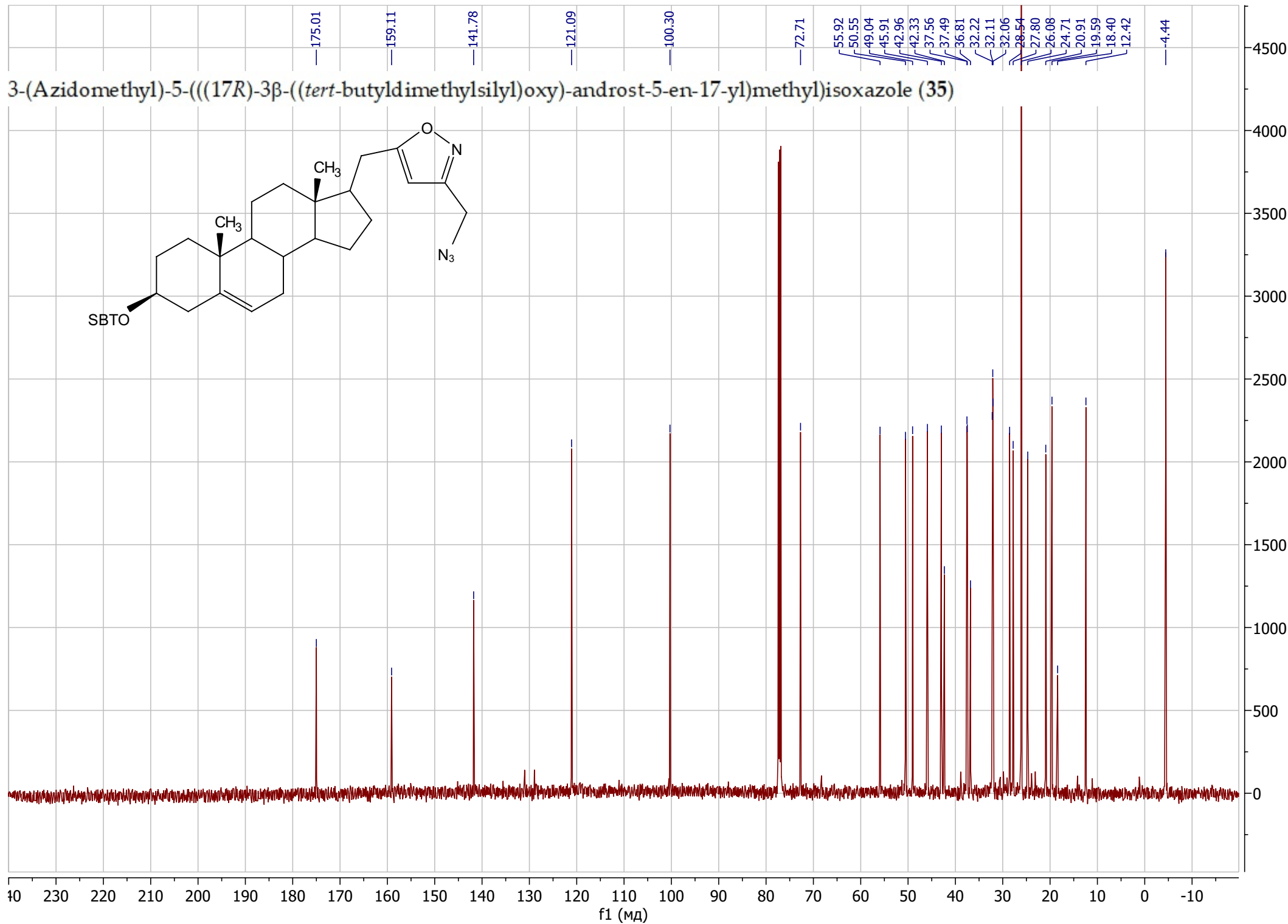
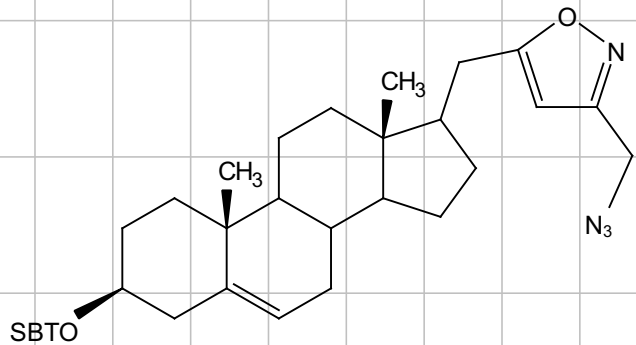
5-((3β-((*tert*-Butyldimethylsilyl)oxy)-androst-5-en-17-yl)methyl)isoxazol-3-yl)methyl methanesulfonate (34)



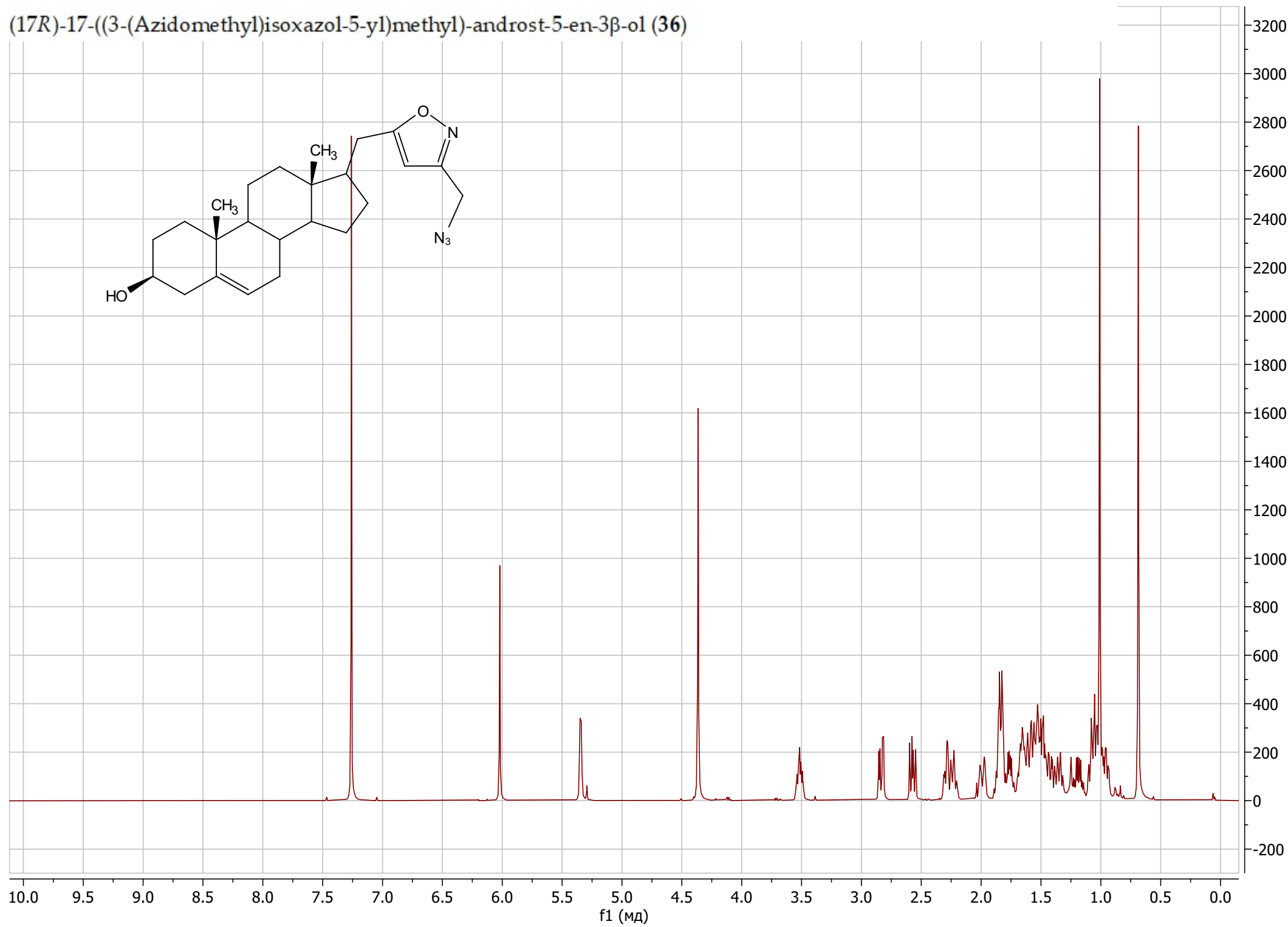
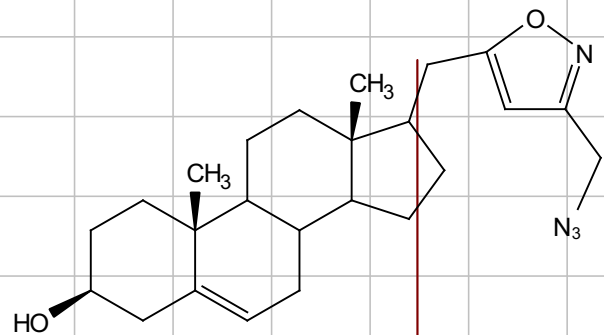
3-(Azidomethyl)-5-(((17R)-3β-((tert-butyldimethylsilyl)oxy)-androst-5-en-17-yl)methyl)isoxazole (35)



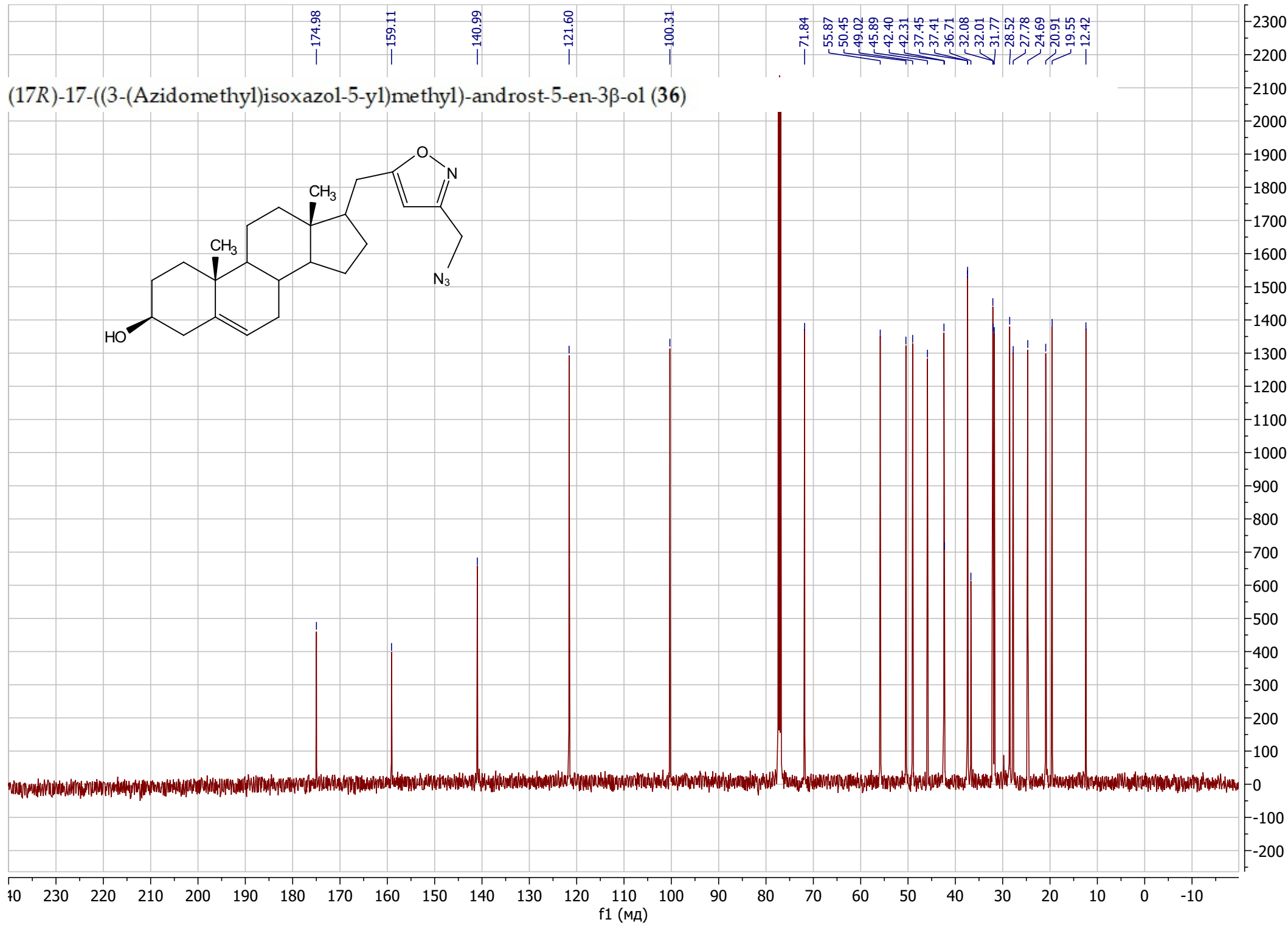
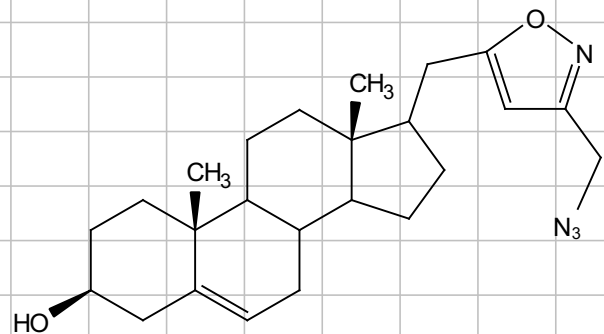
3-(Azidomethyl)-5-(((17R)-3 β -((*tert*-butyldimethylsilyl)oxy)-androst-5-en-17-yl)methyl)isoxazole (35)



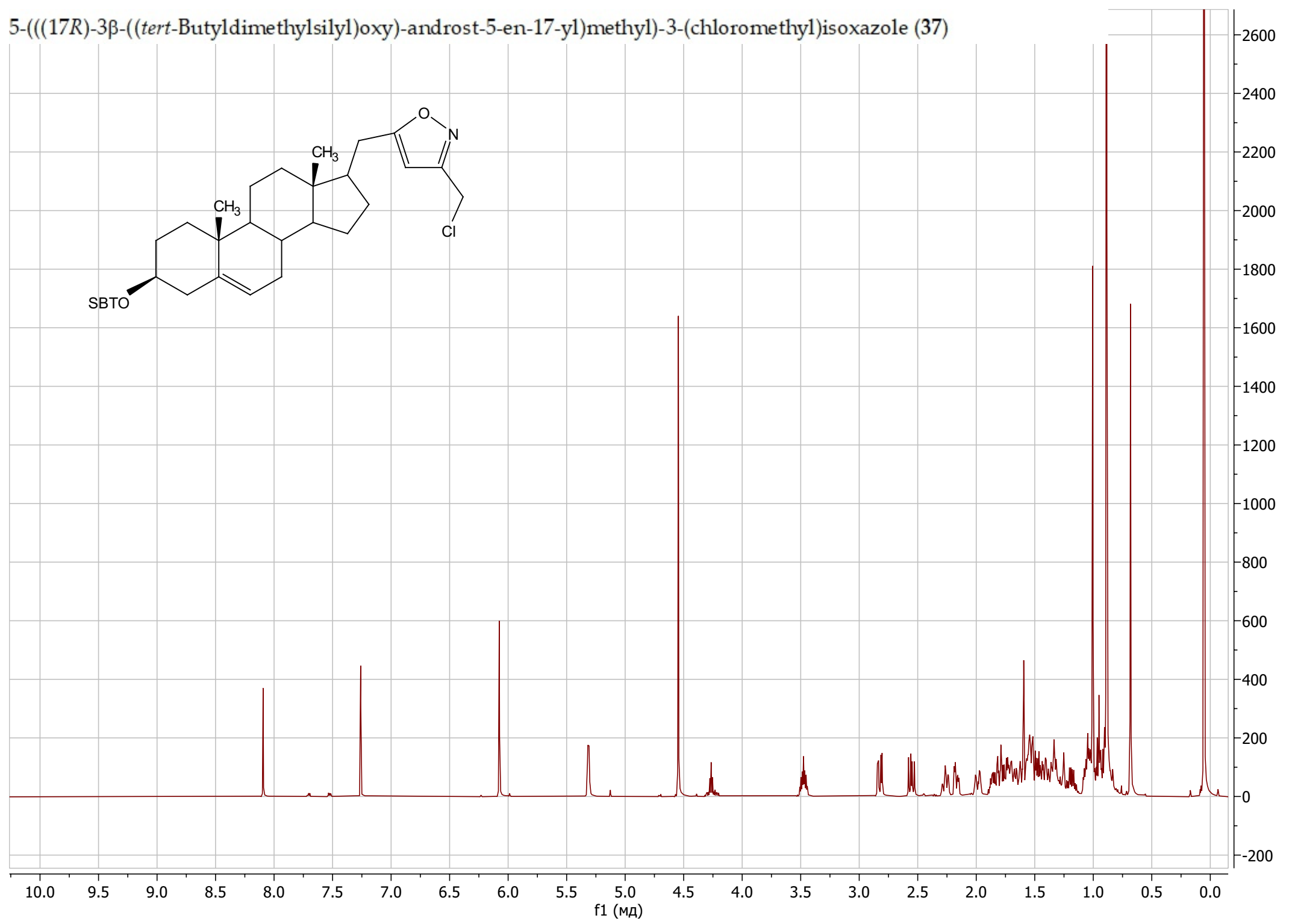
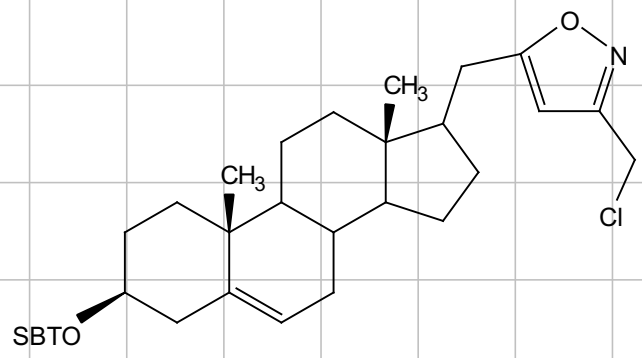
(17R)-17-((3-(Azidomethyl)isoxazol-5-yl)methyl)-androst-5-en-3 β -ol (36)

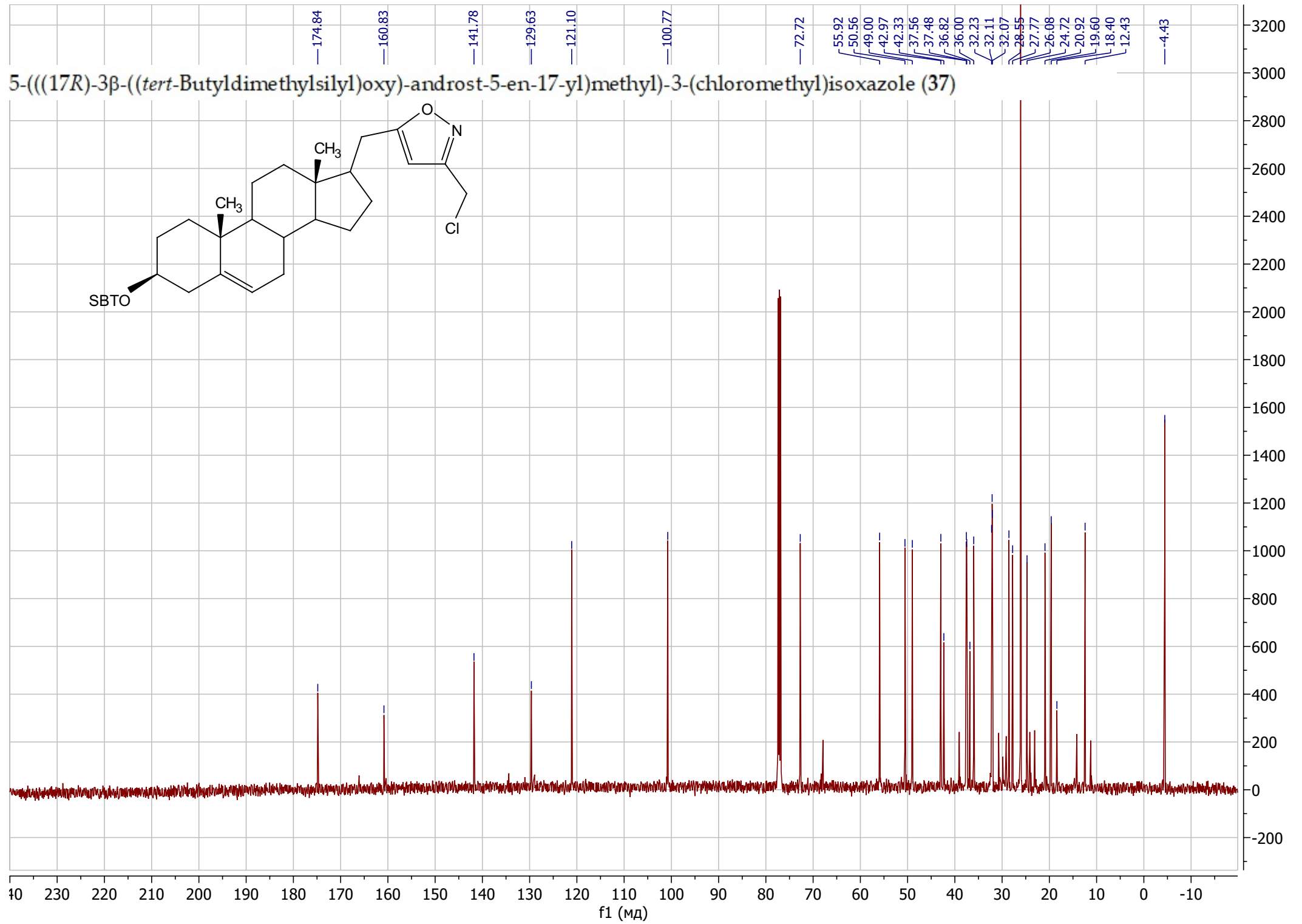


(17R)-17-((3-(Azidomethyl)isoxazol-5-yl)methyl)-androst-5-en-3 β -ol (36)

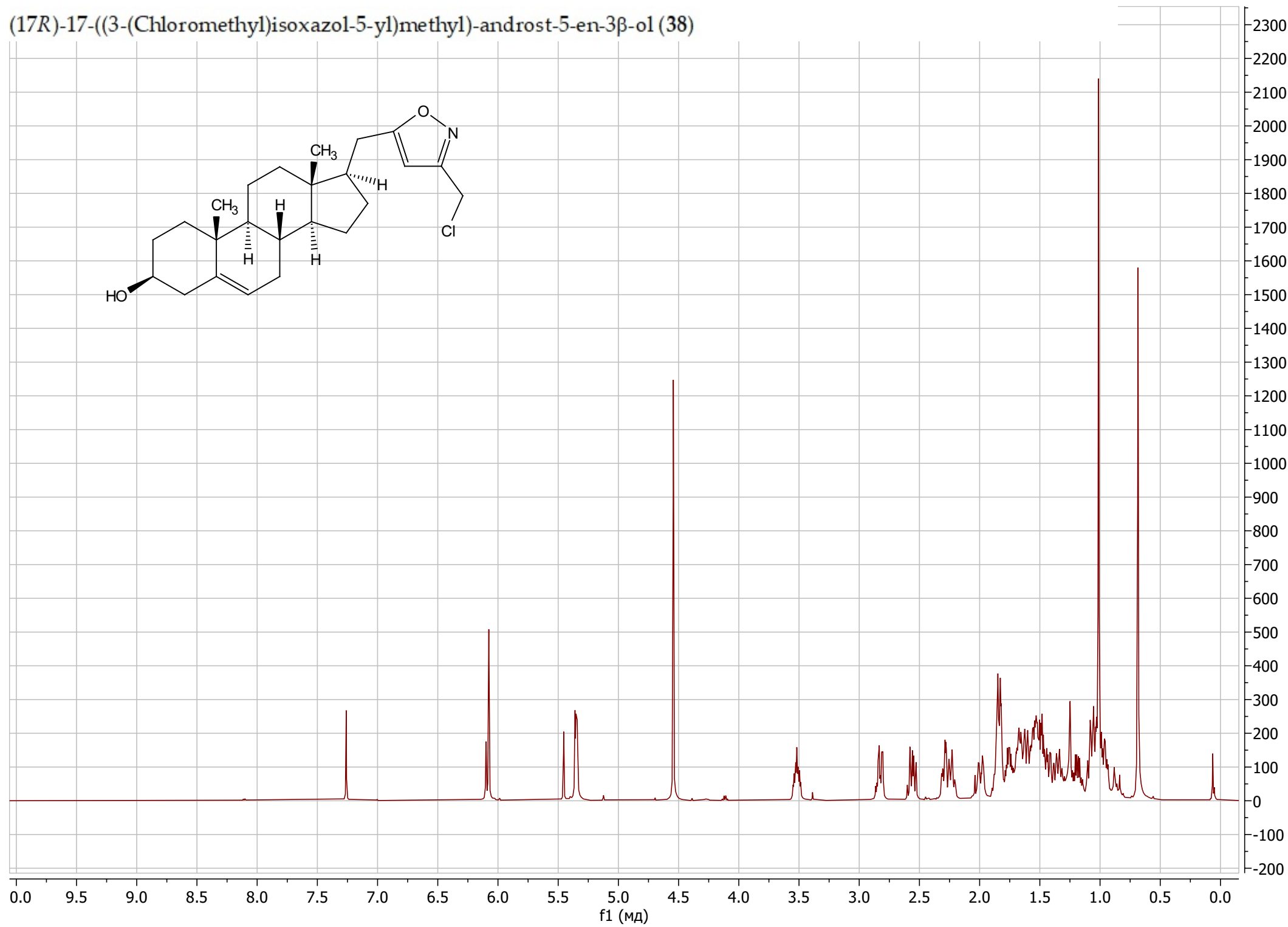
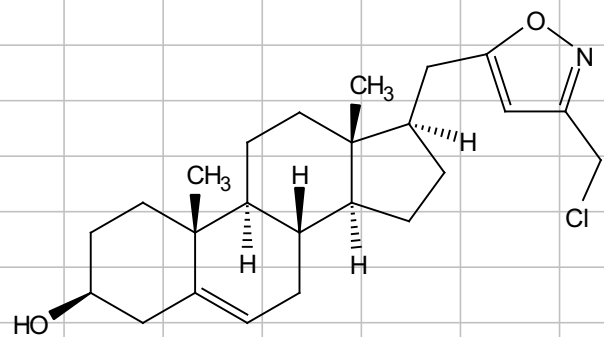


5-(((17R)-3 β -((*tert*-Butyldimethylsilyloxy)-androst-5-en-17-yl)methyl)-3-(chloromethyl)isoxazole (37)

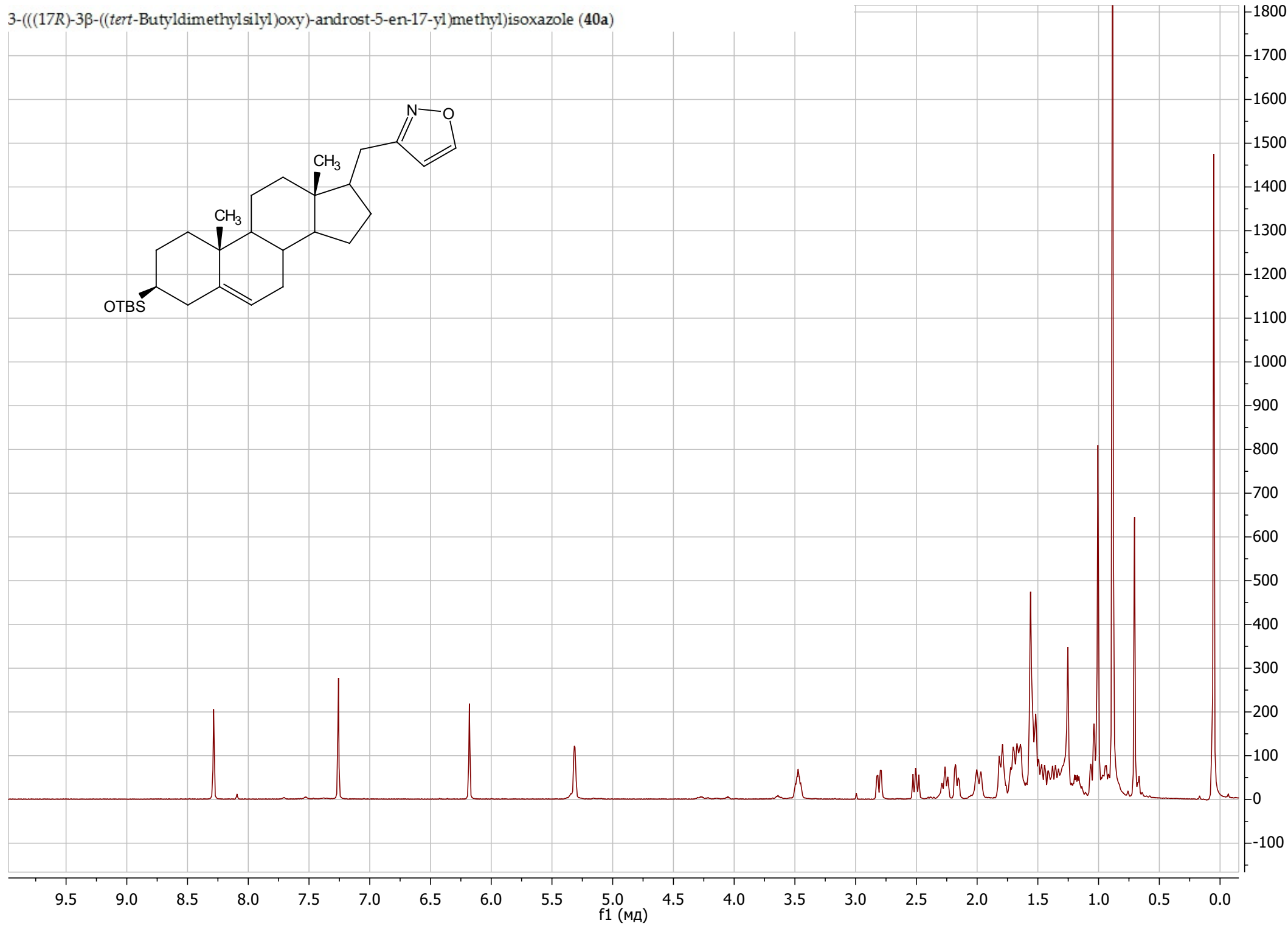
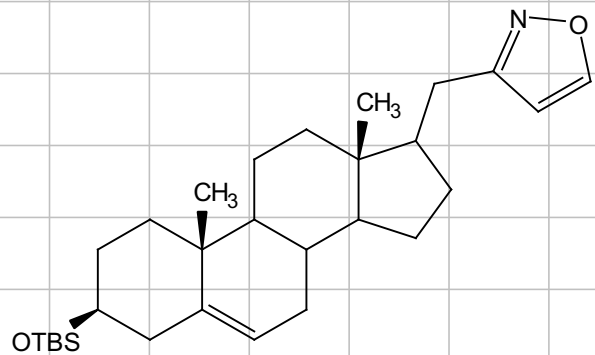




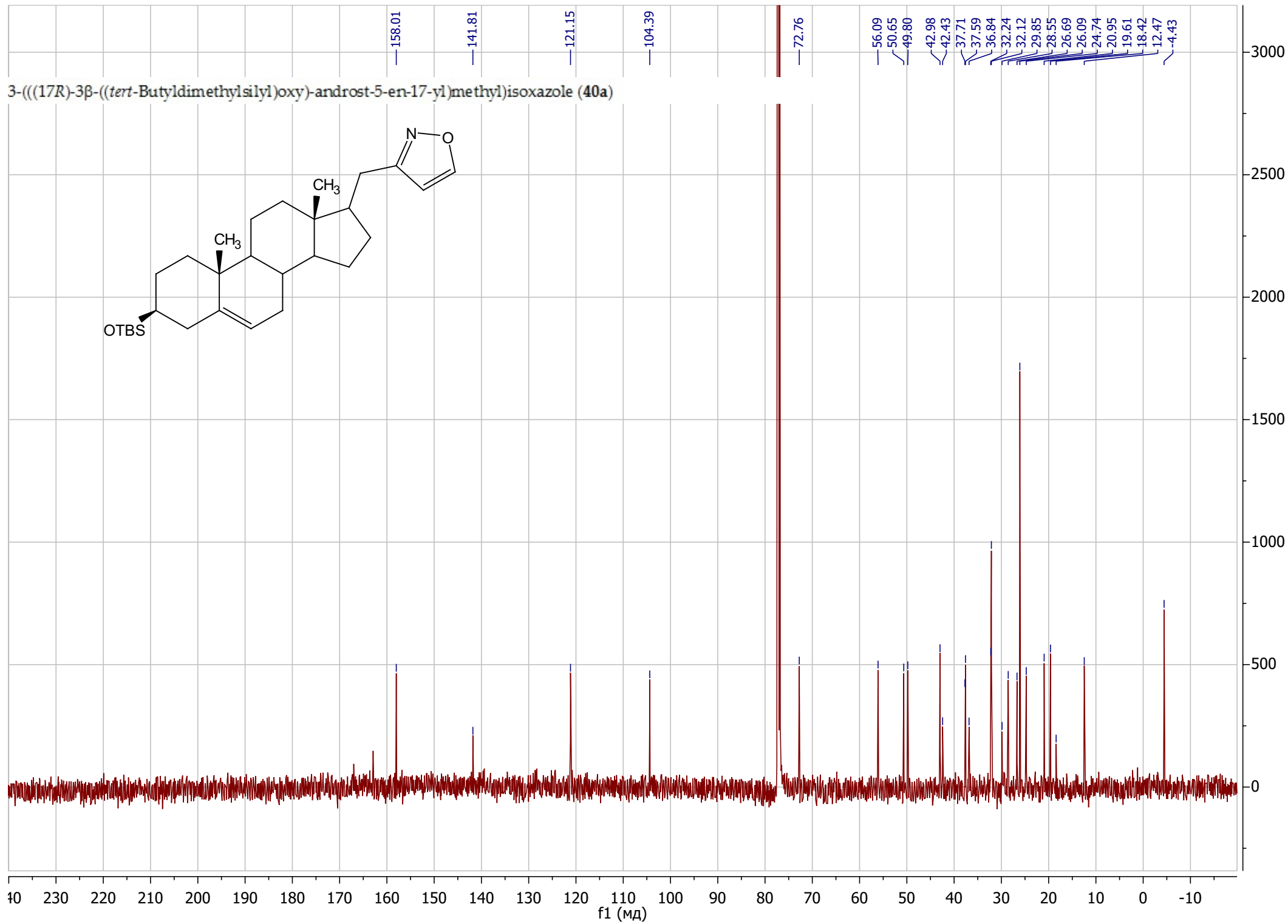
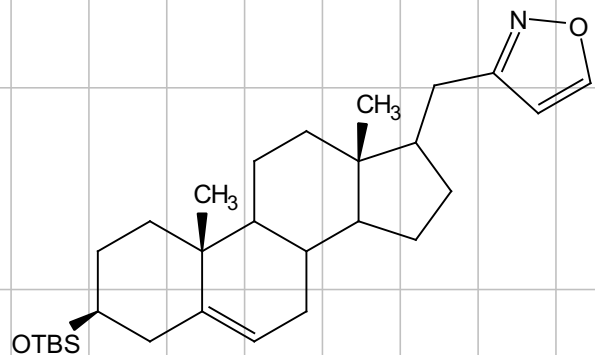
(17R)-17-((3-(Chloromethyl)isoxazol-5-yl)methyl)-androst-5-en-3 β -ol (38)



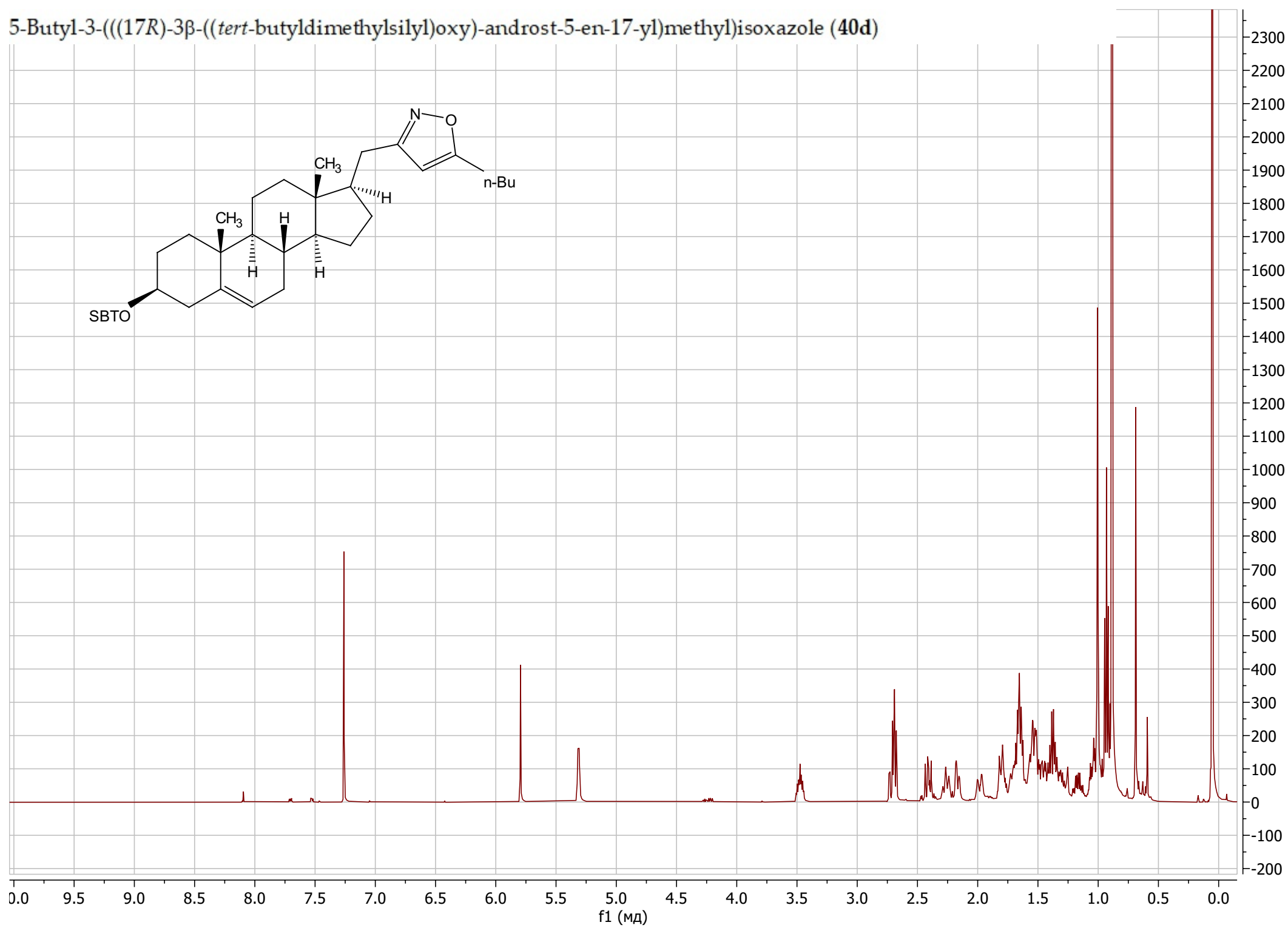
3-(((17R)-3 β -((*tert*-Butyldimethylsilyl)oxy)-androst-5-en-17-yl)methyl)isoxazole (40a)



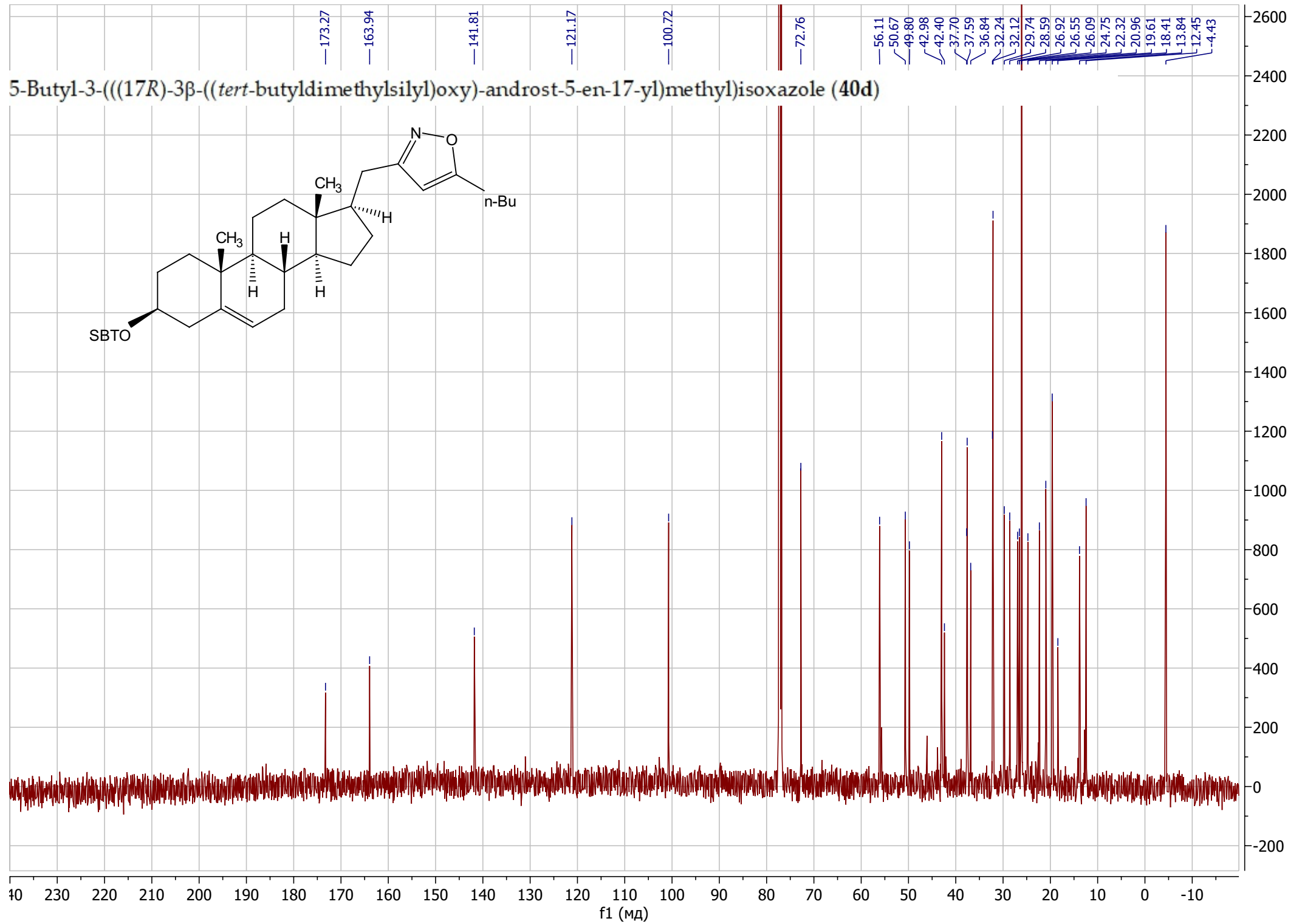
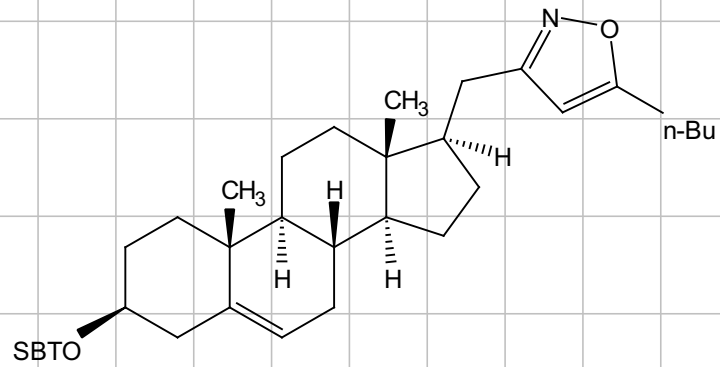
3-(((17R)-3 β -((*tert*-Butyldimethylsilyl)oxy)-androst-5-en-17-yl)methyl)isoxazole (40a)



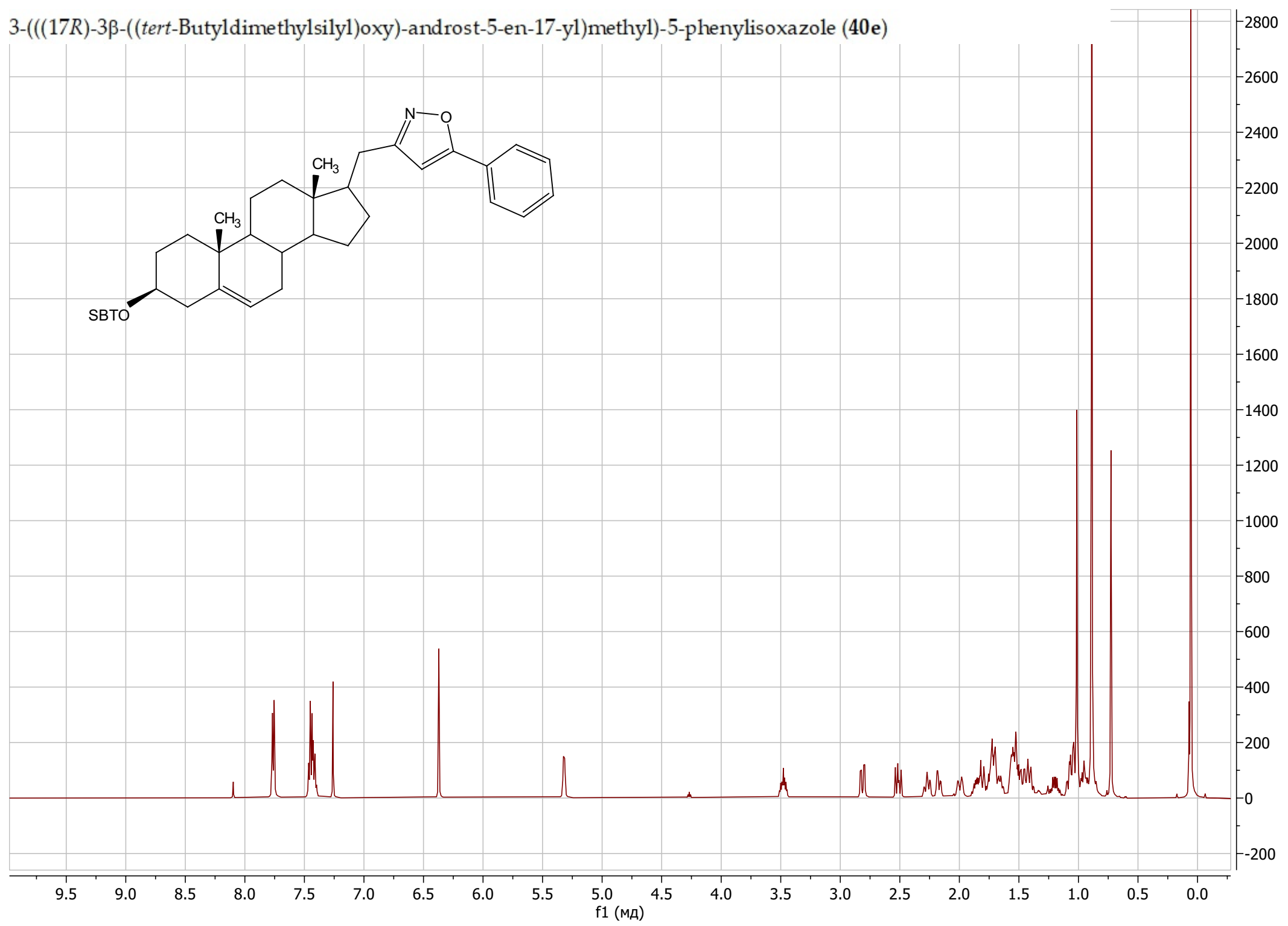
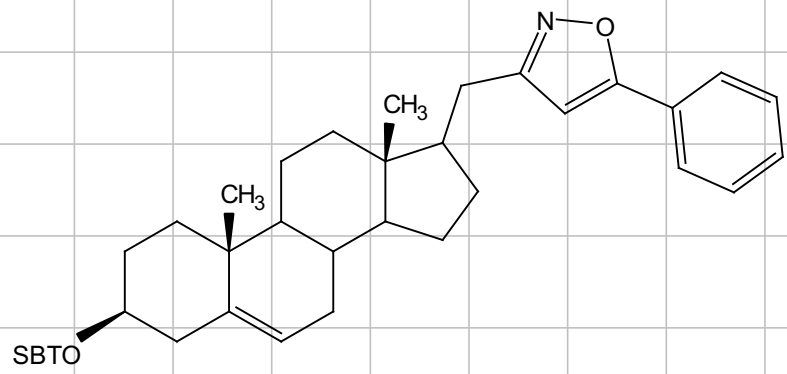
5-Butyl-3-(((17R)-3 β -((*tert*-butyldimethylsilyl)oxy)-androst-5-en-17-yl)methyl)isoxazole (40d)



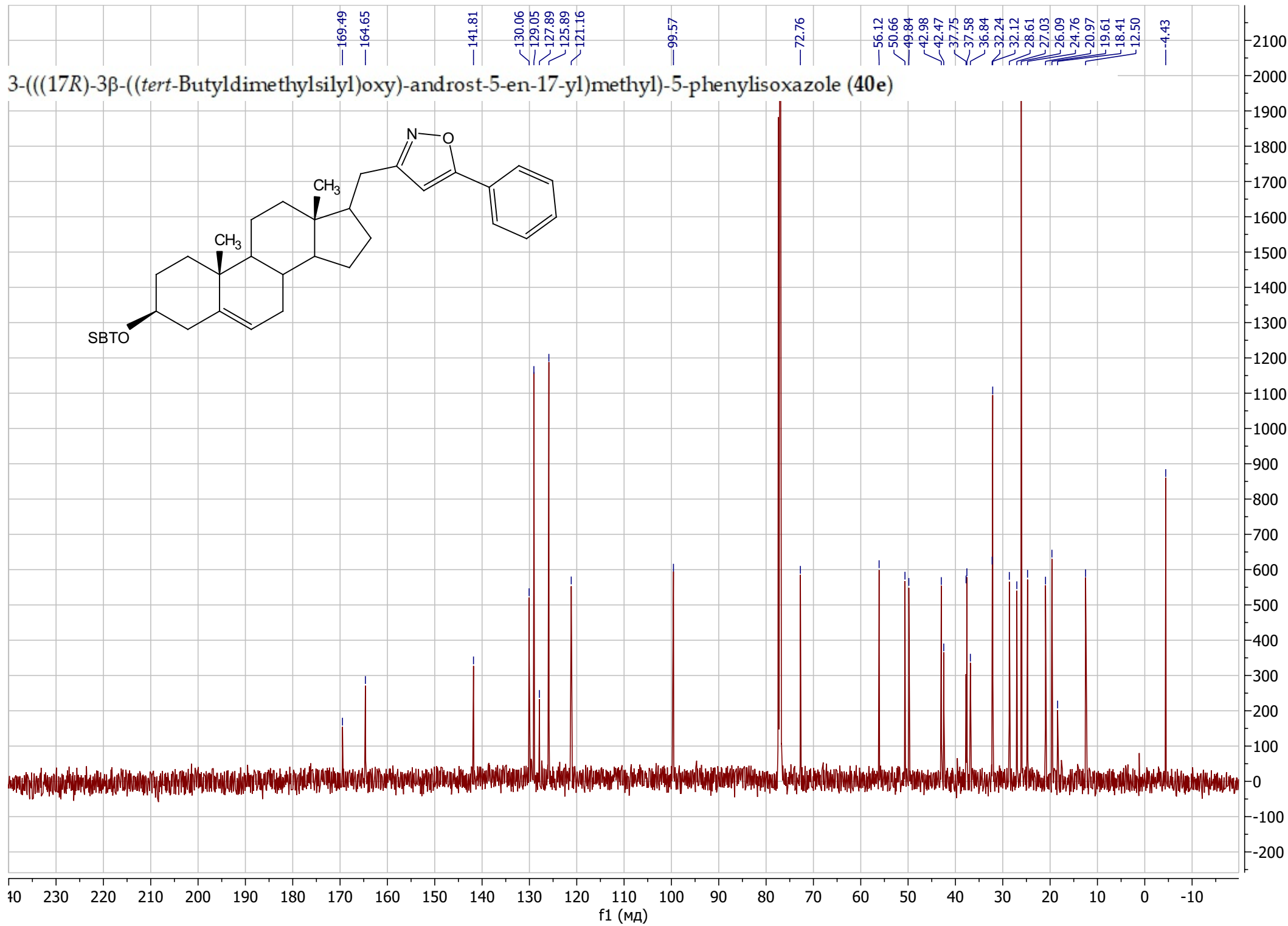
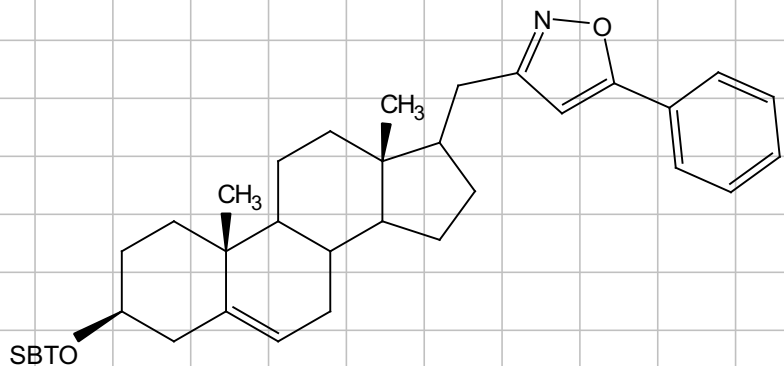
5-Butyl-3-(((17R)-3 β -((*tert*-butyldimethylsilyl)oxy)-androst-5-en-17-yl)methyl)isoxazole (40d)



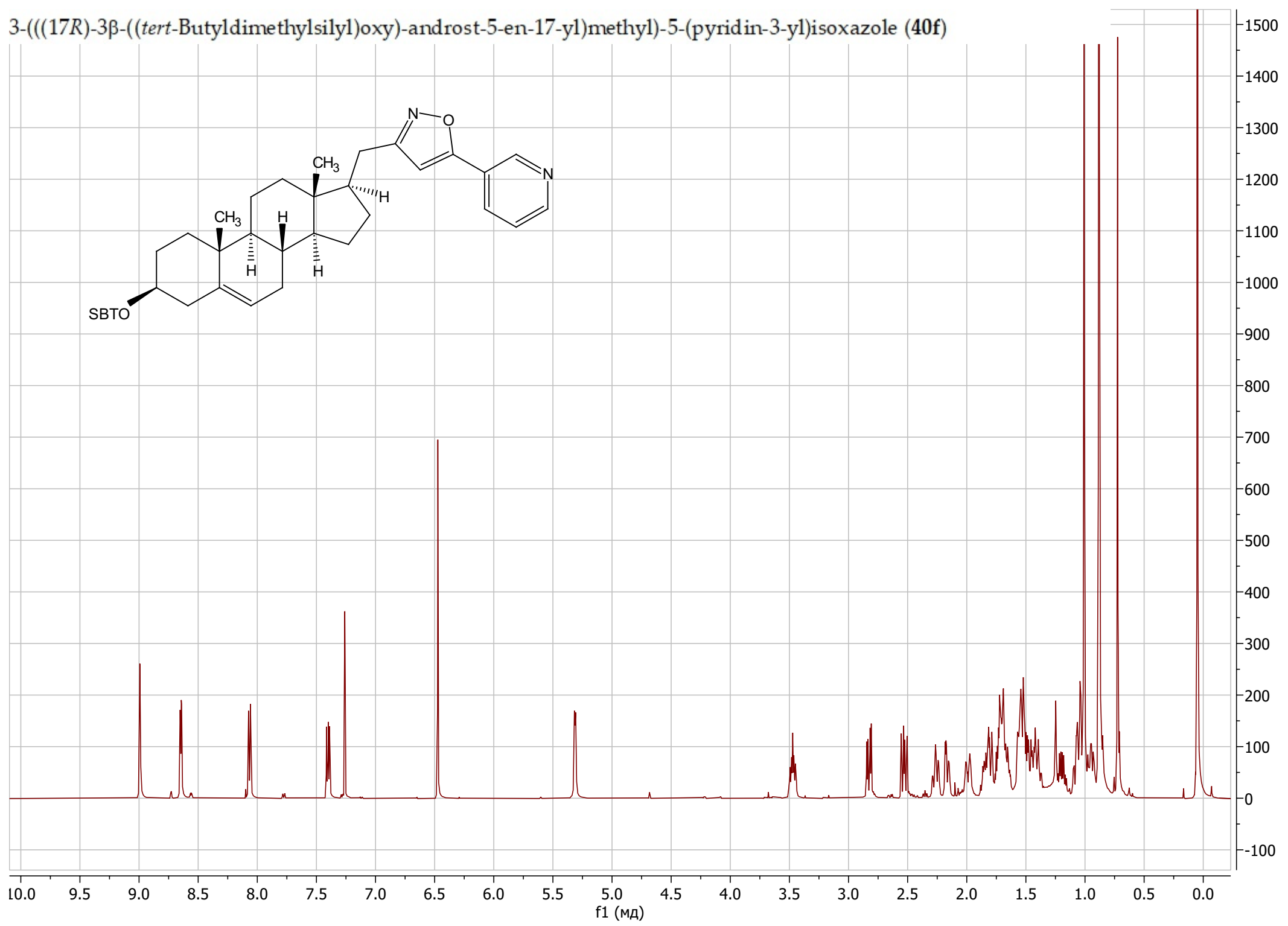
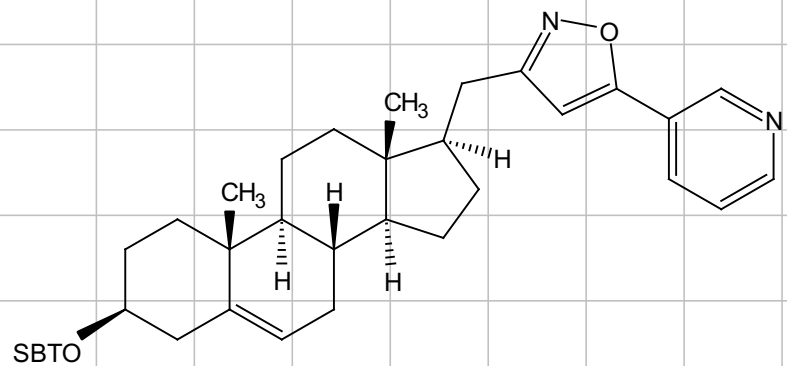
3-(((17R)-3 β -((*tert*-Butyldimethylsilyl)oxy)-androst-5-en-17-yl)methyl)-5-phenylisoxazole (40e)



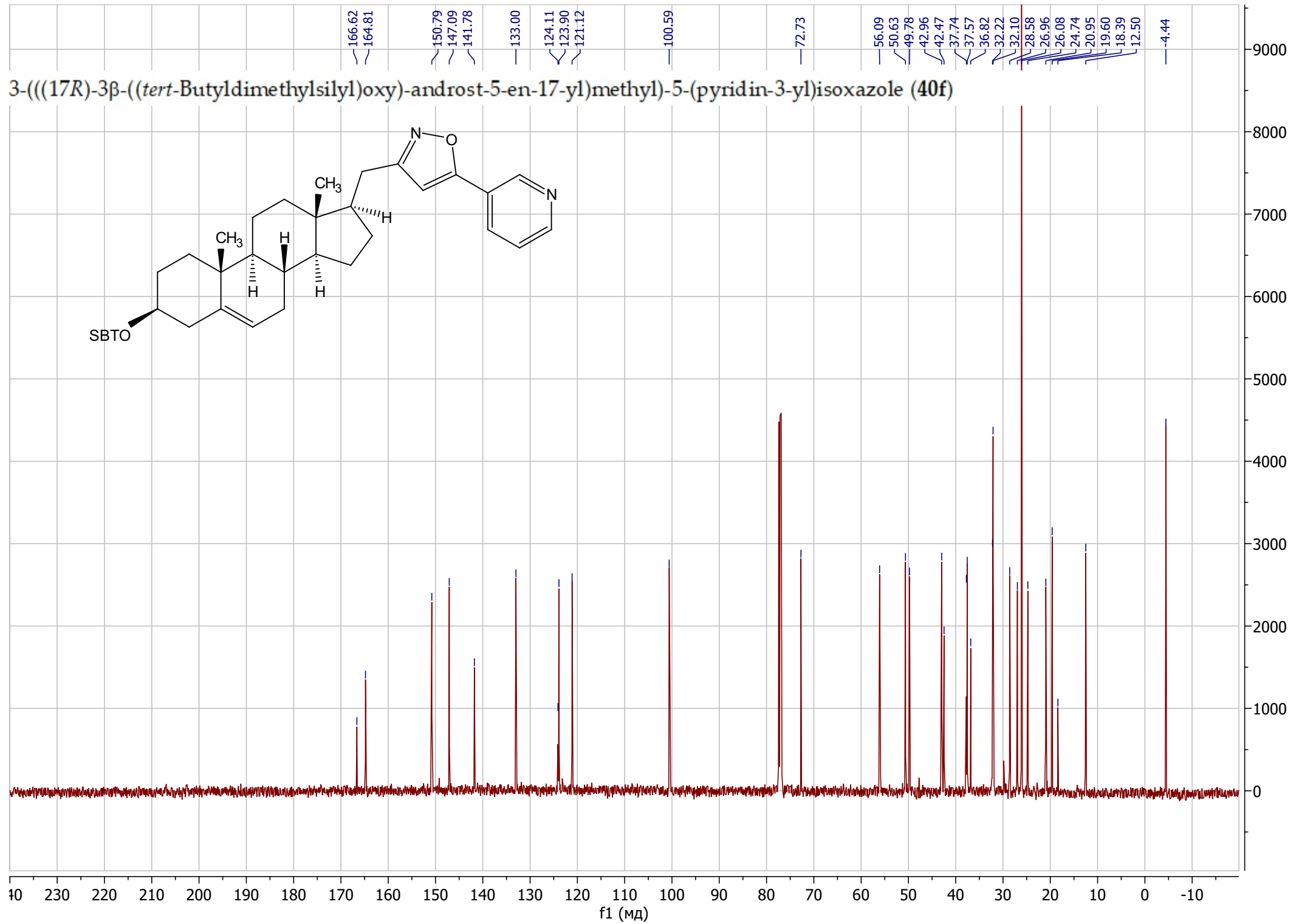
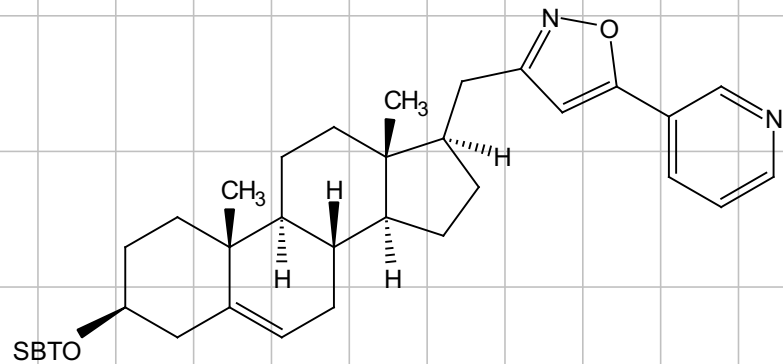
3-(((17R)-3β-((*tert*-Butyldimethylsilyl)oxy)-androst-5-en-17-yl)methyl)-5-phenylisoxazole (40e)



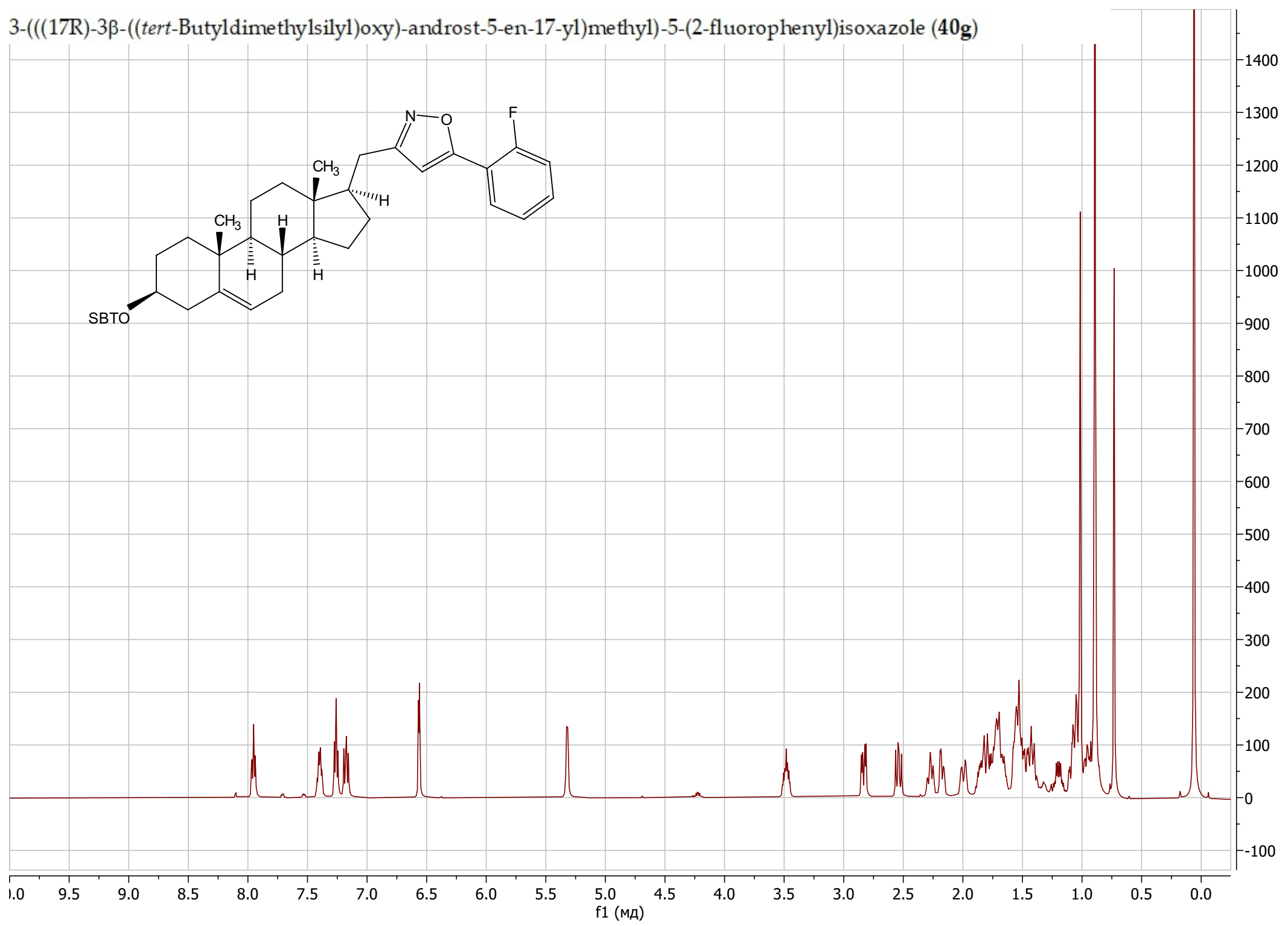
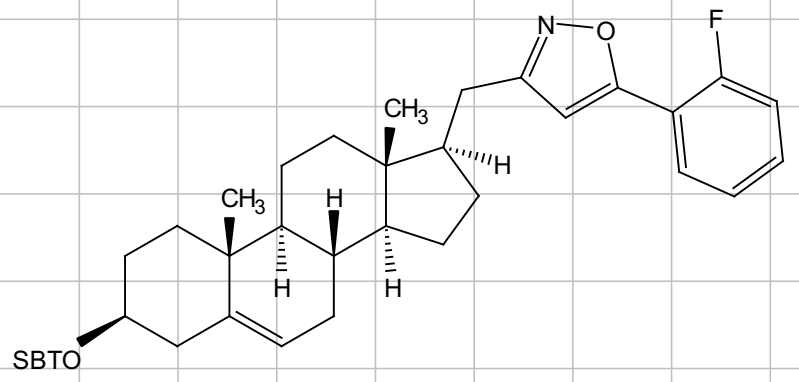
3-(((17R)-3 β -((*tert*-Butyldimethylsilyloxy)-androst-5-en-17-yl)methyl)-5-(pyridin-3-yl)isoxazole (40f)



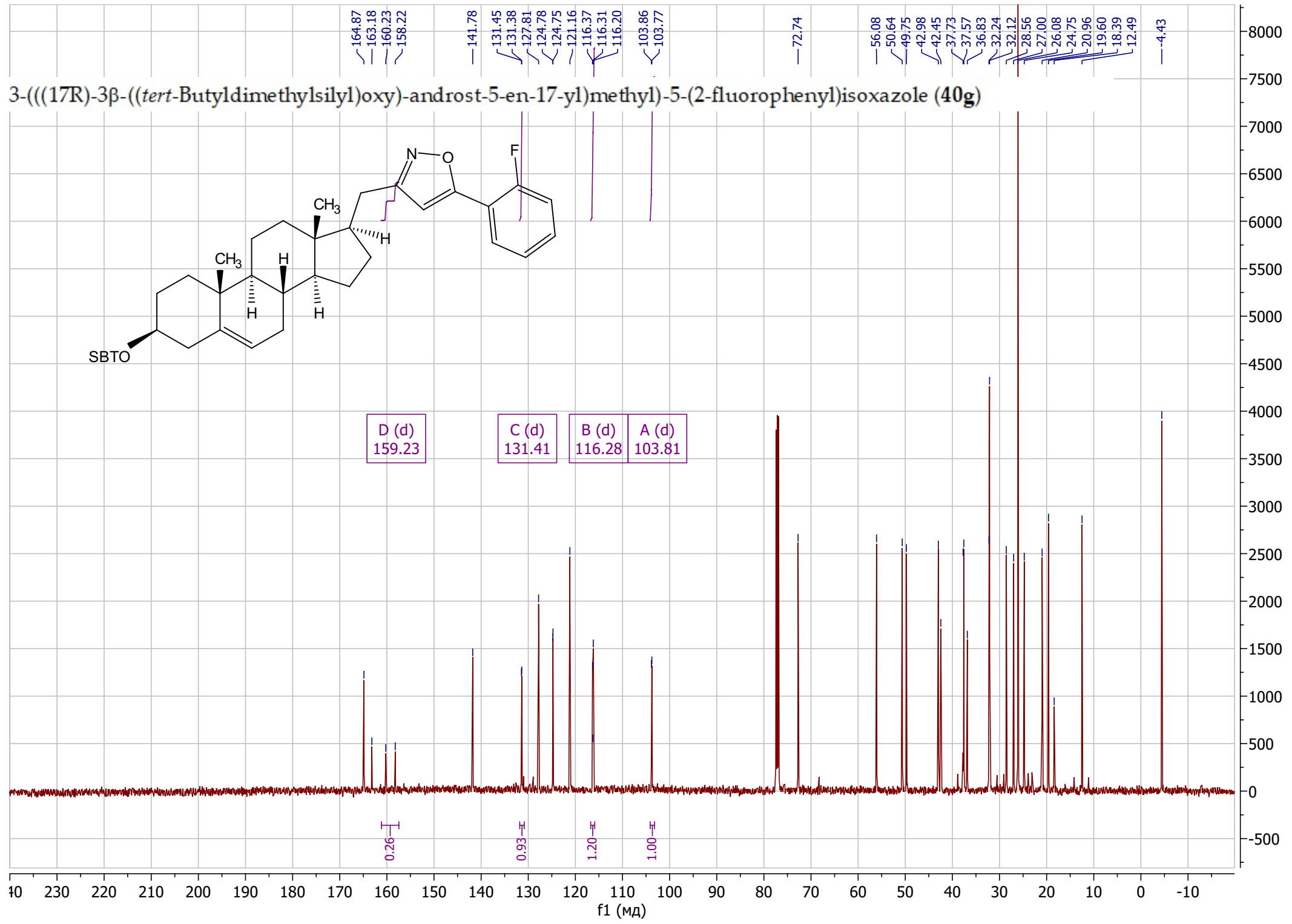
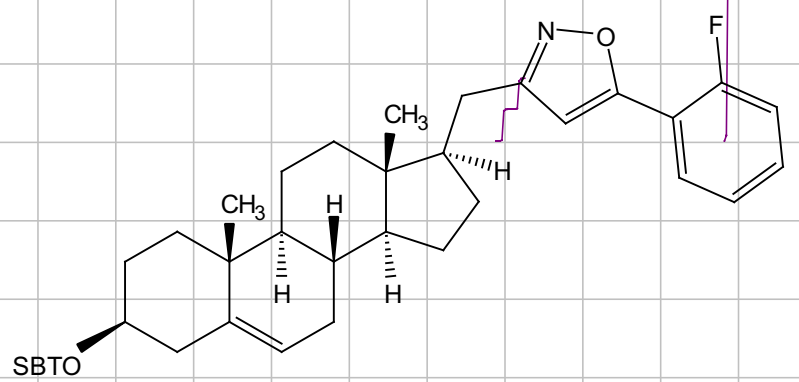
3-(((17R)-3 β -((*tert*-Butyldimethylsilyl)oxy)-androst-5-en-17-yl)methyl)-5-(pyridin-3-yl)isoxazole (40f)



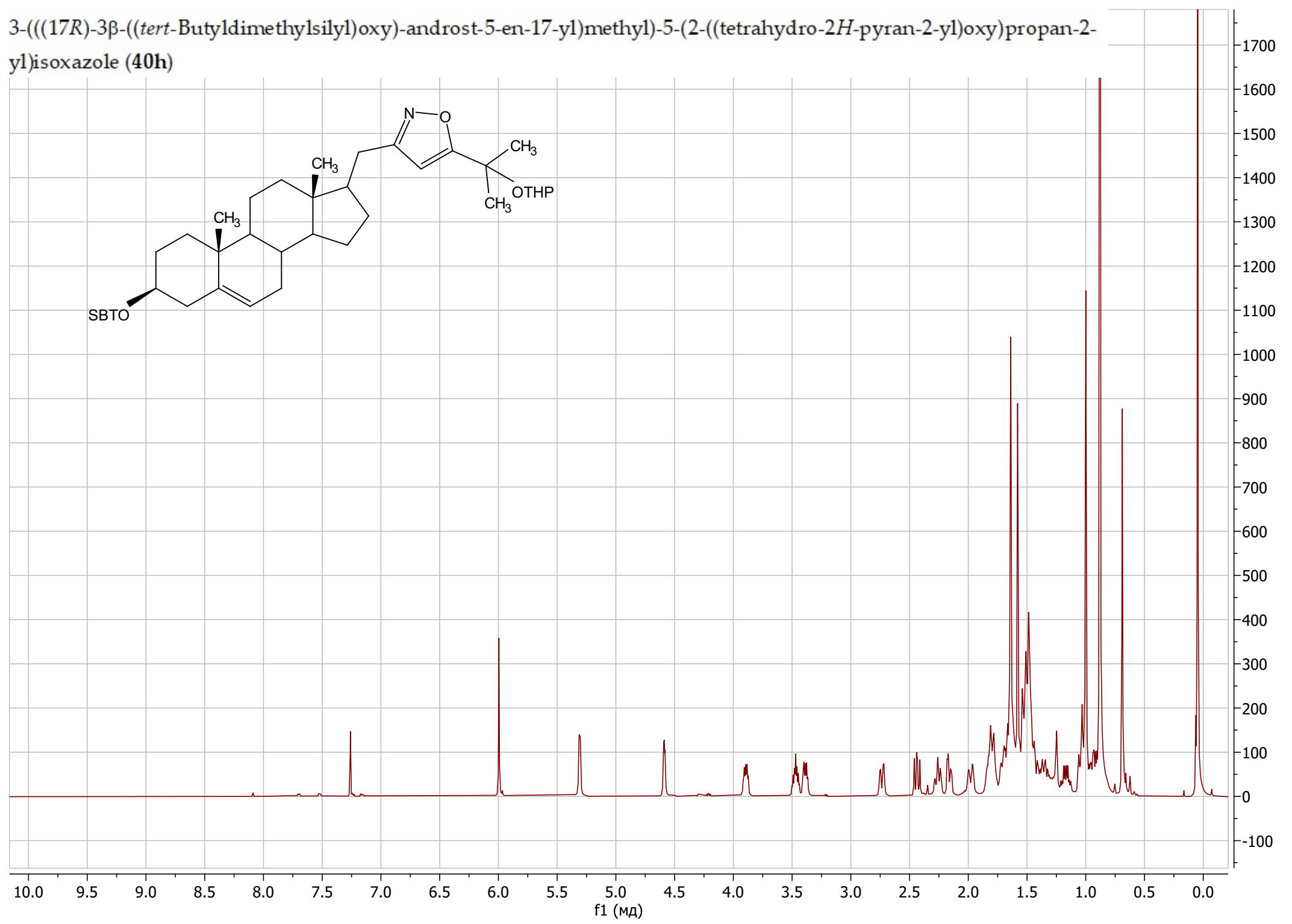
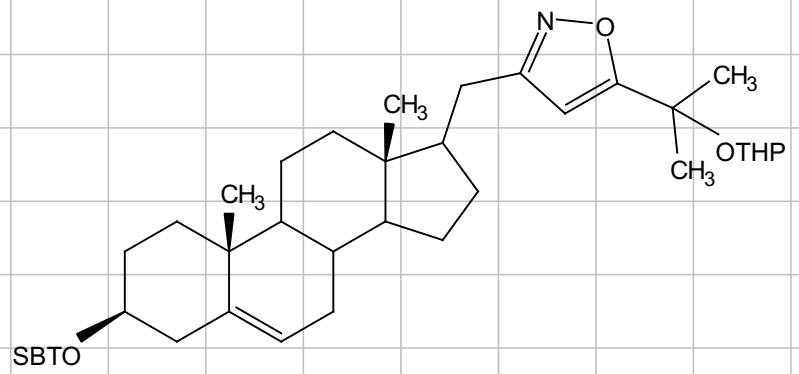
3-(((17R)-3 β -((*tert*-Butyldimethylsilyloxy)-androst-5-en-17-yl)methyl)-5-(2-fluorophenyl)isoxazole (40g)



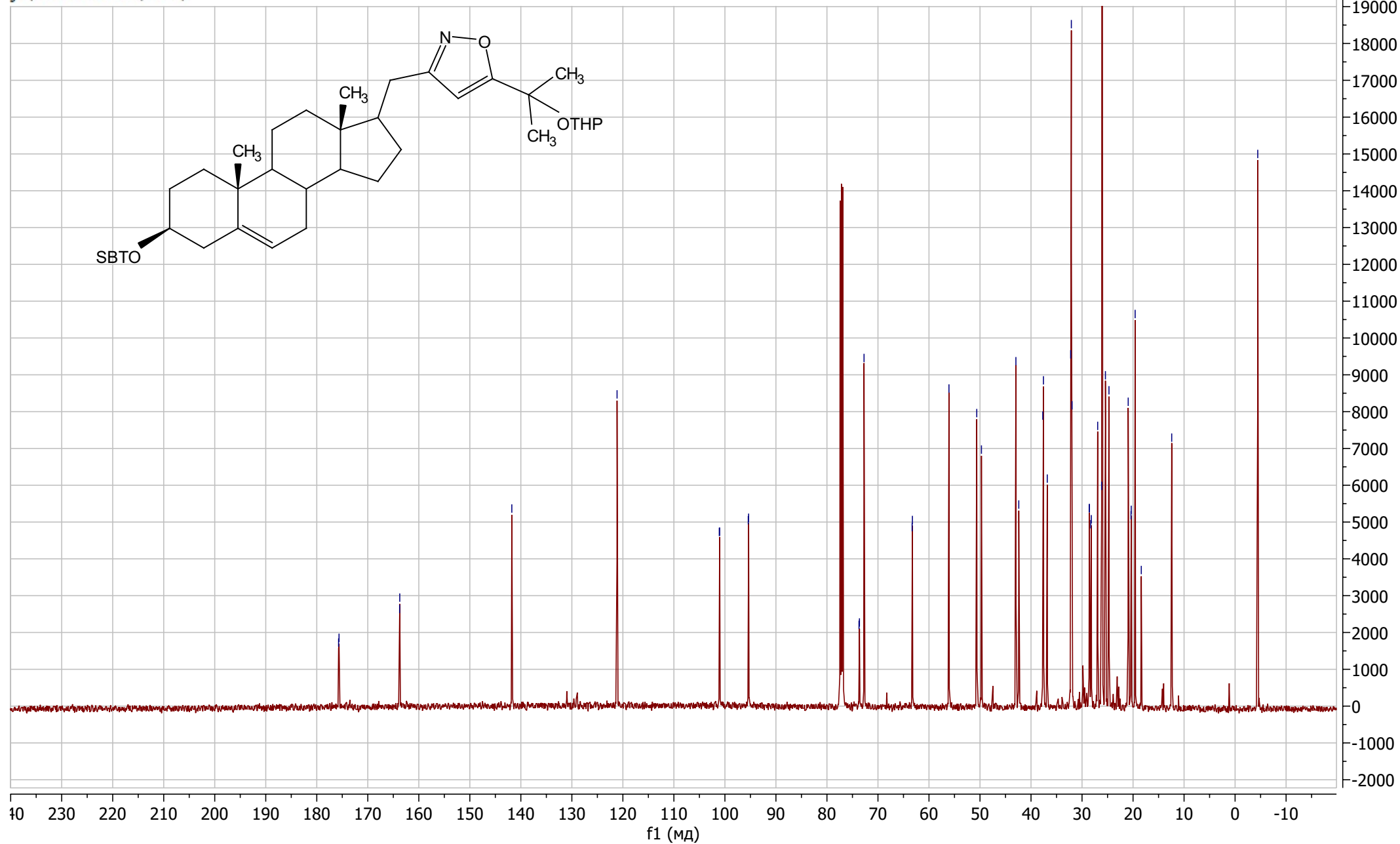
3-(((17R)-3 β -((*tert*-Butyldimethylsilyl)oxy)-androst-5-en-17-yl)methyl)-5-(2-fluorophenyl)isoxazole (40g)



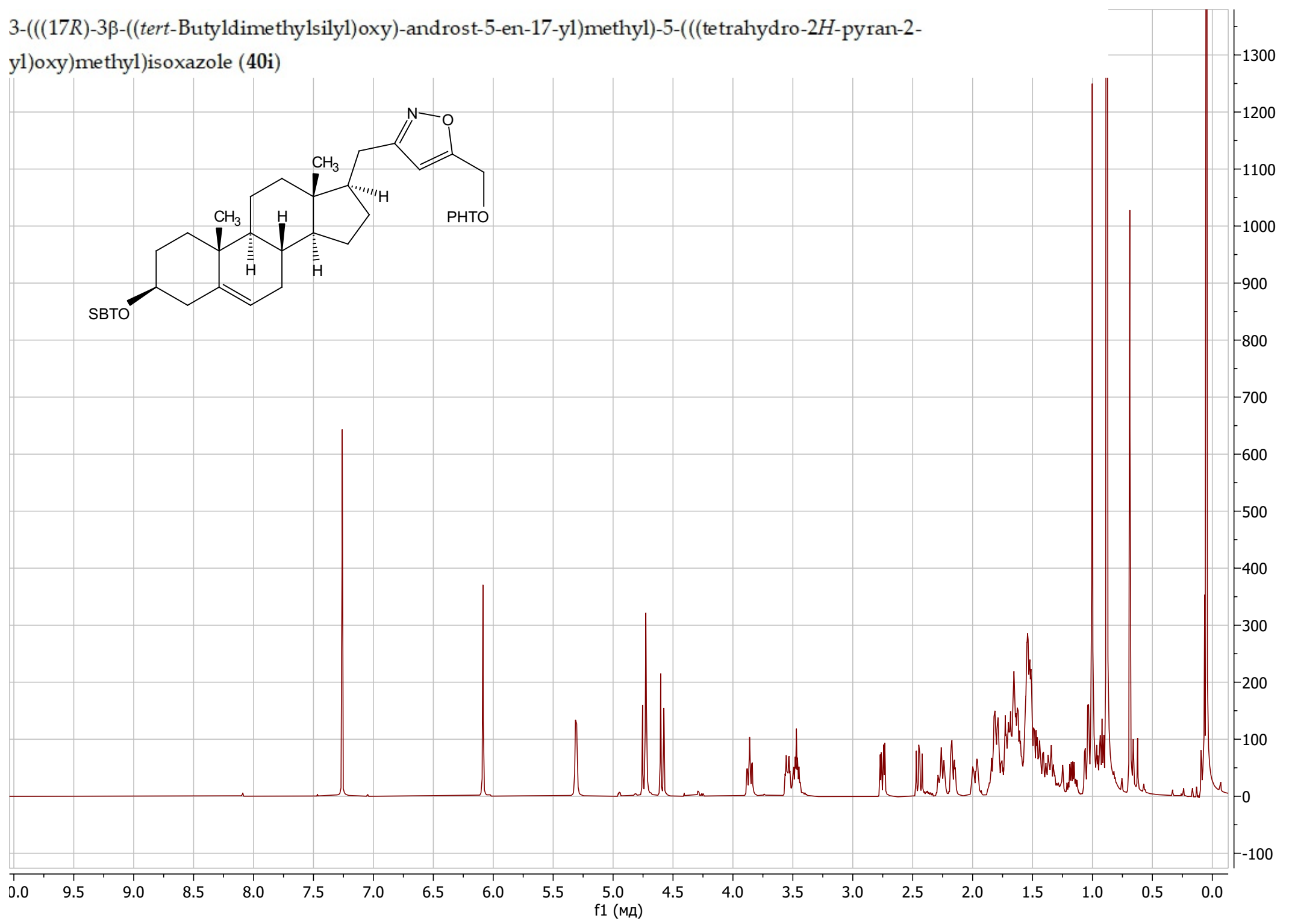
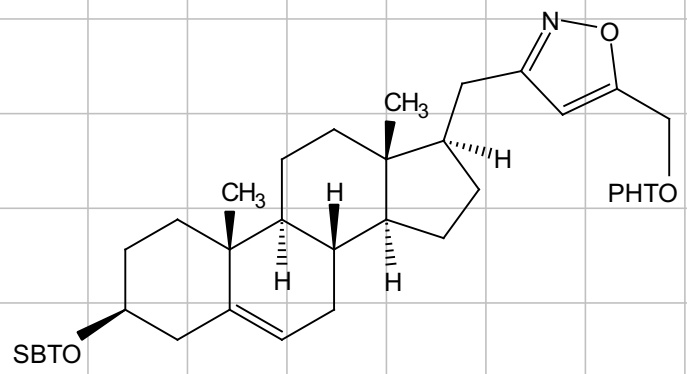
3-(((17R)-3 β -((*tert*-Butyldimethylsilyl)oxy)-androst-5-en-17-yl)methyl)-5-(2-((tetrahydro-2H-pyran-2-yl)oxy)propan-2-yl)isoxazole (40h)



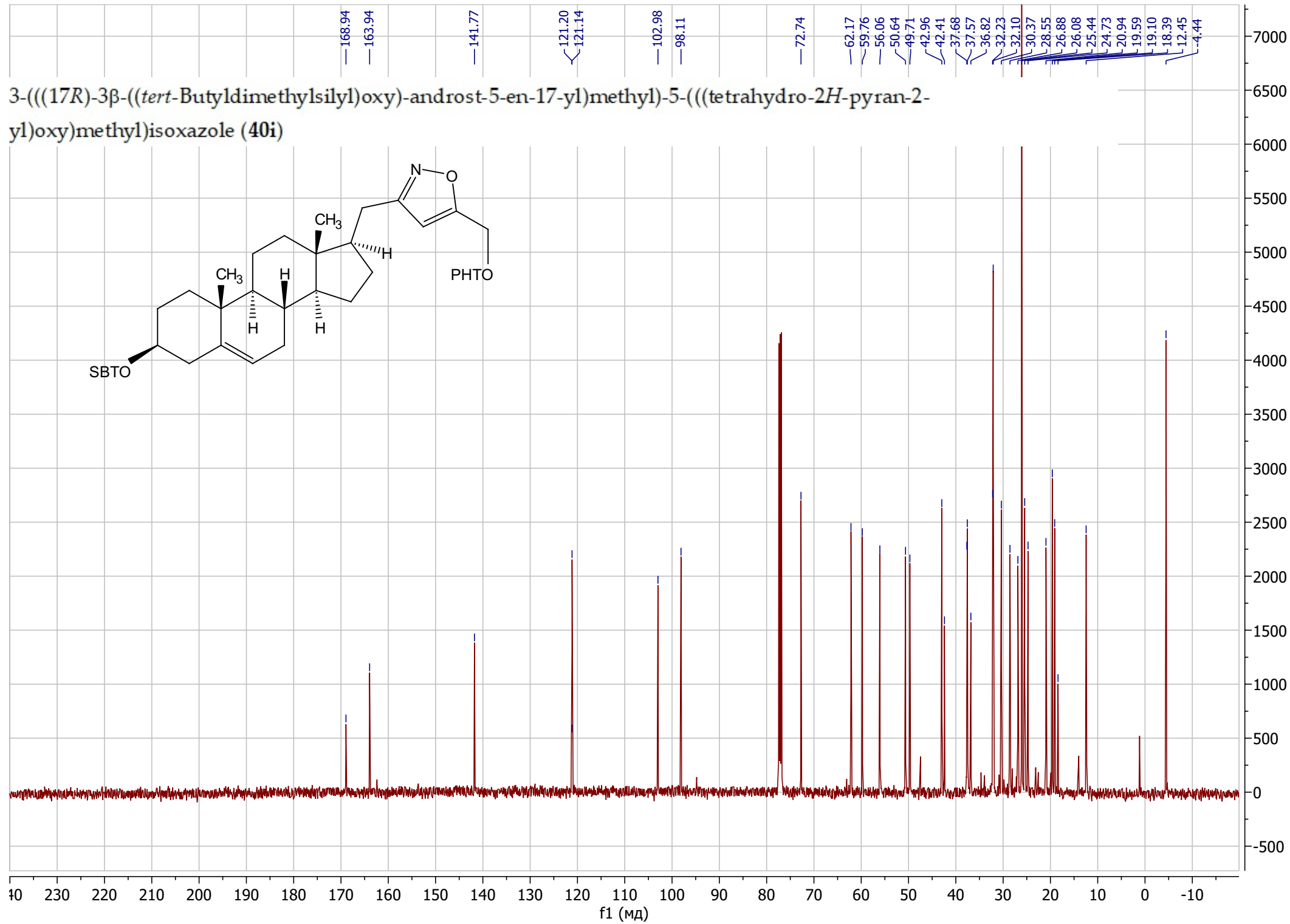
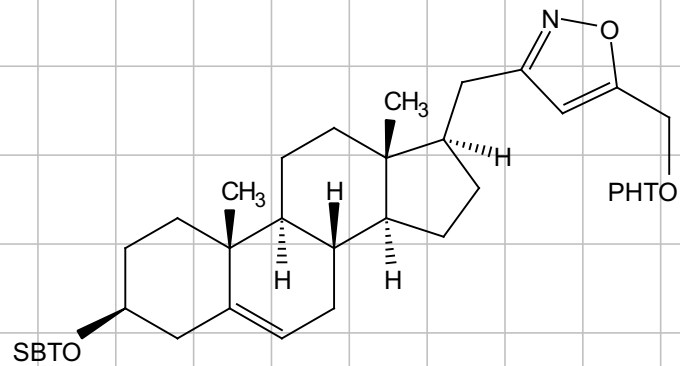
3-(((17*R*)-3β-((*tert*-Butyldimethylsilyl)oxy)-androst-5-en-17-yl)methyl)-5-(2-((tetrahydro-2*H*-pyran-2-yl)oxy)propan-2-yl)isoxazole (40h)



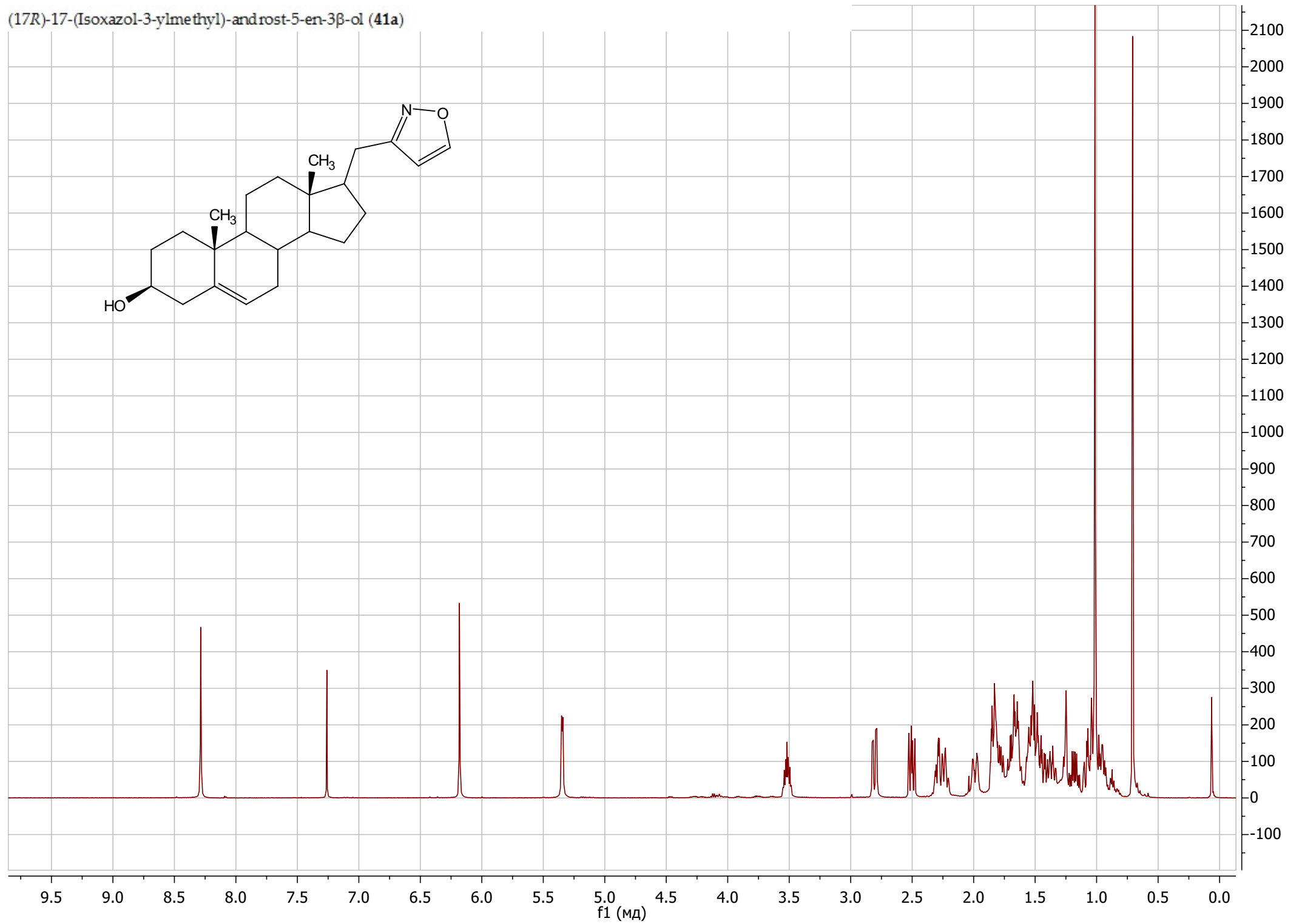
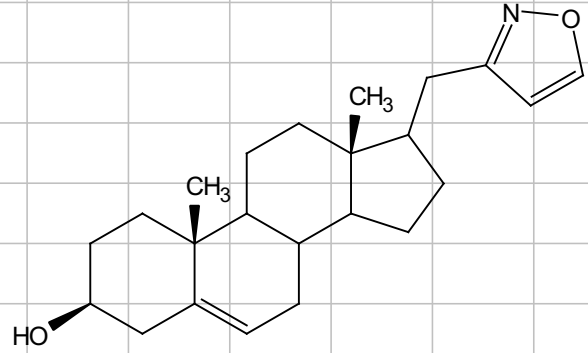
3-(((17R)-3 β -((*tert*-Butyldimethylsilyl)oxy)-androst-5-en-17-yl)methyl)-5-(((tetrahydro-2*H*-pyran-2-yl)oxy)methyl)isoxazole (40i)



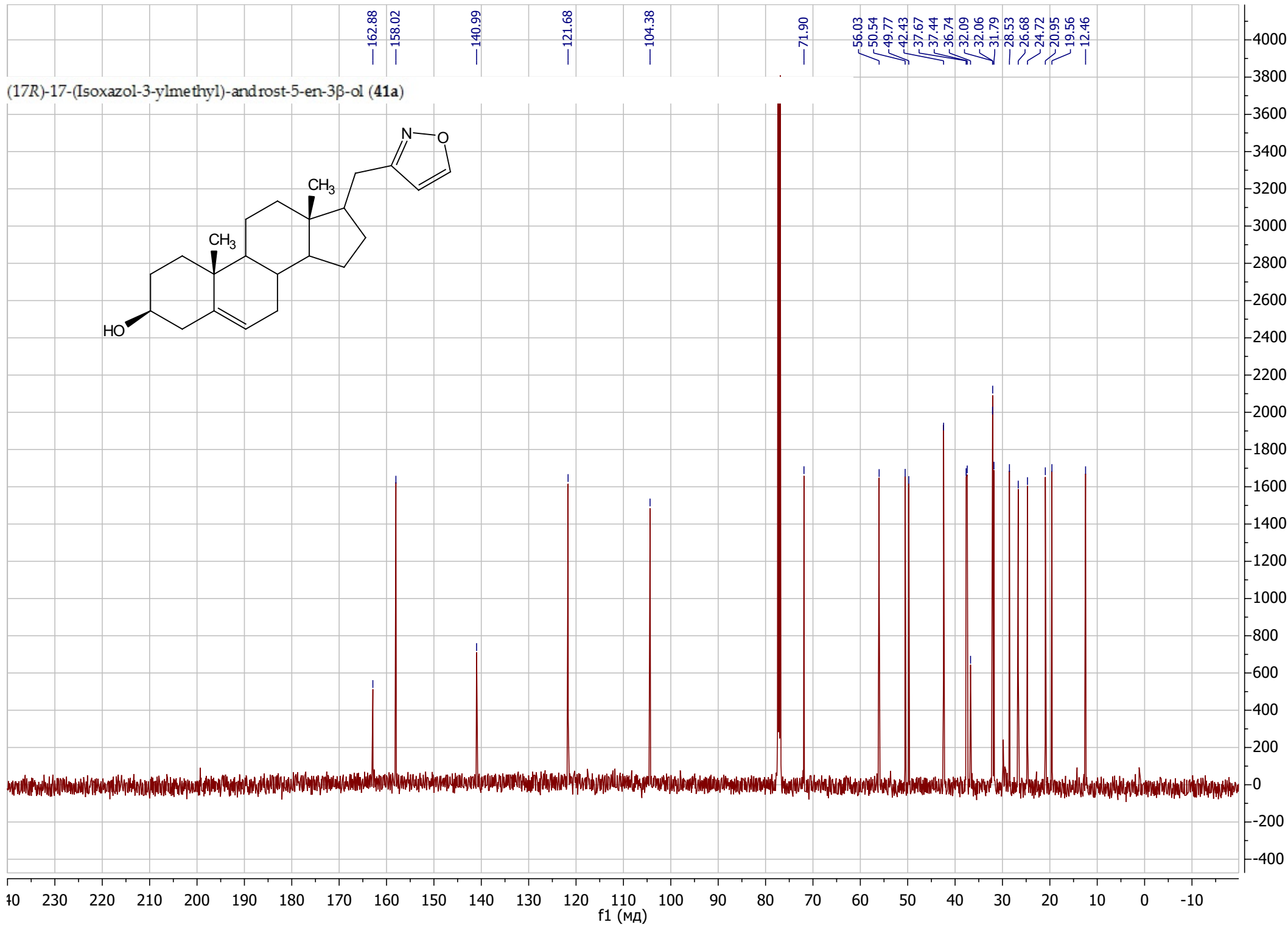
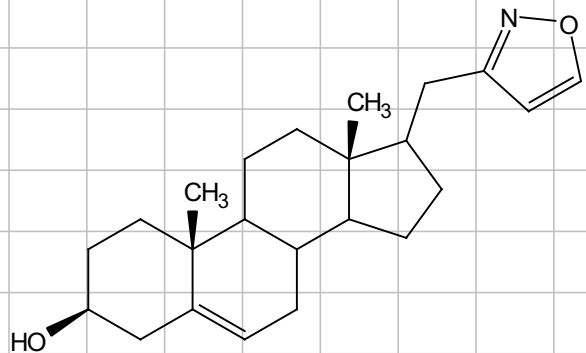
3-(((17*R*)-3β-((*tert*-Butyldimethylsilyl)oxy)-androst-5-en-17-yl)methyl)-5-(((tetrahydro-2*H*-pyran-2-yl)oxy)methyl)isoxazole (40i)



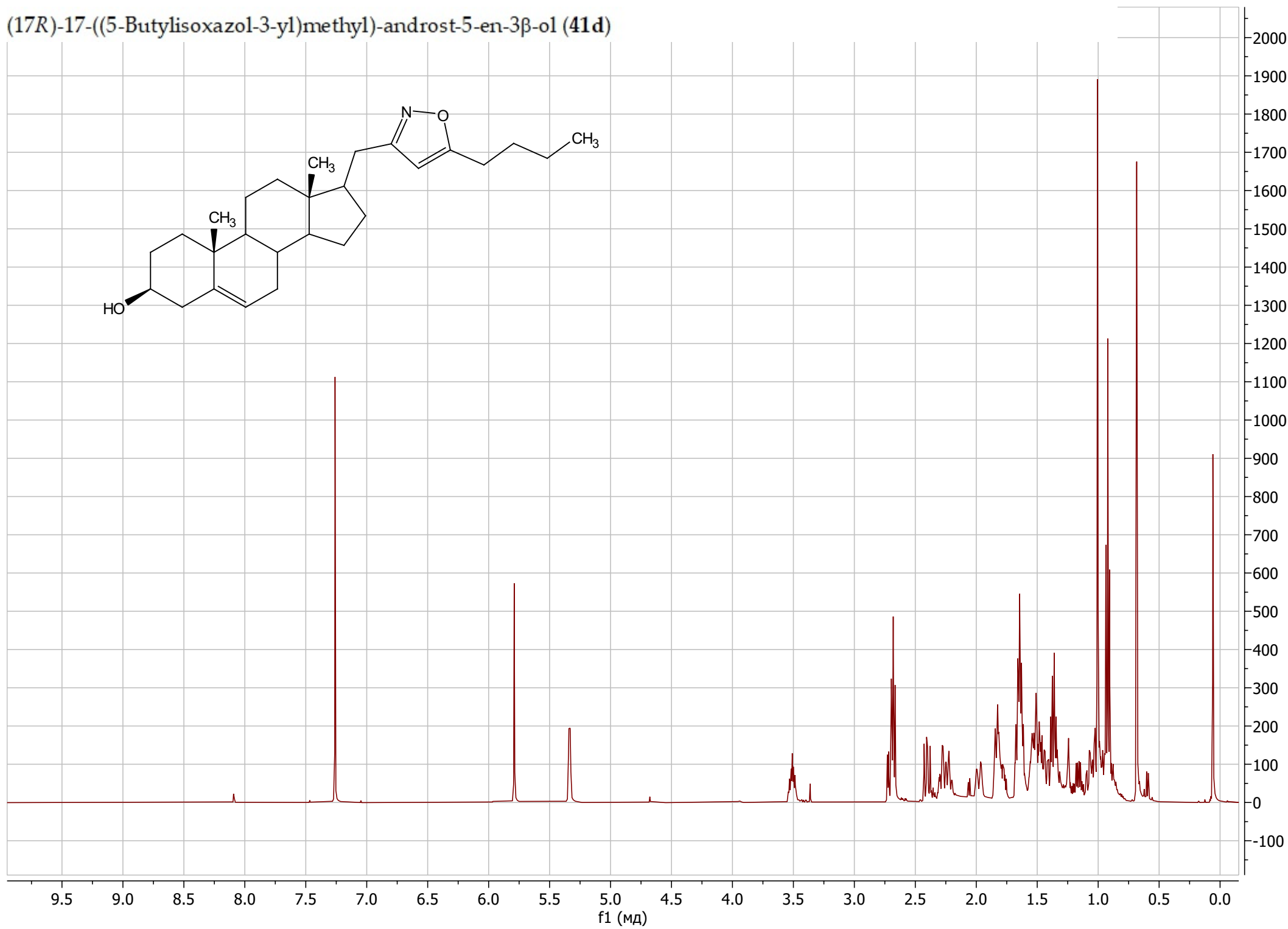
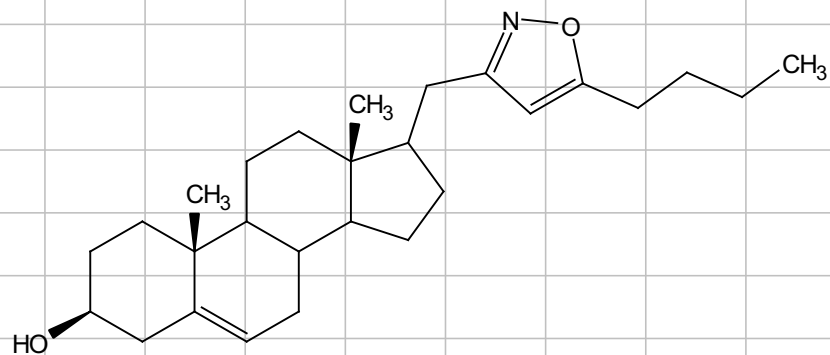
(17R)-17-(Isoxazol-3-ylmethyl)-androst-5-en-3 β -ol (41a)



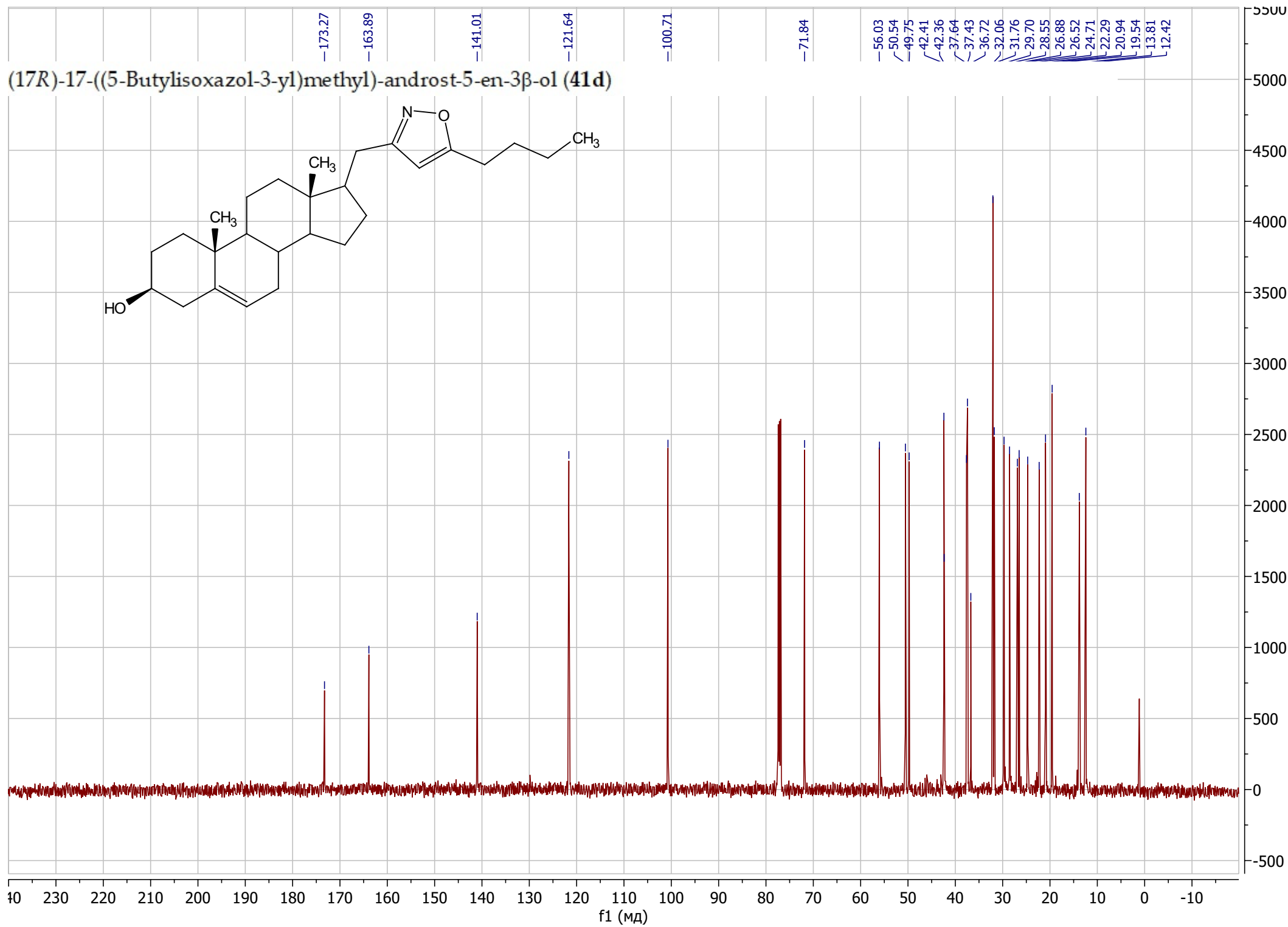
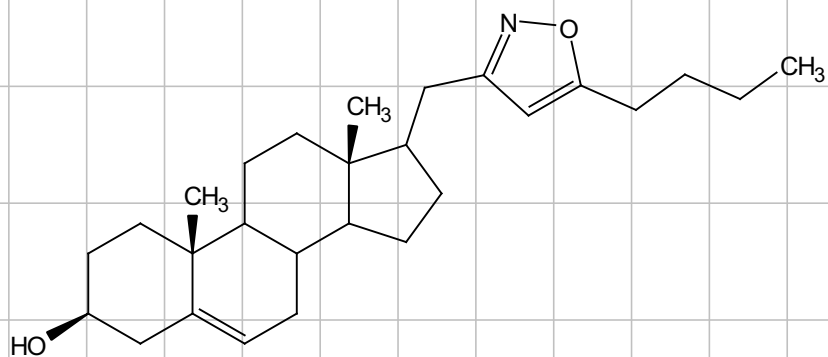
(17R)-17-(Isoxazol-3-ylmethyl)-androst-5-en-3 β -ol (41a)



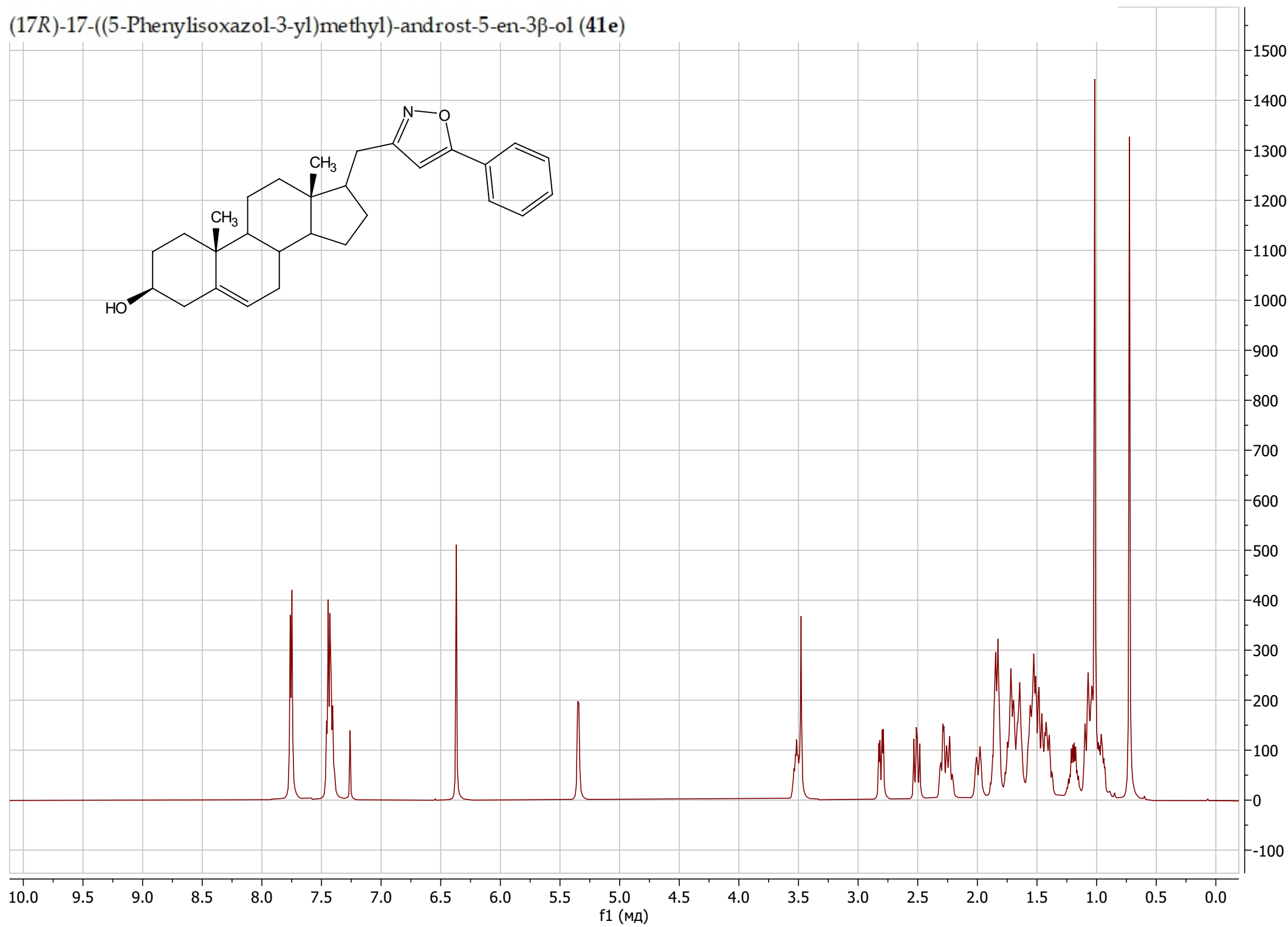
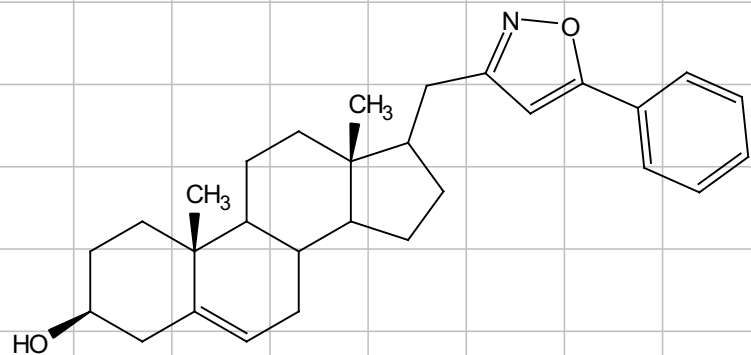
(17R)-17-((5-Butylisoxazol-3-yl)methyl)-androst-5-en-3 β -ol (41d)



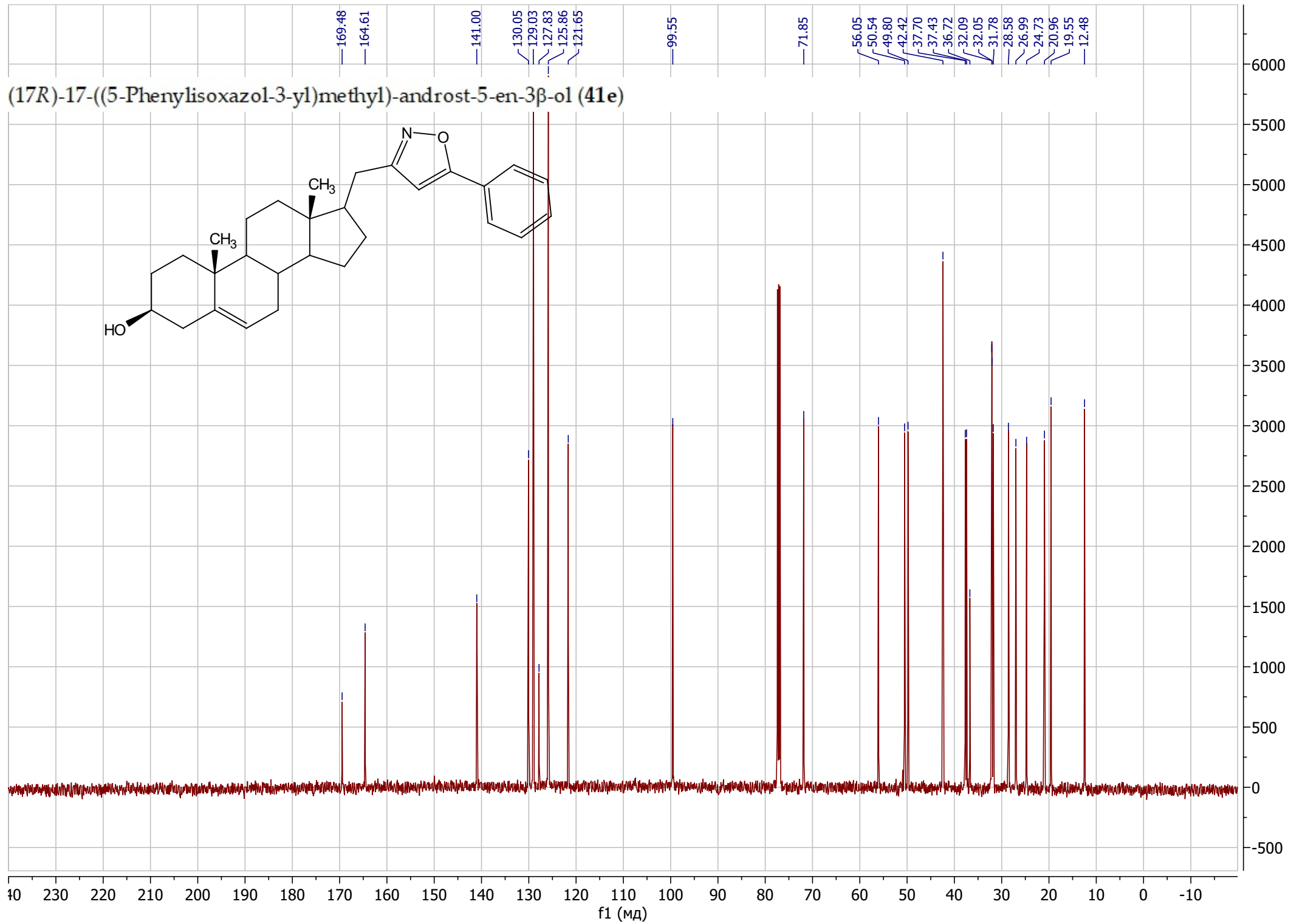
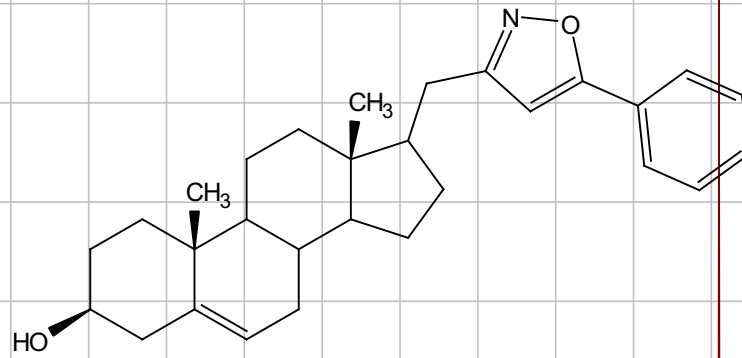
(17R)-17-((5-Butylisoxazol-3-yl)methyl)-androst-5-en-3 β -ol (41d)



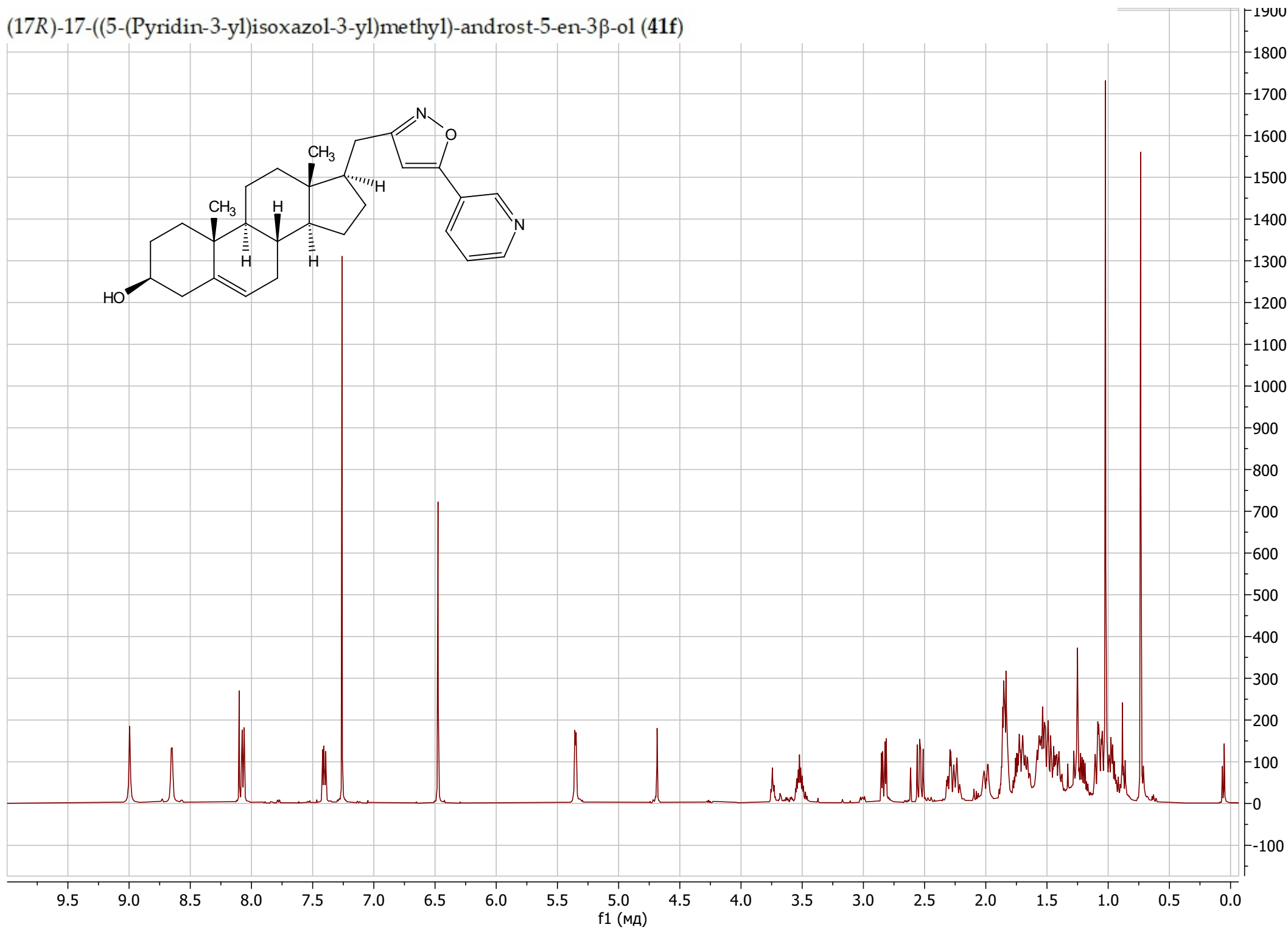
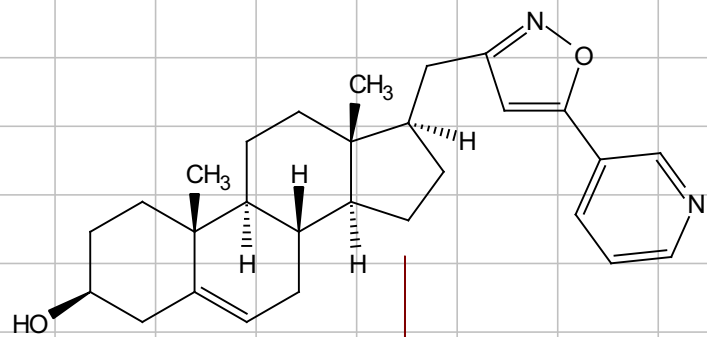
(17R)-17-((5-Phenylisoxazol-3-yl)methyl)-androst-5-en-3 β -ol (41e)



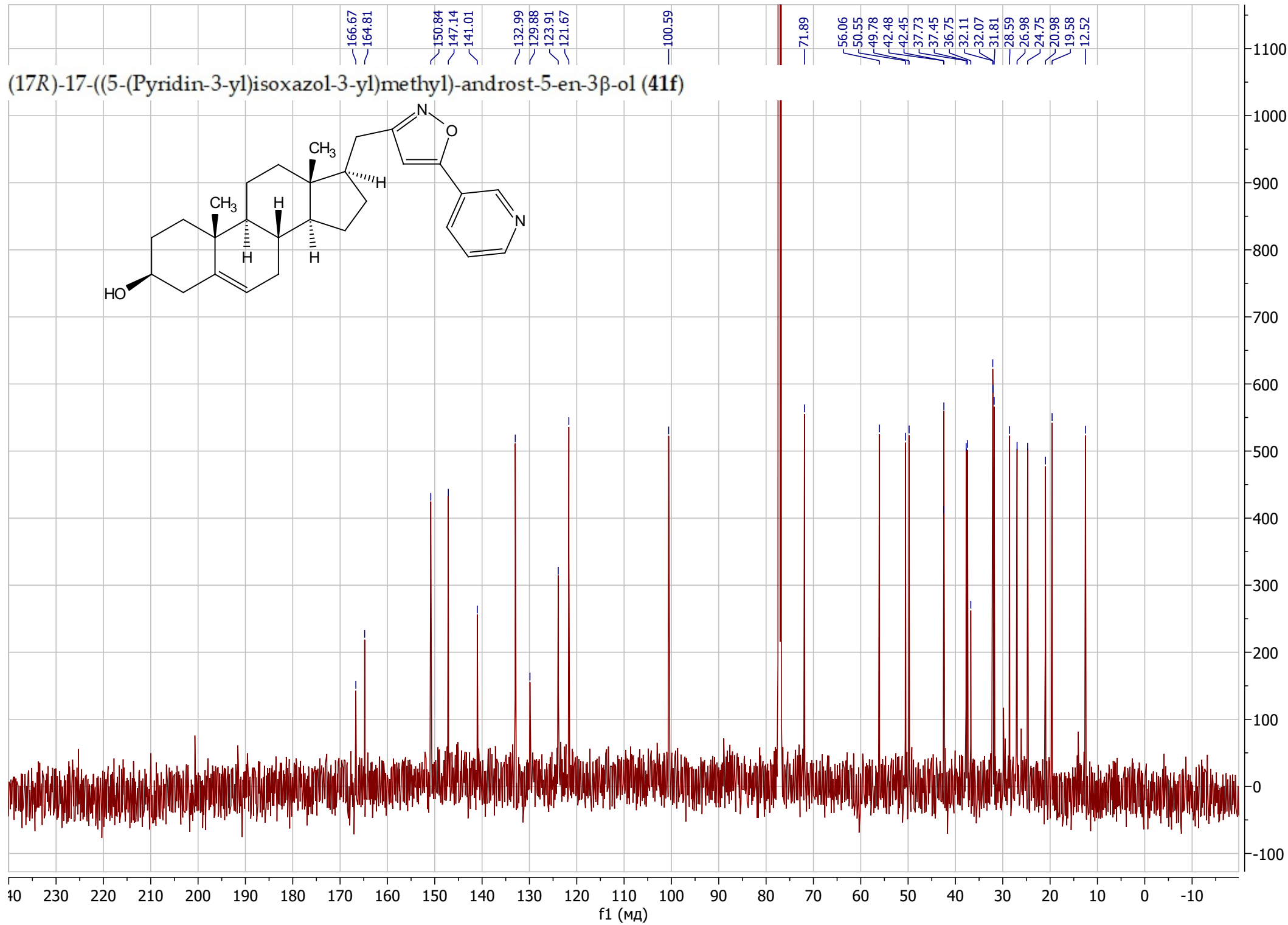
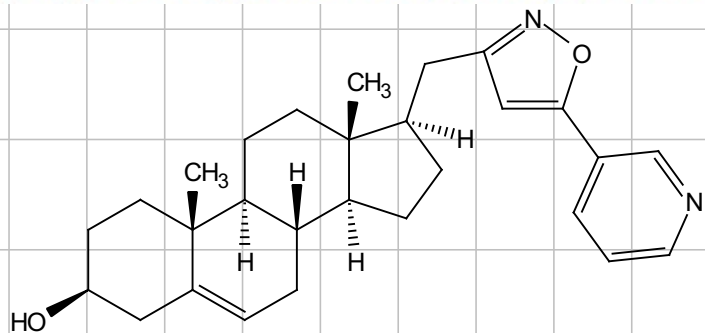
(17R)-17-((5-Phenylisoxazol-3-yl)methyl)-androst-5-en-3 β -ol (41e)



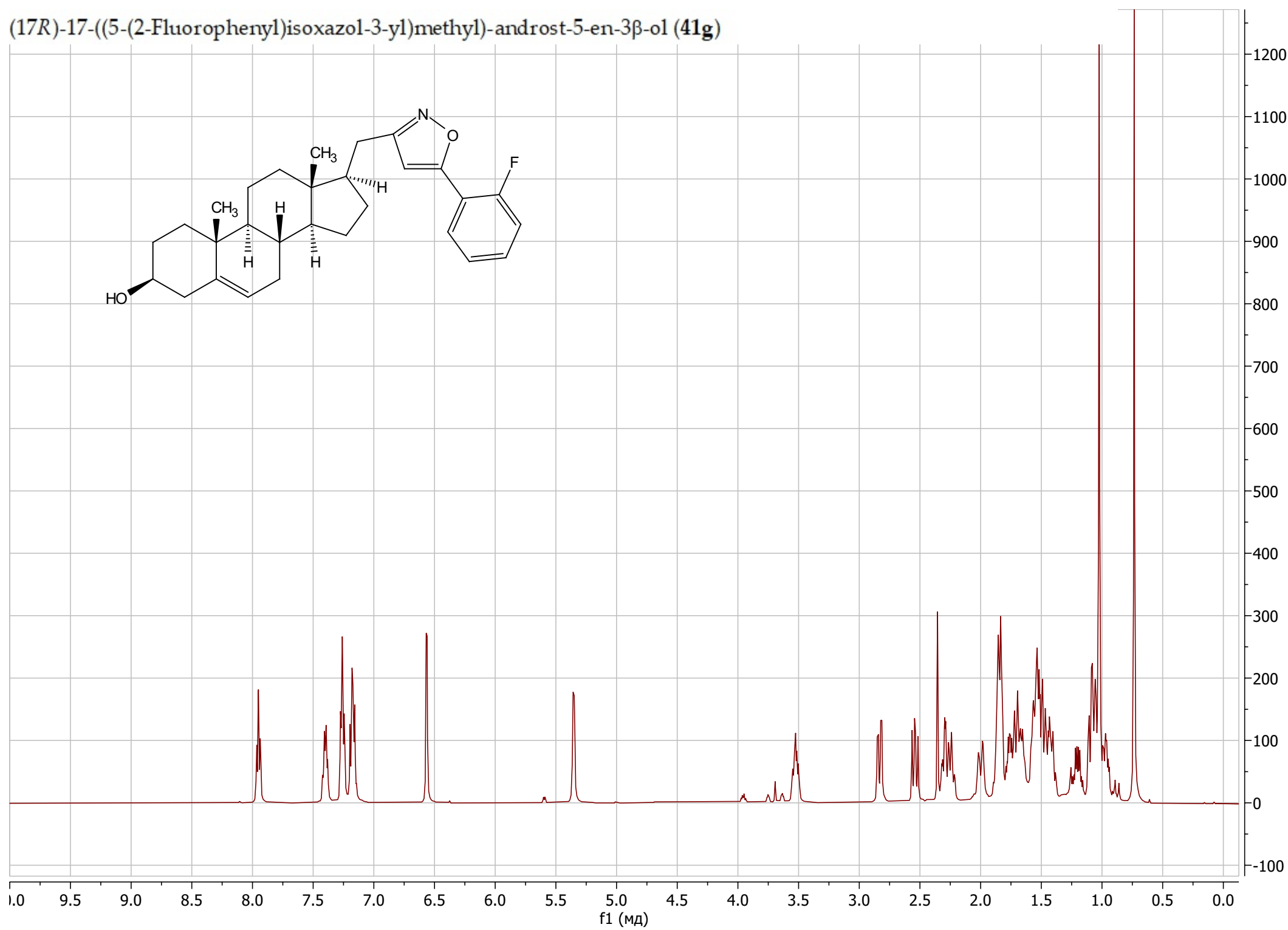
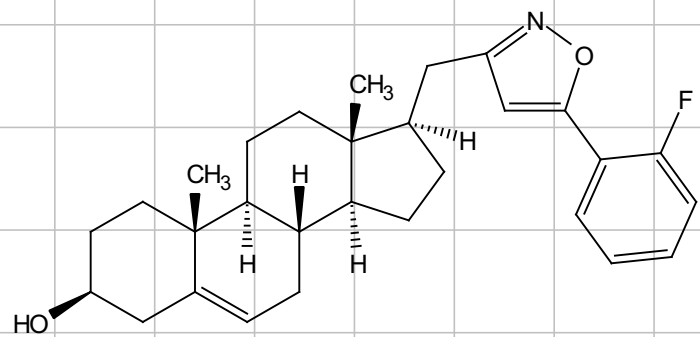
(17R)-17-((5-(Pyridin-3-yl)isoxazol-3-yl)methyl)-androst-5-en-3 β -ol (41f)



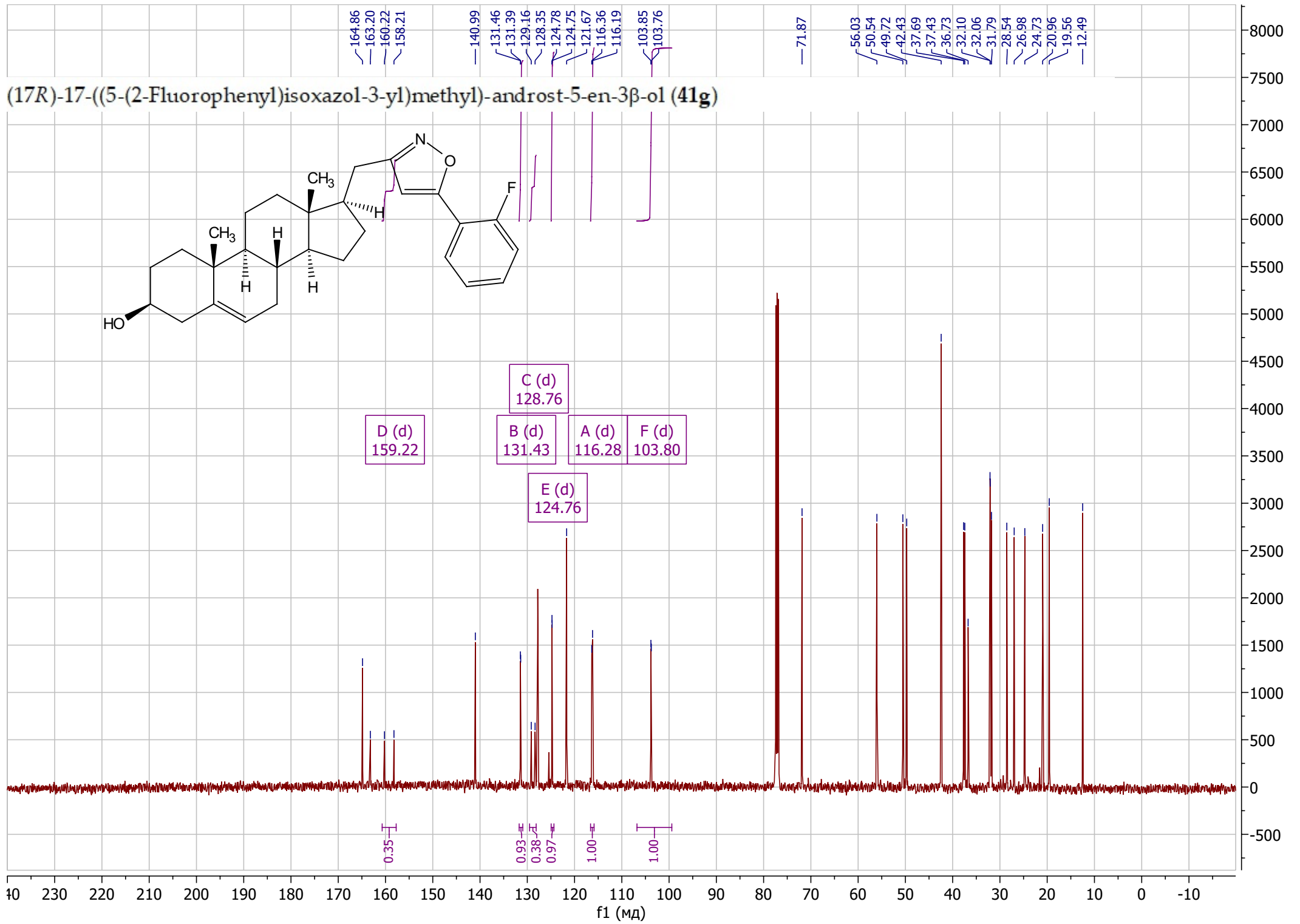
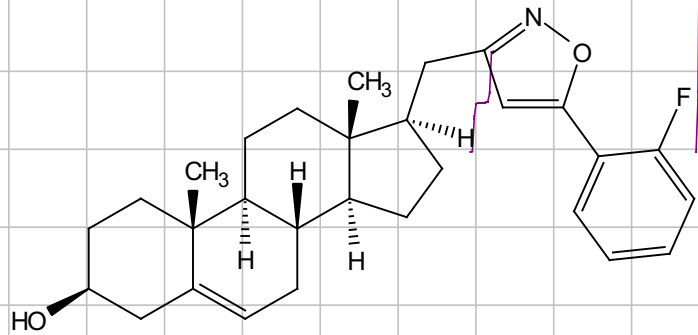
(17R)-17-((5-(Pyridin-3-yl)isoxazol-3-yl)methyl)-androst-5-en-3 β -ol (41f)



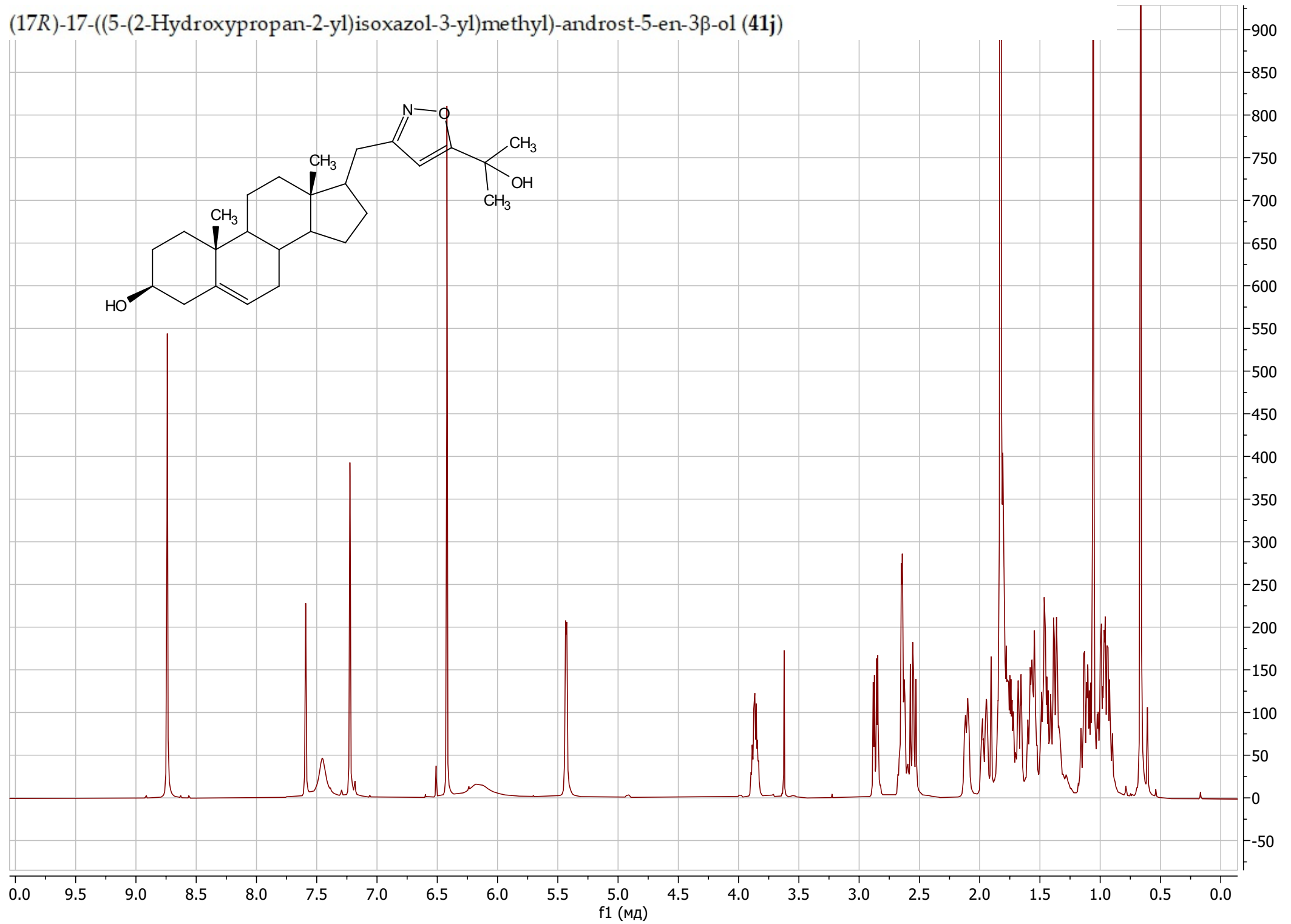
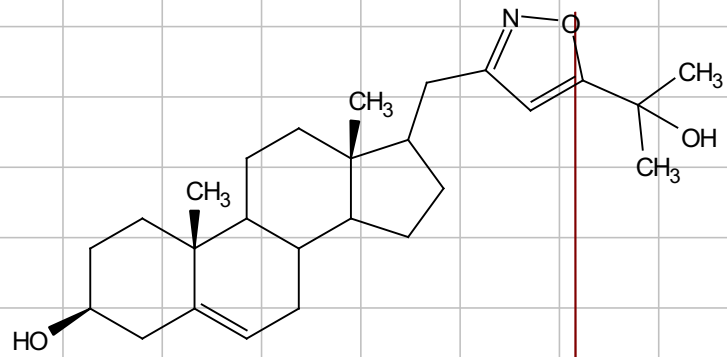
(17R)-17-((5-(2-Fluorophenyl)isoxazol-3-yl)methyl)-androst-5-en-3 β -ol (41g)



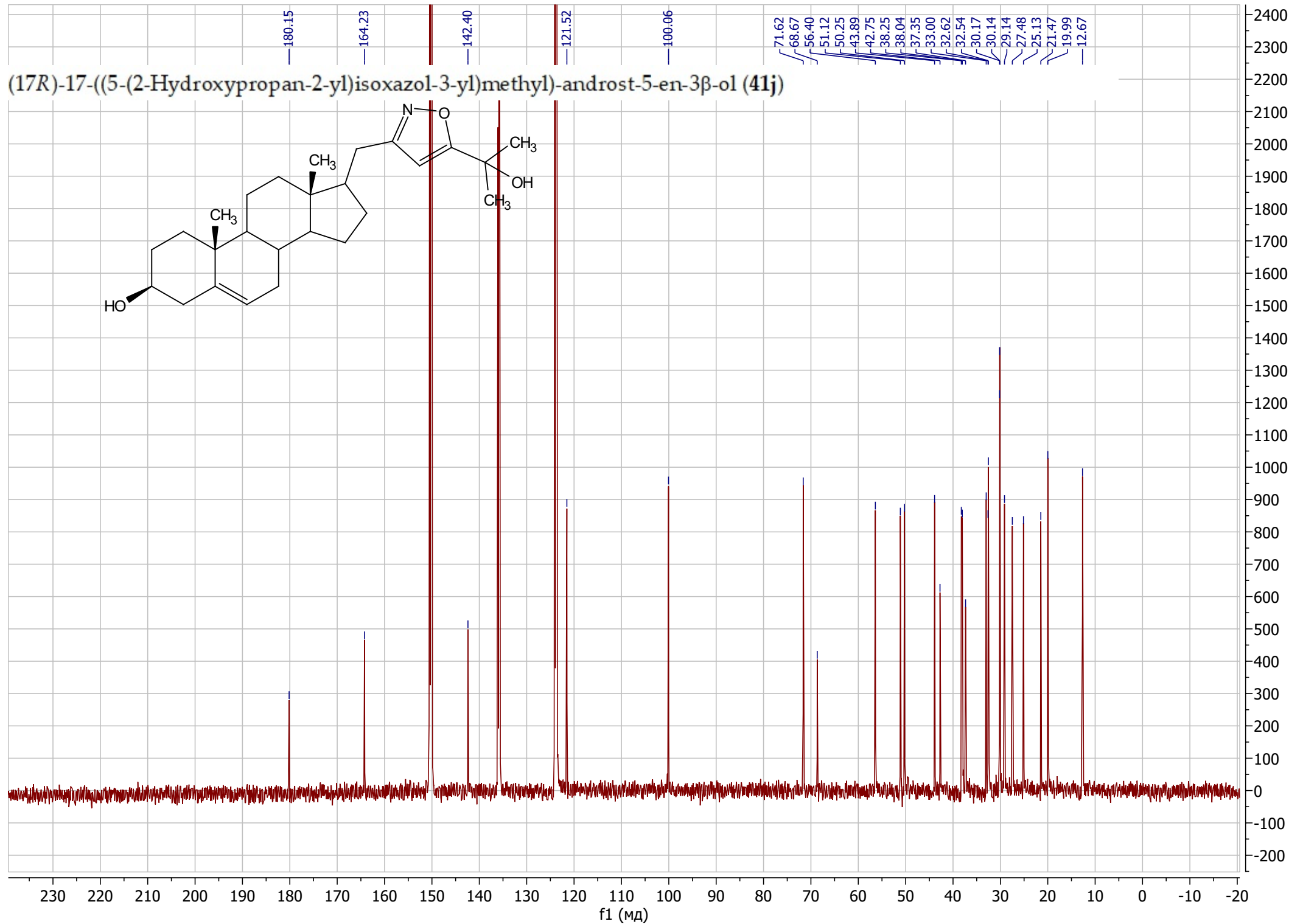
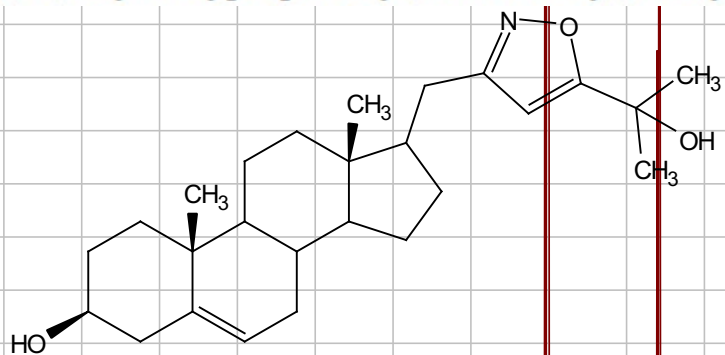
(17R)-17-((5-(2-Fluorophenyl)isoxazol-3-yl)methyl)-androst-5-en-3 β -ol (41g)



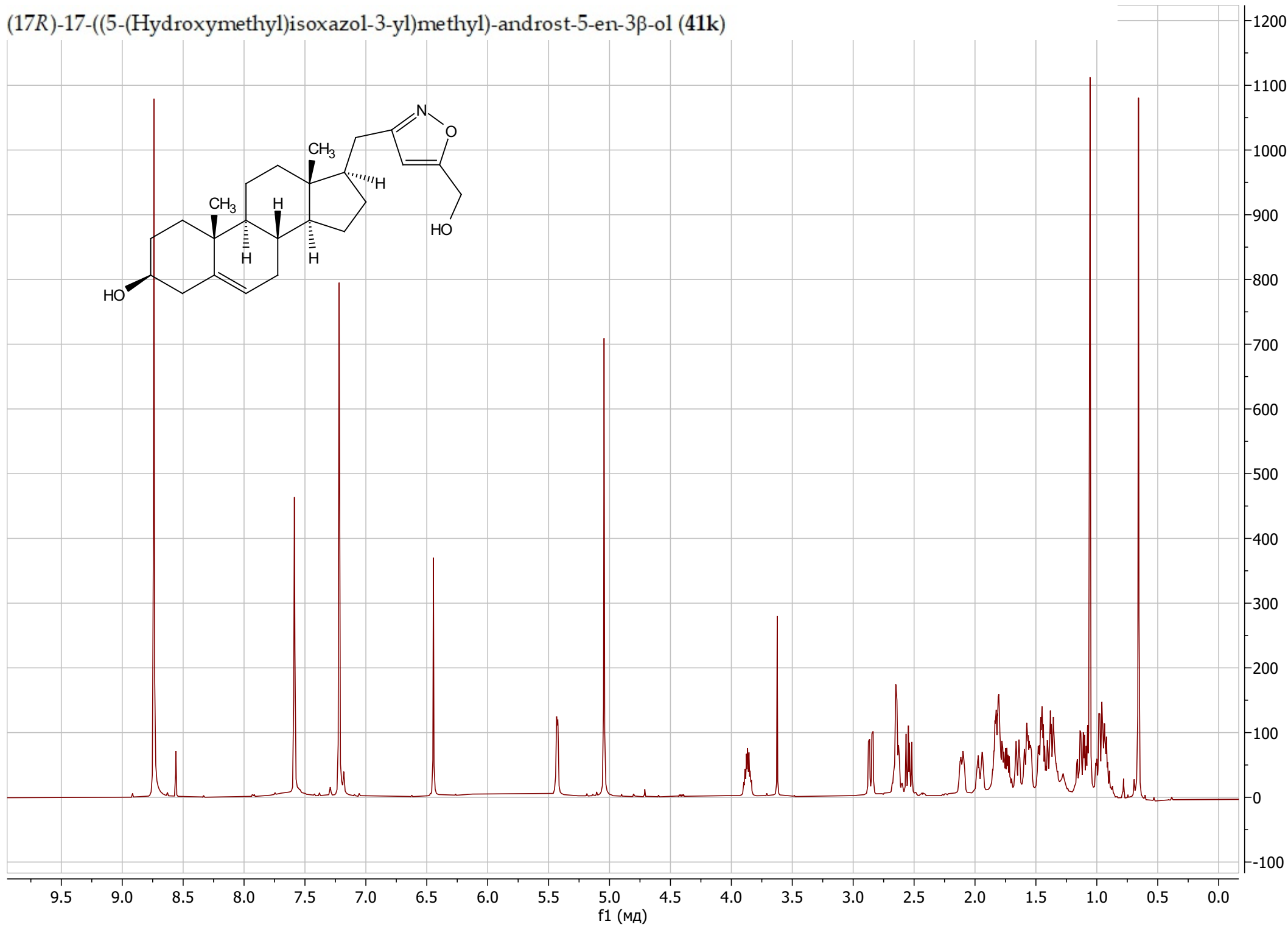
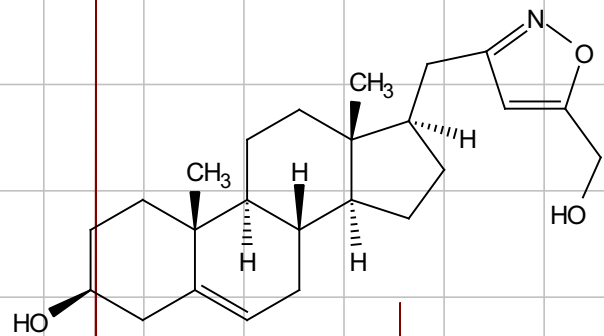
(17R)-17-((5-(2-Hydroxypropan-2-yl)isoxazol-3-yl)methyl)-androst-5-en-3 β -ol (41j)



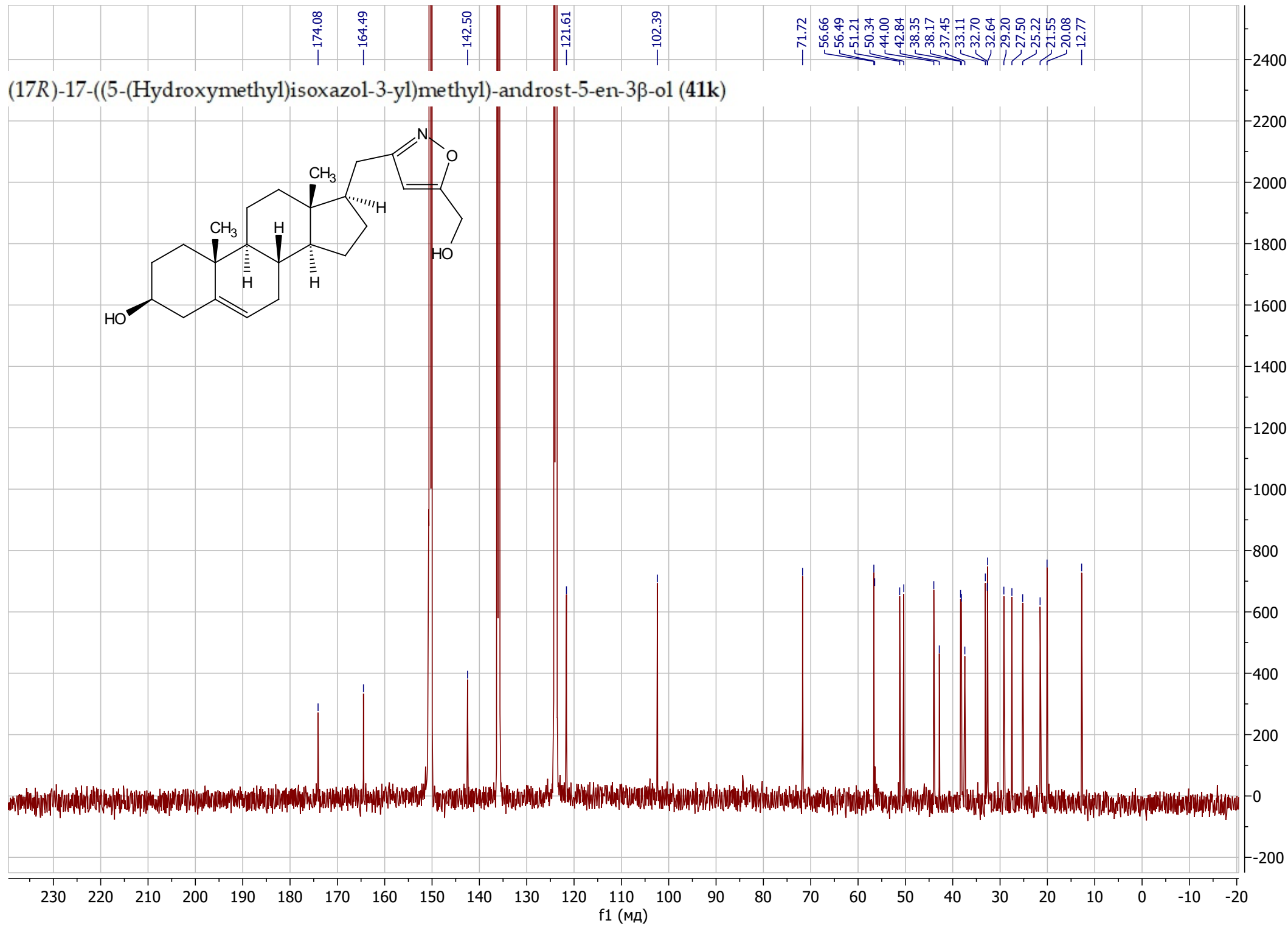
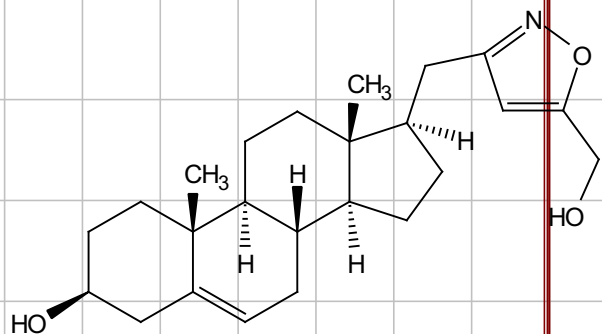
(17R)-17-((5-(2-Hydroxypropan-2-yl)isoxazol-3-yl)methyl)-androst-5-en-3 β -ol (41j)



(17R)-17-((5-(Hydroxymethyl)isoxazol-3-yl)methyl)-androst-5-en-3 β -ol (41k)



(17R)-17-((5-(Hydroxymethyl)isoxazol-3-yl)methyl)-androst-5-en-3 β -ol (41k)



PALACKÝ UNIVERSITY OLOMOUČ

Faculty of Science

Laboratory of Growth Regulators



Summary of the dissertation thesis

**Modulation of nuclear receptors' activity
in relation to human cancer**

Mgr. Miroslav Peřina

B1527 Biology
P0511D030004 Experimental biology

Olomouc, 2024

This dissertation was realized within the framework of the full-time doctoral study of the doctoral study program Experimental Biology P0511D030004 at the Faculty of Science, Palacký University in Olomouc in the years 2020 – 2024. The study was guaranteed by the Laboratory of Growth Regulators, Faculty of Science, Palacký University in Olomouc.

Candidate: **Mgr. Miroslav Peřina**

Supervisor: **Mgr. Radek Jorda, Ph.D.**

Department of Experimental Biology
Faculty of Science, Palacký University in Olomouc
Šlechtitelů 27
783 71 Olomouc

Oponents: **RNDr. Hana Zemková, CSc.**

Institute of Physiology CAS
Vítěňská 1083
142 00 Praha 4

doc. Ing. Radim Vrzal, Ph.D.

Department of cell biology and genetics
Faculty of Science, Palacký University in Olomouc
Šlechtitelů 27
783 71 Olomouc

The evaluation of this Ph.D. thesis was written by **Prof. Ing. Miroslav Strnad, CSc. DSc.**, Laboratory of Growth Regulators, Faculty of Science, Palacký University in Olomouc.

The oral defence will take place on **20. 06. 2024** with the Commission for the Ph.D. thesis of the Study Program Experimental Biology, Palacký University in Olomouc, Faculty of Science, Šlechtitelů 27, Olomouc – Holicе.

The Ph.D. thesis will be available 14 days before the defence in the Library of the Biological Departments of the Faculty of Science, Palacký University, Šlechtitelů 27, Olomouc – Holicе.

Prof. Ing. Miroslav Strnad, CSc. DSc.

Chairman of the Commission for the Ph.D. thesis,
Study Program Experimental Biology,
Faculty of Science, Palacký University in Olomouc

SUMMARY

The treatment of prostate cancer (PCa) has undergone significant advancements and targeting of androgen receptor (AR) by next-generation hormone therapies improved patients' outcomes, but nearly all patients eventually progress to develop resistance. Therefore, the discovery of novel agents is needed to improve the treatment efficacy of PCa.

The main part of the dissertation thesis investigated the biological activity of the library of dihydrotestosterone (DHT)-derivatives with different modifications on the A-ring (119 compounds in total) prepared by Éva Frank's (University of Szeged, Hungary) synthetic group. The A-ring fused pyrazole modification of DHT was generally the most potent structural motif of analysed compounds, with representatives displaying strong antagonist activity against AR transactivation, and potent antiproliferative activity towards PCa, surpassing standard AR antagonists like enzalutamide and galeterone. The potent downregulation and degradation of AR, induced by lead compound must be underscored, as well as its activity in patients' samples *ex vivo*. Molecular docking studies provided the structural basis of compounds' activity, revealing interactions with the AR and potential for further optimization.

In the other part of the dissertation, given the role of the glucocorticoid receptor (GR) in PCa acquired resistance, novel hydrocortisone's derivatives were also analysed and dual antagonists of AR/GR were described. The lead compound suppressed the signalling of both receptors, the interactions were proved in cells and modelled by molecular docking. The findings support the development and characterisation of dual AR/GR antagonists as anticancer agents in PCa cases with upregulation of GR activity.

Overall, the dissertation study provided valuable insights into the design and development of novel AR-targeted compounds for the treatment of PCa, highlighting their potential as alternative or complementary therapies to existing standards of care.

CONTENT

1	INTRODUCTION AND OBJECTIVES	6
2	MATERIALS AND METHODS	8
2.1	Commercial compounds	8
2.2	Cell cultures	8
2.2.1	AR and GR transactivation luciferase reporter assay	8
2.2.2	Cell viability assay	9
2.2.3	Colony formation assay	9
2.2.4	Cell lysis, SDS-PAGE and Western blot	9
2.2.5	Fractionation of cellular compartments	10
2.2.6	Cellular thermal shift assay (CETSA).....	10
2.2.7	Cell cycle analysis.....	10
2.2.8	Analysis of mRNA expression.....	10
2.2.9	AR-ligand binding domain preparation and MST measurements.....	11
2.2.10	Molecular docking	11
3	SURVEY OF RESULTS AND DISCUSSION	12
3.1	Screening and discovery of novel AR antagonists.....	12
3.2	Compounds' effect on AR downstream signalling and the cell cycle	15
3.3	AR downregulation and induction of its degradation	16
3.4	Analysis of compounds' interaction with AR	17
3.5	Optimisation of cell compartment fractionation and CETSA.....	19
3.6	Dual targeting of AR and GR	23
4	CONCLUSION AND PERSPECTIVES	25
5	REFERENCE.....	27
6	LIST OF AUTHOR'S PUBLICATIONS	31
7	SOUHRN	34

1 INTRODUCTION AND OBJECTIVES

Nuclear receptors (NRs) are crucial regulators of physiological processes, including metabolism, immunity, development and cell proliferation. However, they also act as pivotal regulators of diseases and serve as biomarkers for tumour classification and targets for hormone therapy (Dhiman *et al.*, 2017). The androgen receptor (AR) is a nuclear receptor that binds the androgen hormones (testosterone) (Velho *et al.*, 2021), and acts as a transcription factor, playing a crucial role in the physiological development of male sexual characteristics. However, it is also implicated in diseases including muscular atrophy (Brinkmann, 2001), prostate cancer (PCa) or breast cancer (BrCa). In the case of PCa, the dependence on AR signalling is crucial and it has been exploited for therapeutic intervention for decades.

Over the years, the treatment of PCa has undergone significant advancements and targeting of AR has been utilized to improve patients' outcomes (Denmeade and Isaacs, 2002). While the previous standard was androgen deprivation therapy (ADT) and cytotoxic chemotherapy (taxanes), the approved next-generation hormone therapies targeting are the golden standards nowadays (He *et al.*, 2022). Despite the initial effectiveness of PCa treatment, nearly all patients eventually progress to develop resistance. Novel strategies for targeting AR have arisen (binders of other domains except of the ligand-binding ones, targeted degradation), but the discovery of novel agents along with the identification of new predictive biomarkers of resistance is still needed to improve treatment outcomes in PCa patients (Deluce *et al.*, 2022).

Initially, the first antiandrogens incorporated a steroidal skeleton, but their clinical use was limited due to significant adverse effects (hepatotoxicity, potency decrease, cardiovascular limitations) (Schröder *et al.*, 2004). The next development focused mainly on non-steroidal compounds and while the approval of the two generations of non-steroidal antagonists (flutamide, bicalutamide, nilutamide, enzalutamide, apalutamide and darolutamide) was a great success, there is not any approved steroid-based AR antagonist. On the contrary, the steroid-based abiraterone is the only approved drug to block the androgen synthesis by cytochrome P450 17-alpha-hydroxylase, 17,20-lyase (CYP17A1) inhibition. Several other steroidal compounds, mostly modified on the D-ring of the androstane core have been recently investigated as AR modulators or for their anti-PCa properties (Jorda *et al.*, 2019), but apart from abiraterone (Jarman *et al.*, 1998) only galeterone (Njar and Brodie, 2015) entered clinical trials. Despite the promising pre-clinical potency, the phase III clinical trial in mPCa patients did not confirm galeterone's efficacy (Taplin *et al.*, 2019). For the abovementioned reasons, investigation of novel ligands is desirable.

However, compared to D-ring fused or substituted steroid derivatives, compounds containing a heterocycle moiety on the A-ring have been recently much less investigated. In collaboration with Éva Frank's (University of Szeged, Hungary) synthetic group, we aimed to explore the biological activity and SAR of 5 α -dihydrotestosterone (DHT)-derivatives with modifications on the A-ring. Several examples of A-ring fused quinolines (Baji *et al.*, 2016) and 1-aryl-5-methyl A-ring fused pyrazoles (Mótyán *et al.*, 2019) of DHT were previously synthesized by Éva Frank's group, which demonstrated anticancer activity against multiple cell lines including PCa ones, but without any research of AR-targeting.

The main objective of the dissertation thesis was to characterise the biological activity of already published and novel A-ring substituted DHT derivatives, searching for potent and selective AR antagonists (Chen *et al.*, 2022). The compounds were intended for analysis of their agonist and antagonist activities towards AR, their binding into the AR, antiproliferative activity in PCa cell lines (both AR-positive and AR-negative ones), influence of the AR level and downstream signalling etc. A broad library of DHT derivatives with modification on the A-ring (119 compounds in total) were screened at first by the gene-reporter assay and the antiproliferative activity assay and further, the most potent compounds from each series were evaluated in detail (**Appendix I - III**).

The other objective was to evaluate the biological activity of hydrocortisone's derivatives prepared by the synthetic group of Gyula Schneider and Erzsébet Mernyák (University of Szeged, Hungary). Given the crucial role of the glucocorticoid receptor (GR) in resistant PCa and recently described dual and selective antagonists of AR/GR (Puhr *et al.*, 2018; Wu *et al.*, 2019; Li *et al.*, 2024), the aim was to develop and characterise the 17 α - and/or 21-ester or carbamate derivatives of hydrocortisone. Compounds were analysed for their agonist or antagonist activity in both the AR and GR reporter cell lines and the lead compound suppressing the signalling of both receptors was successfully found (**Appendix IV**). As a part of this thesis, several D-ring-attached steroidal isoxazoles and triazoles (similar to abiraterone) were also characterised, displaying CYP17A1 inhibitory effect and moderate AR-antagonist activity (**Appendix V**).

2 MATERIALS AND METHODS

2.1 Commercial compounds

The compounds which were used as standards are listed in **Table 4**.

Table 1 List of commercially available compounds, vendor and their purity.

Compound	CAS number	Vendor	Purity (%), determination
enzalutamide	915087-33-1	MedChemExpress	99.96% (HPLC/MS)
galeterone	851983-85-2	Merck	≥98 %, (HPLC)
R1881	965-93-5	Merck	≥98 % (HPLC)
MG-132	133407-82-6	MedChemExpress	99.97% (HPLC/MS)

2.2 Cell cultures

The PCa cell lines comprised the LNCaP and C4-2 (American Tissue Culture Collection), 22Rv1, LAPC-4, DU145 (generous gift from Assoc. Prof. Jan Bouchal from Faculty Hospital Olomouc) LNCaP-Abl and DuCaP (generous gift from Prof. Zoran Culig, Medical University Innsbruck, Austria) and PC-3 (German Collection of Microorganisms and Cell Cultures). All the PCa cell lines were cultivated in RPMI, supplemented with sera specified for each experiment, only LAPC-4 was routinely cultivated with 1 nM R1881 and LNCaP-Abl with steroid-depleted serum (charcoal-stripped serum, CSS). The AR-positive breast cancer cell lines comprised T47D and MCF7 (European Collection of Authenticated Cell Culture) and SKBR3 (American Tissue Culture Collection) and were cultivated in DMEM. The reporter cell lines 22Rv1-ARE14 and AZ-GR were generous gifts from Prof. Zdeněk Dvořák from the Department of Cell Biology, UP. All the media were supplemented with 100 IU/ml penicillin, 100 µg/ml streptomycin, 4 mM glutamine and 1 mM sodium pyruvate. Cells were cultivated in a humidified incubator at 37 °C and in a 5% CO₂ atmosphere.

2.2.1 AR and GR transactivation luciferase reporter assay

The Nunc™ MicroWell™ 96-well optical flat-bottom plate (Thermo Fisher Scientific) was used for luciferase assays, to which 22Rv1-ARE14 or AZ-GR cells were seeded. On the second day, the cultivation medium was discarded and cells were washed with PBS. Cells were then incubated with analysed compounds dissolved in a medium supplemented with CSS and 1 nM R1881 or 100 nM dexamethasone in the case of 22Rv1-ARE14 or AZ-GR, respectively. Upon 24 h, cells were washed with PBS and lysed for 10 min in a lysis buffer (10 mM Tris pH 7.4, 2 mM DCTA, 1% Nonidet P40, 2 mM DTT) at 37 °C. Next, reaction buffer (20 mM

tricine pH 7.8, 1.07 mM MgSO₄, 5 mM ATP, 9.4 mM luciferin) was added and the luminescence was measured using a Tecan M200 Pro reader (Biotek).

2.2.2 Cell viability assay

For the viability assays, cells were seeded into the 96-well tissue culture plates, the other day, solutions of compounds were added in different concentrations in replicates for 72 h. Upon treatment, the resazurin solution (Sigma Aldrich) was added for 4 h, and the fluorescence of resorufin was subsequently measured at 544 nm/590 nm (excitation/emission) using a Fluoroskan Ascent microplate reader (Labsystems). Percentual viability or GI₅₀ value were calculated and plotted using GraphPad Prism 5.

2.2.3 Colony formation assay

PCa cells 22Rv1 and DU-145 (5000 cells per well), LAPC-4 and PC-3 (10 000 cells per well) were seeded into 6-well plates. After two days of cultivation, the medium was replaced with fresh medium with compounds and cells were further cultivated for 10 days. After the treatment, the medium was discarded and colonies were fixed with 70% ethanol, washed with PBS and stained with crystal violet (1% solution in 96% ethanol) for 1 h. Finally, wells were washed with PBS and colonies' photographs were captured.

2.2.4 Cell lysis, SDS-PAGE and Western blot

After all treatments, cells were harvested by centrifugation, washed twice with PBS, pelleted and kept frozen at - 80 °C. Pellets were resuspended in RIPA lysis buffer supplemented with phosphatase and protease inhibitors on ice. Ultrasound sonication of cells was performed and samples were clarified by centrifugation at 14 000 g for 30 min. Protein concentration in supernatants was measured and balanced within samples, which were denatured in SDS-loading buffer, separated by SDS-PAGE and electroblotted onto nitrocellulose membranes. Immunodetection of proteins was performed as usual, membranes were blocked in 4% BSA, incubated overnight with primary antibodies, washed and incubated with secondary antibodies conjugated with peroxidase. Peroxidase activity was detected by SuperSignal West Pico reagents (Thermo Scientific) using a CCD camera LAS-4000 (Fujifilm). Particular primary antibodies are listed in publications (appendices), and secondary antibodies were purchased from Cell Signalling Technology. All antibodies were diluted in 4% BSA and 0.1% Tween 20 in TBS.

2.2.5 Fractionation of cellular compartments

Cellular fractionation experiments were first performed using the Qproteome Cell Compartment Kit (Qiagen). The protocol was subsequently optimised with in-house buffers, as described in section 3.5. Cells were first harvested by trypsinisation, washed in PBS and the basic cytosolic buffer A (150 mM NaCl, 50 mM HEPES (pH 7.4) with protease inhibitors and 0.1% IGEPAL® CA-630 was added. After the incubation on ice, the suspension was centrifuged at 600 g for 6 min. The supernatant represented the cytosolic fraction, while the pellet was incubated with nuclear buffer B (20 mM HEPES, pH 7.9, 1.5 mM MgCl₂, 0.5 M NaCl, 0.2 mM EDTA, 20% glycerol, 1% Triton™ X100), sonicated and centrifuged at 14 000 g for 15 min. The supernatant represented soluble nuclear proteins, while the pellet contained proteins bound to chromatin and cell debris.

2.2.6 Cellular thermal shift assay

Cellular thermal shift assay (CETSA) experiments were performed according to the optimised protocol (section 3.5). LAPC-4 or C4-2 cells were harvested by trypsinisation, re-suspended in PBS with 5 mM glucose and divided into test tubes, where they were treated with tested compounds for 1 h. Upon the treatment, cells were counted and equally aliquoted into PCR strips, heated at the temperature gradient from 37 °C to 60 °C for 3 min, cooled down to 4 °C and they were snap-frozen in liquid nitrogen. The lysis by freeze-thaw cycles was performed and the supernatants containing soluble proteins were obtained by centrifugation at 14 000 g for 30 min, prepared for SDS-PAGE and immunoblotted for thermostable AR level.

2.2.7 Cell cycle analysis

Cells were treated with test compounds for 24 h, they were harvested by trypsinisation, washed with PBS and fixed with 70% ethanol. After rehydration, cells were permeabilised by 2 M HCl, 0.5% Triton X-100. Following neutralization and washing with PBS, the cells were stained with propidium iodide and analysed by flow cytometry with a 488 nm laser (BD FACS Verse with BD FACSuite software, version 1.0.6.). Cell cycle distribution was analysed using ModFit LT (Verity Software House, version 5.0).

2.2.8 Analysis of mRNA expression

Cells were treated and harvested into lysis buffer and total RNA was isolated using RNeasy plus mini kit (QIAGEN) based on the manufacturer's instruction. RNA concentration and purity were evaluated using a DeNovix DS-11 spectrophotometer, while the quality of RNA was determined by gel electrophoresis. The RNA (0.5–1 µg) was reverse transcribed into cDNA by

SensiFast cDNA Synthesis Kit (Bioline). RNA Spike I template (TATAA) was used as a control. Quantitative RT-PCR was performed on a CFX96 Real-Time PCR Detection System (Bio-rad) with a SensiFAST SYBR No-Rox Kit (Bioline). The suitable primers were designed using Primer-BLAST (Ye *et al.*, 2012) and synthesized by Generi Biotech. Relative gene expression levels were determined using the $\Delta\Delta C_t$ method (Livak and Schmittgen, 2001) in Bio-rad CFX Maestro 2.2. Expression was normalized per *ACTB* and *SDHA* (the most stable housekeeping genes).

2.2.9 AR-ligand binding domain preparation and MST measurements

AR-ligand binding domain (LBD) (with His6-tag) was expressed and purified using recombinant plasmid pET-15b-hAR-663-919, which was a generous gift from Elizabeth Wilson (Addgene plasmid # 89083) by the original protocol (Askew *et al.*, 2007). The recombinant AR was purified into the storage buffer (25 mM Tris, 300 mM NaCl, pH 8.0, 5 mM DTT) and concentrated up to 0.5 mg/ml. The micro-scale thermophoresis (MST) method was used to prove the binding of **3d** in the AR-LBD, which was labelled with the His-Tag Labelling Kit RED-tris-NTA (NanoTemper). The labelled protein was used for MST measurements with or without **3d** in a final concentration of 400 nM His-tagged protein in the storage buffer, supplemented with 0.1% Tween. Measurements were performed on a Monolith NT.115 instrument (NanoTemper Technologies).

2.2.10 Molecular docking

Molecular docking was performed with the crystal structure of AR-LBD with DHT (PDB: 2PIV) or AR-antagonist model (Wahl and Smieško, 2018), for GR the docking was performed into the crystal structure of GR-LBD with mifepristone (PDB:1NHZ). The 3D structures of all compounds were obtained and their energy was minimised by molecular mechanics with Avogadro 1.90.0, a software used for the drawing and characterisation of chemical structures. Polar hydrogens were added to ligands and proteins with the AutoDock Tools program (Morris *et al.*, 2009) and docking studies were performed using AutoDock Vina 1.05 (Trott *et al.*, 2010). Interactions between ligand and amino acid residues were modelled in PLIP software (Adasme *et al.*, 2021). Figures were generated in Pymol ver. 2.0.4 (Schrödinger, LLC).

3 SURVEY OF RESULTS AND DISCUSSION

The results part of the thesis comprises the deep screening of AR antagonists within compounds based on DHT with diverse A-ring substitutions. At first, the effect of compounds on AR-transactivation and their antiproliferative potency towards PCa cell lines was assessed. The potent compounds were analysed in detail for their binding into the AR, the influence of the AR level and downstream signalling (**Appendix I. – III.**) by methods established at the department. The isolation of the cellular fractions and the thermal shift assay were optimised to fit best for the AR's analysis as a part of this thesis.

Next, hydrocortisone's derivatives prepared by the synthetic group of Gyula Schneider and Erzsébet Mernyák (University of Szeged, Hungary) were analysed towards both AR/GR receptors and the effect of their downstream signalling (**Appendix IV.**).

3.1 Screening and discovery of novel AR antagonists

A broad library of DHT derivatives was efficiently prepared in two steps. Altogether, compounds bearing different nitrogen-containing five or six-membered heterocycles as a fusion to the A-ring of DHT with a similar series of terminal substituents (**Figure 1**) (119 compounds in total) were thoroughly characterised.

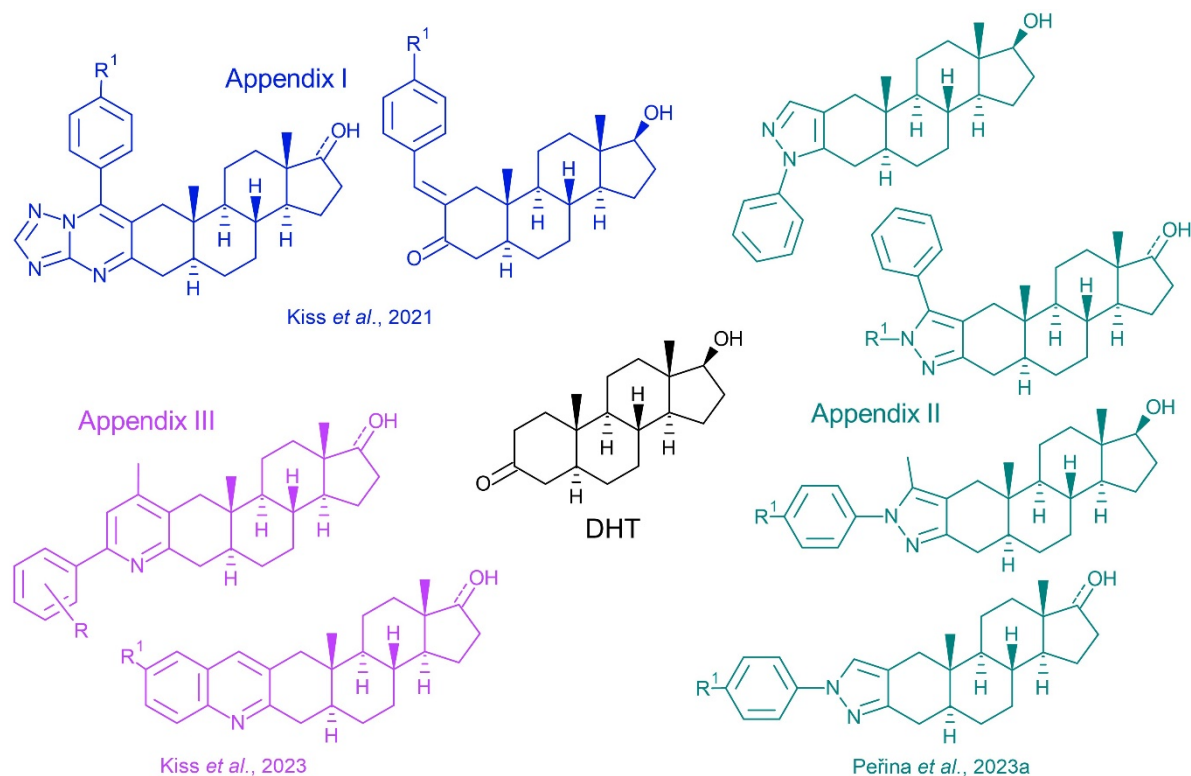


Figure 1 Schematic representation of the A-ring fused DHT derivatives from Éva Frank's synthetic group analysed in publications (**Appendix I. -III.**)

The first part of the analysed library comprised α,β -enones, triazolo[1,5-*a*]pyrimidines and pyrazolo[1,5-*a*]pyrimidines. As shown in **Appendix I., Table 3** α,β -enones belonged to potent antagonists, with no agonist properties. Conversely, triazolo[1,5-*a*]pyrimidines and pyrazolo[1,5-*a*]pyrimidine DHT-derivatives were active only partially and some of them displayed agonist activities. The antagonist activity of *p*-chlorobenzylidene derivative **2f** ($IC_{50} = 3.54 \mu M$) (**Figure 2**) reached the single-digit micromolar values and showed to be comparable with standards, i.e. galeterone ($IC_{50} = 5.82 \mu M$) and enzalutamide ($IC_{50} = 1.50 \mu M$) (Yu *et al.*, 2014; Tran *et al.*, 2009) (**Appendix I., Supplementary Material, S38-S41**). While the majority of the compounds induced no decrease in PCa cells' proliferation, the most potent derivative **2f** displayed mid-micromolar values ($GI_{50} = 9.9 \pm 1.8 \mu M$ and $15.7 \pm 4.4 \mu M$) in 22Rv1-ARE14 and C4-2, respectively and outperformed the standards with $GI_{50} > 50 \mu M$ (**Appendix I., Supplementary Material, S42-S47**). The limited cytotoxicity of AR antagonists (Latysheva *et al.*, 2020; Chen *et al.*, 2022) with rather a cytostatic effect corresponds with previous studies. The prolonged treatment with **2f** showed dose-dependent inhibition of 22Rv1-ARE14 colonies formation (**Appendix I., Fig. 5**).

The next group comprised already published A-ring fused pyrazoles of DHT bearing the mono-substitution in positions N2 or N1 (series **1** and **2**) and 1-aryl-5- methyl pyrazoles (**3** and **4**), together with newly prepared 1-methyl-5-aryl pyrazoles (**8** and **10**). The monosubstituted pyrazoles from series **1** and **2** displayed only a moderate antagonist effect, while most compounds undesirably activated the AR in agonist mode (**Table 6, Appendix II., Table 2**). Representatives from series **3** and **8** that bear the C-17 hydroxy group and combine methyl and aryl substitution at N1 or C5 position of pyrazole (**3a–3h, 8a–8h**) acted as strong antagonists (**Table 6, Appendix II., Tables 3, 4**), with the series **3** being generally more potent than their regioisomers from series **8**. Importantly, none of the compounds displayed agonist activities except **8b**. The most potent derivative was **3d** with 1'-fluorophenyl-5'-methyl pyrazole moiety (**Figure 2**) reached the low micromolar antagonist potency ($IC_{50} = 1.18 \mu M$), outperforming the analysed standards enzalutamide and galeterone (Yu *et al.*, 2014; Tran *et al.*, 2009). Antagonist activities were observed also for series **4** and **10** bearing the C-17 keto group, but they were less potent than their C-17 hydroxy counterparts (series **3** and **8**) (**Appendix II., Tables 3, 4**). The results showed that the combination of a small substituent (Me group) with a bulky one (phenyl moiety) in the 1', and 5' positions of the pyrazole ring is fundamental for strong antagonist activity, which was obvious from the results of derivatives **8l, 10l** (1',5'-dimethyl-substituted) and **8i, 10i** (1',5'-diaryl-substituted) with only agonist activities.

Antiproliferative properties of the pyrazole derivatives were screened on the panel of three PCa cell lines, namely LAPC-4, 22Rv1 (AR-positive) and DU145 (AR-negative). The activity corresponded with previous assays since compounds from series **3**, **4**, **8** and **10** belonged to the most active ones. The results confirmed the selective targeting of AR because DU145 stayed unaffected upon treatment with the majority of compounds (**Appendix II., Table 5**) (Latysheva *et al.*, 2020; Chen *et al.*, 2022). The antiproliferative effect of the most potent compound **3d** in different cell lines was dose-dependent, with selectivity for AR-positive PCa cell lines with GI₅₀ values in low micromolar ranges with LAPC-4 cells being the most sensitive (GI₅₀ = 7.9 ± 1.6 μM) (**Appendix II., Figure S9**).

As shown in **Appendix II., Table 2, Table 3, Table 4, Figures. S4 and S5**, all compounds from series **3**, **4**, **8** and **10** potently blocked the formation of LAPC-4 colonies in 5 μM upon 10 days, the majority outperforming the enzalutamide (Tran *et al.*, 2009).

The last analysed group in the library comprised already published steroidal A-ring-fused quinolines (**1a–1i**) novel A-ring-fused 6'-substituted pyridine derivatives (**2a–2h**) and A-ring-fused 4',6'-disubstituted pyridine derivatives (**3a–3o**). The quinolines included several antagonists, but with lower potency compared to earlier derivatives, with moderately active compounds (**1a**, **1d**, **1i**). In the agonist mode, few compounds displayed agonist activity (**1b**, **1g**, **1c**, **1i**) (**Appendix III., Table 3**) The lead compound **1d** (**Figure 2**) was the most potent quinoline derivative with IC₅₀ = 10.51 μM, comparable to galeterone (7.59 μM) (Yu *et al.*, 2014) (**Appendix III., Figure 7**). There was no clear SAR within series **2** and **3**, of the pyridines, which generally showed few and only weak antagonists. Interestingly in series **3**, the combinations of methyl and aryl substitutions or bi-aryl substitutions followed the same tendency as in the A-ring fused pyrazoles (**Appendix III., Table 3**). The antiproliferative analysis upon 72 h correlated with weak antagonist properties, since the majority of compounds decreased the viability only to 70–80% of the vehicle-treated cells (Latysheva *et al.*, 2020; Chen *et al.*, 2022). Generally, the viability of DU145 was not influenced, showing selective targeting of the AR. The most potent quinoline compounds **1d** and **1i** displayed reasonable antiproliferative activity selective towards AR-positive 22Rv1, LAPC-4 and LNCaP (**Appendix III., Table 4, Figure 7**), outperforming the standard antagonists galeterone and enzalutamide. The prolonged treatment of LAPC-4 in colony-formation assay showed antiproliferative activity of compounds **1a**, **1c**, **1d**, **1g** - **1i** (**Appendix III., Figure 5**).

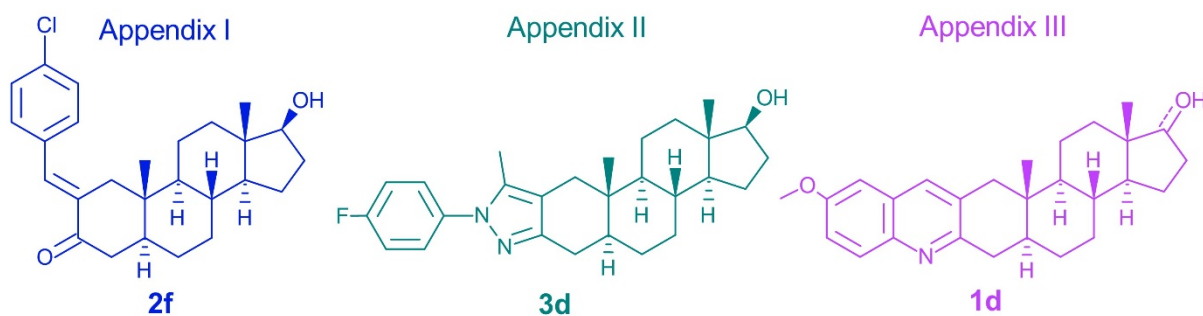


Figure 2 Structures of the most potent compounds from each group.

3.2 Compounds' effect on AR downstream signalling and the cell cycle

AR modulators block the transport of AR to the nucleus (Tran *et al.*, 2009; Yu *et al.*, 2014). Therefore, the effect of **2f** on AR distribution in R1881-stimulated cells was analysed. As shown in **Appendix I., Fig. 7**, compound **2f** and galeterone markedly decreased the transport of AR to the nucleus and while AR remained in cytosol upon the treatment of cells with **2f**, galeterone induced also partial AR degradation (Kwegyir-Afful *et al.*, 2015). The effect of the most potent AR antagonists from the screening to the AR downstream signalling was analysed by western-blot of AR transcription targets, PSA and Nkx3.1. In the case of the *p*-chlorobenzylidene derivative **2f**, the treatment of 22Rv1-ARE14 and C4-2 did not change the protein expression of AR itself, while expression of PSA and Nkx3.1 decreased in a dose-dependent manner. It correlated with the effect on AR-transactivation and it was comparable with galeterone (Yu *et al.*, 2014). Moreover, cleaved PARP (indicating ongoing apoptosis) was not detected, corresponding with mild cytotoxicity of the investigated compound (**Appendix I., Figure 9**).

The candidate pyrazole **3d** displayed potent blockage of AR signalling mainly in LAPC-4 (expressing wt-AR), with sharp decreases in both Nkx3.1 and PSA protein levels and AR-phosphorylation level at S 81 as well as moderate decrease in AR level, in agreement with antagonist activity (Jorda *et al.*, 2018; Lv *et al.*, 2020). Moreover, **3d** displayed activity in LNCaP cells (bearing the AR Thr877Ala mutation) and importantly, even in CRPC model LNCaP – Abl (with AR hypersensitivity (Culig *et al.*, 1999), being able to block the S81 phosphorylation and down-regulate both the AR and PSA (**Appendix II., Figure 4**). Moreover, the changes in AR level and downstream targets were time and dose-dependent with suppression of AR signalling up to 10 μ M concentration of **3d** (comparable to galeterone's effect) in LAPC-4 (**Appendix II., Figure 5**), as well as in 22Rv1 and LNCaP (**Appendix II., Supplementary Figure S6**) (Kwegyir-Afful *et al.*, 2015). Long-term treatment of LAPC-4

showed a significant decrease in the AR expression, which is discussed in section 3.3. The quinoline compounds **1d** and **1a** moderately diminished the AR phosphorylation on S81 and suppressed the AR signalling in LAPC-4, similar to galeterone (Kwegyir-Afful *et al.*, 2015) (**Appendix III., Figure 7**). The lead compound **1d** decreased the PSA level even in LNCaP and 22Rv1 (**Appendix III., Supplementary Figure 4**).

To further describe the mechanism of action of candidate compounds, the cell cycle analysis was performed. The 48-h treatment with pyrazole derivative **3d** reduced the number of cells in S-phase in AR-positive LAPC-4 and 22Rv1 cells, but with no effect in AR-negative DU145 cells (**Appendix II., Supplementary Figure S10**), corresponding with published AR-regulation of the cell cycle (Gregory *et al.*, 2001). The effect of **3d** was comparable with PROTAC bavdegalutamide. The S-phase decrease was compensated by G2/M increase in LAPC-4, but G1 increase in 22Rv1 cells, showing different consequences among the PCa cell lines. The inactivity in DU145 proved the AR selectivity (Puhr *et al.*, 2018). The quinoline derivative **1d** induced an increase in G1 percentage with reduced S-phase percentage in LAPC-4 and LNCaP, more profound compared to galeterone or enzalutamide (**Appendix II., Supplementary Figure S5**).

3.3 AR downregulation and induction of its degradation

Long-term treatment of LAPC-4 with the most potent pyrazole **3d** showed a significant decrease in AR protein level upon 48 and 72 h (**Appendix II., Figure 5B**), as observed for bavdegalutamide (Neklesa *et al.*, 2018), galeterone (Yu *et al.*, 2014) and other monomer AR-degraders. Moreover, the expression of PSA and Nkx3.1 was completely switched off upon 72 h treatment and it caused proliferation inhibition without massive apoptosis (**Appendix II., Supplementary Figure S7**), confirming that the AR downregulation is not evoked by cell death.

Using the rescue experiment (Tang *et al.*, 2009), the ability of **3d** to bind to AR-LBD was verified, showing that **3d**-saturated AR has impaired bavdegalutamide degradation (**Appendix II., Figure 5C**). Further, qPCR analysis of mRNA expression of *AR* and *KLK3* (PSA) was performed. In the 24-h treatment, lead compound **3d** decreased *KLK3* mRNA expression in activated 22Rv1 and LAPC-4 cells more potently than enzalutamide or galeterone (**Appendix II., Figure 7B**). The expression of *AR* transcript decreased moderately, as well (**Appendix II., Supplementary Figure S11**). Further, an experiment with proteasome inhibition was performed to distinguish between targeting the *AR* transcription or the AR-protein stability. The proteasome inhibitor MG-132 treatment led to the accumulation

of ubiquitinated proteins (including AR) (Jin *et al.*, 2020) (**Figure 3A**). Contrary to the effect of **3d** and bavdegalutamide, MG-132 induced an increase in AR protein level and co-treatment with the analysed AR degraders blocked the AR degradation (**Figure 3A**). It proved that the **3d** induced proteasomal degradation and changed the AR turnover, similar to galeterone (Kwegyir-Afful *et al.*, 2015). Additionally, the dose-response treatment with **3d** decreased also the AR mRNA expression below 50 % in 10 μM (comparable to galeterone (Kwegyir-Afful *et al.*, 2015)), while the 1 μM bavdegalutamide (Neklesa *et al.*, 2018) did not influence it (**Figure 3B**). Most importantly, it was shown that compound **3d** induced a clear downregulation of AR (similar to bavdegalutamide) in short-term *ex vivo* culture of patient-derived samples (**Appendix II., Figure 8, Supplementary Figure S12**).

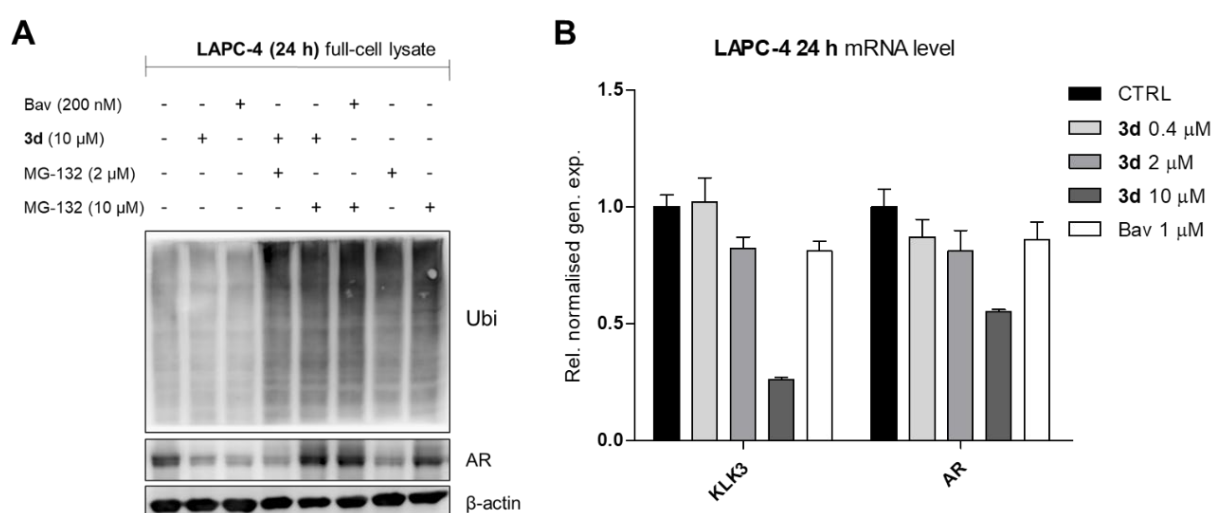


Figure 3 (A) Western blot analysis of AR and overall ubiquitinated proteins. The LAPC-4 cells were treated with **3d**, bavdegalutamide, MG-132 or combinations for 20 h and the full-cell lysate in 1% SDS was prepared. β -actin served as a loading control. **(B)** The dose-dependent effect of compound **3d** and bavdegalutamide (Bav) on relative normalized mRNA expression of AR and downstream KLK3 (PSA). Cells were cultivated in CSS medium and then treated with compounds in the presence of 1 nM R1881 for 24 h.

3.4 Analysis of compounds' interaction with AR

Steroidal agonists induce thermal stabilisation of AR performed by CETSA (Shaw *et al.*, 2018), therefore it was recruited and optimised as described in section 3.5. The assay proved the direct, in-cell binding of **2f** (**Appendix I., Figure 6**) to the AR in a dose-dependent manner. The experiment with R1881 confirmed previously published increase in AR's thermal stability as well (Shaw *et al.*, 2018).

The CETSA is a tedious and time-consuming method. That is why the expression of recombinant human His6-AR-LBD was performed (Askew *et al.*, 2007) and innovatively it was

expressed ligand-free (otherwise expressed with DHT), to bind ligands, analysed by the micro-scale thermophoresis (Nanotemper). The binding of the **3d** induced significant dose-dependent changes in the protein mobility (Wienken *et al.*, 2010) (**Appendix II., Figure S8**). Using the same procedure, the interaction of **1d** was also confirmed and the change was consistent with the effect of 25 μ M galeterone (**Appendix II., Figure 8B**).

To describe interactions of antagonists in the LBD, molecular docking into AR-LBD co-crystal structure with DHT (PDB: 2PIV) was recruited. The key residues in extremities of the cavity (Asn705, Gln711, Arg752, and Thr877) were set flexible. Candidate compound **2f** showed extensive interactions (**Appendix I., Figure 8**) and high binding energy (-12.7 kcal/mol). The lead compound **3d** revealed more extensive binding in AR-LBD with poses similar to steroidal antagonists cyproterone (Bohl *et al.*, 2007) or galeterone (Njar and Brodie, 2015). Moreover, it was confirmed by similar positions as in the antagonist model (Wahl and Smieško, 2018). The first two poses of **3d** displayed high binding energy (-11.8 kcal/mol and -11.6 kcal/mol, respectively) and similar orientation (**Figure 4; Appendix II., Figure 6A, B**), but in the first pose the C-17 β -OH group formed a conserved hydrogen bond with Thr877, while in the second pose with Asn705 (**Figure 4; Appendix II., Figure 8B**). Moreover, it showed similar binding to cyproterone and the pose independent of Thr877 was also observed in non-steroidal antiandrogens (Xu *et al.*, 2022). The docking of the quinoline **1d** in the same setting showed a very similar binding pose, with the binding energy = -10.2 kcal/mol. Overall, it formed hydrogen bonds with Arg752 and Gln711, the steroid core formed conserved interactions (Gim *et al.*, 2021) and the 17 β -OH formed a bond with Thr877, with a possible interaction with Asn705 (**Appendix III., Figure 8C**).

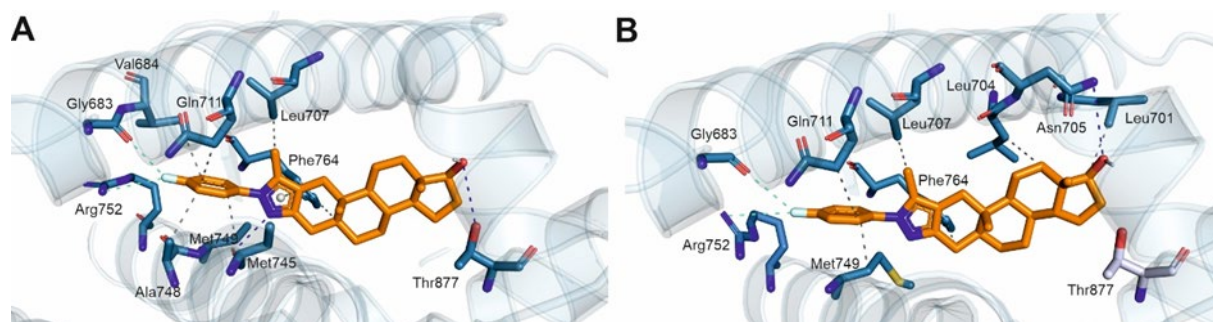


Figure 4 Binding poses of the most potent pyrazole derivative **3d** (orange) in the AR-LBD (light blue), dependent (A) and independent (B) of Thr877. The interacting AR residues are shown as blue sticks. Nitrogen atoms are shown in dark blue, oxygen in red, sulphur in yellow, and fluorine in cyan.

3.5 Optimisation of cell compartment fractionation and CETSA

The trial experiment of cellular fractionation was performed using the Qproteome Cell Compartment Kit (Quiagen) (**Appendix I, Figure 7**). Subsequently, a protocol using in-house buffers was optimised. Inspired by protocols for crude subcellular fractionation (Abmayr *et al.*, 2006; Holden and Horton, 2009), 22Rv1 cells were initially directly lysed from the monolayer on the Petri dish, which was incubated with the lysis buffer A (cytosolic, 150 mM NaCl, 50 mM HEPES (pH 7.4), 45 µg/ml digitonin with protease inhibitors) on ice, which should have released the cytosol fraction (Abmayr *et al.*, 2006; Holden and Horton, 2009), that was collected (sample 1) (**Figure 5A**). Unfortunately, the digitonin did not disrupt cells, which were scratched in another portion of buffer A (sample 2). Upon centrifugation at 600 g for 6 min, the pellet contained all proteins (sample 3), while the supernatant only the cytosolic ones (sample 4). The pellet was further incubated with the RIPA (nuclear) lysis buffer (150 mM NaCl, 50 mM HEPES (pH 7.4) 0.5% sodium deoxycholate, 0.1% sodium dodecyl sulphate) in which it completely dissolved (sample 5), but contained all the types of proteins (**Figure 5A**)

Another protocol was used for the monolayer of 22Rv1 cells (Baghirova *et al.*, 2015), first incubated with the lysis buffer A (cytosolic, 150 mM NaCl, 50 mM HEPES (pH 7.4), 0,1% IGEPAL® CA-630 with protease inhibitors) on ice. Upon the incubation, the cells detached, they were gently collected from the dish bottom (sample 1) (**Figure 5B**) and centrifuged at 600 g for 6 min. The obtained supernatant (sample 2) contained only cytosolic proteins, while the pellet was further incubated with buffer B (nuclear, 20 mM HEPES, pH 7.9, 1.5 mM MgCl₂, 0.5 M NaCl, 0.2 mM EDTA, 20% glycerol, 1% Triton™ X100), sonicated and centrifuged at 14 000 g for 15 min. The obtained supernatant (sample 3) contained soluble nuclear proteins and the insoluble pellet contained DNA-bound proteins (sample 4) (**Figure 5B**).

The previous attempts showed complications with direct lysis on the Petri dish, so for the comparison of different detergents (Baghirova *et al.*, 2015; Senichkin *et al.*, 2021) in the cytosolic buffer, cells were harvested by trypsinisation, washed and divided into aliquots. Then, the basic cytosolic buffer A was applied with three different detergents (45 µg/mL digitonin or 0.1% IGEPAL® CA-630 or 0.1% NP-40). After the incubation on ice, the suspension was centrifuged at 600 g for 6 min. The obtained supernatant should represent the cytosolic fraction (c), while the pellet was further incubated with buffer B, sonicated and centrifuged at 14 000 g for 15 min to obtain soluble nuclear fraction (n). It was shown that Igepal or NP-40 (Baghirova *et al.*, 2015; Senichkin *et al.*, 2021) are suitable for cytosol extraction, while digitonin did not succeed, contrary to published protocols (Abmayr *et al.*, 2006; Holden and Horton, 2009)

(Figure 5C). The combination of the Igepal/Triton buffers was further shown to easily fractionate the cells for the desired fractions (Figure 5D). The optimised buffers (summarised in section 2.2.5) were further used to assess the NR's localisation (Appendix IV., Figure 4).

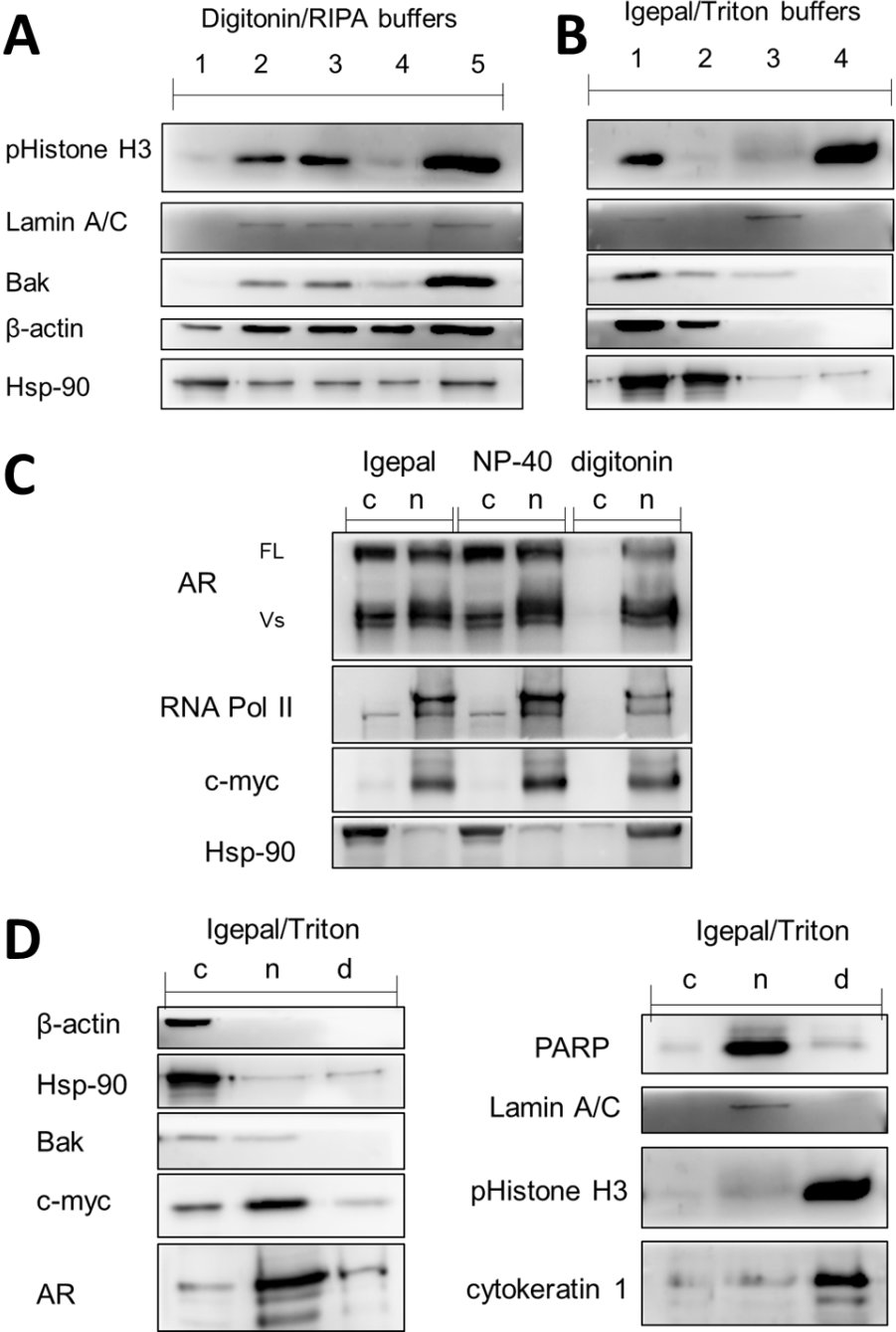


Figure 5 Comparison of digitonin and RIPA buffers (A) with Igepal/ Triton buffers (B) for 22Rv1 cell fractionation from Petri dish with the same procedure (lysis in the first buffer, scratching of the cells, low speed-centrifugation to separate nuclei, their lysis in the second buffer, high-speed centrifugation to separate insoluble parts. Numbers correspond with obtained cellular fraction. (C) Fractionation of trypsinised cells incubated with different combinations of lysis buffers with the same general procedure to obtain cytosolic (c) and nuclear (n) fractions. (D) Igepal/ Triton combination for the best fractionation of cytosol (c), soluble nuclear proteins (n) and DNA-bound nuclear proteins (d) with the membrane debris.

The binding of candidate AR antagonists was first evaluated by CETSA, whose advantage is the use of untagged AR from cell lysate or within intact cells, showing the thermal stabilisation upon target engagement. At first, the CETSA experiment was based on the original publication (Jafari *et al.*, 2014) using a purified AR-FL protein (Merck Millipore) in a protein buffer and a crude cell lysate of C4-2 cells (high AR expression) in RIPA lysis buffer. The aggregation temperature was screened in the range of 40 – 60 °C (3 min in CFX96 Touch (BioRad), then the samples were cooled for 3 min at 4 °C and centrifuged at 14 000 g for 30 min. The supernatants were subsequently mixed with SDS-loading buffer, separated by SDS-PAGE and immunoblotted with AR-antibody.

It was shown that the thermal stability of recombinant protein is insufficient, while the lysate from C4-2 cells displayed an appropriate response, with the aggregation temperature around 44 °C (**Figure 5A**). The optimisation continued with the C4-2 cell lysate from the harvested cells cultivated in full, FBS-supplemented media or in CSS-supplemented media (steroid-depleted). No clear thermal stabilisation was observed upon the incubation of the R1881 or candidate compound **2f** with both lysates for 1 h (**Figure 5B**).

Even that the CETSA can be performed in cell lysate, the presence of detergents might dramatically change the protein solubility. The next setup was the CETSA in treated intact cells (Shaw *et al.*, 2018; Henderson *et al.*, 2020) cultivated in CSS-supplemented media. The cells were harvested by trypsinisation, diluted in PBS with 5 mM glucose, counted and divided into test tubes, and treated with R1881 or **2f** for 3 h. The subsequent procedure followed the same principle, with a temperature gradient from 45 °C to 57 °C. Obtained samples were lysed by 3 freeze-thaw cycles (Almqvist *et al.*, 2016) and processed as usual. R1881 and **2f** apparently increased temperature stability, but after the normalisation of the signal to the control, no effect was observed (**Figure 5C**).

The prolonged incubation of cells in PBS with high concentrations of compounds probably influenced the integrity of the cells and caused an imbalance of the basal AR level. To avoid this effect, finally, C4-2 cells were harvested, re-suspended in PBS with 5 mM glucose and divided into test tubes, treated with R1881 only for 1 h. Upon the treatment, cells were counted and equally aliquoted into PCR strips, heated at the temperature gradient and processed as before. The immunoblotting revealed that 100 nM R1881 induced thermal stabilisation from 43 °C to 54 °C (**Figure 5, D**), corresponding with previous findings (Shaw *et al.*, 2018). The CETSA was also used to confirm the binding of non-steroidal enzalutamide (Shaw *et al.*, 2018), however, by showing the decrease in AR thermal stability, reverting the R1881-induced stabilisation. The candidate compound **2f** displayed the AR-stabilisation in C4-2

in a concentration manner (from 10 μM – 100 μM) (**Appendix I, Figure 6**) and the stabilisation might originate from extensive interactions of the steroid scaffold with AR-LBD.

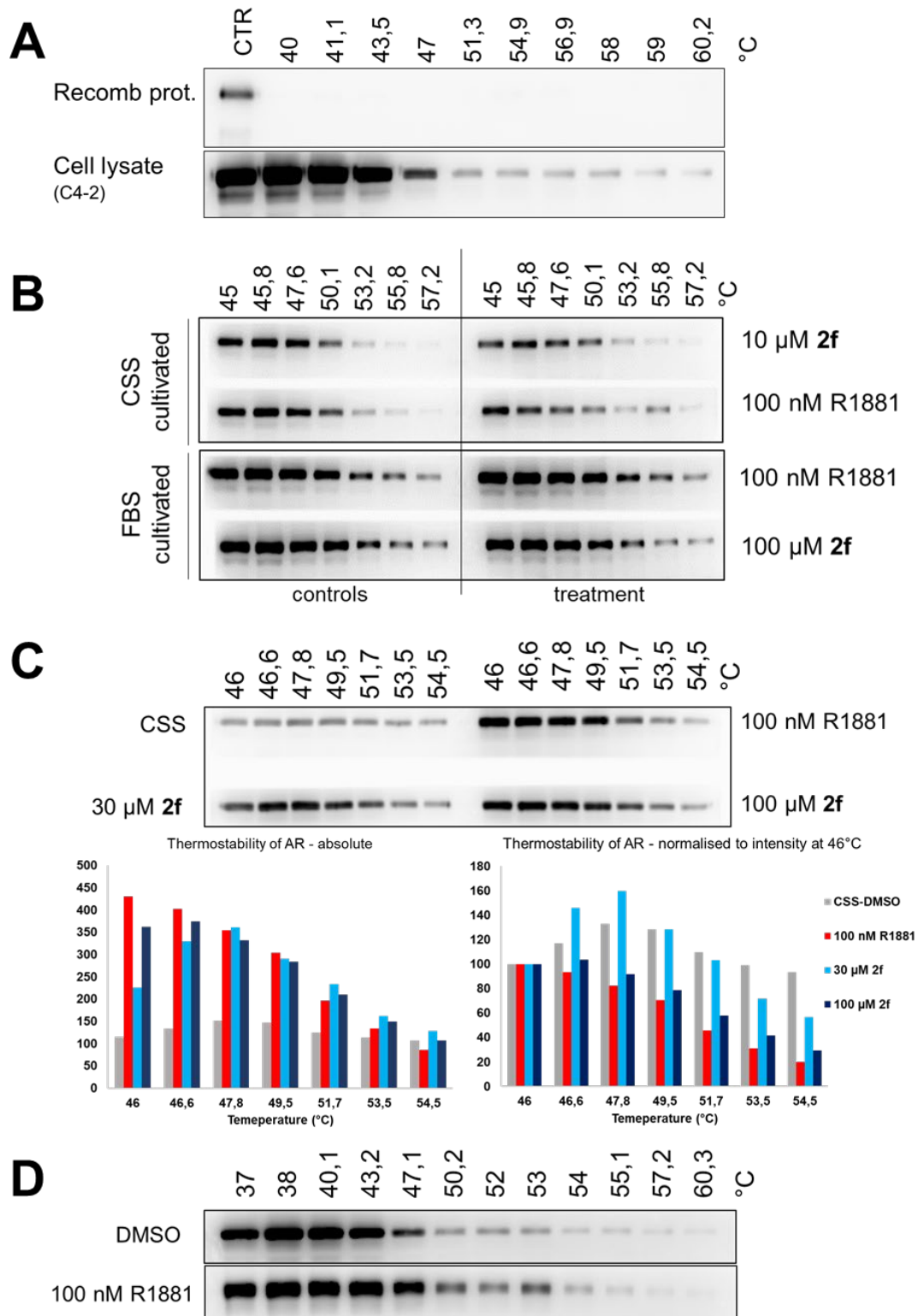


Figure 6 Optimisation of the CETSA protocol. **(A)** First trial of thermal shift using recombinant AR protein and C4-2 cell lysate. **(B)** CETSA with 1 h incubation of compounds with RIPA-buffer lysate from cells cultivated in FBS or CSS-supplemented media **(C)** CETSA performed in cells treated for 3 h with subsequent lysis by freeze-thaw cycles. **(D)** CETSA performed in cells treated for 1 h and normalised after the treatment.

3.6 Dual targeting of AR and GR

To combat the resistance of CRPC and namely the AR-negative PCa with GR upregulation, GR-targeting treatments were recently described with dual and selective antagonists of AR/GR (Rosette *et al.*, 2020). In the frame of this thesis, novel 17 α - and/or 21-ester or carbamate derivatives of hydrocortisone (GR agonist) were developed and evaluated for their biological activity towards AR and GR in different PCa cells. The group of analysed compounds comprised 17 α -monoesters of hydrocortisone, C-21 esters and carbamates. The effect of compounds on both NRs was evaluated using AR and GR reporter cell lines, 22Rv1-ARE14 (Bartonkova *et al.*, 2015) and AZ-GR (Novotna *et al.*, 2012) respectively. Within prepared compounds, several AR agonists were described, in agreement that hydrocortisone can activate AR (Bartonkova *et al.*, 2015) and that glucocorticoids can act as AR agonists in AR-mutants (Zhao *et al.*, 2000). However, the attention was focused on two 17 α -butyryloxy,21-(alkyl)carbamoyloxy derivatives **14** and **15** that displayed strong antagonist properties towards both AR and GR (**Appendix IV., Figure 2**). Antagonist activities of the lead compound **14** (**Figure 7**) towards AR reached low micromolar values ($IC_{50} = 3.96 \mu M$), comparable to standards, i.e. enzalutamide ($IC_{50} = 3.32 \mu M$) and galeterone ($IC_{50} = 7.59 \mu M$) (Norris *et al.*, 2017). Additionally, antagonist activity of **14** towards GR reached single-digit micromolar values ($IC_{50} = 4.44 \mu M$), weaker than for standard mifepristone ($IC_{50} = 0.59 \mu M$) (Du *et al.*, 2019). No clear agonist activity was observed for **14** neither towards the AR nor the GR (**Appendix IV., Figure 2**).

Antiproliferative properties of the hydrocortisone derivatives were tested in four PCa cell lines, namely LAPC-4, 22Rv1 (expressing both AR and GR), C4-2 (only AR), and DU145 (AR-negative and GR overexpressing). While the compounds without clear AR/GR activities did not display antiproliferative activities, the most potent derivatives **14** and **15** displayed mid-micromolar values ($GI_{50} = 25 \mu M - 40 \mu M$ upon treatment for 72 h) in all AR-positive cells, comparable with standards galeterone and mifepristone. Compound **14** was the only one which reached measurable $GI_{50} = 80 \mu M$ in AR-negative DU145 cells (**Appendix IV., Supplementary Figure S6**). In the CFA assay, compound **14** exhibited strong colony-formation inhibition in AR-positive PCa cell lines, comparable with standard galeterone (Kwegyir-Afful *et al.*, 2019), but weaker colony-formation inhibition in AR-negative and GR-overexpressing PCa cell line, compared to both galeterone and mifepristone (**Appendix IV., Figure 3**).

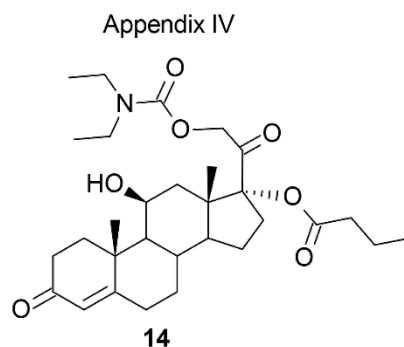


Figure 7 Structure of the most potent AR/GR antagonist **14**.

Interaction with both NRs was confirmed by the optimised CETSA and followed the previous studies. Subsequently, **14** decreased the translocation of AR and GR to the nucleus similarly to galeterone (Yu *et al.*, 2014) and mifepristone (Peeters *et al.*, 2008), respectively (**Appendix IV.**, **Figure 4**). Both compounds **14** and **15** reduced AR a GR downstream signalling (**Appendix IV.**, **Figure 5A, B**; **Supplementary Figure S9**), similar to standards (Yu *et al.*, 2014; Peeters *et al.*, 2008)).

Molecular docking into the GR (PDB 1NHZ) (Kauppi *et al.*, 2003) showed extensive binding of **14** in a similar way as mifepristone, but with stronger binding energy ($\Delta G_{Vina} = -11.5$ kcal/mol and -10.8 kcal/mol, respectively). Direct hydrogen bonds from the 3-carbonyl in the A-ring to Gln570 and Arg611 were found. Interestingly, the 21-(*N,N*-diethylcarbamoyloxy) was orientated in the same direction as the dimethylaniline side chain of mifepristone (**Appendix IV.**, **Figure 6A, B**), disrupting the helix-12 position (Kauppi *et al.*, 2003). Molecular docking into the AR-antagonist model (Wahl and Smieško, 2018) revealed the same binding of compound **14** as cyproterone (Bohl *et al.*, 2007) (**Appendix IV.**, **Figure 6C, D**) with similar binding energy ($\Delta G_{Vina} = -12.5$ kcal/mol and -12.1 kcal/mol, respectively) and key interaction residues.

The enzalutamide resistance is connected with increased GR expression (Culig, 2017) and the first increase in GR level is detectable just 7 days after the treatment with enzalutamide (Isikbay *et al.*, 2014; Puhr *et al.*, 2018). The candidate compounds **14** and **15** did not cause a significant increase in GR or AR levels during the same periods. Importantly, compound **14** reduced the enzalutamide-induced GR upregulation (**Appendix IV.**, **Supplementary Figure S7**). Overall, the findings and the clinical trial of enzalutamide and mifepristone in CRPC (Serritella *et al.*, 2022) support the development and deep characterisation of novel dual AR and GR antagonists (Li *et al.*, 2024) as anticancer agents in PCa cases with upregulation of GR activity.

4 CONCLUSION AND PERSPECTIVES

The approved next-generation hormone therapies targeting AR markedly increased the effectiveness of the PCa therapy (He *et al.*, 2022). Despite the initial effectiveness of treatment of PCa, nearly all patients eventually progress to develop resistance. Therefore, the discovery of novel strategies is needed to improve the effectiveness in resistant PCa cases (Deluce *et al.*, 2022). Since the steroidal compounds containing a heterocycle moiety in the A-ring have been recently much less investigated towards the AR and PCa (Jorda *et al.*, 2019; Njar and Brodie, 2015; Baji *et al.*, 2016; Mótyán *et al.*, 2019), the main part of the dissertation thesis investigated biological activity of library of DHT derivatives with modifications on the A-ring prepared by Éva Frank's (University of Szeged, Hungary) synthetic group. Altogether, DHT derivatives bearing different nitrogen-containing five or six-membered heterocycles as a fusion to the A-ring with a series of terminal substituents (119 compounds in total) were thoroughly characterised, searching for a potent AR antagonist to effectively suppress the growth and proliferation of PCa cells with minimal toxicity to healthy tissue. For a detailed assessment of the compounds' behaviour, methods established at the department were used, while the isolation of the cellular fractions (cytosol and nuclei) and the cellular-thermal shift assay were optimised based on the published protocols.

Divided by the particular groups, it was clear that α,β -enones demonstrated potent antiandrogenic effects, with compound **2f** being particularly effective outperforming standard treatments like enzalutamide and galeterone (Yu *et al.*, 2014; Tran *et al.*, 2009), while triazolo[1,5-*a*]pyrimidines and pyrazolo[1,5-*a*]pyrimidines showed partial activity, with some representatives exhibiting agonist properties. The A-ring fused pyrazoles were generally the most potent group of analysed compounds with representatives bearing the C-17 hydroxy group and 1'-aryl-5'-methyl substitution showing the strongest antagonist properties. Antiproliferative effects were observed, selective for AR-positive cell lines, with the lead compound **3d** displaying significant potency. The potent downregulation and degradation of AR must be underscored, as well as the potent activity of **3d** in patients' samples *ex vivo*. The A-ring-fused quinolines showed moderate antagonist activity, with **1d** which showed reasonable antiproliferative potency, particularly in AR-positive cell lines. The pyridine derivatives exhibited varying activity, with both agonist/antagonist properties.

From the mechanistic point of view, the most potent derivative **3d** displayed strong antagonist activity, surpassing standard AR antagonists like enzalutamide and galeterone, selectively targeted AR-positive cells, sparing AR-negative cell lines. Molecular docking

studies provided insights into the structural basis of compounds' activity, revealing interactions within the AR-LBD and potential for further optimization.

Finally, the biological activity of hydrocortisone's derivatives was also analysed and compounds were described as dual antagonists of AR/GR. The lead compound suppressed the signalling of both receptors, the interactions were proved in cells and modelled by molecular docking. Since GR signalling is a resistance mechanism (Puhr *et al.*, 2018; Wu *et al.*, 2019), the findings support the development and deep characterisation of dual AR and GR antagonists as anticancer agents in PCa cases with upregulation of GR activity (Li *et al.*, 2024).

Overall, the dissertation study provided valuable insights into the design and development of novel AR-targeted compounds for the treatment of prostate cancer, highlighting their potential as alternative or complementary therapies to existing standards of care. Various novel approaches like PROTACs (Alabi and Crews, 2021) and targeting different regions (Li *et al.*, 2019) are explored to overcome resistance mechanisms observed in clinical trials. Based on the frequent LBD mutations and splicing variants (Angulo *et al.*, 2022), the most promising therapies seem to be N-terminal or DNA-binding domains-targeting drugs. However, the development of novel LBD antagonists is also plausible, with emphasis on desired properties such as limited resistance, favourable pharmacokinetics and minimal side effects (He *et al.*, 2022) The structure-based development is however hampered by the absence of a crystal structure of the wt-LBD with an antagonist (Wahl and Smieško, 2018). Apart from the AR axis, there are several other approaches for the PCa treatment, including phototherapy (Shi and Sadler, 2020), targeting prostate-specific membrane antigen (PSMA) by immunotherapy in clinical trials or approved radionuclide therapy (¹⁷⁷Lu-PSMA-617) (He *et al.*, 2022) and many other clinical trials of compounds holding promise for the future.

5 REFERENCE

- Abmayr SM, Yao T, Parmely T, Workman JL. Preparation of nuclear and cytoplasmic extracts from mammalian cells. *Curr Protoc Mol Biol*. 2006 Aug;Chapter 12:Unit 12.1.
- Adasme MF, Linnemann KL, Bolz SN, et al. PLIP 2021: expanding the scope of the protein-ligand interaction profiler to DNA and RNA. *Nucleic Acids Res*. 2021;49(W1):W530-W534.
- Alabi SB, Crews CM. Major advances in targeted protein degradation: PROTACs, LYTACs, and MADTACs. *J Biol Chem*. 2021 Jan-Jun;296:100647.
- Almqvist H, Axelsson H, Jafari R, Dan C, Mateus A, Haraldsson M, Larsson A, Martinez Molina D, Artursson P, Lundbäck T, Nordlund P. CETSA screening identifies known and novel thymidylate synthase inhibitors and slow intracellular activation of 5-fluorouracil. *Nat Commun*. 2016 Mar 24;7:11040.
- Angulo JC, Ciria Santos JP, Gómez-Caamaño A, Poza de Celis R, González Sala JL, García Garzón JM, Galán-Llopis JA, Pérez Sampietro M, Perrot V, Planas Morin J; ANARESISTANCE study group. Development of castration resistance in prostate cancer patients treated with luteinizing hormone-releasing hormone analogues (LHRHa): results of the ANARESISTANCE study. *World J Urol*. 2022 Oct;40(10):2459-2466.
- Askew EB, Gampe RT Jr, Stanley TB, Faggart JL, Wilson EM. Modulation of androgen receptor activation function 2 by testosterone and dihydrotestosterone. *J Biol Chem*. 2007 Aug 31;282(35):25801-16.
- Baghirova S, Hughes BG, Hendzel MJ, Schulz R. Sequential fractionation and isolation of subcellular proteins from tissue or cultured cells. *MethodsX*. 2015 Nov 7;2:440-5.
- Baji A, Gyovai A, Wölfling J, Minorics R, Ocsosvzki I, Zupkó I, Frank É. Microwave-assisted one-pot synthesis of steroid-quinoline hybrids and an evaluation of their antiproliferative activities on gynecological cancer cell lines. *RSC Adv*. 2016; 6: 27501-27516.
- Bartonkova I, Novotna A, Dvorak Z. Novel stably transfected human reporter cell line AIZ-AR as a tool for an assessment of human androgen receptor transcriptional activity. *PLoS One*. 2015 Mar 26;10(3):e0121316.
- Bohl CE, Wu Z, Miller DD, Bell CE, Dalton JT. Crystal structure of the T877A human androgen receptor ligand-binding domain complexed to cyproterone acetate provides insight for ligand-induced conformational changes and structure-based drug design. *J Biol Chem*. 2007 May 4;282(18):13648-55.
- Brinkmann AO. Molecular basis of androgen insensitivity. *Mol Cell Endocrinol* 2001; **179**:105–9
- Chen Y, Zhou Q, Hankey W, Fang X, Yuan F. Second generation androgen receptor antagonists and challenges in prostate cancer treatment. *Cell Death Dis*. 2022 Jul 21;13(7):632.
- Culig Z, Hoffmann J, Erdel M, Eder IE, Hobisch A, Hittmair A, Bartsch G, Utermann G, Schneider MR, Parczyk K, Klocker H. Switch from antagonist to agonist of the androgen receptor bicalutamide is associated with prostate tumour progression in a new model system. *Br J Cancer*. 1999 Sep;81(2):242-51.
- Culig Z. Molecular Mechanisms of Enzalutamide Resistance in Prostate Cancer. *Curr Mol Biol Rep*. 2017;3(4):230-235.
- Deluce JE, Cardenas L, Lalani AK, Maleki Vareki S, Fernandes R. Emerging Biomarker-Guided Therapies in Prostate Cancer. *Curr Oncol*. 2022 Jul 18;29(7):5054-5076.
- Deluce JE, Cardenas L, Lalani AK, Maleki Vareki S, Fernandes R. Emerging Biomarker-Guided Therapies in Prostate Cancer. *Curr Oncol*. 2022 Jul 18;29(7):5054-5076.
- Denmeade SR, Isaacs JT. A history of prostate cancer treatment. *Nat Rev Cancer*. 2002 May;2(5):389-96.
- Dhiman VK, Bolt MJ, White KP. Nuclear receptors in cancer - uncovering new and evolving roles through genomic analysis. *Nat Rev Genet*. 2018 Mar;19(3):160-174.
- Du X, Eksterowicz J, Zhou H, Rew Y, Zhu L, Yan X, Medina JC, Huang T, Chen X, Sutimantanapi D, Jahchan N, Kong W, Sun J, Zavorotinskaya T, Ye Q, Fantin VR, Sun D. Discovery of a Potent Steroidal Glucocorticoid Receptor Antagonist with Enhanced Selectivity against the Progesterone and Androgen Receptors (OP-3633). *J Med Chem*. 2019 Jul 25;62(14):6751-6764.
- Gim HJ, Park J, Jung ME, Houk KN. Conformational dynamics of androgen receptors bound to agonists and antagonists. *Sci Rep*. 2021 Aug 5;11(1):15887.

- Gregory CW, Johnson RT Jr, Presnell SC, Mohler JL, French FS. Androgen receptor regulation of G1 cyclin and cyclin-dependent kinase function in the CWR22 human prostate cancer xenograft. *J Androl.* 2001 Jul-Aug;22(4):537-48.
- He Y, Xu W, Xiao YT, Huang H, Gu D, Ren S. Targeting signaling pathways in prostate cancer: mechanisms and clinical trials. *Signal Transduct Target Ther.* 2022 Jun 24;7(1):198.
- Henderson MJ, Holbert MA, Simeonov A, Kallal LA. High-Throughput Cellular Thermal Shift Assays in Research and Drug Discovery. *SLAS Discov.* 2020 Feb;25(2):137-147.
- Holden P, Horton WA. Crude subcellular fractionation of cultured mammalian cell lines. *BMC Res Notes.* 2009 Dec 10;2:243.
- Iannantuono GM, Chandran E, Floudas CS, Choo-Wosoba H, Butera G, Roselli M, Gulley JL, Karzai F. Efficacy and safety of PARP inhibitors in metastatic castration-resistant prostate cancer: A systematic review and meta-analysis of clinical trials. *Cancer Treat Rev.* 2023 Nov;120:102623.
- Isikbay M, Otto K, Kregel S, Kach J, Cai Y, Vander Griend DJ, Conzen SD, Szmulewitz RZ. Glucocorticoid receptor activity contributes to resistance to androgen-targeted therapy in prostate cancer. *Horm Cancer.* 2014 Apr;5(2):72-89.
- Jafari, R., Almqvist, H., Axelsson, H., Ignatushchenko, M., Lundbäck, T., Nordlund, P., & Molina, D. M. (2014). The cellular thermal shift assay for evaluating drug target interactions in cells. *Nature Protocols*, 9(9), 2100–2122.
- Jarman M, Barrie SE, Llera JM. The 16,17-double bond is needed for irreversible inhibition of human cytochrome p45017alpha by abiraterone (17-(3-pyridyl)androsta-5, 16-dien-3beta-ol) and related steroidal inhibitors. *J Med Chem.* 1998 Dec 31;41(27):5375-81.
- Jorda R, Řezníčková E, Kielczewska U, Maj J, Morzycki JW, Siergiejszyk L, Bazgier V, Berka K, Rárová L, Wojtkielewicz A. Synthesis of novel galeterone derivatives and evaluation of their in vitro activity against prostate cancer cell lines. *Eur J Med Chem.* 2019b Oct 1;179:483-492.
- Jorda R., Buckova Z., Reznickova E., Bouchal J., Krystof V. Selective inhibition reveals cyclin-dependent kinase 2 as another kinase that phosphorylates the androgen receptor at serine 81. *Biochim Biophys Acta Mol Cell Res.* 2018;1865:354–363.
- Kauppi B, Jakob C, Färnegårdh M, Yang J, Ahola H, Alarcon M, Calles K, Engström O, Harlan J, Muchmore S, Ramqvist AK, Thorell S, Ohman L, Greer J, Gustafsson JA, Carlstedt-Duke J, Carlquist M. The three-dimensional structures of antagonistic and agonistic forms of the glucocorticoid receptor ligand-binding domain: RU-486 induces a transconformation that leads to active antagonism. *J Biol Chem.* 2003 Jun 20;278(25):22748-54.
- Kwegyir-Afful A. K., Ramalingam S., Purushottamachar P., Ramamurthy V. P., Njar V. C. (2015): Galeterone and VNPT55 induce proteasomal degradation of AR/AR-V7, induce significant apoptosis via cytochrome c release and suppress growth of castration resistant prostate cancer xenografts in vivo. *Oncotarget* 6, 27440-27460.
- Kwegyir-Afful AK, Ramalingam S, Ramamurthy VP, Purushottamachar P, Murigi FN, Vasaitis TS, Huang W, Kane MA, Zhang Y, Ambulos N, Tiwari S, Srivastava P, Nnane IP, Hussain A, Qiu Y, Weber DJ, Njar VCO. Galeterone and The Next Generation Galeterone Analogs, VNPP414 and VNPP433-3β Exert Potent Therapeutic Effects in Castration-/Drug-Resistant Prostate Cancer Preclinical Models In Vitro and In Vivo. *Cancers (Basel).* 2019 Oct 24;11(11):1637.
- Latysheva AS, Zolottsev VA, Veselovsky AV, Scherbakov KA, Morozevich GE, Pokrovsky VS, Novikov RA, Timofeev VP, Tkachev YV, Misharin AY. New steroidal oxazolines, benzoxazoles and benzimidazoles related to abiraterone and galeterone. *Steroids.* 2020 Jan;153:108534.
- Li C, Han X, Yan Q, Ji Y, Zhang R, Yuan D, Yang F, Wang J, Wu M, Zhou J. Design and Synthesis of Dual-Target Inhibitors Targeting Androgen Receptors and Glucocorticoid Receptors to Overcome Antiandrogen Resistance in Castration-Resistant Prostate Cancer. *J Med Chem.* 2024 Mar 14;67(5):3419-3436.
- Li D, Zhou W, Pang J, Tang Q, Zhong B, Shen C, Xiao L, Hou T. A magic drug target: Androgen receptor. *Med Res Rev.* 2019 Sep;39(5):1485-1514.
- Livak KJ, Schmittgen TD. Analysis of relative gene expression data using real-time quantitative PCR and the 2(-Delta Delta C(T)) Method. *Methods.* 2001 Dec;25(4):402-8.
- Lv S, Song Q, Chen G, Cheng E, Chen W, Cole R, Wu Z, Pascal LE, Wang K, Wipf P, Nelson JB, Wei Q, Huang W, Wang Z. Regulation and targeting of androgen receptor nuclear localization in castration-resistant prostate cancer. *J Clin Invest.* 2021 Feb 15;131(4):e141335.

- Morris GM, Huey R, Lindstrom W, Sanner MF, Belew RK, Goodsell DS, Olson AJ. AutoDock4 and AutoDockTools4: Automated docking with selective receptor flexibility. *J Comput Chem.* 2009 Dec;30(16):2785-91.
- Mótyán G, Gopisetty MK, Kiss-Faludy RE, Kulmány Á, Zupkó I, Frank É, Kiricsi M. Anti-Cancer Activity of Novel Dihydrotestosterone-Derived Ring A-Condensed Pyrazoles on Androgen Non-Responsive Prostate Cancer Cell Lines. *Int J Mol Sci.* 2019 May 2;20(9):2170.
- Neklesa TK, Snyder LB, Willard RR, Vitale N, Raina K, Pizzano J, Gordon D, Bookbinder M, Macaluso J, Dong H, Liu Z, Ferraro C, Wang G, Wang J, Crews CM, Houston J, Crew AP, Taylor I. Abstract 5236: ARV-110: An androgen receptor PROTAC degrader for prostate cancer. *Cancer Res.* 2018 Jul 1;78(13_Supplement):5236.
- Njar VC, Brodie AM. Discovery and development of Galeterone (TOK-001 or VN/124-1) for the treatment of all stages of prostate cancer. *J Med Chem.* 2015 Mar 12;58(5):2077-87.
- Norris JD, Ellison SJ, Baker JG, Stagg DB, Wardell SE, Park S, Alley HM, Baldi RM, Yllanes A, Andreano KJ, Stice JP, Lawrence SA, Eisner JR, Price DK, Moore WR, Figg WD, McDonnell DP. Androgen receptor antagonism drives cytochrome P450 17A1 inhibitor efficacy in prostate cancer. *J Clin Invest.* 2017 Jun 1;127(6):2326-2338.
- Novotna A, Pavek P, Dvorak Z. Construction and characterization of a reporter gene cell line for assessment of human glucocorticoid receptor activation. *Eur J Pharm Sci.* 2012 Dec 18;47(5):842-7.
- Peeters BW, Ruigt GS, Craighead M, Kitchener P. Differential effects of the new glucocorticoid receptor antagonist ORG 34517 and RU486 (mifepristone) on glucocorticoid receptor nuclear translocation in the AtT20 cell line. *Ann N Y Acad Sci.* 2008 Dec;1148:536-41.
- Puhr M, Hoefler J, Eigentler A, Ploner C, Handle F, Schaefer G, Kroon J, Leo A, Heidegger I, Eder I, Culig Z, Van der Pluijm G, Klocker H. The Glucocorticoid Receptor Is a Key Player for Prostate Cancer Cell Survival and a Target for Improved Antiandrogen Therapy. *Clin Cancer Res.* 2018 Feb 15;24(4):927-938.
- Rosette C, Agan FJ, Rosette N, Mazzetti A, Moro L, Gerloni M. The Dual Androgen Receptor and Glucocorticoid Receptor Antagonist CB-03-10 as Potential Treatment for Tumors that have Acquired GR-mediated Resistance to AR Blockade. *Mol Cancer Ther.* 2020 Nov;19(11):2256-2266.
- Schröder FH. Cyproterone acetate--mechanism of action and clinical effectiveness in prostate cancer treatment. *Cancer.* 1993 Dec 15;72(12 Suppl):3810-5.
- Senichkin VV, Prokhorova EA, Zhivotovsky B, Kopeina GS. Simple and Efficient Protocol for Subcellular Fractionation of Normal and Apoptotic Cells. *Cells.* 2021 Apr 9;10(4):852.
- Serritella AV, Shevrin D, Heath EI, Wade JL, Martinez E, Anderson A, Schonhoft J, Chu YL, Karrison T, Stadler WM, Szmulewitz RZ. Phase I/II Trial of Enzalutamide and Mifepristone, a Glucocorticoid Receptor Antagonist, for Metastatic Castration-Resistant Prostate Cancer. *Clin Cancer Res.* 2022 Apr 14;28(8):1549-1559.
- Shaw J, Leveridge M, Norling C, Karén J, Molina DM, O'Neill D, Dowling JE, Davey P, Cowan S, Dabrowski M, Main M, Gianni D. Determining direct binders of the Androgen Receptor using a high-throughput Cellular Thermal Shift Assay. *Sci Rep.* 2018 Jan 9;8(1):163.
- Shi H, Sadler PJ. How promising is phototherapy for cancer? *Br J Cancer.* 2020 Sep;123(6):871-873.
- Taplin ME, Antonarakis ES, Ferrante KJ, Horgan K, Blumenstein B, Saad F, Luo J, de Bono JS. Androgen Receptor Modulation Optimized for Response-Splice Variant: A Phase 3, Randomized Trial of Galeterone Versus Enzalutamide in Androgen Receptor Splice Variant-7-expressing Metastatic Castration-resistant Prostate Cancer. *Eur Urol.* 2019 Dec;76(6):843-851.
- Tran C, Ouk S, Clegg NJ, Chen Y, Watson PA, Arora V, Wongvipat J, Smith-Jones PM, Yoo D, Kwon A, Wasielewska T, Welsbie D, Chen CD, Higano CS, Beer TM, Hung DT, Scher HI, Jung ME, Sawyers CL. Development of a second-generation antiandrogen for treatment of advanced prostate cancer. *Science.* 2009 May 8;324(5928):787-90.
- Trott O, Olson AJ. AutoDock Vina: improving the speed and accuracy of docking with a new scoring function, efficient optimization, and multithreading. *J Comput Chem.* 2010;31(2):455-461.
- Velho PI, Bastos DA, Antonarakis ES. New approaches to targeting the androgen receptor pathway in prostate cancer. *Clin Adv Hematol Oncol.* 2021 Apr;19(4):228-240. PMID: 33989272.
- Wahl J, Smieško M. Endocrine Disruption at the Androgen Receptor: Employing Molecular Dynamics and Docking for Improved Virtual Screening and Toxicity Prediction. *Int J Mol Sci.* 2018 Jun 15;19(6):1784.

- Wienken CJ, Baaske P, Rothbauer U, Braun D, Duhr S. Protein-binding assays in biological liquids using microscale thermophoresis. *Nat Commun.* 2010 Oct 19;1:100.
- Wu M, Xie Y, Cui X, Huang C, Zhang R, He Y, Li X, Liu M, Cen S, Zhou J. Rational drug design for androgen receptor and glucocorticoids receptor dual antagonist. *Eur J Med Chem.* 2019 Mar 15;166:232-242. doi: 10.1016/j.ejmech.2019.01.036. Epub 2019 Jan 26. PMID: 30711833.
- Ye J, Coulouris G, Zaretskaya I, Cutcutache I, Rozen S, Madden TL. Primer-BLAST: a tool to design target-specific primers for polymerase chain reaction. *BMC Bioinformatics.* 2012 Jun 18;13:134.
- Yu Z, Cai C, Gao S, Simon NI, Shen HC, Balk SP. Galeterone prevents androgen receptor binding to chromatin and enhances degradation of mutant androgen receptor. *Clin Cancer Res.* 2014 Aug 1;20(15):4075-85.
- Zhao XY, Malloy PJ, Krishnan AV, Swami S, Navone NM, Peehl DM, Feldman D. Glucocorticoids can promote androgen-independent growth of prostate cancer cells through a mutated androgen receptor. *Nat Med.* 2000 Jun;6(6):703-6.

6 LIST OF AUTHOR'S PUBLICATIONS

Publications included in the dissertation thesis:

- I. Kiss MA*, **Peřina M***, Bazgier V, May NV, Baji Á, Jorda R, Frank É. Synthesis of dihydrotestosterone derivatives modified in the A-ring with (hetero)arylidene, pyrazolo[1,5-a]pyrimidine and triazolo[1,5-a]pyrimidine moieties and their targeting of the androgen receptor in prostate cancer. **J Steroid Biochem Mol Biol.** 2021 Jul;211:105904.

*shared first authorship

IF (2021): 5.0 (Q1, clinical biochemistry, endocrinology; Q2, molecular medicine)
MP (40% contribution), as a shared first author, performed cellular experiments analyzing the biological activity of the tested substances, the effect on the AR, its signalling and the binding of candidate substances. He interpreted the obtained data and participated in writing the manuscript.

- II. **Peřina M***, Kiss MA*, Mótyán G, Szczyrbová E, Eliáš M, Študent V Jr, Kurfürstová D, Kovalová M, Mada L, Bouchal J, Frank É, Jorda R. A-ring-fused pyrazoles of dihydrotestosterone targeting prostate cancer cells via the downregulation of the androgen receptor. *Eur J Med Chem.* 2023a Mar 5;249:115086.

*shared first authorship

IF (2022): 6.7 (Q1, chemistry, medicine, pharmacology)
MP (40% contribution), as shared first author, optimized and performed biochemical and cellular experiments analyzing the biological activity of the tested substances, the effect on the AR and its signalling and degradation, the binding of substances and the viability of prostate cancer cell lines after treatment. Using computer modelling, he created a model of the binding pose. He interpreted the obtained data and significantly participated in the writing of the manuscript and its revision.

- III. Kiss MA, **Peřina M**, Bereczki L, Baji Á, Bělíček J, Jorda R, Frank É. Dihydrotestosterone-based A-ring-fused pyridines: Microwave-assisted synthesis and biological evaluation in prostate cancer cells compared to structurally related quinolines. **J Steroid Biochem Mol Biol.** 2023 Jul;231:106315.

IF (2022): 4.1 (Q2, clinical biochemistry, endocrinology; molecular medicine)
MP (30% contribution), as a co-author, performed biochemical and cellular experiments analyzing the biological activity of the tested substances, the effect on the androgen receptor, its signalling and proof of binding of the substances. Using computer modelling, he created a model of the binding pose. He interpreted the data and participated in the writing of the manuscript.

- IV. Peřina M**, Kiss A, Mernyák E, Mada L, Schneider G, Jorda R. Synthesis of hydrocortisone esters targeting androgen and glucocorticoid receptors in prostate cancer in vitro. **J Steroid Biochem Mol Biol.** 2023b May;229:106269.

IF (2022): 4.1 (Q2, clinical biochemistry, endocrinology, molecular medicine)
MP (40% contribution) as the first author optimised and performed biochemical experiments analyzing the biological activity of the tested substances, the effect on the AR and GR and their signalling and substance binding. He created a model of the binding pose, studied the viability and proliferation of prostate cancer cell lines, interpreted the data and wrote the manuscript and its revision.

- V. Rudovich AS, Peřina M**, Krech AV, Novozhilova MY, Tumilovich AM, Shkel TV, Grabovec IP, Kvasnica M, Mada L, Zavialova MG, Mekhtiev AR, Jorda R, Zhabinskii VN, Khripach VA. Synthesis and Biological Evaluation of New Isoxazolyl Steroids as Anti-Prostate Cancer Agents. **Int J Mol Sci.** 2022 Nov 4;23(21):13534.

IF (2022): 5.6 (Q1, medicine, organic chemistry; Q2, molecular biology)
MP (30% contribution), as a co-author performed biochemical and cellular experiments analyzing the biological activity of the tested substances, the effect on the AR and its signalling, and binding of substances. He created a model of the binding pose, interpreted the data and participated in the writing of the manuscript.

Other publications:

Jorda R, Havlíček L, Štunc A, Tušková D, Daumová L, Alam M, Škerlová J, Nekardová M, **Peřina M**, Pospíšil T, Šíroká J, Urbánek L, Pachtl P, Řezáčová P, Strnad M, Klener P, Kryštof V. 3,5,7-Substituted Pyrazolo[4,3-d]pyrimidine Inhibitors of Cyclin-Dependent Kinases and Their Evaluation in Lymphoma Models. **J Med Chem.** 2019 May 9;62(9):4606-4623.

Jansa J, Jorda R, Škerlová J, Pachtl P, **Peřina M**, Řezníčková E, Heger T, Gucký T, Řezáčová P, Lyčka A, Kryštof V. Imidazo[1,2-c]pyrimidin-5(6H)-one inhibitors of CDK2: Synthesis, kinase inhibition and co-crystal structure. **Eur J Med Chem.** 2021 Apr 15;216:113309.

Dayal N, Řezníčková E, Hernandez DE, **Peřina M**, Torregrosa-Allen S, Elzey BD, Škerlová J, Ajani H, Djukic S, Vojáčková V, Lepšík M, Řezáčová P, Kryštof V, Jorda R, Sintim HO. 3H-Pyrazolo[4,3-f]quinoline-Based Kinase Inhibitors Inhibit the Proliferation of Acute Myeloid Leukemia Cells In Vivo. **J Med Chem.** 2021 Aug 12;64(15):10981-10996.

Vlková K, Gucký T, **Peřina M**, Řezníčková E, Kryštof V. Synthesis and biological activity evaluation of novel 2,6,9-trisubstituted purine conjugates as potential protein kinases inhibitors. **Bioorg Med Chem Lett.** 2022 Mar 15;60:128603.

Jorda R, Havlíček L, **Peřina M**, Vojáčková V, Pospíšil T, Djukic S, Škerlová J, Grúz J, Renešová N, Klener P, Řezáčová P, Strnad M, Kryštof V. 3,5,7-Substituted Pyrazolo[4,3-d]Pyrimidine Inhibitors of Cyclin-Dependent Kinases and Cyclin K Degradors. **J Med Chem.** 2022 Jul 14;65(13):8881-8896.

Řezníčková E, Krajčovičová S, **Peřina M**, Kovalová M, Sural M, Kryštof V. Modulation of FLT3-ITD and CDK9 in acute myeloid leukaemia cells by novel proteolysis targeting chimera (PROTAC). **Eur J Med Chem.** 2022 Dec 5;243:114792.

- Vlková K, Padrtová R, Gucký T, **Peřina M**, Řezníčková E, Kryštof V. Synthesis and biological activity evaluation of novel 3,5,7-trisubstituted pyrazolo[1,5-a]pyrimidines. **Bioorg Med Chem Lett**. 2022 Dec 8;80:129096
- Tomanová M, Kozlanská K, Jorda R, Jedinák L, Havlíková T, Řezníčková E, **Peřina M**, Klener P, Dolníková A, Cankař P, Kryštof V. Synthesis and Structural Optimization of 2,7,9-Trisubstituted purin-8-ones as FLT3-ITD Inhibitors. **Int J Mol Sci**. 2022 Dec 18;23(24):16169.
- Gonzalez G, Kvasnica M, Svrčková K, Štěpánková Š, Santos JRC, **Peřina M**, Jorda R, Lopes SMM, Melo TMVDPE. Ring-fused 3 β -acetoxyandrost-5-enes as novel neuroprotective agents with cholinesterase inhibitory properties. **J Steroid Biochem Mol Biol**. 2023 Jan;225:106194.
- Kovalová M, Havlíček L, Djukic S, Škerlová J, **Peřina M**, Pospíšil T, Řezníčková E, Řezáčová P, Jorda R, Kryštof V. Characterization of new highly selective pyrazolo[4,3-d]pyrimidine inhibitor of CDK7. **Biomed Pharmacother**. 2023 May;161:114492.

Conferences

- Peřina M, Řezníčková E, Jorda R, Kryštof V. Biological differences among CDK4/6 inhibitors. EFMC-ACSMEDI MedChem Frontiers, Kraków, Poland (10. 6. – 13. 6. 2019) poster presentation
- Peřina M, Kiss MA, Bazgier V, May NV, Baji Á, Jorda R, Frank É. Synthesis of dihydrotestosterone derivatives modified in the A-ring with (hetero)arylidene, pyrazolo[1,5-a]pyrimidine and triazolo[1,5-a]pyrimidine moieties and their targeting of the androgen receptor in prostate cancer. CHEMISTRY AND BIOLOGY OF PHYTOHORMONES AND RELATED SUBSTANCES 2021, Malenovice (12. -14. 9. 2021) – oral presentation awarded with a price
- Peřina M, Kiss A, Mernyák E, Mada L, Schneider G, Jorda R. Hydrocortisone esters targeting androgen and glucocorticoid receptors in prostate cancer. CHEMISTRY AND BIOLOGY OF PHYTOHORMONES AND RELATED SUBSTANCES 2022, Malenovice (15. -17. 5. 2022) – oral presentation
- Peřina M, Supíková K, Bělíček J, Kovalová M. Production of transferases for ligand discovery and structural biology. EMBO WORKSHOP: Chemical biology 2022, Heidelberg, Germany (5. 9. – 8. 9. 2022) – poster presentation
- Peřina M, Kiss MA, Mótyán G, Szczyrbová E, Eliáš M, Študent V Jr, Kurfürstová D, Kovalová M, Mada L, Bouchal J, Frank É, Jorda R. A-ring-fused pyrazoles of dihydrotestosterone targeting prostate cancer cells via the downregulation of the androgen receptor. CZECH ANUAL CANCER RESEARCH MEETING 2022, Olomouc (1. - 2. 12. 2022) – poster presentation
- Peřina M, Kiss MA, Mótyán G, Szczyrbová E, Eliáš M, Študent V Jr, Kurfürstová D, Kovalová M, Mada L, Bouchal J, Frank É, Jorda R. A-ring-fused pyrazoles of dihydrotestosterone in prostate cancer. CZECH ANUAL CANCER RESEARCH MEETING 2023, Olomouc (20. - 22. 11. 2023) – oral presentation

7 SOUHRN

Léčba rakoviny prostaty (PCa) prošla významným pokrokem a cílení na androgenový receptor (AR) hormonální terapií nové generace zlepšilo výsledky, ale téměř u všech pacientů nakonec dochází k rozvoji rezistence. Pro zlepšení účinnosti léčby PCa je proto zapotřebí vývoj nových léčiv.

V hlavní část disertační práce byla analyzována biologická aktivita knihovny dihydrotestosteronových (DHT)-derivátů s různými modifikacemi na A-kruhu (celkem 119 sloučenin) připravené syntetickou skupinou Évy Frank (University of Szeged, Maďarsko). Modifikace DHT fúzí s pyrazolem byla obecně nejúčinnějším strukturním motivem analyzovaných sloučenin, jejíž zástupci vykazovali silnou antagonistickou aktivitu vůči transaktivaci AR a silnou antiproliferativní aktivitu vůči PCa, převyšující standardní antagonisty AR, jako je enzalutamid a galeteron. Nejúčinnější látka vyvolala snížení exprese a degradaci AR i ve vzorcích pacientů *ex vivo*. Molekulárním dokováním byl popsán strukturní základ aktivity sloučenin a objasněna interakce s ligand-vazebnou doménou AR i potenciál pro další optimalizaci.

V druhé části disertační práce, vzhledem k roli glukokortikoidového receptoru (GR) u PCa se získanou rezistencí, byly také analyzovány nové deriváty hydrokortizonu a nalezení duální antagonisté AR/GR. Nejúčinnější sloučenina potlačila signalizaci obou receptorů a její interakce s jadernými receptory byly prokázány v buňkách i namodelovány molekulárním dokováním. Zjištění podporují vývoj a charakterizaci duálních antagonistů AR/GR jako protirakovinných léčiv pro případy PCa se zvýšenou aktivitou a expresí GR.

Obecně disertační studie poskytla cenné poznatky o návrhu a vývoji nových sloučenin cílených na AR pro léčbu PCa a zdůraznila jejich potenciál jako alternativní nebo doplňkové terapie ke stávajícím standardním přístupům.